W. Schäberle

Ultrasonography in Vascular Diagnosis

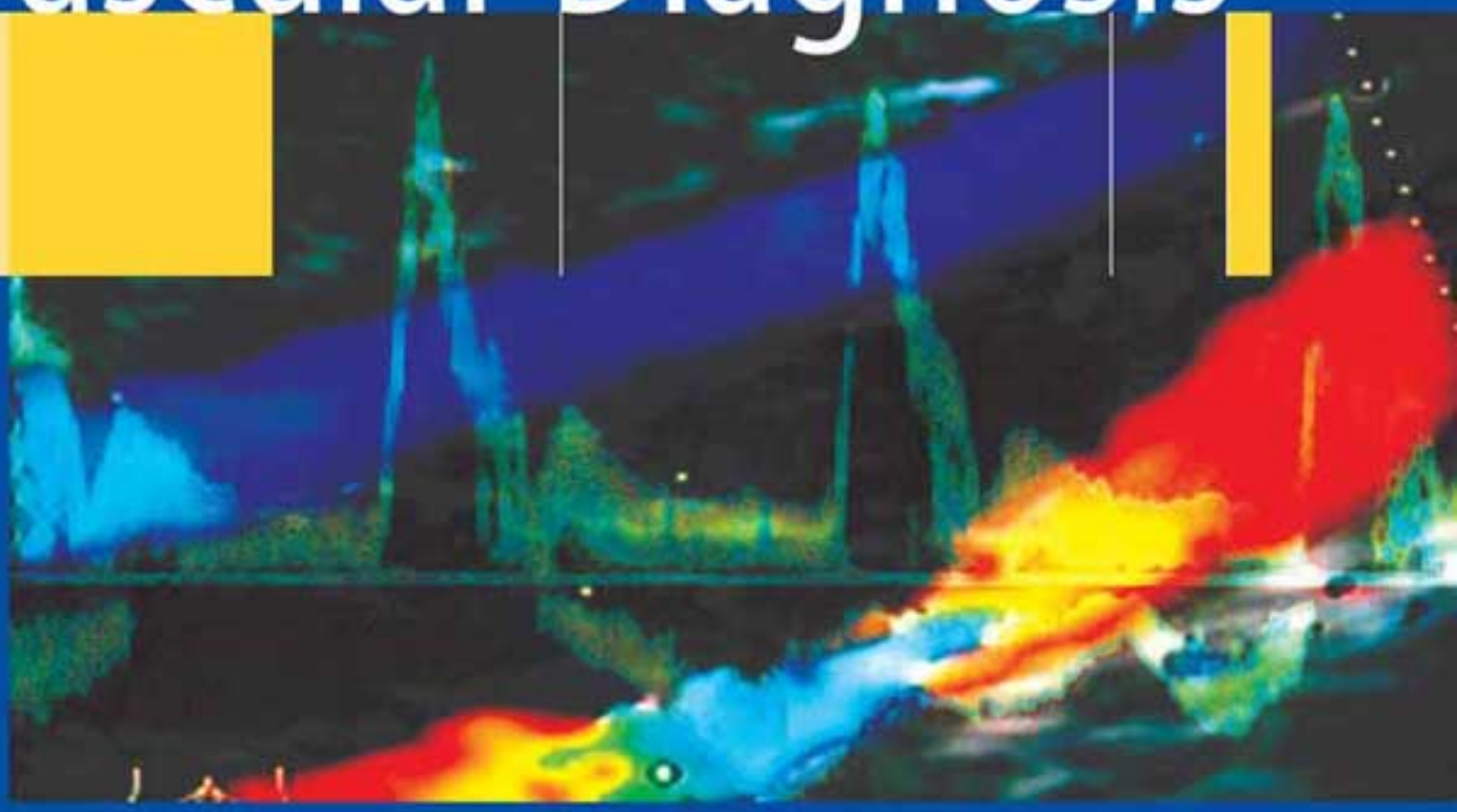

A Therapy-Oriented Textbook and Atlas

Springer

W. Schäberle

Ultrasonography in Vascular Diagnosis

A Therapy-Oriented Textbook and Atlas

With 303 Figures in 818 Parts and 77 Tables

Springer

Dr. Wilhelm Schäberle
Klinik für Viszeral-, Gefäß-, Thorax- und Kinderchirurgie
Klinik am Eichert
P. O. B. 660
73006 Göppingen
Germany

Translator: Bettina Herwig, Hauptstraße 4 H, 10317 Berlin, Germany

Title of the Original German Edition:
Ultraschall in der Gefäßdiagnostik –
Therapieorientiertes Lehrbuch und Atlas

ISBN 3-540-43228-0

ISBN 3-540-23220-6 Springer-Verlag Berlin Heidelberg New York

Library of Congress Control Number: 2005927483

Springer-Verlag Berlin Heidelberg New York
Springer is a part of Springer Science+Business Media
http://www.springeronline.com

Printed in Germany

Editor: Dr. Ute Heilmann
Desk Editor: Wilma McHugh
Production Editor: Joachim W. Schmidt

Cover design: eStudio Calamar, Spain

Typesetting: FotoSatz Pfeifer GmbH, 82166 Gräfelfing, Germany
Printed on acid-free paper – 24/3150 – 5 4 3 2 1 0

To Solange

Preface to the English Edition

Vascular ultrasonography becomes increasingly valuable the more the diagnostic query to be answered is based on the clinical findings and the more the examination is performed with regard to its therapeutic consequences. As with other specialties that make use of ultrasound findings, the diagnostic yield of vascular ultrasound relies crucially on the close integration of the examination into the routine of the clinician or physician treating the patient. That is why in the German-speaking countries, vascular ultrasound is chiefly performed by angiologists and vascular surgeons. Duplex ultrasound can indeed be regarded as an integral component of the angiologic examination or an extension of the clinical examination by fairly simple technical means. Thus the sonographic findings do not simply supplement other imaging modalities but, together with the clinical findings, provide the basis for deciding whether medical therapy, a radiologic intervention, or surgical reconstruction is the most suitable therapy for an individual patient. This means that in a patient with atherosclerotic occlusive disease of the leg arteries, the patient's clinical presentation determines whether or not surgical repair is necessary while the duplex sonographic findings serve to plan the kind of repair required and to confirm the localization and extent of the vascular pathology suspected on clinical grounds. Up to this point, no invasive diagnostic tests are needed. Angiography continues to have a role in planning the details of the surgical procedure, i.e. identification of a suitable recipient vessel for a bypass graft. Some surgical procedures such as thromboendarterectomy of the carotid arteries or femoral bifurcation can be performed without prior angiography, which does not provide any additional information that would affect the surgical strategy. Duplex sonography has evolved into the gold standard for answering most queries pertaining to venous conditions (therapeutic decision-making in thrombosis, planning of the surgical intervention for varicosis, chronic venous insufficiency).

Special emphasis is placed on the therapy-oriented presentation of indications for vascular ultrasonography, including the sonographic differentiation of rare vascular pathology and the role of the ultrasound examination in conjunction with the patient's clinical findings. The abundant images provided are intended to facilitate morphologic and hemodynamic vascular evaluation and put the reader in a position to become more confident in identifying rare conditions as well, which often have a characteristic appearance and are thus recognizable at a glance. The high acceptance of the diagnostic concept advocated here as reflected in the success of the first two editions of the book in the German-speaking countries led to the decision to have an English edition. I would like to thank Springer-Verlag, in particular Dr. Heilmann, for making this English edition possible.

Göppingen, August 2005 *Wilhelm Schäberle*

Preface to the Second German Edition

Vascular duplex sonography is the continuation of the clinical examination of vascular disease by fairly simple technical means. A sonographic examination relies on interaction with the patient and is guided by the clinical findings, therapeutic relevance, and treatment options available. It is highly examiner-dependent and does not easily lend itself to full documentation of the results, which are thus difficult to communicate and verify. For these reasons, sonographers require thorough training, both to avoid inaccurate findings with disastrous consequences for patients and in order not to discredit the method.

The format of the first edition with a text section and an atlas for each vascular territory has been retained as has the subdivision of the individual chapters into sections on sonoanatomy, examination technique, normal findings, abnormal ultrasound findings, and diagnostic role of the sonographic findings. Given the special focus of this textbook on clinically and therapeutically relevant aspects of vascular ultrasonography, each of the main chapters (peripheral arteries and veins, extracranial arteries supplying the brain, hemodialysis shunts, and abdominal and retroperitoneal vessels) has been supplemented with a section on the clinical significance of ultrasound examinations in the respective vascular territory. This addition was considered necessary in order to do justice to the expanding and changing role of diagnostic ultrasound since the first German edition six years ago. While until only a few years ago vascular ultrasound was used for orientation or served as a supplementary diagnostic test only, it has since evolved into a key modality in this field. It has since even become a kind of gold standard in the diagnostic evaluation of veins, in particular in patients with thrombosis and varicosis. In this setting, venography has lost its significance and its use is now restricted to exceptional cases where it serves to obtain supplementary information to answer specific questions.

In patients with arterial disease, duplex ultrasound is an integral part of the step-by-step diagnostic workup. The sonographic findings provide the key to adequate therapeutic management (medical therapy, radiologic intervention, or vascular surgical repair). Together with the patient's clinical status, duplex sonography is thus decisive for establishing the indication for medical therapy or invasive vascular reconstruction. Duplex sonography has replaced angiography in the localization of a vascular obstruction and the evaluation of its significance. The invasive radiologic modality is used only to identify a suitable recipient segment in patients scheduled for a bypass procedure or in combination with a catheter-based intervention (PTA and stenting). The morphologic information provided on the vessel lumen and wall as well as on perivascular structures makes nonatherosclerotic vascular disorders a domain of ultrasound.

Ultrasonography is the method of first choice in evaluating carotid artery stenoses for stroke prevention by identifying those patients who would benefit from surgical repair on the basis of hemodynamic parameters but also taking into account morphologic information. Ultrasound can retain its central role in therapeutic decision-making only if its advantages are fully exploited, which means that the examination should be performed by the angiologist or vascular surgeon who is also treating the patient. This is why this second edition is again intended mainly for angiologists and vascular surgeons.

The revised edition also describes recent developments such as the use of ultrasound contrast media, or echo enhancers, in angiology and the B-flow mode although their role in the routine clinical setting is small from the angiologist's and vascular surgeon's perspective. The use of ultrasound contrast media in differentiating liver tumors is not dealt with in detail since it is mainly of interest to gastroenterologists and visceral surgeons and would therefore go beyond the scope of this textbook.

As in the first edition, great care was taken in selecting illustrative ultrasound scans of high quality for the atlas, following the motto "an ultrasound image must speak for itself". The sonomorphologic context is important for didactic purposes; that is why the pathology of interest is not shown in a magnified view (zoom) but presented in the constellation in which it appears in the course of a routine examination. In those settings where the sonication conditions are poor but an ultrasound examination nevertheless appears to be indicated from a clinical perspective as in postoperative patients, the examples shown were not selected specifically but are such as illustrate this fact. Angiograms, and in individual cases graphic representations, are intended to clarify the situation.

The abundant images contained in the atlas sections reflect the intention not only to present abnormal finding as such but to illustrate more clearly situations that are relevant from a therapeutic perspective and to also show the development of vascular pathology. Adhering to the ultrasound convention of depicting cranial on the left side of the image and caudal on the right, the blood flow direction is color coded in accordance with the defaults settings of the ultrasound equipment. This means, for instance, that the internal carotid artery is coded in blue, indicating arterial blood flow away from the transducer. Following this convention, it is thus not necessary to first have to look for the color key, and orientation is facilitated when complex vascular territories such as the abdominal and retroperitoneal vessels are examined.

The detailed introduction to the fundamental physical principles of diagnostic ultrasound and basic hemodynamics under normal and abnormal conditions as well as the detailed description of vascular anatomy, examination protocols, and of the interpretation of the findings aim at providing the beginner with an introduction to vascular ultrasound. It is hoped that the richly illustrated atlas sections will facilitate the first steps for the beginner. For experienced sonographers, the detailed illustrations also of rare vascular pathology are expected to broaden their knowledge and help them diagnose rare disorders with greater confidence. To this end the role of ultrasound examinations is compared with that of other diagnostic modalities and tips and tricks are described that facilitate the examination and provide a basis for tackling more difficult diagnostic tasks. That is why all diseases in which ultrasonography is indicated and that are of relevance for angiologists and vascular surgeons are represented by images in the atlas. Rare vascular conditions can often be identified sonographically at a glance. Where appropriate, additional angiograms illustrate the role of the respective modality in comparison, and occasionally the situation is further clarified by an intraoperative photograph.

The constant support I received from Professor R. Eisele is gratefully acknowledged. My special thanks are due to the co-workers of Springer-Verlag for their excellent cooperation in preparing the second edition and to Ms. R. Mütschele for her assistance in preparing the graphics.

Göppingen, February 2004 *Wilhelm Schäberle*

Preface to the First German Edition

Conventional and color duplex ultrasonography has evolved into an indispensable tool for the diagnostic evaluation of vascular pathology. As a noninvasive test that can be repeated any time, sonography is increasingly replacing conventional diagnostic modalities that cause more discomfort to the patient. The combination of gray-scale sonographic information for evaluating topographic relationships and morphologic features of vessels with the qualitative and quantitative data obtained with the Doppler technique enables fine diagnostic differentiation of vascular disorders. In particular, the hemodynamic Doppler information is a useful supplement to the findings obtained with radiologic modalities. Being noninvasive and easy to perform any time, duplex sonography precedes more invasive, stressful, and expensive diagnostic tests in the step-by-step diagnostic workup of patients with vascular disease. It provides crucial information for optimal therapy and will replace invasive modalities such as angiography and venography as examiners gain skills and experience and ultrasound equipment becomes more sophisticated.

The significance duplex ultrasonography has gained in the hands of angiologists and vascular surgeons is also reflected in the further education programs for these specialties. This book therefore aims at providing a detailed description of the diagnostic information that can be obtained by (color) duplex sonography in those vascular territories that are relevant to angiologists and vascular surgeons. Each of the main chapters introduces beginners to the relevant vascular anatomy and scanning technique while at the same time offering detailed discussions of the parameters involved and a thorough review of the pertinent scientific literature to help experienced sonographers become more confident in establishing their diagnoses.

The first chapter presents the basic hemodynamic concepts that are relevant to vascular sonography and the fundamental physical and technical principles of vascular ultrasonography. This introductory chapter is intended to help readers grasp the potential and limitations of the method.

The situation in Germany is different from that in many other countries in that duplex sonography is performed primarily by angiologists, internists, and increasingly by vascular surgeons rather than by radiologists. On the basis of a patient's clinical findings, it is thus possible to specifically address therapeutically relevant questions in performing the sonographic examination. Besides general assessment of the vascular status, ultrasound can thus serve to acquire additional diagnostic information important for therapeutic decision-making in general and for planning the surgical procedure in particular. Duplex sonography in the hands of the clinician who is also treating the patient is seen as the continuation of the clinical examination by technical means. That is why the emphasis in this book is on the clinical and therapeutic role of ultrasound findings, and the individual chapters are organized according to such pragmatic aspects.

Each of the six main chapters deals with a specific vascular territory and consists of a text section as well as an atlas section with ample illustrations and detailed descriptions of normal findings, variants, and abnormal findings. Whenever considered appropriate for better illustration of complex pathology, the sonographic images have been supplemented with angiograms or CT scans. The comparison also illustrates the advantages and disadvantages of the respective radiologic modalities. As many rare vascular disorders are diagnosed at a glance by an experienced sonographer, their appearance is shown in numerous figures. Series of ultrasound scans document the course of the examination and complex hemodynamic changes in vascular disorders as well as their clinical significance and changes under therapy. The legends provide detailed descriptions allowing the reader to use the atlas sections independently for reference when looking for information on specific vascular conditions.

Different ultrasound modes are described in detail and their respective merits and shortcomings are discussed for the benefit of readers using different equipment. Gray-scale sonography alone (compression ultrasound) is quite sufficient for the diagnostic assessment of thrombosis while conventional duplex ultrasonography is a valid modality for diagnosing therapeutically relevant abnormal changes of the femoropopliteal territory. In most instances, color flow images are shown together with the Doppler waveform but occasionally "only" the conventional duplex scan is presented to illustrate the fact that many abnormalities can be identified by conventional duplex ultrasound alone. Despite the additional diagnostic information obtained with the color-coded technique, quantitative evaluation relies on the Doppler frequency spectrum. The color duplex mode can facilitate the examination procedure (identification of small vessels, recanalization, differential diagnosis) but the sonographer needs some basic knowledge of the conventional Doppler technique for the proper interpretation of color flow images.

My special thanks are due to Professor R. Eisele for promoting the use of diagnostic ultrasound in the department of vascular surgery at our hospital and for his valuable advice. I thank Ms. G. Rieker and Ms. E. Stieger and Mrs. B. Sihler for typing the manuscript and Ms. R. Uhlig for the photographic work in preparing the figures.

Finally I would like to express my thanks to the publishers, Springer-Verlag, and in particular to Ms. Zeck and Dr. Heilmann, for their excellent cooperation and constructive support.

Göppingen, December 1997 *Wilhelm Schäberle*

Table of Contents

Fundamental Principles 1

1.1 Technical Principles of Diagnostic Ultrasound

All ultrasound techniques rely on the processing of *reflected sound waves*. A wave motion results from the periodic, medium-dependent propagation of the vibration of particles around their resting positions. Sound waves are pressure waves that spread by alternately compressing and decompressing the medium they are traveling in. The speed of sound wave propagation is a function of the compressibility and density of the medium. Various modes of sound propagation are distinguished, again depending on the medium. Transverse waves occur when the particles vibrate around a resting position perpendicular to the direction of propagation, longitudinal waves occur when the vibration is parallel to the direction. In solid media, sound propagates in the form of both transverse and longitudinal waves. In fluids and gases, only longitudinal waves occur because no shearing forces are present in these media. As the human body mostly consists of water, the effect of transverse waves is negligible. Particles excited in the ultrasound range vibrate around their resting positions at a rate of 20,000 to 1 billion times per second. The frequencies used in vascular ultrasonography range from 2 – 10 MHz (frequency f: 1 hertz = 1/s).

The velocity of sound waves, C, is the product of wavelength λ and frequency f:

$$C = \lambda \cdot f$$

Wavelength λ is the shortest distance between two vibrating particles in identical states of motion (Table 1.1). The average speed of sound in human tissue is about 1,540 m/s. The wavelengths occurring in diagnostic ultrasound are determined by the frequency emitted by the transducer (carrier frequency) and range from 0.7 mm at a frequency of 2 MHz to 0.15 mm at 10 MHz.

Table 1.1. Parameters defining a sound wave

Period:	Duration of a complete vibration
Wavelength:	Spatial extension of a period
Frequency:	Number of periods per second
Amplitude:	Measure of sound energy

1.1.1 Physical Factors Affecting the Ultrasound Scan (B-mode Scan)

An ultrasound image is created by processing the echoes returning to the transducer from various depths of the body upon emission of an ultrasound pulse of a specific frequency. A two-dimensional image is generated from adjacent ultrasound lines. Two-dimensional morphologic images are acquired by applying short pulses of energy using only a small number of wavelengths in order to optimize spatial resolution. The *echo arrival time* is the time delay between the emission of an ultrasound pulse and the return of the reflected echo and is a function of the distance between the transducer and the reflecting particle. Reflection occurs at the boundaries between media that differ in their sound propagation properties. Each tissue structure in the human body has a specific sound resistance, or *acoustic impedance*. The impedance is equal to the *speed of sound propagation* multiplied by the *density* of the medium. Hence, an ultrasound scan does not visualize tissue structures directly but rather interfaces between tissues of different acoustic impedance. The greater the difference in impedance, the greater the *reflection* of the ultrasound wave and the smaller its *transmission* into deeper tissue. Other physical processes besides reflection and scattering that affect the ultrasound scan are refraction, interference, diffraction, attenuation, and absorption.

The echo pulses reflected back from an interface between media of different acoustic impedance can be processed for image generation only if the interface is relatively perpendicular to the ultrasound beam (angles of incident and reflected beam). For this reason, structures such as vessel walls perpendicular to the beam appear fairly bright compared to vessel walls tangential to the beam since most echo pulses are reflected back to the transducer by the former. Reflection occurs at the surfaces of particles that are larger than the wavelength, while scattering predominates when they are smaller. Since structures perpendicular to the beam are rare in clinical ultrasound examinations, an ultrasound image is chiefly generated from a mixture of reflected and scattered echoes. Aggregations of tissue cells scatter the beam diffusely in all directions but with a low energy only. Therefore, a structure appears bright and is clearly defined when it is perpendicular to the ultrasound beam because the image information is mainly derived from reflected echoes; its visualization is weaker and less bright when the ultrasound beam strikes

tangentially and only diffusely reflected echoes are available to generate the image, although the impedance is identical in both cases.

The intensity of the returning echoes is dependent on the emitted frequency. Attenuation increases with frequency and limits the penetration depth of the ultrasound pulse. The emitted intensity decreases exponentially with distance and is influenced by an attenuation coefficient that varies with the type of tissue through which the beam travels in the human body (fat, muscle, blood). The average intensity in the body ranges from 0.3 to 0.6 decibels/MHz cm. The energy is converted into absorption heat.

Higher carrier frequencies result in a lower penetration depth because attenuation is more pronounced. The increasing attenuation can be compensated for to some extent by adjusting amplification (gain). Using transducers with a wide frequency range results in the predominance of lower frequencies with greater penetration depths because attenuation of higher frequencies is more pronounced.

In addition to scattering and reflection, there is *refraction* at the interface between different media. Refraction in the direction of the normal to the interface occurs when there is an increase in sound velocity in the next medium, refraction away from the normal when the velocity decreases. Refraction may lead to misinterpretation of the location and size of the structure visualized.

Interferences of sound waves can change the amplitude and thus the brightness of an image despite an identical acoustic impedance in the boundary zone. Depending on the momentary phase of the wave, the amplitude is either amplified or diminished.

Resolution describes the spatial discrimination of two structures differing in acoustic impedance. A distinction is made between *axial resolution* (resolution in the direction of sound propagation) and *lateral resolution*. Axial resolution solely depends on the wavelength and increases as the wavelength decreases, i.e. the frequency increases. It ranges from 0.2 to 1 mm, depending on the emitted frequency.

Lateral resolution refers to the ability of discriminating two points located side by side on the image. It is likewise determined by the transmit frequency and the resulting wavelength but also by the array of the transducer elements. Only in a certain area does the ultrasound beam have a high resolution while in front of and behind this area the resolution is much poorer. The slow speed of sound in human tissue (1,540 m/s) and the aim of achieving a high frame rate (real-time display) limit the number of ultrasound scan lines that can be used per image. In order to relate the echoes to a specific depth, it is necessary to wait for the arrival of the returning echo from the respective depth of the preceding pulse before emission of the next ultrasound pulse. The transmitted or received pulse is focused in a longitudinal direction relative to the transducer, and focusing of the returning pulse in the scan plane is optimized in smaller steps (dynamically, almost continuously with the arrival time of the pulse).

The possible resolution is proportional to the wavelength. It is $1/2\lambda$ (wavelength) for axial resolution and much poorer for lateral resolution with a value of 4λ. Depending on the wavelength, axial and lateral resolution increase with the ultrasound frequency. However, greater penetration depths are achieved only by using transducers with lower transmit frequencies (attenuation). When deeper vessels are scanned, a compromise must be found at the expense of an adequate discrimination of the vessel structures of interest (poorer spatial resolution resulting from a lower transmit frequency).

The *scanning depth* encoded in the B-mode image is calculated from the echo arrival time. As attenuation increases with the penetration depth (arrival time), progressively increasing amplification is applied to the echo signals as they arrive from deeper in the body in order to visualize them with the same intensity. This electronic correction is referred to as "time-gain compensation" or "depth-gain compensation". Overall gain and depth gain are chosen according to the localization of the vessel of interest. The gain is crucial for the amplitude or intensity of the signal, together with the output energy and the signal-to-noise limit, and must be set properly when assessing vascular structures.

Lateral resolution is limited by the proximity of the transducer elements emitting the ultrasound pulses. Resolution along the longitudinal axis can be improved by exciting a small number of elements at a time rather than operating on the whole array. A more focused beam is achieved by later excitation of the transducer elements in the center. Dynamic focusing is accomplished by applying small time delays to the excitation pulses driving the individual transducer elements. Resolution in the third direction, or slice thickness, depends on the position in the image.

1.1.2 Basic Physics of Doppler Ultrasound

Sound waves change in frequency as a result of relative expansion between the transmitter and receiver. This frequency shift is called the Doppler effect, named after the Viennese mathematician Christian Doppler (1803 to 1852), and is proportional to the velocity between the transmitter and receiver. In addition, the frequency shift is influenced by the direction of motion: the frequency increases as the transmitter and receiver approach each other and decreases as they move apart.

In diagnostic ultrasound, the Doppler effect is used to measure blood flow velocity. In this application, when the emitted ultrasound beam strikes moving blood cells, the latter reflect the pulse with a specific Doppler shift frequency that depends on the velocity and direction of blood flow. The shift is detected by the transducer. The direction of blood flow relative to the transducer determines whether the returning echoes have a higher or lower frequency and flow velocity determines the magnitude of the frequency shift (Fig. 1.1). On the other hand, the Doppler frequency shift is proportional to the carrier frequency. This relationship is summarized by the Doppler equation:

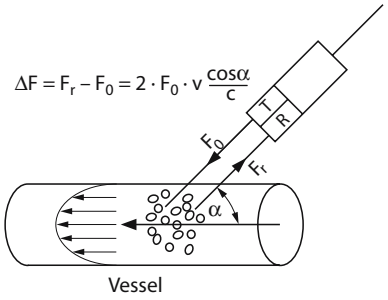

Fig. 1.1. Schematic representation of Doppler interrogation of a vessel with laminar flow. The arrows in the vessel are vectors representing different flow velocities. Blood flow is fastest in the center of the vessel and decreases toward the wall. The drawing illustrates the effect of the angle of incidence on the Doppler measurement. In the equation for calculating the Doppler shift, this angle is represented by the cosine function. The Doppler shift increases with the acuity of the angle (cosine of 90° = 0). (*T* transmitter, *R* receiver, F_o emitted frequency, F_r reflected frequency)

$$F_d = F_0 - F_r = \frac{2F_0 \cdot v \cdot cos\ \alpha}{c}$$

F_d Doppler frequency shift,
F_o emitted frequency,
F_r reflected frequency,
v mean flow velocity of the reflecting red blood cells,
c speed of sound in soft tissue (about 1,540 m/s),
α angle between ultrasound beam and direction of blood flow.

In the transcutaneous measurement of blood flow by Doppler ultrasound, *angle correction* is necessary to calculate the flow velocity since the axis of the ultrasound beam is not in line with the longitudinal axis of the vessel or the direction of flow. The transformation with representation of the different velocity vectors is expressed mathematically as a cosine function of the angle between the sound beam and the blood vessel (cos α).

F_d is proportional to the velocity of blood flow, cos α, and the carrier frequency of the ultrasound beam.

For angles of about 90°, the cosine function yields values around 0, at which there is no Doppler frequency shift, and the Doppler shift increases as the angle decreases (with a maximum cos α of 1 at α = 0°).

The blood flow velocity is calculated by solving the Doppler shift equation for V:

$$V = (F - F_o) \cdot \frac{c}{cos\ \alpha \cdot 2F_0}$$

This formula allows one to calculate the *blood flow velocity* from the Doppler frequency shift occurring at a given transmit frequency and angle of incidence. The accuracy of velocity measurements increases with the acuity of the angle. Ideally, a small angle should be used (less than 60°) since larger angles will result in unacceptably high errors in the velocity estimate. At angles above 60°, even minor errors in determining the Doppler angle (which are unavoidable in the clinical setting, especially when curved vessels are scanned) unduly distort the velocity calculation. At angles around 90°, a Doppler shift is no longer detectable and the flow direction cannot be determined. This is reflected in the color duplex scan by the absence of color-coded flow signals although flow is present.

1.1.2.1 Continuous Wave Doppler Ultrasound

Continuous wave (CW) Doppler ultrasound (Fig. 1.2) uses two transducers, with one continually transmitting and the other continually recording the ultrasonic waves. Blood flow velocity is calculated from the frequency shift of the signal reflected by the moving red blood cells.

A major limitation of CW Doppler is that the signals from all moving reflectors along the path of the ultrasound beam are detected with their respective frequency shifts. Consequently, CW Doppler lacks axial resolution as it cannot differentiate flow signals from two vessels of which one lies behind the other along the beam path. The advantage of CW Doppler lies in the detection of high flow velocities without aliasing, which is accomplished by the use of separate transmit and receive crystals for the simultaneous emission and recording of ultrasound signals.

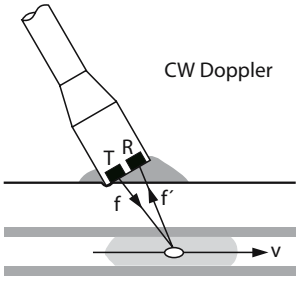

Fig. 1.2. Schematic representation of continuous wave (CW) Doppler ultrasound. Ultrasound pulses are continuously emitted by the transmitter (*T*) and return to the receiver (*R*) with the respective frequency shifts after reflection by the red blood cells moving at different velocities

1.1.2.2 Pulsed Wave Doppler Ultrasound/Duplex Ultrasound

In pulsed wave (PW) Doppler ultrasound (Fig. 1.3), a single crystal intermittently emits short pulsed Doppler signals in rapid succession, referred to as the *pulse repetition frequency* (*PRF*), and records the reflected signals in between. Sound waves travel through the human body at a fairly constant speed of about 1,540 m/s. Hence, the echo arrival time varies with the distance of the reflector from the transmitter. Using a time filter, the operator can select a specific scan depth, or sample volume, and an electronic gate then opens briefly to pass only the signals from this site. With all interfering echoes coming in earlier or later being eliminated, it is thus possible to record Doppler signals from the specified depth only. The

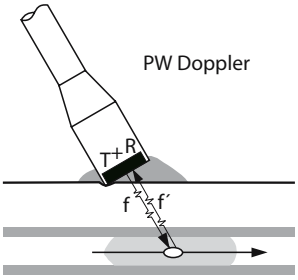

Fig. 1.3. Schematic representation of pulsed wave (PW) Doppler ultrasound. The transducer alternately emits short ultrasound pulses (*T* transmitter) and records the reflected echoes at defined intervals (*R* receiver)

combination of PW Doppler with real-time gray-scale imaging is the basis for *duplex ultrasonography*. PW Doppler has the advantage of providing axial resolution (discrimination of vessels along the ultrasound beam) but is limited by the fact that it fails to adequately record high velocity signals (depending on the transmit frequency and penetration depth). Using a single crystal for transmitting and receiving signals requires a delay between pulses for the processing of returning echoes. The longer the pulse delay, the lower the peak flow velocity that can be detected.

Duplex ultrasound combines two-dimensional real-time imaging with pulsed Doppler and thus provides flow information from a sample volume at a defined depth. Duplex scanning enables calculation of blood flow velocity from the Doppler frequency shift as the angle of incidence between the ultrasound beam and the vessel axis can be measured in the B-mode image.

1.1.2.3 Frequency Processing

In a blood vessel, blood components move with different velocities which are represented in the Doppler spectrum by a range of frequencies with different amplitudes reflecting the distribution of flow velocities in the vessel. The technique that has established itself for spectral analysis is an algorithm known as *fast Fourier transform (FFT)*, which breaks down the waveform into a series of sinusoidal waveforms. For the individual frequency values, the corresponding amplitudes are calculated and displayed in different shades of gray.

According to Fourier's theorem, any periodic waveform can be reconstructed from its component waveforms. Conversely, in spectral analysis, a complex waveform of a given frequency (Doppler shift frequency) is decomposed into its frequency components. In this case, the fast Fourier transform yields the amplitudes of the individual frequencies of the respective sine and cosine functions, which together make up the waveform. The individual frequencies thus separated are continuously displayed over time in the *Doppler frequency spectrum* (*spectral waveform*). The Doppler spectrum contains the following information on blood flow (Fig. 1.4):

- vertical axis representing different flow velocities as Doppler frequency shifts,
- horizontal axis representing the time course of the frequency shifts,
- density of points, or color intensity, on vertical axis representing the number of red blood cells moving at a specific velocity (may also be plotted in the form of a histogram).

Flow toward and away from the transducer is processed simultaneously and respectively represented above and below the baseline (zero flow velocity line).

Alternatively, some ultrasound devices display the magnitudes of the different velocity components in a separate *power spectrum*. This is done by measuring the signal intensities of the individual Doppler frequencies at a specific time in the cardiac cycle and displaying the spectral distribution in a histogram (Fig. 1.5; Table 1.2).

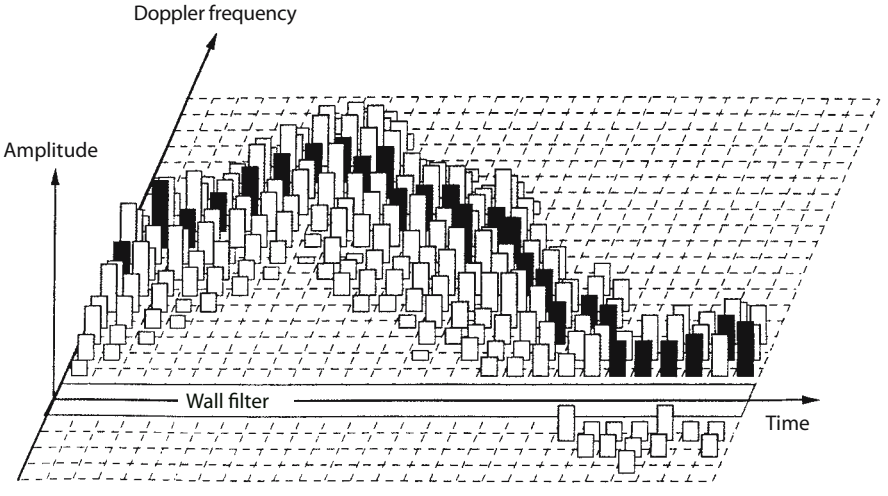

Fig. 1.4. Three-dimensional Doppler frequency spectrum showing the distribution of individual Doppler shifts (amplitudes), flow directions (above and below the time axis), and flow velocities (computed from Doppler frequency shifts). The heights of the boxes correspond to the amplitudes of the respective Doppler frequencies. A Doppler frequency spectrum represents amplitudes by different levels of brightness. In color-coded duplex ultrasound (black boxes), the averaged flow velocity at a specific point in time is displayed in color according to the flow direction and superimposed on the two-dimensional gray-scale image in real time. (According to P.M. Klews, in Wolf and Fobbe 1993)

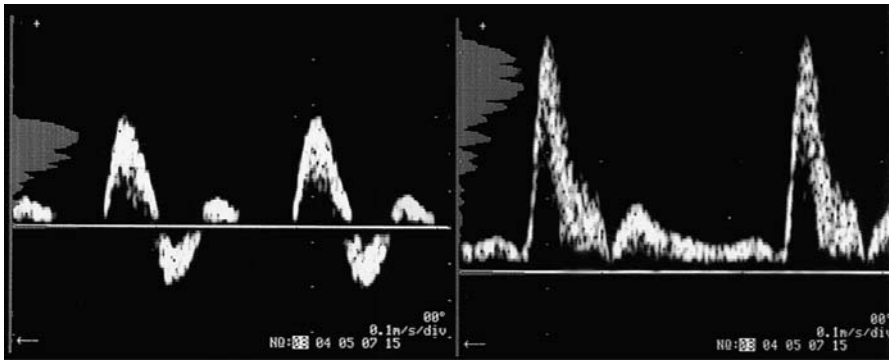

Fig. 1.5. Doppler frequency spectrum of the superficial femoral artery (*left section*). The histogram plotted on the vertical axis on the left represents the distribution of the different Doppler frequency shifts during systole. In the Doppler waveform, this distribution is represented by different levels of brightness (laminar flow). The *right section* shows the corresponding distribution during systole in the common carotid artery, which has less pulsatile flow

Table 1.2. Spectral displays

Power spectrum:	Quantitative frequency distribution in terms of amplitude
Frequency spectrum:	Temporal distribution of frequencies or velocities
Usual mode of display:	Frequency spectrum
Levels of brightness or color represent the density of a given frequency in the frequency band	

1.1.2.4 Blood Flow Measurement

The most important parameters for evaluating blood flow that can be derived from the Doppler frequency spectrum are:

- the peak systolic frequency (mainly relevant for quantifying stenosis),
- the peak end-diastolic frequency (stenosis, flow character),
- the average flow velocity,
- the mean or intensity-weighted flow velocity (which is the basis for calculation of the volume flow rate), and
- the variance (spectral broadening due to disturbed flow).

Based on these parameters, the following quantitative determinations can be performed:

- Angle-corrected peak systolic and end-diastolic velocities can be calculated from the Doppler waveform. Mean flow velocity is calculated on the basis of the signal intensities.
- The volume flow rate is calculated from the *mean flow velocity* and the *cross-sectional area* according to the following equation:

$$Q\,(ml/min) = 60 \cdot mean\ flow\ velocity\ (cm/s) \cdot cross\text{-}sectional\ area\ (cm^2)$$

Quantitative evaluation of blood flow requires accurate setting of the Doppler angle of insonation. The Doppler shift alone does not provide information on blood flow behavior. Determination of the Doppler angle is necessary to calculate the angle-corrected blood flow velocity. To minimize errors in the calculation of blood flow velocity and other quantitative determinations, the angle must be as small as possible and should not exceed 60°.

An angle setting error of ± 5° causes a 20% error in the velocity measurement at a Doppler angle of 60°. Higher angles of incidence lead to a rapid progression in the magnitude of the error (Fig. 1.6 a, b).

Various measures are available to optimize the angle of incidence for Doppler measurement:

- Use of a unilateral waterpath (linear-array transducer);
- Activation of beam steering: successive firing of the elements in the linear-array transducer produces an ultrasound wave that is emitted from the transducer at a specific angle, which makes the color box appear tilted;
- Shifting and angling of the transducer (sector and curved-array transducers): curved-array transducers with a small radius enable a wide range of motion including angulation for optimization of the Doppler angle. However, the examiner must be aware that the color coding may change as a result of a change in the flow direction relative to the sector-shaped ultrasound beam. In this case, the area of transition between red and blue is black in contrast to aliasing, where it is yellow. No Doppler frequency shift information is obtained from this black zone because the ultrasound beam is at a 90° angle to the vessel axis.

In-vitro measuring series in waterbath experiments in which two precision pumps generated different flow profiles demonstrated a good correlation of r = 0.98 between the volume flow rate measured by duplex scanning and the volumetrically determined rate (Schäberle and Seitz 1991; Fig. 1.7).

Highly reproducible measurements are obtained even in deeper abdominal vessels by minimizing the effect of errors in angle determination through interrogation of the vessel at an angle as close to 0° as possible. Repeated ultrasound measurements of flow in the superior mesenteric artery performed in 28 fasting subjects in the morning revealed a day-to-day variation of 11% in peak systolic flow velocity and of 9.7% for peak end-diastolic flow velocity (Fig. 1.8). The vascular diameter repeatedly determined using the leading-edge method showed a day-to-day variation of 2.2% (Schäberle and Seitz 1991).

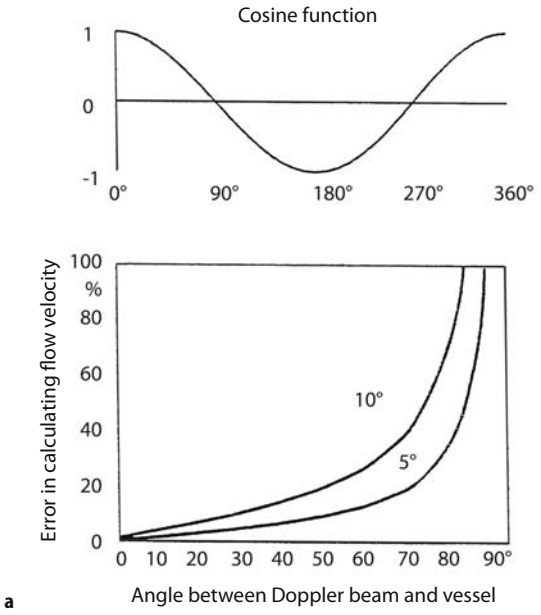

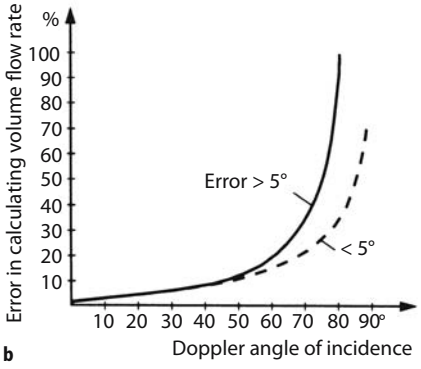

Fig. 1.6. a The equation for calculating the Doppler frequency shift incorporates the angle between the ultrasound beam and the blood flow direction in the form of the cosine function (cos α) with the shift being highest when the beam strikes the vessel tangentially (cosine of 0° = 1) and lowest when the beam is perpendicular to the vessel (cosine of 90° = 0). The larger the Doppler angle, the greater the resulting error in the velocity estimate in case of incorrect angle determination (graphically shown for errors of 5° and 10°). Such errors in setting the angle are unavoidable, in particular when aligning the angle correction cursor with the vessel wall in curved vessel segments.
b The figure shows the angle-dependent error in calculating the volume flow rate for an assumed error of ± 5°. Overestimation of the Doppler angle results in a greater error than underestimation

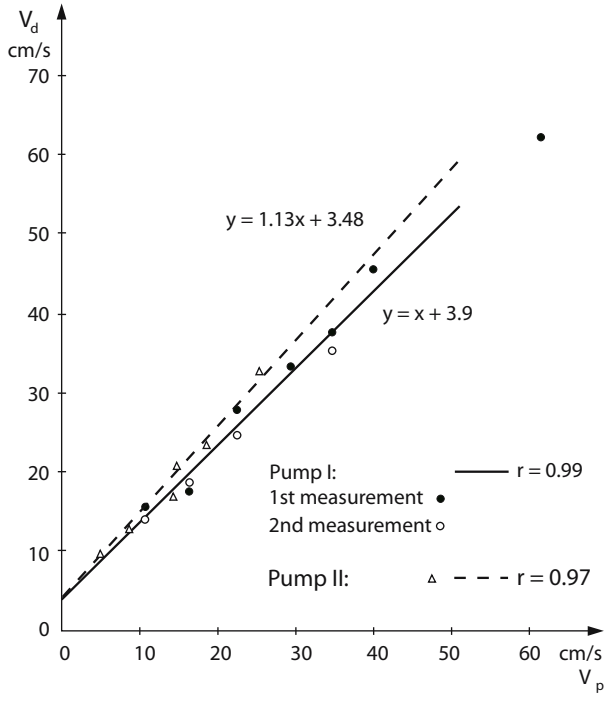

Fig. 1.7. In vitro flow measurement by duplex ultrasound. Comparison of mean flow velocity determined by duplex ultrasound (V_d) and volumetry (V_p). Different flow profiles were generated by two precision pumps (I and II). The mean axis shift of 3.75 cm/s with shift of the zero line was due to a software error and was corrected by the manufacturer following these experiments. V_p mean actual flow velocity calculated from volumetrically determined flow rate/cross-sectional area of the tube; V_d mean flow velocity determined by duplex ultrasound (mean of 5 individual measurements). (Schäberle and Seitz 1991)

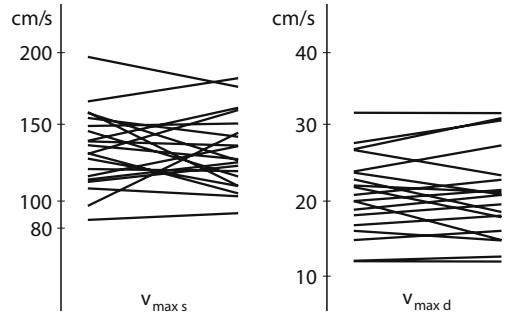

Fig. 1.8. Peak systolic ($V_{max\,s}$) and late diastolic ($V_{max\,d}$) velocities measured in the superior mesenteric artery of fasting subjects on 2 successive days (n = 28)

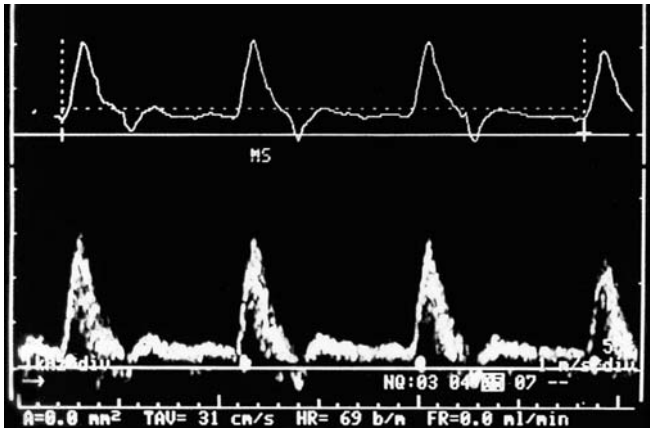

Fig. 1.9. Doppler waveform sampled in the superior mesenteric artery with adequate instrument settings (*bottom*) with the corresponding mean flow velocities calculated by the device (*top*). The mean velocity averaged over 3 cardiac cycles is 31 cm/s

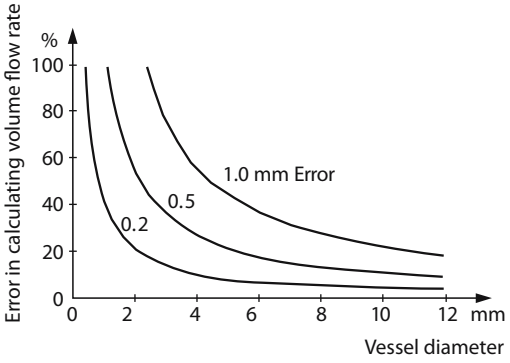

Fig. 1.10. Errors in flow rate estimation resulting from different measurement accuracies in determining vessel diameter (for errors ranging from 0.2 – 1.0 mm)

Another source of error is the inadequate setting of transmit and receive gain, resulting in over- or underestimation of the mean flow velocity (Fig. 1.9).

The major source of errors in flow measurements, however, is the inaccurate determination of the vascular diameter and the resulting inaccuracy in calculating the cross-sectional area (Fig. 1.10; Table 1.3). In B-mode scans, the vessel walls appear larger than their true anatomic size. This is due to the so-called blooming effect resulting from the strong reflection of the ultrasound beam at the boundary between tissues of different acoustic impedance (Fig. 1.11 b).

The measurement errors described above can be minimized and systematized by using the leading-edge method and a low gain setting.

Using the *leading-edge method*, the diameter is measured from the reflection of the outer wall to that of the opposite inner wall (Fig. 1.11 a). In-vitro experiments demonstrated a greater accuracy for diameters below 13 mm and showed the overestimation of diameters to be less pronounced than the underestimation associated with diameter measurement from inner wall to inner wall (Smith 1984). Moreover, use of the leading-edge method systematizes the unavoidable measurement error, thereby improving the reproducibility of measurements.

Fluctuations in diameter during the cardiac cycle are taken into account by measurement of both systolic and diastolic diameters, which enter the equation for calculating flow volume with different weighting.

The resistance indices – the *pulsatility index (PI)* and the *resistance index (RI)* according to Pourcelot – can be calcu-

Table 1.3. Sources of error in flow rate determination with duplex ultrasound

- Determination of mean flow velocity
- Error in determining the Doppler angle
- Measurement of vessel cross-section
  - Measuring accuracy (blooming effect)
  - Assumption of a circular cross-section
  - Variation in cross-section during cardiac cycle
  - Respiratory variation of vessel cross-section (veins)

Fig. 1.11 a, b. Determination of vessel diameter.
a Schematic representation of the leading-edge method. The vessel diameter is measured from the beginning of the reflection from the outer vessel wall to the beginning of the echo reflected from the opposite inner wall

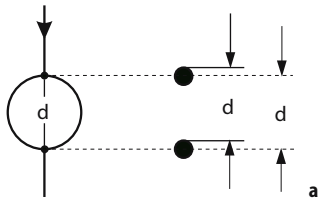

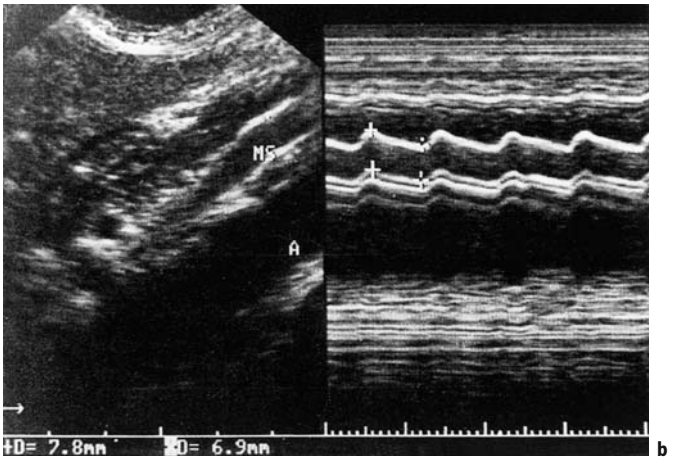

b Determination of the diameter of the superior mesenteric artery (*MS*) using the leading-edge method: The figure illustrates how the vessel wall is overemphasized as a result of the blooming effect. Systolic-diastolic variation in diameter: The gray-scale scan on the *left* coincidentally depicts the maximum systolic extension of 7.8 mm while the time-motion display shows the variation in diameter from 7.8 mm in systole to 6.9 mm in diastole

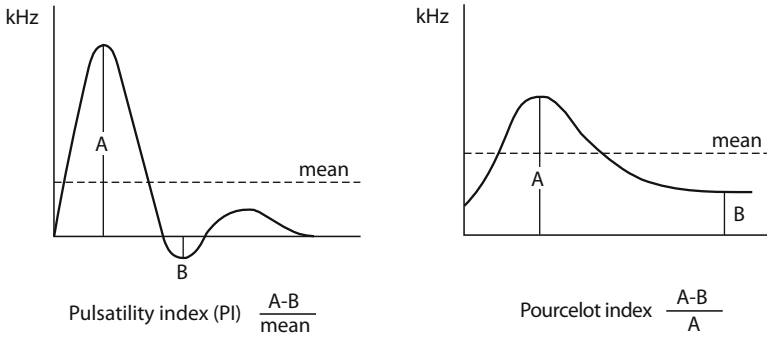

Fig. 1.12. Schematic representation of the resistance indices. The Pourcelot index is calculated from peak systolic and end-diastolic velocities while the pulsatility index can only be calculated when the ultrasound equipment allows determination of mean flow velocity

lated independently of the Doppler angle. The resistance indices, in particular the Pourcelot index, also reflect wall elasticity as well as the peripheral resistance of the organ supplied (Fig. 1.12).

In vessels with greater peripheral resistance, the Pourcelot index is higher and end-diastolic velocity decreases. Stenoses or occlusions in peripheral arteries with triphasic flow alter the Doppler waveform and the pulsatility index. The index can thus serve as a semiquantitative parameter for the evaluation of stenoses. In a vessel supplying a parenchymal organ, a relevant decrease in the Pourcelot index between the prestenotic and the poststenotic segment can be interpreted as indicating a hemodynamically significant stenosis, for instance, when looking for a renal artery stenosis.

1.1.3 Physical Principles of Color-coded Duplex Ultrasound

1.1.3.1 Velocity Mode

Color-coded duplex ultrasound combines the presentation of two-dimensional morphologic information with superimposed flow data of a defined area displayed in color. The frame rate is much lower for the color-coded, two-dimensional display of flow information than for the conventional (black-and-white) display because it takes much longer to compute the two-dimensional distribution of flow.

In conventional duplex ultrasound, a small gate (sample volume) is defined in the real-time gray-scale image for which Doppler frequency shift data is obtained by analyzing separate scan lines. This information is displayed in the form of a Doppler waveform. In pulsed *multigate Doppler*, not one but several sample volumes are placed along the Doppler beam, from which the respective Doppler frequency shift information is gathered and analyzed simultaneously by several independent channels. The flow information can thus be analyzed and displayed without delay compared to the conventional duplex scan. This technique is used in color-coded M-mode echocardiography and is the basis of color-coded duplex sonography. An ultrasound line with several measuring gates is swept over the B-mode scan or a defined part thereof in 50 – 150 ms. The number of scan lines is limited by the geometric arrangement of the crystals in the transducer and the available lines must be divided into those for generation of the gray-scale image (B-mode image lines) and those for blood flow velocity measurement (Doppler lines). Most scan lines are reserved for generation of the B-mode image with only every third or fourth line being available for acquiring Doppler information. Due to the lower number of Doppler lines, the missing information between two Doppler lines must be interpolated. Using the multigate technique with placement of several sample volumes along the Doppler beam path a two-dimensional display of blood flow distribution is generated. About 10 pulse packets are necessary for each color Doppler line to obtain precise enough information (as opposed to only one pulse packet for each B-mode scan line). Before emission of each new pulse packet, the return of reflected echoes from the maximum penetration depth must be awaited in order to be able to assign the echo signals to the respective pulses. Hence, the time required for generating a color Doppler scan line is 10 times that needed for a B-mode scan line. The information from the 50 – 250 measuring gates along each scan line is processed and analyzed simultaneously by separate channels.

Based on a mean ultrasound propagation velocity in the human body of 1,540 m/s, an echo signal reflected from a depth of 10 cm has an arrival time of 130 μs, which is the time required for the generation of a B-mode scan line. It takes 10 times longer, i.e. 1.3 ms, to generate a color Doppler scan line. If 50 color Doppler scan lines are used to generate a color Doppler image, the overall time required is about 65 ms, resulting in a frame rate of 15 images per second. The frame rate decreases when more color Doppler scan lines are required, which in turn depends on the width of the color box selected. A frame rate of at least 20/s is necessary for a smooth display with good temporal resolution.

When deeper structures are scanned, as in abdominal ultrasound, the longer delay of the echo pulses makes it necessary to use lower pulse repetition frequencies for precise spatial resolution of the echo pulses, which likewise decreases the frame rate.

In *triplex scanning*, a Doppler waveform from a defined site in the B-scan that provides detailed information on flow velocity is obtained in addition to the gray-scale morphologic data and two-dimensional flow velocity information of the duplex technique. The pulse repetition frequency for sampling of the color flow information must be kept constant in addition to the Doppler spectrum, which heavily restricts the arrangement of the pulse sequences. The frame rate is reduced further in the triplex mode because of the scan lines required for generating the Doppler spectrum. The maximum pulse repetition frequency that can be used in triplex scanning is markedly lower than that for the generation of a Doppler frequency spectrum while the B-scan or color flow display is frozen. Therefore, at higher flow velocities, the Doppler frequency spectrum should be sampled in the mono mode following color duplex scanning for orientation and placement of the sample volume in the B-mode scan.

Some improvement is possible with use of the *interleave technique*, in which a Doppler pulse echo cycle is processed after each second to fourth B-mode scan line. This technique thus enables a rather fast frame rate at low pulse repetition frequencies, e.g. when scanning deep body structures. A much higher frame rate is possible with this technique compared to the analysis of one Doppler scan line after each B-mode line.

With use of a conventional processing technique, the color-coded flow image is generated from the Doppler frequency shift of the ultrasound echoes reflected by flowing red blood cells. The frequency shift information can be analyzed and displayed in relation to velocity (velocity mode) or in relation to power (power mode).

In contrast, the *color-velocity imaging technique*, which is a so-called time-domain technique, determines flow velocity

from the echo arrival times. This is done by comparing changes in the patterns of the reflected echoes between two successive B-scan line pulses and deriving blood flow information from changes in the echo pattern over time.

Quantitatively, the direction and velocity of flow can be determined using a *cross-correlation technique*. However, this procedure makes high demands on computing capacity and has not established itself although it is superior to shift-based techniques because there is no aliasing and angle dependence and it enables higher frame rates. The cross-correlation technique does not determine the Doppler frequency or phase shift of an echo compared to the transmitted pulse but compares two successive pulse echo cycles in a defined space and at a predetermined time delay. In other words, the positional change of two pulse echo cycles is determined in relation to time. The velocity of the moving medium with its characteristic echo pattern is then calculated from the temporal shift. This technique relies on the recognition of the echo pattern, which requires an excellent signal-to-noise ratio. The only factor that limits the pulse repetition frequency is the scanning depth.

The *autocorrelation technique* compares demodulated Doppler signals. The accuracy of determining the mean Doppler shift is higher when blood flow is constant and decreases when flow becomes more turbulent. The bandwidth of the different flow components is given by the variance, which can be displayed in color by adding a green shade. Analysis of several pulse cycles will yield a more accurate value of mean flow velocity.

The amount of Doppler information collected from the large number of sample volumes along the scan line (in contrast to a single, circumscribed gate in conventional duplex scanning) is too large to be processed by spectral analysis using the fast Fourier transform with decomposition of the spectrum into its component parts and display of the proportions of different flow velocities at a given location. Instead, the faster autocorrelation technique is used to calculate the mean frequency shift and the corresponding mean velocity. Averaging of the frequencies reduces the spectral information to a color pixel that represents an intensity-weighted mean Doppler frequency shift in a direction-dependent manner. Blood flow toward the transducer is displayed in red, flow away from the transducer in blue. Less saturated hues indicate higher flow velocities. The instrument alternately displays the gray-scale scan and the color flow information whenever a Doppler frequency shift occurs.

In the inverse color mode, veins can be displayed in blue and arteries in red regardless of the true flow directions relative to the transducer. The use of this mode will cause problems when there is abnormal reversal of flow or when scanning abdominal regions with a complex vascular anatomy. The ultrasound convention of depicting cranially directed segments on the left side of the monitor and caudal segments on the right allows direct identification of the flow direction (toward the heart or toward the periphery) from the color coding if the transducer position is known (without first having to look for the information that indicates the inverse color display and varies from one manufacturer to the next).

1.1.3.2 Power (Angio) Mode

In contrast to the more widely used velocity mode, the *power mode* determines the frequency shift of the reflected echoes from the ultrasound energy (Fig. 1.13 a, b). In the power-mode display, the sum of the Doppler signal intensities reflected by moving particles is represented by levels of brightness while the magnitude of the flow velocity and different velocities as well as flow direction (in older devices) are ignored. The color intensity in the power mode is determined by the density of the moving reflectors. The power mode is more sensitive to slow flow and flow with only few reflectors as compared with the velocity mode. The more gates sampled along each color Doppler line, the better the signal-to-noise ratio. Lighter shades indicate higher densities of reflecting flow-

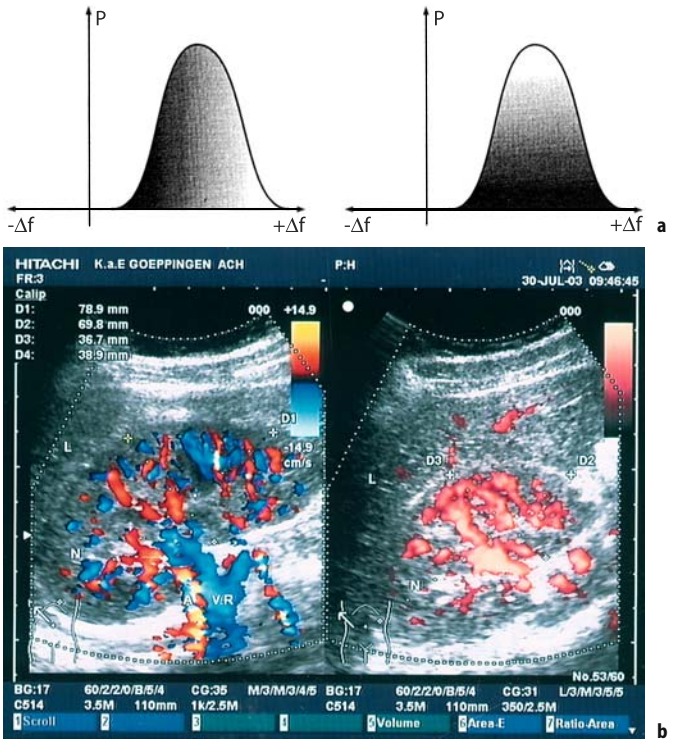

Fig. 1.13. a Types of color coding used to display flowing blood: In the velocity mode (*left*), red and blue represent the flow direction and lighter shades a higher Doppler shift. In the power/angio mode (*right*), higher amplitudes of the reflected ultrasound echoes are displayed in lighter shades irrespective of the frequency and flow direction.
b Depiction of the right kidney by color duplex ultrasound in the velocity mode on the *left* and in the power Doppler mode on the *right*. In the velocity mode, the color coding of the vessels indicates the blood flow direction with veins being shown in blue (flow away from the transducer) and arteries in red (toward the transducer). Vessels to the level of the interlobar vessels are depicted. The power Doppler mode provides no information on the flow direction of blood but enables evaluation of slow flow and is less angle dependent, which is why this mode is superior in depicting parenchymal blood flow in small vessels. The kidney (*N*) is marked with *plus signs*. Part of the liver (*L*) is depicted near the abdominal wall with visualization of peripheral vessels in the power Doppler mode. (For Fig 1.13c see p.11)

ing blood cells. While the power mode is similar to other techniques in that it only registers reflected echo signals within a certain range of Doppler frequency shifts, it is largely independent of the angle between the ultrasound beam and the blood vessel. Since blood does not flow strictly in one direction, there will always be some reflection of echo pulses even at an unfavorable insonation angle but color intensity is reduced at an angle around 90°. The power Doppler mode is particularly suitable for evaluating slow flow in small vessels and can thus be used to examine peripheral perfusion as well as perfusion in small tumor vessels or in parenchymal organs.

The power mode is limited by the fact that it does not provide qualitative or semiquantitative information on flow velocity. Moreover, it is more susceptible to artifacts induced by organ movement and has a poorer temporal resolution. There is no aliasing because the power mode is independent of the magnitude of the Doppler frequency shift. The main advantage of the power mode lies in the fact that it uses very low pulse repetition frequencies (in the range of some 100 hertz), which in turn enables the resolution of very small Doppler frequency shifts (slow flow). Such low pulse repetition frequencies would be highly susceptible to aliasing in velocity-dependent color coding (Table 1.4).

The power mode represents the intensities of the signals reflected by moving blood by different levels of brightness based on their amplitudes. The so-called bidirectional power mode offered by the manufacturers of state-of-the-art scanners enables simultaneous color coding of flow direction (blue and red). This is achieved by the activation of some additional ultrasound beams which solely serve the purpose of sampling and processing flow direction information using the autocorrelation technique.

1.1.3.3 B-flow Mode

The B-flow mode is not a Doppler technique based on the processing of the Doppler shift but a B-mode scanning technique that compares gray-scale scans over time to identify changes in the spatial positions of reflectors (blood cells) by the successive emission of coded pulse packets. The echo signals are subtracted from one another, and the brightness is determined by the number of reflectors and partly also by their velocity. The conventional B-scan generated from the stationary echoes is displayed around the flow information. Since the successive pulses are emitted at defined intervals and in digitally encoded form, it is possible to eliminate interfering echoes and use only the encoded echoes in the subtraction procedure. Hence, only the amplitude signal reflected by moving particles is processed in the interval between two pulses. As the signal strength increases not only with the number of reflecting particles (volume flow) but also with flow velocity, a jet within a stenosis is depicted with a higher signal intensity. The advantage of this technique lies in the simultaneous display in a single image of hemodynamic parameters (comparable to angiography) and morphologic details of the vessel wall with a high resolution while showing no or only little angle dependence. Disadvantages of B-flow imaging are the occurrence of artifacts in highly pulsatile, atherosclerotic vessels, the susceptibility to artifacts caused by wall motion, and the still limited scanning depth.

With further technical advancement, B-flow imaging will, in principle, enable morphologic quantification of stenoses and differentiation of the vessel wall from the patent lumen even if only slow flow is present (e.g. in ulceration). The B-mode provides a high-resolution display of the vessel wall contour with separate representation of blood flow in the B-flow mode. There is no superimposition of blood flow information as in color duplex scanning (see Fig. A 5.23).

1.1.3.4 Intravascular Ultrasound (IVUS)

Intravascular ultrasound (IVUS) is a catheter-based imaging modality that has increasingly been used to assist peripheral interventions. Originally a cardiology tool, IVUS is now used in peripheral angioplasty, stenting, and endoluminal grafting because of its advantageous diagnostic and interventional properties. In recent years, an improved image quality has transformed IVUS into a highly practical instrument. Both 3-dimensional reconstruction and color flow IVUS have made the images in the operating room much easier to understand and apply. It is a sensitive and useful technology for interventionists that tends to be underused because of perceived expense.

Images in IVUS are acquired by means of high-frequency, single-use probes based on various mechanical and electronic phased-array systems. Higher frequencies limit the scanning depth but improve the axial resolution of those structures that lie within the tissue depth reached. On a 360° IVUS view, the normal arterial wall architecture has a three-layer appearance resulting from the reflection of the ultrasound beam at interfaces between structures of different acoustic impedance in the

Table 1.4. Comparison of the two methods of flow encoding: velocity mode and power Doppler (angio) mode

Mode	Advantages	Disadvantages
Velocity mode	Detection of flow velocity and direction, high temporal resolution	Angle-dependent evaluation of flow (which in turn affects color filling of lumen), aliasing
Power Doppler mode (angio mode)	Evaluation of flow largely angle-independent (resulting in good color filling), depiction of slow flow, sensitivity to small flow volumes, few artifacts, good color filling improves discrimination of patent lumen from mural structures	No determination of flow velocity and direction, more difficult differentiation of arteries and veins, no hemodynamic information

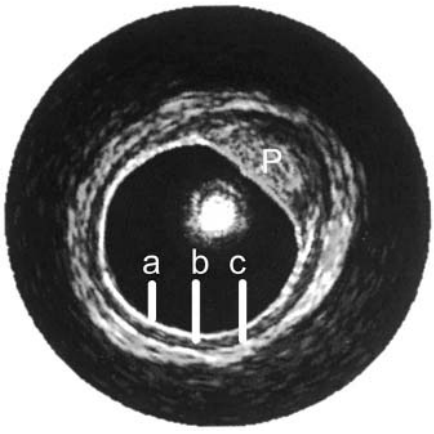

Fig. 1.13c Three-layer apperarance of the arterial vessel wall in intravascular ultrasound. *P* plaque; *a* reflection of blood-intima interface; *b* muscularis; *c* reflection of interface between adventitia and periadventitial tissue

vessel wall. The intima has a normal histologic thickness that is below the axial resolution of the currently available IVUS systems and is therefore visualized only when it is thickened in the presence of atherosclerotic lesions. The bright innermost reflection corresponds to the blood-intima interface. The outer echogenic ring represents the reflection of the interface between the adventitia and periadventitial tissue (Fig. 1.13c). This outer layer is clearly distinct from a less echogenic middle layer, which corresponds to the muscularis and contributes to the characteristic three-layer appearance of arteries of the muscular type. The higher spatial resolution of IVUS improves the evaluation of intimal thickness and plaque morphology including differentiation of fibrous plaques or necroses as compared with conventional transcutaneous ultrasonography.

1.1.4 Factors Affecting (Color) Duplex Scanning – Pitfalls

The pitfalls of duplex ultrasonography are summarized in Table 1.5.

Table 1.5. Pitfalls of duplex ultrasound. (Modified according to Seitz and Kubale 1988; Wolf and Fobbe 1993)

- Errors in angle determination (primarily with angles >60°), chiefly in curved vessels and branchings
- Errors in determining vessel diameter (blooming effect, diameter variation during cardiac cycle)
- Limitation of maximum velocity detectable (Nyquist limit)
- Limitation of minimum velocity detectable (wall filter, inadequate PRF)
- Position and size of sample volume
- Inclusion of accompanying vessels (high PRF, CW Doppler, large sample volume)
- Overmodulation resulting from unfavorable signal-to-noise ratio (gain)
- Impairment by scattering structures (plaque, intestinal gas, edema)

1.1.4.1 Scattering, Acoustic Shadowing

Air (in the intestine and lungs) and calcified structures (bones, calcified plaque) produce scattering and acoustic shadowing. These structures are not penetrated by the ultrasound beam and thus prevent collection of morphologic and Doppler flow information from body regions behind them. Bowel gas can be pushed out of the way by firmly pressing the transducer against the bowel, thereby enabling visualization of retroperitoneal structures and flow. In all other cases, the examiner must try and circumvent such structures by changing the transducer position.

1.1.4.2 Mirror Artifacts

The mirror artifacts known from gray-scale ultrasound occur at strongly reflecting surfaces (interfaces between structures with large differences in acoustic impedance) and mimic structures behind the reflector (e.g. liver behind diaphragm) in gray-scale imaging or patent vessels in color duplex scanning (e.g. subclavian artery behind pleura). The artifacts will disappear when the reflector is scanned in oblique orientation (Fig. 1.14).

1.1.4.3 Maximum Flow Velocity Detectable – Pulse Repetition Frequency

The pulse repetition frequency (PRF) limits the maximum Doppler shift frequency for which precise determination of the direction and amplitude is possible. The PRF is the rate at

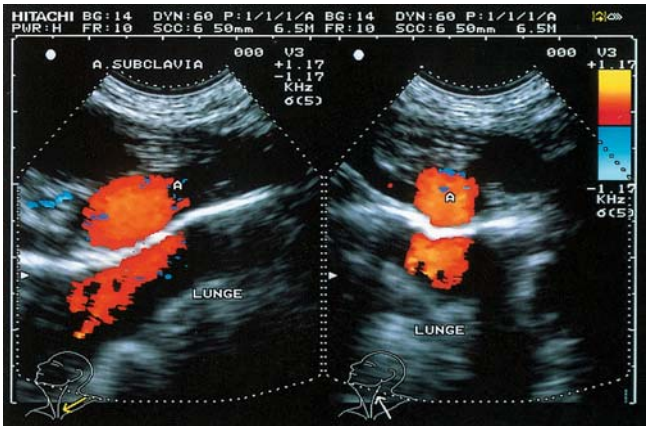

Fig. 1.14. Mirror artifacts (subclavian artery scanned from supraclavicular approach). Here the strongly reflecting pleura (*bright reflection*) mirrors the subclavian artery (*A*), producing the impression of a second artery ("ghost vessel") posterior to the true artery. Mirroring can be prevented by oblique interrogation of the mirroring structure (longitudinal (*left*) and transverse (*right*) scans of subclavian artery)

which ultrasound pulses are emitted from the transducer. In pulsed Doppler (conventional and color duplex), only echoes reflected from a predefined depth are accepted and processed (determination of mean flow velocity or FFT analysis) in the interval between transmissions. In color duplex ultrasound this is accomplished by using multiple gates to which the returning Doppler shift frequency packets are assigned. The relatively low Doppler shift frequencies (some kHz with a period of about 1 ms) are extracted from short, successive ultrasound pulses less than 1 μs in duration. A minimum number of ultrasound pulses is necessary for correct frequency determination. The Nyquist limit states that only Doppler shifts below half the pulse repetition frequency can be unambiguously processed in terms of direction and flow velocity. Doppler shifts exceeding the Nyquist limit lead to aliasing. Depending on the degree of aliasing, the high frequencies "wrap around" and are displayed on the opposite side of the baseline, so that blood appears to be flowing in the wrong direction. Under these conditions, the color duplex image likewise shows an apparent flow reversal by a change in the color coding. In aliasing, the transition to the opposite color progresses from increasingly lighter shades to yellow, followed by a light shade of the opposite color (e.g. from light red, through yellow, to light blue). In contrast, true flow reversal is characterized by a color change from a dark shade of the initial color (or black for a transient period during which no flow information is obtained) to the opposite color. Aliasing can be prevented by a higher pulse repetition frequency or various other options such as repositioning of the baseline, reduction of the transmit frequency, and interrogation of the vessel at a larger angle.

The lower the transmit frequency, the lower the Doppler shift frequency. The latter can thus be reduced to below half the pulse repetition frequency by lowering the transmit frequency. Larger angles between the ultrasound beam and the blood vessel will also decrease the Doppler shift frequency, however, the extent to which this can be done is limited by the fact that errors in velocity measurement will increase unacceptably at angles above 70°. Shifting of the baseline enables doubling of the Doppler frequencies that can be displayed above or below the line, depending on the direction of the shift. Enlarging the positive frequency range in this way automatically reduces the negative frequency range by the same amount and vice versa.

Another parameter is the scanning depth, but this is difficult to manipulate. The greater the penetration depth, the longer the pulse delay. As the echo arrival time increases, the pulse repetition frequency must be reduced as successive pulses can only be emitted after all reflected echoes of the preceding pulse have been received.

Mathematically, the Nyquist limit is expressed in the following equation:

$$\delta F_{max} = \frac{1}{2} PRF$$

The maximum flow velocity that can be measured is then calculated using the Doppler equation:

$$V_{max} = \frac{c}{4 \cdot T \cdot F_0 \cdot cos\ \alpha}$$

The maximum flow velocity is thus inversely proportional to echo arrival time T, or to scan depth and transmit frequency F_0 (Figs. 1.15, 1.16, 1.17).

The options available to overcome these limitations can be summarized as follows:

- Use of a higher pulse repetition frequency in order to register higher Doppler shift frequencies, but this will reduce the scan depth (longer pulse delays with greater depth; Fig. 1.18).
- Use of a lower transmit frequency, but this will reduce the spatial resolution of the gray-scale scan.
- Shifting of the baseline, both in the spectral display and on the color scale, by which the frequency range in one direction can be doubled while flow in the opposite direction is no longer depicted.
- Some ultrasound machines have a high PRF option for the detection of faster flow. The higher frequency is achieved by emitting ultrasound pulses before the preceding signals have been processed. Processing is done using additional Doppler lines. However, this approach is associated with some unreliability in terms of spatial resolution as Doppler information from a larger number of gates must be processed to generate the spectral display.
- CW Doppler using separate crystals for continuously transmitting and receiving signals is not limited by an upper Doppler shift threshold. This technique does not

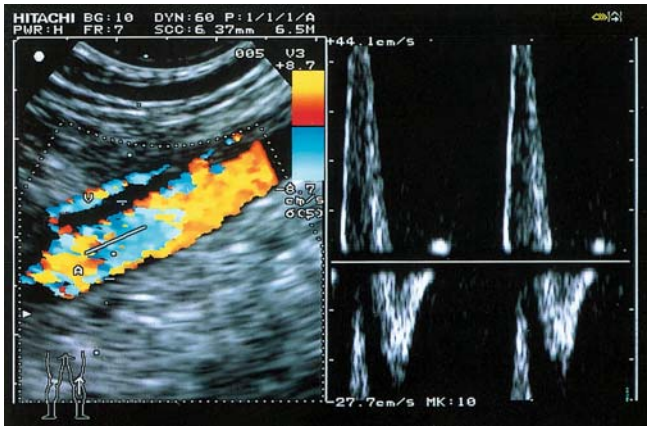

Fig. 1.15. Examination of the popliteal artery with the pulse repetition frequency set too low. There is aliasing because the Doppler shift frequencies are above the Nyquist limit. Aliasing is seen in the color duplex image as a color change from light red, through yellow, to blue. In the Doppler waveform, the peak velocity is cut off and these signals are displayed below the baseline. Aliasing can be prevented by repositioning the baseline and increasing the PRF

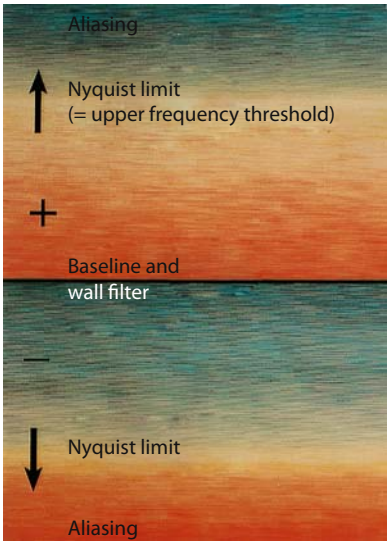

Fig. 1.16. In color duplex scanning, a positive Doppler shift is displayed in red and a negative shift in blue with lighter shades indicating higher flow velocities. When the upper velocity threshold set on the color scale is exceeded, aliasing will occur and the faster flow is depicted in the color of the opposite flow direction. In aliasing, the color change from red to blue or vice versa progresses through a lighter shade (faster flow) and a yellow to white zone of transition. In contrast, true flow reversal is characterized by a dark transition zone. Absence of color (black) may be due to a short cessation of flow or change in flow direction relative to the transducer (curved-array transducer) with failure to detect flow at a Doppler angle of 90°

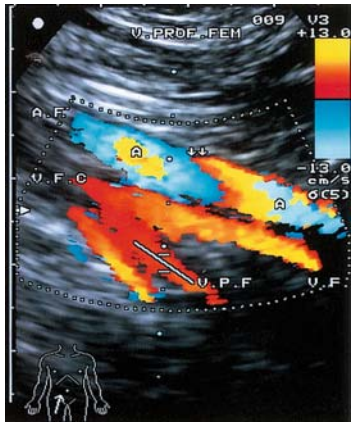

Fig. 1.17. The pulse repetition frequency is adequately set for evaluating venous flow (confirmed here in the deep femoral vein). The figure illustrates the pitfalls of color duplex scanning in the superficial femoral artery. Color-coded flow signals are depicted throughout the lumen of the deep femoral vein (duplicated in the example shown, *V.P.F.*), in the area of its opening, and in the superficial femoral vein. Flow is toward the transducer (red). The superficial femoral artery (*A.F*) is shown with flow in the opposite direction (blue). The PRF is too low to depict arterial flow signals, resulting in aliasing indicated by the color change through yellow to red. As a result of the low frame rate (proportional to the PRF), the change in flow direction from systole to early diastole is displayed in the *center* of the image (indicated by *arrows*). The changed flow direction is reflected by the color change from dark blue to dark red. In the further course of the vessel, there is a second area of aliasing with color changing from red, through yellow, to blue. The increasingly smaller Doppler angle of incidence also contributes to these phenomena and is also responsible for the lighter color in the superficial femoral vein running posteriorly

allow local differentiation of the reflected signals since all frequencies reflected back from along the beam path are processed to generate the Doppler waveform.

1.1.4.4 Minimum Flow Velocity Detectable – Wall Filter, Frame Rate

Doppler frequency shifts are caused not only by flowing blood but also by the motion of the vessel wall. Shifts due to wall motion typically have a high amplitude but low frequency and affect the velocity spectrum. In contrast, the Doppler shifts resulting from flowing blood have higher frequencies and lower amplitudes. *Wall filters* are therefore used to remove the interfering low-frequency signals. The cutoff can be selected from 100 to 400 Hz, or up to 1,600 Hz in some devices. The filter eliminates all frequencies below the selected cutoff, including Doppler shift frequencies caused by slow flow (Fig. 1.19 a, b). When the filter choice is inappropriate, the elimination of signals from slow-flowing venous blood may suggest absence of flow. Also, the mean flow velocity may be overestimated if slow flow components with low Doppler shifts are filtered out. To overcome these problems, devices have been introduced that eliminate only low frequencies with high amplitudes (typical of wall motion) or that identify and eliminate typical patterns of tissue motion.

The *frame rate* is the number of color-coded ultrasound

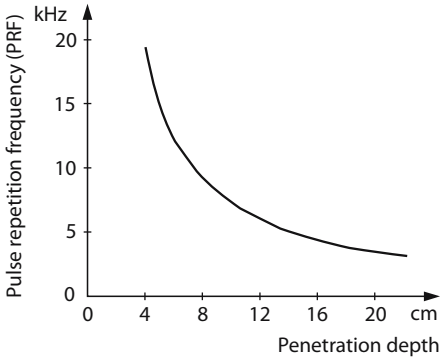

Fig. 1.18. The penetration depth in duplex ultrasound is limited by the pulse repetition frequency

scans that can be generated per second and determines the minimum flow velocity that is detectable. It is mainly dependent on the width of the color box and scan depth selected by the examiner. A larger color box requires more color Doppler lines to be processed for image generation. Moreover, image generation is slower when deeper structures are scanned due to the longer echo arrival time (Table 1.6). Lower frame rates result in a poorer temporal resolution with failure to detect

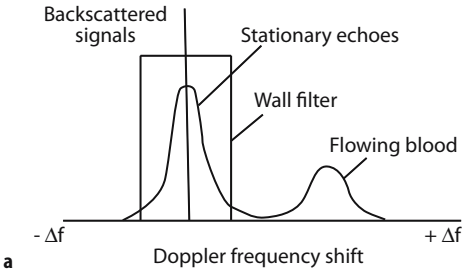

a

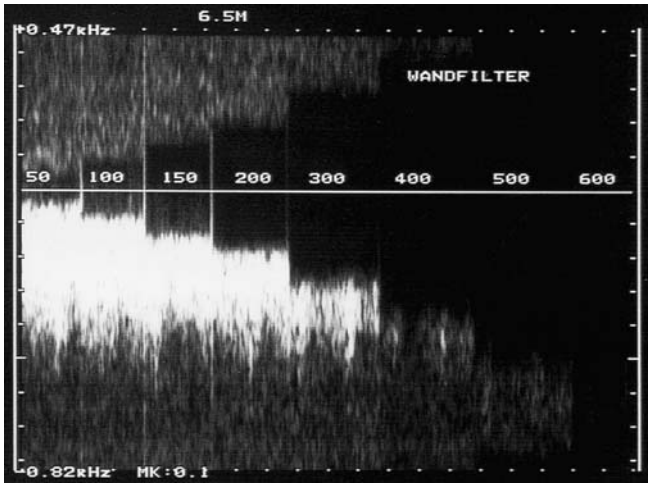

b

Fig. 1.19. a Wall filters are used to eliminate the low-frequency signals caused by motion of the vessel wall. The cutoff should be selected so as not to inadvertently remove flow-related low-frequency signals, for instance, when evaluating slow venous flow. **b** By increasing the cutoff in a stepwise manner, at first only the low Doppler shift frequencies are eliminated while further increments will eliminate venous flow signals as well. A wall filter of 500 Hz eliminates venous flow signals up to 450 Hz while slower flow is already eliminated at lower cutoff values

Table 1.6. Color Doppler – frame rates

	Frame rate	
	Higher	Lower
Size of color box	Smaller	Larger
Number of scan lines	Fewer	More
Scan depth	Smaller	Greater
Lower frequency limit	Higher	Lower

Table 1.7. Options for improving color filling of the vascular lumen

- Lower Doppler transmit frequency
- Lower pulse repetition frequency
- Lower wall filter
- Optimization of insonation angle
- Higher color gain

rapid changes or short interruptions of flow. Cardiac perfusion and flow in peripheral arteries can only be examined with high frame rates (at least 20 images per second). Lower frame rates, on the other hand, improve the spectral Doppler display and the sensitivity for low Doppler shift frequencies because more Doppler information can be sampled. Despite the poorer temporal resolution, low frame rates yield better results in scanning veins and small arteries (Table 1.7).

1.1.4.5 Transmit and Receive Gain

The receive gain must be set so as to ensure that all information from the reflected echo pulses is displayed while at the same time preventing artifacts due to overmodulation. The gain is adjusted separately for B-mode, Doppler, and color duplex scanning because different pulses are used for each of these modes. Readjustment during the examination may be

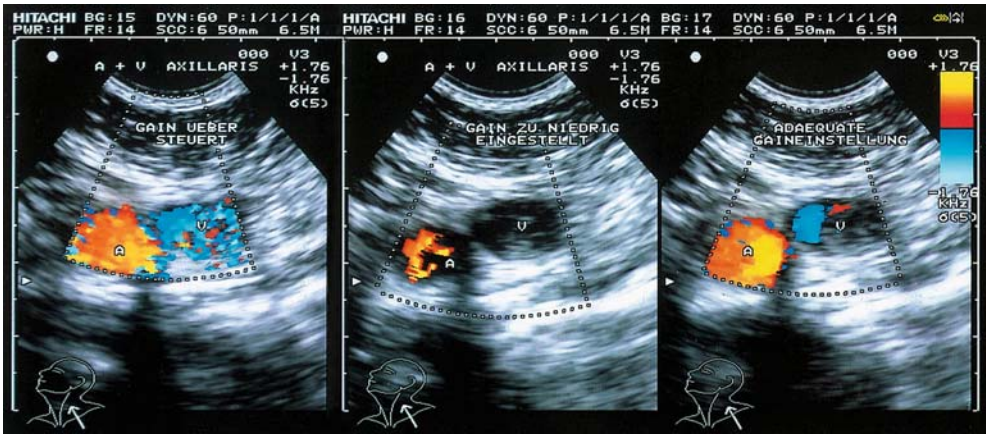

Fig. 1.20. Effect of different gain settings on the depiction of mural thrombosis in the axillary vein at an identical pulse repetition frequency. The scan on the *left* obtained with gain overmodulation shows the mural thrombus to be largely obscured by artifacts extending beyond the patent lumen (blue). In the next scan (*middle section*), no flow signals are depicted along the thrombus in the axillary vein because the gain is too low. In addition, there is incomplete color filling of the axillary artery (red) cranial to the vein. The scan on the *right* illustrates adequate gain setting. There is proper color coding of the artery (red) and the thrombus in the axillary vein is depicted with adjacent blue venous flow signals

required, for instance, when measuring the intima-media complex. Correct measurement requires careful tuning of the receive gain so that boundary lines are visible and overestimation resulting from the blooming effect is avoided.

Receive gain setting for the acquisition of Doppler information must ensure that, in the presence of laminar flow, the clear systolic window in the display of the Doppler spectrum contains no artifacts while not eliminating signals from slow flow. Conversely, some overmodulation of the receive gain may be necessary in the presence of subtotal occlusion to determine the correct peak systolic flow velocity (high-frequency Doppler shifts with low amplitudes due to the small number of reflecting red blood cells in the stenosis jet), even if this results in more artifacts. In color duplex scanning, overmodulation of the gain will lead to color overflow and may obscure thrombi and arterial plaques in partially occluded veins (Fig. 1.20). This phenomenon contributes to the unreliability of planimetric measurement of stenoses based on the vessel cross-section depicted in color duplex scans.

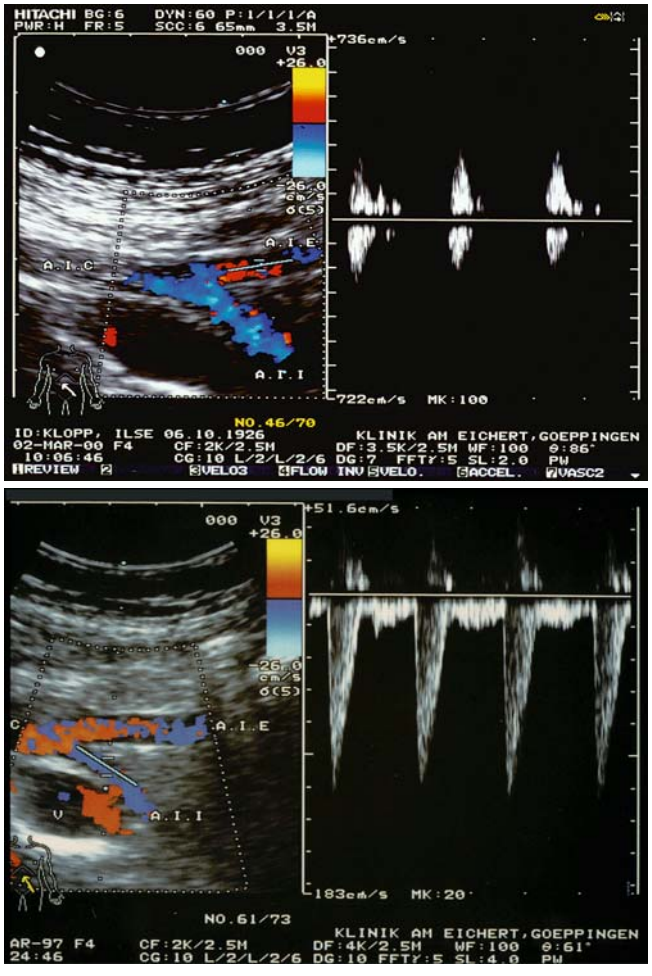

Fig. 1.21. a An optimal gray-scale scan is obtained with a beam perpendicular to an interface between tissues of different acoustic impedance. In contrast, angles of 80 to 90° yield the lowest frequency shifts according to the Doppler equation and thus provide poor (color) duplex information. Therefore, interrogation of the iliac bifurcation at the preferred site of stenoses of the external iliac artery (*A.I.E*) poses a problem as adequate Doppler angles can be achieved only by tilting the transducer and moving it up or down (see also Fig. 2.1 a). In the color duplex scan, the change between red and blue at the origin of the external iliac artery illustrates the problem of determining the flow direction. The Doppler waveform is not helpful either, showing flow in both directions. As a result of the error in setting the Doppler angle, an iliac artery stenosis with a peak systolic flow velocity of 250 cm/s is suggested. **b** The posterior origin of the internal iliac artery (*A.I.I*), on the other hand, can be interrogated with a Doppler angle of less than 60° from the same transducer position, yielding a diagnostic Doppler waveform, from which a correct peak systolic flow velocity of 120 cm/s is calculated

1.1.4.6 Doppler Angle

The depiction of the vessel course in the B-mode image combined with the spectral Doppler information obtained with a defined ultrasound beam and known angle of insonation enables calculation of the true flow velocity from the Doppler shift. To select a proper Doppler angle relative to the flow direction, a long stretch of the vessel of interest must be depicted in the longitudinal plane (parallel vessel walls along the width of the monitor). The smaller the angle between the Doppler beam and the direction of the flowing blood, the higher the Doppler frequency shift of the reflected echo and the higher the sensitivity for flow detection. At angles of 60 to 90°, the Doppler frequency shift decreases and flow velocity measurement becomes progressively unreliable and no flow signals are depicted when the Doppler beam is perpendicular to the vessel wall (Fig. 1.21 a, b). Conversely, perpendicular insonation of a reflecting surface provides optimal B-mode information. In the clinical setting, the examiner must find a compromise between optimal B-mode imaging and optimal flow evaluation. The usual procedure is to first try and achieve a perpendicular beam angle for morphologic evaluation of the vessel wall and to then sample the Doppler information either by activation of beam steering (lateral beam deflection) or with a smaller angle through shifting and angling of the curved-array or sector probe and placement of the Doppler gate at the edge of the imaging field.

In color duplex scanning with a curved-array transducer, different shades of color that do not reflect different flow velocities are displayed when interrogating a vessel coursing parallel to the skin surface (e.g. carotid or femoral artery) with the transducer held perpendicular to the skin surface. Under these conditions, flow near the wall is displayed in lighter shades due to higher Doppler shifts and in increasingly darker colors toward the center where the frequency shift decreases as the insonation angle increases. This phenomenon is relevant only in the velocity mode and not in the power mode, as the latter is virtually independent of the Doppler angle.

1.1.4.7 Physical Limitations of Color Duplex Ultrasound

As a result of the vast amount of information to be processed, color duplex scanning has a much poorer spatial and temporal resolution than pure B-mode imaging. Axial resolution is proportional to the wavelength in B-mode imaging while it is dependent on the number of sample volumes placed along the color Doppler scan line in the color duplex mode. The use of smaller sample volumes improves axial resolution but at the expense of sensitivity and accuracy in Doppler shift evaluation as the signal-to-noise ratio deteriorates. Lateral resolution in color-coded duplex scanning is determined by the number of color Doppler lines processed per centimeter. The frame rate decreases as the number of Doppler lines increases, resulting in a lower temporal resolution, in particular at greater scan depths.

As a result of these limitations, the axial resolution of color duplex ultrasound is on the order of 0.4 – 1.0 mm with a lateral resolution of only 1.0 – 2.0 mm, which is 4 – 10 times lower than B-scan resolution (Widder 1995).

The frame rate in the color duplex mode ranges from 50 – 200 ms (corresponding to an image repetition rate of 5 Hz), depending on the scanning depth and size of the color box. When a low pulse repetition frequency is selected, the speed at which the color Doppler scan lines sweep the sector is similar to or slightly below the mean flow velocity in arteries. Therefore, a single ultrasound scan may simultaneously depict systolic flow (e.g. displayed in red) and early diastolic flow (e.g. displayed in blue) (cf. Fig. 1.17). Due to the low temporal resolution, however, the color coding does not fully reflect the pulsatile character of flow.

Slow flow produces smaller Doppler frequency shifts, which have to be extracted from short echo pulse packets for each scan line consisting of a number of individual pulses. The scan lines must be processed successively.

Though the insonation angle should ideally be as small as possible for optimal Doppler scanning, this is not always practical because there will be a longer delay when the color box is tilted (beam steering). This is why one must find a compromise, in particular when examining deeper vessels. Tilting the color box 20° and 30° prolongs the echo arrival time by 13 % and 31 %, respectively.

Color duplex imaging, like all diagnostic ultrasound techniques, is impaired by scattering and acoustic shadowing caused by bowel gas or calcified structures (bone or calcified plaques on vessel walls). The examiner can circumvent such interfering structures by moving the transducer, but this is frequently achieved only at the cost of a longer echo arrival time due to a greater distance from the structure of interest.

Strong reflectors that are oblique to the beam axis act like mirrors and generate phantom images in another area of the scan. Such mirror images can be identified by angling the transducer, which will make the mirror artifacts disappear or appear in a different location. When the ultrasound beam strikes interfaces of high acoustic impedance at a right angle, reverberations (repeat echoes) may occur with the ultrasound pulses being reflected to and fro, resulting in a kind of ping-pong effect. Slight angulation of the transducer prevents reverberations but will also reduce reflection from the interface and thus degrade image quality.

1.1.5 Ultrasound Contrast Media

Ultrasound contrast media, or echo enhancers, are intravascular agents that enhance the reflection of ultrasound signals by the flowing blood for a short period of 3 – 5 min after intravenous administration. They improve the identification of vessels and the demonstration of flow in vessels with slow flow that are notoriously difficult to scan. Ultrasound contrast media are primarily employed in evaluating organ perfusion, especially for characterizing of tumors such as focal liver lesions. In the routine clinical setting, echo enhancers have no role in evaluating patients with angiologic or vascular surgical conditions. Exceptions are the evaluation of small peripheral vessels and lower leg arteries with slow, postocclusive flow, transcranial duplex scanning, and the search for endoleaks after stenting of the aorta. With the use of contrast media, ultrasound to some extent gives up its crucial advantages over other imaging modalities such as low cost, short examination time, and noninvasiveness. Moreover, in those body regions where diagnostic improvement is achieved through the administration of echo enhancers, other competing imaging modalities already have a high or higher accuracy and often enable better documentation of the findings. Since the focus of this book is on the role of ultrasound in vascular surgery and angiology, the basic principles, advantages, and limitations of ultrasound contrast media will only be discussed briefly below.

Ultrasound contrast media act by enhancing the echogenicity of the solid components in flowing blood and by increasing the proportion of scattered and reflected ultrasound pulses, thereby improving the Doppler signal and the signal-to-noise ratio. Most echo enhancers consist of gas-filled microbubbles that improve sound backscatter as a result of the large difference in acoustic impedance that exists between the gas and the liquid blood. The extent of backscatter depends on the microbubble concentration and the reflection capacity of the individual bubbles. This capacity is a function of the scatter cross-section of the bubbles. The maximum bubble size is limited by the fact that they must pass the lungs (bubble size < 8 μm). Studies have shown that backscatter enhances the echo signal intensity of blood by 15 – 25 dB (Kaps and Seidel 1999).

In addition to producing backscatter, the gas-filled bubbles are induced to resonate at higher ultrasound energies, producing harmonic vibrations that are fractions or multiples of the transmitted frequency. With the resonance frequencies of the 2 – 7 μm gas bubbles being in the range of the transmitted frequencies of 2.5 – 10 MHz typically used in ultrasound, the vibrations of the bubbles produce an additional signal amplification. The corresponding frequencies are received

and processed in addition to the backscattered Doppler shift frequencies. The resonance effect of the microbubbles improves the signal-to-noise ratio by a further 30 – 35 dB, provided that the ultrasound system is equipped for receiving and processing the harmonic vibrations (Correas et al. 1997).

Short pulses of high energy can be applied to make the microbubbles burst, producing ultrasound signals that can be detected with a high degree of sensitivity. In contrast to the enhancing mechanisms outlined in the preceding sections, bursting is independent of flow and the resulting signals merely show the distribution of the collapsed microbubbles at that time. This procedure has been referred to as sonoscintigraphy (Cosgrove et al. 1998) and is increasingly being used in differentiating and characterizing focal liver lesions.

Echo enhancers with different compositions and properties are commercially available from various manufacturers. Basically, however, they consist of a gas particle stabilized by a coat or carrier medium. Levovist, for instance, is a preparation of air-bubble-like galactose microparticles that are stabilized by a film of palmitic acid. Levovist is injected as a bolus or short infusion with echo enhancing occurring 1 – 4 min after administration, first in arteries, then in the veins. The Doppler signal is enhanced by 20 – 30 dB after bolus administration.

Another echo enhancer, Sonovist, is composed of air bubbles stabilized by cyanoacrylate and has a mean diameter of 1 µm. Both Sonovist and Levovist are taken up and eliminated by the reticuloendothelial system of the liver. In the liver, the Sonovist bubbles burst when exposed to a high-energy beam and thus contribute to the differentiation of liver metastases, which do not have a reticuloendothelial system. In addition, focal liver lesions may be differentiated on the basis of their blood supply (predominantly portal venous versus arterial) and differences in contrast medium arrival times after bolus administration. Other echo enhancers are available as suspensions (some of which contain human albumin) of particles stabilized with other materials for specific applications.

The use of echo enhancers has been investigated in the evaluation of slow flow in peripheral vessels, including postocclusive flow, and of carotid artery stenoses. The investigations show that echo enhancers improve the accuracy of color duplex ultrasound in identifying pseudo-occlusion (Fürst et al. 1999; Ferrer et al. 2000). In the vertebral artery territory, echo enhancers are beneficial in evaluating a hypoplastic vessel branch and in patients with poor scanning conditions.

Echo enhancers have been advocated as improving the signal-to-noise ratio in the examination of deep vessels such as the pelvic or renal arteries. Using state-of-the-art ultrasound equipment, however, these vascular areas rarely pose diagnostic problems. On the other hand, a study of renal artery stenoses investigating duplex scanning with echo enhancer administration demonstrated the diagnostic yield to increase from 64 to 84 %, while the improvement in the sensitivity and specificity for identifying high-grade stenosis was negligible (Claudon et al. 2000).

Specific instrument settings using echo enhancers. The administration of echo enhancers in color duplex ultrasound leads to overmodulation of the color Doppler signal with color overflow obscuring perivascular structures and parts of the vessel wall, in particular when larger vessels are examined. This effect can be eliminated by downregulating the receive gain. On the other hand, the strong reflection produced by the contrast bubbles leads to sound attenuation in structures farther away from the transducer than the enhanced vessel. In Doppler scanning after echo enhancer administration, there will be spectral broadening with almost complete filling-in of the systolic window. This effect can likewise be counteracted by downregulating the receive gain.

1.2 Hemodynamic Principles

1.2.1 Laminar Flow

Although blood flow is subject to specific conditions due to the solid components in plasma and the elasticity of the vessel wall, it basically follows the laws of hemodynamics. These laws govern the flow of a fluid in tubes and apply to watery or oily solutions of a constant viscosity (Newtonian fluid) and assume that flow velocity under these conditions is primarily a function of the pressure difference that exists between the two ends of the tube. These ideal conditions for continuous laminar flow are typically not met in a living organism because various factors like elasticity of the vessel wall, pulsatility resulting from cardiac activity, curving of vessels, and branching affect blood flow, resulting in changing velocity distributions in the different layers. Moreover, blood is not a watery or oily solution of constant viscosity but a suspension of solid blood cells in plasma. The viscosity of blood is primarily dependent on its hematocrit and is fairly constant only at levels below 10 but increases exponentially above this level. Other factors affecting blood viscosity are plasma viscosity and vessel diameter. In the terminal capillary bed, viscosity is additionally influenced by the deformation of the red blood cells. Despite these specific features of blood flow, some basic hemodynamic terms and laws are useful and will make it easier to understand normal and abnormal flow in arteries and veins. In addition, in vitro experiments and blood flow measurements in vivo performed in recent years using duplex scanning have provided new insights into the flow behavior in specific vessels under normal and abnormal conditions as well as under the influence of pharmacologic agents.

Continuous or *laminar flow* is characterized by a constant velocity over time. Flow in a tube is brought about by a pressure difference between the two ends of the tube. The pressure difference (P_1–P_2) is proportional to the volume flow rate. The volume flow rate (I) is proportional to the tube diameter (r) and inversely proportional to its length (l) and the viscosity of the fluid (η). Mathematically, this relationship is expressed in the Hagen-Poiseuille law.

$$I = \frac{(P_1 - P_2) \cdot \pi \cdot r^4}{8 \cdot l \cdot \eta} = \frac{(P_1 - P_2)}{R}$$

By analogy with Ohm's law, *flow resistance* can be calculated from the Hagen-Poiseuille equation.

$$R = \frac{8 \cdot l \cdot \eta}{\pi \cdot r^4}$$

It follows that resistance is proportional to the length of the tube (l) and the viscosity of the liquid (η).Overall resistance is most strongly affected by the radius (r), which enters the equation in the fourth power. This means that decreasing the vessel radius by one-half, for example, increases the flow resistance by a factor of 16. Peripheral resistance in the vascular system is regulated according to demand, primarily by the tone of the arterioles, and affects the pulsatility depicted in the Doppler waveform of large vessels.

The *flow profile* of laminar flow is determined by inertial and frictional forces. Friction produces a laminar, or, in the three-dimensional model, parabolic flow profile. Flow is fastest toward the center of a vessel and decreases toward the wall, where it approximates zero.

Color duplex ultrasound reflects this flow profile by lighter color shades in the center (fast flow) and darker shades near the wall (slow flow) (Fig. 1.22 a). The following factors determine the shape of the flow profile of blood:

- velocity,
- viscosity (internal friction), and
- adhesion of the blood to the vessel wall (external friction),
- cohesion (forces that occur between adjacent molecules of like composition).

Blood differs from Newtonian fluid in that its viscosity is not an inherent property that only varies with temperature but is mainly determined by the hematocrit level and other factors such as plasma viscosity (which in turn is predominantly dependent on the fibrinogen concentration), red blood cell deformability, and the degree of shearing. In laminar flow, shearing forces, like thrust, are least pronounced at the center of the vessel and strongest near the wall (Fig. 1.22 b).

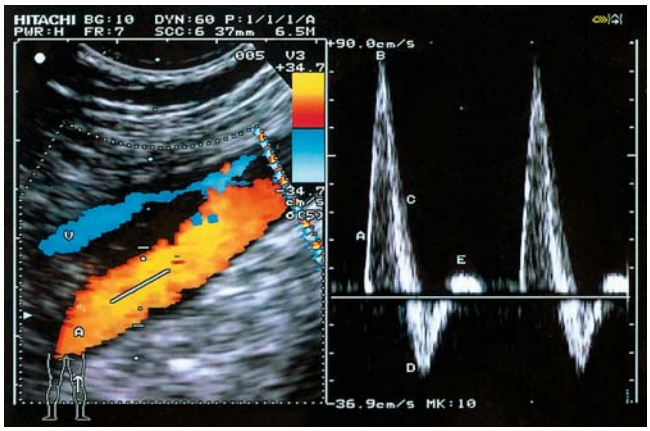

a

Fig. 1.22. a Typical triphasic Doppler waveform of the popliteal artery. The color duplex scan depicts laminar flow with lighter coloring in the center darker colors toward the margins represent. The slow flow near the vessel wall. Red indicates blood flow toward the transducer. A vein closer to the transducer is displayed in blue, indicating blood flow away from the transducer. The triphasic waveform consists of a steep upslope (*A*), a deceleration phase (*C*) following peak systolic flow (*B*), a short phase of early diastolic backward flow (*D*), and forward flow from mid-diastole to end-diastole (*E*). The magnitude and duration of diastolic forward flow (*E*) are determined by the peripheral resistance (sympathetic tone) and the thrust generated by the compliant aorta (windkessel effect). Blood flow toward the transducer is displayed above the baseline, flow away from it below the line. The Doppler angle of insonation is 59°, and peak systolic flow velocity is 85 cm/s. The different intensities of the individual pixels in the Doppler waveform

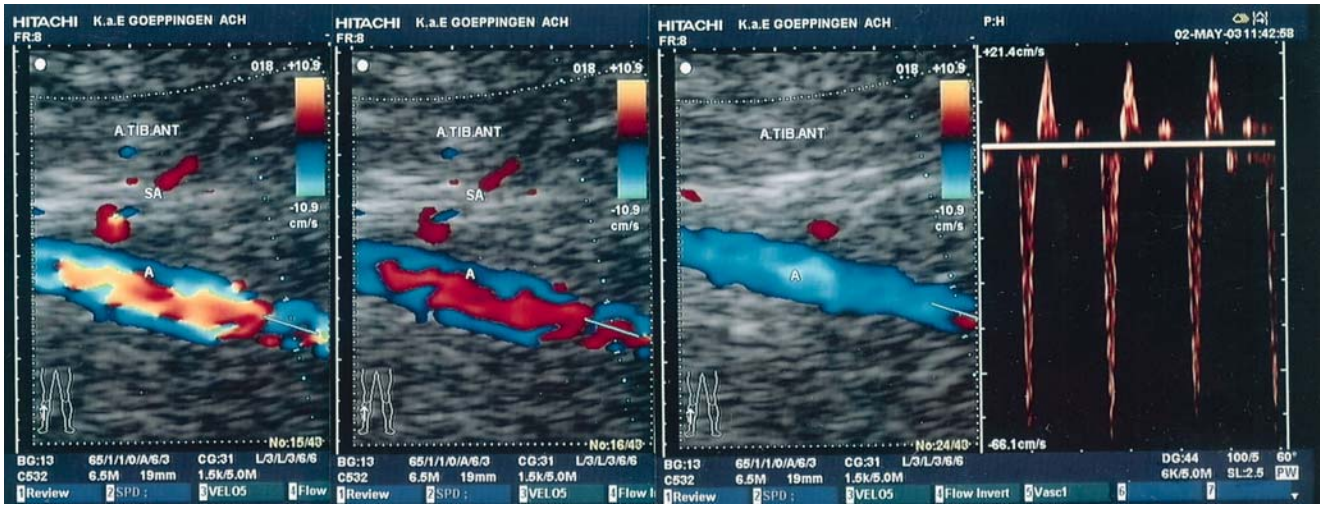

b

(Fig. 1.22 cont.) reflect the number of red blood cells at a given point in time. The amplitude can also be represented in the form of a histogram. **b** Use of a low pulse repetition frequency to ensure good color filling of arteries with slow flow in the lower leg. In the first color image (*leftmost section*), the anterior tibial artery (blue, flow toward the periphery, away from the transducer) is depicted with central aliasing (color change from blue, through yellow, to red). This example illustrates a laminar flow profile with fast flow in the center and lower flow velocities near the arterial wall due to friction. The second color scan depicts blood flow during early diastole at the same site as a result of the low frame rate. In the center, arterial reflux due to high peripheral resistance is seen as a superimposed wave (red, toward transducer) while flow toward the periphery predominates nearer the walls (blue, away from transducer). The view illustrates true flow reversal relative to the ultrasound beam rather than aliasing. True flow reversal is characterized by a color change from blue, through black, to red. The third color scan depicts blood flow (blue, away from transducer) toward the periphery and without aliasing in mid-diastole. The blood flow in a peripheral artery during one cardiac cycle as depicted by these three color duplex scans is additionally represented in the Doppler frequency spectrum (*rightmost section*), which presents the flow changes over time

According to the continuity law, a decrease in the cross-sectional area in the course of a vessel segment leads to an increase in mean flow velocity. Blood flow through a vessel segment with an abrupt change in caliber becomes flattened (plug flow) upon entering the narrower vessel segment. In plug flow inertial forces are stronger than frictional forces, resulting in the same flow velocity of all fluid layers in the vessel except for a thin layer near the wall. So-called turbulent flow results when the inertial forces become even stronger compared to the frictional forces, which bring order to the course of flow. Turbulent flow is characterized by an irregular flow pattern with flow in different directions. The typical parabolic flow pattern develops after a certain stretch along which frictional forces predominate. Physiologically, this occurs when blood leaves the left ventricle and enters the ascending aorta. The sharp velocity gradient between central portions and the thin boundary layer near the wall in plug flow is associated with strong shearing forces.

The abrupt reduction of the cross-sectional area in a stenotic vessel segment and the resulting increase in flow velocity are associated with progressive disturbance of laminar flow, which will finally become turbulent. Turbulent flow above a critical velocity is characterized on color duplex ultrasound by a mosaic-like flow pattern reflecting the different flow directions. The transition from laminar to turbulent flow can be calculated by means of the dimensionless Reynolds number, which depends on mean flow velocity (v), vessel diameter (d), density of the fluid (p), and viscosity (η):

$$Re = \frac{v \cdot d \cdot p}{\eta}$$

Turbulent flow occurs at Reynolds numbers above 2,000. Blood flow becomes turbulent when the vessel lumen is narrowed by a stenosis. The details are highly complex but need not be taken into account by the sonographer in determining the degree of stenosis.

In turbulent flow, part of the kinetic energy is converted into sound energy, which can be auscultated as a characteristic bruit.

In vessels with pulsatile flow, which normally is laminar, turbulent flow may occur at specific points in the cardiac cycle under physiologic conditions. This phenomenon depends on the flow profile (high pulsatility) and pulse rate.

A sudden increase in the vessel diameter results in a longer flow profile and greater velocity gradient across the vessel lumen. If the difference between a narrow and wide (poststenotic) vessel segment exceeds a certain value, *flow separation* and eddy currents will occur near the wall. Flow separation near the wall is also observed in branching vessel segments (Fig. 1.23).

Flow separation is associated with areas of recirculation in which relative stasis of flow in conjunction with shear forces induces platelet aggregation with release and adhesion of procoagulative agents, which in turn can trigger local atherogenic processes. This is a possible mechanism contributing to

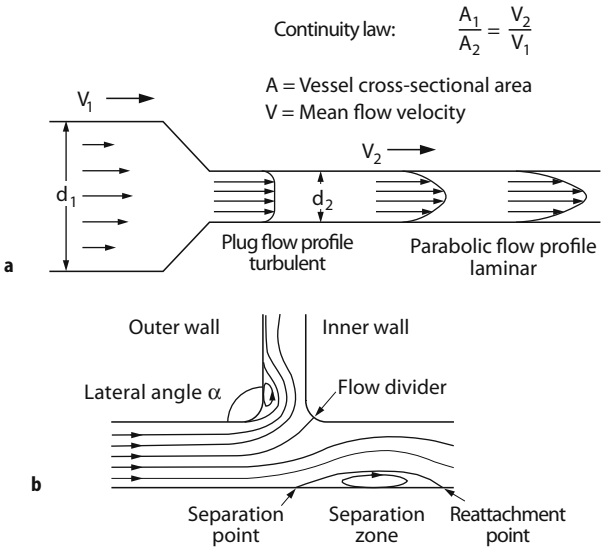

Fig. 1.23. a When a fluid such as blood enters a narrower lumen, parabolic flow changes into plug flow and returns to its original profile only after having traveled some distance under the influence of shear forces. According to the continuity law, flow velocity increases in proportion to the decrease in diameter. **b** Flow pattern at a vessel branching. Thrust and shearing are highest at the inner wall of the branching. Separation occurs at the outer wall, where thrust is rather low. Physiologic flow separation is depicted sonographically in the carotid bulb (cf. Fig. A 5.1). (According to Lanzer and Yoganathan 1991)

the preferred occurrence of atherosclerotic lesions at vessel divisions and branchings.

The phenomenon of flow separation is depicted most impressively by color duplex scanning at the origin of the internal carotid artery, where it occurs as a result of both widening in the bulb area and vessel branching (cf. Fig. A 5.1). Flow separation may also be observed in poststenotic vessel segments as a result of the abrupt increase in the cross-sectional area (cf. Fig. 1.26 a, b).

1.2.2 Pulsatile Flow

In contrast to laminar flow, *pulsatile flow* changes periodically over time. Phases of acceleration and deceleration vary in relation to changes in pressure. The pressure amplitude generated by the left ventricle is reduced by the compliance of the aorta and other large vessels (windkessel effect), resulting in a more steady flow. Another factor affecting the flow profile is the peripheral resistance.

Flow is highly pulsatile in the extremity arteries due to the high peripheral resistance at rest, resulting in the typical triphasic Doppler waveform. An increase in the peripheral blood demand leads to dilatation of the arterioles and the resulting decrease in peripheral resistance changes the Doppler waveform. Peripheral resistance may decrease under normal (muscle activity) or abnormal conditions (local inflammation, postocclusive ischemia, tumor perfusion) and is associated with an increase in the diastolic flow component in the waveform. Moreover, the character of the waveform is affected by central regulatory processes (increase in heart rate, blood pressure) and vessel wall elasticity (diabetes mellitus).

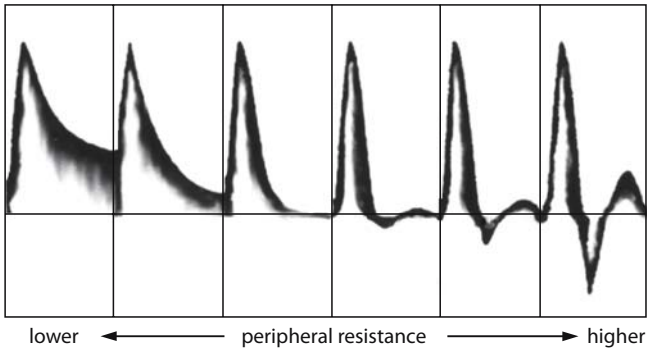

Fig. 1.24. Effect of peripheral resistance on the Doppler waveform. Pulsatility increases with peripheral resistance

As the peripheral resistance is a crucial factor affecting the waveform, a distinction is made between low-resistance flow and high-resistance flow (Fig. 1.24).

The windkessel effect of large vessels including the aorta leads to a continuous diastolic flow in arteries supplying parenchymal organs due to a lower peripheral resistance of the terminal vascular territories supplied by these arteries.

1.2.2.1 Low-resistance Flow

Arteries supplying parenchymal organs and the brain are characterized by a fairly steady blood flow as a result of low peripheral resistance. In these arteries, a moderate systolic rise is followed by a steady flow that persists throughout diastole. This flow profile is typical of the renal, hepatic, splenic, internal carotid, and vertebral arteries.

The windkessel effect thus ensures a more continuous flow than would result from the action of the left ventricle and aortic valve alone. As a result, flow will become more pulsatile when this effect and the normal elasticity of the vessels are lost.

1.2.2.2 High-resistance Flow

A high peripheral resistance results in a more pulsatile flow with a steep systolic upslope during the acceleration phase, followed by deceleration and a significant reflux in early diastole and short backward flow in mid-diastole. Zero flow is typically seen in end diastole. This pattern is referred to as triphasic flow.

The systolic pulse wave is in part reflected by the high peripheral resistance and thus moves backward through the arterial system until the flow is again redirected toward the periphery by the influx of blood during the next cardiac cycle.

This flow component is small due to the high peripheral resistance.

As a result of the high pressure in the arterioles supplied by the limb arteries, significant blood flow in these vessels occurs only during systole when systemic pressure is higher than peripheral pressure. The pressure during diastole is too low to produce blood flow toward the periphery.

High-resistance flow is typical of the arteries supplying muscles and the skin. These are the leg and arm arteries and the external carotid artery. The ratio of skin to muscle supply determines the extent of diastolic forward flow. When the peripheral demand increases (muscle activity, inflammation), the arterioles reduce the peripheral resistance, and forward flow, primarily during diastole, increases.

Transitions between these two flow patterns may occur under normal and abnormal conditions. Besides, there are vessels with mixed flow. A typical example is the superior mesenteric artery, which has pulsatile flow like a limb artery but also a significant end-diastolic flow component. A iatrogenically created arteriovenous (AV) shunt will turn high-resistance flow into low-resistance flow. A change from low-resistance to high-resistance flow in the renal artery is a criterion for kidney graft rejection.

1.2.3 Determining the Degree of Stenosis

According to the continuity law, the volume flow rate (cross-sectional area multiplied by mean flow velocity) is identical in all vessel segments. Therefore, a sudden decrease in the vessel diameter is associated with an increase in blood flow velocity (a 50% decrease in diameter, corresponding to a 75% decrease in cross-sectional area, will result in a 4 times higher flow velocity). The flow profile flattens out (plug flow) when the blood enters a narrower vessel segment. If the increase in flow velocity is known, it is possible, in principle, to calculate the degree of stenosis according to the continuity equation:

$$X = 100 \cdot \left(1 - \frac{V_1}{V_2}\right)$$

X percentage stenosis grade (cross-sectional area reduction)
V_1 prestenotic velocity
V_2 intrastenotic velocity

This equation for estimating the degree of stenosis does not take into account other systemic factors (blood pressure, wall elasticity, peripheral resistance) that may affect the ultrasound measurement. A sudden decrease in the cross-sectional area is associated with pronounced acceleration forces, which turn laminar flow into plug flow along the constricted segment. The increase in kinetic energy resulting from the increase in mean flow velocity in the stenotic area is associated with a decrease in static (lateral) pressure. This conservation of energy is expressed in the Bernoulli equation as the sum of lateral pressure energy and kinetic energy:

$$P_1 + \frac{1}{2} \cdot \rho \cdot V_1^2 = P_2 + \frac{1}{2} \cdot \rho \cdot V_2^2$$

P_1 prestenotic lateral pressure
P_2 intrastenotic lateral pressure
V_1 prestenotic flow velocity
V_2 intrastenotic flow velocity
ρ density of blood

Using the Bernoulli equation, the conversion of static pressure energy into kinetic energy resulting from a reduction of the vessel cross-sectional area is expressed as follows:

$$P_1 - P_2 = \frac{1}{2} \cdot \rho \cdot (V_2^2 - V_1^2)$$

The poststenotic increase in the cross-sectional flow area leads to turbulent flow, flow separation, and vortexing. The pronounced turbulence occurring in the presence of high-grade stenoses is associated with eddy currents and backward flow, resulting in the irreversible loss of most of the kinetic energy while the loss due to inertial and frictional forces is negligible (Weber et al. 1992). The pressure drop over a stenosis (substantial portion of the measured Doppler blood pressure) thus predominantly reflects the lost kinetic energy in the stenosis. Therefore, the kinetic energy expressed as peak systolic velocity in the stenosis can serve as a measure of the pressure drop over the stenosis (according to the simplified Bernoulli equation: $P_1 - P_2 = 4 \cdot V_2^2$; neglecting prestenotic velocity P_1 in favor of intrastenotic velocity V_2) and the grade of stenosis (cf. Sect. 2.1.6.1.1, "Pelvic Arteries").

Blood flow resumes its laminar profile only farther downstream of the stenosis as a result of decreasing turbulence and the influence of mural friction. The conversion of much of the remaining kinetic energy into static pressure energy promotes the dilatation of an atherosclerotically damaged vessel wall behind the stenosis.

In determining the degree of stenosis, the examiner must be aware that, due to friction losses inside the stenosis, the measured grade may be lower than expected. In high-grade stenoses that reduce the volume flow rate, flow velocity is already decreased in the prestenotic vessel segment, resulting in an intrastenotic increase in velocity that is lower than expected from the diameter reduction. The peak intrastenotic velocity may thus be lower in high-grade stenoses associated with a reduced volume flow rate than in intermediate-grade stenoses that cause less pronounced flow reduction.

In the presence of two or more sequential stenoses, the respective pressure drops reduce peak flow velocity upstream of the next (second or third) stenosis, so that no absolute flow velocity levels can be used as thresholds for stenosis grading. In these cases, one should use quotients of flow velocities measured upstream of and within the stenosis. Quotients greater than 2, corresponding to an increase in peak systolic

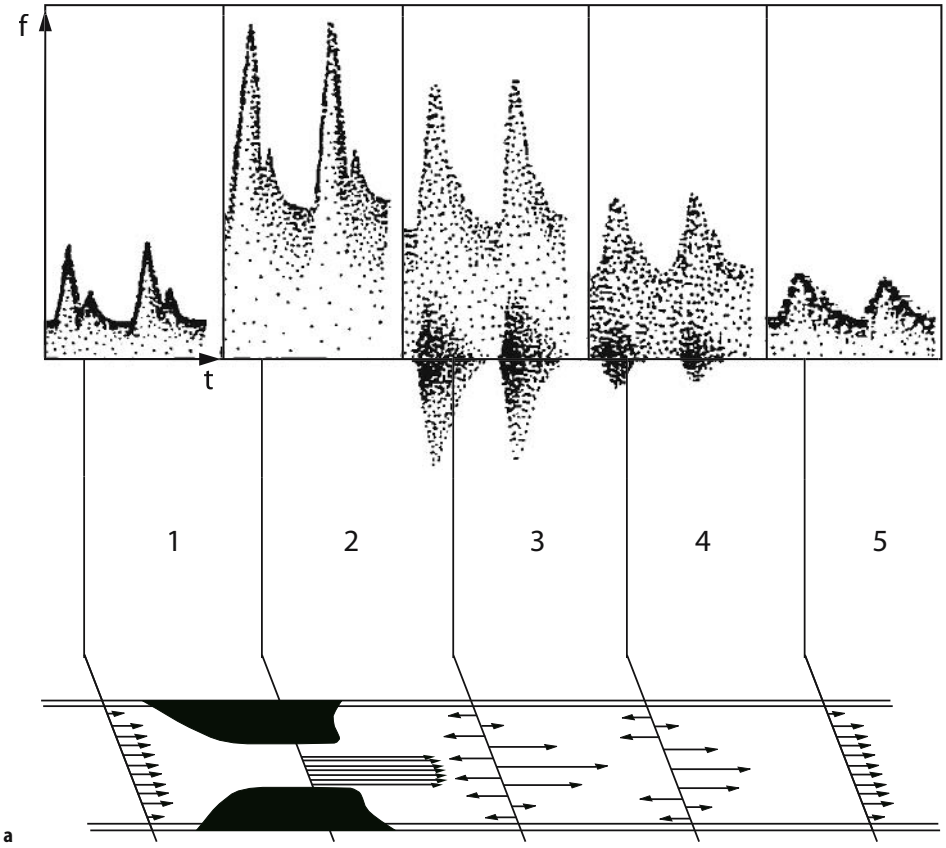

a

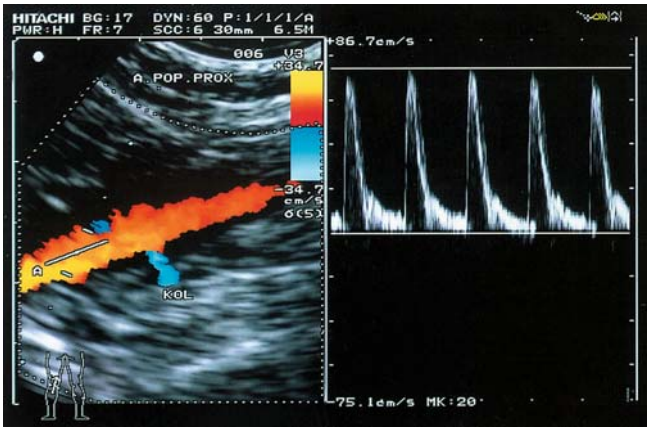

b

Fig. 1.25. a Impact of flow in and around a stenosis on the Doppler waveform (A.carotis interna stenosis):
1 prestenotic (laminar, pulsatile);
2 intrastenotic (plug profile, maximum acceleration of flow depending on diameter reduction);
3 immediately poststenotic (pronounced turbulence, accelerated flow);
4 poststenotic (deceleration of flow, residual turbulence);
5 further downstream from stenosis (relamination of flow but decreased pulsatility, flattened waveform with larger diastolic component).
The spectral waveforms schematically represented in **a** show the flow patterns occurring in the course of a stenosis of the carotid artery but are similar to the waveforms obtained in stenotic peripheral arteries (see Table 2.9), except for a higher pulsatility in the latter. **b** (Stenosis of the Arteria poplitea) Proximal to the origin of hemodynamically significant collaterals in a stenotic artery, the normally triphasic prestenotic waveform may show reduced pulsatility. The extent to which pulsatility is decreased depends on the amount of collateral flow and the poststenotic, ischemic widening of the arteries and arterioles. When the sample volume is placed upstream of the origin of a collateral (*KOL*), there is only a subtle incisure in the Doppler waveform in early diastole and continuous blood flow throughout diastole. Farther away from the transducer, a collateral arising from the popliteal artery is depicted, which provides significant compensatory circulation. The hemodynamic effects of collateralization are rarely depicted in such an impressive manner

velocity inside the stenosis of over 100 %, suggest a hemodynamically significant stenosis (> 50 %). This method cannot be used for grading stenoses occurring immediately downstream of vessel divisions, which are clinically relevant because they are predilection sites for stenoses (origins of deep femoral vein or renal arteries, carotid bifurcation). For these vessel areas, empirical threshold velocities (reference value, angiography) must be determined to diagnose hemodynamically significant stenoses. Such thresholds are affected by systemic factors (hypercirculation, hypertension).

Note that for calculating the flow velocity it is important to correct the angle of insonation for Doppler scanning, which should ideally be smaller than 60°. Angles above 70° should not be used because the measurement error will be too large. Proper angulation of the ultrasound beam may be difficult to achieve in curved or branching vessels.

Peak flow velocity is measured during systole in the stenosis or the jet visualized in the color duplex image. The intrastenotic increase in flow velocity in a high-grade stenosis results in an increase of the Reynolds number and is associated with turbulent flow. Turbulence is characterized on color duplex images by a typical mosaic pattern around the central stenosis jet with backward flow near the wall. Depending on the increase in flow velocity, eddy currents may be seen over a length of some centimeters downstream of the stenosis (Fig. 1.25 a–f).

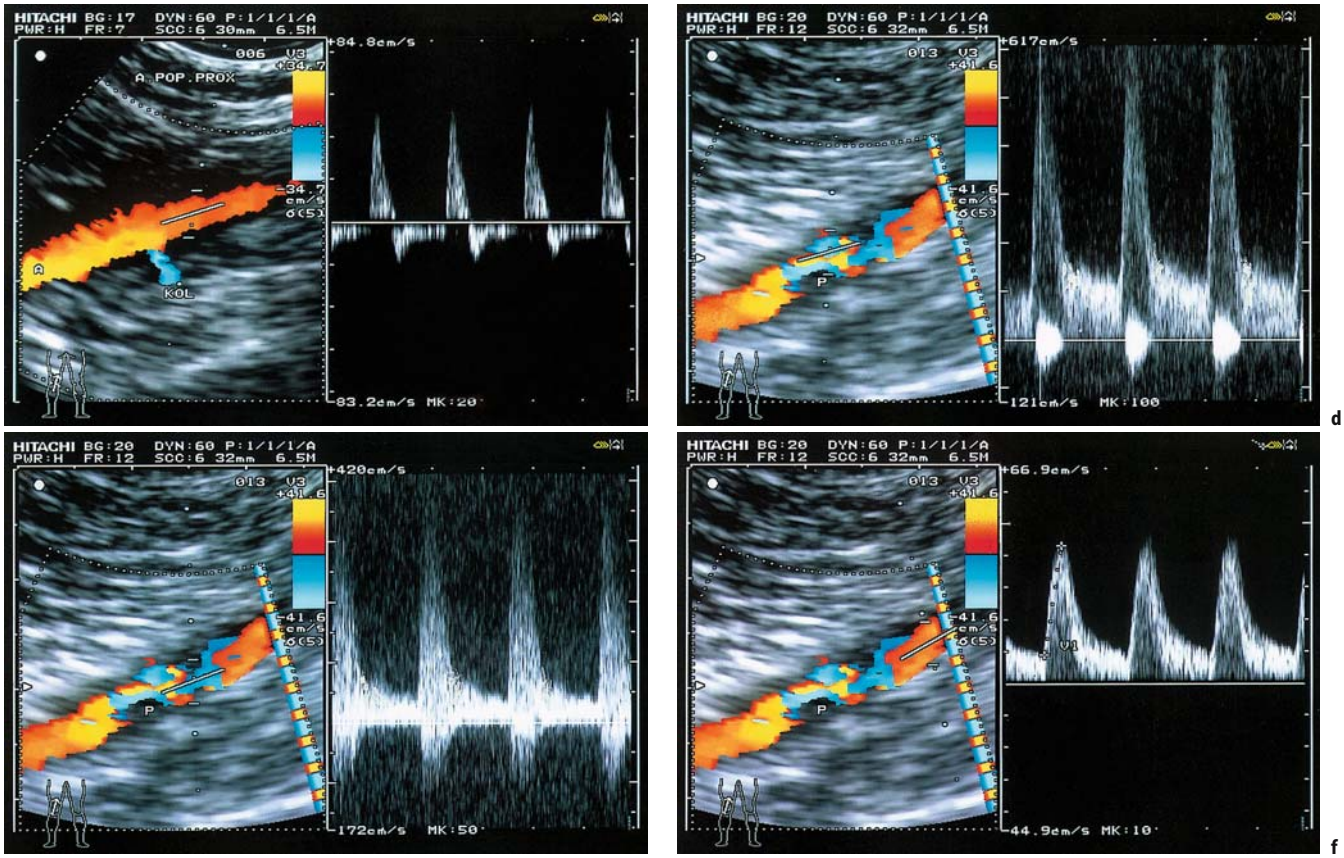

(Fig. 1.25. cont.) c Downstream of the collateral, the increased pulsatility reflects the flow resistance in the popliteal artery immediately after the stenosis. The abnormal diastolic flow is not only a function of the stenosis-related peripheral resistance but also of vessel elasticity. Proximal to the sample volume, the hemodynamically significant collateral (*KOL*) arising from the popliteal artery is displayed in blue. The stenotic popliteal artery segment is not depicted but is likely to be located to the right of the view presented. **d** The high-grade stenosis caused by a hypoechoic plaque produces aliasing in the color duplex scan. The Doppler spectrum shows the flow velocity to be increased to over 600 cm/s (see *2* under **a**). In the segment depicted in the B-mode scan, the popliteal artery stenosis appears to be less severe because the plaque predominantly involves the lateral vessel wall as compared with the spectral display, which reflects the hemodynamic significance of the stenosis (cf. Fig. 5.7 a, b). Like angiography, the B-mode scan reduces the three-dimensional lumen to a two-dimensional, longitudinal plane. Depending on the scan level chosen for gray-scale ultrasound, the extent of the stenosis caused by plaques may be underestimated and differ from the hemodynamic degree of stenosis. **e** In the immediate poststenotic zone, turbulent flow is predominant both in the color duplex image and in the Doppler waveform. Peak systolic flow velocity is still increased at 300 cm/s (see *3* under **a**). **f** Three cm downstream of the stenosis, flow is monophasic with a delayed systolic rise and reduced peak systolic velocity (see *5* under **a**)

The jet tapers off distal to the stenosis while the zone of turbulent flow widens until it occupies the entire lumen. Further downstream, flow becomes laminar again. The pressure drop over a stenosis is determined by its length and degree. These two parameters, together with poststenotic turbulence, govern the loss of kinetic energy. The extent of the pressure drop over a stenosis correlates with the kinetic pressure energy present in the stenosis jet. Based on measurement of the stenosis jet, the pressure drop over the stenosis can be estimated using the simplified Bernoulli equation (neglecting prestenotic flow velocity) as

$$P_1 - P_2 = 4 \cdot V_2^2 \text{ (jet velocity)}$$

The jet axis is usually not parallel to the vessel wall, especially when the stenosis is eccentric. Depiction of the stenosis jet in the B-mode image enables good adjustment of the angle and thus fairly accurate measurement of the flow velocity in the jet (Fig. 1.26).

A study correlating the invasively measured mean catheter pressure gradient over stenoses with the pressure gradient determined from the stenosis jet by means of duplex ultrasound (Strauss et al. 1993) found a correlation for stenoses of the iliac artery of R = 0.77. This investigation was based on preceding model calculations and neglected viscous friction losses and energy losses due to poststenotic turbulence.

In vitro measurements in a model of pulsatile peripheral flow demonstrated good agreement for the pressure decrease over the stenosis measured invasively and that determined by Doppler ultrasound. The correlation found for different grades of stenosis was R = 0.98 (Strauss et al. 1990; Weber et al. 1992). Still, quantitative evaluation of a stenosis using only

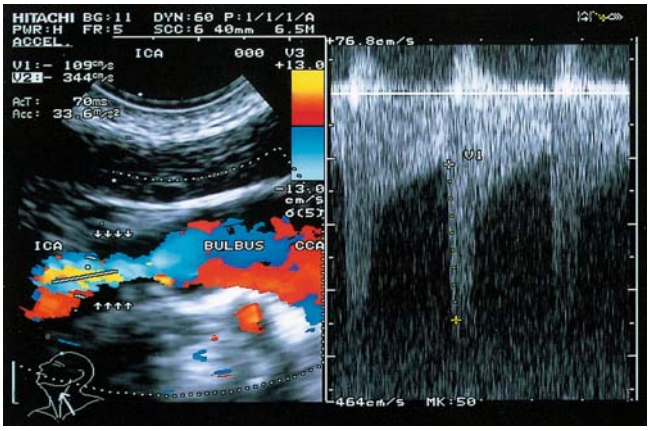

Fig. 1.26. In the eccentric high-grade stenosis of the internal carotid artery shown, the Doppler angle adjusted relative to the vessel wall differs by about 10° from the angle relative to the stenosis jet. Flow in the vessel is displayed in blue (away from transducer) with aliasing due to the stenosis jet. Distal to the hypoechoic plaque, blood flow is depicted in red, indicating flow reversal resulting from flow separations and eddy currents. The color change in the common carotid artery and the bulb (red to blue) is due to the change in flow direction relative to the ultrasound beam (flow toward and away from transducer) and flow separation in the bulb (blue). Proper alignment of the Doppler angle with the stenosis jet would have yielded a higher flow acceleration. The turbulent flow components are reflected more adequately in the Doppler waveform

the absolute values of peak intrastenotic frequency shifts or peak flow velocities is discouraged, as the magnitude of intrastenotic flow velocity is also affected by various other factors such as central regulatory mechanisms (blood pressure), collateral pathways, and peripheral resistance.

Empirical data suggests that a stenosis becomes hemodynamically significant and causes clinical symptoms when the vessel diameter is reduced by over 50 % (corresponding to a cross-sectional area reduction of over 75 %). The pressure drop over a stenosis increases with its degree and length and is reflected by a decrease in the peripheral blood pressure determined by Doppler sonography.

The examiner must be aware, however, that a decrease in peripheral resistance, for example during muscle activity, is associated with a relative increase in the degree of stenosis. The increased blood volume required in the periphery per unit time leads to a relatively greater reduction of the blood flow through the stenosis above a certain degree of stenosis, resulting in a greater discrepancy between the flow volume required in the periphery and the volume that can pass the stenotic vessel segment. As a result, the peripheral dilatation associated with muscle activity can reduce the stenosis-related perfusion pressure to such an extent that relative or absolute ischemia may occur. The hemodynamic effects of an exercise-induced, hemodynamically significant perfusion reduction in the presence of a stenosis that is not hemodynamically significant at rest are also reflected in the Doppler waveform: there is a more pronounced increase in the diastolic component during exercise but, above all, a longer rest after exercise is required before the postocclusive Doppler waveform returns to its normal triphasic pattern (as compared with the contralateral side). In addition to the local degree of stenosis, the reduction in peripheral perfusion is also affected by other occlusive processes and above all by cardiac function (in particular systolic pressure) and the extent of collateralization.

The decrease in pulsatility is primarily due to the high pressure gradient associated with luminal narrowing. The changes in the spectral waveform proximal to a vessel obstruction vary with collateral perfusion and the distance between the site of sampling and the vessel lesion. Close to the lesion, pulsatility increases as a result of the high resistance. When the Doppler information is sampled proximal to the origin of relevant collateral vessels, peripheral resistance causes a less pulsatile flow profile (cf. Fig. 1.25 b–f). The hemodynamic changes resulting from the dilatation of the arterioles, which decrease their tone as the blood supply drops, affect the flow pattern in the prestenotic vessel segment through the collateral connections.

Downstream of a stenosis, the slower systolic pressure build-up is seen in the Doppler waveform as a less steep systolic upslope (acceleration), which can be expressed as the acceleration time. A longer acceleration time in the poststenotic waveform is an indirect sign of a hemodynamically significant stenosis. Behind high-grade stenoses, the delayed equalization of central and peripheral (prestenotic and poststenotic) pressure during the cardiac cycle also contributes to the persistent diastolic flow. This postocclusive increase in diastolic pressure is due to the decreased peripheral resistance resulting from arteriolar dilatation secondary to reduced blood flow. Obtaining Doppler spectra at selected sites and evaluating them for prestenotic and poststenotic criteria can shorten the examination. The resistance index (pulsatility index) proximal and distal to a vessel segment with a suspected stenosis that is difficult to interrogate directly can be determined to calculate the so-called damping factor to demonstrate a hemodynamically significant flow obstruction.

$$\text{Damping factor} = \frac{\text{proximal pulsatility index}}{\text{distal pulsatility index}}$$

Stenoses of less than 60 % have little effect on the poststenotic Doppler waveform. Only higher-grade stenoses are associated with an increasing reduction of peak systolic flow velocity, a less steep systolic upslope, and delayed diastolic decrease with persistent flow to the periphery. The decreased peak systolic velocity and delayed systolic rise are primarily due to the preceding flow obstruction while the monophasic flow profile results from peripheral vasodilatation secondary to a mismatch of blood supply and demand. The latter can thus influence the prestenotic waveform via the collateral vessels.

To grade stenoses at the origins of vessels (internal carotid, deep femoral, and renal arteries), one has to rely on empirical data as the continuity equation does not apply to vessel divisions. In most cases, an exact percentage quantification of a stenosis is not necessary in the clinical setting since the therapeutic management of a hemodynamically significant steno-

sis is guided by the clinical symptoms and the vessel segment affected.

On color duplex images acquired with adequate instrument settings, aliasing will already suggest a stenosis. Nevertheless, quantitative evaluation must be performed by analysis of the Doppler waveform with angle-corrected velocity measurement using the criteria outlined above.

Again and again it has been proposed to measure the degree of a stenosis planimetrically by determining the residual patent lumen visualized in the color flow mode in relation to the vessel lumen (wall). However, this approach is often impaired or yields unsatisfactory results due to inaccuracies resulting from color overflow (few color scan lines with interpolation) and scattering or acoustic shadowing due to intrastenotic structures such as calcified plaques. Under ideal conditions with complete direct visualization of the stenotic segment, absence of aliasing, and localization of the stenosis outside of vessel bifurcations, however, determination of the residual lumen by color duplex ultrasound has a satisfactory diagnostic accuracy of 85 % in comparison with angiography (Steinke et al. 1997). Methodological considerations indicate that planimetric measurement is most suitable for evaluating low-grade to intermediate-grade stenoses (cf. Fig. A 5.5).

1.3 Instrument Settings

Proper adjustment of the scanning parameters is of utmost importance in color-coded duplex ultrasound (Table 1.8). Adjustment is done individually for the respective vessel to be interrogated, in particular when spectral Doppler information is collected. The most important aspects are summarized below.

Transducer
- Selection of a suitable frequency
- Adequate presetting (magnification, gain, focusing, PRF, wall filter etc.)

Table 1.8. Optimal instrument settings for specific diagnostic tasks

Color-coded duplex ultrasound		
Setting	Evaluation of flow pattern Diagnosis of stenosis	Evaluation of small vessels Measurement of slow flow
PRF	As high as possible	Low
Color box	Small	Fairly large
Doppler angle	Intermediate (30° – 60°)	As small as possible
Wall filter	Intermediate	Low
Color gain	Intermediate	High
Pulsed Doppler ultrasound		
Setting	Depiction of fast flow	Depiction of slow flow
PRF	As high as possible	As low as possible
Wall filter	Intermediate	Low
Doppler angle	70° – 90°	As small as possible
Transducer	Low frequency	Higher frequency

Adjustment of B-mode scanning parameters
- Identification of the vessel in the transverse plane
- 90° clockwise rotation of the transducer to depict the vessel in the longitudinal plane
- Optimization of the image size
- Optimization of gain and time-gain compensation: black vessel lumen, walls sharply delineated

Color Doppler
- Angling of the transducer to interrogate the vessel in the longitudinal plane (to improve angle of incidence)
- Positioning of the color box, possibly tilting it (parallel scanner), to ensure the smallest angle possible in relation to the vessel axis
- Selecting the size of the color box in such a way as to ensure a high enough frame rate
- Optimizing gain
- Adjusting PRF (Fig. 1.27 a, b):
  - higher PRF when aliasing occurs
  - lower PRF when no flow is detected but slow flow is expected
- Adjusting high-pass filter (HPF; rarely necessary as mostly coupled to PRF):
  - lower cutoff to detect very slow flow
  - higher cutoff when motion artifacts occur
- If color filling of the vessel is insufficient, a *lower-frequency transducer* should be selected to improve penetration depth. The poorer spatial resolution is negligible in the color mode as it is compensated for by the superior color signal.

Pulsed Doppler
- Placing the Doppler gate in the center of the lumen in the color-mode viewfinder at an angle $< 70°$ relative to the longitudinal vessel axis
- Angle correction
- Optimizing the Doppler gate width to cover the entire lumen
- If the Doppler signal is poor, the color mode should be frozen in triplex scanning to improve Doppler resolution
- Optimizing the spectral waveform:
  - Gain:
  - absent or sketchy curve: *gain* ↑
  - overmodulation (complete filling-in of systolic window, mirror image): *gain* ↓
  - PRF:
  - peak frequency/velocity cut off (aliasing): *PRF* ↑
  - spectrum too “small”: *PRF* ↓
  - Filter:
  - depiction of slow flow: *HPF* ↓
  - elimination of interfering low frequencies: *HPF* ↑

An optimal waveform can be sampled from the site interrogated by minimally changing the transducer position using for orientation the Doppler tracing but above all the *acoustic Doppler signal*. An abnormal signal is often heard before the

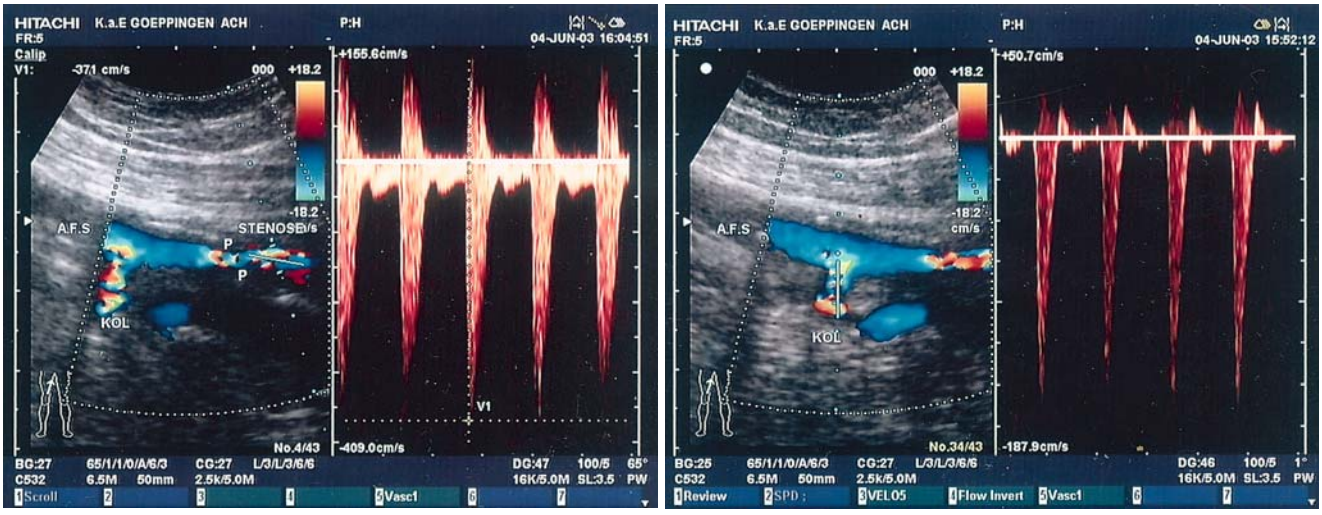

a b

Fig. 1.27 a, b. a Semiquantitative measurement of flow velocity by color duplex ultrasound requires proper instrument setting, in particular of the pulse repetition frequency. Aliasing should not occur in vessels with normal flow. A compromise between different requirements may occasionally be necessary. In color duplex scanning, aliasing occurs if the pulse repetition frequency is too low to register high Doppler shifts. The Doppler frequency is affected by the flow velocity of the reflecting particles and the size of the Doppler angle. The scan shows the superficial femoral artery in blue (flow away from transducer toward periphery) with aliasing (on the right side of the scan), which suggests a stenosis unless instrument settings are inadequate. The Doppler waveform generated with an angle of 65° confirms the stenosis with a peak systolic velocity of 371 cm/s. **b** Aliasing due to a small angle of insonation. The collateral (*KOL*) arising from the posterior aspect of the superficial femoral artery (*A.F.S*) has a normal Doppler waveform with an angle-corrected peak systolic flow velocity of 170 cm/s (very small Doppler angle of 1°)

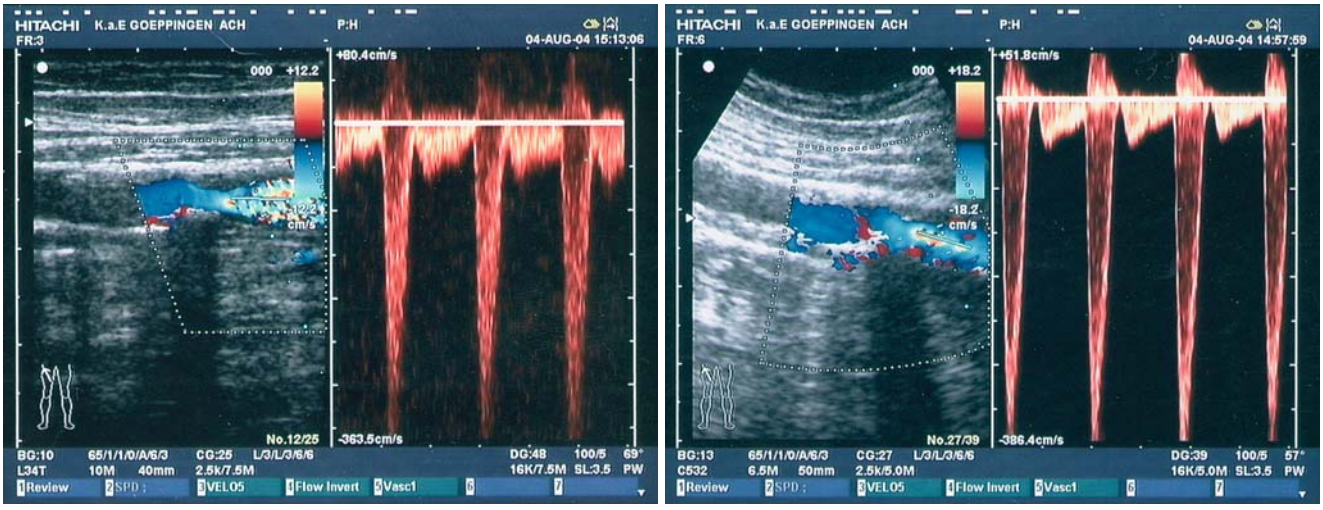

a b

Fig. 1.28 a, b
Determination of Doppler angle
Small angles of incidence below 70° are a prerequisite for minimizing the error in flow velocity measurement in Doppler ultrasonography (hemodynamic evaluation of stenosis). At Doppler angles of 70° or above, small angle setting errors that are unavoidable under clinical conditions (e.g. 5°) introduce unacceptably large errors in velocity measurement (cf. Fig. 1.6).
Selection of a proper transducer assists in achieving an adequate Doppler angle.
a A linear-array transducer with a maximum beam deflection of 20° does not enable insonation angles of less than 70° when scanning a vessel running parallel to the skin surface and will lead to the above-described errors
b A curved-array transducer with a small radius can be tilted to record the Doppler frequency spectrum with a small angle if the sample volume is placed at the edge of the scan sector. This improves the spectrum obtained and reduces the measurement error because vessels parallel to the skin surface can be interrogated with an angle of incidence of 50–60° (57° in the example shown). The intermediate-grade stenosis depicted in **a** and **b** has a peak systolic flow velocity of 380 cm/s

transducer provides the corresponding graphic information (in particular when there is scattering due to plaque).

Note: In areas of high-grade stenoses with pronounced turbulence, high-energy frequencies from slow flow are predominant. For stenosis grading, however, it is important to register the fast flow that often has a low energy and is concentrated in a thin jet. The following measures are recommended *to determine peak flow velocity in high-grade stenoses*:

1. selection of a high PRF,
2. overmodulation of the spectrum by a higher gain to also depict the low-energy, high Doppler frequencies,
3. localization of the jet by minimally and carefully changing the transducer position under acoustic and optical guidance.

Peripheral Arteries

2

With the longer life expectancy, atherosclerotic occlusive processes gain in clinical relevance. Atherosclerosis affects not only the coronary arteries and extracranial cerebral vessels but also the arteries of the extremities. The prevalence of symptomatic arterial occlusive disease (AOD) in men and women aged 55 to 75 is 4.5 % and over 20 % when asymptomatic disease is included. Atherosclerosis reduces an individual's quality of life causing immobility and disability. Life expectancy is reduced, by about 10 years in male AOD patients. Major causes of death are coronary heart disease (55 % of patients with AOD versus 36 % without AOD) and cerebral conditions (11 % with AOD and 4 % without). AOD is the manifestation of generalized atherosclerosis affecting all vascular territories but with a high rate of concomitant involvement of the coronary and extracranial cerebral vessels, in particular in AOD of the pelvic type. Patients in whom peripheral AOD has been diagnosed require not only individual therapeutic management based on the stage of the disease and the suitability of their vascular system for surgical repair but also further prophylactic diagnostic and therapeutic measures (coronary heart disease/CHD, carotid stenosis). The wider range of therapeutic options available today, in particular the percutaneous interventions, can help to prevent the loss of a limb through reconstruction or recanalization of occluded vessel segments and to improve the patient's quality of life through the early elimination of stenotic processes. Early diagnosis is essential for the initiation of proper treatment. Duplex ultrasonography is a well-suited noninvasive modality for an efficient and low-risk primary diagnostic workup.

2.1 Pelvic and Leg Arteries

2.1.1 Vascular Anatomy

2.1.1.1 Pelvic Arteries

At the level of lumbar vertebrae (L) 4/5, or the umbilical level when scanning from the anterior approach, the abdominal aorta divides into the two *common iliac arteries*. They descend into the true pelvis taking an arched course along which they bifurcate at about the most posterior point (Fig. 2.1 a). The common and external iliac veins course behind the respective arteries. The *internal iliac artery* arises at the level of the sacroiliac joint, coursing in a posterior direction to supply the pelvic organs, pelvic wall, and buttocks. The *external iliac artery* is the continuation of the common iliac artery and arches into the lacuna vasorum under the inguinal ligament. It runs medial to the iliopsoas muscle and gives off the inferior epigastric and deep circumflex iliac arteries shortly before it reaches the inguinal ligament. These two arteries can serve as collaterals in pelvic artery occlusion.

The vessel diameters vary between 0.6 to 1.4 cm in the common iliac artery, 0.5 to 1.0 cm in the external iliac artery, and 0.4 to 0.8 cm in the internal iliac artery.

2.1.1.2 Leg Arteries

The *common femoral artery* is about 2 – 4 cm long and below the inguinal ligament divides into the profunda femoris artery, which typically branches off on the posterolateral aspect, and the superficial femoral artery (Fig. 2.1 b).

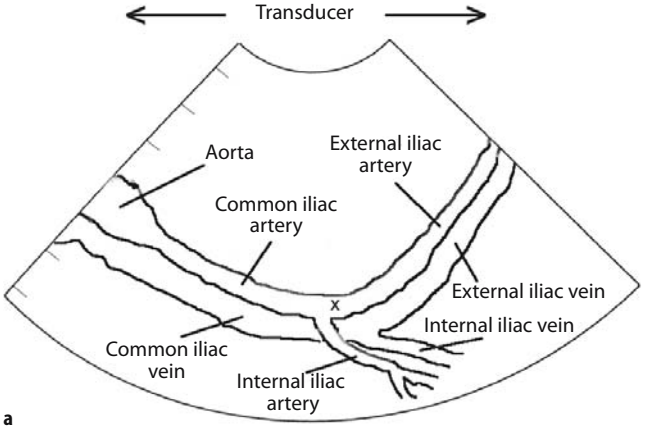

a

Fig. 2.1. a Schematic representation of the arched course of the iliac vessels through the true pelvis. The iliac bifurcation is situated at the most posterior point where the common iliac artery gives off the internal iliac artery. The common and external iliac veins run posterior to the arteries of the same name. The origin of the external iliac artery is a preferred site of atherosclerotic stenosis (*X*). From the normal anterior transducer position, however, stenosis cannot be assessed due to an extremely poor Doppler angle of about 90°. To improve the angle, the transducer must be moved upward or downward (*arrows*) and angled (cf. also Fig. 1.21 and Fig. 2.2)

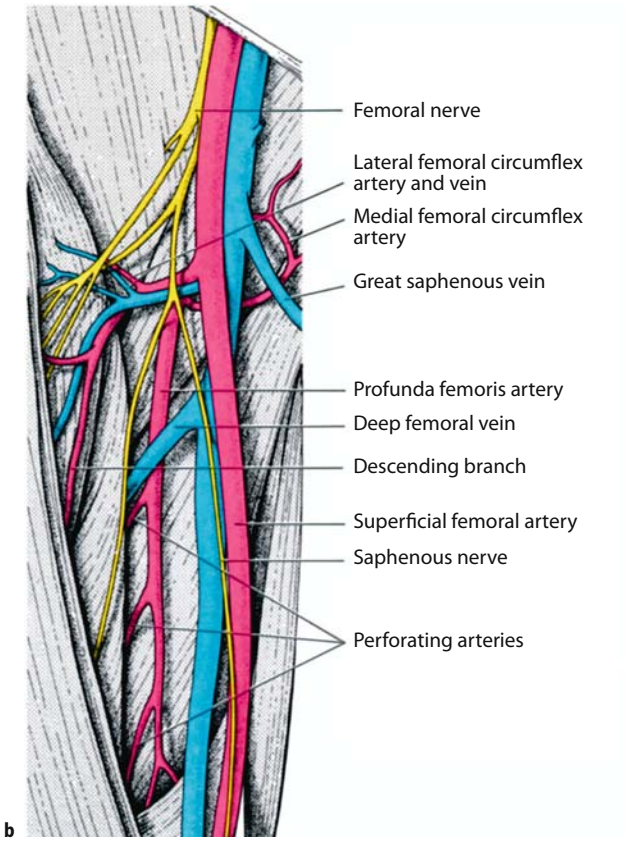

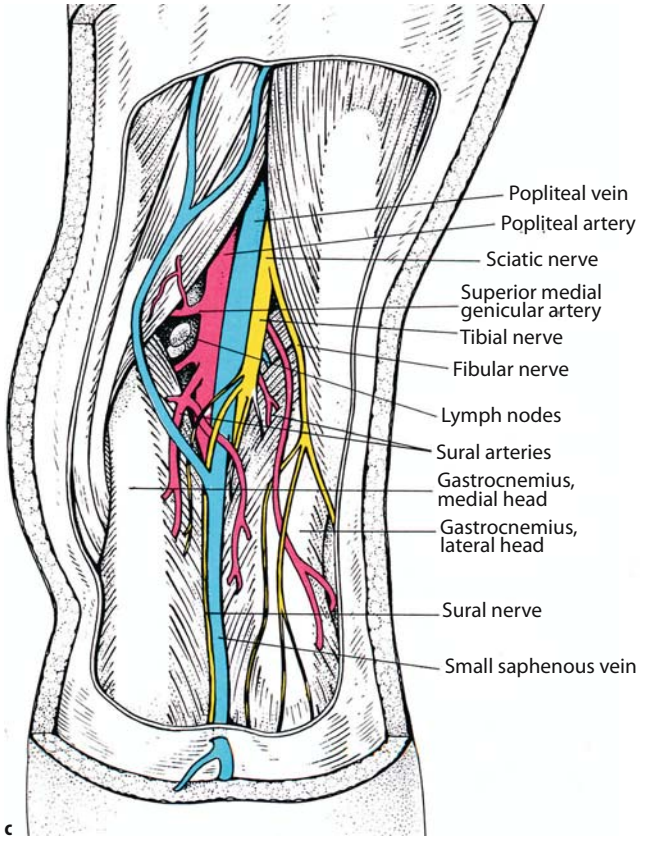

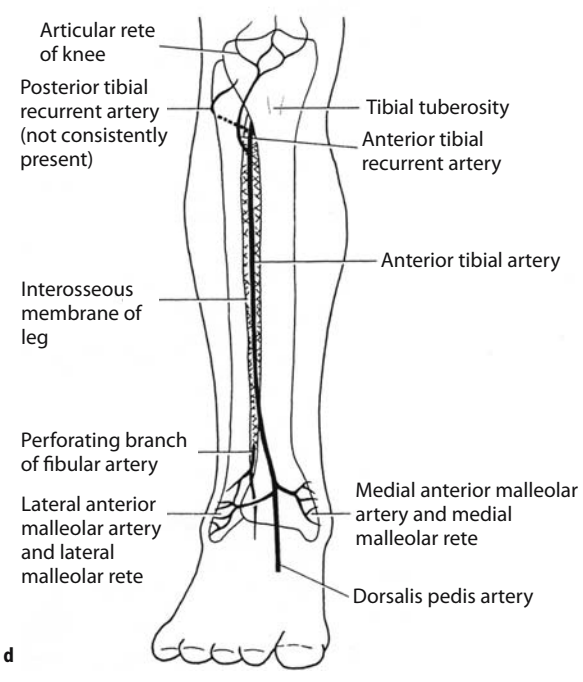

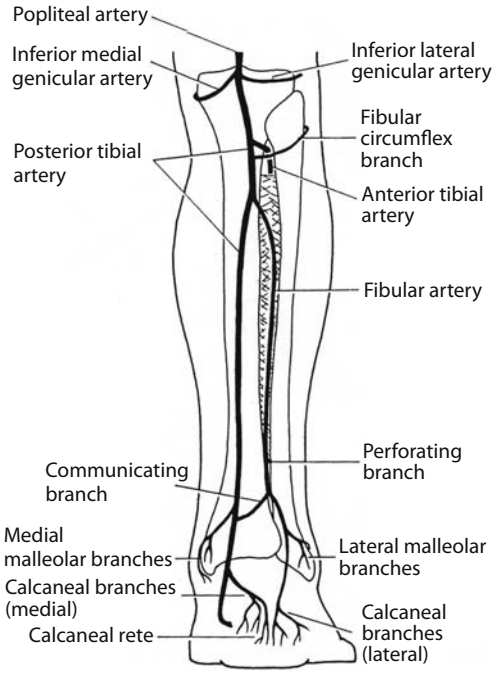

Fig. 2.1. b Schematic representation of the vessels in the groin (from Heberer and van Dongen 1993). **c** Schematic representation of the vessels in the popliteal fossa (from Heberer and van Dongen 1993). **d** Schematic representation of the lower leg arteries

The origin of the *profunda femoris artery* is variable and several branches may arise directly from the common femoral. Typically, one branch arises posteriorly while the main branch arises posterolaterally or, in rare cases, posteromedially. Branches of the medial and lateral circumflex arteries open into the femoral bifurcation and form the main collateral pathways in pelvic artery stenosis or occlusion. The profunda femoris artery is the most important collateral route in occlusion of the femoropopliteal segment. Somewhat distal to the femoral bifurcation, the *deep femoral veins* converge and unite with the *superficial femoral vein*. The deep veins cross the bifurcation. The superficial femoral vein runs behind the artery on its course to the distal thigh. The plexus passes posteriorly through the vasoadductor membrane at the level of the adductor canal (Hunter's canal) and the superficial femoral artery continues as the *popliteal artery*.

Interventional radiologists and vascular surgeons subdivide the popliteal artery into 3 segments with the P1 segment in angiography extending to the upper edge of the patella and the P2 segment to the knee joint cleft. The P3 segment extends to the origin of the *anterior tibial artery*, which passes anteriorly through the interosseous membrane at the lower edge of the popliteal muscle. It continues through the extensor compartment anterior to the interosseous membrane to the upper edge of the ankle joint with its proximal segment coursing relatively close to the fibula. The popliteal artery continues as the highly variable *tibiofibular trunk* with a length of about 1 – 5 cm (Fig. 2.1 c), branching into the posterior tibial and fibular arteries. The *posterior tibial artery* is the main artery of the lower leg and passes through the deep crural fascia between the superficial and deep flexors. It continues posterior to the medial ankle to the sole of the foot, where it divides into the larger lateral plantar artery and the smaller medial plantar artery. The lateral plantar artery extends to the deep plantar arch, which completes the arch of foot via its collaterals to the dorsalis pedis artery establishing a connection to anterior tibial branches. The *fibular artery* courses posteromedial to the fibula, also at the level of the deep crural fascia. It ends at the distal lower leg and gives off several arteries supplying the muscles and serving as collaterals when other lower leg arteries become occluded.

The lower leg arteries vary widely in caliber. In cases of hypoplasia or, very rarely, aplasia, the other arteries act as collaterals. Collateralization through the rete malleolare at the level of the upper ankle joint has an important role in atherosclerotic occlusion or hypoplasia.

2.1.2 Examination Protocol and Technique

2.1.2.1 Pelvic Arteries

The depth of penetration required for scanning of the pelvic arteries makes it necessary to use *convex transducers* with frequencies of *3.5 – 5 MHz*. The proper pulse repetition frequency (no aliasing) and gain are selected in a healthy vessel segment. The examination is performed with the patient in the supine position and after an adequate period of rest in order to prevent false-positive findings due to reactive hyperemia. Exercise-induced hyperemia takes longer to return to normal in the presence of atherosclerotic occlusive processes.

A hemodynamically significant stenosis above the inguinal ligament can be identified quickly by obtaining a spectral Doppler tracing from the common femoral artery. A triphasic waveform with a peak systolic velocity above 70 cm/s (side-to-side comparison) excludes a higher-grade stenosis at the pelvic level with a high degree of likelihood.

For closer evaluation, the aortic bifurcation is located in the transverse plane at the umbilicus and the common and external iliac arteries are tracked along their courses and searched for stenotic lesions in longitudinal orientation (Fig. 2.2). Bowel loops, in particular when filled with air, produce marked scattering and *attenuation*, impairing continuous scanning of the pelvic vessels. Air-filled bowel loops can be displaced from the insonation window by exerting continuous pressure with the transducer, or the transducer is shifted to circumvent such attenuating structures.

The iliac arteries take an arched course through the true pelvis, which makes it more difficult to achieve a small angle of incidence, in particular at the deepest point, the iliac bifurcation, where the origin of the external iliac artery is a predilection site for the occurrence of pelvic artery stenoses. The Doppler angle is optimized by moving the transducer along the course of the vessel and angling it (cf. Figs. 2.1 a and 1.21). In patients with a poor insonation window, at least the origin of the common iliac artery from the aorta and the external iliac artery after the bifurcation and just proximal to the inguinal ligament should be scanned including spectral analysis of these vessel segments, as they are *predilection sites for pelvic artery stenoses*. Besides the analysis of the spectral Doppler tracings for established stenosis criteria, the comparison of the spectra from different sites will also yield indirect evidence of stenotic processes in between.

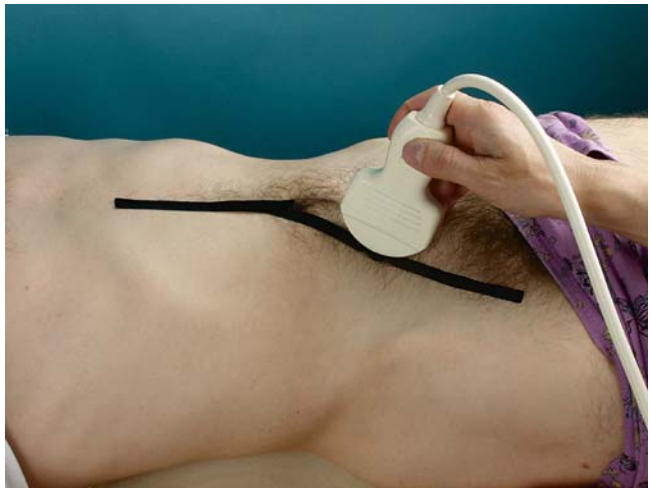

Fig. 2.2. Positioning of transducer for pelvic artery examination (aortic bifurcation at the umbilical level) (cf. also Fig. 2.1a)

2.1.2.2 Leg Arteries

The superficial course of the leg arteries makes it possible to use higher-frequency transducers of 5 – 7.5 MHz, depending on the thickness of the soft-tissue coat. Linear transducers require the activation of beam steering and careful alignment with the course of the vessel to achieve an adequate Doppler angle. Curved-array transducers with a small radius yield B-mode scans with somewhat poorer detail resolution but have the advantage of enabling fast optimization of the Doppler angle ($<60°$) by angling of the transducer and placement of the sample volume at the lateral edges of the imaging field. In contrast, beam steering in most ultrasound devices enables a maximum deflection of the emitted beam of only 20°, resulting in a Doppler angle of 70° when interrogating vessels running parallel to the skin surface. Evaluation of spectral tracings for indirect signs of occlusive lesions in the vicinity of the sample volume requires an angle of less than 60°.

The femoral (Fig. 2.3 a) and anterior tibial arteries are examined in the supine position, all other lower leg arteries and the popliteal artery in the prone position with slight elevation of the distal lower leg by a support placed under the ankles.

In general, vessels are visualized in two planes. First, the vessel is identified in the *transverse plane*. The pulse repetition frequency and gain are set so as to ensure good color filling of the arterial lumen while avoiding aliasing. For a preliminary overview in transverse orientation, the transducer must be angled distally or cranially to achieve a small angle of insonation relative to the vessel. A survey in the transverse plane has the advantage of enabling rapid identification of vessel dilatations, stenoses that produce aliasing, and occlusions once adequate setting has been achieved. Abnormal findings need to be confirmed and quantified in the *longitudinal plane*. An adequate angle of insonation and verification of the Doppler angle in the B-mode scan are prerequisites for quantification of a stenosis. As in gray-scale scanning, the monitor display in vascular imaging in longitudinal orientation depicts the cranial vessel segment on the left and the distal segment on the right.

With the patient in the supine position and after an adequate period of rest (>5 min), the common femoral artery is identified in the transverse plane and traced along its course to the bifurcation. The transducer is positioned (in most cases on the inner thigh) to view the bifurcation in such a way that the profunda femoris artery, which typically arises from the posterolateral aspect, comes to lie exactly behind the superficial femoral artery. In this way, the bifurcation is depicted as a fork in longitudinal orientation, which facilitates vessel identification and proper angle setting for evaluation of a stenosis at the origin of the profunda femoris. Especially when occlusions have been identified in the femoropopliteal segment, the profunda femoris artery should be traced to the level of second order branches and checked for the presence of more distal stenoses. The superficial femoral artery is traced in longitudinal orientation down the inner thigh. Scattering and attenuation due to connective tissue structures within the adductor canal may require readjustment of the gain in the B-scan and Doppler modes.

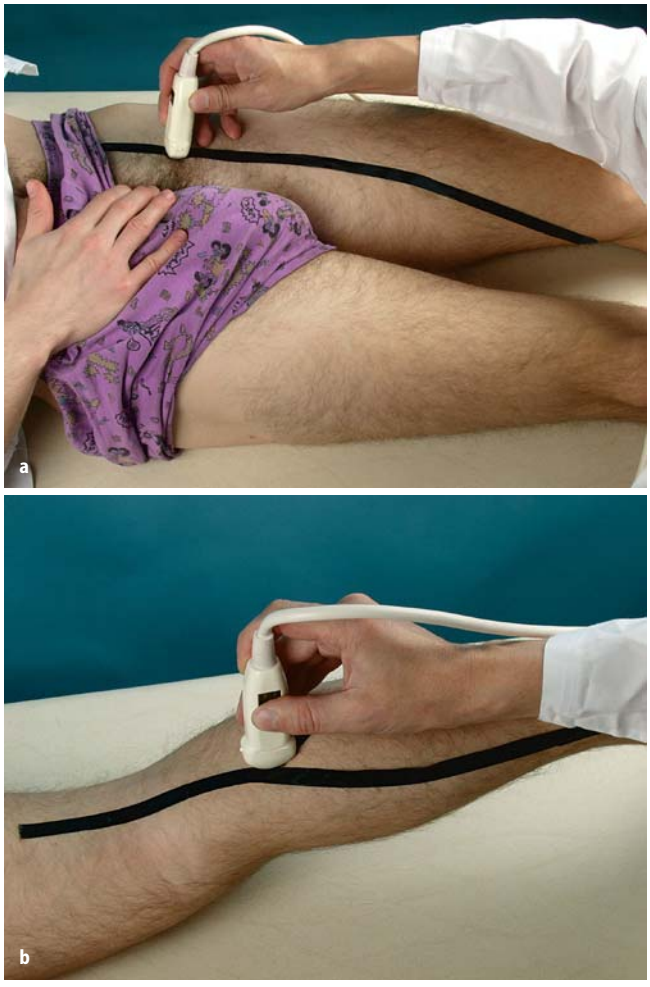

Fig. 2.3. a Positioning of transducer for examination of the femoral arteries (transverse plane for identification of vessel, longitudinal plane for determining flow velocity). **b** Positioning of transducer for examination of the popliteal vessels (at the junction of the P3 segment and tibiofibular trunk)

The vessel course inside the adductor canal is easier to follow with the leg turned outwardly and the knee slightly bent. The popliteal artery and vein are best examined with the patient lying prone. The vein runs posterior to the artery. As the anterior tibial artery arises from the anterolateral aspect of the popliteal artery, its origin is seen farther away from the transducer when scanning from the popliteal fossa (Fig. 2.3 b). The origin may be relatively high in individuals with a short P3 segment or very low when P3 is long. In about 4% of the population, all 3 lower leg arteries jointly arise in a trifurcation (Lippert and Pabst 1998). After having penetrated the interosseous membrane, the anterior tibial artery is traced distally along its anterolateral course in longitudinal orientation.

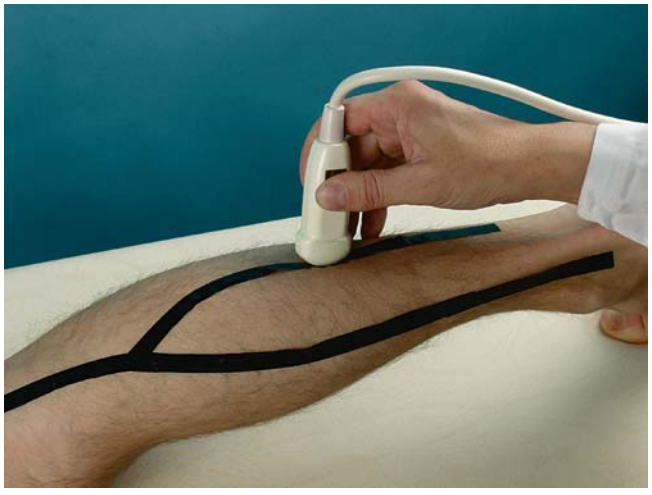

Fig. 2.4. Positioning of transducer for examination of fibular and posterior tibial arteries (course marked by thick black line)

The tibiofibular trunk varies in length from 1 – 5 cm, depending on the level of origin of the anterior tibial artery. Its division into the posterior tibial and fibular arteries is identified in the transverse plane. In the longitudinal view, the vessels are continuously scanned for stenosis or occlusion by following their courses distally (Fig. 2.4). If a vessel disappears from the scanning plane, it can easily be identified again by changing to a transverse view. The tibia and fibia cast acoustic shadows and can serve as landmarks. Further orientation is provided by the hyperechoic band of the deep crural fascia. Under good insonation conditions, the lower leg arteries can be visualized down to the ankle region. Time can be saved by obtaining two spectral tracings, one in the proximal and the other in the distal segment of the respective lower leg artery, which in general excludes a hemodynamically significant obstruction between the two sampling sites when both show the same flow profile and normal peak systolic velocity.

The dorsalis pedis artery and the posterior tibial artery behind the medial ankle are examined in the supine position using a high-frequency transducer (7.5 – 10 MHz). These vessels are first identified in the transverse plane to then obtain the Doppler spectrum in the longitudinal plane. From there, the course of the plantar artery can be tracked in transverse orientation and its patency determined down into the interdigital arteries.

2.1.3 Specific Aspects of the Examination from the Angiographer's and Vascular Surgeon's Perspective

As the therapeutic approach to peripheral artery disease is symptom-oriented (versus prognosis-oriented for the carotid territory), the diagnostic evaluation is guided by the clinical query, and vessel mapping is not done (Table 2.1). Efficient vascular evaluation is performed in stages (Fig. 2.5). If the patient's history, clinical examination with full evaluation of peripheral pulses, and Doppler blood pressure measurement suggest arteriosclerotic occlusive disease (AOD), the next test is noninvasive duplex scanning to identify vessel obstructions and evaluate their localization and causes (embolism, atherosclerosis, compression syndrome). The ultrasound findings serve to determine the therapeutic procedure (medical treatment, radiologic intervention, surgical reconstruction). Angiography is performed only as part of a therapeutic intervention (diagnostic angiography plus angiographically guided percutaneous intervention) or in planning surgery (evaluation of outflow tract for bypass implantation and identification of the most suitable vessel segment for distal anastomosis). The use of further diagnostic procedures, in particular invasive modalities such as angiography, must always be guided by their therapeutic consequences. Hence, angiography has been abandoned for diagnosing peripheral AOD or evaluating the vascular status in patients with definitive or inconclusive symptoms of claudication because the therapeutic consequences are still unclear.

Adequate therapeutic measures in relation to the stage of disease are initiated on the basis of the clinical presentation in conjunction with the (noninvasive) duplex findings (cf. also Table 2.5, Fig. 2.6). In some cases, the site of obstruction and clinical stage allow surgical repair without prior angiography.

For instance, the indication for thromboendarterectomy (TEA) can be established without performing angiography if duplex ultrasound demonstrates a stenosis of the common femoral artery or of the origin of the profunda femoris artery – with occlusion of the superficial femoral – and excludes a vessel obstruction of the pelvic artery territory or, in occlusion of the superficial femoral, confirms refilling of the P1 popliteal segment without major obstruction. In these cases, TEA at the inguinal level is indicated with subsequent evaluation of the clinical improvement. Vessel mapping, in particular with evaluation of the lower leg arteries, does not affect therapeutic decision making, and the benefit of determining collateral flow in the thigh by preoperative anteroposterior

Table 2.1. Vascular surgical and endovascular interventions

Vascular disease	Therapy
Peripheral AOD	Symptom-oriented
Nonatherosclerotic peripheral vessel disease	Prevention-oriented
Carotid artery stenosis	Prevention-oriented
Aneurysm	Prevention-oriented
Diagnostic procedure prior to: Symptom-oriented therapy:	Levelwise duplex scanning guided by therapeutic options contemplated/step-by-step diagnostic management
Prevention-oriented therapy:	Duplex sonographic vessel mapping of predilection sites based on clinical suspicion or in high-risk patients

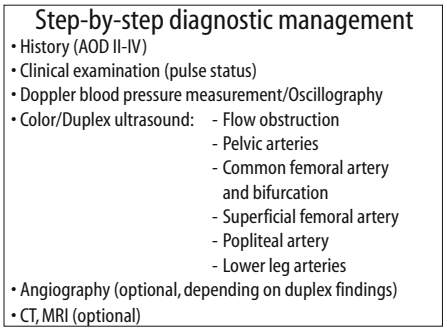

Fig. 2.5. Step-by-step diagnostic management and algorithm for diagnostic and therapeutic management based on the clinical presentation and localization of flow obstruction demonstrated by duplex ultrasonography. Symptom-oriented therapy → symptom-oriented diagnostic procedure. In the step-by-step approach, no subsequent diagnostic test is performed unless it is therapeutically relevant

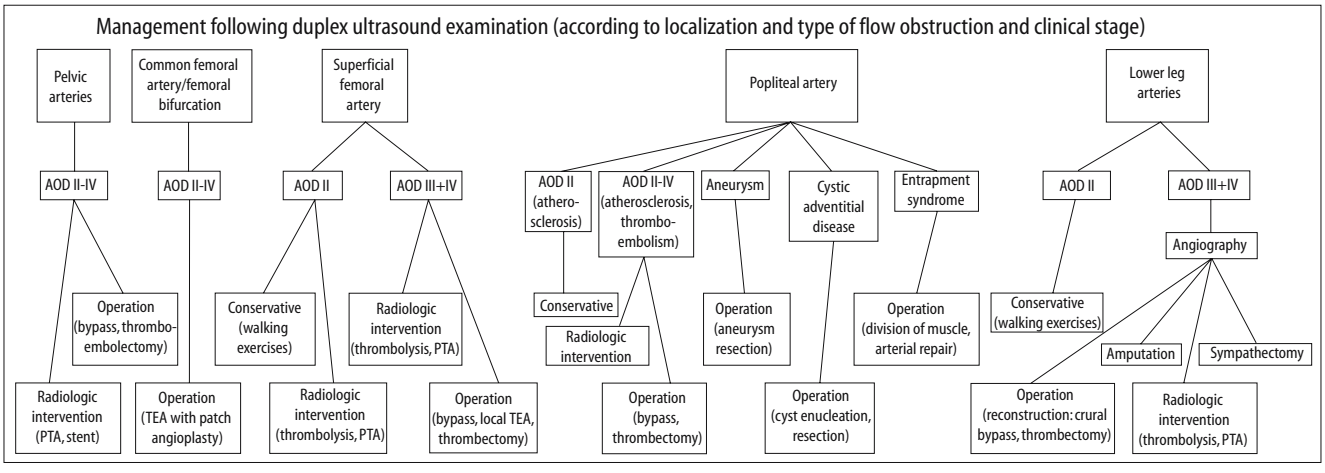

angiography in occlusion of the superficial femoral artery is disputed. This is confirmed in a study by our group including 38 patients with clinical stage II and III AOD in whom duplex scanning performed in the framework of step-by-step diagnostic workup demonstrated high-grade stenosis or occlusion of the common femoral artery (14 patients) or high-grade stenosis of the profunda femoris artery in occlusion of the superficial femoral (24 patients). Angiography identified plaque with mild to moderate luminal narrowing in some of these patients and confirmed high-grade stenoses in 86% of the cases. Intraoperatively, high-grade stenosis was confirmed in all cases. The popliteal artery was included in the duplex evaluation, which excluded pelvic stenosis, while dilatation with stenting was performed before or during surgery in 4 cases. The crucial question to be answered by this study was whether preoperative angiography can be done without in patients with stenosis of the common femoral or profunda femoris. In no case did the preoperative angiography findings alter the therapeutic procedure determined on the basis of duplex ultrasonography. However, 3 patients had to be excluded from the analysis due to a poor insonation window that prevented reliable exclusion of pelvic artery stenosis, which is the crucial prerequisite for dispensing with angiography.

An exception to the restrictive use of diagnostic angiography are patients with longstanding diabetes and secondary macro- and microangiopathy. Medial sclerosis in these patients may preclude continuous scanning of the lower leg arteries and peripheral outflow tract. Possible sequential stenoses may thus be overlooked. Still, identification of all macro- and microangiopathic lesions is necessary for initiation of appropriate therapeutic measures.

The hemodynamic effect of arterial stenoses is evaluated using hemodynamic parameters. Flow models and studies indicate that a reduction in vessel diameter of 50% or more becomes hemodynamically significant and is associated with an increase in peak systolic velocity and, in higher-grade stenosis, an increase in peak end-diastolic velocity as well. The increase in peak velocity correlates with the grade of stenosis (cf. also Fig. 5.5).

In contrast to the evaluation of the carotid artery system, evaluation of plaque morphology in the B-mode for estimating the risk of embolism has no role in examining the peripheral arteries. This is obvious given the difficulties one faces in assessing the risk of embolism associated with carotid artery stenoses in B-mode sonography and the rare occurrence of interdigital artery embolism (blue toe). Nevertheless, one must be aware that, as in the carotid territory, the risk of embolism increases with the degree of stenosis and plaque thickness.

Determining the degree of stenosis from the vessel diameter and the residual perfused lumen on transverse color duplex scans is less accurate than the hemodynamic estimation from the Doppler waveform. The former is done only for preliminary orientation and is susceptible to artifacts due to calcified plaques. Moreover, the interpolation necessary

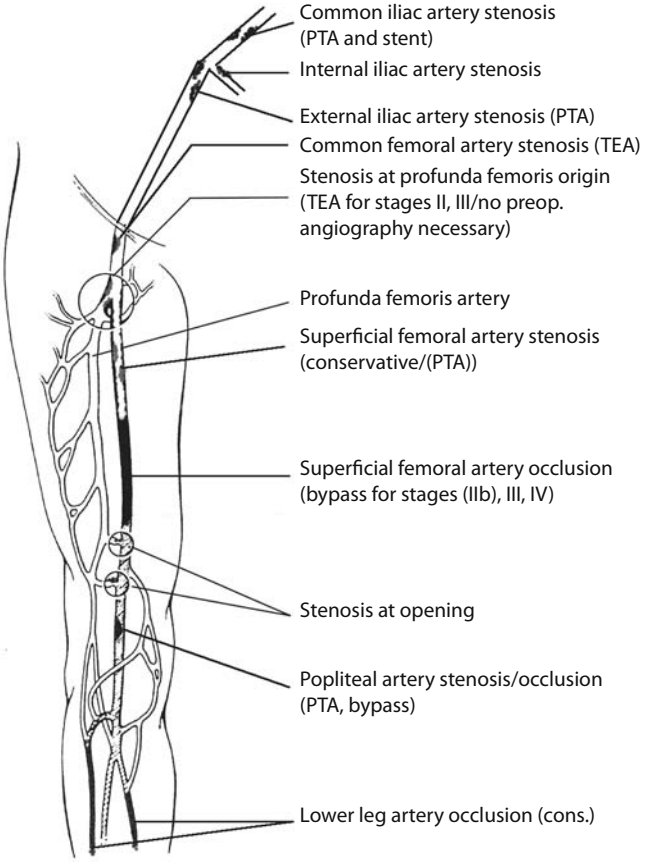

Fig. 2.6. Schematic representation of stenotic and atherosclerotic processes diagnosed by duplex ultrasound and primary therapeutic procedures that can be initiated on the basis of the duplex ultrasound findings (alternative therapeutic strategies may be required according to the clinical stage or in patients with multilevel involvement)

because of the wider spacing of the color scan lines due to physical and technical limitations often leads to overestimation of the patent lumen and underestimation of the stenosis.

2.1.4 Interpretation and Documentation

Reporting and documentation of the duplex ultrasound findings of the leg arteries is guided by the assessment of the key sites. These are the common femoral artery, the origins of the deep and superficial femoral arteries, and the popliteal artery in longitudinal B-mode views and the corresponding Doppler spectra obtained with proper angles of incidence. If the findings at these levels are inconclusive or a specific clinical question has to be answered, angle-corrected time-velocity spectra are sampled in longitudinal orientation from the common and external iliac arteries, possibly the lower leg arteries as well, and documented together with longitudinal scans from these vessels. In addition, all abnormal findings (stenosis or occlusion) are documented on a longitudinal view with a corresponding angle-corrected spectral waveform. The intrastenotic and poststenotic Doppler waveforms are analyzed (see also Table 2.9) to quantify the stenosis (magnitude of peak systolic flow velocity, extent to which triphasic flow profile is lost poststenotically). An aneurysm must be documented in two planes and its diameter measured on the transverse scan. Partial thrombosis, if present, should be documented as well. Optional documentation of corresponding color duplex scans (transverse view of aneurysm, longitudinal view of stenosis) is useful.

The report should describe the morphologic and Doppler ultrasound appearance of the abnormal vascular findings that led to the diagnosis (Table 2.2).

Table 2.2. Duplex ultrasound criteria for arterial evaluation

B-mode:	Assessability	
	Anatomy	(course, variants)
	Vessel contour	(aneurysm, stenosis)
	Wall structures	(calcifications, plaque, cysts)
	Pulsation	(axial, longitudinal)
	Perivascular structures	(hematoma, abscess, tumor, other compressing structures)
Doppler:	Demonstration of flow	
	Flow direction	
	Flow pattern	(laminar, turbulent)
	Flow character	(monophasic/triphasic)
	Flow velocity	

2.1.5 Normal Duplex Ultrasound of Pelvic and Leg Arteries

Flow in the limb arteries is pulsatile and nearly laminar, due to the high peripheral resistance, which is reflected in the Doppler waveform by a narrow bandwidth with a clear systolic window. The typical triphasic waveform is characterized by a steep systolic upslope and rapid return to the baseline, followed by a short early diastolic reversal of flow and subsequent diastolic forward flow depending in magnitude and duration on the vessel area supplied (see also Fig. 1.22). The early diastolic backward flow component is due to the high peripheral resistance. The slight but variable forward flow in late diastole depends in magnitude not only on peripheral resistance (which in turn is dependent on sympathetic tone) but above all also on aortic compliance (windkessel effect).

The character of the Doppler waveform varies with the elasticity of the vessel wall and peripheral resistance (Table 2.3) and is influenced by systemic or local hypercirculatory effects (fever, hyperthyroidism, phlegmon). The more or less pronounced flow persisting during diastole is affected by physiologic parameters such as sympathetic tone and heart rate. In addition, the flow pattern is influenced by the ratio of skin to muscle supply, which is why diastolic flow is higher in the profunda femoris than in the superficial femoral artery (Fig. A 2.2). The vessel diameter and peak systolic velocity show wide interindividual variation and decrease toward the

Table 2.3. Factors influencing the flow profile (Doppler waveform)

Elasticity of the vessel wall (atherosclerosis, medial sclerosis)		
Peripheral resistance	Normal:	Muscle activity
	Abnormal:	Inflammation (stage IV AOD)
		Hypercirculation
		Pharmacologic therapy
		Postocclusive vasodilatation (AOD)

Table 2.4. Normal diameters (D) and peak systolic velocities (V_{max} and standard deviation) of the pelvic and leg arteries determined in 30 healthy subjects

	D [cm]	V_{max} [cm/s]
External iliac artery	0.85 ± 0.11	116 ± 29.7
Common femoral artery	0.81 ± 0.17	112.2 ± 22.7
Proximal superficial femoral artery	0.65 ± 0.14	93.95 ± 15.9
Profunda femoris artery	0.55 ± 0.14	95.1 ± 21.5
Popliteal artery	0.58 ± 0.12	71.6 ± 12.4

periphery (Table 2.4) while the triphasic flow profile is preserved.

Investigations of normal flow velocity in the pelvic and leg arteries (Jäger et al. 1985; Kohler 1990; Karasch et al. 1990; Polak et al. 1992) show wide variation between different study populations as well as between individual subjects within a study population. These observations make it somewhat difficult to determine an absolute systolic velocity threshold above which a hemodynamically significant stenosis should be assumed, as is the case for the diagnosis of carotid and renal artery stenosis. Alternatively, a hemodynamically significant stenosis is assumed when there is doubling of the mean normal velocity of the respective artery. The normal values determined by our group are presented in Table 2.4 and are comparable to those reported by others (Jäger et al. 1985; Kohler et al. 1990).

In addition to peak systolic velocity and changes in the normal triphasic flow profile, the acceleration index has established itself as a further parameter for describing occlusive and postocclusive changes in blood flow. Higher-grade stenoses and occlusions are associated with a postocclusive decrease in peak systolic velocity and a lengthened systolic acceleration time. The acceleration time is the quotient of peak systolic velocity and the pulse rise time from the onset of systole to the first peak.

Moreover, the pulsatility index (PI) is used to describe the pulsatility of flow (for its calculation cf. Fig. 1.12). As the poststenotic decrease in peak systolic velocity and increase in end-diastolic velocity become more pronounced through dilatation of the arterioles and the resulting decrease in peripheral resistance, triphasic flow becomes monophasic and the extent of this change correlates with the decrease in PI (cf. Figs. 1.12, A 2.2, and A 2.3).

2.1.6 Abnormal Findings – Clinically Oriented Ultrasound Examination, Ultrasound Findings and Measurement Parameters, Diagnostic Role

2.1.6.1 Atherosclerotic Occlusive Disease

Most atherosclerotic lesions affect the thigh vessels (about 40 %), followed by the pelvic and calf vessels, each with an incidence of about 20 – 30 % (Schoop 1988). However, over 20 % of the patients already have obstruction of more than one level at the time of diagnosis. Since vascular sclerosis is a generalized process, it typically involves both legs, though often not to the same extent.

Duplex ultrasound is mainly used to evaluate patients with typical AOD symptoms in the framework of step-by-step diagnostic workup (cf. Fig. 2.5), to help in therapeutic decision making, and to differentiate atherosclerotic from non-atherosclerotic vascular disease (Table 2.5).

The further diagnostic and therapeutic management depends on the duplex ultrasound findings and the clinical dis-

Table 2.5. Indications for (color) duplex ultrasound of the peripheral arteries

Step-by-step diagnostic workup of AOD
- Localization of flow obstruction (upper leg, lower leg, pelvis, vessel origin)
- Identification of type of flow obstacle (stenosis, occlusion)
- Length of flow obstacle (length of occlusion, sequential stenoses)
- Grading of stenosis (high-grade, low-grade)
- Cause of occlusion (embolism, atherosclerosis, trauma, compression, dissection)
- Evaluation of postocclusive outflow tract
- Therapeutic decision making: medical treatment, radiologic intervention, surgery

Diagnostic evaluation of aneurysm
- Localization
- Characterization (saccular, spindle-shaped, false)
- Extension (infrarenal, aortoiliac, popliteal)
- Thrombosis (partial, complete)
- Therapy: compression therapy of false aneurysm, thrombin injection

Arterial compression
- Entrapment syndrome
- Cystic adventitial disease
- Thoracic outlet syndrome
- Tumor compression

AV fistula
- Localization
- Flow volume in fistula

Follow-up after vessel reconstruction
- Bypass procedure (anastomotic stenosis, suture aneurysm, infection, occlusion, flow velocity inside bypass: prognosis)
- PTA (residual stenosis, restenosis, puncture aneurysm, hematoma)
- Endoluminal stents (patency, stenosis)

ease stage (cf. Fig. 2.5) and is guided by the motto: No further (invasive) diagnostic tests without therapeutic consequences.

2.1.6.1.1 Pelvic Arteries

Occlusions and stenoses of the extremity arteries occur in the pelvic arteries in 11 % of cases. Single pelvic vessel occlusions affect the common iliac artery in about 54 % of cases, the external iliac in 21 %, and the internal iliac in 13 % (Schoop 1988). The clinical presentation of pelvic artery occlusion varies with the presence of collateral pathways and concomitant obliteration of more distal vessels (40 – 50 % incidence of combined femoropopliteal obliteration). Reconstruction of the occluded pelvic artery to improve inflow of blood is particularly important in patients with additional superficial femoral occlusion. Moreover, pelvic artery repair has a good long-term prognosis and patency rate.

Collateral flow in pelvic artery occlusion mainly occurs through the internal iliac artery circulatory systems and through the inferior mesenteric artery when the common iliac artery is occluded as well. Collateral supply to the distal segment of the common femoral is ensured by the lateral and medial circumflex arteries (via the profunda femoris). In addition to the typical claudication symptoms of the lower leg, pelvic artery occlusion is associated with specific claudication pain of the gluteal, hip, and thigh muscles.

Other etiologic factors in pelvic artery stenosis, apart from atherosclerosis, are aneurysmal changes (in particular in association with distal aortic aneurysm) and fibromuscular dysplasia.

As for the thigh arteries, a peak intrastenotic flow velocity of 180 cm/s has been identified as a cutoff value for hemodynamically significant stenoses both in flow models and in vivo (Whyman et al. 1993). On the other hand, ROC (receiver operating characteristic) curve analysis yielded markedly lower velocity thresholds of 120 cm/s for 50 % stenosis and 160 cm/s for 70 % stenosis (Sacks 1994) but these turned out to be unsuitable in the routine clinical setting. The threshold velocities identified by ROC analysis vary greatly with the study population investigated (e.g. incidence of hypertension, proportion of diabetics).

If direct demonstration of a stenosis through flow acceleration in the stenotic segment is not possible, in particular when scanning is impaired by overlying bowel gas or in obese patients, the poststenotic waveform from the proximal common femoral or distal external iliac artery can be analyzed for the presence of indirect criteria. In general, a triphasic flow profile with a steep systolic upslope and peak velocities greater than 80 cm/s excludes a hemodynamically significant obstruction in the pelvic area. However, in cases of good collateralization of common iliac stenoses (and in higher-grade stenoses or occlusions that have developed chronically), the triphasic flow profile is damped but preserved. Pulsatility is less pronounced and peak systolic velocity is decreased compared to the unaffected side (cf. Fig. A 2.4).

Stenoses of less than 60 % do not affect the poststenotic waveform. Only higher-grade stenoses produce grade-related flow changes including a decreased peak systolic velocity, less steep systolic rise, and delayed diastolic drop with persistent flow toward the periphery. The diminished peak systolic velocity and the delayed systolic rise are primarily due to the upstream flow obstruction while the monophasic profile indicates peripheral vasodilatation in response to a mismatch of blood supply and demand. This peripheral situation in turn also affects the prestenotic waveform through the collaterals.

Therefore, a hemodynamically significant, higher-grade stenosis can also be excluded by determining the pulsatility index (cf. Fig. 1.12) of the common femoral artery as an indirect criterion. A significant stenosis in the aortoiliac segment is excluded if the pulsatility index exceeds 5.5 (Johnson et al. 1983; Neuerburg et al. 1991). The following pulsatility indices have been determined: 8.5 ± 3.5 in a normal population, 2.8 ± 1.6 in isolated stenosis at the pelvic level, 2.3 ± 1.0 in combined pelvic and upper leg occlusion, and 6.3 ± 2.6 in isolated femoral artery occlusion. The pulsatility index increases with the extent of collateralization (cf. Fig. 2.9), giving rise to false-negative results. Using a pulsatility index with a cutoff value of 4, a sensitivity of 94 % and a specificity of 82 % were found in identifying isolated aortoiliac obstructions (Thiele et al. 1983).

Stenoses can be diagnosed indirectly when the insonation conditions in the true pelvis are poor. Whenever abnormal findings are encountered, however, an attempt should be made to also demonstrate and localize the stenosis directly. Under normal scanning conditions, the direct demonstration of a stenosis or occlusion is often faster than the determination of the indirect criteria if state-of-the-art (color) duplex ultrasound equipment is used.

When the external iliac artery is occluded, refilling may occur through the lateral circumflex artery, which will lead to backward flow in the proximal profunda femoris and common femoral arteries. This is seen in the Doppler examination as reversed flow with a monophasic character.

Strauss et al. (1995), investigating stenoses of the external iliac artery, found the following correlations between the flow velocity measured by duplex ultrasound and various other parameters:

- Reduction of cross-section determined densitometrically and the hemodynamic stenosis grade calculated as the ratio of prestenotic to intrastenotic flow velocity: R = 0.64;
- Peak systolic flow velocity and densitometrically determined cross-section reduction: R = 0.56;
- Pressure drop calculated from the flow velocity determined by color duplex ultrasound using the Bernoulli equation (Fig. 2.7) and the pressure drop measured intraarterially by catheter: R = 0.86.

The highest correlation (R = 0.86) was found for the pressure drop determined noninvasively by ultrasound and that measured invasively (cf. Fig. 2.7). The pressure measured over a stenosis also takes into account collateralization, as pelvic

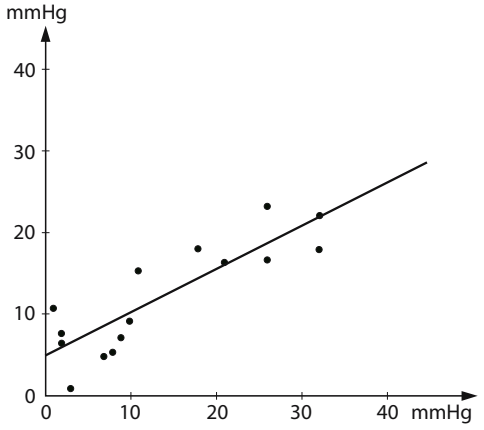

Fig. 2.7. Correlation (R = 0.86) of the mean pressure drop over pelvic artery stenoses calculated from color duplex ultrasound using the Bernoulli equation and the drop measured by intraarterial catheter. (Strauss et al. 1995)

artery stenoses of identical degree will show slower transstenotic flow when they are collateralized and hence a smaller pressure drop.

2.1.6.1.2 Leg Arteries

Preferred sites of atherosclerotic stenoses of the femoral arteries are the origins of the superficial and profunda femoris arteries at the bifurcation and the adductor canal.

Isolated stenoses or occlusions of the common femoral artery are uncommon (about 4%); most stenoses of the common femoral are associated with obstructions of the superficial femoral and lower leg arteries. Occlusion of the common femoral artery or femoral bifurcation is of considerable clinical significance and should be treated by surgical repair (TEA) whenever possible because there is only poor compensation by collateral flow, as all collateral pathways (via the iliac arteries and the profunda femoris artery) comprise the femoral bifurcation and auxiliary collaterals have a low capacity. The profunda femoris artery supplies the thigh muscles and is the most important collateral vessel in all arterial obstructions distal to the femoral bifurcation. As a phylogenetically old vessel, the profunda femoris artery is rarely affected by sclerotic changes distal to its origin. All isolated obstructions of the profunda femoris are due to embolism or are associated with diabetes mellitus. Stenoses of the origin of the profunda femoris in association with atherosclerosis of the femoral bifurcation, however, are more common and clinically relevant due to the above-described key role of the profunda femoris as a collateral in obstruction of the femoropopliteal circulation. Surgical repair of the profunda femoris artery is the treatment of choice. The superficial femoral artery is the preferred site of atherosclerotic obstructions and is the most common site of isolated occlusions, which have an incidence of 27%. Combined femoropopliteal occlusions occur in 40–45% of cases. In all cases of isolated popliteal artery occlusion, thrombosed popliteal aneurysm and nonatherosclerotic vascular disorders (which preferably affect the popliteal artery) must be excluded in the differential diagnosis.

The treatment of femoropopliteal artery occlusion depends on the clinical presentation, cause, site, and length of the obstruction. These frequently affected and hence clinically significant vessels are easily accessible to duplex scanning as they lie close to the surface and scatterers are absent. Many studies have shown the high accuracy of duplex ultrasound in evaluating femoropopliteal occlusion (Table 2.6). The precise information on the site and length of an obstruction provided by duplex ultrasound is necessary for therapeutic decision making based on what is clinically required.

Atherosclerotic processes of the vessel wall are already seen on the gray-scale scan as irregularities of the wall contour, intimal thickening, or plaques. In case of echogenic, noncalcified plaques in larger vessels, the B-mode image also allows a rough estimate of the extent of luminal narrowing but precise quantitative determination of the hemodynamic significance is always done in the Doppler mode.

An occlusion is caused by atherosclerosis if extensive intraluminal plaques are visualized and the wall is no longer delineated. External structures compressing the vessel wall can be depicted, identified, and differentiated from atherosclerotic stenoses by gray-scale ultrasound.

Medial sclerosis in diabetics is characterized by diffuse calcifications of the middle coat of the vessel wall. Sonographically, the calcifications produce inhomogeneous wall thickening with scattering and acoustic shadowing and impair the recording of flow signals from the vessel lumen.

In the limb arteries, the high peripheral resistance produces pulsatile, nearly laminar flow, which is reflected in the Doppler display by a narrow bandwidth with a clear systolic window. The typical triphasic waveform is characterized by a steep systolic rise and subsequent decrease, followed by a short early-diastolic reflux and forward flow depending in magnitude and duration on the vessel area supplied. Physiologic changes of the laminar flow profile can occur at vessel origins and curvatures.

Flow obstruction due to stenosis or vessel compression leads to flow acceleration in proportion to the cross-sectional area reduction (cf. Fig. 1.23; continuity law), and the flow becomes turbulent (cf. Fig. 1.25). Flow is already somewhat faster when there is luminal narrowing of 40–50% but a relevant reduction of peripheral arterial blood pressure (Doppler pressure) is unlikely or will occur during exercise only. Mild stenoses of less than 50% have only little effect on the flow profile. With increasing narrowing, however, flow becomes less pulsatile with development of turbulence and eddy currents downstream of the stenosis. A reduction of the cross-sectional area exceeding 75% (>50% diameter reduction) is associated with an intrastenotic increase in flow velocity of more than 100% compared with the prestenotic vessel segment (Jäger et al. 1985; Moneta et al. 1992). Flow becomes less and less pulsatile, ultimately resulting in a monophasic waveform typical of flow within and behind a high-grade stenosis

Table 2.6. Sensitivity, specificity, and diagnostic accuracy of duplex ultrasonography compared with angiography in the diagnosis of hemodynamically significant stenoses (>50 %), occlusions, and aneurysms of the pelvic and leg arteries

Author	Vessel region	Duplex technique	Reference method	Sensitivity [%]	Specificity [%]	Accuracy [%]
Kohler et al. 1987	Femoropopliteal	Conventional	Conventional angio	82	92	–
Legemate et al. 1991	Aortoiliac	Conventional	IA DSA	89	92	91
Allard et al. 1994	Aortoiliac	Conventional	Conventional angio	83	96	92
	Femoropopliteal			87	93	90
Cossman et al. 1989	Iliac	Color	Conventional angio	81	98	92
	Common femoral			70	97	93
	Superficial femoral			87	85	87
	Profunda femoris			71	95	93
	Popliteal			85	97	93
Mulligan et al. 1991	Femoropopliteal	Color	Conventional angio	89	91	
Moneta et al. 1992	Iliac	Color	Conventional angio or IA DSA	89	99	
	Common femoral			76	99	
	Superficial femoral			87	98	
	Profunda femoris			83	97	
	Popliteal			67	99	
Strauss et al. 1994	Iliac	Color	Conventional angio or IA DSA	87	73	83
	Common femoral			75	91	86
	Superficial femoral			94	72	88
	Profunda femoris			79	96	86
	Popliteal			94	92	93
Schäberle 1998	Femoropopliteal, iliac, proximal segments of crural arteries	Color	Conventional angio or IA DSA; intraoperative	97	98	97
Polak et al. 1990	Femoropopliteal	Color	Angiography or IA DSA	88	95	93
Landwehr 1990	Femoropopliteal	Color	Angiography or IA DSA	92	99	96
Koennecke et al. 1989	Femoropopliteal	Color	Angiography or IA DSA	97	97	97
Legemate et al. 1991		Color	Angiography	84	96	
Ranke et al. 1992		Color	Angiography	87	94	

(Cossman et al. 1989; Polak et al. 1991). The changes depicted by (color) duplex scanning within a stenosis are referred to as direct stenosis criteria and the poststenotic changes in the flow profile as indirect stenosis criteria (Table 2.7).

The examiner must be aware that the indirect criterion of monophasic flow merely indicates peripheral dilatation that may also be caused by other factors such as peripheral infection (Table 2.8).

Duplex ultrasound using the direct stenosis criteria has an accuracy ranging from 83 – 97 % in identifying hemodynamically significant stenoses and occlusions of the aortoiliac and femoropopliteal vascular systems compared to angiography (cf. Table 2.6).

Color duplex ultrasound depicts the subtle flow acceleration associated with low-grade to intermediate-grade stenoses in lighter color shades (primarily within the stenosis jet). As the grade of stenosis increases, retrograde flow components associated with eddy currents and flow separations are depicted as color changes. High-grade stenoses with turbulent flow are characterized by a mosaic-like color pattern and

Table 2.7. Duplex ultrasound of peripheral arteries – stenosis criteria

Direct stenosis criteria	Turbulent flow Flow acceleration $V_{max} \rightarrow 180$ cm/s Abrupt doubling of V_{max} Perivascular vibration
Indirect stenosis criteria	Flow profile: Damping (triphasic/monophasic) Delayed systolic rise

Table 2.8. Factors damping the triphasic waveform (change from high-resistance to low-resistance flow)

Normal:	Muscle activity
Abnormal:	Fever Hypercirculation Downstream infection Postocclusive dilatation

Table 2.9. Grading of peripheral arterial stenoses (cf. Fig. 1.25). The grade is defined as the percentage reduction in cross-sectional area. The grading system is not fully valid for obstructions located at vessel branchings. There are no strict boundaries between the different grades as the hemodynamic effects of a stenosis depend on a complex interaction of different factors. (Modified according to Wolf and Fobbe 1993; Cossman et al. 1989; Polak et al. 1991)

Stenosis grade	(Color) duplex (intrastenotic)	(Color) duplex (just distal to stenosis)	Waveform far distal to stenosis	Waveform proximal to stenosis	Ratio[a]
No stenosis	Triphasic waveform ($V_{max} < 150$ cm/s)	Clear spectral window Markedly pulsatile flow Steep systolic upslope	Unchanged	Unchanged	< 1.5
20 – 50 % Low-grade stenosis	Increase in V_{max} (150 – 200 cm/s)	Only mild turbulence Moderate spectral broadening may occur	Same as prestenotic	Normal	1.5 – 2
51 – 75 % Intermediate-grade stenosis	Further increase in V_{max} (200 – 380 cm/s) Slight reduction in pulsatility	Eddy currents Possibly slight turbulence Partial filling-in of systolic window	Slightly reduced pulsatility	Normal	2 – 4
76 – 95 % High-grade stenosis	Very pronounced increased in V_{max} (> 380 cm/s) Reduction in pulsatility	Considerable turbulence Complete filling-in of systolic window	Lengthened systolic acceleration time Reduced pulsatility	Amplitude normal or slightly reduced (compared to other side) Pulsatility may be reduced before sites of origins of collaterals	> 4
95 % Subtotal occlusion	Nearly complete loss of pulsatility Marked increase in peak systolic and end-diastolic flow velocity	Pronounced turbulence Completely filled-in systolic window	Flattened systolic peak Considerably reduced pulsatility	Reduced amplitude Increased pulsatility immediately before stenosis Normal prestenotic pulsatility but reduced before sites of origins of collaterals	> 4
Occlusion	No flow signal detectable	Very reduced flow in distal segment Marked damping of waveform	Very flat systolic peak	Low amplitude Blunt waveform immediately before occlusion: increased pulsatility, small complex with large negative component Decreased pulsatility before sites of origins of collaterals	

[a] Ratio: quotient of intrastenotic/prestenotic peak systolic flow velocity

aliasing. Color duplex scanning performed with proper instrument setting thus enables rapid identification of the site of a stenosis and semiquantitative estimation of its grade.

For precise quantification of a stenosis, however, the *Doppler frequency spectrum* must be recorded, which is highly sensitive in depicting the hemodynamic changes occurring in the prestenotic, intrastenotic, and poststenotic vessel segments (Table 2.9).

Upstream of a high-grade stenosis, flow may become less pulsatile due to changes in peripheral resistance. In the spectral display, however, the steep systolic rise remains unchanged (in contrast to flow in the postocclusive segment). The closer the sample volume is placed to a high-grade stenosis (or occlusion), the less it is affected by collateral flow. When no hemodynamically significant collaterals arise between the sample volume and the flow obstruction, there may be very pronounced pulsatility or even *to-and-fro flow* (blunt waveform; cf. Fig. 1.25).

Downstream of a stenosis with flow acceleration (according to the continuity law) and higher-grade stenosis with loss of the triphasic flow profile, the monophasic pattern persists and flow additionally becomes turbulent. Depending on the degree of stenosis, the poststenotic waveform will show a decreased peak systolic flow velocity, a lengthened systolic acceleration time, and reduced pulsatily or even monophasic flow (Table 2.9).

The loss of pulsatility distal to high-grade stenoses and obstructions is due to a decrease in peripheral resistance (widening of collateral vessels, reduced arteriolar tone) and a pressure drop over the stenosis. The pressure difference between the heart and the periphery is no longer equalized during a single cardiac cycle and there may be flow throughout diastole.

Most study groups comparing duplex or color duplex ultrasound and angiography in patients with peripheral arterial occlusive disease found good agreement with sensitivities and specificities ranging between 85 and 99 % (Table 2.6). More recent studies report values of over 90 % but earlier studies using only conventional duplex ultrasound show surprisingly good results as well: As early as 1986 Jäger et al.

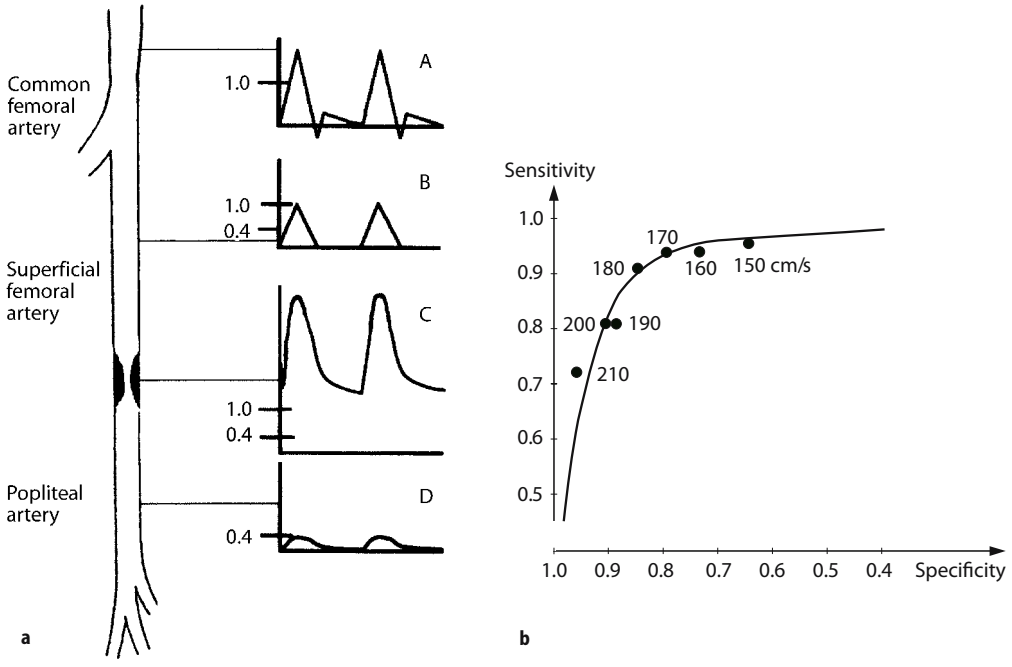

Fig. 2.8. a Schematic representation of the stenosis-induced changes of the Doppler waveform in peripheral arteries (cf. Fig. 1.25); stenosis of superficial femoral artery
A: Fairly normal triphasic waveform from common femoral artery (far away from stenosis)
B: Prestenotic waveform from proximal superficial femoral artery with slightly reduced peak systolic flow velocity and reduced or absent early diastolic dip
C: Monophasic flow profile with peak intrastenotic flow velocity increased to more than twice the prestenotic velocity
D: Monophasic poststenotic waveform from distal superficial femoral artery with delayed systolic upslope and slow peak systolic flow
2.8. b Profunda femoris artery stenosis: ROC curve for determining the sensitivity and specificity at different velocity thresholds in the profunda femoris artery measured by duplex ultrasound in comparison with angiography

found a sensitivity of 96% and a specificity of 81% for the demonstration of abnormal changes of the pelvic and leg arteries by duplex ultrasound compared to angiography. Surprisingly, the sensitivity was the same and the specificity higher in relation to the agreement between two radiologists interpreting the same angiographies (sensitivity 97%, specificity 68%).

To diagnose a hemodynamically significant stenosis (>50%), some study groups use mainly qualitative, indirect criteria but the majority of investigators use either a peak systolic flow velocity of 1.8 or 2 m/s as a cutoff or the sudden doubling of peak systolic flow velocity over the stenosis relative to the prestenotic velocities (Fig. 2.8a).

In a study by our group comparing (color) duplex ultrasound with angiography in 125 patients with typical symptoms of arterial occlusive disease (grades II-IV), the ultrasound examination was found to have a sensitivity of 96%, a specificity of 98%, and a diagnostic accuracy of 97%. The vascular territories involved in the study population were the femoropopliteal arteries in 31%, the pelvic level in 12%, the lower leg arteries in 18%, and several levels in 39% of the cases.

The criterion used to diagnose a hemodynamically significant stenosis was a peak systolic velocity of over 180 cm/s in vessel branchings (e.g. origin of profunda femoris; Fig. 2.8b) and a sudden doubling of the peak systolic velocity for stenoses in straight vessel segments. The indirect criteria listed in Table 2.7 (prestenotic and poststenotic waveform changes) served as supplementary criteria.

The comparison of two examination modalities based on different criteria will necessarily yield slightly discrepant results. Angiography (as well as IA DSA and X-ray densitometry) primarily relies on morphologic features while duplex ultrasound uses functional parameters to assess the hemodynamic significance of stenoses. Selective angiography continues to be the gold standard against which any newly introduced method is measured. Note, however, that angiographic methods also have their limitations in grading stenoses because they depict only the perfused lumen and not the vessel wall. Moreover, they reduce the three-dimensional lumen to the two dimensions of the film. In particular, the posterior wall plaques frequently occurring in the pelvic arteries may be underestimated on anteroposterior views (cf. Fig. 5.7).

The *main trunk of the profunda femoris artery* is of particular significance in the diagnostic evaluation as it is the most important collateral vessel in occlusion or stenosis of the superficial femoral artery. It is often involved in obstruction of the superficial femoral artery; blood supply to the lower leg can be improved by a minor surgical intervention (profunda femoris repair, TEA). The origin of the profunda femoris artery has a crucial clinical role, but is difficult to assess angiographically due to superimposition of vessels. Reliable assessment is possible only if an *additional oblique projection* is obtained.

In a study by our group (Strauss and Schäberle 1989), investigating the hemodynamics at the origin of the profunda

femoris with determination of the degree of stenosis on the basis of peak systolic flow velocity, the positive and negative predictive values were 86 % and 91 %, respectively, compared to angiography as the reference method. ROC curves identified a peak systolic velocity of 180 cm/s as the optimal cutoff for differentiating normal vessels and low-grade stenosis from higher-grade (> 50 %) stenoses (cf. Fig. 2.8b).

The more distal an occlusion, the more the examiner has to take into account the collateral function of the vessel examined. For instance, the profunda femoris artery as the main collateral in occlusion of the superficial femoral may show an increase in mean flow velocity of over 100 % at its origin without being stenosed itself. Moreover, a vessel serving as a collateral in an occlusive process has a reduced pulsatility due to the decrease in peripheral resistance. In this situation, only an increase in peak velocity above a defined upper limit (see above) and a monophasic flow profile are valid criteria for diagnosing a stenosis.

The postocclusive perfusion pressure in the periphery is affected by the preocclusive systemic pressure and, above all, by the flow resistance in the collateral vessels (Fig. 2.9). Collateral resistance, in turn, is determined by the number and size of the collateral vessels, the length of the occluded segment that has to be bypassed, and blood viscosity. When collateral resistance is low, the situation in the periphery is less dramatic and there is only moderate postocclusive vasodilatation; the Doppler waveform has a fairly normal appearance

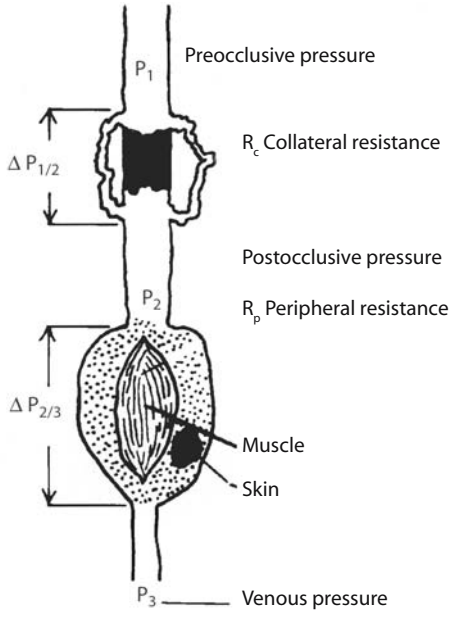

Fig. 2.9. Postocclusive arterial pressure depends on the degree of stenosis or length of occlusion as well as on collateral resistance. The pressure increases when collateral resistance is low due to extensive collateralization. In the presence of good collateralization, the spectrum is less abnormal and exhibits a higher peak systolic velocity and low end-diastolic velocity. Triphasic flow may even be almost completely preserved in pelvic artery occlusion with good collateralization. (From Rieger and Schoop 1998)

and pulsatility. Hence, postocclussive pulsatility is determined not only by the grade of stenosis or length of obstruction but also by the extent of collateralization. When there is good collateralization (e.g. in pelvic artery stenosis), the Doppler waveform is less abnormal with only little damping of the triphasic flow profile. The magnitude of the postocclusive blood pressure measured by Doppler is likewise a function of both the occlusive process and collateral resistance. Moreover, good collateralization with division of the blood flow can lead to a lower peak systolic velocity in the stenotic segment than would be expected from the degree of stenosis alone.

The usual stenosis criteria may also lead to misinterpretation when there is multilevel occlusion with sequential stenoses or occlusions. In grading a second stenosis, the examiner has to take into account the hemodynamic changes produced by the preceding stenosis: The postocclusive decrease in velocity after the first stenosis will lead to a less pronounced increase in peak systolic velocity in the second stenosis. Therefore, a sequential stenosis is classified as hemodynamically significant if the peak systolic velocity is twice the interstenotic velocity (cf. Table 2.6: some investigators also use doubling of peak systolic velocity as a criterion for the hemodynamic significance of single stenoses).

Stenosis grading by comparison of intrastenotic and prestenotic flow velocities is rather unreliable in stenoses at vessel origins because the prestenotic segment has a different diameter and different hemodynamics. In cases where direct color duplex scanning of a stenotic segment is not possible due to acoustic shadowing by calcified plaques, the proximal and distal Doppler waveforms have to be compared (Table 2.10). If the peak velocity and the waveform character are unchanged, the plaque does not produce hemodynamically significant narrowing.

Color duplex scanning and Doppler ultrasound demonstrate vascular occlusion as an absence of flow signals. Note, however, that the failure to demonstrate flow may also be due to inadequate instrument settings (gain, PRF) or technical limitations of (color) duplex ultrasound in the area of calcified plaques (cf. Table 2.10). The problem of posterior acoustic shadowing due to calcifications in the vessel wall is mainly encountered in diabetic patients with medial sclerosis and can be overcome by comparing the Doppler waveforms before and after the calcified area (monophasic profile downstream of occlusion) and searching for collaterals arising upstream of the obstruction and emptying downstream (see Figs. A 2.13 and A 2.14).

Table 2.10. Duplex scanning of the peripheral arteries – methodological limitations

B-scan:	Calcified plaque: posterior acoustic shadowing Edema: scattering
Doppler:	Calcified plaque: posterior acoustic shadowing Maximum flow velocity detectable: limited by pulse repetition frequency

Duplex scanning is highly accurate in determining the *length of occlusion*. A study of our group including 40 legs with femoropopliteal occlusion demonstrated a correlation of 0.96 between angiography and duplex ultrasound. The length of the occlusion was less than 5 cm in 21 %, 5 to 10 cm in 54 %, and over 10 cm in 25 %. Pelvic artery occlusion (n = 30) was correctly identified by duplex ultrasound in all cases; however, due to the poorer scanning window, the peripheral extent was sometimes overestimated by several centimeters ("dead water zone"). A similar correlation (R = 0.95 in 98 extremities) between the sonographically and angiographically measured length of occlusion was reported by other authors (Karasch et al. 1993).

The slow postocclusive flow may lead to overestimation of the length of the occlusion, in particular when collateralization is poor. Further downstream, evaluation by duplex scanning is better due to the increased flow resulting from emptying collaterals. In regions that are difficult to scan, blood flow detection can be improved by the intravenous administration of an ultrasound contrast medium (Langholz et al. 1992). In the routine clinical setting, however, ultrasound contrast media are used in individual cases only.

In order to precisely identify the distal end of an occlusion, a fairly low pulse repetition frequency and high gain are needed as the slow flow downstream of an occlusion would otherwise be missed.

Occlusions, like high-grade stenoses, affect the preocclusive and postocclusive Doppler waveforms. When using a duplex ultrasound unit without a color option, the examiner can approach the occluded zone by sampling Doppler information at both ends. Signals from collaterals coursing parallel to the occluded artery may be misinterpreted as patency shortly before the refilled segment of the artery is actually reached, giving rise to underestimation of the length of the occlusion. Collaterals emptying into the main artery can be identified by an apparent sudden flow acceleration resulting from the different insonation angle and above all by the change in flow direction indicated by the Doppler signal. Once an origin or opening of a collateral has been identified, a Doppler tracing obtained with a suitable angle of incidence will enable diagnosis of a stenosis. Evaluation of the postocclusive flow also contributes to therapeutic decision making (medical therapy or repair).

The flow rate downstream of multilevel occlusions with poor collateralization may occasionally drop below the lower limit of detection of (color) duplex scanning even when a high-resolution scanner is used with proper settings. In cases where no flow is detected by color duplex, a flow signal will often be obtained by a Doppler tracing recorded with a high gain and low pulse repetition frequency.

2.1.6.2 Arterial Embolism

Arterial embolism with ischemia is typically of cardiac origin (80 – 90 %) with the remaining cases being accounted for by arterioarterial emboli, chiefly arising from a partially thrombosed aneurysm and rarely from an atherosclerotic lesion.

The site and length of an embolic occlusion are identified in the Doppler waveform or by the absence of flow signals in the color duplex mode. In the less common cases of subtotal occlusion, some residual flow will be detected along the hypoechoic thromboembolus near the wall (cf. Fig. A 2.29). An embolic occlusion is suggested by the depiction of a fairly hypoechoic and homogeneous mass in the vessel lumen, good delineation of the wall with preservation of its smooth contour, and the absence of plaques.

Embolic occlusions typically affect vessel bifurcations, where the embolus creates a nidus for the formation of appositional thrombi that may extend proximally to the site of the nearest hemodynamically significant vessel branching. The distal end of the occlusion is identified with a low pulse repetition frequency and a high gain to depict the slow flow due to inadequate collateralization. In addition to identifying and characterizing the embolic occlusion, searching for the source of the embolus is an integral part of the examination (echocardiography, duplex ultrasound of the aorta and peripheral arteries with special emphasis on the identification of a possible popliteal artery aneurysm).

2.1.6.3 Aneurysm

Aneurysms most commonly affect the aorta and the popliteal artery but may also occur in the femoral and iliac vessels, in particular in patients with dilated angiopathy (Schuler et al. 1993). Aneurysms are identified on gray-scale scans as saccular or spindle-shaped dilatations of the vessel lumen. Mural thrombi in the aneurysm are often identified by their slightly higher echogenicity relative to flowing blood in the patent lumen. Confirmation is obtained by color duplex ultrasound, which indicates thrombosis by the absence of color coding. The thrombotic deposits can cause stenosis, in particular when they occur at the distal end of an aneurysm. No flow signals will be depicted in a completely thrombosed aneurysm. Angiography is not the method of reference for assessing a partially thrombosed aneurysm while *computed tomography (CT)* depicts the morphology and extent of an aneurysm but provides no hemodynamic information. Patients with an isolated occlusion in the popliteal territory should be examined ultrasonographically for exclusion of a thrombosed aneurysm or compression syndrome prior to a radiologic intervention.

Aneurysms of the popliteal artery often occur bilaterally and a concomitant aneurysm of the abdominal aorta is present in 25 – 30 % of cases. Aneurysms can occlude or rupture or cause embolic occlusion of peripheral vessels with the necessity of amputation.

Surgery is indicated for all aneurysms with a diameter greater than 2 cm and smaller ones when they are saccular or contain thrombotic deposits. Thrombotic aneurysms in the knee area carry a higher risk of arterial embolism even when they are small because they are exposed to the shearing forces of the bending knee.

Duplex scanning is the method of first choice, yielding reliable information on the diameter of the aneurysm, its shape,

and the presence of thrombosis (cf. Fig. A 2.31) and thus providing the foundation for planning the surgical procedure. Scanning of the superficial aneurysm is performed with a high-resolution transducer. The diameter is measured and thrombotic material identified in the lumen (absence of color coding) in transverse orientation while the shape is assessed in the longitudinal plane.

False aneurysms (pseudoaneurysms) are a typical complication of arterial puncture performed for diagnostic angiography or interventional procedures. Their incidence is up to 4% after percutaneous transluminal angioplasty (PTA) and cardiac catheterization (Hust and Schuler 1992; Moll et al. 1991). A subgroup of false aneurysms are suture aneurysms developing after vascular surgery, in particular after bypass operations.

A false aneurysm must be differentiated from a perivascular hematoma with transmitted pulsation but this is difficult on clinical grounds (Thomas et al. 1989). Using duplex ultrasound, an aneurysm can be differentiated from hypoechoic, perivascular structures such as hematoma, seroma, or lymphocele by the depiction of to-and-fro flow, which is diagnostic of a false aneurysm and requires no angiographic confirmation. To-and-fro flow occurs in the neck of an aneurysm due to changing pressures: At the high intraluminal pressure during systole, blood flows through the narrow neck into the aneurysm at a rather high velocity. Under the reversed pressure conditions during diastole, the blood flows back into the vessel at a slightly lower flow rate. Reflux is typically turbulent.

Before ultrasound enabled the precise localization of the aneurysmal neck relative to the skin surface, the therapy of choice was surgical revision with closure. With the ultrasound scanners now available, it is possible to occlude over 90% of the aneurysms by ultrasound-guided compression of the neck (Fellmeth et al. 1991; Hust et al. 1993). Thrombosis occurs after 10 to 30 minutes of compression of the neck (cf. Fig. A 2.26).

Alternatively, thrombosis of a false aneurysm can be induced by injecting thrombin into the aneurysm under ultrasound guidance (Table 2.11).

The hyperechoic signal reflected by the needle ensures reliable placement of the needle tip inside the hypoechoic aneurysm for instillation of 5,000 IU thrombin dissolved in 3 – 5 ml saline solution. Injection produces immediate thrombosis and there are no publications reporting thrombus dislocation into a peripheral vessel induced by this procedure. Nevertheless, some investigators recommend to first inject thrombin near the wall before proceeding to the neck. Thrombin injection has the advantage of rapidly inducing thrombosis while compression therapy is less expensive and has the added advantage of reducing the aneurysm volume, leaving a smaller hematoma that produces less swelling and pressure (cf. Fig. A 2.27 and Fig. A 2.25).

Table 2.11. Ultrasound-guided diagnostic and therapeutic vascular interventions

False aneurysm (typically iatrogenic):	Compression of neck, thrombin injection
Postoperative fluid collection around implants:	Puncture (infection, abscess?)

2.1.6.4 Rare Stenosing Arterial Diseases of Nonatherosclerotic Origin

The popliteal artery is the preferred site not only of atherosclerotic stenoses and occlusions or embolism but also of rare vascular disorders, in particular *compression syndromes*. Though venography or angiography remains the gold standard, these modalities may be limited in identifying the cause of a compression syndrome, especially when occlusion has already occurred (Table 2.12).

(Color) Duplex scanning provides information on the extent of luminal narrowing and its hemodynamic significance and enables evaluation of the vessel wall and perivascular structures, thus allowing identification of the cause of nonatherosclerotic vessel diseases (Table 2.13).

Suspected vessel compression by muscular structures (entrapment syndrome) can be confirmed by functional tests and its hemodynamic significance can be determined by spectral Doppler (Figs. A 2.36 to A 2.38). Another domain of duplex scanning is the evaluation of vascular complications in compression syndromes such as development of mural thrombosis or postocclusive aneurysm and vessel occlusion.

Many nonatherosclerotic conditions predominantly affect the popliteal artery. Duplex scanning is mandatory to identify the cause and initiate proper therapeutic management, in particular in patients with isolated popliteal artery occlusion. Such an occlusion may be caused by complete thrombosis of an aneurysm. The popliteal artery is the second most common site of aneurysm after the aorta. In a study of 1,190 patients with stage II-IV arterial occlusive disease according to Fontaine, angiography demonstrated isolated popliteal artery occlusion in 51 patients.

Table 2.12. Nonatherosclerotic vascular diseases

- Embolism
- Aneurysm
- Intimal dissection
- Arteritis
- Wall tumor
- Compression syndrome (entrapment syndrome)
- Cystic adventitial disease

Table 2.13. Duplex ultrasound in nonatherosclerotic vascular disease

B-scan (morphology):	Vessel lumen (thrombotic deposits)
	Vessel wall (cysts, concentric inflammatory wall thickening; differential diagnosis: plaques)
	Perivascular structures (vessel compression)
Doppler (hemodynamics):	Stenosis (hemodynamic significance of narrowing due to perivascular or mural structures)
	Function test (plantar flexion: more pronounced stenosis)
	Occlusion
	(Collaterals)

The consecutive ultrasound examination of these popliteal occlusions identified atherosclerotic changes with pronounced plaques in 47% of the cases. Embolic occlusions were diagnosed by ultrasound in 21.5%. These were characterized by a fairly homogeneous content of the occluded lumen and good delineation of the wall without major plaque. Thrombotic aneurysms accounted for 27.5% of the isolated popliteal artery occlusions and an entrapment syndrome for the remaining 4%.

In a study by our group comprising 11,500 duplex ultrasound examinations of the popliteal fossa, among them patients with typical complaints of occlusive arterial disease (stage II), the following rare vascular conditions were identified:

- Entrapment syndrome: 11 patients (0.1%), including:
  - occlusion of the popliteal artery: 5 patients, among them 4 with malformation of the medial head of the gastrocnemius muscle or popliteal artery (Insua I) and one with postocclusive aneurysm and additional compression of the popliteal vein due to atypical attachment of the popliteal muscle,
  - compression and stenosis of the popliteal artery during plantar flexion: 5 patients (Insua I and II),
  - compression of the popliteal artery and vein through hypertrophic heads of the gastrocnemius muscle without malformation: 1 patient;
- Cystic adventitial disease: 6 patients (0.05%);
- Traumatic intimal dissection: 2 patients (0.02%);
- Tumor compression: 1 patient (0.01%);
- AV fistula of the popliteal artery (traumatic, large shunt volume): 1 patient (0.01%);
- Large false aneurysm with compression of artery and vein (iatrogenic after arthroscopic resection of meniscus): 1 patient (0.01%).

The compression syndrome predominantly affects vessels in narrow anatomic passages such as the popliteal fossa and predominantly occurs in individuals with atypical variants. In contrast, cystic adventitial disease predominantly affects arterial segments near joints.

2.1.6.4.1 Cystic Adventitial Disease

Cystic adventitial disease is a rare condition in which cystic structures in the outermost coat of arteries close to joints (Leu et al. 1977) and very rarely of veins (20 case reports in the literature until 2002) cause variable stenosis according to their state of filling. In a review of the literature and earlier overviews, we identified a total of 196 reported cases (Schäberle and Eisele 1996). The disorder affects the popliteal artery in over 90% of the cases (Dunant and Eugenidis 1973; Flanigan et al. 1979; Flückiger et al. 1991). There is no agreement in the literature about the etiology and the underlying pathoanatomic changes of the condition. Histologic sections of affected vessels show zones of mucoid degeneration in the adventitia. The cysts resemble articular ganglions with regard to their contents and wall structures. Some investigators postulate a direct connection to the joint space but no such connection was seen in any of the patients operated on by the author. The cysts arise from mesenchymal cell formations dispersed to the arterial adventitia near joints during embryonic development. Among our patients with cystic adventitial disease, a 45-year-old man with typical claudication symptoms had variable cysts that increased in size with the sonographically demonstrated extent of knee joint effusion. Following arthroscopic repair of the meniscal tear causing the effusion, the patient was free of complaints and sonographic follow-up demonstrated only minimal filling of the cysts.

Isolated or multiple cysts can occur and they may be uniloculated or multiloculated. The clinical manifestation and the ischemic symptoms may vary widely and occasionally there is a rapid succession of asymptomatic intervals and episodes during which the walking distance is reduced to a few meters. This pattern is due to the variable vessel compression resulting from changes in cystic filling. The typical hourglass stenosis depicted by angiography may be absent during complaint-free intervals or just barely visible as a subtle impression. In the sonographic duplex examination, other hypoechoic lesions in the popliteal fossa must be differentiated from adventitial cysts by carefully evaluating their relationship to the vessel wall (Table 2.14).

Ultrasonography provides direct evidence of the cysts and thus confirms the tentative diagnosis made on the basis of the clinical presentation and angiographic findings. Moreover, ultrasound identifies the cysts and their variable size even during symptom-free intervals, and the Doppler information enables precise determination of the degree of stenosis. The ultrasound findings thus provide the foundation for therapeutic decision making.

Surgical enucleation of the cyst or resection of the affected vessel segment with replacement by a venous bypass graft is the therapy of choice. If an operation is not possible or refused by the patient, the cystic fluid can be aspirated under ultrasound guidance (Schäberle and Eisele 1996).

2.1.6.4.2 Popliteal Entrapment Syndrome

Entrapment of the popliteal artery was first described in 1879 by a medical student in Edinburgh. Little data is available on the incidence of this syndrome but it seems to be more com-

Table 2.14. Differential diagnosis of sonographically hypoechoic vascular and perivascular structures in the popliteal fossa

- Aneurysm of the popliteal artery (true/false)
- Hematoma, seroma, abscess
- Hemangioma
- Baker's cyst
- Cystic adventitial disease
- Dissection with thrombosis of false lumen
- Tumor
- Venous aneurysm

mon than assumed in the past. A study performed in members of the Greek army yielded an incidence of 0.17 % (Bouhoutsos and Daskalakis 1981) and an autopsy study an incidence of 3.5 % (Gibson 1977). In the above-quoted study by our group, the incidence was 0.1 % in symptomatic patients with typical symptoms of claudication or pain at rest. Intermittent claudication chiefly associated with walking uphill is the cardinal clinical symptom. Paresthesia and rest pain or trophic disorders have been observed but are uncommon. Both our results and published data indicate that thrombosis or segmental arterial occlusion is already present at the time of diagnosis in 50 – 70 % of the patients. Bilateral involvement was reported to occur in 30 – 50 % of cases but was seen in only one patient (9 %) of our series (of symptomatic patients).

The popliteal artery courses through the center of the intercondylar fossa together with the popliteal vein and the tibial nerve and gives off a variable number of branches along this course (sural arteries). An atypical course of the popliteal artery, and possibly of the popliteal vein as well, or abnormal attachment of the medial head of the gastrocnemius muscle can lead to compression of the vessels during muscle contraction.

Plantar flexion compresses the popliteal artery and may induce intermittent reduction of lower leg perfusion and claudication with secondary damage to the vessel wall in the form of intimal proliferation. Intimal damage may give rise to the formation of mural thrombi with subsequent complete occlusion of the vessel while compression of the artery may be associated with poststenotic dilatation. The mural thrombi developing in the aneurysm may cause arterial embolism with occlusion of peripheral vessels. These complications can be prevented by early surgical division of the structure compressing the vessel.

Insua et al. (1970) distinguish four types of popliteal entrapment syndrome according to the relationship between artery and muscle (Fig. 2.10 a–f):

- In *types I and Ia* the popliteal artery courses on the medial side of the medial head of the gastrocnemius muscle. Type I refers to a malformation of the artery, type Ia to the malformation of the medial head of the gastrocnemius, which attaches to the femur more laterally and cranially than under normal conditions, thereby displacing the artery from its normal path. Sonographi-

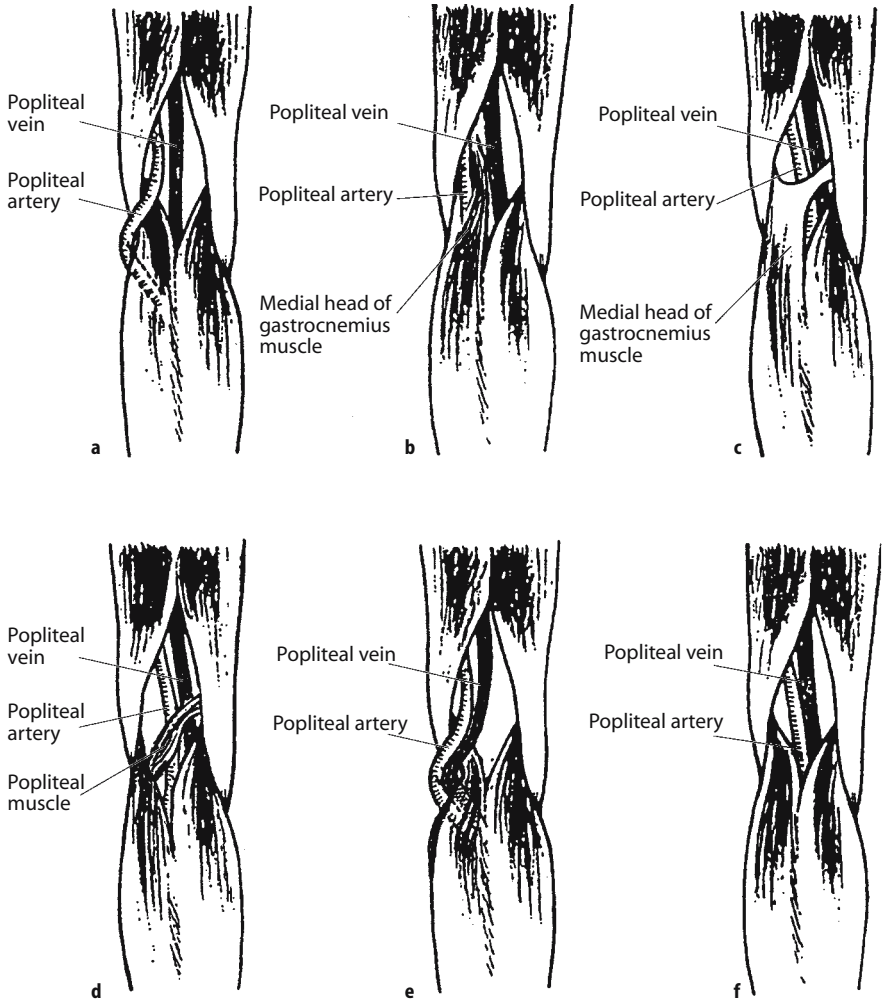

Fig. 2.10 a–f. Types of popliteal entrapment syndrome (modified according to Insua). **a** The popliteal artery courses medially over the posterior aspect of the normal attachment of the medial head of the gastrocnemius to return to its normal course in front of the muscle (corresponding to Insua type I). **b** The medial head of the gastrocnemius attaches more cranially and laterally, thus forcing the popliteal artery to take an abnormal course around the head (cf. Figs. A 2.36 and A 2.38; corresponding to Insua type Ia); the popliteal vein may be compressed as well. **c** The attachment of the medial head of the gastrocnemius has an accessory lateral extension, or the plantar muscle takes an abnormal course. The path of the popliteal artery is normal but the artery and vein may be compressed to variable degrees, depending on the strength of the muscle fibers (Fig. A 3.45a) coursing to the lateral femoral condyle (corresponding to Insua types II and IIa). **d** The popliteal artery and vein are compressed by the popliteal muscle, an abnormal branch of the tibial nerve, or a fibrous ligament (according to Rich). **e** In rare cases, the popliteal vein follows the artery along its abnormal path and is compressed as well. Only one case of an isolated abnormal course of the popliteal vein has been reported so far. **f** Normal course of the popliteal artery and vein through the popliteal fossa but excessive hypertrophy of the gastrocnemius muscle with compression of both vessels during muscle contraction, giving rise to intermittent claudication or venous congestion (cf. Figs. A 2.37 and A 3.45b, c)

cally, these two types are suggested by the depiction of muscle tissue between the artery and vein, which usually course through the popliteal fossa together.
- In *types II und IIa* the artery and vein have a normal course but are compressed by structures crossing the popliteal fossa (abnormal attachment of a lateral extension of the medial head of the gastrocnemius, abnormal course of plantar muscle).

Rarely, excessive hypertrophy of the gastrocnemius can cause intermittent claudication. During contraction, the hypertrophied heads compress the popliteal artery and occasionally the vein as well.

Younger persons presenting with typical claudication should be examined for the presence of popliteal entrapment. This is done sonographically by carefully following the course of the popliteal artery with evaluation of its relationship to muscular structures and performing the plantar flexion test (Table 2.15).

The appearance of stenosis signals in the popliteal artery during plantar flexion confirms muscle-induced arterial compression. Angiography does not yield any relevant additional information that may affect therapeutic management (Table 2.16), especially since ultrasound also depicts the vascular complications such as occlusion and poststenotic dilatation (Table 2.17). The examiner should bear in mind that isolated popliteal occlusion may be due to popliteal entrapment, in particular in younger persons, and that aneurysmal changes of the popliteal artery may be due to poststenotic dilatation (Fig. A 3.45a).

Therapeutic management consists in division of the structure compressing the popliteal artery and repairing the artery in case of secondary occlusion (Steckmeier et al. 1989). In Insua type I popliteal entrapment syndrome, the atypically attaching medial gastrocnemius head is divided.

Table 2.15. Differential diagnosis – nonatherosclerotic vessel diseases

Vessel wall:	Cystic adventitial disease: cysts in adventitia Arteritis: concentric wall thickening
Morphology – (hemodynamics)	
Vessel compression:	Popliteal entrapment syndrome Compression syndrome of upper thoracic aperture (Compression by perivascular structures)
Hemodynamics in functional tests – (morphology)	

Table 2.16. Diagnostic workup of nonatherosclerotic vessel disease prior to surgical repair

Compression syndrome, cystic adventitial disease:	Mandatory: duplex ultrasound (morphology and hemodynamics during provocative maneuver) Optional: angiography (not necessary in: cystic adventitial disease and popliteal entrapment syndrome without occlusion) May be supplemented by MRI, CT
Vascular inflammation:	Duplex scanning to confirm the diagnosis and prevent unnecessary vessel repair

Table 2.17. Vascular complications of compression syndrome

- Mural thrombi secondary to local vessel wall lesions
- Poststenotic development of aneurysm
- Thrombotic occlusion secondary to vascular damage or aneurysmal dilatation

Method of choice for diagnosing and evaluating complications: duplex ultrasound (morphology and hemodynamics)

2.1.6.4.3 Raynaud's Disease

Raynaud's disease is characterized by intermittent attacks of ischemia of the fingers and toes, brought on characteristically by cold and enhanced by emotional stress, local compression, and conditions that are associated with an increased sympathetic tone. The vasospasm is relieved by heat or drug treatment. Primary or idiopathic Raynaud's disease (no underlying disease; no occlusion of finger arteries) is distinguished from a secondary form (underlying conditions such as scleroderma; simultaneous finger artery occlusion). Ischemic attacks often occur bilaterally, affecting the second to fifth fingers while sparing the thumb in most cases. The toes are involved in only about 2% of the cases. Women are affected 2 to 5 times more commonly than men, primarily at the age of 20 to 50 years.

The diagnosis of Raynaud's disease chiefly relies on the typical clinical presentation, while further diagnostic procedures are required only to identify vasospasm as the underlying cause of the clinical symptoms. Again, Doppler and duplex ultrasound with spectral analysis provide useful information. The examination is performed with exposure to cold to provoke the vasospasm and exposure to heat to relieve the spasm. Under exposure to cold, the systolic finger artery pressure in Raynaud's disease drops markedly by 20–50% compared to only up to 10% in healthy persons. Duplex scanning typically demonstrates residual perfusion in the common digital arteries while there is no or only partial flow in the distal finger arteries during spasm. The vasospasm produces a markedly pulsatile flow pattern with a short systolic peak and absence of diastolic flow in the hand arteries and the common digital arteries. In contrast to the flow signal seen in the presence of distal finger artery occlusion, heat exposure induces vasodilatation with hyperemia, resulting in pronounced diastolic flow in the proximal finger arteries. Other helpful diagnostic procedures are oscillography and pressure measurement in the finger arteries. Raynaud's disease must be differentiated from vascular disorders of larger proximal vessels as well as arterial embolism (popliteal artery aneurysm, aortic aneurysm, thoracic outlet syndrome with poststenotic subclavian aneurysm), in particular if color duplex ultrasound demonstrates occlusion of interdigital arteries and the clinical picture of trash foot is present.

2.1.6.4.4 Paraneoplastic Disturbance of Acral Perfusion

Tumor-related disturbances of blood flow may be caused by the following pathomorphologic and pathophysiologic mechanisms:

1. local displacement and compression (tumors of soft tissue, nerves, vessels, and bones as well as metastases) or tumor infiltration of the vessel wall, which may be associated with arterial tumor embolism;
2. paraneoplastic vasculitis;
3. paraneoplastic hyperviscosity of the blood and hypercoagulable state.

Duplex scanning will identify the site of external compression or infiltration of the arterial wall by the tumor and provide information on the hemodynamic significance of the narrowing for therapeutic decision making. Arteries, with their strong muscle coat and intramural pressure, are much less susceptible to local tumor compression than veins.

2.1.6.4.5 Buerger's Disease

Buerger's disease, or thromboangiitis obliterans, is a vascular condition with an intermittent course that is characterized by segmental and multilocular occlusions of small and medium-sized arteries of the extremities. As a panangiitis, it can be differentiated from atherosclerosis and other inflammatory vascular diseases. Though the etiology of Buerger's disease is unknown, there is an association between the onset and progression of the disease and cigarette smoking; 93 – 99 % of the patients smoke. Remission is seen in most patients who quit for good. The severity and frequency of disease episodes correlate with the patient's smoking habits. The clinical symptoms depend on the extent and localization of occlusions. Pain at rest and acral necrosis occur at an early stage while typical intermittent claudication of the calf muscles is rare. Based on the duplex ultrasound findings, other disorders such as arterial embolism, aneurysms of the aorta and popliteal artery, popliteal entrapment syndrome, atherosclerosis, and macroangiopathy must be excluded. In Buerger's disease, the walls of the large arteries appear normal without hyperechoic atherosclerotic plaques or thickening on B-scan ultrasound performed with a high-resolution transducer. Duplex ultrasound often depicts corkscrew-like collateral vessels or revascularization with repeat flow reversal over a short distance. This flow pattern is also reflected in the Doppler waveform. Specific sonomorphologic criteria for Buerger's disease do not exist.

2.1.6.4.6 Inflammatory Conditions

Inflammatory vascular disease may be localized or generalized. The primary form originates from the vessel wall while the secondary form refers to inflammatory vascular involvement in systemic diseases (rheumatoid arthritis, collagen disease). The following primary inflammatory vascular diseases are distinguished according to the vessels affected:

- inflammation of large vessels (giant cell arteritis, Takayasu's arteritis),
- inflammation of medium-sized vessels (polyarteritis nodosa, Kawasaki disease), and
- inflammation of small vessels (Wegener's granulomatosis, microscopic polyangiitis, Schoenlein-Henoch purpura, Churg-Strauss syndrome).

The clinical diagnosis is suggested by the complaints and findings occurring in the areas supplied by the affected vessels. The findings range from pathognomonic local skin changes with palpable purpura to organ loss (kidney) or disturbed limb perfusion when peripheral arteries are affected. During the active stage of vascular inflammation, a pronounced elevation of the erythrocyte sedimentation rate will be seen in most cases (typically above 100 during the first hour) with only a slight increase in C-reactive protein. Additional findings are anemia, mild to moderate leukocytosis, and pronounced thrombocytosis. Supplementary tests are protein electrophoresis, complement determination, and antibody serology. Duplex ultrasound allows localization and quantification of vascular narrowing but its crucial role is to noninvasively demonstrate the typical inflammatory thickening of the vessel wall. This is done using a high-resolution transducer (7 – 10 MHz), which will depict the characteristic "macaroni sign" consisting of a higher-level echo from the lumen/intima interface surrounded by a concentric, homogeneous tube-like structure of lower echogenicity (intima-media complex) (Maeda et al. 1991). If the scanner resolution is not high enough, the macaroni sign may be visualized only in large and medium-sized vessels. In the further course, vessel thickening progresses to concentric and rather long stenoses and subsequent obliteration.

The sonomorphologic differentiation of intimal thickening and sclerotic changes (calcifications) from the concentric wall thickening of long vessel segments (macaroni sign) in inflammatory disease has a crucial diagnostic role and is highly accurate in those vessels that can be evaluated with high-resolution transducers (superficial vessels such as the carotid, subclavian, axillary, and femoral arteries).

Reference modalities for evaluating changes of the vessel wall are computed tomography and magnetic resonance imaging (MRI). Angiography maps the vessel areas affected by inflammatory lumen reduction but does not demonstrate wall thickening (cf. also Table 2.16 and Fig. A 2.40).

2.1.7 Follow-up after Vascular Repair

With its proven validity in comparison to the gold standard and intraoperative findings, duplex scanning provides the foundation for planning the therapeutic procedure in obstructions of the pelvic, femoral, and popliteal territories including the trifurcation. The duplex ultrasound informa-

tion on the localization and type of vessel obstruction in conjunction with the clinical manifestation helps the physician to decide whether conservative management with walking exercises, an interventional radiologic procedure, or surgical repair (TEA or bypass) is the most suitable therapy in the individual patient. Surgical vessel reconstruction in the infrainguinal area can be planned with the same accuracy as with angiography (Wain et al. 1999; Ligush et al. 1998). In patients with adequate scanning conditions, no preinterventional angiography is necessary for planning reconstructive procedures in this territory including the P1 segment. Evaluation of the recipient vessel segment is an important component of the preoperative workup. As this can be done very accurately by duplex ultrasound including evaluation of the trifurcation and segmental evaluation of lower leg arteries, the indication for a P1 femoral artery bypass can be established without preoperative angiography on condition that an inflow obstacle (pelvic artery obstruction) has been excluded.

In pelvic artery occlusion the most suitable sites for proximal and distal anastomosis of a planned bypass graft can be selected on the basis of the sonographically identified localization and length of the obstruction.

2.1.7.1 Thromboendarterectomy (TEA)

An important indication for TEA are stenoses of the femoral artery bifurcation, which is easily accessible to ultrasound examination. The indication for TEA can thus be established and the procedure planned on the basis of the duplex findings.

Duplex ultrasonography thus enables very detailed planning of TEA or profundaplasty for obstructive processes at the origin of the profunda femoris. Moreover, hemodynamic evaluation by duplex ultrasound overcomes the limitations of angiography in this area, which is impaired by overlying vessels and posterior wall plaques.

Ultrasound is likewise the appropriate imaging modality for postoperative follow-up. For example, the collateral function of the profunda femoris artery in superficial artery occlusion can be demonstrated after surgical elimination of a profunda stenosis by the improved flow in the refilled popliteal artery with higher peak systolic and diastolic flow velocities (Fig. A 2.10).

2.1.7.2 Percutaneous Transluminal Angioplasty and Stent Implantation

Angioplasty aims at improving peripheral perfusion by widening narrow vessel areas. The therapeutic procedure in patients with occlusion (percutaneous transluminal angioplasty or bypass surgery) can be planned beforehand once the length of the occluded segment has been determined. In angioplasty atherosclerotic plaques are fragmented and pressed into the vessel wall, often resulting in intimal or medial tears. The irregular vessel surface is susceptible to the deposition of thrombotic material. In addition, recurrent stenosis may occur after angioplasty due to fragmented plaques extending into the lumen, dissection, or elastic rebound forces, and, in the further course, intimal hyperplasia or progressive atherosclerosis. Residual stenoses persisting after intra-arterial thrombolytic therapy with dissolution of thrombotic material by administration of plasmin activators are likewise treated by dilatation. Other interventional procedures apart from standard PTA are arterectomy, rotational angioplasty, and laser angioplasty.

Duplex scanning is the first-line diagnostic modality to follow up patients after PTA (with or without stent implantation) or bypass surgery for the early identification of those who require reintervention. A study showed that patients with a postinterventional peak velocity ratio above 2 had restenoses in 85 % of the cases (Mewissen 1992).

The role of *duplex ultrasound* in the follow-up after interventional procedures is to identify complications (dissection, aneurysm, perforation) and to diagnose residual or recurrent stenoses caused by thrombotic deposits or fragmented plaques protruding into the lumen. The hemodynamic information is most important for identifying restenosis besides the morphologic appearance of the vessel wall in the widened area. Subintimal hemorrhage due to intimal or medial tears may be identified as hypoechoic wall thickening in the dilated area while thrombotic deposits appear as hypoechoic intraluminal areas without color coding.

Stents are identified on B-scans as ribbed or mesh-like structures in the vessel wall. The crucial criterion for a residual or recurrent stenosis after PTA, stenting (where special attention must be paid to the two stent ends), and bypass grafting (primarily at the anastomotic sites) is a localized acceleration of flow (cf. Fig. A 2.4e).

In most cases, flow evaluation within a stent requires a higher color gain. Eddy currents and turbulent flow at the proximal and distal ends suggest that the stent is imperfectly adapted to the wall, which can promote restenosis.

The postinterventional patency rate is primarily affected by residual and recurrent stenoses besides complications such as arteriovenous (AV) fistula, false aneurysm, and hematoma. The sonographic criterion for a hemodynamically significant residual or recurrent stenosis is the sudden doubling of the flow velocity in the dilated segment. The diagnosis of a hemodynamically significant stenosis by duplex sonography is a predictor of the 1-year patency rate, which is 83 % in the absence of stenosis as opposed to only 15 % when a hemodynamically significant stenosis is diagnosed (Mewissen et al. 1992). In this study, duplex ultrasound was found to be superior in quantifying residual stenosis.

2.1.7.3 Bypass Procedures

The appearance of a bypass on the gray-scale scan depends on the material used.

The thin wall of an *autologous* venous bypass graft is very difficult to delineate in case of occlusion. Such a bypass is easier to identify, in particular in older occlusion, if the sonogra-

pher has information on its course (anatomic, extra-anatomic). In the follow-up of a venous bypass graft, the entire length must be scanned because the former valves are predilection sites for stenoses, especially in an in-situ bypass with incomplete valve destruction with the valvulotome. AV fistulae developing from perforating veins that have not been ligated are identified by the presence of perivascular vibration artifacts and in the color duplex mode.

In contrast, the wall of a *synthetic bypass graft* is always clearly delineated. PTFE (polytetrafluoroethylene) prostheses have the typical echogenic double contour and Dacron bypasses a sawtooth-like appearance.

In the postoperative evaluation and follow-up of a synthetic graft, special attention must be given to possible anastomotic stenoses. Narrowing within the bypass is due to neointimal hyperplasia and occurs later. About 20–30% of venous bypass grafts develop strictures on the basis of neointimal hyperplasia within the first year of surgery.

Different factors can cause occlusion of a bypass at different times after surgery:

- *Immediate postoperative occlusion* within the first days may be due to an inadequate surgical technique resulting in anastomotic stenoses or to a poor outflow tract. The latter can be identified by assessing the patency and hemodynamics of the recipient vessel.
- *Early occlusion* within the first year is chiefly caused by neointimal hyperplasia, which predominantly causes proximal or distal anastomotic stenoses, or a disturbed outflow due to progression of atherosclerosis distal to the bypass. If the occlusion is due to an impaired inflow as a result of atherosclerotic lesions of the proximal artery with loss of the triphasic waveform, the sonographer must carefully evaluate this area to identify the site of the lesion.
- *Late occlusion* is predominantly caused by progression of atherosclerosis.

Liquid structures around a bypass graft should be punctured under ultrasound guidance for microbiologic testing, in particular in patients with clinical signs of infection. Before puncture, a suture aneurysm should be excluded by color duplex scanning (cf. Fig. A 2.18).

Hematoma, seroma, and suture aneurysm, which are noted as pulsatile protrusions around the anastomosis have a characteristic appearance in the color duplex scan that enables their differentiation at first glance.

The criteria for stenosis grading are based on those used for the peripheral arteries. It must be noted, however, that the hemodynamic changes within a bypass may occasionally lead to a monophasic waveform that has no pathologic value. Eddy currents at the sites of anastomoses cause spectral broadening, which is likewise normal (cf. Figs. A 2.20 to A 2.24).

The normal peak velocity is a function of the relation of the cross-sections of the bypass, the upstream vessel, and the downstream vessel. The complex relationships make it difficult to give a reliable general threshold velocity. Still, one can exclude a hemodynamically significant stenosis with some confidence if the peak systolic velocity in the anastomotic area is below 2 m/s and the vascular surgeon has chosen an adequate bypass.

Since stenoses in synthetic grafts chiefly occur at the anastomoses, the quotient of peak systolic velocity in the stenosis and proximal to the stenosis as proposed by several investigators must be used with caution due to differences in the cross-section and elasticity of the bypass and proximal vessels. With these limitations in mind, it may be assumed that a quotient above 2.5 indicates a greater than 60% stenosis. Differences in caliber between the bypass and the recipient vessel often result in a flow acceleration downstream of the distal anastomosis, in particular when the anastomosis is located below the knee. Under these conditions, an even higher quotient (>3) must be used as a cutoff to prevent false-positive results (Polak 1992).

Mapping of an entire bypass graft with spectral Doppler tracing at the proximal and distal anastomoses is too time-consuming. The sonographer can therefore attempt to perform a more efficient examination by intermittent recording of Doppler information and analysis of the waveforms using the same criteria as for native peripheral arteries (Fig. 2.11 and Fig. 2.8). The flow profile and peak systolic flow velocity

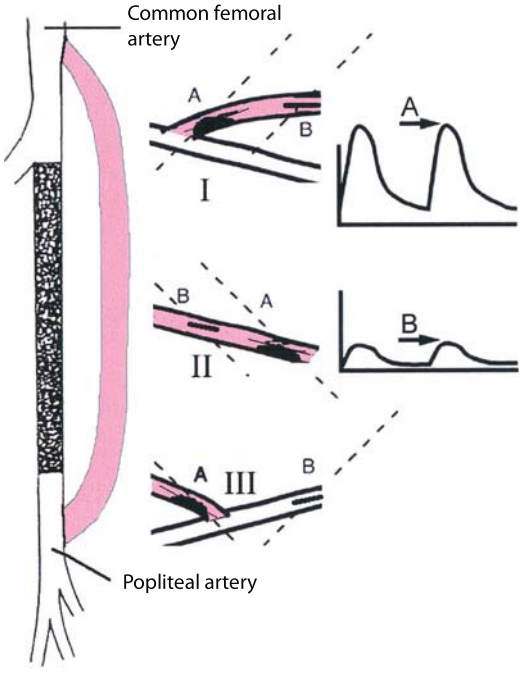

Fig. 2.11. Preferred sites of bypass graft stenoses and the corresponding changes of the Doppler waveform (*A, B*). Occlusion of superficial femoral artery bridged by femoropopliteal bypass graft (cf. also Fig. A 2.19 to Fig. A 2.24)
I: Stenosis of proximal bypass anastomosis (*A*) with poststenotic waveform (*B*)
II: Stenosis within the bypass graft (at site of former venous valve) with sudden doubling of flow velocity (*A*) compared to prestenotic waveform (*B*) and postocclusive flow profile distal to the stenosis
III: Stenosis of distal bypass anastomosis (*A*) with poststenotic flow profile in the popliteal artery onto which the graft is anastomosed (*B*)

are evaluated. If a triphasic flow profile with a peak systolic flow velocity of over 55 cm/s is recorded inside the bypass graft, a stenosis within the graft or at the anastomoses is extremely unlikely, especially if the bypass was established for critical ischemia of the leg. In contrast, a stenosis in the graft would lead to a demand-adjusted reduction of peripheral resistance with widening of the arterioles, reflected in the flow profile by a change from triphasic to monophasic. If the intermittently recorded Doppler spectrum in the bypass does not show triphasic flow and there is slow blood flow, the entire bypass must be scanned for the presence of stenosis with special attention paid to the anastomoses. However, a monophasic waveform from within the bypass may also be obtained if no stenosis is present, especially if the bypass was established to improve inflow in patients with multilevel obstruction and persistent reduction of peripheral perfusion due to more distal stenoses in the lower leg. In contrast, an initially triphasic flow profile in a bypass graft that becomes monophasic at later follow-up indicates peripheral widening as a result of reduced peripheral perfusion. This again warrants sonographic evaluation of the entire bypass and the anastomoses. Another possible cause of impaired peripheral perfusion is progressive atherosclerosis with stenotic narrowing of the segments proximal or distal to the bypass graft.

The long-term patency rate is determined by stenotic changes in the bypass (predominantly involving the anastomoses) and the condition of the peripheral outflow tract. The latter affects the velocity in the bypass, which can lead to occlusion in combination with systemic factors such as a hypercoagulable state. Several investigators regard the peak systolic velocity as the most important parameter in the follow-up after bypass surgery (Bandyk et al. 1985, 1989; Buth et al. 1991; Calligaro et al. 1996; Grigg et al. 1988; Lundell et al. 1995; Passman et al. 1995). Postoperative mean or median peak systolic velocities reported in the literature range from 0.68 to 1.12 m/s (Belkin et al. 1994; Nielsen et al. 1995; Wölfle et al. 1994) and decrease in the further course if no occlusive changes develop (from 1.125 m/s to 1 m/s after one year according to Wölfle and by 30 % within the first 6 months according to Nielsen 1993). There is agreement that an increase in the peak systolic velocity in the bypass or anastomosis (indicating stenosis) is associated with a poorer prognosis. The cutoff points proposed for a significant stenosis requiring bypass revision range from 2 m/s (Passman et al. 1995) to 3 m/s (Westerband et al. 1997). In our opinion, however, there is no single cutoff point that applies throughout a bypass. For example, velocities of 2.5 – 3 m/s may be considered normal at the distal anastomosis, in particular when there is a transition from a wide bypass lumen to a narrow recipient vessel as in crural bypasses, but are abnormal when they occur at the proximal anastomosis or in the course of the bypass.

As already mentioned, some authors use a quotient, termed the peak velocity ratio (PVR), of the abnormal peak velocity to that in the normal upstream vessel segment. However, the quotient above which >70 % stenosis requiring revision is assumed varies from 3 (Calligaro et al. 1996; Dougherty et al. 1998) to 4 (Idu et al. 1999). A quotient of 3.5 has now become the accepted threshold (Zwolak 2000).

Intermediate-grade stenoses (50 – 70%) in a bypass graft are characterized by a PVR of 2 – 3.5 and a peak systolic flow velocity of 2 – 3.5 m/s.

Some authors propose a markedly reduced overall peak systolic velocity in the bypass as a supplementary indicator of a poor prognosis in addition to a local increase (Calligaro et al. 1996; Hoballah et al. 1997). Slow flow suggests an outflow obstacle, either a stenosis of the distal anastomosis or an impaired outflow tract (stenosis of the recipient segment, poor collateral flow). Hence, various velocity thresholds have been suggested as predictors of bypass occlusion. Most authors assume a threshold of 45 cm/s as an indicator of a failing bypass (Calligaro et al. 1996; Hoballah et al. 1997; Mohan et al. 1995), others 40 cm/s (Green et al. 1990) or 55 cm/s (Nielsen et al. 1995). More recent studies have shown that assuming a single velocity threshold as an indicator of imminent bypass occlusion for all types of bypass grafts and recipient vessels is not sensitive and specific enough (Chang et al. 1990; Hoballah et al. 1997; Idu et al. 1998; Mohan et al. 1995; Treiman et al. 1999). Since flow velocity in a bypass is determined by the diameter of the bypass and by the diameter and outflow of the recipient vessel, crural bypass grafts with fairly peripheral anastomoses have low flow velocities already under normal conditions (Fig. A 2.19). Still, slow flow in a bypass is a risk factor for occlusion, in particular when combined with other predisposing factors such as a hypercoagulable state, increased blood viscosity, and low systemic blood pressure. This is why it has been proposed to combine an increased local flow velocity and a decreased global flow velocity in a single prognostic factor (Calligaro et al. 1996). In a study of 85 PTFE bypass grafts, this combined criterion was found to have a sensitivity of 81 %, a specificity of 93 %, a positive predictive value of 63 %, and a negative predictive value of 93 % (similar results are reported by Green et al. 1990). Other investigations (Hoballah et al. 1997; Mohan et al. 1995) did not confirm these results. In the study by Hoballah et al., 24 of 27 patients with occlusions showed neither a decrease in peak velocity below 45 cm/s nor a threefold increase in preceding examinations.

Despite these inconsistent results, patients who have undergone a bypass procedure (especially those with venous grafts) should be followed up by duplex scanning (Table 2.18), at least during the first postoperative year when the risk of occlusion is highest and revision can be performed with a fairly good prognosis (Passmann et al. 1995; Taylor et al. 1990).

In the examination the sonographer should compare the pulsatility and flow velocity in the bypass graft with the initial postoperative ultrasound findings obtained during the first three months after the operation. If there is a decrease in peak systolic flow velocity in the bypass or triphasic flow becomes monophasic, the examiner must look for proximal or distal stenoses, applying the criteria described above. Even if a stenosis can be identified and localized with duplex ultrasound, intra-arterial DSA should be performed prior to surgery to

Table 2.18. Sonographic follow-up after bypass procedures

Identification of bypass complications (suture aneurysm, abscess, early occlusion)	
Imminent bypass occlusion (failing bypass):	Duplex criteria: decrease in peak systolic velocity in the bypass resulting from slow flow due to poor outflow tract (stenosis of distal anastomosis, stenosis or occlusion distal to bypass), monophasic waveform
Anastomotic stenosis:	Duplex criteria: flow acceleration in the stenotic area

plan the extent of the revision and to identify possible stenoses upstream of the graft or in the distal recipient segment.

Follow-up of patients after bypass surgery with duplex ultrasound with revision as required results in a one-year patency rate of 93 % as opposed to only 57 % without monitoring, and the amputation rate is likewise lower than in patients in whom no measures are taken to prevent imminent occlusion (Wixon et al. 2000). Especially in patients with critical ischemia of the leg at the time of bypass grafting, sonographic follow-up with bypass revision as required can reduce the major amputation rate (Visser 2001). Patients with follow-up by duplex ultrasound had a major amputation rate of 1.7% as compared with 7.7% in patients undergoing only clinical follow-up supplemented with the ankle-brachial index. The cost of diagnosis and treatment was only half as high in the patient group followed up by duplex sonography. The subgroup of patients with intermittent claudication at the time of bypass surgery benefited less from sonographic follow-up. Although some discrepancy exists in published results, there is a clearcut advantage of duplex ultrasound follow-up for autologous vein grafts while the results are much poorer for synthetic grafts. Many studies investigating populations of patients with venous and synthetic bypass grafts found a 25 % higher patency rate for venous grafts monitored by duplex ultrasound. In contrast, duplex ultrasound is of little prognostic value in the follow-up of patients with a synthetic bypass, where which occlusion is due to multiple factors.

If, for cost-efficiency reasons, not all patients are monitored by duplex scanning, at least grafts with low intraoperative flow and an increased outflow resistance (crural bypasses) should be followed up (Mercer et al. 1999). A venous bypass should be examined 3 and 6 months after surgery and then at 6-month intervals. Moreover, the proposed threshold velocities have to be used more flexibly and adjusted to the individual bypass diameter and outflow tract. Future studies should try and establish different threshold values for different types of grafts (autologous vein versus synthetic material, recipient vessel above or below the knee, status of outflow tract, bypass diameter).

The Doppler frequency spectrum recorded in a bypass is affected by several factors that have to be taken into account, especially in patients with severe atherosclerosis and in assessing a graft connected to a lower leg artery. Pulsatility is physiologically dependent on the demand-oriented widening of the arterioles (monophasic flow). In a bypass, pulsatility is further affected by differences in elasticity (depending on the material used for grafting) and an increase in outflow resistance if there is stenosis distal to the bypass (more pulsatile flow). These opposing effects on the flow profile preclude simple monocausal interpretation of the waveform obtained from a bypass graft. Hence, the examiner must check both the distal anastomosis and the recipient artery for the presence of stenosis even if the waveform shows triphasic flow (cf. Fig. A 2.19).

While a synthetic graft should primarily be inspected for stenoses at the proximal and distal ends, an autologous venous graft must be scanned throughout its course to identify stenoses at the sites of former valves. As with native vessels, it may be helpful and reduce the length of the examination if Doppler spectra are recorded at specific intervals and compared to localize a stenosis. When scanning an autologous in-situ venous bypass, the examiner must also look for any patent perforating veins, which function as AV fistulae and must be ligated after they have been localized sonographically.

2.1.7.4
Ultrasound Vein Mapping prior to Peripheral Bypass Surgery

Autologous venous bypass grafts having higher short-term and long-term patency rates are superior to other procedures in peripheral bypass surgery. However, vein preparation may be time-consuming in patients with variants such as an aberrant path or duplication and in obese patients. When the great or small saphenous vein is considered, the superficial course can be identified with a high-resolution transducer (6.5 – 10 MHz) and marked on the skin before surgery. Moreover, duplicated veins can be localized and the most suitable branch selected for grafting. When an in-situ bypass is planned, perforating veins can likewise be marked for intraoperative ligation to prevent AV fistulae. The vein diameter is measured in transverse orientation with the great saphenous vein normally having a diameter of 3 – 4 mm in the lower leg; very small veins (< 2 mm) are unsuitable for grafting. If two branches are present, the larger one is selected. Moreover, unnecessary preparation can be avoided by discarding varicose or postthrombophlebitic veins with wall thickening and sclerosis. Altogether, preoperative sonographic vein mapping for selection of a suitable graft shortens the length of surgery and helps prevent unnecessary incisions and extensive exposure.

2.1.8
Role of (Color) Duplex Ultrasound Compared to other Modalities – Problems and Pitfalls

In the step-by-step diagnostic workup of peripheral AOD, the patient's history, clinical examination with evaluation of pulses, and Doppler blood pressure measurement come before noninvasive duplex scanning, which may then be fol-

Table 2.19. Advantages and disadvantages of duplex scanning

Advantages	Disadvantages
Noninvasiveness Multilevel evaluation Evaluation of wall morphology surrounding structures intraluminal structures plaque Stenosis grading based on morphology hemodynamics Low cost	Documentation of findings Evaluation of collateral pathways Long training period Long examination time Evaluation of terminal vascular bed Specific methodological limitations (calcifications, air, obesity, edema)

Table 2.20. Advantages and disadvantages of angiography

Advantages	Disadvantages
Documentation of findings	Invasiveness and complications (false aneurysm, embolism, bleeding, local thrombosis, AV fistula)
Visualization and evaluation of collateral pathways	Visualization of patent lumen only
Evaluation of terminal vascular bed	Projection-related problems: stenosis grading evaluation of bifurcation
Fairly short training period	Nonvisualization: vessel wall surrounding structures High cost Radiation exposure and contrast medium administration

lowed by invasive angiography (cf. Table 2.4). The stage of AOD and the sonographic findings provide the foundation for the further management, either initiation of treatment or ordering of specific supplementary diagnostic tests (Table 2.19; cf. Fig. 2.7).

For example, patients with a stenosis in the iliac or femoropopliteal territory can undergo diagnostic angiography which may be extended to PTA, depending on the findings. In contrast, patients with longer occlusions of the pelvic or thigh arteries can be scheduled for bypass surgery without angiography if ultrasound has demonstrated an adequate outflow tract as well as patency of the popliteal vessels and lower leg arteries. Angiography is likewise not necessary in patients in whom an aneurysm has been confirmed sonographically.

If ultrasound demonstrates vessel compression (popliteal entrapment syndrome, cystic adventitital disease), surgical management can likewise be initiated without prior angiography, which provides no additional information and only serves to document the vascular status. Depicting only the vessel lumen, angiography is inferior to ultrasound in evaluating structures around the vessel. A further drawback of angiography is the reduction of the three-dimensional vessel lumen to the two-dimensional plane of the film (cf. Fig. 5.7). With this limitation, the diameter reduction randomly depicted in the imaging plane is not necessarily representative of the effective cross-sectional area reduction, as the wall changes may vary along the length of the stenosis (concentric – eccentric; regular – irregular). Stenosis grading by angiography may thus differ from the Doppler grading on the basis of hemodynamic parameters. There may also be discrepancies in plaque evaluation by gray-scale ultrasound, which depicts plaques as intraluminal color gaps, and their hemodynamic evaluation by Doppler ultrasound with determination of flow acceleration. For accurate and reproducible quantification, it is thus necessary to consistently depict a stenosis in different planes both sonographically and angiographically (Table 2.20).

A projection-related source of error in angiography results from posterior wall plaques which are especially common in the pelvic territory and may obscure a stenosis on anteroposterior views (cf. Fig. 5.7). Evaluation of stenoses at the origin of the profunda femoris artery by angiography may be impaired by superimposed vessels. Ultrasound is superior here when performed with an adequate angle of insonation. In a study of 30 patients scheduled for TEA of the profunda to improve collateralization of superficial femoral occlusion, the high-grade stenosis demonstrated by ultrasound and confirmed intraoperatively was definitely identified by angiography in only 70 % of the cases and there was considerable variation in the degree of stenosis determined by different examiners.

Diagnostic angiography is required only if the sonographic findings are inconclusive, in patients with diabetes, and before vascular surgery, especially in patients with involvement of the crural vessels (cf. Fig. 2.5).

Follow-up of reconstructive procedures is done with ultrasonography, which will identify residual or bypass stenoses and thus ensure timely revision (cf. Table 2.14).

Calcified plaques impair sonographic assessment because *acoustic shadowing* obscures affected vessel segments and other structures behind them on B-mode scanning and impairs the color display in the color duplex mode. Long calcified plaques may prevent the acquisition of an adequate Doppler signal even at a higher gain. In such cases, the degree of a stenosis is determined by comparing the changes in the waveforms from the upstream and downstream vessel segments. An unchanged peak systolic velocity and preservation of the triphasic flow profile suggest plaques without hemodynamic significance (cf. Fig. A 2.14).

Proper angulation of the ultrasound beam for quantifying a stenosis may be difficult to achieve despite changing the transducer position. This applies in particular to the arched segment of the common iliac artery at the junction with the external iliac. Also, there may be aliasing in vessels interrogated at a very small Doppler angle and peak systolic velocity is cut off. This holds especially for deeply situated vessels such as the internal iliac artery.

In older stenosis, extensive collateral pathways may have developed. In such cases, the reduced blood flow and altered hemodynamics in the main artery resulting from a division of the blood volume between the collaterals and the artery can lead to *underestimation* of the stenosis because duplex ultra-

sound solely relies on hemodynamic parameters (cf. also Fig. 2.9).

Color duplex scanning with a high-resolution transducer enables assessment of collaterals, in particular when the occluded segment is short, and detection of stenoses at the sites of opening of the collaterals (cf. Fig. A 2.13). Nevertheless, ultrasound is inferior to angiography in providing a full overview of the collateral circulation of an occlusion. The hemodynamic situation distal to an occlusion provides clues to the quality of collateralization. A relatively high peak systolic velocity in the postocclusive vessel area distal to the emptying of the collaterals suggests good collateralization. However, this criterion must be interpreted with caution as peak systolic velocity is also increased in diabetics with rigid arterial walls due to medial sclerosis.

If two or more sequential stenoses are present, the more distal ones may be underestimated or difficult to assess (cf. Fig. A 2.12), especially in *diabetic macroangiopathy*. Moreover, the *hemodynamic changes* associated with diabetic medial sclerosis and peripheral vessel occlusions further impair stenosis grading by duplex ultrasound. Angiographically, such sequential stenoses are identified by their typical goose throat appearance.

When diagnostic ultrasonography and vascular repair are performed by different persons or even by different departments, the lack of *continuous documentation* of the findings – in particular in patients with complex patterns of involvement – limits the communication of the findings to the surgeon. Ultrasonography is an invaluable tool in the hands of the radiologist or vascular surgeon who also treats the patient and benefits from the additional hemodynamic information. What one must also bear in mind is that ultrasound is highly examiner-dependent.

An experienced examiner is able to asses the lower leg arteries throughout their course using a high-resolution transducer. Extra time is required for the separate evaluation of an occlusion or stenosis. What ultrasound fails to provide is an overview of complex patterns of disturbed perfusion with multiple occlusions of the lower leg arteries that collateralize each other, especially with regard to evaluation of peripheral outflow (Table 2.21).

The studies comparing duplex scanning with digital subtraction angiography (DSA) in the assessment of the cruropedal arteries report widely divergent results (Karacagil et al. 1996; Koelemay et al. 1997) with sensitivities and specificities for the detection of occlusion ranging from 50 to 90 %. However, the investigators used 5 MHz transducers, which are inadequate for the pedal vessels, resulting in a low resolution that may explain the poor results. Other study groups (Boström et al. 2002; Hofmann et al. 2001) describe limitations of nonselective IA DSA in the visualization of the outflow vessels of the foot (cf. Fig. A 2.17). In a consecutive series of 49 patients reported by Hofmann et al. (2001), the pedal vessels in 32 cases (65.3 %) were hardly – or not at all – visualized by DSA. Based on the sonographic evaluation of the pedal vessels using a high-resolution transducer (13 MHz), all 32 patients underwent pedal bypass grafting with a 2-year patency rate of 69.5 %. Boström et al. (2002) compared 157 vascular surgical procedures (32 inguinal TEA, 91 femoropopliteal bypass, 34 femorocrural bypass) performed solely on the basis of the ultrasound findings and 172 procedures (28 inguinal TEA, 144 femoropopliteal and femorocrural bypass) planned on the basis of angiography. The second group were patients with inadequate ultrasound results (in particular also patients with femorofibular bypass procedures). Cruropedal bypass grafts (ratio of 1:2 [ultrasound versus angiography group]) and femorocrural bypass grafts (ratio of 1:1) were likewise established solely on the basis of the ultrasound findings. The primary patency rate of the bypass grafts was 59 % in the ultrasound group versus 64 % in the angiography group. No intraoperative revision of the planned procedure was necessary in 98 % of the patients examined by preoperative ultrasound (not even on the basis of intraoperative DSA).

Selective DSA with positioning of the catheter in the superficial femoral artery or further distal continues to be the gold standard. When technically adequate DSA is not possible or there is poor visualization of the crural and pedal vessels, a supplementary high-resolution duplex ultrasound examination is required. Provided the necessary infrastructure and ultrasound equipment are available and there is adequate communication between the sonographer and the operator (ideally the same person), TEA and femorpopliteal and femorocrural bypass procedures will increasingly be performed on the basis of the duplex ultrasound findings alone in those patients with good insonation conditions.

Table 2.21. Different indications for angiography and color duplex ultrasonography. More plus signs indicate a more favorable rating

Diagnostic task	Angiography	Color duplex
Atherosclerosis screening	Not possible	+++
Therapeutic decision making (medical, PTA, surgery)	++	+++
Planning of surgical procedure	+++	+
Follow-up: PTA, surgery	+	+++
Critical ischemia	Mandatory	+++
Vessel wall evaluation (aneurysm/inflammatory conditions)	(+)	+++
Evaluation of surrounding structures	Not possible	+++
Analysis of occlusion (cause)	(+)	+++
Evaluation of collaterals	+++	+
Analysis of plaque morphology, progression, regression	(+)	+++
Atypical arteries	+++	+
Diabetic foot	+++	+
Documentation of findings	+++	–

2.2 Arm Arteries

2.2.1 Vascular Anatomy

The innominate artery (brachiocephalic trunk) arises from the aortic arch on the right and behind the sternoclavicular joint divides into the subclavian and common carotid arteries. On the left, the *subclavian artery* arises directly from the aortic arch as does the common carotid artery at a more proximal site. Along its course, the subclavian artery first gives off the *vertebral artery* cranially. Further along the course, the thyrocervical trunk arises, likewise from the posterior aspect, and at once divides into a branch supplying the thyroid and other branches supplying the skin and soft tissue. Together with the brachial plexus, the subclavian artery (Fig. 2.12) passes through the scalene triangle (between the anterior and medial scalene muscles and cranial to the first rib) and arches over the pleural dome, crossing under the clavicle, to continue as the *axillary artery*. In individuals with a cervical rib, the subclavian artery is displaced cranially and anteriorly. Distal to the thyrocervical trunk, the internal thoracic (mammary) artery arises and descends behind the anterior chest wall and about one fingerbreadth lateral to the sternum.

The branches of the axillary artery have extensive collateral connections to the branches of the subclavian artery and supply the region of the shoulder girdle. The axillary artery courses along the lower border of the pectoralis muscle through the axilla and continues as the *brachial artery*. The latter runs through the medial bicipital groove near the humerus to the elbow and divides into the radial and ulnar arteries at the level of the joint space. There are anatomic variants in which the brachial artery already gives off the radial artery in the upper arm (in about 15 %) or arises directly from the distal axillary artery (1 – 3 %). The ulnar artery may likewise originate from the axillary artery (in about 1 %).

The radial artery continues through the forearm on the ulnar side of the radius to the wrist where it unites with the deep branch of the ulnar artery to form the deep palmar arch. The radial artery primarily feeds the deep arch and the ulnar artery the superficial arch. The main branches of the superficial arch give off the common palmar digital arteries, which in turn give rise to the proper palmar digital arteries, the main vessels supplying the fingers. A complete connection between the superficial and deep palmar arches is present in only about 80 – 90 % of individuals.

2.2.2 Examination Protocol and Technique

The subclavian and axillary arteries are scanned at *5 to 7.5 MHz* while higher-frequency transducers are appropriate more distally where the arteries lie closer to the surface. The finger arteries are examined with *7.5 – 10 MHz transducers*. Especially in the supraclavicular fossa, curved array or sector transducers are superior to linear transducers. The subclavian and axillary arteries are scanned best in the supine position with the examiner behind the patient's head, as in the examination of the carotid arteries. The forearm and finger arteries are examined in the sitting patient with the hand supinated.

The arm arteries are traced along their course from the supraclavicular area to the palmar arch. In the upper arm, the arteries are easily identified by B-mode scanning based on sonoanatomic knowledge. The vessels of the palmar arch and fingers are localized with the aid of color duplex ultrasound. Spectral Doppler information is sampled in longitudinal orientation with a smaller angle of insonation.

The proximal portion of the subclavian artery is interrogated with the transducer in the supraclavicular position. In

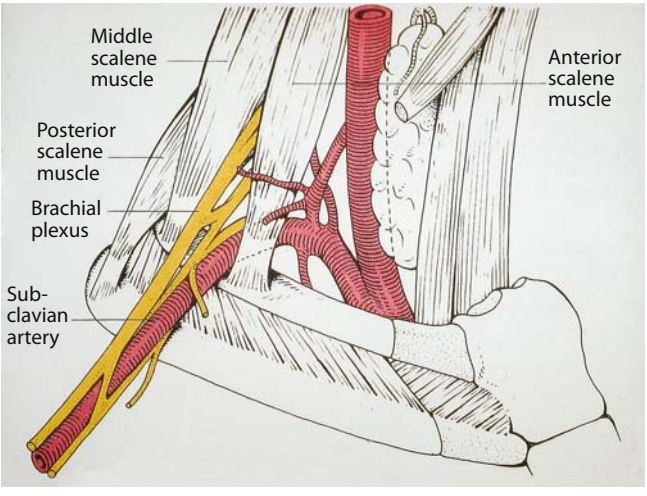

Fig. 2.12. Course of the subclavian artery through the scalene triangle. The subclavian runs between the first rib, medial scalene muscle, and anterior scalene muscle. (From Heberer and van Dongen 1993)

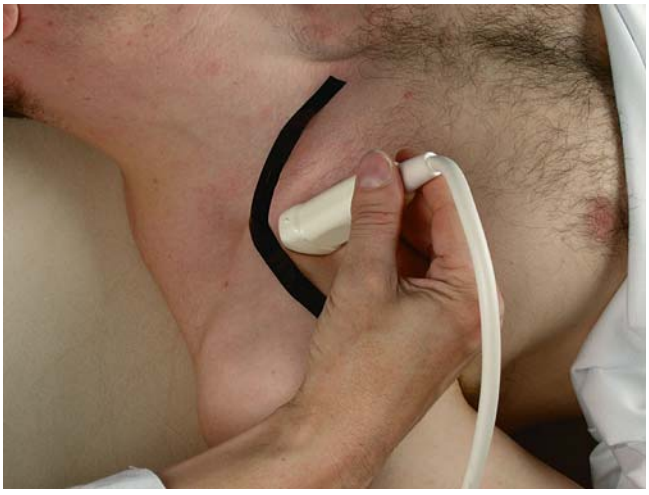

Fig. 2.13. Transducer position for examination of the axillary artery (transducer placed in Mohrenheim's fossa) and subclavian artery (course indicated by black line)

evaluating the supra-aortic branches, the examiner should pay special attention to the origin of the vertebral artery, which must be differentiated from the thyrocervical trunk. Rhythmical tapping of the vertebral artery suboccipitally will be transmitted and appear in the Doppler waveform of the proximal segment of the artery.

The axillary artery is identified with the transducer placed in Mohrenheim's fossa cranial to the axillary vein (Fig. 2.13) and scanned along its path to the axilla. The brachial artery is examined in the upper arm from a medial position.

Depending on the clinical query, special attention must be paid to the presence of aneurysm or stenosis of the subclavian artery. When the color duplex findings are inconclusive, a spectral Doppler tracing is recorded. Under normal conditions, the subclavian, axillary, and brachial arteries have a triphasic flow profile (high-resistance flow of arteries supplying soft tissue and skin).

2.2.3 Clinical Role of Duplex Ultrasound

2.2.3.1 Atherosclerosis

Stenoses of the upper extremity arteries chiefly affect the proximal subclavian artery and are four times more common in the longer left subclavian artery (especially at its origin from the aorta). If a subclavian stenosis or occlusion is suspected, scanning should always include the vertebral artery as well to identify flow reversal as a sign of the subclavian steal syndrome. Prior to coronary bypass surgery, color duplex ultrasound can serve to noninvasively assess the internal thoracic artery as a candidate for grafting. Stenoses of the arm arteries distal to the subclavian artery are rare and typically have no clinical significance, except in patients with a long history of diabetes mellitus or after creation of an AV shunt.

Repeat traumatic pushing of the ulnar artery against the hamate bone can damage the vessel wall and give rise to an aneurysm, which may become partially thrombosed and then embolize to the interdigital arteries.

2.2.3.2 Compression Syndromes

Various factors such as abnormal congenital osseous and fibromuscular structures, postural anomalies, and trauma are involved in the development of the thoracic outlet syndrome. The nerves and vessels coursing through the narrow space of the upper thoracic aperture may become compressed if they take an atypical course or in the presence of osseous or fibrous anomalies. The clinical manifestation is very heterogeneous and varies with the structure compressed. The vast majority of patients (97%) suffer from more or less severe neurogenic symptoms due to compression of the brachial plexus (Roos 1987, 1989). The most common vascular symptoms are insidious episodes of microembolization that may lead to occlusion of the interdigital arteries. Larger emboli, chiefly arising from poststenotic dilatations or aneurysms of the subclavian artery, may cause occlusion of the larger arteries, namely the ulnar, radial, and brachial arteries.

The thoracic outlet syndrome predominantly occurs in patients aged 20 to 50 and affects females at a ratio of 3:2.

Compression of the subclavian artery can occur in three narrow spaces that lie along its course:

- the anterior scalenus muscle gap (scalene triangle),
- the narrow passage between the first rib and clavicle (costoclavicular space), and
- the narrow space below the pectoralis minor muscle at its site of attachment to the coracoid process (pectoralis minor space).

As already mentioned, several anatomic variations or pathologic processes can compromise these already narrow spaces, resulting in mechanical irritation or compression of vessels and nerves. Prolonged compression of a vessel can lead to downstream aneurysm formation with development of mural thrombi and embolism of the arm arteries.

The term *thoracic outlet syndrome* encompasses three neurovascular syndromes distinguished according to the site of vessel or nerve compression:

- *Scalenus anterior or cervical rib syndrome*: In this syndrome, the brachial plexus and the subclavian artery are compressed due to thickening or an abnormal position of the anterior or medial scalenus muscle at its attachment to the first rib, exostosis of the first rib, or a cervical rib. The subclavian vein is not involved as it does not pass through the scalene triangle (Figs. A 2.42 to A 2.44).
- *Costoclavicular syndrome*: The narrow passage between the clavicle and first rib is the preferred site of venous compression caused by a sagging shoulder girdle, rib callus, or exostosis. The subclavian artery and the brachial plexus are rarely compressed at this site (Fig. A 3.51).
- *Hyperabduction syndrome*: At the third site, mechanical nerve damage predominates. It is due to compression of the neurovascular bundle by the tendon of the pectoralis minor muscle or the coracoid process when the arms are stretched above the head (Fig. A 2.45).

2.2.4 Documentation

Documentation of the findings is the same as for the leg arteries and is comprised of longitudinal B-scan views of the subclavian, axillary, and brachial arteries with the corresponding angle-corrected Doppler waveforms. An aneurysm is documented in two planes and its diameter measured on a transverse view. In case of stenosis, the angle-corrected intrastenotic peak flow velocity is recorded. If no adequate Doppler tracing can be sampled from a central subclavian stenosis, the monophasic waveform distal to the lesion is documented.

2.2.5 Normal Findings

As with the leg arteries, the arm arteries have a triphasic waveform with a steep systolic rise and subsequent decrease with some retrograde flow (due to high peripheral resistance) and slight flow persisting during diastole. The diameter of the arm arteries decreases toward the periphery (6 – 7 mm subclavian artery, 5 – 6 mm axillary artery).

2.2.6 Abnormal Findings, Duplex Ultrasound Measurements, and Clinical Role

2.2.6.1 Atherosclerosis

Due to the poor insonation window in this anatomic region, a central subclavian stenosis can often be diagnosed only indirectly through the demonstration of a monophasic flow profile and turbulent flow in the poststenotic segment. In patients with good scanning conditions, however, the subclavian artery can be traced with a low-frequency transducer to its origin from the aorta and a stenosis near the origin can be demonstrated directly by accelerated flow in the angle-corrected Doppler waveform.

As in the leg arteries, peak systolic flow velocity in the subclavian and axillary arteries has a high standard deviation in the normal population. Therefore, sudden doubling of the peak velocity serves as a diagnostic criterion for a hemodynamically significant stenosis. However, this criterion does not apply to the proximal subclavian artery, the preferred site of arterial stenosis in the upper extremity. Here, a peak systolic velocity greater than 2 m/s is assumed to indicate stenosis (cf. Fig. A 2.41).

Interdigital artery occlusion is suggested by the clinical presentation and confirmed by duplex ultrasound. It may be caused by cardiac disease or a thoracic outlet syndrome. Moreover, such occlusions may be due to the hypothenar hammer syndrome if they involve the ulnar supply area and the patient has a history of chronic repetitive blunt trauma of the hypothenar with arterial wall damage. When the latter is suspected, the examiner must specifically look for an aneurysmal dilatation of the distal ulnar artery in the hypothenar area. Ultrasonography depicts corkscrew-like changes already at an early stage and demonstrates the intra-aneurysmal thrombi responsible for embolization to the interdigital arteries as well as the patent lumen in the color duplex mode (cf. Fig. A 2.46).

2.2.6.2 Compression Syndromes

The great variability of clinical symptoms and the problem of definitively confirming the thoracic outlet syndrome by means of provocative maneuvers make it difficult to diagnose this condition. A study in a German patient population shows that on average 6.5 specialists were consulted before the syndrome was diagnosed after a mean of 4.3 years (Gruss et al. 1989 and Gruss and Geissler 1997).

Prior to apparative tests, a vascular examination is performed with determination of pulses, auscultation, and bilateral Doppler blood pressure measurement. Unilateral pulse reduction or obliteration with elevation or abduction of the arm is not a very specific symptom and is seen in 30 – 60 % of asymptomatic young adults. The AER (abduction external rotation) test continues to have a significant clinical role: arms in 90 degree AER position with fist clenching every 2 sec for 3 min. Most subjects will experience fatigue, pain, and heaviness before the end of the 3-minute test period. Formication suggests compression of the upper plexus. Additional pain and pallor of the fingers indicate arterial compression. The diagnosis of a thoracic outlet syndrome further requires measurement of the nerve conduction velocity of the ulnar and median nerves. A clearcut delay in proximal ulnar and median nerve conduction in the plexus/axilla segment is diagnostic of compression but normal conduction does not exclude the thoracic outlet syndrome. Ulnar motor velocities above 65 m/s are normal and velocities below 45 m/s indicate damage to the plexus (Urschel 1976).

In cases where the (color) duplex findings confirm interdigital artery occlusion, the examiner must look for the source of embolism, primarily a partially thrombosed aneurysm (cf.Fig. A 2.43 and A 2.44).

Such aneurysms primarily occur secondary to compression-induced wall damage in thoracic outlet syndrome or as a result of traumatic damage to the distal ulnar artery in hypothenar syndrome. The intermittent compression in thoracic outlet syndrome may also give rise to intraluminal thrombus formation. The specific type of thoracic outlet syndrome (Table 2.22) is diagnosed by ultrasonography of the respective sites of compression as suggested by the patient's history and clinical symptoms using the following provocative tests:

- *Scalenus muscle test* (*Adson test*) in combination with the hyperabduction test to identify arterial compression in the scalene triangle: the hyperextended head is turned

Table 2.22. Compression syndromes of the upper thoracic aperture and arm vessels

- Cervical rib syndrome
- Scalenus anterior syndrome (arterial: Adson test)
- Scalenus minimus syndrome
- Costoclavicular compression syndrome (venous: hyperabduction test)
- Pectoralis minor syndrome
- Compression syndrome of the brachial artery

toward the affected side (Schoop 1988) with the neck muscles tensed and possibly with additional hyperabduction and rotation of the arm.

- *Costoclavicular* or *hyperabduction test* to identify venous compression in the costoclavicular space: gliding of the clavicle over the first rib with the arm hyperabducted narrows the passage, thereby inducing venous compression. However, the more common cause of venous compression in this area are weak shoulder muscles, which are better identified by a downward pull on the posteriorly turned arm (with the shoulder drawn back, inspiration).

During the provocative maneuvers, the Doppler spectrum is recorded from the target site or distal to it if the vessel is not accessible to scanning. The test is positive if there is flow acceleration in the compressed artery or if an altered flow profile is obtained distal to the compressed segment. The examiner can also move the scanner toward the compressed segment from the periphery, intermittently recording the Doppler information. As clinical symptoms are often unspecific, the provocative tests are necessary to differentiate and localize the clinically relevant, though rare, compression syndromes (Table 2.23). If there is occlusion of the forearm or finger arteries, it is crucial to identify the partially thrombosed aneurysm of the subclavian artery, which typically develops on the basis of a scalene muscle or cervical rib syndrome. In rare cases, emboli may arise from thrombotic deposits of the damaged wall of the axillary artery in hyperabduction syndrome. These changes are caused by intermittent compression of the axillary artery and will be identified with the transducer placed in the axilla (cf. Fig. A 2.45).

Table 2.23. Compression syndromes of the upper thoracic aperture. Duplex scanning with confirmation by angiography, venography, intraoperative findings. Tentative clinical diagnosis: arterial and/or venous compression (n = 680)

Compression syndrome	Number
Cervical rib syndrome (arterial)	3
Scalenus anterior syndrome (arterial)	6
with poststenotic aneurysm	2
Costoclavicular compression syndrome (venous)	8
with venous thrombosis	5
Pectoralis minor syndrome (arterial)	2

Patients with venous compression and the corresponding clinical symptoms should initially be treated by physical therapy to strengthen the shoulder muscles or by resection if bony abnormalities such as a cervical rib or exostosis are present.

In the thoracic outlet syndrome with compression or mechanical irritation of the arteries or nervous plexus, the first rib should be resected before secondary damage to the vessel wall with development of aneurysm occurs. In cases where secondary damage has already occurred, the affected arterial segments must be resected as well.

Inflammatory conditions of the vessel wall primarily affect the subclavian artery (Takayasu's arteritis) and are characterized by hypoechoic concentric wall thickening over long segments. If the clinical presentation and patient's history suggest Raynaud's syndrome, this must be confirmed by provocative tests with heat and cold exposure after exclusion of interdigital artery occlusion (see above, Sect. 2.1.6.4.3).

2.3 Atlas

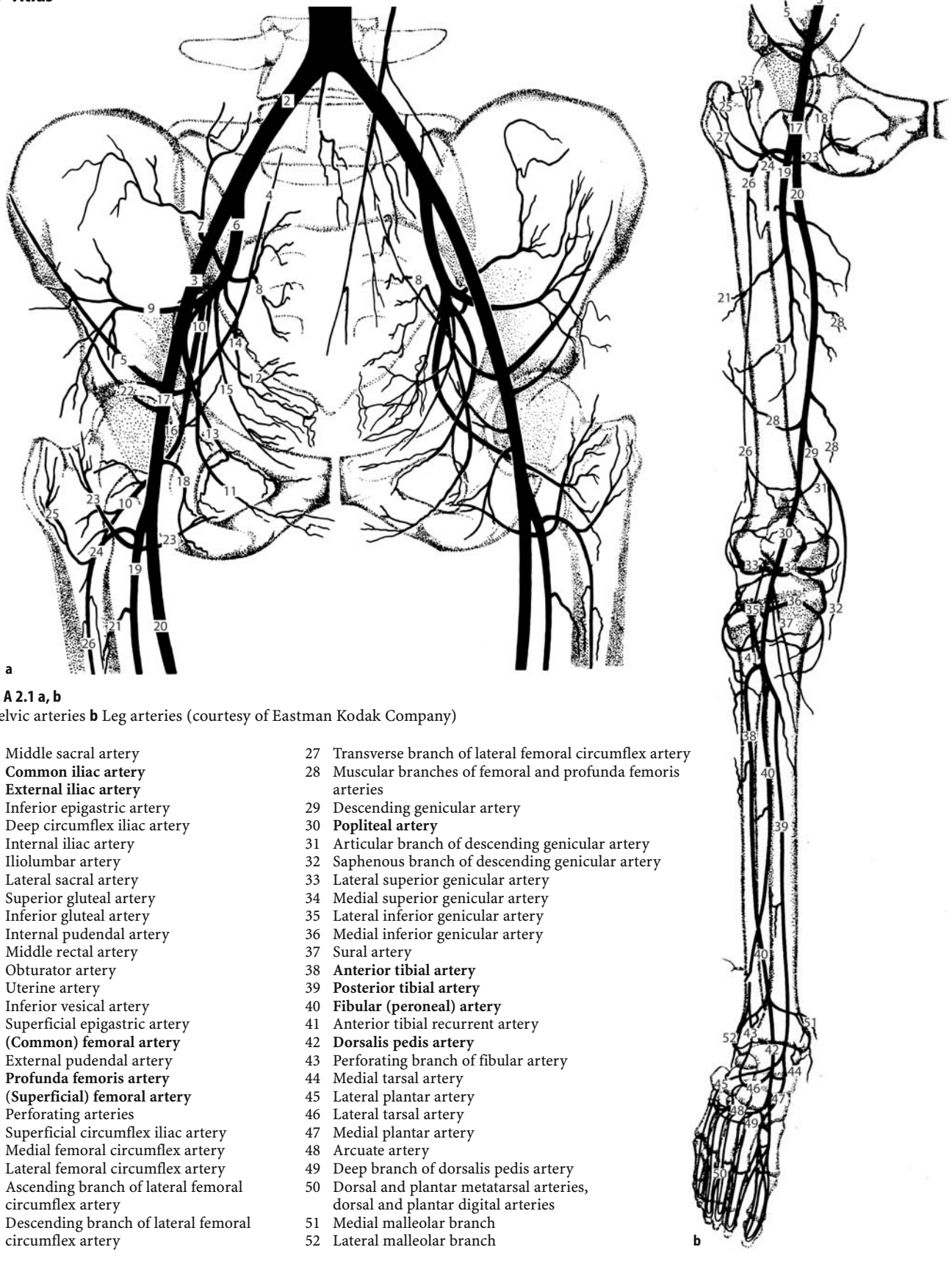

Fig. A 2.1 a, b
a Pelvic arteries **b** Leg arteries (courtesy of Eastman Kodak Company)

1 Middle sacral artery
2 **Common iliac artery**
3 **External iliac artery**
4 Inferior epigastric artery
5 Deep circumflex iliac artery
6 Internal iliac artery
7 Iliolumbar artery
8 Lateral sacral artery
9 Superior gluteal artery
10 Inferior gluteal artery
11 Internal pudendal artery
12 Middle rectal artery
13 Obturator artery
14 Uterine artery
15 Inferior vesical artery
16 Superficial epigastric artery
17 **(Common) femoral artery**
18 External pudendal artery
19 **Profunda femoris artery**
20 **(Superficial) femoral artery**
21 Perforating arteries
22 Superficial circumflex iliac artery
23 Medial femoral circumflex artery
24 Lateral femoral circumflex artery
25 Ascending branch of lateral femoral circumflex artery
26 Descending branch of lateral femoral circumflex artery
27 Transverse branch of lateral femoral circumflex artery
28 Muscular branches of femoral and profunda femoris arteries
29 Descending genicular artery
30 **Popliteal artery**
31 Articular branch of descending genicular artery
32 Saphenous branch of descending genicular artery
33 Lateral superior genicular artery
34 Medial superior genicular artery
35 Lateral inferior genicular artery
36 Medial inferior genicular artery
37 Sural artery
38 **Anterior tibial artery**
39 **Posterior tibial artery**
40 **Fibular (peroneal) artery**
41 Anterior tibial recurrent artery
42 **Dorsalis pedis artery**
43 Perforating branch of fibular artery
44 Medial tarsal artery
45 Lateral plantar artery
46 Lateral tarsal artery
47 Medial plantar artery
48 Arcuate artery
49 Deep branch of dorsalis pedis artery
50 Dorsal and plantar metatarsal arteries, dorsal and plantar digital arteries
51 Medial malleolar branch
52 Lateral malleolar branch

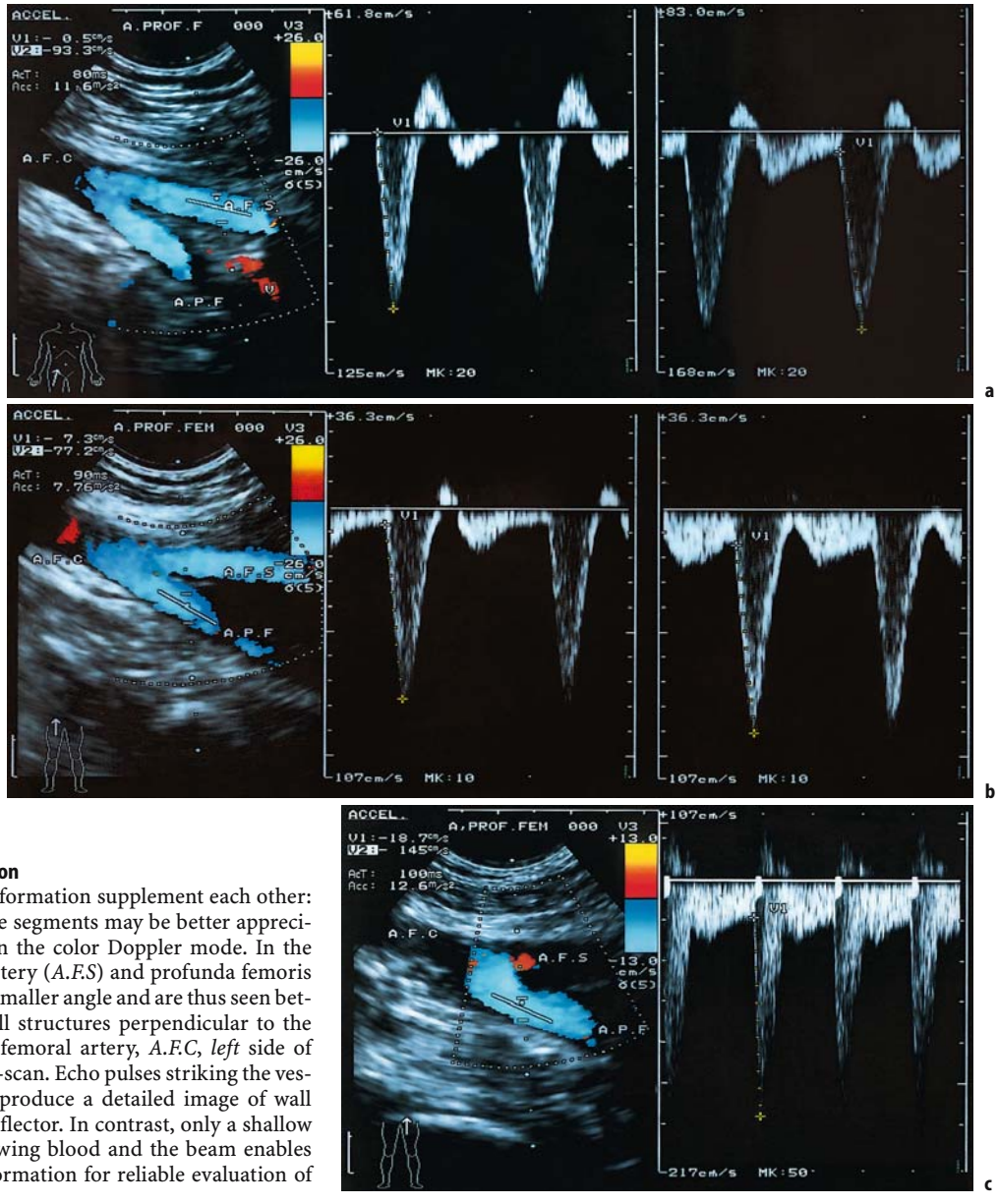

Fig. A 2.2 a–f
Femoral bifurcation – normal perfusion

a Gray-scale scan and color flow information supplement each other: Along the course of an artery, some segments may be better appreciated in the B-mode scan, others in the color Doppler mode. In the example, the superficial femoral artery (*A.F.S*) and profunda femoris artery (*A.P.F*) are insonated with a smaller angle and are thus seen better in the color mode whereas wall structures perpendicular to the ultrasound beam (here: common femoral artery, *A.F.C*, *left* side of scan) are seen more clearly in the B-scan. Echo pulses striking the vessel wall at a perpendicular angle produce a detailed image of wall structures as the wall is a strong reflector. In contrast, only a shallow angle between the direction of flowing blood and the beam enables adequate sampling of Doppler information for reliable evaluation of flow

Although all extremity arteries have a triphasic pulsatile flow profile under normal conditions resulting from the high peripheral resistance at rest, different spectral waveforms may be obtained, depending on the territory supplied by the vessel interrogated. A vessel with high-resistance flow like the superficial femoral artery, which mostly supplies skin and subcutaneous tissue but only a small proportion of muscle, has a triphasic waveform with pronounced pulsatility and zero flow in end-diastole

The example shows the femoral bifurcation with the Doppler sample volume placed in the superficial femoral artery (*A.F.S*). Blue indicates arterial flow away from the transducer, red the flow in the superficial femoral vein toward the transducer. The corresponding Doppler tracings illustrate the hemodynamic situation at rest (*left* waveform) and after exercise (*right* waveform). Peak systolic velocity increases from 90 cm/s at rest to 141 cm/s after exercise (10 tiptoe movements)

The increased muscular blood demand during exercise is met by a decrease in peripheral resistance and is reflected in the Doppler waveform by an increase in peak end-diastolic flow velocity from 0 (*left* waveform) to 16 cm/s (*right* waveform)

b Femoral bifurcation (longitudinal scan): The profunda femoris (*A.P.F*) supplying more muscle tissue has a slightly less pulsatile flow but the profile is still triphasic. Peak velocity at rest (*left* waveform) is 77 cm/s in systole and 7 cm/s at end-diastole

After exercise (*right* waveform) peak systolic flow increases to 90 cm/s with end-diastolic velocity doubling to 15 cm/s. The color change in the color duplex image from red, through black, to blue reflects the change in flow direction relative to the ultrasound beam (toward transducer: red; away from transducer: blue). (*A.F.S* superficial femoral artery, *A.F.C* common femoral artery)

c When there is occlusion of the superficial femoral artery (*A.F.S*), the profunda femoris is the main collateral vessel to compensate for this loss. The increased blood flow in the profunda femoris circulation is reflected by a higher flow velocity, which may increase by 50 – 80 % even if there is no stenosis at the origin of the profunda femoris

The Doppler waveform from the profunda femoris artery (*A.P.F*) illustrates peak velocity in case of occlusion of the superficial femoral, which is 145 cm/s in systole and 18 cm/s in diastole. Reversed flow due to eddy currents at the origin of the occluded superficial femoral is displayed in red

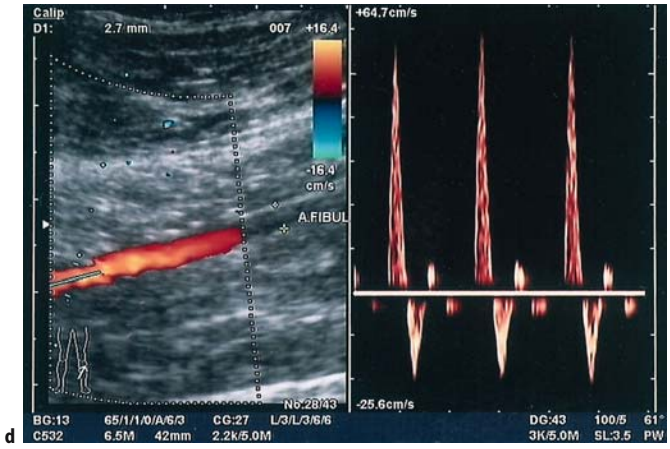

d

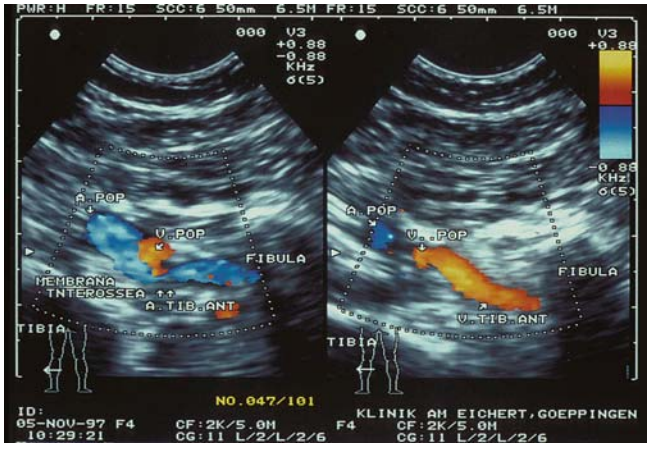

e

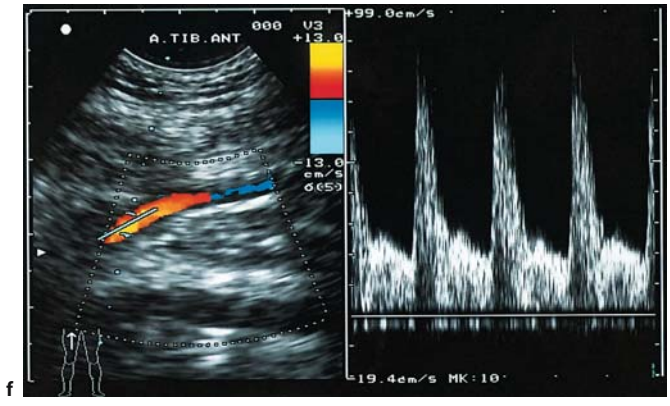

f

(Fig. A 2.2 a–f cont.)

d The leg arteries have a triphasic waveform down into the periphery as illustrated here by the normal fibular artery. The artery has a diameter of 2.7 mm

Sonoanatomy of the origin of the anterior tibial artery

e The popliteal artery gives off the anterior tibial artery, which courses anteriorly to pierce the interosseous membrane in front of which it descends, initially taking a course close to the fibula. The scan depicts the anterior tibial artery insonated from a posterior transducer position (popliteal fossa) in blue (flow away from transducer) downstream of its origin from the popliteal artery (*A.POP*) as it pierces the interosseous membrane (hyperechoic structure between tibia and fibula). With the transducer slightly angled, the anterior tibial vein is depicted in blue (flow toward transducer) along its course parallel to the artery and as it empties into the popliteal vein

Hyperemia

f Peripheral inflammation is another factor affecting the character of the Doppler waveform besides an increased flow resulting from exercise-induced hyperemia or collateral function of a vessel. In the case depicted here, a phlegmon of the foot results in a monophasic waveform with reduced pulsatility and a rather high end-diastolic flow velocity of 22 cm/s. The fact that the steep systolic upslope is preserved excludes an upstream stenosis. In contrast, the normal anterior tibial artery has a triphasic flow profile with short diastolic forward flow after the incisure and zero end-diastolic flow (cf. Fig. A 2.2 d)

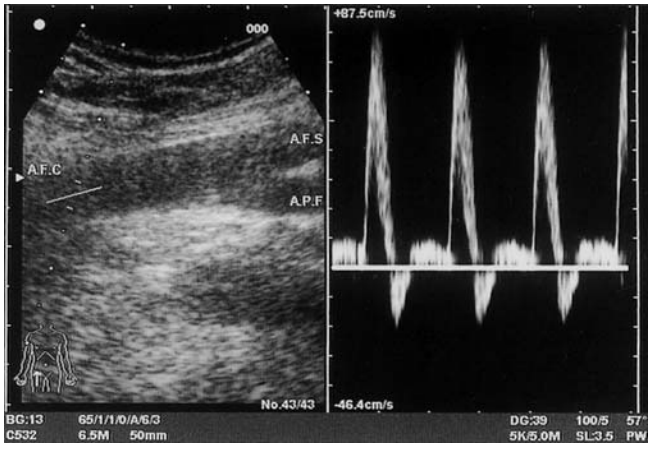

a

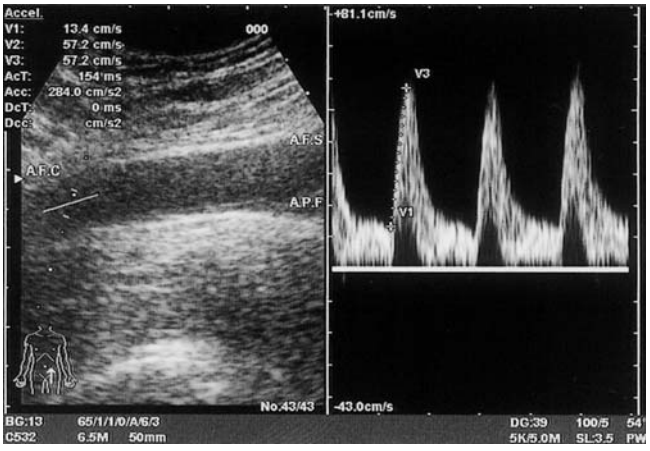

b

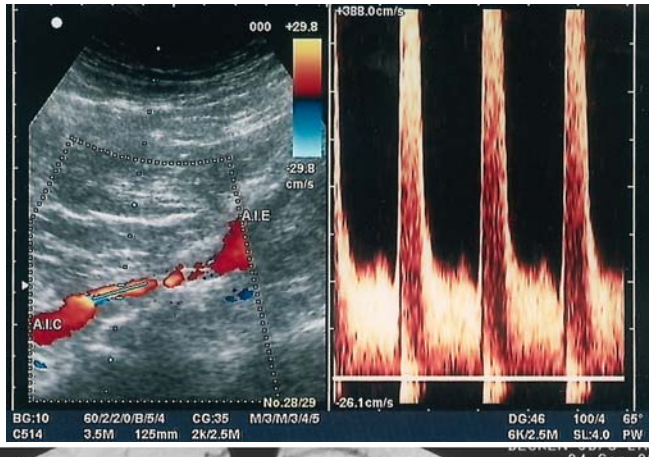

c

Fig. A 2.3 a–d
Pelvic artery stenosis

a In evaluating a patient with suspected pelvic artery obstruction, the examiner first obtains Doppler tracings from both common femoral arteries to compare these in terms of triphasic flow, steep systolic upslope, and magnitude of peak systolic velocity. Reliable Doppler shift analysis requires an insonation angle below 60°. In this example, the angle is 50° on the right and 54° on the left. The waveform from the right groin shows triphasic flow with a systolic upslope and a peak systolic velocity of over 80 cm/s

b The Doppler waveform from the left common femoral artery illustrates postocclusive flow with a monophasic profile, reduced peak systolic velocity (57 cm/s), and delayed systolic rise

c Monophasic flow profile caused by a high-grade stenosis of the common iliac artery (*A.I.C*) due to plaque, mainly of the posterior wall. Criteria for a stenosis are aliasing in the color duplex image and a peak systolic flow velocity of over 5 m/s in the Doppler frequency spectrum

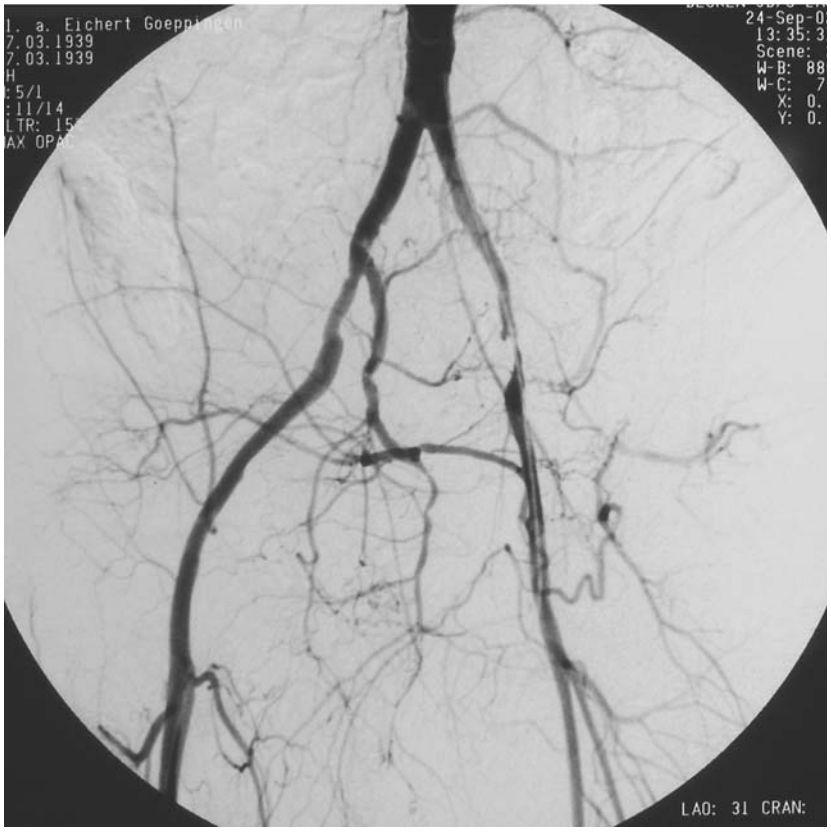

d

d Angiography demonstrates the high-grade iliac stenosis as a filling defect in the lumen

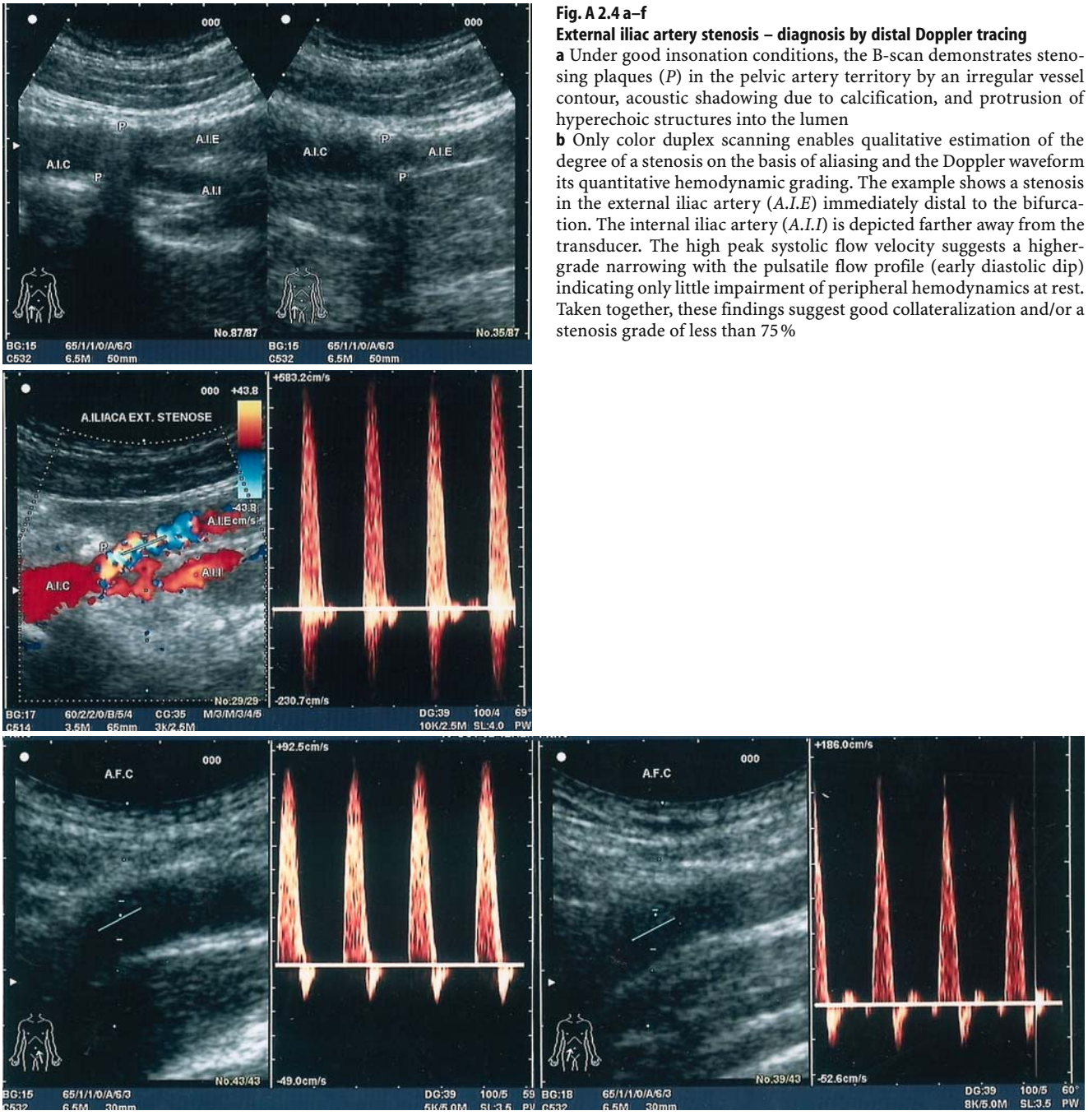

Fig. A 2.4 a–f
External iliac artery stenosis – diagnosis by distal Doppler tracing

a Under good insonation conditions, the B-scan demonstrates stenosing plaques (*P*) in the pelvic artery territory by an irregular vessel contour, acoustic shadowing due to calcification, and protrusion of hyperechoic structures into the lumen

b Only color duplex scanning enables qualitative estimation of the degree of a stenosis on the basis of aliasing and the Doppler waveform its quantitative hemodynamic grading. The example shows a stenosis in the external iliac artery (*A.I.E*) immediately distal to the bifurcation. The internal iliac artery (*A.I.I*) is depicted farther away from the transducer. The high peak systolic flow velocity suggests a higher-grade narrowing with the pulsatile flow profile (early diastolic dip) indicating only little impairment of peripheral hemodynamics at rest. Taken together, these findings suggest good collateralization and/or a stenosis grade of less than 75 %

c Such stenoses will be noted in the Doppler waveforms from the groin and a more peripheral site only if the examination is performed carefully and the Doppler information is acquired with an angle as small as possible and a meticulous spectrum analysis is done with comparison of both sides. In this case, the waveform from the stenotic side shows an early diastolic retrograde flow component, indicting that high peripheral resistance is preserved, while peak systolic velocity is markedly decreased compared to the unaffected side (80 cm/s versus 150 cm/s). Moreover, the waveform from the unaffected side displays the preserved diastolic flow resulting from the windkessel effect of the aorta

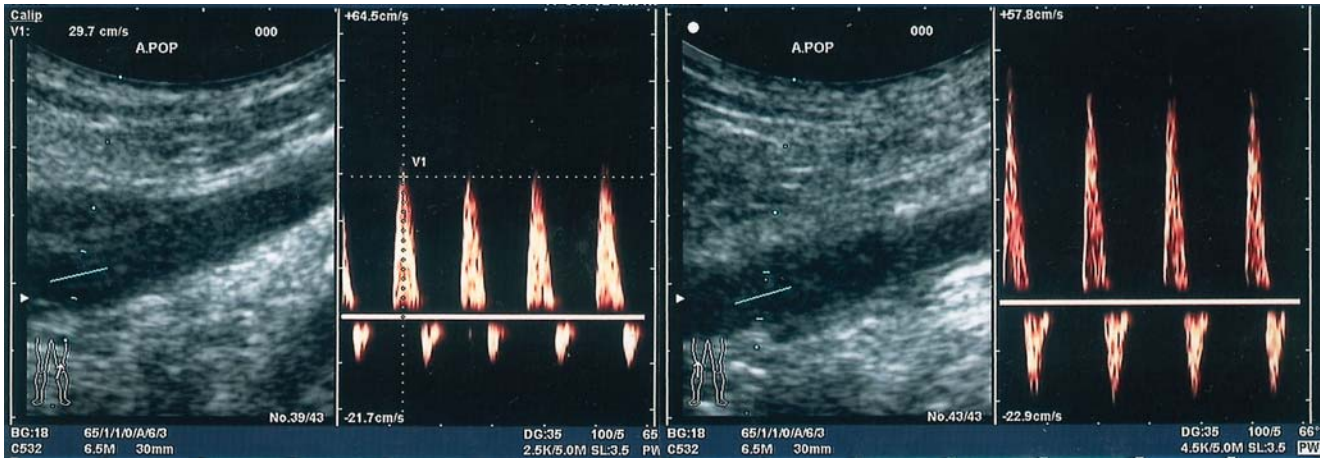

d

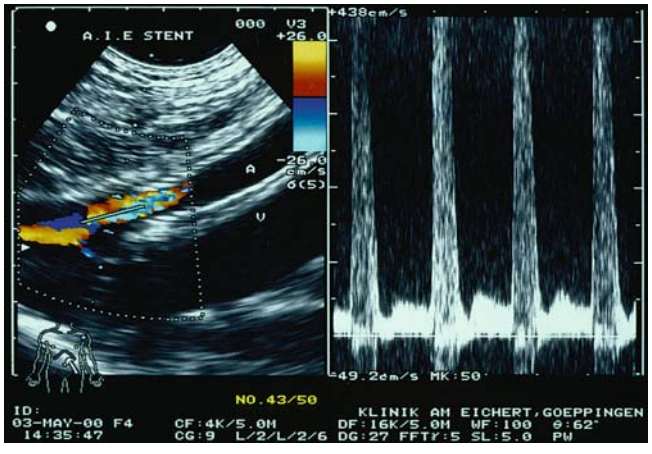

e

(Fig. A 2.4 cont.)

d The upstream stenosis on the left is likewise apparent in the popliteal waveform as a dampened flow signal that is also audible and a post-occlusive peak systolic velocity of 29 cm/s versus 45 cm/s on the non-stenotic side

Another way of demonstrating a stenosis is to sample the Doppler information after exercise: After 10 knee bends, the Doppler waveforms from the groin and popliteal artery are monophasic on both sides (due to exercise-induced peripheral widening). On the unaffected side, the waveform returns to its normal triphasic shape within a minute. A delayed return to this normal profile indicates a stenosis, which prevents an adequate blood supply during and after exercise. The length of the delay varies with the stenosis grade and collateralization

e Status after dilatation and stenting of a proximal external iliac artery stenosis with a a high-grade stenosis at the proximal end of the stent (aliasing, peak systolic flow above 4 m/s). The meshlike structure enables good estimation of the extent of the stent

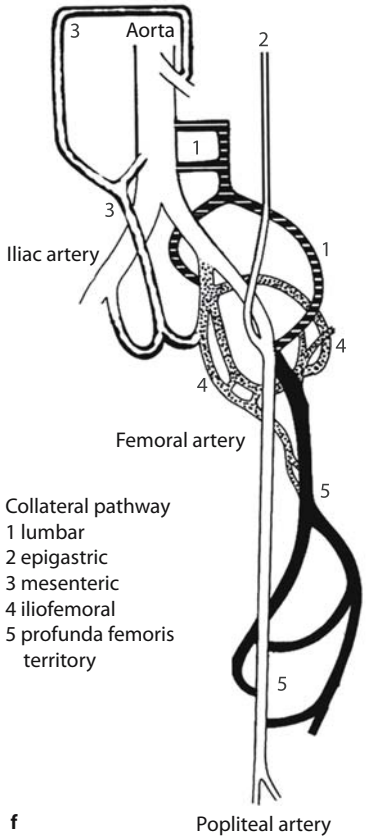

f

Collateral pathways in stenosis and occlusion of the aortoiliac and iliofemoral territories

f The better the collateralization, the less pronounced the postocclusive changes of the Doppler waveform

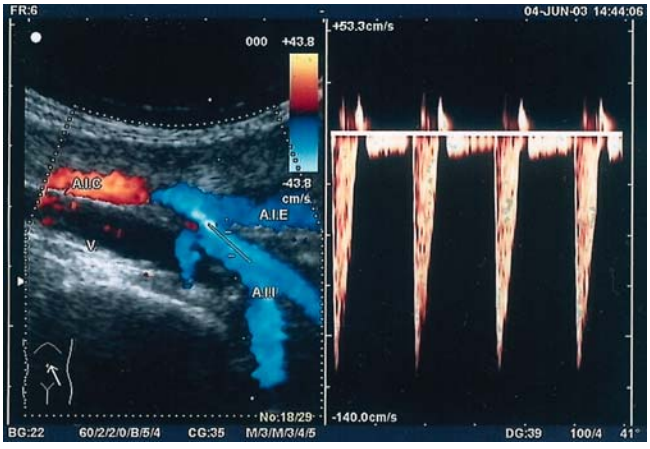

a

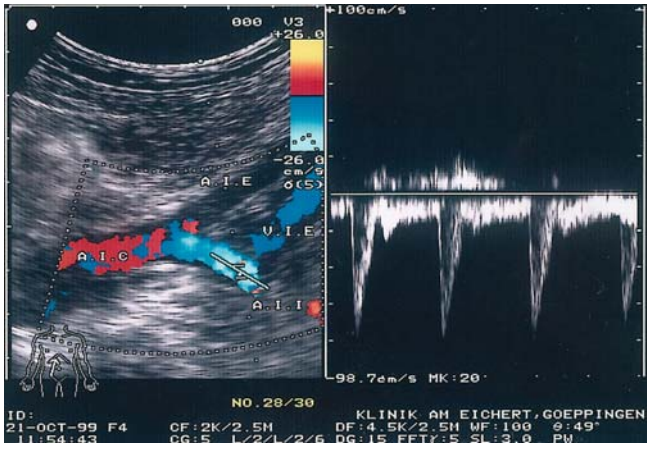

b

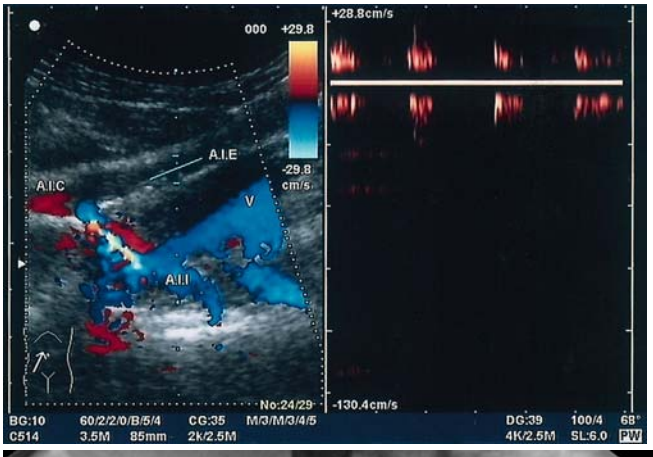

c

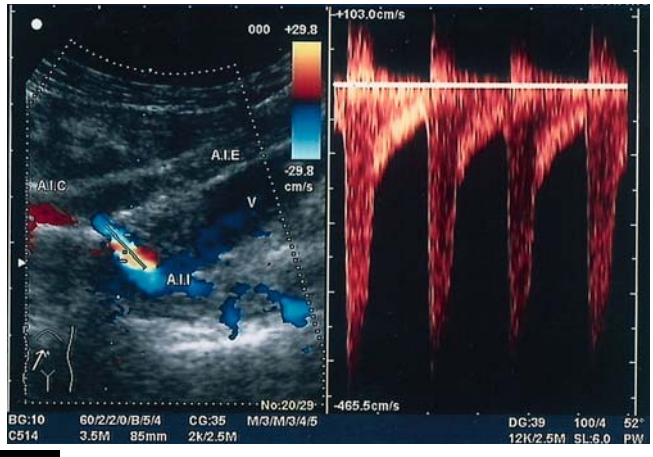

d

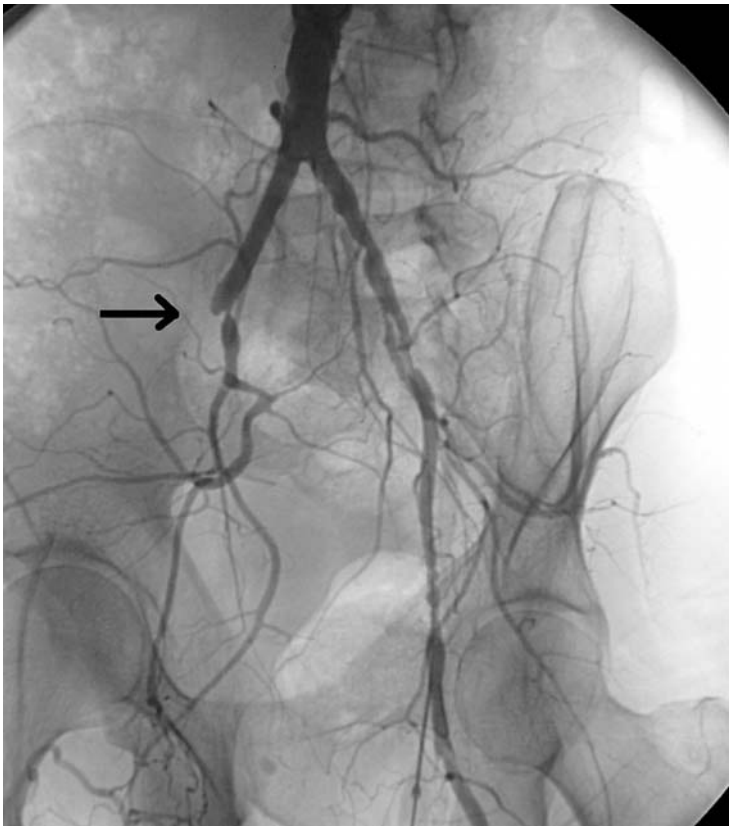

e

Fig. A 2.5 a–h
Iliac artery – stenosis – occlusion – collateral pathways
a The iliac bifurcation with the origin of the internal iliac artery (*A.I.I*) is situated at the deepest point of the true pelvis. The internal iliac courses posteriorly (blue, away from transducer, toward periphery). The waveform shows a pulsatile profile but with diastolic flow because the internal iliac empties into the pelvic vessels. The color change from red to blue in the bifurcation is due to the changed flow direction relative to the ultrasound beam. With the high pulse repetition frequency selected to depict fast arterial flow, no flow signals are obtained from the iliac vein (*V*) posterior to the artery. (*A.I.E* external iliac artery, *A.I.C* common iliac artery)
b Exact localization of an occlusion is crucial for planning a bypass procedure. In case of external iliac artery occlusion (*A.I.E*), the internal iliac artery (*A.I.I*; blue, away from transducer) is an important collateral pathway
c, d 54-year-old patient with intermittent claudication with a short walking distance and impotence (see also Ch. 7) due to external iliac artery occlusion (Doppler waveform with wall pulsation but no flow signals) and concomitant high-grade internal iliac stenosis (aliasing and peak systolic velocity of 4 m/s)
e Oblique angiographic projection depicting right-sided occlusion of the external iliac artery and internal iliac stenosis. The internal iliac artery stenosis on the left is obscured by superimposed structures

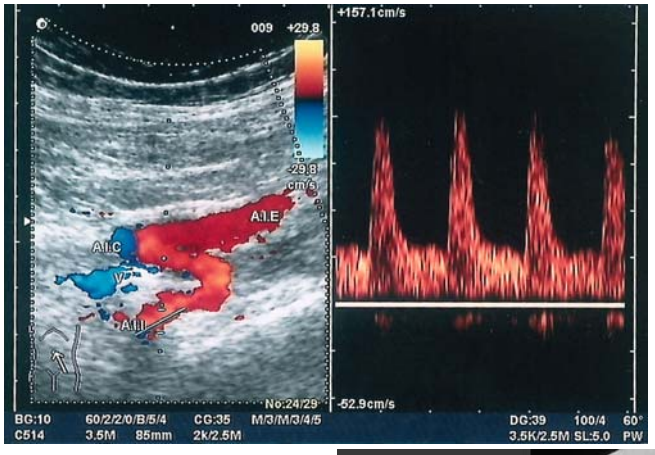

f

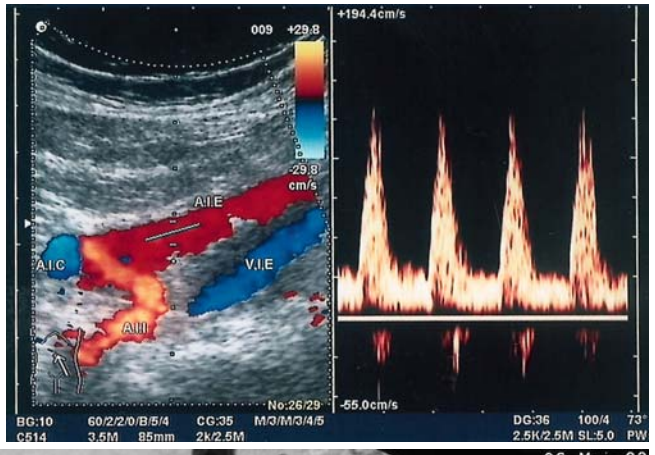

g

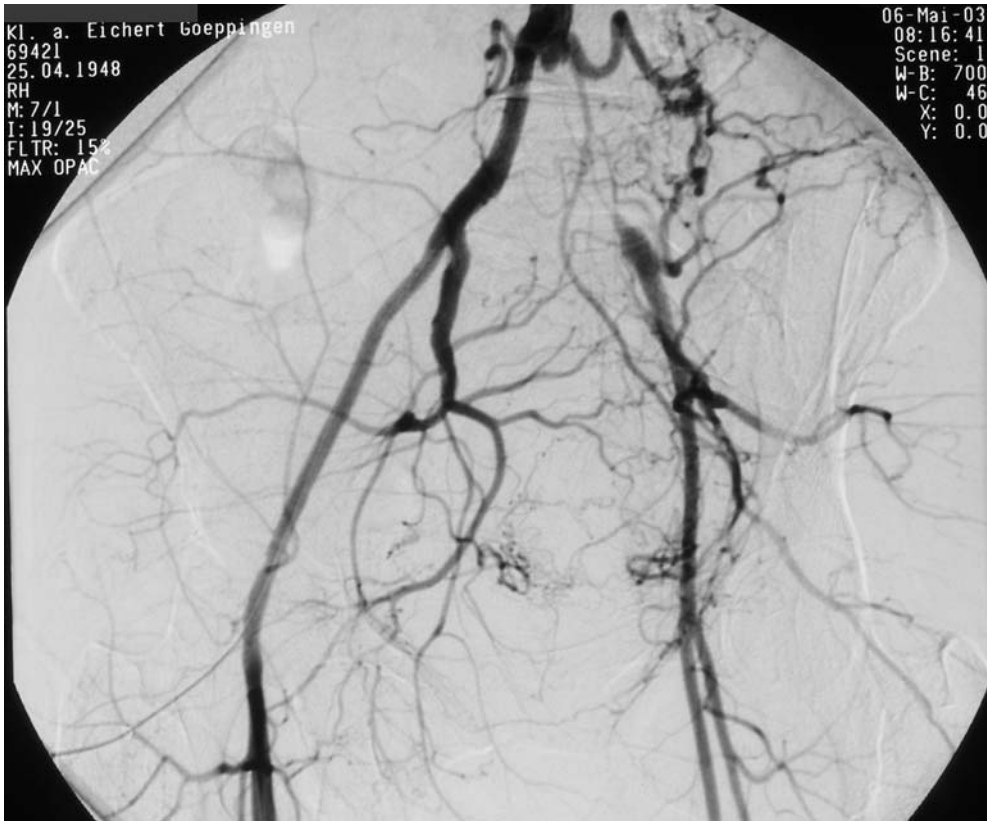

h

(Fig. A 2.5 cont.)

f In common iliac artery occlusion, the internal iliac fills the external iliac and shows retrograde flow (red, toward transducer). No flow signal in the common iliac artery (*A.I.C*)

g The refilled external iliac artery (*A.I.E*) is depicted with normal flow toward the periphery (red). The waveform is monophasic, corresponding to postocclusive flow

h Angiography showing common iliac artery occlusion

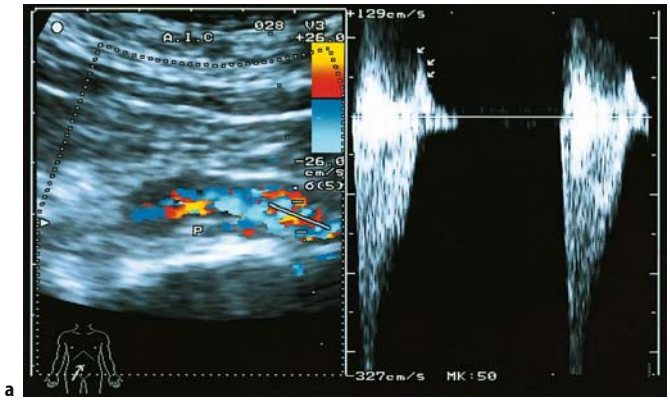

a

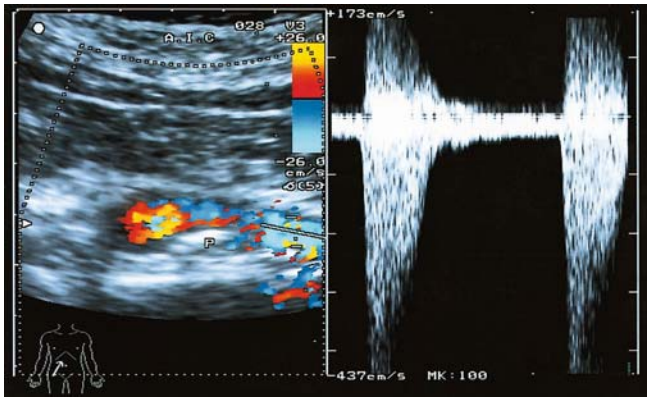

b

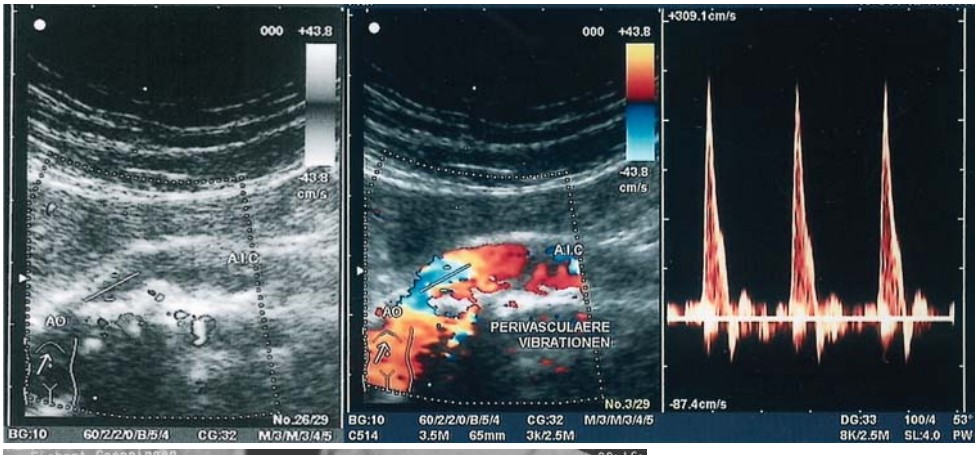

c

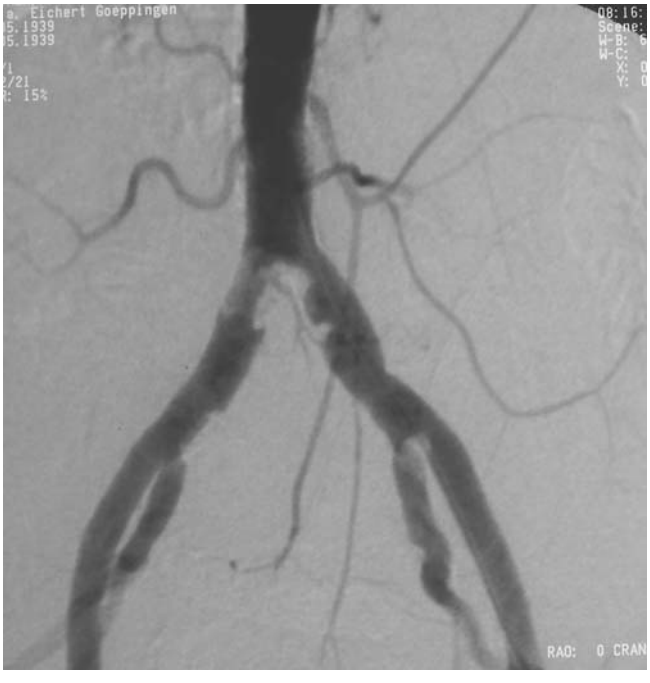

d

Fig. A 2.6 a–d
Common iliac artery stenosis
a Morphologic evaluation of the pelvic territory is frequently precluded by scattering structures and the great scanning depth necessitating the use of low-frequency transducers with a poor resolution. Therefore, only hemodynamic parameters can be determined to diagnose a stenosis. In the case presented, a stenosis of about 60% in the mid-portion of the common iliac artery produces aliasing in the color flow image. In the Doppler tracing, peak systolic velocity is increased to 330 cm/s while pulsatility is preserved. The early diastolic incisure (*arrows*) is obscured by retrograde flow during systole (turbulence)
b The decreased peripheral resistance shortly after exercise induces an increase in flow velocity (440 cm/s in systole and 30 cm/s at end diastole). The waveform and the reduced pulsatility suggest a high-grade stenosis. The increased arterial blood flow resulting from the higher peripheral demand leads to overestimation of the degree of stenosis. The rather low overall diastolic flow is, in this case, due to diabetes-related vascular damage. This example underlines the importance of 3 to 5 minutes of rest prior to stenosis grading in order to prevent overestimation
c Stenoses of the iliac and common femoral arteries are often more difficult to assess by angiography in anteroposterior projection because plaques of the posterior wall may impair evaluation of the hemodynamic significance. The gray-scale scan depicts the posterior wall plaque with acoustic shadowing. Aliasing in the color duplex image and the Doppler tracing with a peak systolic velocity of 250 cm/s but preserved triphasic flow suggest a stenosis becoming hemodynamically significant
d Angiography demonstrating wall irregularities of the common iliac artery and luminal narrowing at its origin

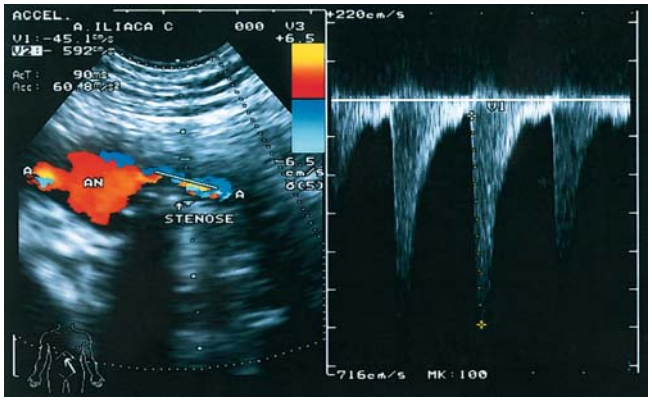

a

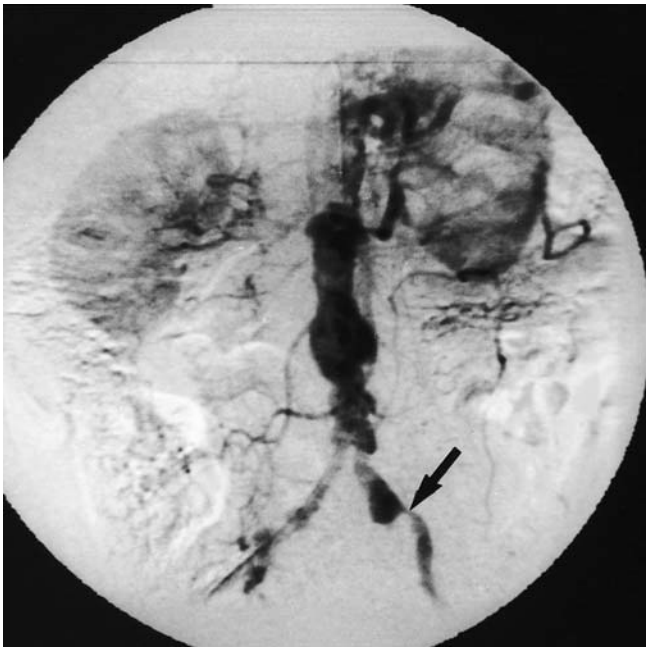

b

Fig. A 2.7 a, b
Iliac artery aneurysm

a The common iliac artery (*left* side of scan) shows circumscribed dilatation at its origin from the aorta (red, flow toward transducer). The aneurysm (*AN*) has a diameter of 2.5 cm and contains no thrombus. There is aliasing in the color duplex scan distal to the aneurysm. Along its further course, the common iliac artery is depicted in blue indicating flow away from the transducer. The peak velocity is 590 cm/s during systole and 45 cm/s at end-diastole. These velocities, together with the monophasic flow profile, indicate a high-grade stenosis at the distal end of the aneurysm

b Angiography: Aortic aneurysm and stenosis at the origin of the common iliac artery (*arrow*)

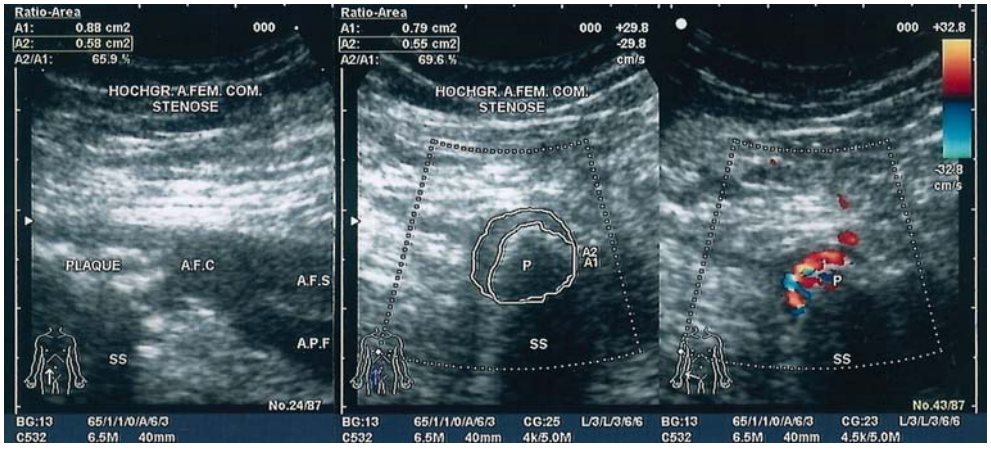

a

Fig. A 2.8 a–d
Common femoral artery stenosis

a In the common femoral artery, stenosing plaques chiefly affect the posterior wall. The B-scan depicts the extent and morphology of the plaque with acoustic shadowing (*SS*). The transverse scans (B-scan in the *middle*, color duplex scan on the *right*) illustrate the problem of estimating the degree of stenosis on the basis of cross-sectional area reduction (vessel cross-section/plaque cross-section; planimetric measurement: 69.9 %). Acoustic shadowing impairs visualization of the vessel and plaque contour in the B-mode and thus makes it difficult to precisely differentiate the atherosclerotic wall thickening from the patent lumen. In the color duplex mode, perivascular vibration artifacts and poor color resolution with interpolation lead to "color overflow" beyond the patent lumen

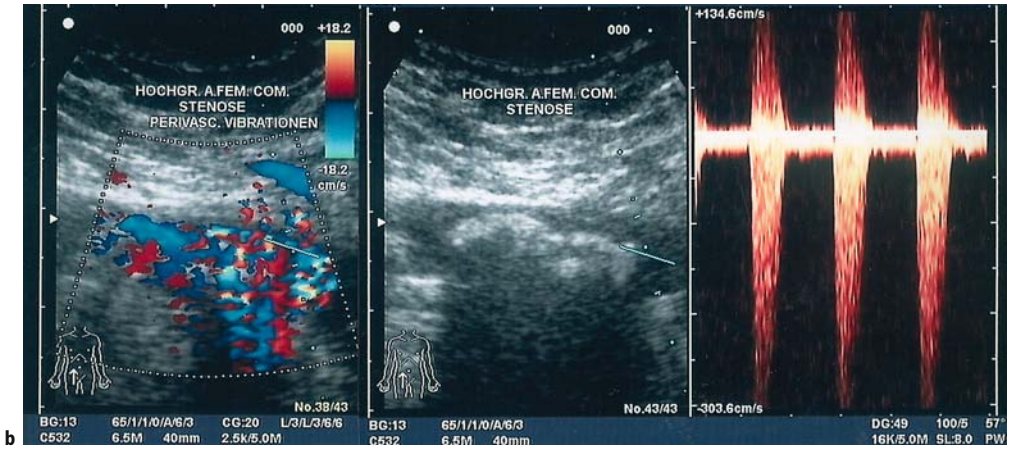

b

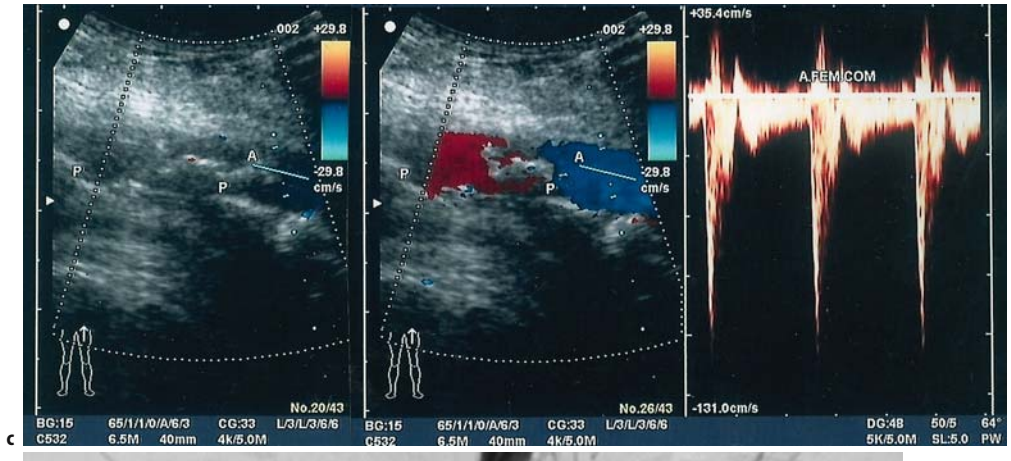

c

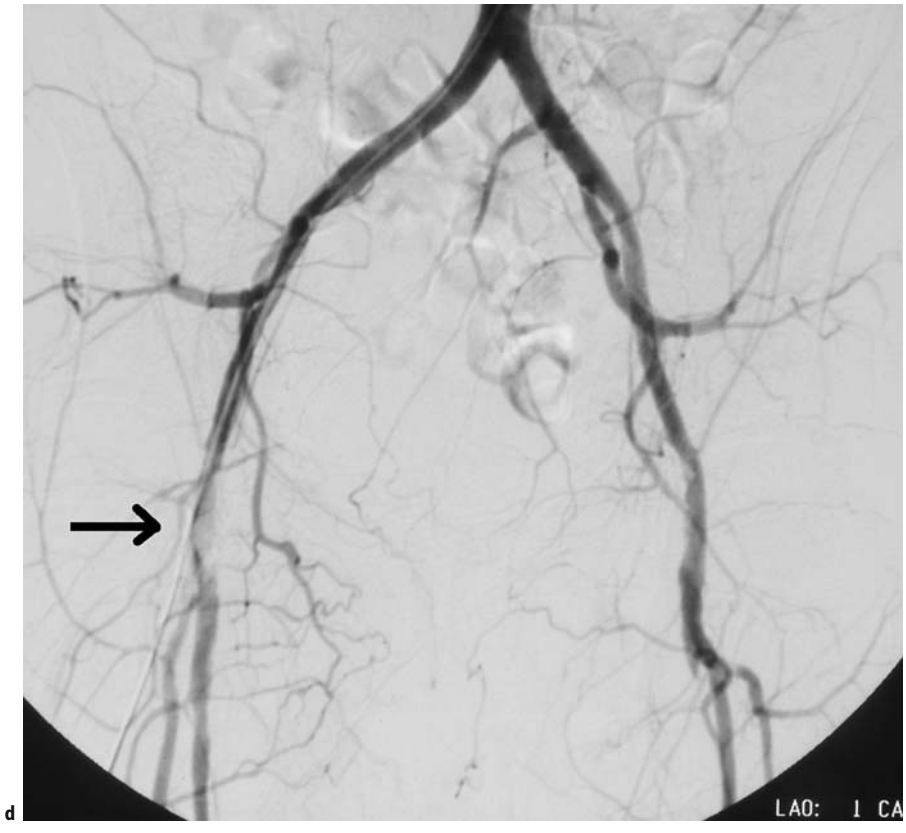

d

(Fig. A 2.8 cont.)
b Perivascular vibration artifacts may prohibit the differentiation of the patent lumen from plaque by color duplex scanning in large vessels with high-grade stenosis *(left section*: longitudinal color scan; *middle section*: corresponding B-scan). The combination of plaque localization in the B-scan and color duplex visualization of the stenosis jet facilitates placement of the sample volume in the jet for recording of a representative Doppler spectrum. Here, peak systolic flow over 3.5 m/s, pronounced turbulence, and monophasic flow suggest high-grade stenosis
c B-scan on the *left* and color duplex scan in the *middle* demonstrate a similar situation in the common femoral artery on the contralateral side with plaques protruding into the vessel lumen. However, the Doppler tracing fails to demonstrate a hemodynamic effect (triphasic flow with normal waveform and no increase in peak systolic velocity)
d Angiography depicting plaques with luminal narrowing of the common femoral artery, which is more pronounced on the right side

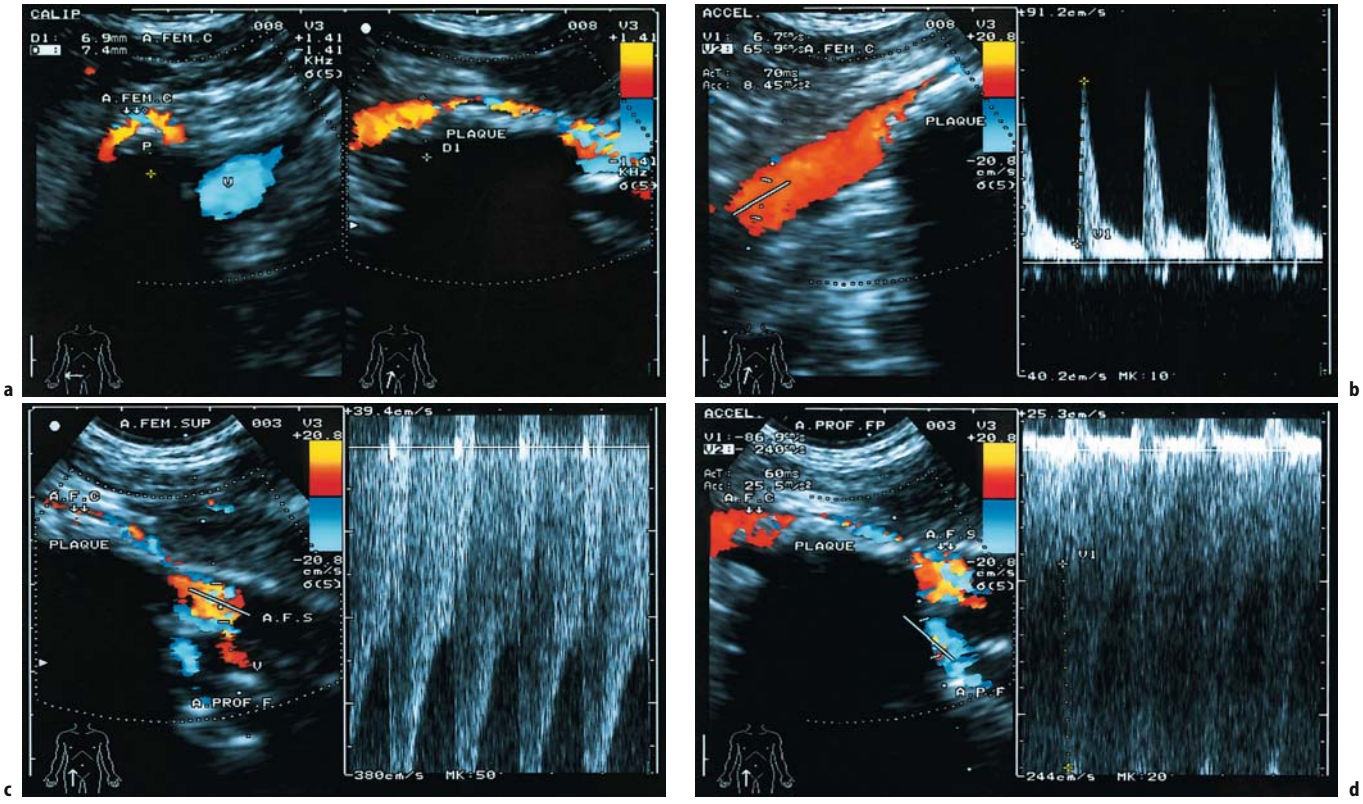

Fig. A 2.9 a–h
Common femoral artery stenosis

a The high-grade stenosis of the common femoral artery involves the bifurcation and is caused by a calcified plaque (*P*) with posterior shadowing and protrusion into the lumen. Transverse view of the artery on the *left* and longitudinal view on the *right*. The common femoral vein (*V*) is shown in blue on the medial side of the artery. The high hemodynamic grade of the stenosis is reflected by the color change from red, through yellow, to blue (aliasing)

b The effects of the high-grade stenosis on the prestenotic waveform (pulsatility) in the external iliac artery are chiefly caused by the collaterals arising upstream of the stenosis and by peripheral dilatation

c The Doppler waveform from the proximal superficial femoral artery (*A.F.S*) immediately distal to the plaque reflects the high-grade stenosis of the bifurcation. The peak systolic velocity is cut off by aliasing. It is over 380 cm/s with an end-diastolic velocity of over 200 cm/s. Posterior to the artery, the vein (*V*) is shown in red and the profunda femoris in blue (*A.PROF.F*)

d Acoustic shadowing due to the calcified plaque makes it very difficult to assess the stenosis involving the origin of the profunda femoris both in the gray-scale scan and the color image. A very high gain is required to obtain a Doppler tracing with a stenosis signal. The monophasic flow has a peak systolic velocity of 240 cm/s and end-diastolic velocity of 86 cm/s

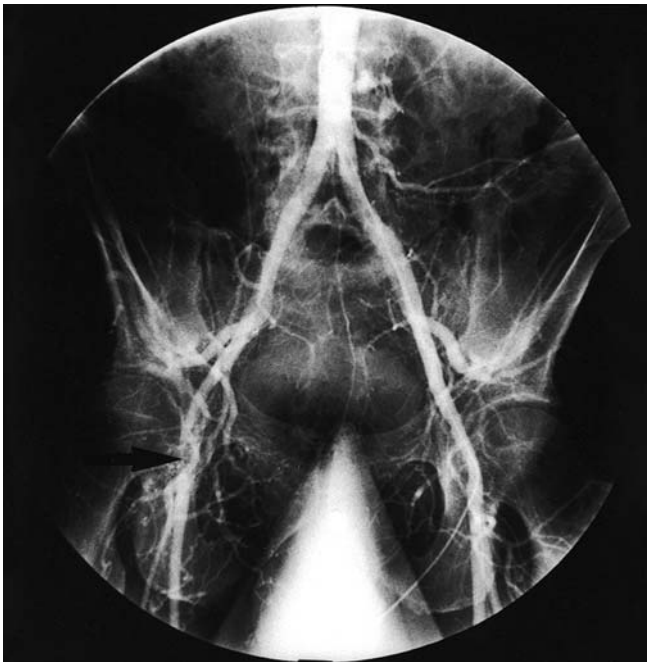

e

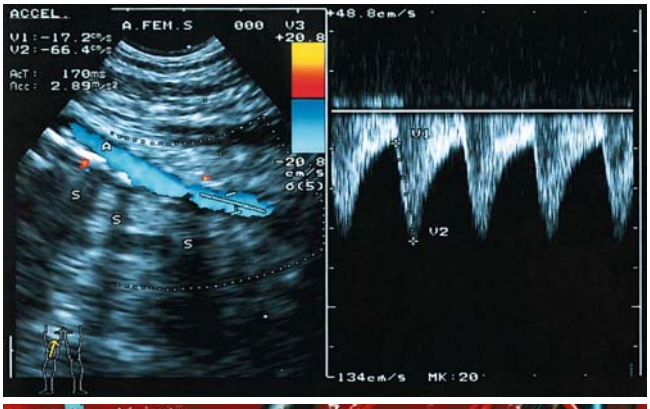

f

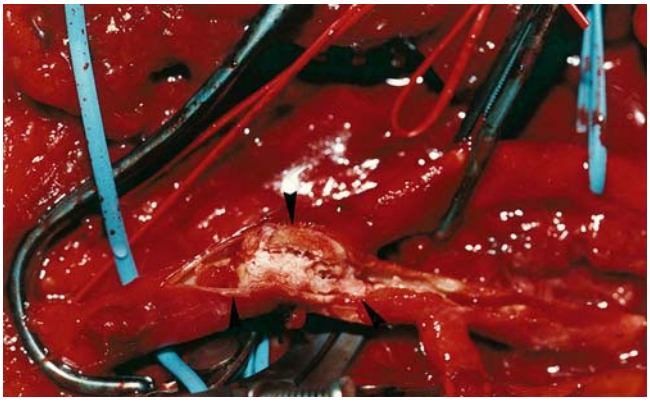

g

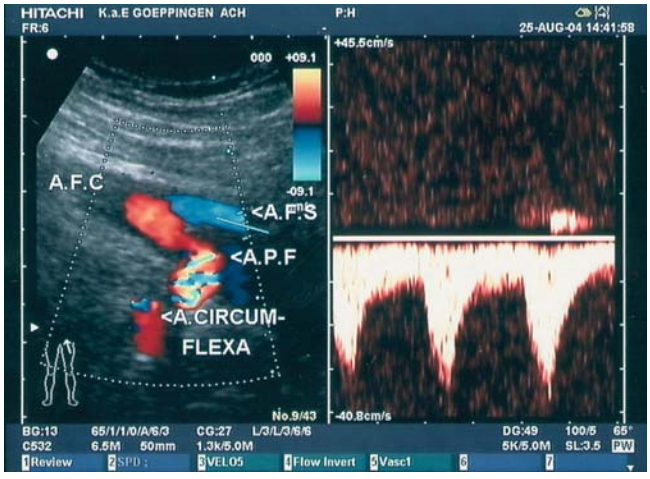

h

(Fig. A 2.9 cont.)

e Angiography: The high-grade stenosis of the common femoral artery on the right has led to extensive collateralization compared to the unaffected side. The stenosis caused by the posterior wall plaque is difficult to grade in the anteroposterior projection alone and would require a second imaging plane

f The flow profile of the superficial femoral artery has the typical poststenotic appearance with markedly reduced pulsatility, delayed and reduced systolic upslope, and monophasic flow. The gray-scale scan on the *left* depicts the nonstenotic atherosclerotic changes as hyperechoic plaques with acoustic shadowing (*S*)

g With duplex scanning ruling out pelvic artery stenosis and demonstrating patent vessels down to the popliteal artery, the planned TEA with patching of the femoral bifurcation could be performed without preoperative angiography. As illustrated by this example, angiography does not add any relevant therapeutic information and merely serves to document the findings

The intraoperative site confirms the high-grade stenosis caused by calcified plaques (*arrowheads*). The artery is exposed from the common femoral to the profunda femoris. The origin of the superficial femoral artery with the lumen still constricted by the plaque is clamped off with straight forceps (*right side* of photograph). A round clamp is fixed around the proximal common femoral artery

Collateral arteries in case of occlusion of the Arteria femoralis communis

h Occlusion (absence of flow signals) of the common femoral artery (*A.F.C*) with refilling of the superficial femoral artery (*A.F.S*; forward flow coded in blue, away from transducer) through the profunda femoris artery (*A.P.F*), which exhibits backward flow at its origin (red, toward transducer) and is supplied by the femoral circumflex artery. The flow profile is postocclusive (monophasic waveform with delayed systolic upstroke)

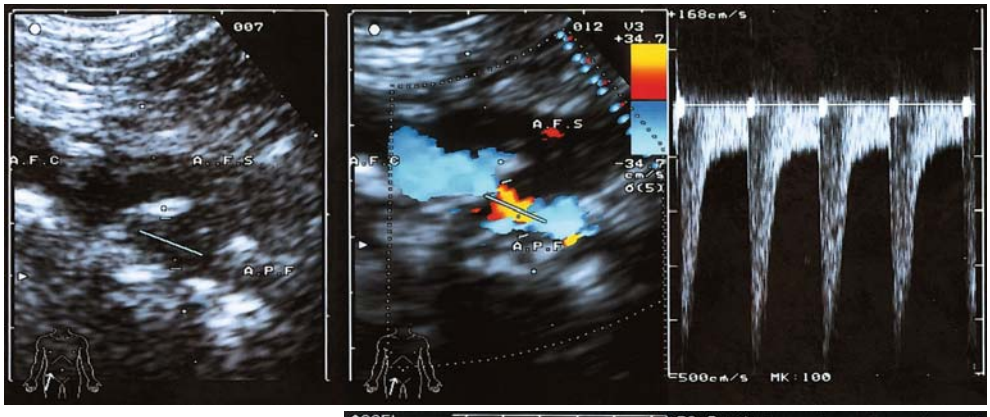

a

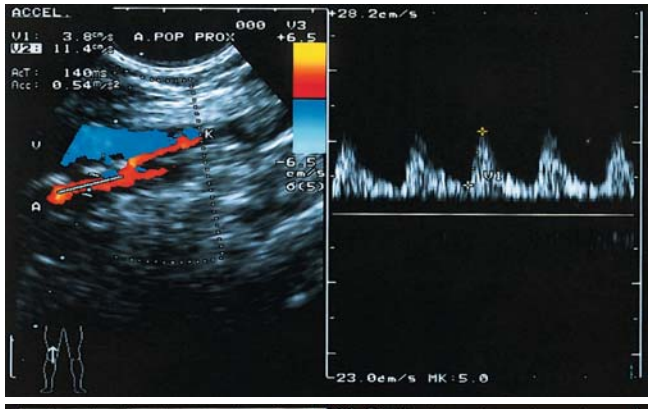

b

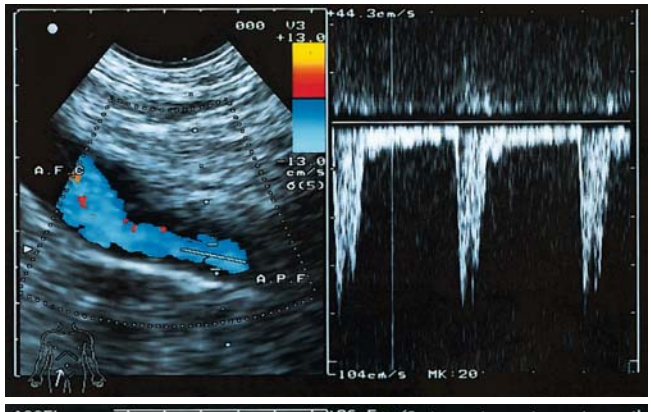

c

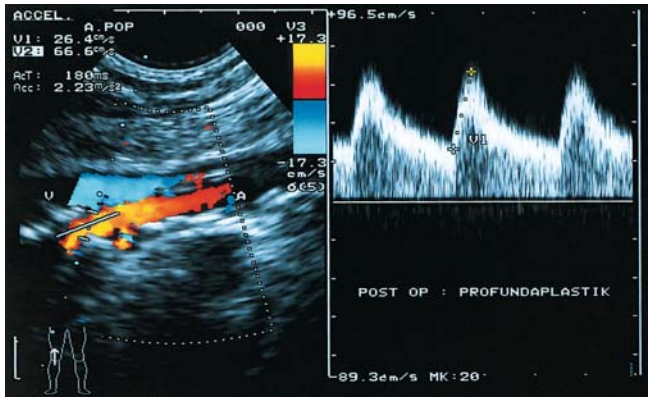

d

Fig. A 2.10 a–d
Stenosis at origin of profunda femoris artery – TEA

a High-grade stenosis of the profunda femoris artery (*A.P.F*) with a monophasic flow profile and a peak velocity of 480 cm/s in systole and 90 cm/s in end-diastole. In the color duplex image (*middle section*), the flow acceleration produces aliasing (color change through yellow). The superficial femoral artery (*A.F.S*) is occluded; only a residual segment about 1 cm in length is patent at the end but the slow flow is not detected with the high PRF used and only some retrograde flow (red) is recorded. The gray-scale scan (*left section*) depicts plaques of different echogenicity with marked wall irregularities. Some of the plaques produce posterior acoustic shadowing. (*A.F.C* common femoral artery)

b As a result of the proximal occlusion of the superficial femoral artery and the high-grade stenosis in the main collateral (profunda femoris), the blood volume in the refilled popliteal artery is markedly reduced. This is reflected by the small lumen of the popliteal artery with chronic narrowing and the markedly reduced flow velocity in the Doppler waveform (11 cm/s peak systolic flow and 3 cm/s end-diastolic flow). The vessel moves out of the scan plane. When insonated from the popliteal fossa, a collateral arising from the posterior aspect is seen (*K*). In addition, the popliteal vein (*V*) is depicted in blue posterior to the popliteal artery (*A*)

c The stenosis is treated by femoral profundaplasty with severing of the ipsilateral superficial femoral. Following the intervention, the profunda femoris artery (*A.P.F*) shows a peak velocity in the area of the patch of 80 cm/s during systole and 10 cm/s at end-diastole. The diastolic flow component and the reduced pulsatility are due to collateral flow in the profunda femoris and the difference in wall elasticity in the area of the patch. (*A.F.C* common femoral artery)

d The improved perfusion following profunda femoris repair with persistent superficial femoral occlusion is reflected in the waveform obtained from the refilled femoral artery at about the same site as the preoperative waveform presented above, now showing a peak velocity of 66 cm/s in systole and 26 cm/s at end-diastole. The postocclusive flow character is due to persistent superficial femoral occlusion

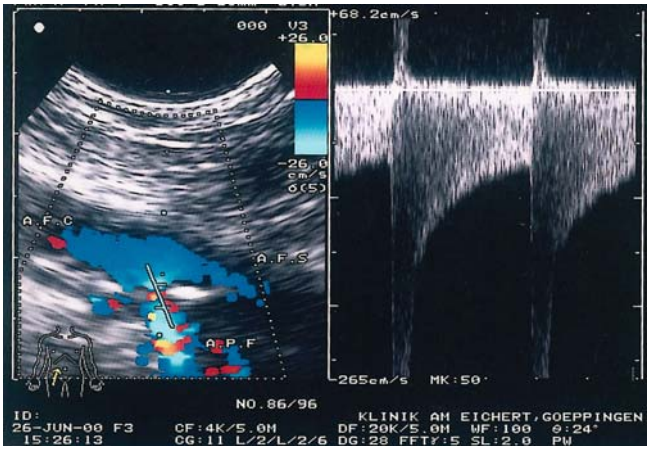

a

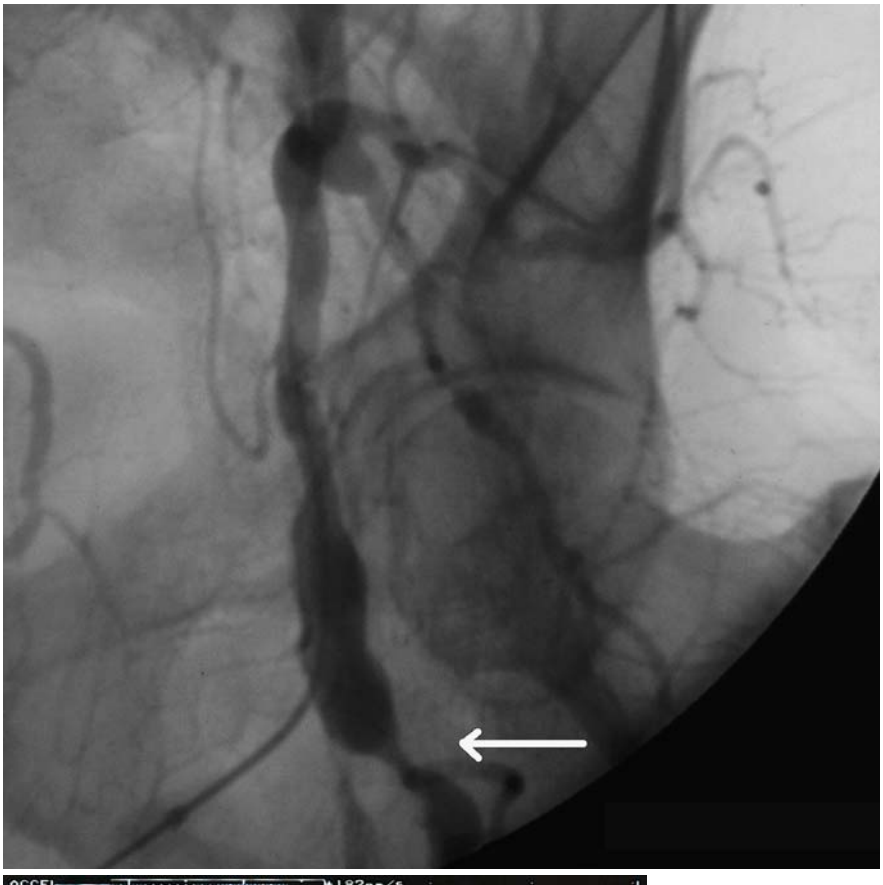

b

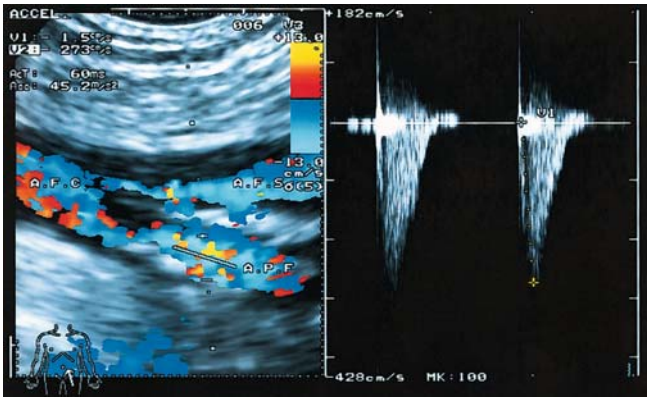

c

Fig. A 2.11 a, b
Stenosis at origin of profunda femoris artery (recurrence)
a Duplex ultrasound has become the method of choice for diagnosing and grading stenoses of the profunda femoris artery, as angiography in the anteroposterior projection is limited in estimating the degree of stenosis in the femoral bifurcation by overlying vessels or variants in the course of the artery and stenoses caused by posterior wall plaque. In this patient with prior TEA of the common femoral artery, aliasing in the color duplex scan and a peak systolic velocity of over 3 m/s with a monophasic flow profile indicate recurrent high-grade stenosis
b The corresponding angiogram depicts the stenosing plaque at the origin of the profunda femoris. Recurrent stenosis and wide lumen of the common femoral artery following TEA

Stenosis at origin of profunda femoris artery in diabetes
c The plaque has a highly irregular surface, which leads to very turbulent flow with backward flow components, reflected both in the color scan and in the Doppler waveform. However, in this patient with diabetes, the failure to obtain flow signals at end-diastole is due to the reduced wall elasticity caused by medial sclerosis. The superficial femoral artery (*A.F.S*) is occluded 5 cm distal to its origin from the common femoral artery (*A.F.C*)

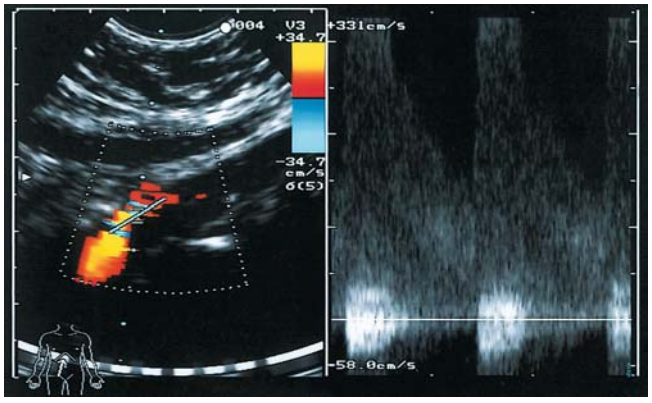

a

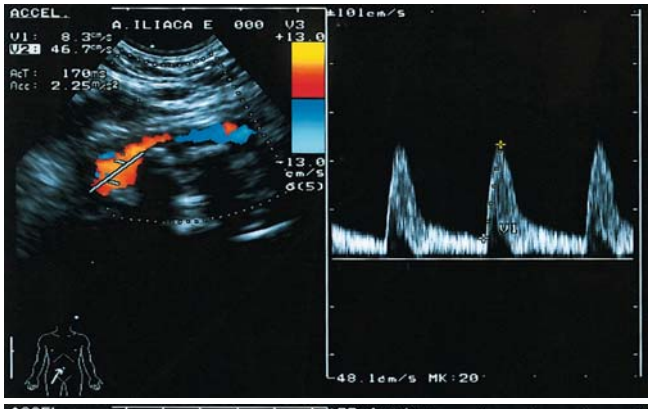

b

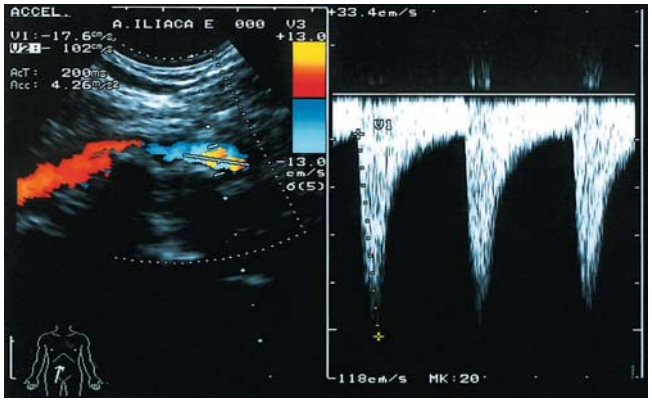

c

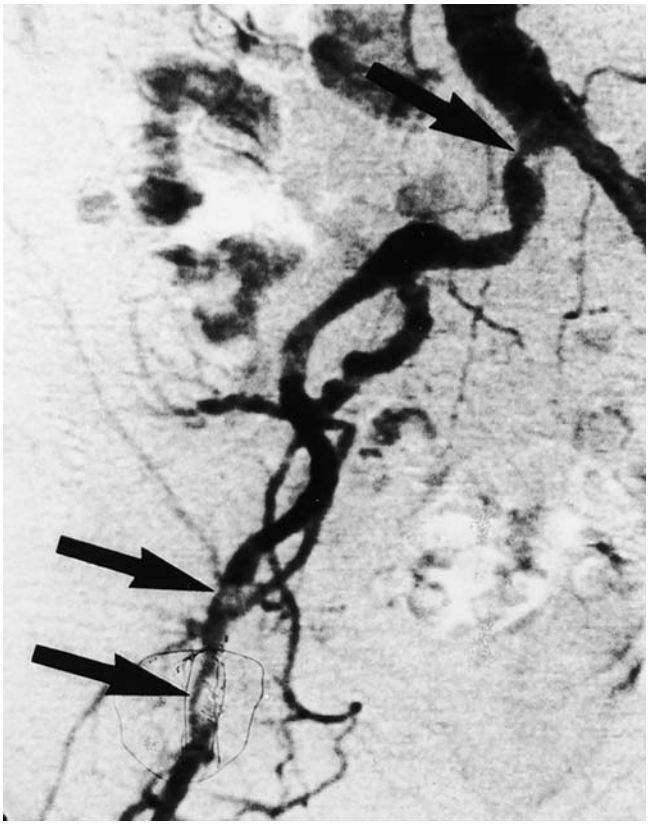

d

Fig. A 2.12 a–f
Multilevel obstruction

a In cases of sequential stenoses, threshold velocities become unreliable as grading criteria. Grading of a subsequent stenosis must take into account the decrease in peak velocity resulting from the poststenotic pressure drop after the preceding stenosis. In these cases, a stenosis is considered hemodynamically significant if there is a 100% increase in peak systolic velocity relative to the velocity in the same vessel upstream of the stenosis

Here, the high-grade stenosis at the origin of the common iliac artery is demonstrated on the oblique color duplex scan by aliasing and by flow acceleration in the Doppler waveform. Due to aliasing, the peak systolic velocity is cut off and must be interpolated (about 4.5 m/s). The simplified Bernoulli equation, $P = 4 \cdot V_{2max}$, yields a maximum pressure drop of 81 mm Hg over the stenosis, resulting in a poststenotic decrease in systolic velocity

b The poststenotic peak systolic flow velocity in the external iliac artery is 46 cm/s. The sample volume is placed upstream of a stenosing plaque in the distal external iliac artery

c Because of the plaque, systolic flow velocity is increased to 102 cm/s, corresponding to an increase by a factor of 2.2 compared to the prestenotic velocity. This increase makes the stenosis hemodynamically significant although the absolute peak systolic velocity is still in the normal range of the distal external iliac at the junction with the common iliac. Flow upstream and downstream of the stenosis is monophasic; this is due to the pressure drop over the common iliac artery stenosis

d Angiography: Poor visualization of the stenosis due to posterior wall plaque in the distal external iliac artery at the junction with the common iliac artery. Only subtle brightening of opacification is seen (*middle arrow*). The common iliac artery stenosis is indicated by the *proximal arrow* and a stenosis of the common femoral by the *distal arrow*

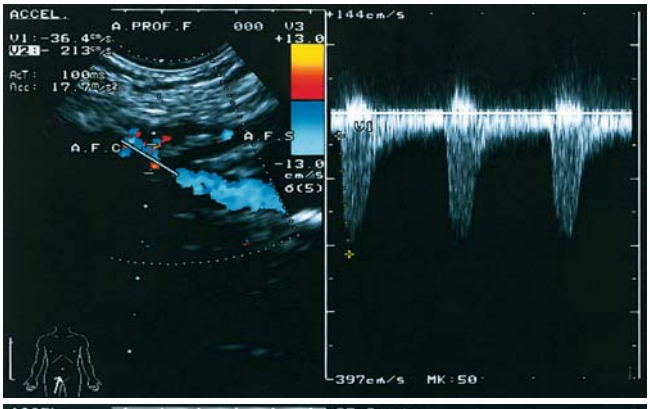

e

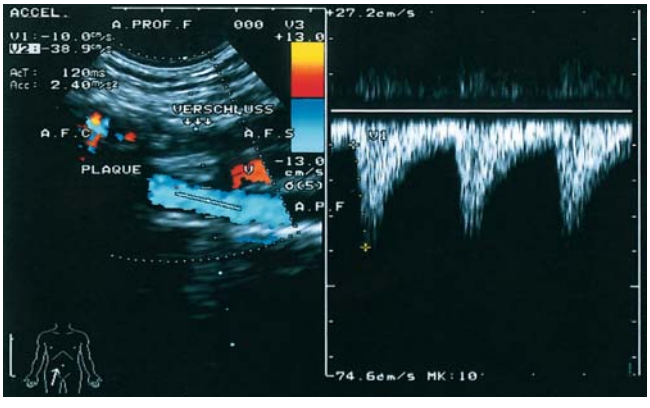

f

(Fig. A 2.12 cont.)

e The common femoral artery stenosis (*A.F.C*) at the junction with the profunda femoris is associated with a peak vecolity of 213 cm/s during systole and 26 cm/s at end-diastole. Calcified plaques with acoustic shadowing eliminate both the gray-scale echo pattern and the color coding. The occluded superficial femoral artery (*A.F.S*) is depicted close to the transducer

f Downstream of the stenosis, the profunda femoris artery (*A.P.F*) shows the typical monophasic waveform with a reduced flow velocity and delayed systolic increase. Peak velocity is 38.9 cm/s during systole and 10 cm/s at end-diastole. Anterior to the blue profunda femoris artery, part of the superficial femoral artery is depicted in red and further anteriorly the occluded segment of the superficial femoral artery (*A.F.S*). Visualization of the common femoral artery (*A.F.C*) is impaired by plaque-induced acoustic shadowing but there is aliasing

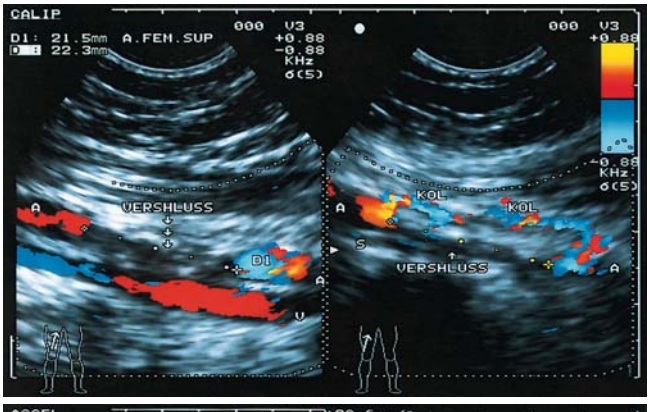

a

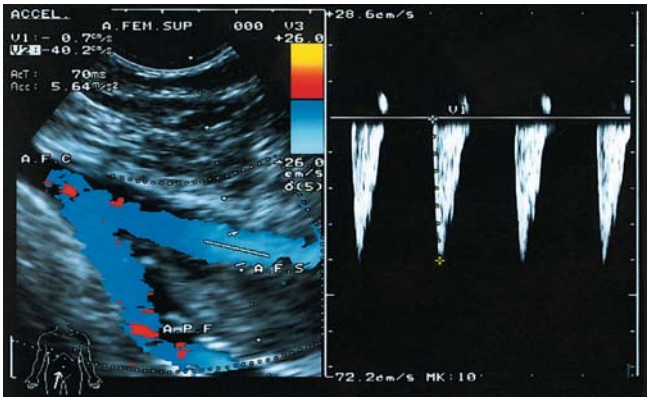

b

Fig. A 2.13 a–g
Femoral artery occlusion

a Color duplex scanning is superior to conventional duplex in that it enables rapid identification of an occlusion and fairly reliable determination of its length

In the example, there is a 2 cm occlusion of the distal femoral artery just above the adductor canal. The scan on the *left* shows the proximal and distal ends of the occlusion with absence of flow signals in between. The absence of flow signals is due to actual absence of flow rather than inadequate instrument setting or calcified plaques, as shown by the presence of backward flow signals in the femoral vein posterior to the artery

Parallel shifting of the transducer leads to disappearance of the femoral vein from the scanning plane while the collateral arising from the femoral artery upstream of the occlusion and emptying into it downstream comes into view. In the color mode the collateral (*KOL*) is depicted closer to the transducer than the occlusion. In this scan plane the plaques in the occluded artery cause posterior acoustic shadowing

b Femoral bifurcation: The Doppler waveform from the proximal superficial femoral artery already suggests a flow obstacle distal to the sample volume. Flow is pulsatile but the early-diastolic forward flow component is absent. In this case, the flow profile cannot be explained by diabetic medial sclerosis. Moreover, peak systolic velocity is reduced to 40 cm/s although there is no proximal stenosis. Collateral flow is mainly through the profunda femoris artery (see angiogram)

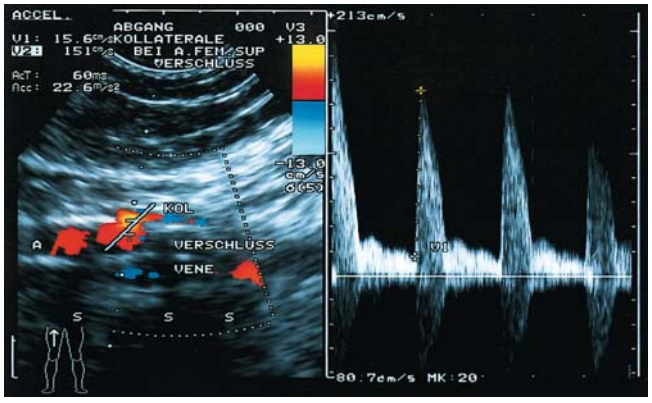

c

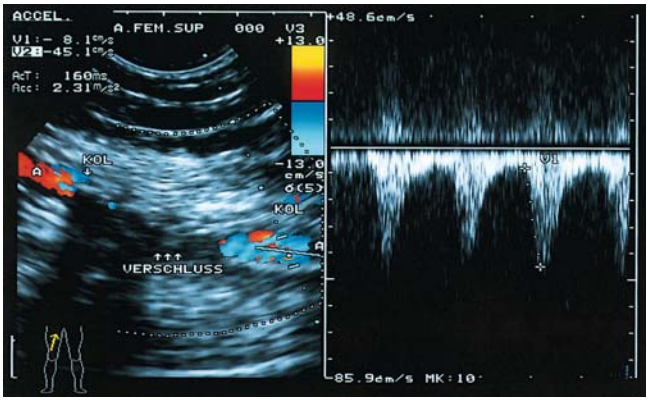

d

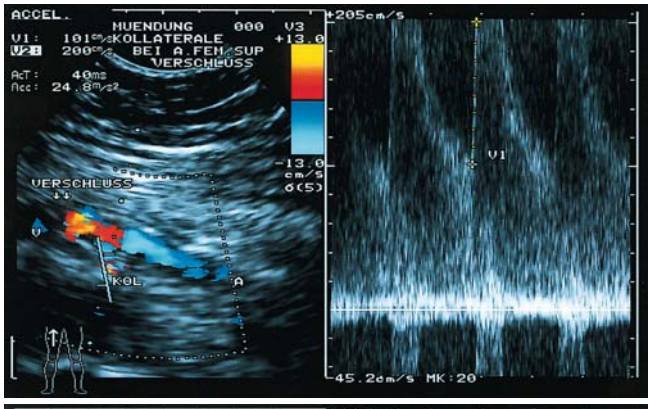

e

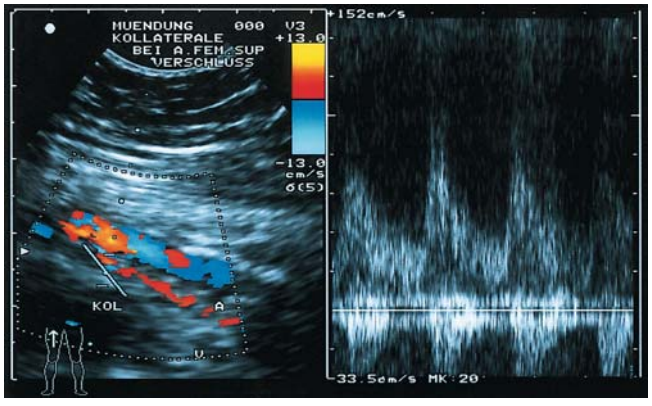

f

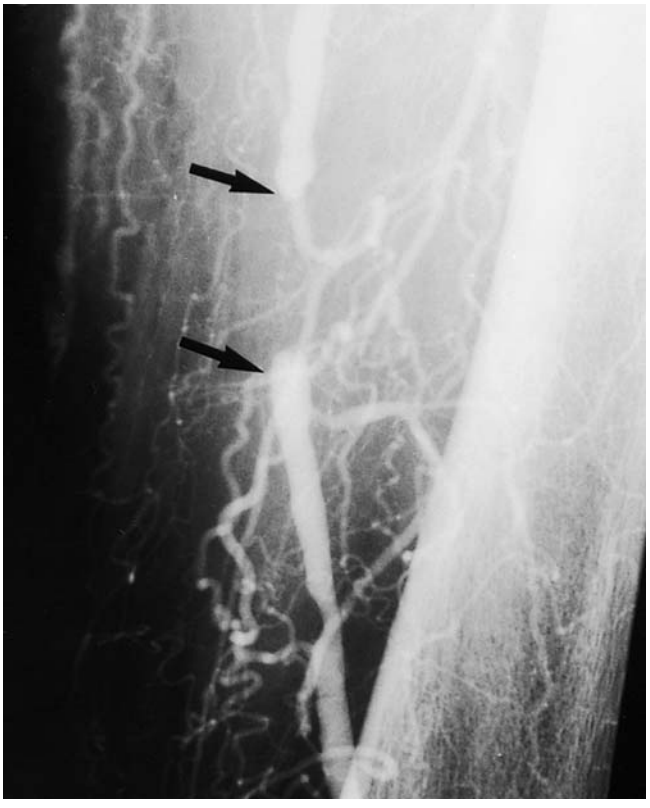

g

(Fig. A 2.13 cont.)

c Superficial femoral occlusion: The Doppler spectrum recorded at the origin of the collateral (*KOL*) from the superficial femoral artery just upstream of the occlusion shows a peak velocity of 150 cm/s. The higher flow velocity toward the superficial femoral is not caused by a stenosis at the origin but by different vessel calibers. The occluded superficial femoral is depicted posterior to the collateral and the vein posterior to the artery. The color-coded blood columns in the artery and vein are disrupted by plaques (*S*)

d The postocclusive waveform of the refilled superficial femoral artery shows monophasic flow with a peak systolic velocity of 45 cm/s

e, f Just proximal to the refilled segment, two further collaterals (*KOL*) empty into the superficial femoral on its posterior aspect with flow toward the transducer. In **f** a long segment of the collateral is depicted in red while the superficial femoral is shown in blue (flow away from transducer). With a peak systolic velocity of 95 cm/s, this collateral is not stenosed whereas the second collateral (**e**) entering the artery more proximally shows criteria of stenosis at its site of entry on duplex ultrasound and in the Doppler waveform (aliasing, peak velocity of 100 cm/s at end-diastole and over 250 cm/s in systole). The occlusion is indicated by *arrows* in **e**. Retrograde flow components in the superficial femoral artery are displayed in red

g Angiography: Confirmation of the 2 cm long occlusion of the superficial femoral artery. Also shown are the anterior collateral vessel and the two collaterals emptying into the artery on its posterior aspect (*distal arrow*). The latter are supplied by profunda femoris collaterals

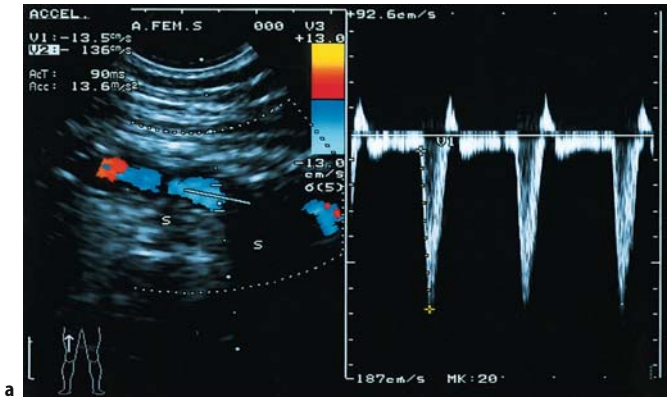

a

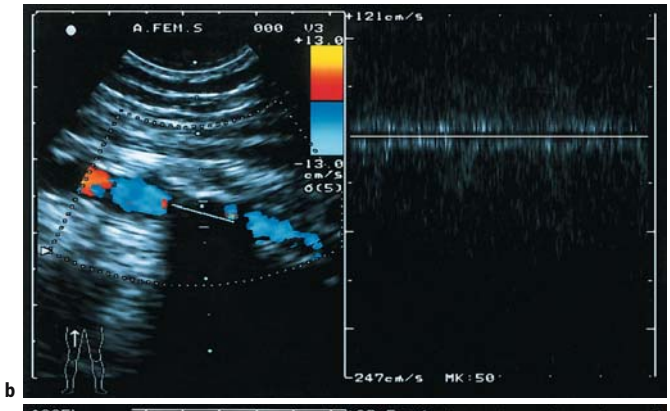

b

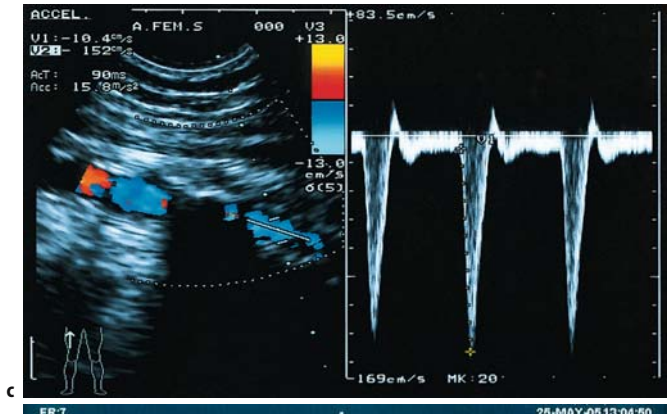

c

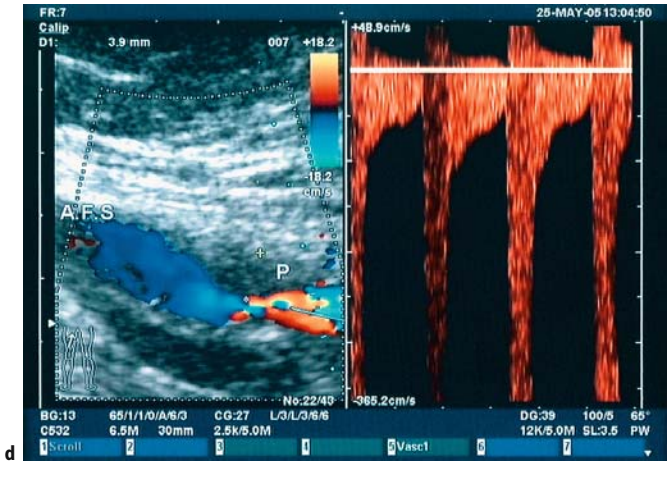

d

Fig. A 2.14 a–c
Artifact due to acoustic shadowing
a In contrast to the example presented in Fig. A 2.13 a–g, the absence of flow signals along a 1-cm segment of the superficial femoral artery in this case is not due to occlusion but to acoustic shadowing produced by a calcified plaque. Just proximal to this segment, there is pulsatile, triphasic flow with a peak systolic velocity of 136 cm/s
b Neither color duplex scanning nor the Doppler waveform depicts flow in the area of acoustic shadowing
c The Doppler waveforms distal and proximal to the obscured segment are identical, excluding a higher-grade stenosis or occlusion of the nonvisualized segment. The slightly higher flow velocity of 152 cm/s may be due to a moderate lumen reduction or an angle-related measurement error

Hypoechoic plaque – stenosis
d Visualization and quantification of a stenosis in the presence of noncalcified plaque is much easier. The example shows a high-grade stenosis of the superficial femoral artery (*A.F.S.*) caused by a hypoechoic plaque (*P*) without calcification. PTA of a stenosis due to such hypoechoic plaques has a better long-term prognosis and lower recurrence rate than one caused by an extensively calcified plaque

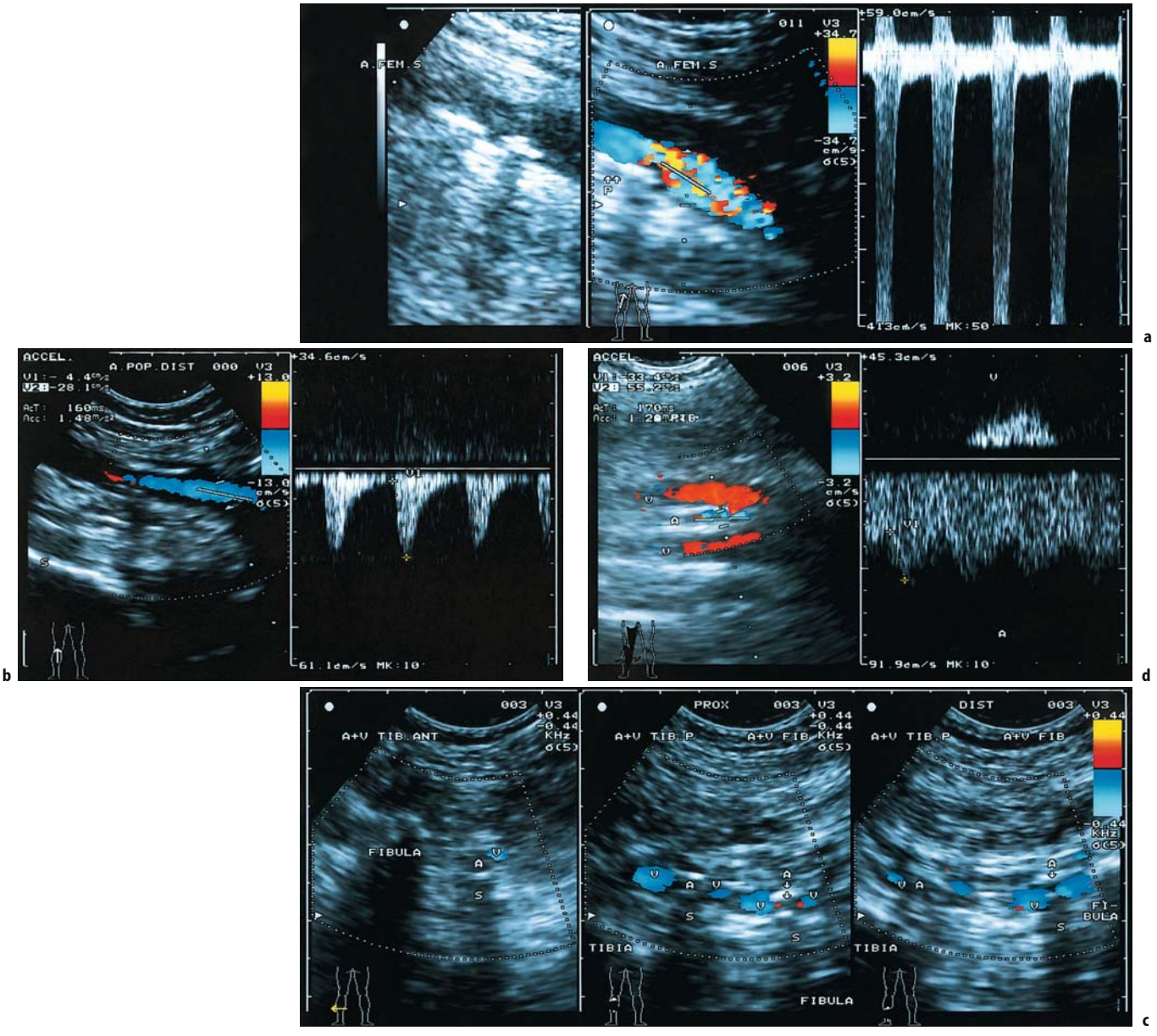

Fig. A 2.15 a–i
Follow-up after PTA

a Patient with a long history of diabetes mellitus and stage III AOD. Besides medial sclerosis, there is a high-grade stenosis at the junction of the superficial femoral and popliteal arteries. The stenosis is associated with monophasic flow with a peak systolic velocity of over 400 cm/s in the Doppler waveform and aliasing with color changing through yellow to red. Near the transducer, a short segment of the femoral vein is seen as a hypoechoic structure in this plane but the high PRF does not depict flow signals from the slowly flowing venous blood

b In the distal popliteal artery downstream of the stenosis, the Doppler waveform shows the typical changes consisting of delayed systolic rise, reduced peak flow velocity (28 cm/s), and monophasic flow profile

c The only patent vessel in the lower leg is the fibular artery. The anterior view (*left section*) depicts the anterior tibial artery (*A*) on the medial side of the fibula; there is acoustic shadowing posterior to the artery due to medial sclerosis with calcifications. The good color filling of the vein (*V*, blue) confirms adequate instrument setting for the detection of the slower poststenotic flow

The posterior view (*middle section*) depicts the posterior tibial and fibular arteries in the distal lower leg in transverse orientation. With the transducer tilted, the veins are shown with flow away from the transducer (blue). Only residual flow near the wall displayed in red is detected in the fibular artery, due to plaque-induced acoustic shadowing involving the central vessel segment. As a result of acoustic shadowing, the proximal fibular artery (*right section*) appears to be occluded in the color duplex mode

d To confirm the patency of the fibular artery, the vessel must be interrogated in longitudinal orientation and the Doppler tracing obtained with an adequate angle of incidence. Here, an attempt was made to avoid the acoustic shadows by moving and rotating the transducer. It was thus possible to also depict flow signals in the distal fibular artery There is only sparse coloring of the arterial lumen despite a low PRF and a high gain. In this view of the distal fibular artery, the accompa-

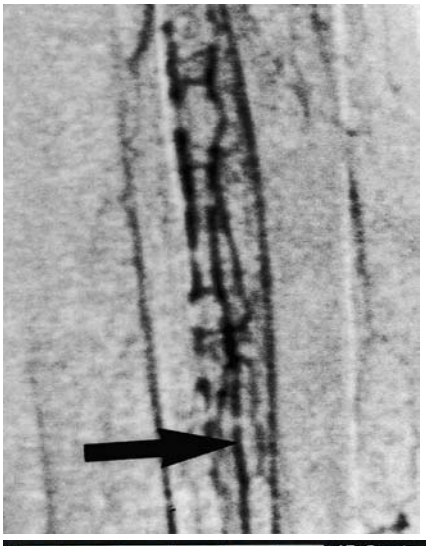

e

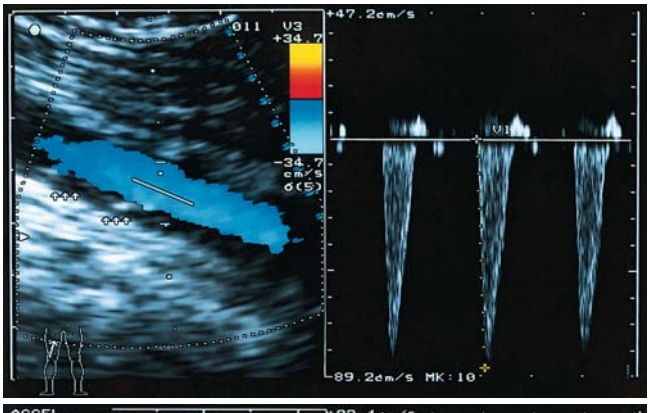

f

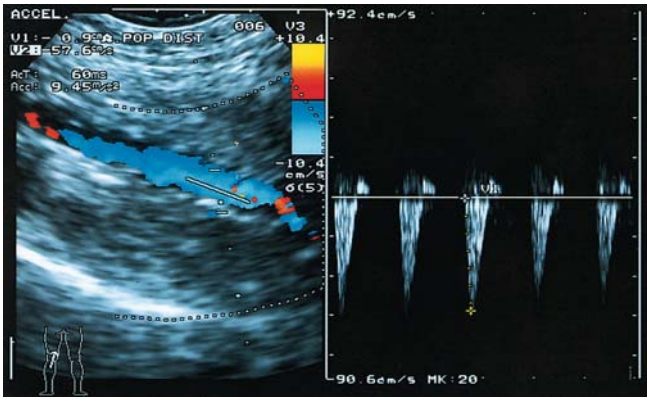

g

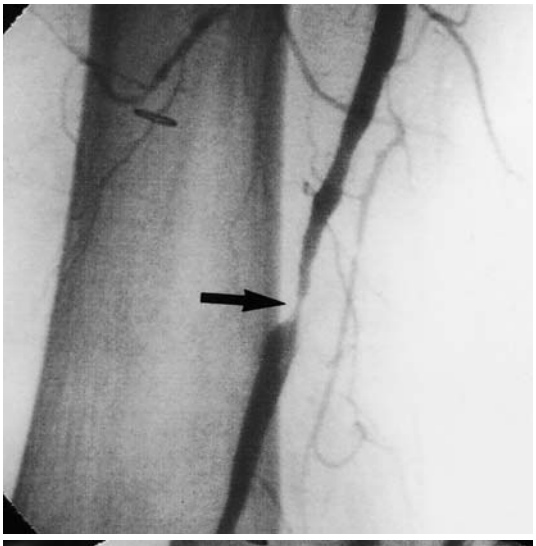

h

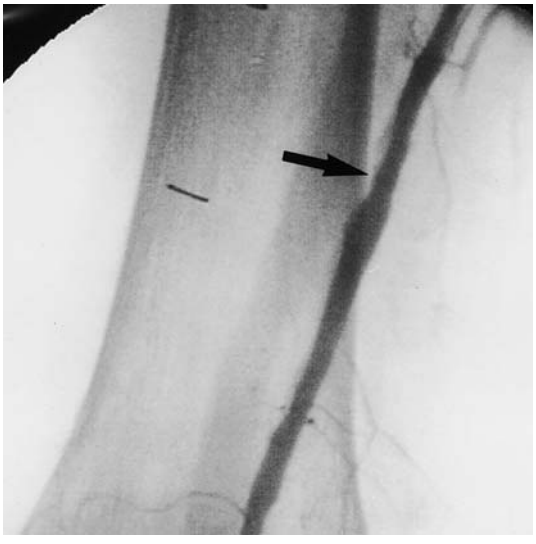

i

(Fig. A 2.15 cont.)
nying veins anterior and inferior to the artery are displayed in red. The poststenotic Doppler waveform displays the arterial flow below the baseline (away from transducer) with an almost venous poststenotic character. The flow signal represented above the baseline is from an accompanying vein with flow toward the transducer

e Angiography: The patent distal segment of the fibular artery is indicated by an arrow. The posterior tibial artery is occluded and the anterior tibial artery is filled with blood only along a short stretch of its middle segment, supplied by collaterals from the fibular artery

f Duplex scanning is an excellent follow-up modality for patients having undergone vascular interventions. After angioplasty, a peak systolic velocity of 88 cm/s is measured at the site of the former stenosis (compare **a**); the plaques are fragmented (*arrows*). The hypoechoic wall thickening may be due to subintimal hemorrhage

g The Doppler waveform now shows pulsatile flow with a steep systolic rise in the distal popliteal artery compared to the preinterventional waveform (**b**). This waveform rules out a hemodynamically significant stenosis

h Angiography: High-grade stenosis at the femoropopliteal junction (compare findings in **a**)

i Angiography after angioplasty of the stenosis at the femoropopliteal junction (*arrow*) demonstrates successful dilatation. The angiogram corresponds to the duplex ultrasound findings in **f**

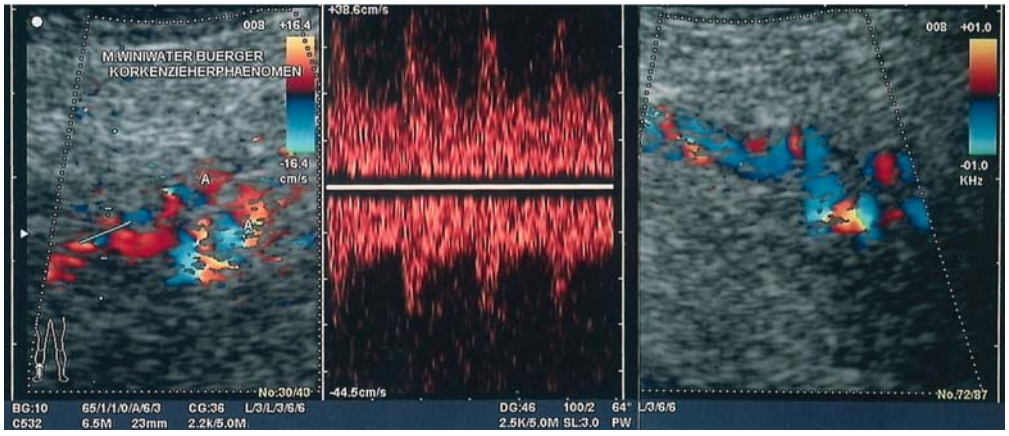

a

b

Fig. A 2.16 a–c
Buerger's disease (thromboangiitis obliterans)
a Typical color duplex ultrasound appearance of corkscrew collaterals in Buerger's disease (*left* and *right* sections with vessel branching). The changes from red to blue reflect the changing flow directions of the blood relative to the ultrasound probe. The Doppler waveform obtained with placement of the sample volume in this vessel depicts the typical pulsatile flow with flow components toward and away from the transducer (*middle section*)
b Angiographic appearance of corkscrew collaterals
c Doppler waveform from a very thin collateral illustrates the changes in flow direction. With subtle movement of the transducer (spectrum showing beginning and end of the movement), signals indicating flow in the opposite direction are depicted. This is pathognomonic and should not confuse the sonographer during the examination

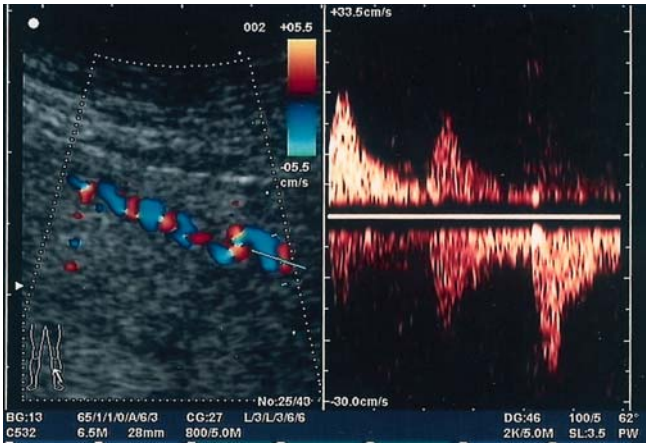

c

Fig. A 2.17 a–k
Planning of bypass procedure, graft selection (vein mapping), recipient segment
a Suitable veins for grafting can be selected preoperatively. This includes measurement of the diameter, which should be over 2 mm for a crural bypass. Preoperative marking of the course of the selected vein on the skin reduces the length of incision and shortens operation time. In case of duplication, the most suitable branch in terms of diameter and course is selected sonographically. The transverse view on the *left* shows a suitable small saphenous vein with a diameter of 4 mm and the scan on the *right* obtained more distally a duplicated vein with a thicker (3.4 mm) and a thinner branch (2.6 mm)
b Veins with postthrombophlebitic changes are unsuitable for grafting. These can be identified by sonography, which will demonstrate a patent lumen with sclerotic wall thickening, as illustrated here for the small saphenous vein. A recanalized thrombophlebitic vein shows the same features as a postthrombotic deep vein: wall sclerosis and thickening, residual thrombi, and valve incompetence. In the example, transverse and longitudinal views (*left* and *right*, respectively) depict

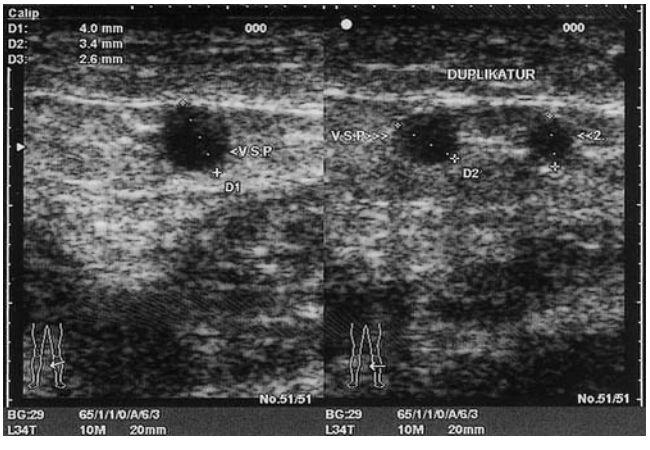

a

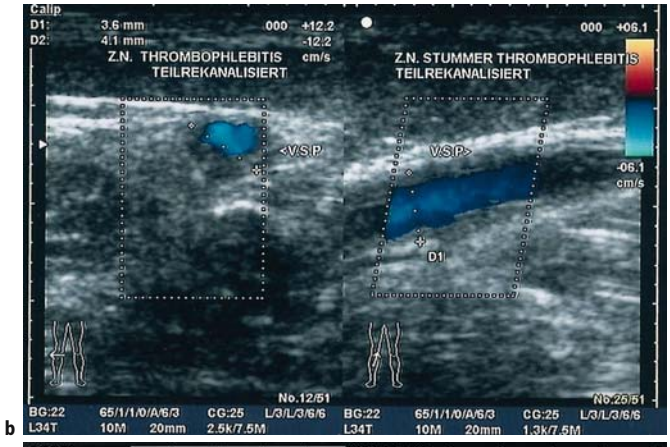

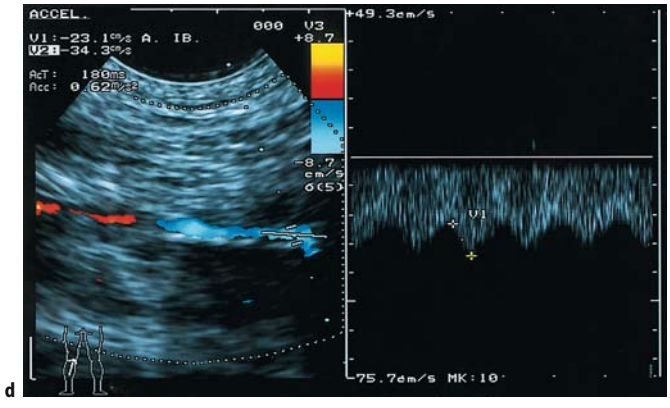

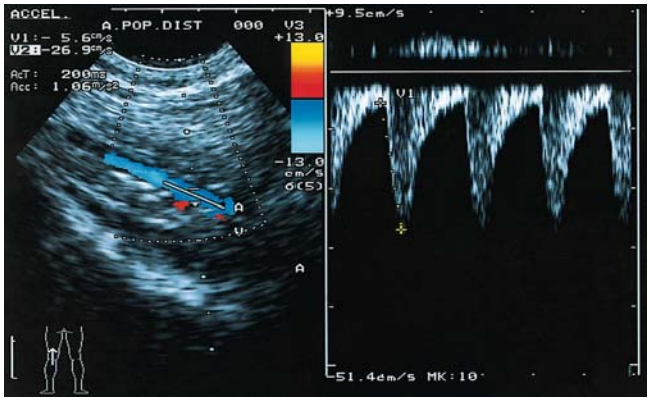

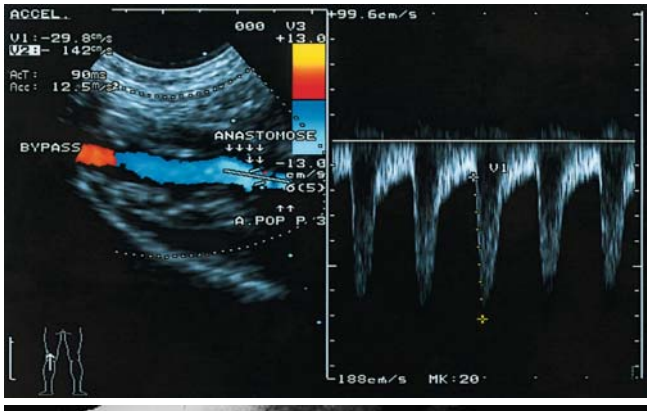

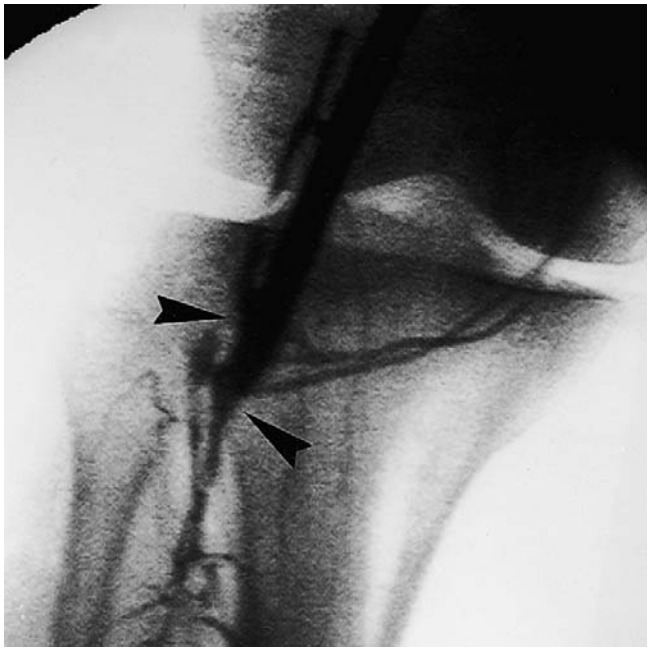

(Fig. A 2.17 cont.)
flow in the patent lumen of the small saphenous vein (blue) and hypoechoic wall thickening

Bypass recipient segment

c Refilled distal popliteal artery with only a minor calcified plaque downstream of the occlusion. This gray-scale appearance suggests that segment 3 is suitable for connection of the femoropopliteal bypass graft

d Continuous scanning of the vessels down the leg reveals that only the fibular artery is patent. The color duplex scan shows color reversal from red, through black, to blue, which is due to the changing flow direction relative to the transducer. The peak systolic velocity measured down to the distal lower leg is still fairly high (34 cm/s measured in a nonstenotic segment) in view of the multiple proximal occlusions

Together with a diastolic velocity of 23 cm/s, these findings suggest a satisfactory outflow tract in the distal lower leg. Evaluation of the hemodynamic situation in the lower leg arteries is crucial for estimating the prognosis if a bypass procedure is contemplated

e Duplex ultrasound is the ideal modality for follow-up after bypass surgery. The femoropopliteal PTFE bypass connected onto the P3 segment is suggested by the just barely visible double contour (*left section*); the color change is again due to the changed flow direction relative to the ultrasound beam. There is no anastomotic stenosis (peak systolic flow velocity of 142 cm/s). The steep systolic rise rules out an upstream stenosis. The monophasic flow profile is due to the different elasticity of the bypass wall and the changed peripheral resistance resulting from the presence of only a single patent lower leg artery providing collateral flow. The anastomosis is indicated by *arrows*. Intraoperative inspection of the arterial segment confirmed the presence of only little plaque and hence suitability as a recipient segment for the bypass

f Intraoperative angiography: The large-caliber bypass is depicted on the *right* and the thin native popliteal artery on the *left*. The artery is disrupted by multiple occlusions. The occlusion at the level of the knee joint cleft is depicted over a length of 1 cm. No anastomic stenosis (length of anastomosis indicated by *arrowheads*). The bandlike structure is a vessel loop and not an artifact

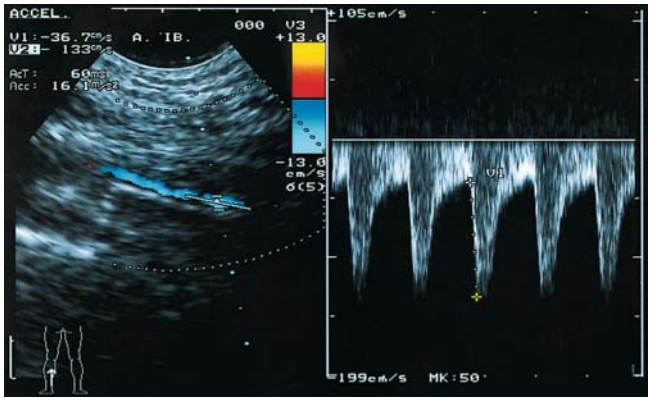

g

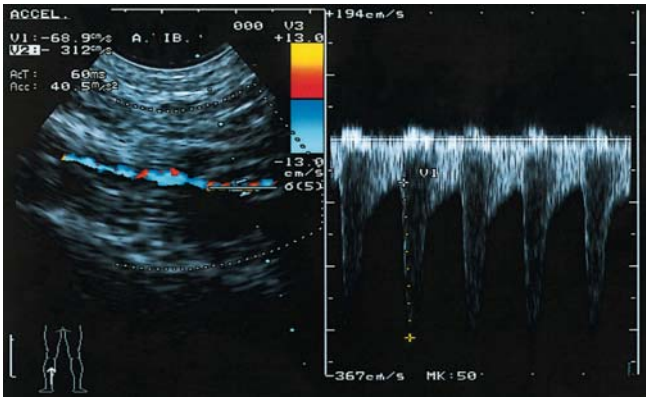

h

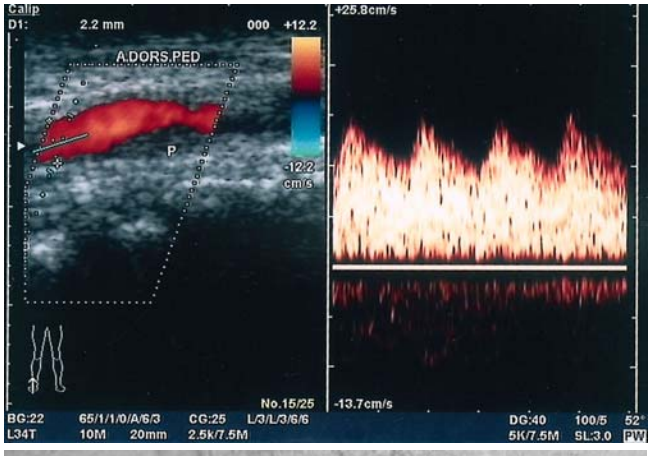

i

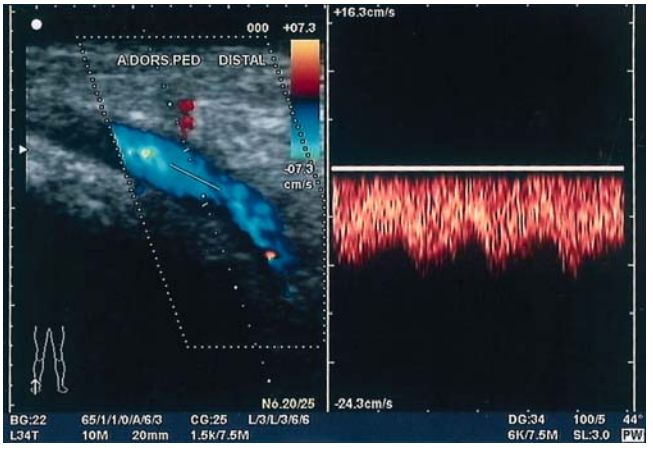

j

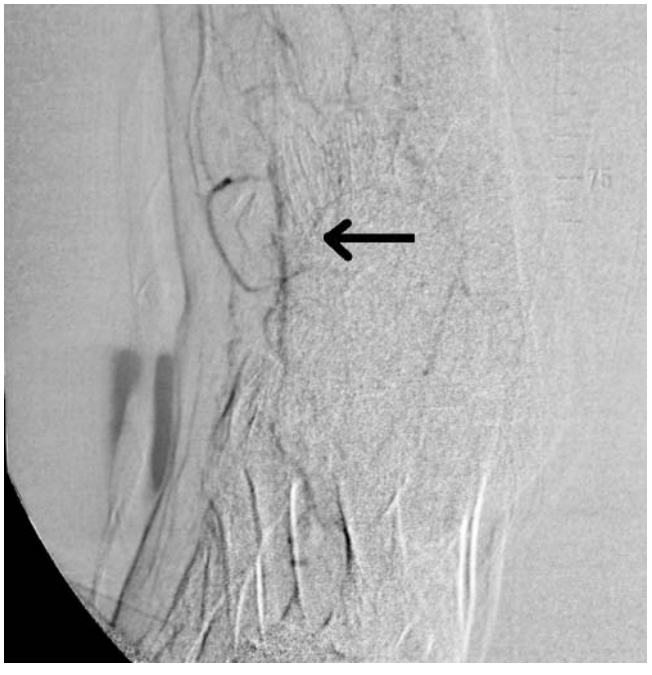

k

(Fig. A 2.17 cont.)

g The Doppler tracing obtained in the fibular artery after bypass surgery nicely depicts the improved perfusion (cf. **d**) with a peak flow velocity of 133 cm/s during systole and 36 cm/s at end-diastole (waveform similar to that recorded at the anastomosis and depicted in **e**)

The rather fast flow is due to the diameter mismatch between the bypass graft and the fibular artery, the only patent vessel of the lower leg in this patient

h There is a circumscribed flow acceleration to 312 cm/s during systole and 312 cm/s at end-diastole 12 cm above the ankle joint. The quotient of peak systolic velocity in the stenosis and distal to it is 2.3, corresponding to a hemodynamically significant stenosis with a grade of 50 to 75%

Recipient segment of pedal bypass

i Slow flow in the superficial pedal vessels is detected by high-resolution duplex scanning using a high-frequency transducer and a low pulse repetition frequency. Plaques and stenoses are depicted, and a Doppler waveform showing the typical postocclusive monophasic flow, often with an almost venous profile, indicates upstream occlusion. Moreover, the mean flow velocity or magnitude of peak systolic flow velocity and the diastolic flow component are important parameters in determining whether the vessel would provide adequate outflow if used as the recipient segment of a planned bypass. This information is important to estimate bypass patency prior to surgery. The patient presented has stage IV AOD. The dorsalis pedis artery shows monophasic, postocclusive flow just above the ankle joint. There is some luminal narrowing from a hypoechoic, central plaque

j Further down, shortly before it enters the arch of foot, the dorsalis pedis artery has an unchanged monophasic flow profile with good perfusion, suggesting that the artery is a suitable candidate for connection of a pedal bypass graft. In this patient with multiple upstream occlusions, a more pulsatile flow profile would suggest poorer outflow

k Angiography of the pedal vessels demonstrates patency of the artery though there is poor opacification due to the multiple proximal occlusions. Angiography is inferior to color duplex scanning in determining whether the artery provides suitable runoff for a pedal bypass

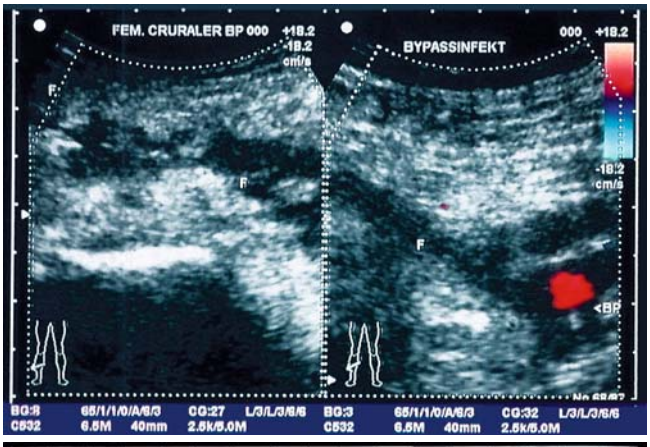

a

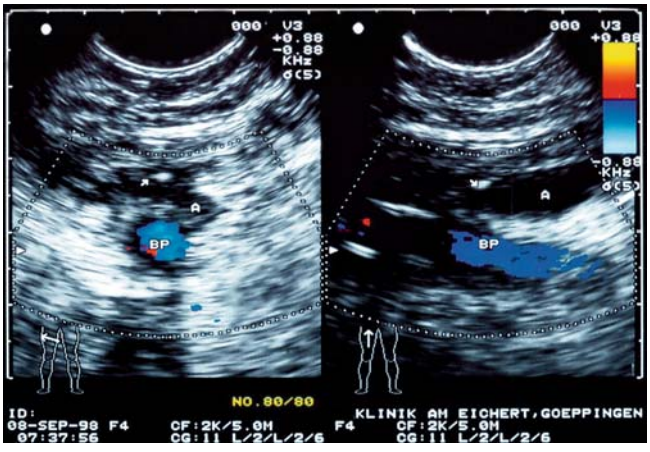

b

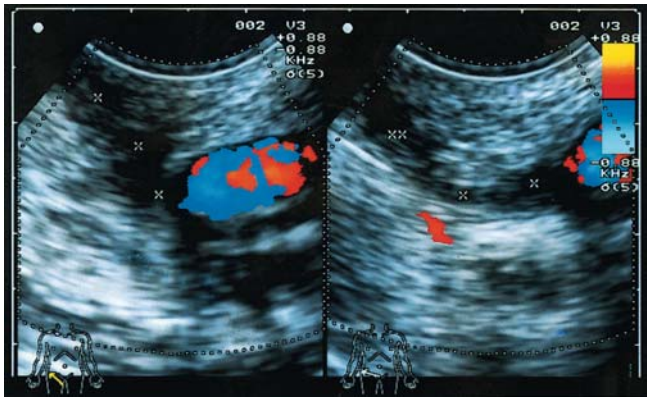

c

Fig. A 2.18 a–c
Follow-up after bypass procedure – graft infection
a A hypoechoic fistula some centimeters in length extends from below the skin to the distal anastomosis of a P2 bypass, indicating graft infection although the initial clinical appearance of the wound suggested a superficial, subcutaneous infection only
b If gray-scale ultrasound depicts elongated hypoechoic to anechoic areas around a bypass graft, an infection of the bypass has to be excluded, in particular if the respective clinical signs are present. The simplest test is ultrasound-guided aspiration with placement of the hyperechoic needle tip (*N*) in the hypoechoic zone adjacent to the graft. The needle may have to be moved about a bit under suction to reach a fluid collection
c Six days after crossover bypass grafting, a hypoechoic fistula (*X*) is seen extending from the site of the anastomosis to the subcutaneous tissue. There is only mild reddening of the skin in the scar area. In this patient, Staphylococcus aureus was isolated from the cloudy fluid aspirated under ultrasound guidance

The slightest clinical suspicion of bypass infection should prompt a sonographic control examination so that early bypass revision can be initiated as required

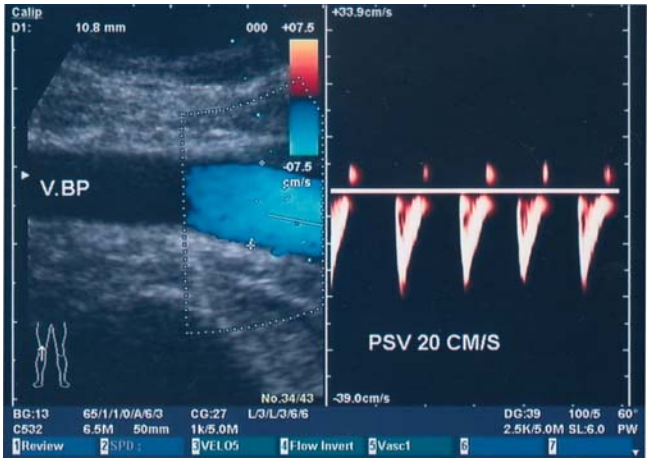

a

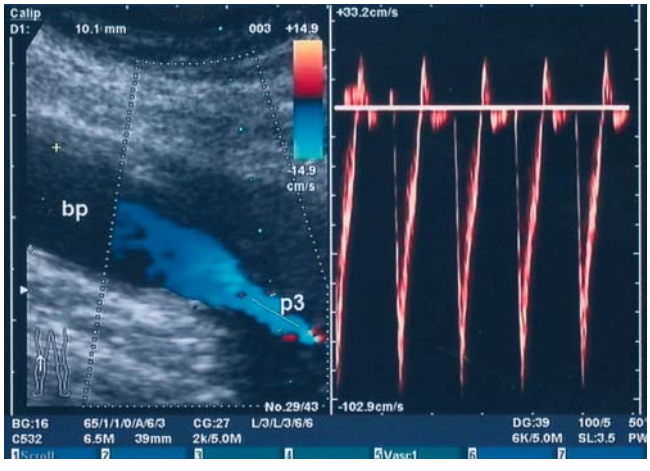

b

Fig. 2.19 a, b. Blood flow velocities in relation to bypass graft diameter
a The blood flow velocity within a bypass graft is largely determined by its diameter and the distal recipient segment. In the example shown, the peak systolic flow velocity in the dilated venous bypass graft (*V.BP*; diameter of 11 mm) is only 20 cm/s although there is no stenosis distal to the sampling site. The waveform is pulsatile and exhibits a steep systolic upstroke
b There is no stenosis of the distal anastomosis onto the distal popliteal artery (P3). The sudden diameter reduction at the junction of the dilated bypass graft (*bp*; see also **a**) and the normal-caliber distal popliteal artery is associated with a sudden increase in peak systolic flow velocity to 102 cm/s, which does not indicate an anastomotic stenosis in this setting. The triphasic and pulsatile waveform recorded in the popliteal artery distal to the anastomosis is that of a normal peripheral artery. The sonographer performing follow-up examinations of bypass grafts should compare the pulsatility and flow velocity with the baseline values determined sonographically within the first three months of the bypass procedure

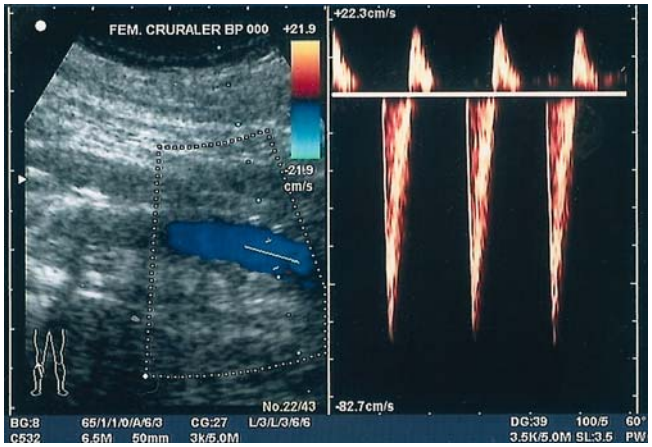

c

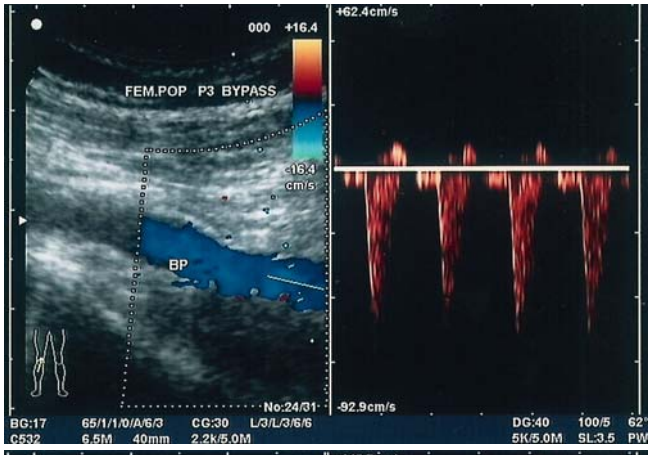

d

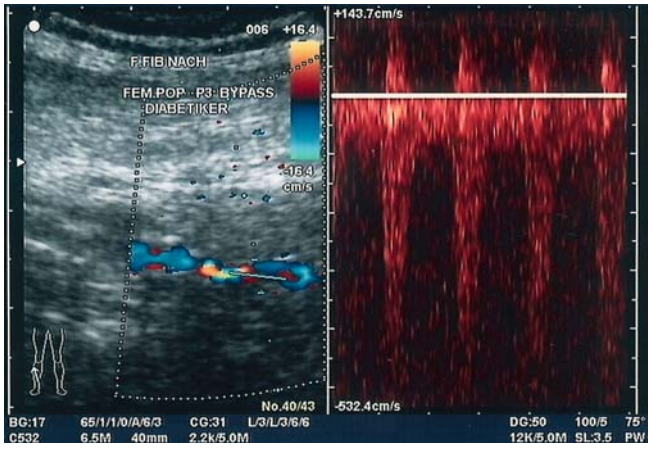

e

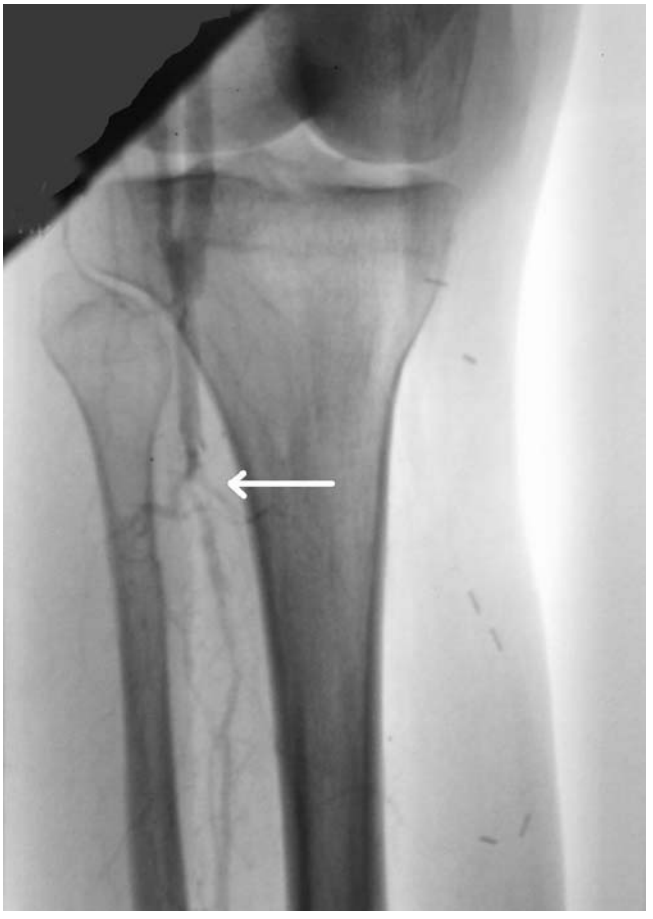

f

(Fig. A 2.19 cont.)
Flow through bypass graft – outflow obstacle

c A triphasic flow profile with a steep systolic upslope and a peak systolic velocity of over 60 cm/s (in the present case 65 cm/s) suggest good bypass function. Nevertheless, the examiner should check the anastomoses, in particular the distal one, for the presence of stenosis and evaluate run-off in the arterial recipient segment

d In contrast, the 1-year ultrasound follow-up of this femoropopliteal bypass graft at the P2 level demonstrates a reduced peak systolic flow velocity of only 45 cm/s while the flow profile is still triphasic. These findings may be indicative of an outflow obstruction. The patient is a diabetic with a necrotic great toe, which should produce a monophasic flow profile due to widening of peripheral vessels

e In the lower leg, only the fibular artery is patent, and color duplex scanning demonstrates a high-grade stenosis at the junction between the tibiofibular trunk and the fibular artery with aliasing and a peak systolic flow velocity of about 5 m/s. The stenosis obstructs bypass outflow

f Control angiography confirms a high-grade stenosis (*arrow*) of the tibiofibular trunk at the junction with the fibular artery

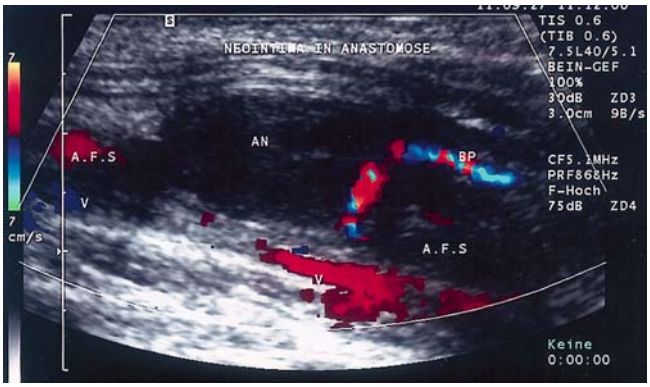

Fig. A 2.20
Neointima at site of anastomosis
Neointima formation at the site of an anastomosis (*AN*: proximal stenosis of a femorocrural bypass graft) can obstruct flow and thus lead to bypass occlusion. In the example, with the bypass still patent, a thin trickle along the neointima can be identified by scanning in different planes

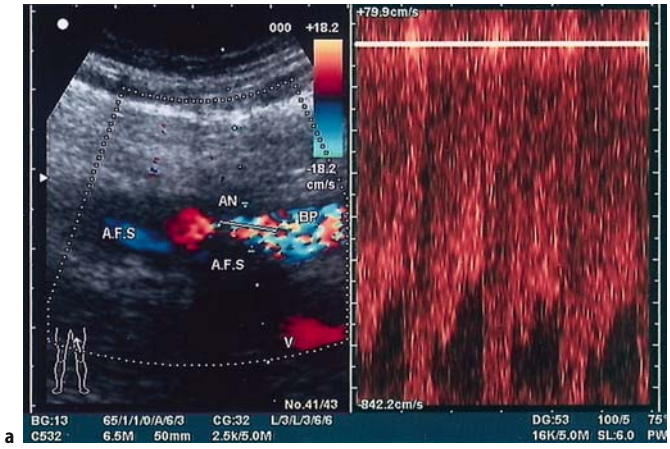

a

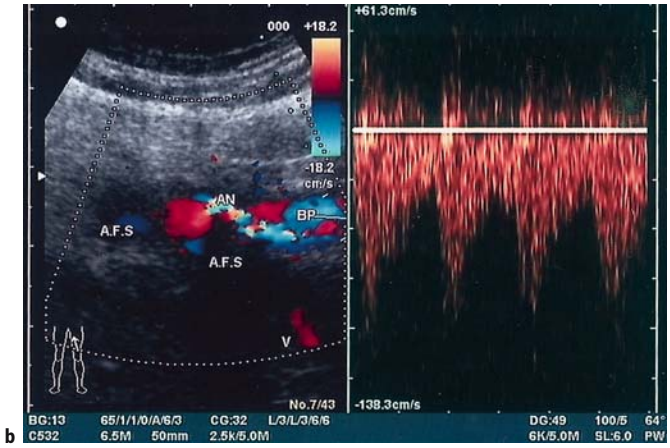

b

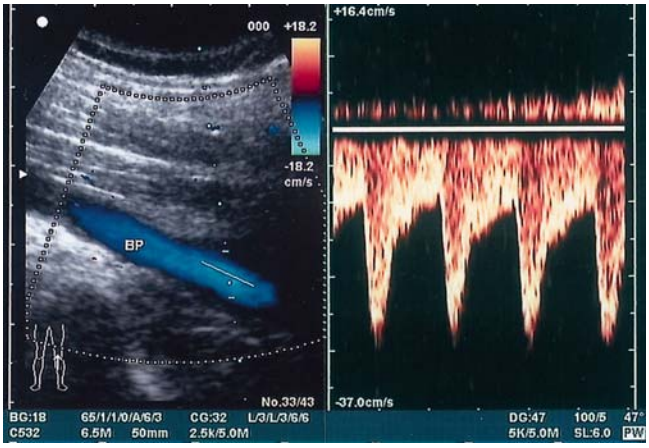

c

Fig. A 2.21 a–c
Stenosis of bypass anastomosis
a Routine 6-month follow-up of a femorocrural bypass graft in a patient with grade IV AOD demonstrates a high-grade stenosis at the proximal anastomosis (aliasing, peak systolic flow velocity >700 cm/s) due to neointima in this area (hypoechoic intraluminal wall deposit at anastomotic site)
b Flow profile somewhat distal to the stenosis shows pronounced turbulence
c The bypass is patent but exhibits a postocclusive flow profile (monophasic, delayed systolic rise, peak flow velocity <30 cm/s). The slow flow in the bypass due to stenosis of the proximal anastomosis suggests that there is a risk of imminent bypass occlusion

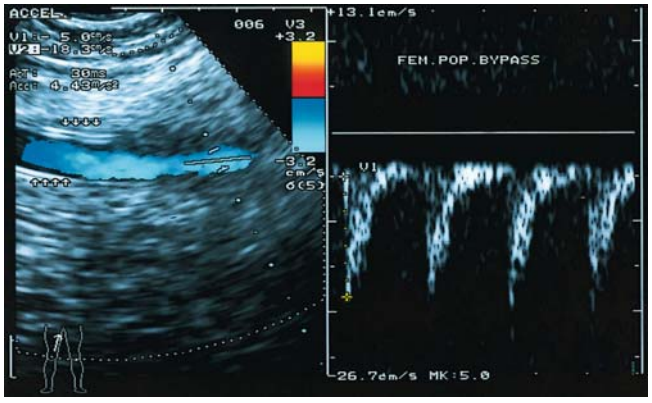

a

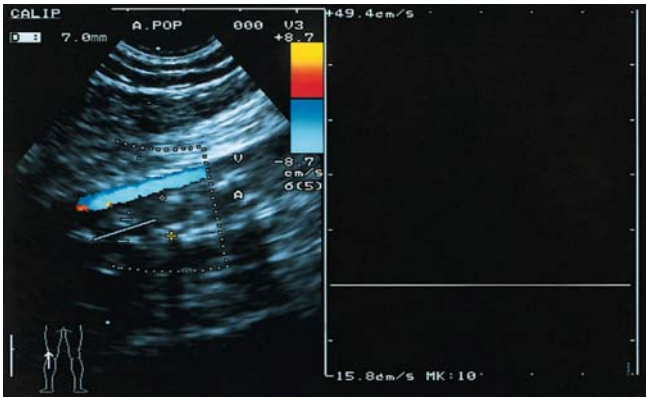

b

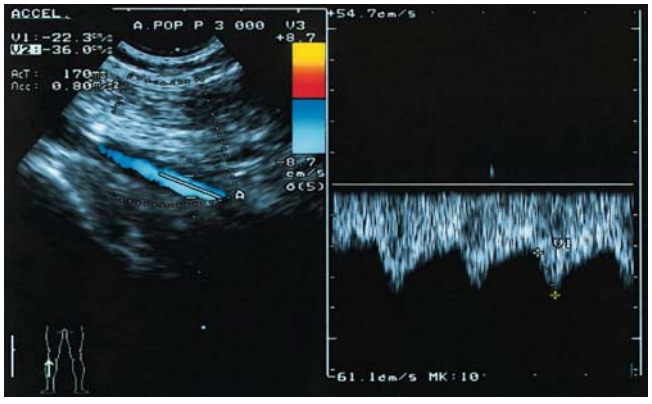

c

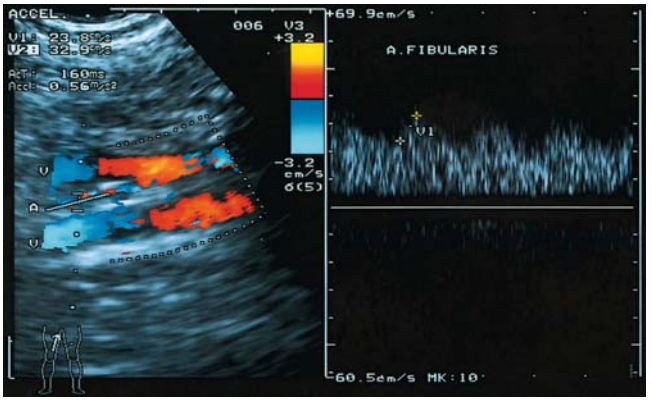

d

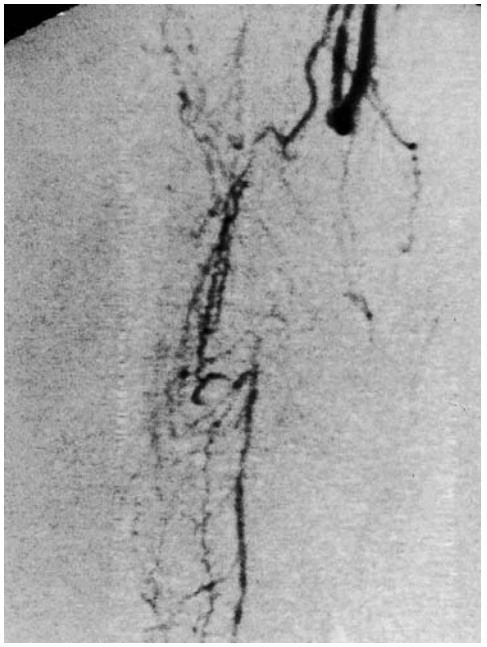

e

Fig. A 2.22 a–j
Bypass graft occlusion

a The markedly reduced peak systolic velocity of 18 cm/s in the PTFE bypass graft (double contour) is an indicator of imminent occlusion (threshold velocity: 35 – 40 cm/s). In interpreting flow velocities measured in a bypass, one must take into account whether a suitable bypass diameter was selected for the respective vascular territory by the surgeon

b The slow flow in the femoropopliteal bypass anastomosed to the proximal popliteal artery is due to newly occurring occlusion of the popliteal artery (*A*) distal to the anastomosis 3 years after bypass grafting. The poor delineation of the artery from surrounding tissue due to plaques with acoustic shadowing suggests progression of atherosclerosis as the cause of the occlusion. Thrombectomy is not promising in this case; instead, a suitable recipient segment should be identified for an extension of the bypass

c The P3 segment of the popliteal artery is refilled and shows the typical postocclusive Doppler waveform (markedly delayed systolic rise and peak systolic velocity decreased to 36 cm/s)

d Duplex evaluation of the outflow segment shows the fibular artery to be the only patent major artery. Only sparse flow signals are obtained from the artery despite adequate instrument setting as shown by the good color filling of the accompanying veins

Besides the low peak flow velocity of 32°cm/s, the Doppler waveform shows a low amplitude despite a rather high gain. The waveform is much like a venous waveform but is typical of an artery with flow to the periphery toward the transducer (Doppler angle 70°). Blue indicates that flow in the veins is away from the transducer at the level of the sample volume (color change resulting from flow reversal relative to the transducer)

e Control angiography: With the popliteal artery occluded, the bypass (*top right*) fills the superficial femoral artery (*to the left of it*) retrogradely. Collaterals arising from the superficial femoral artery bridge the occluded popliteal artery and refill the distal popliteal and the fibular arteries

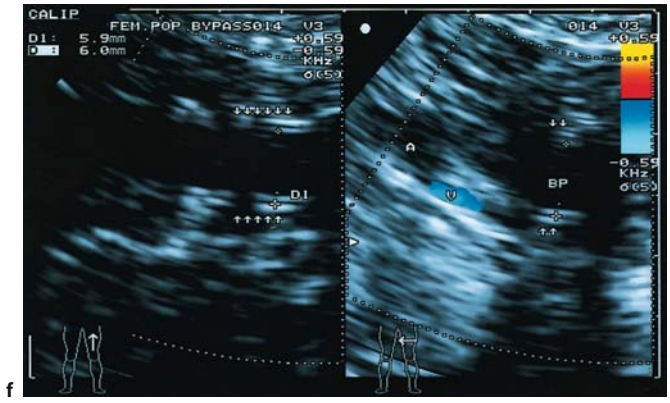

f

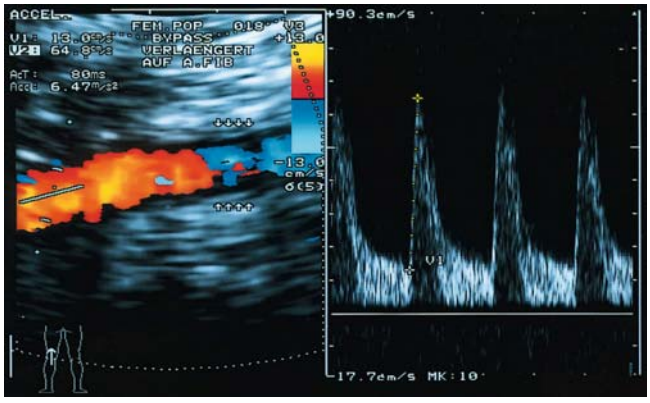

g

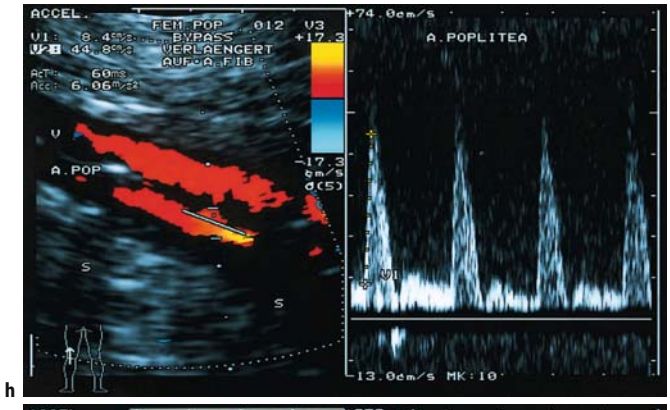

h

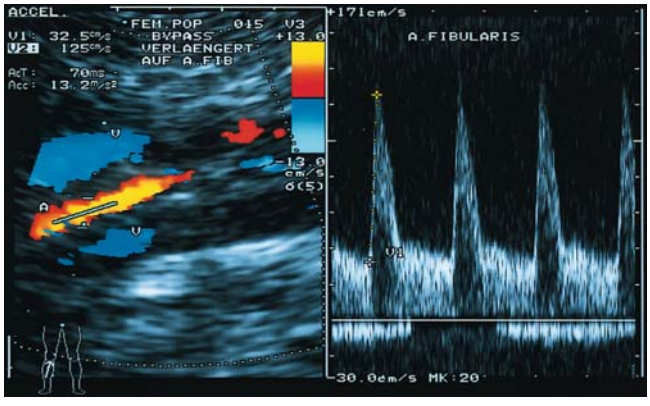

i

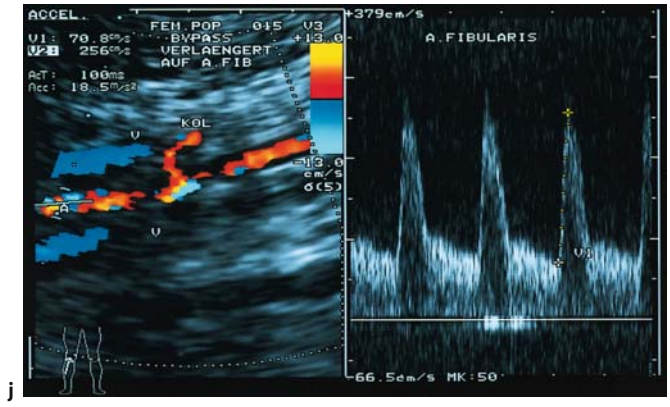

j

(Fig. A 2.22 cont.)

f A few days later occlusion of the bypass occurs. The longitudinal view on the *left* shows no flow signals; the transverse view on the *right* depicts the vein in blue (*V*) to the left of the occluded bypass (*BP*) and, anterior to it, the proximal superficial femoral, which is also occluded (*A*)

g After thrombectomy of the bypass graft and extension to the tibiofibular trunk, both color duplex and the Doppler waveform demonstrate good flow in the graft with a peak systolic velocity of 64 cm/s. The monophasic flow profile is due to peripheral dilatation rather than a bypass stenosis as the steep systolic upslope is preserved

h Following bypass extension to the tibiofibular trunk, there is retrograde flow coded red in the distal popliteal artery (flow toward transducer as in the accompanying artery). Flow is triphasic and pulsatile

i A rather high flow signal with a peak systolic velocity of 125 cm/s and an end-diastolic flow of 30 cm/s is obtained from the proximal fibular artery after bypass extension. As this flow velocity is not circumscribed but detectable over a longer graft segment, it is not due to a stenosis but to the sudden decrease in diameter from the graft to the fibular artery, which is the only patent lower leg artery serving as a collateral in this case

j However, there is aliasing in the distal fibular artery with a color change from red, through yellow, to blue in the duplex scan and flow acceleration with a peak systolic flow of 256 cm/s. The circumscribed doubling of the flow velocity compared to the prestenotic velocity suggests a hemodynamically significant peripheral stenosis. Besides the fibular vein displayed in blue (flow away from transducer), a collateral (*KOL*) with flow toward the transducer is depicted in red, supplying blood to the distal territory of the occluded posterior tibial artery

Fig. A 2.23 a, b
Stenosis of anastomosis
a A coiled crural bypass graft anastomosed onto the anterior tibial artery shows rather slow flow of 45 cm/s during systole and 8 cm/s at end-diastole. The coil is identified by the absence of signal (*X*). The slow flow may be due to the pronounced mismatch in diameter between the bypass (6 mm) and the rather thin anterior tibial artery. The sonographer must exclude a distal stenosis
b The bypass graft was connected to the anterior tibial artery over a long segment. In the *left section*, the proximal end of the anastomosis to the anterior tibial artery is indicated by *arrows*. The anterior tibial artery arises posterior to the bypass graft and shows retrograde flow in its proximal portion

In a crural bypass graft with a long end-to-side anastomosis, the distal end of the anastomosis is the chief site of stenosis. The transducer is tilted to optimize the Doppler angle for interrogation of the junction of the bypass with the anterior tibial artery (*middle section*). There is aliasing at the distal end and flow acceleration with a peak velocity of 260 cm/s during systole and 63 cm/s at end-diastole. The magnitude of the flow acceleration suggests a hemodynamically significant stenosis of the anastomosis

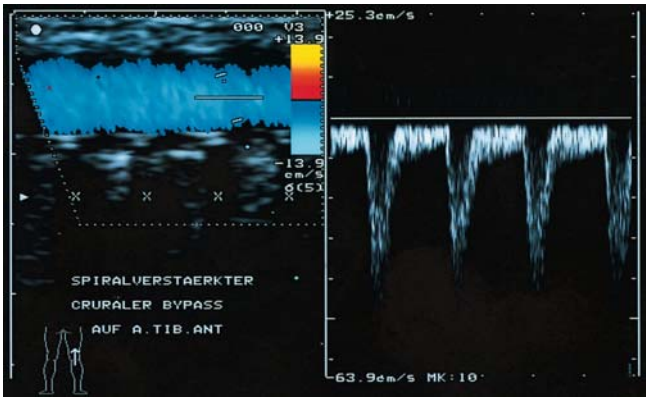

a

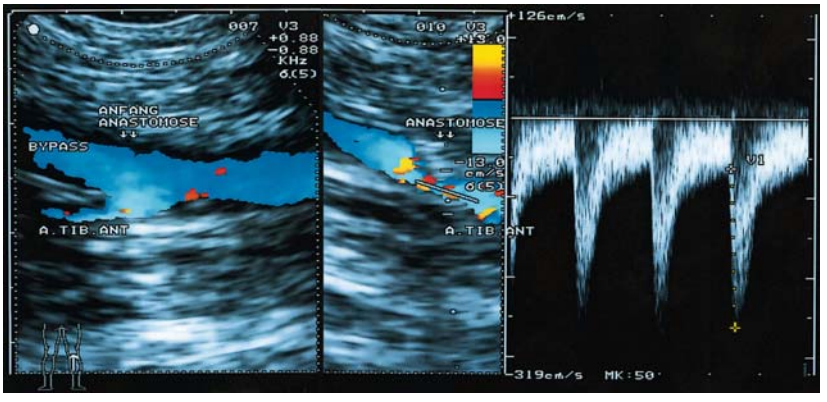

b

Fig. A 2.24 a, b
Saphenous vein bypass graft – anastomotic stenosis
An autologous bypass graft (great saphenous vein) is more difficult to identify, especially when it is occluded, due to the thin venous wall and the frequent extra-anatomic course. Color duplex helps in localizing the graft but spectral Doppler scanning is necessary for quantitative evaluation
a The postocclusive waveform with a peak systolic velocity of 12 cm/s and end-diastolic velocity of 4.6 cm/s indicates an upstream stenosis

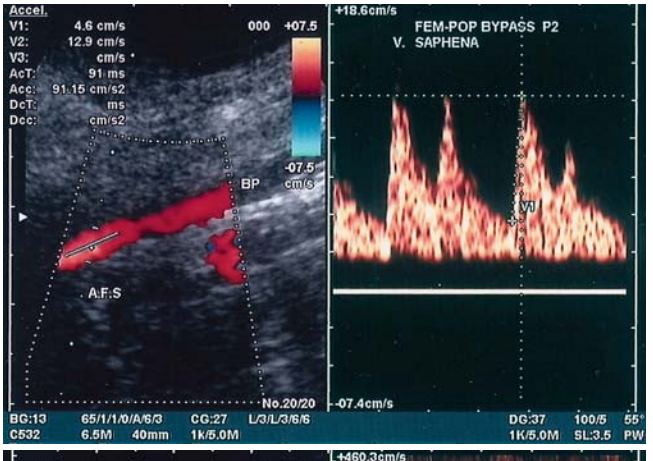

a

b Stenoses predominantly affect the anastomoses. In the case shown, a stenosis signal with a peak systolic velocity of 4 m/s is obtained at the anastomosis immediately after the bypass graft arises from the superficial femoral artery (*A.F.S*). While stenoses along the course of a bypass are rare when synthetic material is used, venous bypass grafts must be checked throughout their course because stenoses may develop at the sites of the former valves as a result of intimal proliferation

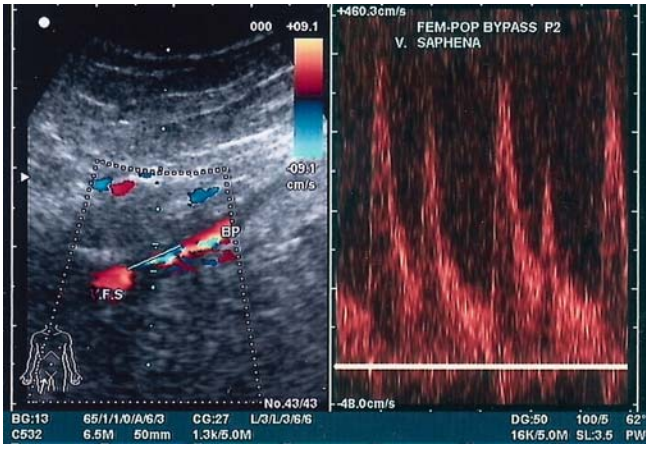

b

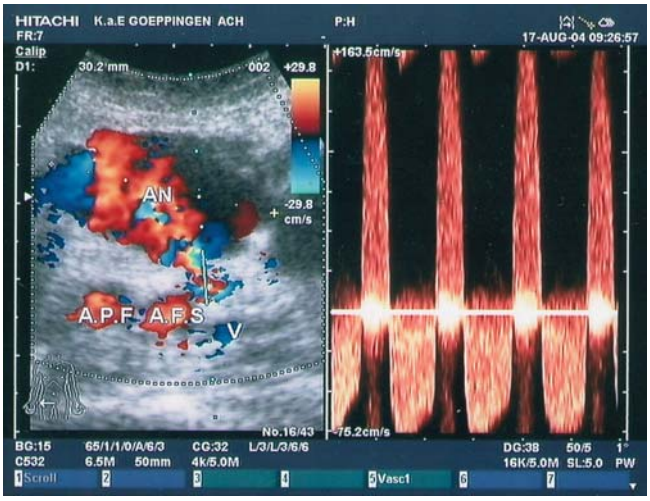

a

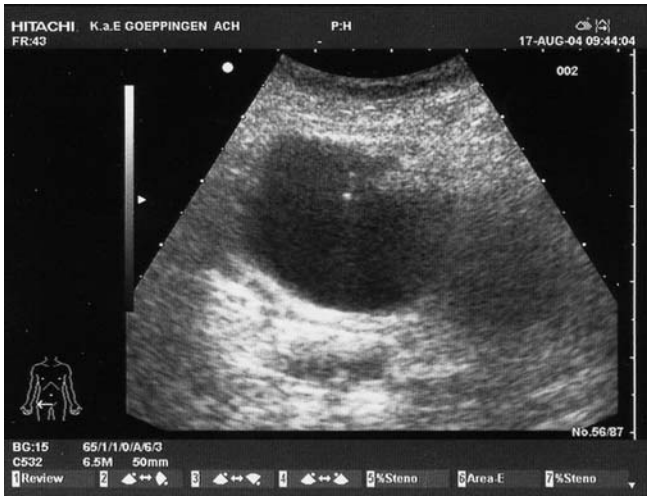

b

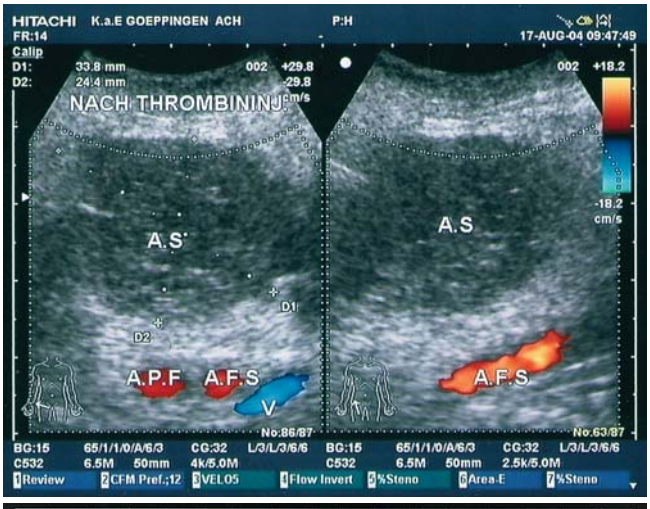

c

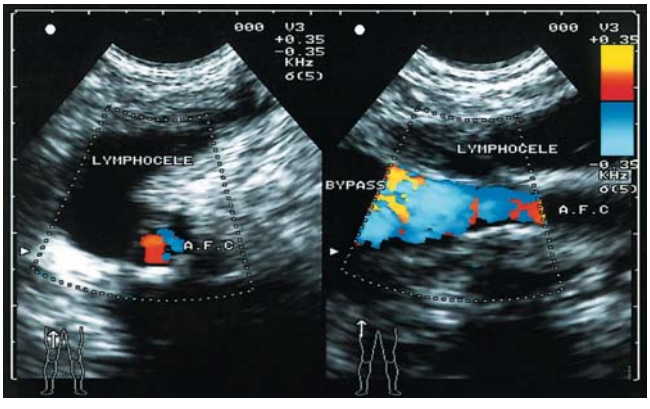

d

Fig. A 2.25 a–d
False aneurysm – treatment by thrombin injection

a Transverse view of the thigh depicting a false aneurysm (*AN*) and its neck arising from the superficial femoral artery (*A.F.S*). With the sample volume placed in the neck, Doppler ultrasonography depicts the characteristic to-and-fro flow with a high-frequency flow into the aneurysm in systole and backward flow into the vessel throughout diastole

b For treatment of the aneurysm by thrombin instillation, a needle is advanced into the center of the aneurysm under ultrasound guidance (bright echo indicating the needle tip)

c A total of 5,000 IU of thrombin dissolved in 2 ml of saline solution is instilled. Complete thrombosis of the aneurysm (*AN*) occurs after instillation of 1 – 2 drops as demonstrated by color duplex monitoring, in transverse orientation on the *left* and in longitudinal orientation on the *right* (*A.F.S* superficial femoral artery, *A.P.F* profunda femoris artery, *V* femoral vein). No flow signals are depicted from the aneurysm in the color flow mode

Lymphocele

d Alternatively, a pulsatile mass developing in the groin after bypass grafting may be a seroma, hematoma, lymphocele, or abscess. All of these entities show transmission of arterial pulsation to the skin surface and can be differentiated by ultrasound. The transverse view on the *left* depicts a lymphocele extending to the anastomosis between the common femoral artery and the iliofemoral bypass graft. A lymphocele differs from an aneurysm in that no flow signals can be obtained from the hypoechoic or anechoic lumen

The longitudinal view (*right section*) depicts the bypass graft on the left side and the common femoral artery on the right with the anastomosis roughly in the middle. The lymphocele is located near the transducer. Since the differential diagnosis also includes infected fluid or an abscess, with extension to the bypass anastomosis in this case, ultrasound-guided puncture for bacteriological testing is indicated. At the same time, an attempt should be made to drain all of the fluid

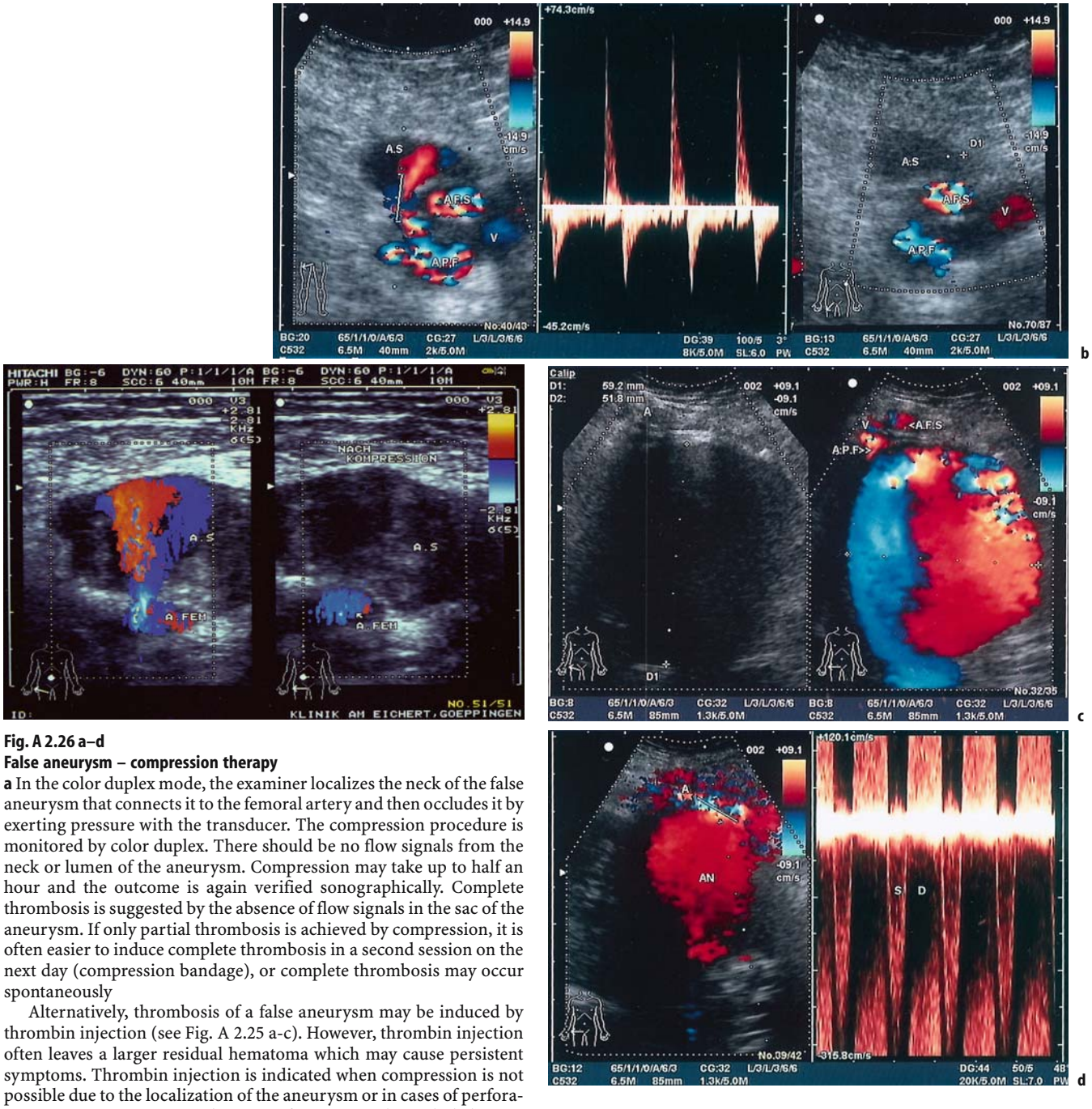

Fig. A 2.26 a–d
False aneurysm – compression therapy

a In the color duplex mode, the examiner localizes the neck of the false aneurysm that connects it to the femoral artery and then occludes it by exerting pressure with the transducer. The compression procedure is monitored by color duplex. There should be no flow signals from the neck or lumen of the aneurysm. Compression may take up to half an hour and the outcome is again verified sonographically. Complete thrombosis is suggested by the absence of flow signals in the sac of the aneurysm. If only partial thrombosis is achieved by compression, it is often easier to induce complete thrombosis in a second session on the next day (compression bandage), or complete thrombosis may occur spontaneously

Alternatively, thrombosis of a false aneurysm may be induced by thrombin injection (see Fig. A 2.25 a-c). However, thrombin injection often leaves a larger residual hematoma which may cause persistent symptoms. Thrombin injection is indicated when compression is not possible due to the localization of the aneurysm or in cases of perforation or suture aneurysm (where an infection must be excluded)

b A small false aneurysm (*A.S*) measuring only 2 cm but not occluding spontaneously arises somewhat atypically from the profunda femoris artery (*A.P.F*) about 2 cm distal to the femoral bifurcation (*left section*). With the sample volume placed in the neck, the typical systolic-diastolic to-and-fro flow is recorded. On the medial side of the neck, the superficial femoral artery (*A.F.S*) and vein (*V*) are depicted in the transverse plane. Compression of the neck with the transducer in a more lateral position brings about complete thrombosis of the aneurysm after 15 min (*right section*)

c Large traumatic false aneurysm (5.5 cm in diameter; gray-scale scan on the *left* and color duplex scan on the *right*) developing after perforation of a branch of the profunda femoris artery (*A.P.F*) by the lesser trochanter in association with a fracture of the neck of femur

d The false aneurysm is confirmed by the Doppler waveform with the characteristic systolic(*S*)-diastolic(*D*) to-and-fro flow in the aneurysmal neck between the profunda femoris branch (*A*) and the aneurysmal sac (*AN*), causing the typical “steam engine sound”

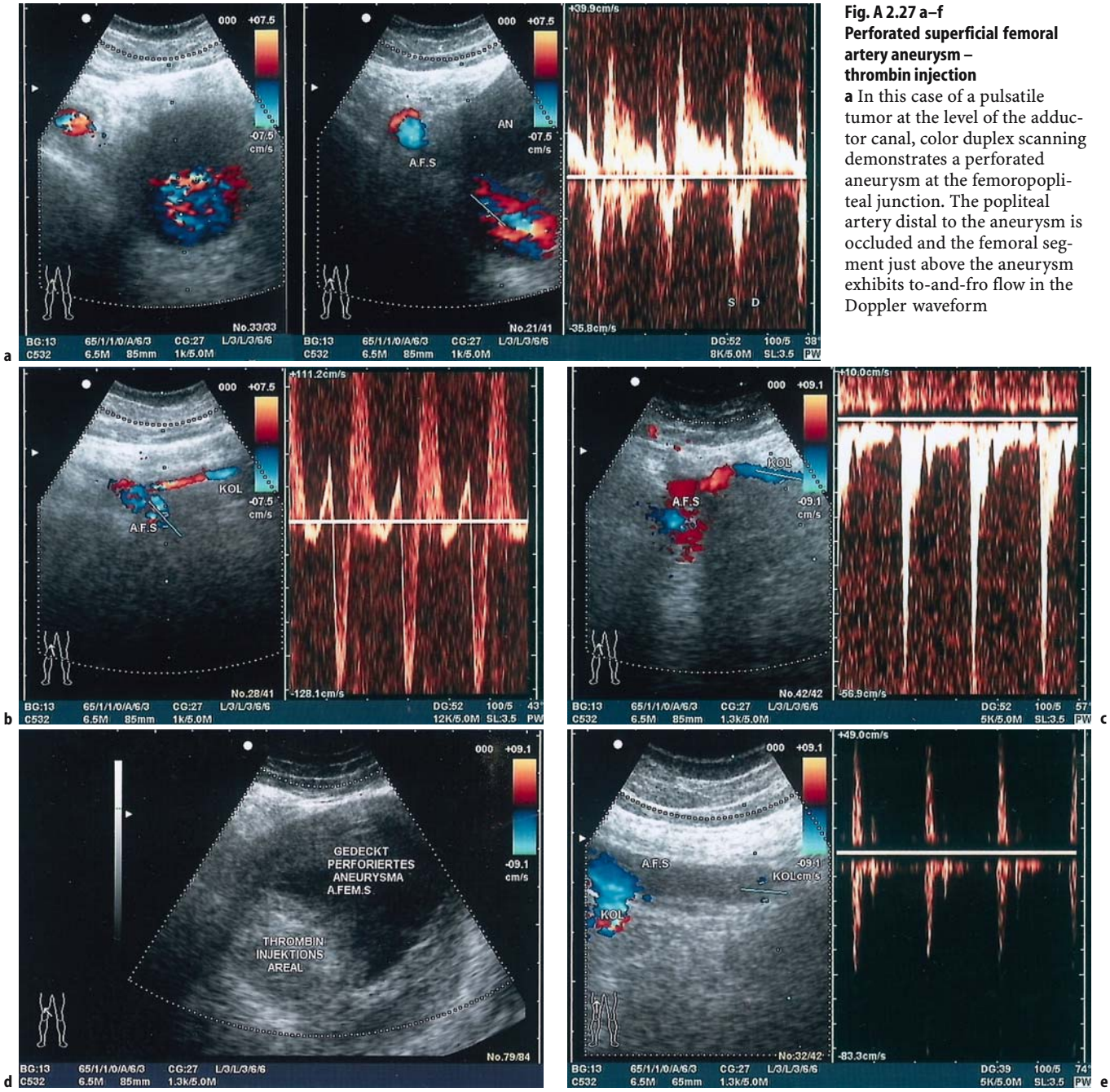

Fig. A 2.27 a–f
Perforated superficial femoral artery aneurysm – thrombin injection

a In this case of a pulsatile tumor at the level of the adductor canal, color duplex scanning demonstrates a perforated aneurysm at the femoropopliteal junction. The popliteal artery distal to the aneurysm is occluded and the femoral segment just above the aneurysm exhibits to-and-fro flow in the Doppler waveform

b The to-and-fro flow can be followed back into the distal superficial femoral artery (*A.F.S*) to the site of origin of a larger collateral (*KOL*). Systolic inflow (toward the periphery, away from transducer) is followed by early-diastolic outflow (toward transducer) and a further diastolic to-and-fro movement

c The Doppler waveform from the main collateral vessel in this case of presumably older popliteal occlusion has a just barely visible incisure but persistent diastolic flow (peripheral dilatation). The patient with considerable comorbidity and clinical stage II AOD did not require vascular repair; therefore, the perforated and only partially thrombosed aneurysm was treated with thrombin injection to induce complete thrombosis

d Thrombin at a dose of 5,000 IU dissolved in 5 ml saline solution was injected after ultrasound-guided placement of the needle in the aneurysm. The fresh thrombus has a higher echogenicity

e Following thrombin injection, the superficial femoral artery was likewise thrombosed to the level of the origin of the collateral with a blunt signal in the proximal segment ("knocking" waveform). The hematoma caused no pressure-related symptoms, and there was no progression of stage II AOD

(Fig. A 2.27 cont.)
f Angiography prior to thrombin injection: Aneurysm of the superficial femoral artery and popliteal artery occlusion with refilling of the lower leg arteries through the collateral vessel already demonstrated by ultrasonography

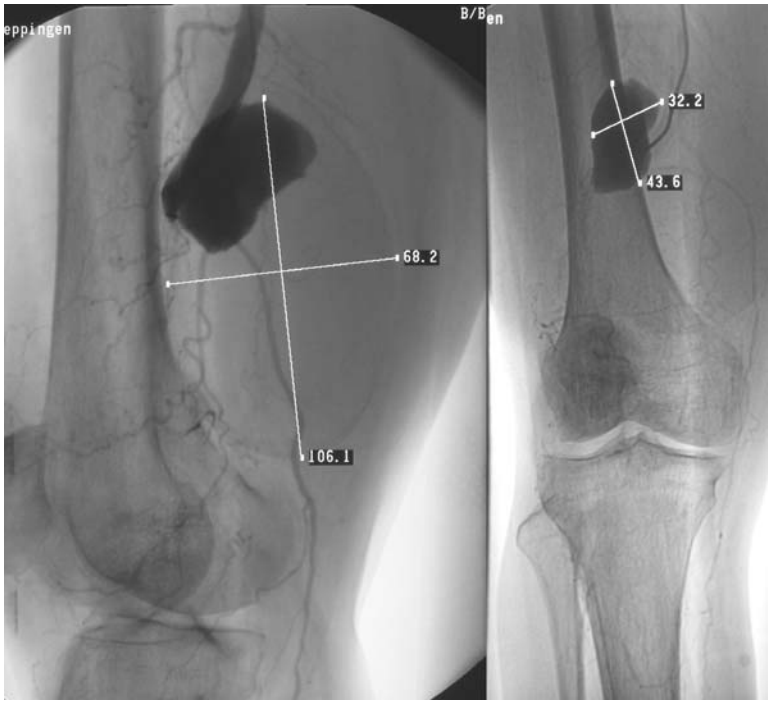

f

Fig. A 2.27g, h
Internal iliac artery – false aneurysm – thrombin injection
g Routine abdominal diagnostic assessment prior to gastrectomy for cancer in a 78-year-old patient reveals a spontaneous false aneurysm (no trauma, no iatrogenic cause) arising from the internal iliac artery and measuring 6 x 6 cm. Under ultrasound guidance, a thin needle is passed somewhat below the iliac bifurcation between the internal and external iliac arteries to puncture the aneurysm for instillation of 5,000 IU of thrombin dissolved in 3 ml saline solution. Only marginal thrombosis is achieved (*right section*). Much of the lumen still shows eddy flow (color coding). Injection of a second dose of 5,000 IU of thrombin into the false aneurysm (*A.S*) results in complete thrombosis (*left section*). Even at a low pulse repetition frequency, no flow signals are detected in the color duplex mode. There is flow in the external iliac (*A.I.E*) and internal iliac (*A.I.I*) arteries. The patient has no clinical symptoms

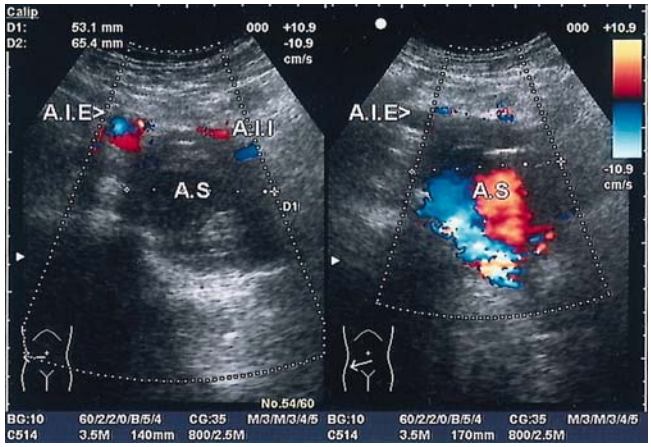

g

h *Left section*: Control angiography showing large false aneurysm arising from the internal iliac artery (detail with iliac bifurcation in oblique projection) prior to thrombin injection

Right section: Angiography of the aortic bifurcation and pelvic circulation (both iliac bifurcations) after ultrasound-guided thrombin injection into the false aneurysm (oblique projection similar to preinterventional angiogram). Absence of contrast medium in the area of the aneurysm as evidence of complete thrombosis

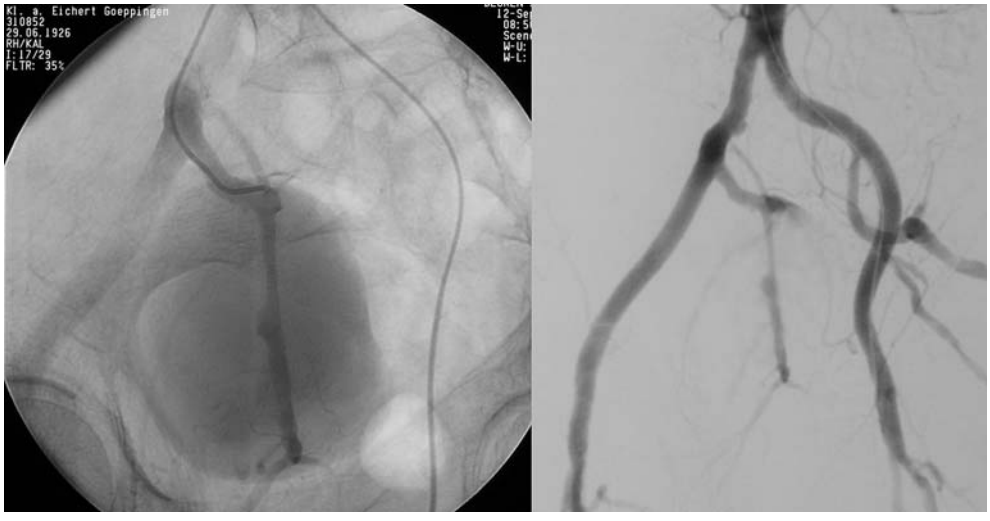

h

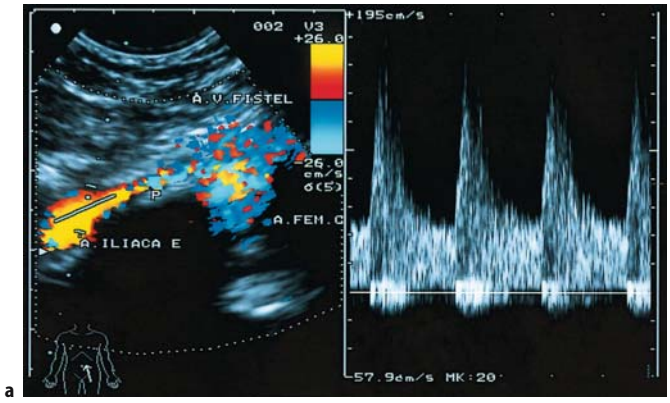

a

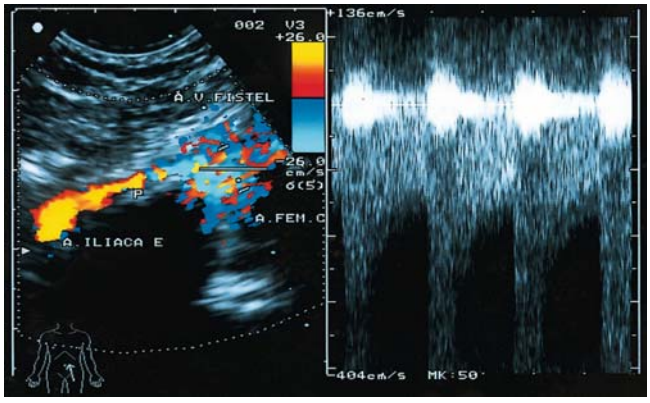

b

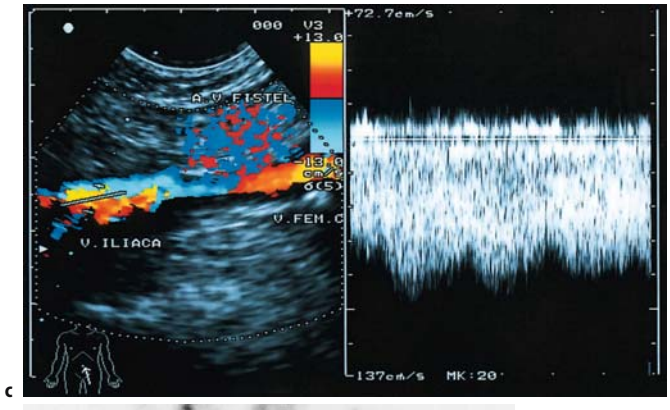

c

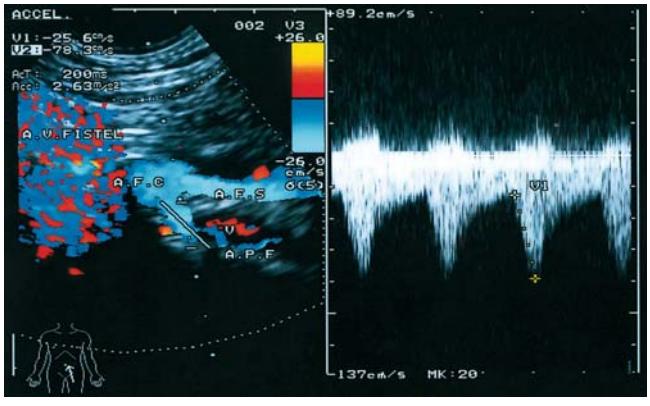

d

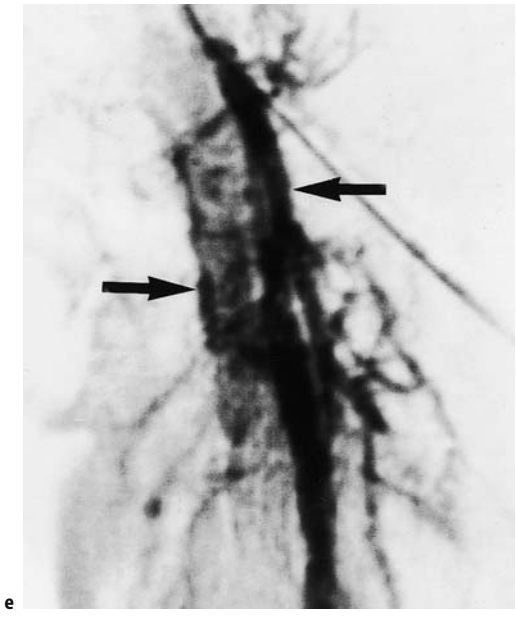

e

Fig. A 2.28 a–e
Arteriovenous fistula

a Patient with stage IV AOD in whom color duplex ultrasound after puncture in the left groin shows a mosaic-like "color cloud" at the junction of the external iliac and common femoral arteries. The distal external iliac artery shows the high-frequency flow typical of an artery feeding a fistula with a peak flow velocity of 160 cm/s during systole and 50 cm/s at end-diastole (monophasic)

b Just proximal to the color cloud there is a calcified and stenosing plaque with posterior acoustic shadowing. The high-frequency flow signal recorded in the area of the cloud (end-diastolic: 80 cm/s; systolic: >400 cm/s) may be related to a stenosis or fistula. For further clarification, venous drainage and the femoral artery distal to this area must be examined

c The iliac vein exhibits the venous flow signal typical of an AV fistula: high-frequency flow (angle-corrected: 90 cm/s) with pulsatile variation. Adjustment of the PRF to venous flow leads to aliasing (*left* side of color scan)

d The Doppler waveform from the profunda femoris artery distal to the AV fistula has a delayed and flattened systolic upslope and a monophasic profile with a fairly large diastolic flow component. This is a typical poststenotic profile, caused by the puncture-induced AV fistula and the high-grade stenosis resulting from the plaques shown in **a**. For differentiation of the cause of the perivascular vibration artifacts, the downstream circulation must be evaluated (fistula: venous; stenosis: arterial). As illustrated here, vessel manipulation by puncture may not only induce fistula formation but also cause stenosis through detachment of a plaque from the vessel wall

e Angiography: Contrast medium outflow in the iliac vein typical of a fistula. Angiography does not allow precise localization of the fistula nor does it provide clearcut evidence of the additional presence of a stenosis in this area (superimposition)

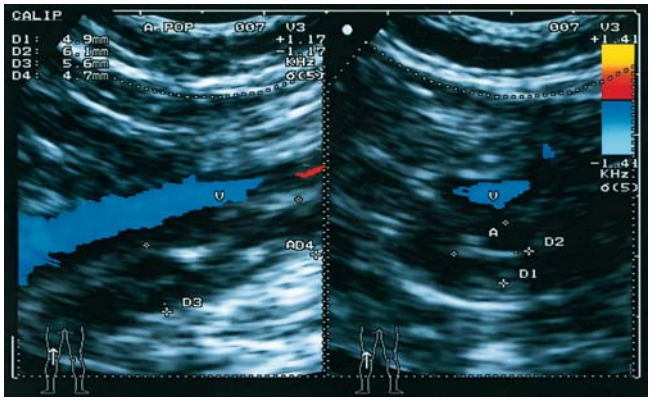

a

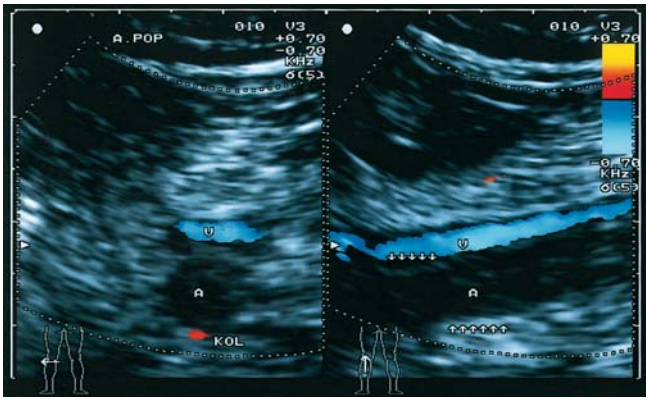

b

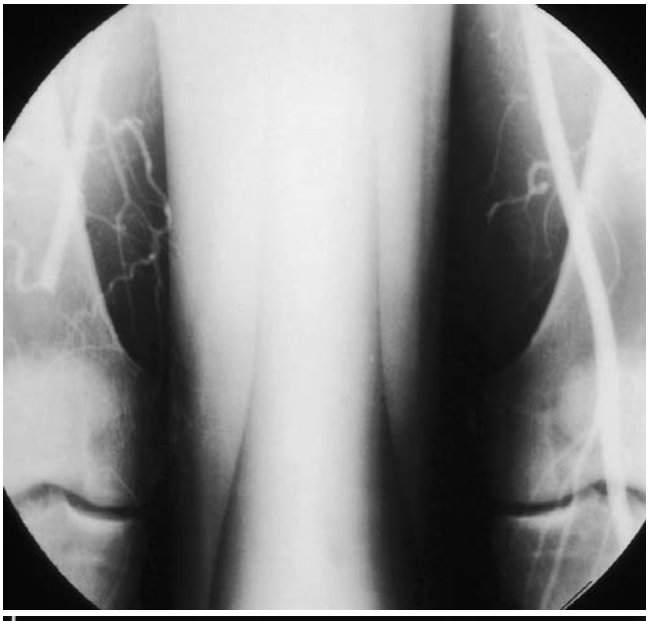

c

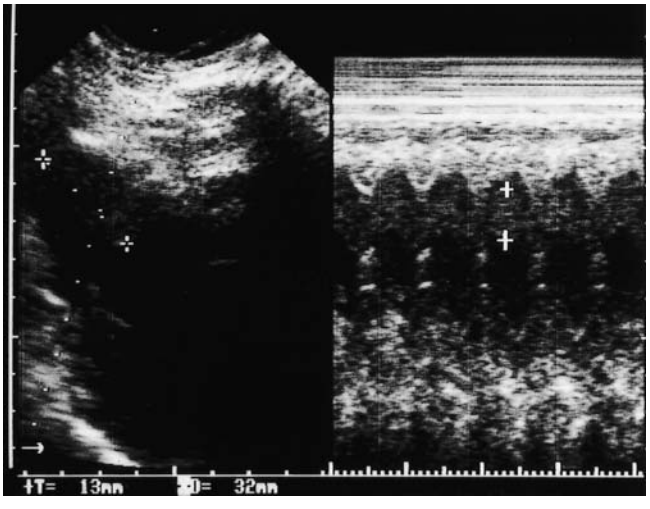

d

Fig. A 2.29 a–g
Popliteal artery occlusion – atherosclerosis versus embolism
a Atherosclerotic occlusion of the popliteal artery, longitudinal view on the *left*, transverse view on the *right*: Popliteal vein displayed in blue close to transducer. The pronounced plaques throughout the vessel with poor demarcation of the wall contour as well as the inhomogeneous and partially very hyperechoic vessel lumen suggest an atherosclerotic process. Based on these ultrasound findings, catheter thrombolysis, possibly with PTA, is not promising. Instead, bypass grafting is indicated, if clinically necessary
b Embolic occlusion: The lumen of the popliteal artery is filled with a hypoechoic, homogeneous thrombus or embolus. There is good delineation of the vessel wall without signs of plaque. Anterior to the popliteal artery, the popliteal vein is depicted in blue; posterior to it, a red arterial collateral (*KOL*) is shown
c Angiography: Popliteal artery occlusion
d Further diagnostic workup reveals a thrombus at the tip of the left ventricle as the source of embolic occlusion. The floating thrombus is indicated by *plus signs* in the two-dimensional view on the *left* and in the time-motion display on the *right*

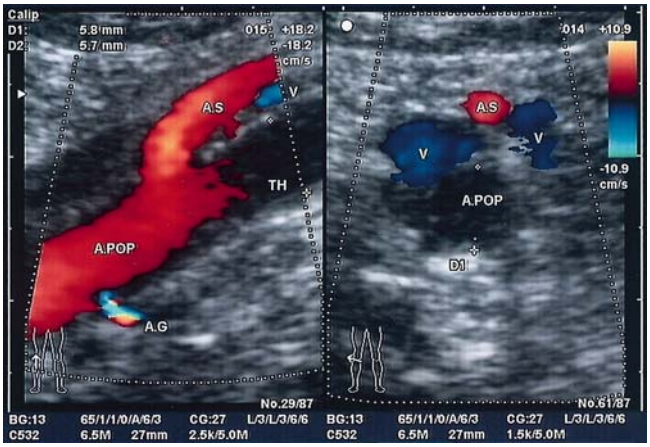

e

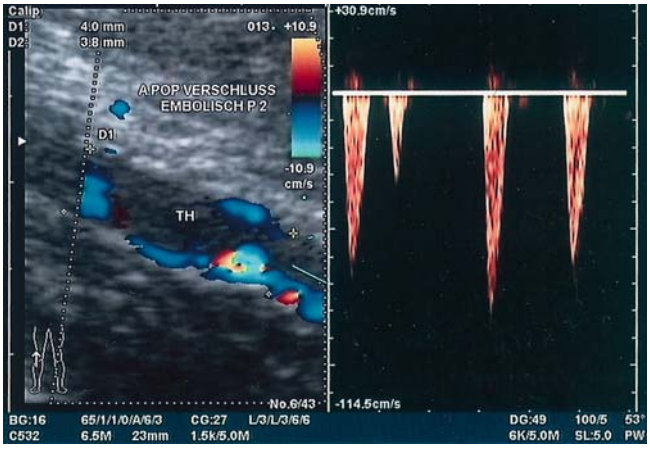

f

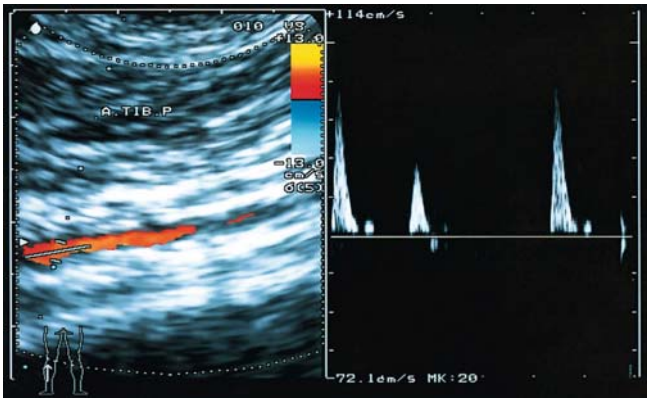

g

(Fig. A 2.29 cont.)
Embolic occlusion

e Emboli grow in a cranial direction by thrombotic apposition up to the next branching of a hemodynamically significant collateral or become lodged in a bifurcation. In the case of embolic popliteal artery occlusion presented here (longitudinal view on the *left* and transverse view on the *right*), the artery is patent down to the origin of the sural artery while the distal portion is occluded (*TH*). The vessel wall is smoothly delineated and shows no atherosclerotic changes

f When there is spontaneous partial or complete recanalization of thromboembolic occlusions, the Doppler waveform at follow-up will show flow signals near the arterial walls. In the example, flow (blue, away from transducer) along the intraluminal thromboembolic material is demonstrated in the distal popliteal artery. The thrombus (*TH*) is homogeneous and clearly delineated from the wall, which shows no atherosclerotic changes

g Despite flow obstruction through the popliteal artery thrombus, the Doppler tracing (arrhythmia) from the patent lower leg arteries shows triphasic flow (as illustrated here in the distal posterior tibial artery). With compensation through collateral perfusion, the flow obstruction in the popliteal artery has only little effect on peripheral perfusion

After two days of heparin therapy, there was complete recanalization of the popliteal artery

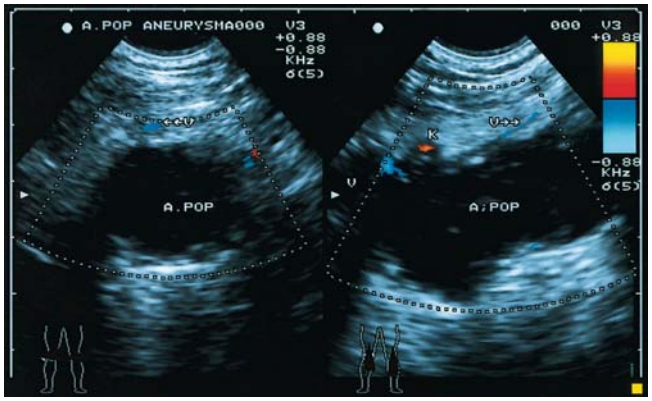

a

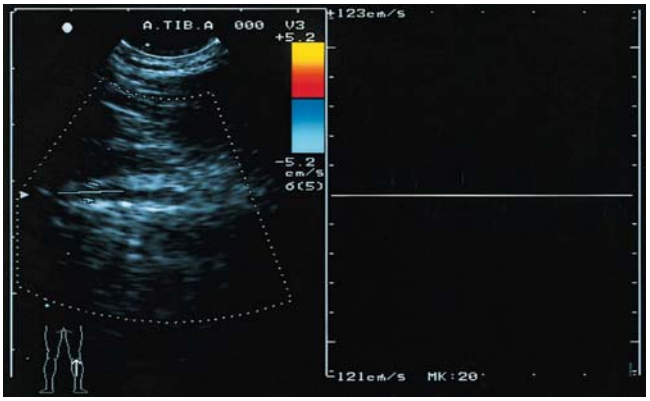

b

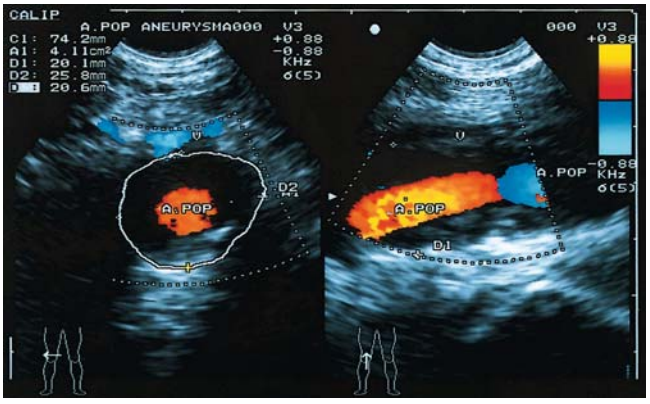

c

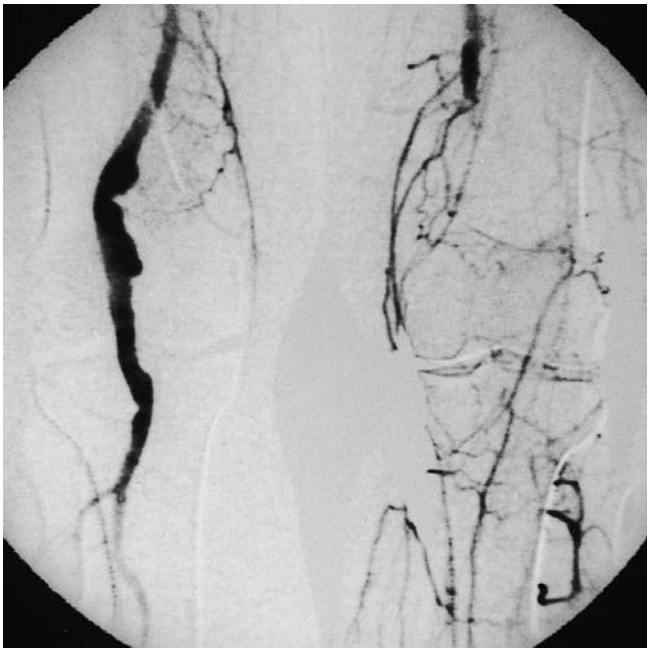

d

Fig. A 2.30 a–d
Aneurysm

a Patient with ischemic rest pain due to popliteal artery occlusion caused by a completely thrombosed aneurysm. Segments of the compressed vein displayed in blue are seen near the transducer. No flow signals are obtained from the lumen of the popliteal aneurysm. Transverse view of the aneurysm on the *left* (*A.POP*) and longitudinal view on the *right*

b Apart from the risk of perforation, a partially thrombosed popliteal artery aneurysm tends to embolize into distal vessel segments. Chronic recurrent emboli can lead to occlusion of a main lower leg artery, as illustrated here for the mid-third of the anterior tibial artery. Neither color duplex nor the Doppler waveform shows a flow signal. In this example, a femoropopliteal or crural bypass graft to bridge the aneurysm has an unfavorable prognosis due to embolic impairment of the outflow tract

c On the contralateral side, the patent lumen of the popliteal artery (red) is surrounded by the hypoechoic thrombotic deposits of the partially thrombosed aneurysm. The patent lumen of the aneurysm roughly corresponds to the lumen of a normal popliteal artery, as shown on the transverse scan on the *left* and the longitudinal scan on the *right*. The white line indicates the extent of the aneurysm (*left section*)

d Angiography: Popliteal artery with occlusion on the *left* and aneurysmal dilatation on the *right*. An estimate of the length and diameter of the aneurysm is not possible

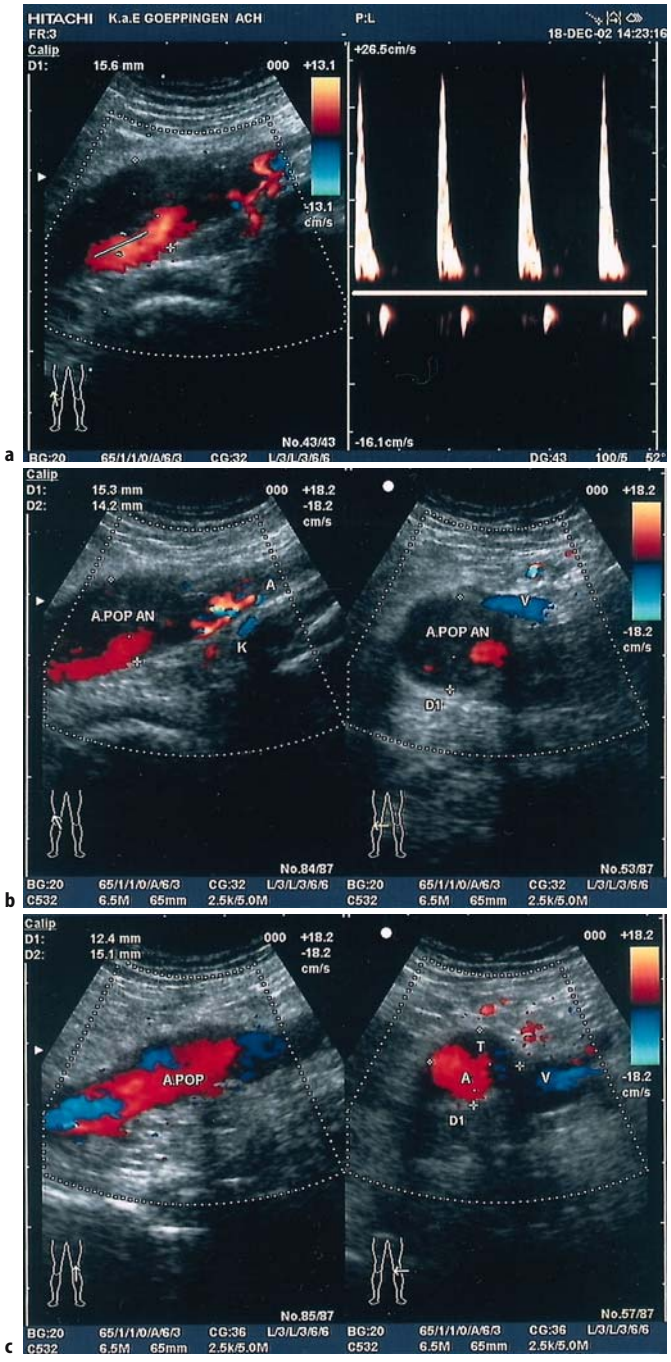

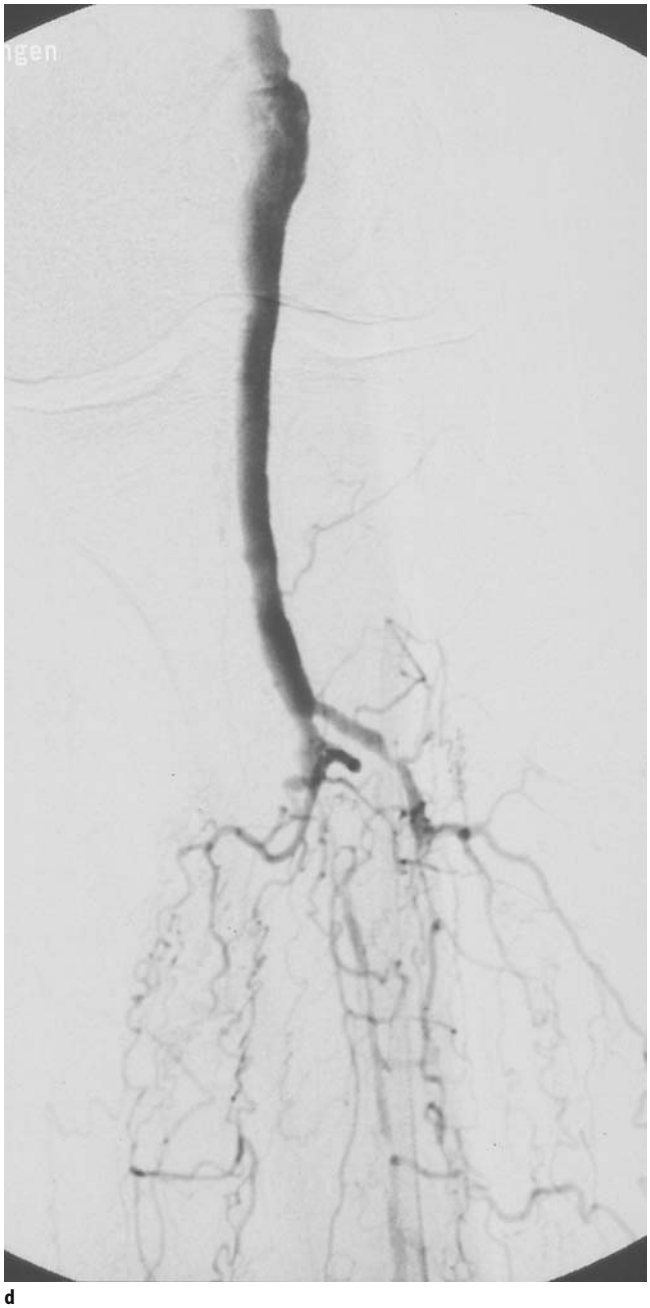

Fig. A 2.31 a–d
Small popliteal artery aneurysm with arterial embolism
a, b Patient with small popliteal aneurysms on both sides. Ultrasonography demonstrates occlusion of the popliteal artery distal to the aneurysm on the right. The aneurysm is partially thrombosed and has a diameter of 1.5 cm. There is only residual flow through the aneurysm via collaterals (arising from the popliteal artery in the distal aneurysm). These are patent but outflow is obstructed. This situation is reflected by a blunt waveform with a peak systolic velocity reduced to 22 cm/s
c Scans of the left popliteal artery (longitudinal view on the *left*, transverse view on the *right*) depict the small aneurysm (diameter of 1.5 cm) with only little thrombosis (clearly seen on the transverse view only) and a patent residual lumen of normal width. The lower leg arteries are still patent. The control examination performed prior to elective aneurysm resection showed an unchanged configuration of the aneurysm, but lower leg artery occlusions due to arterial embolism
d Left-sided angiography showing occlusions of lower leg arteries without significant dilatation of the popliteal artery. Only at the upper margin of the image does the popliteal artery appear somewhat ectatic (corresponding ultrasound scans in **c**)

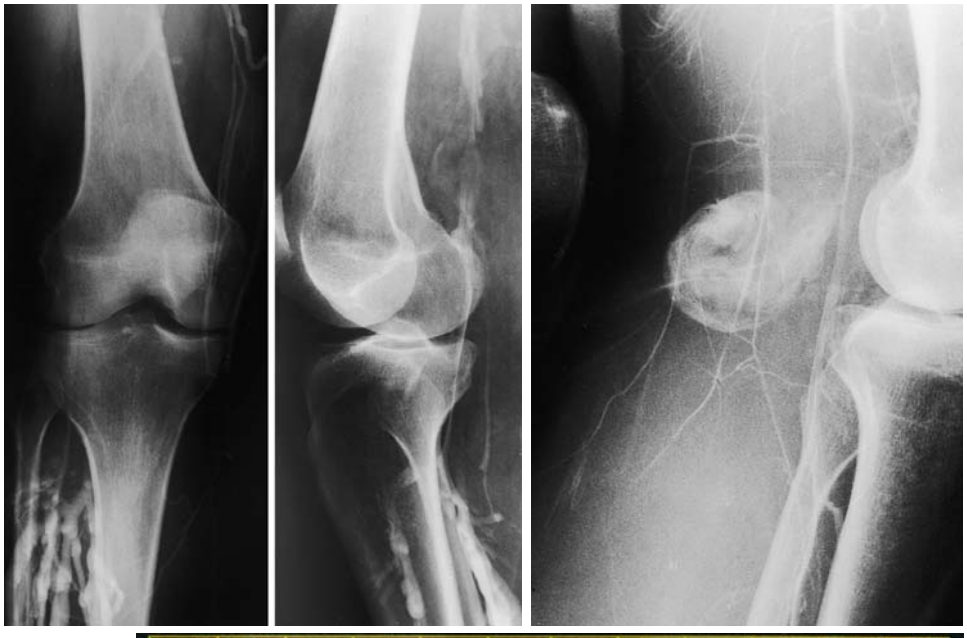

a d

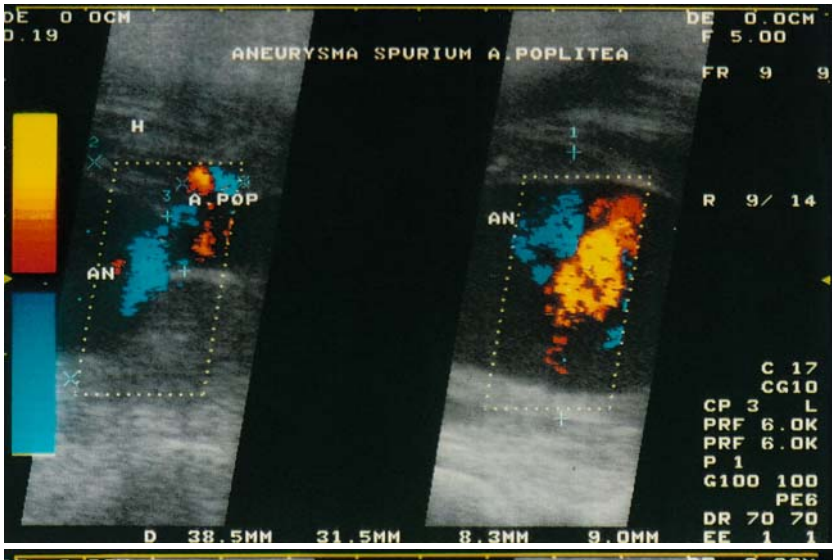

b

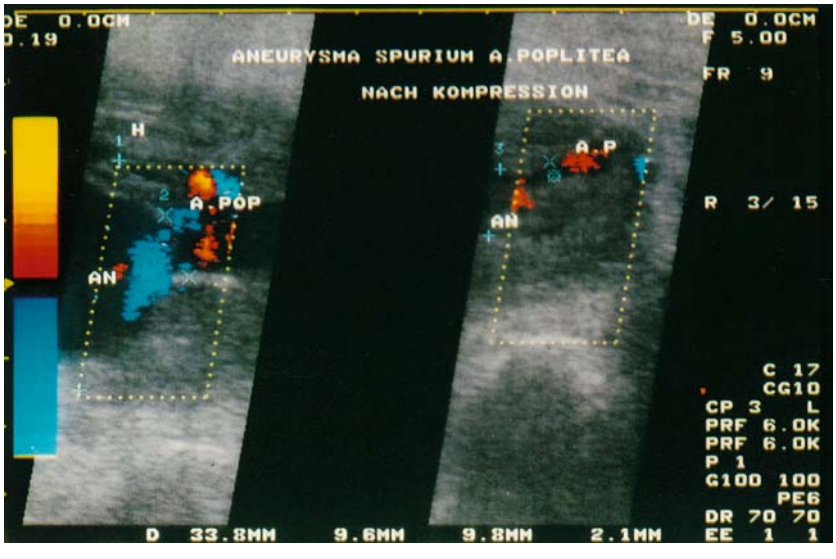

c

Fig. A 2.32 a–d
False aneurysm

a Iatrogenic damage to the vessels of the popliteal fossa is a rare but serious complication of knee arthroscopy. In the case presented, a large false aneurysm developed after outpatient arthroscopy with partial resection of the medial meniscus. Venography performed for swelling of the calf showed contrast gaps in the popliteal vein, which were misinterpreted as popliteal vein thrombosis

b Duplex scanning performed after initiation of anticoagulation therapy demonstrates the false aneurysm. In the aneurysm there is flow toward and away from the transducer (*right section*). Black areas without flow signals either indicate stasis in the aneurysm or are due to the failure to obtain flow signals at an angle of 90° (cos 90° = 0)

The scan on the *left* depicts the canal connecting the popliteal artery (*A.POP*) and the aneurysm (*AN*) in blue, indicating flow from the artery into the aneurysm. The aneurysm is surrounded by a hematoma (*H*). Ultrasound shows the popliteal vein to be compressed by the aneurysm rather than thrombosed

c The attempt to induce thrombosis of the aneurysm by compression failed because the neck is too wide and there is no adequate structure against which to compress it. The *right section* shows persistent flow signals after attempted compression. Thrombin injection would have been an alternative in this case but experience with this therapy was still limited when this patient was seen 10 years ago

d Angiography: False aneurysm of the popliteal artery

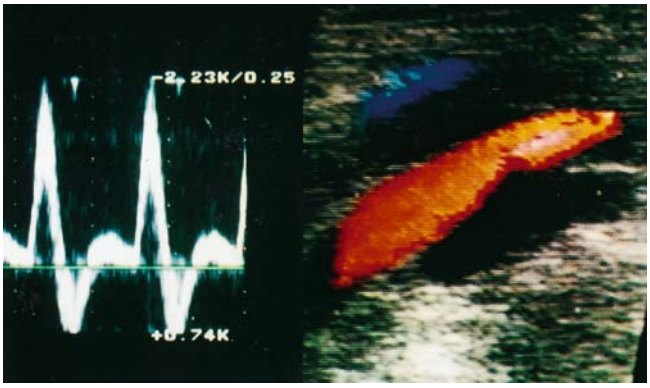

a

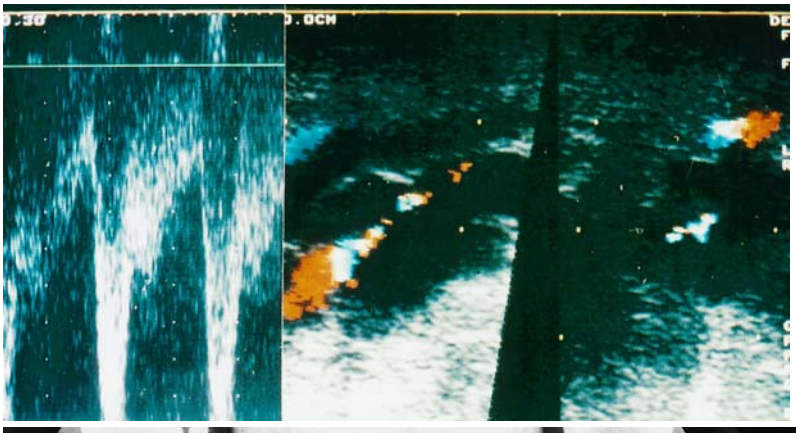

b

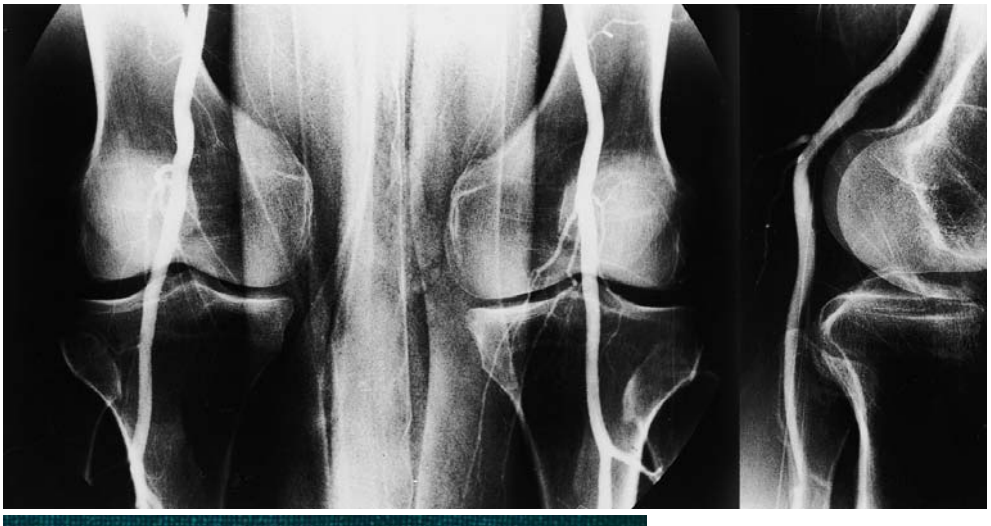

c

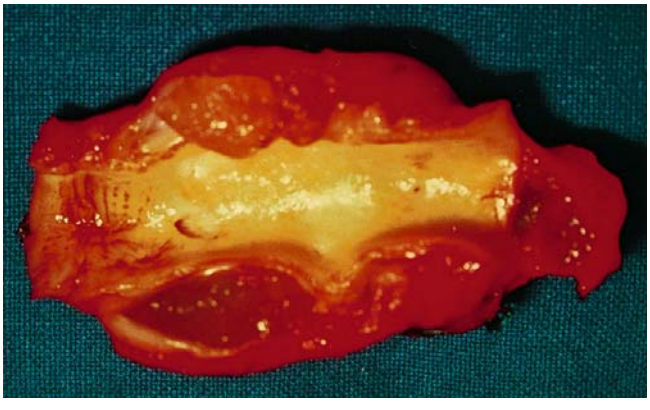

d

Fig. A 2.33 a–d
Cystic adventitial disease
a The popliteal artery (displayed in red) is surrounded by hypoechoic cystic structures, which produce slight indentation of the patent lumen but no hemodynamically significant narrowing. The Doppler waveform shows triphasic flow. The patient reports intermittent claudication with a highly variable walking distance
b Seven days after the first examination the patient presents with severe claudication and a maximum walking distance of 30 m. Ultrasound shows a markedly increased cyst volume with high-grade stenosis of the popliteal artery (*middle section*: longitudinal view; *right section*: transverse view). Color duplex ultrasound depicts a small residual lumen between the cysts with accelerated flow and aliasing. The Doppler tracing is presented in the inverted mode with arterial flow displayed below the baseline. The waveform indicates stenosis with monophasic flow and a flow velocity of over 3 m/s
c Angiography performed 2 weeks later: Fairly inconspicuous popliteal artery with only slight anterior indentation, identified on a lateral view. Duplex scanning performed at this time shows a marked decrease in cyst size without hemodynamically significant stenosis corresponding to the situation depicted in **a**
d The therapy of choice is surgical resection of the cyst-bearing arterial segment or enucleation of the cysts if the intima is still intact. In the example presented, gross inspection of the surgical specimen shows the adventitial cysts to be filled with gelatinous material. (Courtesy of Schwilden)

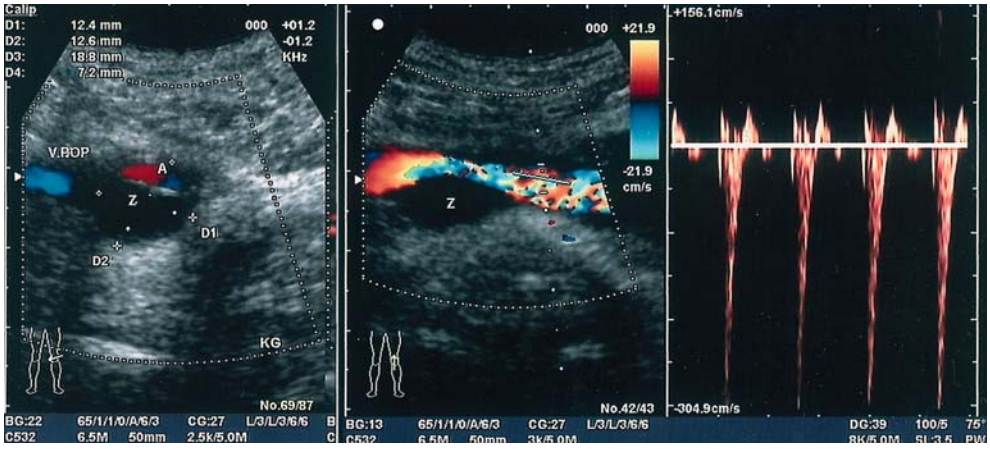

Fig. A 2.34 a–c
Cystic adventitial disease – variable cyst size
a This patient with intermittent claudication of variable severity due to cystic adventitial disease (*Z*) shows a highly variable cyst size over a period of 2 weeks. The transverse view (*left*) demonstrates compression of the popliteal artery with a residual lumen of 20 – 30 %. Aliasing (*middle section*) and a flow velocity of 3 m/s in the Doppler waveform confirm stenosis due to cystic vessel compression

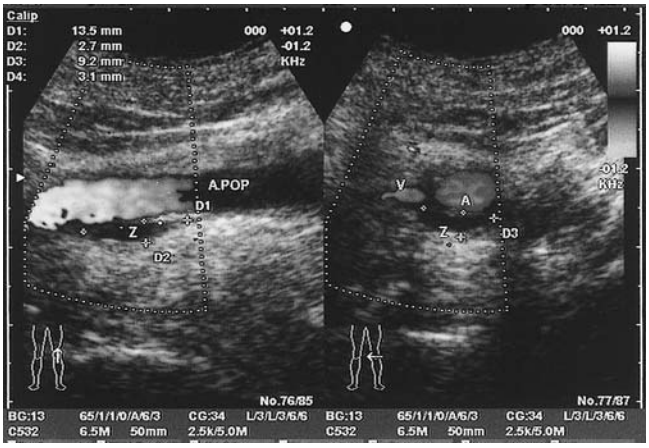

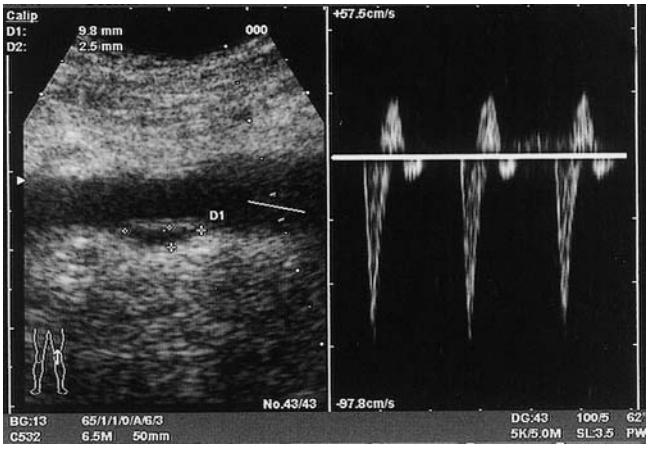

b, c The cyst has become so small that it is easily overlooked on routine ultrasound if one is unaware of the earlier findings (**b**, longitudinal view on the *left*, transverse view on the *right*). The diameter of the cyst has decreased from 1 cm to 2.7 mm and the vessel lumen is no longer compromised (not seen angiographically). The Doppler waveform is normal

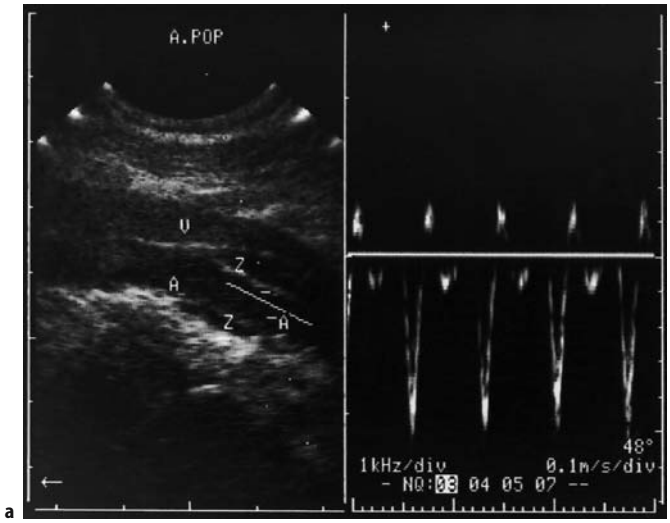

a

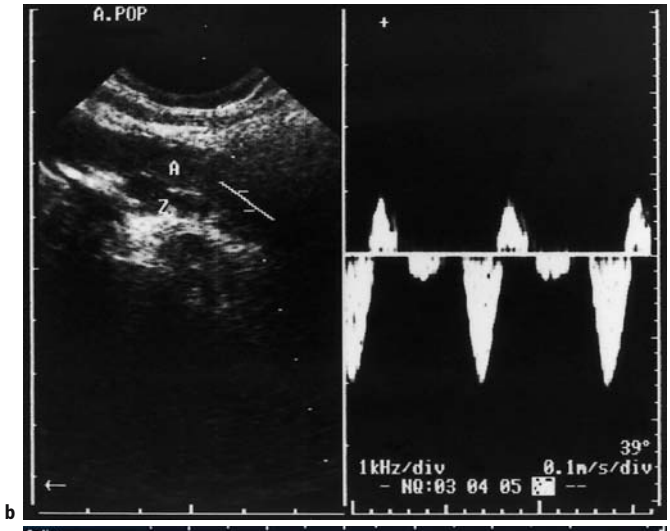

b

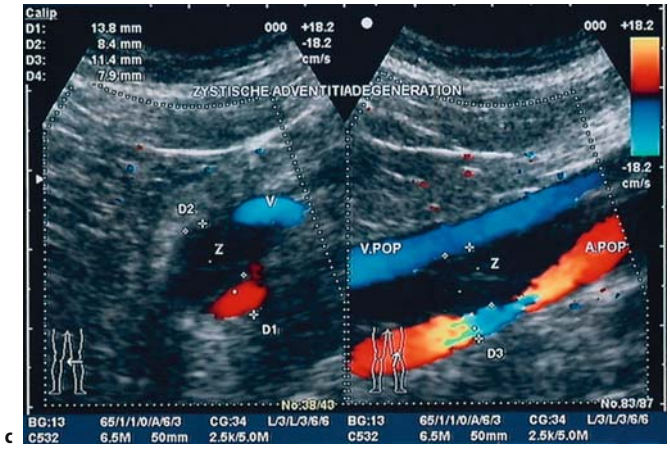

c

Fig. A 2.35 a, b
Cystic adventitial disease – ultrasound-guided aspiration
a 44-year-old patient with 2 cysts around the popliteal artery and intermittent claudication. As the patient refuses surgery (enucleation or resection of cystic vessel segment), an attempt is made to aspirate the contents under ultrasound guidance. At the time of examination, the cysts do not cause narrowing of the popliteal artery, the Doppler frequency spectrum is triphasic, and there is no flow acceleration. The popliteal vein depicted near the transducer is not compressed either
b The posterior cyst near the transducer can be emptied under ultrasound guidance; 2 ml of viscous fluid is aspirated. The anterior cyst cannot be punctured without perforating the vessel wall. In the view presented the popliteal vein is compressed by the transducer. Follow-up ultrasound showed an unchanged anterior cyst and no recurrence of the posterior cyst; the patient has been free of complaints for 5 years

Cystic adventitial disease – differentiation from dissection
c Single or multiple cysts as well as cysts extending over a long vessel segment may occur in cystic adventitial disease. A cyst involving a long popliteal segment as in this example may be difficult to differentiate from dissection with complete thrombosis of the false lumen (compare Figs. A 2.39 a and A 5.18 d,e). The popliteal artery (*A.POP*) is shown in transverse orientation on the *left* and in longitudinal orientation on the *right* with the cyst (*Z*) narrowing a long segment of the artery (confirmed intraoperatively). There is aliasing as a result of cystic narrowing of the lumen. The popliteal vein (*V.POP*) is depicted closer to the transducer with flow coded in blue

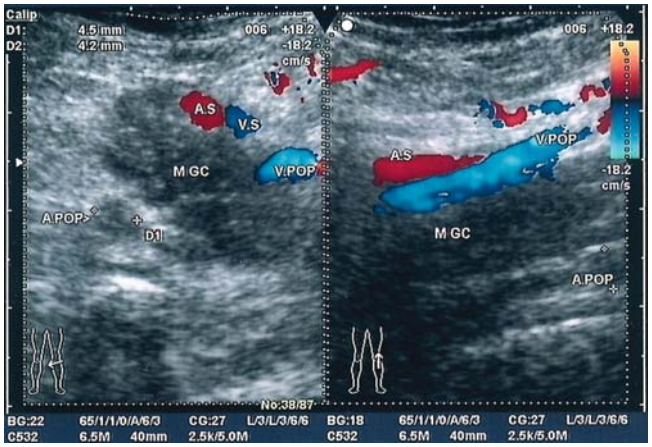

a

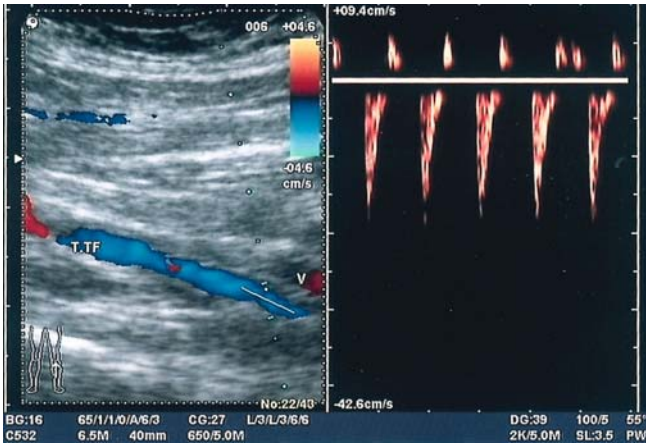

b

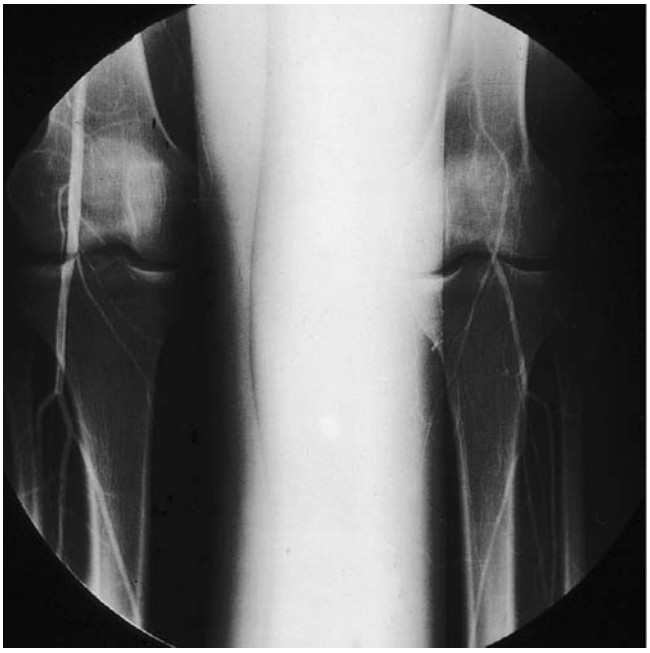

c

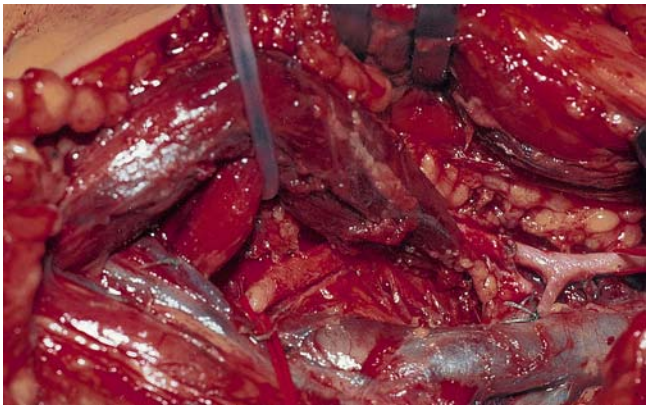

d

Fig. A 2.36 a–d
Popliteal entrapment syndrome (Insua type I, cf. Fig. 2.10 a)
a Isolated popliteal artery occlusion due to malformation of the medial head of the gastrocnemius muscle forcing the artery to course around the head on the medial side. In this type of malformation, the medial head of the muscle is located between the popliteal artery and vein – which thus do not pass through the popliteal fossa together – and compresses the artery against the femur with each plantar flexion. Intermittent compression damages the vessel wall with deposition of thrombotic material, which may ultimately progress to occlusion. No color duplex signal is obtained from the popliteal artery (*A.POP*). Posterolateral to the head of the gastrocnemius, the patent popliteal vein (*V.POP*) is depicted closer to the transducer with a blue flow signal. Posterior to it, the artery (red) supplying the soleus muscle and serving as a collateral and the vein are shown. The arteries acting as collaterals are markedly dilated due to the chronic occlusion process and may thus be confused with the popliteal artery. The sonoanatomic situation (transverse section on the *left* and longitudinal section on the *right*) is as follows: The popliteal artery courses anterior to the popliteal vein and is depicted farther away when scanning is performed from the posterior approach. The muscle-supplying arteries acting as collaterals arise from the posterior aspect of the popliteal artery and course posterior to the popliteal vein and are thus closer to the transducer than the vein
b In this case with good collateralization of a chronic occlusive process, the flow profile in the refilled tibiofibular trunk does not show the typical postocclusive monophasic flow but is triphasic, though damped. Peak systolic velocity is just under 20 cm/s. Additional collaterals enter distally. There is no postocclusive peripheral dilatation at rest
c Angiography: Short occlusion of the left popliteal artery with refilling at the level of the knee joint cleft (lateral collateral)
d The intraoperative site confirms the ultrasound findings. The popliteal artery and vein do not pass through the popliteal fossa together because the medial gastrocnemius head (encircled with transparent vessel loop) attaches between the artery (distal segment encircled with red vessel loop) and the vein (at *lower margin*). The proximal popliteal artery (on the *right*) gives off the collateral already identified sonographically and accompanying the vein

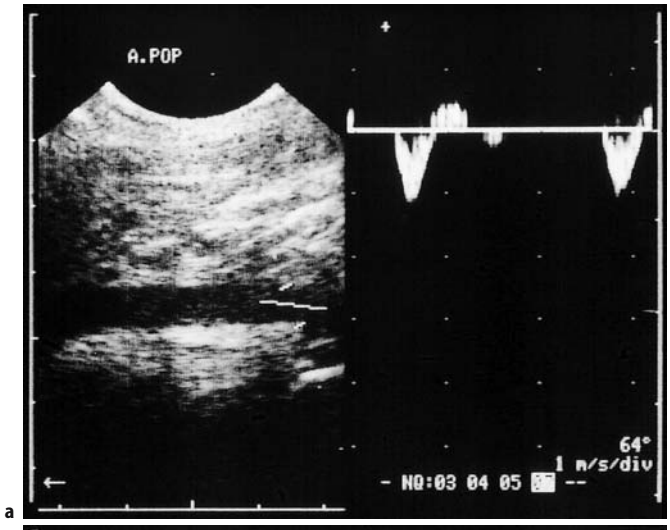

a

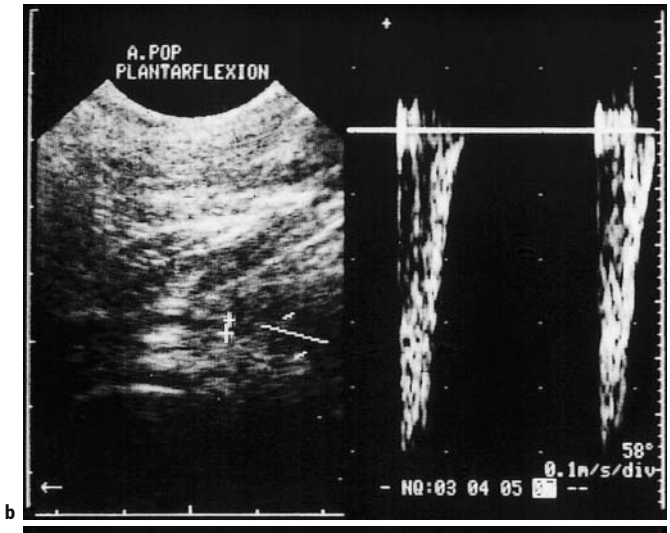

b

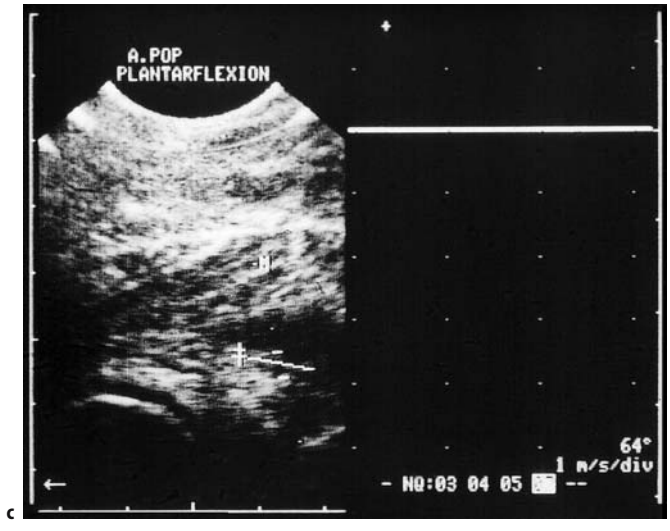

c

Fig. A 2.37 a–c
Popliteal entrapment syndrome (cf. Fig. 2.10 f)
a Calf swelling with occasional pain in a young patient caused by compression of the vessels in the popliteal fossa due to a hypertrophied head of the gastrocnemius with normal attachment. The popliteal artery and vein pass through the popliteal fossa together and the vein is already compressed by the relaxed muscle (cf. Fig. A 3.45 b, c). The popliteal artery is not stenosed and shows triphasic flow in the Doppler tracing

b Progressive compression of the popliteal artery occurs with increasing plantar flexion, producing a stenosis signal in the Doppler waveform with loss of triphasic flow and a peak flow velocity of 300 cm/s
c Further plantar flexion leads to complete occlusion of the popliteal artery through muscular compression (cf. also Fig. A 3.45 a–c: Popliteal entrapment syndrome with arterial and venous compression)

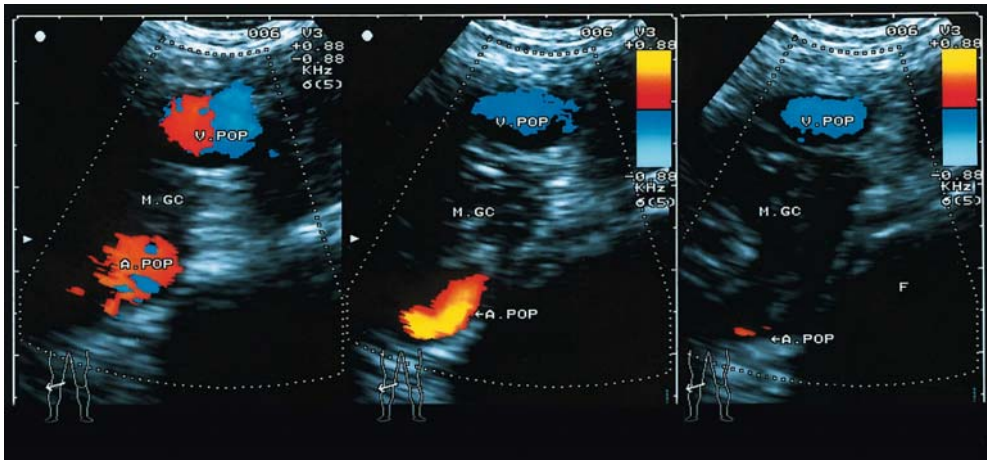

Fig. A 2.38
Popliteal entrapment syndrome – functional test
38-year-old athletic patient with entrapment syndrome caused by an abnormal lateral extension of the gastrocnemius muscle with muscle fibers coursing from the medial head to the bone attachment of the lateral head (Insua type II). The transverse views from left to right show the progressive compression of the popliteal artery by the gastrocnemius muscle (*M.GC*) with increasing plantar flexion. The muscle attachment between the popliteal artery and vein (*V.POP*) forces them apart, thereby compressing the artery (subtotal occlusion on *rightmost scan*)

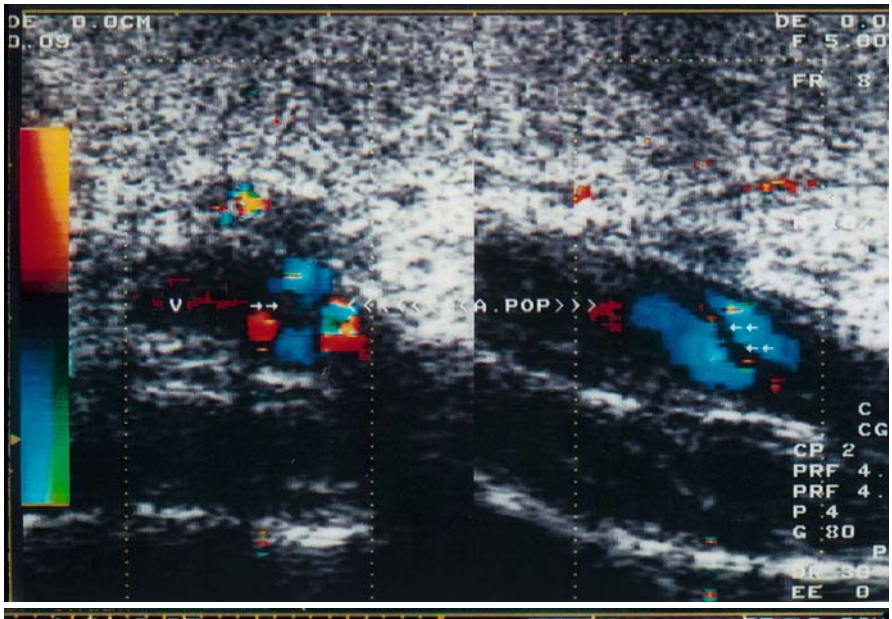

a

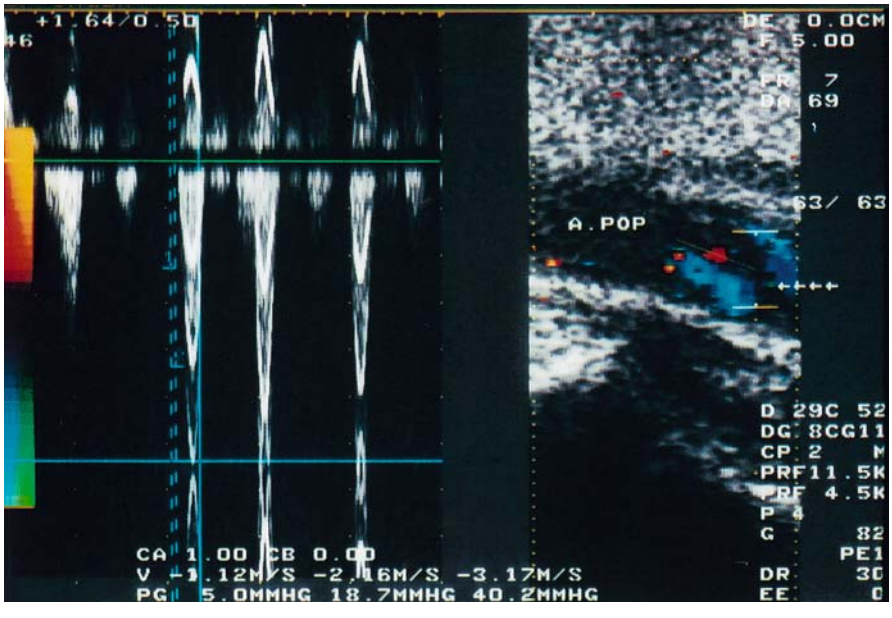

b

Fig. A 2.39 a, b
Dissection
a Popliteal trauma can cause arterial wall dissection with ischemia-related symptoms of varying severity. A tear of the intima with detachment is depicted as a disruption of the color-coded arterial flow column in the color duplex mode. In the arteries below the inguinal ligament, dissection rarely leads to the development of 2 lumina over a long segment but gives rise to intimal flaps that can block the lumen. The transverse view of the artery is shown on the *left* and the longitudinal view on the *right*; *arrows* indicate the dissection. The transverse view of the popliteal artery depicts at least two lumina with different color coding
b The Doppler waveform from the dissected popliteal artery simultaneously depicts flow signals of different velocity and direction. There is proper blood flow to the periphery but a "knocking" waveform consistent with several blood columns with different flow velocities

Intraoperative inspection revealed a partial tear of the intima and two lumina with forward flow and flow-obstructing intimal flaps more distally. The resected arterial segment was replaced by a venous graft

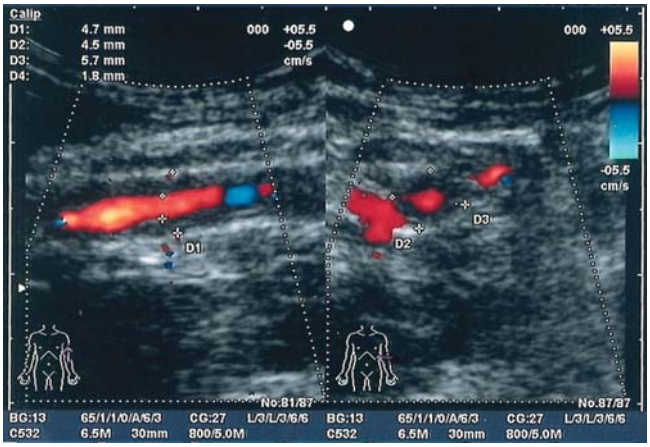

Fig. A 2.40
Inflammatory vascular disease
Vascular inflammation – Takayasu's arteritis of the subclavian and common carotid arteries or polyarteritis nodosa – leads to concentric wall thickening with a centrally perfused lumen in extremity vessels as in the case presented here and is identified on ultrasound by the macaroni sign. There is a normal echo reflected from the wall interface while the remainder of the arterial wall is depicted as a concentric, hypoechoic structure (wall thickening) over a long segment without signs of atherosclerotic plaques. Progressive inflammatory wall thickening may ultimately lead to occlusion of the affected vessel. Aneurysmal changes may also occur. The longitudinal view on the *left* and the transverse view on the *right* show the concentric wall thickening of a lower leg artery in a patient with polyarteritis nodosa. (Due to reflux caused by postthrombotic venous changes, the veins depicted to the left and right of the artery are likewise displayed in blue)

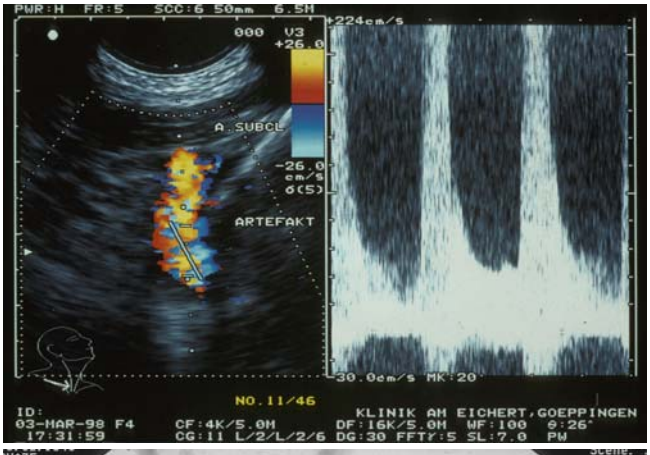

a

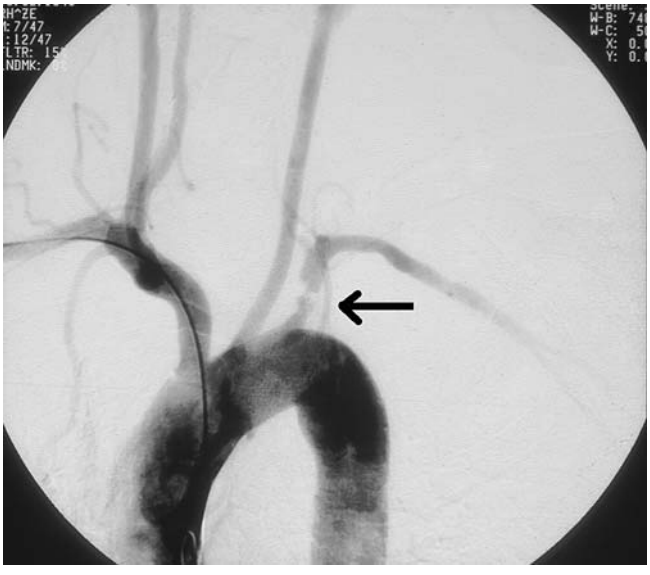

b

Fig. A 2.41 a–c
Subclavian artery stenosis due to atherosclerosis
a Scanning of the subclavian artery from the supraclavicular position demonstrates direct signs of stenosis: increased peak systolic flow, aliasing, and perivascular vibration artifacts. Atherosclerotic stenoses of the arm arteries typically affect the origin of the subclavian artery and cannot be identified on the basis of direct criteria in all cases. Instead, the diagnosis has to rely on indirect criteria such as monophasic postocclusive flow
b Angiography showing stenosis of the subclavian artery on the *left*
c The aneurysm (*AN*) of the right subclavian artery (longitudinal view on the *left*, transverse view on the *right*) is not depicted angiographically (cf. **b**) due to thrombosis

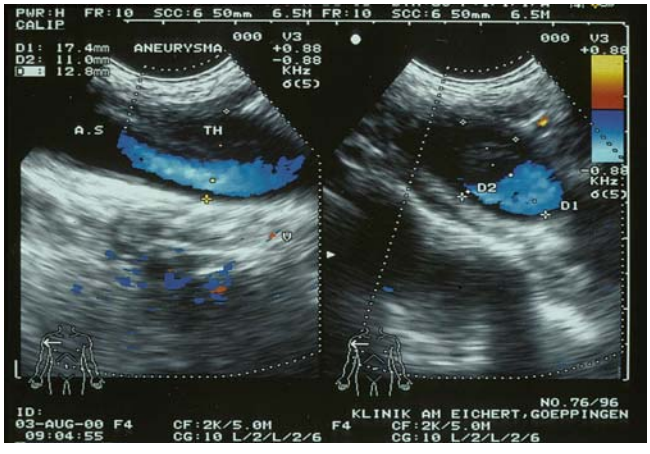

c

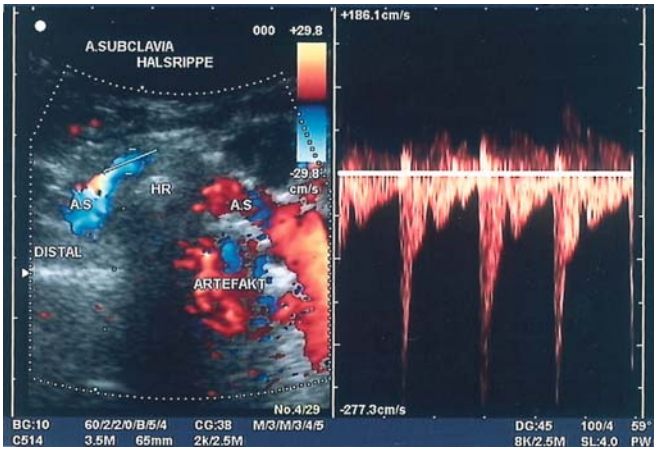

a

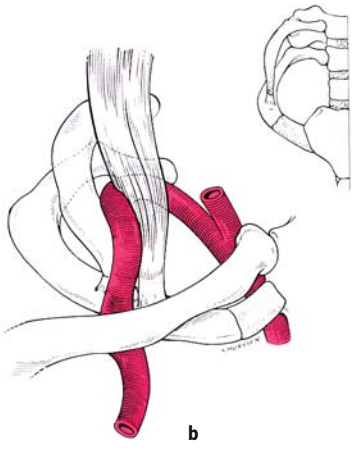

b

Fig. A 2.42 a, b
Cervical rib syndrome
a A cervical rib (*HR*) forces the subclavian artery (supraclavicular transducer position) to take an abnormal, arched course ("the artery is riding the rib"). In the case presented here, the artery is narrowed by an intermediate-grade stenosis with a peak systolic flow velocity of 2.5 m/s. Due to its abnormal course, the artery is not depicted completely in a single scan plane. Mirror artifacts (with superimposed vibration artifacts) are seen posterior to the proximal subclavian artery
b Schematic representation of the mechanism causing the cervical rib syndrome: Displacement and compression of the subclavian artery by the cervical rib. (From Heberer and van Dongen 1993)

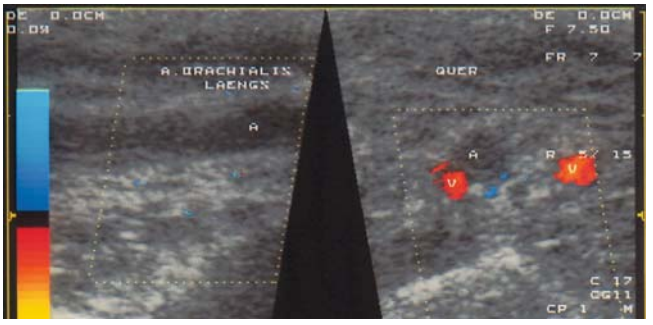

a

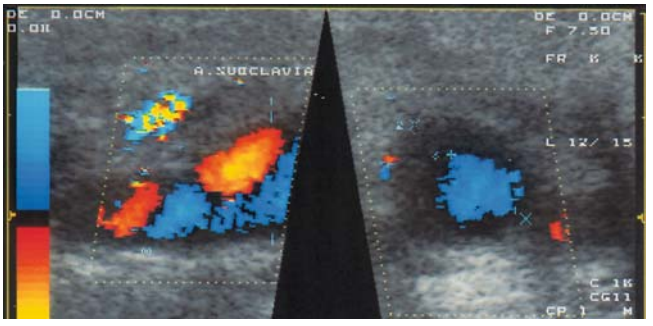

b

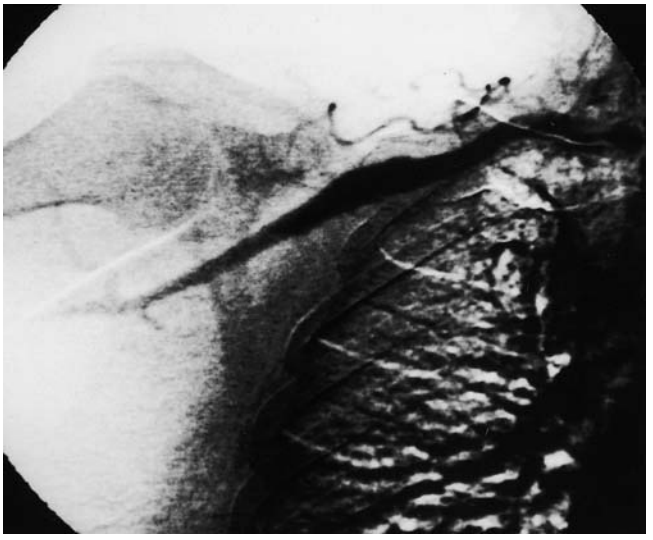

c

Fig. A 2.43 a–c
Aneurysm of subclavian/axillary artery
a 62-year-old patient presenting with acute onset of a sensation of cold and pallor of the right hand and increasing pain unrelated to exercise. The radial and ulnar arteries are not palpable

Duplex scanning demonstrates an occluded brachial artery (*A*) as the cause of the patient's complaints with the absence of plaques and the hypoechoic homogeneous lumen suggesting an embolic mechanism. The veins (*V*) are coded red
b The brachial occlusion in this case is caused by emboli from a 14-mm aneurysm of the subclavian artery at the junction with the axillary artery. Due to mural thrombosis, the patent lumen is only slightly dilatated compared to the proximal, normal vessel segment (hypoechoic rim around the blue, patent lumen of the artery on the transverse scan, *right section*). The longitudinal view on the *left* shows the proximal end of the aneurysm with retrograde flow components (eddy currents)
c Angiography: Due to mural thrombosis, the aneurysm is seen only as a mild dilatation of the subclavian artery at the junction with the axillary artery. The aneurysm in this patient is caused by mechanical irritation due to an exostosis of an old clavicular fracture

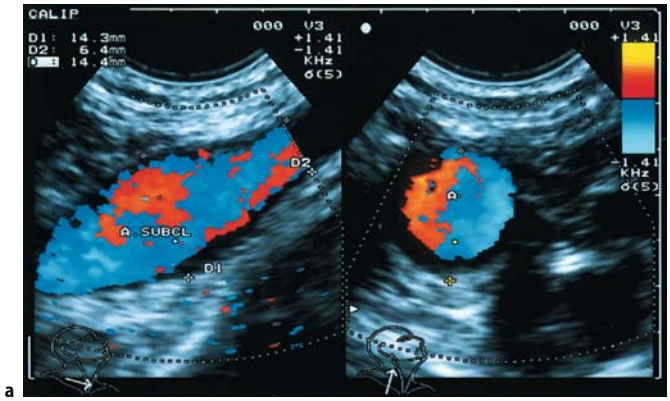

a

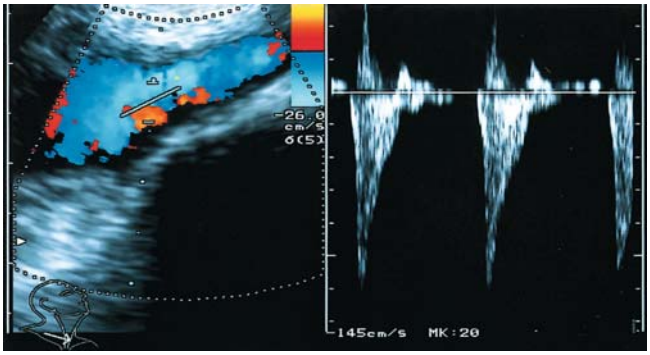

b

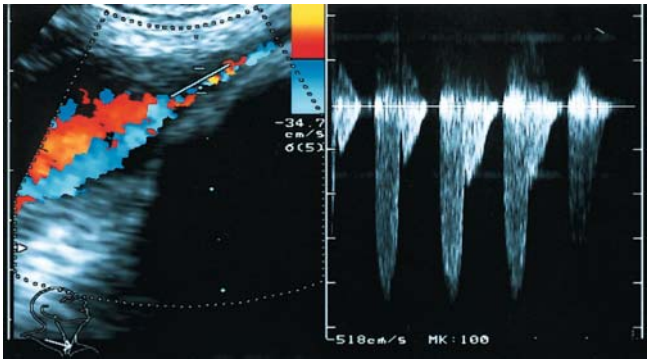

c

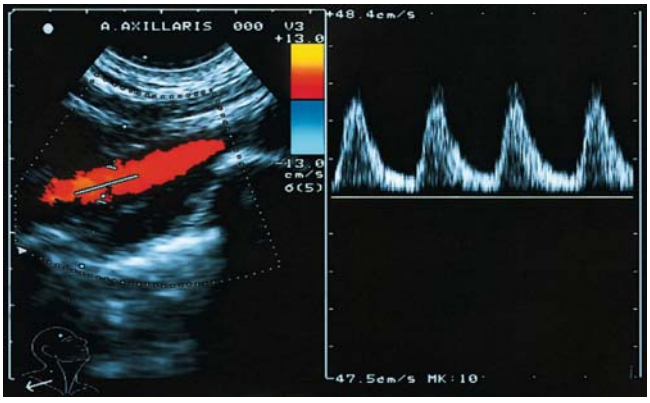

d

Fig. A 2.44 a–d
Thoracic outlet syndrome with poststenotic dilatation
a 45-year-old patient with recurrent pain of the right hand during work (painter). With the transducer in the supraclavicular position, the transverse scan (*left*) and the longitudinal scan (*right*) show aneurysmal dilatation of the subclavian artery. No mural thrombi are depicted. The aneurysm has a maximum diameter of 14 mm; eddy currents in the aneurysm give rise to blue and red flow signals
b The Doppler waveform recorded with the patient lying in a relaxed position (without provocative maneuver) shows disturbed flow but a triphasic profile without signs of a hemodynamically significant stenosis
c Examination during Adson's test reveals compression of the subclavian artery with aliasing on color duplex scanning and a peak systolic flow velocity of over 400 cm/s in the Doppler waveform (stenosis signal). The test is positive for a compression syndrome with poststenotic dilatation
d Specific anatomic conditions (obesity and short neck) may prohibit proper placement of the transducer during Adson's test. In such cases, compression during provocation can be demonstrated by the presence of the typical poststenotic changes in the Doppler waveform sampled in the axillary artery with the transducer placed in Mohrenheim's fossa

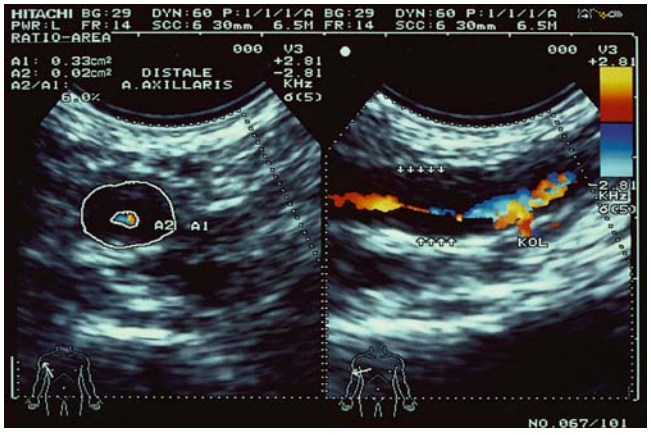

a

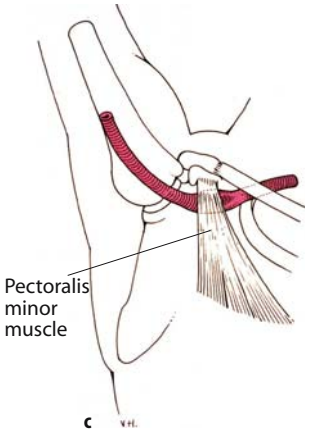

c

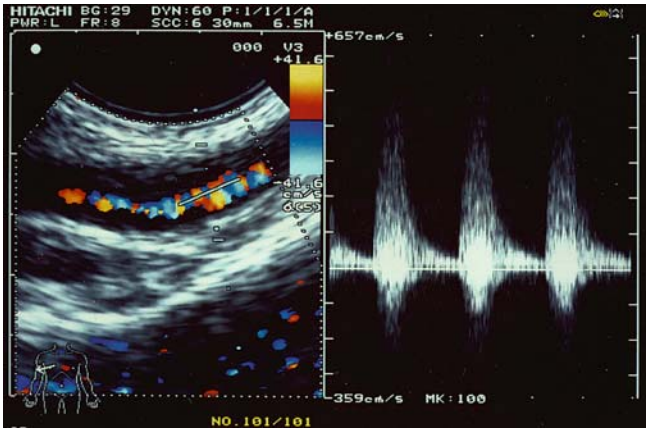

b

Fig. A 2.45 a–c
Pectoralis minor syndrome
a The scan of the axillary artery obtained during hyperabduction with the transducer in the armpit shows the compression-induced stenosis as well as the complications of longstanding compression syndrome: extensive, though circumscribed, wall damage with thickening and local thrombus formation. In the transverse view on the *left*, the normal vessel diameter is marked; aliasing in the color duplex mode enables differentiation of the perfused lumen from mural thrombus
b Doppler waveform showing high-grade stenosis with a flow velocity of over 3 m/s, monophasic flow, and turbulence
c Schematic representation of the compression of the axillary artery between the pectoralis minor muscle and the coracoid process during hyperabduction. (From Heberer and van Dongen 1993)

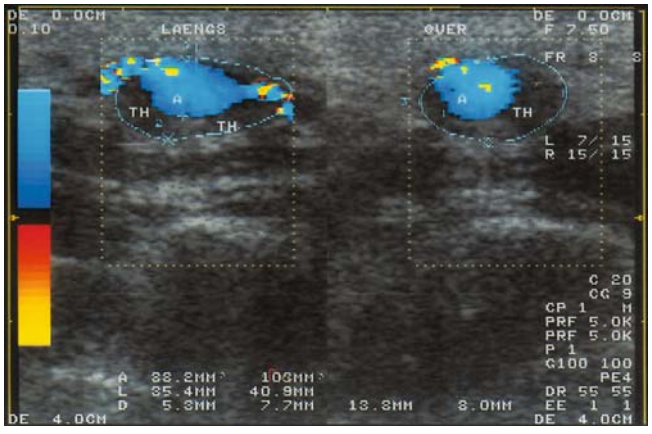

a

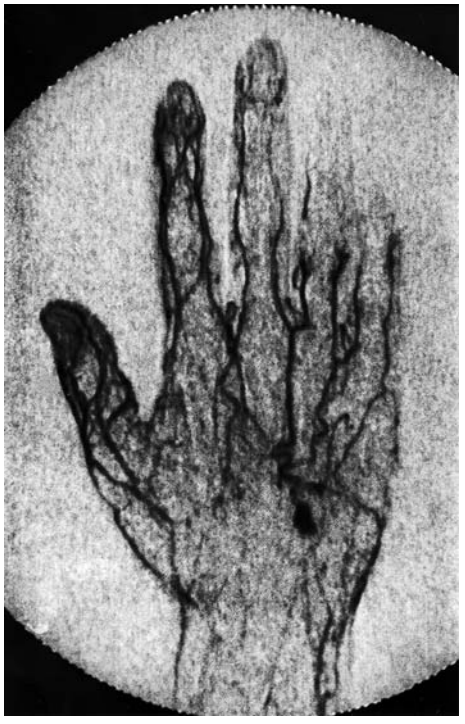

b

Fig. A 2.46 a, b
Aneurysm of the ulnar artery (hypothenar syndrome)
a Patient with ischemia of the pads of fingers 4 and 5 due to arterial emboli from an aneurysm of the distal ulnar artery proximal to the palmar arch. The extent of the aneurysm is outlined in the color duplex scans (longitudinal on the *left*, transverse on the *right*) to illustrate the difference between the overall size of the partially thrombosed aneurysm (20 × 18 mm) and the perfused lumen
b Angiography: Aneurysmal dilatation with a rather small caliber of the distal ulnar artery at the junction with the palmar arch and peripheral occlusions of the digital arteries of fingers 4 and 5. The largely thrombosed aneurysm of the ulnar artery is confirmed intraoperatively

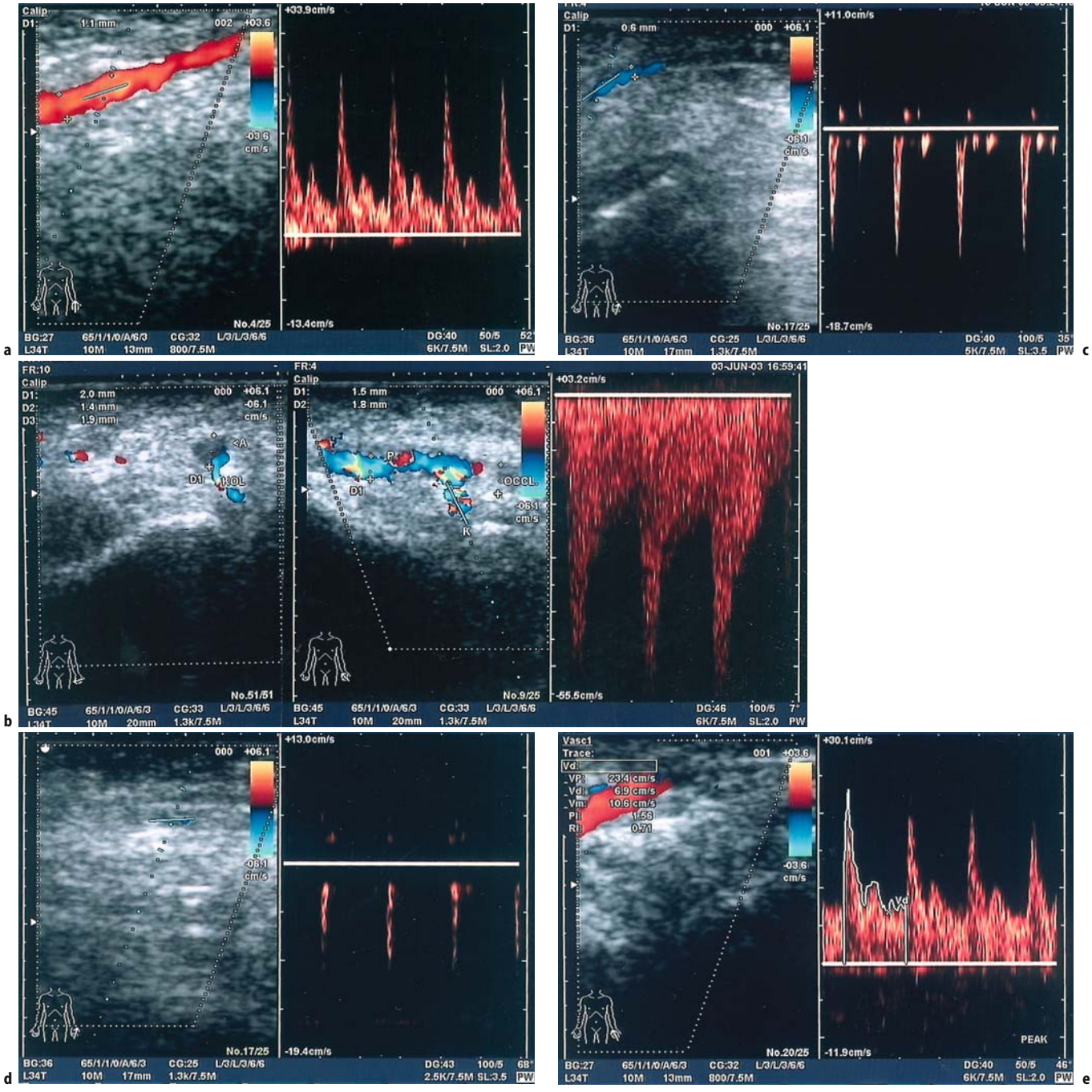

Fig. A 2.47 a–e
Interdigital artery occlusion – Raynaud's disease

a Interdigital arteries to the right and left of the metacarpal bones scanned from the palm show pulsatile flow (pulsatility dependent on sympathetic tone)

b In case of interdigital artery occlusion, the small collateral vessels show monophasic flow due to peripheral dilatation. The occluded interdigital artery with the origin of a collateral is depicted in transverse orientation in the *left section* and in a longitudinal plane in the *middle section*. It has a diameter of 2 mm and a plaque (*P*) is depicted

c A common digital artery in Raynaud's disease with a diameter of 0.6 mm and very pulsatile flow due to vasospasm (atypically displayed in blue because the transducer had to be rotated to visualize the artery)

d A "knocking" waveform is recorded from the affected distal interdigital artery due to peripheral spasms associated with Raynaud's disease

e Arterial dilatation induced by bathing of the hand leads to less pulsatile flow with a large diastolic component

Peripheral Veins

3

3.1 Pelvic and Leg Veins

3.1.1 Vascular Anatomy

Three groups of leg veins subject to different abnormalities of clinical relevance can be distinguished:

- epifascial veins,
- subfascial veins, and
- transfascial veins.

The epifascial veins belong to the superficial venous system of the leg and the subfascial veins to the deep venous system with the transfascial or perforating veins establishing connections between these two venous systems. The deep veins accompany the arteries of the same name (Fig. 3.1).

The iliac vein runs through the true pelvis posterior to the iliac artery, pierces the inguinal ligament, and then immediately passes to the medial side of the artery, where it continues as the common femoral vein. Just below the inguinal ligament, the great saphenous vein enters the common femoral vein on its anteromedial aspect. Along its further course, the common femoral vein receives the deep femoral vein just after the division of the common femoral artery into the deep and superficial branches. The deep femoral vein runs between the arterial branches of the femoral bifurcation. Distally, the superficial femoral vein courses along the posterior aspect of the artery of the same name. In most individuals, a second, large branch of the deep femoral vein opens into the superficial femoral vein. Different variants exist as to where, how, and how many deep femoral vein branches enter the superficial femoral vein.

A single superficial femoral vein is present in 62 % of individuals only, 21 % have a duplicated vein, and in another 14 % even three or more branches are present. If there is more than one vein, these may vary in caliber and course lateral or anterior to the artery rather than posterior to it. While the iliac vein has no valves, the superficial femoral vein has about 4 to 5 (Weber and May 1990). After its passage through the adductor canal, the superficial femoral vein becomes the popliteal vein, which runs posteriorly along the artery of the same name (closer to the transducer when scanning from the popliteal fossa). The small saphenous vein enters the proximal popliteal vein (cf. Fig. 3.1) on its posterior aspect at a highly variable level. Just below its opening, the small saphenous vein perforates the deep fascia and descends along the back of the calf. Distal to the opening of the small saphenous vein, the popliteal vein receives the muscular veins of the lower leg (soleus and gastrocnemius veins) at various levels about the knee joint cleft. Just before emptying into the popliteal vein, the proximal small saphenous vein gives off a connecting branch to the deep muscular veins of the thigh, the femoropopliteal vein (Fig. 3.2 a).

The popliteal vein may be present as a single or paired vessel and is formed by the union of the posterior tibial and the fibular veins. It receives the anterior tibial vein as the first lower leg vein at a variable level. The main lower leg veins typically follow the arteries of the same name. The anterior tibial veins penetrate the interosseous membrane and course along its anterior aspect. The fibular veins run close to the fibula in the deep crural fascia between the superficial and deep flexors, as do the tibial veins, but on the posteromedial aspect of the tibia.

The superficial (epifascial) venous drainage system consists of two subsystems, that of the great saphenous vein and that of the small saphenous vein, which receive the larger arch veins and side branches. The great saphenous vein extends from the back of the foot to the medial malleolus and takes a medial course through the lower and upper leg to about 2 – 3 cm below the inguinal ligament, where it opens into the popliteal vein. There is variation in the tributaries to the great saphenous vein in the lower leg but these are mainly the following: the posterior arch vein, which is connected to the major deep veins, in particular the posterior tibial vein, through the perforating veins (Cockett I, II und III); the great saphenous branch from the back of the foot; and the anterior tributary vein. In the thigh, connections to the deep venous system are established by Dodd's perforators. Just before its junction with the common femoral vein, the great saphenous vein receives tributary veins of the upper leg and lateral branches that establish collateral connections to the abdominal (epigastric) veins and become important as collaterals in pelvic vein thrombosis (Fig. 3.2 b).

The small saphenous vein drains the lower leg and arises at the lateral dorsum of the foot, coursing behind the lateral malleolus to the posterior side of the lower leg, where it ascends between the heads of the gastrocnemius and pierces the fascia to open into the popliteal vein above the knee joint cleft. The gastrocnemius veins enter the small saphenous vein

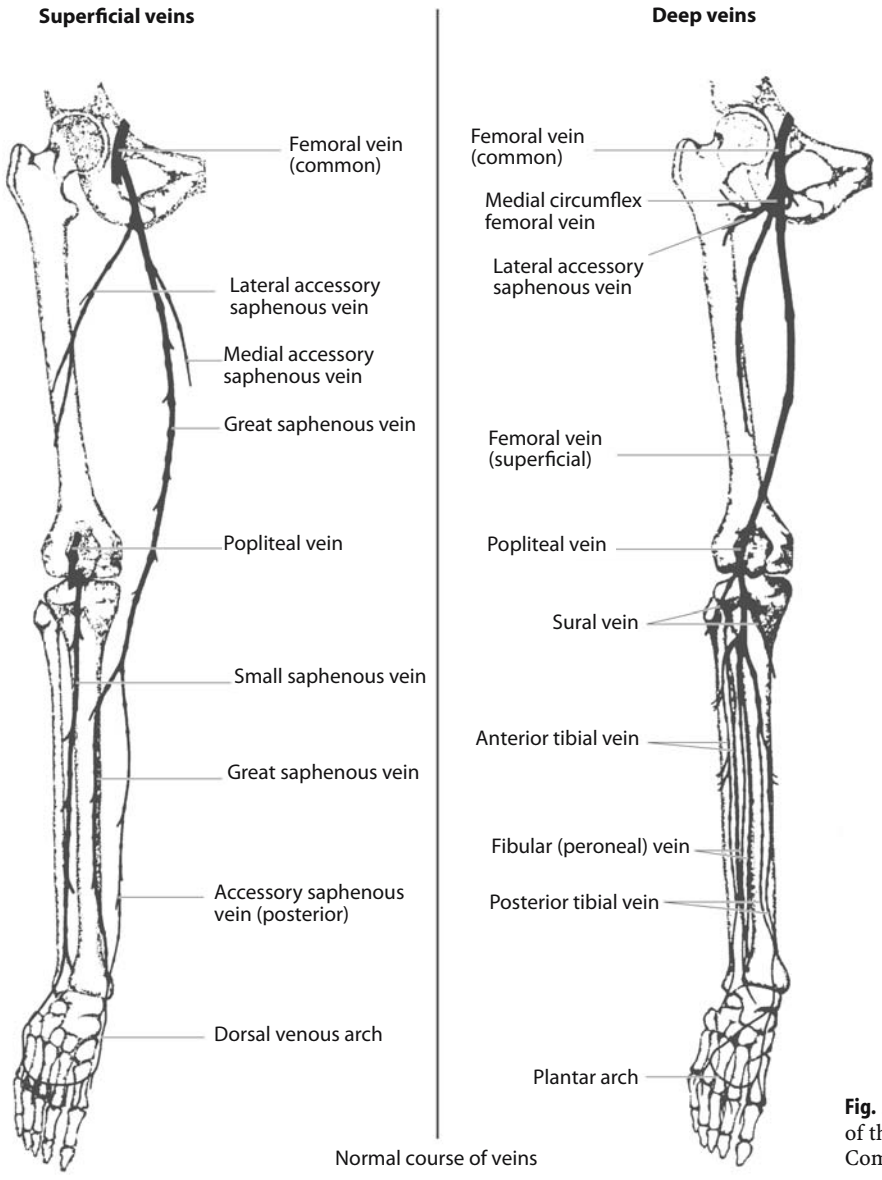

Fig. 3.1. Radiographic anatomy of the large veins of the lower limb. (Courtesy of Eastman Kodak Company)

shortly before its opening or enter the popliteal vein directly. The femoropopliteal vein passes from the small saphenous vein (just before it opens into the popliteal vein) as a collateral to the deep veins of the upper leg.

Both the great and small saphenous veins have valves. In comparison to the deep veins, the superficial veins have thicker walls with a thin muscular layer. The lumen varies with the intravenous pressure and can be compressed by external structures. There is wide variation in the course of individual veins and the connections they form.

The perforating veins are transfascial veins that drain blood from the superficial venous system into the major deep veins. About 150 such short veins exist between the superficial and deep venous systems, among which the Cockett groups I-III, the Sherman vein, and the Boyd vein are of clinical importance in the lower leg, the Dodd group in the upper leg, and the May perforator between the small saphenous vein and deep lower leg veins. Under normal conditions, valves ensure blood flow from the superficial to the deep venous system while the blood is propelled toward the heart by muscular contraction with compression of the deep veins. This mechanism prevents backward flow into the superficial veins.

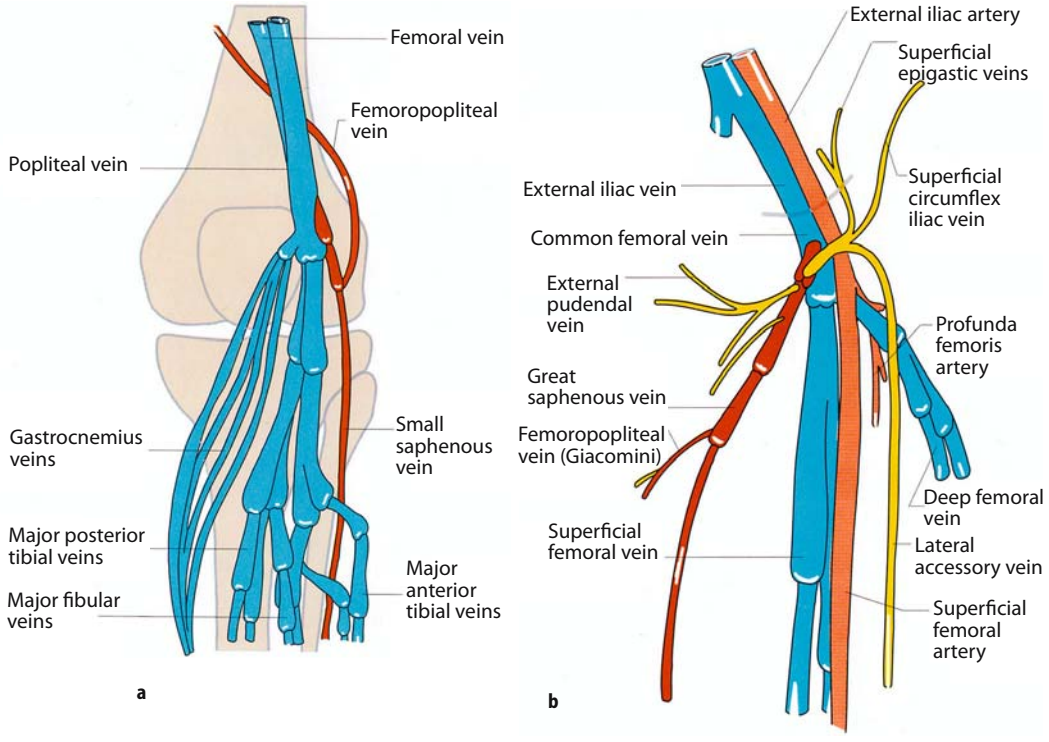

Fig. 3.2. a Anatomic relationship between the small saphenous vein opening into the popliteal vein in the popliteal fossa and the gastrocnemius veins. The sural veins (not shown) enter more distally and further along is the confluence of the main lower leg veins.
b Schematic representation of the vessels in the groin. Just below the saphenofemoral junction, the great saphenous vein receives the lateral accessory pudendal vein and the superficial epigastric veins. Further down, the deep femoral vein opens into the femoral vein. The arteries of the same name (*orange*) lie anterolateral to the veins. (From Stritecky-Kähler 1994)

3.1.2 Examination Protocol

3.1.2.1 Thrombosis

Instrumentation. The ultrasound examination of the peripheral veins depends on the clinical question to be answered. If thrombosis is suggested by the clinical symptoms, compression ultrasound of the upper and lower leg veins of the affected side is indicated, while in patients with suspected chronic venous insufficiency, valve function tests of the vein segments involved are performed during recording of Doppler information. The subfascial leg veins are scanned using transducers operating at 5 – 7.5 MHz while the pelvic veins and the vena cava are examined at 3.5 – 5 MHz (depending on the scanning depth required). Assessment of the epifascial veins and in particular of the perforating veins requires a transmitter frequency of 7.5 – 10 MHz.

The question as to whether a linear or curved array transducer should be used is secondary. However, the footprint for compression ultrasound should not be too small in order to achieve compression of muscular and major lower leg veins in transverse orientation. To depict the slow venous flow, scanning is performed with a low wall filter and a low pulse repetition frequency. Many scanners have the slow-flow mode as the preset option.

Patient Positioning. The inferior vena cava and iliac vein are examined with the patient in the supine position. If there is overlying air, improvement may be achieved by repositioning the patient on the right or left side; bowel gas can be pushed aside by applying pressure with the transducer. The femoral vein is scanned in the supine patient with the leg slightly rotated outwardly and the knee slightly bent. An experienced examiner can scan the popliteal vein and lower leg veins with the patient in the supine or semilateral position and the knee slightly bent. Alternatively, the popliteal vein can be examined with the patient in the prone position. However, to avoid collapse of the veins due to hyperextension of the knee, the ankle should be slightly elevated by placing a cushion underneath. When the patient is sitting or standing, there is better filling of the veins, which makes it easier to localize the veins in the lower leg and evaluate their compressibility. Valve incompetence in the popliteal vein, the superficial lower leg veins (varicosis), and the perforating veins is best evaluated in the sitting patient. The proximal great saphenous vein and the femoral vein are scanned in the supine position (like the femoral artery, cf. Fig. 2.3 a).

Examination Technique (Table 3.1). In the diagnostic evaluation of thrombosis, the subfascial veins are continuously scanned from the groin to the ankle and checked for absence of intraluminal thrombi by intermittent compression (cf. Figs. 2.3 a, b and 3.12). First, the common femoral vein is identified on the medial side of the common femoral artery below the inguinal ligament and followed in transverse orientation down to its junction with the superficial femoral vein. Along the course of the common femoral vein, the openings of the great saphenous vein and of the deep veins from the upper leg muscles are tested for compressibility as well.

In evaluation of the pelvic veins, compression ultrasound does not yield valid results because a continuous structure against which to compress the veins is not available and the

Table 3.1. Ultrasound examination of the veins

B-mode scanning	Orientation:	Transverse (except for external iliac vein)
	Criteria:	Compressibility Lumen width Wall morphology Internal structures
	Note:	Reversed compression maneuver in adductor canal
	Documentation:	Split scan: without/with compression Normal findings as outlined in the text, abnormal findings according to the situation
(Color) duplex scanning	Orientation:	Longitudinal plane, overview in transverse plane
	Criteria:	Spontaneous flow, augmented flow (Valsalva, compression-decompression) Luminal filling (defects?) Wall contour abnormalities, perivascular structures
	Note:	Doppler tracing in longitudinal plane only
	Documentation:	B-scan with corresponding waveform, color Doppler scan as needed

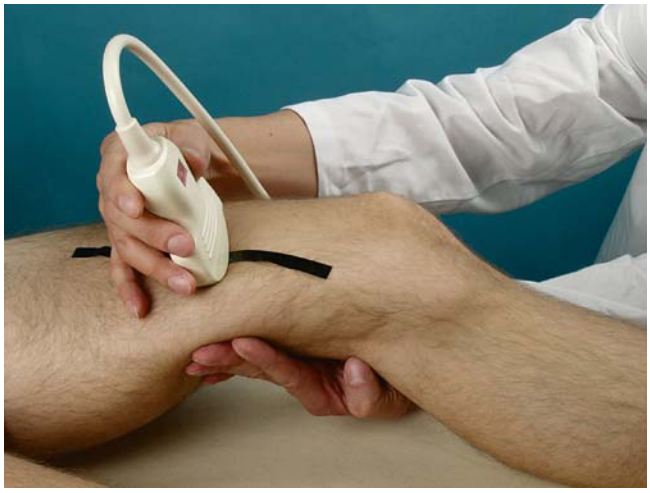

Fig. 3.3. The compression test applying pressure with the transducer only is inadequate at the level of the adductor canal. Rather, the examiner additionally presses the vein against the transducer from below with the flat hand

abdominal organs and fatty tissue prohibit reliable compression, in particular in obese patients. Nevertheless, compression ultrasound can be performed, especially in slender patients. The arched iliac veins in the true pelvis are tested with the transducer in transverse orientation with additional longitudinal scanning as required. If adequate evaluation of compressibility is not possible in this way, patency must be evaluated by spectral Doppler.

If the scanning conditions are limited, occluding thrombosis of the pelvic veins can be ruled out by obtaining a Doppler spectrum from the junction of the common femoral and external iliac veins, where the insonation window is good. In the presence of an obstruction, respiratory phasicity of flow is absent or reduced compared to the unaffected side. This is evaluated by analyzing the Doppler waveform recorded in the external iliac vein (posterior to the artery) somewhat above the inguinal ligament in the longitudinal plane and with a low pulse repetition frequency. With the patient stretched in the supine position, the common femoral vein may be compressed along its course under the inguinal ligament, especially in slender patients. In such cases, visualization can be improved by slight outward rotation of the hip joint.

Next, with the patient in the supine position, the superficial femoral vein is traced along its course down the leg in transverse orientation and intermittently compressed (every 1 – 2 cm) with the transducer. In its distal segment, at the level of the adductor canal, compression is difficult due to the absence of a bony structure and interfering connective tissue. Instead, the examiner must press the muscle and vessels against the transducer from below with his or her other hand to achieve adequate compression (Fig. 3.3).

Below the adductor canal, the popliteal vein is scanned from posteriorly. This part of the examination is performed with the patient supine and the knee slightly bent or in the prone position with a support under the ankles. The slightly bent knee ensures better filling and hence improves visualization. With the knee joint stretched or even overstretched in the flat position, the popliteal vein is often collapsed or compressed by surrounding connective tissue structures pushing the vein against the artery and bony structures.

Following evaluation of the popliteal vein for compressibility in transverse orientation, it is traced downward to the confluence of the fibular and posterior tibial veins. The anterior tibial vein entering at a higher level is often identified at its point of entry by means of color duplex only. After having been identified, the vein is evaluated for compressibility from an anterior approach. The accompanying veins are then continuously scanned downward and intermittently compressed using the anterior tibial vein as a landmark.

For scanning of the anterior tibial vein, the transducer is placed on the extensors and then moved so as to achieve a beam direction roughly perpendicular to the interosseous membrane between the tibia and fibula. The procedure is the same for scanning of the fibular and posterior tibial veins, except that the transducer is in a posterior position on the gastrocnemius muscle. The two veins are traced distally with intermittent compression (Fig. 3.4).

While the popliteal and femoral veins are reliably identified by B-mode ultrasound, the lower leg veins may have to be localized using the arteries of the same name visualized by color duplex as landmarks. The hyperechoic interosseous membrane is an anatomic landmark for identifying the anterior tibial artery and vein coursing in it whereas the deep crural fascia between the deep flexors and the soleus and gastrocnemius muscles is not always depicted well enough to serve as a landmark for identifying the posterior tibial and fibular veins coursing in it (Fig. 3.5). The fibular vein is easier to identify from the posterior approach (as is the proximal ante-

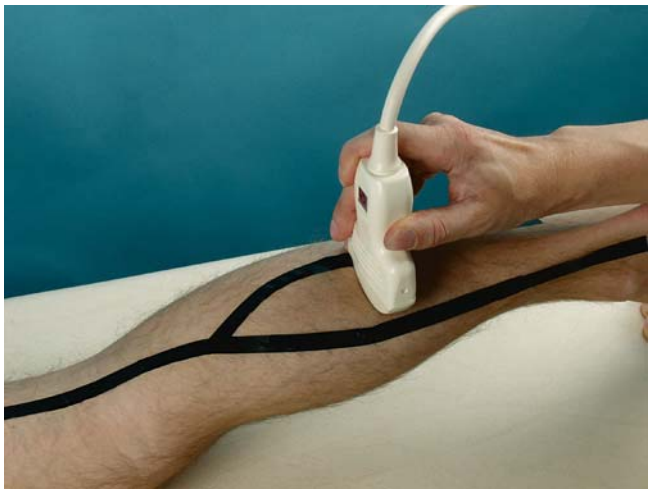

Fig. 3.4. Compression ultrasound of the lower leg veins (course marked). The transducer is positioned on the calf so that the ultrasound beam is perpendicular to the interosseous membrane between the tibia and fibula

rior tibial vein from the anterior approach) as it courses close to the fibula. Diagnostic assessment of thrombosis can be performed with the patient in the supine or prone position but better filling facilitates visualization of the veins in the sitting patient.

In addition to the main veins of the lower leg, evaluation of thrombosis also includes compression scanning of the muscular veins (the gastrocnemius veins opening into the popliteal vein) and the soleus veins entering the main veins of the lower leg, in order to exclude muscular vein thrombosis (the same applies to the deep femoral vein in the thigh). The muscular veins can be traced in a distal direction from their sites of entry into the main vein, especially when there is adequate venous filling with the patient sitting.

The ultrasound examination in thrombophlebitis serves to determine the extent, in particular the cranial extent, and involvement of the deep venous system (openings into deep venous system). This is done by performing compression ultrasound of the great or small saphenous vein in transverse orientation after identification of the clinically inflamed segment and using the same criteria as in the diagnostic assessment of thrombosis.

In thrombophlebitis, special attention must be paid to the sites of entry of the small and great saphenous veins into the popliteal and common femoral artery, respectively, which are checked for compressibility in transverse plane.

In patients examined for thrombosis, the compression tests are always performed in transverse orientation. On the one hand, this facilitates identification and tracking of the vein down the leg; on the other hand, false-negative findings are prevented: longitudinally, a noncompressible vein may be displaced and disappear from the scanning plane when pressure is applied, thereby mimicking compressibility.

3.1.2.2 Chronic Venous Insufficiency and Varicosis

In patients with chronic venous insufficiency of the deep veins or varicosis of the superficial veins, the affected venous segments are scanned longitudinally for the presence of

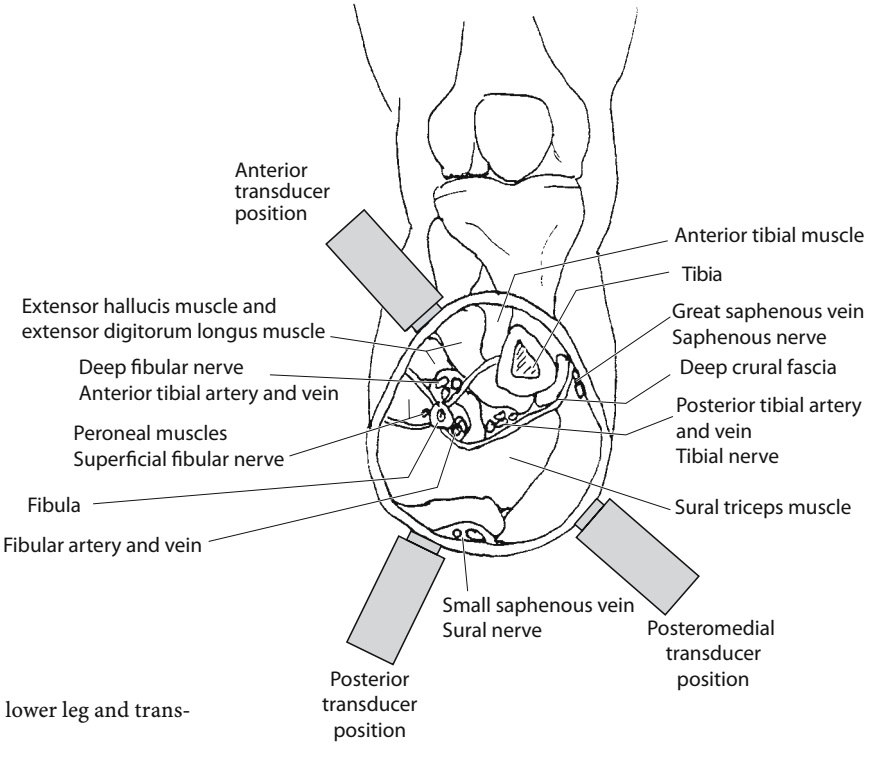

Fig. 3.5. Schematic anatomic cross-section of the lower leg and transducer positions

venous reflux, which is induced by applying the respective provocative tests. For the demonstration of valve incompetence of the deep veins, the tests for reflux diagnosis are performed with Doppler recording in longitudinal orientation at specific sampling sites (key sites) in the common femoral, superficial femoral, and popliteal veins.

Function of the proximal valves is evaluated during Valsalva's maneuver in the recumbent patient and Doppler sampling in the common and superficial femoral veins during increased abdominal pressure. Valve incompetence is demonstrated by persistent backward flow to the periphery, indicated by a corresponding color change in the color flow image. If this test is positive for proximal valve incompetence, the test is progressively extended to the popliteal vein and lower leg veins to determine the distal extent of the valve incompetence.

In patients with competent proximal valves (common femoral and proximal superficial femoral veins), distal insufficiency is diagnosed by the demonstration of persistent flow reversal (over 1 s) in the Doppler waveform (Fig. 3.6) or on color duplex scanning in the popliteal vein (longitudinal scan) during compression-decompression with the patient sitting or standing.

Incompetence of the terminal valve of the great saphenous vein is assessed longitudinally during Valsalva's maneuver (Fig. 3.7 a). In case of truncal varicosis, the great saphenous vein is tracked distally to identify the lowest point of incompetence through intermittent Valsalva maneuvers (grading according to Hach). In case of sufficiency of the proximal segment, the extent of distal varicosis of the great saphenous vein is determined by intermittent compression-decompression

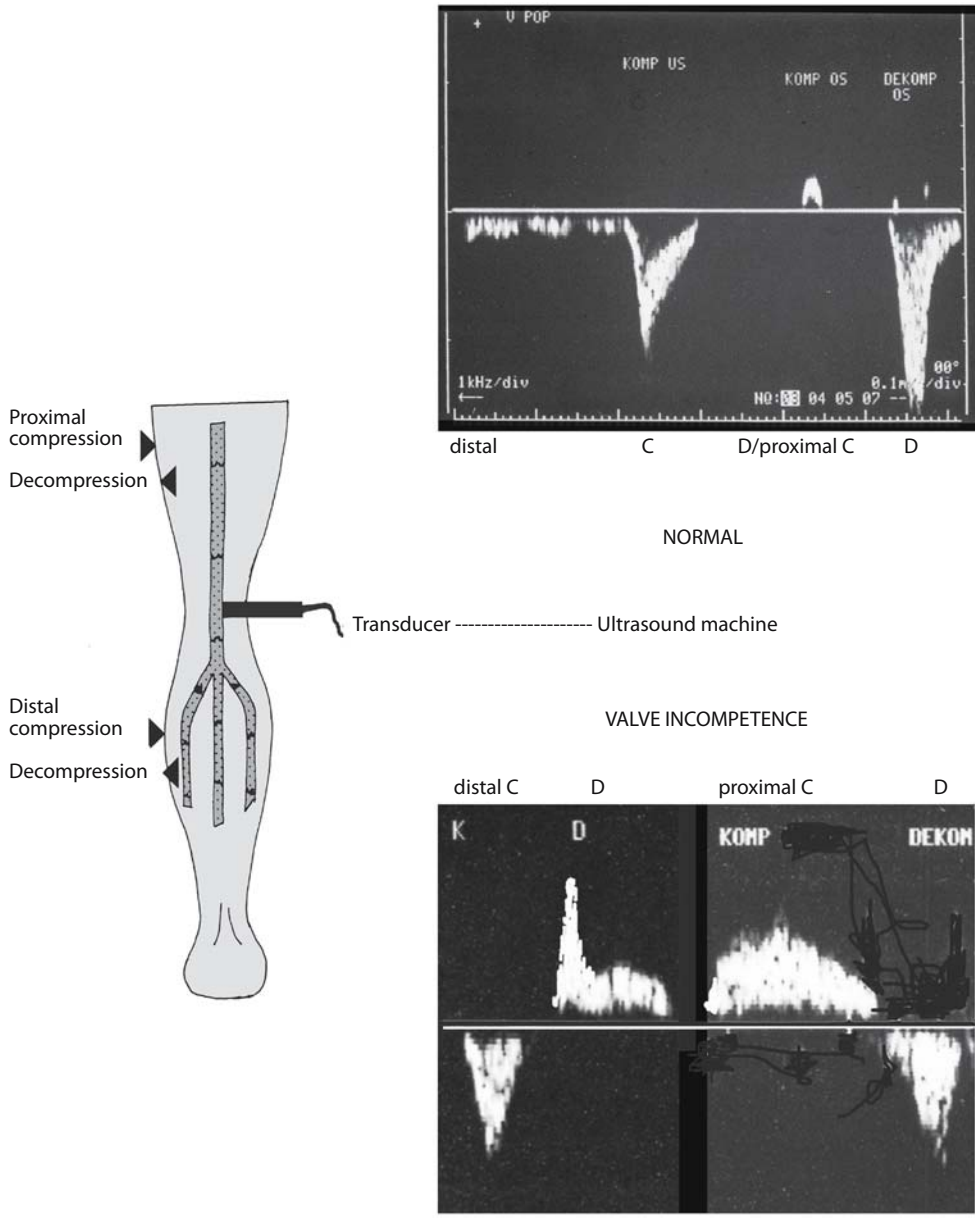

Fig. 3.6. Representation of the proximal and distal compression-decompression test – here illustrated for Doppler recording in the popliteal vein. The waveform *above* shows the normal findings obtained when there is proper valve closure (distal compression-decompression on the *left*; proximal compression-decompression on the *right*); the waveform *below* shows the changes in valve insufficiency with reflux (*C* compression, *D* decompression)

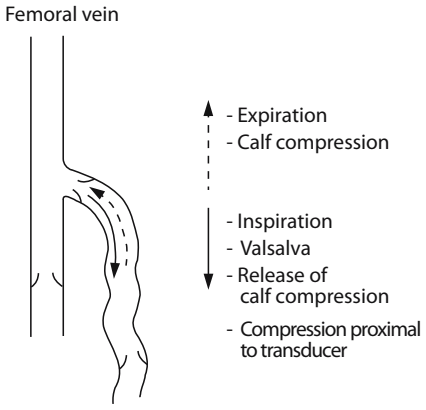

a Great saphenous vein

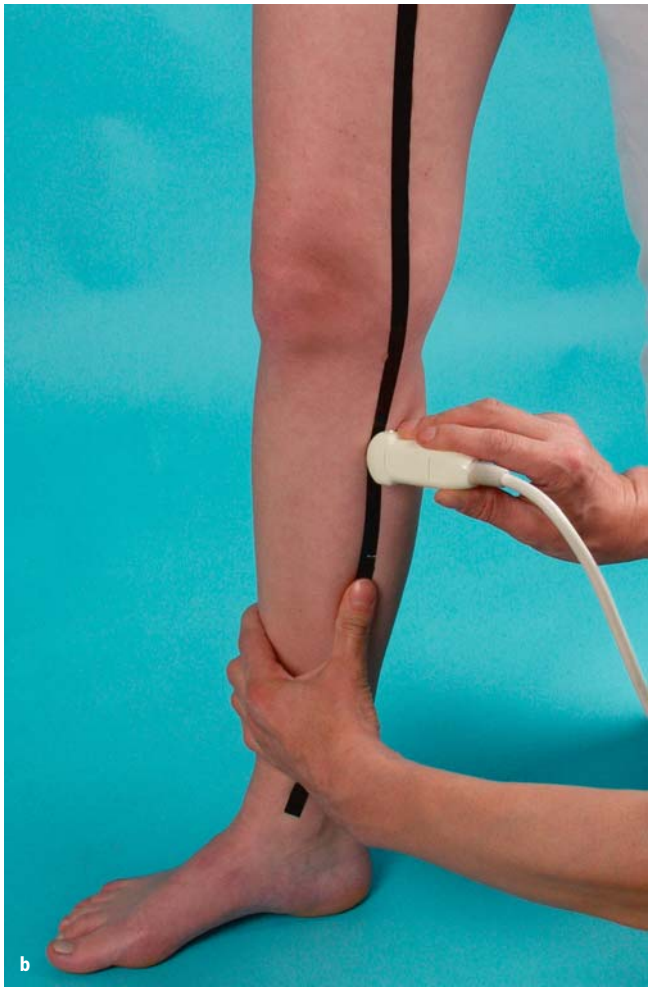

Fig. 3.7. a Schematic representation of the valve function test in the great saphenous vein. **b** Transducer position for evaluating valve competence of the distal great saphenous vein in the compression-decompression test. Alternating distal compression and decompression of the vein during recording of the Doppler spectrum is performed with the left thumb

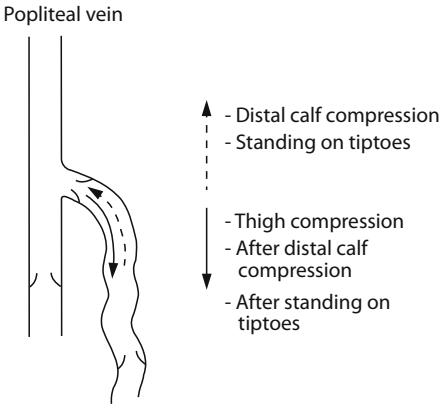

a Small saphenous vein

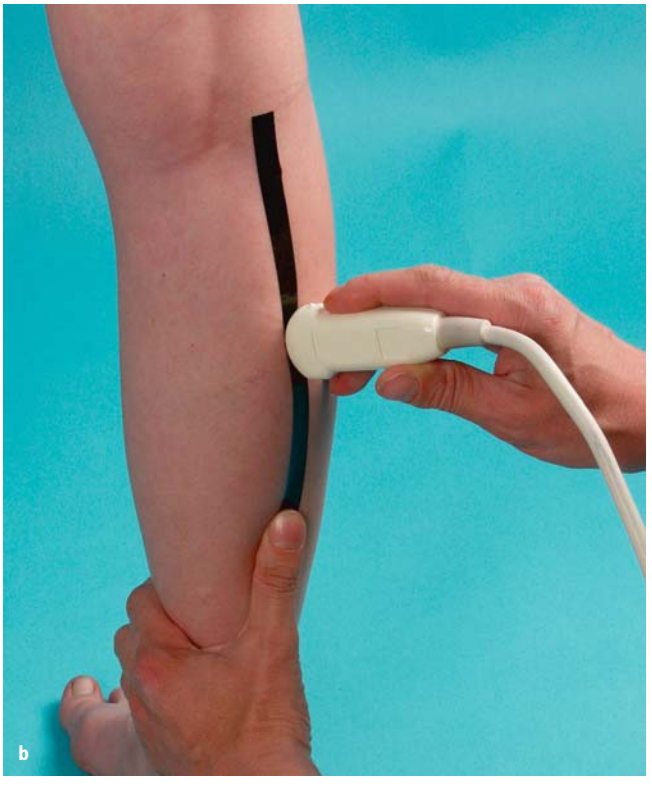

Fig. 3.8. a Schematic representation of the valve function test in the small saphenous vein. **b** Transducer position for evaluating valve competence of the small saphenous vein (cf. legend to Fig. 3.7 b)

testing along the vein in the cranial direction (Fig. 3.7 b: compression with the thumb distal to the transducer) to identify the proximal and distal points of insufficiency (transition from persistent reflux to absent reflux in the compression-decompression test) in the sitting or standing patient. The same test is used to diagnose reflux in the small saphenous vein (Fig. 3.8 a, b).

To assess valve competence of the perforating veins, these are first identified in their typical locations (e.g. Cockett's group in the distal medial lower leg, Boyd's group in the proximal lower leg, or Dodd's group in the upper leg) (Fig. 3.9).

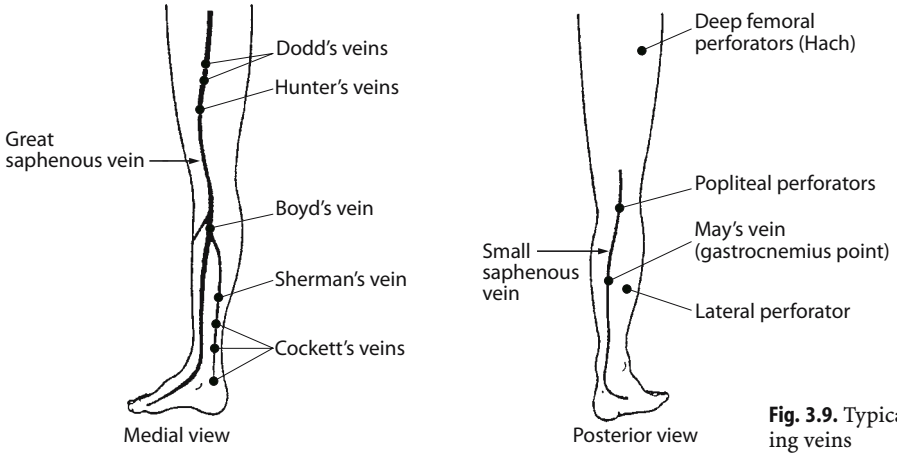

Fig. 3.9. Typical locations of clinically important perforating veins

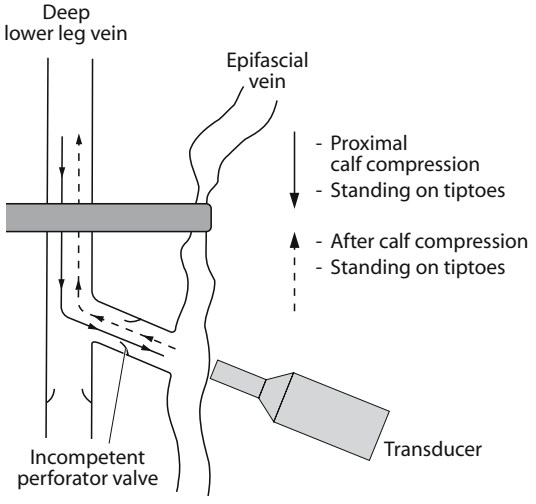

Fig. 3.10. Schematic representation of the valve function test in the perforating veins

In B-mode scanning, the perforating veins are identified as hypoechoic, tubular structures that pass through the deep fascia from the superficial to the deep veins. Once identified, the compression-decompression test is performed as outlined in Fig. 3.10.

If there is incompetence, color duplex or duplex scanning with the sample volume placed in the perforating vein depicted on the B-scan will demonstrate reflux (retrograde flow from the deep into the superficial vein) during compression of the calf just proximal to the Doppler sample volume. If the valves function properly, there is no backward flow from the deep to the superficial vein. Compression of the calf will induce stoppage of flow but no reversal. Application of a tourniquet proximal to the site of scanning can prevent interference from flow in insufficient superficial veins.

3.1.3 Normal Findings

The leg veins, with their delicate walls and low intraluminal pressure, can be completely compressed with the transducer, so that normal veins become nearly invisible on ultrasound or only a hyperechoic reflection indicating the wall but no lumen is seen. The breathing-related intra-abdominal pressure changes lead to respiratory fluctuation of venous flow with faster flow during expiration due to lower intra-abdominal pressure (upward movement of diaphragm) and slower flow during inspiration due to higher intra-abdominal pressure (downward movement of diaphragm). This pressure-dependent flow pattern is transmitted through the upper leg veins into the major deep veins in the distal lower leg and into the major superficial veins (great and small saphenous veins) in the recumbent patient. Respiratory fluctuation of venous flow may be overridden by cardiac pulsatility (changes in atrial pressure) in the iliac and proximal femoral veins, especially in young patients (Table 3.2).

The pocket-like vein valves ensure undisturbed flow from the periphery to the center. When there is pressure reversal with backward flow, flow ceases upon closure of the valves (after a short reflux of 0.3 s on average). Proper valve closure is demonstrated by Valsalva's maneuver or in the compression-decompression test (cf. Fig. 3.6).

Table 3.2. Factors affecting venous reflux

- Vis-a-tergo
- Changes in intra-abdominal and intrathoracic pressure (suction pump)
- Cardiac suction pump (systole, early diastole)
- Musculovenous pump (requires competent valves):
  Competent perforating veins prevent blood flow into superficial veins
  Competent valves distal to the contracting muscle prevent backward flow

3.1.4 Documentation

As with the examination protocol, the documentation of findings is dictated by the clinical query.

In Germany, the Deutsche Gesellschaft für Ultraschall in der Medizin (DEGUM; German Society of Ultrasound in Medicine) issued guidelines for documenting the findings of venous ultrasound of the legs based on clinical experience and requirements. The routine sites for which the duplex ultrasound findings (B-scan and Doppler waveform) should be documented in all cases are the superficial femoral, deep femoral, common femoral, and popliteal veins. Additional results are documented according to the abnormal findings in the individual case.

3.1.4.1 Deep Vein Thrombosis of the Leg

Transverse scans of the common femoral vein at about the level of the opening of the great saphenous vein, the superficial femoral vein somewhat distal to the site of entry of the deep femoral vein, and the popliteal vein are documented with and without compression.

Supplementary scans of the major lower leg veins (posterior tibial and fibular veins) obtained in the proximal lower leg should be documented, again with and without compression, together with a Doppler spectrum recorded at the junction of the external iliac vein with the common femoral vein to show unobstructed venous return of the pelvic veins. If the duplex ultrasound findings are documented, these should comprise longitudinal scans with the corresponding Doppler spectra confirming preserved respiratory phasicity of blood flow in the common femoral, superficial femoral, and deep femoral veins near their openings, and in the popliteal vein.

In addition, if venous thrombosis is diagnosed, the abnormal findings have to be documented (noncompressible venous segment) in transverse views with and without compression or by means of the Doppler waveform obtained in longitudinal orientation and showing absence of flow or an abnormal flow profile. If the absence of flow is documented by means of a color duplex scan, the scan must contain information to the effect that proper instrument settings including a low pulse repetition frequency and adequate gain were used.

3.1.4.2 Chronic Venous Insufficiency and Varicosis

Longitudinal scans of the common femoral, superficial femoral, and great saphenous veins (at the sites of their openings) are documented with the corresponding Doppler spectra recorded during normal breathing and Valsalva's maneuver. The openings of the popliteal and small saphenous veins are likewise documented on longitudinal scans with the corresponding Doppler spectra during compression-decompression testing. Color duplex scans alone are inadequate for documenting reflux because the duration must be quantified to differentiate abnormal reflux from the short backward flow normally occurring before valve closure.

3.1.5 Clinical Role of Duplex Ultrasound

3.1.5.1 Thrombosis and Postthrombotic Syndrome

The incidence of deep vein thrombosis of the leg is 1 – 2 ‰ per year and increases with age. Various noninvasive tests have been proposed for the diagnosis of this common condition which often takes an asymptomatic or unspecific clinical course but has serious early (pulmonary embolism) and late complications (chronic venous insufficiency in about 50 % of cases). These modalities comprise plethysmography, thermography, iodine fibrin test, and Doppler ultrasonography (Bollinger et al. 1982; Hull et al. 1984; Kakkar 1972; Lepore 1978; Neuerburg-Heusler and Hennerici 1995; Sandler et al. 1984; Strandness 1977).

The methods were either very time consuming or provided reliable results only in specific vessel segments. CW Doppler ultrasound used to be the noninvasive modality of first choice in the diagnostic assessment of valvular incompetence of the superficial and deep veins and, as a functional modality, showed good results in diagnosing pelvic and upper leg venous thrombosis including popliteal artery thrombosis with reported accuracies of up to 90 %. However, isolated lower leg venous thrombosis and central thrombi surrounded by flowing blood are difficult to detect. A review of 2,060 patients who underwent additional venography yielded a sensitivity of 84 % and a specificity of 88 % for CW Doppler ultrasound in demonstrating venous thrombosis (Wheeler 1985).

Combining morphologic information (B-scan) and functional information (Doppler), duplex ultrasound has become the central noninvasive modality for venous diagnosis.

Stasis is an important risk factor for the development of deep vein thrombosis of the leg, in addition to a hypercoagulable state and damage of the vessel wall. Thus, immobilization plays a crucial role in the pathogenesis of thrombosis of the deep veins, which primarily arises in the muscular veins in bedridden patients or in patients with cast immobilization of the leg. The risk of thrombosis without heparin prophylaxis is 10 – 30 % in general surgery and up to 54 % in hip surgery (Lippert and Pabst 1998). Venous thrombi are ascending in over 90 % of cases and have an annual incidence of 160/100,000 inhabitants in Germany with pulmonary embolism occurring in 60/100,000 inhabitants per year. Thrombosis of the deep pelvic and leg veins is the source of pulmonary embolism in over 90 % of cases. The importance of isolated lower leg venous thrombosis should not be underestimated as it may cause pulmonary embolism, though often asymptomatic, in 15 – 26 % of cases. In contrast, iliofemoral thrombosis has an incidence of pulmonary embolism of 56 – 85 %. The mortality of pulmonary embolism ranges from 0.1 – 5 %, depending on the risk group (Polak 1992).

Data in the literature on the localization of venous thrombosis of the legs are not very consistent. In a study of 1,084 lower extremities with acute venous thrombosis, the thrombosis was localized above the knee in 51 %, below the knee in 32 %, and in a superficial vein in 17 % (Kerr et al. 1990). A venographic study (Schmitt et al. 1977) of deep venous thrombosis of the leg showed concomitant involvement of the common iliac vein in 16 %, external iliac vein in 33 %, common femoral vein in 46 %, deep femoral vein in 45 %, superficial femoral vein in 65 %, popliteal vein in 66 %, anterior tibial vein in 73 %, posterior tibial vein in 82 %, and fibular vein in 77 %. The generous use of diagnostic ultrasound in patients with clinically suspected thrombosis of the deep leg veins can help reduce the incidence of thrombosis of the pelvic and femoral veins.

Thrombi typically arise in venous sinusoids of the lower leg muscles or in zones of relative stasis of blood flow behind the pocket-like valves (cf. Fig. A 3.18) of the popliteal and femoral veins (Fig. 3.11 a). Most deep venous thromboses of the leg (over 50 %) arise from the valves of the muscular veins (cf. Fig. A 3.23) of the lower leg (soleus or gastrocnemius veins) or the valves of the fibular vein. Recirculation in the cusps induces platelet activation and the release of procoagulant substances that may lead to the formation of a red thrombus. It is estimated that 20 – 30 % of such thrombi undergo spontaneous thrombolysis through the simultaneous activation of the fibrinolytic system and that about 50 % of the thrombi become organized and thus remain clinically asymptomatic. About 20 – 30 %, however exhibit appositional growth with extension into the deep venous system, from where they may continue to grow cranially. With increasing growth into the major deep veins, the thrombi may become floating and lead to pulmonary embolism without causing any major local clinical symptoms such as swelling and pain. The thrombi become clinically apparent only when they occlude a main vein or obstruct flow through protrusion from a muscular or superficial vein into a major vein. Only then will the symptoms lead to the initiation of diagnostic measures.

Depending on flow in the partially thrombosed tributary vein and the flow obstruction caused by the growing thrombus in the main vein, further growth is ascending or descending (Fig. 3.11 b). Descending venous thrombosis is less common and, in primary pelvic vein thrombosis, is twice as frequent on the left side than on the right. This is attributed to a pelvic vein spur, a connective tissue structure producing narrowing of the lumen through chronic wall trauma as the vein is compressed against the spur by the pulsation of the common iliac artery. The spur is not easily accessible to imaging procedures.

In case of complete thrombotic occlusion of the deep leg veins, venous return is through superficial veins, chiefly the great saphenous vein. The increased blood flow from the great saphenous vein stops the growth of most ascending thrombi in the common femoral vein at the level of its opening. Some superficial femoral vein thrombi do not extend beyond the opening of the deep femoral vein or ascending thrombi are surrounded by blood from the deep femoral veins (Fig. 3.11 c). In isolated descending pelvic vein thrombosis, the blood is drained through epigastric collaterals or suprapubic pudendal veins (Fig. 3.11 d). On duplex scanning, this collateralization is identified by retrograde flow at the opening of the great saphenous vein (cf. Fig. A 3.8).

The incidence of early deep vein thrombosis of the legs is much higher than suspected on clinical grounds due to its fairly asymptomatic course. Moreover, thrombosis carries the risk of serious early complications (pulmonary embolism) and late complications (chronic venous insufficiency with crural ulceration). For these reasons, the indication for diagnostic measures to identify deep venous thrombosis of the legs should be established generously and also in patients presenting with unspecific symptoms only. This is underscored by the fact that compression duplex scanning offers an inexpensive, noninvasive, and accurate diagnostic modality for the evaluation of these patients and that anticoagulant ther-

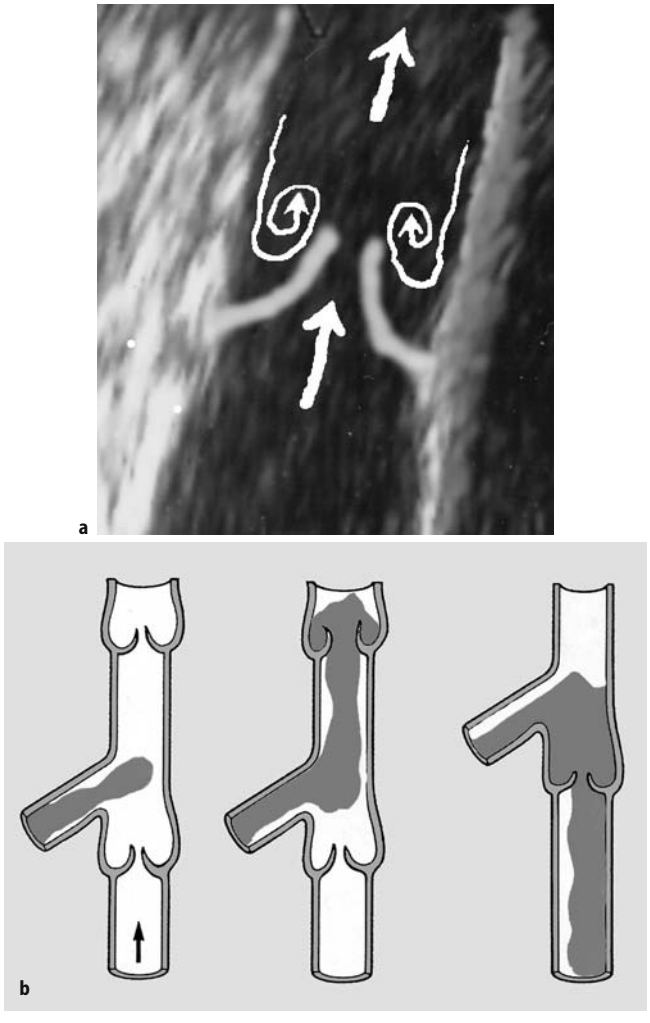

Fig. 3.11. a Turbulent flow and eddy currents in the pocket-like venous valves can lead to local stasis with release of procoagulant substances. **b** Schematic representation of a thrombus (*left*) protruding from a tributary (e.g. lower leg muscular vein) and ascending (*center*) or descending (*right*) in the main vein

(Fig. 3.11 cont.)
c Venous blood flow in thrombotic femoral vein occlusion with venous return from the periphery occurring primarily through the great saphenous vein (*indicated by arrows*). (From Stritecky-Kähler 1994)
d Collateral pathways in descending (isolated) pelvic vein thrombosis: suprapubic pudendal and epigastric collaterals. (From Stritecky-Kähler 1994)

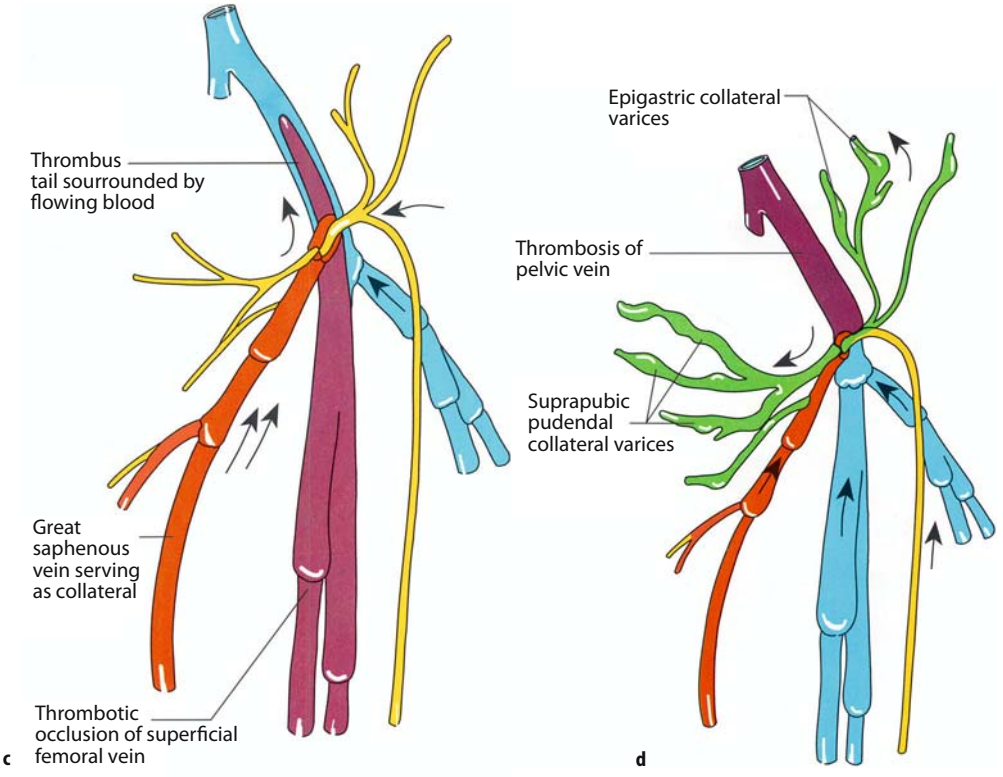

e Grades of truncal varicosis of the great saphenous vein according to Hach:

A Normal blood flow toward the heart in the great saphenous vein,
B Grade I: incompetent terminal valve of great saphenous vein, possibly associated with lateral branch varicosis of accessory veins,
C Grade II: varicosis of great saphenous vein in upper leg, possibly associated with lateral branch varicosis,
D Grade III: varicosis of great saphenous vein extending to proximal lower leg, possibly associated with varicosis of anterior or posterior tributary vein of lower leg,
E Grade IV: varicosis of great saphenous vein extending down to ankle region with more or less pronounced lateral branch varicosis. (From Stritecky-Kähler 1994)

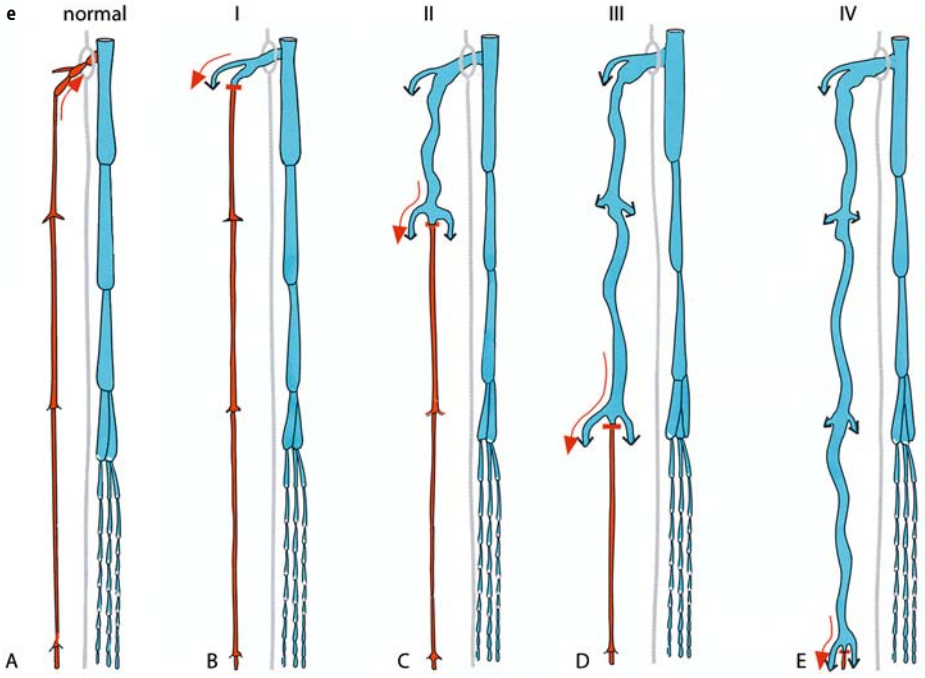

apy is an effective regimen to reduce the risk of pulmonary embolism and prevent further thrombus growth.

With most venous thromboses arising from the lower leg veins, assessment of the muscular and main veins in this area is an integral part of diagnostic sonograhy in these patients.

Ultrasound has the advantage of "illuminating the blind spots" of venography. In the elderly, stasis due to degenerative ectasis of gastrocnemius and soleus veins is a common source of ascending thrombosis. For technical reasons (valve function), such thromboses of the lower leg muscular veins and

the less common deep femoral vein thromboses cannot be identified by venography, because these veins take up the contrast medium only through retrograde flow or not at all. Sonographic findings suggest that ascending thrombophlebitis with thrombus extension from a muscular or perforating vein into the deep venous system as a cause of deep venous thrombosis of the leg is much more common than has been assumed so far.

The fibular vein is a typical source of error in venography because failure to visualize this vein may be due to technical limitations or to a thrombus. At the same time, the fibular vein is the most common site of isolated venous thrombosis of the lower leg with ascending thrombus growth. In an analysis of 105 cases of isolated venous thrombosis of the lower leg (without involvement of the popliteal vein) by our group, the fibular vein alone was affected in 48 instances, the posterior tibial vein in 36, and the posterior tibial and fibular veins in 21. Only one case of anterior tibial vein thrombosis was due to a trauma-induced large hematoma of the anterior compartment. Spontaneous thrombosis of the anterior tibial vein is always caused by descending thrombus growth from the popliteal vein.

Soft tissue lesions such as abscess, hematoma, or perforated Baker's cyst are associated with similar clinical symptoms but are sonographically differentiated from deep venous thrombosis at first glance and may possibly be confirmed by ultrasound-guided puncture.

Thrombus organization begins on day 3 to 4 with attachment to the venous wall, and ingrowth of capillaries occurs after 8 – 12 days (Leu 1973). At the end of the first week, lipoblasts and fibrocytes start to induce the formation of collagen fibrils that fill the hollow and intercapillary spaces left after liquefaction and absorption (Rotter 1981). As cellular infiltration is an ongoing process, a thrombus is composed of layers reflecting the different stages of development from the vessel wall to the lumen. Further organization is associated with shrinkage of the vein, which is demonstrated by ultrasound. Hemolysis with partial degradation of fibrin occurs after days to weeks.

Complete thrombus organization over a few weeks may transform superficial and small veins into strands of fibrous scar tissue. In most cases, however, there will be recanalization of the lumen through the ingrowth of capillaries. The latter dilate and become merged, thereby re-establishing patency after several months. However, recanalization is associated with shrinkage and destruction of the valves as well as fibrosis and thickening of the wall. The main mechanism involved in the recanalization of a thrombosed vein is the high fibrinolytic potential of the venous wall.

The duration of thrombus organization depends on the vessel diameter and intraluminal pressure and may additionally be affected by external factors such as application of compression bandages. Attachment of the thrombus to the wall by collagen fibers will invariably have occurred by day 8 to 10. Thrombolytic therapy (e.g. with streptokinase) performed at this time or later will recanalize the vessel but cannot prevent venous valve destruction in most cases. When surgical thrombectomy is performed at this stage, only central thrombus portions can be removed while mural residues remain and may give rise to the postoperative development of recurrent thrombi through appositional growth. Residual thrombotic material near valves induces valve incompetence. Late sequelae are calcifications of the venous wall.

Collateralization and recanalization following acute deep venous thrombosis lead to the more or less complete reconstitution of venous drainage. Long segments of an occluded vein are recanalized in most cases (endogenous thrombolysis). Recanalization starts in the first weeks and takes six months to one year. Recanalization may begin after 3 – 4 weeks in small vessels but as late as 3 – 9 months after occlusion of large veins such as the popliteal and femoral veins (Irninger 1963). The patency of a deep vein is re-established three months after the onset of thrombosis in about half of all cases (Killewich et al.1989).

Venographic studies demonstrate that complete recanalization occurs in up to 35 % of all venous thromboses within one year and partial recanalization in another 55 % with only 10 % showing persistent occlusion. The clinical severity of the postthrombotic syndrome mainly depends on the degree of valve incompetence, in particular of the popliteal vein, while a persisting lumen reduction after thrombosis has only a minor effect. The insufficient venous return is further compromised by secondary damage (widening with subsequent valve incompetence) to superficial and perforating veins resulting from the higher pressure and volume overload due to collateral flow (secondary varicosis).

Anticoagulation and compression therapy are major components in the management of thrombosis. The latter serves to limit the extent of progressive dilatation of the collateral veins induced by the increased outflow resistance, in particular during the first three months. In summary, chronic venous insufficiency (disturbed venous return from peripheral veins) can have the following causes:

- obstruction of the deep veins,
- valve incompetence of the subfascial veins,
- valve incompetence of the epifascial veins,
- valve incompetence of the perforating veins,
- impairment of the calf muscle pump.

The superficial system (varicosis) and deep system (chronic venous incompetence) may develop secondary changes in response to disease of the respective other system. These secondary changes result from the compensatory increase in pressure and volume and further contribute to the progressive impairment of the existing drainage insufficiency.

The morphologic changes associated with the postthrombotic syndrome can be demonstrated in part by B-mode ultrasound but above all by venography while the functional parameters reflecting the severity of reflux are reliably determined by duplex ultrasound. These parameters have a crucial role in selecting the proper therapeutic procedure (type, extent, and duration of compression therapy).

3.1.5.2 Varicosis

Truncal varicosity of the great or small saphenous vein is caused by valve incompetence due to constitutional or external factors in the primary form or due to a pressure and volume overload of the superficial venous system secondary to pathology (e.g. thrombosis) of the deep venous system (Table 3.3).

Four grades of stem varicosis of the great saphenous vein are distinguished according to Hach, depending on the length of involvement from its termination to its origin (Fig. 3.11 e). Grade I is varicosis of the terminal valve, grade II extension to the distal upper leg, grade III to the proximal lower leg, and grade IV complete incompetence of the vein down to the ankle.

Primary superficial varicosis can in turn lead to pressure and volume overload of the deep venous system with secondary damage resulting from recirculation. Under these conditions, the blood is drained in the deep veins to the proximal point of insufficiency of the superficial system (typically the terminal valve of the great saphenous vein) and then flows back in the superficial veins down to the distal point of insufficiency. There, the blood is again drained into the deep venous system and back toward the heart (cf. also Fig. 3.15 a–c). The resulting overload of the perforating veins and deep venous system induces secondary valve incompetence in these venous segments. This condition is referred to as compensated recirculation when the deep veins have competent valves and as decompensated recirculation when they become incompetent.

Careful assessment of the extent of varicosis with determination of the upper and lower insufficiency points, secondary damage of the deep venous system, and the presence of recirculation is crucial for proper therapy of varicosis (obliteration, surgery, compression). Surgery aims at removal of the insufficient portion of the affected deep vein between the upper and lower insufficiency points, sparing uninvolved venous segments for later arterial reconstruction. Insufficient superficial segments and perforating veins will invariably lead to recurrent varicosis if they are not removed. This is why precise determination of the distal point of insufficiency and the identification of insufficient perforating veins is crucial for the outcome of therapy. Duplex ultrasound is the method of choice and gold standard for this indication.

Thrombophlebitis is a typical complication of varicosis and is diagnosed by B-mode sonography using the same criteria as in the assessment of deep venous thrombosis. Since thrombophlebitis often extends beyond its clinically apparent boundaries, identification of the proximal thrombus end by imaging modalities is clinically relevant to exclude involvement of the deep system.

Moreover, further progression of thrombophlebitis into the deep system must be prevented by high ligation of the saphenofemoral junction in cases where the disease process already extends close to the deep veins. Alternatively, transient anticoagulation in combination with local symptomatic measures can be performed to prevent further progression in such cases.

B-mode ultrasonography is the most suitable imaging modality both to identify the upper end of the thrombus for the initiation of adequate therapeutic management and to follow up therapy.

A retrospective analysis of the ultrasound findings in 363 patients with thrombophlebitis demonstrated growth of the thrombus into the deep venous system over an observation period of 10 days in 11 % of the cases. Seventy percent of these cases were accounted for by great saphenous vein thrombophlebitis with thrombus growth into the common femoral vein (Foley et al. 1989).

More recent ultrasound studies of thrombophlebitis show thrombotic involvement of the deep venous system in 11 – 44 % of the cases, which is a much higher rate than suspected on the basis of the clinical appearance (Blättler 1993; Blättler et al. 1996; Gaitini 1990; Gaitini et al. 1988). Since therapeutic management must be extended to the deep veins in these patients, the indication for ultrasonography of the deep leg veins should be established generously.

In the routine clinical setting, chronic venous insufficiency always gives rise to the question of whether it is a sequela of great or small saphenous vein stem varicosis or whether it is due to the postthrombotic syndrome. As the therapeutic consequences are different, adequate diagnostic workup always includes evaluation of the morphologic and functional status of the major deep veins. Primary valve incompetence of the superficial veins (varicosis) without involvement of the deep veins is treated by surgical removal of the affected superficial vein segments to prevent dermatologic damage as well as secondary involvement of the deep leg veins due to pressure and volume overload (so-called Trendelenburg private circulation; Hach and Hach-Wunderle 1994). In secondary valve incompetence of the superficial veins with simultaneous deep vein involvement (postthrombotic), on the other hand, excision of the varices will bring only little improvement of insufficient venous return. With few exceptions, surgery is not indicated in this situation. Instead, patients, including those operated on, are treated by a rigorous compression regimen (which must also be continued after surgery).

Incomplete recanalization or pronounced postthrombotic occlusion of deep veins is a contraindication to the surgical removal of incompetent superficial vein segments. Tailoring therapeutic procedures to the individual patient relies on precise information regarding the localization and extent of morphologic and hemodynamic abnormalities. Duplex scanning is superior to all other imaging modalities in providing this information (Table 3.4).

Table 3.3. Causes of valve incompetence

- Destruction (postthrombotic)
- Dilatation with incomplete coaptation
  weakness of the venous wall (acquired, congenital)
  pressure overload
  volume overload (secondary, varicosis)
- Malformations

Table 3.4. Diagnostic information required for tailored approaches to treating varicosis

- Localization and function of recirculation (upper/lower insufficiency points)
- Incompetence of main superficial vein
- Incompetence of main deep vein
- Morphologic variants
- Quantification of insufficient venous return
- Identification of incompetent perforating veins

If sclerotherapy is planned for the treatment of varicosis of a side branch or mild truncal varicosis, the ultrasound examination can additionally serve to guide the puncture for injection of the sclerosing agent, particularly in obese patients. The outcome can likewise be assessed immediately.

3.1.6 Duplex Ultrasound – Diagnostic Criteria, Indications, and Role

3.1.6.1 Thrombosis

The chief sonographic criterion for the presence of venous thrombosis (of the deep and superficial systems) is the failure to compress the affected vein with the transducer in transverse orientation (Table 3.5; Fig. 3.12).

Table 3.5. Criteria for identifying fresh deep venous thrombosis of the leg by compression ultrasound in the B-mode

- Compressibility of the vein
- Dilatation of the vein (excluding breathing-related lumen changes)
- Hyperechoic intraluminal structure
- Perivascular structures (to identify extravascular causes of disturbed drainage)

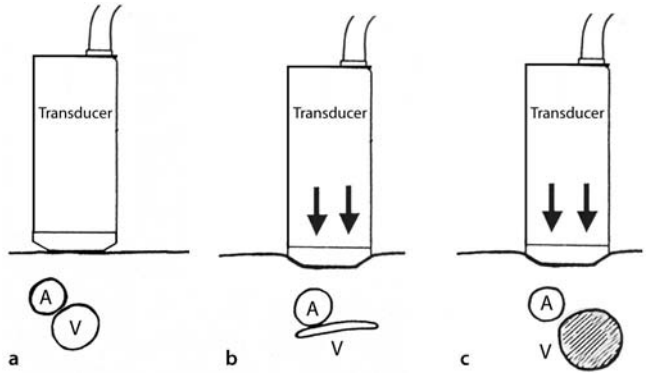

Fig. 3.12. Schematic representation of compression ultrasound. A patent vein is completely compressed and virtually disappears when pressure is exerted with the transducer (**b**). A thrombosed vein retains its shape upon compression (**c**) while a partially thrombosed or partially recanalized vein can be compressed to some degree. A very fresh venous thrombus in a larger vessel may also be compressible to some extent while the vein itself often has a wider lumen than the unaffected vein or the accompanying artery. A more or less hyperechoic intraluminal structure may be depicted (cf. Fig. A 3.3)

Many studies have demonstrated the high accuracy of B-scan ultrasound in the detection of thrombosis in comparison with venography. In symptomatic patients, compression ultrasound has a sensitivity of 95 % and a specificity of nearly 100 % in demonstrating fresh thrombosis of the upper leg and popliteal vein. The failure to compress a vein is both a necessary and sufficient condition for the diagnosis of deep venous thrombosis of the leg. Additional color duplex scanning does not improve the accuracy and the use of color duplex alone tends to have a poorer specificity than compression ultrasound due to false-positive findings as a result of slow venous flow or a poor insonation window in the lower leg.

In the rare cases of isolated pelvic vein thrombosis, compression ultrasound alone is often unreliable due to the lack of an adequate structure against which to compress the vein and interfering overlying structures. In these cases, a thrombosis is diagnosed on the basis of absent flow or an abnormal flow signal (compared to the unaffected side) in the Doppler waveform or a gap in color filling in color duplex scanning.

A thorough evaluation of the pelvic axis is indicated if an abnormal Doppler waveform with reduced respiratory phasicity and slower flow compared to the contralateral side is recorded in the distal external iliac vein in the longitudinal plane. However, since even isolated pelvic vein thrombosis typically involves the entire external iliac vein (including outflow through veins of the saphenofemoral junction and abdominal wall), the thrombosis can be demonstrated by B-mode and compression ultrasound over the inguinal ligament. The only pitfalls are thrombi protruding from the internal iliac vein into the common iliac vein, which escape detection by indirect hemodynamic flow analysis in the groin as they represent no flow obstacle. This also applies to incomplete mural thrombi in a partially patent pelvic vein.

The vessels of the lower legs with their smaller lumen are less well demarcated from the inhomogeneous echotexture of muscle tissue. Still, the criteria for isolated lower leg venous thrombosis are the same as in the upper leg: dilatation of the vessel lumen, failure to compress the vein, and possibly depiction of an inhomogeneous, hypoechoic intraluminal structure. Better filling of the veins is achieved if the examination is performed in the sitting or standing patient. Since a tubular structure distended by fresh thrombosis can be identified more easily than a normal vein, nonvisualization can be interpreted to indicate absence of fresh thrombosis. Note, however, that this only holds true for fresh venous thrombosis whereas older thrombi shrink and often become more hyperechoic and inhomogeneous with the venous lumen returning to its normal diameter. Hence, the vein is again more difficult to differentiate from surrounding muscle tissue, rendering the method less accurate in identifying older thrombosis in the lower leg.

In the diagnosis of fresh (clinically relevant) lower leg thrombosis in patients with clinical symptoms, compression ultrasound has a sensitivity of 85 – 90 % and a specificity of over 95 % (cf. Table 3.6 and page 133). Besides inspection of the main lower leg veins, which are identified on B-mode or color flow images using the arteries of the same name as landmarks, the examiner must pay special attention to the muscular veins

Table 3.6. Studies investigating the role of compression ultrasound, duplex ultrasound, and color-coded duplex ultrasound in larger patient populations with deep leg thrombosis compared with venography

Authors/Year	Patients [n]	Thromboses [n]	Sensitivity [%]	Specificity [%]
Compression ultrasound				
Appelman 1987	112	52	96	97
Dauzat 1986[b]	145	100	94	100
Elias 1987[b]	430	303	98	95
Habscheid 1990[a]	238	153	96	99
Krings 1990	182	–	95	97
Lensing 1989[a]	220	66	99	100
Pederson 1991	215	113	89	97
Herzog 1991[a]	113	57	88	98
Langholz 1991	64	25	76	88
Compression ultrasound: analysis of lower leg veins only (thrombosis)[a]				
Habscheid 1990	37	–	89	99
Elias 1987	92	–	91	96
Duplex ultrasound				
De Valois 1990	180	61	92	90
Comerota 1990	103	44	96	93
Killewich 1989[a]	47	38	92	92
Van Ramshorst 1991	117	64	91	95
Schäberle 1991[a,c]	125	56	97	98
Betzl 1990	66	–	97	72
Color-coded duplex ultrasound				
Schindler 1990	97	54	98	100
Grosser 1990[a]	180	154	94	99
Van Ramshorst 1991	117	64	91	95
Schönhofer 1992	100	63	97	98
Miller 1996	216	98	99	100
Fürst 1990	102	39	95	99
Persson 1989[a]	264	16	100	100
Rose 1990[a]	69	32	79	88
Van Gemmeren 1991	114	74	96	97
Langholz 1991	116	65	100	94
Fobbe 1989	103	58	96	97
Lensing 1989	220	–	91	99
Krings 1990	235	–	93	96
Schweizer 1993 (with ultrasound contrast medium)	78	70	96	100

Note that the lower leg veins were not included in the examination in all cases.

[a] Lower leg included in examination and analysis.
[b] Compression ultrasound, in part supplemented by CW Doppler.
[c] Primary compression ultrasound with optional duplex scanning (primarily for pelvic vein assessment and inconclusive lower leg findings)

Table 3.7. Prospective therapeutic studies of patients with clinically suspected thrombosis of leg veins. Use of different diagnostic approaches but compression ultrasound only of the proximal leg veins including popliteal vein. (According to Bounameaux 2002)

Study	Cogo 1998	Bernardi 1998	Wells 1997	Perrier 1999
Algorithm (see Fig. 3.13a):	rCUS	rCUS+DD	rCUS+PP	CUS+DD+PP
[n]	1	2	4	3
	1,702	946	593	474
Prevalence of thrombosis	24 %	28 %	16 %	24 %
PP	–	–	Score	Empirical
DD	–	Yes	–	Yes
CUS	100 %	100 %	100 %	73 %
rCUS	76 %	9 %	28 %	0 %
Abnormal rCUS	0.9 %	5.7 %	1.8 %	–
Venography	0 %	0 %	6 %	0.4 %
Risk of thromboembolism in untreated group after 3 months	0.7 %	0.4 %	0.6 %	2.6 %

CUS compression ultrasound, *rCUS* repeat compression ultrasound, *DD* D-dimer test, *PP* prediction of pretest probability

of the gastrocnemius and soleus groups, because they often give rise to deep venous thrombosis, especially in immobile patients. Stasis of flow may occur in old age with ectatic degeneration of the muscular veins. The diagnostic criteria are the same as for the main veins (dilatation and failure to compress the vein seen as a tubular structure in the respective muscle).

There is some remaining diagnostic uncertainty, which may require supplementary venography in some cases, especially in patients with a poor insonation window in the lower leg. Nevertheless, venography has its limitations as well and does not achieve 100 % certainty either because some veins of the lower leg, especially the fibular vein group, are notoriously difficult to image.

Different algorithms have been proposed to compensate for the diagnostic uncertainty of compression ultrasound in the lower leg (sensitivity of 85 – 90 %) and to thus optimize the diagnostic and therapeutic management of patients. The options available to reduce the diagnostic uncertainty are application of the highly sensitive but rather unspecific D-dimer test, repeat ultrasound after one week, and venography in high-risk patients. Based on empirical and clinical experience, patients with suspected venous thrombosis can be assigned to a high-probability or a low-probability group on the basis of their risk factors, the severity of clinical signs, and the likelihood of alternative conditions that may explain the symptoms. These factors are assessed by means of scores assigning patients to different probability groups, which determines the further diagnostic procedure if the ultrasound findings are inconclusive. Thus, for instance, patients with a high risk will undergo supplementary venography or a D-dimer test while no further diagnostic measures will be taken in patients with a low risk (Fig. 3.13a).

Compression ultrasonography of the lower leg veins should be a mandatory component of the diagnostic workup of all patients with thrombosis, especially as the most common type of thrombosis, the ascending type, arises in the veins of the lower leg. Hence, the clinical significance of diagnosing lower leg thrombosis lies in the prevention of ascending popliteal or femoral vein thrombosis. Nevertheless, the necessity of careful assessment of the lower leg veins is still a matter of controversy since only one study, which was performed in a rather small patient population, found a significantly higher rate of thromboembolic complications in patients without long-term coagulation of venous thrombosis

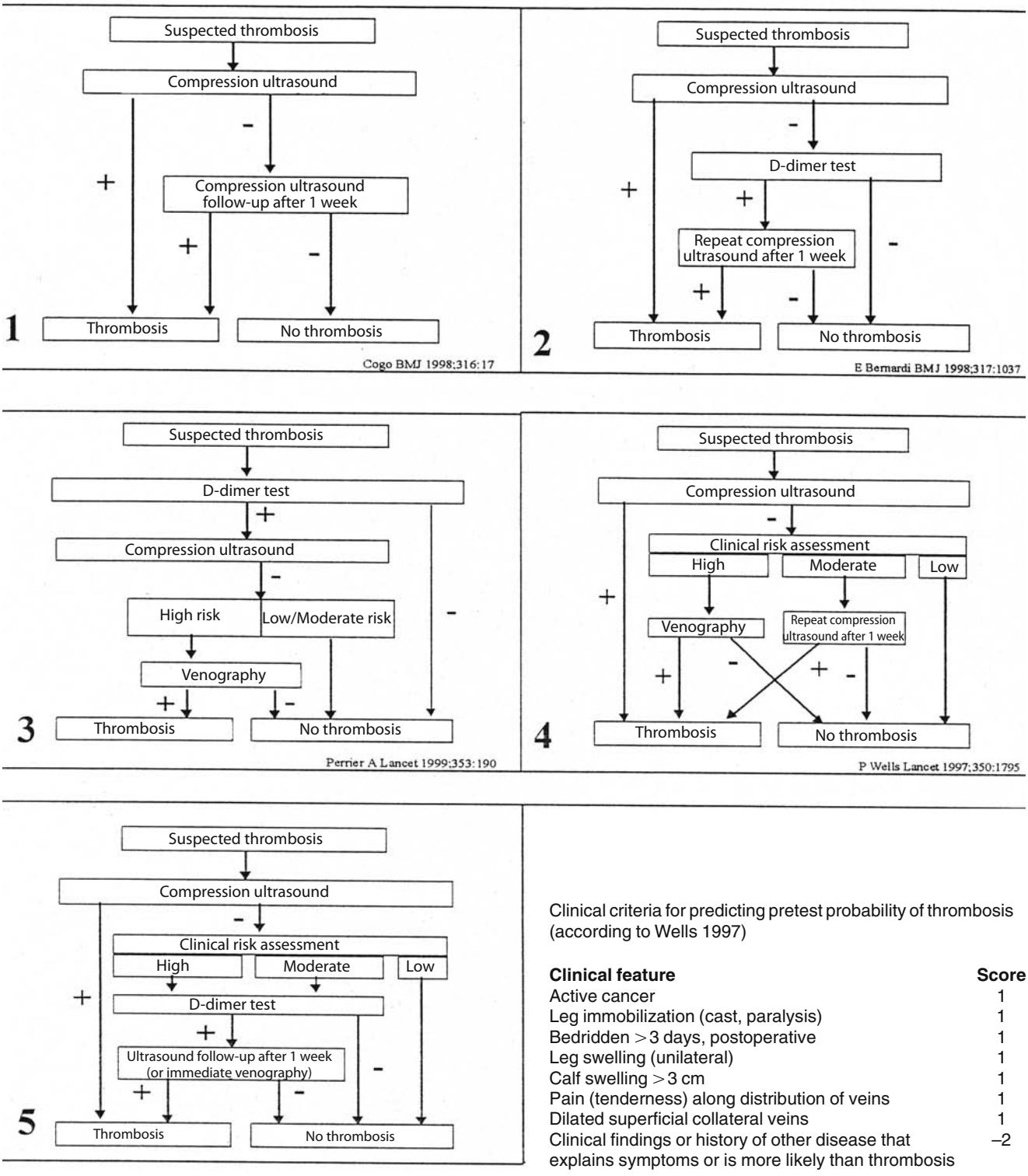

Clinical criteria for predicting pretest probability of thrombosis (according to Wells 1997)

Clinical feature	Score
Active cancer	1
Leg immobilization (cast, paralysis)	1
Bedridden >3 days, postoperative	1
Leg swelling (unilateral)	1
Calf swelling >3 cm	1
Pain (tenderness) along distribution of veins	1
Dilated superficial collateral veins	1
Clinical findings or history of other disease that explains symptoms or is more likely than thrombosis	–2

Fig. 3.13 a Algorithms for the diagnostic management of deep vein thrombosis of the leg. The risk of thrombosis is assessed by means of a scale with a score of over 2 indicating a high risk of thrombosis and a score of 1 to 2 a moderate risk. Charts 1 – 4: Algorithms used in prospective studies with compression ultrasound restricted to the upper leg veins including the popliteal vein. Chart 5: Diagnostic algorithm including compression ultrasound of the upper and lower leg veins and procedure in case of inconclusive findings in the lower leg (according to W. Habscheid). No further diagnostic measures are required in patients with a moderate risk and negative ultrasonography of the lower legs performed by an experienced examiner

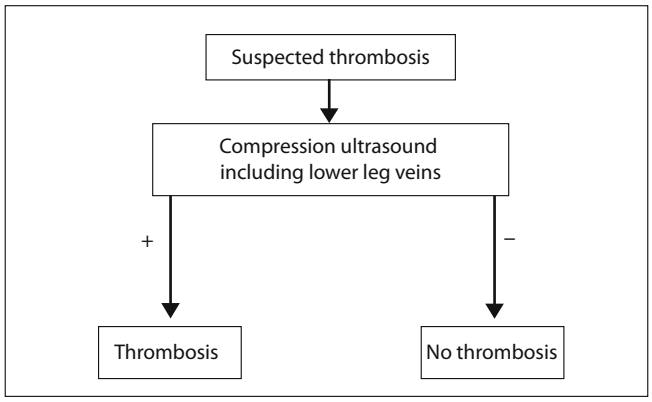

Fig. 3.13 b Algorithm for the diagnostic management of deep vein thrombosis including evaluation of the lower leg veins; 3-month thrombosis rate of 0.3 % in the group with negative findings

of the lower leg (Lagerstatt et al. 1985). Surprisingly, a review of therapeutic studies including a total of more than 3,500 patients with suspected thrombosis in whom only the iliac, femoral, and popliteal veins were examined by compression ultrasound (Table 3.7) identified a 3-month rate of thromboembolism of only 0.4 – 2.6 % in the untreated patients (Bernardi et al. 1998; Cogo et al. 1998; Perrier et al. 1999; Wells et al. 1997). The lower legs were not evaluated by compression ultrasonography, from which the conclusion is drawn that isolated lower leg thrombosis is of little clinical relevance. However, an algorithm for diagnostic management (Fig. 3.13) was used which included repeat examinations in patients with an increased risk of thrombosis.

The only prospective study with long-term follow-up in which the lower leg veins were included in a meticulous evaluation by compression ultrasound identified a rate of thrombosis or thrombembolic complications of 0.3 % after 3 months in the patient group with negative findings in the initial compression ultrasound examination (Fig. 3.13b; Schellong et al. 2003).

There is also disagreement about the additional examination of the asymptomatic leg when deep venous thrombosis has been diagnosed in the other. While an incidence of thrombi of up to 20 % has been described for the asymptomatic leg, their diagnosis may not be necessary as they will be covered by systemic anticoagulation therapy anyway.

Color duplex scanning has no advantages over compression ultrasound in diagnosing fresh thrombi of the deep veins (Table 3.8) but is helpful in evaluating recanalization processes and in identifying thrombi surrounded by flowing blood or floating thrombi. Documentation of the patency of all relevant veins by duplex ultrasound is time-consuming and would prohibit the generous use of this procedure advocated above. All ultrasound laboratories should implement a standardized and efficient algorithm for the diagnostic management of patients with suspected acute venous thrombosis of the legs. Such an algorithm can be based on compression ultrasound, which enables examination of both legs in about 10 – 15 min.

Initial hopes of determining thrombus age by means of sonomorphologic criteria and of thus selecting the most promising therapeutic option (surgery, thrombolysis, anticoagulation) have been disappointed. What is possible is to differentiate very fresh thrombi from markedly older ones, which are characterized by an increasing inhomogeneity and echogenicity while the vessel diameter returns to its original size. Altogether, however, there is wide interindividual variation in the development of thrombi and the criteria are not reliable enough for therapeutic decision making. This holds true especially for the clinically relevant identification of thrombi that are still amenable to recanalization measures, i.e. thrombi not older than one week. Nevertheless, the sonomorphologic criteria can contribute to the therapeutic decision in individual cases. For instance, homogeneous thrombi with a lower echogenicity in markedly dilated veins with good demarcation of the wall and thrombus portions surrounded by flowing blood are more likely to undergo rapid recanalization under thrombolytic therapy.

An outflow obstacle (thrombosis, external compression) is associated with an increase in intravascular pressure in venous segments peripheral to it with demonstration of slower flow by duplex scanning.

The increased venous flow resistance associated with occlusion, compression, or persisting postthrombotic obstruction eliminates the respiratory fluctuation of venous return. This is reflected in the Doppler examination by an unchanging flow velocity in the vein distal to the obstruction

Table 3.8. Venous ultrasound

Indications for gray-scale ultrasound/compression ultrasound:
- Evaluation of thrombosis (exclusion, confirmation, extent, age) with localization and differentiation (main veins, muscular veins)
- Thrombophlebitis (extent, thrombus protrusion into major deep vein)
- Follow-up (spontaneous resolution, thrombolysis, thrombectomy)
- Differential diagnosis of perivascular structures compressing the vein (Baker's cyst, soft tissue tumor, hematoma, abscess, wall tumor)

Indications for color duplex ultrasound:
- Follow-up after thrombosis (spontaneous or thrombolysis-induced recanalization)
- Pelvic vein thrombosis
- Floating thrombi
- Chronic venous insufficiency/postthrombotic syndrome (valve incompetence of deep leg veins: severity of reflux, extent, degree of recanalization)
- Varicosis (extent, severity of reflux, secondary incompetence of main veins; preoperative evaluation: determination of upper and lower points of insufficiency, identification of incompetent perforating veins)
- Vein mapping prior to bypass surgery (suitability of saphenous vein for venous bypass grafting)
- Venous aneurysm (extent; characterization: spindle-shaped, saccular, intraluminal thrombosis)

and a reduced flow velocity that is best appreciated by comparison with the contralateral side (Fig. 3.14; Table 3.9).

3.1.6.2 Chronic Venous Insufficiency

While thrombosis can be evaluated by B-mode scanning alone, Doppler ultrasound is mandatory for the hemodynamic assessment of the severity of disturbed drainage in chronic venous incompetence besides providing information on the postthrombotic morphologic changes. High-resolution transducers nicely demonstrate venous wall sclerosis by an increased echogenicity and thickening in the presence of a patent lumen as well as the incompetent valves that have become fixed through the sclerotic process. Nevertheless, B-mode scanning alone is insufficient because the formerly thrombosed and then recanalized venous segments will have a normal sonomorphologic appearance in about 30 % of cases. The other 70 % show wall irregularities and thickening, a strand-like vein with a reduced lumen, or a vein that has become dilated after recanalization through pressure and volume overload due to incompetent valves (cf. Figs. A 3.26 to A 3.29).

These changes are best seen in comparison with the unaffected side. The thickened wall will hinder complete compression of the vein, leaving a hypoechoic rim in the soft tissue. The degree to which a vein can be compressed depends on the extent of recanalization and the presence of intraluminal structures, which are inhomogeneous and mostly hypoechoic relative to the surrounding connective tissue. Especially the femoral vein is often depicted as a thin strand only that is identified on poststhrombotic B-scan ultrasound using the adjacent artery as a landmark. However, a recanalized and incompetent femoral vein will widen during Valsalva's maneuver.

B-mode scanning does not allow evaluation of the recanalization process as it does not depict flow in sclerotic segments with wall thickening and compression may be inhibited by wall sclerosis (Table 3.10).

The clinical manifestation of the postthrombotic syndrome is chiefly influenced by the extent to which venous drainage is disturbed, which in turn varies with the degree of thrombosis and recanalization as well as collateral blood flow. Valve incompetence in the main veins determines the extent of reflux, which correlates well with the extent of the initial thrombosis. Duplex ultrasound studies demonstrate abnormal reflux after recanalization of thrombotic deep vein segments in about 45 – 70 % of cases after 1 – 3 years, while normal findings with preserved valve function are seen in 12 – 30 % after recanalization (Johnson et al. 1995; Markel et al. 1992) and 10 – 20 % of vessel segments remain completely obstructed (Johnson et al. 1995).

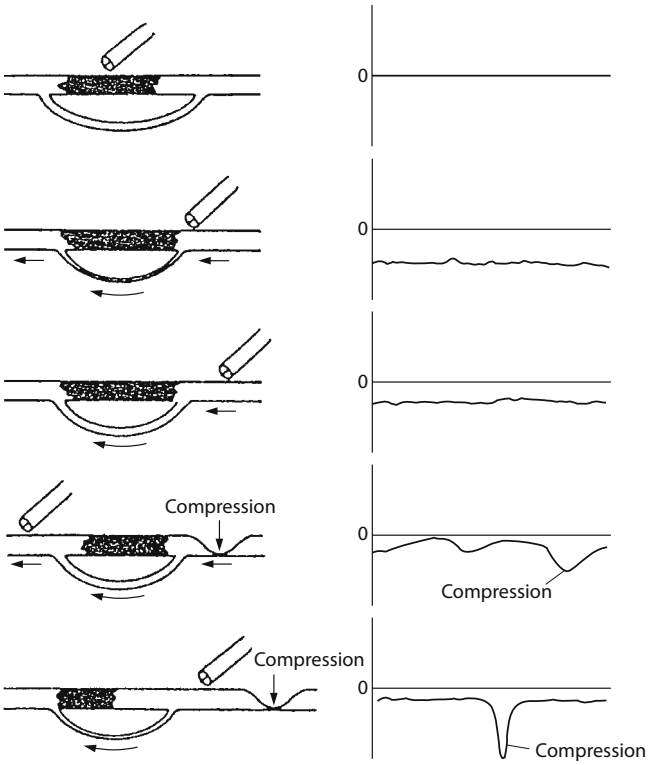

Fig. 3.14. Schematic representation of Doppler waveforms in thrombosis – functional tests

Table 3.9. Evaluation of flow obstruction by duplex scanning using criteria known from CW Doppler ultrasound

- Zero flow in the thrombotically occluded vein
- Decreased flow velocity with reduction or elimination of respiratory phasicity due to a proximal thrombus or venous compression by surrounding structures
- Flow signal unaffected by respiration, possibly of high frequency, along partially thrombosed or compressed vessel segments or along thrombi surrounded by flowing blood (differential diagnosis: flow signal from collateral vein not subject to respiratory fluctuation)
- Augmented flow abnormally reduced in compression-decompression test distal or proximal to thrombosis or flow obstruction

Table 3.10. Ultrasound criteria in evaluating postthrombotic syndrome

B-scan (normal in 30 – 40 %):	Narrowing of vessel lumen Blurred wall structure Thickened wall Wall sclerosis, intramural calcifications Intraluminal connective-tissue strands, adhesions Echogenic vessel lumen Not fully compressible
Color duplex scanning:	Degree of recanalization Incompetence of major veins Better visualization of wall sclerosis Identification of collaterals Incompetence of superficial veins (secondary) Incompetence of perforating veins

Venous reflux is measured using Valsalva's test to evaluate the proximal valves and the compression-decompression test to evaluate distal insufficiency. The increase in intra-abdominal pressure induced by the Valsalva maneuver produces a short, physiologic backward flow with a mean duration of 0.3 s. Reflux persisting for over 1 s is abnormal. Studies in patients with stage II or III chronic venous insufficiency demonstrated sensivities of 77 – 91 % and specificities of 85 – 100 % for reflux assessment by duplex scanning (Araki et al. 1993; Neglen and Raju 1992). Moreover, the duplex findings showed a better correlation with the clinical stage than the findings obtained with ascending venography.

The Valsalva test can be performed in the recumbent patient while the compression-decompression test should be performed with the patient sitting or standing, which increases the diagnostic accuracy by 10 %. The compression-decompression test can be performed manually distal to the ultrasound probe or in a standardized manner using a cuff for compression. Standardized spectral Doppler recordings of reflux in the popliteal vein are obtained upon sudden deflation of a blood pressure cuff placed around the calf and inflated to 100 mmHg. The use of such standardized provocative maneuvers is a prerequisite for interindividual comparison of results and scientific studies. The compression-decompression test reproduces the flow variations resulting from the alternating compression and decompression of the venous wall by the calf muscle pump.

The muscular compression of the main veins embedded in the muscle not only brings about drainage to the center but also induces flow toward the periphery, which is prevented by competent valves. The muscle pump is also responsible for abnormal reflux from the deep into the superficial veins in patients with valvular incompetence of the perforators.

Therefore, incompetent valves reduce the efficiency of the muscle pump because the venous pressure, normally decreasing upon muscular activity, remains unchanged or drops only little. These complex interactions must be taken into consideration in order to select a proper site for placing the Doppler sample volume but also in interpreting the flow data obtained.

In severe valvular incompetence, as in the postthrombotic syndrome, reflux can be induced not only by Valsalva's maneuver but also by normal inspiration or deep inspiration in the horizontal position. Persisting reflux throughout inspiration indicates valvular incompetence. Under normal conditions, the craniocaudal pressure gradient ensures rapid valve closure and thus prevents reflux.

Pressure and volume overload occurring distal to postthrombotically altered veins can lead to secondary damage through hyperextension of the valvular rings in the formerly unaffected vessel segments (Killewich et al. 1989). The same pathomechanism leads to secondary, non-postthrombotic valvular incompetence of the deep veins in patients with a long history of truncal varicosity (Trendelenburg private circulation; Fig. 3.15 a–c). In this secondary form as well as in primary chronic venous insufficiency of the deep leg veins, the B-scan shows dilatation of the affected vein but no wall thickening and no inhomogeneous structures in the lumen. Moreover, the vein can be completely compressed. Under good insonation conditions, mobility of the valve is demonstrated, which distinguishes this condition from the postthrombotic syndrome with valve immobility due to fibrotic thickening (cf. Figs. A 3.5 and A 3.6).

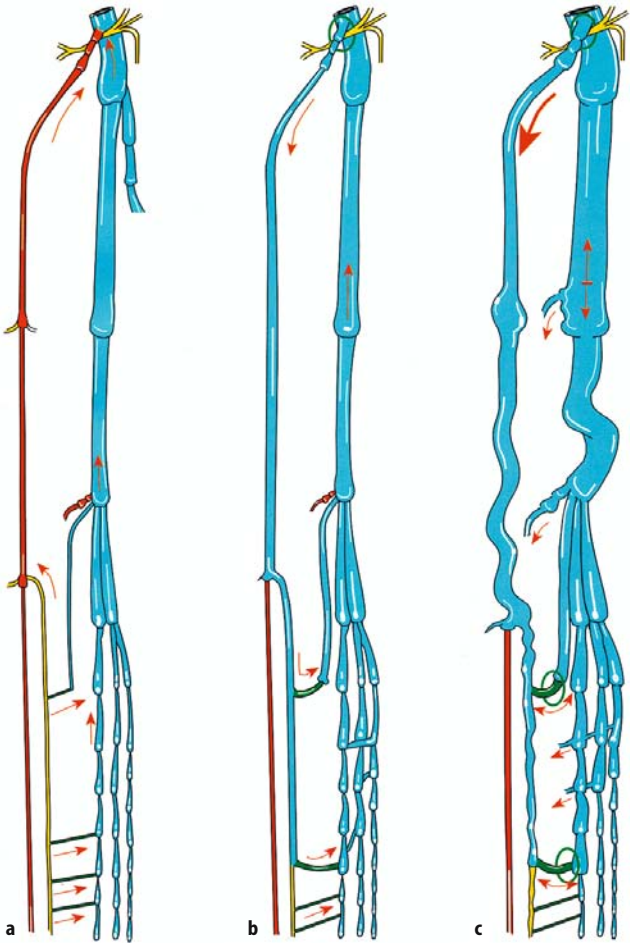

Fig. 3.15 a–c. Development of chronic venous insufficiency with valvular incompetence of the deep veins secondary to truncal varicosity of the great saphenous vein. **a** Physiologic blood flow direction in deep and superficial veins (*red arrows*). Perforating veins drain the blood from the superficial to the deep venous system. **b** Truncal varicosis of the great saphenous vein is associated with retrograde flow through the perforators back into the superficial venous system. This hypercirculation (Trendelenburg private circulation) is compensated as long as the valves of the deep veins remain competent but leads to dilatation of superficial side branches and perforators as well as volume-induced dilatation of the deep veins. **c** In the further course, the hypercirculation becomes decompensated through valve failure of the deep veins due to overload-induced dilatation. This valve failure in turn leads to pressure-induced dilatation and secondary valve incompetence of further perforating veins (Cockett's Boyd's, and Dodd's perforating veins). Finally, the muscle pump becomes insufficient and full-blown drainage insufficiency occurs. (From Stritecky-Kähler 1994)

The cause of valvular incompetence influences the character of reflux (Evers and Wuppermann 1995, 1997). Reflux in postthrombotic valve incompetence sets in immediately with the provocative maneuver (without signs of valve movement), increases rapidly, peaks during the first seconds, and then decreases (type B). In contrast, in primary chronic venous insufficiency and primary varicosis, the abnormal reflux occurs with a short delay after physiologic reflux (which normally leads to valve closure) and is continuous (cf. Fig. A 3.29) and slower (type A). In severe venous dilatation without any residual valve function, however, even primary chronic venous insufficiency of the superficial or deep venous system results in immediate high-frequency reflux.

Reflux velocity can serve as a semiquantitative measure of postthrombotic valvular damage. The velocity increases during the first year and then reaches a plateau. Moreover, the reflux velocity and duration may be increased by secondary postthrombotic changes caused by pressure and volume overload.

3.1.6.3 Varicosis

The procedure for evaluating valvular incompetence of the superficial veins is the same as for the deep veins, namely recording of Doppler frequency tracings during provocative tests. The flow reversal thus induced can also be demonstrated by the color change in the color duplex scan but only the Doppler waveform enables precise determination of the duration of reflux. Clinically, it is important to determine the proximal extent of insufficiency. In complete insufficiency of the great saphenous vein, which is the more common type, the proximal point is identified by repeated Doppler sampling beginning just below the termination of the vein. Valve incompetence is indicated by reflux persisting for more than 1 sec upon increased intra-abdominal pressure during Valsalva's maneuver. This test is performed intermittently along the course of the great saphenous vein until the distal point of insufficiency is identified (transition from reflux to normal flow), which determines the grade of great saphenous vein varicosis according to Hach (Fig. 3.16). In Hach grades I to III, varicose side branches often enter the vein in the area of the distal point of insufficiency.

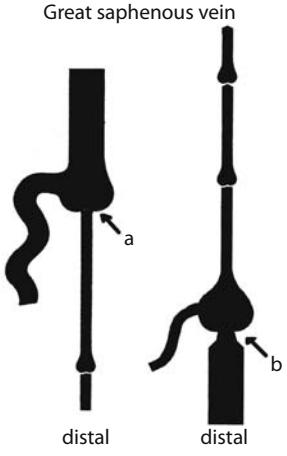

Fig. 3.16. Valve incompetence of major superficial veins. *Left drawing*: schematic representation of the distal point of insufficiency (*a*) with pressure-induced dilatation of a side branch or perforating vein (varicose degeneration) originating from the insufficiency point. Normal segment of main vein with functioning valves distal to this point. *Right drawing*: schematic representation of the proximal point of insufficiency (*b*). Normal vein with competent valves proximal to the point and valve insufficiency distal to it

Clinically apparent varicose changes of the great saphenous vein are often restricted to the lower leg. Nevertheless, duplex scanning frequently demonstrates valve incompetence of the great saphenous vein in the upper leg as well where dilatation is less pronounced due to the lower intravascular pressure. A study by our group including 103 patients with great saphenous vein varicosis demonstrated involvement of the saphenofemoral junction in 66 % of the cases with clinically normal findings of the upper leg. Therefore, evaluation of the junction is mandatory in duplex scanning of patients with lower leg varicosis.

In the incomplete form of varicosis of the great saphenous vein, valve incompetence is confined to the distal segments while the terminal valves in the proximal segment are intact.

Four main types of incomplete truncal varicosis are distinguished:

- In incomplete varicosis of the perforator type with a properly functioning valve at the saphenofemoral junction, distal incompetence of the great saphenous vein originates from an insufficient perforating vein, e.g. a Dodd vein in the upper leg (cf. Fig. A 3.33).
- In incomplete varicosis of the lateral branch type with proximal competence, the distal great saphenous vein varicosis is maintained by varicosis in a side branch, e.g. an insufficient lateral accessory vein in the upper leg (cf. Fig. A 3.30 d–g).
- In the posterior type, venous incompetence extends from the small saphenous vein, through the popliteal vein, to an accessory great saphenous vein and hence to the great saphenous vein (Giacomini anastomosis) (cf. Fig. A 3.21 b).
- Distal varicose lateral branches such as the communicating veins between the great and small saphenous veins can maintain secondary varicose changes of the distal saphenous vein.

Preoperative identification of the upper point of insufficiency in distal varicosis by duplex scanning is important to achieve complete surgical removal of the incompetent vein segments and to thus prevent recurrence as well as to spare competent venous segments for possible later bypass procedures. The dilated varicose segments are identified in the standing patient and traced up to the point of insufficiency and marked on the skin. Surgeons will benefit most from real-time imaging of venous morphology and function by duplex scanning if they perform the examination themselves.

In incomplete distal great saphenous insufficiency, the Valsalva test yields no valid results because the proximal valves still function properly. Instead, the compression-decompression test is performed with the patient standing. The incompetent great saphenous vein depicted by B-mode imaging is followed upward to identify the proximal point of insufficiency for tailoring the surgical procedure. Divisions into arch veins can thus be identified by duplex scanning as well and evaluated for incompetent valves. The ultrasound exami-

nation thus enables accurate identification of all incompetent venous segments prior to surgical removal.

Moreover, the perforating veins can be identified sonographically in their typical locations (Cockett's, Boyd's, and Dodd's perforators) and evaluated for competence. Demonstration of reflux from the deep into the superficial veins in the compression-decompression test with compression of superficial veins by means of a tourniquet indicates perforator incompetence.

In a comparative study, 95.5 % of a total of 252 insufficient perforating veins diagnosed by color duplex ultrasound were confirmed intraoperatively. In comparison, venography identified only 65 % of these insufficient perforating veins (Stiegler et al. 1994). The accuracy of palpation alone is 49 % and that of CW Doppler 75 %.

The ultrasound examination for incompetence of the small saphenous vein is likewise performed with the patient standing. If the deep veins are still competent, however, insufficiency can be evaluated only with the compression-decompression test and not with Valsalva's maneuver. After identification of the highly variable opening of the small saphenous vein into the popliteal vein, a Doppler tracing is recorded during intermittent compression and decompression with the hand or a cuff distal to the transducer. The course of the small saphenous vein is then traced downward applying intermittent pressure to identify the distal point of insufficiency. Valve incompetence is suggested by dilatation – primarily in the popliteal fossa – and a tortuous course resulting from elongation of the vein.

3.1.7 Rare Venous Abnormalities

3.1.7.1 Venous Aneurysm

Venous aneurysms are true aneurysms that develop by dilatation of an intact venous wall. Their etiology is unknown (Fischer et al. 1996; Smets et al. 1997). Only individual cases of secondary posttraumatic aneurysms of the popliteal vein have been reported (Aldrige et al. 1993).

Thrombosed aneurysms of the popliteal vein are rare but are a potential source of recurrent pulmonary embolism.

More aneurysms of the popliteal vein have been discovered since compression ultrasound and duplex scanning became widely accepted as the first-line modalities for the evaluation of deep venous thrombosis and valve incompetence of the leg.

As with arterial aneurysms, fusiform or spindle-shaped and saccular aneurysms are distinguished. Experimental investigations in models have shown that quasilaminar flow is predominant in fusiform aneurysms while turbulent flow with flow separations occurs in saccular aneurysms (Brunner et al. 1997; Haaverstad et al. 1995). Stasis in dead water zones in an aneurysm can give rise to thrombus formation (cf. Fig. A 3.35 a). Only anecdotal cases of pulmonary embolism caused by venous aneurysms have been reported (Biesseaux et al. 1994; Seino et al. 1994).

One case of paradoxical embolism has been described (Manthey et al. 1994). Most venous aneurysms are incidentally detected in patients examined for exclusion of deep venous thrombosis of the lower extremity. The patients typically report pain and swelling. In a study by our group, 4 saccular aneurysms and 4 spindle-shaped aneurysms of the popliteal vein were detected in 11,500 ultrasound examinations of the deep leg veins performed in patients with suspected thrombosis (Schäberle and Eisele 2001). Two of the saccular aneurysms were partially thrombosed and the patients suffered pulmonary embolism. The other two saccular aneurysms were incidental findings without pulmonary embolism, and one of them was associated with deep venous lower leg thrombosis. The four spindle-shaped aneurysms were not thrombosed and there was no evidence of prior pulmonary embolism in these patients (cf. Figs. A 3.35 to A 3.38).

Venography is limited in assessing the size and extent of mural thrombosis of an aneurysm in the popliteal fossa due to interference from overlying muscular veins and the small saphenous vein. Real-time ultrasound, on the other hand, provides definitive information on the relationship of an aneurysm to the veins opening into it, the aneurysm diameter, its shape, and intra-aneurysmal thrombus formation. The shape (saccular of spindle-shaped) and thrombus formation are crucial criteria for therapeutic management. Based on the sonographic findings, the four saccular aneurysms in our study were resected and the ultrasound diagnosis confirmed. The spindle-shaped aneurysms were followed up and treated by combined anticoagulation and compression or compression alone according to their size.

These cases underline that the noninvasive duplex findings provide the basis for a differentiated approach to the treatment of the rare popliteal vein aneurysms (incidence of 0.07 % of all patients examined for suspected deep venous leg thrombosis in our study). The intraoperative findings confirm the validity of duplex scanning, which is the method of first choice in the diagnostic evaluation of venous aneurysm.

3.1.7.2 Tumors of the Venous Wall

Venous stasis or obstruction of inflow with unilateral leg edema of unclear origin may be caused by a benign or malignant tumor of a venous wall. Such tumors may give rise to the development of appositional thrombi as wall compression or infiltration progresses. The tumor can be demonstrated directly as circumscribed wall thickening and differentiated from venous thrombosis by ultrasound, which thus serves as a basis for establishing the indication for surgical resection. Benign venous wall tumors comprise papillary endothelial hyperplasia, hemangioma, leiomyoma, and fibroma. Malignant tumors are angiosarcoma and leiomyosarcoma. Sonomorphologic criteria for differentiating benign and malignant tumors are invasive growth and tumor vascularization (cf. Fig. A 3.44).

3.1.7.3 Venous Compression

The venous wall has only a thin muscle coat and is therefore easily compressed by lymphoma (predominantly in the true pelvis and groin), perivascular tumors, hematoma, abscess, and arterial aneurysm (above all of the popliteal artery), causing flow obstruction with the clinical signs of thrombosis. With its ability to visualize both the vein itself and the surrounding structures, ultrasound will either demonstrated the cause of disturbed drainage directly or lead to further, more specific diagnostic measures such as ultrasound-guided aspiration or biopsy.

In rare cases, a popliteal entrapment syndrome involves both the artery and the vein, for instance in the presence of an ectopic popliteal muscle or pronounced hypertrophy of the heads of the gastrocnemius muscle. In such cases, the outflow obstruction can be elicited by active plantar flexion (cf. Fig. A 3.45).

A vein compressed by external structures will only show augmented flow (A-sound) upon distal compression while spontaneous flow is absent. Normal respiratory phasicity is lost distal to the flow obstacle. When a small residual lumen is still patent, spectral Doppler depicts a high-frequency flow signal resembling a stenosis signal (cf. Figs. A 3.41 and A 3.42).

3.1.8 Vein Mapping

Autologous saphenous vein grafts have the best patency rate of all materials used in peripheral bypass surgery. However, the vein may be unsuitable for bypass grafting for several reasons (cf. Fig. A 2.17 a, b):

- small lumen,
- postthrombophlebitic changes,
- ectatic, varicose degeneration.

These criteria can be assessed in the preoperative ultrasound examination, which will thus shorten the length of surgery and prevent unnecessary vein exposure. Moreover, preoperative marking of the course of the vein on the skin helps prevent large incisions and is especially helpful in obese patients. Duplex scanning is highly reliable in identifying suitable vein segments for grafting as demonstrated by intraoperative confirmation of the findings in 98 % of cases (Krishnabhakdi 2001).

3.1.9 Diagnostic Role of Ultrasound

3.1.9.1 Thrombosis

The value of a diagnostic test is determined in comparison with the other methods available. Apart from venography, the current standard, other modalities that have been used in the diagnostic assessment of thrombosis include thermography, scintigraphy, plethysmography, and CW Doppler. All of these modalities rely on the demonstration of indirect criteria and have a fairly poor specificity. Moreover, each of these is restricted to a specific vascular territory and none of them enables evaluation of the entire venous system. Scintigraphy is highly sensitive in diagnosing thrombosis of the lower leg whereas CW Doppler ultrasound is reliable only in identifying upper leg and pelvic thrombosis.

In patients with clinically suspected lower extremity deep vein thrombosis, duplex scanning is the preferred initial imaging modality. Its high diagnostic accuracy with a sensitivity and specificity of nearly 100 % in assessing the veins in the upper leg and the popliteal vein as well as the proximal segments of the lower leg veins ensures a confident diagnosis, provided the scanning conditions are adequate. In lower leg venous thrombosis, on the other hand, duplex sonography has a sensitivity of only 85 – 90 %. Here, additional venography should be performed if the sonographic findings are inconclusive and the patient has a high risk of thrombosis or if ultrasound visualization is inadequate. Alternatively, the D-dimer test can be performed, which is highly sensitive but not very specific. Due to the low specificity, a positive D-dimer test is of little use, especially in postoperative patients with suspected thrombosis but a negative result excludes thrombosis in combination with compression sonography.

Venography is no longer necessary in patients with patent femoral and popliteal veins on compression ultrasound. Instead, these patients undergo close sonographic follow-up to ensure early identification of thrombus growth into the popliteal vein in those patients in whom lower leg thrombosis may have been missed due to poor scanning conditions in the initial examination. The high specificity of compression ultrasound results in a high positive predictive value, i.e., an abnormal finding (noncompressibility of the vein) is diagnostic of deep venous thrombosis of the leg.

Duplex scanning, on the other hand, has a lower accuracy in diagnosing suspected symptomatic recurrent thrombosis and in screening asymptomatic high-risk patients for thrombosis.

Compression ultrasound is less specific in diagnosing recurrent thrombosis because the failure of the vessel walls to completely coapt in a postthrombotic vein that is not fully recanalized may give rise to false-positive results. Early recurrent thrombosis is suggested if a more markedly dilated venous segment is demonstrated proximal to a partially recanalized segment (flow signals on color duplex ultrasound). Another criterion is the complete noncompressibility of a vein segment having shown postthrombotic recanalization in an earlier examination. Careful documentation and recording of the findings thus ensures a nearly 100 % accuracy in diagnosing recurrent thrombosis (Prandoni et al. 1993). Color duplex sonography performed 6 months (at the time of discontinuation of anticoagulant therapy) and 12 months after the occurrence of thrombosis serves as a basis for the diagnosis of recurrent thrombosis.

Compression sonography is the noninvasive gold standard in evaluating symptomatic patients but has a much poorer sensitivity in identifying thrombosis in asymptomatic high-risk patients after orthopedic, urologic, or general surgery. Such screening examinations are clinically justified as 17 – 20 % of patients develop deep venous thrombosis of the leg after hip or knee replacement despite antithrombotic prophylaxis (Hamulyak et al. 1995). A review of 11 studies performed in asymptomatic patients after hip and knee surgery demonstrated a sensitivity of only 62 % for compression ultrasound but a specificity of 97 % for identifying femoropopliteal venous thrombosis (Wells et al. 1995). An even lower accuracy was found for the diagnostic assessment of lower leg vein thrombosis (Lensing et al. 1997).

In studies performed in neurosurgical patients in the mid-1990s, ultrasound was found to have a sensitivity of only 56 % in asymptomatic proximal thrombosis and of only 50 % in distal thrombosis compared to venography (Jongbloets et al. 1994; Lausen et al. 1995).

Venous thrombi in asymptomatic patients often cause no occlusion or are very short (cf. Fig. A 3.18a) and are easily overlooked in the presence of postoperative edema. Venography is superior, especially in depicting minute clots in the pocket-like valves of the femoral and popliteal veins. The poor results in asymptomatic high-risk patients are also due to a lack of compliance and a less thorough examination in this patient population. The results may be improved by exploiting the flexibility of ultrasound and testing the compressibility of poorly visualized vessel segments with different transducer orientations.

Mural thrombi in a partially compressible vein can be identified if the vein is insonated posterior to the artery, which can thus serve as an acoustic window unless it shows atherosclerotic changes. The clinical relevance of such thrombi is controversial but they may be the source of further thrombus growth. Therefore, postoperative patients should be assessed by compression sonography of the deep leg veins prior to mobilization despite the limitations outlined above.

The term “floating thrombus” is based on the venographic appearance of a thrombus segment surrounded by flowing blood: The convoluted tail suggests swimming motion but is due to thrombus growth in the blood stream and gives the thrombus the appearance that it is floating. Floating thrombi were considered to carry a high risk of embolism and therefore used to be operated on much more frequently in the past. More recent ultrasound and CT studies suggest that actual movement of floating thrombi is overestimated due to their morphologic structure. Floating thrombi are diagnosed three times more often on venography than on ultrasound and even less frequently on CT (Gartenschlager et al. 1996). This overestimation of floating thrombi is also confirmed by our experience. For these reasons, a floating thrombus should only be diagnosed if an unattached thrombus segment is seen on gray-scale ultrasound, color duplex scanning demonstrates a thrombus tail several centimeters in length, or the thrombus is seen in the center of the vessel and surrounded by flowing blood on all sides (without wall adherence) during a gently performed Valsalva maneuver.

The simultaneous visualization of perivascular structures by ultrasound enables the differentiation of abnormal soft-tissue changes that may lead to thrombosis-like clinical symptoms. A hematoma occurring after trauma or in association with a coagulation disorder is seen as a hypoechoic area more or less clearly delineated from the surrounding muscle. If the findings are inconclusive or abscess is suspected, the diagnosis can be confirmed by ultrasound-guided puncture.

Baker’s cysts are caused by the escape of synovial fluid. They are located in the popliteal fossa and typically arise from the medial knee joint space. Depending on their size, they cause swelling and tension. Cyst rupture is associated with acute pain of the calf and is demonstrated on ultrasound as an anechoic, leaking fluid collection under the fascia. Ultrasound-guided aspiration confirms the diagnosis and also leads to rapid improvement or complete elimination of the complaints.

In case of a tumorous soft-tissue lesion, ultrasound additionally provides direct information on vein compression by the tumor and allows hemodynamic assessment of the outflow obstruction. The sonographic examination thus enables precise preoperative determination of the extent and localization of disturbed drainage and identification of possible vascular infiltration, which is important for surgical tumor removal. In establishing the cause of thrombosis, the ultrasonographer must also search for a tumor to exclude a paraneoplastic origin, especially in older patients. The site of compression of a vein by a lymphoma can be identified and the severity of the outflow obstruction estimated by spectral Doppler recording (spontaneous and augmented signal) distal to the compressed vein.

The accuracy of compression and duplex ultrasound must be measured against that of venography, the traditional gold standard. It is noteworthy that venography itself was never validated in comparison with another modality. Opacification of the veins by the contrast medium enables direct assessment of the lumen but no extravascular information is provided. Moreover, filling defects may give rise to misinterpretation because they may be due to occlusion or methodological limitations, especially in the lower leg. The lower leg veins are depicted incompletely in 15 % of cases and inadequately in 4 % (Schmidt 1974, 1977). Complete visualization of the venous segments of the lower extremity varies from 61 – 96 %. Repeat venography in patients with clinical signs of venous thrombosis of the leg performed due to progression of symptoms within 5 days of a negative initial venography enabled definitive diagnosis of thrombosis in 1.3 % of cases (Hull 1981 et al.).

These results put into question the suitability of venography as the gold standard in the diagnosis of thrombosis. In a study performed by our group in 159 patients with clinically suspected deep vein thrombosis who were independently examined by duplex scanning and venography (Schäberle and Eisele 1991), venography yielded inconclusive or false results or failed to identify the cause of leg swelling in 21 cases due to methodological limitations. In these cases, duplex scanning demonstrated an AV fistula, thrombophlebitis,

muscular vein thrombosis, and venous compression by pelvic tumors, Baker's cysts, or arterial aneurysms. In five instances, venography yielded false-negative results compared to ultrasound (deep femoral vein thrombosis; complete thrombosis of one branch of a paired superficial femoral vein; lower leg venous thrombosis; mural thrombosis of venous aneurysm). False-positive venograms were seen in three cases (compression of the popliteal vein and proximal lower leg veins by a ruptured Baker's cyst and a large false aneurysm; misinterpretation of filling defect). The ultrasound findings were confirmed intraoperatively or through additional examinations. In this study, venography had an accuracy of 95% compared to duplex ultrasound.

In a large study of 430 consecutively examined patients, the 5% discrepancy between venography and ultrasound (including the lower legs) is attributed to false-negative venograms, which are represented in the study as false-positive ultrasound findings (Elias et al. 1987). Part of the false-negative venograms were accounted for by sonographically identified venous thrombi in the lower leg and misinterpretation of filling defects.

Complete evaluation of all deep lower leg veins is often not possible by venography because thrombi producing complete occlusion of small veins are missed, as these are not apparent as filling defects.

Several studies conducted since the late 1980s found sensitivities and specificities of compression ultrasound ranging from 87 to 100% compared with venography as the gold standard (cf. Table 3.6). In one of these studies, performed by our group and including 131 legs with clinically suspected deep venous thrombosis (confirmed by venography in 73 legs) in 125 patients (72 female, 53 male; mean age 55 ± 18.5 years), ultrasound had a sensitivity of 97% and a specificity of 98% (Schäberele and Eisele 1991). Discrepancies mainly involved the lower leg veins.

Despite the controversy about the clinical importance of lower leg venous thrombosis symptomatic patients should undergo early diagnostic assessment and treatment in order to prevent appositional thrombus growth. Compression ultrasound is a valid diagnostic modality in isolated lower leg venous thrombosis as well, where it has sensitivities and specificities of 85% to 90% (cf. Table 3.6; Elias et al. 1987; Habscheid et al. 1990). Even isolated thrombosis of the muscular veins is highly conspicuous on compression ultrasound and is identified with a high degree of accuracy as an accessory finding.

Conventional duplex scanning did not lead to a statistically significant improvement in the diagnosis of thrombosis while flow assessment by means of spectral Doppler tracings facilitates diagnostic evaluation in venous segments notoriously difficult to scan such as the pelvic veins. The demonstration of flow signals adjacent to central thrombi or in early recanalization can contribute to therapeutic decision making.

To assess *valve function*, gray-scale imaging is supplemented by Doppler scanning (duplex or color duplex). The postthrombotic assessment of valve function in the superficial veins is the key to proper therapeutic management besides evaluation of spontaneous or thrombolysis-induced recanalization. The evaluation proceeds from the openings of the great and small saphenous veins down the leg to determine the distal extent of reflux.

As a supplementary tool in the hands of the surgeon, *color duplex scanning* was found to have an accuracy of 95.4% in demonstrating the exact localization of insufficient perforating veins as confirmed by the intraoperative findings (Stiegler et al. 1994). Moreover, duplex scanning can be used to assess the outcome of therapy, as in sclerotherapy of varices.

The risk of *appositional thrombus growth* with protrusion into major deep veins secondary to superficial thrombophlebitis was first noted and documented by ultrasonography. Patients with local thrombophlebitis treated conservatively should undergo sonographic follow-up to identify appositional growth, if indicated on the basis of their symptoms. High ligation of the saphenofemoral junction aimed at preventing further appositional growth and pulmonary embolism is indicated in thrombosis extending to the opening of the saphenous vein or if a thrombus protrudes from a superficial vein into a major deep vein. Unlike venography, ultrasound enables very reliably evaluation of the opening areas of the great and small saphenous veins (Barrelier 1993; Schuler et al. 1995; Schönhofer et al. 1992). Since thrombophlebitis additionally correlates with silent lower leg venous thrombosis, the latter should be excluded specifically by ultrasound (Jorgensen 1993).

Precise determination of thrombus age is crucial for optimizing the therapeutic approach (thrombolysis, surgery, or conservative therapy). Thrombus age is often underestimated if based on the clinical findings and history alone. Venography chiefly relies on indirect criteria (collateralization) to estimate thrombus age while the morphologic appearance is of limited value in venographic age determination. The ultrasonographic evaluation of thrombus morphology provides the most reliable data for estimating thrombus age despite the variations that exist in echotexture and extent of venous dilatation in relation to thrombus genesis and localization (Table 3.11; Fobbe et al. 1991).

Early recanalization is suggested by the presence of spontaneous or augmented flow in the venous lumen. Incompetent valves in recanalized thrombotic veins are identified by functional tests (Valsalva's maneuver, compression-decompression test). Wall irregularities and hyperechoic deposits as well as a rigid vessel wall in the compression test already suggest the postthrombotic syndrome in the gray-scale scan. Noninvasive color duplex scanning can be repeated any time and therefore is an excellent modality for monitoring the outcome of thrombolytic therapy and deciding when therapy can be discontinued. Moreover, this modality can be used to evaluate the outcome of thrombectomy and to quantitatively estimate the flow volume after creation of a bucket handle shunt by determining blood flow in the common femoral artery proximal to the shunt in comparison with the contralateral side.

Close sonographic follow-up of the *natural history* (in patients undergoing heparinization with subsequent phenprocoumon administration) in comparison with thrombo-

Table 3.11. Sonographic findings in the diagnostic evaluation of venous thrombosis and estimation of thrombus age

Thrombosis	Findings
Absent	Complete compressibility of vein Thin wall Breathing, Valsalva's maneuver, and distal compression elicit identical changes in flow on both sides No elicitation of retrograde flow (indicating adequate valve closure)
Fresh thrombus (< 8 days)	Noncompressibility of vein Venous diameter increased to at least twice that of accompanying artery Flow signals near the wall if thrombus is still surrounded by blood or in the presence of a floating thrombus Thrombus tends to be homogeneous and hypoechoic Good delineation of vessel wall, in part with hypoechoic halo No demonstration of collateral veins by color duplex scanning
Older thrombus (> 2 – 3 weeks)	*Total occlusion:* Noncompressibility of vein Diameter shrinks to less than twice that of accompanying artery No flow signals, thrombus tends to become more hyperechoic and inhomogeneous Poor delineation of vessel wall, hyperechoic halo may still be present *Partial occlusion:* Partial compressibility of vein Vessel lumen comparable in diameter to that of accompanying artery Signs of marginal and central recanalization Collaterals begin to form
Postthrombotic lesions	*Persistent occlusion:* Reduced venous lumen (same as or smaller than diameter of accompanying artery) Vessel wall poorly demarcated against surrounding soft tissue Fully developed collateral vessels *Partial recanalization:* Meandering flow signal in center of vein Little or no respiratory fluctuation of flow Short residual occlusions Sclerotic thickening and rigidity of vessel wall; incomplete compressibility *Recanalization:* Flow signal throughout lumen Sclerotically altered segments and sonographically normal wall segments Incompetent valves demonstrated by Valsalva's maneuver and compression-decompression test Variable lumen with widened and narrowed segments

lysis or thrombectomy provides data for a critical appraisal of these therapies and may lead to changes in the currently established therapeutic approaches. The fact that patients undergoing thrombolytic therapy for more than 10 days develop valve incompetence casts doubt on this approach, although it leads to recanalization (but fairly late). Moreover, one must take into account the increasing bleeding risk associated with longer thrombolytic therapy. Valve damage occurs with increasing thrombus organization; the valves immobilized by residual thrombotic material can be depicted in the recanalized veins if the scanning conditions are good. Comparative studies of the late outcome of thrombolytic therapy according to thrombus age, treatment duration, and thrombus localization in comparison with the natural history would be desirable but require a complex study design.

Our preliminary observations suggest that *isolated pelvic vein thrombosis* has a high rate of spontaneous recanalization. Twelve of 15 patients with isolated pelvic vein trhombosis treated conservatively (full-dose heparin with subsequent phenprocoumon and compression therapy) showed complete recanalization after six months. Because the iliac veins have no valves, these patients are unlikely to develop a postthrombotic syndrome as long as the thrombosis does not descend into the femoral vein or such extension is prevented by heparin and compression therapy.

The sonographic examination yields very detailed information on the *extent and localization of thrombosis*. It provides direct evidence as to whether a thrombus is localized in a lower leg muscular vein or a main vein or if a thrombus protruding into the femoral vein originates from the great saphenous vein or the deep femoral vein. Pulmonary emboli may arise from the proximal deep femoral vein, especially if an appositional thrombus protruding into the common femoral vein is dislodged. Venographically, the deep femoral vein is often not depicted or only after retrograde contrast filling, which does not occur in most patients with competent valves. Evaluation of the first 4 – 8 cm of the deep femoral vein, which are easily amenable to scanning, is an integral part of the diagnostic ultrasound examination. Another source of embolism is thrombosis at the opening of the internal iliac vein. This area should be assessed by duplex scanning for the presence of a floating thrombus, in particular in patients with pulmonary embolism. However, sonographic assessment of this area is limited in obese patients or when there is scattering and acoustic shadowing due to overlying bowel gas. If visualization of the pelvic veins is limited, occluding pelvic vein thrombosis can be excluded indirectly by analysis of a Doppler waveform from the common femoral vein in comparison with the contralateral side.

Ultrasound, not involving radiation exposure and not requiring contrast medium administration, is the method of choice in pregnant women, children and adolescents, and patients allergic to contrast medium. Another advantage of this noninvasive modality is the short examination time of 5 – 10 min per leg in the diagnostic assessment of thrombosis. Some extra time is required for the valve function tests in patients with the postthrombotic syndrome and varicosis.

As with arterial aneurysms, ultrasonography enables more precise assessment of the extent, localization, and presence of mural thrombosis of *venous aneurysms* as compared with radiographic tests that rely on the opacification of the patent lumen (angiography, venography). The decision for conservative management or surgical resection is mainly based on

the presence of partial thrombosis, the shape of the aneurysm, and its extent.

Venous compression syndromes of the upper and lower extremities can be assessed sonographically by analyzing the flow patterns elicited by provocative tests.

3.1.9.2 Chronic Venous Insufficiency

In the evaluation of patients with the postthrombotic syndrome, duplex scanning is a highly valid modality both for depicting morphologic changes of the venous wall (B-scan) and for identifying insufficiency of the main vein (Doppler). Recanalization is visualized with a high degree of accuracy and drainage insufficiency is evaluated semiquantitatively by measuring flow velocity and the duration and extent of reflux. It is important to differentiate reflux from persisting occlusion because the latter has important prognostic implications with regard to insufficient venous drainage. Careful documentation of the findings is crucial for comparison and diagnosing recurrent thrombosis at follow-up. In the occasional patient, venography is required to confirm morphologic wall changes and recurrent thrombosis.

Noninvasive duplex scanning would also be a suitable modality for determining functional parameters in monitoring the effectiveness of *pharmacologic treatment*. However, for adequate evaluation and monitoring of chronic venous insufficiency, it would be desirable to have threshold values, e.g. of the vessel diameter above which abnormal venous dilatation should be assumed.

To overcome this lack, various parameters were determined by duplex scanning in 30 subjects with normal vessels (18 male, 12 female; mean age 34.7 ± 7.3 years). Mean values were calculated for each leg from 5 individual measurements. The measurements were performed with the subjects in the flat supine position and the feet lowered 10°. The following values were measured in the common femoral vein just above the termination of the great saphenous veins (n = 60 legs):

- Diameter: 11.7 ± 2.1 mm during expiration, 12.4 ± 2.2 mm during inspiration,
- Planimetrically determined cross-sectional area: 1.07 ± 0.28 cm^2 during expiration, 1.16 ± 0.31 cm^2 during inspiration,
- Peak flow velocity: 23.5 ± 8.3 cm/s during expiration; mean flow velocity averaged over 3 respiratory cycles with normal inspiration depth and abdominal breathing: 7.7 ± 1.9 cm/s.

During Valsalva's maneuver the femoral vein diameter increased to 1.82 ± 0.6 cm^2. The mean intraindividual diurnal variation in the cross-sectional area from morning to evening was 19.2 % in expiration and 17.7 % in inspiration. Peak expiratory flow velocity varied by 18.9 % and mean flow velocity by 17.3 %. Measurements performed on different days demonstrated a variation in the cross-sectional area of 24.6 % during expiration and of 27.8 % during inspiration while peak expiratory flow velocity varied by 24.7 % and mean flow velocity by 21.4 %. Other diameters determined in the 30 subjects were 8.9 ± 1.8 mm in the superficial femoral vein just after the origin of the deep femoral vein and 8.7 ± 1.6 mm in the popliteal vein at about the level of the knee joint cleft. The mean diameter of the great saphenous vein measured just below its opening in standing subjects was 5.6 ± 1.9 mm.

The parameters show wide intraindividual variation in repeat measurements performed on the same day or from day to day. Blood flow velocity as well as the diameter and cross-sectional area of large veins vary with breathing. Our results are confirmed by Marshall (1990), Hirschl et al. (1990), and Ludwig (1991), who report similar variations in diameter and cross-sectional area. Taking these factors into account, the mean flow rate determined for the common femoral vein just above the opening of the great saphenous vein is 503 ± 137 ml/min calculated as mean cross-sectional area multiplied by mean flow velocity (V_{mean}).

The respiration-induced variations in cross-sectional area are incorporated in this calculation as follows:

> Mean cross-sectional area = 1/3 × (2 × venous cross-section in expiration + cross-section in inspiration)

Arterial blood flow shows less variation. In experimental measurement series performed in waterbaths by our group, the correlation between the average arterial flow velocity calculated from mean arterial flow velocities repeatedly measured by duplex scanning and the actual flow velocity was R = 0.98 (Schäberle and Seitz 1991). In the calculation, the pulsatile diameter variation is accounted for according to the formula:

> Radius = $1/3 \times (2\ R_{diastolic} + R_{systolic})$

Measurements in the superior mesenteric artery showed good reproducibility with a day-to-day variation of 10 % for blood flow velocity and of 2.2 % for vessel diameter. In contrast, quantitative determination of venous flow is much less precise because venous diameter measurement is subject to errors that are difficult to control. The diameters of large veins vary with breathing and the proximal iliac vein even shows pulsatile diameter variation. These variations are difficult to quantify and respiratory maneuvers do not easily lend themselves to standardization. The large veins are typically not circular but elliptical.

Another source of error is the use of high-pass filters that eliminate slow venous flow components from the Doppler spectrum, resulting in overestimation of mean blood flow velocity. In the above-described measurement series in 30 subjects with normal vessels, comparison of flow in the common femoral artery and in the common femoral vein just after the opening of the great saphenous vein surprisingly showed mean venous flow to be 21 % faster than arterial flow. In a series by Ludwig (1991) venous blood flow in the common femoral vein was about 32 % higher than in the artery. These results are attributable to the above-described sources of error.

Cross-sectional areas or diameters markedly exceeding the above-described normal values suggest chronic venous incompetence but the wide variation already seen under normal conditions prohibits a reliable separation by means of cutoff values. Moreover, the observed day-to-day variation in cross-sectional area and mean flow velocity makes such measurements unsuitable for monitoring the outcome of pharmacologic therapy. Other studies, however, suggest that such parameters (Jäger et al. 1986; Eichlisberger and Jäger 1989) can indeed be used to identify physiologic variations or to objectively follow up the effectiveness of pharmacologic therapies aimed at altering venous tone.

The severity of drainage insufficiency in chronic venous incompetence can be determined more reliably on the basis of morphologic criteria depicted by venography compared to the wall changes seen on gray-scale ultrasound. Although dilatation in primary chronic venous incompetence or shrinkage of the vessel lumen in the postthrombotic syndrome with wall thickening, sclerosis, residual thrombi, or persistent occlusion are important descriptive criteria, the severity of drainage insufficiency can be evaluated more reliably using hemodynamic parameters such as extent, type, and length of reflux. Moreover, postthrombotic gray-scale sonography shows normal vein morphology in 20–30% of cases.

Sonographic evaluation after thrombosis with determination of the degree of recanalization helps decide the duration of anticoagulant therapy. Moreover, the findings serve as a basis for identifying recurrent thrombosis in later follow-up examinations. Since there will be no persisting incompetence of the major vein after deep vein thrombosis in about 20–30% of cases (probably because some valves retain their function), the evaluation of reflux by duplex scanning identifies those cases with persistent insufficiency that require treatment with compression stockings. Wearing of compression stockings reduces postthrombotic trophic skin damage but does not affect the rate of recurrent thrombosis.

Disadvantages of ultrasound (Table 3.12) are the lack of full documentation of the findings and the greater examiner dependence. It is limited in the presence of large edemas or vessel and soft tissue calcifications and if the scanning window is small or inadequate due to surgical wounds, skin defects, or overlying bowel gas. A patient's inability to cooperate and thoracic breathing can lead to misinterpretation of Doppler frequency spectra; no cooperation is required in compression ultrasound.

The wall changes associated with recanalization after thrombosis make the vessel more resistant to compression and may mimic a fresh thrombus if not enough pressure is applied. The question as to whether there is recurrent thrombosis or appositional growth on the basis of earlier thrombosis with or without partial recanalization may be difficult to answer using venographic and sonographic criteria. Fresh, nonoccluding thrombotic deposits are differentiated from older, mural residues of thrombotic material by searching for other residual changes in the form of wall thickening or incompetent proximal valves, which are demonstrated during Valsalva's maneuver. The demonstration of flow signals near the wall suggests a fresh thrombus surrounded by flowing blood while meandering flow in the center of the vessel is a sign of early recanalization.

Table 3.12. Comparison of venography and color duplex ultrasound in assessing disturbed drainage/thrombosis of the leg veins. The more plus signs given for an entry, the more favorable the rating of the procedure. (Modified according to Koppenhagen and Fobbe 1993)

	Venography	Color duplex
Pelvic veins	++	++
Femoral muscle vein	+++	+++
Deep femoral muscle veins	–	+++
Popliteal vein	+++	+++
Major veins of lower leg	++	++
Muscular veins of lower leg	–	+++
Superficial veins	++	+++
Patency	+++	+++
Wall changes postthrombotic	++	+++
Complete/partial occlusion	++	+++
Extent of thrombosis	++	+++
Thrombus age determination	+	++
Recanalization	++	++
Collaterals	+++	++
Function of venous valves	+++	+++
Cause of vein compression	+	+++
Venous aneurysm	++	+++
Evaluation of varicosis	++	+++
Impairment by edema/skin defects/ postoperative changes	++	+
Soft tissue calcifications	+	+
Documentation	+++	+
Examiner dependence	++	+
Patient cooperation	+	+++
Side effects	+	+++
Cost	+	+++
Complexity of procedure, duration	+	+++

CT and MRI can be used to assess the veins of the extremities but their main indication is in the evaluation of the pelvic veins. CT requires contrast medium administration. MRI is complex and time-consuming and thus unlikely to gain a place in routine venous diagnosis. Although ultrasonography is a highly accurate method providing extensive information on venous abnormalities, the examiner must always retain a critical stance and be aware of its limitations, which may make it necessary to order supplementary diagnostic tests in individual cases.

3.1.9.3 Varicosis

Color duplex scanning is a reliable tool for determining the extent of venous varicosis (upper and lower points of insufficiency) and identifying incompetent perforators prior to surgical interventions. In the localization of incompetent perforators, duplex ultrasound was found to have a significantly higher sensitivity than venography (96% versus 65%; Stiegler

et al. 1994) although only venograms with a good image quality were included in the analysis. Venograms of poor quality depicted only 16% of the insufficient perforators identified sonographically. Ultrasound of the perforating veins is performed with the patient standing since small incompetent veins may be missed in the recumbent patient, just as during surgery.

Additional evaluation of the deep venous system by duplex ultrasound enables differentiation of primary from secondary, postthrombotic varicosis. Duplex ultrasound is thus superior to all other imaging modalities in establishing the indication for surgery and determining the extent of the surgical procedure. Identification of the upper and lower insufficiency points spares nonvaricose vein segments, which are thus available for possible later arterial reconstruction.

Apart from cosmetic reasons, treatment of varicosis primarily aims at preventing secondary incompetence of major veins. Duplex ultrasound is the most reliable imaging modality to determine the proximal and distal points of insufficiency and to identify incompetent perforating veins, which must be eliminated in order to stop extrafascial recirculation. Duplex ultrasound information on involvement of the saphenous vein and its extent is important for choosing between sclerotherapy and surgical stripping.

In patients with varicosis complicated by thrombophlebitis, duplex ultrasound is the preferred method for identifying the proximal end of the thrombus, which determines whether anticoagulant therapy or high ligation of the saphenofemoral junction is indicated. Moreover, it serves to exclude concomitant involvement of the deep venous system. By demonstrating varicose as well as postthrombophlebitic changes in vein mapping prior to bypass procedures, ultrasonography can help to identify suitable segments for grafting and these can be marked on the skin prior to surgery.

3.2 Arm Veins and Jugular Vein

3.2.1 Vascular Anatomy

As in the leg, superficial and deep veins can be distinguished in the arm. The most important superficial vein is the cephalic vein, which has a crucial role in establishing a hemodialysis access. It courses from the wrist to the bend of the elbow on the radial side of the arm and continues on this side to the shoulder, from where it passes anteriorly to Mohrenheim's fossa. The deep veins accompany the arteries of the same name and have multiple connections with the superficial veins. The deep veins of the lower arm join at the bend of the elbow to continue as the brachial vein. The latter often has multiple branches and courses along the medial aspect of the humerus to the axilla. The axillary vein begins at the lower border of the teres major muscle as the continuation of the basilic vein, from where it passes to the clavicle. Along its course, it receives the cephalic vein at the level of Mohrenheim's fossa. Proximal to the clavicle, the axillary vein continues to the superior vena cava as the subclavian vein. Along its course, the subclavian vein relates anteriorly with the clavicle and subclavius muscle and above with the subclavian artery. Inferiorly, the vein rests on the first rib. The subclavian vein passes in front of the scalene triangle (in front of the scalenus anterior) and unites with the internal jugular vein to form the brachiocephalic vein (Fig. 3.17).

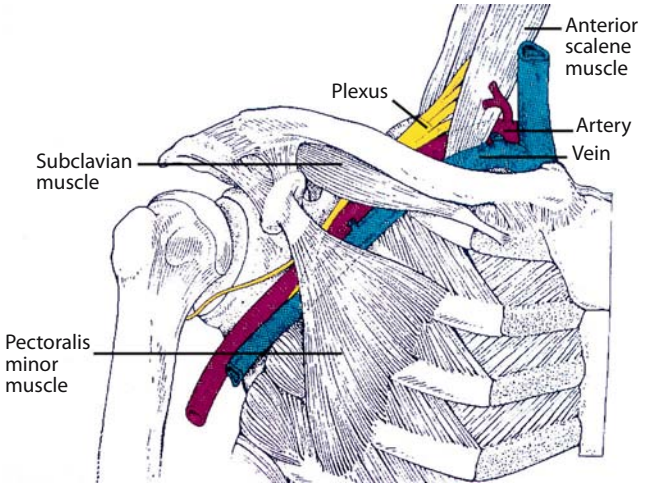

Fig. 3.17. Courses of the subclavian and axillary veins. (From Heberer and van Dongen 1993)

3.2.2 Examination Protocol and Technique

The subclavian, axillary, and brachial veins are examined with a 7.5 MHz transducer. These veins are scanned with the examiner positioned at the patient's head. Morphologic assessment and the compression test are performed as with the deep leg veins. Note, however, that the compression test is reliable only for the axillary and brachial veins but not for the subclavian vein when interrogated from the supraclavicular approach. First, the axillary vein coursing below the artery is tested for compressibility in transverse orientation with the transducer in Mohrenheim's fossa. Next, the Doppler spectrum is recorded in the longitudinal plane to exclude a central outflow obstruction due to thrombosis or compression. The further course of the vein is traced, and the compressibility of the brachial vein is tested in the upper arm from medially pressing the vein against the humerus. The subclavian vein is scanned longitudinally from the supraclavicular position with recording of a Doppler spectrum and evaluation of the opening of the jugular vein. The internal jugular vein can be tracked along its course parallel to the carotid artery in transverse orientation with intermittent compression to exclude thrombosis. The color duplex mode in longitudinal planes enables assessment of recanalization, identification of central thrombi surrounded by flowing blood, and detection of partial thrombosis after implantation of a portal catheter, central venous catheter, or pacemaker probe.

3.2.3 Normal Findings

As with the pelvic and leg veins, undisturbed flow in the arm veins shows respiratory phasicity. In addition, flow in the subclavian and axillary veins varies during the cardiac cycle (W-shaped profile with two peaks, one during systole and a second upon opening of the AV valves; markedly reduced flow during atrial contraction with short transient reflux). Moreover, the typically elliptical lumen of the subclavian and axillary veins shows respiratory diameter variations on longitudinal or transverse views (cf. Fig. A 3.46).

3.2.4 Documentation

The findings in the subclavian, axillary, and brachial veins are documented on longitudinal views together with the corresponding angle-corrected time-velocity spectra. In case of venous thrombosis, an additional transverse view of the abnormal vessel segment without and during compression is documented.

3.2.5 Clinical Role

Thrombosis of the arm veins is rare compared to venous thrombosis of the legs and can be caused by

- paraneoplasia,
- obstructed drainage in the narrow costoclavicular space,
- tumor compression in the thoracic outlet, or
- thrombogenic effects of portal catheters, central venous catheters, or pacemaker probes in the axillary and subclavian veins.

The narrow costoclavicular space through which the vein must pass is formed by the first rib, the clavicle, and the subclavian muscle. Venous drainage may be obstructed when the already narrow passage is constricted further by weak shoulder muscles, rib callus, or exostosis. Obstruction can be reproduced during the examination by hyperabduction of the arm. Following recanalization after thrombolytic therapy, the indication for resection of the first rib is established by demonstration of an outflow obstruction in the costoclavicular space by means of the hyperabduction test.

Ultrasound can be used to evaluate patency prior to insertion of a pacemaker probe or a central venous catheter, especially in patients with clinical signs or a history of previous venous thrombosis of the upper extremity. Prior to placement of a central venous catheter in the jugular vein, ultrasound can in addition serve to identify the correct vessel in order to preclude misplacement or complications in patients with an abnormal course of the vein.

The risk of pulmonary embolism in venous thrombosis of the arm is very low. Clinically relevant postthrombotic damage is unlikely because there is good collateralization. Nevertheless, early examination by noninvasive duplex scanning is indicated in patients with clinical signs of thrombosis in order to stop further progression by full-dose heparin therapy. Thrombophlebitis is typically caused iatrogenically and is rarely associated with thrombus extension into major deep veins.

3.2.6 Duplex Ultrasound Findings and their Diagnostic Significance

The ultrasound findings in thrombosis are the same as in deep vein thrombosis of the legs: The vein appears markedly dilated and contains homogeneous or inhomogeneous structures, it cannot be compressed, and (color) duplex scanning fails to depict flow signals or depicts flow only near the wall in the presence of a central thrombus surrounded by flowing blood. Any internal or external obstruction of venous drainage eliminates cardiac pulsatility and eliminates or reduces respiratory fluctuation of flow. Therefore, a significant flow obstacle can be excluded by means of a Doppler waveform recorded in the axillary vein (from Mohrenheim's fossa) in cases where methodological limitations prohibit adequate evaluation of the subclavian vein from the supraclavicular position. Apart from the subclavian vein, the easily accessible axillary vein may be affected by thrombosis because blood from the arms is emptied into this vein through thoracic wall collaterals. Compression ultrasound is used to exclude thrombosis of the axillary vein (with the transducer in Mohrenheim's fossa) and of the peripheral veins. As already mentioned, the compression test is unreliable in the subclavian vein, where flow has to be demonstrated directly by means of a Doppler tracing. Sonographically, thrombophlebitis can be distinguished from subfascial thrombosis on the basis of the course of the vessel affected and its relationship to anatomic landmarks (accompanying artery of the same name) (cf. Fig. A 3.54).

We analyzed 610 patients with arm swelling examined by duplex ultrasound, which demonstrated arm vein thrombosis in 96 cases. In 61 of the patients, thrombosis was attributable to paraneoplasia, central venous catheters, or pacemaker probes. Nine of the remaining 35 patients, in particular younger ones, underwent thrombolytic therapy, which led to recanalization in 7 cases. Subsequently, flow obstruction was demonstrated in the costoclavicular space by duplex scanning with provocative maneuvers in 5 of the patients.

In the hyperabduction test, the arm on the affected side is raised above the head while the Doppler spectrum is recorded in the axillary vein with the transducer in Mohrenheim's fossa. Note, however, that there may be some physiologic flow obstruction during extreme hyperabduction, especially in slender patients. A more reliable way to demonstrate clinically significant narrowing of the passage between the clavicle and the first rib is to use a modified "apron grip" test in which the Doppler spectrum in the axillary vein is recorded while pulling on the ipsilateral arm that is turned backward and rotated to the side. Flow reduction with elimination of

cardiac and respiratory fluctuation is abnormal (cf. Figs. A 3.51 and A 3.52).

The underlying mechanism is complex. Typically, however, the clinical symptoms are caused by weakness of the shoulder muscles. Under normal conditions, the muscular tone elevates the clavicle above the neurovascular bundle. If the muscles are too weak, however, the bundle is compressed by the movement of the clavicle over the first rib during abduction with rotation.

Obstruction in the costoclavicular space primarily affects the vein while the scalenus and cervical rib syndromes do not affect venous drainage as the subclavian vein passes in front of the scalenus anterior muscle. The costoclavicular compression syndrome is primarily treated by physical therapy aimed at strengthening the muscles of the shoulder girdle. The outcome can be followed up by duplex scanning. If the symptoms persist after physical therapy, or after recanalization following thrombolytic therapy of compression-induced thrombosis, resection of the first rib is indicated.

Color duplex scanning provides precise information on both spontaneous and thrombolytic recanalization after arm vein thrombosis as well as on lesions persisting after thrombosis such as luminal variations, residual mural thrombi, or wall sclerosis (cf. Fig. A 3.53). Postthrombotic valvular incompetence is of little clinical relevance in the arm. Ultrasound is superior to all other imaging modalities in providing the information on morphologic wall lesions and their hemodynamic effects necessary for initiating the most appropriate therapeutic measures.

3.2.7 Diagnostic Role of Duplex Ultrasound Compared with other Modalities

Duplex ultrasound is equal to the current gold standard, venography, in evaluating the arm veins for thrombosis, as their superficial course provides good insonation conditions. It is superior to venography in evaluating the wall of the axillary vein for postthrombotic lesions persisting after recanalized thrombosis. Moreover, ultrasound provides highly accurate information on the hemodynamic effects of vein compression by tumor or in the costoclavicular compression syndrome, especially through the Doppler frequency spectrum recorded distally during provocative maneuvers. Since scanning of the thoracic outlet is limited, CT is superior in assessing tumor-related inflow obstruction. As in the legs, venography is superior in evaluating the extent of collateralization. In controlled studies using venography as the reference procedure, duplex ultrasound was found to have a sensitivity of 94% and a specificity of 96% in detecting arm vein thrombosis (Koksoy et al. 1995; Haire et al. 1991).

3.3 Atlas

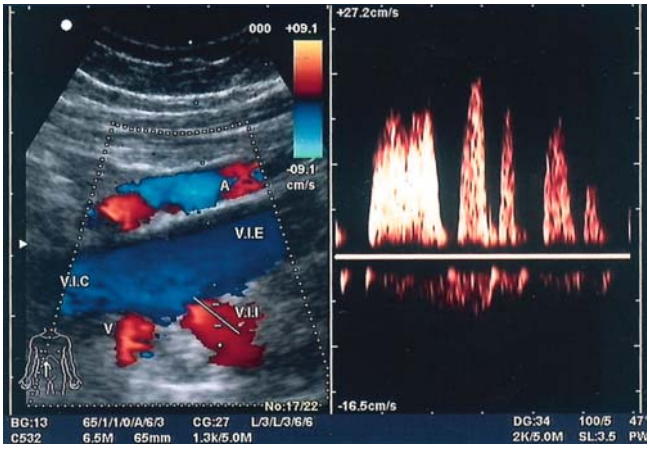

Fig. A 3.1
Course of the pelvic veins
The pelvic veins (common iliac vein/*V.I.C* and external iliac vein/*V.I.E*) take an arched course through the true pelvis posterior to the arteries (cf. Fig. 2.1a) of the same name (*A*). The internal iliac vein (*V.I.I*) enters the common iliac vein on its posterior aspect at its lowest point (flow toward transducer, coded in red). There is respiratory phasicity of the flow profile and younger individuals may additionally show cardiac pulsatility. In the case presented, a second leg vein (red) enters the common iliac vein (blue) slightly above the internal iliac vein

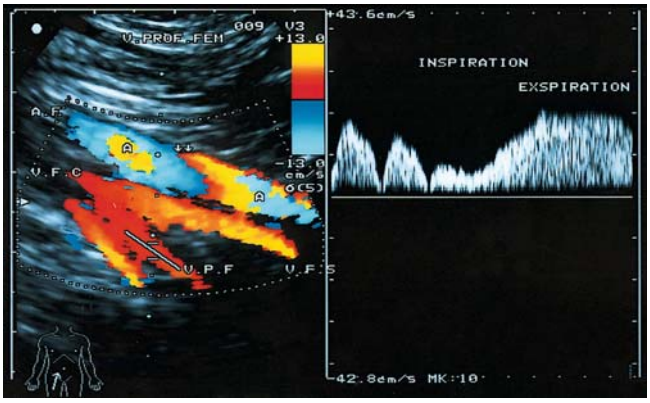

Fig. A 3.2
Venous Doppler waveform
Just below the inguinal ligament, the common femoral vein (*V.F.C*) divides into the deep femoral vein (*V.P.F*) and the superficial femoral vein (*V.F.S*). Flow in the veins is characterized by respiratory fluctuation when no proximal obstruction (thrombus, compression) is present. The Doppler waveform on the *right* illustrates the respiratory variation of flow velocity in the deep femoral vein

Venous flow velocity is decreased due to an increase in intra-abdominal pressure during abdominal inspiration. There is cardiac modulation even during expiration (waveform obtained in a young woman). With the pulse repetition frequency adjusted to venous flow, the femoral artery close to the transducer shows aliasing (*A*) and flow reversal at diastole (*arrows*)

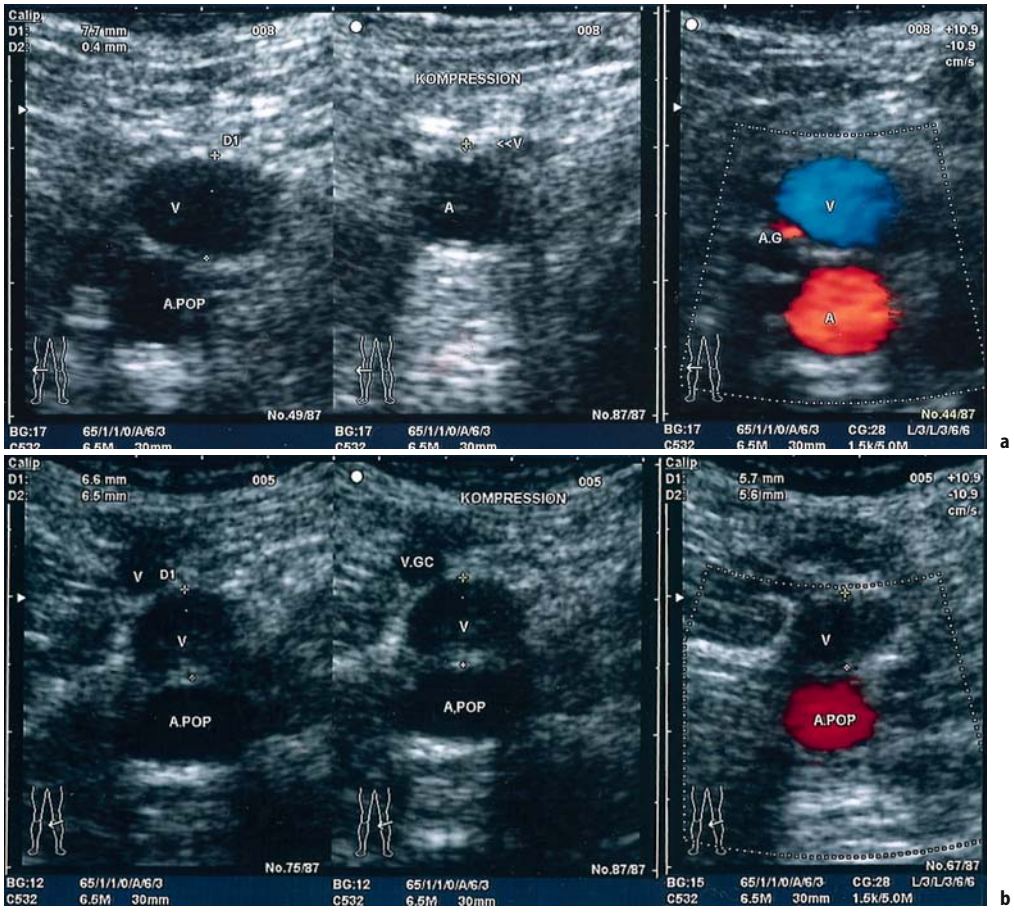

Fig. A 3.3 a, b
Popliteal vein thrombosis: evaluation by compression and color duplex ultrasound
a The transverse gray-scale scan on the *left* depicts the popliteal artery (farther away from transducer, which is placed in the popliteal fossa) anterior to the popliteal vein. In the *middle section*, the vein becomes invisible as it is completely compressed by the transducer, indicating absence of an intraluminal thrombus. The transverse scan on the *right* obtained at the same level in the popliteal fossa confirms patency of the popliteal artery (red) and vein (blue) **b** In this example, a somewhat older thrombus is already depicted in the gray-scale scan (*left section*) as a more hyperechoic intraluminal structure compared to the artery. Applying pressure with the transducer does not compress the vein (*middle section*). The color-duplex scan (*right section*) depicts flow only in the popliteal artery (red) and no flow signals in the vein (despite a low pulse repetition frequency)

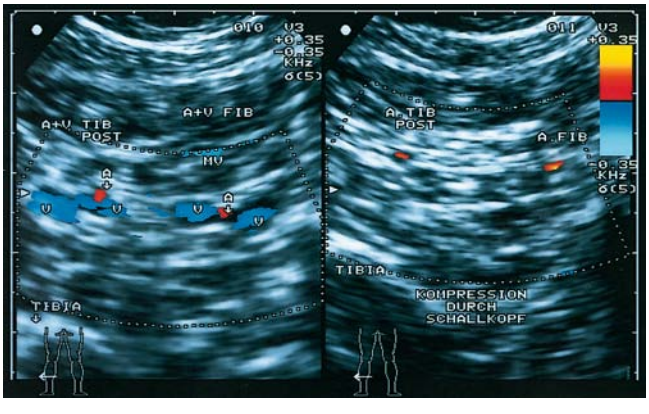

Fig. A 3.4
Lower leg veins
The main veins in the lower leg are identified using the corresponding arteries as landmarks. The veins typically occur in pairs that run on both sides of the respective artery with color coding indicating flow in the opposite direction. Taking the popliteal vein as a point of departure, the examiner follows the veins toward the periphery in transverse orientation. Below the confluence, the courses can be followed continuously, that of the fibular vein close to the fibula and that of the posterior tibial vein along the more hyperechoic deep crural fascia

The *left* scan depicts the posterior tibial veins in blue (close to the left margin) above the tibia with the artery coded in red running in between. The fibular artery and vein are seen to the right and a muscular vein (*MV*) above. Upon compression with the transducer (*right section*), the veins collapse and flow signals are depicted from the arteries only (coded in red)

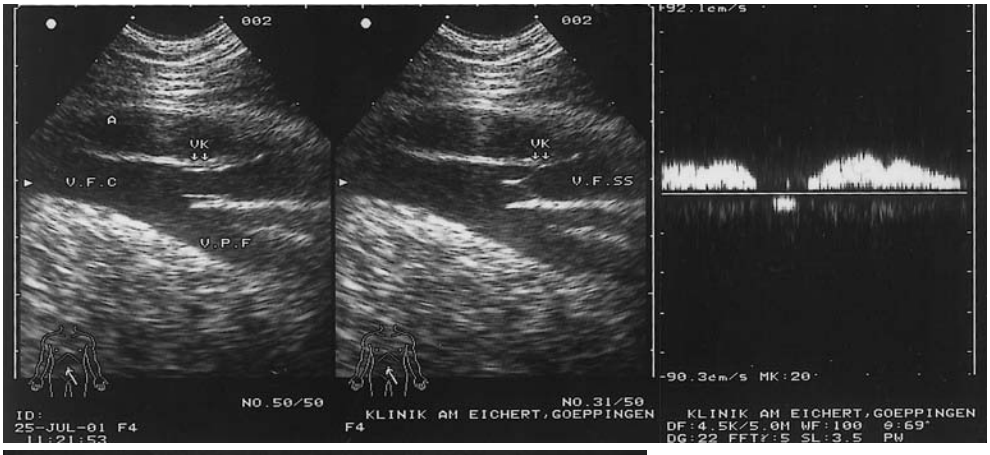

a

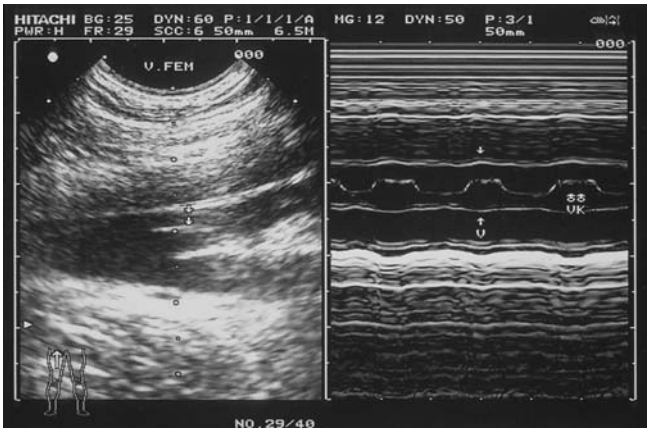

b

Fig. A 3.5 a, b
Normal venous valve function – morphology

a Under good insonation conditions, normal valve function is apparent in the gray-scale scan. The valve (*VK*) depicted in the superficial femoral vein (*V.F.S*) shortly before the opening of the deep femoral vein (*V.P.F*) is shown during expiration (valve open) on the *left* and during inspiration (valve closed) in the *middle section*. The cusps prevent flow reversal during the inspiration-induced increase in intra-abdominal pressure

The respiratory variation in blood flow is documented in the Doppler waveform. Flow toward the transducer is increased in expiration and decreased in inspiration. Flow may even decrease to zero and the short transient reflux until valve closure may be absent if the sample volume is placed near a valve

b The time-motion display documents the course of valve movement from inspiration to expiration: The hyperechoic line in the lumen represents the closed valve during inspiration with subsequent expiratory opening shown as movement of the valve leaflet toward the vessel wall

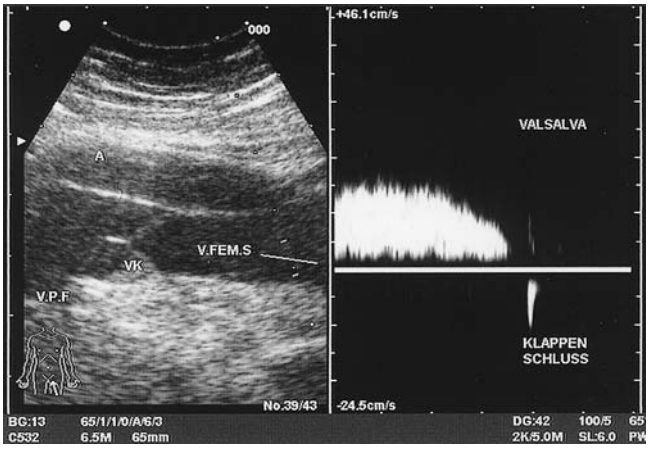

a

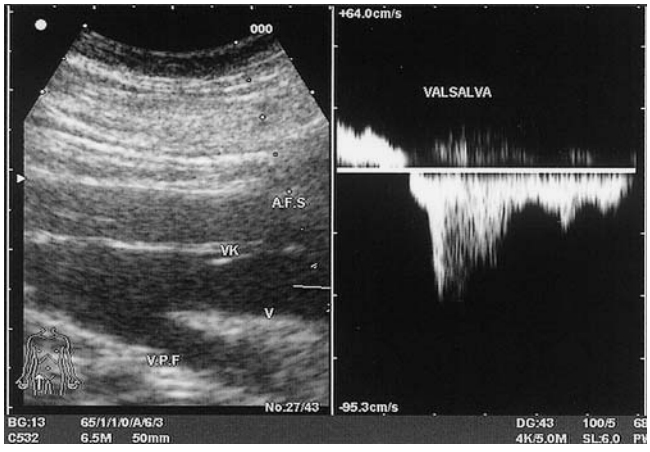

b

Fig. A 3.6 a, b
Venous valve function – hemodynamics

a Competent valves (*VK*) in the superficial femoral vein (*V.FEM.S*) close upon Valsalva's maneuver after a short reflux and thus prevent further retrograde flow

b Posthrombotically sclerosed valves (*VK*) that have become attached to the wall do not close upon Valsalva's maneuver, thereby enabling continuous reflux toward the periphery (away from transducer)

Fig. A 3.7
Compression-decompression test
Doppler frequency data sampled during functional tests provides information on proximal or distal flow obstacles and valve function. The femoral vein is commonly evaluated using Valsalva's test

Illustration of the effect of alternating compression and decompression in the popliteal vein. The respiration-modulated flow signal is followed by augmented flow (upon compression of the lower leg soft tissue distal to the sample volume) toward the heart. No flow signal is recorded upon decompression. Compression of the muscle and vein in the upper leg (*KOMP OS*) induces a short signal indicating distal flow that persists until valve closure

Valve incompetence would be associated with persistent reflux

The example shows an induced signal indicating flow toward the heart (A-sound) after decompression of the upper leg (*DEKOMP OS*), i.e. proximal to the sampling site. In the absence of flow obstruction, there is a steep upstroke of the Doppler waveform whereas a flow obstruction between the site of compression and the sample volume would be associated with a less pronounced augmentation (cf. Fig. A 3.41 a, b)

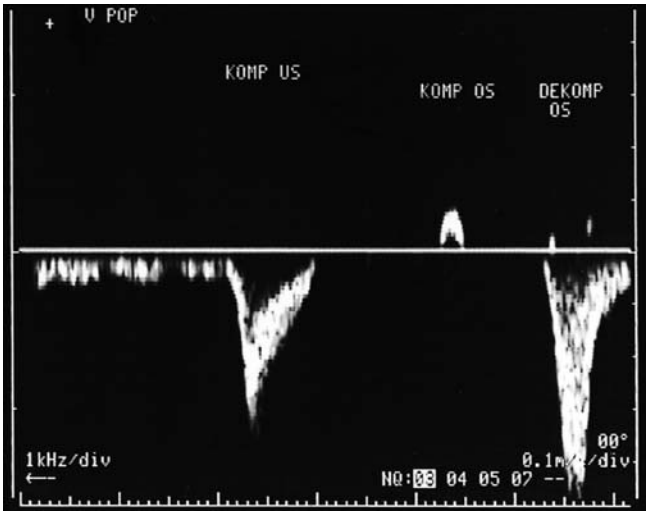

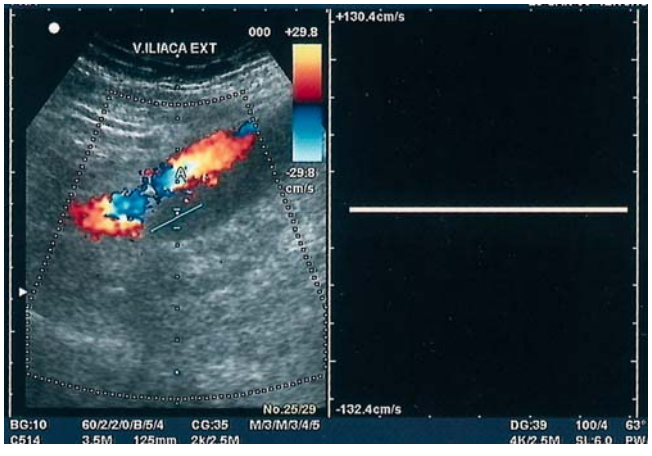

a

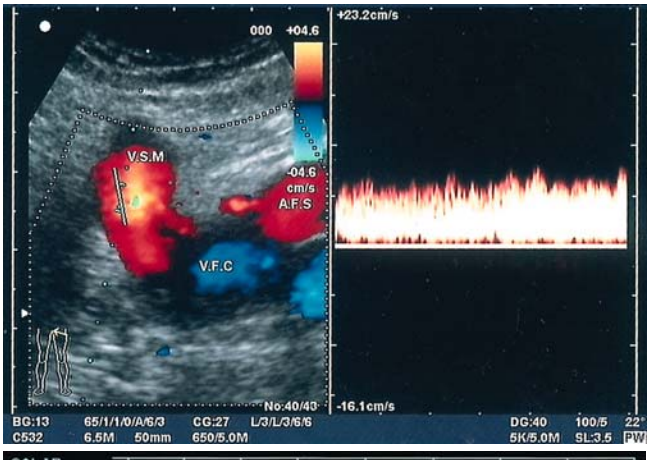

b

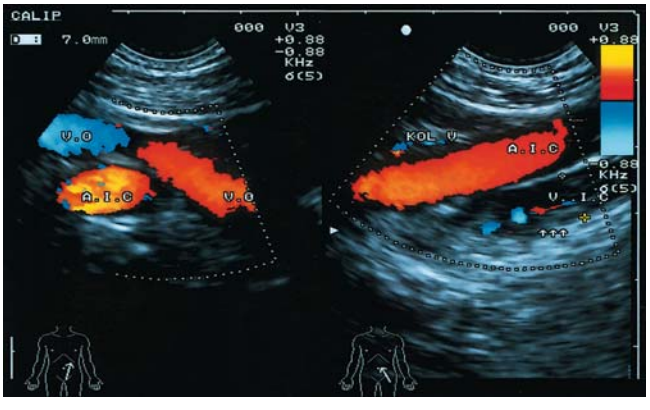

c

Fig. A 3.8 a–e
Pelvic vein thrombosis
a Compression ultrasound is unreliable, especially in obese patients, because an adequate structure against which to compress the vein is not available and a greater scanning depth is required. Sonographically, the vein is identified posterior to the iliac artery and thrombosis is demonstrated by failure to obtain a flow signal in the color flow mode. The occlusion is confirmed by the absence of flow signals in the Doppler frequency spectrum
b In pelvic vein occlusion, venous return must be ensured by collaterals. An important collateral pathway includes the saphenofemoral junction (termination of the great saphenous vein in the groin), which shows a retrograde flow signal (displayed in red, toward transducer, not affected by respiration) and drains into the abdominal wall collaterals (epigastric vein). The latter are not subject to intra-abdominal pressure changes
c Early recanalization 3 months later is difficult to identify by conventional duplex scanning in the pelvic territory. The scan on the *right* demonstrates central flow signals in the common iliac vein (*V.I.C*), which is still markedly thrombosed. Anteriorly, the common iliac artery is depicted with flow coded red (*A.I.C*). The scan on the *left* depicts the dilated ovarian vein (*V.O*) coursing over the common iliac artery (*A.I.C*). The color change from red to blue is due to the change in flow direction relative to the ultrasound beam

While thrombosis can be diagnosed by gray-scale or conventional duplex ultrasound, the detection of early signs of recanalization falls in the domain of color duplex

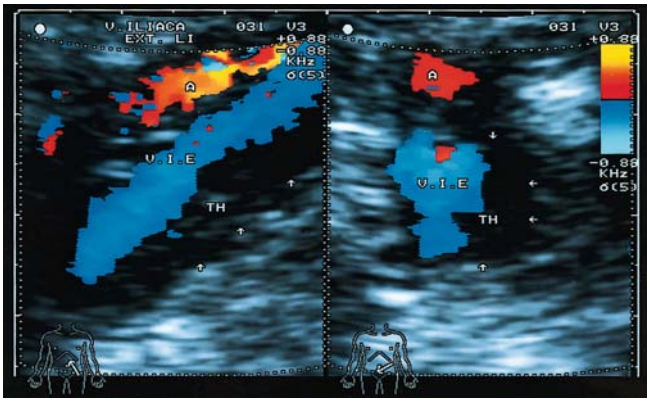

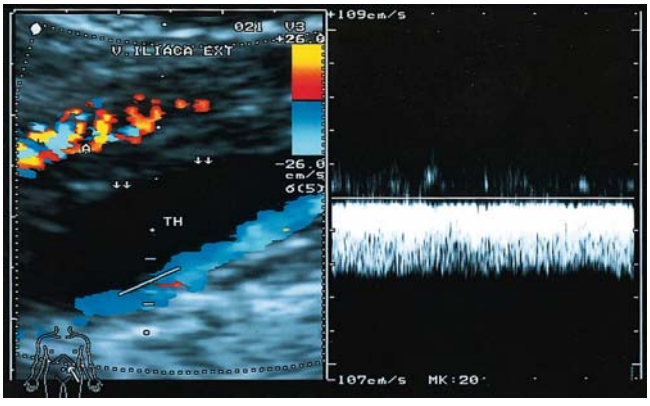

(Fig. A 3.8 cont.)

d In this young patient with scintigraphically proven pulmonary embolism, ultrasound showed patent subfascial leg veins while there were thrombi in the iliac vein. In contrast to recanalization with central flows signals as shown in **c**, the fresh thrombus (*TH*) in the external iliac vein (*V.I.E*) is attached to the wall and surrounded by flowing blood

e Proximally, near the opening of the internal iliac vein, the thrombus is surrounded by flowing blood posteriorly. The flow obstruction produces a high-frequency, continuous signal (with loss of respiratory phasicity) typical of venous stenosis. The peak flow velocity is 50 cm/s. With the pulse repetition frequency adjusted to venous flow, there is aliasing in the artery anterior to the vein. The thrombus is indicated by *arrows*. Not shown is the Doppler waveform obtained in the uninvolved common femoral vein distal to the thrombus. The patent lumen of the common femoral vein is relatively wide and there is only little reduction of respiratory fluctuation. A thrombus in an otherwise patent lumen as in this case may be overlooked if only the Doppler frequency spectrum from the common femoral vein is analyzed, even if a side-to-side comparison and functional tests are done. Routine venography may likewise fail to identify such mural thrombi in an otherwise patent iliac vein or to differentiate them from flow phenomena

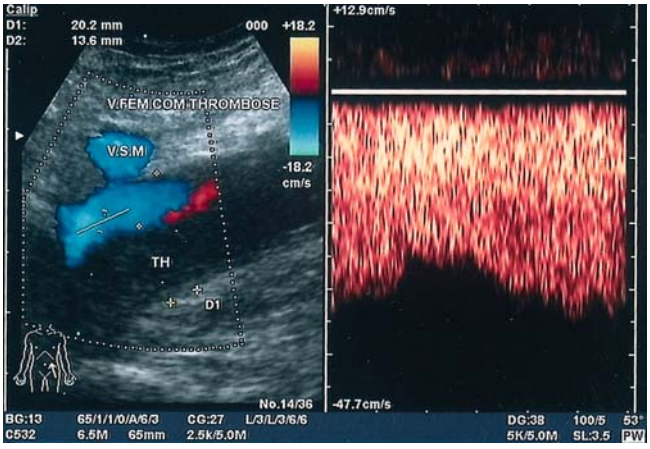

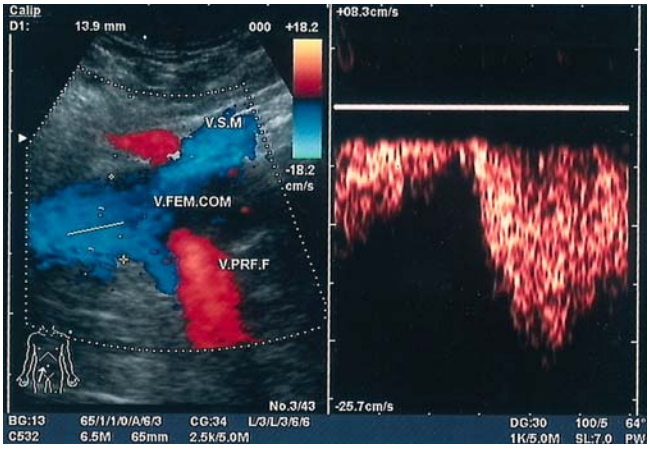

Fig. A 3.9 a, b

Elimination of respiratory phasicity by flow obstacle

a Flow obstruction along a thrombus in a partially thrombosed vein eliminates or reduces respiratory phasicity and results in a higher-frequency flow signal in the Doppler waveform, unless the blood is drained through collaterals (according to the continuity law, as in arterial stenosis)

b Since some residual respiratory variation may still be depicted in the Doppler waveform, both sides must be compared. In the example, respiratory fluctuation is much less pronounced on the left than on the unaffected right side. Common femoral vein(*V.FEM.COM*) with the opening of the great saphenous vein (*V.S.M*) coded in blue and the opening of a deep femoral vein (*V.PRF.F*) coded in red (toward transducer)

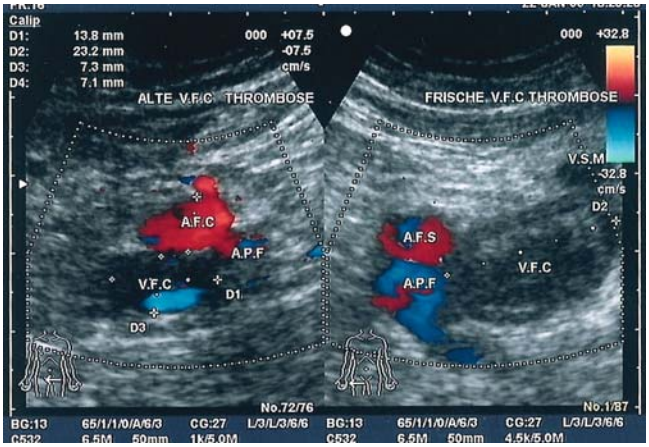

Fig. A 3.10
Criteria for estimating thrombus age
The major signs of fresh deep venous thrombosis of the leg are pronounced dilatation of the vein and good delineation of the homogeneous, often hypoechoic, thrombosed venous lumen from perivascular connective tissue. The two scans obtained in the same patient show fresh deep venous thrombosis with the venous lumen dilated to well over twice that of the accompanying artery on the right and an old thrombosis of the common femoral vein already partially recanalized in the area of the femoral bifurcation at the same level on the left (flow in the *V.F.C* displayed in blue). (*A.F.C* common femoral artery, *A.P.F* deep femoral artery, *A.F.S* superficial femoral artery)

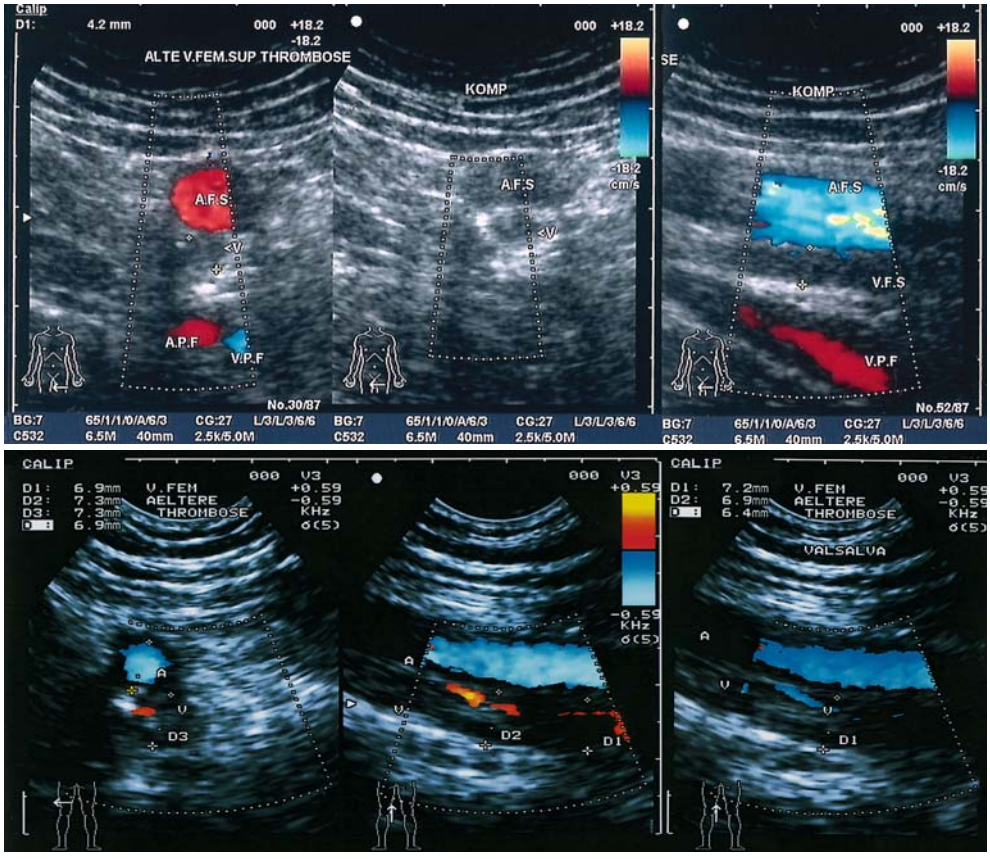

Fig. A 3.11 a, b
Older femoral vein thrombosis
a Older thrombosis is associated with shrinkage of the lumen (relative to the corresponding artery). The scan on the *left* shows the thrombotically occluded superficial femoral vein (*V*) posterior to the red superficial femoral artery (*A.F.S*). Demarcation is much poorer than in fresh thrombosis. The compression scan (*middle section*) shows noncompressibility of the vein depicted posterior to the artery. The longitudinal scan (*right section*) of the occluded superficial femoral vein (*V.F.S*) shows absence of flow in the vein posterior to the artery shortly before the opening of the deep femoral vein (*V.P.F*). The deep femoral vein is recanalized with flow toward the transducer coded in red. However, marginal hypoechoic thrombosis still persists along the patent venous lumen

Femoral vein thrombosis, early recanalization
b While color duplex scanning contributes only little to the diagnostic evaluation of thrombosis and thrombus age, it has its role in demonstrating early recanalization. In the older femoral vein thrombosis presented here (poor demarcation of the wall, venous diameter identical to that of the artery), color duplex scanning demonstrates meander-like flow within the thrombosed lumen as a sign of early recanalization

Flow in the vein posterior to the artery is depicted in red (directed toward the heart) on the transverse scan (*left section*) and longitudinal scan (*middle section*). The scan on the *right* demonstrates flow reversal after Valsalva's maneuver, indicating impaired valvular function. Early recanalization in patients on thrombolytic therapy is identified in the same way. The depiction of flow in the center of the vessel differentiates recanalization in older thrombosis from fresh thrombus with residual flow near the wall

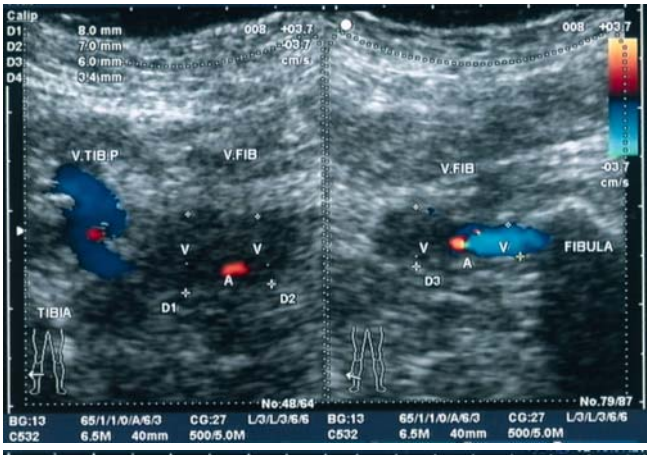

a

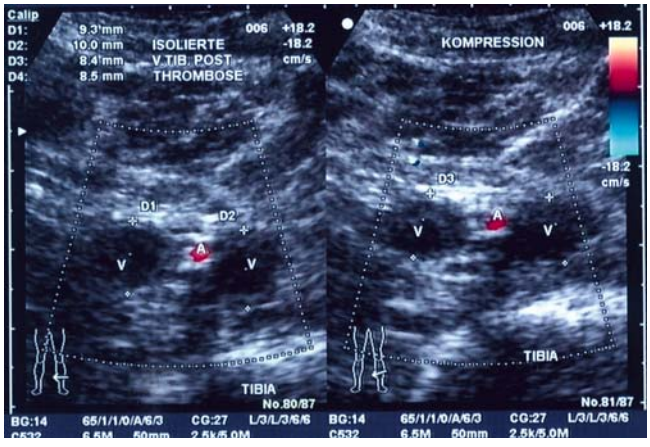

b

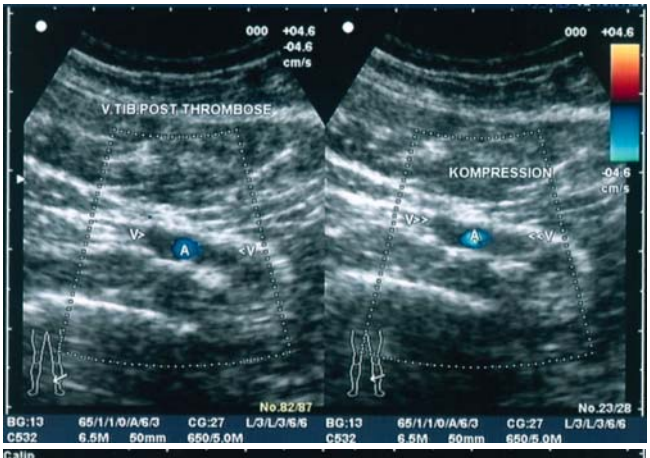

c

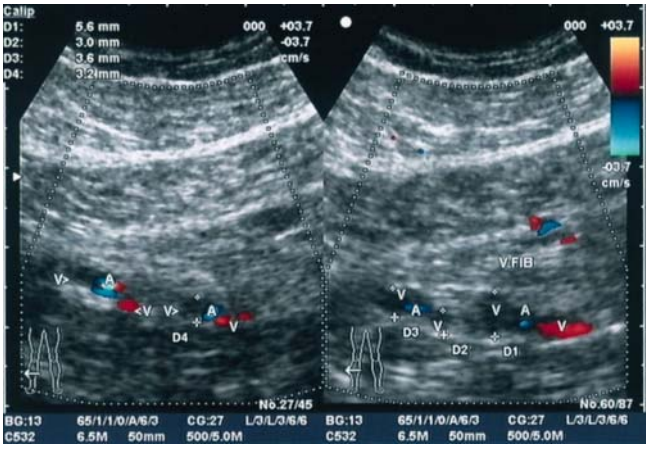

d

Fig. A 3.12 a–e
Lower leg venous thrombosis (fresh – older)
a Under adequate insonation conditions, fresh venous thrombosis in the lower leg is easily identified as a hypoechoic tubular structure in the soft tissue in the typical locations of the veins. The lumen is wider than that of the corresponding artery. The fibular artery and vein course along the medial aspect of the fibula. Compression and color duplex scanning differentiate patent and thrombotic segments with a high degree of accuracy. The scan on the *right* shows one patent vein and one thrombosed vein, the *left* scan thrombosis of both fibular veins while both adjacent posterior tibial veins are patent with flow coded in blue

Fresh isolated thrombosis of the posterior tibial vein
b Paired posterior tibial vein to the left and right of the artery. The vein is not compressible (right) and the lumen is increased to more than twice that of the artery as a sign of fresh thrombosis. The thrombus is hypoechoic and has a homogeneous echotexture; color duplex depicts no flow signals in the vein

Older isolated thrombosis of the posterior tibial vein
c Hypoechoic tubular structures are seen to the left and right of the anterior tibial artery. The structures cannot be compressed (compression scan on the *right*) and have about the same diameter as the artery, indicating older thrombosis with shrinkage of the lumen. Color duplex depicts flow in the artery in blue while there are no flow signals in the thrombosed vein, suggesting that recanalization has not yet occurred
d Older thrombosis is more difficult to demarcate from surrounding soft tissue, as the diameter of the vein decreases with thrombus age and the thrombotic lumen may become more hyperechoic. Residual thrombosis is difficult to detect if parts of the vessel have already undergone recanalization and can be compressed or show flow signals in the color duplex mode. It is not clear, however, whether the identification of such residual thrombosis is clinically relevant. The scan on the *left* shows red venous flow to the right of the fibular and posterior tibial arteries (blue in this example). The hypoechoic tubular structures to the left reflect older venous thrombosis. Occluded lower leg veins that have undergone persistent fibrotic transformation are very difficult to identify (*right scan*). In such cases, the examiner must very thoroughly search the vicinity of the artery for tubular structures. No flow signal will be obtained next to the artery (venous A-sound) during distal compression in the standing patient

(Fig. A 3.12 cont.)
Lower leg venous thrombosis, older
e Older isolated lower leg venous thrombosis may occasionally be more difficult to detect due to poor scanning conditions. Differentiation from surrounding muscle is impaired by poor demarcation of the wall, greater echogenicity of the thrombus, and receding luminal dilatation. Such cases require careful evaluation of the area around the arterial landmark

An attempt must be made to identify spontaneous flow as well as augmented flow (A-sound) by color duplex scanning and spectral Doppler recording. The compression scan on the *left* depicts the posterior tibial artery in red with the thrombotic posterior tibial vein appearing as a hypoechoic structure to the left and right of the artery

The longitudinal scan on the *right* shows the same area without compression by the transducer. The posterior tibial vein is depicted proximal to the posterior tibial artery. The vein is thrombosed and difficult to distinguish from surrounding tissue

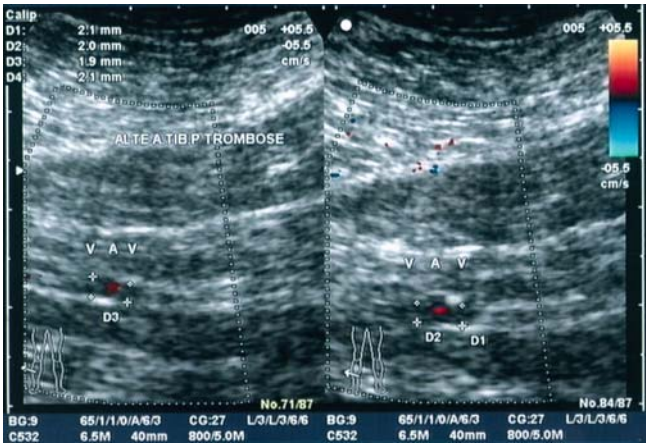

e

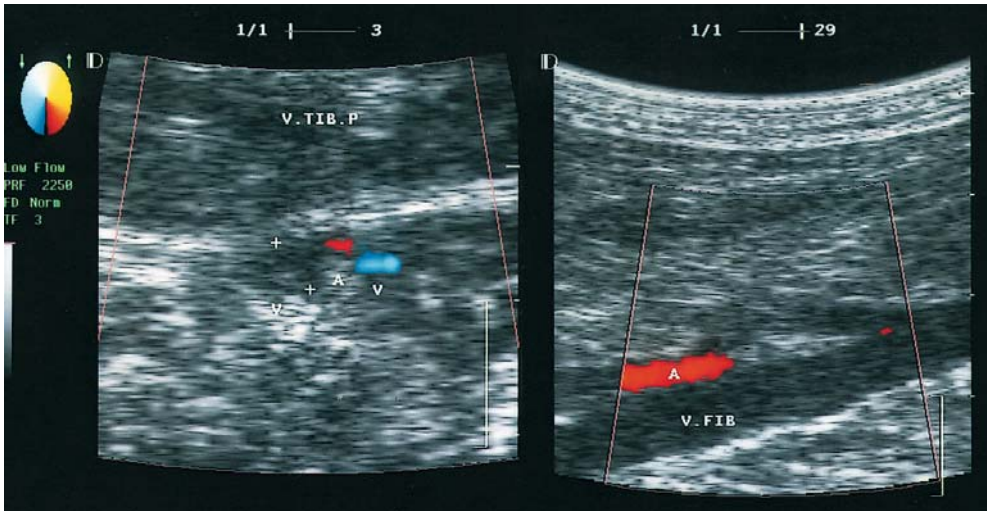

a

Fig. A 3.13 a, b
Lower leg venous thrombosis, fresh
a Isolated lower leg thrombosis of a single vein group may be overlooked or misinterpreted on venography. Moreover, small filling defects are difficult to locate to a muscular vein or a major vein. B-scan sonography identifies fresh thrombosis of a lower leg vein as a hypoechoic tubular structure along the respective artery

Color duplex scanning corroborates the diagnosis by the failure to demonstrate flow when performed with a low pulse repetition frequency. Residual flow may be indicated by a signal elicited by muscle compression distal to the transducer (A-sound). The scan on the *left* shows a patent posterior tibial vein (*V*) with blue-coded flow to the right of the red artery (*A*) while the second vein (*V*) to the left of the artery is thrombosed. Marked dilatation of the vein (>twice arterial lumen) and the low-level echo of the thrombus suggest fresh thrombosis

The longitudinal scan on the *right* shows the fibular vein to be thrombosed as well. The lumen is much wider than that of the corresponding artery (*A*) with flow depicted in red. The thrombotic vein is hypoechoic and homogeneous, clearly demarcating it from the surrounding soft tissue
b Venography: Filling defect in the posterior tibial vein. The fibular vein is not depicted

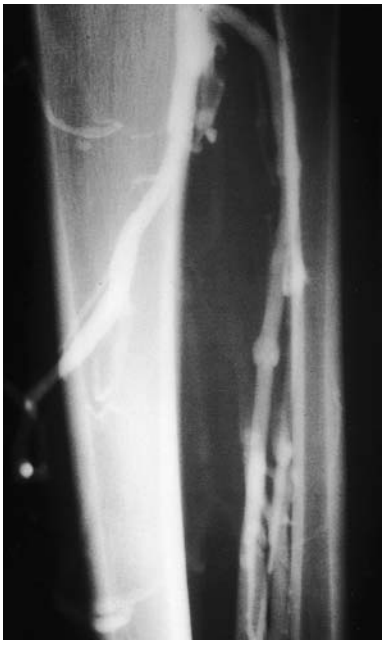
b

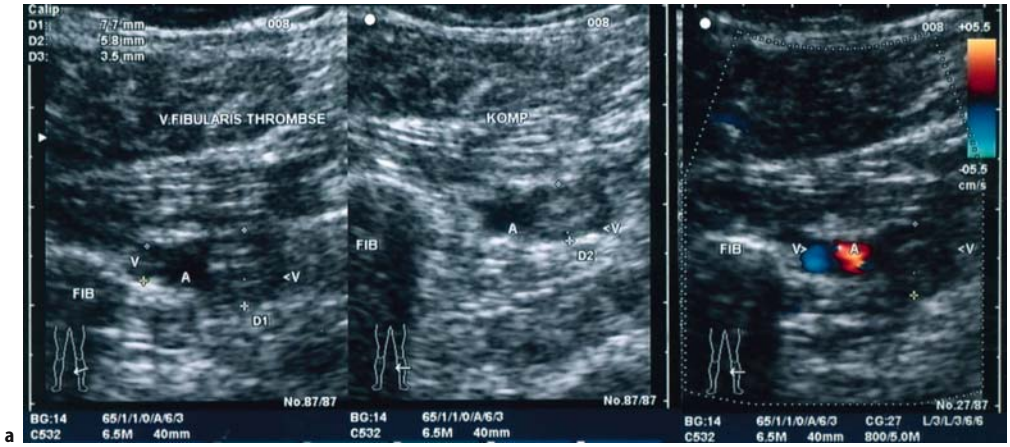

a

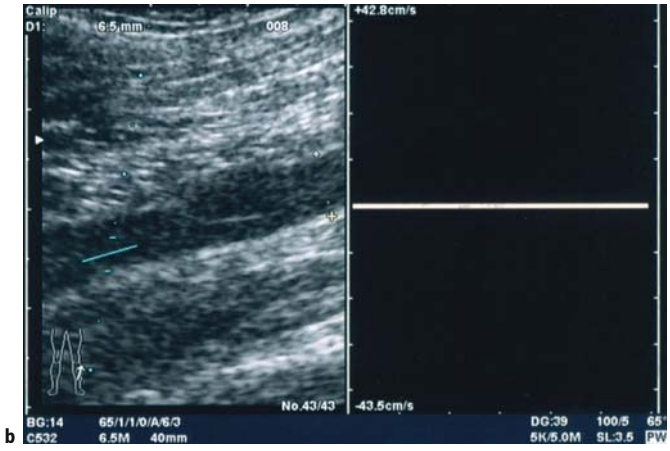

b

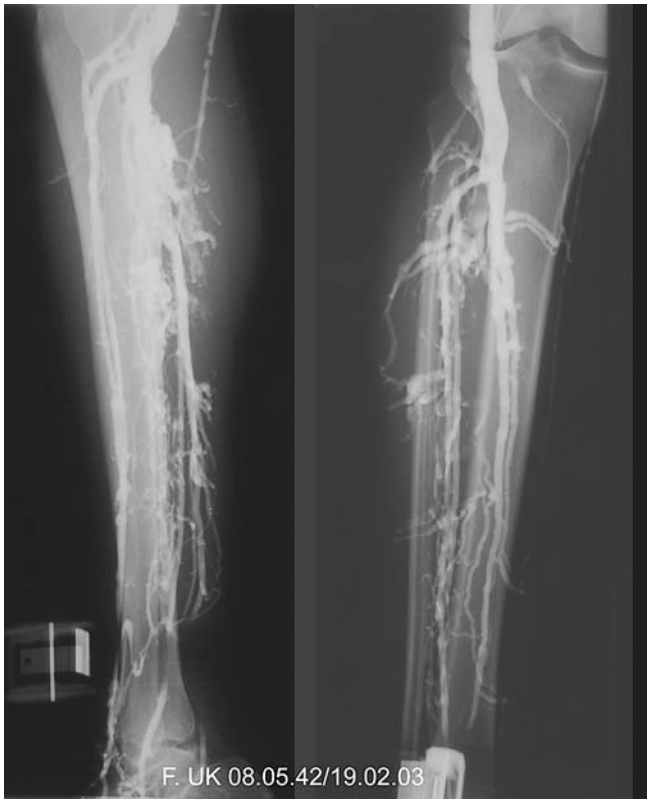

c

Fig. A 3.14 a–c
Lower leg venous thrombosis
Venography is limited in the evaluation of the fibular vein. A filling defect in this vein may be due to a technical limitation or thrombosis
a Sonographic depiction of fresh thrombosis of a fibular vein with patency of the second fibular branch. The transverse view (*left section*) depicts round, tubular structures to the left and right of the artery and the fibula (*FIB*) to the left. The veins are indicated by *plus signs*; the thrombosed vein (right) is markedly dilated (7.7 mm) while the patent vein (left) has a diameter of 3.5 mm.

The compression scan (*middle section*) fails to depict the vein to the left of the artery (*A*) because its lumen is completely compressed. The vein to the right shows only little compressibility (diameter reduced from 7.7 to 5.8 mm), indicating fresh thrombosis.

The color duplex scan (*right section*) depicts the patent vein in blue to the left of the artery (red), the thrombosed vein (*V*) to the right (marked with *plus signs*). The thrombosed vein is hypoechoic, markedly dilated, and shows no flow
b Longitudinal duplex scan of the markedly dilated vein without flow signals in the Doppler waveform. The B-mode view shows a valve with its leaflet immobilized by the thrombus
c The venogram fails to depict the fibular veins. Based on the duplex sonographic demonstration of one patent and one thrombosed branch of the fibular vein, this example illustrates that absence of opacification may be due to thrombosis or technical limitations

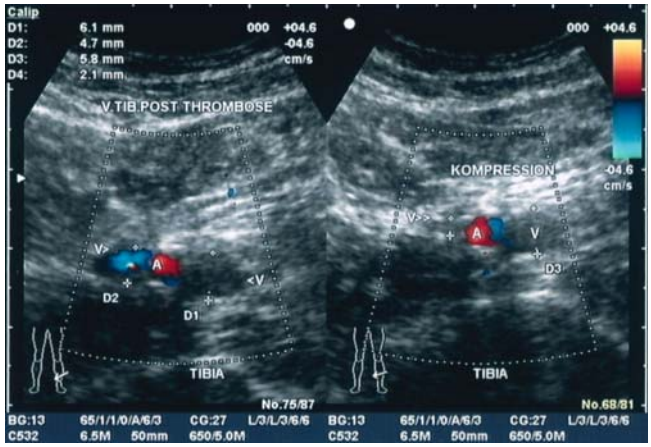

Fig. A 3.15
Recurrent thrombosis after recanalization
The posterior tibial vein to the right of the artery (*A*, red) is markedly dilated (6.1 mm) and shows no flow, suggesting fresh thrombosis. The vein to the left exhibits flow coded in blue with a surrounding hypoechoic margin corresponding to wall thickening as a sign of recanalized thrombosis

The compression scan (*right section*) shows only little compressibility of the thrombosed vein. No venous flow signals are depicted to the left of the artery during compression. However, the vein is not fully compressed. There is a hypoechoic area in the connective tissue indicating the postthrombotically thickened walls. The vein is surrounded by hyperechoic connective tissue of the deep crural fascia, and the tibia is depicted farther away from the transducer

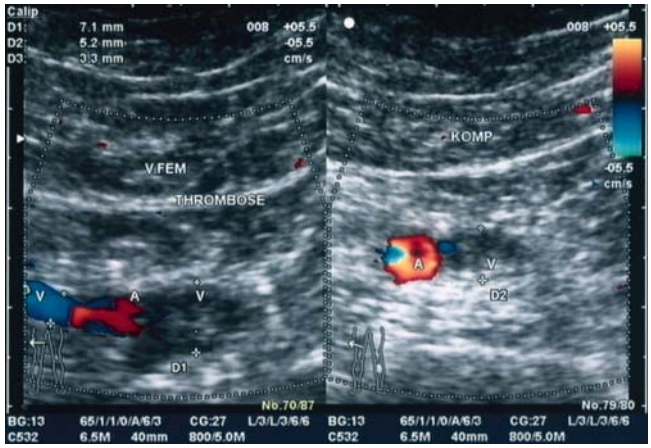

Fig. A 3.16
Paired femoral vein
A paired vein with one patent branch and one completely occluded branch is a pitfall in venography. Color duplex scanning shows a perfused vein (*V*) to the left of the artery (*A*) and a markedly dilated vein (*V*) without flow to the right. The compression scan (*right section*) demonstrates complete compressibility of the vein to the left of the artery with only little compression of the vein to the right, which is still seen as a hypoechoic tubular structure

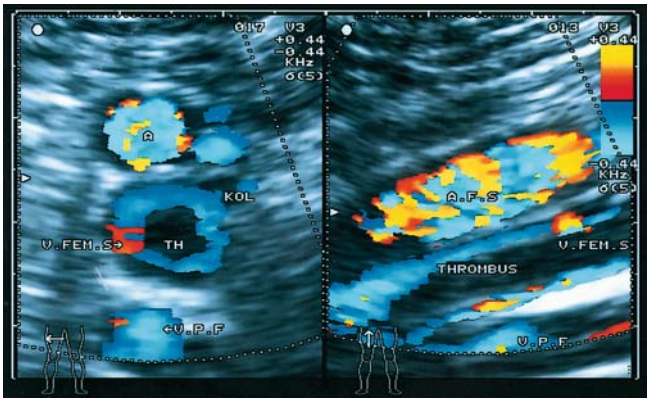

a

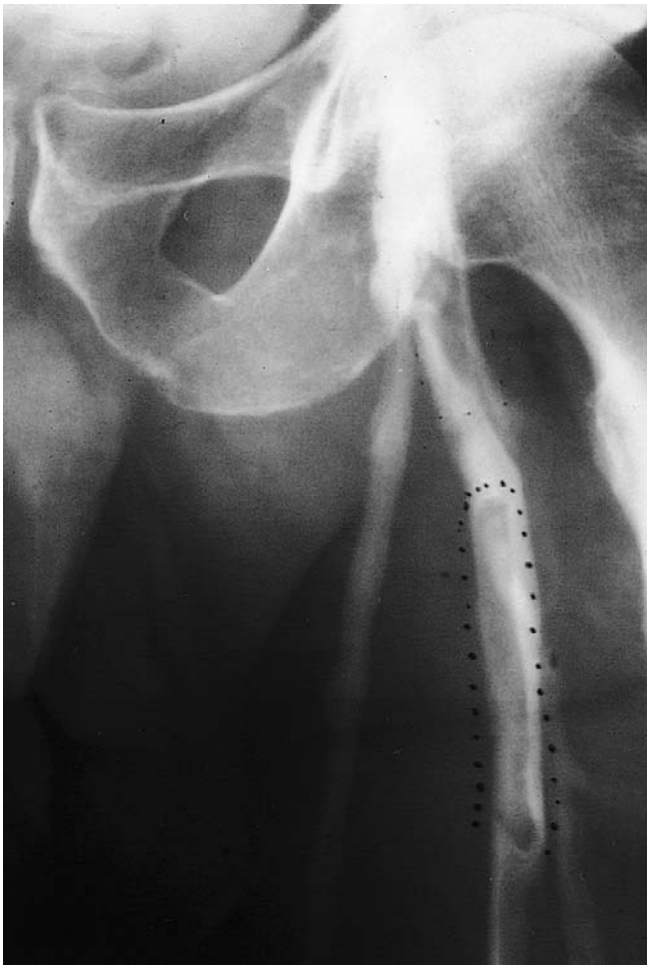

b

Fig. A 3.17 a, b
Floating thrombus of femoral vein

a Floating thrombus in the superficial femoral vein (*V.FEM.S*), transverse view on the *left* and longitudinal view on the *right*. A circular flow signal around a thrombus in the color flow mode is diagnostic of a floating thrombus (*TH*) and enables determination of the extent of the free-floating tail

The slow flow around the floating tail proximal to the occlusion may be difficult to depict despite adequate instrument settings (high gain, low PRF). The problem can be overcome by attempting to induce augmented flow (A-sound) by means of a Valsalva maneuver. Instrument adjustment to slow venous flow leads to aliasing in the superficial femoral artery (*A*, anterior to the vein). Collaterals with flow in blue (*KOL*) are depicted anterolaterally and the deep femoral vein (*V.P.F*) posteriorly

b Venography: The femoral vein is thrombosed; the length of the floating tail can only be assessed in a second plane

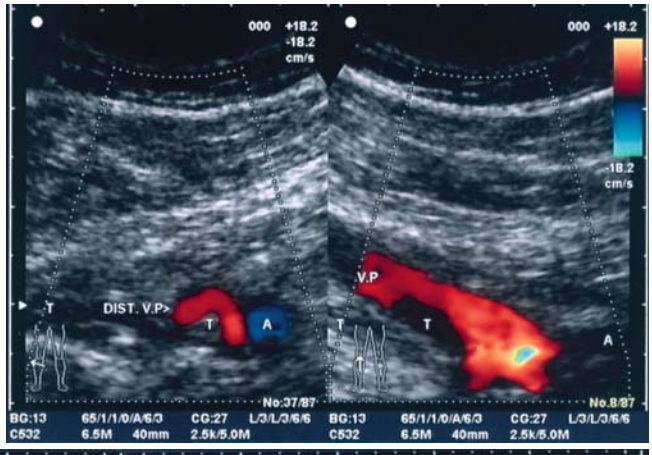

a

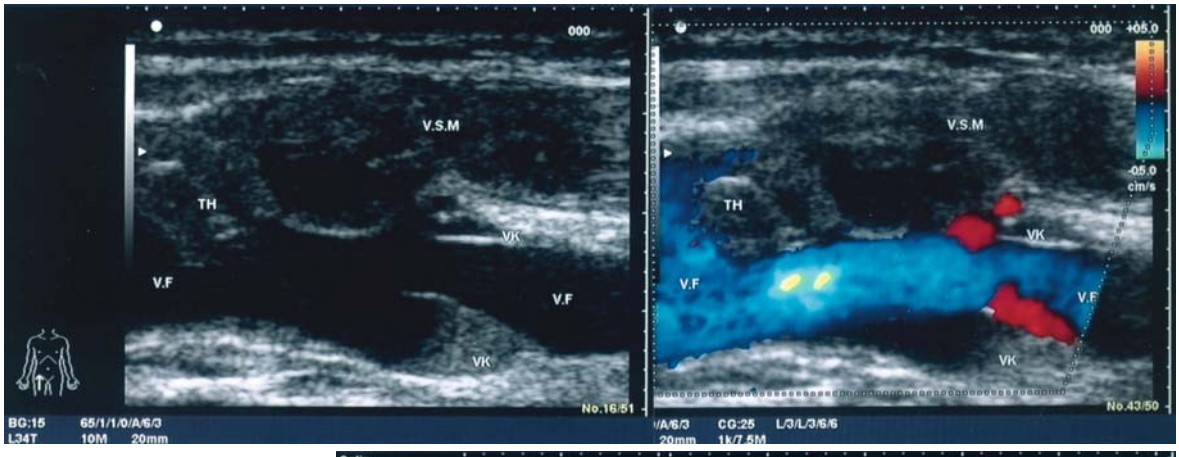

b

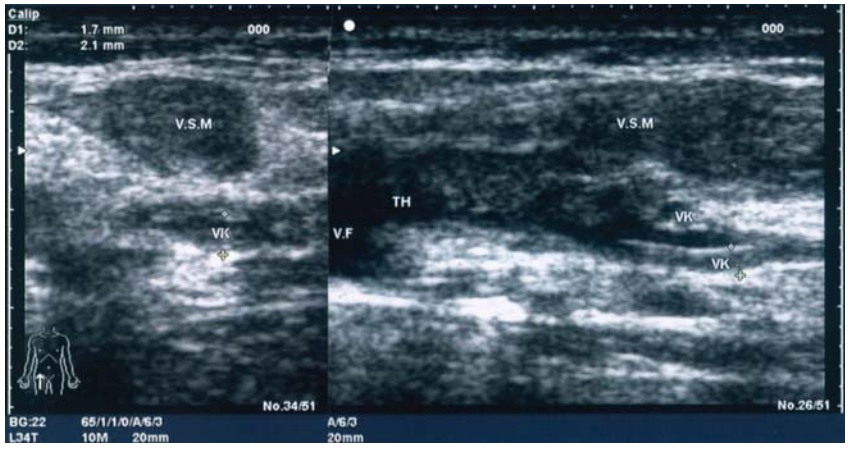

c

Fig. A 3.18 a–c
Asymptomatic venous thrombosis

a Ultrasound has a markedly lower sensitivity in asymptomatic thrombosis than in symptomatic thrombosis. This is due to the fact that thrombi surrounded by flowing blood may be overlooked in lower leg areas notoriously difficult to scan, especially if there is only little dilatation and partial compressibility, or if the thrombus is confined to valve pockets. The transverse (*left*) and longitudinal views (*right*) depict the distal popliteal vein with a patent lumen (red, flow toward transducer) but with absent color coding in the area of a valve leaflet. Color duplex scanning facilitates the identification of such subtle abnormalities in problematic areas. However, to exclude flow phenomena as a possible cause of the filling defect, the thrombus must be confirmed by a compression scan of this area

b Duplex scanning performed in a clinically asymptomatic patient prior to stripping of varicose veins demonstrates thrombophlebitis of the great saphenous vein (*V.S.M*) with a thrombus (*TH*) protruding into the common femoral vein (*V.F*). The gray-scale scan (*left*) shows a hyperechoic structure in a valve (*VK*) somewhat distal to the termination of the saphenous vein. On the color duplex scan, absence of color coding indicates the thrombus (*TH*) and the valvular thrombus, which prevents proper opening of the valve (despite augmented flow elicited by compression of the upper leg/A-sound). Red color in the valve area indicates eddy flow (cf. also Fig. 3.11 a), in particular in the pocket of the valve (*VK*) depicted closer to the transducer. To exclude a flow-related cause of this subtle change in the color coding, the thrombus must be confirmed by a compression scan

c The compression scans (transverse view on the *left* and longitudinal view on the *right*) show noncompressibility of the great saphenous vein (*V.S.M*) and incomplete compression of the femoral vein at the level of the thrombotic valve (residual diameter of 2 mm, see *markings*). The example illustrates two main sources of thrombosis of the major deep veins: thrombus development in a valve pocket (for its pathogenesis see Fig. 3.11 a) and extension of thrombi from superficial or muscular veins

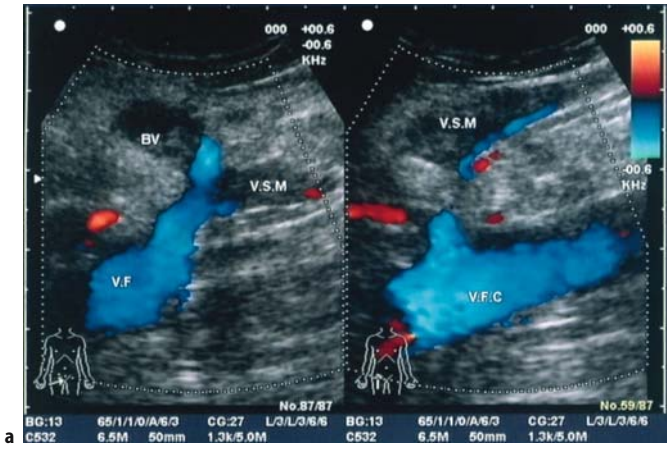

a

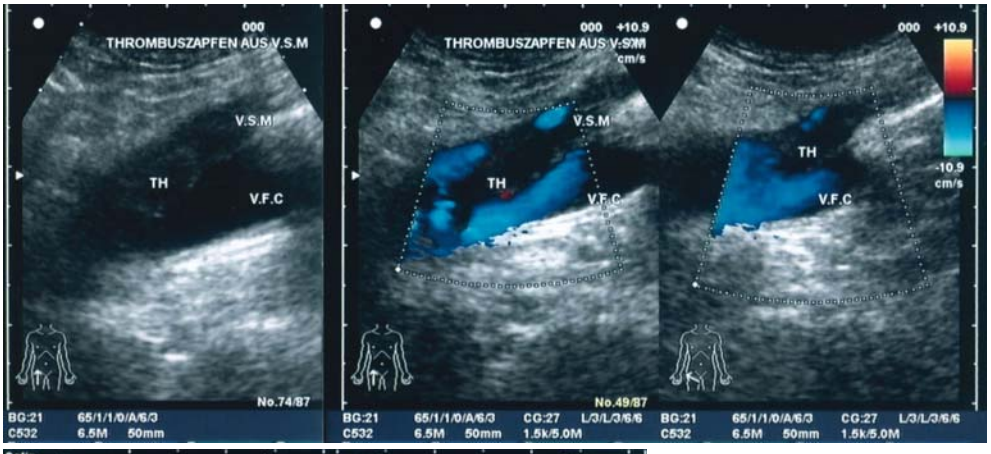

b

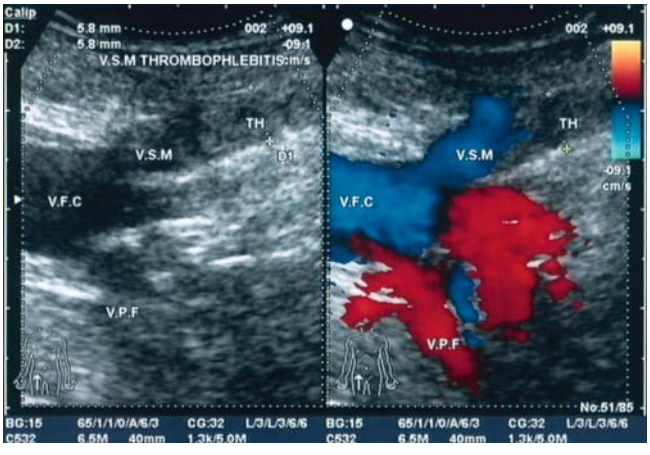

c

Fig. A 3.19 a–c
Thrombophlebitis

a The proximal extent of thrombophlebitis may be greater than suggested by the clinical findings. The patient shown presented with reddening along the course of the great saphenous vein up to the midthigh, while color duplex scanning (transverse view on the *left* and longitudinal view on the *right*) demonstrates gaps in the color coding extending up to 1.5 cm below the saphenofemoral junction. The longitudinal view depicts flow in blue along the thrombus. Ultrasound also demonstrates thrombophlebitic involvement of the clinically normal anterior tributary vein (*BV*). Surgical ligation is indicated to prevent further thrombus growth into deep veins

b Ascending thrombophlebitis can extend into a deep vein as a cone-shaped thrombus. The B-scan (*left section*) already depicts a slightly more hyperechoic thrombus (*TH*) protruding into the anechoic lumen of the common femoral vein (*V.F.C*) from the great saphenous vein (*V.S.M*). On the color duplex scan (*right*), the thrombus (*TH*) protruding into the common femoral vein is identified by the absence of color in the blue-coded lumen

c Based on the duplex findings, high ligation of the great saphenous vein is indicated but refused by the patient. Therefore, the course of endogenous thrombolysis under heparin therapy can be followed in this case. After three weeks, the thrombus in the great saphenous vein has receded to 1 cm below the termination. The scan on the *left* demonstrates the thrombus (*TH*) in the lumen of the great saphenous vein (*V.S.M*). The color scan on the *right* depicts flow in the great saphenous vein in blue (away from transducer, toward center) and a branch of the deep femoral vein (*V.P.F*) coming from posteriorly with flow toward the transducer coded in red

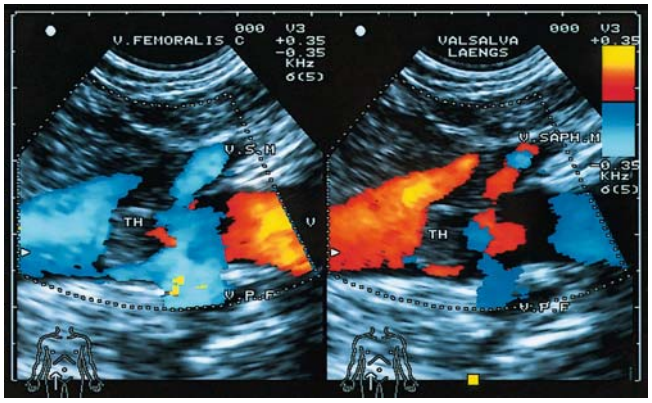

a

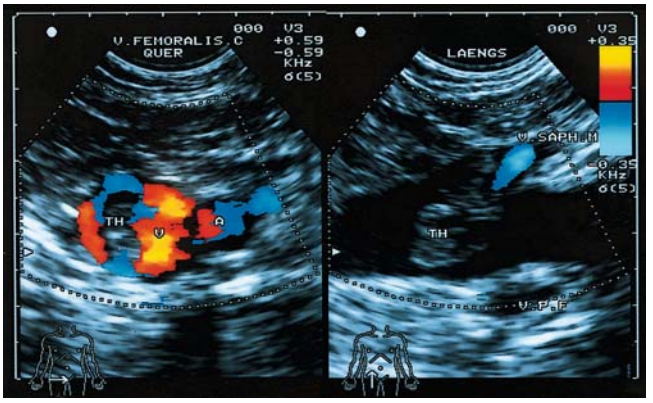

b

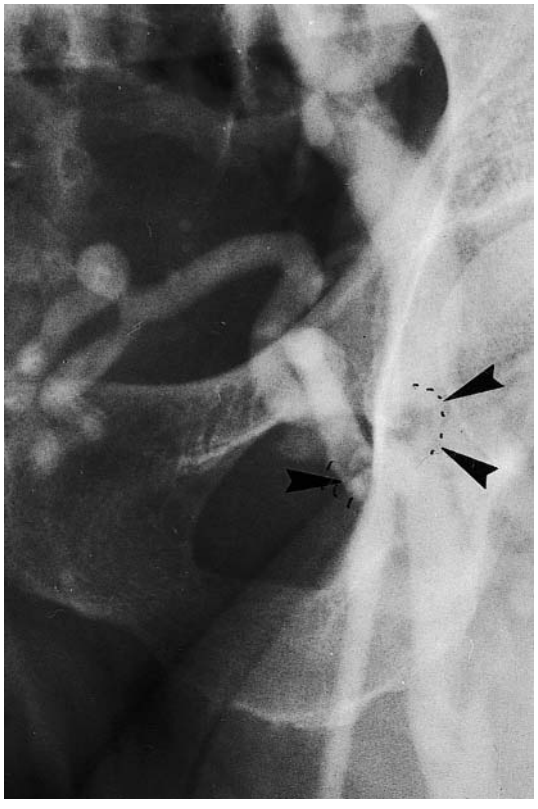

c

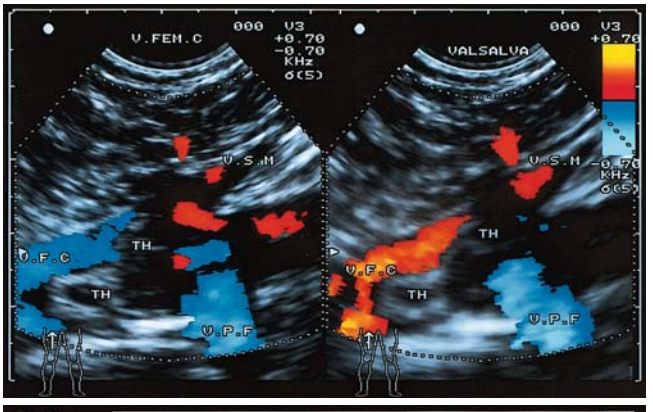

d

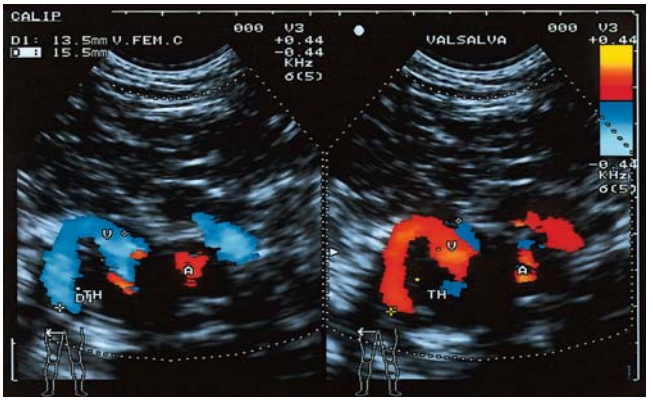

e

Fig. A 3.20 a–e
Thrombus protrusion from superficial vein

a Floating thrombus (*TH*) protruding into the common femoral vein from a tributary vein entering the saphenofemoral junction. The scan on the *left* depicts the common femoral vein with flow toward the heart (blue). The scan on the *right* obtained during Valsalva's maneuver shows retrograde flow extending into the common femoral and great saphenous veins (color change from blue to red)

The great saphenous vein is patent below the terminal valve (depicted with flow in blue close to the transducer at the right margin of both scans)

b The longitudinal (*right*) and transverse (*left*) views obtained during Valsalva's maneuver show the thrombus protruding into the common femoral vein to be surrounded by flowing blood on all sides. During inspiration there is zero flow without flow signals in the common femoral vein and only some residual, obstructed flow in the patent great saphenous vein. The extent of the floating tail is clearly seen as there is no color overflow

c Venography: Confirmation of the protruding thrombus

d, e High ligation of the great saphenous vein is recommended but refused by the patient. Follow-up demonstrates further growth of the thrombus extending from the junction into the common femoral. Moreover, the longitudinal (**d**) and transverse (**e**) scans obtained during Valsalva's maneuver now show the thrombus (*TH*) to adhere to the posterior wall (cf. **b**). It is surrounded by flowing blood only at the anterior wall and laterally (blue flow toward the heart, away from transducer). Reflux during Valsalva's maneuver is depicted in red. Blue flow away from the transducer indicates collateral drainage through a deep femoral vein. The flow obstruction caused by the thrombus has led to the establishment of collateral pathways to the lateral thigh and along the hip parallel to the accompanying circumflex arteries

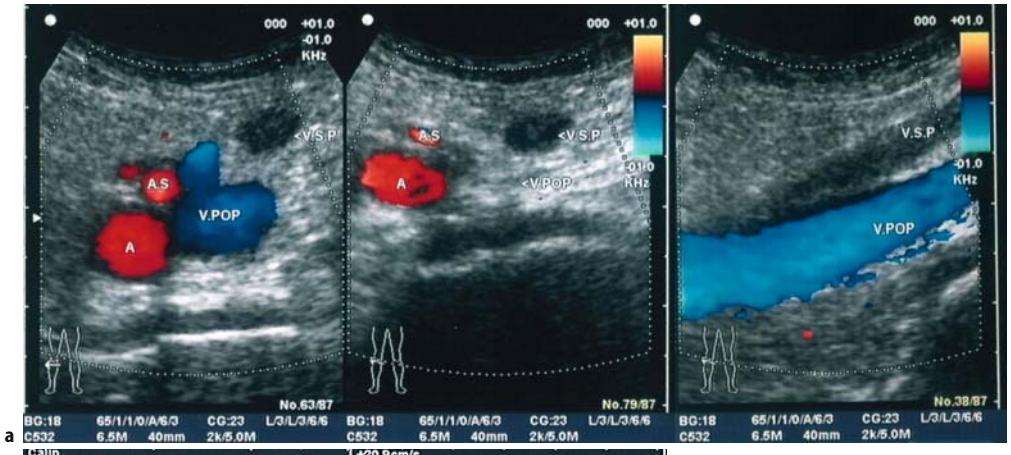

Fig. A 3.21 a, b
Thrombophlebitis of small saphenous vein

a Patients with thrombophlebitis of the small saphenous vein often present with unspecific clinical symptoms that may mimic deep venous thrombosis of the leg. For this reason, diagnostic evaluation of patients for exclusion of deep vein thrombosis must also include the small saphenous vein. The transverse view on the left depicts the small saphenous vein (*V.S.P*) as a nonperfused hypoechoic tubular structure posterior to the popliteal vein (*V.POP*). The compression scan (*middle section*) shows noncompressibility of the vein. The longitudinal scan (*right section*) depicts the small saphenous vein (*V.S.P*) without flow to the level of its opening into the popliteal vein. There is no thrombus extension into the popliteal vein shown with flow in blue (*V.POP*)

Femoropopliteal vein

b The femoropopliteal vein (*V.FP*) passes posteriorly from the small saphenous vein (*V.S.P*, dilated by fresh thrombus) shortly before the latter opens into the popliteal vein. Despite thrombophlebitis of the small saphenous vein distal to the site of entry of the femoropopliteal vein, the proximal compression-decompression test demonstrates reflux at the opening of the small saphenous vein due to femoropopliteal valve incompetence

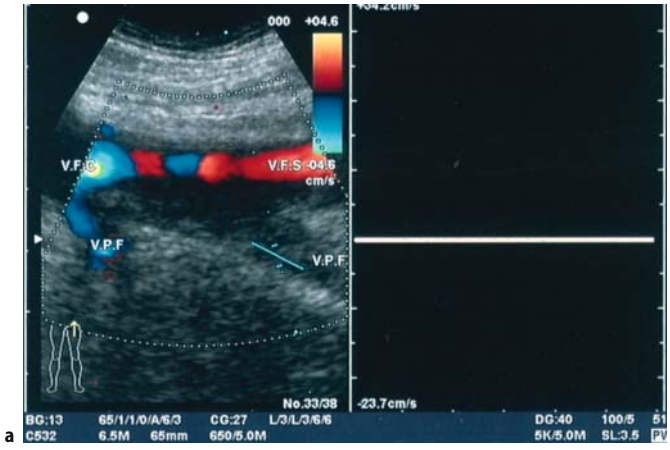

Fig. A 3.22 a–d
Deep femoral vein thrombosis

a The deep femoral veins (*V.P.F*) open into the superficial femoral vein on its posterolateral aspect. Deep femoral vein thrombosis is rare but can cause pulmonary embolism if there is ascending thrombus protrusion into the common femoral vein. The color duplex scan depicts the superficial femoral vein (*V.F.S*) with flow toward the transducer on the *right* (red) and with flow away from it on the *left* (blue). Several branches of the deep femoral vein (*V.P.F*) enter the superficial femoral posteriorly. Neither color duplex nor the Doppler spectrum depict flow in the deep femoral vein entering distally. The mural thrombus protrudes into the superficial femoral vein at the junction with the common femoral vein. The second deep femoral vein entering more proximally is not thrombosed (at *left* margin)

(Fig. A 3.22 cont.)
b The transverse scan (*left*) and longitudinal scan (*right*) depict the thrombus (*TH*) growing appositionally from the deep femoral vein (*V.P.F*) into the common femoral vein. The superficial femoral vein (*V.F.S*) is not thrombosed. (*A.F.S* superficial femoral artery; *K* venous valve)
c Transverse view of the femoral venous confluence at a slightly higher level. The power mode (*right scan*) shows the thrombus extending from the deep femoral vein (*V.P.F*) to be partially surrounded by flowing blood. In the common femoral vein, the blood from the patent superficial femoral vein (*V.F.S)* flows along the floating thrombus tail anteriorly. The superficial femoral artery (*A*) is depicted above

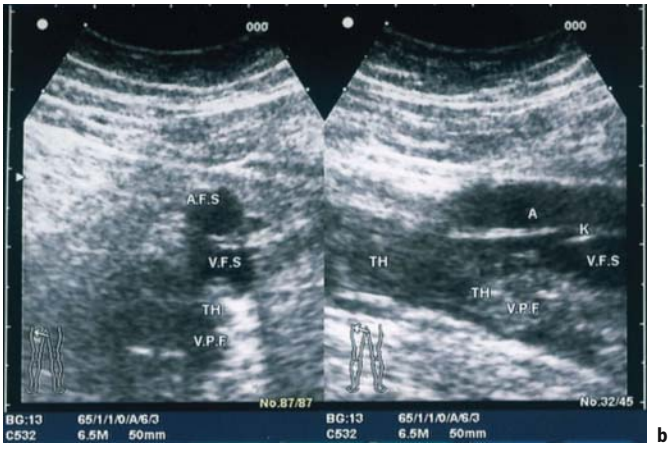

b

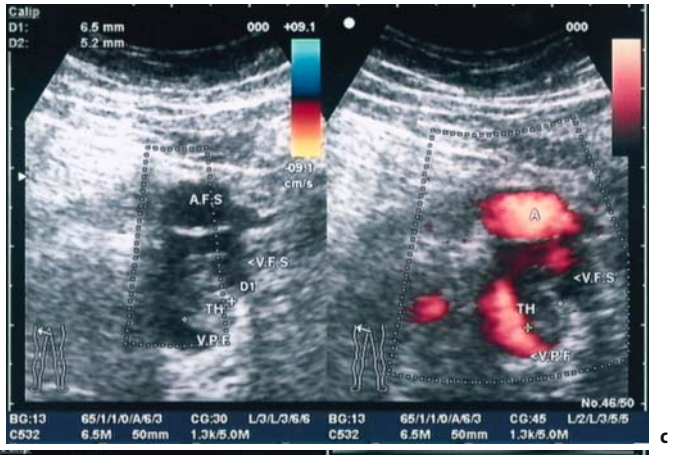

c

d Depiction of the floating thrombus in the common femoral vein at the level of the femoral artery bifurcation (*left section*) and 1 cm above it (*middle section*). The color duplex scan depicts a rim of blue-coded flow signals around the thrombus (*TH*)
The time-motion display (*right section*) nicely shows the floating movement of the thrombus in the bloodstream.
(*A.F.S* = superficial femoral artery, *A.P.F* = deep femoral artery, *V.F.C* = common femoral vein, *V.P.F* = cranial branch of deep femoral vein entering the common femoral vein between the deep and superficial femoral arteries)

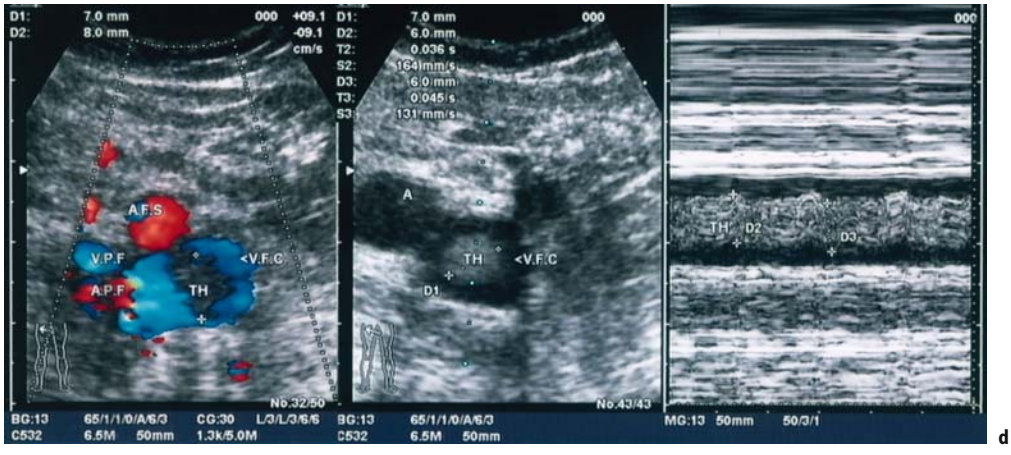

d

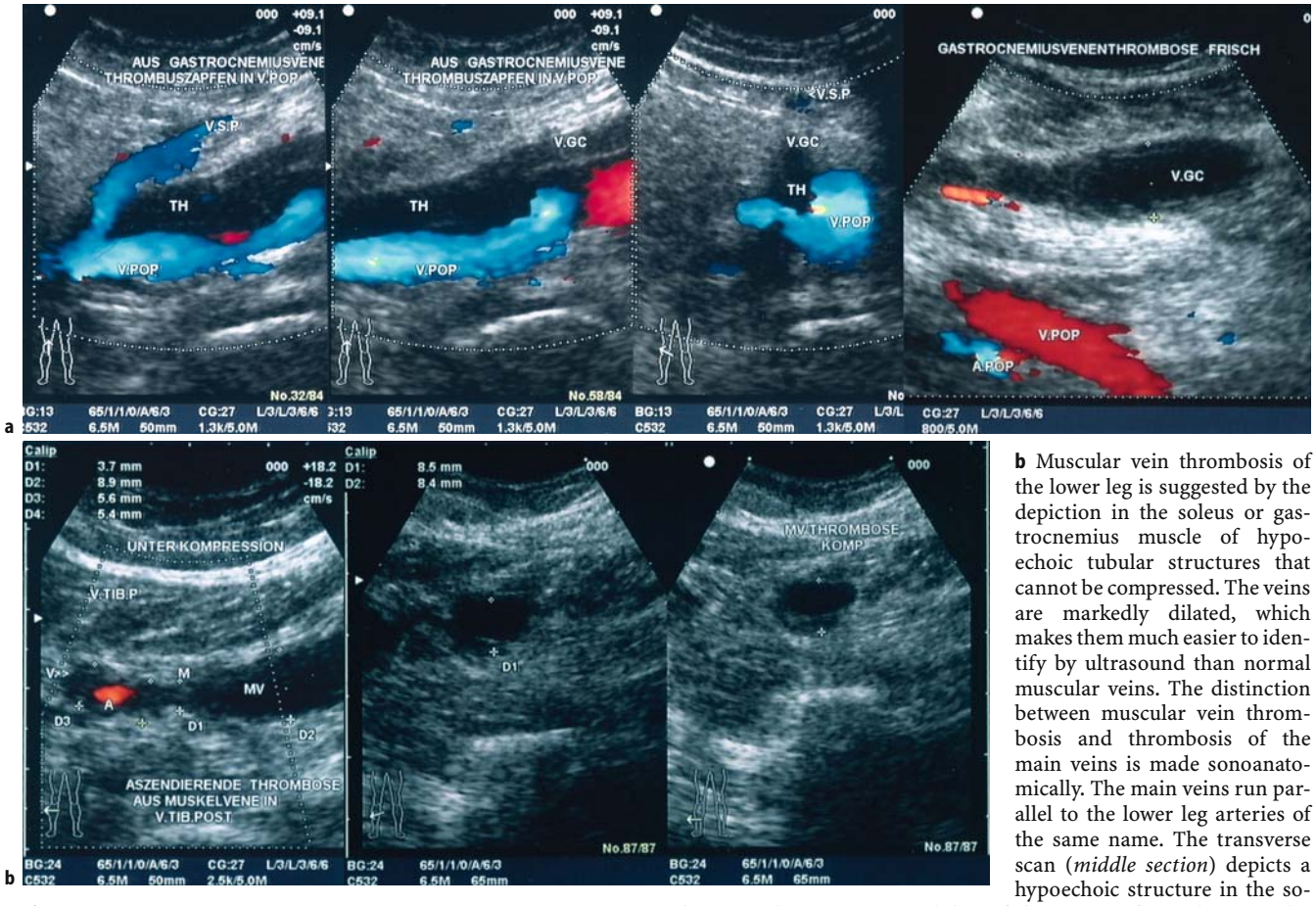

b Muscular vein thrombosis of the lower leg is suggested by the depiction in the soleus or gastrocnemius muscle of hypoechoic tubular structures that cannot be compressed. The veins are markedly dilated, which makes them much easier to identify by ultrasound than normal muscular veins. The distinction between muscular vein thrombosis and thrombosis of the main veins is made sonoanatomically. The main veins run parallel to the lower leg arteries of the same name. The transverse scan (*middle section*) depicts a hypoechoic structure in the soleus muscle. Noncompressibility of the vein confirms the muscular vein thrombosis (*right section*). The oblique color duplex scan on the left depicts the thrombosed soleus vein (*MV*, labeled as D2) along its course from the mid-calf to the knee and its opening (labeled as D1) into the posterior tibial vein. The latter is likewise thrombosed up to the tibiofibular confluence through appositional thrombus growth but is compressible somewhat distal to the opening of the muscular vein. The scan on the *left* was obtained during compression and depicts the hypoechoic, noncompressible posterior tibial veins (labeled as D3 and D4) to the left and right of the posterior tibial artery (red)

Fig. A 3.23 a, b
Muscular vein thrombosis
a The two longitudinal views (*leftmost* and *left center*) and the transverse view (*right center*) show a gap (*TH*) in the color-coded flow in the popliteal vein (*V.POP*). An ascending thrombus (*TH*) protrudes into the popliteal vein from the opening of a thrombosed gastrocnemius vein (*V.GC*). More cranially, the small saphenous vein (*V.S.P*) is depicted with blood flow in blue. The mural thrombosis ascending from the gastrocnemius vein into the popliteal vein ends at the opening of the small saphenous vein (*leftmost* and *left center*). The gastrocnemius vein thrombosis cannot be traced further distally (*rightmost section*)

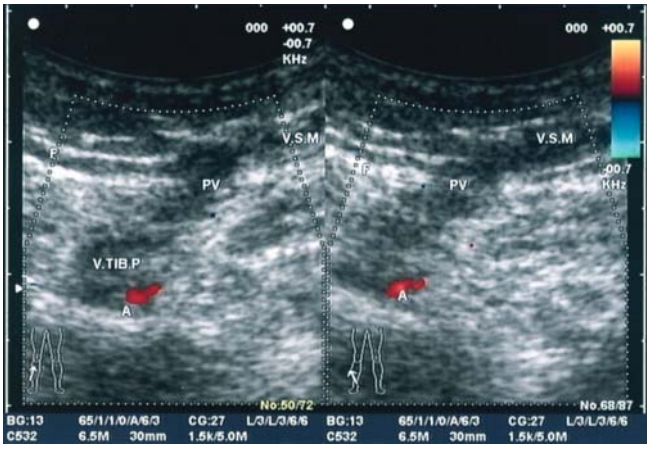

Fig. A 3.24
Thrombosis arising from thrombophlebitis extending through perforator
Extension of thrombophlebitis into the deep venous system can also occur through a perforating vein. In the case presented, extensive thrombophlebitis of the great saphenous vein (*V.S.M*) gives rise to a thrombus extending through a perforating vein (*PV*) into the posterior tibial vein (*V.TIB.P*) where it causes a circumscribed thrombosis 3 cm in length. Next to the vein, the artery is depicted with flow in red. The great saphenous, perforating, and posterior tibial veins are markedly dilated by the thrombus and not compressible (*right section*). The hyperechoic reflection indicates the site at which the vein pierces the fascia (*F*)

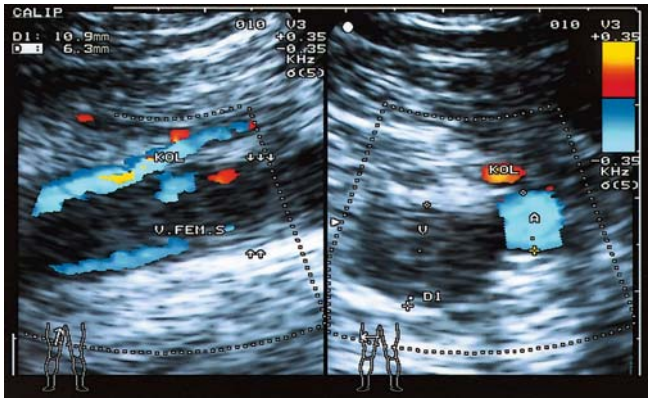

a

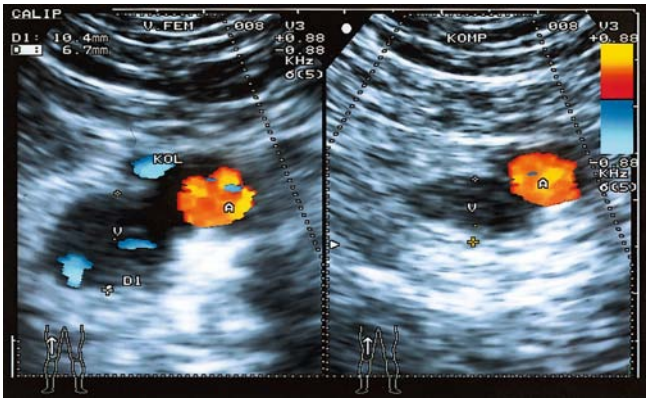

b

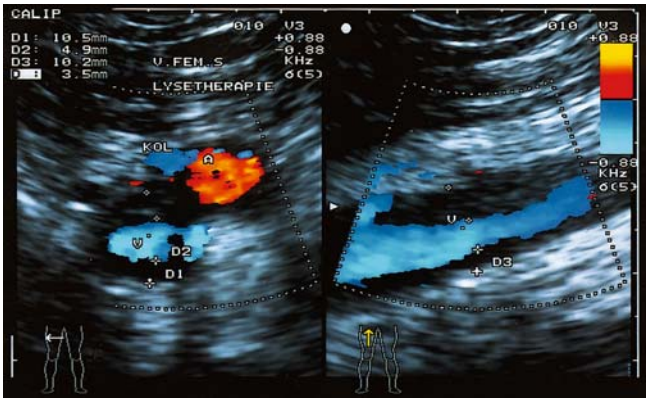

c

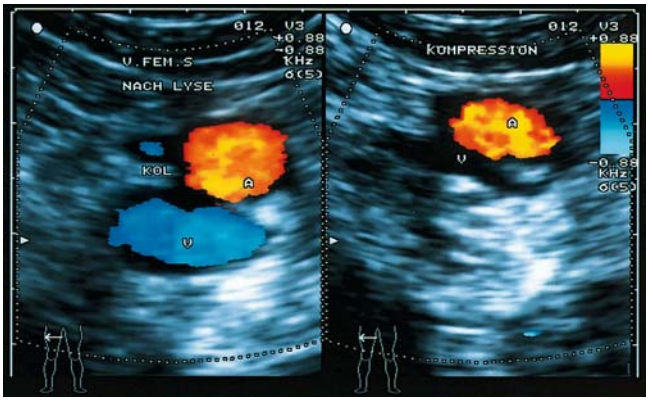

d

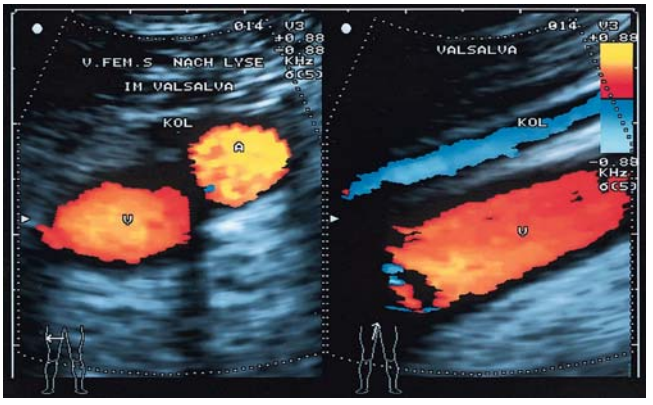

e

Fig. A 3.25 a–e
Follow-up of thrombolytic therapy

a The marked dilatation of the superficial femoral vein (compared to the corresponding artery) and the hypoechoic, homogeneous thrombus with a just barely visible hypoechoic halo suggest fresh thrombosis. The transverse view depicts a collateral (*KOL*) with flow in red anterior to the superficial femoral artery (*A*). The longitudinal view on the *left* shows a more proximal segment of the superficial femoral vein (*V*). The thrombus proximal to the opening of a collateral vein is surrounded by residual flow near the walls (blue)

b Both central and peripheral segments of the thrombosed superficial femoral vein (*V*) show flow coded in blue as a sign of beginning recanalization after 3 cycles of thrombolytic therapy with streptokinase. The scan was obtained in the same plane as the transverse scan in **a** but with the transducer angled superiorly. The scan on the *right* shows that flow signals disappear from the collateral vein and the partially recanalized femoral vein upon compression. The patent lumen collapses and only the thrombosed portion is still visible

c Complete recanalization of the vein after another 3 cycles of thrombolytic therapy. The transverse view (*left*) and the longitudinal view (*right*) depict only some residual mural thrombi of low echogenicity around the patent lumen. Also shown is the collateral (*KOL*, blue) anterior to the superficial femoral vein (*V*, blue)

d After another cycle of thrombolysis, the residual mural thrombi have almost completely dissolved. Upon compression (*right section*) of the vein (*V*), only a thin, hypoechoic band is depicted posterior to the artery, indicating reactive inflammatory wall thickening and intimal edema

e Despite complete recanalization after streptokinase therapy, there is persistent reflux after Valsalva's maneuver. Valve damage is due to the delay of more than 10 days between the onset of thrombosis and complete recanalization. The scan on the *left* demonstrates blood flow in the same direction (coded red) in the vein (*V*) and the corresponding artery (*A*). The scan on the *right* shows flow toward the heart (blue) in the competent collateral vein (*KOL*) during Valsalva's maneuver. This forward flow in the competent collateral is induced by the calf muscle pump because some patients inadvertently also contract their muscles during the Valsalva maneuver

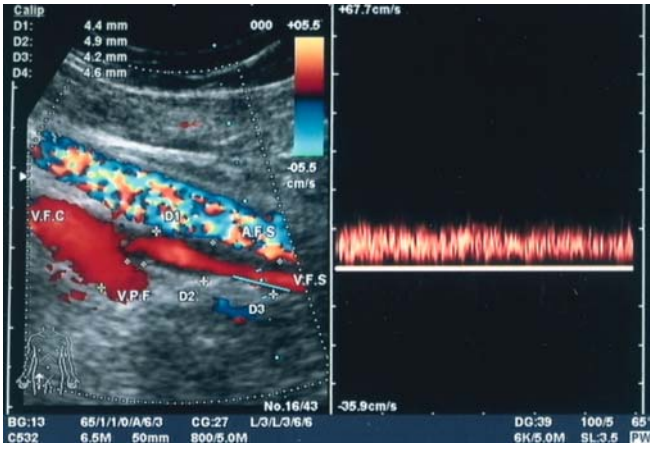

a

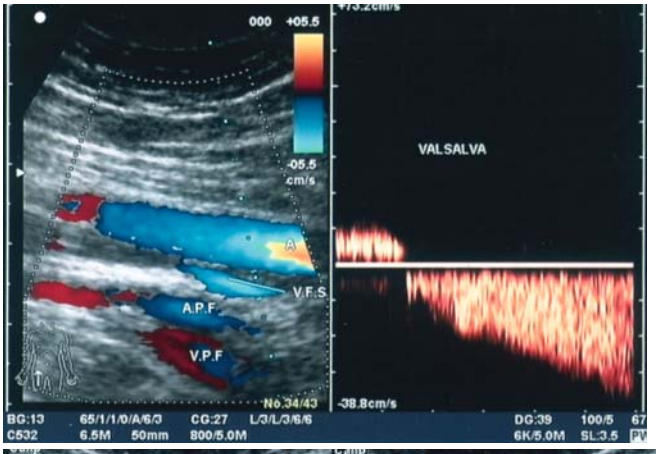

b

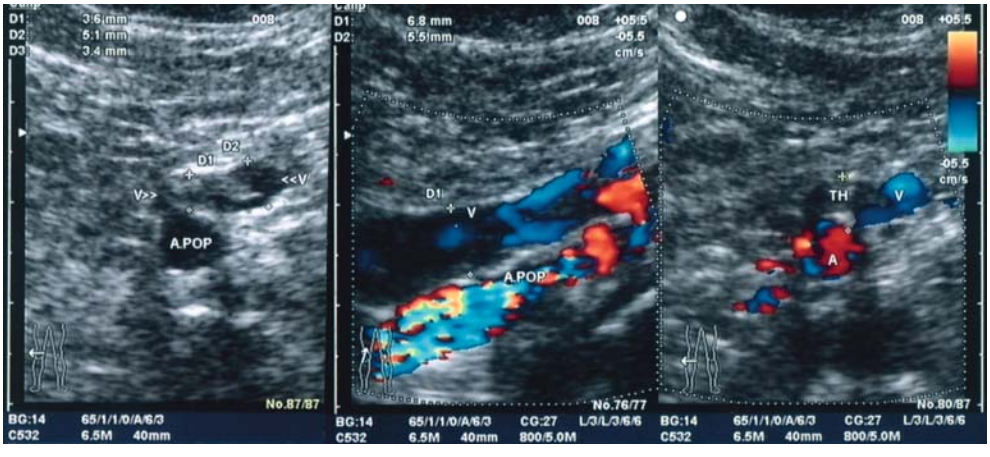

c

Fig. A 3.26 a–g
Postthrombotic syndrome – recanalized lumen
a In about 10 % of cases, thrombosis leads to permanent damage of the vein, depicted sonographically as a hypoechoic, tubular strand with a thin caliber adjacent to the artery (as in Fig. A 3.11). In most cases, however, there is postthrombotic recanalization but often with a smaller lumen. In the example shown, the superficial femoral vein is patent 4 months after thrombosis but only trickling flow is present. Hypoechoic thrombotic wall deposits and sclerotic wall lesions persist. Aliasing in the superficial femoral artery closer to the transducer confirms the pulse repetition frequency to be adequate for the detection of slow venous flow. The continuous flow signal resulting from the loss of respiratory phasicity indicates persistent flow obstruction in the recanalized vein
b Flow in the superficial femoral vein (*V.F.S*) during Valsalva's maneuver is coded in blue (away from transducer), and the Doppler waveform shows flow reversal
c Only meandering flow is detectable between residual thrombi (*TH*) in the popliteal vein (*V*) in the longitudinal color flow scan in the *middle* (with aliasing in the popliteal artery due to the low PRF). The transverse gray-scale scan (*left*) depicts hyperechoic residual thrombi adjacent to the anechoic recanalized lumen, which shows flow displayed in blue in the color duplex image (*right*)

(Fig. A 3.26 cont.)

d In this recanalized superficial femoral vein 4 months after thrombosis, the patent lumen (blue) has shrunk to about 20% of its original diameter. The poorly delineated walls of the vein are marked on the transverse view (*left*) and the longitudinal view. Posterior to the artery, a muscular vein is depicted with collateral flow (*KOL*) in blue

e The flow obstruction is reflected by a continuous flow profile without respiratory variation in the Doppler frequency spectrum. The color change from red to blue in the recanalized superficial femoral vein (wall indicated by *arrows*) is due to flow reversal in the vessel relative to the ultrasound beam. The low PRF produces aliasing in vessel segments insonated at a small angle. A collateral is depicted close to the transducer (*KOL*)

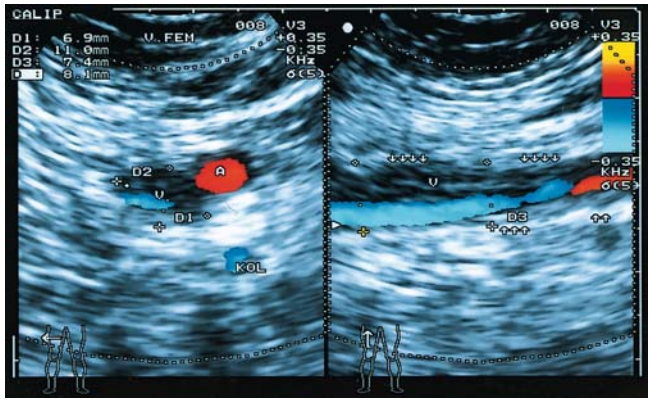

d

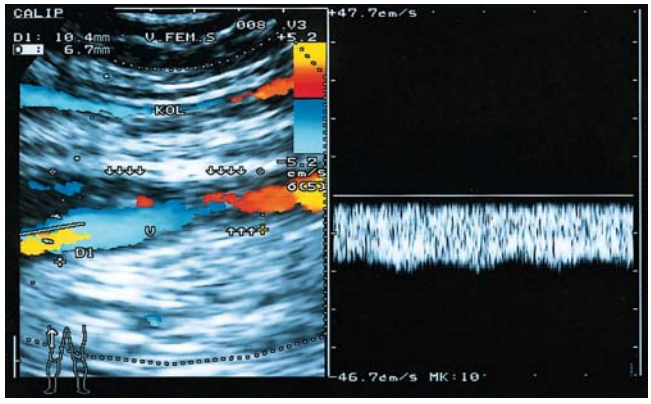

e

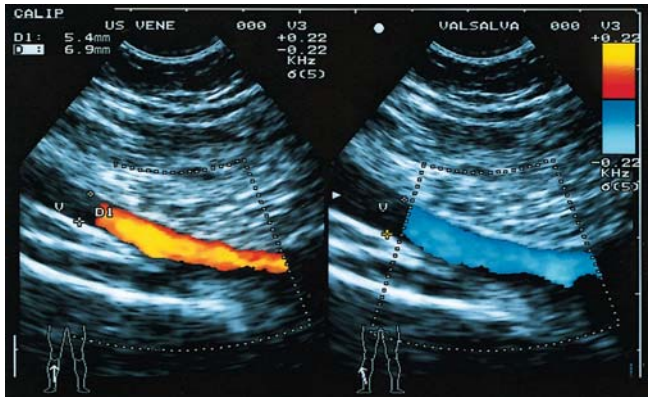

f

f The postthrombotic syndrome is distinguished from primary chronic venous insufficiency of the deep leg veins, in which valve failure is due to dilatation of the veins. The walls are delicate and free of deposits and therefore easy to compress. In the example shown, valve incompetence in the proximal posterior tibial vein is associated with persistent reflux during Valsalva's maneuver, indicated by the color change from red to blue

In case of pronounced incompetence of all venous valves proximal to the transducer, deep abdominal inspiration can already induce a reflux and normal rhythmical inspiration and expiration may induce to-and-fro flow

Valve incompetence of lower leg veins

g The duration of reflux can be determined in the Doppler frequency spectrum, which thus enables differentiation of short physiologic reflux prior to valve closure from persistent reflux due to incompetent valves. Blue indicates reflux in the posterior tibial vein away from the transducer. Repeated and somewhat longer compression and decompression lead to alternating flow toward the transducer during compression (*KOMP*) and away during decompression (*DEKOMP*)

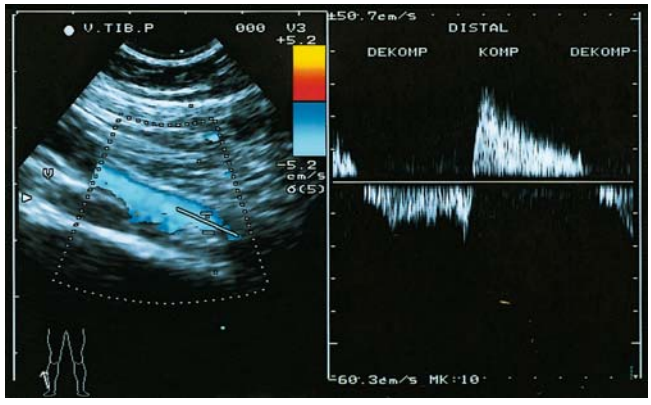

g

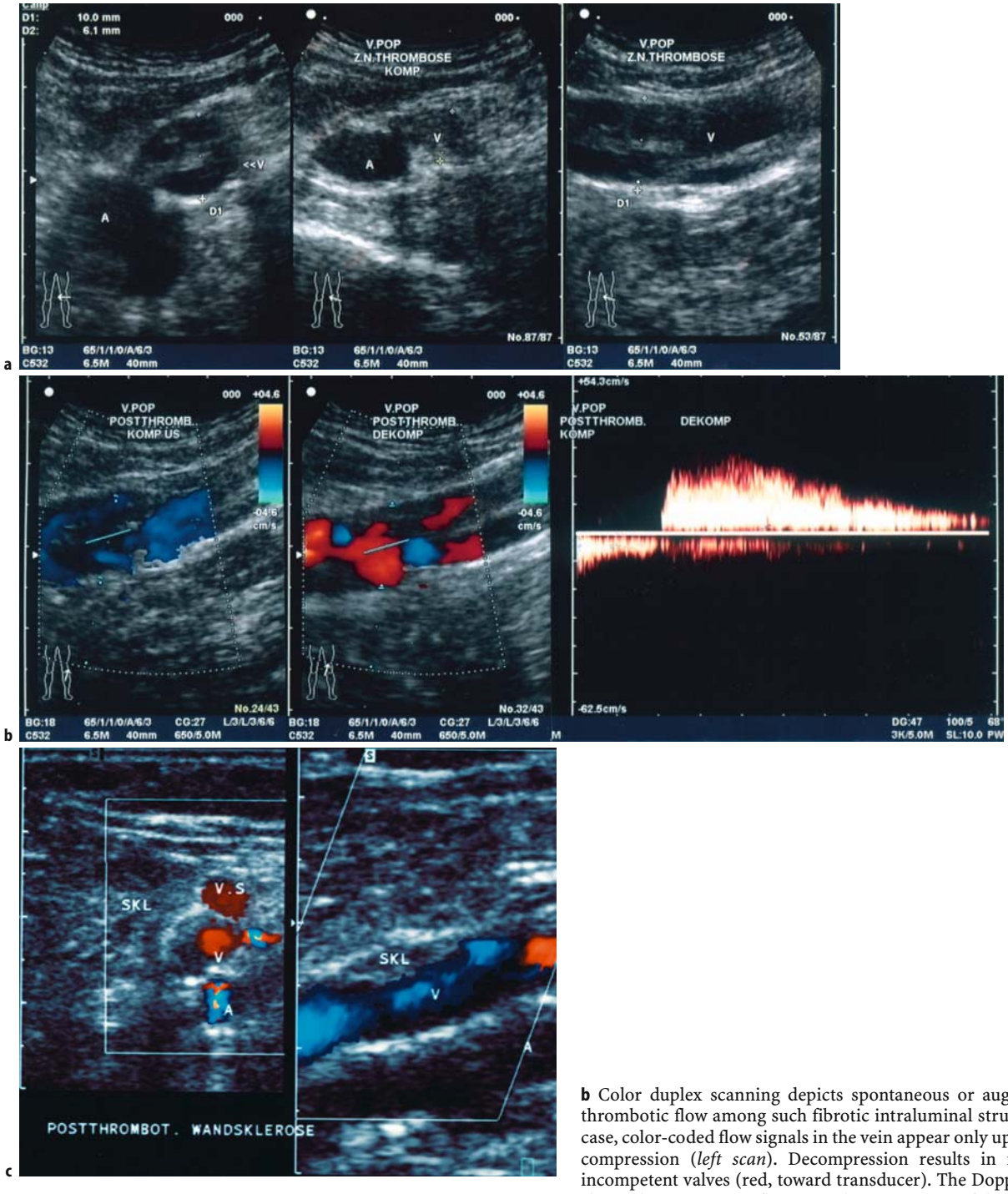

Fig. A 3.27 a–e
Postthrombotic syndrome – residual morphologic lesions
a The compression scan (*middle section*) shows an inhomogeneous, mostly hypoechoic structure in the soft tissue at the site of the incompletely recanalized vein. The scan on the *left* depicts hyperechoic threadlike structures in the partially recanalized (more hypoechoic) lumen. These structures, which occasionally may have a honeycomb appearance, are sclerotic strands persisting after thrombosis. The scan on the *right* shows these structures in longitudinal orientation

b Color duplex scanning depicts spontaneous or augmented postthrombotic flow among such fibrotic intraluminal structures. In this case, color-coded flow signals in the vein appear only upon peripheral compression (*left scan*). Decompression results in reflux due to incompetent valves (red, toward transducer). The Doppler waveform shows the persistent reflux upon decompression of the calf
c The popliteal vein is completely patent but there is postthrombotic wall sclerosis depicted as hyperechoic thickening of the wall (*SKL*, shown in longitudinal orientation on the *right*). The transverse scan on the *left* also depicts more hypoechoic areas in the lumen, corresponding to residual thrombotic deposits on the wall or wall thickening. These abnormalities appear to the left of the recanalized patent lumen displayed in red and farther away from the transducer. The more superficial small saphenous vein appears normal shortly before it enters the popliteal vein

(Fig. A 3.27 cont.)
d Postthrombotic wall lesions can lead to wall sclerosis and calcifications with acoustic shadowing on ultrasound. The Doppler waveform shows reflux due to incompetent valves
e Vasosclerotic changes with wall thickening and calcification may also occur after thrombophlebitis. In the example, the longitudinal view on the *right* shows the hyperechoic sclerotic wall lesions with intraluminal deposits that are partially calcified as shown by posterior acoustic shadowing (*SS*). The longitudinal scan in the *middle* and the transverse scan on the *left* also depict the thin recanalized lumen of the postthrombophlebitic small saphenous vein with flow in blue

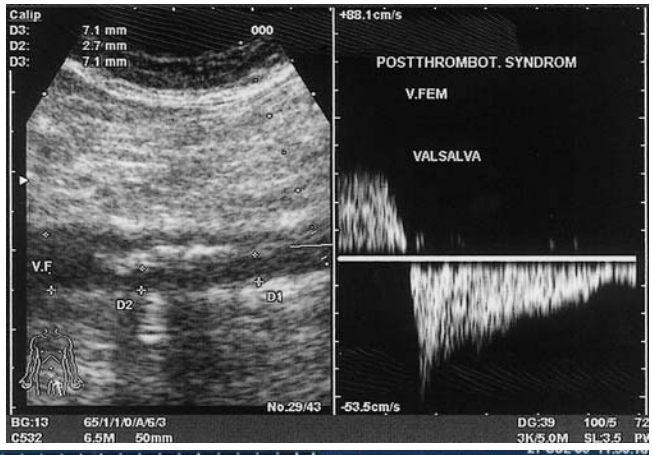

d

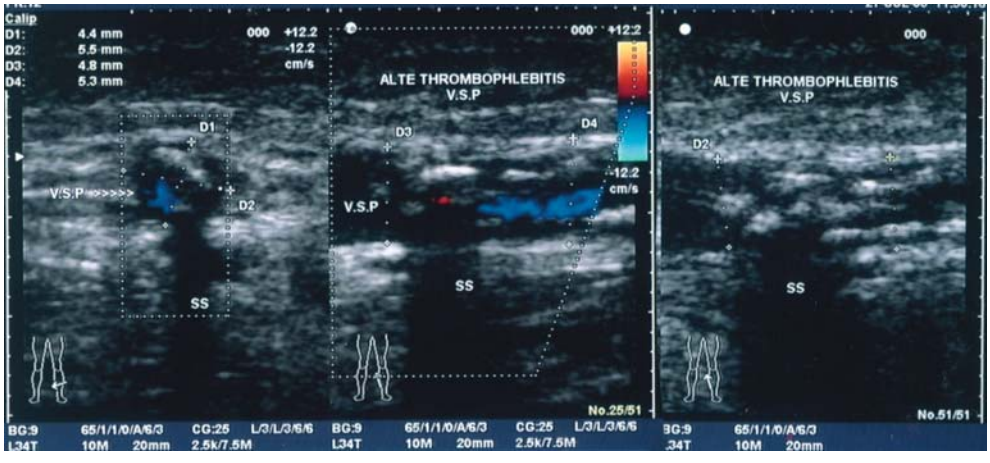

e

Fig. A 3.28
Postthrombotic lower leg vein
The diagnosis of older lower leg vein thrombosis or residual postthrombotic lesions relies on the examiner's sonoanatomic knowledge, as the affected veins will no longer be visualized as markedly dilated tubular structures. The corresponding arteries serve as landmarks. It is often difficult to detect spontaneous flow in (partially) recanalized lower leg veins. In the case presented, a flow signal (A-sound) can be recorded with adequate instrument settings in the duplicated posterior tibial vein (depicted to the left and right of the artery of the same name) following distal compression (lower calf). A vein with a normal lumen would have become invisible upon compression. The hypoechoic small-caliber structures persisting upon compression in the soft tissue along the course of the veins to the left and right of the artery indicate residual thrombotic lesions or fibrotic wall changes

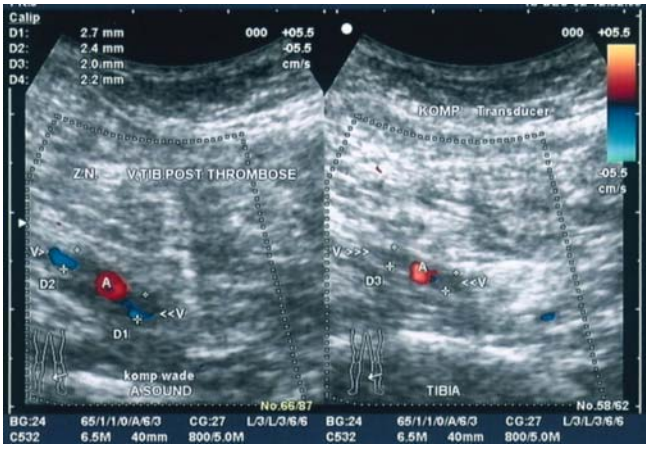

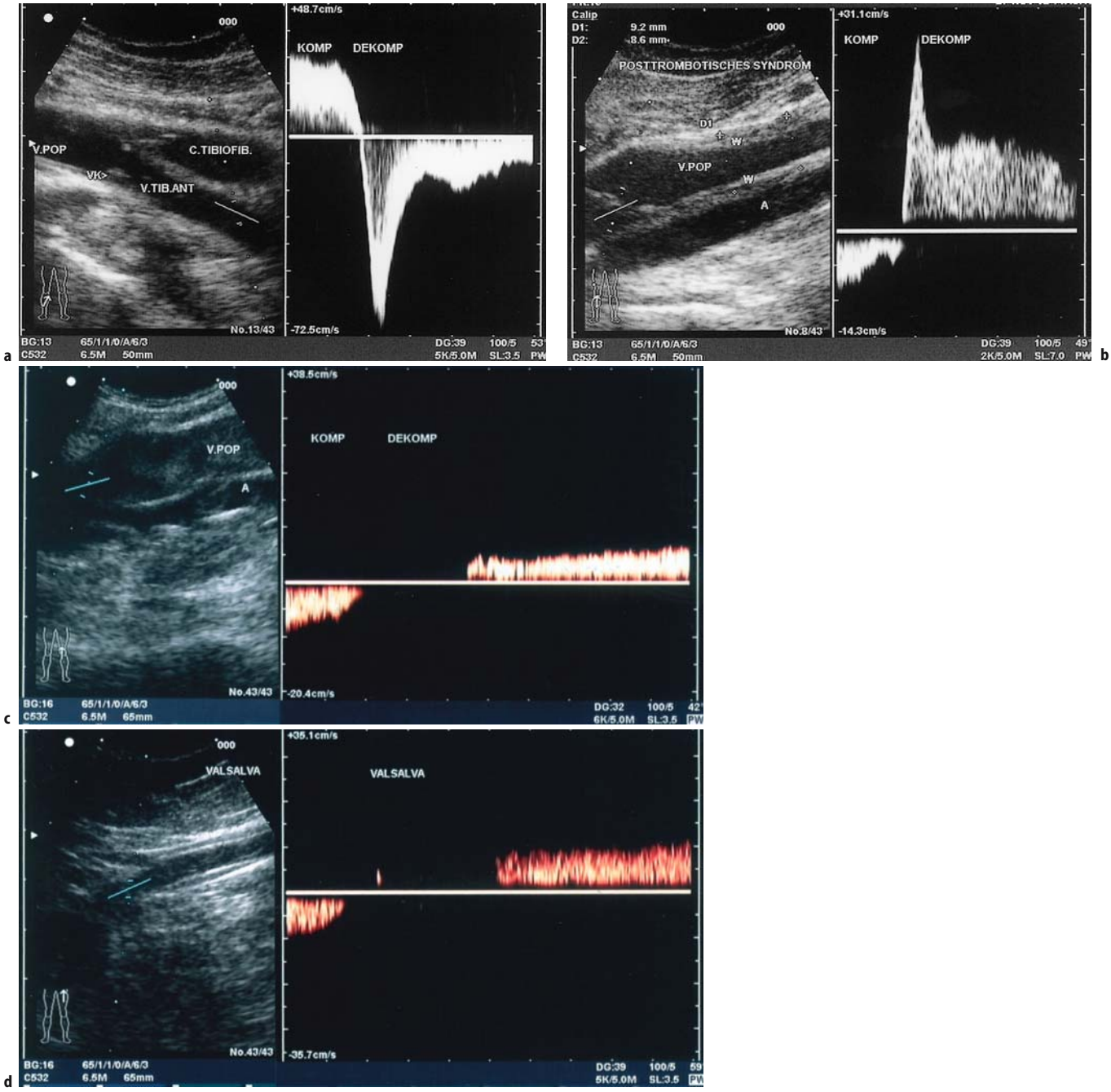

Fig. A 3.29 a–g
Degrees of valvular incompetence

a Postthrombotic thickening of a venous valve (*VK*) with adhesion to the wall prevents closure, which is indicated by reflux during Valsalva's maneuver or in the compression-decompression test. Here, postthrombotic sclerosis and valve incompetence of the popliteal and lower leg veins lead to immediate backward flow with a high signal upon compression of the calf (*KOMP*) with subsequent decompression (*DEKOMP*). This finding indicates complete valve failure. Once the blood column expulsed from the calf has flowed back, the flow signal decreases in the further course of decompression. The example presented illustrates valve incompetence of the anterior tibial vein (*V.TIB.ANT*) before its opening into the popliteal vein (*V.POP*)

b The popliteal vein also shows postthrombotic valvular adhesion and wall sclerosis (*W*), reflected sonographically as hyperechoic wall thickening (wall near transducer). The Doppler waveform from the popliteal vein (*V.POP*) depicts the prompt and pronounced reflux (toward transducer) upon decompression (*DEKOMP*) as a sign of complete valve failure

c Primary chronic venous insufficiency with dilatation but some residual valve function is associated with delayed reflux in the Valsalva or compression-decompression test. The example shows the delayed reflux (toward transducer) with a lower but constant flow in the popliteal vein

d A similar pattern of backward flow is seen in this case of varicosis of the great saphenous vein with early, mild valvular incompetence. There is delayed but constant reflux through the leaking valve after Valsalva's maneuver

(Fig. A 3.29 cont.)
e Marked varicose dilatation produces severe valvular incompetence without residual function, as in the postthrombotic syndrome, resulting in immediate and pronounced reflux with high-velocity flow toward the periphery in Valsalva's test

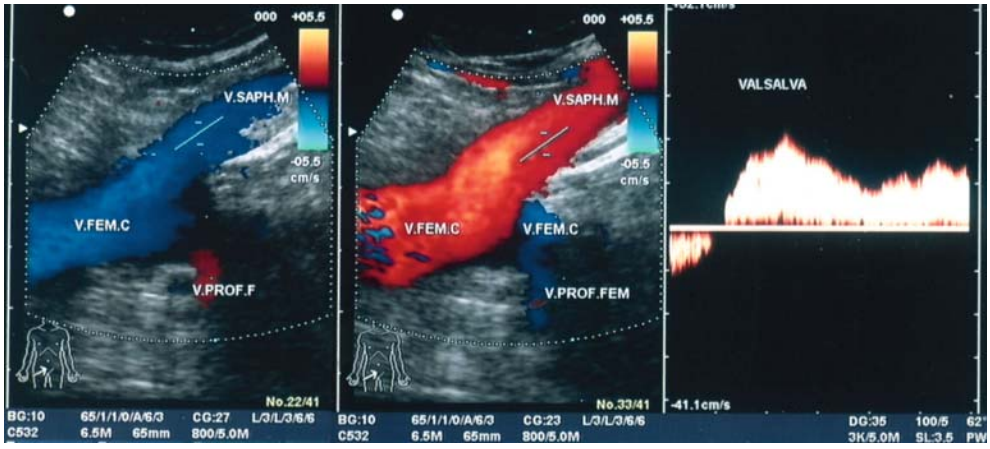

e

f The reflux resulting from postthrombotic valve incompetence is additionally influenced by flow obstruction due to residual thrombi. In the example, the popliteal vein is still partially thrombosed (*TH*) with only slow spontaneous flow. Compression (*KOMP*) of the calf induces constant flow from the periphery to the heart while the backward flow occurring upon decompression (*DEKOMP*) is less pronounced and less persistent than would be expected in extensive, recanalized thrombosis. The reduced backward flow is due to flow obstruction by the residual thrombi

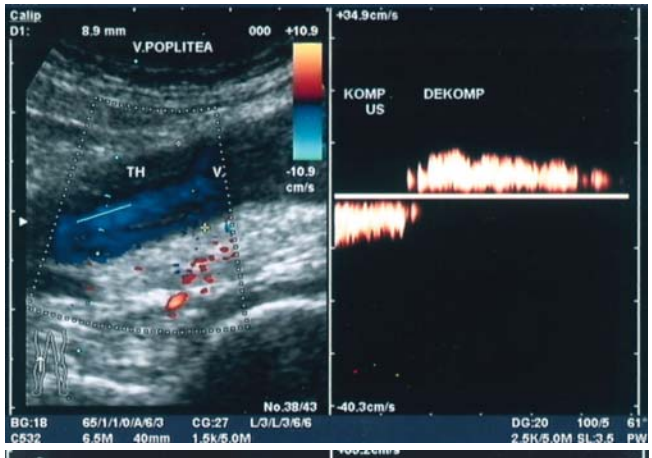

f

g Slight reflux through a small leak in a valve leaflet during prolonged Valsalva's maneuver can be detected using a high-resolution transducer with a low pulse repetition frequency or in the power mode (for detection of slow flow). The power-mode scan on the *left* shows only little flow (red) directly behind the leaking valve leaflet in the proximal superficial femoral vein. If there is only little leakage, the sample volume must be placed close to the valve in order to depict the slight reflux during Valsalva's maneuver (flow toward periphery, away from transducer). As only little blood leaks back into the vein, no flow signals are detectable in the remaining venous segments. Such slight leakage as in this case should not be overinterpreted as valve incompetence but merely illustrates the high sensitivity of high-resolution ultrasound scanners for the detection of small flow volumes. However, repeat Doppler sampling along the course of the vein with provocative maneuvers is necessary to definitely exclude any clinically relevant reflux. Anterior to the vein, the superficial femoral artery (*A.F.S*, red) is depicted; and posterior to it, the opening of the deep femoral vein (*V.P.F*, without flow signals during Valsalva's maneuver)

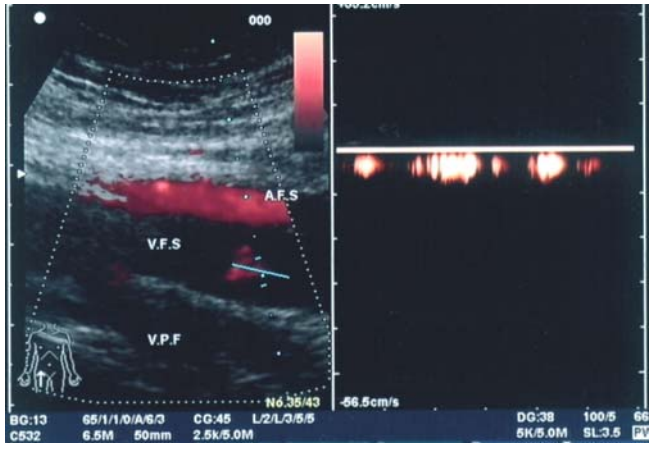

g

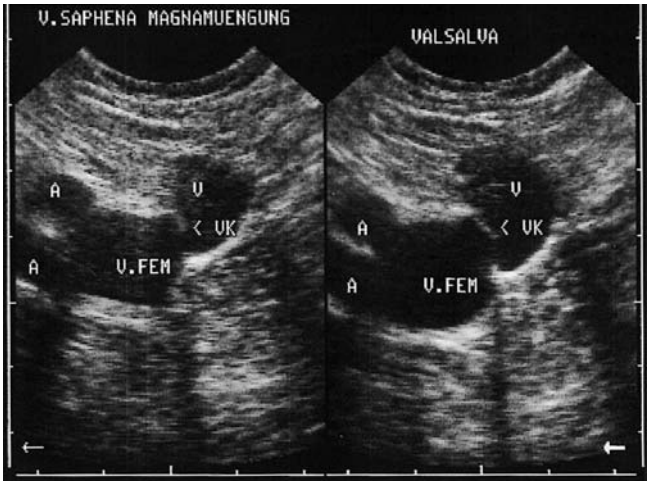

a

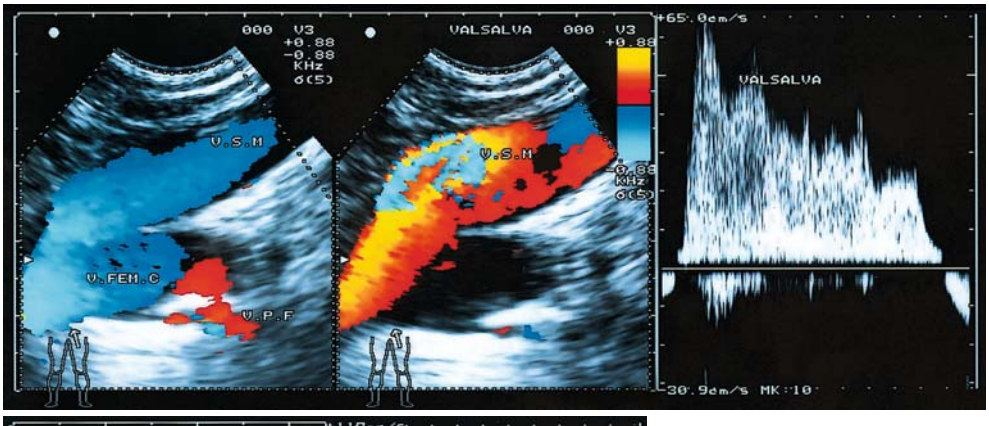

b

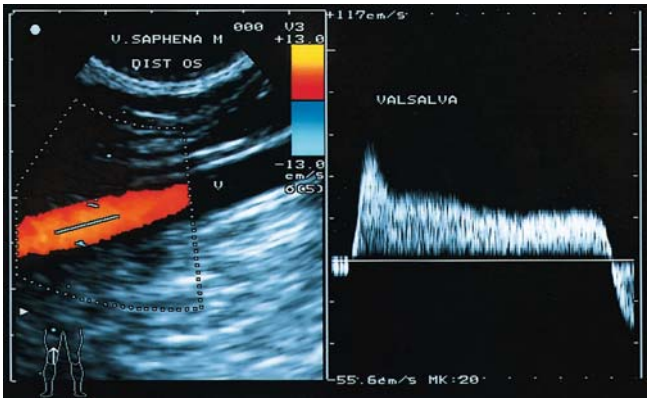

c

Fig. A. 3.30 a–g
Truncal varicosis of great saphenous vein (distal extent)
a The transverse B-mode scans show dilatation of the proximal great saphenous vein during Valsalva's maneuver with the incompetent valve leaflet turning distally and thus becoming visible (*VK*)
b Incompetent terminal valve of the great saphenous vein. The scan on the left shows blood flow toward the heart (blue). The great saphenous vein (*V.S.M*) courses close to the transducer, and a deep femoral vein (*V.P.F*) with flow displayed in red is seen entering the common femoral vein (*V.FEM.C*) posteriorly. Valsalva's maneuver (*middle section*) induces reflux (red) with aliasing due to the low PRF adjusted to slow venous flow. Proper valve closure in the common femoral vein prevents reflux into the deep venous system. The Doppler frequency spectrum (*right*) recorded at the termination of the great saphenous vein during Valsalva's maneuver shows flow to the periphery (toward transducer)

c The distal point of insufficiency of the great saphenous vein for grading according to Hach is identified by determining reflux during Valsalva's maneuver (toward transducer) in the color duplex mode or in the Doppler tracing obtained along the course of the vein from above the knee (*V*) to the lower leg

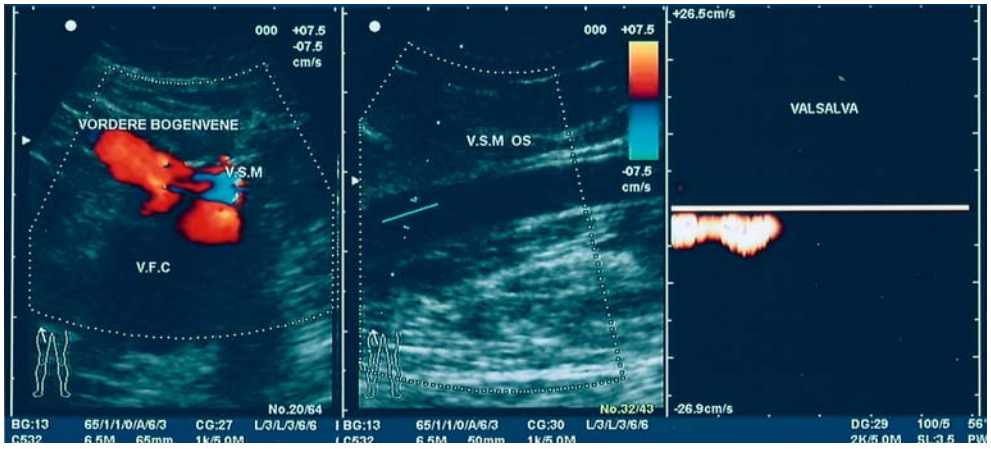

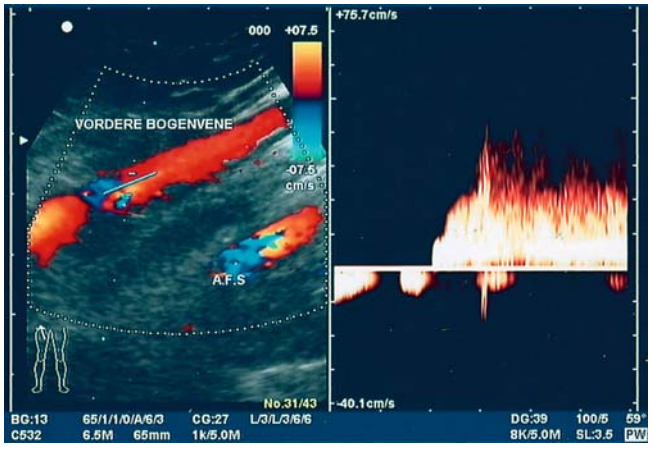

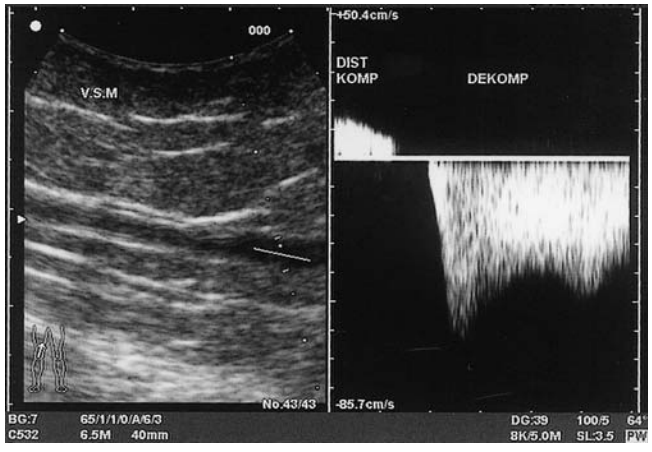

(Fig. A 3.30 cont.)
Incomplete truncal varicosis of great saphenous vein

d The scan on the *left* depicts retrograde flow toward the periphery (red) in the lateral accessory saphenous vein during Valsalva's maneuver. The great saphenous vein itself does not show signs of valve incompetence in the form of retrograde flow during Valsalva's maneuver on color duplex (*middle section*) or in the Doppler waveform (*right section*). There may even be some forward flow (in blue) during Valsalva's maneuver as suggested by the scan on the *left*. This is due to recirculation of the lateral accessory saphenous vein through the bucket handle anastomosis into the great saphenous vein (with retrograde flow in its peripheral, incompetent segment but antegrade flow in its proximal, competent segment)

e Color duplex scanning and the Doppler waveform document flow toward the periphery (toward transducer) in the lateral accessory saphenous vein during Valsalva's maneuver

f Incomplete truncal varicosis of the great saphenous vein of the lateral branch type is demonstrated by reflux in the vein above the knee (below opening of the bucket handle anastomosis)

g Incomplete truncal varicosis of the great saphenous vein of the lateral branch type: *1* lateral accessory saphenous vein, *2* bucket handle anastomosis, *3* superficial femoral vein, *4* great saphenous vein

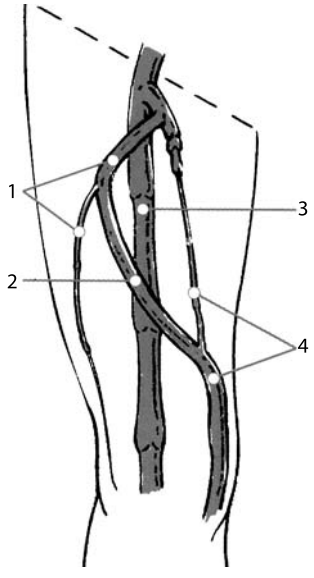

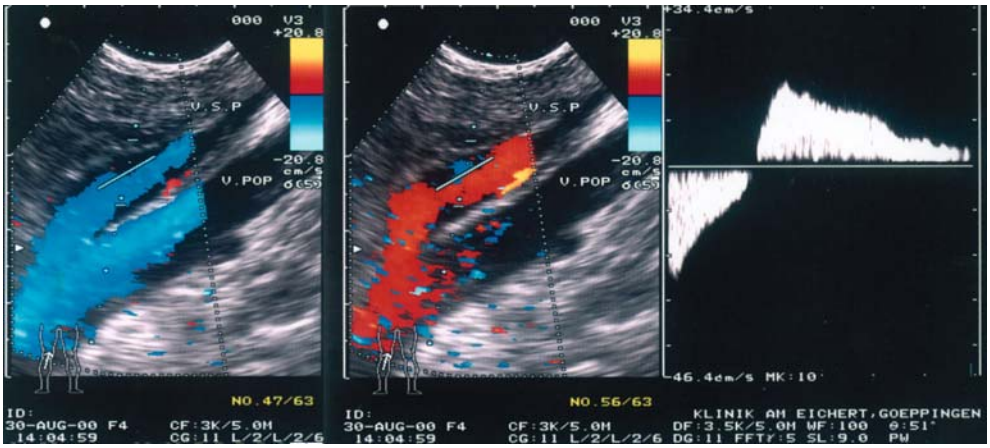

Fig. A 3.31
Truncal insufficiency of small saphenous vein
Valve function of the small saphenous vein (*V.S.P*) is assessed by means of the compression-decompression test in the sitting or standing patient. After compression of the calf (*left section*), blood flow displayed in blue (toward the heart, away from transducer) is seen followed by red-coded reflux into the small saphenous vein (*middle section*). The Doppler waveform on the *right* shows flow away from the transducer during compression and reflux during decompression (flow above baseline)

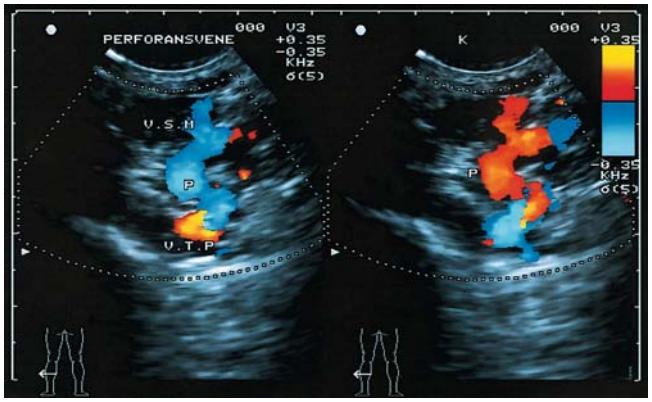

a

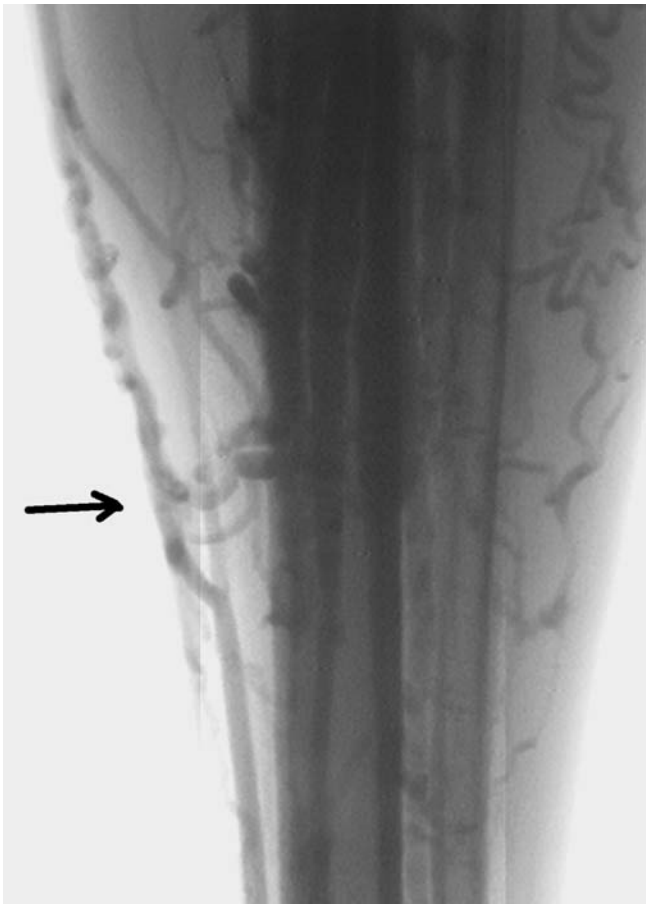

b

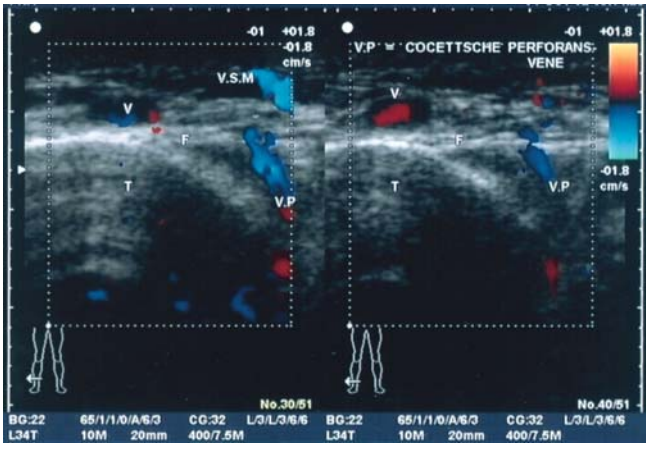

c

Fig. A 3.32 a–c
Valve incompetence of perforating vein
a Incompetent perforating veins are identified by looking for transfascial tubular structures originating from branches of the great or small saphenous vein in transverse orientation using a high-frequency transducer. In the example, compression of the calf proximal to the probe with elimination of flow in the superficial veins by means of a tourniquet induces retrograde flow (displayed in red) from the posterior tibial vein (*V.T.P*) into the great saphenous vein (*V.S.M*) with a return to forward flow (blue, away from transducer) upon decompression. Reflux from the deep venous system into the superficial system in this test confirms an incompetent perforating vein
b Venography depicting an incompetent perforating vein between the great saphenous vein and the posterior tibial vein
c Widening associated with valve incompetence makes it much easier to identify an abnormal perforating vein than a normal one. A very small perforating vein (*V.P*) of the lower leg is depicted along its transfascial course (*F*) with flow coded in blue

During compression there is flow in the perforating vein (*V.P*) from the superficial into the deep system coded in blue and no reflux upon decompression. The scan on the *left* depicts a perforator, the one on the *right* a Cockett perforator. Between the fascia (*F*) and the skin, the great saphenous vein and lateral branch veins (*V*) are depicted

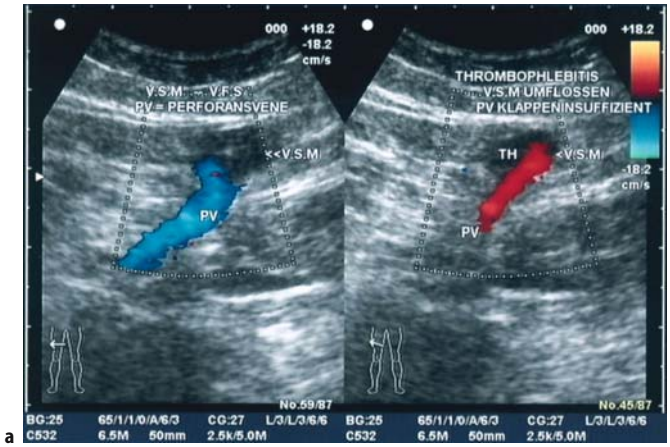

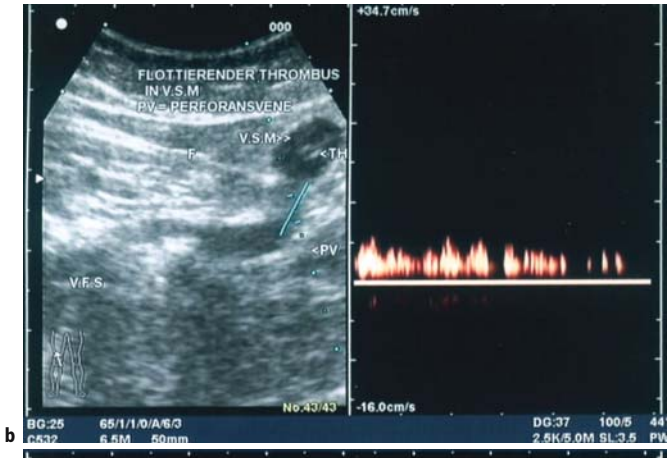

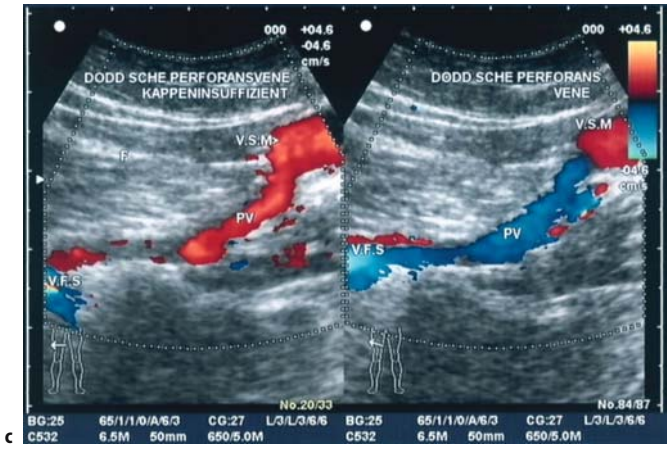

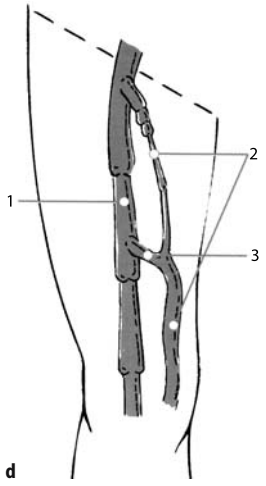

Fig. A 3.33 a–d
Thromboembolism of great saphenous vein and Dodd perforator incompetence

a Patient with thrombophlebitis clinically extending to the knee and sonographic demonstration of a thrombus in the great saphenous vein with proximal extension to the level of the mid-thigh. The proximal 3 cm are surrounded by flowing blood. At this level, the transverse view depicts a Dodd perforator (*PV*) with normal flow into the deep venous system and an increase in flow velocity upon compression of the great saphenous vein just above the thrombophlebitic segment. Release induces reflux into the superficial system (displayed in red, scan on the *right*), indicating valve incompetence of the perforating vein. The thrombus in the great saphenous vein (*TH*) is identified by the absence of color coding

b B-mode scan depicting the thrombus (*TH*) in the great saphenous vein (*V.S.M*). The Doppler spectrum recorded in the perforating vein demonstrates reflux from the superficial femoral vein (*V.F.S*) upon decompression

c The Valsalva maneuver inadvertently dislodged the thrombus in the great saphenous vein, inducing asymptomatic pulmonary embolism. Scintigraphy showed a small perfusion defect in the right lower lobe. Following this incident, the great saphenous vein was patent in the area of the Dodd perforator with forward flow from the great saphenous vein (*V.S.M*) into the superficial femoral vein (*V.F.S*) and persisting reflux after a provocative maneuver as definitive evidence of perforator incompetence (*PV*, coded red, toward transducer)

d Incomplete truncal varicosis of the great saphenous vein of the perforator type: *1* superficial femoral vein, *2* great saphenous vein, *3* Dodd's perforating vein

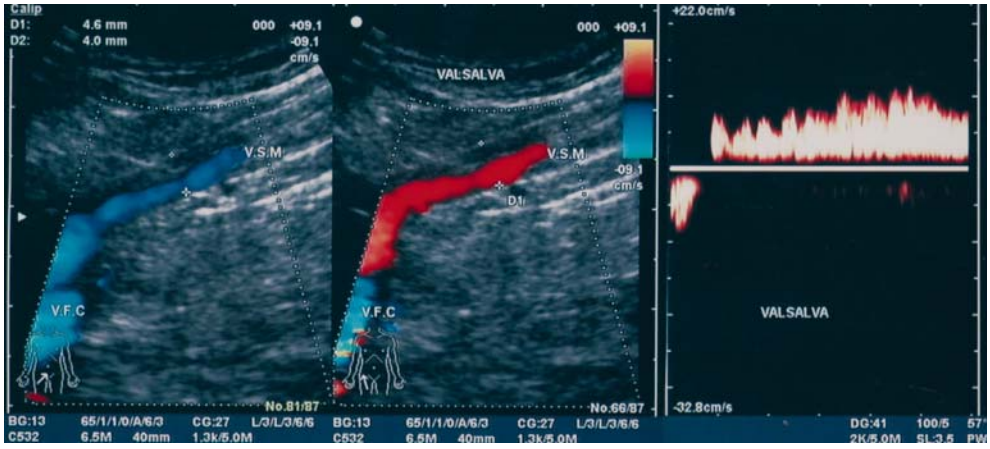

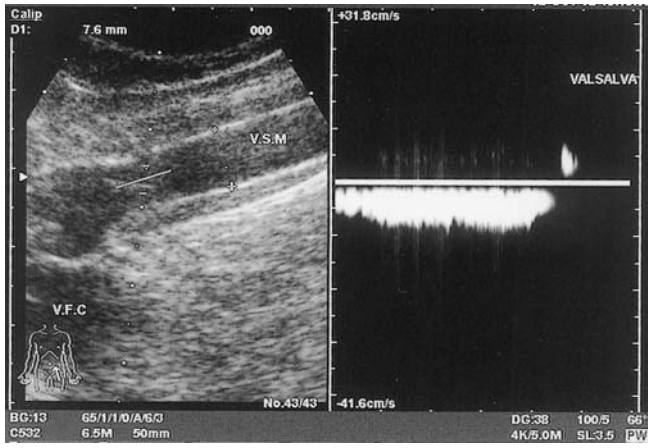

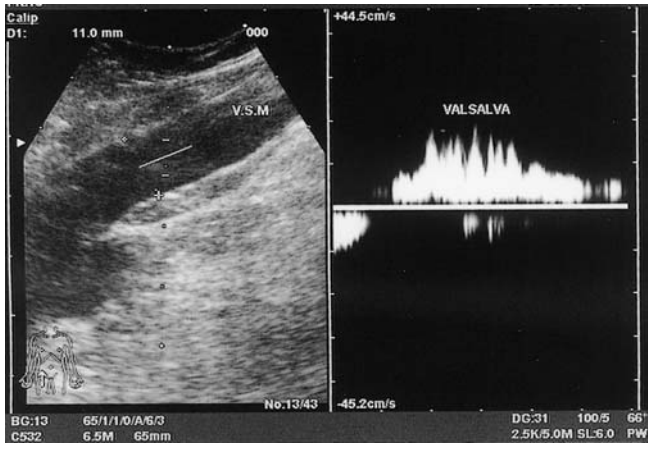

Fig. A 3.34 a–c
Recanalized great saphenous vein after thrombophlebitis
a Only about half of the lumen of the great saphenous vein (*V.S.M*) is patent just below the junction with the common femoral vein (*V.F.C*) and shows normal flow displayed in blue (lumen indicated by plus signs). Reflux in the great saphenous vein during Valsalva's maneuver (red). In addition, hypoechoic areas are depicted along the patent lumen. The Doppler waveform demonstrates reflux during Valsalva's maneuver. The exclusion of venous segments with postthrombophlebitic changes is important in preoperative vein mapping for identifying a suitable vein segment for bypass grafting
b The great saphenous vein (*V.S.M*) not affected by varicosis takes a straight course and has a regular, nonectatic lumen. At its opening into the common femoral vein (*V.F.C*), Valsalva's maneuver induces only a short reflux until valve closure occurs
c In contrast, an insufficient great saphenous vein is dilated, elongated, and tortuous with a variable lumen width. At the same site as depicted in **b**, the insufficient vein shows the typical persistent reflux during Valsalva's maneuver (flow toward transducer)

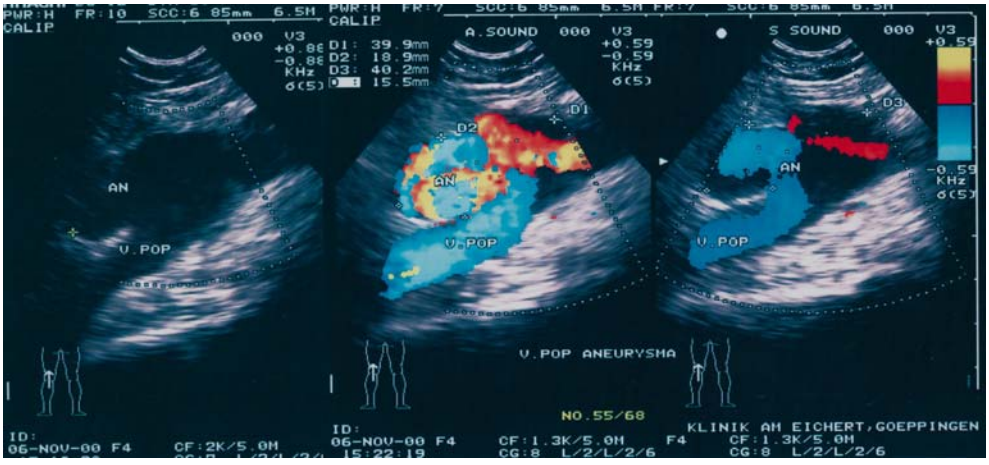

a

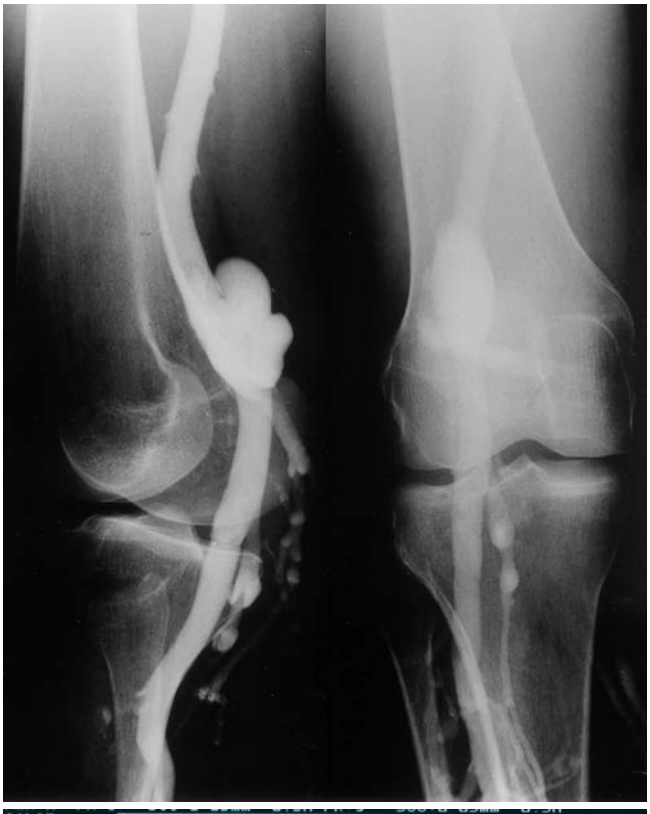

b

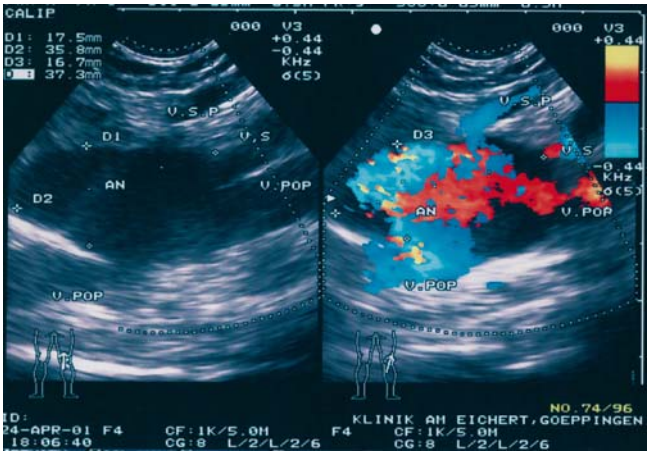

c

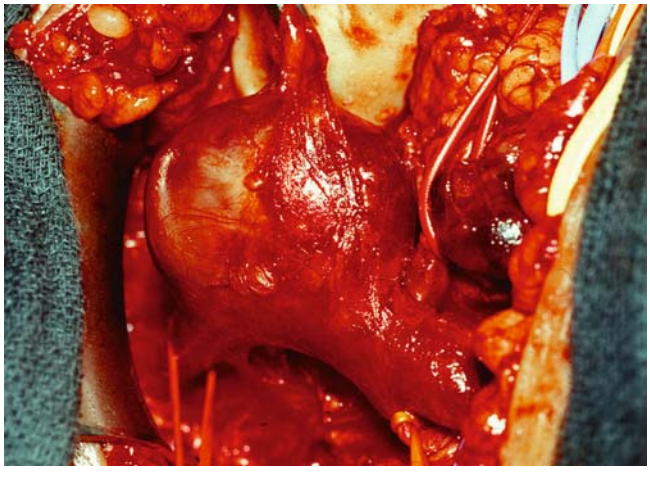

d

Fig. A 3.35 a–d
Venous aneurysm
a Gray-scale scan depicting a saccular aneurysm (*AN*) as a distended sac at its preferred site, the popliteal vein (*V.POP*). Color duplex evaluation (*right section*) of spontaneous flow demonstrates zones of nearly complete stasis (S-sound). Compression of the calf (A-sound) induces pronounced eddy currents in the popliteal vein aneurysm (*middle section*)
b Venography demonstrating saccular aneurysm of the popliteal vein. In a nonthrombosed aneurysm, as in the case shown, opacification corresponds to the sonomorphologic appearance (cf. *left section* in **a**)
c With a different transducer orientation, the small saphenous vein (*V.S.P*) and a gastrocnemius vein (*V.S*) opening into the aneurysm are depicted. The maximum cross-sectional diameter of the aneurysm is 2.5 cm
d The intraoperative site confirms the sonomorphologic appearance of the saccular aneurysm. The saccular cranial end is exposed on the left and the two veins (gastrocnemius vein and small saphenous vein) opening into the aneurysm are seen in the center. The popliteal vein (*left margin*) and a vessel opening into the distal popliteal vein (*right*) are encircled with red vessel loops

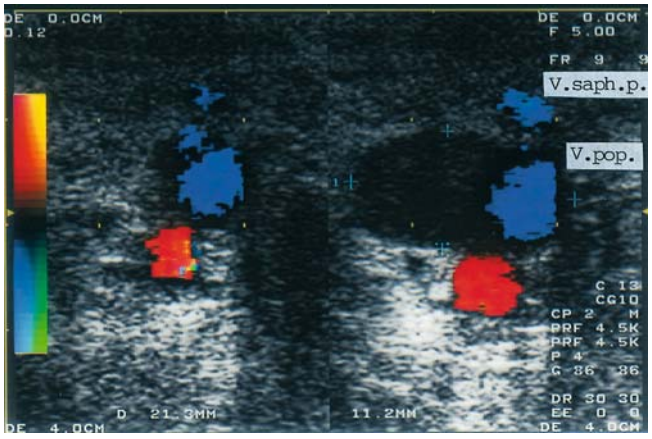

a

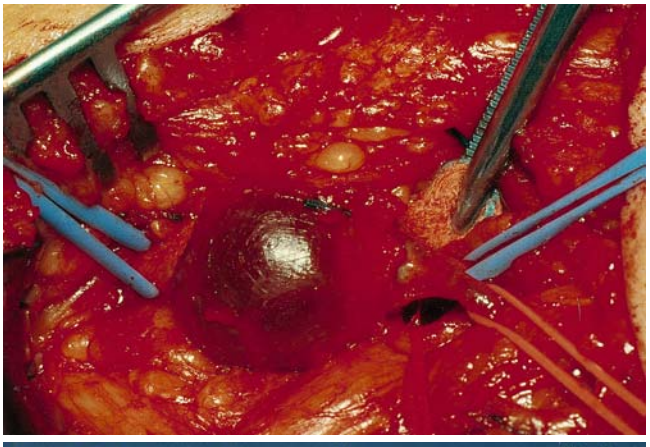

c

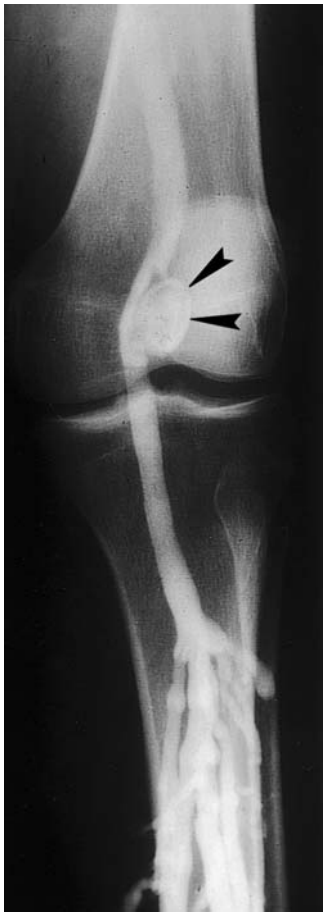

b

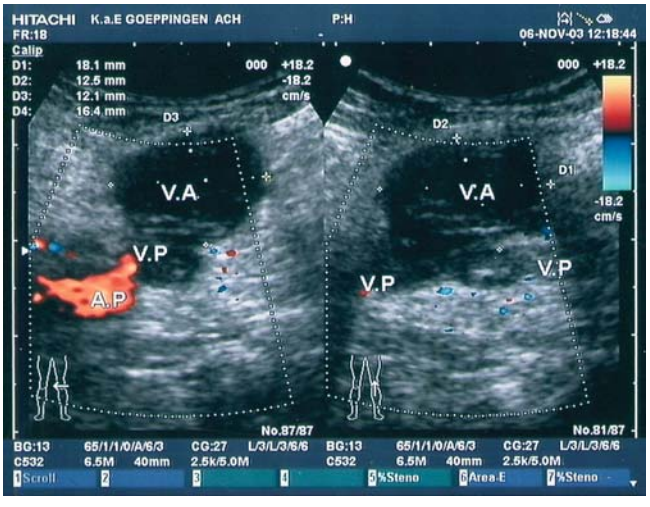

d

Fig. A 3.36 a–d
Venous aneurysm
58-year-old patient with scintigraphically proven pulmonary embolism. Saccular popliteal vein aneurysm extending into the opening of the sural vein with mural thrombosis of the aneurysmal venous segment and patency only of the normal popliteal lumen
a The scan on the *left* depicts the popliteal vein with flow in blue proximal to the aneurysm; the scan on the *right* shows the dilated segment of the popliteal vein (*V.POP*) with mural thrombosis
b Venography: Mural thrombosis precludes visualization of the popliteal vein aneurysm and only aneurysmal dilatation of the opening area of a tributary vein is demonstrated (above knee joint cleft)
c The intraoperative site confirms the ultrasound findings of popliteal vein aneurysm (*middle*) with mural thrombosis of the saccular portion and aneurysmal dilatation of the opening of the sural vein. Popliteal vein encircled with blue vessel loops proximally and distally and sural vein with red vessel loop

Venous aneurysm and deep venous thrombosis of leg
d There is complete thrombosis of the popliteal vein (*V.P*). Both the transverse scan (*left*) and the longitudinal scan (*right*) additionally demonstrate a saccular venous aneurysm (*VA*) with a diameter of nearly 2 cm. The aneurysm is thrombosed as well. This young patient had no other risk factors for venous thrombosis, suggesting that thrombosis from the venous aneurysm caused secondary popliteal vein thrombosis. Venous aneurysm must be differentiated from an ectatic opening of a varicose small saphenous vein or an ectatic gastrocnemius vein

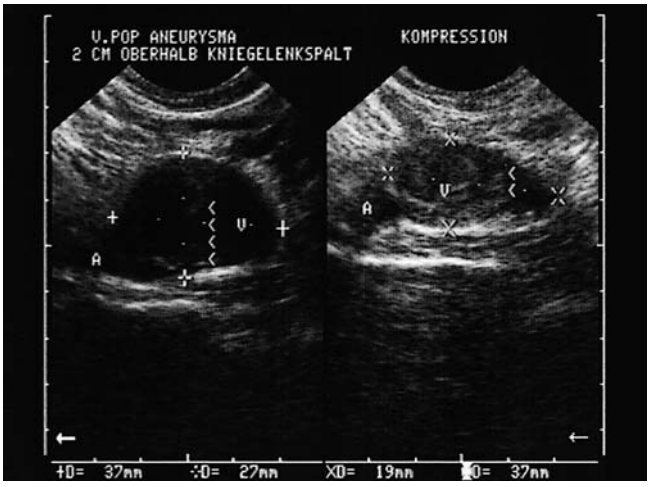

a

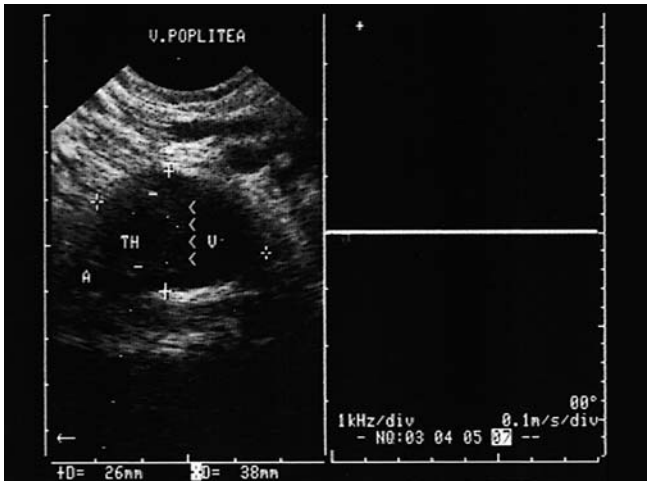

b

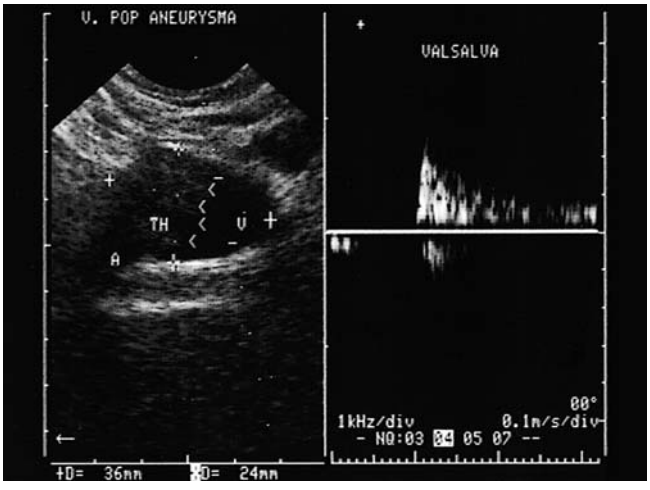

c

Fig. A 3.37 a–c
Saccular popliteal vein aneurysm
a 45-year-old patient with recurrent pulmonary embolism; saccular popliteal vein aneurysm with nearly complete thrombosis leaving only a small residual lumen demonstrated by sonography and venography
b, c The aneurysm has a maximum cross-sectional extent of 38 mm. Duplex ultrasound enables differentiation of the thrombotic portion (**b**) from the nonthrombotic residual lumen. Flow is depicted in the patent lumen and there is reflux during Valsalva's maneuver indicating valve incompetence (**c**). The patient had additional valve incompetence of the femoral vein and therefore underwent ligation of the superficial femoral vein to prevent further pulmonary embolism

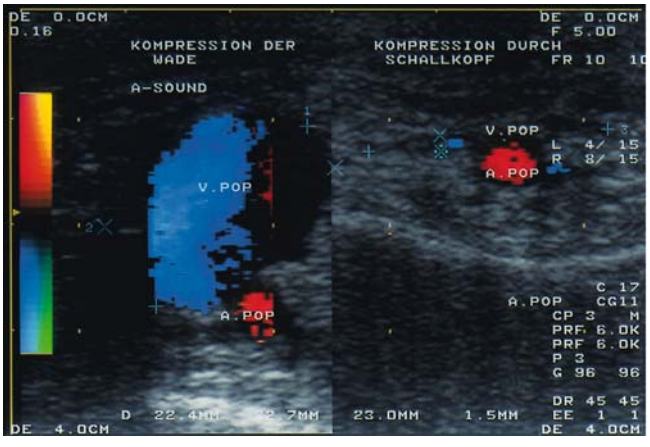

a

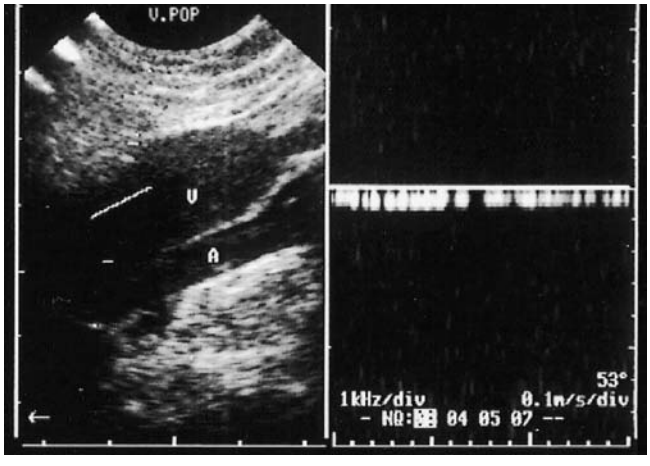

b

Fig. A 3.38 a, b
Spindle-shaped popliteal vein aneurysm
a Spindle-shaped aneurysm in a patient presenting with a tendency for calf swelling. The aneurysm has a maximum width of 28 mm and can be completely compressed with the transducer. Although there is no rich color filling throughout the patent lumen due to the slow venous flow, partial thrombosis is excluded by complete compressibility
b The spindle shape of the popliteal vein aneurysm is depicted on the longitudinal scan; calf swelling is caused by valve incompetence in this area. Surgery was not indicated; the patient underwent compression therapy. Sonographic follow-up over 5 years showed an unchanged aneurysm without mural thrombosis

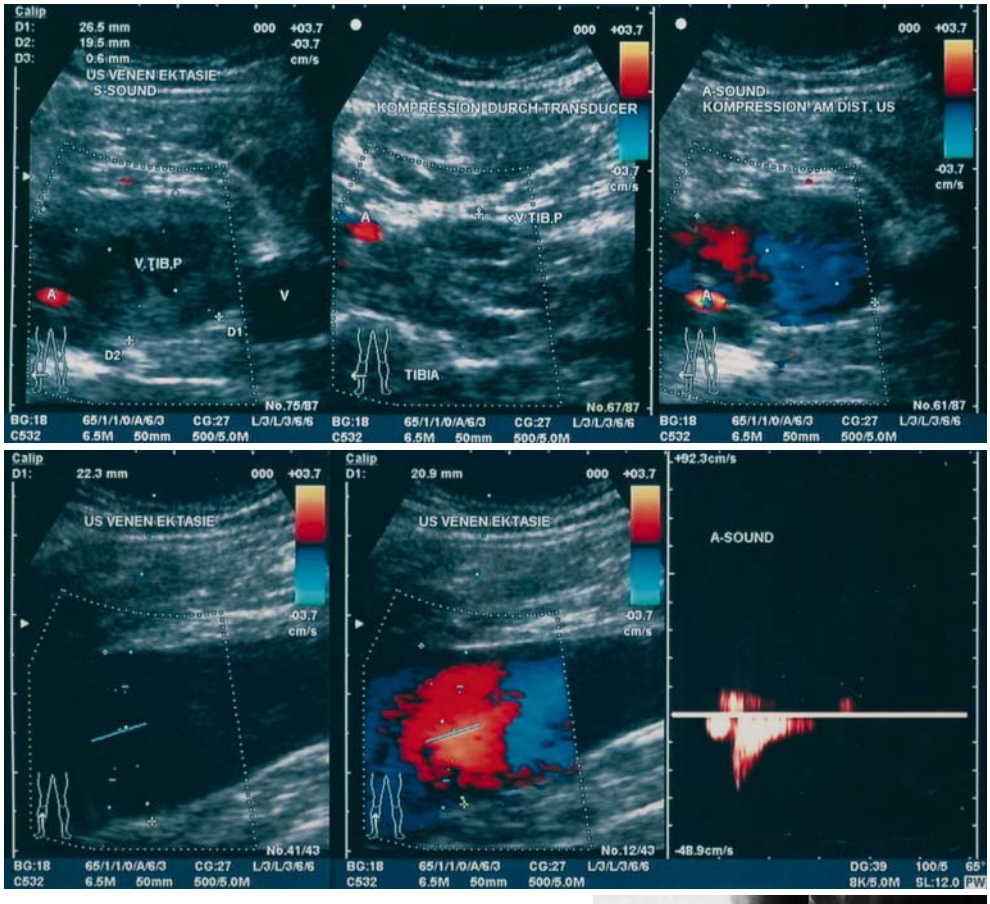

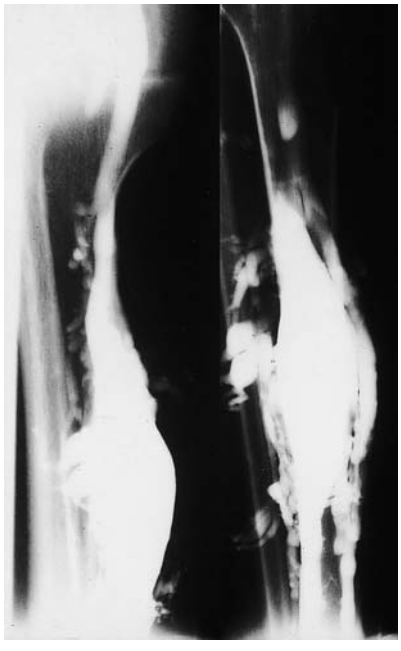

Fig. A 3.39 a–c
Ectasia of lower leg veins

a Ectatic degeneration chiefly affects the muscular veins of the gastrocnemius group while severe ectasia of the major lower leg veins is rare. In the 50-year-old patient presented here, spindle-shaped ectatic changes of the posterior tibial vein (*V.TIB.P*) were the source of scintigraphically proven pulmonary embolism. The B-scan appearance suggests thrombosis. The ectatic veins have a diameter of up to 2.5 cm and can be completely compressed (*middle section*); the lumen of the posterior tibial vein is indistinguishable (marked). To the left of the vein the posterior tibial artery is depicted with flow in red. There is no spontaneous flow in the vein (S-sound, *left section*) but augmented flow signals can be obtained upon distal compression of the calf (A-sound)

b The longitudinal scan likewise fails to depict flow in the spindle-shaped ectatic posterior tibial vein (*middle section*). Augmented flow (A-sound) is demonstrated by color duplex scanning and in the Doppler waveform following compression distal to the transducer

c Venography: Spindle-shaped ectatic muscular and main veins in the lower leg

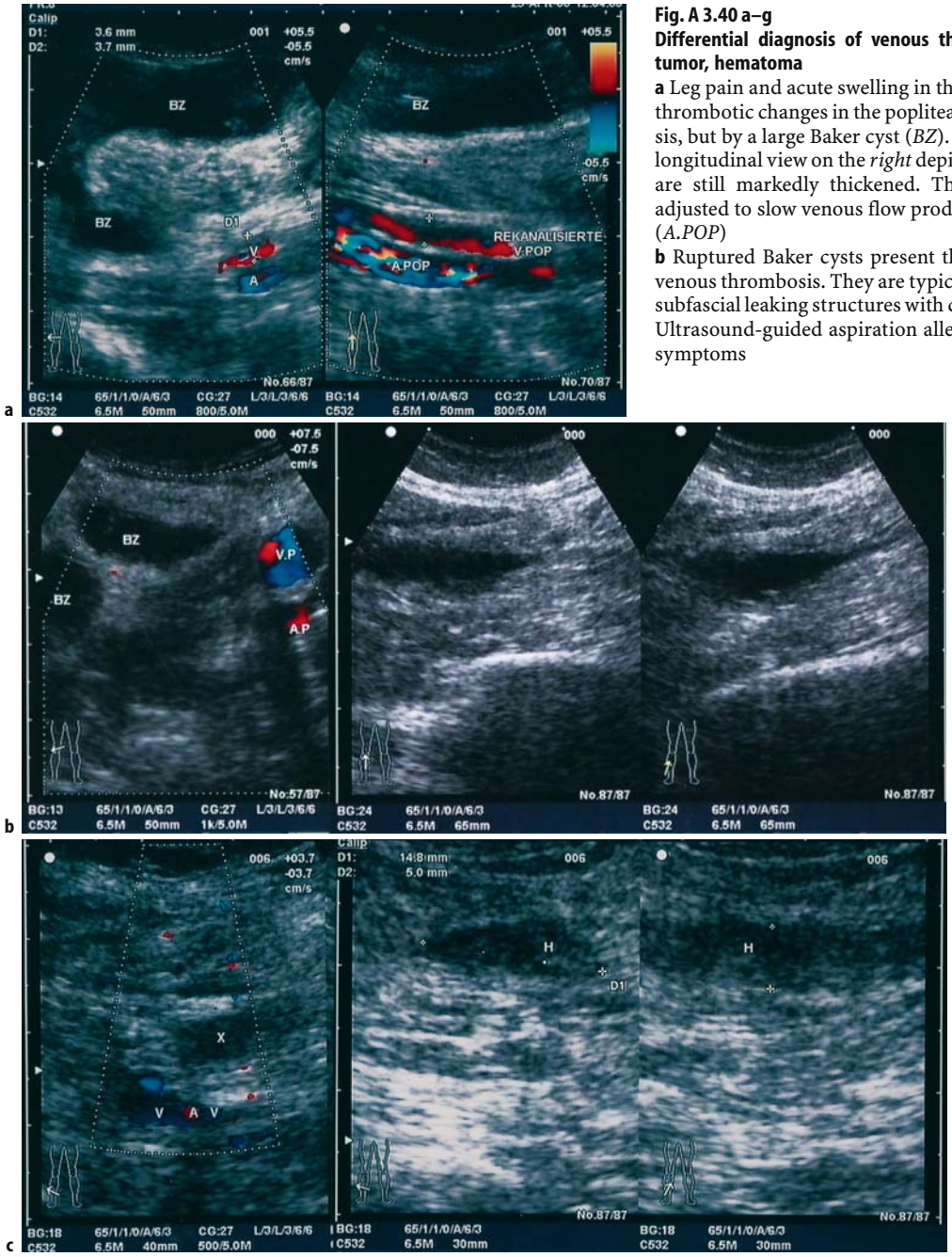

Fig. A 3.40 a–g
Differential diagnosis of venous thrombosis – Baker's cyst, soft-tissue tumor, hematoma

a Leg pain and acute swelling in this patient is not caused by the post-thrombotic changes in the popliteal vein (*V*) or by recurrent thrombosis, but by a large Baker cyst (*BZ*). The transverse view on the *left* and longitudinal view on the *right* depict the recanalized vein but the walls are still markedly thickened. The low pulse repetition frequency adjusted to slow venous flow produces aliasing in the popliteal artery (*A.POP*)

b Ruptured Baker cysts present the classical symptoms of lower leg venous thrombosis. They are typically seen as hypoechoic or anechoic subfascial leaking structures with cystic residues in the popliteal fossa. Ultrasound-guided aspiration alleviates or completely eliminates the symptoms

c Another cause of soft-tissue swelling and pain to be considered in the differential diagnosis is hematoma, caused for instance by torn muscle fibers. Behind the posterior tibial vein, a hypoechoic structure (*X*) is depicted in two planes, which explains the local tenderness. A second hematoma is seen in the scan on the *right*. It is located in the gastrocnemius muscle more distally and closer to the surface

(Fig. A 3.40 cont.)

d Compression of the popliteal vein (*V.POP*) by a sarcoma in the popliteal fossa. External compression of the vein is reflected in the Doppler waveform by a high-frequency signal (flow velocity of 90 cm/sec, absence of respiratory phasicity)

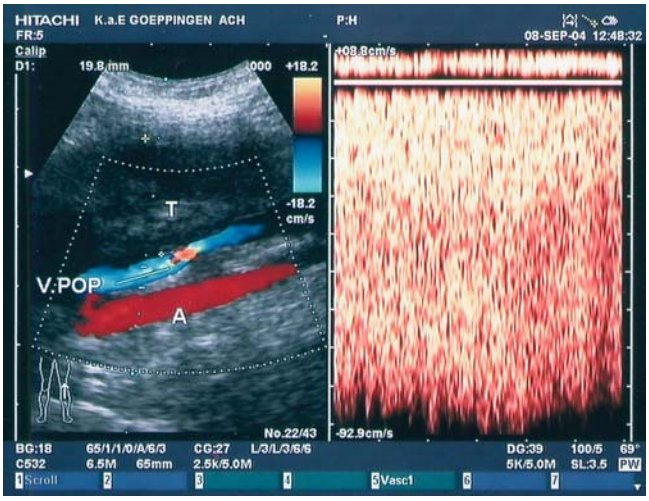

d

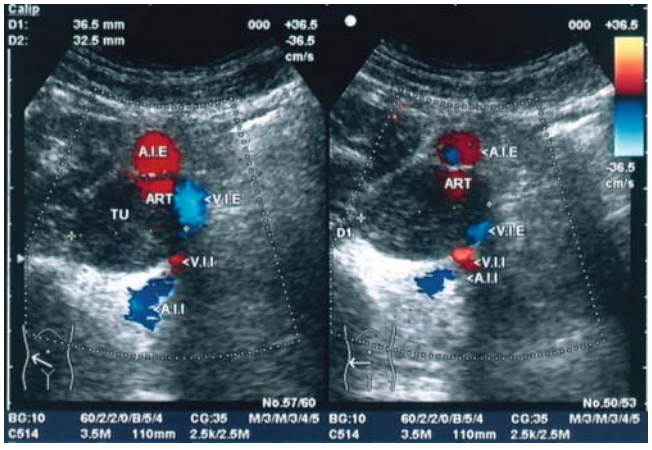

e

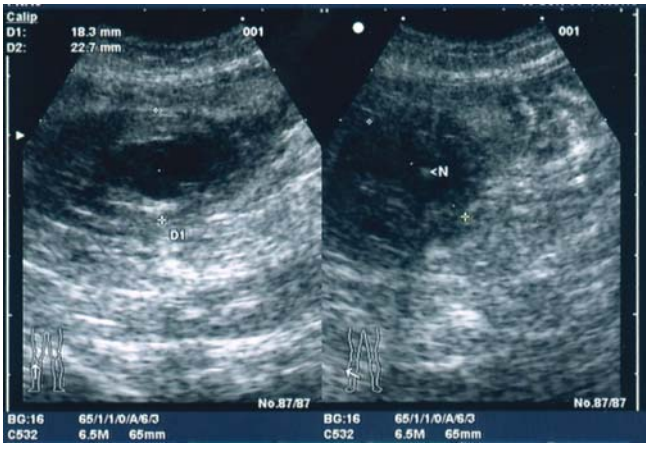

f

e Painful leg swelling caused by a tumor in the iliac bifurcation. Transverse views of the lower abdomen depict the external iliac vein (*V.I.E*, blue, flow away from transducer) and artery (*A.I.E*, red, toward transducer) anterior to the tumor and the internal iliac vein (*V.I.I*, red, toward transducer) and artery (*A.I.I*, blue, away from transducer) posterior to it. The hypoechoic tumor lies in the bifurcation and primarily compresses the external iliac vein (scan on the *right* obtained more cranially). Posterior to the external iliac artery, a mirror artifact is seen caused by the interface of high acoustic impedance

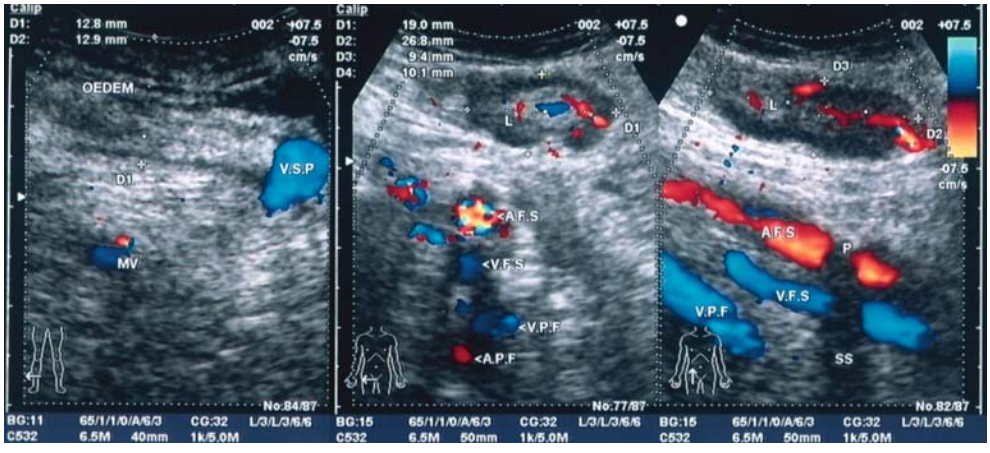

g

f An intramuscular abscess is not always associated with inflammation of the skin but may be diagnosed incidentally in patients undergoing ultrasonography for suspected venous thrombosis. It is seen on gray-scale scans as a hypoechoic, inhomogeneous structure and is confirmed by ultrasound-guided aspiration (*N* = needle tip)

Edema, lymphoma

g Another cause of leg swelling is cardiac, inflammatory, or lymphogenic edema with epifascial fluid collections in fatty or connective tissue clefts. Edema causes scattering and thus impairs evaluation of deeper subfascial areas and detection of thrombosis in the lower leg. In the case presented, there is edematous subcutaneous thickening (indicated by *plus signs*, 12 mm). The small saphenous vein (*V.S.P*) and a gastrocnemius vein (*MV*) are seen in transverse orientation

Inflammatory edema is associated with reactively enlarged lymph nodes in the groin. They are depicted as hypoechoic, inhomogeneous structures that can be differentiated from thrombophlebitis by gray-scale ultrasound in 2 planes, which will demonstrate their round shape. Color duplex scanning with a low pulse repetition frequency depicts the supply and perfusion of the lymph node. Atherosclerosis with wall irregularities and calcified plaque (*P*) with acoustic shadowing (*SS*) is seen as an accessory finding

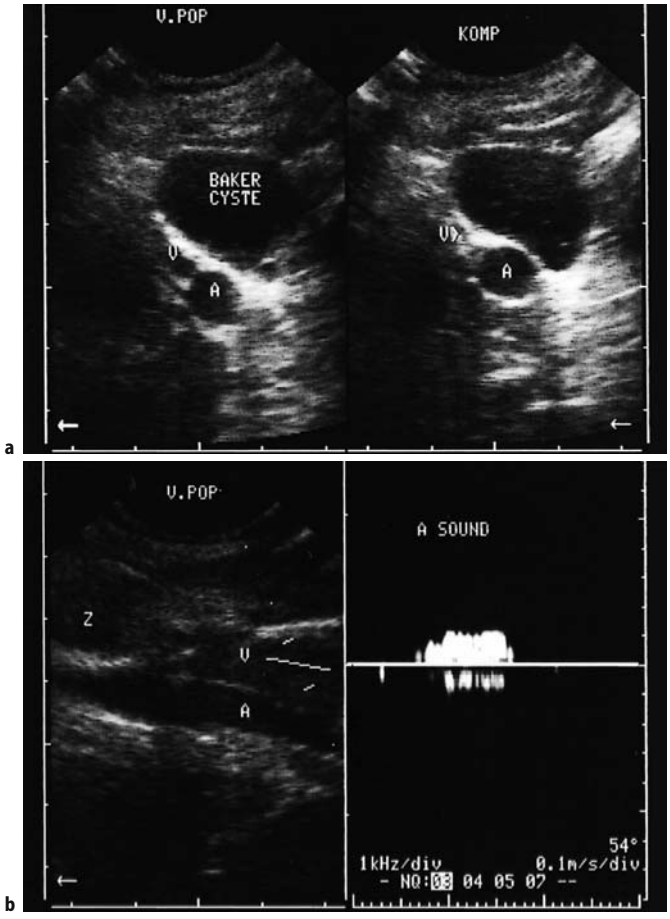

Fig. A 3.41 a, b
Vein compression by Baker's cyst
Patient with calf swelling caused by a large Baker's cyst compressing the vein. The lumen of the vein is still patent but reduced. Pressure applied with the transducer causes complete compression of the vein as seen on the transverse scan (*right*) in **a**. A month later, the cyst has increased in size, now compressing not only the vein but also displacing the artery. The Doppler waveform (**b**) shows no spontaneous flow signals but only a reduced A-sound upon strong compression of the calf muscles. The sample volume is placed in the vein (longitudinal scan); *Z* indicates the cyst

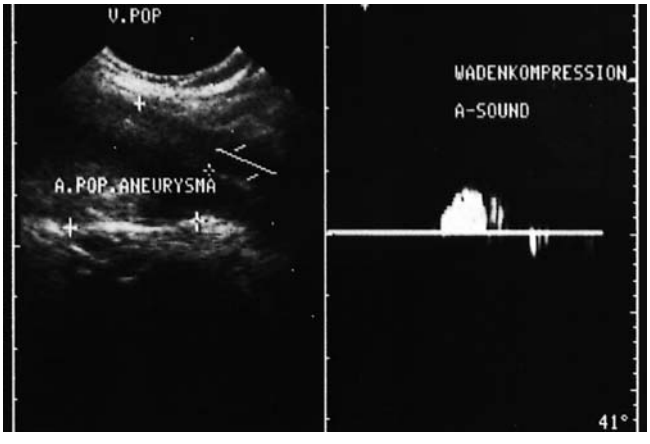

Fig. A 3.42
Vein compression by aneurysm
Swelling of the lower leg caused by proximal vein compression as a differential diagnosis of vein thrombosis. In this case the popliteal vein is compressed by an aneurysm of the popliteal artery. The Doppler waveform shows no spontaneous flow in the popliteal vein distal to the aneurysm. Calf compression only elicits a reduced signal (A-sound) due to the downstream flow obstruction. The sample volume placed in the venous lumen is shown above the popliteal artery with the *plus signs* indicating the extent of the aneurysm

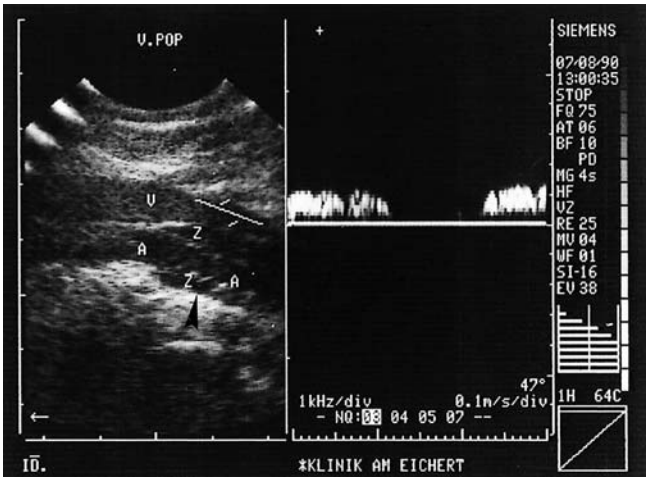

Fig. A 3.43
Venous wall impression due to adventitial cysts
Cystic adventitial disease of the popliteal artery causes indentation of the popliteal vein seen on venography and ultrasonography. The Doppler waveform shows preserved respiratory phasicity and normal flow velocity (no stenosis signal)

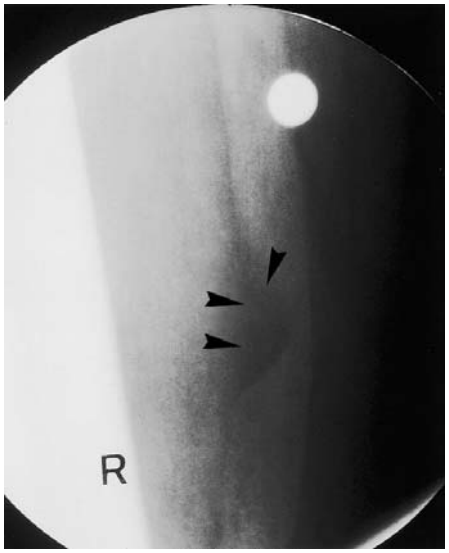

a

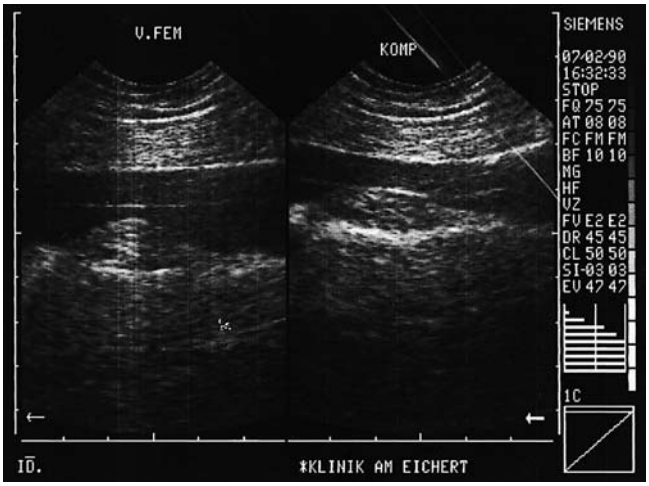

b

Fig. A 3.44 a, b
Venous wall tumor
The contrast medium filling defect in the venogram (**a**) is caused by a tumorous lesion of the venous wall depicted by ultrasound (**b**). The wall is delineated and not disrupted (longitudinal scan). Scanning from an anteromedial position depicts the artery near the transducer and adjacent to the vein, which is compressible (*KOMP, right section* in **b**). Histologic workup of the surgical specimen yields the diagnosis of a venous wall fibroma

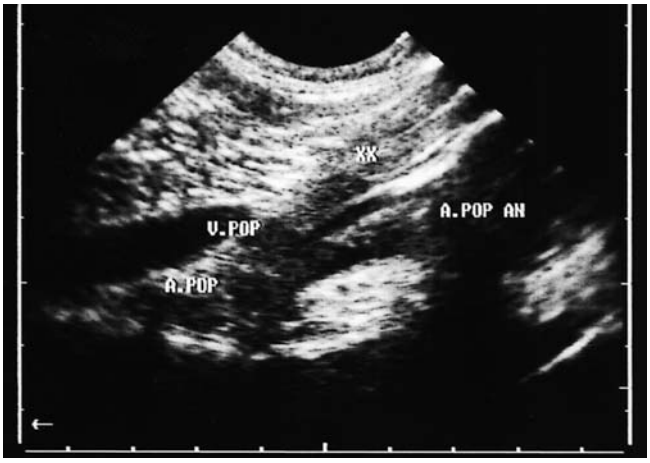

a

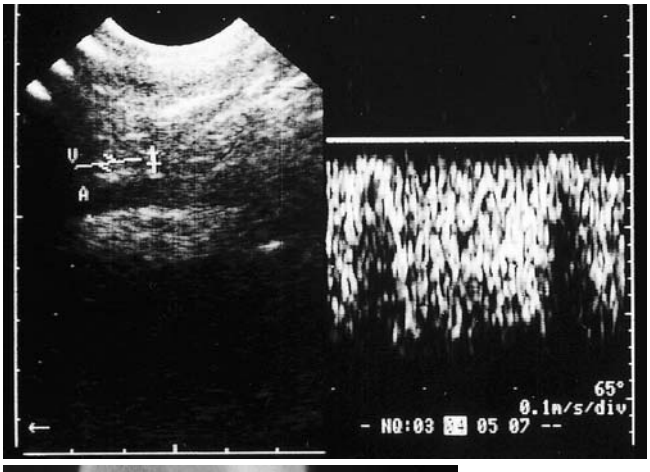

b

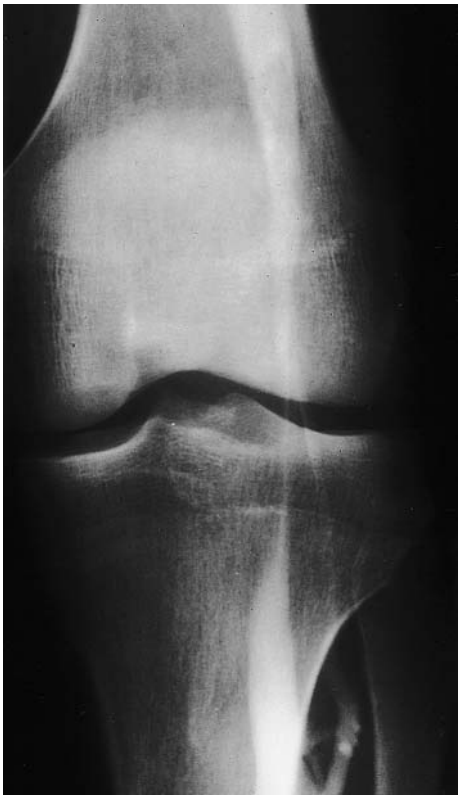

c

Fig. A 3.45 a–c

Popliteal entrapment syndrome with arterial and venous compression (Insua type II, cf. Fig. 2.10 c)

a An entrapment syndrome of the popliteal artery very rarely involves the popliteal vein as well (cf. Sect. 2.1.6.4.2). In a 45-year-old patient, malformation of the medial head of the gastrocnemius with a lateral extension (*XX*) to the lateral condyle of the femur (Insua type II) causes stenosis of the popliteal artery with poststenotic, thrombotic dilatation (*A.POP AN*). The atypical lateral gastrocnemius extension in this case also impairs venous return in the popliteal vein (*V.POP*) due to compression between the dilated artery and the lateral muscle extension (*XX*)

Popliteal entrapment syndrome with arterial and venous compression (cf. Fig. 2.10 f)

b 35-year-old athletic patient (strong calf muscles) presenting with calf swelling and exercise-induced pain. Ultrasound demonstrates compression of the popliteal vein by a hypertrophied gastrocnemius muscle with two strong heads but normal courses in the popliteal fossa

The Doppler spectrum sampled in the compressed popliteal vein with the patient lying in a relaxed position shows a stenosis signal interrupted by arterial pulsation. The vein has a lumen of 2 mm. The angle-corrected flow velocity is over 100 cm/s and respiratory variation is lost (same patient as in Fig. A 2.37 a–c)

In this patient with the rare combination of arterial and venous compression, calf swelling was caused by compression of the popliteal vein at rest and exercise-induced pain by compression of the artery during plantar flexion

c Venography: The vein appears compressed. A large popliteal artery aneurysm or a large Baker cyst may have a similar venographic appearance

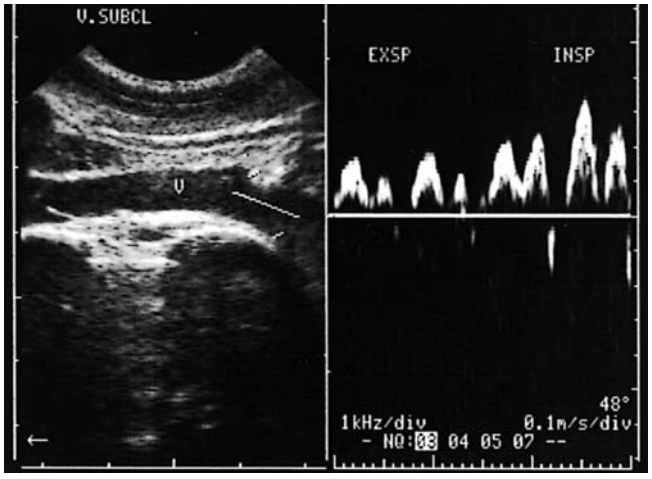

Fig. A 3.46
Axillary vein – normal findings
Junction of axillary and subclavian veins with respiratory and typical cardiac fluctuation of blood flow velocity. The B-mode scan on the *left* depicts a venous valve

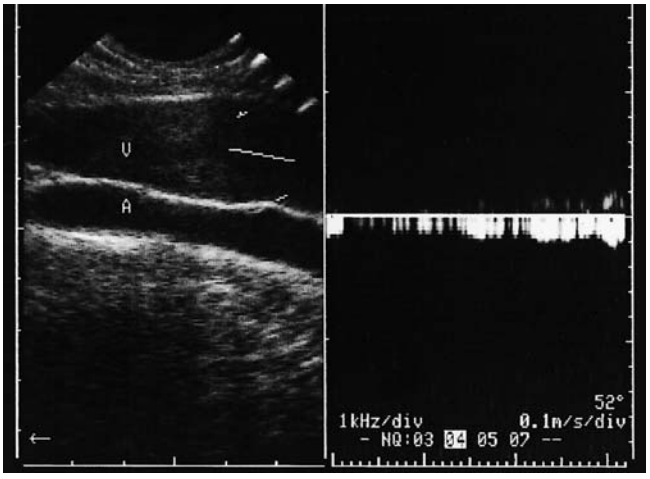

Fig. A 3.47
Obstruction of thoracic inflow
Obstruction of venous inflow in the upper thoracic aperture by a mediastinal tumor is seen on the B-mode scan as a dilatation of the veins (shown here for the jugular vein). Blood flow is slower and cardiac pulsatility is eliminated

Fig. A 3.48 a–e
Jugular vein thrombosis (central venous catheter)
a Foreign bodies in a vein (pacemaker, central venous catheter) have thrombogenic effects. In the example, the double contour indicates the central venous catheter (*KAT*) in the thrombosed jugular vein with residual flow near the wall depicted in blue on the transverse scan (*left*). The common carotid artery is seen medial to the thrombosed jugular vein (*arrowheads*; transverse scan on the *left*, longitudinal scan on the *right*). Flow in the artery is in the opposite direction. The color change from red, through black, to blue in the artery is due to the change in flow direction relative to the ultrasound beam

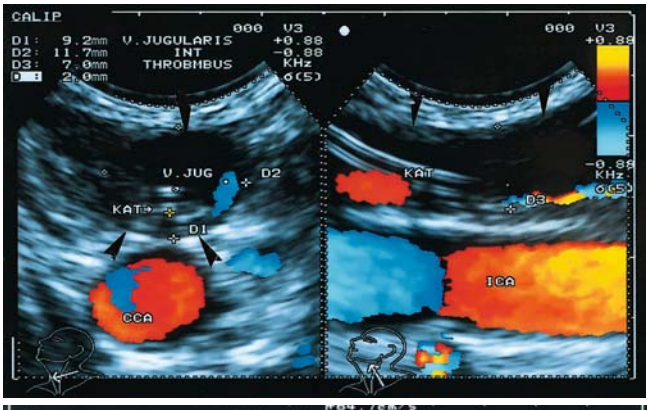

a

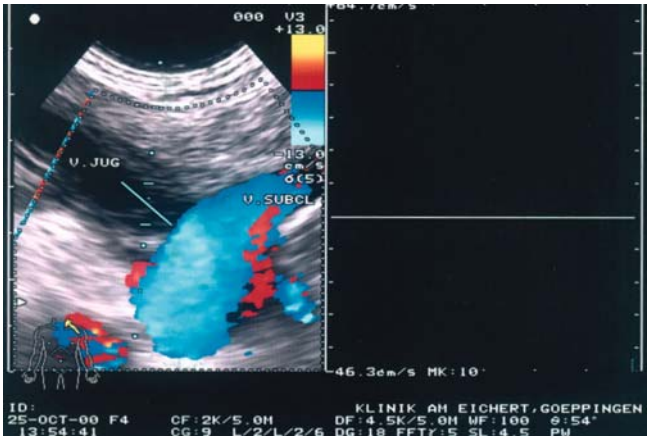

b

b Due to the thrombosis, flow signals are absent from the jugular vein scanned along its course toward the center to the level of its opening into the subclavian vein (*V.SUBCL*); the subclavian vein is patent

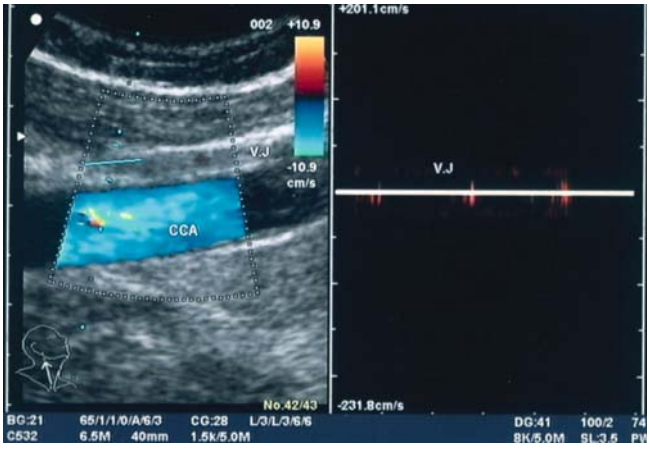

c

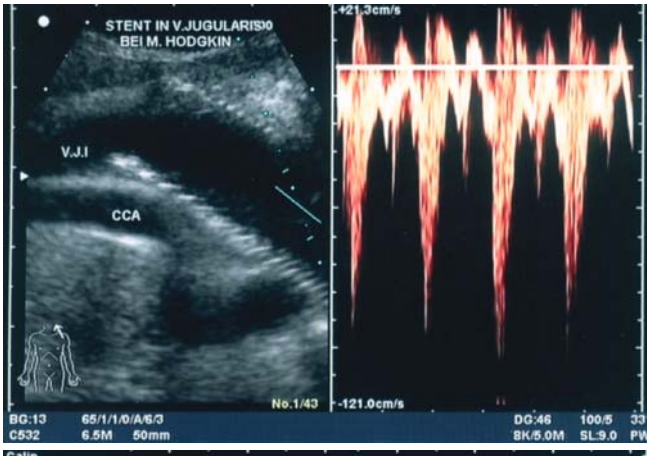

d

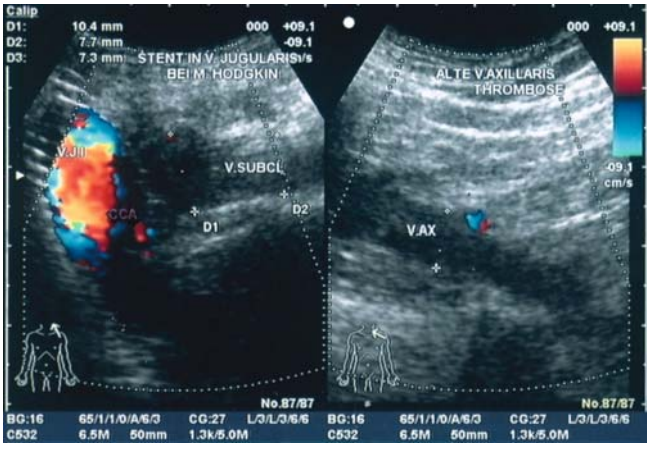

e

(Fig. A 3.48 cont.)

c In older jugular vein thrombosis, there may be partial recanalization or persistent obstruction with depiction of the vein as a connective tissue strand with a rather thin lumen adjacent to the carotid artery. An ultrasound examination of patients in whom implantation of a central venous catheter is planned can thus prevent unnecessary puncture

d The meshlike pattern indicates a stent placed to maintain patency of the jugular vein obstructed in the upper thoracic aperture by Hodgkin lymphoma

e After stenting of the compressed jugular vein (*left section*), the patient developed thrombosis of the subclavian (*V.SUBCL*) and axillary veins (*V.AX*, *right section*)

Fig. A 3.49 a–c
Axillary vein thrombosis (thrombolytic therapy)

a Hypoechoic and homogeneous thrombi in the axillary and subclavian veins with clear demarcation from the wall indicate fresh thrombosis. The vein is markedly dilated compared to the artery posterior to it. Collateral veins are depicted anteriorly

b Following 2 cycles of thrombolytic therapy with ultrahigh-dose streptokinase administration, beginning recanalization is shown by color duplex scanning. There is complete recanalization of the distal axillary vein (flow depicted in red, toward transducer). In the proximal axillary vein (scan on the *left*), there is flow along one side of the thrombus (blue, due to change in flow direction relative to transducer). A chest wall collateral is seen anteriorly. The transverse view (*middle section*) depicts a second, larger hypoechoic mural thrombus in an otherwise patent axillary vein with flow in blue. The compression test confirms a thrombus and excludes a flow phenomenon due to inadequate instrument settings (scan on the *right*; cf. Fig. 1.20). The patent lumen is collapsed and only the thrombosed, noncompressible portion is still identifiable as a hypoechoic structure. The transverse scans depict the axillary artery (*A*) posterocranially (*CL* = clavicle)

c There is full recanalization of the vein after another cycle of thrombolytic therapy. The Doppler waveform demonstrates respiratory as well as cardiac fluctuation of flow (M-shaped profile). The presence of cardiac pulsatility indicates that the thrombus was still very fresh when thrombolytic therapy was initiated; an older thrombus would have caused inflammatory changes and rigidity of the venous wall

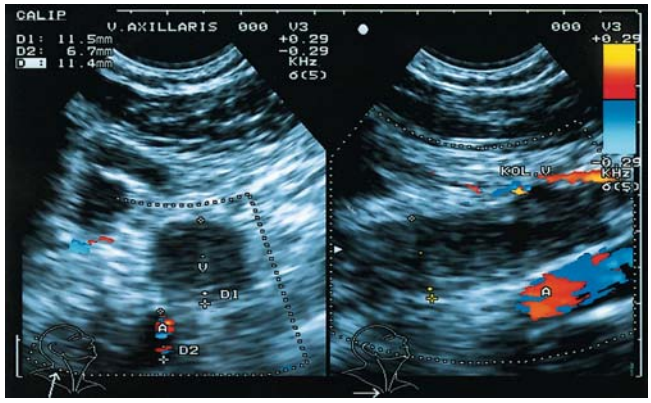

a

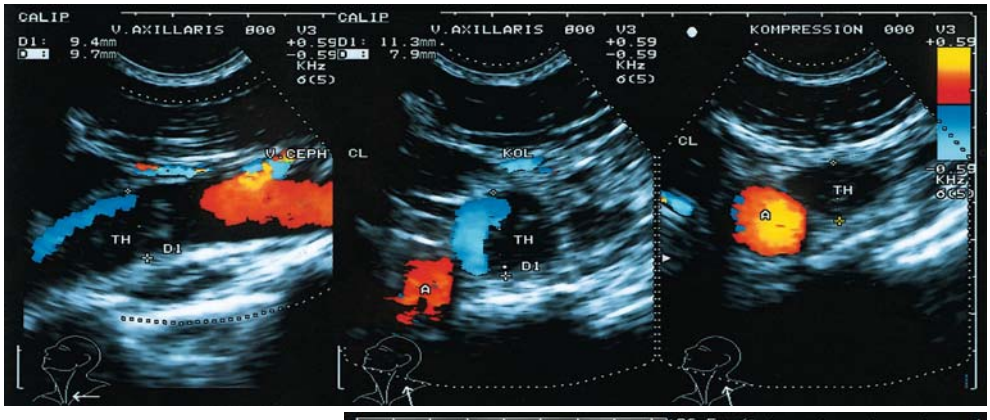

b

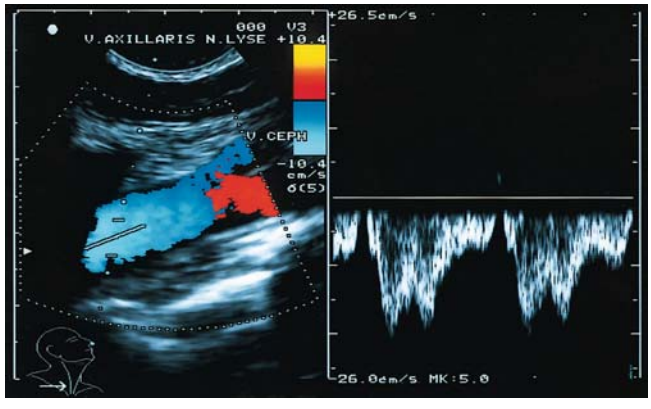

c

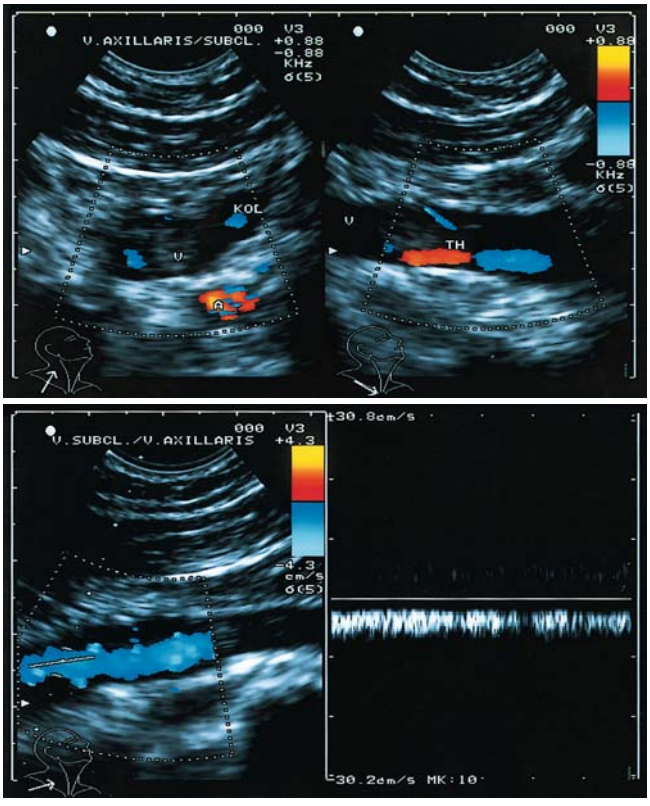

Fig. A 3.50 a, b
Recanalization

a Thrombosis of the axillary vein as in the case presented in Fig. A 3.49 a–c but 5 cycles of thrombolytic therapy are necessary before signs of recanalization are seen (transverse scan on the *left*, longitudinal scan on the *right*)

b Recanalization of the axillary vein is complete after another 3 cycles but the wall is still markedly thickened as indicated by the hypoechoic structure surrounding the patent lumen (blue). The Doppler waveform shows no cardiac variation. Postthrombotic inflammatory changes, possibly associated with thrombotic deposits, lead to rigidity of the wall. In the case shown, the thrombogenic wall lesions carry a high risk of early recurrence of thrombosis. In this patient, recurrent thrombosis of the axillary vein with occlusion was seen 2 days later despite adequate heparinization

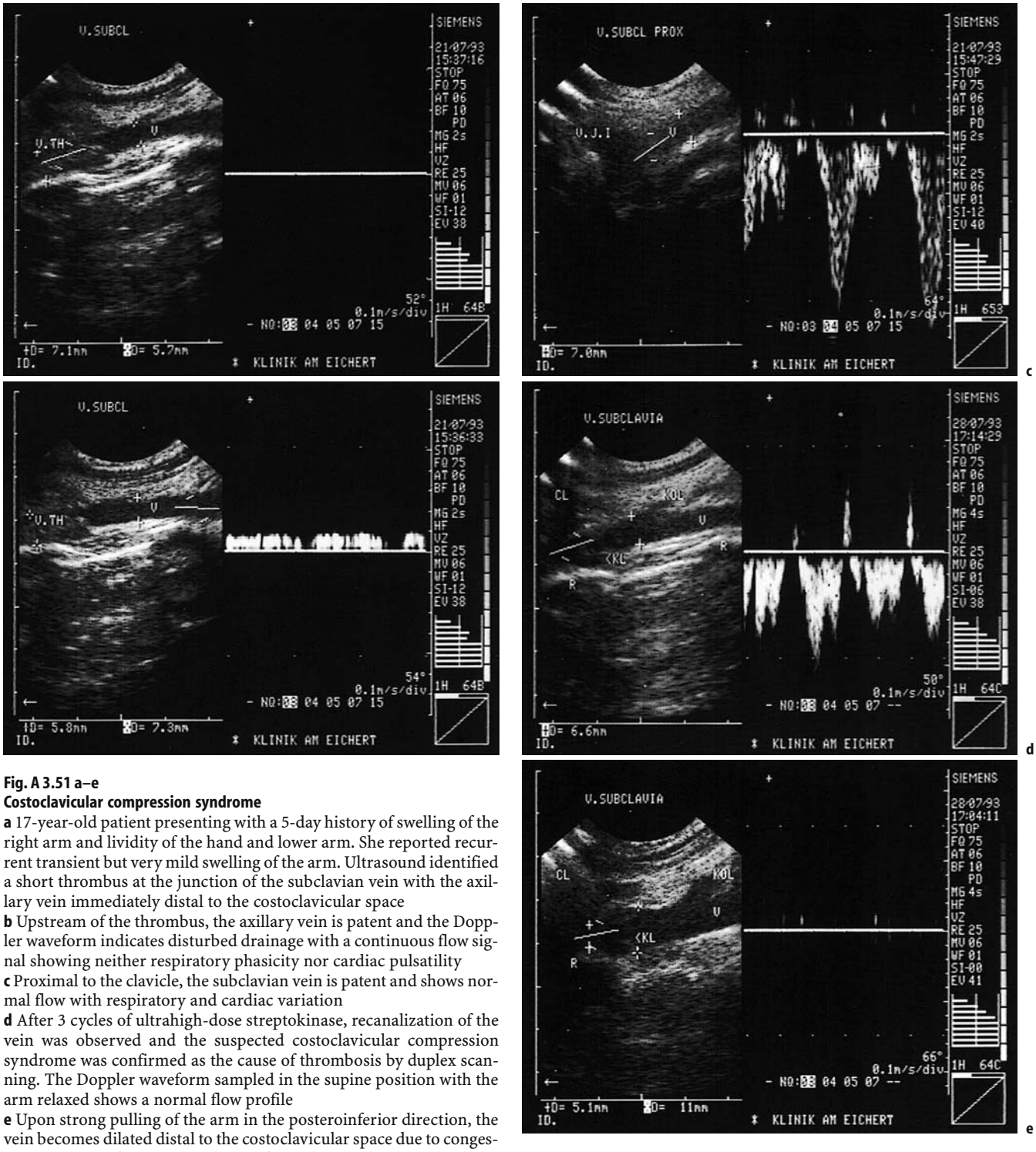

Fig. A 3.51 a–e
Costoclavicular compression syndrome
a 17-year-old patient presenting with a 5-day history of swelling of the right arm and lividity of the hand and lower arm. She reported recurrent transient but very mild swelling of the arm. Ultrasound identified a short thrombus at the junction of the subclavian vein with the axillary vein immediately distal to the costoclavicular space
b Upstream of the thrombus, the axillary vein is patent and the Doppler waveform indicates disturbed drainage with a continuous flow signal showing neither respiratory phasicity nor cardiac pulsatility
c Proximal to the clavicle, the subclavian vein is patent and shows normal flow with respiratory and cardiac variation
d After 3 cycles of ultrahigh-dose streptokinase, recanalization of the vein was observed and the suspected costoclavicular compression syndrome was confirmed as the cause of thrombosis by duplex scanning. The Doppler waveform sampled in the supine position with the arm relaxed shows a normal flow profile
e Upon strong pulling of the arm in the posteroinferior direction, the vein becomes dilated distal to the costoclavicular space due to congestion. Scanning from Mohrenheim's fossa depicts the dilated subclavian and axillary veins as well as collateral veins (*KOL*). No flow signal is detected immediately distal to the costoclavicular space, indicating compression-induced occlusion of the subclavian vein. Valves (*KL*) are seen in the dilated lumen. (*CL* = clavicle)

A Doppler frequency spectrum should be obtained to document the costoclavicular compression syndrome because the color duplex findings are difficult to quantify and are more susceptible to artifacts as a result of the maneuvers performed to induce compression

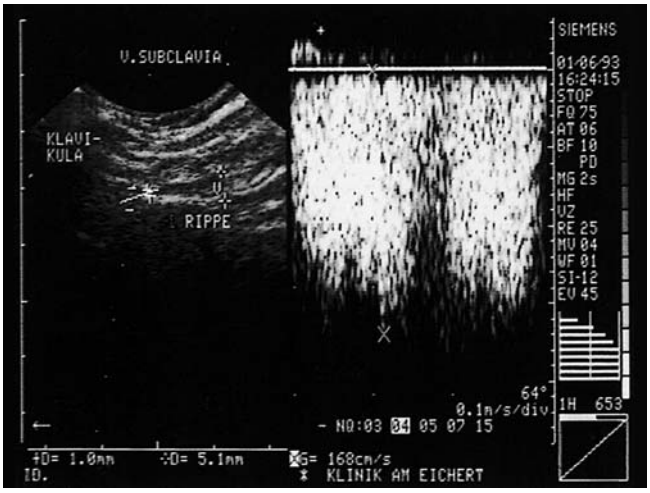

Fig. A 3.52
Costoclavicular compression syndrome
The passage of the vein through the costoclavicular space between the clavicle and the first rib is difficult to depict due to bone-induced acoustic shadowing. Scanning of the vein in this area is possible only if tangential beam orientation can be achieved in slender patients. Under these conditions, a continuous high-frequency stenosis signal will be obtained from this vein segment with increasing abduction of the arm, possibly until complete occlusion of the subclavian vein has occurred. The findings presented were obtained in a 29-year-old patient with costoclavicular compression syndrome. As in most cases of this syndrome, the subclavian artery was not compressed and showed triphasic flow in the duplex examination

In this patient, the same duplex findings could be elicited when the outwardly rotated arm was pulled in the posteroinferior direction. Extreme hyperabduction can induce compression of the subclavian vein in the costoclavicular space with demonstration of disturbed venous return in the Doppler waveform also in subjects without clinical symptoms of compression syndrome. For this reason, the hyperabduction test must be interpreted with caution. An abnormal Doppler waveform sampled while the outwardly rotated arm is being pulled posteroinferiorly is a more specific sign of the costoclavicular compression syndrome

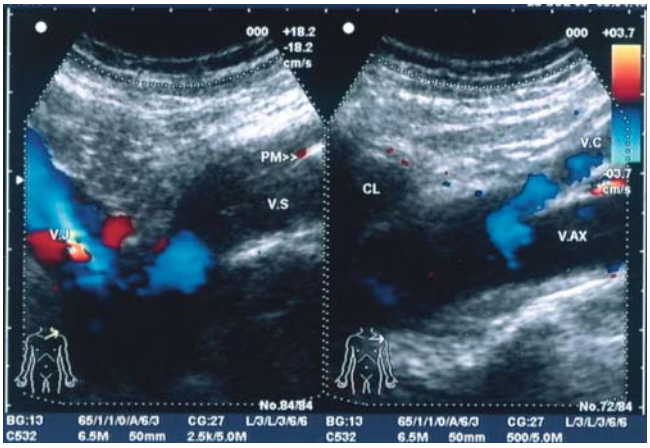

Fig. 3.53 a–e
Follow-up of subclavian vein thrombosis after pacemaker implantation
a One week after pacemaker implantation, ultrasound demonstrates thrombosis of the subclavian vein (*left section*) and of the axillary vein (*right section*). Only isolated segments of the partially thrombosed axillary vein show flow signals when scanned with a low pulse repetition frequency. The subclavian vein (*V.S*) is completely thrombosed to the level of the opening of the jugular vein (*V.J*). The pacemaker probe (*PM*) is identified by the hyperechoic double reflection in the lumen

b The Doppler waveform of the brachial vein shows the bandlike flow profile with absence of respiratory phasicity typical of upstream flow obstruction (thrombosis)

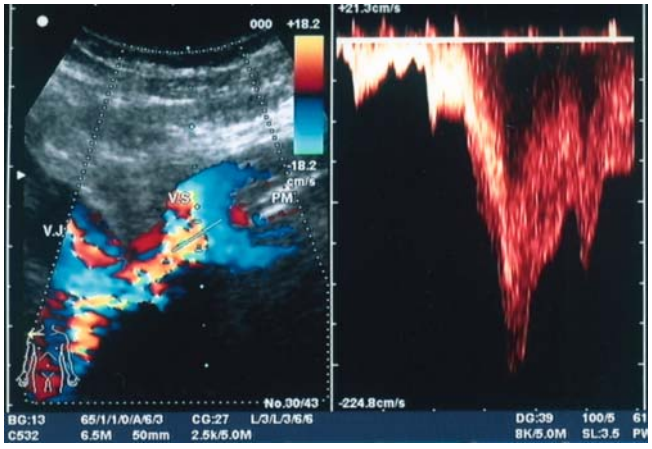

c

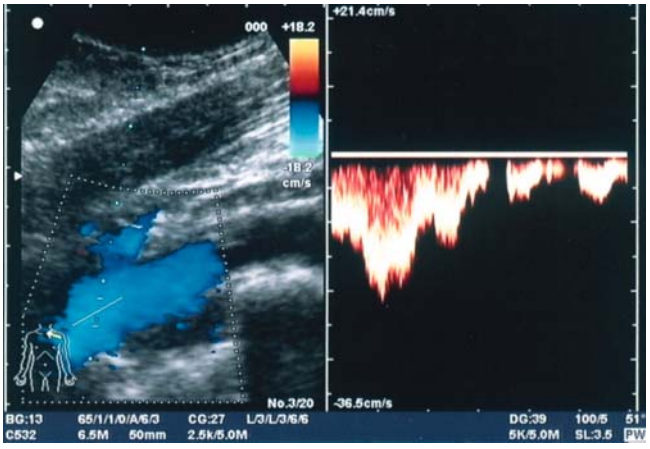

d

(Fig. A 3.53 cont.)

c After only 2 days of low-molecular heparin (weight-adjusted therapeutic dose), the patient shows surprisingly early spontaneous recanalization. Residual thrombi are only seen around the pacemaker probe (*PM*). Moreover, there is narrowing of the subclavian vein as it enters the confluence (aliasing, but without demonstration of flow obstruction in the Doppler waveform)

d The axillary vein is completely recanalized with restoration of respiratory and cardiac flow variation (no central flow obstruction)

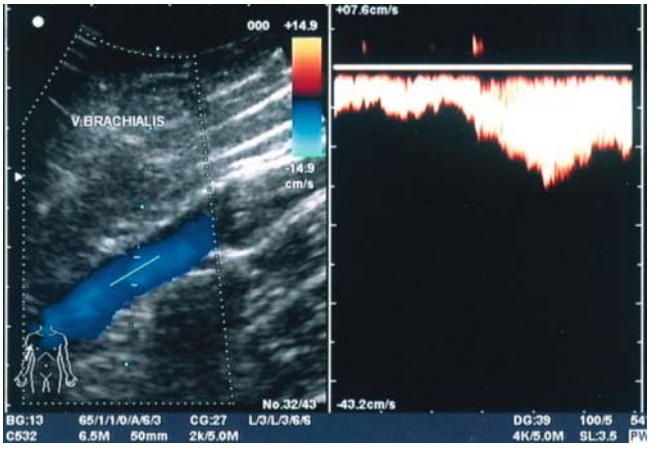

e

e The brachial vein now exhibits respiratory phasicity of flow with slight cardiac pulsatility, indicating absence of a flow obstruction (sampling at the same site as in **b**)

Fig. A 3.54
Thrombophlebitis of arm veins

The arteries serve as landmarks to distinguish the deep veins from the superficial veins, thereby enabling differentiation of thrombosis and thrombophlebitis. In the example, venous thrombosis is excluded (brachial vein with flow displayed in blue, compressible as shown on the *right*) while thrombophlebitis is confirmed (basilic vein not compressible, superficial course, no accompanying artery)

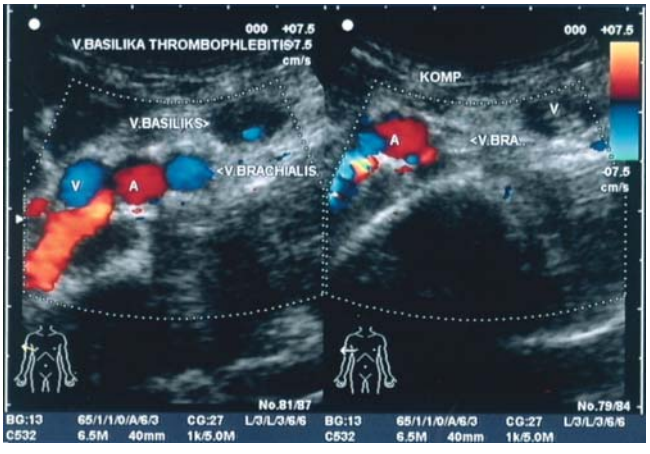

Shunts

4

4.1 Spontaneous versus Therapeutic Shunts

An arteriovenous (AV) shunt is a direct communication between an artery and a vein that bypasses the capillary bed. Such short circuits may be *congenital* or *acquired*. The latter usually develop after trauma or as complications after puncture procedures or catheter examinations (Table 4.1).

In addition, an AV fistula or shunt may be created for *therapeutic* reasons, chiefly to provide access for hemodialysis tubing or as a transient connection in the groin after thrombectomy for pelvic vein thrombosis.

The wrist or the bend of the elbow is the most suitable site for establishing a hemodialysis shunt, both in terms of surgical technique and ease of access. If the vein caliber at the wrist is inadequate, the fistula is created in the bend of the elbow between the brachial artery and the cephalic or the basilic vein. A minimum shunt volume of 300 ml/min is required for dialysis while a volume exceeding 15 – 20 % of the cardiac output may lead to cardiac insufficiency.

In cases where the vein is not adequate for creating a direct AV connection, a synthetic graft (polytetrafluoroethylene/PTFE or Gore-Tex) may be interposed. The classic AV connection for hemodialysis is the Brescia-Cimino fistula consisting of an end-to-side anastomosis between the cephalic vein and radial artery at the level of the wrist (Fig. 4.1). Synthetic shunts are established as loops from the brachial artery at the elbow to the basilic or brachial vein, most commonly as a U-shaped loop implanted subcutaneously in the lower arm. Alternatively, a shunt can be established with interposition of a straight graft between the brachial artery and the cephalic, axillary, or jugular vein (Fig. 4.2).

Table 4.1. Types of arteriovenous fistulae

Congenital AV fistula:	Direct anatomic communication between the arterial and venous system or indirect communication through bypasses in the soft tissue
Acquired AV fistula:	Iatrogenic: complication of arterial catheter examinations or renal transplant biopsy Traumatic Spontaneous
Therapeutic AV fistula:	Transient: after thrombectomy for pelvic vein thrombosis For hemodyalsis access in renal failure

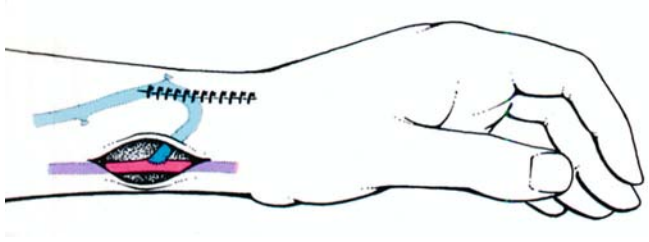

Fig. 4.1. Distal cephalic vein fistula of the lower arm: side-to-end anastomosis of the radial artery and distal cephalic vein. (From Heberer and van Dongen 1993)

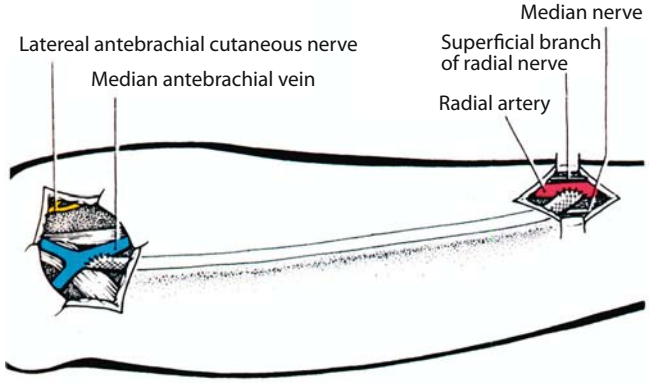

Fig. 4.2. Example of a synthetic shunt with alloplastic interposition graft. (From Heberer and van Dongen 1993)

The standard diameter of a PTFE prosthesis is 5 or 6 mm. It can be punctured for hemodialysis access immediately after implantation, as opposed to direct AV shunts, which require a maturation period of 3 to 4 weeks to undergo sufficient dilatation and wall thickening before they can be used.

Natural AV shunts have a better prognosis than synthetic implants as the latter may be affected by various functional problems requiring repeat revision (cf. Table 4.4).

Both the unphysiologically high flow rates and repeat puncture of the access vein induce intimal proliferation, frequently leading to stenosis and occlusion. Published shunt patency rates range widely, depending on the patient population, inclusion criteria, and type of shunt investigated. The patency rate reported for Brescia-Cimino shunts is 80 – 90 % after one year, 63 – 87 % after 2 years, and about 65 % after 4 years (Ahmad et al. 1998; Brittinger et al. 1966; Harnoss et al. 1991; Keller et al. 1991, 1988). In contrast, synthetic AV shunts

have patency rates of 62 – 90 % after one year, 50 – 79 % after 2 years, and about 40 % after 4 years (Haimov 1979; Munda 1983; Tellis 1979). Since the morbidity and quality of life of patients on chronic hemodialysis depend on good shunt function, the timely recognition and proper interpretation of shunt problems is an important clinical task. Noninvasive modalities such as color duplex ultrasonography are the most suitable diagnostic tests and enable early identification of the causes of a reduced flow rate through the fistula or other shunt complications and prompt initiation of adequate therapeutic measures.

Clinically, shunts are recognized by a palpable thrill and a more or less persistent high-frequency bruit that is present throughout the cardiac cycle and varies with the shunt flow.

Congenital, acquired, and therapeutic AV fistulae are distinguished:

- Congenital AV fistulae in the form of direct anatomic communications between the arterial and venous system (malformation) or as blood-conducting structures between the two systems such as aneurysmal changes or multiple short circuits in the soft tissue or bone.
- Acquired AV fistulae:
  - spontaneous fistulae without an apparent cause in the patient's history or clinical presentation,
  - traumatic,
  - iatrogenic as a complication of arterial puncture or biopsy of a parenchymal organ such as a kidney graft.
- Therapeutic AV fistulae:
  - transient AV fistula after thrombectomy for pelvic vein thrombosis,
  - for improved patency of femorocrural bypass grafts with a poor outflow tract (controversial),
  - AV fistula for hemodialysis.

Color duplex ultrasound has the following indications in the assessment of AV fistulae:

- Congenital or acquired AV fistulae:
  - demonstration of the fistula,
  - localization,
  - identification of the feeding artery and draining vein,
  - estimation of shunt flow.
- Therapeutic AV fistulae:
  - estimation of shunt flow,
  - evaluation of shunt complications:
    shunt occlusion,
    stenosis (at site of anastomosis or along course of shunt),
    stenosis of proximal artery or of shunt vein,
    peripheral ischemia (steal phenomena) in high-flow shunts and follow-up after shunt banding,
    puncture aneurysm,
    perivascular complications: abscess, hematoma.

Congenital or acquired (nontherapeutic) AV fistulae are characterized on color duplex scanning by a cloud-like mosaic of colors resulting from highly turbulent flow in the fistula and perivascular vibration. Moreover, the higher flow velocity will cause aliasing if the scan parameters are set for depicting normal venous flow.

Doppler scanning of the feeding artery shows a monophasic flow profile with a large diastolic component due to the lower peripheral resistance. The draining vein has an arterialized flow profile with pronounced turbulence.

The (color) duplex examination enables precise localization of the feeding artery and draining vein.

In therapeutically established shunts, ultrasonography enables noninvasive assessment of shunt complications and is useful for estimating shunt flow. Determination of blood flow in the feeding artery has been found to be the most reliable measure for estimating the fistula flow rate due to pronounced turbulence in the shunt or the draining vein and the variability of the shunt diameter. Based on this measurement, the fistula flow rate is determined by comparing the value measured in the feeding artery with the contralateral side or by subtracting the blood flow in the artery distal to the shunt. The volume flow rate is calculated from the mean velocity and the cross-sectional area of the vessel.

4.2 Examination Protocol, Technique, and Diagnostic Role

4.2.1 Congenital and Acquired Fistulae

Precise localization of a fistula with its feeding artery and draining vein is helpful for planning the surgical procedure.

Based on the clinical suspicion, the fistula is located by color duplex scanning and its feeding and draining vessels are identified. The transducer frequency must be adjusted to the required scanning depth. The rather high flow velocities and perivascular vibration artifacts make it necessary to use a fairly high pulse repetition frequency.

The transducer choice, patient positioning, and procedure depend on the region of the body in which the fistula is suspected clinically (palpable thrill or swelling of the affected limb due to disturbed venous return). If the color duplex mode is available, the examiner scans the area of interest to identify the typical color cloud indicating perivascular tissue vibration.

In the periphery, which typically has high-resistance flow, the feeding artery is identified by an abnormal Doppler waveform showing low-resistance flow and increased diastolic flow. Distal to the fistula, the artery resumes its normal triphasic flow profile.

An AV fistula with a hemodynamically significant shunt flow is identified by intermittent sampling of the arterial Doppler frequency spectrum in front of and behind the suspected site. Since the low peripheral resistance associated with an AV fistula leads to persistent diastolic flow in the upstream vessel segment, while the typical pulsatile and triphasic flow of extremity arteries predominates distal to the fistula, the site of the fistula is identified as the point of transition between these two arterial flow patterns. At the same time, venous return proximal to this point will show pulsatile

variation. In addition to precise localization, which is relevant for planning the surgical procedure, the shunt flow may have to be calculated as well. This is done on the basis of the diameter of the feeding artery determined in the B-mode scan and its mean flow velocity (from the angle-corrected Doppler frequency spectrum), from which its normal flow rate is subtracted. The normal flow rate is determined in the artery of the same name on the contralateral side. Veins supplied by a fistula are characterized by an arterialized flow profile.

4.2.2 Hemodialysis Shunts

In the sonographic evaluation of therapeutic AV shunts and their clinical complications, it is not the morphologic or hemodynamic changes as such that are crucial for therapeutic decision making, but rather the way in which they affect the clinical manifestation. The indication for therapy is chiefly established on the basis of the clinical problems while the most suitable therapeutic approach is selected on the basis of the findings obtained by duplex scanning or other imaging modalities (shunt PTA, creation of a new shunt, shunt revision, ligation of collateral veins, resection of aneurysm, banding of fistula, shunt closure).

The clinical query determines the extent of the sonographic examination. For instance, shunt flow must be determined in case of peripheral ischemia or cardiac insufficiency. If dialysis flow has become insufficient, the examiner must look for stenoses of the shunt artery or vein.

A *shunt of the lower arm* is best examined in the sitting patient with the elbow slightly bent and the lower arm resting on a support. The superficial course of the arm vessels enables their examination with a high-frequency transducer (7.5–10 MHz) with a linear transducer having the advantage of providing better contact to the arm. Shunts of the upper arm are examined in the supine patient with the arm comfortably positioned on a support in such a way as to ensure good accessibility of the shunt area with the transducer. A high pulse repetition frequency is necessary to depict the fast flow resulting from the high flow volume in the shunt whereas the gain must be downregulated to prevent vibration artifacts. A lower pulse repetition frequency is necessary to assess slow postocclusive flow. First, the examiner tracks the course of the fistula in transverse orientation followed by hemodynamic evaluation in the longitudinal plane with sampling of Doppler spectra in the feeding artery, the shunt vein (along the access segment) or the synthetic loop graft, and in the draining vein. Additional Doppler tracings may be obtained from the anastomotic sites. Based on the clinical query and the hemodynamic findings obtained in the shunt (flow character), the examiner then searches for the site of the abnormality by continuously scanning the course of the shunt. Due to the high shunt-related diastolic flow, the indirect criteria of arterial obstruction (monophasic flow profile) are not reliable. Therefore, in inconclusive cases, the feeding limb must be scanned continuously from the subclavian artery to the brachial or radial artery in longitudinal orientation with spectral Doppler sampling in order to detect flow acceleration as a sign of stenosis.

In patients with a Cimino shunt, the shunt veins must be followed along their course toward the center to identify dilatation or narrowing (Fig. 4.3 a–c).

To avoid the false-positive diagnosis of a stenosis due to compression of the venous limb, the transducer should be applied with very light pressure. This is achieved by bracing several fingers or the edge of the hand holding the transducer against the arm outside the course of the shunt. The transducer can thus be moved with very subtle pressure. Moreover, undue pressure is avoided by placing the transducer somewhat lateral to the apex of the vein wall and then angling it to interrogate the vein. Synthetic grafts are less susceptible to compression.

Apart from palpation, the course of a shunt is most easy to track sonographically in transverse orientation. Spectral Doppler tracings are recorded in the longitudinal plane from sites suspicious of stenosis. The known thrill in the shunt area may produce perivascular vibration and thus impair assessment. This problem can be overcome by carefully compressing the area next to the transducer with the flat hand while at the same time avoiding excessive compression of the vein. When an intricate shunt is examined, an overview of flow directions in the different venous limbs can be obtained in the color duplex mode.

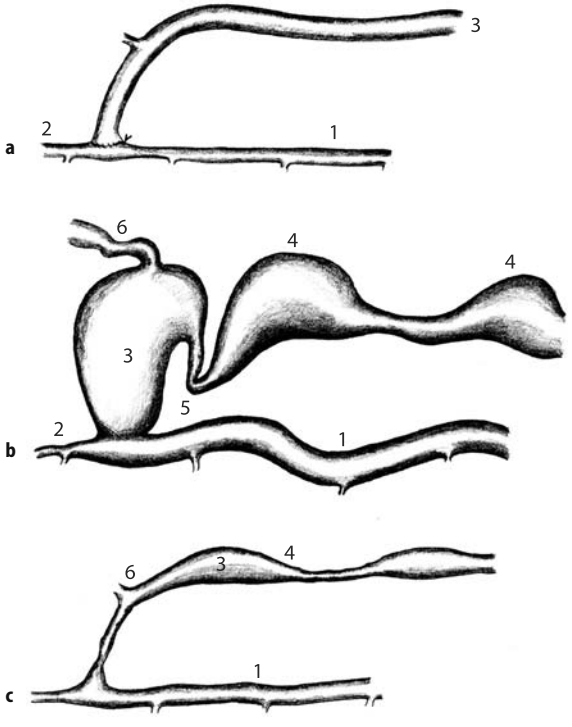

Fig. 4.3 a–c. Schematic representation of the morphologic changes of a hemodialysis shunt: **a** shortly after creation of the AV shunt, **b** dilatation, **c** stenosis (*1* feeding artery, *2* draining artery, *3* shunt vein, *4* dilatation or stricture at site of frequent venipuncture, *5* kinking-induced stenosis, *6* side branch of the shunt vein). (From Scholz 1995)

When a narrowing is encountered in the B-mode examination or color duplex scanning with adequate settings shows aliasing or perivascular vibration artifacts (mosaic-like appearance), a Doppler waveform is obtained from the respective site in the shunt in longitudinal orientation to confirm a stenosis. Artifacts caused by perivascular vibration can be avoided by slight soft-tissue compression. Proper positioning is verified in the B-mode by slightly changing the pressure exerted with the transducer. Tortuous veins are better appreciated transversely but the Doppler waveform is nevertheless recorded in longitudinal orientation.

In addition to vascular assessment, the sonographer also evaluates perivascular structures to differentiate hematoma, abscess, and shunt aneurysm on longitudinal and transverse views as well as in the color duplex mode as required.

4.3 Typical Shunt-related Changes of the Doppler Waveform

The low peripheral resistance associated with an AV short circuit leads to a monophasic flow profile with continuous systolic and diastolic flow and a fairly large diastolic flow component in the feeding artery (Table 4.2). A return to pulsatile flow in a therapeutic AV shunt indicates a low shunt volume due to disturbed venous runoff, shunt stenosis, or shunt occlusion.

Perivascular tissue vibration around the shunt primarily occurring during systole may be seen as a mosaic-like pattern. The smaller the shunt caliber and the larger the jet, the more pronounced the perivascular vibration artifacts. The turbulent flow in the shunt area is identified by a mix of colors on color duplex sonography and by pronounced spectral broadening in the Doppler waveform, possibly with additional retrograde flow components during systole.

The vein draining the shunt is dilated and, due to arterialization, shows pulsatile flow velocity changes and spectral broadening (primarily close to the fistula) due to turbulence. Vibration of the vessel wall and adjacent soft tissue in the color duplex scan can be reduced by slight manual throttling of arterial inflow, thus ensuring fairly artifact-free visualization, which is especially important when recording Doppler spectra for comparison of flow velocities before and after a suspected stenosis.

Table 4.2. Characteristics of arteriovenous fistulae on color duplex scanning

- Monophasic flow profile due to continuous systolic and diastolic flow with a large diastolic component in the feeding artery
- Pulsatile flow in the runoff vein due to arterialization
- Markedly turbulent flow in the fistula (over long stretch in hemodialysis shunts)
- Perivascular tissue vibration at site of fistula
- Dilatation of feeding artery and draining vein of hemodynamically significant fistulae after several years' use

All draining veins have arterialized flow. Lateral venous branches that divert blood away from the access vein but are unsuitable for hemodialysis access can thus be identified and ligated.

The flow changes occurring in a hemodialysis shunt that has been used for many years may lead to intricate flow patterns in arteries that are only indirectly connected to the feeding arteries through collaterals (e.g. steal phenomena, supply of a radial artery shunt by the palmar arch and ulnar artery). Evaluation of color-coded blood flow directions allows correct interpretation and identification of shunt problems (such as ischemia of the fingers, reduced shunt flow) under such complex flow conditions as well.

4.4 Determination of Flow Rate

A decreased flow through the fistula due to complications such as stenoses impairs hemodialysis function. Only high-grade shunt stenoses become functionally relevant, which, according to Kathrein (1988, 1991), is defined as a decrease in the volume flow rate below 250 ml/min. Although this would seem to be the most obvious thing to do, blood flow is not measured directly in the affected access vein because sudden changes in diameter, especially in older shunts, and changes in the lumen shape (elliptical) give rise to errors while measurement of the mean velocity within the fistula is impaired by turbulent flow (spectral broadening). For these reasons, the volume flow rate of the fistula is most reliably determined from the mean flow velocity measured in the main feeding artery (typically the brachial artery). The flow rate is determined as the mean velocity (calculated from the Doppler waveform of the feeding artery by means of the implemented software) multiplied by the cross-sectional area (cf. Sect. 1.1.2.4). The flow rates measured with different ultrasound machines may vary by up to 30 %. One reason is the use of different methods for determining the cross-sectional area (direct planimetric measurement or calculation from diameter, leading-edge method). Another is the way of determining flow velocity, which may be calculated as the mean velocity integrated over the vessel cross-section or as the median velocity. Inadequate setting of the receive gain can thus produce measurement errors. Calibration measurements to determine possible correction factors are rarely done prior to determining blood flow rates. The deviations are less relevant if follow-up measurements are performed with the same ultrasound scanner.

Grosser et al. (1991) investigated shunt flow rate measurements performed in the brachial artery, radial artery, and shunt vein and found the best reproducibility for measurements in the brachial artery. Pitfalls are the calculation of the cross-sectional areas of small arteries (blooming effect) and the determination of mean flow velocity in the presence of pronounced turbulence.

The most accurate results are obtained by calculating the difference in arterial flow rates before and after the shunt

anastomosis. Alternatively, the flow rate in the artery supplying the shunt can be determined relative to that of the contralateral artery. It should be noted, however, that the blood flow to the arm is negligible in most cases compared to the high shunt flow.

Determination of the flow rate in the shunt vein should be done in exceptional cases only as it is subject to the above-mentioned errors. However, when there is complex branching of veins, an attempt can be made to determine the functionally relevant shunt flow of the access vein. To do so, the Doppler sample volume must be placed in a fairly straight vessel segment with little turbulence and without major caliber variation.

Another indication for measuring the fistula flow rate is to evaluate the "maturity" of a newly created shunt. A shunt is considered suitable for hemodialysis over a wide range of flow rates of 300 to 1,200 ml/min.

4.5 Documentation

The documentation of findings depends on the clinical question to be answered or the type of shunt complication suspected. Individual ultrasound scans often give only a poor representation of the intricate vascular patterns that may be encountered, especially in hemodialysis patients having undergone repeat shunt revision. To facilitate follow-up evaluations, the following views should be documented in addition to the shunt complication (such as degree of stenosis):

- a longitudinal view and Doppler waveform of the feeding artery,
- a longitudinal view and Doppler waveform of the anastomotic region, and possibly
- a longitudinal view with Doppler waveform of the shunt vein.

Further documentation depends on the clinical question to be answered. Prior to shunt revision, all vessel segments involved have to be assessed and the findings documented, e.g. the axillary or jugular vein if insertion of a synthetic shunt is planned. A drawing of the vessels in the shunt area indicating the parameters determined can facilitate the documentation of complex vascular relationships for subsequent follow-up and reporting of the findings to colleagues.

4.6 Abnormal Findings (Dialysis Problems)

Poor shunt flow and inadequate dialysis have many causes with typical changes on duplex scanning. These are:

- decreased inflow due to stenosis or occlusion of the feeding arteries,
- decreased outflow due to obstruction of runoff veins (thrombi, stenoses of venous limb),
- cardiac insufficiency,
- insufficient blood flow in the access segment due to diversion of blood into venous branches,
- partial shunt thrombosis with reduction of patent lumen,
- anastomotic stenosis.

In addition, the function and prognosis of a hemodialysis fistula can be impaired by the following factors:

- shunt aneurysm (true or false),
- steal phenomena and peripheral ischemia,
- local infection, hematoma,
- difficult access due to deep or small vessels.

4.6.1 Shunt Stenosis

The clinical presentation, palpation findings, and type of problem encountered during hemodialysis (adherence of the needle – insufficient inflow; increased venous pressure – outflow obstruction) suggest the type of shunt complication and site of obstruction to be expected. Based on these clues, the suspected shunt segment is located in the color duplex mode and evaluated for the presence of stenosis by means of the Doppler frequency spectrum sampled in longitudinal orientation and analyzed using basically the same criteria as in the peripheral arteries. The direct criteria comprise local flow acceleration, turbulent flow, and perivascular vibration artifacts. Changes in the flow profile are of limited value as monophasic flow is predominant in the shunt area due to the low resistance resulting from the venous short circuit. Still, a high-grade constriction will induce an increased upstream pulsatility and decreased downstream pulsatility. Local vessel obstructions can be identified in the B-mode if a high-resolution transducer is used. Their hemodynamic significance is subsequently evaluated in the Doppler frequency spectrum. Moreover, the B-mode information enables differentiation of intramural and extramural causes of luminal narrowing. An example of an intramural process is intimal proliferation. Other obstructing lesions are local thrombotic deposits. These can be differentiated from extramural structures such as hematomas. Early intimal proliferation is seen as a hypoechoic wall deposit or a gap in the color coding. In the further course, the proliferated intima becomes inhomogeneous and may show calcifications.

Because the flow velocity is already unphysiologically high in the fistula under normal conditions, a higher cutoff value must be defined for a hemodynamically significant stenosis. A circumscribed increase in peak systolic velocity exceeding 2.5 m/s indicates a stenosis. Moreover, doubling of the peak velocity compared to the upstream velocity can serve as a criterion for stenosis in recently established shunts but not in older shunts, where it becomes unreliable due to caliber irregularities. Indirect criteria for a shunt stenosis are a triphasic flow profile in the feeding artery and a decrease in shunt flow to less than 250 ml/min (Table 4.3).

Stenoses predominantly develop in the *anastomotic area* (Kathrein 1991) or along the *access vein* (Fig. 4.4). Causes may

Table 4.3. Criteria for a significant stenosis of hemodialysis shunts. (Modified according to Trodoir et al. 1989; Kathrein 1991; Grosser et al. 1991)

- Circumscribed systolic flow velocity > 2.5 m/s
- Return to triphasic flow in the feeding artery (increased resistance)
- Fistula flow rate < 250 ml/min

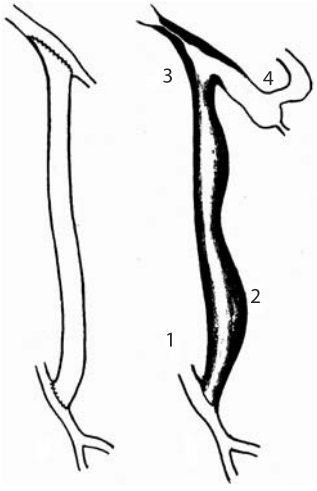

Fig. 4.4. Schematic representation of late morphologic changes in an AV shunt (*right*): stenosis at site of venous anastomosis (*3*), dilatation of access segment due to frequent puncture (*2*), dilatation of distal venous limb (*4*), stenotic changes of feeding limb due to progressive atherosclerosis (*1*). (From Scholz 1995)

be intimal hyperplasia, chiefly near valves, or puncture-induced wall dissection. The costoclavicular space representing no flow obstruction under normal conditions may become hemodynamically significant in hemodialysis patients due to the abnormally high venous flow.

Shunt stenoses are mainly caused by intimal proliferation beginning 4–8 weeks after creation of a shunt but showing wide interindividual variation in further progression. Intimal proliferation may be induced by turbulent flow at the anastomotic sites and puncture-induced intimal damage as well as increased wall pressure due to the unphysiologically high shunt flow. Shearing forces lead to chronic injury, which in turn triggers repair processes with stimulation of smooth muscle cells.

An outflow obstacle is identified indirectly by an increased pulsatility in the upstream vessel segment or even re-establishment of triphasic flow in high-grade stenosis or shunt occlusion. Therefore, a high-resistance waveform obtained in a feeding artery or in the shunt vein near the anastomosis is diagnostic of a relevant outflow obstacle in the further course of the vessel.

Shunt thrombosis may lead to a partial lumen reduction or complete occlusion and is caused by pre-existing stenoses, puncture complications (dissection, wall hematoma), shunt infections, or local compression, especially in patients with episodes of hypovolemia or hypotension.

When no stenosis has been detected at the anastomotic site or in the shunt vein to explain the decreased shunt flow, the search must be continued proximally along the *shunt artery* (axillary artery), which is susceptible to atherosclerosis after many years of hemodialysis. Also, a central stenosis of the shunt vein must be excluded. Since all vessels communicating with the fistula have a monophasic flow profile, the latter cannot serve as a criterion for stenosis. The same holds true for turbulent flow. Therefore, *flow acceleration* is the only direct criterion for shunt stenosis but an absolute threshold is difficult to define due to the wide variation that exists in flow velocities within a shunt. However, a significant shunt stenosis is suggested if there is abrupt doubling of peak systolic velocity in a circumscribed shunt segment. Trodoir et al. (1989), comparing digital subtraction angiography and duplex scanning, identified a peak systolic velocity of over 2.5 m/s as the most reliable indicator of a stenosis.

While stenoses in the course of a hemodialysis fistula, the upper arm, and in the subclavicular axillary vessels can be identified directly, one has to rely on indirect signs (turbulence, reduced pulsatility) to identify central stenoses (proximal subclavian artery).

4.6.2 Peripheral Ischemia

The creation of an AV fistula may lead to critical hypoperfusion of the hand, in particular in patients with pre-existing arterial occlusive disease or in diabetics with macro- and microangiopathic medial sclerosis and stenoses. In addition to the blood drained through the low-resistance shunt, blood may be diverted from the arteries supplying the lower arm and the hand (steal phenomena). A pronounced steal syndrome may lead to retrograde flow from the vessels supplying the hand or an increased flow in the ulnar artery if the fistula is supplied by the arteries of the palmar arch. Hypoperfusion of the fingers or even of the whole hand may ensue. The risk of ischemia in the fingers or the hand increases with the severity of arterial occlusive disease and the magnitude of shunt flow.

A drop in peripheral perfusion pressure below the critical threshold with pain and vital risks to finger areas is dependent on several factors (Fig. 4.5):

- systemic blood pressure,
- atherosclerosis of peripheral arteries (micro- and macroangiopathy) with an increase in outflow resistance distal to the shunt,
- peripheral resistance distal to the shunt,
- collateralization around the shunt,
- width of anastomosis,
- steal phenomena,
- venous outflow resistance downstream of the shunt,
- reduced inflow through stenosis upstream of the shunt.

Macroangiopathic causes of ischemia of the shunt-bearing arm or excessive shunt flow can be diagnosed by duplex scan-

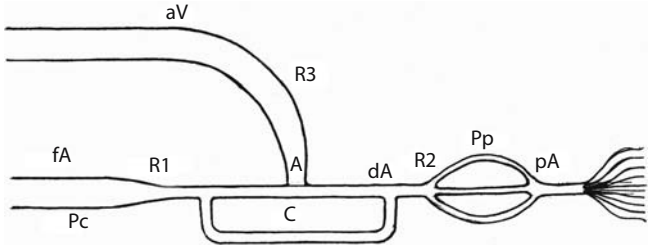

Fig. 4.5. Schematic representation of the factors affecting peripheral perfusion after creation of an AV shunt (*fA* feeding artery, *Pc* central arterial pressure, *dA* draining artery, *Pp* peripheral arterial perfusion pressure, *pA* peripheral arteries, R_1 resistance of feeding artery, R_2 resistance of peripheral vessels, R_3 total resistance of anastomosed vessel, *A* anastomosis, *aV* anastomosed vessel, *C* collateral. (From Scholz 1995)

ning. Based on the sonographic findings, the following therapeutic measures can be initiated: reduction of flow rate (banding, purse-string suture), elimination of hemodynamically significant stenoses, or creation of a new AV fistula at an appropriate level as identified by ultrasound.

4.6.3 Shunt Aneurysm

Shunt occlusion or aneurysm can be diagnosed clinically in the superficially located hemodialysis shunts. Duplex ultrasonography may be performed to confirm the clinical diagnosis and to identify the origin and extent of an aneurysm (suture aneurysm, puncture aneurysm) for planning the therapeutic procedure.

A false aneurysm is a typical puncture complication that develops as a result of blood escaping into a subcutaneous hollow space. A subtype is suture aneurysm, which is especially common after infection. Color duplex ultrasound identifies a false aneurysm as a perivascular space with pulsatile flow.

True shunt aneurysms are localized outpouchings that develop on the basis of degenerative changes of the shunt wall. They are defined as circumscribed increases in diameter to over 15 mm or to twice that of the preceding shunt segment. Aneurysms are differentiated from mere dilatations caused by turbulent flow and an increased wall pressure due to arterialization of the access vein. Such dilatations may extend over long segments of the vein if a hemodialysis access has been used for many years (cf. Fig. 4.3 a–c).

4.6.4 Excessive Shunt Flow

Shunt flow rates of over 1,500 – 2,000 ml/min chiefly occur in proximal shunts (bend of the elbow) if the cephalic vein is dilated and the anastomosis is too wide. Such high flow rates may lead to decompensation of compensated cardiac insufficiency or pre-existing cardiac damage. These complications

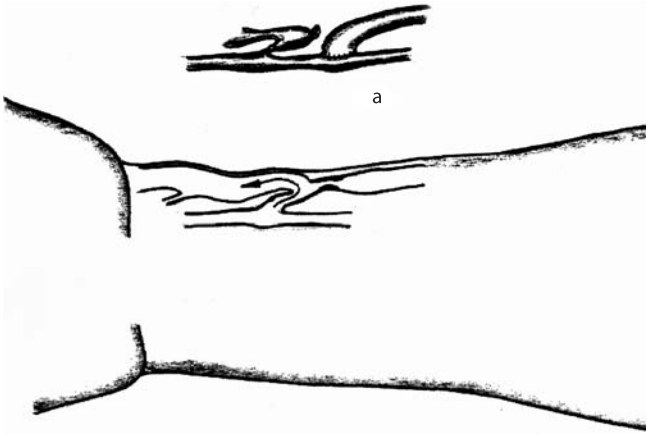

Fig. 4.6. Retrograde arterialization via backward supply of a lateral branch with reduction of the shunt flow: ligation of the branch after sonographic identification. (According to Scholz 1995)

can be avoided in cases with suspected excessive shunt flow rates (hemodialysis device) by measuring blood flow, for which duplex sonography is the most reliable procedure.

As shunt flow rates vary widely, a range of 300 to 1,200 ml/min is considered suitable for hemodialysis. Rates exceeding 1,600 ml/min (Grosser et al. 1991) or 20 % of the cardiac output are associated with the risk of cardiac insufficiency or ischemia distal to the shunt. Calculation of the shunt flow after banding serves to assess the blood flow reduction achieved by this measure.

Most shunt stenoses become functionally significant only when they are associated with high-grade narrowing, which is the case if the shunt flow rate decreases to less than 250 ml/min (Kathrein 1988, 1991). The most accurate method for determining the shunt volume is to calculate the difference in flow rates of the feeding artery upstream and downstream of the shunt. A simpler alternative is to compare the flow rates of the brachial arteries in the shunt-bearing arm and in the contralateral arm.

Central venous obstruction with impaired venous runoff can lead to swelling of the arm, especially when there is poor collateralization and shunt flow is high. The site of the obstruction is identified by duplex scanning of the axillary and subclavian veins.

A low shunt flow not caused by a stenosis may be due to drainage of blood through collateral veins coursing parallel to the access vein. Such veins can be identified by ultrasound and labeled for ligation (Fig. 4.6).

4.7 Diagnostic Role of Duplex Ultrasound Compared with other Modalities

Gray-scale ultrasound demonstrates perivascular changes (hematoma, abscess) and morphologic changes of a hemodialysis shunt (dilatation, aneurysm, strictures, thrombosis). (Color) duplex scanning provides quantitative information

Clinical problem	Possible cause	Diagnostic role of duplex scanning
Inadequate flow during dialysis (< 200 – 300 ml/min) but dialysis may still be possible (cf. Fig. A 4.6 and 4.7)	Stenosis of the artery Stenosis of the anastomosis Stenosis of the shunt vein Puncture of lateral vein instead of main access vein (branching shunt)	+++ +++ +++ +
No or little flow (< 100 ml/min) during dialysis (cf. Fig. A 4.13)	As above or occlusion	+++
Access vein difficult or impossible to palpate/auscultate	Occlusion	+++
Increased venous outflow pressure (> 150 mm Hg at maximum pump speed) (cf. Fig. A 4.11)	Proximal venous stenosis/occlusion	+++
Cardiac insufficiency and/or steal syndrome (cf. Fig. A 4.4)	Excessive fistula flow	++
Local swelling	Hematoma Aneurysm (cf. Fig. A 4.5) Abscess	+++ +++ +++
Swelling of arm	Relative proximal stenosis of vein due to excessive fistula flow	++
Reddening, fever, pain	Shunt infection	++
Ischemia distal to the shunt (cf. Fig. A 4.8)	Microangiopathy Excessive fistula flow Arterial occlusive disease	– ++ ++
Insufficient dialysis despite adequate flow	Proximal stenosis with circulation of partially dialyzed blood into peripheral veins	+

Table 4.4. Important clinical dialysis access problems, possible causes, and diagnostic role of duplex scanning (the more plus signs given, the better the rating for identifying the cause). (Modified according to Wolf and Fobbe 1993)

on shunt flow and enables identification of stenoses in the shunt and the upstream artery. Ultrasonography thus allows a more comprehensive evaluation of possible shunt complications and their differential diagnosis than the mere visualization of vascular morphology by angiography. Angiography, on the other hand, has the advantage of providing a better overview of the vascular anatomy around a shunt although evaluation of complex vascular patterns may be impaired due to overlying vessels. Abnormal findings such as a stenosis, extent of dilatation, or venous short circuits demonstrated by ultrasound can be directly marked on the skin for surgical management. Ultrasound has a sensitivity and specificity of 91 – 98 % in identifying stenoses of the shunt artery and vein compared to angiography. The early identification of shunt problems and complications (Table 4.4) enables timely and specific operative or interventional management, thereby improving the prognosis, function, and long-term patency of a hemodialysis access.

4.8 Atlas

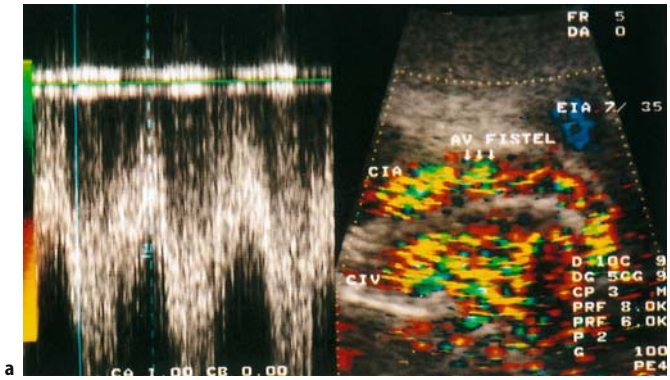

a

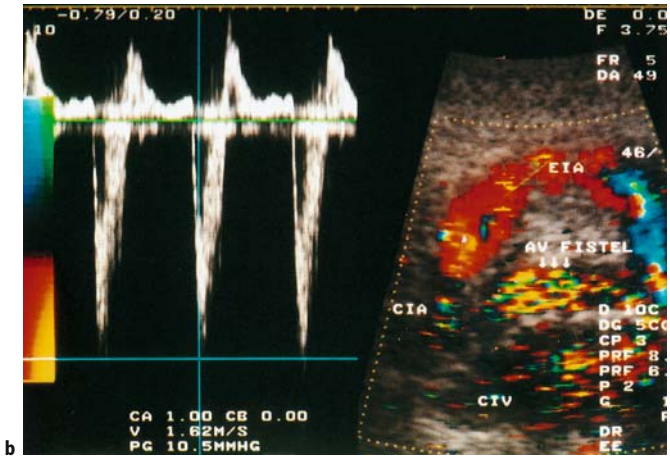

b

b Unlike the internal iliac artery supplying the fistula, the external iliac artery (*EIA*) shows pulsatile, triphasic flow on color duplex and in the Doppler waveform. Repeatedly recording Doppler frequency spectra along the internal iliac artery and vein, the examiner can gradually approach the site of the fistula, which is identified by an abrupt increase in peak systolic and especially diastolic velocities

Fig. A 4.1 a–c
Spontaneous AV fistula
a Ultrasound examination to exclude thrombosis in a patient with leg swelling. Scanning of the pelvic veins shows pronounced perivascular vibration in the left lower abdomen (typical appearance of an AV fistula). There is highly turbulent flow in the feeding common iliac artery (*CIA*) and in the internal iliac artery with the Doppler frequency spectrum sampled in the internal iliac artery near the fistula showing the high diastolic flow typical of a fistula. The arched internal iliac artery is depicted with turbulent flow to the level of the fistula (mosaic-like color clouds). Turbulent flow is also depicted in the common iliac vein (*CIV*) posterior to it. The elongated external iliac artery (*EIA*) is seen anteriorly

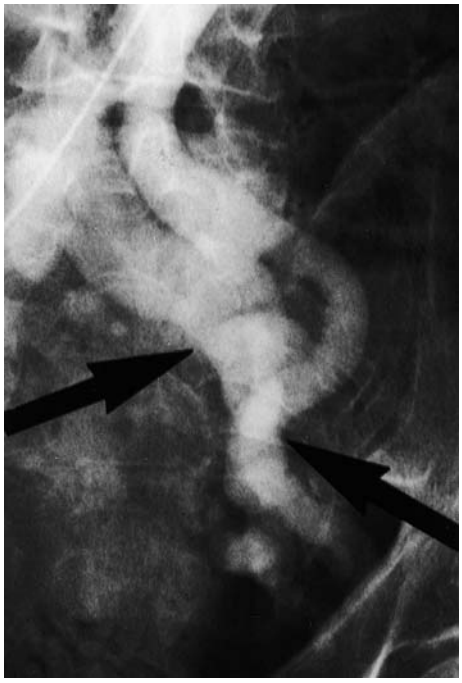

c

c The contrast medium flow in angiography demonstrates the AV short circuit in the pelvis. Ultrasonography is superior to angiography in precisely localizing the fistula. The *arrows* indicate the iliac artery and vein

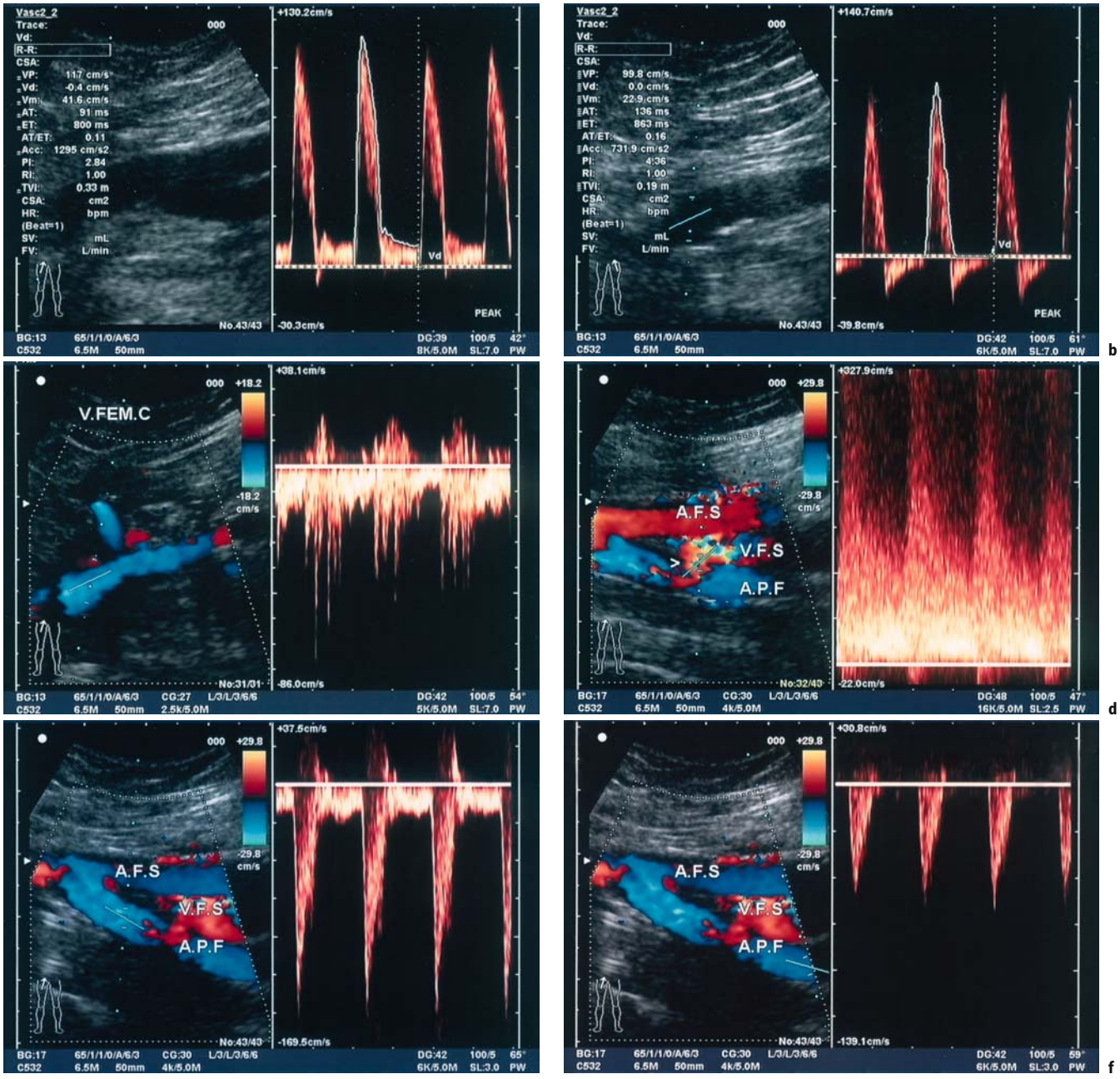

Fig. A 4.2 a–f
Arteriovenous fistula (iatrogenic)

a There is continuous diastolic flow in the common femoral artery on the right compared to the contralateral side. The peak velocity is 117 cm/s during systole and 10 cm/s at end-diastole with a mean flow velocity of 47.6 cm/s

b Comparison with the unaffected side shows flow in the left common femoral artery to be triphasic with a peak systolic velocity of 99.8 cm/s and a mean peak velocity of 22.9 cm/s. The common femoral artery diameter is the same on both sides

c The common femoral vein on the right has a pulsatile flow profile (with flow toward the center displayed in blue) as a sign of its serving as the draining limb of an AV fistula

d As illustrated by the case presented, a iatrogenic AV fistula (as a complication of cardiac catheterization) nearly always develops between the superficial femoral vein and the profunda femoris artery. This complication typically occurs when the access site in the groin is chosen too low. The search for the fistula reveals a connection extending from the profunda femoris artery (*A.P.F*; blue flow away from transducer) to the superficial femoral vein (*V.F.S*) with a high-frequency flow signal (aliasing, red) and a flow velocity of over 3.5 m/s in the Doppler frequency spectrum. Anteriorly, the superficial femoral artery is depicted (*A.F.S*; red, toward transducer)

e The Doppler frequency spectrum sampled cranial to the AV fistula in the profunda femoris artery (*A.P.F*) shows a large diastolic flow component and the same flow profile as the common femoral artery

f Distal to the AV fistula (cf. **d**), the profunda femoris artery (*A.P.F*; coded in blue) shows a triphasic profile without end-diastolic flow. This change in flow profiles proves that the AV fistula is located between the two sampling sites (in **e** and **f**)

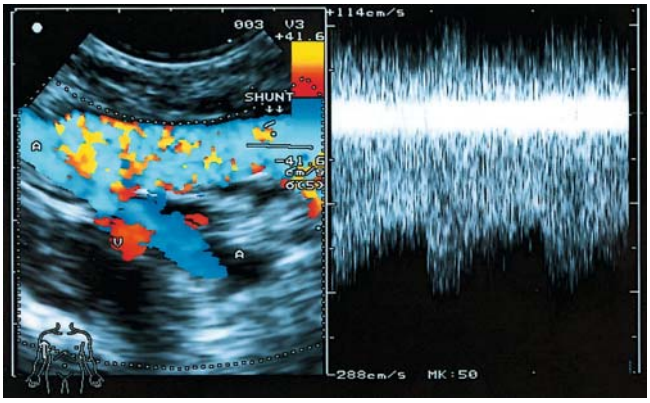

a

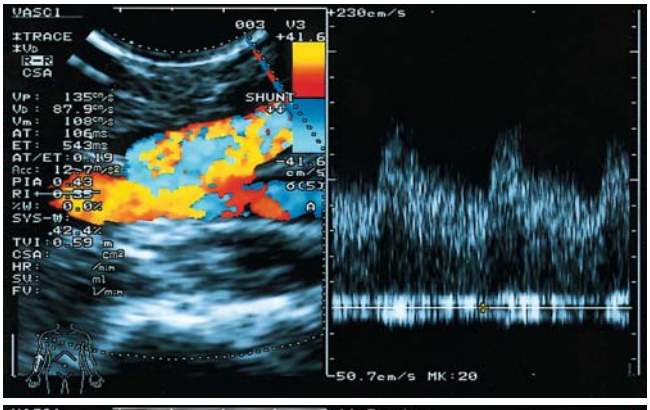

b

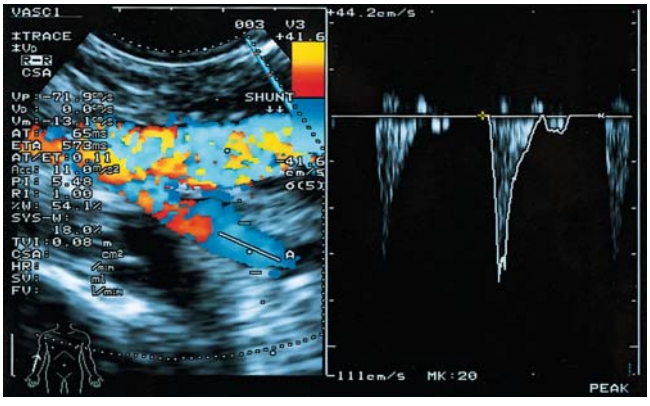

c

Fig. A 4.3 a–c
Hemodialysis access – flow measurement
a Oblique view of the anastomosis of a Cimino shunt (end-of-vein-to-side-of-artery anastomosis) in the bend of the elbow with marked turbulence at the anastomotic site. Stretched brachial artery coursing posterior to the anastomosis
b The color scan (*left section*) shows the brachial artery with flow in the cranial direction coded in red and mild aliasing on the *left* and the distal brachial artery on the *right* (coded blue). The sharp transition from red to blue appears to indicate flow reversal but is due to a change in flow direction relative to the transducer. The faster blood flow in the feeding artery is indicated by the lighter color

The Doppler frequency spectrum sampled from the feeding artery (*right section*) shows shunt flow with a large diastolic flow component (peak end-diastolic flow velocity of 95 cm/s). With a calculated mean flow velocity of 108 cm/s and a diameter of the brachial artery of 4.8 mm, a flow rate of 1,170 ml/min is calculated for the feeding artery

Flow measurement before and after shunt
c The continuation of the brachial artery distal to the shunt has the triphasic flow profile without an end-diastolic component typical of arm arteries. The flow rate calculated for the vessel segment immediately after the shunt origin is 129 ml/min (0.16 cm^2 x 60 x 13 cm/s). The flow rate of the shunt calculated as the difference in flow in the brachial artery before and after the shunt origin is 1,040 ml/min

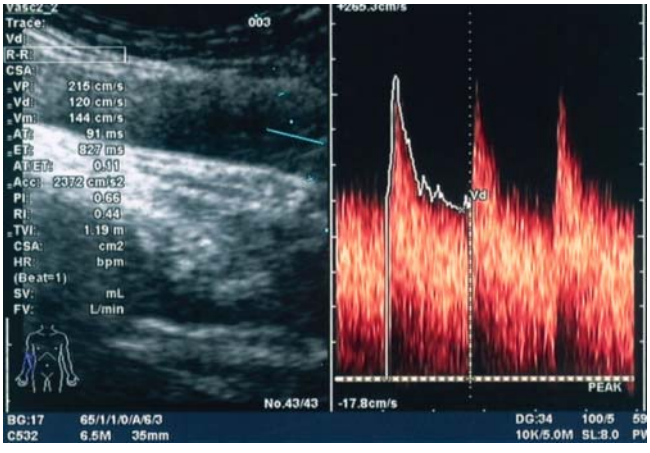

a

Fig. A 4.4 a–d
Complications of hemodialysis access – flow measurement in both arms
Excessive shunt flow can lead to steal phenomena or cardiac insufficiency with subsequent ischemia of the hand. Since hemodialysis patients often have considerable comorbidity, the shunt must be examined as a possible cause of newly occurring signs of cardiac insufficiency. Duplex ultrasound is the simplest and most reliable method for measuring shunt flow. As an alternative to the method presented in Fig. A 4.3 c, flow in the brachial artery is determined on both sides and the shunt flow calculated as the difference between the shunt-bearing arm and the non-shunt-bearing arm
a Mean flow velocity is calculated with the integrated software from the Doppler frequency spectrum that should be sampled with an angle of less than 60° (here: 144 cm/s)

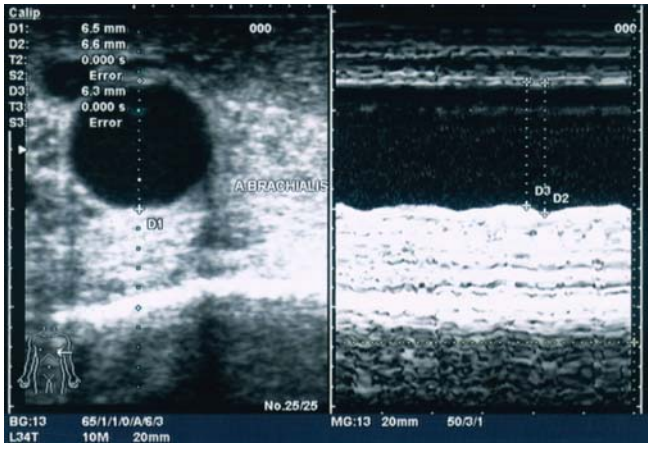

b

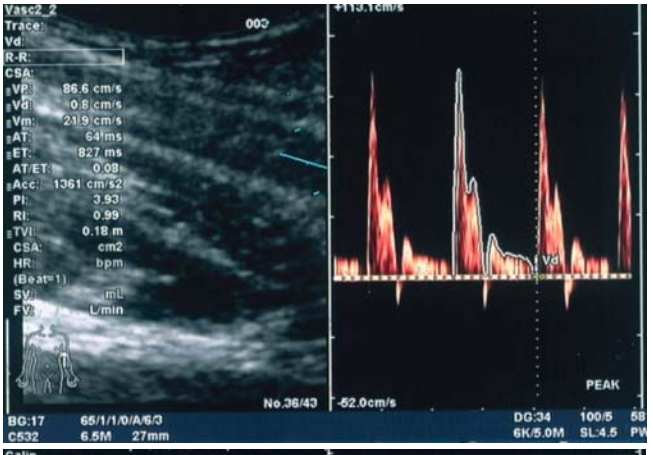

c

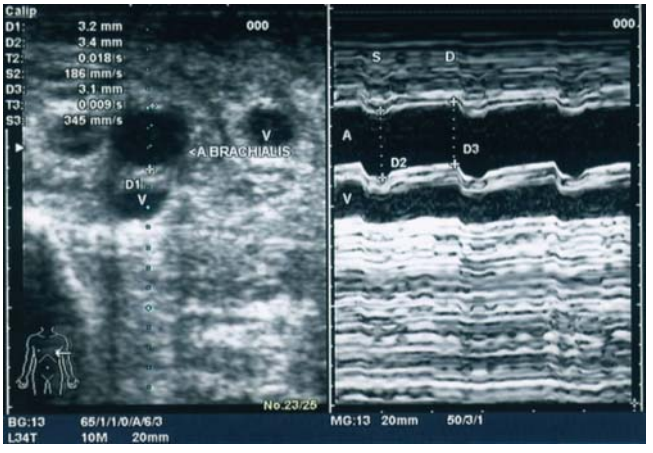

d

(Fig. A 4.4 cont.)
b At the same site, the vessel diameter is measured in the B-mode scan (6.5 mm). For precise measurement, the systolic and diastolic diameters have to be determined and weighted at a ratio of 1:2. This is done in the time-motion mode with scanning of the vessel at an angle as close to 90° as possible. In the example, a flow of 2,778 ml/min is calculated from the mean flow velocity and cross-sectional area
c The same measurements are performed in the brachial artery of the non-shunt-bearing arm, where a mean flow velocity of 21.9 cm/s is calculated. The flow profile is triphasic
d After determination of the mean cross-sectional area from the systolic and diastolic diameters, a mean flow of 108 ml/min is calculated

The example also illustrates the flow-induced dilatation of the arterial vessels as a cause of increased flow in long-standing shunts [the diameter differences between the views with spectral recordings (**a**, **c**) and those with time-motion displays (**b**, **d**) are due to the use of different scales]

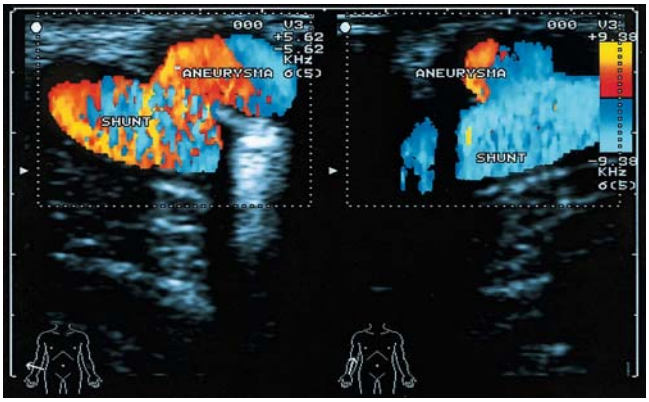

Fig. A 4.5
Puncture aneurysm
Puncture aneurysms of shunt veins are depicted on ultrasound as local dilatations with flow signals. They are unlikely to produce spontaneous occlusion in synthetic shunts. The scan on the *left* depicts the synthetic shunt with hyperechoic walls, from which a puncture aneurysm arises. The corresponding longitudinal scan on the *right* documents a fairly small puncture aneurysm

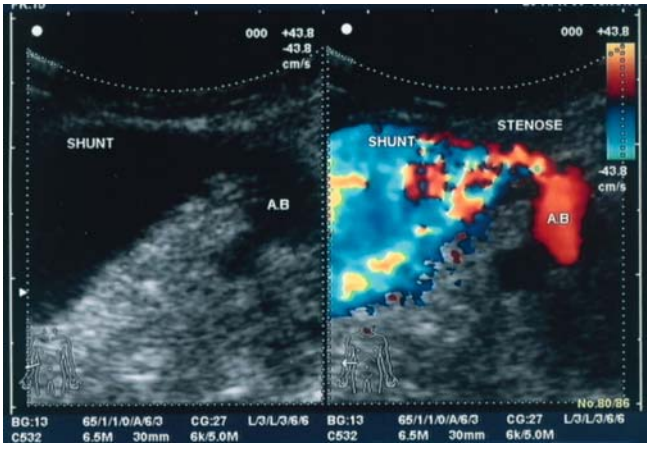

a

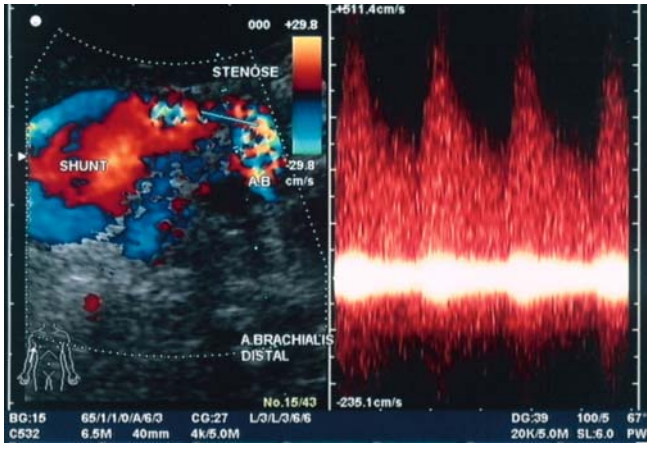

b

Fig. A 4.6 a, b
Stenosis of dialysis access
a, b A Cimino shunt established in the bend of the elbow many years before shows marked variations in caliber with a high-grade stenosis upstream of an aneurysmal dilatation. Color duplex scanning demonstrates turbulence and aliasing and the Doppler waveform a peak systolic velocity of over 500 cm/s. The red flow signals in the aneurysm are due to eddy currents

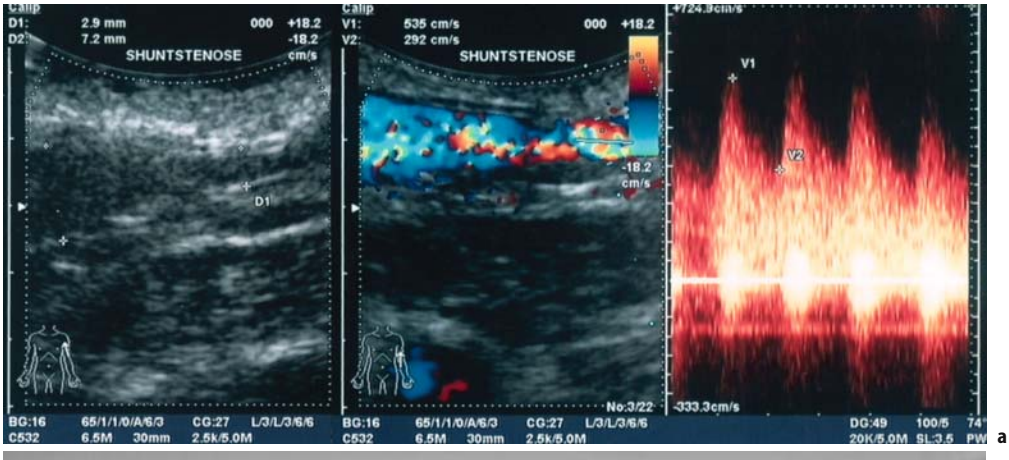

a

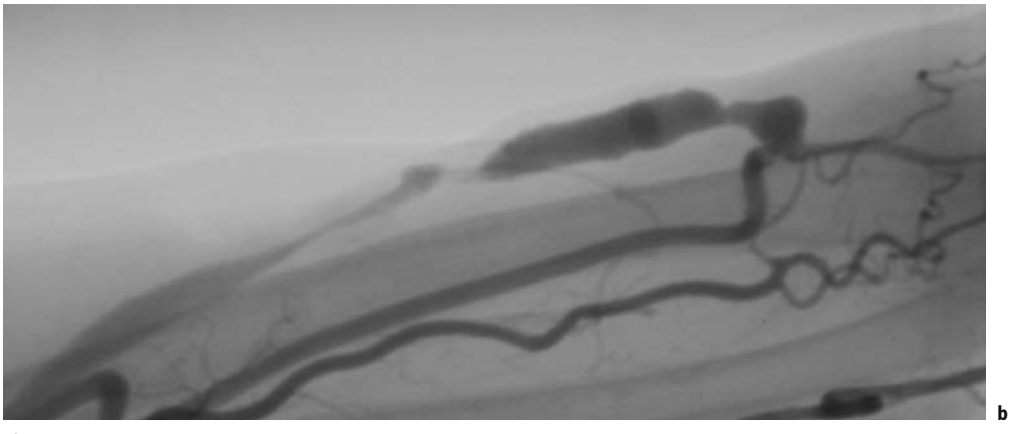

b

Fig. A 4.7 a, b
Stenosis of dialysis access
a Perivascular vibration artifacts impair morphologic as well as hemodynamic assessment of a shunt stenosis by color duplex scanning. Therefore, morphologic assessment is done on the basis of the B-mode scan without activation of the color mode (*left section*). Assessment in the color duplex mode may be improved by throttling shunt flow through controlled compression of the feeding artery. A high-grade stenosis is indicated by the Doppler frequency spectrum with a peak flow velocity of 536 cm/s in systole and 292 cm/s at end-diastole
b Angiography demonstrating shunt stenosis (after revision and synthetic graft interposition)

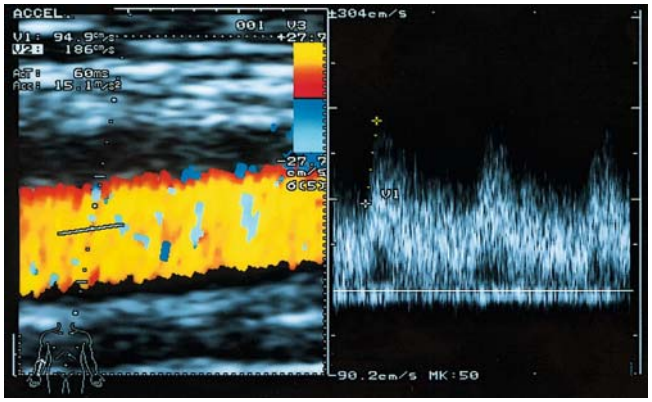

a

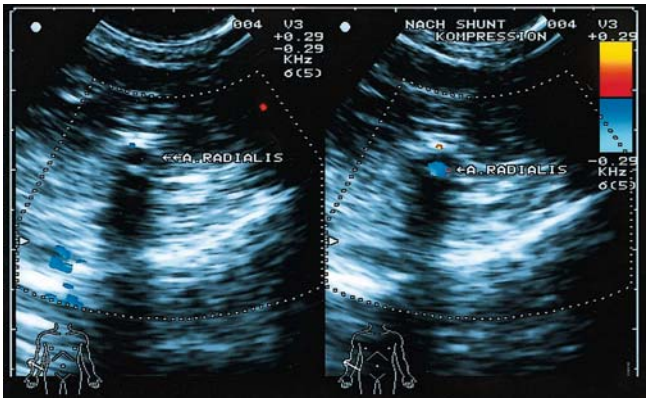

b

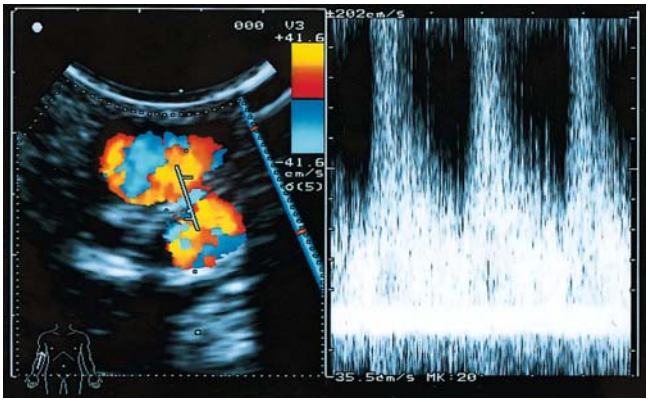

c

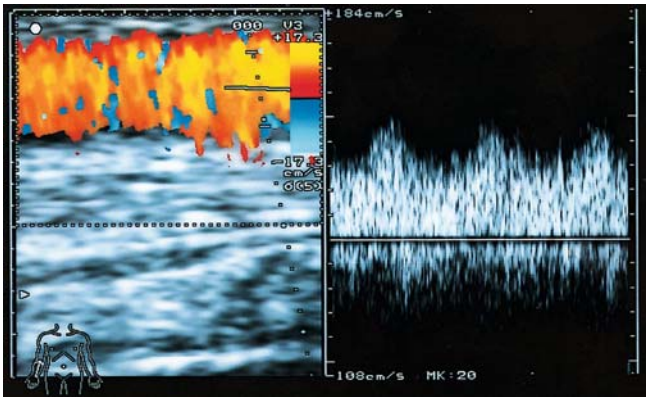

d

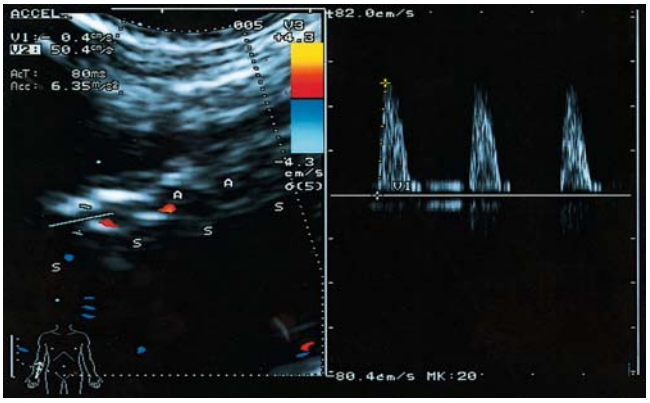

e

Fig. A 4.8 a–e
Steal phenomenon

a A patient with a hemodialysis shunt in the bend of the elbow which functioned for many years developed ischemic necrosis of the finger pads. The shunt was found to be patent and showed a high flow rate with peak velocities of 186 cm/s in systole and 94 cm/s at end-diastole over a long stretch

b With the shunt patent, no flow is detected in the radial artery by color duplex or in the Doppler frequency spectrum. The transverse view of the radial artery on the *left* demonstrates marked medial sclerosis with posterior acoustic shadowing impairing the detection of flow. The scan on the *right* shows blood flow coded in blue in the radial artery upon compression of the shunt

Angiography likewise visualizes the distal radial artery only while the shunt is being compressed in the bend of the elbow

c After banding of the shunt, a stenosis is demonstrated in this area with a peak flow velocity of 280 cm/s in systole and 100 cm/s at end-diastole

d The peak flow velocity in the shunt is reduced to 95 cm/s in systole and 60 cm/s at end-diastole

e Although scanning is impaired by medial sclerosis, flow with a systolic velocity of 50 cm/s is detectable in the radial artery (*A*) after banding. However, only isolated spot-like flow signals are depicted in the radial artery despite a high gain (indicated by posterior artifacts due to overmodulation) and a low pulse repetition frequency. The calcified plaques and medial sclerosis induce acoustic scattering and shadowing (*S*)

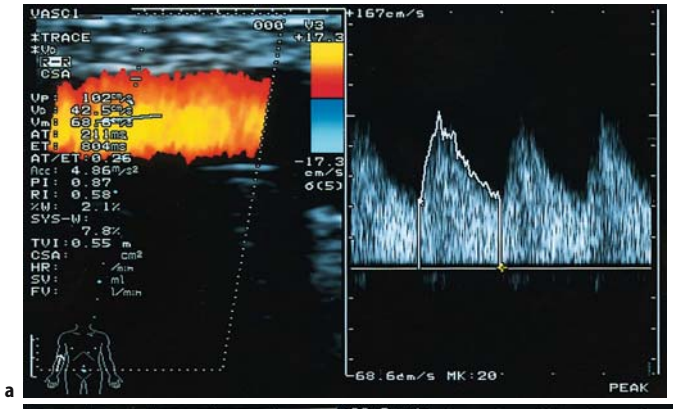

a

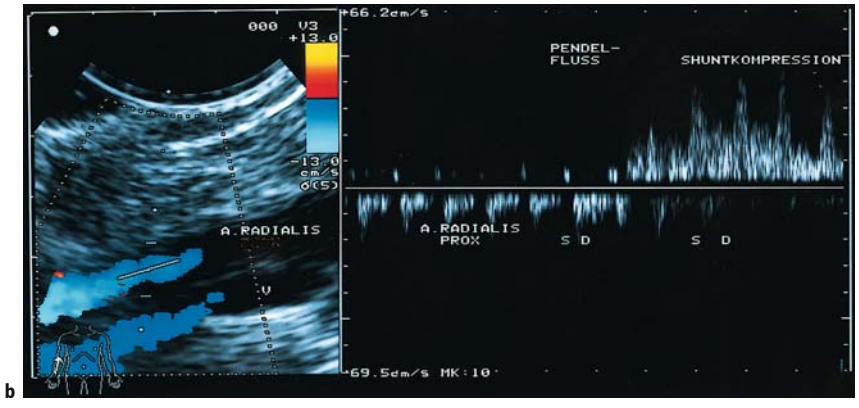

b

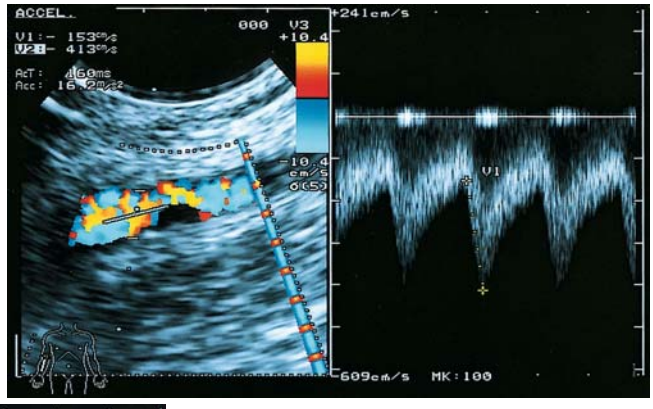

c

Fig. A 4.9 a–c
Stenosis of shunt artery

a Synthetic loop with a diameter of 6 mm implanted for hemodialysis between the brachial artery and the basilic vein in the bend of the elbow. The shunt has a flow rate in the upper normal range: flow rate of 1,153 ml/min calculated from a mean flow velocity of 68.8 cm/s derived from the Doppler frequency spectrum. Nevertheless, the patient presents with ischemia-induced pain of the fingers

b Color duplex scanning demonstrates retrograde flow in the proximal radial artery (depicted in blue, away from transducer, same flow direction as in the parallel vein shown posteriorly). The shunt diverts blood away from the periphery, which is why there is retrograde flow in the brachial artery distal to the shunt anastomosis and in the radial artery (proximal is on the *left*). These arteries are filled through cutaneous and muscular collaterals

The Doppler waveform (*right section*) shows the flow pattern associated with the steal phenomenon: there is to-and-fro flow with a short forward flow during systole (*S*) and persistent retrograde flow during diastole (*D*) with flow reversal upon compression of the shunt. The flow reversal leads to forward flow in the distal brachial artery and in the radial artery. The abnormal diastolic flow is due to ischemia-induced dilatation of the arterioles

c The retrograde flow in the proximal radial artery distal to the shunt is due to a stenosis of the brachial artery somewhat proximal to the shunt anastomosis (distal is on the *left*). With the shunt showing a normal flow rate, there is flow through collateral arteries from the proximal brachial artery to the lower arm arteries and shunt flow causes a steal phenomenon with retrograde flow in the proximal lower arm arteries

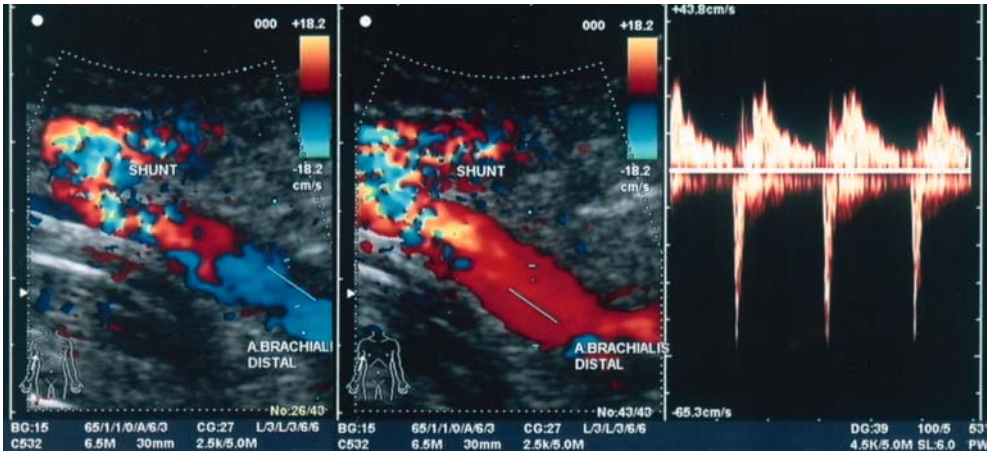

Fig. A 4.10
Peripheral ischemia

A high shunt flow (shunt in bend of elbow) causes to-and-fro flow in the brachial artery distal to the shunt with peripheral ischemia manifesting as pain of the hand. The systolic-diastolic flow alternation is demonstrated both on color duplex scanning (systolic flow away from transducer depicted in blue and diastolic flow toward transducer and shunt depicted in red) and in the Doppler waveform

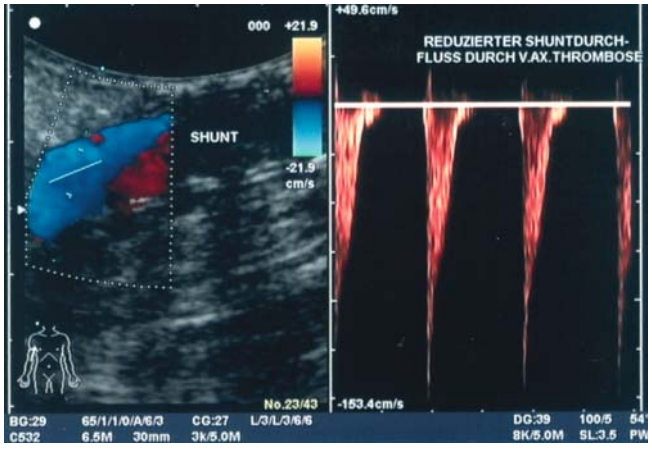

a

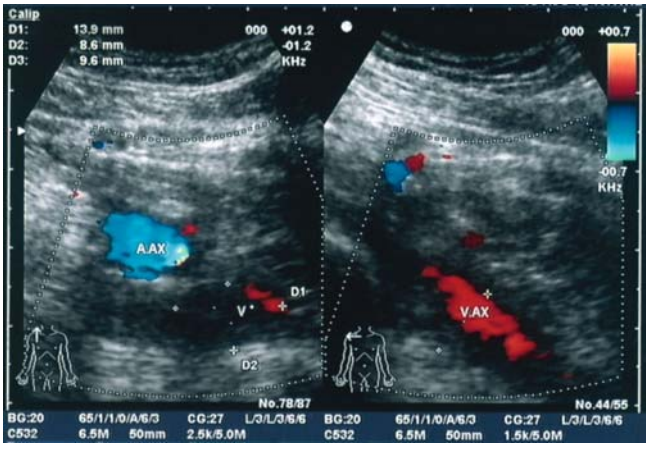

b

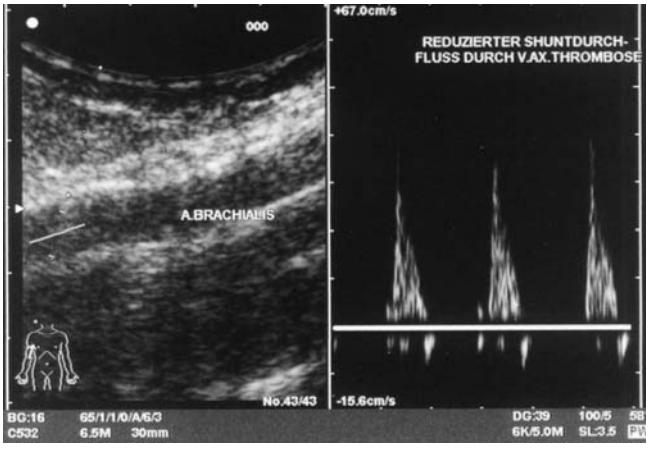

c

Fig. A 4.11 a–c
Outflow obstruction – central venous thrombosis proximal to dialysis access
In the presence of a stenotic process upstream of a hemodialysis shunt, the Doppler spectrum sampled in the shunt is less pulsatile with a delayed systolic rise and an increased diastolic flow component whereas obstruction of venous outflow (thrombosis, stenosis, compression) results in a more pulsatile flow profile
a The abnormal Doppler waveform from the shunt lacks a diastolic component, suggesting an increased flow resistance (flow obstacle) distal to the sample volume
b Color duplex scanning demonstrates thrombosis of the axillary vein with little residual flow near the walls coded in red. The lumen of the vein (*V*) is nearly completely filled by the thrombus
c The outflow obstruction leads to high-resistance flow as indicated by the typical triphasic arterial flow profile in the brachial artery feeding the shunt

In cases of inadequate shunt flow during hemodialysis, a drainage obstruction can be diagnosed from the Doppler frequency spectrum sampled in the brachial artery or in the shunt. The cause of the outflow obstruction can then also be searched for ultrasonographically. In the case presented, thrombosis of the axillary vein was identified. In patients with a synthetic loop graft, the same flow profile may indicate a stenosis of the venous anastomosis

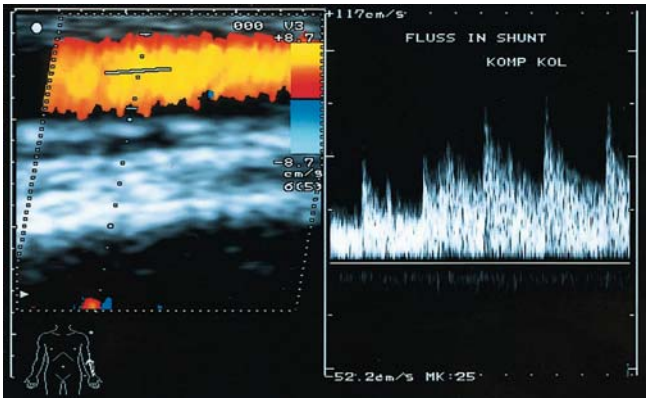

Fig. A 4.12
Inadequate shunt flow due to branching shunt veins
Cimino shunt at the wrist with inadequate flow for hemodialysis. Once stenosis has been excluded, the examiner must search for venous collaterals that reduce the fistula flow available for dialysis and therefore need to be ligated surgically. In this case, compression of a sonographically identified collateral with relevant flow leads to doubling of flow in the main shunt vein. The increase in flow velocity is documented in the Doppler frequency spectrum, which shows that this increase is chiefly due to the larger diastolic flow component

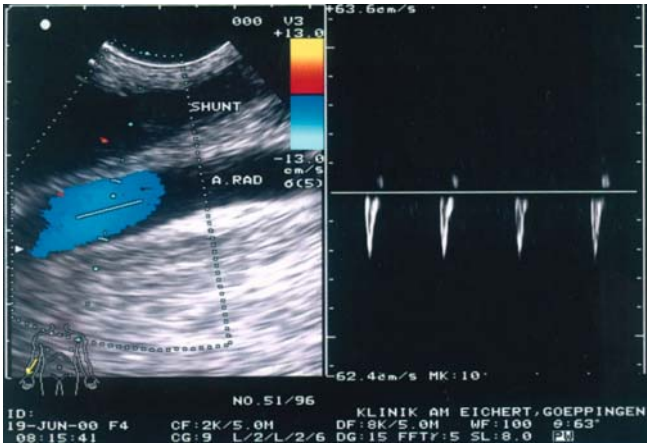

a

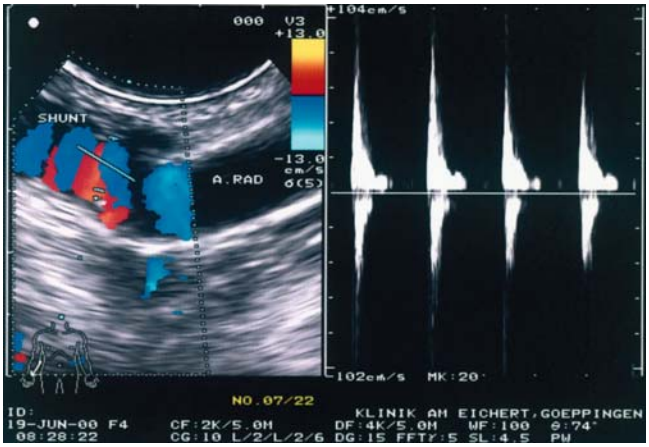

b

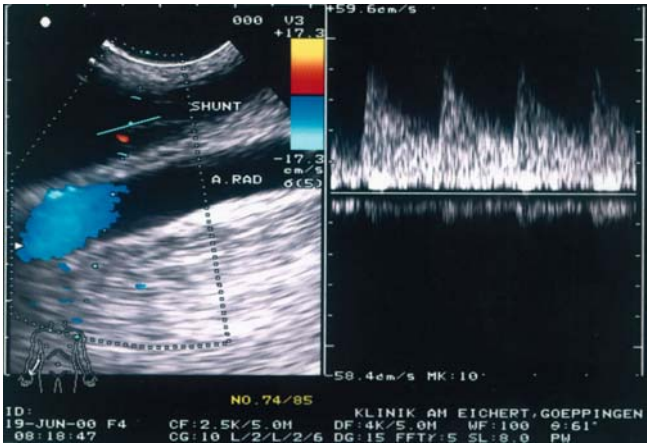

c

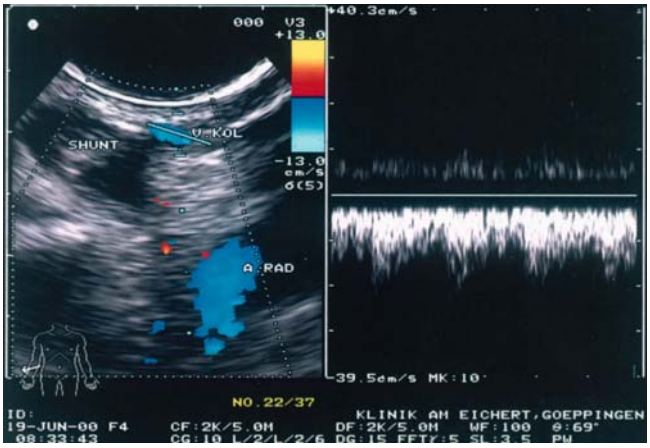

d

Fig. A 4.13 a–d
Occlusion of dialysis access
Progressive formation of neointima and thrombi in the shunt reduces flow, which is identified indirectly as high-resistance flow in the Doppler spectrum sampled in arterial segments upstream of the shunt
a View of the lower arm depicting the radial artery and the nearly completely thrombosed Cimino shunt (closer to transducer) in one scanning plane. The artery has a triphasic flow profile with a low peak systolic velocity
b The shunt is patent at the anastomotic site but there is a blunt flow signal with a "knocking" waveform
c Inside the shunt, color duplex scanning demonstrates meandering flow with a typical shunt profile but markedly reduced velocity
d Along the course of the shunt, there are thrombi surrounded by flow signals proximal to the origin of a small venous branch (*V.KOL*). Distal to it, the shunt is occluded by thrombosis

Extracranial Arteries Supplying the Brain 5

Cardiovascular disease constitutes the most common cause of death in western industrialized countries. The most serious cerebrovascular manifestation is stroke with its complications, which are fatal in one third of cases. Patients surviving cerebral infarction often suffer from irreversible damage and paralysis and will be in need of permanent care. With atherosclerosis of the carotid system becoming more common in old age, cerebral infarction gains in relevance as the population ages. Over 60 – 70 % of all ischemic cerebral infarctions are caused by arterial embolism, typically arising from the carotid artery (Bock et al. 1993; Evans 1999; Roederer et al. 1984).

Carotid thromboendarterectomy (TEA), first performed by De Bakey in 1953, is a highly effective surgical measure to reduce the risk of stroke in patients with atherosclerosis of the carotid system. This has been confirmed in several large trials in individuals with symptomatic carotid stenoses performed in Europe (European Carotid Surgery Trial, ECST) and the USA (North American Symptomatic Carotid Endarterectomy Trial, NASCET) as well as in an asymptomatic population (Asymptomatic Carotid Atherosclerosis Study, ACAS) (Table 5.1). These studies compared the natural history with the morbidity and mortality after carotid surgery stratified by clinical stage and grade of carotid stenosis. The results of all three studies suggest that carotid reconstruction is beneficial in individuals with symptomatic high-grade stenoses (> 70 %) and in certain cases with 60 – 70 % symptomatic stenoses. In high-grade asymptomatic stenosis, on the other hand, surgical repair has advantages over the natural history only in individuals with a low risk of perioperative morbidity and a plaque morphology suggesting a high risk of embolism.

Table 5.1. Results of randomized multicenter trials comparing surgical versus medical treatment of symptomatic (NASCET, ECST) and asymptomatic carotid artery stenosis(ACAS)

	NASCET	ECST	ACAS
No. of patients	659	778	1659
surgical	328	455	825
medical	331	323	834
Perioperative stroke rate	2.1 %	6.6 %	1.4 %
Morbidity/mortality rate (natural history)	5.8 %	7.5 %	2.3 %
Risk reduction (relative)	65 %	43 %	53 %
men			66 %
women			17 %

Suitable diagnostic procedures are necessary to identify those patients who will benefit from the therapeutic measures whose advantages have been confirmed in these large trials. More specifically, this involves identifying subjects with carotid stenosis with a high risk of embolism who will benefit from carotid TEA. Color duplex ultrasound is a noninvasive method that can be repeated any time and has evolved as a highly accurate method for grading carotid stenosis (the risk of embolism increases with the degree of stenosis). Moreover, sonography provides information on plaque morphology, which is the second factor affecting the risk of embolism.

The superficial course of the carotid vessels without interfering structures enables detailed sonographic evaluation of the vessel segment accounting for the majority of cerebral infarctions. Given these ideal scanning conditions and the fact that the vast majority of carotid stenoses occur at the origin of the internal carotid artery, CW Doppler ultrasound was already highly accurate in detecting higher-grade carotid stenoses.

Duplex ultrasonography enables precise morphologic evaluation of vessel pathology and its location and yields information on the hemodynamic significance of a stenosis on the basis of the angle-corrected frequency shift in the Doppler spectrum. In addition, assessment of plaque morphology helps estimate the risk of embolism. Using these ultrasound techniques, it is possible to establish the indication for surgery or medical management of carotid artery stenosis without the need for additional invasive evaluation.

5.1 Normal Vascular Anatomy and Important Variants

The brain derives its blood supply from the two carotid arteries and the two vertebral arteries. The latter unite at the inferior border of the pons to form the basilar artery. In over 70 % of individuals, the left *common carotid artery* arises directly from the aortic arch before the origin of the subclavian artery (Fig. 5.1 a). The right common carotid artery originates from the *innominate artery* (*brachiocephalic trunk*), which arises from the aortic arch and additionally gives off the subclavian artery. The most important variants of the supra-aortic arteries, which originally developed from the branchial arches, are:

- common origin of the innominate artery and left common carotid artery from the aortic arch (13 %);

- persisting communicating trunk arising from the aortic arch and giving off first the left common carotid artery and then the innominate artery (9%);
- bilateral innominate artery dividing into the common carotid and subclavian arteries (1%);
- situs inversus (very rare).

The normal innominate artery on the right has a length of 4–5 cm. It crosses under the brachiocephalic vein and behind the right sternoclavicular joint divides into the right subclavian and right common carotid arteries.

The two common carotid arteries course cranially accompanied by the vagus nerve and the internal jugular vein, which runs anterolateral to the carotids. The *carotid bifurcation* is usually situated at the level of the 4th to 5th cervical vertebra, i.e. at about the level of the thyroid cartilage, but there is wide variation in its location. Typically, the larger internal carotid artery arises from the posterolateral aspect. It has a widened portion at its origin, called the carotid bulb. Unlike the external carotid, the internal carotid does not give off branches along its extracranial course.

Elongation of the internal carotid artery is associated with kinking (90° angle between adjacent segments) or coiling (360° loop) (Fig. 5.1 b). Carotid elongation develops with age. Arterial hypertension is considered a predisposing factor. Kinking or coiling results from the limited space available between the two points of fixation, the bifurcation and base of skull. Pronounced kinking can lead to a stenosis that may become hemodynamically significant in rare cases (cf. Fig. A 5.2).

The external carotid artery arises from the anteromedial aspect of the internal carotid; in about 10% of cases its site of origin is lateral or posterolateral. Along its course, it first gives off the superior thyroid artery and then branches supplying the skin and extracranial organs.

The two *vertebral arteries* originate from the ipsilateral subclavian arteries at the level of the 6th cervical vertebra and pass through the transverse foramina of the corresponding vertebrae, thus taking a partly intraosseous course on their way to the skull base. The two vertebral arteries often differ in caliber and may exhibit unilateral hypoplasia or aplasia compensated for by contralateral hypertrophy. Typically, the left vertebral artery that may occasionally arise directly from the aortic arch has a larger caliber.

Somewhat distal to the vertebral artery, the thyrocervical trunk arises from the subclavian artery. The differentiation is significant in the duplex ultrasound examination. For a precise description of the site of lesions, the vertebral artery is divided into 4 segments:

- the V1 segment, which extends from the origin to the site of entry into the transverse foramen of the 6th cervical vertebra;

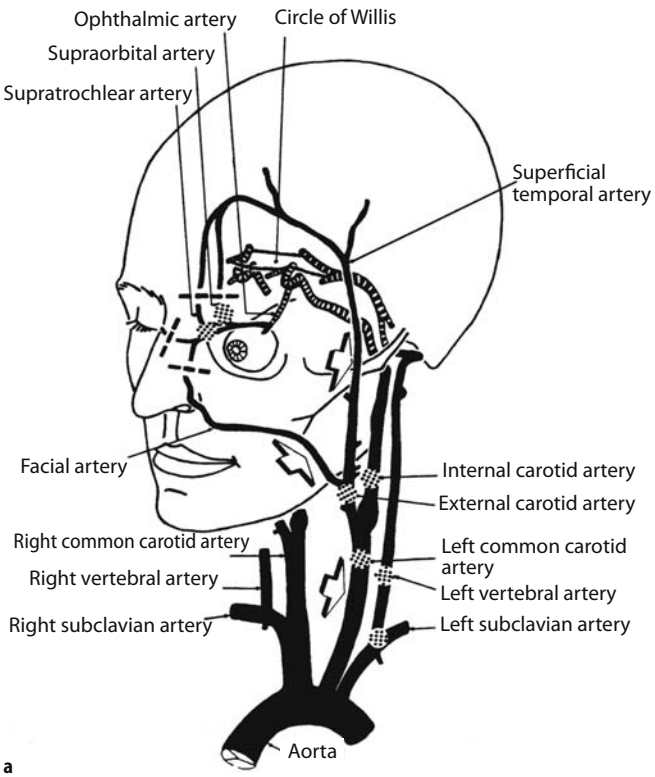

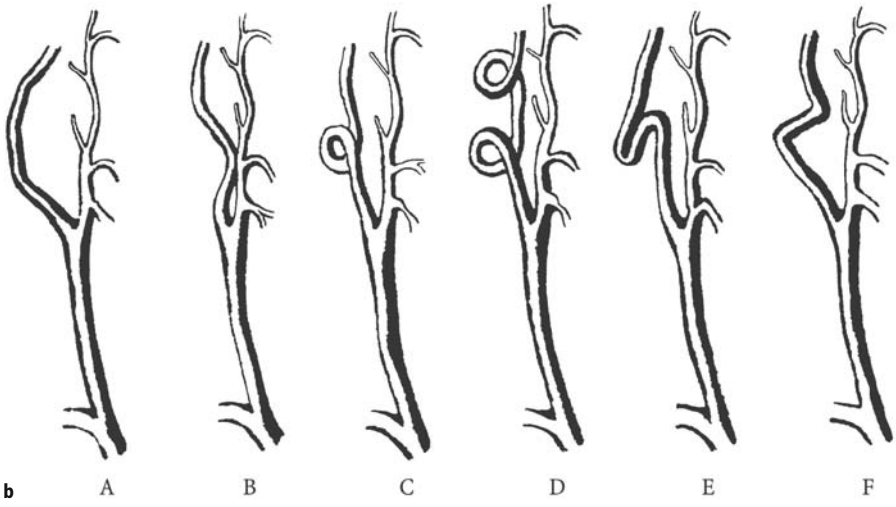

Fig. 5.1. a Schematic representation of the arteries supplying the brain (documentation sites marked).
b Variants resulting from elongation of the internal carotid artery (shown for the left artery): *A* C-shaped course, *B* S-shaped course, *C* coiling, *D* double coiling, *E* kinking, *F* double kinking

- the V2 segment, which is the part coursing through the cervical vertebral foramina;
- the V3 segment, which takes an arched course around the atlas and is therefore also referred to as the atlas loop;
- the V4 segment, which is the intracranial part of the vertebral artery.

5.2 Examination Technique and Protocol

The superficial location of the cervical vessels enables their examination with a high-frequency transducer (5–7.5 MHz or even 10 MHz), yielding B-mode images with a high spatial resolution. The patient is in the supine position with the head slightly hyperextended, and the examiner sits at the patient's head. The course of the vessels and the carotid bifurcation are identified in the transverse section and the Doppler spectrum is sampled longitudinally. The spatial orientation is the same as in the examination of other body regions with display of cranial on the left side of the image and caudal on the right.

5.2.1 Carotid Arteries

The examination begins by obtaining a survey of the *carotid bifurcation in transverse orientation* to determine the location and course of the internal and external carotid arteries in relation to each other. The following variants may be encountered:

- In about 90% of the population, the internal carotid courses posterolateral to the external carotid artery.
- In about 10% of cases, the internal carotid is seen at the same level and medial to the external carotid.
- In rare cases, the internal carotid lies in front of the external carotid artery.

For adequate angulation of the beam and precise localization of a stenosis or plaque, the examiner must move the transducer around to obtain a view depicting the carotid bifurcation as a fork. Three standardized approaches for longitudinal imaging are distinguished:

- positioning of the transducer between the larynx and sternocleidomastoid muscle for sagittal anteroposterior sections (Fig. 5.2 a);
- lateral approach through the sternocleidomastoid muscle;
- posterolateral approach with the transducer behind the sternocleidomastoid muscle (Fig. 5.2 b).

The posterolateral transducer position will lay the bifurcation out beautifully in most individuals with a normal course of the internal carotid. In this position the internal carotid artery is depicted near the transducer.

B-mode scanning serves to identify the course of the vessels and provides initial information on the vessel wall in

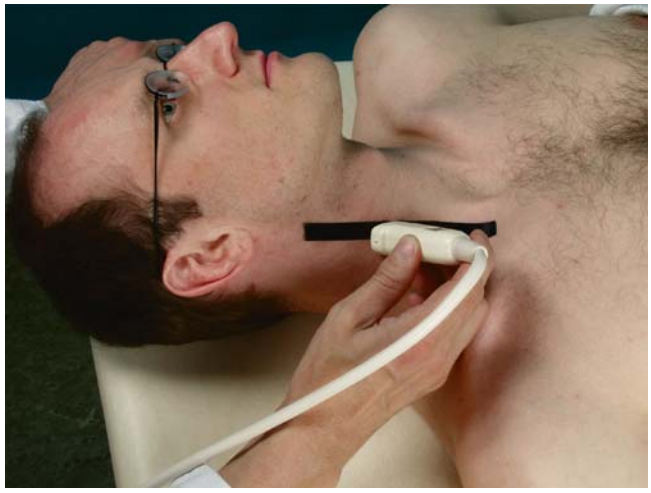
a

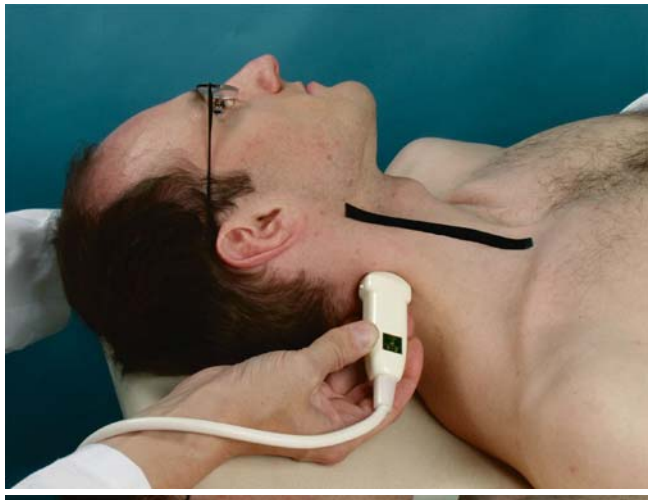
b

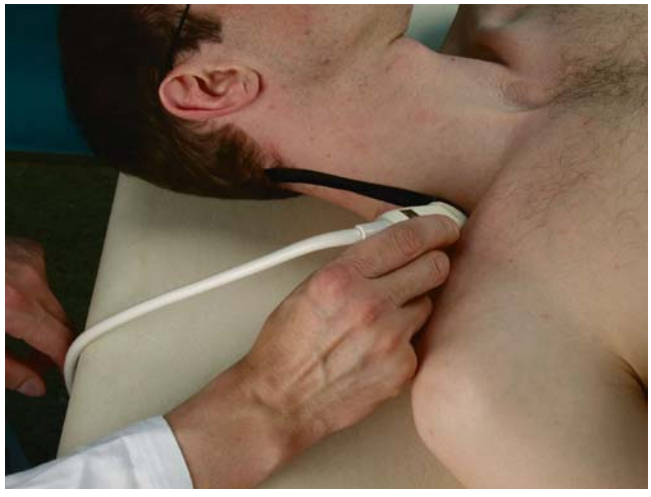
c

Fig. 5.2. a Scanning of extracranial carotid vessels from the anterolateral transducer position (in front of sternocleidomastoid muscle). **b** Scanning of carotid vessels (course marked by black line) from the posterolateral probe position (behind sternocleidomastoid muscle). **c** Transducer position for scanning of vertebral artery (at its origin; course marked)

transverse orientation and the above-described longitudinal views.

Sonographically, three layers of the normal vessel wall can be distinguished: an inner layer depicted as a hyperechoic line next to the lumen; a middle zone seen as a somewhat broader, hypoechoic layer; and an outer layer of slightly higher echogenicity and poorly demarcated from the perivascular fatty tissue. Since ultrasound does not visualize tissues or tissue layers directly but echoes reflected by interfaces between zones of different acoustic impedance, the three layers seen do not exactly match the three anatomic vessel layers – the intima, media, and adventitia. It is therefore not possible to evaluate the intima directly on the basis of the reflection from the interface.

In the search for sonographic features that could serve to identify progressive or regressive changes in the follow-up of atherosclerotic lesions after the elimination of risk factors or in patients undergoing pharmacologic therapy, it has been proposed to measure the thickness of the so-called intima-media complex. This complex comprises the reflection from the innermost interface and the adjacent hypoechoic zone, and it is assumed that thickening has prognostic implications. Although this kind of measurement for assessment of the vessel wall is highly dependent on the ultrasound equipment and examiner, an interface reflection of over 1 mm in thickness is assumed to indicate diffuse wall lesions as they occur in lipopathy or diabetes mellitus. A plaque is assumed when the reflection is 2 mm or wider.

Following evaluation of the vessel wall and possible plaques, blood flow is assessed in the Doppler mode. In color duplex scanning performed with proper instrument settings, a stenosis is suggested by the occurrence of aliasing and an occlusion by the absence of color filling in the lumen. Moreover, the color duplex mode facilitates tracing of the course of a kinked or coiled internal carotid artery.

While color duplex scanning can be performed optionally for initial orientation, Doppler spectra with qualitative determination of angle-corrected flow velocities in longitudinal orientation must be obtained from the common, internal, and external carotid arteries. Spectral Doppler sampling should be performed in the internal carotid artery at short intervals. Use of a larger sample volume will often enable continuous examination of the common and internal carotids in the duplex mode, especially from the posterolateral approach. In this way, a continuous spectrum can be obtained and analyzed throughout the common and internal carotid arteries, similar as with CW Doppler ultrasound. The external carotid artery is scanned only at its origin for differentiation from the internal carotid and identification of possible stenosis.

The posterolateral transducer position is preferred to the anterior position in most cases for sampling of the Doppler frequency spectrum because it enables depiction of the bifurcation as a fork with visualization of the common carotid artery, the bulb, and long segments of the internal and external carotids in a single scan. Moreover, angle correction is easier and the intervening soft tissue improves visualization in this transducer position. In contrast, variable scanning planes are necessary to trace a maximum segment of the carotid when there is kinking and coiling.

To avoid errors in flow velocity measurement in the internal carotid artery, the examiner should try to achieve an insonation angle of less than 60°. This requires selection of an adequate transducer. Scanning with a linear transducer is performed using beam steering with maximum cranial deflection. Linear transducers provide the best resolution for morphologic assessment of the vessel wall in the B-mode while curved-array transducers with a small radius are superior for spectral Doppler recording with an adequate angle, especially when the transducer must be tilted along the arched course of the internal carotid artery. Curved-array transducers are also superior to linear transducers in patients with short necks and in interrogating vessel segments near the base of the skull. The view is optimal when the artery is depicted with parallel walls over the entire width of the monitor. In the 10% of cases with a medial origin of the internal carotid artery, the bifurcation is occasionally seen as a fork from the anterior approach. If not, the transducer is first angled for selective visualization of the origin of the external carotid artery and then angled laterally for visualization of the origin of the internal carotid artery.

Longitudinally, the *internal carotid artery* is continuously traced to the base of the skull, for which the posterolateral transducer position is most suitable in the majority of cases. Different approaches may be required to follow a coiled or kinked internal carotid artery and to identify associated stenoses. In all inconclusive cases, a Doppler frequency spectrum with adequate angle correction must be obtained.

When color-coded duplex ultrasound is used, the gain and pulse repetition rate must be chosen so as to ensure rich color filling of the vessel lumen without aliasing (color change from red to blue or vice versa). Transverse views are obtained with the transducer slightly tilted to achieve an adequate Doppler angle. With proper instrument setting, changes in the color-coded flow pattern suggest pathology, which must then be confirmed by spectral Doppler analysis.

Calcified plaques completely reflect the ultrasound pulse and thus cast *acoustic shadows*, impairing both color duplex and conventional duplex as well as B-mode scanning. Color coding is most severely affected by acoustic shadowing. In such cases, the pulsed Doppler enabling focused application of a higher beam intensity with a high gain will usually provide a Doppler frequency spectrum with a weak amplitude that still allows assessment of flow. If the calcifications are noncircular, the examiner can try and evaluate the blood flow in the lumen by moving the transducer to a position that depicts the calcification in the wall away from the transducer.

Under normal conditions, the internal and external carotid arteries are easily differentiated on the basis of their sonoanatomic relationship, the demonstration of branches arising from the external carotid but not the internal carotid, and the widened bulb area at the origin of the internal carotid. The external carotid exhibits a more pulsatile flow with a smaller diastolic component in the Doppler spectrum. In case of high-grade stenosis of the bifurcation, acoustic scattering

Table 5.2. Criteria for differentiating the internal and external carotid arteries

Criterion	Reliability
Internal carotid artery lies posterolateral to external carotid	Fairly unreliable: in only 90 % of cases; in the remaining 10 % medial course of the internal carotid
Less pulsatile flow (large diastolic flow component) in internal carotid compared to external carotid	Reliable under normal conditions but external carotid may also exhibit large diastolic flow component in the presence of stenosis
Larger lumen of internal carotid artery, especially of bulb	Fairly reliable under normal conditions but not valid in the presence of multiple (calcified) plaques
Doppler waveform of external carotid artery shows pulsation transmitted upon intermittent tapping of temporal artery	Reliable
External carotid gives off arterial branches (1st branch: superior thyroid artery) and external carotid does not	Reliable if origins can be depicted but often impaired by multiple plaques with acoustic scattering and shadowing

and shadowing may impair differentiation on the B-mode scan and also in the Doppler spectrum, where the external carotid will show a larger diastolic component due to the stenosis. When the external carotid provides collateral flow in occlusion of the internal carotid, its flow profile becomes less pulsatile and resembles that of the internal carotid. In such cases, the external carotid can be identified by rhythmical tapping of the temporal artery (anterior to the ear). The pulsation will be transmitted to the Doppler waveform of the external carotid, especially in diastole (Table 5.2).

5.2.2 Vertebral Arteries

In slender patients with good insonation conditions, the vertebral artery is identified at its origin from the subclavian artery (Fig. 5.2 c), where stenosis is excluded by recording of a Doppler spectrum in *longitudinal orientation*. If the scanning window is poor, the common carotid artery is located longitudinally to then identify the vertebral artery between the transverse processes of the cervical vertebrae by slight parallel posterolateral movement and medial angulation of the transducer (cf. Fig. A 5.24). Acoustic shadowing by the transverse processes at regular intervals precludes complete evaluation of the vertebral artery. Following the vessel downward, its origin is identified. The atlas loop will come into view when the transducer is moved cranially and angled.

Doppler evaluation of the vertebral artery is important to determine the flow direction. In patients with forward vertebral artery flow and suspected exercise-induced subclavian steal syndrome due to subclavian stenosis or occlusion, the clinical situation can be reproduced during the examination. With continuous spectral Doppler recording in the vertebral artery, a blood pressure cuff around the upper arm is inflated to over 250 mm Hg and then released after 3 – 5 min to induce reactive hyperemia in the arm. If high-grade stenosis or occlusion of the proximal subclavian artery with a subclavian steal phenomenon and vertebrovertebral crossover is present, this maneuver will induce flow reversal in the ipsilateral vertebral artery and an increase in flow velocity in the contralateral vertebral artery.

5.3 Documentation

Normal findings should be documented in longitudinal views (B-mode) of both common carotid, internal carotid, and external carotid arteries with the corresponding Doppler frequency spectra or angle-corrected velocity spectra. Abnormal findings are documented on additional B-mode images and the corresponding Doppler spectra recorded in longitudinal orientation from the affected sites. The angle-corrected velocity measurement must reflect the degree of stenosis. Moreover, the report should contain information on the localization of nonstenotic plaques as well as on the vascular segments (according to the documentation sites given in Fig. 5.1 a) in which the systolic and end-diastolic Doppler shift frequencies or angle-corrected velocities were obtained.

5.4 Normal Findings

5.4.1 Carotid Arteries

The common carotid artery has a constant luminal diameter of about 7 mm to the level of the bulb. Flow is pulsatile with a large diastolic component. Peak systolic flow velocity ranges from 60 to 100 cm/s. The wider lumen and vessel branching lead to eddy currents in the carotid bulb already under normal conditions, which is shown both by color duplex and in the Doppler tracing. The peak systolic flow velocity is decreased in the bulb and flow separation may lead to retrograde flow on the side opposite the external carotid, seen as changes in the color coding in the color duplex scans (cf. Figs. A 5.1 and 1.23 b).

The normal thickness of the intima-media complex measured in the B-mode (from the lumen-intima interface, the first hyperechoic line, to the media-adventitia interface, the second hyperechoic line) is 0.5 – 0.6 mm and increases somewhat with age.

As a brain-supplying vessel, the internal carotid artery has low-resistance flow with a Doppler waveform that is characterized by a steep systolic upslope followed by monophasic flow with a fairly large diastolic component. In contrast, flow in the external carotid artery is more pulsatile with a smaller

diastolic component. The common carotid supplying both vessel territories has a mixed waveform. As in all other vascular territories, the pulsatility in the carotid system is determined by peripheral resistance and vessel elasticity and therefore increases with age.

5.4.2 Vertebral Arteries

The flow velocity in the vertebral artery reported in different studies varies widely from 19 to 98 cm/s in systole and from 6 to 30 cm/s at end-diastole. The resistance index ranges from 0.62 to 0.75 (Tratting et al. 1992). Assessment of the artery, especially at its origin, is impaired by caliber variation and the occurrence of congenital hypoplasia. At the same time the origin is the preferred site of stenosis.

The normal diameter of the vertebral artery is 3 to 5 mm but there may be asymmetry with hypoplasia on one side and compensatory hyperplasia of the contralateral artery, resulting in right-left diameter differences of over 2 mm.

In case of lateral differences in flow velocity and poor visualization of the origin, the examiner must differentiate a *proximal stenosis* from *hypoplasia*. Hypoplasia is suggested by an unchanged waveform, possibly with diminished diastolic flow, and pronounced widening of the contralateral artery (cf. Fig. A 5.10).

In contrast, a stenosis is indicated by a less pulsatile flow with a smaller systolic component and more pronounced diastolic flow.

5.5 Clinical Role of Duplex Ultrasound

5.5.1 Carotid Arteries

The aim of sonographic assessment of the extracranial cerebral vessels is to prevent cerebral infarction with its harmful sequelae and permanent deficits (Table 5.3).

While diagnostic ultrasound and treatment of peripheral vessels are symptom-oriented, the purpose of carotid artery evaluation is prognosis-oriented in that it aims at identifying patients at risk for stroke and initiating adequate preventive measures in these high-risk patients (Table 5.4).

Over the last decades, TEA has evolved into a suitable method for treating high-grade internal carotid artery stenosis, which accounts for the majority of cerebral infarctions. The main drawback of carotid TEA is that it may cause what it is supposed to prevent, namely stroke or death. This is why the surgical risk must be weighed against the risk of untreated stenoses. Several prospective randomized multicenter studies have been performed in recent years that compared the natural history and the surgical risk for symptomatic and asymptomatic carotid stenoses of different grades. Endarterectomy in symptomatic carotid stenosis aims at eliminating the vascular source of emboli and/or the hemodynamic obstacle in individuals having suffered cerebral infarction with mild residual deficits. The European Carotid Surgery Trial (ECST) and the North American Symptomatic Carotid Endarterectomy Trial (NASCET) compared antiplatelet therapy versus endarterectomy in patients with symptomatic carotid artery stenoses. A recent reanalysis of this data demonstrates that

Table 5.3. Updated classification of extracranial carotid artery stenoses

Stage	Clinical presentation/Symptoms
Stage I	Asymptomatic carotid artery stenosis
IA	Asymptomatic stenosis without high-grade contralateral carotid stenosis or contralateral occlusion
IB	Asymptomatic stenosis with high-grade contralateral carotid stenosis or contralateral occlusion
Stage II	Symptomatic carotid stenosis: ipsilateral transient deficit within the preceding 6 months
IIA	Amaurosis fugax
IIB	Hemispheric symptoms reversible within 24 h (TIA)
Stage III	Indications for emergency carotid TEA
IIIA	Crescendo TIAs
IIIB	Progressive/Acute stroke
Stage IV	Symptomatic carotid stenosis: ipsilateral stroke within the preceding 6 months
Rankin 0	Stroke with fully reversible neurologic deficits (duration > 24 h, prolonged reversible ischemic neurologic deficit [PRIND])
Rankin 1	Stroke without significant disability
Rankin 2	Mild stroke with slight disability and/or slight aphasia
Rankin 3	Moderate stroke with moderate disability with preserved ability to walk and/or moderately severe aphasia
Rankin 4	Severe stroke, unable to walk without assistance, and/or complete aphasia
Rankin 5	Stroke with severe disability: patient bedridden or requiring wheelchair (exceptional indication)

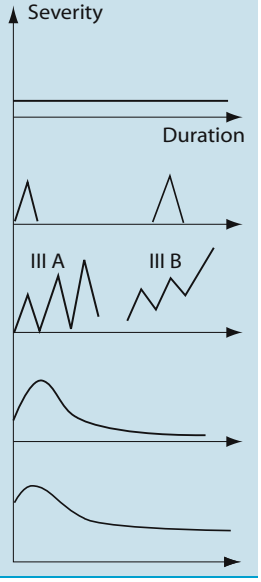

High-grade carotid stenoses ≥ 70 % (NASCET criterion) or ≥ 80 % (ECST criterion), determined angiographically or sonographically. Graphic representation of the duration (horizontal axis) and severity (vertical axis) of the respective neurologic deficits

Table 5.4. Indications for duplex scanning of the extracranial cerebral vessels

- After TIA, PRIND, stroke: identification of underlying cause; additional CT and echocardiography
- Diagnostic evaluation for asymptomatic carotid stenosis suspected on clinical grounds (auscultation, risk factors, atherosclerosis with coronary heart disease or pelvic artery stenosis)
- Indication for operative treatment of carotid stenosis: plaque morphology, hemodynamic stenosis grading
- Diagnostic evaluation of pulsatile neck mass (aneurysm, transmission of pulsation through extravascular tumor)
- Diagnostic evaluation of traumatic intimal dissection
- Diagnostic evaluation of inflammatory disease (Takayasu's arteritis, temporal arteritis)
- Diagnostic evaluation of disturbed perfusion in the posterior circulation (vertebral artery stenosis, subclavian steal syndrome due to subclavian artery occlusion)
- (Diagnosis of brain death)
- Follow-up after surgical repair (TEA) or PTA with stenting (immediately after intervention, then at 6-month intervals)

carotid TEA statistically highly significantly reduces the risk of ipsilateral stroke by 16% after 5 years in individuals with 70–99% stenoses. This means that 6 operations have to be performed to prevent one ipsilateral stroke over a 5-year period (number needed to treat). In individuals with 50–69% stenoses, the absolute risk reduction diminishes to 4.6%. TEA has no advantage in individuals with stenoses <50% and is harmful in those with <30% stenosis compared to the natural history. The rate of severe perioperative complications (stroke, death) was 6.2% for stenoses greater than 70% and 8.4% for 50–69% stenoses (Table 5.5 a).

The wider use of validated noninvasive diagnostic modalities such as Doppler and duplex sonography as well as the known coincidence of coronary heart disease and carotid stenosis with the associated risk of stroke make it more and more important to decide which patients with asymptomatic carotid artery stenoses would benefit from surgery as well. However, in this population with a lower risk of spontaneous stroke (annual rate of less than 1% in stenosis <70% versus 2–5% in those with >70% stenoses, depending on comorbidity), it is more difficult to demonstrate a statistical benefit of therapeutic measures. While earlier studies revealed no benefit of operative treatment, the Asymptomatic Carotid Atherosclerosis Study (ACAS) demonstrated an advantage for the patients operated on for carotid stenoses of 60 to 99% compared to the patients undergoing medical treatment. The 5-year stroke risk was 5.1% in the surgical group versus 11% in the medical care group. The perioperative risk of stroke and death was 2.3% including the rate of 1.2% of preoperative angiography. Based on this data, the American Heart Association recommends surgery for asymptomatic carotid artery stenoses >60% if the center performing the intervention has a perioperative risk of less than 3%. Patient management is dictated by the degree of stenosis determined by duplex scanning and the clinical stage (Table 5.5 b).

Table 5.5 a Comparison of the risk of stroke for surgical versus medical management. Perioperative risk (stroke/death) and absolute risk reduction of ipsilateral stroke over a 5-year period in patients with symptomatic carotid artery stenosis[a]

Degree of stenosis	Operative risk[b]	Risk of stroke surgical	medical	ARR[c]	P	NNT
<30%	6.7%	12%	10.0%	–2.2%	0.05	–
30–49%	8.4%	15%	18.2%	3.2%	0.6	31
50–69%	8.4%	14%	18.6%	4.6%	0.04	22
70–99%	6.2%	10%	26.0%	15.9%	<0.001	6

[a] Summary of results obtained in 6029 randomized patients from the ECST (n=3018), the VA (Veterans Affairs) trial 309 (n=189), and the NASCET (n=2885); stenosis grade according to NASCET criteria.
[b] All strokes/deaths occurring within 30 days in a total of 3248 patients operated on.
[c] Including perioperative stroke/death. *ARR* absolute risk reduction, *NNT* number needed to treat

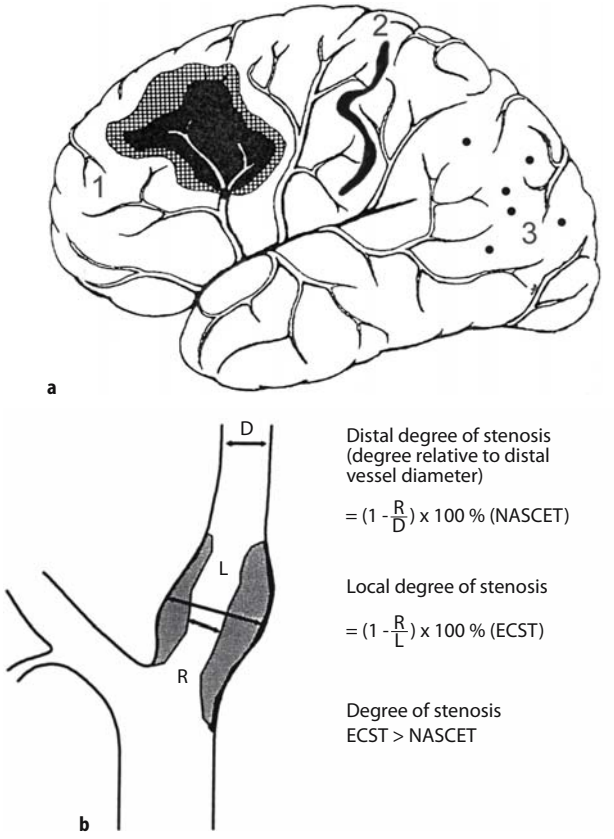

Fig. 5.3. a Types of cerebral infarction. *1* Territorial infarction: due to arterioarterial embolism (carotid, cardiac). *2* Borderzone infarction: hemodynamic origin, reduced perfusion in terminal vascular bed, chiefly in patients with multiple-vessel disease. *3* Lacunar infarction: microangiopathy. **b** Methods of stenosis grading (local versus distal degree of stenosis). Due to the larger vessel diameter in the bulb, a stenosis classified as mild to moderate using the local grading method may not be graded as a stenosis by the distal grading method. Since the stenosis-induced decrease in perfusion only has a minor role in the development of cerebral ischemia whereas plaque thickness is crucial for the associated risk of embolism, the local degree of stenosis is of greater clinical significance. For instance, eccentric plaques causing only moderate stenosis of the bulb may already carry a considerable risk of embolism based on their thickness

Plaque morphology is the other major determinant of the risk of stroke apart from the stenosis grade. Ulcerated plaques with superimposed thrombi, intraplaque hemorrhage, and atheromatous plaques are associated with a higher risk of stroke as compared with smooth, fibrous plaques. However, no imaging modality exists that enables a reliable estimate of the risk of embolism on the basis of plaque morphology.

Yet, in individual cases, the sonomorphologic appearance may provide information as to the risk of embolism. Some studies suggest that hypoechoic plaques have a 2 to 5 times greater tendency to embolize than hyperechoic ones.

In a study of plaque morphology, patients with neurologic deficits scheduled for carotid disobliteration were found to have markedly inhomogeneous plaques in 80 % of the cases while only 22 % of the patients with internal carotid stenoses

Table 5.5 b. Extracranial cerebral vessels – duplex ultrasound findings and therapeutic consequences

Sonographic findings	Clinical presentation	Therapy
Plaques	Not stenotic hemodynamically, asymptomatic or symptomatic	Medical management
Internal carotid artery stenosis	Hemodynamically significant stenosis < 70 %, asymptomatic	Medical management
	Stenosis > 70 %, asymptomatic	Surgical reconstruction (TEA) acceptable but only proven if perioperative risk is low (according to ACAS study): • if perioperative morbidity/mortality rate < 3 % • annual stroke rate of 2 % in medical care group versus 1 % in surgical group surgery only if life expectancy > 5 years
	50 – 70 % stenosis, symptomatic	Surgical reconstruction (TEA): • acceptable but not proven • in TIA < 6 months and plaque morphology suggesting a high risk of embolism (ulceration, hypoechogenicity, irregular surface)
	> 70 % stenosis, symptomatic	Indication for surgery (TEA): • proven • risk reduction relative to natural history increases as the perioperative morbidity and mortality rate decreases (target: < 5 %; Table 5.5a)
	> 70 % stenosis, stage IV	Surgery only after nearly complete resolution of symptoms about 2 – 6 weeks after acute event. Prophylactic surgery of asymptomatic side may be indicated if there is stenosis on this side as well
Internal carotid artery occlusion	Stages I-IV	Usually no operation, emergency operation may be contemplated only immediately after the event (mortality of up to 9 %); otherwise medical management
Subclavian artery stenosis/occlusion	Steal syndrome, symptomatic	PTA, extrathoracic bypass procedure or transposition
External carotid artery stenosis	High-grade	External carotid angioplasty indicated only in multiple-vessel disease (occlusion of ICA) with borderzone ischemias and proven extracranial and intracranial collateralization
Carotid artery dissection	Mostly due to trauma, asymptomatic, patent or thrombosed false lumen	Medical management, anticoagulation (intimal flap becomes attached or false lumen undergoes obliteration or thrombosis in most cases). Fixation or resection of intimal flaps only in exceptional cases with pronounced neurologic deficits and floating flaps
Kinking or coiling	Asymptomatic if nonstenotic Symptomatic if associated with stenosis	Medical management Resection
Inflammatory vessel disease (Takayasu's arteritis, temporal arteritis)	Wall thickening (macaroni sign) with or without hemodynamically significant stenosis	Cortisone therapy, no surgical reconstruction
Carotid body tumor	Well perfused tumor in the carotid bifurcation (color duplex)	Complete tumor resection
Vertebral artery stenosis	High-grade stenosis, asymptomatic High-grade stenosis, symptomatic	Medical management Chiefly located at origin, local TEA or transposition into common carotid artery

caused by homogeneous plaques had neurologic deficits (Banafsche et al. 1995).

Arterial emboli from atherosclerotic plaques in carotid stenosis account for 55 – 60 % of all strokes (territorial infarction; Fig. 5.3 a). Another 30 – 35 % are due to cardiogenic embolism and less than 5 % are due to hemodynamically reduced perfusion, especially in multiple-vessel disease (borderzone infarction). Other rare causes accounting for less than 5 % of cases are inflammatory vessel disease, microangiopathy, and dissection.

5.5.1.1 Defining the Degree of Stenosis

Despite the clinical relevance of internal carotid artery stenoses, there is no agreement about their quantification and various methods have been proposed. This is chiefly attributable to the physiologic widening at the bulb, the preferred site of internal carotid stenoses. Pronounced plaques in this area may be associated with considerable luminal narrowing without becoming hemodynamically effective.

Basically, two methods exist to grade an internal carotid artery stenosis. The *local degree of stenosis* is defined as the ratio of the patent residual lumen to the local vessel lumen without the plaque and gives the best estimate of plaque thickness (which is relevant for the ensuing risk of embolism) and the true extent of vessel constriction. However, angiography enables only a rough and indirect estimate of the local degree of a stenosis because, unlike duplex ultrasound, it does not depict the original vessel diameter.

The *distal degree of stenosis* is calculated from the diameter of the residual lumen in the stenotic area and the diameter of the distal internal carotid artery (which is fairly constant up to the base of the skull). This method allows precise assessment of the hemodynamic effect of a stenosis and classifies mild to moderate stenoses of the carotid bulb as hemodynamically nonsignificant (Fig. 5.3 b).

The distal grading method is primarily used in the United States while determination of the local degree is more common in Europe. Hence the NASCET used the former and the ECST the latter. This must be borne in mind when the results of studies are compared. As the relation between the diameter of the carotid bulb and that of the distant internal carotid is fairly constant, the two degrees of stenosis can be easily converted into each other using the following formulae:

Local (ECST) degree of stenosis (%) = 0.6 × distal (NASCET) degree (%) + 40 %

These formulae yield the following correspondences between the distal and local degrees of stenosis:

Distal (%)	0	50	60	67	70	75	85	90	(NASCET criterion)
Local (%)	40	70	75	80	82	85	90	95	(ECST criterion)

In Germany, the local grading method was recommended as the standard by the German Society of Ultrasound in Medicine (*Deutsche Gesellschaft für Ultraschall in der Medizin*, *DEGUM*) many years ago (Widder et al. 1986). Plaques associated with luminal narrowing of up to 40 % in the bulb area are classified as nonstenosing according to the distal quantification method because stenoses with a local grade of up to 30 % reduce the bulbous lumen only to the diameter of the distal carotid artery. Note, however, that hemodynamic alterations are less relevant for the risk of cerebral infarction than the risk of embolism, which increases with the plaque thickness. Therefore, eccentric plaques in the bulb may already pose a considerable risk of embolism before they become hemodynamically effective.

Angiography, the traditional gold standard for carotid assessment, has methodological limitations as it grades a stenosis on the basis of purely morphologic criteria. It is an invasive procedure that involves radiation exposure and contrast-medium-related side effects as well as the risk of minor stroke in 1.3 – 4.5 % of cases and major stroke in 0.6 –1.3 % (Davies et al. 1993; Dion et al. 1987; Hankey et al. 1990; Moore 2003). The risk of angiography is higher in symptomatic stenoses than in asymptomatic ones and the risk of inducing stroke may increase to up to 12.5 % in patients with bilateral high-grade carotid stenoses (Theodotou 1987). The ACAS provides the most detailed analysis. According to this study, angiography performed at radiologic centers is associated with a combined neurologic morbidity and mortality of 1.2 % in asymptomatic patients, which is only slightly lower than the 1.52 % risk associated with carotid TEA in the same patient population. Given the fact that diagnostic angiography has a stroke risk similar to the therapeutic intervention, it is becoming more and more common to perform carotid TEA without prior diagnostic angiography (Chervu et al. 1994). This is made possible, among others, by the use of high-resolution ultrasound, which has been shown in comparative studies with histologic workup to be superior to angiography in assessing plaque morphology and the risk of embolism (Fontenelle et al. 1994; O'Donell et al. 1985).

5.5.1.2 Plaque Morphology

Risk factors such as longstanding hypertension or hyperlipoproteinemia damage the intima, first becoming manifest as thickening of the intima-media complex. Thickening above 1 mm is considered abnormal and a thickness of 2 mm or more is defined as plaque (Li et al. 1996). Once a plaque has reached a certain thickness, it disturbs the nutrition of the intima, which is not supplied by vessels of its own but through diffusion from the vessel lumen. The initial plaque continues to grow through the accumulation of lipids, lipoproteins, and cholesterol. The interruption of the nutrient supply can lead to central necrosis with formation of an atheroma, which may become organized through fibroblast invasion and thus develop into a stable lesion. Alternatively, there may be rupture of the covering intimal layer with discharge of degenera-

tive atheromatous debris into the bloodstream and embolization to the brain. As a result of lipid inclusion and central necrosis, a plaque can increase in size to such an extent that it represents a considerable obstacle to pulsatile blood flow. Sonographically, such a plaque is identified by pulsatile longitudinal movement with the blood flow. Fibroblast invasion leads to sclerosis, ultimately resulting in calcification of the plaque.

A rapid increase in plaque size may also be due to internal hemorrhage, which is attributed to very minute, vulnerable vessels growing in from the adventitia. Exposure to flowing blood can lead to rupture of the thin plaque cap (intima) with embolization to the brain of necrotic or thrombotic plaque components (Fig. 5.4 a–f). Plaque rupture triggers repair processes with re-endothelization of the former plaque area resulting in a rather smoothly covered niche that poses no risk of embolization. Unfortunately, this fairly harmless state may be difficult to differentiate from ulceration by angiography and ultrasound alike.

Less harmless sequelae are ulcerative defects with incomplete re-endothelialization that may still release thrombotic material into the bloodstream.

The turbulent flow occurring in stenotic areas can induce the deposition of thrombotic material, especially at the distal end of a plaque, with ultimate progression to occlusion of the internal carotid artery.

The risk of embolism is determined not only by the degree of stenosis but also by plaque morphology as such. The following types of plaques can be distinguished in the carotid system on the basis of their macroscopic appearance:

- flat, fibrous plaque,
- atheromatous or soft plaque,
- calcified or hard plaque,
- ulcerative plaque,
- hemorrhagic plaque.

A large consecutive study compared the carotid TEA specimens with the clinical symptoms in 1252 consecutive patients. The incidence of plaque ulceration was 77% in patients with transient ischemic attacks (TIAs) and 79% in those with prior stroke, which was significantly higher than in asymptomatic patients with an ulceration rate of 60%. The incidence of intraplaque hemorrhage did not differ significantly between symptomatic and asymptomatic patients but was significantly higher in patients with greater than 90% carotid stenosis (Park et al. 1998).

For estimation of the risk of embolism, it would be desirable to have an imaging modality that provides reliable information on plaque morphology. This is difficult, however, since most atherosclerotic lesions are chiefly composed of variable amounts of atheromatous material with a high lipid content and fibrous material rich in collagen. The inhomogeneous composition of plaques is reflected in their ultrasound appearance, but it is not possible to identify individual plaque components on the basis of their different echo levels and to thus make use of this information for predicting the risk of embolism. Ulcerated plaques are difficult to differentiate from washed-out cavities that have become re-endothelialized.

5.5.2 Vertebral Arteries

Transitory ischemic attacks or strokes involving the vertebrobasilar system are much less common than those arising from the carotid territory. Stenoses at the origin of the vertebral artery rarely require surgical or interventional treatment, in particular because they have a lower risk of embolism. In patients with multiple-vessel disease and a global reduction of cerebral perfusion, repair is mainly done in the carotid territory.

While lesions in the carotid system present with highly specific hemispheric symptoms, the clinical manifestation is much less specific when the vertebrobasilar system is affected. Dizziness is the chief symptom, but may also be caused by numerous nonvascular conditions. Apart from atherosclerotic lesions, acute symptoms of vertebrobasilar insufficiency may be due to dissection, typically occurring after trauma.

In patients with subclavian artery occlusion, the vertebral artery is scanned to evaluate its collateral function in patients with the subclavian steal syndrome (complete – incomplete).

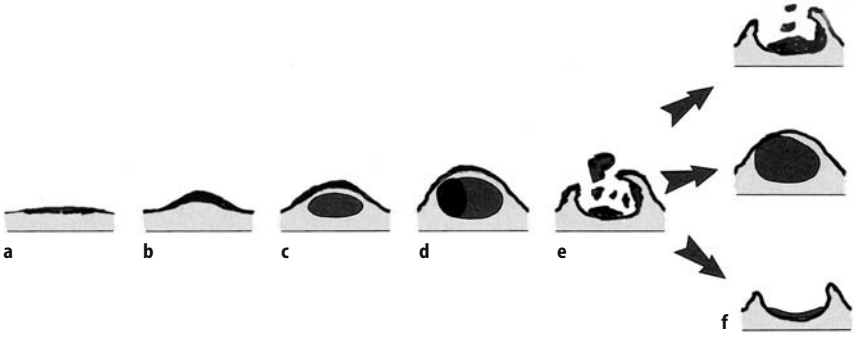

Fig. 5.4 a–f. Stages of plaque development. **a** Initial atherosclerotic wall thickening (intima-media complex thickening). **b** Further increase in wall thickness with development of plaque. **c** Plaque increases in size through lipid inclusion and may undergo central necrosis (atheroma); disturbed nutrition of the plaque. **d** Intramural hemorrhage through rupture of ingrowing vessels. **e** Rupture of the plaque cap induced by pulsatile blood flow (longitudinal pulsation) with ulceration mainly of proximal portions. **f** Re-endothelialization of the ulcer with formation of a washed-out niche as a fairly stable residue (*bottom*), re-endothelialization of the ulcerative plaque (*middle*), or persisting ulcerative plaque with recurrent embolism and only partial repair of the vulnerable surface (*top*)

Ultrasonography is the method of choice for morphologic assessment as well as demonstration of atherosclerotic lesions and dissection. Published data suggests that the vertebral artery is amenable to sonographic assessment in over 80 – 90 % of cases, depending on the segments included in the analysis.

5.6 Ultrasound Criteria, Measurement Parameters, and Diagnostic Role

5.6.1 Carotid Arteries

5.6.1.1 Plaque Evaluation and Morphology

Plaques and stenoses mainly affect the bifurcation and the first 2 cm of the internal and external carotid arteries. Their superficial location enables scanning with high-resolution, high-frequency transducers that also allow evaluation of plaque morphology. The morphologic description of a plaque comprises the following features:

- Localization:
  - anterior/posterior wall,
  - proximal/distal;
- Extension:
  - circular/semicircular,
  - plaque diameter;
- Plaque surface:
  - clearly delineated/moderately delineated/not delineated,
  - smooth/irregular (0.4 – 2.0 mm deep craters)/ulcer (> 2.0 mm deep);
- Internal structure:
  - homogeneous/inhomogeneous;
- Echogenicity:
  - hyperechoic (with or without acoustic shadowing)/hypoechoic/not visualized.

A growing plaque is typically seen as a structure of inhomogeneous echotexture on the vessel wall. Further progression of the atherosclerotic process is associated with luminal narrowing. The next step is a soft plaque resulting from the deposition of atheromatous material and typically exhibiting a low echogenicity. Calcification of the plaque produces scattering and acoustic shadowing. Rupture of the plaque cap can lead to ulceration, which is characterized on the B-mode scan by a heterogeneous echotexture with disruption of the surface or a bowl-shaped gap.

As already mentioned, plaque morphology is a crucial determinant of the risk of embolism apart from the stenosis grade. It would therefore be highly desirable to identify sonographic plaque features associated with an unfavorable prognosis and their respective risk of embolism. Unfortunately, detailed descriptions of plaques have contributed only little to the identification of objective prognostic criteria. Although hyperechoic plaques with a smooth surface correlate with the intraoperative or histologic finding of fibrous plaques (with or without calcifications) while hypoechoic plaques with an irregular surface often correspond to atheromatous, soft plaques with or without thrombotic deposits, caution is in order here because plaque appearance may vary widely with the scanner and ultrasound machine used and its evaluation is examiner-dependent. Therefore, it is recommended that the ultrasonographer merely describe the plaque as long as the correlations between the sonographic appearance and histologic makeup of a plaque are still vague (Woodcock et al. 1992).

Color-coded duplex ultrasound enables assessment of the carotid system with 3 modes: B-mode scan, spectral Doppler, and color flow imaging. The vessel wall should be assessed on the B-scan without activation of the other modes. The thickness of the intima-media complex is measured at the site of maximum thickening in the wall away from the transducer. Thickening above 1 mm is considered abnormal and thickening above 2 mm is assumed to indicate a plaque. Plaques mainly occur in the carotid bifurcation and along the first 2 – 3 cm of the internal carotid artery.

Longitudinal pulsatile movement of a plaque also appears to contribute to the risk of embolism. Shearing forces acting on the plaque increase with plaque thickness and may cause rupture of the vulnerable cap with discharge of embolic material. Progressive lumininal narrowing due to plaque thickening leads to higher flow velocities in the stenotic area (> 350 cm/s), which is associated with an increased risk of ulceration (Beach et al. 1992). The risk of necrosis and ulceration with embolization also increases with the occurrence of necrosis, which in turn results from an insufficient nutrient supply as the plaque increases in length and thickness.

A number of criteria can be derived from the sonographic appearance of plaques that suggest a favorable or unfavorable prognosis:

Favorable in prognosis:	Fairly hyperechoic and homogeneous plaque Plaque surface smooth and clearly delineated Calcification Short plaque (< 1 cm) Thin plaque (< 4 mm)
Unfavorable in prognosis:	Mostly hypoechoic internal signal with plaque suggested only by a small intraluminal area of low echogenicity; surface poorly delineated Long plaque (> 1 cm) Plaque diameter > 4 mm Longitudinal pulsatile movement of the plaque in a cranial direction

Based on these criteria and the descriptions of plaques given by other authors (Geroulakos et al. 1994; Gray-Weale 1988; Langsfeld et al. 1989; Lusby 1993; Widder 1995), plaques can be classified as follows:

- *Type I*: hyperechoic and homogeneous plaque with a clearly delineated surface;
- *Type II*: plaque of mixed echogenicity with a predominance of hyperechoic portions and with a moderately delineated surface;

- *Type III*: very hypoechoic or markedly heterogeneous plaque with a poorly delineated surface;
- *Type IV*: plaque not visualized or suggested only by isolated echogenic spots in an otherwise anechoic lumen. Plaque extent visualized only in the color flow mode (flow in patent residual lumen).

Type IV plaque corresponds to atheroma with lipid inclusions and intraplaque hemorrhage, which make the plaque unstable and have been shown in studies to be associated with a significantly increased risk of stroke. Hyperechoic and homogeneous plaques with a clearly delineated surface (type I), on the other hand, have a low risk of embolization (cf. Figs. A 5.9 to A 5.11). Unfortunately, the most common types II and III are difficult to assess in terms of prognosis, and sonomorphologic risk assessment has disappointingly low accuracies of 50 – 70 %, which is comparable to angiography (Estol et al. 1991; Friedrich et al. 1988; Streitzler et al. 1994). Eccentric plaques carry a higher risk of embolism than concentric plaques because they are thicker yet cause the same degree of stenosis (diameter reduction).

Despite its rather disappointing overall accuracy, sonographic assessment of plaque morphology does provide some information for establishing the indication for surgery in individual patients, especially those with high-grade asymptomatic stenoses or symptomatic 50 – 70 % stenoses with type I or IV plaque. Hopes were set on ultrasound contrast media but their use did not overcome the difficulties in differentiating a low-risk niche remaining after defect healing from fresh ulceration.

Prediction of the risk of embolism on the basis of the sonographically visualized plaque morphology in relation to the clinical differentiation of symptomatic and asymptomatic patients is confronted with a general problem, namely that studies already fail to yield consistent results regarding the correlation of pathomorphologic features of plaques such as ulceration, soft atheromatous deposits, and hemorrhages with the clinical stage. While some investigators (Park et al. 1998; Sterpetti et al. 1991) demonstrated a statistically significant correlation between plaque ulceration and the occurrence of transient or persistent neurologic deficits, others did not find such a correlation (Hill et al. 1994; Van Damme et al. 1992). This explains why the sonographic evaluation of plaque morphology yields so widely discrepant results in terms of risk assessment.

Results reported in the literature are difficult to compare and often contradictory with regard to the assessment of subgroups since the studies comparing the sonomorphologic appearance of plaques and their surface with the clinical stage (and the ensuing risk of embolism associated with the plaque) differ widely in their design or use highly subjective criteria for differentiating hyperechoic from hypoechoic plaques or in defining an irregular surface. Therefore, suggestions have been made to standardize the description of plaques. De Bray et al. (1997) recommend using the echo levels of the following structures as reference values in describing plaque echogenicity: a hypoechoic plaque corresponds to the echogenicity of flowing blood, an intermediate echogenicity to that of the sternocleidomastoid muscle, and a hyperechoic plaque to that of bony structures. Moreover, the authors suggest to describe the plaque surface as smooth or irregular, with an irregular surface being defined as the presence of fissures 0.4 – 2.0 mm deep while ulceration is assumed when craters with a depth of over 2 mm are present. Plaque ulceration has been reported to be associated with an increased risk of ipsilateral cerebrovascular ischemia (Sitzer et al. 1995; De Bray et al. 1997; AbuRahma et al. 1998; Pedro et al. 2000). Other investigators deny such an association (Meairs and Hennerici 1999), failing to identify significant differences in plaque surface between symptomatic and asymptomatic patients.

An *irregular plaque surface*, *plaque ulceration*, or poststenotic *"dead-water zones"* can lead to local platelet aggregation with release of small thrombi into the bloodstream. It is possible, in principle, to depict ulcerated areas as crater-like defects within hyperechoic plaques. However, since plaques are frequently heterogeneous and a fresh ulcer is difficult to differentiate from a washed-out niche (with any imaging modality), the sensitivity in identifying plaque ulcers is very poor with reported values of about 50 % (Katz et al. 1983) and 29 – 93 % in a review by Merritt and Bluth (1992). In contrast, another study reports a surprisingly high sensitivity of 90 % and specificity of 94 % for the sonographic criteria of ulceration (Banafsche et al. 1993). A rapid increase in overall size and in the hypoechoic portions at follow-up suggests a marked increase in the risk of embolism and is an indication for surgery.

Subintimal intraplaque hemorrhage depicted on B-mode ultrasound as hypoechoic and heterogeneous areas can lead to rupture of the plaque cap (ulceration) and will increase the risk of stroke. Surgical specimens from symptomatic patients were shown to have a 6-fold higher incidence of hemorrhage than specimens from asymptomatic patients. Fresh hemorrhage is demonstrated by ultrasonography with a sensitivity of 72 – 91 % and a specificity of 65 – 88 % (Bluth et al. 1986; Widder et al. 1990).

Another prognostic criterion in addition to the plaque surface is the echogenocity. Atheromatous material and lipid inclusions are often identified by their low-level echoes when scanned with a high-frequency transducer but more recent studies yield contradictory results regarding the value of gray-scale ultrasound in plaque analysis. For instance, it has been reported that inhomogeneous and hypoechoic plaques are unstable (Bräsen et al. 1997), and prospective studies confirm that plaques with these features and predominantly heterogeneous portions are associated with a significantly higher risk of ipsilateral cerebrovascular ischemia than hyperechoic, homogeneous plaques (El-Barghouti et al, 1996; Geroulakos et al. 1994; Bock et al. 1993; Langsfeld et al. 1989). Other authors deny a significant association between clinical symptoms and the sonographic plaque structure (Meairs and Hennerici 1999; Hill and Donato 1994).

Computer-assisted techniques of sonographic analysis have been proposed to standardize the assessment of plaque

echogenicity (El-Barghouti et al. 1995 and 1996; Pedro et al. 2000). The studies investigating these techniques demonstrated an increased risk of stroke for hypoechoic plaques. Moreover, an increasing plaque inhomogeneity was found to be associated with neurologic symptoms and with higher-grade stenoses (Banafsche 1993). Based on the high accuracy of duplex ultrasound in determining plaque inhomogeneity (predictive value of 94.7) and the proven correlation with the clinical stage, it was recommended to give more weight to sonomorphologic plaque assessment in establishing the indication for carotid disobliteration.

On the other hand, a standardized gray-scale analysis of plaque morphology demonstrated good interobserver agreement but a poor correlation between plaque sonomorphology and the histopathologic findings in the surgical specimens from patients having undergone eversion TEA (Denzel 2003).

Ultrasonography does not depict tissues or tissue structures directly but the reflection of ultrasound beams at interfaces between areas of different acoustic impedance. A more heterogeneous tissue contains more interfaces and thus has a higher echogenicity. This is why hemangiomas in the liver are hyperechoic. Inhomogeneous tissue is more hyperechoic than homogeneous tissue regardless of its consistency (hard – soft). Applied to plaques with their variable pathomorphologic composition, this means that the echogenicity of plaques with a high risk of embolism resulting from a high lipid content or intraplaque hemorrhages (as such predominantly hypoechoic) is not uniform but dependent on how the lipid and blood are integrated into the plaque matrix and on the resulting plaque structure. This is a method-specific limitation of the sonographic evaluation of plaque morphology.

Recent investigations of the nature and composition of atherosclerotic plaque have brought about the concept of "vulnerable" plaque. The newly introduced methods of sonographic image processing may improve the differentiation of such vulnerable plaques from stable plaques in the future. While conventional B-mode ultrasonography processes the amplitude of the reflected beam, a recently introduced technique using high-resolution transducers as in intravascular ultrasound (IVUS) differentiates the reflected echo pulses according to their frequencies. This technique is based on the assumption that different tissues (necrosis, fibrosis, or tissue with a high lipid content) reflect the beam with different frequencies. The sonographic evaluation of plaque morphology using this new technique is expected to improve tissue differentiation and to thus help discriminate vulnerable plaques with necrotic portions and a high lipid content from more stable, fibrotic plaques (Reid et al. 2005).

Virtual histology IVUS is the latest advance in the field of IVUS and is likely to change patient management in the future. The frequencies reflected from different plaque types (fibrous, fibrolipidic calcium, and lipid core) are collated, and a color assigned to each plaque type is then superimposed on the original IVUS image. Thus the plaque is demonstrated by ultrasound; a necrotic lipid core is colored red and designated as "vulnerable plaque." While this development is particularly likely to influence coronary interventions, the role of virtual histology IVUS is also likely to affect interventions in other vascular territories, especially the carotid and renal arteries. A worldwide registry to identify the clinical role for virtual histology IVUS is commencing.

5.6.1.2 Quantification of Stenosis

For *stenosis grading*, the plaque is identified in the B-mode and the Doppler frequency spectrum sampled from the stenotic area. Mild stenoses without hemodynamic effects (< 50 % diameter reduction) can be quantified in transverse orientation in the gray-scale mode by determining the patent lumen after proper adjustment of the scan plane. The morphologic method is inferior to hemodynamic grading in *intermediate-* and *high-grade* stenoses. Hypoechoic plaques can lead to grading errors. Therefore carotid stenoses with 50 % luminal narrowing or greater are graded on the basis of the Doppler frequency or angle-corrected flow velocity measurement. As in other vessel territories, low-grade carotid stenoses are characterized by eddy currents and spectral broadening. In hemodynamically significant stenoses, systolic and diastolic flow velocities increase in proportion to the stenosis grade (Table 5.6; Fig. 5.5).

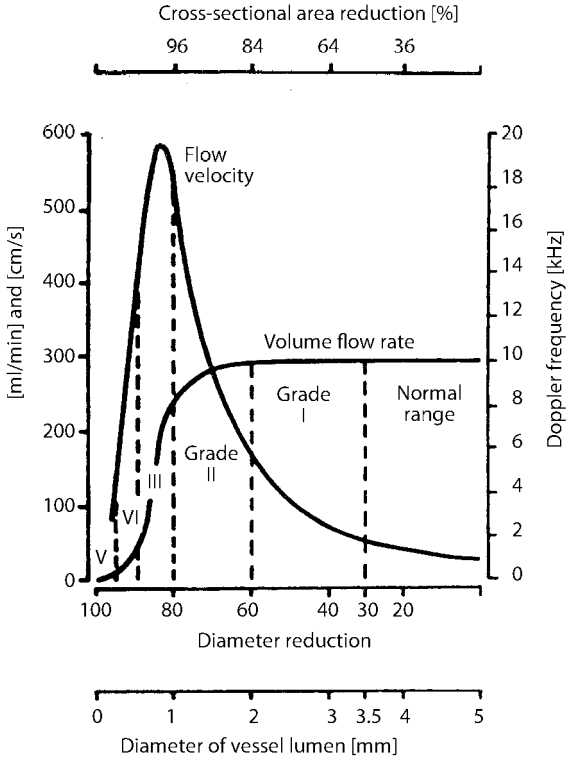

Fig. 5.5. Flow in the carotid artery under idealized conditions: Changes in peak systolic flow velocity (given as Doppler shift frequency in KHz) and volume flow rate (in ml/min) with progressive stenosis of the internal carotid artery (expressed as percentage diameter and cross-sectional area reduction). Relevant flow acceleration occurs at diameter reductions of over 50 %

Table 5.6. Duplex ultrasound criteria for classifying internal carotid artery stenoses. (Modified according to Jacobs et al. 1985; Bluth et al. 1988; Zwiebel et al. 1997, Neale et al. 1994; Faught et al. 1994; Moneta at al. 1995; AbuRahma et al. 1998)

Local diameter reduction [%] (ECST)	Cross-sectional area reduction [%] (ECST)	Distal diameter reduction [%] (NASCET)	Peak systolic flow velocity [cm/s]	Peak diastolic flow velocity [cm/s]	ICA/CCA velocity ratio	Waveform, color duplex
0 – 49	0 – 74	0 – 15	< 110	< 40	< 1	Normal to disturbed flow
50 – 59	75 – 82	16 – 32	110 – 139	40 – 50	1.0 – 1.8	Spectral broadening, increasing fill-in of spectral window
60 – 69	83 – 90	33 – 49	140 – 199	> 50	1.8 – 2.5	Turbulence, poststenotic flow separation, and flow jet
70 – 79	91 – 95	50 – 65	200 – 250	> 70	2.5 – 3.8	
80 – 95	96 – 99	66 – 99	> 250	> 100	> 3.8	Pronounced turbulence, reduced poststenotic flow velocity, and eddy currents
Subtotal occlusion			250 – 500	variable		

Calculation of the percentage diameter reduction as the difference between normal lumen and residual lumen from the gray-scale scan is rarely possible and very unreliable due to the low echogenicity of most plaques and acoustic shadowing of calcified plaques. Evaluation in the color mode, on the other hand, often overestimates the perfused residual lumen because interpolation of the wider-spaced color lines leads to color coding of the outer plaque portions extending into the lumen. Therefore, this method alone should only be used to grade clinically less significant stenoses with less than 50 % diameter reduction. In higher-grade stenoses hemodynamic quantification by spectral Doppler is superior. Hemodynamically, the diameter reduction is calculated from the angle-corrected flow velocity according to the continuity law. Cerebral autoregulation reduces the peripheral resistance through dilatation of arterioles, thereby ensuring a fairly constant flow even in the presence of a greater than 50 % stenosis. Stenoses with a diameter reduction of less than 50 % are not associated with marked flow acceleration.

Flow is disturbed, however, by plaques with an irregular surface protruding into the lumen. The flow disturbance is reflected in the Doppler waveform by eddy currents, turbulence, and flow reversal, especially in systole. Moreover, the waveform shows spectral broadening with filling-in of the clear window. According to the continuity law, intrastenotic flow acceleration does not occur until there is greater than 50 % diameter reduction, which corresponds to an area reduction of 75 % (cf. Fig. A 5.5).

The intrastenotic flow velocity increases in proportion to the degree of stenosis and is highest in subtotal occlusion. At the same time, friction occurring at the high velocities associated with subtotal occlusion acts as a decelerating force (decreasing the velocity of most reflecting blood components). Nevertheless, a high gain will depict isolated high-frequency signals in the flow jet as an indicator of the high grade of the stenosis. Distal to a high-grade stenosis (measured in the internal carotid artery close to the base of skull), the systolic flow velocity decreases with the stenosis grade (postocclusive flow reduction).

The following parameters are used to describe flow velocity in the diagnostic evaluation of a stenosis:

- *Peak systolic flow velocity*: The highest flow velocity derived from the angle-corrected Doppler tracing obtained by continuous scanning of the stenotic area. A hemodynamically significant stenosis (> 50 % stenosis) is assumed at peak systolic flow velocities > 120 cm/s and intermediate- to high-grade stenosis (> 70 – 80 % stenosis) at 180 – 240 cm/s. Recent studies of color duplex ultrasound demonstrated sensitivities of 90 – 96 % and specificities of 86 – 93 % (Faught et al. 1994; Grant et al. 2000; Neale et al. 1994; Moneta et al. 1993; Polak et al. 1992).
- *Minimum end-diastolic flow velocity*: This parameter likewise increases with the stenosis grade for stenoses with a diameter reduction of at least 50 %. In stenoses greater than 50 %, end-diastolic flow velocity is increased to > 40 cm/s. Velocities of over 80 – 100 cm/s suggest a high-grade stenosis. This parameter is especially useful for quantifying subtotal occlusion, in which peak systolic velocity is more difficult to determine.
- *Internal carotid artery to common carotid artery velocity ratio*: Absolute flow velocities are influenced by physiologic and abnormal systemic factors (hypertension, aortic valve stenosis, medial sclerosis, contralateral occlusion). The effect of these factors can be reduced by calculating the ratio of peak systolic velocity in front of and within the stenosis (Moneta et al. 1993; Ranke et al. 1999). However, as the external carotid artery also arises from the common carotid, the ratio is altered if the external carotid is stenosed or acts as a collateral in the presence of an internal carotid artery stenosis.

Technical advances in recent years and the advent of high-resolution transducers have led to improved sensitivities and specificities of 90 – 95 % with regard to the correct identification of hemodynamically significant carotid stenoses. The correlation of intra-arterial angiography and color-coded duplex scanning is 0.8 – 0.9 (Faught et al. 1994; Sitzer et al. 1993). The poststenotic waveforms sampled downstream of high-grade stenoses may show reduced peak systolic flow and filling of the spectral window (cf. Table 5.6 and Fig. 1.25 a–f).

Atherosclerotic elongation of the internal carotid artery leads to tortuosity, kinking, and coiling due to the limited space available between the bulb and the base of the skull.

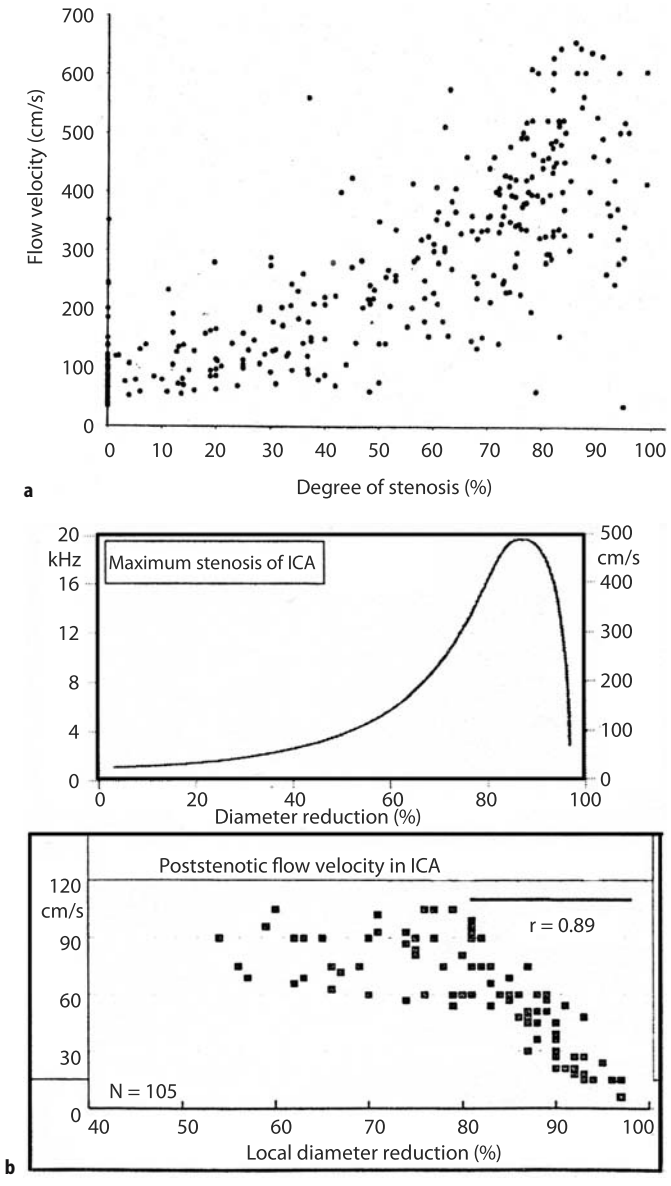

Fig. 5.6. a Internal carotid artery stenosis: Relationship between angiographic degree of stenosis and intrastenotic peak systolic flow velocity (from Moneta et al. 1995). **b** Increases in flow velocity with degree of stenosis. Peak systolic velocity increases as the diameter decreases (continuity law). In stenoses of the highest grades, in particular subtotal occlusion and long stenoses, peak intrastenotic velocity decreases again due to friction losses. Higher-grade stenoses (especially 85% or greater) are associated with a decrease in poststenotic peak systolic velocity (*bottom*). (According to Görtler 1998, personal communication)

Such changes typically do not require treatment and are often incidental findings that impair duplex evaluation. Only kinking stenoses, in particular symptomatic ones, require surgical resection (cf. Fig. A 5.2).

Even severe kinks or coils will lead to stenoses only if the artery takes a sharp turn but may impair flow velocity measurements due to the difficulty of achieving an adequate Doppler angle. Therefore, indirect criteria such as turbulent flow must be considered as well. If there is pronounced kinking, the constriction may vary with different functional positions of the cervical spine.

The above-discussed parameters for grading stenoses of the internal carotid artery have accuracies of 83–97% compared to intra-arterial angiography as the gold standard. When determination of the absolute parameters yields borderline results, effects of systemic conditions such as hypertension or hypercirculation (fever, hyperthyroidism) have to be taken into account. The pulsatile flow in medial sclerosis in longstanding diabetes is associated with a larger systolic component and a smaller diastolic component. Contralateral carotid occlusion, high-grade stenosis, or multiple-vessel disease with vertebral artery involvement also leads to higher flow velocities in the carotid system, depending on collateralization (cf. Fig. A 5.14). Therefore, the cutoff for discriminating between low-grade and hemodynamically significant (>50%) stenoses must be increased to a peak systolic velocity of 140–150 cm/s (modified according to AbuRahma et al. 1995). Not taking these factors into account will lead to false-positive findings and overestimation of carotid stenosis (Horrow et al. 2000).

The effects of systemic factors such as hypertensive episodes or greater pulsatility due to reduced wall elasticity can be minimized by using the internal carotid artery to common carotid artery velocity ratio (V_{max} ICA/V_{max} CCA ratio) as a criterion for stenosis grading. This ratio can be calculated as a supplementary parameter in cases where such systemic factors are suspected and peak velocity measurement yields inconclusive results. It must be noted, however, that larger studies of sonographic stenosis grading in comparison with angiography suggest that the velocity ratio shows similar variations as peak systolic velocity (Moneta et al. 1995; Fig. 5.6 a, b).

Despite the range of flow velocities associated with a given stenosis grade as determined by angiography there is good agreement between duplex ultrasound grading on the basis of peak velocity and angiographic grading (Tables 5.7, 5.8, and 5.9). Another factor limiting the quantification of stenoses is the interindividual variation in intrastenotic peak systolic velocities associated with 80% or 90% stenoses, which

Table 5.7. Accuracies of color duplex ultrasound (CDUS) in identifying and classifying hemodynamically significant internal carotid stenoses determined in studies using angiography as the gold standard (angio)

Author/year	Accuracy of CDUS versus angio [%]	
Hallam et al. 1989	(>50% stenosis)	91
Polak et al. 1992	(>50% stenosis; V_{sys} >125 cm/s)	83
Moneta et al. 1993	(>70% stenosis; $Vsys_{ICA/CCA}$ >4)	88
Faught et al. 1994	(>70% stenosis; V_{end} >130 cm/s)	93
Neale et al. 1994	(>70% stenosis; V_{end} >110 cm/s)	93
Moneta et al. 1995	(>70% stenosis; V_{sys} >250 cm/s and V_{end} >70 cm/s)	90
Ranke et al. 1999	(>70% stenosis; $Vmean_{ICAst/ICA}$)	97
Grant et al. 2000	(>70% stenosis; V_{sys} >225 cm/s)	90

The cutoff points used for angiography and color duplex scanning are given in brackets (some according to NASCET, some in ECST criterion).

Table 5.8. Agreement between 2 independent radiologists in identifying and classifying hemodynamically significant carotid stenosis on angiography

Author/year	Agreement between 2 independent radiologists [%]
Croft et al. 1980	88
Moneta et al. 1993	93

Table 5.9. Accuracy of angiography in comparison with pathologic workup of surgical specimens

Author/year	Accuracy of angiography relative to pathology [%]
Croft et al. 1980	79

depends on the individual extent of collateral blood flow and which also affects the risk of embolism as a result of different shearing forces acting on the plaque.

The gold standard, angiography, also has pitfalls even if a stenosis is evaluated in different projections and quantification is done in the plane with the most pronounced luminal narrowing. Independent interpretation of the findings by two radiologists shows variations in accuracy from 80 to 93%. Errors in angiographic stenosis grading arise from the fact that the three-dimensional plaque is projected onto the two-dimensional film, where the resulting degree of narrowing varies with the imaging plane (Fig. 5.7 a, b). Moreover, plaques of different configuration which produce the same diameter reduction differ in the magnitude of cross-sectional area reduction.

When comparing duplex scanning and angiography, one must also take into account whether the angiographic findings are based on local or distal stenosis grading. As already mentioned, the distal degree of stenosis was used in the NASCET and the local degree in the ECST. The distal degree of stenosis is easier to determine angiographically than the local degree as the latter requires estimation of the bulb diameter through interpolation. Distal quantification would be more appropriate if the hemodynamic effect of a stenosis had a role in the development of stroke [the hemodynamic significance, or flow reduction, depends on the luminal narrowing relative to the (distal) normal internal carotid artery]. Since this is not the case and the majority of strokes are caused by arterial emboli arising from plaques, the *German Society of Ultrasound in Medicine* recommends use of the local quantification method.

The risk of embolism of a plaque increases with its thickness, and eccentric plaques in the bulb may reach a dangerous thickness with a higher risk of rupture due to longitudinal pulsatile movement of the plaque even if no high-grade stenosis is present according to distal quantification. Due to the greater width of the bulb, localized narrowing of about 30% in this area does not have any stenotic effect because it merely reduces the luminal size to that of the more distal internal carotid artery. The local degree of stenosis can be calculated from the distal degree according to the formula: Local degree (ECST criterion, in %) = 0.6 x distal degree (NASCET criterion, in %) + 40% (cf. Sect. 5.5.1.1).

Compared with the internal carotid artery, the external carotid has a more pulsatile flow profile with a smaller diastolic component. Stenoses typically occur at its origin but become clinically relevant only in association with internal carotid occlusion and collateral blood supply to the brain through extracranial branches such as the supratrochlear artery.

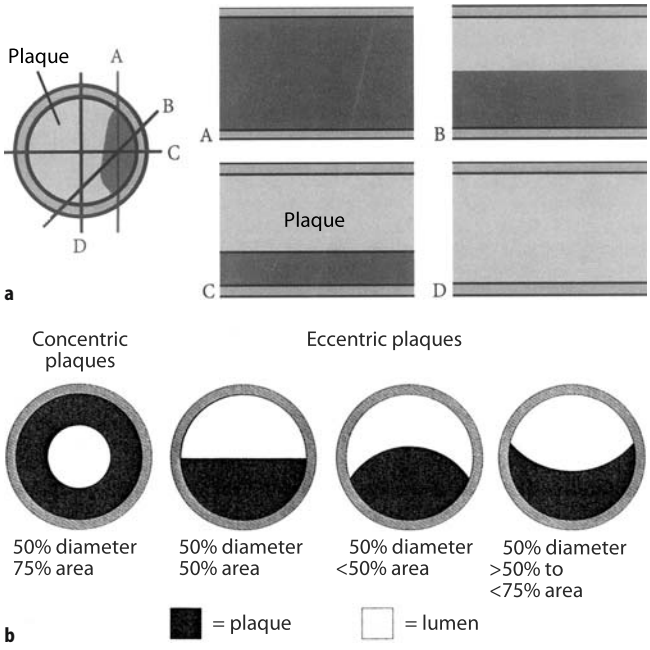

Fig. 5.7. a Eccentric luminal narrowing can vary widely in appearance and suggest different degrees of stenosis, depending on the imaging plane (angiography and B-mode ultrasound). The plaque shown may yield the following stenoses grades: A: 0%, B: about 50%, C: about 70%, D: 100%. This source of misinterpretation results from the reduction of the three-dimensional vascular lesion to the two-dimensional imaging plane. Color duplex facilitates evaluation of eccentric plaques, which, if possible, should be assessed in transverse and longitudinal orientation. **b** Plaque morphology (concentric – eccentric) can lead to variable degrees of cross-sectional area reduction despite identical diameter reduction. Eccentric plaques are thicker than concentric ones while producing identical stenosis grades and are therefore associated with a higher risk of stroke because they are more susceptible to rupture, as they are exposed to greater shearing forces (longitudinal pulsation).
These two factors (reduction to two planes and differences in plaque configuration) explain the discrepancies in stenosis quantification between duplex ultrasound and angiography in case of eccentric plaques. Differences in plaque configuration lead to problems when stenosis grading on the basis of hemodynamic criteria with duplex ultrasound is compared with angiography using diameter reduction as a morphologic criterion. For instance, a 50% diameter reduction measured angiographically and indicating a 50% stenosis corresponds to a 50% stenosis based on hemodynamic grading expressed as cross-sectional area reduction when the plaque is eccentric, but to a 75% stenosis when the plaque is concentric. The stenosis grade determined hemodynamically by spectral Doppler and expressed as area reduction reflects the extent of blood flow reduction more adequately. This is also relevant in evaluating peripheral or renal artery stenoses

Stenoses of the common carotid artery are rare compared to internal carotid stenoses. Preferred sites are its origin from the aortic arch or from the innominate artery and its distal segment just in front of the bifurcation. In case of subtotal or total occlusion of the common carotid artery, the internal carotid can be supplied through branches of the external carotid (such as the superior thyroid artery). Depending on the course of the collateral pathways, the external carotid will show variable retrograde filling. The hemodynamic stenosis criteria for the common carotid are the same as for the internal carotid.

Pulsatility is influenced by the peripheral resistance and wall elasticity. A stenosis causes more pulsatile flow in the prestenotic segment and less pulsatile flow in the poststenotic segment. Causes of decreased pulsatility are AV fistulae, hyperperfusion due to hyperthyroidism, and tachycardia. An increased pulsatility may be due a decreased wall elasticity as in medial sclerosis, an increased intracranial pressure, aortic insufficiency, and bradycardia (cf. Fig. 5.8 a, b).

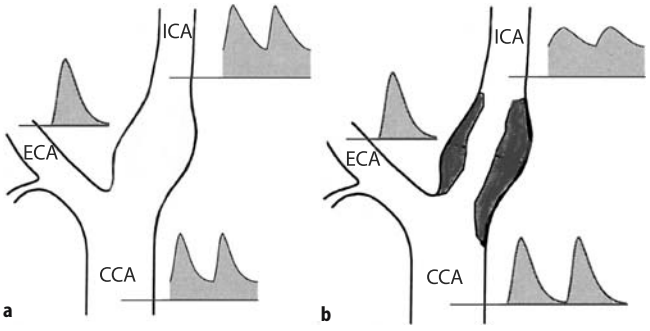

Fig. 5.8 a, b. Schematic Doppler waveforms of the carotid system: **a** Normal waveforms: Internal carotid artery (*ICA*) with low-resistance flow indicated by little pulsatility and a large diastolic flow component. External carotid artery (*ECA*) with more pulsatile flow due to higher peripheral resistance of skin and muscles, the primary area supplied by this carotid branch. The common carotid artery (*CCA*) dividing into the internal and external carotids has a mixed pulsatility. **b** High-grade stenosis or occlusion of the internal carotid artery leads to an increasingly pulsatile flow in the common carotid with a character resembling that of the external carotid (as the effect of the internal carotid is reduced or eliminated). If, in addition, the external carotid contributes to brain supply through vessels connecting the internal and external carotids (supratrochlear artery), its waveform becomes less pulsatile due to lower peripheral resistance. Downstream of a high-grade stenosis of the internal carotid, the waveform reflects postocclusive changes: delayed systolic upslope and less pulsatile flow, i.e. a larger diastolic component and reduced peak systolic velocity. The change is less pronounced than in peripheral vessels as the internal carotid supplying a low-resistance area already has a monophasic flow profile under normal conditions

5.6.1.3 Occlusion

Occlusions of the carotid territory are chiefly due to local thrombus formation on the basis of stenosing atherosclerosis at the origin of the internal carotid artery. As there are no arteries emptying into or arising from the internal carotid artery along its extracranial path, the occlusion extends to the level of the next branching in the petrous bone or intracranially to the ophthalmic artery. Embolic occlusions mainly affect the distal, intracranial segments of the internal carotid system. In the most severe form, there will be to-and-fro flow in the Doppler tracing (blunt waveform) and the thrombus may extend cranially to the level of the bifurcation. Differentiation of subtotal and total occlusion of the internal carotid artery is crucial for the surgical procedure. Unfortunately, the ingrowth of vessels into the connective tissue of an organized occlusion will impair differentiation from subtotal occlusion. Thus, depiction of color-coded flow signals in the internal carotid artery segment near the base of the skull indicating a patent lumen is the decisive criterion for establishing the differential diagnosis.

Adequate instrument setting (low wall filter, low pulse repetition frequency, high gain) is important do detect slow flow and small blood volumes in pseudo-occlusion. With adequate setting, failure to detect flow distal to the atherosclerotic lesion is the most reliable evidence of an occlusion. Since no vessels arise from the internal carotid artery extracranially, the Doppler waveform sampled far distal to the bulb (near base of skull) provides the most reliable information for differentiation, in particular as there are no structures interfering with the Doppler signal. Blood flow distal to a subtotal occlusion often assumes a venous character with a slow systolic velocity (Fig. 5.8 a, b). Based on these criteria, color duplex scanning has a positive predictive value of 92.5 – 96.7 % in demonstrating occlusion of the internal carotid artery (Kirsch et al. 1994).

B-mode scanning is fairly unreliable in demonstrating occlusions, in particular fresh ones, which often do not show any major intraluminal structures. Older occlusions, on the other hand, may already be noted in the B-mode, which will demonstrate internal echoes from the connective tissue in the shrunken volume. However, an occluded vessel is often difficult to distinguish from surrounding tissue.

In the rare cases of common carotid artery occlusion, the internal carotid may be refilled through branches of the external carotid serving as collaterals (superior thyroid artery and others; cf. Fig. A 5.13). The corresponding Doppler spectrum shows retrograde flow in the proximal external carotid artery with reversal to forward flow, though with a highly postocclusive character, in the internal carotid artery.

Bypass grafting is indicated only in multiple-vessel disease with reduced global perfusion that carries the risk of border-zone infarctions.

5.6.1.4 Postoperative Follow-up

Three operative techniques are available for thromboendarterectomy (TEA) of the internal carotid artery (Fig. 5.9 a–c).

In patients with a wide bulb, TEA can be performed with direct closure of the arteriotomy. A possible complication of this procedure is the inadvertent creation of a relative stenosis

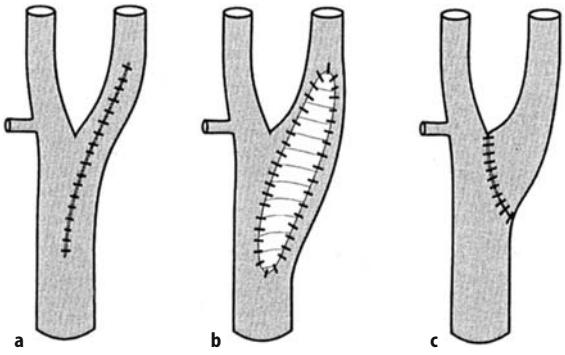

Fig. 5.9 a–c. Techniques of vessel repair in internal carotid artery stenosis. **a** TEA with direct closure. **b** TEA with patch angioplasty. **c** Eversion TEA

compared to the distal lumen of the internal carotid by pulling the vessel wall too tight.

This complication can be prevented by interposing a synthetic or venous patch after TEA to compensate for the relative narrowing that may be created by primary closure. Too wide a patch, on the other hand, will lead to ectasia or even aneurysm with development of turbulent flow.

In eversion TEA, the internal carotid is transected at its origin and the outer coat over the stenosing plaque-intima cylinder is everted and dissected along the vessel until the intima appears fairly normal again. At this point the cylinder is transected and the outer wall coat is re-inserted into the common carotid.

Each of these three surgical techniques is prone to specific complications that must be carefully excluded by postoperative ultrasonography. The complications of the primary closure technique, apart from relative narrowing as an early complication, are an intimal step or an intimal flap. Elongation of the internal carotid artery can lead to kinking with development of a stenosis unless the excessive segment is resected.

Patch angioplasty is susceptible to thrombotic deposits but these may resolve, even after days, following treatment with heparin and platelet aggregation inhibitors (cf. Fig. A 5.20). However, such thrombotic deposits can also induce TIAs or early occlusion. Aneurysmal dilatation due to excessive correction gives rise to turbulent flow. Suture aneurysms primarily occur in association with infection and after insertion of a synthetic patch. At the junction of the patch with the distal internal carotid artery, detachment of the intima can lead to the same complications as direct closure. Use of a venous patch can give rise to the formation of a true aneurysm due to the physiologically weaker venous wall. In the further course, recurrent stenosis may occur. Hence, in the follow-up examination, special attention must be paid to the suture area in order to identify stenosing intimal hyperplasia.

Suture line complications are rare in eversion TEA, while step formation at the transition to the native intima is somewhat more common (Table 5.10).

The specific complications of the individual operative techniques as just outlined must be borne in mind when performing the mandatory postoperative duplex ultrasound examination. Postoperative sonography is impaired by scattering through edema, which may affect both B-mode scanning and spectral Doppler recording. The use of a lower-frequency transducer (5 or even 3.5 MHz) yields B-scans with a poorer resolution but often facilitates both the identification of the vessel within the edematous tissue and spectral Doppler sampling for exclusion of early occlusion, residual stenosis, or stenosing thrombotic deposits.

Table 5.10. Sonographic evaluation of postoperative complications after surgical internal carotid artery reconstruction

Operative technique	Operative site	Distal internal carotid
TEA with direct closure	Relative stenosis, recurrent or residual stenosis	Intimal step, intimal flap, intimal dissection, kinking, intimal hyperplasia
TEA with patch angioplasty	Thrombotic deposits in the patch area without/with hemodynamically significant stenosis, suture aneurysm, ectasia, infection, recurrent stenosis	Intimal step, intimal flap, intimal dissection, kinking, intimal hyperplasia
Eversion TEA	Retraction of suture line, suture aneurysm, recurrent stenosis	Intimal flap, intimal step, intimal dissection, intimal hyperplasia

The development of recurrent stenosis has been investigated in numerous studies with postoperative follow-up by duplex scanning. However, the studies do not address the problem of the diagnostic accuracy of ultrasound in detecting the above-described early complications under the poorer postoperative insonation conditions as just outlined. Experience suggests that perioperative TIAs are often associated with thrombotic deposits on the synthetic patch, which are in part identified by a hemodynamic stenosis signal in the Doppler waveform and may be completely resolved within days to weeks under heparin and antiplatelet therapy. No studies have investigated these complications in terms of their possible impact on patch selection. Unfortunately, B-mode scanning can identify intimal flaps and dissection only after a few days when swelling has subsided. Intimal flaps are then often seen as hyperechoic floating structures in the bloodstream.

The flow pattern in a suture aneurysm is the same as in a false aneurysm. To-and-fro flow is demonstrated by color duplex scanning or in the spectral waveform (see also Sect. 2.1.6.3 and Figs. A 5.15 and A 5.16).

If semiclosed endarterectomy of the external carotid artery is performed, intimal flaps or dissection may give rise to external carotid stenosis or occlusion. These are rarely significant functionally and clinically but must be considered in the differential diagnosis when examining the internal carotid artery.

The intimal step remaining at the proximal end of the TEA in the common carotid is often highly conspicuous on the B-mode scan but has no clinical or functional relevance as the step flattens out in the direction of the flowing blood.

Following carotid PTA with stenting, ultrasound depicts the stent as a meshlike structure. A diagnostic spectral waveform is difficult to obtain from the stented vessel segment by (color) duplex scanning during the first days, presumably because the stent is not yet incorporated. After this initial period, the insonation conditions are the same as before stent placement. Stents are also prone to thrombotic deposits that may become stenotic and recede under treatment with heparin and platelet antiaggregators. The distal stent end is especially prone to recurrent stenosis (cf. Figs. A 5.21 and A 5.22).

Recent follow-up studies of carotid artery stenting procedures have shown that higher velocity thresholds have to be assumed for the adequate diagnosis of recurrent stenosis. Blood flow is altered in the stented carotid artery. Peak systolic flow velocity and the ICA/CCA velocity ratio increase with stenosis to a greater extent in stented carotid arteries.

To differentiate $\geq 70\,\%$ from $< 70\,\%$ angiographic stenosis, a peak systolic velocity ≥ 350 cm/s had 100 % sensitivity, 96 % specificity, 55 % positive predictive value, and 100 % negative predictive value. An ICA/CCA velocity ratio ≥ 4.75 had 100 % sensitivity, 95 % specificity, 50 % positive predictive value, and 100 % negative predictive value. Optimal thresholds to differentiate $\geq 70\,\%$ stenosis in unstented arteries were a positive predictive value of 250 cm/s and an ICA/CCA ratio of 3.50 (Stanziale et al. 2005).

The optimal threshold for 50 % stenosis, i.e. stenosis becoming hemodynamically significant, was 225 cm/s for recurrent stenosis in stented carotid arteries. This threshold had 90 % sensitivity, 97 % specificity, and 96 % diagnostic accuracy. These results were obtained using the distal stenosis grade according to the NASCET criteria. If the local grading system (based on ECST criteria) presented above is used, the thresholds are lower as the local system assigns a higher degree to the same stenosis as compared with the distal degree (NASCET). Moreover, it must be noted that the study included only 118 stented arteries with recurrent stenosis in 20 of them. Larger studies are not yet available and the data is quoted here merely to show that standard velocity criteria that are valid for unstented vessels need to be revised and replaced by higher cutoff values to diagnose significant recurrent stenosis in stented internal carotid arteries.

5.6.2 Vertebral Arteries

5.6.2.1 Stenosis

Virtually all stenoses of the vertebral artery occur at its origin from the subclavian artery. Since there is wide fluctuation in peak systolic flow velocities and perfusion in the vertebral artery resulting from marked caliber differences (hyperplasia, hypoplasia), no absolute cutoff value can be given to discriminate between low-grade and hemodynamically significant stenosis as in the carotid (Fig. 5.10). Instead, the diagnosis of a vertebral artery stenosis relies on indirect criteria such as turbulent flow at the origin or markedly reduced pulsatility compared to the contralateral vessel. A pronounced local increase in peak systolic flow velocity at the origin compared to more distal segments suggests a vertebral artery stenosis ($> 50\,\%$ difference). A high-grade stenosis is identified on the basis of a marked increase in peak systolic velocity (> 150 cm/s; cf. Fig. A 5.25).

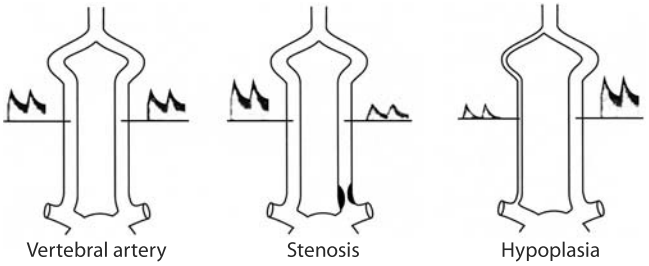

Fig. 5.10. Schematic Doppler waveforms of the vertebral artery. Normal waveform on the *left*. The postocclusive waveform in the *middle* shows a delayed systolic rise and lower peak systolic velocity but a relatively large diastolic component. The waveform in a hypoplastic vertebral artery (*right*) differs from the poststenotic waveform in that the diastolic velocity is decreased as well. (Modified according to Widder 1995)

5.6.2.2 Occlusion

Occlusion of the vertebral artery can occur if the vertebral artery itself is affected by progressive atherosclerosis or if it is involved in atherosclerosis of the subclavian artery. An occlusive process of the proximal vertebral artery segments is diagnosed as the absence of flow signals from the vessel demonstrated after adjustment of the scanner to slow flow. Intracranial occlusion downstream of the origins of the first intracranial branches leads to a markedly higher pulsatility of the upstream segment with a diminished diastolic flow velocity. The higher pulsatility – possibly combined with to-and-fro flow – gives rise to the tentative diagnosis of basilar artery occlusion.

5.6.2.3 Subclavian Steal Syndrome

The vertebral artery system is of special significance in the subclavian steal syndrome. Proximal stenoses or occlusions of the subclavian artery lead to diversion of blood from the basilar territory when the ipsilateral arm is used. Clinically, the steal phenomenon is characterized by symptoms of intermittent brain stem and cerebellar ischemia in the form of dizziness, ataxia, or drop attacks. Flow reversal in the ipsilateral vertebral artery is typically triggered by exercise but can also occur at rest. In this situation, blood is supplied to the affected arm by other cerebral arteries, in particular the contralateral vertebral artery.

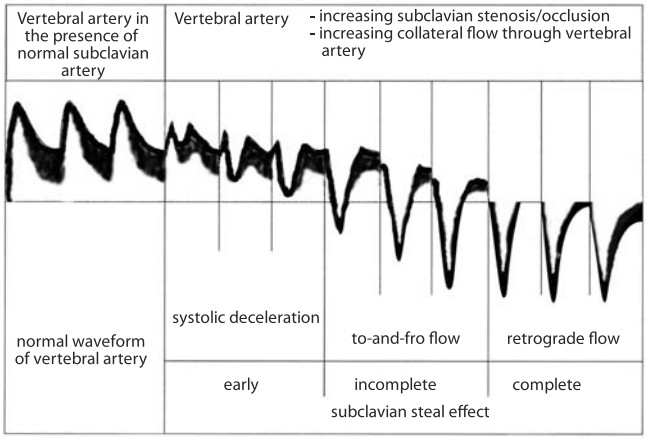

Fig. 5.11. Changes in the Doppler waveform of the ipsilateral vertebral artery in subclavian artery occlusion with subclavian steal. Depending on collateralization and the hemodynamic role of the vertebral artery as a collateral pathway, changes already occurring without provocative maneuvers may range from systolic deceleration, through to-and-fro flow, to retrograde flow (in case of pronounced vertebrovertebral crossover). The provocative test may induce more pronounced changes in the postischemic phase, e.g. an increase in the retrograde flow component or a change from systolic deceleration to retrograde flow

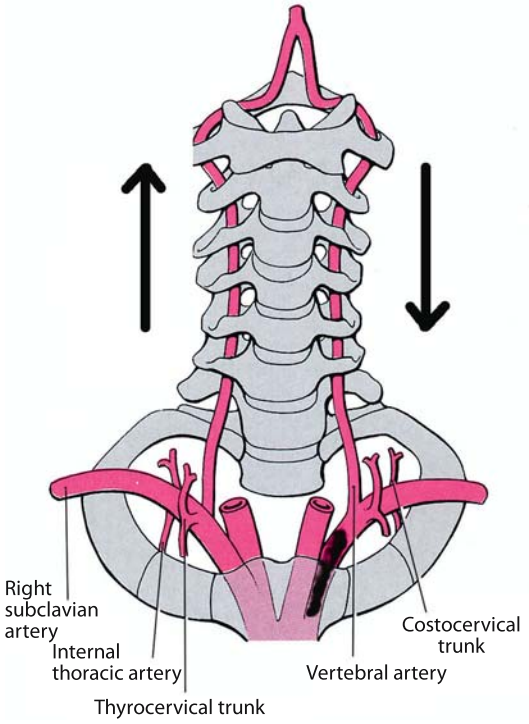

Fig. 5.12. Schematic representation of the course of the vertebral arteries and blood flow direction (*arrows*) in occlusion of the left subclavian artery (*marked in black*). Flow in the ipsilateral vertebral artery is reversed. Other collateral pathways are the internal thoracic artery, thyrocervical trunk, and costocervical trunk. (Modified according to Heberer and van Dongen 1993)

The subclavian steal syndrome is diagnosed by the demonstration of reversed flow in the vertebral artery at rest or upon provoked hyperemia in the ipsilateral arm (cf. Figs. A 5.28 to A 5.30).

The severity of the subclavian steal syndrome varies with the extent of the occlusive process in the subclavian artery and the role of the vertebral artery in collateral flow to the arm. The increasing significance of the ipsilateral vertebral artery as a collateral is reflected in the Doppler waveform by changes ranging from increasing systolic deceleration, through to-and-fro flow with retrograde systolic flow and antegrade diastolic flow, to complete retrograde flow (Fig. 5.11).

In vertebrovertebral crossover, a steal effect chiefly occurs in the contralateral vertebral artery as the feeding vessel (Fig. 5.12), which is above all identified by an increase in diastolic flow in the provocative test. Further collateral pathways are the thyrocervical trunk, chest wall vessels, and cervical vessels supplying soft tissue.

The provocative test for demonstration of the steal effect in case of less pronounced collateral flow through the vertebral artery is performed by inducing ischemia in the ipsilateral arm by means of an upper arm cuff inflated to over 200 mm Hg for 3 to 5 minutes. Subsequent deflation will lead to a postischemic increase in flow velocity in the arm arteries, resulting in an increase of the steal effect in the vertebral artery. This is reflected in the waveform by an increase in the retrograde flow component or even complete flow reversal despite a predominance of antegrade flow at rest.

Duplex ultrasound is the method of choice for evaluating patients with subclavian occlusion and symptoms of subclavian steal. It enables detailed evaluation of the steal effect in the vertebral artery with differentiation of the stages of incomplete steal. However, occlusion of the subclavian artery, just as of the carotid artery, may have no therapeutic relevance if no neurologic symptoms or clinical complaints are present.

5.7 Diagnosis of Brain Death

An elevated intracranial pressure associated with trauma, hemorrhage, or edema is reflected by signs of increased peripheral resistance in the upstream vessel segments. In the Doppler spectrum of the internal carotid artery, increasing intracranial pressure is indicated by a corresponding decrease in the diastolic flow component or even to-and-fro flow with a systolic forward and diastolic backward component (Fig. 5.13). However, the correlation between intracranial pressure and the pulsatility index varies as it is affected by individual factors and autoregulatory processes as well as the underlying disease. Therefore, no reproducible absolute values of intracranial pressure can be derived from the Doppler waveform or the pulsatility index.

Nevertheless, interpretation of the Doppler waveform will yield information on relevant elevations of intracranial pressure. When intracranial pressure exceeds diastolic blood pressure, the diastolic flow component disappears or be-

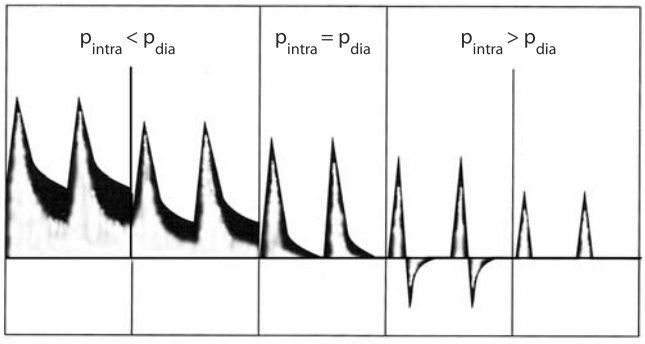

Fig. 5.13. Changes in the pulsatility of the extracranial segments of the cerebral arteries with increasing intracranial pressure. The schematic Doppler waveforms from left to right reflect the increase in the diastolic component (P_{dia} = diastolic blood pressure) resulting from increasing intracranial pressure (P_{intra}). In the middle, the end-diastolic component has disappeared. The right waveform first shows to-and-fro flow and then only early-diastolic peaks as signs of cerebral circulatory arrest. (According to Widder 1995)

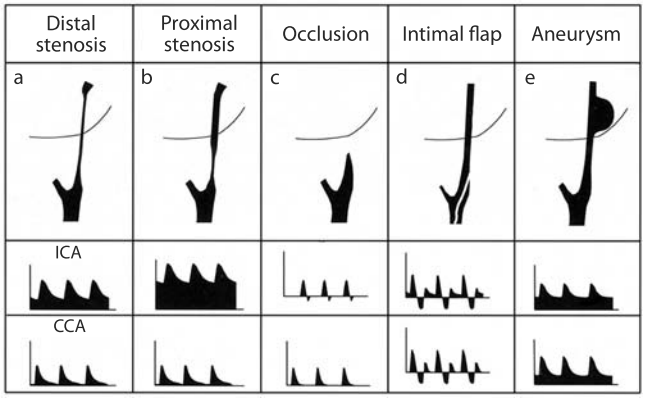

Fig. 5.14 a–e. Different flow profiles in the internal carotid artery in dissection, depending on localization, extent, thrombosis, and sites of entry and re-entry (from Widder 1995). **a** Long internal carotid dissection with varying flow velocities in the patent segment. **b** Short dissection with circumscribed flow acceleration at the site of luminal narrowing. Differentiation of atherosclerotic lesions and fibromuscular dysplasia may be difficult. **c** Dissection-induced occlusion of the internal carotid artery with blunt signal (to-and-fro sign) in the patent segment. Flow in the common carotid artery assumes the character of the external carotid. **d** If the true and false dissection lumina are patent, flow profiles vary widely with the sites of entry and re-entry. The waveform of the true lumen is highly dependent on the flow obstruction caused by the dissection. Fluttering of the intimal flap leads to a multiphasic waveform. **e** Distal formation of a pseudoaneurysm (typically beneath base of skull) cannot be detected by ultrasound because proximal flow is normal

comes retrograde (to-and-fro flow), suggesting cessation of cerebral blood flow. In Germany, transcranial Doppler sonography has been an accepted diagnostic modality to shorten the waiting time for diagnosing cerebral circulatory arrest since the end of 1991. If the typical changes in the Doppler waveform cannot be demonstrated in the basal cerebral arteries due to technical limitations, cerebral circulatory arrest can be diagnosed by demonstrating these changes in the flow profile (Fig. 5.13) of the extracranial segments of the internal carotid or vertebral arteries using duplex sonography. In doing so, care must be taken to clearly identify the arteries supplying the brain and to differentiate them from other segments such as the external carotid artery.

5.8 Rare (Nonatherosclerotic) Vascular Diseases of the Carotid Territory

5.8.1 Dissection

Carotid dissection due to intramural hemorrhage as a cause of cerebral infarction primarily affects adolescents. It is typically due to trauma and rarely occurs spontaneously. Dissection chiefly occurs in areas where a vessel segment is subject to injury from bony structures such as the skull base or the transverse foramina. Following an acute phase with a relatively high risk of embolization and occlusion, dissection has a good long-term prognosis with regard to spontaneous repair through recanalization.

B-mode scanning may already identify dissection by depiction of an intimal flap or a long stretch of eccentric luminal narrowing, typically extending along the entire length of the extracranial internal carotid. Thrombosis of the false lumen is usually identified by a somewhat higher echo level compared to the patent lumen. The Doppler waveform varies widely with the extent and type of dissection. In case of dissection-induced occlusion with a patent origin, a blunt waveform is obtained and the profile of the common carotid assumes the character of the external carotid. Dissection with luminal narrowing is characterized by a waveform with a higher Doppler shift frequency and an increased angle-corrected flow velocity in the residual lumen over a long stretch of the internal carotid. With only minimal luminal narrowing, the spectral Doppler tracing from the internal and common carotids appears fairly normal (Fig. 5.14 a–e).

Dissection of the common carotid artery may also result from blunt trauma to the neck or hyperextension of the cervical spine. Moreover, it may be caused iatrogenically by puncture of the cervical veins or secondarily in aortic dissection with extension into the common carotid (type I according to De Bakey). Rarely, common carotid dissection extends into the internal carotid with patency of long stretches of both vessels. In this form there may be forward flow in both vessels but also to-and-fro flow or retrograde flow in the false lumen, depending on the site of re-entry (cf. Fig. A 5.18).

5.8.2 Inflammatory Vascular Disease (Takayasu's Arteritis)

Takayasu's arteritis, also known as pulseless disease, is a rare chronic inflammatory condition, typically affecting the common carotid and subclavian arteries while the internal carotid is not involved. In this condition, the inflammatory process

leads to concentric thickening of the vessel wall. Its etiology is unknown but an immunologic basis is likely. The disease predominantly occurs in younger women. General symptoms include weakness, headache, fever, and loss of weight. These symptoms as well as unspecific signs of inflammation are present before vascular stenosis or occlusion occurs, and an ultrasound examination of the subclavian and common carotid arteries should be performed in cases of suspected Takayasu's arteritis. If the suspicion is confirmed by sonography, cortisone therapy is initiated to prevent vascular complications.

Highly characteristic of Takayasu's arteritis is the concentric, homogeneous, and fairly hypoechoic thickening of the inner vessel wall, the macaroni sign (cf. Fig. A 5.19). In contrast, atherosclerotic lesions exhibit focal variation, are more hyperechoic, and have an irregular surface. The Doppler spectrum will show a continuously but only moderately increased flow velocity, depending on the degree of concentric narrowing. Ultrasound has a markedly higher accuracy than angiography, in particular in early disease. In advanced disease, there may be vascular occlusion due to inflammatory wall thickening. Medical therapy with administration of anti-inflammatory and immunosuppressive agents is the treatment of choice. Bypass surgery is discouraged, even in occlusion, as the patency rate is poor.

5.8.3 Aneurysm

Aneurysms of the internal carotid artery are rare and may occur in atherosclerosis or inflammatory vascular disease. B-mode scanning depicts the focal dilatation of the vessel lumen (saccular or spindle-shaped) and color duplex can differentiate mural thrombotic deposits from the patent lumen. Embolism from the thrombotic deposits can lead to cerebral infarction. Color duplex ultrasound is the method of choice, enabling precise evaluation of the diameter and extent of the aneurysm as well as differentiation of thrombotic deposits (which is not possible with angiography) (cf. Fig. A 5.17).

A suture aneurysm is a false aneurysm that may be noted as a pulsatile mass of the neck or is detected at sonographic follow-up after carotid TEA. Color duplex ultrasound differentiates flow within the aneurysm from thrombotic material and the Doppler spectrum recorded in the neck area exhibits the characteristic "steam engine sound" with a high-frequency systolic signal and retrograde flow throughout diastole (cf. Fig. A 5.16). The indication for surgical revision can be established without preoperative angiography.

5.8.4 Arteriovenous Fistula

An *AV fistula* is typically caused by trauma or iatrogenically and is recognized on color duplex at first glance as a mosaic of colors due to perivascular vibration artifacts. In the Doppler spectrum, the fistula is identified by the high flow velocity and the arterialized flow pattern in the draining vein.

5.8.5 Tumorous Vessel Compression, Carotid Body Tumor

Compression of a carotid segment by cervical *tumors* or *lymph node metastases* is rare and more commonly affects the internal jugular vein. Carotid body tumors are highly vascularized masses located at the carotid bifurcation, where they cause the typical saddle deformity (splaying of the internal and external carotid branches by the tumor mass) on ultrasound. In the color duplex mode, multiple small tumor vessels are demonstrated.

The tumors arise from the 3 – 4 mm carotid body, a structure in the bifurcation that functions as a chemoreceptor and regulates PO_2, PCO_2, and the pH value. They are primarily supplied with blood from external carotid branches and rarely also from the thyrocervical trunk. Only 10 – 20 % of the carotid body tumors are diagnosed before surgery (Geiger et al. 1991). They are assumed to develop from paraganglial tissue, probably a residue of the neural crest. Hence, there may be multiple tumors and rarely also parajugular or paravagal tumors as well as tumors at the aortic arch. Histologically, an adenomatous and angiomatous subtype can be distinguished. The latter is extremely highly vascularized with an impressive appearance on color duplex scanning. Tumor growth in the area of the carotid bifurcation can lead to vessel encasement and compression. Color duplex evaluation of the localization and vascularization of the tumor contributes to the preoperative differentiation, and the information on tumor extension facilitates radical surgical removal.

5.9 Diagnostic Role of Duplex Ultrasound in Evaluating the Cerebral Arteries

As a noninvasive procedure, *duplex ultrasound* is the method of choice to confirm or exclude suspected obstructive changes of the carotid system following in the step-by-step diagnostic workup after clinical examination and history. The formerly widely used CW Doppler technique is less expensive, easy to perform, and has an accuracy of over 90 % in detecting the therapeutically relevant higher-grade stenoses (Keller 1990; Neuerburg-Heusler 1984). It is a suitable screening procedure for patients with a reasonable suspicion of carotid stenosis if abnormal findings are subsequently verified by duplex scanning. However, *atypical vessel courses* and sudden changes in the angle of incidence due to *kinking* or *coiling* of the carotid may lead to false-positive findings. Low-grade stenoses escape detection by CW Doppler.

Duplex ultrasonography has a sensitivity and specificity of over 90 % in quantifying internal carotid artery stenoses. Angiography, the current gold standard, has its limitations as well. Its accuracy, determined by comparing image interpre-

tation by two independent radiologists, is 88 to 93 %, which is similar to the comparison of duplex ultrasound and angiography. This agreement is surprising since duplex ultrasound is based on hemodynamic evaluation while angiography is a morphologic method. One drawback of angiography is the fact that the three-dimensional plaque protruding into the vessel lumen is reduced to the two film dimensions, which impairs the reliability of stenosis measurement despite mandatory assessment in 2 or 3 planes.

Duplex sonography is also the method of choice for evaluation of all nonatherosclerotic vascular conditions (inflammatory disease, dissection, aneurysm) because B-mode scanning depicts not only the luminal narrowing but also wall changes and perivascular structures.

The complications of angiography include a stroke rate of 1 – 3 % (Waugh et al. 1992), which is almost as high as the rate of complications experienced centers achieve with surgical management by carotid TEA. For this reason, the indication for carotid TEA is increasingly based on duplex ultrasound alone. In addition to the preoperative localization and quantification of carotid stenoses, sonography is also the diagnostic procedure of choice for the postoperative follow-up after carotid TEA or dilatation with stenting.

Numerous investigators have tried to identify sonographic criteria of plaque morphology that would enable preoperative estimation of the risk of embolism. However, in view of the controversial results of the studies on plaque evaluation and the methodological problems, predicting the risk of embolism on the basis of the sonomorphologic appearance must be regarded with caution. Further studies, in particular prospective ones, are needed for a definitive appraisal and identification of more accurate criteria. Such criteria are still lacking and have not even been identified by computer-based analysis. The retrospective analysis of patients operated on does not allow any conclusions to be drawn regarding plaque ulceration and its prognosis. Prospective studies on the natural history and the search for criteria to differentiate ulceration from a stable niche would be desirable but face numerous methodological problems. In view of the known risk of embolism of ulcerative plaques in high-grade stenosis, their follow-up observation in randomized studies is precluded on ethical grounds.

In addition, a methodological limitation of ultrasound has to be taken into account, namely that it does not visualize tissue directly but only the reflection of echoes at interfaces of different acoustic impedance. Although plaque composition is heterogeneous, the individual components do not necessarily differ in their acoustic impedance. Despite these limitations, sonographic plaque analysis can contribute additional information for estimating the risk of stroke. Rapidly progressive stenoses are four times more likely to cause TIAs and cerebral infarction than less progressive stenoses of a similar grade (Widder et al. 1992). Heterogeneous, mostly hypoechoic plaques have a greater tendency to progress. A more definitive association between the sonomorphologic plaque type and stroke cannot be established. Moreover, one also has to be aware that similar plaques may develop differently. Plaques that are considered harmless on the basis of their sonomorphologic and macroscopic appearance may rapidly become vulnerable, high-risk plaques, for instance, through intraplaque hemorrhage. This is why plaques should be monitored by ultrasound.

Initial CW Doppler scanning, as it used to be advocated by some investigators, is no longer necessary since color duplex performed with proper instrument settings enables continuous hemodynamic evaluation. Supplementary transcranial ultrasonography provides useful additional information on intracranial vessel anomalies and stenoses. A severe intracranial vascular process such as occlusion of the middle cerebral artery may occasionally be suggested by indirect signs demonstrated by continuous Doppler scanning or in the spectral waveform. However, the extracranial Doppler waveform may appear normal when there is good collateralization of a high-grade stenosis of the main trunk of the middle cerebral artery.

Duplex or color-coded duplex sonography is highly reliable in diagnosing and evaluating a carotid stenosis at its preferred site, the bifurcation. Angiography does not yield any additional information in this area. The hemodynamic assessment by duplex ultrasound is superior in grading carotid stenoses compared to angiography, which merely depicts the perfused lumen in relation to the adjacent vessel segment. Only ultrasound provides information on plaque morphology (cf. Sect. 5.6.1.1 and Fig. 5.7). Angiography is likewise insufficient in evaluating plaque ulceration (i.e. surface properties), as shown by the NASCET results in comparison with the intraoperative findings.

The advantages of *angiography* include the continuous visualization of the vasculature and better documentation of the findings. Whether angiography is necessary prior to carotid surgery in addition to duplex scanning performed by an experienced examiner depends on the communication between the surgeon and the sonographer and the technical quality of the ultrasound examination. Another advantage of angiography is the detection of stenoses near the aortic arch and base of the skull as well as intracranially. If the sonographic findings in these vessel areas are inconclusive, angiography should be performed.

The sonographer must work very conscientiously if no angiography is performed prior to carotid TEA. This comprises reliable identification of the internal and external carotid arteries. A high gain is required to differentiate subtotal and total occlusion. In particular if the examination is impaired by calcified plaques, the sonographer must attempt to depict flow signals in the vessel up to the base of the skull. However, a control angiography should be done in such cases and also if pronounced calcification impairs stenosis grading.

Angiography or intra-arterial DSA is no longer necessary unless the sonographic examination is inconclusive or shows indirect criteria of intracranial vascular pathology. If the indication for surgery is established on the basis of the duplex scan alone (as it is possible in experienced centers), supplementary magnetic resonance (MR) angiography can be performed for assessment of the intracranial internal carotid segments. MR angiography provides a good overview of the

extracranial and intracranial cerebral vasculature but overestimates the degree of stenosis due to turbulence, in particular when the time-of-flight technique is used. Nevertheless, with a sensitivity of 92% and specificity of 74%, contrast-enhanced MR angiography has a poorer accuracy in identifying stenoses requiring surgical management and is less accurate in determining the degree of stenosis than duplex ultrasound. The two modalities are supplementary with duplex ultrasound enabling adequate evaluation of the extracranial carotid system and MR angiography providing information on the intracranial vessels as well as on the supra-aortic origins of arterial branches. Together, the two modalities enable comprehensive diagnostic evaluation prior to surgical repair of a carotid stenosis.

The indication for surgical management in patients with the subclavian steal syndrome can be established if the clinical suspicion is confirmed by duplex scanning but only angiography will enable exact determination of collateral pathways.

If first-line treatment of a carotid stenosis is conservative (e.g. antiplatelet therapy), follow-up ultrasonography should be performed every 6 months for timely initiation of surgery in case of rapid progression. Follow-up after carotid TEA is performed immediately after the operation and then at 6-month intervals in order to detect recurrent stenosis or complications such as suture aneurysm.

5.10 Atlas

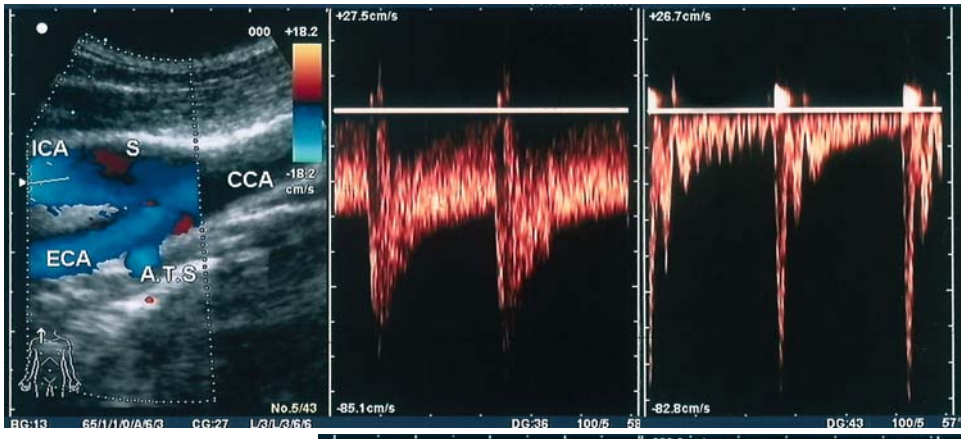

Fig. A 5.1 a, b
Carotid bifurcation
a Longitudinal view of the carotid bifurcation obtained with the transducer in the posterolateral position. The internal carotid artery (*ICA*) is closer to the transducer. The color change in the bulb indicates retrograde flow components due to flow separation (*S*) (cf. Fig. 1.23 b). The Doppler waveform of the internal carotid artery is characterized by a fairly large end-diastolic flow component

The external carotid artery (*ECA*) is depicted further away from the transducer with flow separation at its origin (red) and the superior thyroid artery (*A.T.S*) arising from it

Doppler waveforms recorded in the internal carotid (*middle section*) and external carotid (*right section*). The waveform of the ECA differs from that of the ICA by a more pulsatile flow and the pulsation transmitted from the temporal artery upon rhythmical tapping anterior to the ear (left part of the waveform)

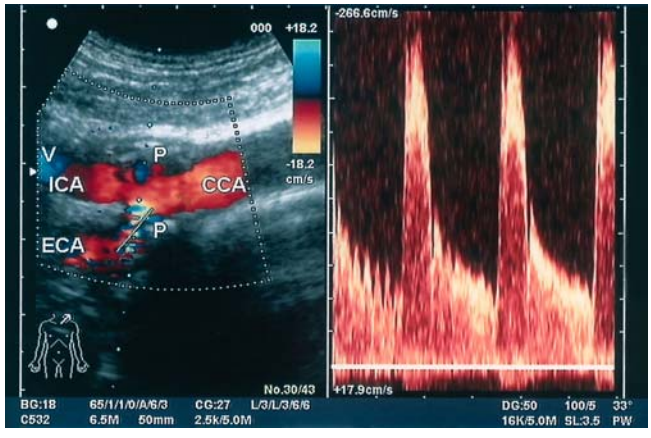

External carotid artery stenosis
b A stenosis of the external carotid artery is associated with less pulsatile flow in the stenotic area, which may make it difficult to assign a stenosis to the internal or external carotid branch. The temporal tap sign enables reliable differentiation of the two arteries even if the external carotid waveform is altered by stenosis. (Inverted color encoding of flow direction compared to **a**)

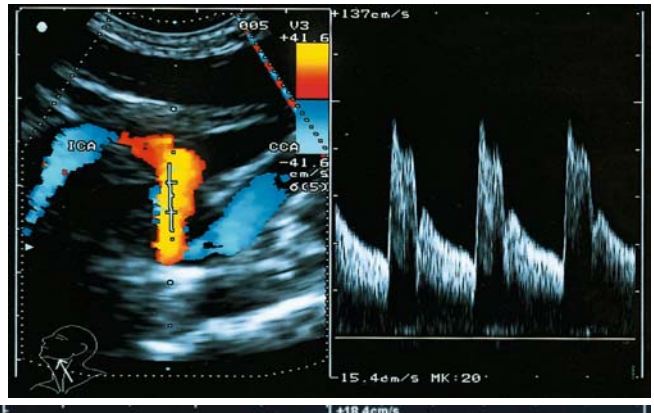

Fig. A 5.2 a, b
Kinking with stenosis
a Elongation of the internal carotid artery may lead to kinks or coils (cf. Fig. 5.1 b). The localized increase in the Doppler shift frequency is due to a changed insonation angle and must not be misinterpreted as indicating stenosis. In the color duplex mode, a stenosis causes aliasing in vessel segments insonated at a small angle. Depending on the insonation angle, kinks or coils with flow toward the heart in short vessel segments may mimic flow reversal

The color scan (*left section*) depicts the junction of the common carotid artery (*CCA*) with the internal carotid on the *right* and the distal internal carotid artery (*ICA*) on the *left*. The Doppler waveform obtained after careful adjustment of the insonation angle shows a peak flow velocity of 95 cm/s and laminar flow, confirming that aliasing in the color mode is due to a small insonation angle. The color change from red to blue is caused by the changed flow direction relative to the transducer

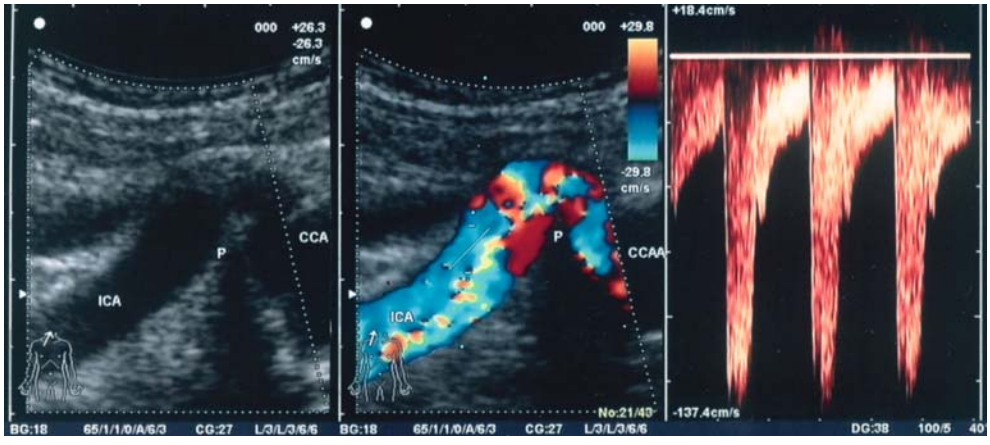

b Stenosis due to kinking of the internal carotid artery is rare. Such a stenosis may be caused by sclerotic wall changes with plaque (*P*) at the site of the kink. Here, a peak systolic flow velocity of 145 cm/s indicates a stenosis of approximately 60 %

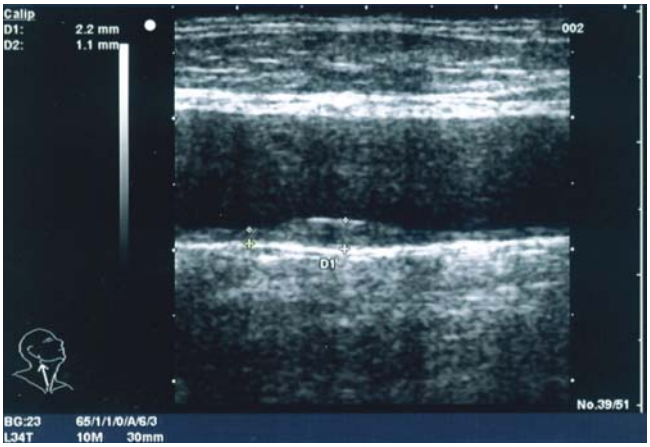

Fig. A 5.3
Measurement of the intima-media complex
The thickness of the intima-media complex is measured in the wall away from the transducer, where the interface between the perfused lumen and the intima produces a sharp reflection due to the intervening flowing blood. The intima and media cannot be differentiated because the next hyperechoic reflection occurs only at the transition from the adventitia to the connective tissue. The layer between these two reflections is the intima-media complex that is measured. The example shows abnormal thickening (1.1 mm) and a plaque with a thickness of 2.2 mm in the middle of the scan

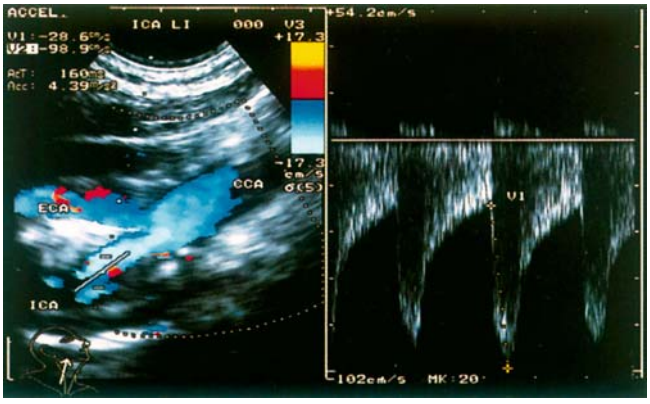

a

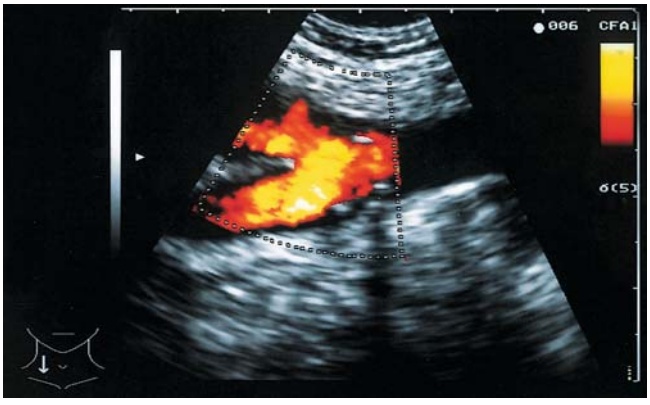

b

Fig. A 5.4 a, b
Plaque – grade of stenosis
a Sagittal scan from the anteromedial approach depicting the origin of the internal carotid artery. The plaques on the posterior wall are not hemodynamically significant, as suggested by a peak systolic velocity of 99 cm/s. However, both the color scan and the Doppler waveform show backward flow

Plaque contour
b Bowl-shaped gaps in the plaque (in the *middle* of the image at the origin of the internal carotid away from the transducer) suggest niches. Color duplex scanning or power (angio) mode as in this example is superior in depicting the patent lumen as compared with B-mode scanning. However, based on the ultrasound appearance, it is not possible to say whether the hypoechoic areas at the bottom of the gap correspond to thrombotic deposits with a risk of embolism or simply reflect the heterogeneous plaque composition. The plaque is not stenotic. The origin of the inferior thyroid artery arising from the external carotid artery and coursing toward the transducer is just barely visible

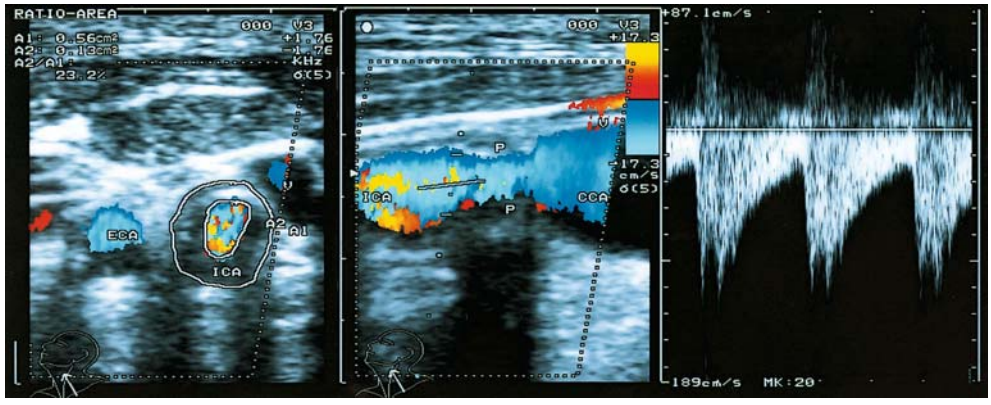

a

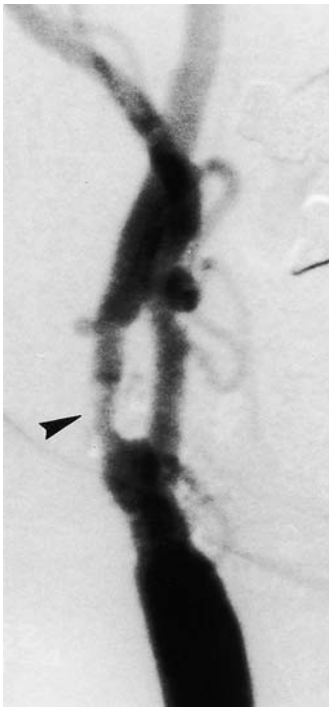

b

Fig. A 5.5 a, b
Stenosis with mild hemodynamic significance
a A circular plaque in the internal carotid artery (*ICA*) reduces the cross-sectional area by 75 % (*left section*). To achieve complete color filling of the perfused lumen in the transverse plane, a fairly low pulse repetition frequency is employed, which produces aliasing. The *middle section* depicts central flow acceleration in lighter coloring (yellow) and eddy currents as a change in color coding (red)

The hemodynamic stenosis grade with a peak systolic flow velocity of 128 cm/s and spectral broadening correlates with the cross-sectional area reduction measured. (A 65 – 83 % cross-sectional area reduction corresponds to a 40 – 60 % diameter reduction and hence to a stenosis just becoming hemodynamically significant.) Morphologically, the plaque is mostly hyperechoic and smoothly marginated. The sonographic criteria suggest a stable plaque type
b Angiography: Intermediate-grade stenosis of the origin of the internal carotid artery

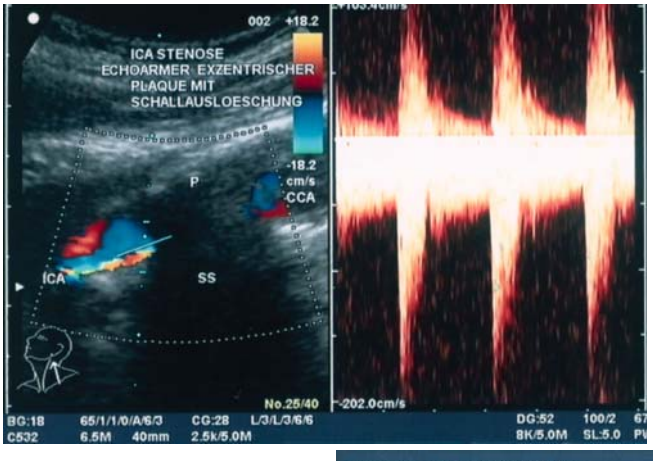

a

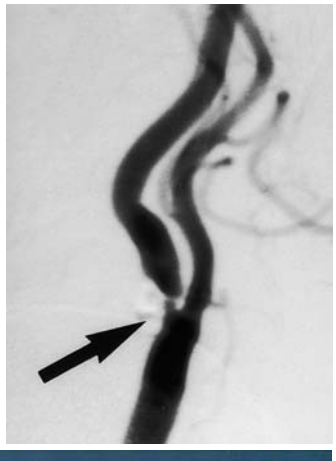

b

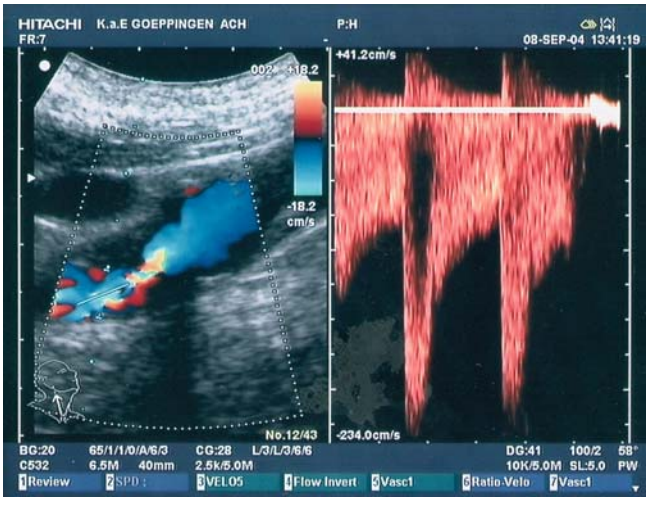

c

Fig. A 5.6 a–c
Intermediate-grade stenosis at origin of internal carotid artery
a The extent of luminal narrowing caused by the plaque at the internal carotid origin cannot be evaluated in the gray-scale scan due to calcification with posterior acoustic shadowing (SS). Color flow imaging is likewise impaired. Next to the acoustic shadow, there is an eccentric jet with aliasing (yellow) and turbulent flow. Flow velocity is increased to 180 cm/s in systole and 60 cm/s at end-diastole, indicating a 60 – 80 % stenosis by diameter reduction, which corresponds to an 84 – 95 % cross-sectional area reduction. In this case, it was not possible to depict flow by moving the transducer and thus avoiding the calcification. Instead, a high gain was used to obtain a Doppler spectrum from the area of acoustic shadowing for hemodynamic quantification of the stenosis
b Angiography: 60 – 80 % diameter reduction
c The plaque causes a similar degree of stenosis as in **a** but there is better visualization of the stenosis because the plaque is not calcified. In this example, the hypoechoic plaque that is vulnerable on the basis of sonographic criteria but has a smooth surface causes an intermediate- to high-grade stenosis in the bulb area (aliasing, flow velocity in the Doppler spectrum of 210 cm/s in systole and 80 cm/s at end-diastole). The B-mode scan (*left section*) depicts the common carotid artery on the right and the internal carotid artery on the left, both with flow coded in blue

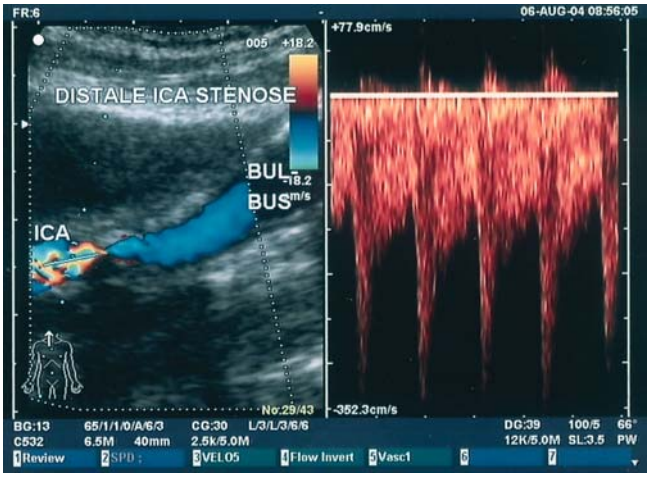

a

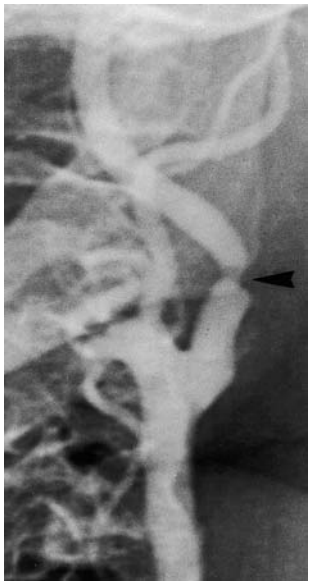

b

Fig. A 5.7 a, b
High-grade stenosis of distal internal carotid artery
a From a posterolateral transducer position, a stenosis is depicted in the internal carotid artery (*ICA*) about 3 cm from the origin of the external carotid artery (*ECA*). In the color duplex mode, the stenosis is indicated by aliasing; the plaque is hypoechoic. The peak systolic velocity is 380 cm/s, corresponding to a high-grade stenosis. The vessel cannot be traced more distally due to acoustic shadowing and scattering produced by connective tissue structures at the base of the skull. In the postoperative evaluation after carotid TEA, it is important to exclude stenosis at the distal patch end

b Angiography: Filling defect (*arrowhead*) just below the skull base and normal origin of the internal carotid artery

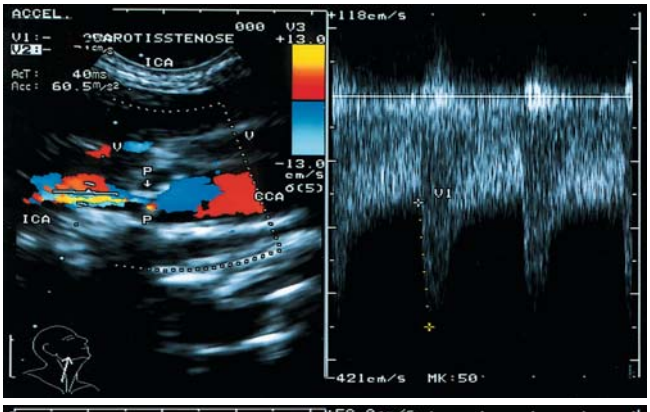

a

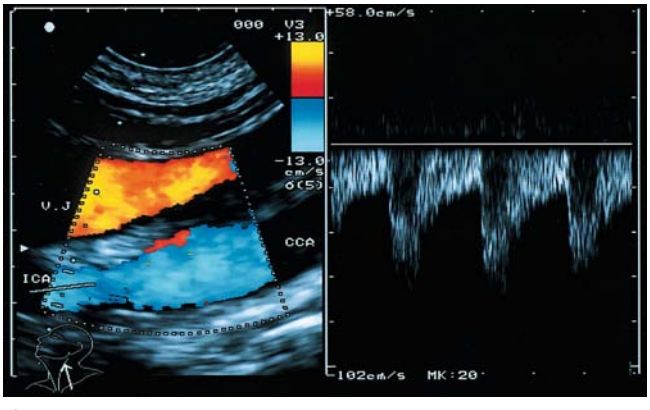

c

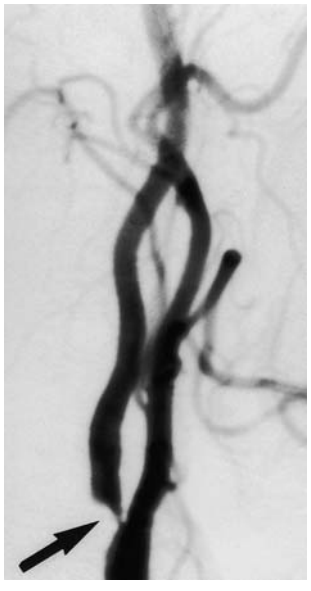

b

Fig. A 5.8 a–c
High-grade stenosis at origin of internal carotid artery
a The high-grade stenosis in the proximal internal carotid artery (*ICA*) is documented by a peak systolic flow of 350 cm/s with an end-diastolic flow velocity of 162 cm/s. These velocities correspond to an 81–99% diameter reduction. Stenosing, smoothly marginated eccentric plaques (*P*) of mixed echogenicity are seen with downstream color reversal from light blue to yellow indicating the stenosis jet. The sonomorphologic features suggest a stable plaque (mostly of high echogenicity, smooth surface) but its eccentric configuration is associated with an increased risk of embolism due to stronger shearing forces. In this scan, forward flow in the internal carotid artery is displayed in blue, away from the transducer. Color reversal occurs in the area of the junction with the common carotid artery, which is displayed in red with flow toward the transducer. Poststenotic eddy currents and flow separations with retrograde flow components displayed in red are seen above the stenosis jet. Additionally, flow signals from the jugular vein are depicted near the transducer
b Angiography: Eccentric high-grade stenosis (*arrow*) of the internal carotid artery

Internal carotid artery after TEA
c Postoperative follow-up after TEA with venous patch angioplasty shows a smoothly delineated vessel wall and laminar flow in the Doppler waveform. The larger cross-sectional area at the site of the patch leads to slower flow in this area

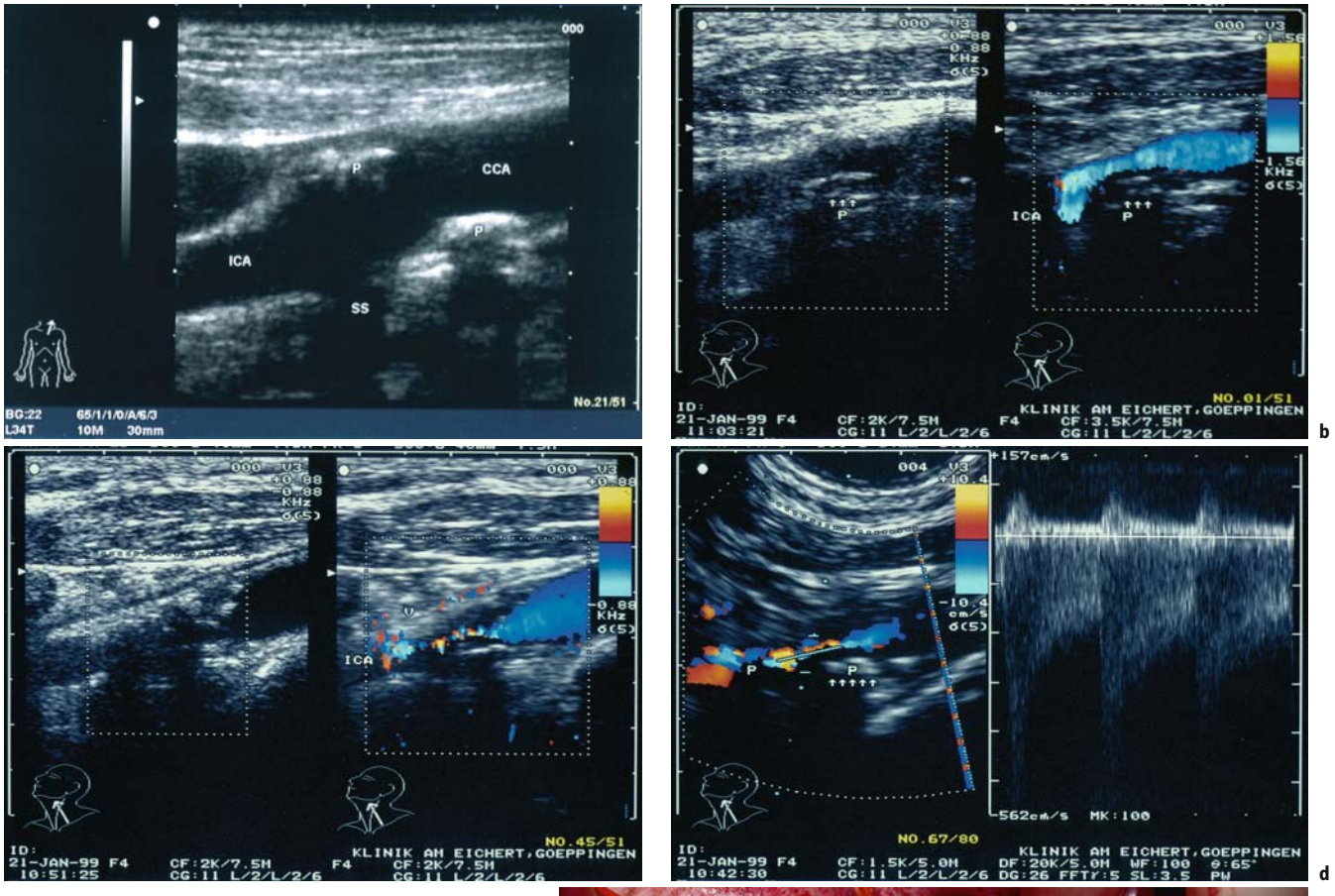

Fig. A 5.9 a–e
Plaque morphology

a A fairly homogeneous and hyperechoic plaque with smooth contours (*P*; wall away from transducer) is depicted in a more central vessel segment at the level of the bulb. This appearance suggests a fibrous plaque with a low risk of embolism. More distally, an inhomogeneous and mostly hypoechoic plaque with a surface poorly delineated from the lumen is depicted. In part, only isolated hyperechoic spots indicate the plaque border within the lumen. This appearance often correlates with an atheromatous plaque

b B-mode scan (*left section*) depicting a plaque with 40–50% diameter reduction in the sagittal plane. Fairly homogeneous plaque with a regular surface (type I). Color duplex confirms the smooth delineation of the plaque from the vessel lumen

c Sagittal B-mode scan showing inhomogeneous plaques that cast acoustic shadows and are poorly delineated from the vessel lumen. The hyperechoic spots extending almost to the center of the lumen suggest plaque extension to this area. Only the color duplex scan clearly depicts the very small residual lumen between the two plaques, one away from the transducer and the other close to it. The flow acceleration is indicated by aliasing. Type IV plaque: hypoechoic, inhomogeneous, surface not delineated from vessel lumen

d The sample volume placed in the jet documents the high-grade stenosis with a peak systolic flow velocity of over 4 m/s

e Intraoperative confirmation of high-grade stenosis with a long plaque, predominantly of the atheromatous type (corresponding to **c** and **d**)

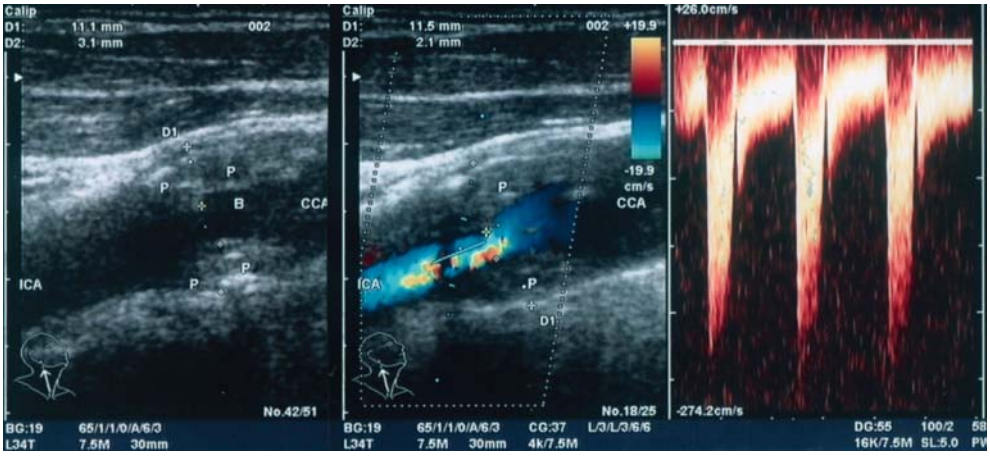

a

Fig. A 5.10 a–c
Plaque morphology – long concentric carotid stenosis
a Gray-scale scan depicting a concentric, fairly homogeneous and smoothly marginated plaque in the center with a just barely visible, extremely hypoechoic extension in the cranial direction. Only the color duplex scan enables differentiation of the hypoechoic wall deposit and perfused lumen in the distal portion of the plaque. Spectral Doppler yields a peak systolic flow velocity of 230 cm/s

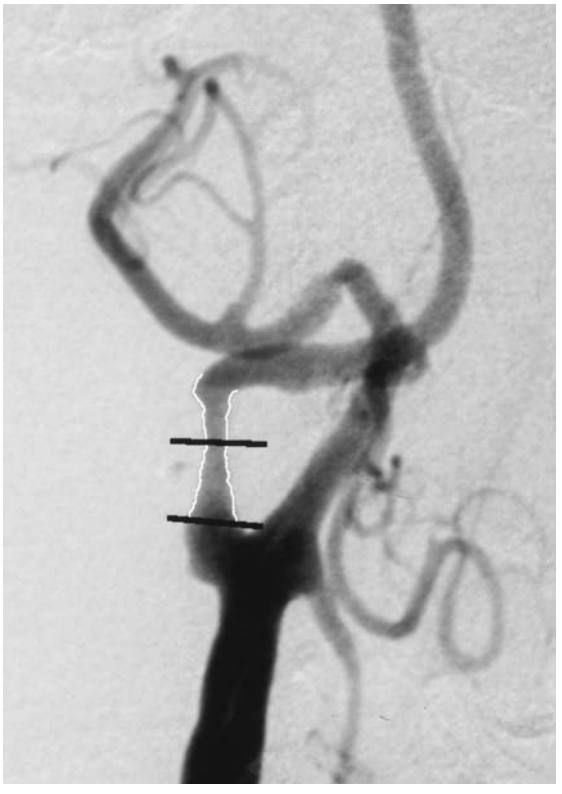

b

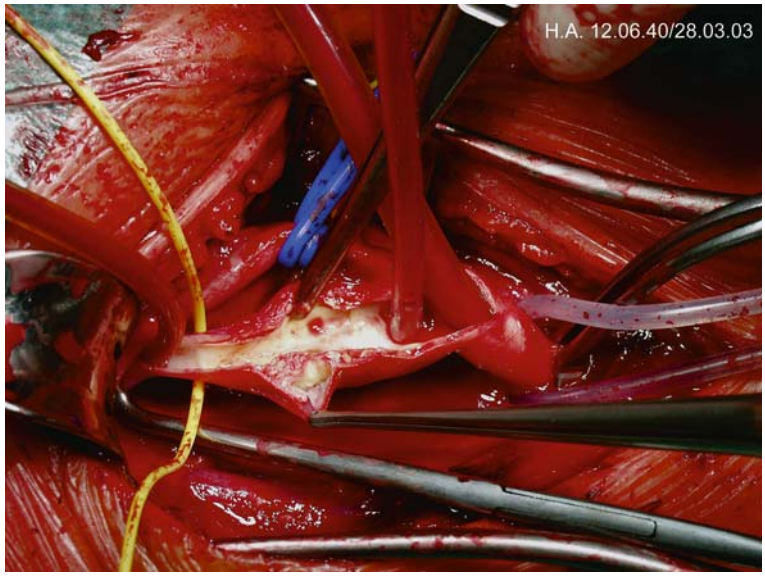

c

b Angiography demonstrating a long concentric, smooth stenosis
c Intraoperative photograph showing mostly fibrous plaque with a smooth surface

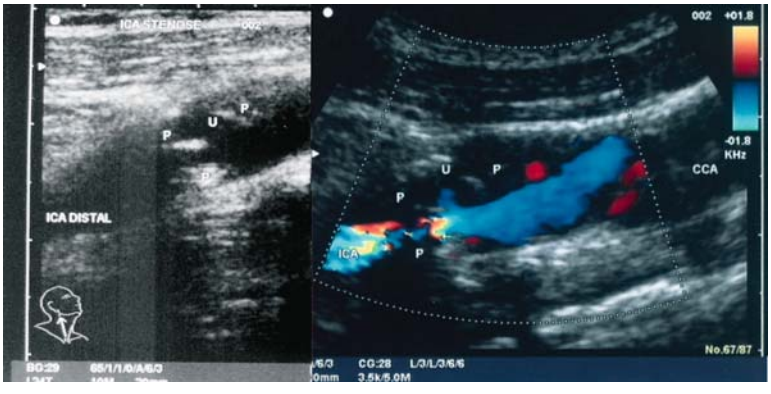

a

Fig. A 5.11 a–e
Plaque morphology – high-grade stenosis with ulceration
a B-scan (*left section*) depicts an inhomogeneous plaque with a poorly demarcated surface and hyperechoic spots extending far into the lumen. The anechoic gap may indicate ulceration. The color duplex scan (*right section*) shows an eccentric, long, and fairly hypoechoic plaque beginning far proximally in the bulb and causing high-grade stenosis that extends to the distal end of the bulb between a plaque close to the transducer and one away from it (*P*). The anechoic bowl-shaped defect in the hypoechoic plaque in the B-mode scan with flow in the color mode (*U*) suggests ulceration

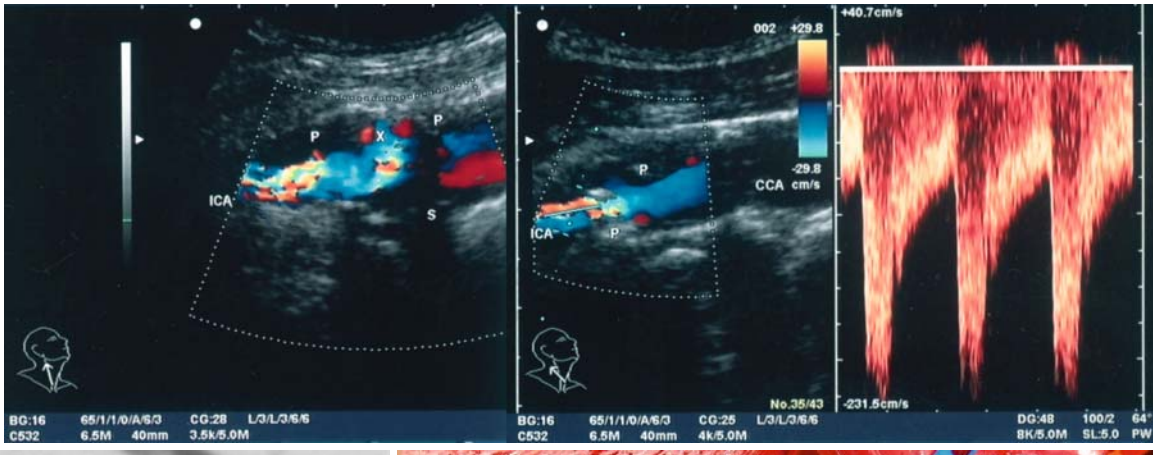

b

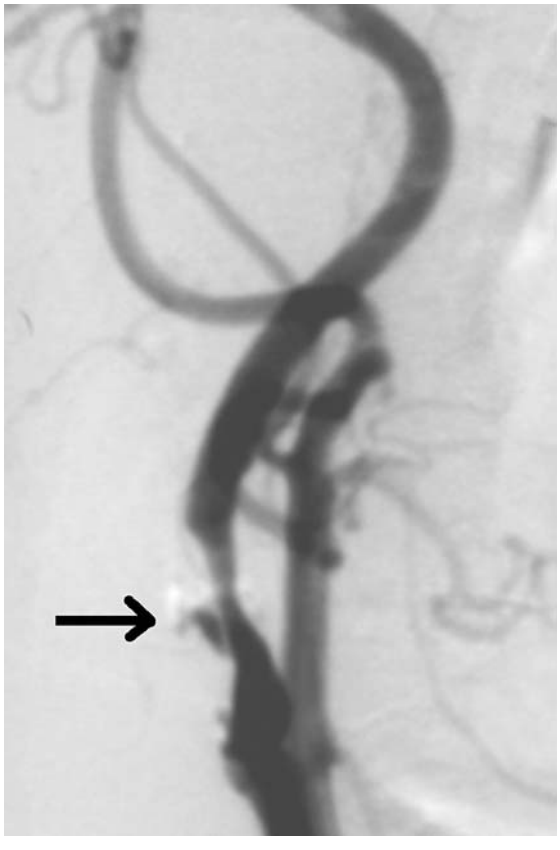

c

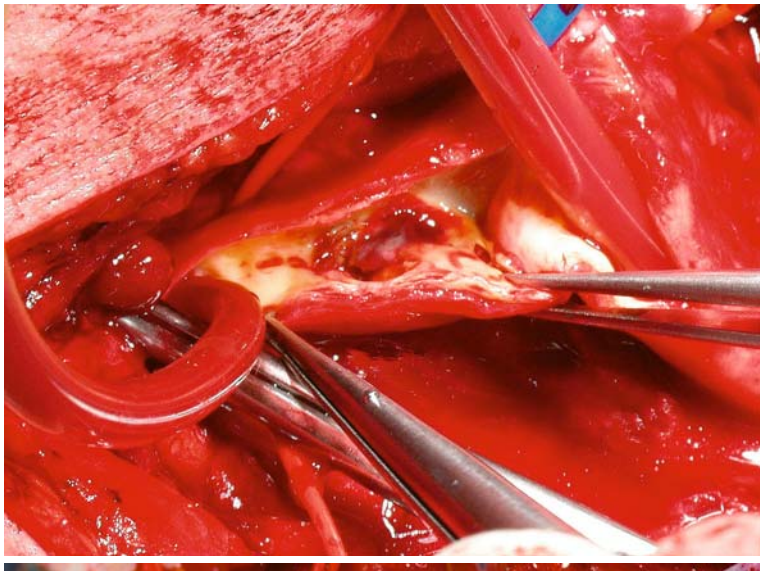

d

e

(Fig. A 5.11 cont.)
b The concentric plaque causing the high-grade stenosis begins directly distal to the ulceration (cf. *U* in **a**). Ulceration often occurs in the proximal portion of a highly stenotic plaque protruding far into the lumen. The arriving pulse wave (often depicted as longitudinal pulsatile plaque movement by gray-scale scanning) may cause rupture of the vulnerable plaque cap. In the example, the peak systolic velocity in the stenosis jet (aliasing) is 220 cm/s
c Angiography with a filling defect confirming the plaque contour demonstrated by ultrasound and also the ulceration
d Intraoperatively, the atheromatous plaque and adjacent ulceration are confirmed at the sites already identified by ultrasonography and angiography (corresponding to **a**–**c**)
e Different case with the intraoperative finding of a washed-out niche, which is difficult to differentiate from ulceration by ultrasound and angiography

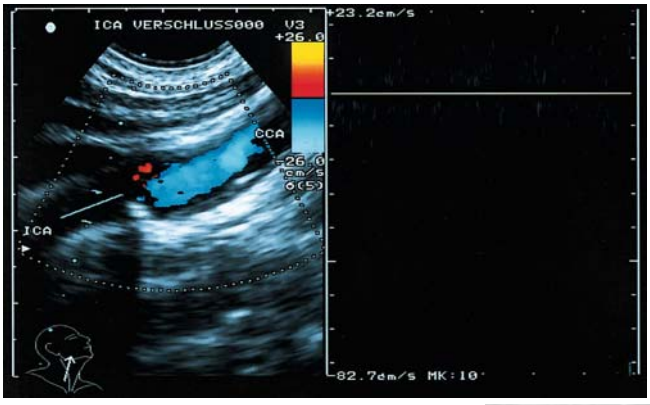

a

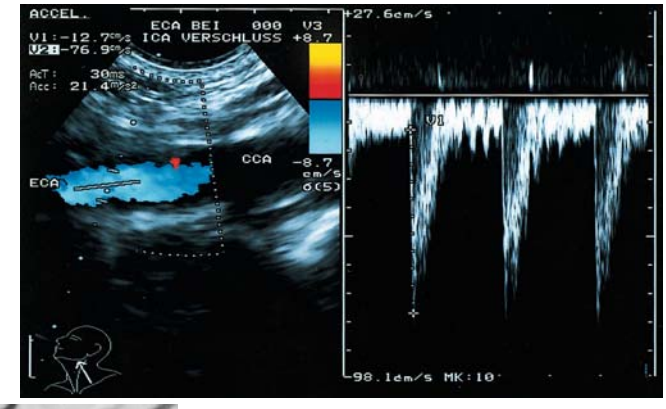

b

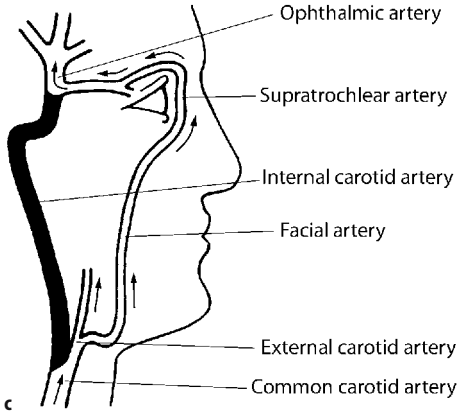

c

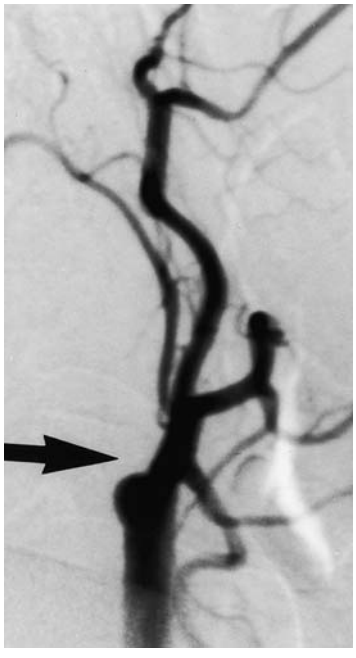

d

b When the external carotid artery (*ECA*) provides collateral flow via the supratrochlear artery, its spectral waveform shows a larger diastolic flow component. To avoid confusion with the internal carotid in this setting, the identity of the external carotid should be confirmed by rhythmical tapping of the temporal artery (branch of external carotid) and transmission of the pulsation to the Doppler spectrum (here seen in the middle cardiac cycle represented in the waveform)

c Schematic representation of collateralization through the external carotid and supratrochlear arteries (with retrograde flow in CW Doppler examination) in occlusion of the internal carotid artery

d Angiography: Internal carotid artery occlusion (*arrow*)

Fig. A 5.12 a–e
Internal carotid artery occlusion

a Neither spectral Doppler nor color duplex depicts flow signals in occlusion of the internal carotid artery. Calcified plaque with acoustic shadowing at origin. The *left section* shows the patent common carotid artery (*CCA*) on the *right*. To differentiate occlusion from subtotal occlusion, the internal carotid artery (*ICA*) must be scanned for depiction of flow signals with a high gain to the level of the mandibular angle

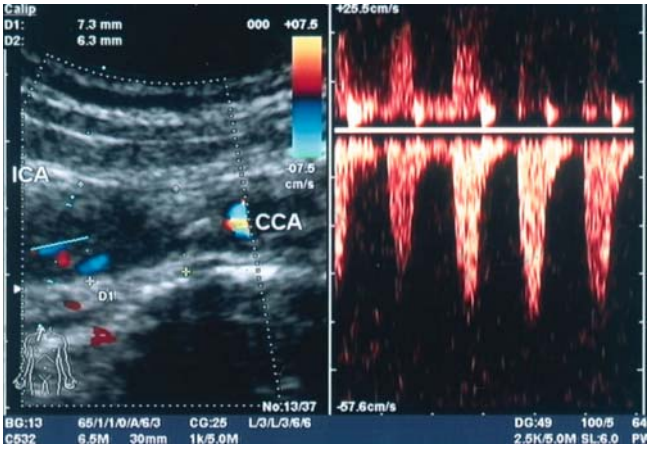

e

Signs of recanalization in internal carotid artery occlusion

e In the setting of internal carotid artery (*ICA*) occlusion, the examiner must search for flow signals using a low pulse repetition frequency. Recanalization is uncommon and must be differentiated from pseudo-occlusion. In subtotal occlusion (which may be identified by isolated high-frequency flow signals when scanning with a high gain), there will be very slow flow in the poststenotic segment filling most of the lumen. In occlusion with recanalization (as shown in this example), flow signals indicating a thin, meandering current are depicted throughout the otherwise occluded extracranial internal carotid artery. In contrast to stenotic narrowing, recanalization is characterized by low flow velocities (30 cm/s in the example with atypical ICA flow signal due to changed resistance). Partial corkscrew-like flow is depicted in the color scan as an apparent change in flow direction (blue – red). This is reflected in the spectral waveform by a change in flow direction when the transducer is slightly angled or moved (flow partly toward the transducer in the left part of the spectrum, away from it on the right). The meander-like course of blood flow in the recanalized ICA precludes depiction of the flow signals in the bulb in a single scan plane

Fig. A 5.13 a–c
Common carotid artery stenosis/ occlusion

a In the setting of common carotid artery occlusion with a patent bifurcation, the internal carotid artery (*ICA*) will be refilled through branches of the external carotid artery (*ECA*), primarily the superior thyroid artery, which in turn is supplied through branches of the thyrocervical trunk

b Distal external carotid branches may likewise contribute to the supply of the internal carotid artery. In this case there is retrograde flow along long segments of the external carotid (displayed in red, toward the heart, same flow direction as in accompanying internal jugular vein)

c Internal carotid artery with forward flow (displayed in blue, away from transducer). The postocclusive waveforms of the external and internal carotids show a delayed systolic increase and damped arterial flow profile

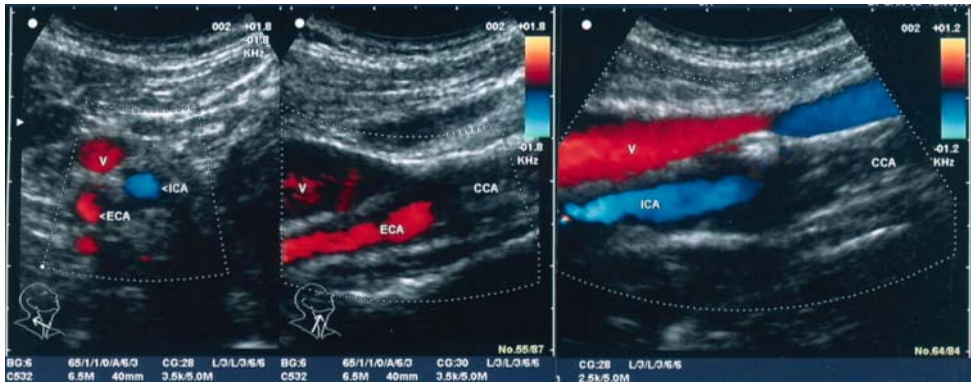

a

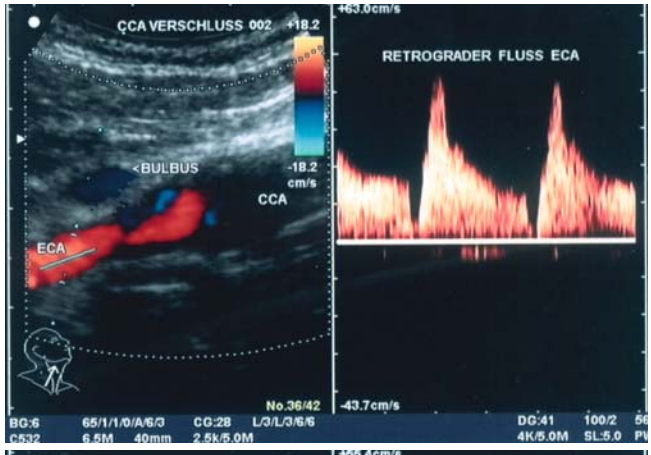

b

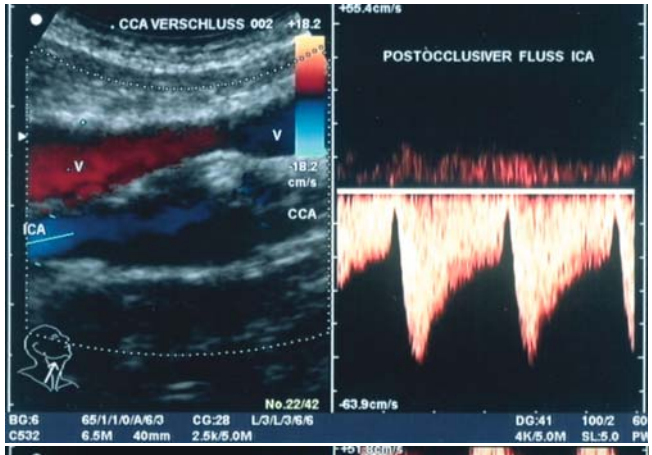

c

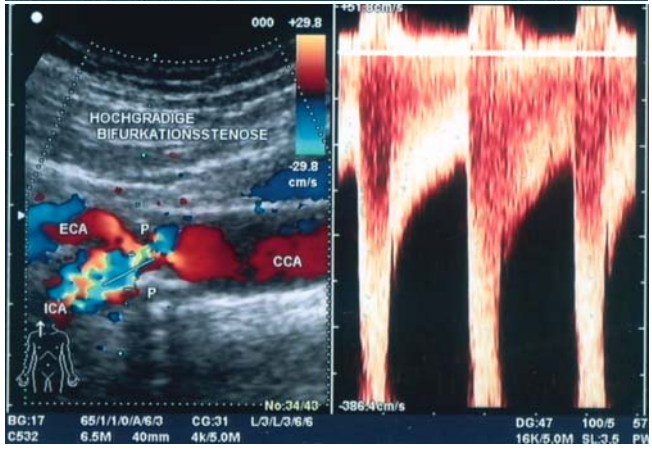

d

d–f Common carotid artery stenosis

d Preferred sites of common carotid artery (*CCA*) stenoses are the origin proximally and the area of the bifurcation distally. Concentric plaques (*P*) cause a high grade-stenosis just before the CCA divides into the internal carotid artery (*ICA*) and external carotid artery (*ECA*). The stenosis is indicated by aliasing and a peak systolic flow velocity of over 4 m/s as determined by spectral Doppler

e Angiography of the high-grade stenosis of the distal common carotid just before the bifurcation (same patient as in **d**)

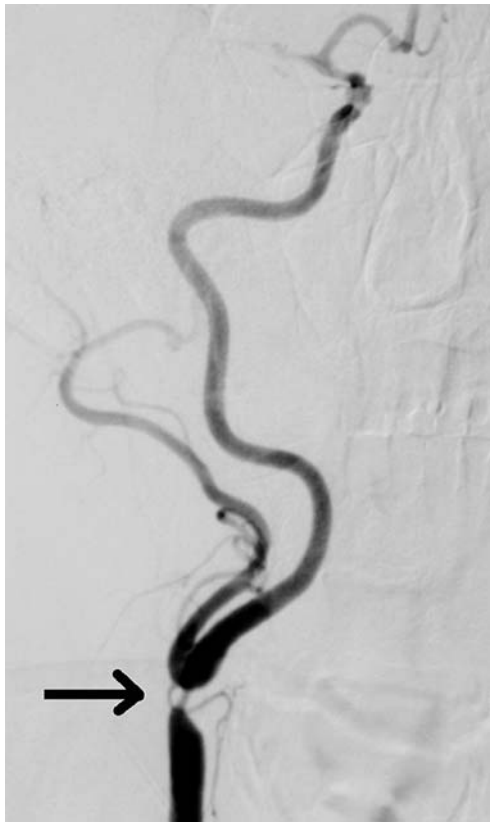

e

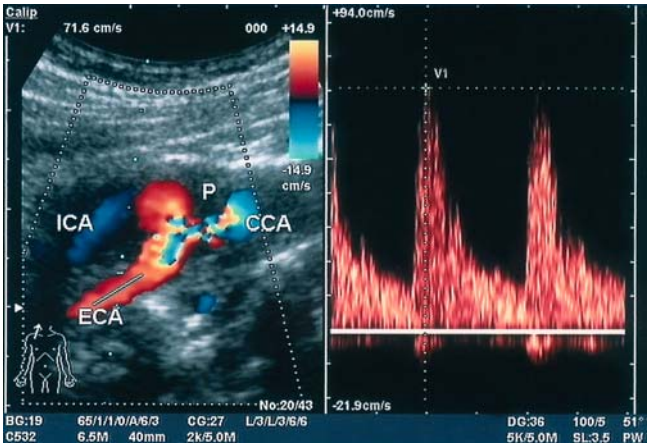

f

(Fig. A 5.13 cont.)
f With increasing stenosis of the distal common carotid artery (*CCA*), connecting vessels opening into the external carotid artery, e.g. via the superior thyroid artery, serve as collaterals. In the example, a high-grade stenosis of the common carotid artery (*P*) is indicated by aliasing. There is retrograde flow in the external carotid artery (*ECA*; displayed in red, toward transducer) with refilling of the internal carotid artery (*ICA*). The Doppler waveform from the external carotid depicts backward flow to the heart (toward transducer). The large diastolic component reflects the fact that the external carotid supplies the brain indirectly via the internal carotid in this setting. (Posterior transducer position as opposed to anterior position in **d**)

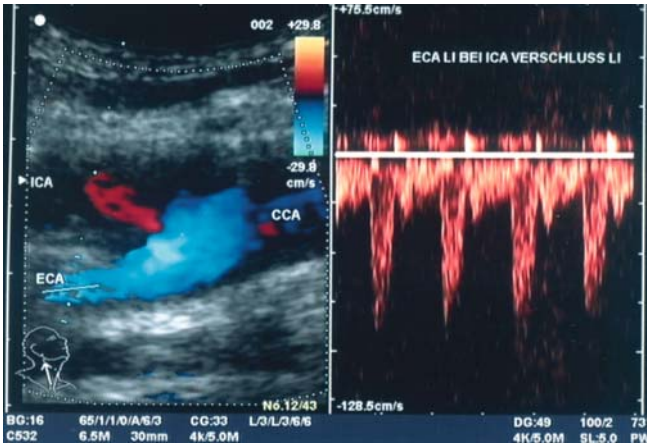

a

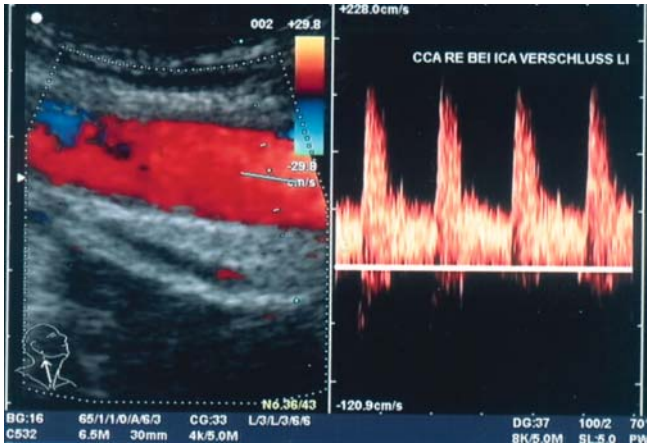

b

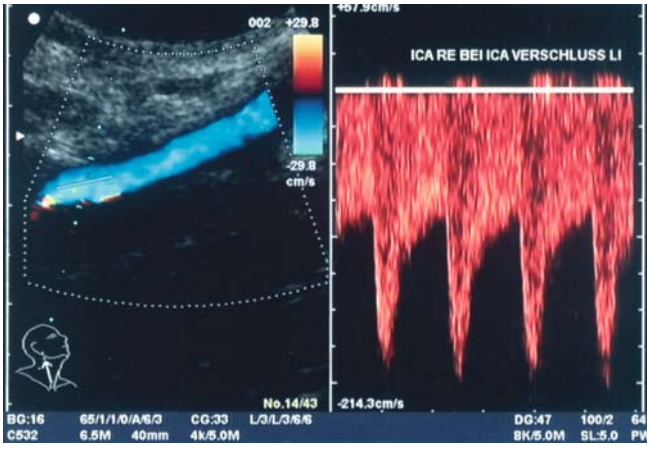

c

Fig. A 5.14 a–c
Compensatory flow increase in collateral pathways
The absent flow in internal carotid occlusion is compensated for by higher flow rates in the collateral arteries. The resulting higher flow velocities must not be misinterpreted as indicating stenosis. Faster flow is detected over long stretches of the collaterals while no stenotic structures are identified
a The ipsilateral external carotid artery can become a collateral, assuming a flow profile resembling that of the internal carotid
b Occasionally, there may be an increased compensatory flow in the contralateral common carotid artery as well (flow velocity increased to 150 cm/s over long stretch)
c Peak systolic velocity of 200 cm/s along long segment of contralateral internal carotid artery. The flow velocity is influenced by collateral flow in other vessels, and the increase is rarely as pronounced as in this example

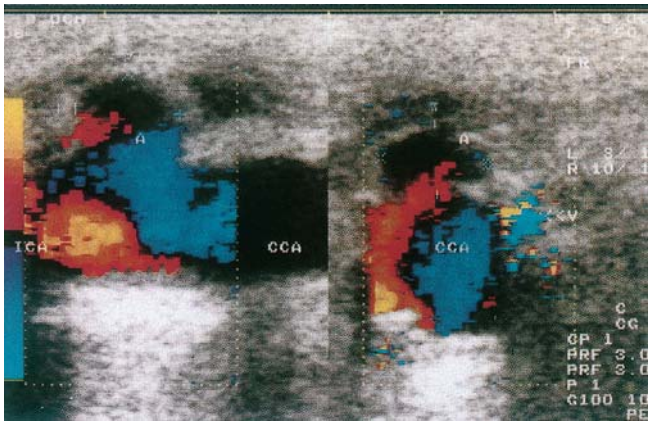

a

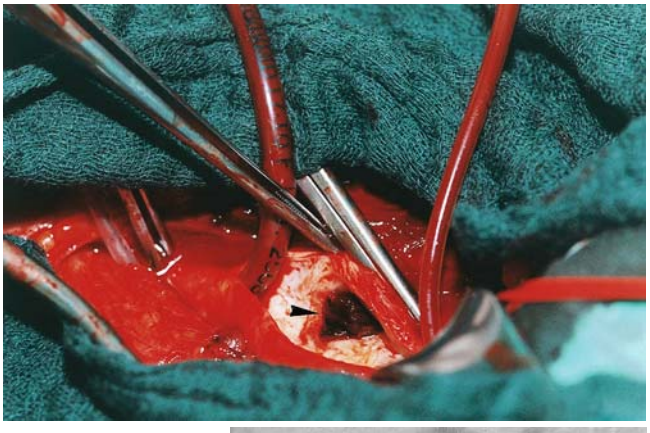

c

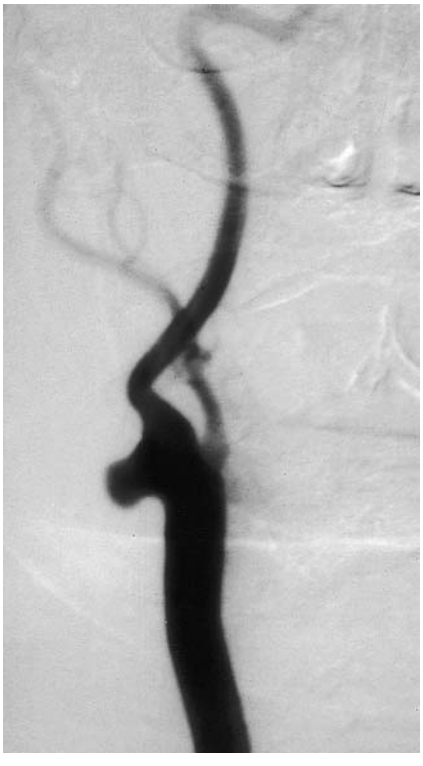

b

Fig. A 5.15 a–c
Suture aneurysm
a Pulsatile mass of the neck 3 years after carotid TEA. Color-coded duplex sonography demonstrates a circumscribed outpouching with flow signals in the patch area at the origin of the internal carotid artery (*ICA*). Incomplete color filling of the pouch suggests partial thrombosis. No demonstration of stenosis
b Control angiography confirms saccular aneurysm of the bulb
c Intraoperatively, a suture aneurysm covered by connective tissue structures is seen with thrombotic deposits in the aneurysmal sac (*arrowhead*)

Fig. A 5.16
Complications after carotid TEA
Virtually all false aneurysms of the carotid system are due to trauma or occur in the form of suture aneurysms after carotid TEA, in particular in patients who have undergone synthetic patch angioplasty. Suture aneurysms often indicate infection of the patch. Color duplex scanning shows a conspicuous mushroom-like structure protruding from the vessel, which can be palpated as a pulsating tumor in most cases. The color coding varies with the presence of thrombosis. The spectral waveform of the aneurysmal neck shows the typical to-and-fro sign indicating high-frequency systolic flow into the aneurysm and flow into the carotid lumen throughout diastole (*left section*: longitudinal scan; *middle section*: vessel cross-section; *right section*: Doppler waveform)

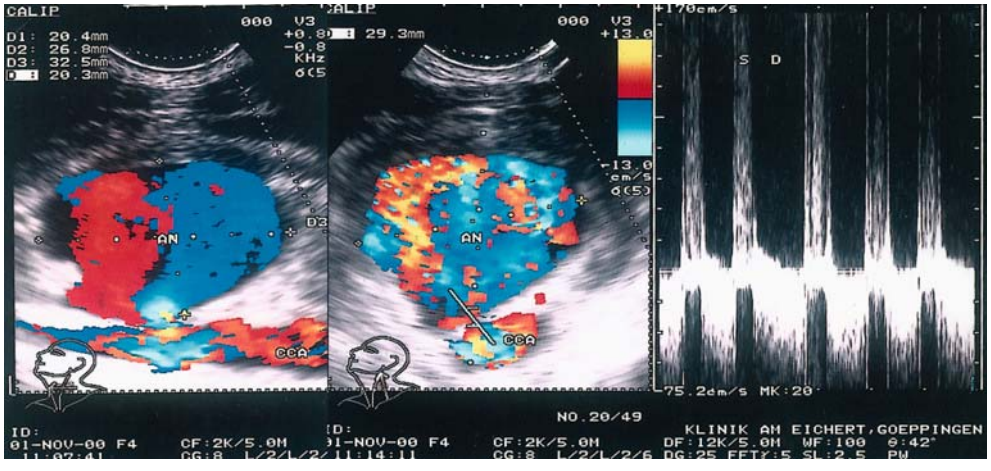

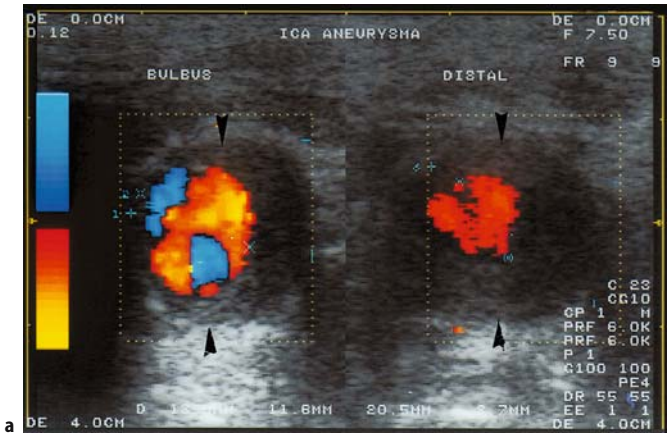

a

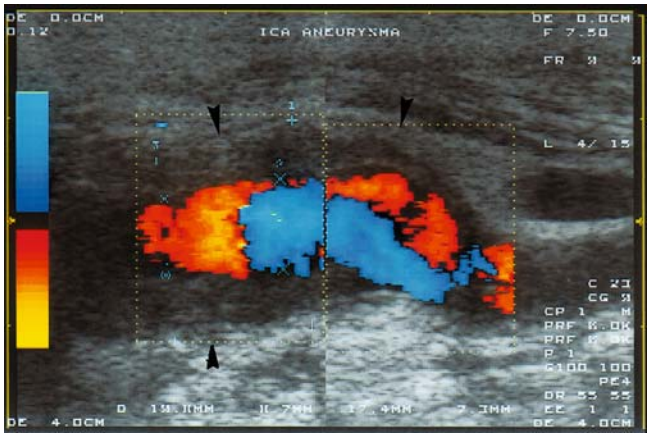

b

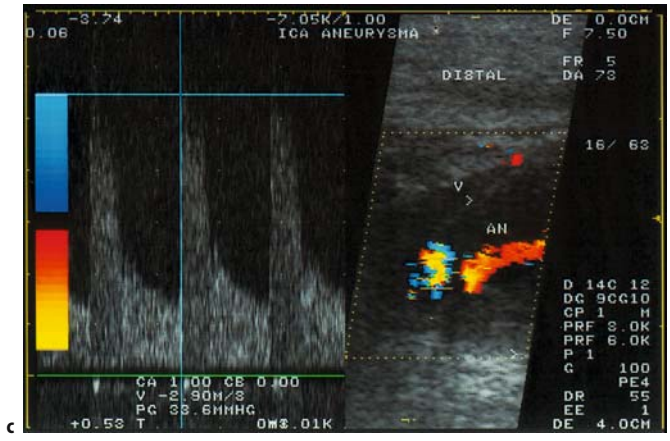

c

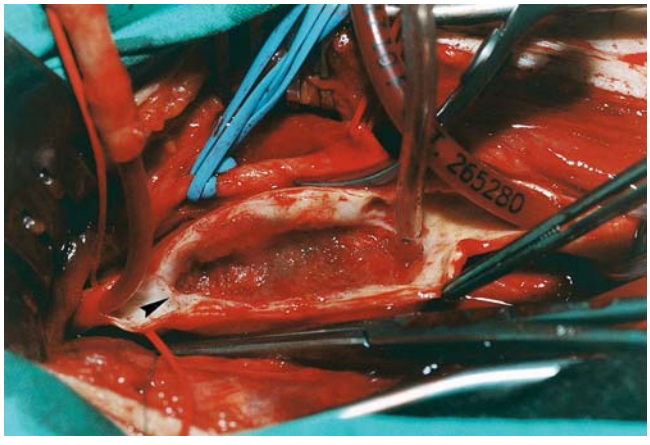

e

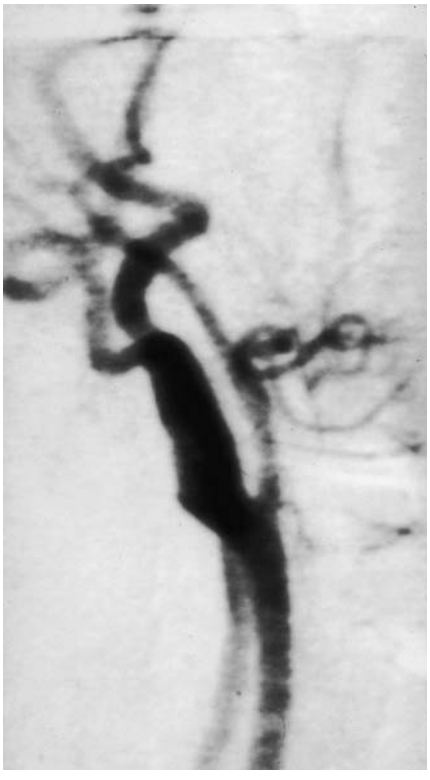

d

Fig. A 5.17 a–e
Internal carotid artery aneurysm (true)
a Transverse section showing the patent lumen of the internal carotid artery surrounded by hypoechoic aneurysmal thrombotic deposits (*arrowheads*) both in the bulb area (*left*) and in the distal segment (*right*). The aneurysm has a diameter of 2 cm
b The longitudinal scan depicts the shape of the internal carotid artery aneurysm (common carotid artery on the *right* and internal carotid artery on the *left*). The longitudinal scan also clearly demonstrates the size of the aneurysm (*arrowheads*) with hypoechoic mural thrombosis in relation to the color-coded flow in the patent lumen. The color change indicates eddy currents
c At the distal end of the aneurysm there is flow acceleration with turbulence and aliasing (inverted display). Flow velocity is increased to 2.9 m/s as determined by spectral Doppler (inverted display depicting flow away from transducer above the baseline)
d Angiography: Ectasia of the internal carotid artery. The mural thrombi make the aneurysm appear smaller than it actually is, and angiography does not provide information on the hemodynamic significance of the stenosis at the distal end of the aneurysm; all that is seen is less pronounced opacification due to luminal narrowing in the anteroposterior projection
e Intraoperative site confirming the spindle-shaped aneurysm in the proximal internal carotid artery with mural thrombosis and fibrotic stenosis at its distal end (*arrowhead*). Common carotid artery with shunt on the *right* and distal internal carotid on the *left* with the aneurysm of the proximal internal carotid in between. The aneurysm is thrombosed and shows fibrous luminal narrowing at its distal end. External carotid artery encircled with blue vessel loop

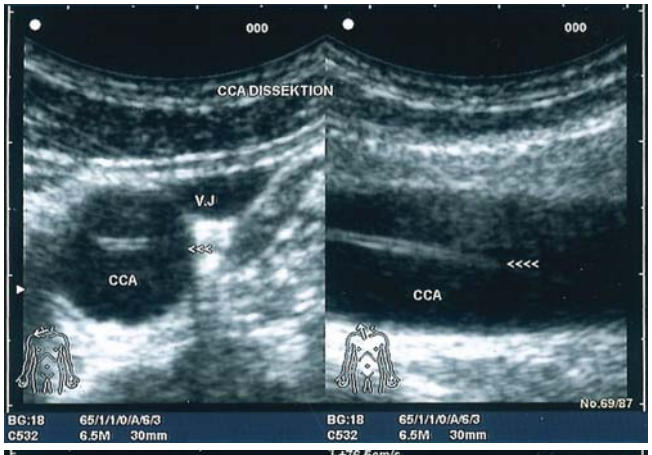

a

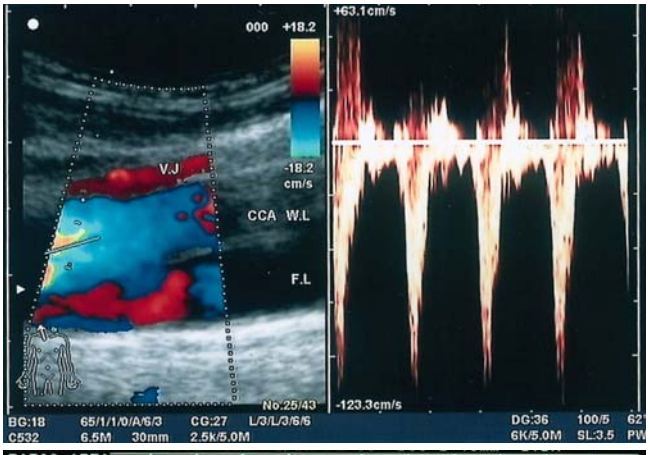

b

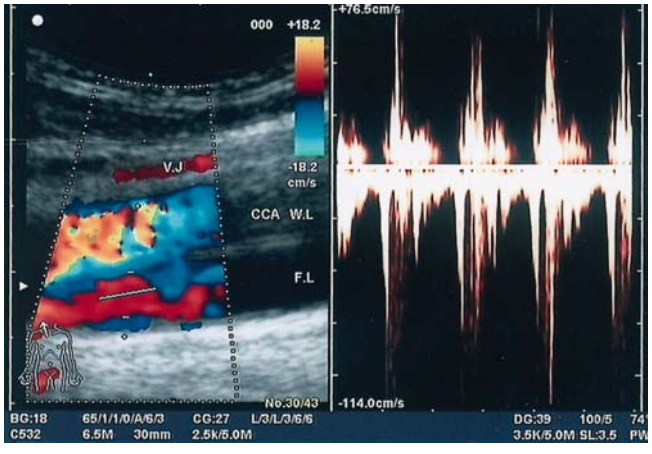

c

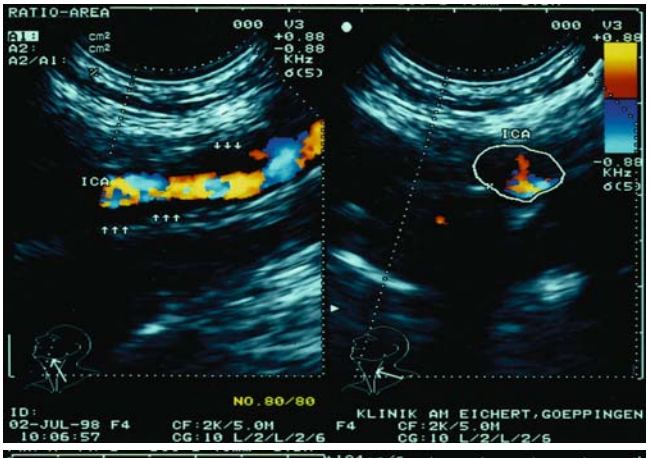

d

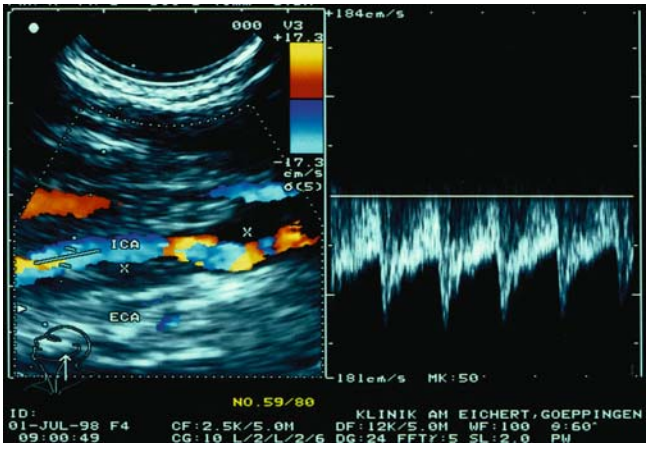

e

Fig. A 5.18 a–e
Dissection of common carotid artery

In type I aortic dissection according to De Bakey, the dissection extends into the common carotid artery

a The B-scan depicts the dissection in longitudinal and transverse planes as an intraluminal flap oscillating during the cardiac cycle

b In the color mode, the true lumen of the common carotid artery (*CCA WL*) can be differentiated from the false lumen (*FL*) as it shows flow in the cranial direction. (*V.J*, jugular vein)

c The flow direction demonstrated in the false lumen varies with the placement of the sample volume relative to the re-entry site. Forward flow is demonstrated if the re-entry is distal to the volume and to-and-fro flow, as in the example, if it is proximal

The scan shows flow in the true lumen displayed in blue (toward the periphery, away from transducer) and aliasing while there is to-and-fro flow in the false lumen (here displayed in red, toward transducer)

Posttraumatic dissection of internal carotid artery

d Long posttraumatic dissection of the internal carotid artery extending from the bifurcation to the base of the skull with thrombosis of the false lumen. In contrast to atherosclerotic changes, thrombotic dissection is characterized by a homogeneous and hypoechoic sonomorphologic appearance. The thrombotic false lumen is long and tortuous and partly attaches to the vessel wall. Occasionally, as in the example, the entry site can be identified by the depiction of pulsatile flow signals in the color duplex mode (*right section*)

e As shown by spectral Doppler, the luminal narrowing due to dissection does not cause a higher-grade stenosis

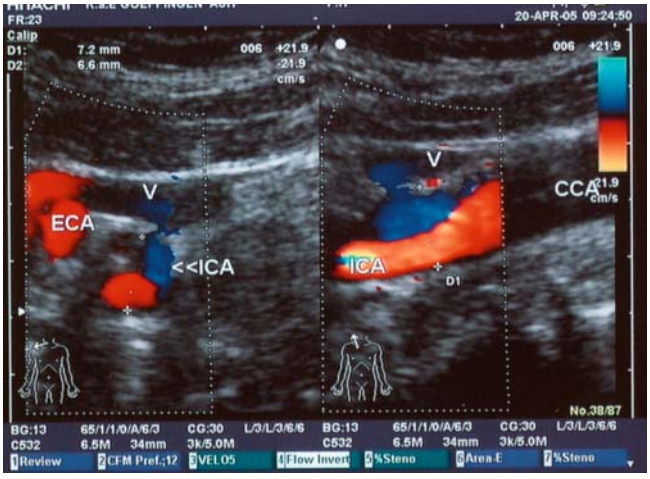

f

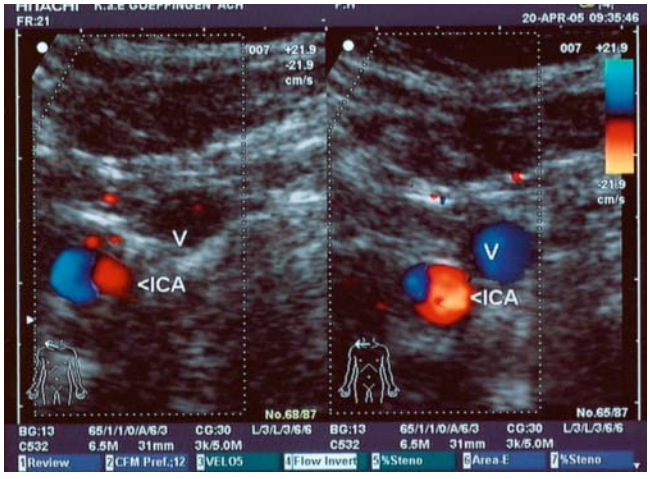

g

(Fig. A 5.18 cont.)
Posttraumatic dissection of internal carotid artery
f The dissection starts in the bulb of internal carotid artery (*ICA*). The longitudinal scan on the *right* (red-coded true lumen, blue-coded false lumen) depicts the dissection with a less than 50 % reduction in diameter. The transverse scan on the *left* shows the dissection membrane and partial thrombosis of the false lumen
V internal jugular vein, *ECA* external carotid artery
g The dissection extends to the intracranial segment of the internal carotid artery (*ICA*). The variable diameter of the false lumen (blue) is seen in the middle portion of the extracranial ICA (*right section*) and its distal portion (*left section* with visible dissection membrane)

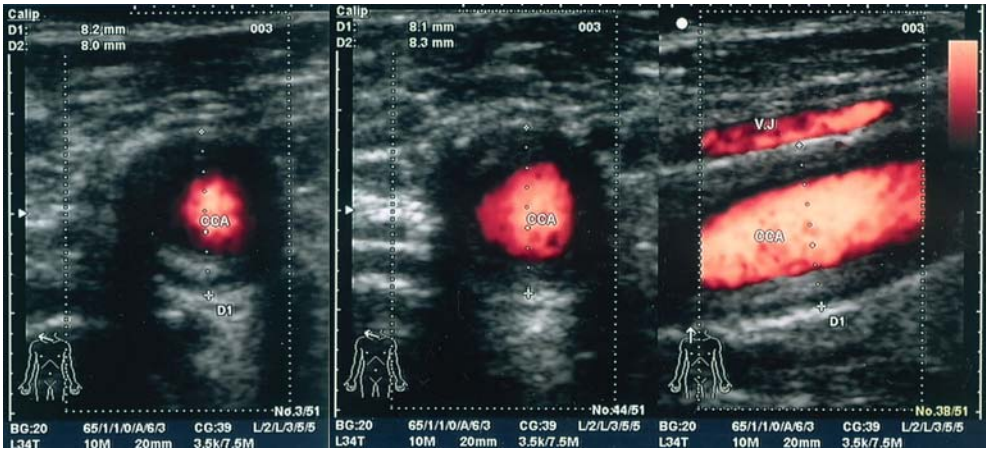

Fig. A 5.19
Takayasu's arteritis
Concentric wall thickening is pathognomonic of arteritis. Takayasu's arteritis predominantly affects the subclavian and common carotid arteries. The example shows the common carotid artery (*CCA*) in the power Doppler mode. The transverse scan (*left section*) demonstrates concentric diameter reduction greater than 50 % involving a long vessel segment. The transverse scan in the *middle* and the longitudinal scan on the *right* obtained after two weeks of cortisone treatment show slightly reduced but persistent concentric wall thickening of the common carotid artery

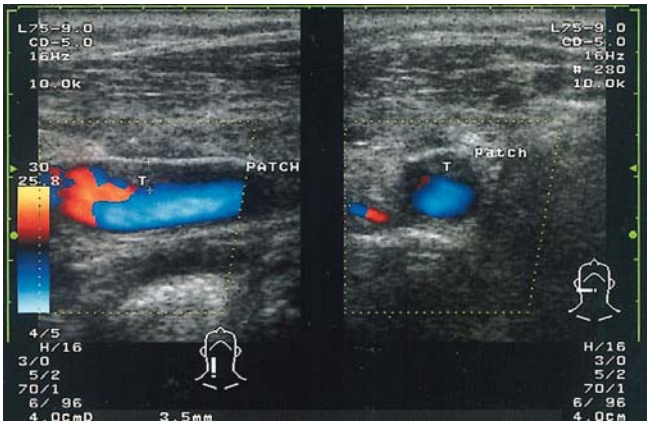

Fig. A 5.20
Postoperative follow-up after TEA
Postoperatively, there may be luminal narrowing due to thrombotic deposits, in particular when a synthetic patch has been interposed. Thrombotic deposits protruding far into the lumen with hemodynamically significant narrowing are a source of embolism. The patch itself is seen as a hyperechoic interface (wall near transducer) with a hypoechoic deposit on the luminal side (*T*)

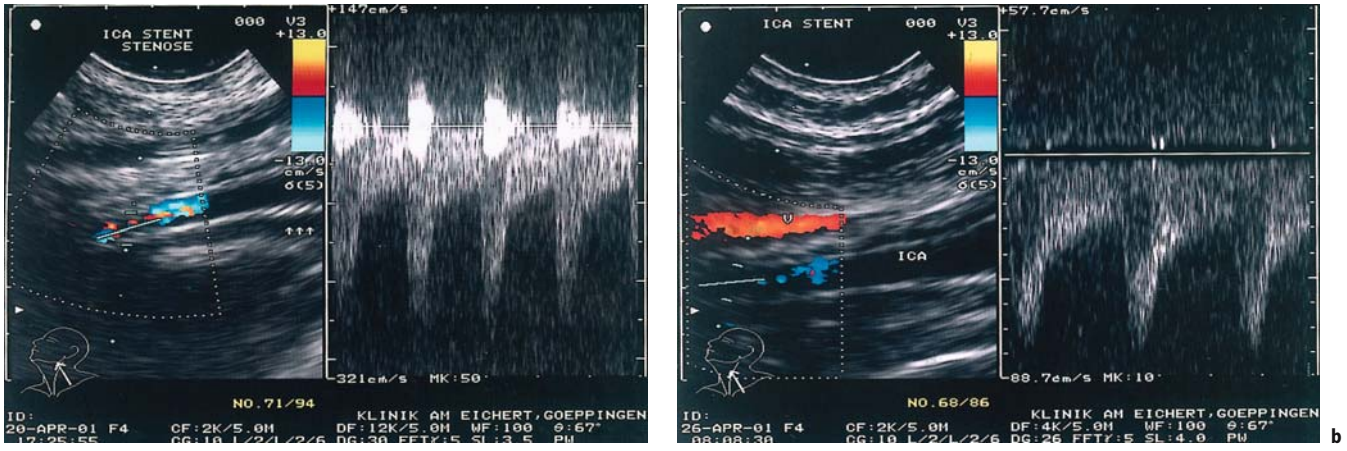

a b

Fig. A 5.21 a, b
Stenosis after carotid stenting
a Sonographic visualization, in particular in the color duplex mode, may be impaired during the first days after stenting due to poor tissue coupling. Visualization can be improved by use of a lower-frequency transducer. Thrombotic deposits within the stent will lead to flow acceleration in the spectral display if there is hemodynamically significant luminal narrowing (250 cm/s PSV that means >70% stenosis)
b Such thrombotic deposits will recede after some days of heparin and aspirin therapy. In the example shown, the peak systolic velocity measured at identical sites decreased from 250 cm/s before treatment (**a**) to 80 cm/s after 5 days of treatment

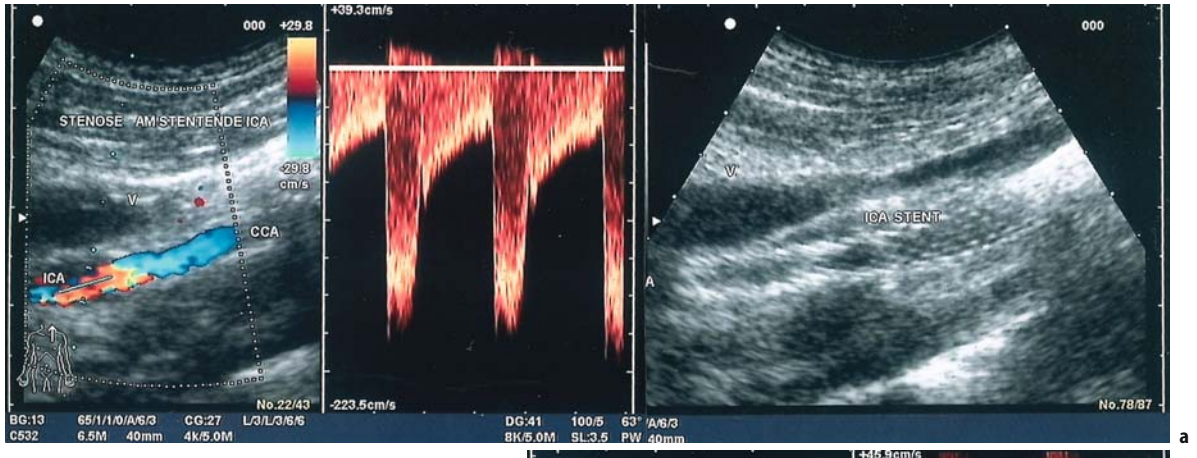

a

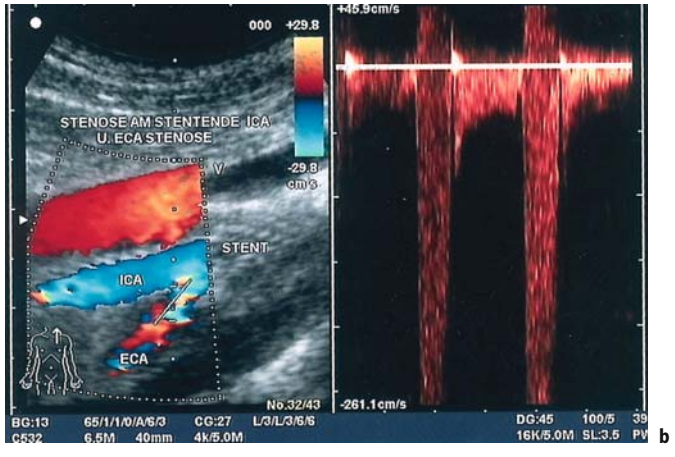

b

Fig. A 5.22 a, b
Carotid artery stent
In the follow-up of carotid artery stent implantation, the sonographer must in particular check the junction between stent and normal vessel for residual or recurrent stenosis and the stent position
a The B-scan depicts the stent as a meshlike structure in the vessel lumen. In the bulb the stent does not fit tightly to the vessel contour because the plaque has been pressed into the wall. B-mode scanning is highly unreliable in depicting thrombotic deposits or neointima shortly after stent placement. Evaluation for stenosis is done by color duplex or spectral Doppler. In the example, there is recurrent stenosis of 60–70% with a peak systolic velocity of 170 cm/s
b The stent extends over the origin of the external carotid artery. The external carotid is patent but the Doppler waveform indicates a high-grade stenosis

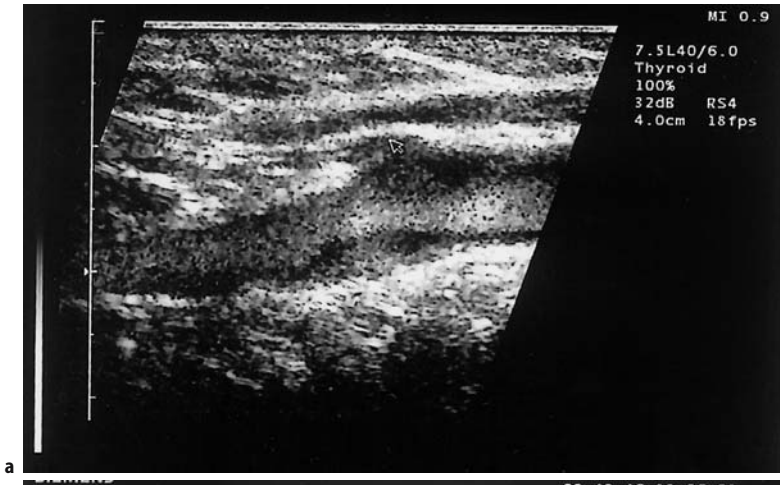

a

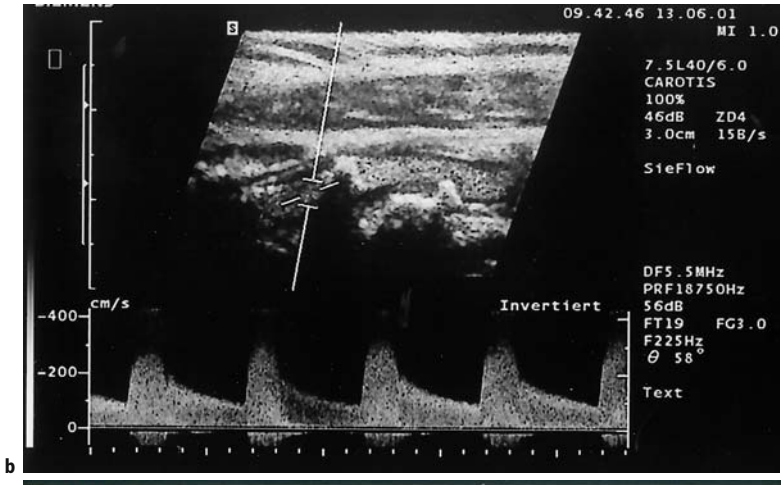

b

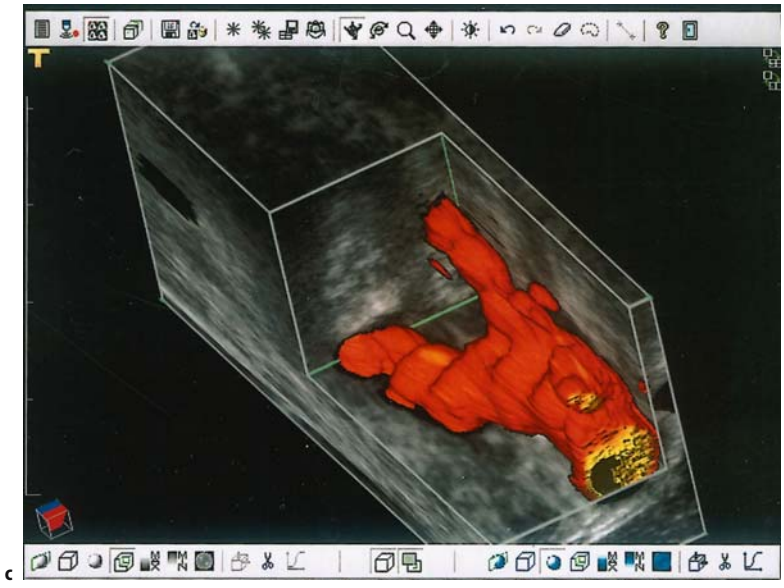

c

Fig. A 5.23 a–c
New ultrasound techniques: B-flow mode, 3D ultrasound
a In the B-flow mode, the amplitude signal of the reflecting particles is analyzed in the interval between 2 pulses. The movement of reflecting particles is encoded in terms of their flow direction, velocity, and number. Vessel narrowing is visualized with a higher signal intensity as a result of the larger number of reflecting particles and faster flow in segments with a reduced cross-sectional area. In addition to hemodynamic parameters, the B-flow mode also provides morphologic images with a high resolution of plaques and the vessel wall, enabling good differentiation of the plaque surface and surface irregularities (ulceration) from the patent lumen. In the example, a plaque near the transducer and another away from it are depicted in the bulb. The luminal narrowing resulting from these plaques is indicated by the higher signal intensity of the perfused lumen in this area
b Advantages of the B-flow mode are its little angle dependence and the good morphologic discrimination of the vessel wall from the patent lumen. Its major drawback is the susceptibility to artifacts induced by highly pulsatile wall motion occurring in the presence of high-grade stenoses caused by plaques. Moreover, like all ultrasound techniques, the B-flow mode is impaired by signal scattering and acoustic shadowing due to calcified structures. This is why the B-flow mode has not replaced the hemodynamic spectral Doppler technique, in particular in the presence of pathology. The figure illustrates the impairment of the B-flow mode display by plaque-induced acoustic shadowing. The higher signal in the vessel lumen indicates the stenosis jet. Still, the Doppler spectrum continues to be the most reliable method for quantifying high-grade stenosis
c Three-dimensional displays can provide a good overview of vascular relationships in the presence of atypical variants or in case of elongation. At its current state of development, however, this technique contributes little to stenosis grading and evaluation of plaque morphology. Due to artifacts caused by vessel pulsation and atherosclerotic plaques, the 3D displays have no advantage over 2D displays in answering relevant angiologic and vascular surgical questions. The example depicts the common carotid artery on the right with the superior thyroid artery above and the internal carotid (*bottom*) and external carotid (*top*) on the left

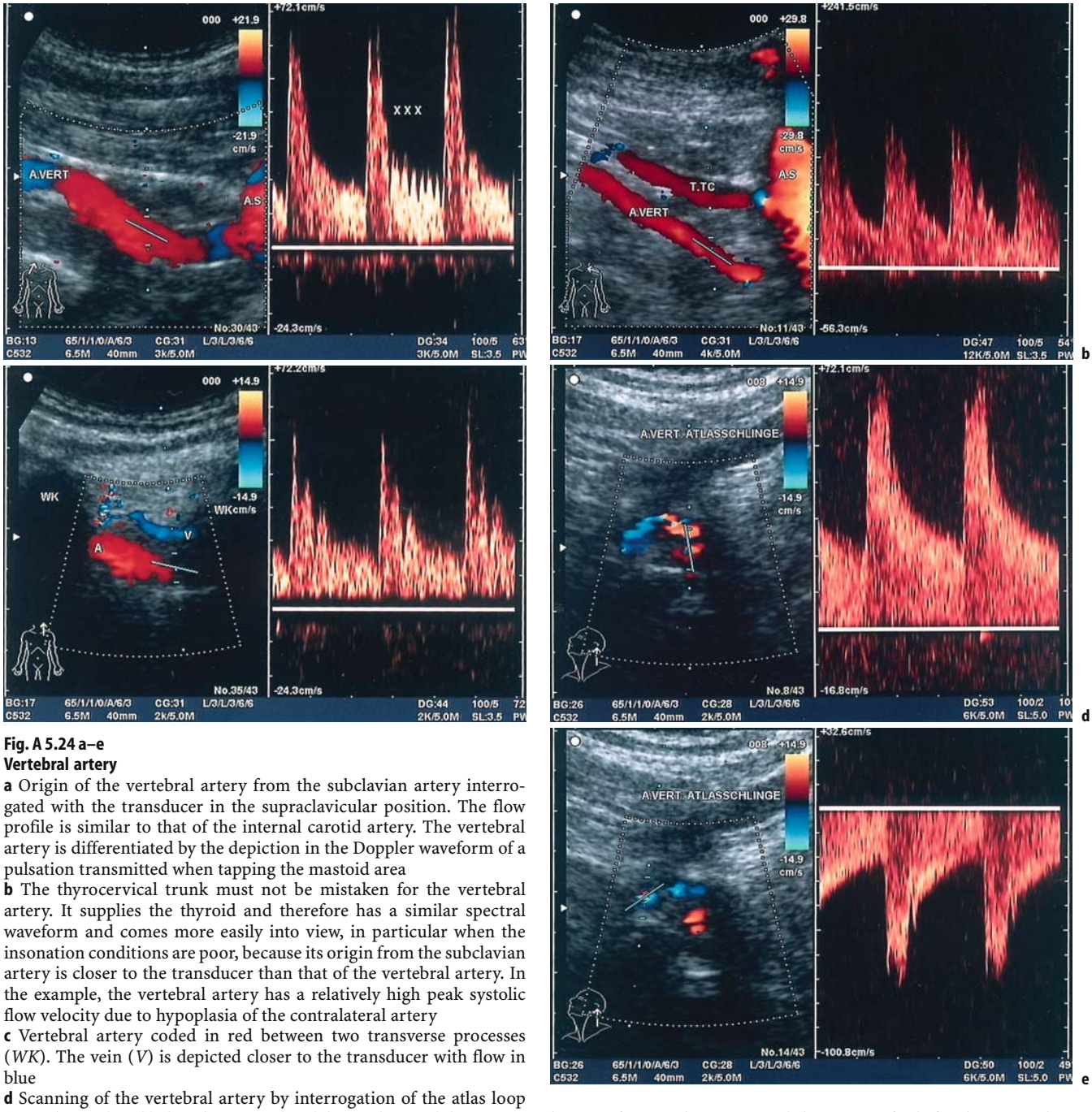

Fig. A 5.24 a–e
Vertebral artery

a Origin of the vertebral artery from the subclavian artery interrogated with the transducer in the supraclavicular position. The flow profile is similar to that of the internal carotid artery. The vertebral artery is differentiated by the depiction in the Doppler waveform of a pulsation transmitted when tapping the mastoid area

b The thyrocervical trunk must not be mistaken for the vertebral artery. It supplies the thyroid and therefore has a similar spectral waveform and comes more easily into view, in particular when the insonation conditions are poor, because its origin from the subclavian artery is closer to the transducer than that of the vertebral artery. In the example, the vertebral artery has a relatively high peak systolic flow velocity due to hypoplasia of the contralateral artery

c Vertebral artery coded in red between two transverse processes (*WK*). The vein (*V*) is depicted closer to the transducer with flow in blue

d Scanning of the vertebral artery by interrogation of the atlas loop (transducer placed below the mastoid and directed toward the contralateral eye) stems from CW Doppler ultrasound and has lost in importance in duplex ultrasound. However, this approach is useful to sample the vertebral artery Doppler spectrum during functional tests performed to diagnose postural compression of the vertebral artery by a vertebral body. In this setting, evaluation of the atlas loop enables follow-up of postocclusive spectral changes in a fairly fixed position during movements of the neck. As with CW Doppler, changes in flow direction are reflected in the Doppler waveform. In the example, there is flow toward the transducer in the proximal portion of the atlas loop

e In the distal portion, flow is away from the transducer, in a distal direction

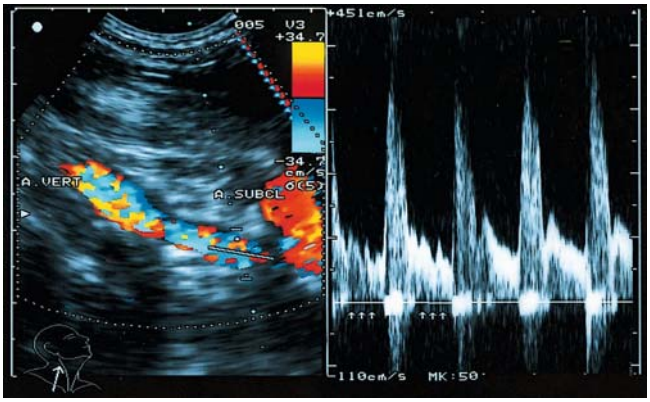

a

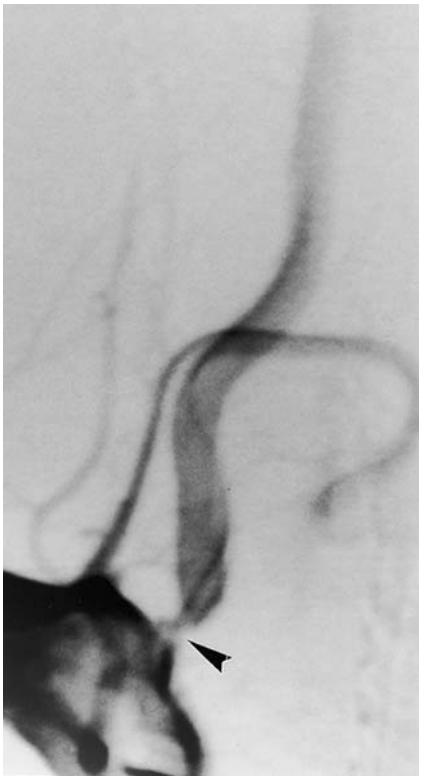

b

Fig. A 5.25 a, b
Stenosis at origin of vertebral artery
a The color duplex scan shows aliasing due to turbulence at the origin of the vertebral artery (coursing leftward in the display) from the subclavian artery (*A.SUBCL*). At the origin, color coding is absent from the lumen due to plaque with acoustic shadowing. The spectral waveform documents the stenosis with a peak systolic velocity of 320 cm/s and an end-diastolic velocity of 80 cm/s. The vertebral artery is distinguished from the thyrocervical trunk, which has a similar flow profile, by the transmission of the pulsation from rhythmical tapping of the distal vertebral artery below the mastoid (indicated by *arrows* in the spectral display)
b Angiography: Stenosis (*arrowhead*) at origin of vertebral artery

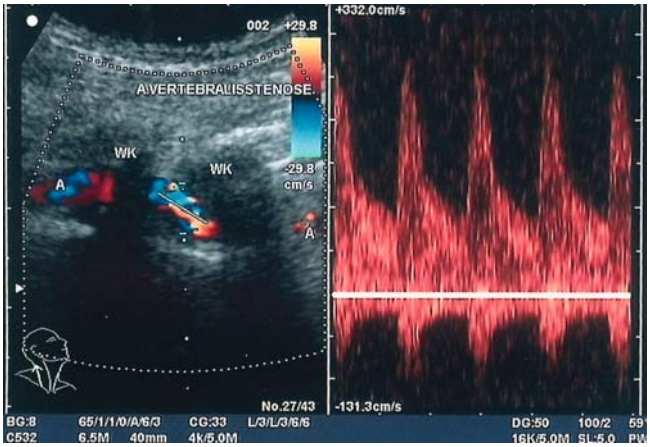

Fig. A 5.26
Distal vertebral artery stenosis
Atherosclerotic vertebral artery stenoses typically occur at the origin from the subclavian artery. A more distal stenosis (in the V2 segment between C4 and C5 in the example presented) is more likely due to other causes such as constriction of the passageway through the transverse processes by exostosis or dissection. An increase in flow velocity (here 250 cm/s) indicates stenosis only if it is localized. Increased flow throughout the vertebral artery suggests a compensatory increase in perfusion due to hypoplasia of the contralateral branch or atherosclerotic occlusion of other arteries supplying the brain

Fig. A 5.27
Vertebral artery occlusion
Both color duplex and spectral Doppler fail to depict flow signals throughout the tubular structure including its origin from the subclavian artery. The course of the structure corresponds to that of the vertebral artery: vertebral artery occlusion

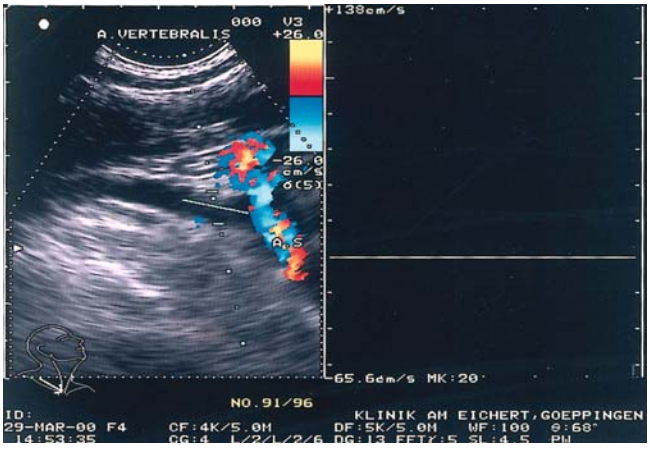

Fig. A 5.28 a, b
Subclavian steal syndrome – to-and-fro flow in vertebral artery
a The steal phenomenon in the vertebral artery varies with the grade of the subclavian stenosis, the collateral pathways, and the role of the vertebral artery in the collateral supply. The corresponding changes can be seen in the Doppler spectrum sampled after provoked ischemia. To-and-fro flow may be preserved and only change from primarily cranial flow to primarily central flow (toward subclavian artery). During compression of the ipsilateral arm, there is high diastolic flow in the cranial direction with only little retrograde flow in systole. Upon deflation of the arm cuff, there is a change in to-and-fro flow with a large retrograde systolic flow component (*S*) and only little antegrade flow in diastole (*D*)

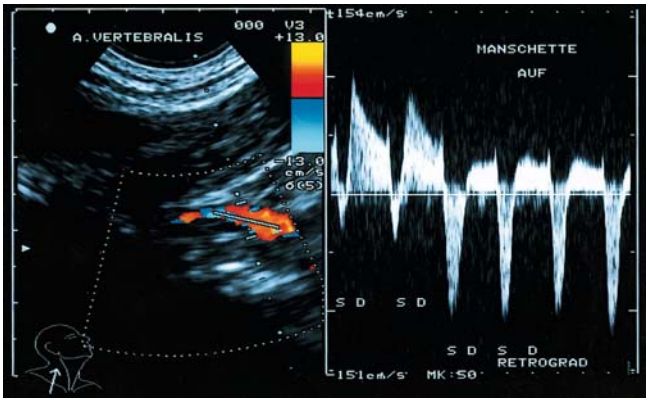

a

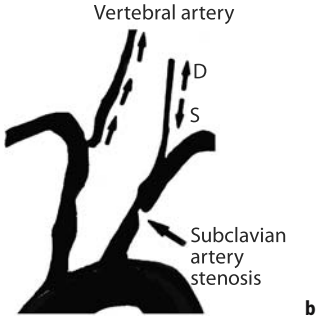

b Schematic representation of to-and-fro flow in the vertebral artery in ipsilateral subclavian artery stenosis **b**

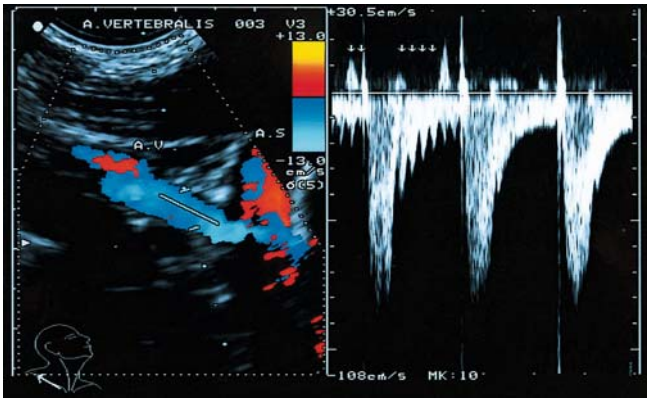

a

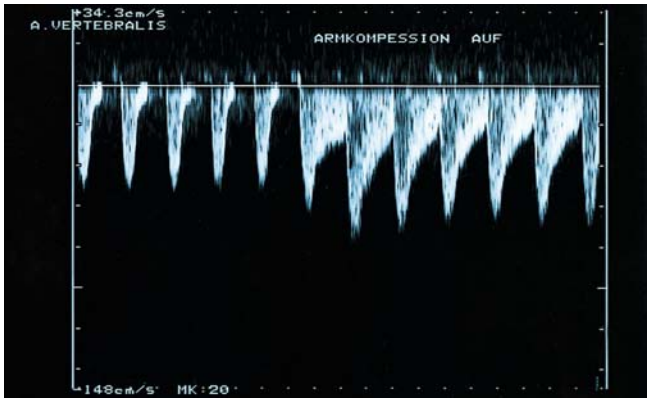

b

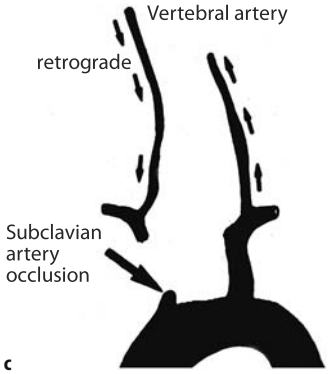

c

Fig. A 5.29 a–c
Subclavian steal syndrome – retrograde flow in the vertebral artery
a In severe subclavian steal syndrome, retrograde flow from the ipsilateral vertebral artery (*A.V*) into the subclavian artery (*A.S*) will already be seen at rest (displayed in blue). This is verified by the spectral Doppler tracing with confirmation of the identity of the vertebral artery by transmission of pulsation upon tapping in the mastoid region. The subclavian artery is occluded proximal to the site of emptying of the vertebral artery
b Following ischemia upon release of the arm cuff, there is a marked increase in retrograde flow, in particular in diastole
c Schematic representation of retrograde flow in the vertebral artery in ipsilateral subclavian artery occlusion with complete subclavian steal syndrome

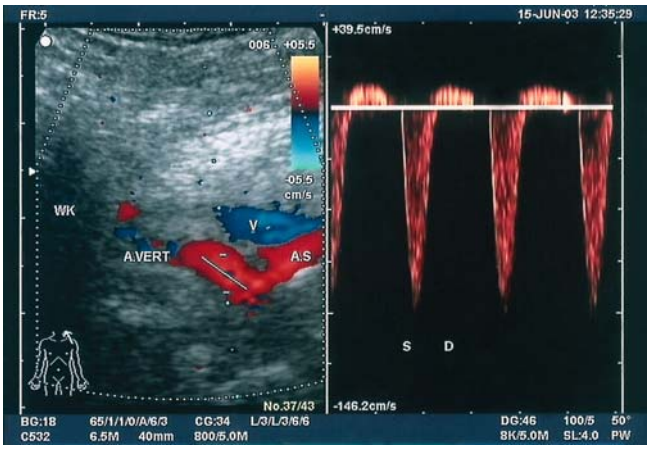

a

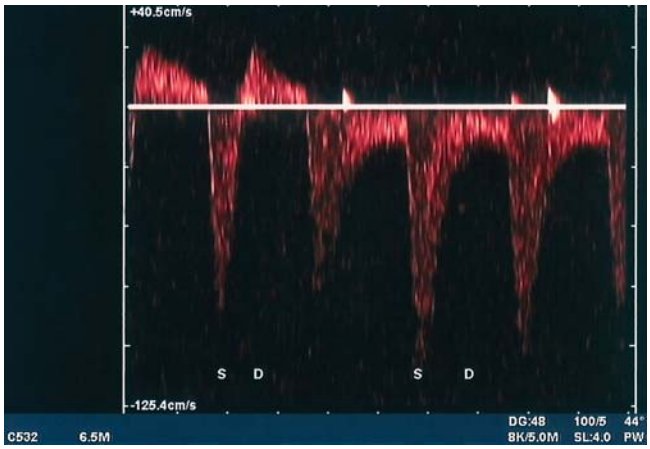

b

Fig. A 5.30 a–d
Subclavian steal syndrome with vertebrovertebral crossover
a Depiction of the origin of the vertebral artery in central subclavian artery occlusion. The spectral waveform recorded at the origin of the vertebral artery (*A.VERT*) from the subclavian artery (*A.S*) demonstrates to-and-fro flow with a retrograde systolic component (away from transducer, toward heart) and an antegrade diastolic component (toward transducer, toward brain). The passage of the artery through the transverse process (*WK*) is shown at the left margin
b In the provocative test, compression of the ipsilateral brachial artery with reduction of blood flow into the arm arteries leads to an increase in antegrade diastolic flow in the ipsilateral vertebral artery compared to rest (see **a**). Ischemia induced by release of the cuff (middle of the spectrum) results in a change from to-and-fro flow to a constant reversed flow from the vertebral artery into the subclavian artery (away from transducer)

(Fig. A 5.30 cont.)
c An increase in systolic and diastolic flow velocity (*S* = systole, *D* = diastole) in the vertebral artery on the opposite side of subclavian artery occlusion upon release of the cuff around the brachial artery on the side of occlusion proves vertebrovertebral crossover in the subclavian steal syndrome. In the example shown, the increase in velocity is not very pronounced, suggesting that there are other collateral routes to bypass the occluded subclavian artery
d Angiography with depiction of contrast medium crossover in occlusion of the left subclavian artery. The temporal course of the contrast medium passage shows flow from the right subclavian artery (*left*) into the right vertebral artery (*middle*) and into the left vertebral artery (*right*)

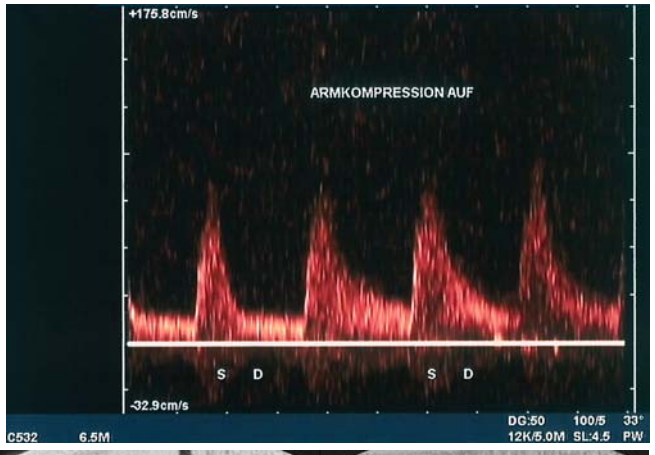

c

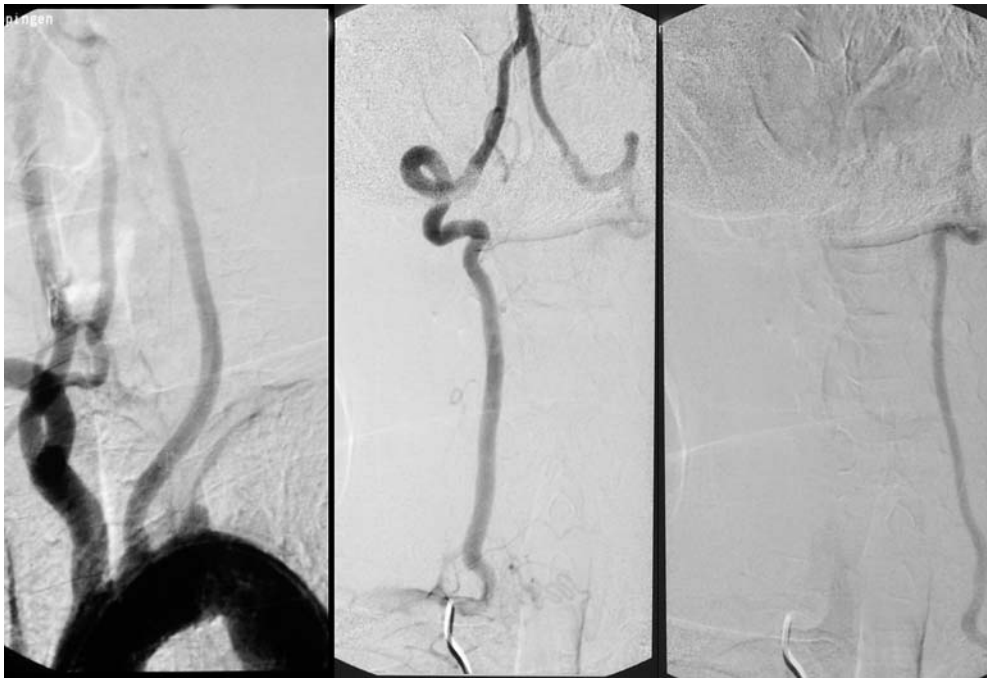
d

Fig. A 5.31
Carotid body tumor
A carotid body tumor typically lies in the carotid bifurcation, causing the characteristic saddle deformity resulting from splaying of the two arteries. The tumor is highly vascularized, chiefly supplied by branches of the external carotid artery, and usually confined to the space between the internal and external carotids. Occasionally, a carotid body tumor may also extend laterally (as in the example shown) or encase the vessels. Carotid body tumors in atypical locations must be differentiated from the more common lymphomas, which is accomplished by duplex ultrasound primarily on the basis of their good vascularization. The longitudinal scan on the *left* obtained in anterior orientation depicts the well-perfused carotid body tumor anterior to the internal carotid artery (*ICA*). The transverse scan (*right*) shows the tumor in atypical location somewhat lateral to the external (*ECA*) and internal carotid arteries (*ICA*). The external carotid is slightly compressed by the tumor (aliasing). Histologic confirmation of the tumor after surgical removal

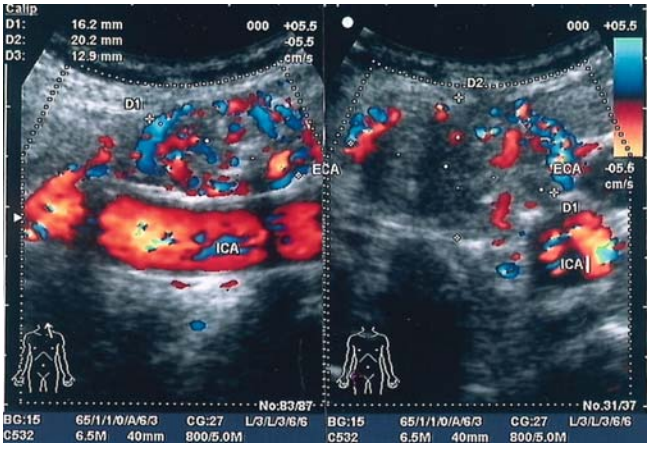

Visceral and Retroperitoneal Vessels 6

6.1 Abdominal Aorta, Visceral and Renal Arteries

6.1.1 Vascular Anatomy

6.1.1.1 Aorta

The *abdominal aorta* begins at the aortic hiatus in the diaphragm at the level of the T12 vertebra and descends in front of or slightly to the left of the vertebral column. The diameter of the aorta decreases on its downward course from 25 to 20 mm. A diameter of up to 30 mm as a result of age-related dilatation is considered normal. An abrupt increase in diameter to more than 1.5 times that of the normal proximal segment is regarded as evidence of an aneurysm. The abdominal aorta divides into the two *common iliac arteries* at the level of the L4/5 vertebrae. The intestine is supplied with blood from the three large visceral branches arising from the anterior aspect of the aorta. Their pattern of supply is complex and has numerous variants. The lumbar arteries originate from the lateral aspect and the two renal arteries course in a retroperitoneal direction. The arteries arising from the aorta from superior to inferior are described in detail below (Fig. 6.1).

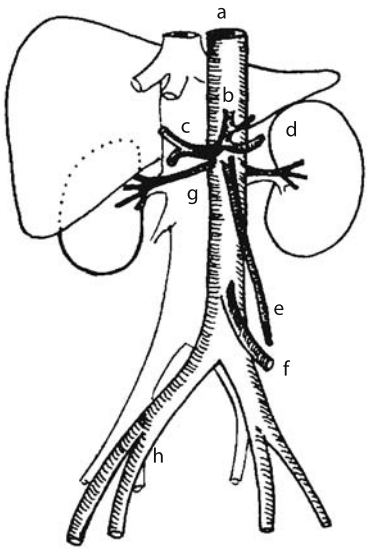

Fig. 6.1. Schematic representation of the sonographically and surgically significant visceral and retroperitoneal arteries: *a* aorta, *b* celiac trunk, *c* hepatic artery, *d* splenic artery, *e* superior mesenteric artery, *f* inferior mesenteric artery, *g* renal artery, *h* iliac arteries (common, internal, external)

6.1.1.2 Visceral Arteries

Just below the aortic aperture of the diaphragm, the aorta gives off the *celiac trunk*, which, after 2 – 3 cm, divides into its two main branches, the common hepatic and splenic arteries. The *common hepatic artery* courses between the head of the pancreas and the lower edge of the liver into the hepatoduodenal ligament, where it gives off the gastroduodenal artery, an important collateral that connects to the superior mesenteric artery. It continues to the liver as the *proper hepatic artery*. The *splenic artery* is in part markedly tortuous on its course along the upper border of the pancreas to the splenic hilum and supplies not only the spleen but also the body and tail of the pancreas as well as the greater curvature of the stomach.

About 0.5 – 2 cm below the celiac trunk lies the origin of the *superior mesenteric artery* at the level of the L1/2 vertebrae. It arises anteriorly at an acute angle of 15 – 30° relative to the aorta and its proximal segment runs parallel to the aorta between the pancreas and renal vein. After about 4 – 5 cm it gives off the inferior pancreaticoduodenal and middle colic arteries, which supply the transverse colon. Along its further course, the superior mesenteric divides into the jejunal, ileal, and ileocolic arteries that supply the small intestine.

Many anatomic variants exist. A normal celiac trunk is present in about 70% of the population. Alternatively, the hepatic or splenic artery may arise from the superior mesenteric artery, which has hemodynamic consequences for the affected vessels. A rare variant is a common origin of the hepatic, splenic, and superior mesenteric arteries from the aorta. In about 24% of cases, the liver is supplied by the superior mesenteric artery. Due to the good collateralization of the visceral arteries, chronic proximal occlusions of individual visceral arteries usually are tolerated well.

The *inferior mesenteric artery* originates at the level of the L3 vertebra, about 4 – 5 cm above the aortic bifurcation, and descends anterior to and somewhat to the left of the aorta. It is not visualized consistently due to its small caliber of about 2 – 4 mm.

6.1.1.3 Renal Arteries

The renal arteries arise from the aorta at right angles at the level of the L2 vertebra about 1 – 2 cm below the mesenteric artery. The right renal artery arises somewhat above the left renal artery and undercrosses the inferior vena cava while the left renal artery takes an almost horizontal course to the left renal hilum. Two or more renal arteries are present in about 25 % of the population. The renal arteries divide into the segmental arteries just before the hilum. The segmental arteries successively split into interlobar, arcuate, and interlobular arteries.

6.1.2 Examination Protocol and Technique

With a scanning depth of up to 20 cm, a valid and diagnostic duplex scan of the intra-abdominal and retroperitoneal arteries can only be obtained using a low-frequency transducer with a higher receive gain and a high enough frame rate. Slender patients can be examined with a 5 MHz transducer but 3.5 – 2 MHz transducers will be necessary in most cases. Sector scanners or curved-array transducers with a small radius make it easier to achieve a suitable Doppler angle ($<70°$, ideally $<60°$). Spectral Doppler sampling is impaired by the longer pulse delay with increasing depth of the vessel of interest.

The sonographer is confronted with a dilemma here since a high pulse repetition frequency is required to detect fast flow while the depth of the target vessels necessitates use of a low pulse repetition frequency, making aliasing a more common problem in evaluating stenoses of the abdominal vessels. This problem can be overcome by reducing the transmit frequency and scanning at a smaller insonation angle. To achieve an adequate frame rate in the color mode, a small color box just large enough to cover the area of interest must be chosen (as the frame rate is lower when more scan lines are processed).

The examination of the abdominal and retroperitoneal vessels begins with the identification of the aorta just below the diaphragm. It is scanned in transverse orientation down to the division into the iliac arteries, localizing the origins of the visceral and renal arteries on the way.

6.1.2.1 Aorta

The aorta is evaluated for dilatations and intraluminal structures on transverse B-mode scans along its course. To measure an aneurysm, the examiner first localizes the largest diameter and then moves the transducer around to identify a plane depicting a circular structure with a small diameter. This maneuver will avoid overestimation of the aneurysm that would result from measuring the size in oblique orientation, which is a common pitfall, especially in the presence of dilatative atherosclerotic processes with elongation and arching of the aorta. With its flexible selection of scan planes, ultrasound is superior to computed tomography and its reliance on the acquisition of standardized transverse slices.

The length of an aneurysm is secondary. What must be determined is whether the aneurysm is suprarenal or infrarenal in location. If the aneurysm is infrarenal and stenting is contemplated, the distance between the origin of the renal artery and the proximal end of the aneurysm is important and should be measured in longitudinal orientation. The origins of the common iliac arteries are evaluated in transverse and oblique planes to identify possible extension of the aneurysm into the iliac artery.

In the diagnostic evaluation of patients with a suspected stenosis, a spectral Doppler tracing of the aorta is recorded longitudinally. Occlusion of the aorta is most easily identified by the absence of flow in the color flow image and then confirmed by acquisition of a Doppler spectrum. The vena cava to the right of the aorta can serve as a landmark.

6.1.2.2 Visceral Arteries

The short celiac trunk with the division into the hepatic and splenic arteries is often identified in the transverse view as a conspicuous palm-leaf-shaped structure. Slight angulation of the transducer may be necessary to identify and visualize the origins of these arteries. The proper hepatic artery can be traced along its course anterosuperior to the portal vein in the hepatoduodenal ligament.

Also in *transverse orientation*, the splenic artery can be visualized along its course. The hepatic and splenic arteries supplying parenchymal organs have a fairly high diastolic flow. From a clinical point of view, the search for an aneurysm is most relevant in evaluating these vessels because aneurysms of this territory most commonly affect the splenic artery, followed by the hepatic artery. Aneurysms of the visceral arteries are altogether uncommon.

The superior mesenteric artery is identified at its origin in longitudinal orientation and tracked along its course parallel to the aorta as far as possible. A smaller angle for quantitative evaluation is achieved by downward angulation of the transducer while keeping the mesenteric origin in view.

In inflammatory bowel disease, B-mode scanning also enables evaluation of accompanying intestinal wall thickening and of inflammatory activity, which is associated with an increased peak systolic flow velocity and diastolic velocity.

The superior mesenteric artery arises at the level of the celiac trunk or as far as 2 cm below it. It descends parallel to the aorta and is thus seen as a round structure with a smaller diameter anterior to the aorta on transverse sections. Doppler spectra are sampled in transverse planes in the celiac trunk and the hepatic and splenic arteries and longitudinally in the superior mesenteric artery. The Doppler angle can be optimized by downward movement and tilting of the transducer (Fig. 6.2). To improve the angle, the patient can be asked to breathe in slightly, which will stretch the elongated and arched origin of the superior mesenteric further and shift the mesentery downward.

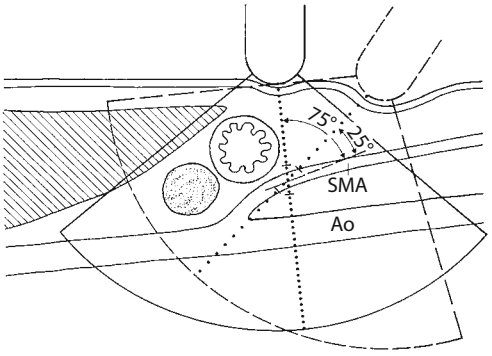

Fig. 6.2. Schematic representation of the origin of the superior mesenteric artery (*SMA*) from the aorta (*Ao*), illustrating how the Doppler angle can be improved from 75° to 25° by moving the transducer distally and then tilting it cranially

An atypical origin of the hepatic artery from the superior mesenteric artery must be identified because it affects the hemodynamics of the superior mesenteric. Therefore, the celiac trunk must always be included in an examination of the mesenteric arteries in order to identify such an atypical origin if the hepatic artery does not originate from the celiac trunk. In the evaluation of suspected acute mesenteric occlusion, the main trunk is evaluated including spectral Doppler sampling and subsequently the artery is tracked downward into its branches, the jejunal, middle colic, ileocolic, and right colic arteries. After adequate instrument adjustment with a high but artifact-free gain and low pulse repetition frequency, the origins of these vessels are located in the mesentery to then confirm or exclude embolic occlusions in these branches. Absence of flow in the color duplex mode must be verified by spectral Doppler recording.

The inferior mesenteric artery is less relevant clinically and is most easily depicted about halfway between the origin of the renal artery and the aortic bifurcation in the transverse plane or in an oblique orientation with the transducer directed toward the left lower abdomen (Fig. 6.3). If involvement of multiple visceral arteries is suspected, Doppler spectra are obtained from the vessel origins to identify a stenosis or occlusion.

To obtain reproducible measurements, the visceral arteries, just like the extremity arteries, should not be scanned during periods of hyperemia. This means that the examination should be performed after a period of fasting since the flow velocity is markedly increased after a meal.

Scatterers such as bowel gas can be pushed aside by applying pressure with the transducer. A small Doppler angle is achieved by moving and tilting the transducer, so that the sample volume in the target vessel comes to lie at the lateral edges of the B-mode scanning field displayed on the monitor.

The respiratory mobility of the intra-abdominal organs including the intra-abdominal and retroperitoneal vessels makes it necessary to scan the vessels during maximum inspiratory breath-holding or during shallow breathing with little respiratory motion. Proper breathing must be practiced with the patient before the examination.

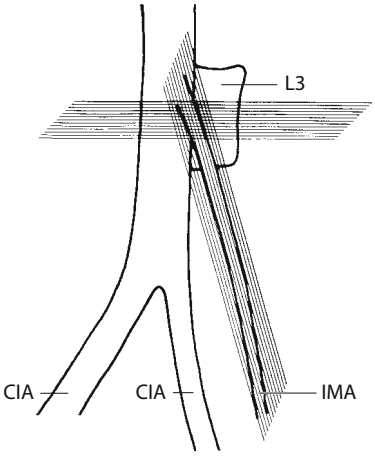

Fig. 6.3. Schematic representation of the origin of the inferior mesenteric artery about 3 cm above the aortic bifurcation. It arises from the left anterolateral aspect of the aorta. The inferior mesenteric artery (*IMA*) is identified with the transducer in transverse orientation and applying slight pressure while moving it upward from the bifurcation until the proximal IMA comes into view. The IMA can then be scanned over a length of 2 – 5 cm in most cases but will not be visualized under poor insonation conditions (*CIA* common iliac artery)

6.1.2.3 Renal Arteries

One way of identifying the renal arteries at their origins just below the easily visualized superior mesenteric artery is to localize the latter in transverse orientation and to then move the transducer 1– 2 cm downward and look for the renal arteries as they arise from the aorta to the left and right (Fig. 6.4). A second landmark is the left renal vein (hypoechoic, broader band) which overcrosses the aorta before opening into the vena cava and along its route passes between the superior mesenteric artery and the aorta. The left renal artery typically arises some millimeters below the right renal artery and both do not usually take a strictly horizontal

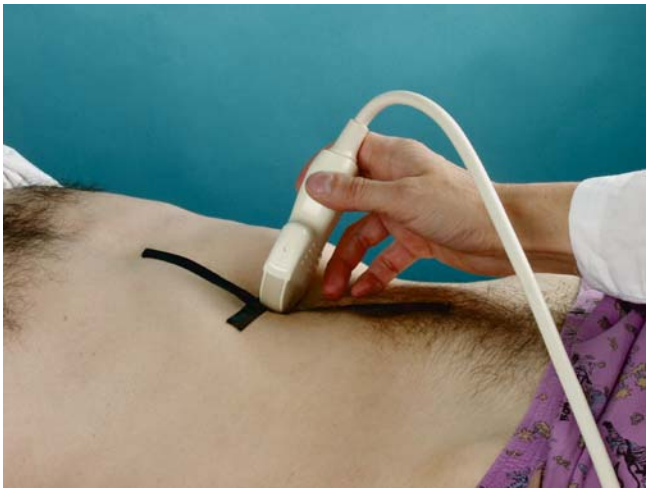

Fig. 6.4. Epigastric transducer position (transverse view of upper abdomen) for scanning of the renal arteries

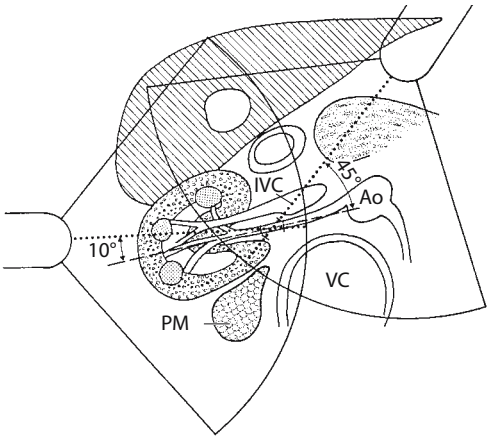

Fig. 6.5. Schematic representation of the right renal artery as it arises from the aorta (*Ao*) and of the renal vein entering the inferior vena cava (*IVC*). Anterior transducer position with a Doppler angle of 45°, lateral position with a Doppler angle of 10° (*VC* vertebral column, *PM* psoas muscle)

course but move slightly downward. The right renal artery first courses anteriorly in a slightly curved fashion and then arches underneath the vena cava. The origins as well as the first 3 cm of the renal arteries can be visualized and evaluated in over 90 % of cases while visualization of the middle third is often incomplete due to overlying bowel gas, especially on the left. The middle segment of the renal artery is easier to scan on the right where the vena cava can serve as an acoustic window. Interfering bowel gas can be displaced by pressing the transducer against the bowel until the vessel is seen. The transducer is then moved to the right or left to achieve an optimal angle for sampling of the Doppler spectrum.

The distal third can be scanned continuously from the flank starting at the renal hilum and following the course of the vessel proximally (Fig. 6.5). From this transducer position, it is also possible to continuously record an adequate Doppler spectrum with a relatively small angle. The individual segmental arteries are identified in the color flow mode and evaluated for stenoses at their origins during shallow breathing or breath-holding. If renal artery infarction is suspected, the renal parenchyma is evaluated for perfusion defects that are seen on color duplex scans as wedge-shaped areas without color coding (high but artifact-free gain, low pulse repetition frequency).

6.1.3 Normal Findings

6.1.3.1 Aorta

The aorta changes in diameter and pulsatility from superior to inferior. The flow profile shows continuous diastolic flow immediately below the diaphragm and becomes triphasic, as in peripheral arteries, below the origins of the renal arteries. The diameter of the aorta decreases from a mean of 25 mm to 15 – 20 mm just above the bifurcation. Progressive age-related dilatation with diameters of up to 30 mm of the infrarenal portion is considered normal, in particular in individuals with atherosclerotic vascular lesions (Rieger and Schoop 1998).

6.1.3.2 Visceral Arteries

Supplying parenchymal organs (liver and spleen) with a low peripheral resistance, the celiac trunk and hepatic and splenic arteries have Doppler waveforms with a monophasic flow profile and a relatively large diastolic component, resulting in a low pulsatility index of 0.6 – 0.8. Studies demonstrate wide interindividual variation in systolic and end-diastolic velocities and in vessel diameters (Table 6.1). This situation makes

	V_{max} [cm/s]	V_{diast} [cm/s]	V_{mean} [cm/s]	RI	Diameter [mm]
Celiac trunk Bowersox et al. 1991; Jäger et al. 1992; Moneta et al. 1988	100 – 237	23 – 58	45 – 55	0.66 – 0.82	6 – 10
Splenic artery Nakamura et al. 1989; Sato et al. 1987	70 – 110		15 – 40		4 – 8
Hepatic artery Jäger et al. 1992; Nakamura et al. 1989; Sato et al. 1987	70 – 120		20 – 40		4 – 10
Superior mesenteric artery* Jäger et al. 1986; Sato et al. 1988; Sabba et al. 1991; Bowersox et al. 1991; Schäberle and Seitz 1991	124 – 218	5 – 30	15 – 35	0.75 – 0.9	5 – 8

Table 6.1. Normal parameters of visceral arteries

* Values including preprandial and postprandial measurements
Duplex parameters: V_{max} peak systolic velocity, V_{diast} diastolic velocity, *RI* Pourcelot index, V_{mean} mean flow velocity

it difficult to define a cutoff value for discriminating hemodynamically significant stenoses.

The Doppler waveform of the superior mesenteric artery reflects a mixed type combining the high pulsatility of peripheral arteries and the low pulsatility of arteries supplying parenchymal organs. At the same time, the waveform of the superior mesenteric artery is a good example of demand-adjusted changes in pulsatility. After a meal, there is an increase in peak systolic flow velocity, but above all in diastolic flow velocity, due to the reduced peripheral resistance, which is the main factor responsible for a lower pulsatility index under these conditions.

In a study of normal vessels in 30 volunteers performed by the author as early as 1987, measurements in the superior mesenteric artery yielded a peak systolic velocity of 134 ± 22.8 cm/s and a peak diastolic velocity of 20.8 ± 4.4 cm/s. The mean flow velocity was 23.4 ± 5.6 cm/s. During digestion-related hyperemia one hour after eating, the peak systolic flow velocity was increased to 196 ± 25 cm/s and peak diastolic velocity to 47.5 ± 8.3 cm/s. The mean postprandial flow velocity was 46 ± 7.4 cm/s. In the time-motion display, the diameter of the superior mesenteric artery varied on average between 8.04 cm during systole and 7.4 cm during diastole (Fig. 6.6). Based on these values, mean blood flow increased by 126 %, from 639 ml/min preprandially to 1447 ml/min postprandially.

Apart from mechanical, metabolic, and neural mechanisms, mesenteric artery perfusion is affected by *vasoactive substances*, in particular gastrointestinal hormones like gastrin, secretin, and glucagon as well as other vasoactive hormones like catecholamines, histamine, and bradykinin. The effect on mesenteric perfusion of drugs like nitrates, ergotamine, narcotic agents, or calcium antagonists can be demonstrated by flow measurements performed with duplex ultrasound. In the above-quoted study, it was also shown that mean blood flow velocity after nifedipine administration increased from 23.9 cm/s to 41.8 cm/s, corresponding to a 75 % increase. The Pourcelot index decreased from 0.84 to 0.77, which is comparable to the postprandial decrease. These observations suggest that the increased mesenteric perfusion is primarily attributable to a reduced peripheral resistance in the mesenteric territory (cf. Fig. A 6.4).

In patients with anatomic variants (hepatic artery arising from the superior mesenteric artery), higher threshold velocities must be defined (cf. Fig. A 6.5). Moreover, blood flow in the superior mesenteric artery is also altered when the artery acts as a collateral in stenosis or obstruction of the celiac trunk.

Diagnostic evaluation of the inferior mesenteric artery is of little clinical significance. Systolic and diastolic flow velocities are comparable to those in the superior mesenteric but flow tends to be somewhat more pulsatile. Angle-corrected measurements in 20 subjects performed by our group yielded an average peak systolic velocity of 109 cm/s and a peak diastolic velocity of 10 cm/s but with wide interindividual variation. The flow profile was found to resemble that of the superior mesenteric artery but with a small diastolic component in most cases.

6.1.3.3 Renal Arteries

Supplying a low-resistance parenchymal organ, the renal arteries have a flow profile with little pulsatility and a large diastolic component. Measurements performed in 102 renal arteries without abnormalities on control angiography yielded a mean peak systolic velocity of 84.7 ± 13.9 cm/s and an end-diastolic velocity of 31.2 ± 7.8 cm/s. The Pourcelot index was 0.66 ± 0.07 (findings by our group, 1988). Visualization of the renal arteries for exclusion of a stenosis by duplex scanning is possible in 85 – 90 % of cases; the proximal third as the preferred site of atherosclerotic stenoses can be evaluated in over 90 % of cases. The flow velocities reported in the literature vary widely from one study to the next but also within the studies. The range is < 60 – 140 cm/s for peak systolic velocity and 20 – 65 cm/s for end-diastolic velocity with a Pourcelot index of 0.6 – 0.8. Reported diameters range from 5 – 8 mm (Karasch et al. 1993; Hoffmann et al. 1991; Schäberle et al. 1992; Sievers et al. 1989).

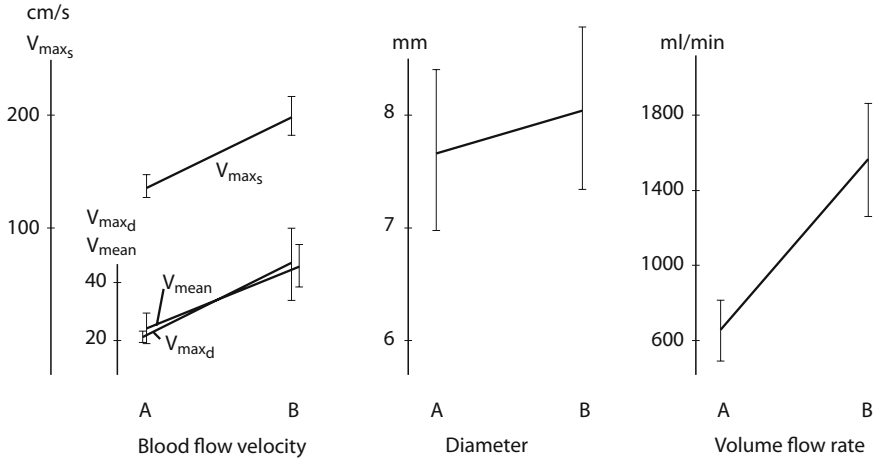

Fig. 6.6. Preprandial (*A*) and postprandial (*B*) mean values (± 15) of peak systolic velocity ($V_{max}s$), late diastolic velocity ($V_{max}d$), and mean blood flow velocity (V_{mean}) in the superior mesenteric artery in 30 healthy subjects. Also shown are the corresponding preprandial and postprandial vessel diameters and volume flow rates

The peak systolic and diastolic velocities and the Pourcelot index are affected by vessel elasticity and peripheral resistance. Moreover, they are influenced by systemic blood pressure. In diabetics, medial sclerosis with decreased wall elasticity and parenchymal changes result in a decreased diastolic flow and a higher Pourcelot index. Peak systolic velocity is slightly higher than in subjects with normal vessels.

6.1.4 Interpretation and Documentation

The ultrasound examination and the subsequent documentation of relevant findings of the visceral and retroperitoneal vessels depend on the clinical question to be answered. If an aortic aneurysm is diagnosed, the measurement is documented in the transverse plane, and the report must provide information on the localization and extent (infrarenal, relation to iliac arteries) as well as on the presence of thrombosis. Blood flow in the aorta should be documented by a longitudinally sampled Doppler waveform, but a color duplex scan may also be sufficient. In patients with suspected visceral artery stenosis, a Doppler spectrum is obtained from the origin of the respective vessel, the preferred site of visceral stenosis, and the vessel is scanned over a long stretch. The findings in patients evaluated for renal artery stenosis are documented by means of angle-corrected Doppler waveforms of the origins of both renal arteries. An angle-corrected waveform from the aorta is required as well. In fibromuscular dysplasia, either the findings in the middle thirds of both renal arteries are documented or Doppler waveforms from the origins and distal thirds (at the renal hilum) with comparison of resistance indices.

6.1.5 Clinical Role of Duplex Ultrasound

6.1.5.1 Aorta

The most important clinical indication for the sonographic evaluation of the retroperitoneal and intra-abdominal arteries is a suspected aneurysm of the abdominal aorta. Morphologically, an aneurysm is characterized by concentric or eccentric luminal dilatation. The vast majority of aneurysms begin infrarenally (95 %) and show variable degrees of thrombosis. The underlying causes in Europe are as follows (in order of descending frequency):

- 70 – 90 % atherosclerosis,
- 8 – 10 % idiopathic medial necrosis (Bollinger 1979),
- 4 – 5 % microbial infection including syphilis (which accounted for 20 – 30 % of aneurysms in the 1960s),
- 3 – 5 % nonbacterial inflammatory aneurysms (arteritis),
- 3 – 5 % inflammation, and
- 1 – 3 % congenital.

Aneurysms predominantly occur in the elderly or in patients with multiple morbidity. Aneurysms with mural thrombosis tend to grow more slowly and are more stable. An aneurysm develops on the basis of rarefaction and fragmentation of the elastic membranes and atrophy of the muscular media of the vessel wall. Although the dilatative process primarily involves the media rather than the intimal and subintimal layers (the site of atherosclerotic lesions), aneurysms in Europe are typically associated with atherosclerosis. In other regions such as Africa, a much larger proportion of aneurysms is due to nonbacterial inflammatory conditions such as arteritis (20 – 30 %) and more younger persons are affected. The sonographic evaluation of the vessel wall can provide information on the pathogenesis, on the basis of which specific therapeutic management can be initiated.

Ultrasound studies performed in Europe and the USA revealed a prevalence of 2.4 % in the normal population aged 65 to 74 (> 4 cm; Collin 1988) and a prevalence of 4.9 % (> 3 cm) in an investigation of 1800 subjects over 50 years of age without accompanying vascular disease (Akkersdijk et al. 1991). The prevalence increases to 10 – 14 % in individuals with arterial occlusive disease or hypertension (Galland et al. 1991; Twomey et al. 1984).

Most aneurysms of the abdominal aorta are incidentally detected in patients undergoing an ultrasound examination for an unrelated problem (Allenberg et al. 1997). The therapeutic management of aortic aneurysms is guided by the risk of rupture, which increases with the diameter. When surgical repair is contemplated, the risk of rupture of the untreated aneurysm must be weighed against the intraoperative and postoperative risk, which is considerable because the patients are often older and may have multiple morbidity. The mortality risk is less than 5 % in patients undergoing elective surgical resection and increases to over 50 – 60 % in emergency surgery for a ruptured aneurysm. Moreover, about 50 % die from aneurysmal rupture before they reach the hospital.

Several follow-up studies of subjects with aneurysms (Limet 1991; Nevitt et al. 1989; Zöllner et al. 1991) demonstrated a markedly higher risk of rupture for aneurysms greater than 5 cm, which is why a size of 5 cm evolved as the cutoff value for the surgical resection of abdominal aortic aneurysm. Based on the UK Small Aneurysm Trial (1998), which compared the natural history and the risk of surgery, the cutoff diameter for surgical management was even elevated to 5.5 cm. Patients with an aneurysm smaller than 5.5 cm require close follow-up and elective surgery is recommended if there is rapid growth of the aneurysm (> 5 mm in 6 months), embolization to the periphery, pain, or the shape is highly saccular. Further complications associated with an aneurysm are compression of surrounding structures (veins, bowel) or fistulization.

Prevention of rupture is the guiding principle of therapeutic management. Therefore, identification of factors contributing to the stabilization of an aneurysm is of crucial importance. Morphology seems to play a role (saccular aneurysms are more susceptible to rupture than spindle-shaped ones) as does thrombosis. Aneurysms with a thrombotic lining seem to grow more slowly whereas growth appears to be accelerated by local pressure peaks associated with turbulent flow, which primarily occurs in saccular aneurysms.

The clinical usefulness as well as cost effectiveness of B-mode scanning as the only screening procedure was impressively demonstrated in the recent English Multicentre Aneurysm Screening Study (MASS 2002). In this study, a total of 67,900 men aged 65 to 74 were screened for aortic aneurysms greater than 3 cm from 1997 to 1999. The results of this study suggest that a single ultrasound examination at the age of 65 with assignment of aneurysms to follow-up or repair reduces the risk of rupture by 53 %.

No studies have yet demonstrated the usefulness of the sonographic examination in cases where stenting of the aorta is contemplated. Here, the ultrasound evaluation can help decide between stenting and surgery. In general, the following criteria are contraindications to an endovascular procedure: a short and conical proximal neck, proximal kinking $>60°$, mural thrombi at the level of the origins of the renal arteries, accessory lower pole renal arteries, pronounced kinking of iliac vessels, and extension of the aneurysm to the origin of the internal iliac artery.

In the close follow-up of patients having undergone stent placement for an aortic aneurysm, color duplex scanning can contribute to the early identification of stent migration and endoleaks (types I, II, III) and thus help prevent complications.

Arteritis may also involve the aorta. Inflammation (e.g. giant cell arteritis, inflammatory aortic aneurysm) is suggested by thickening in the wall as opposed to thickening around the wall in retroperitoneal fibrosis (Ormond's disease). To make the distinction, the sonographer must carefully evaluate the vessel origins and the first centimeters and their relationship to the thickened segment (cf. Fig. A 6.31).

Aortic stenoses are amenable to ultrasound evaluation because they mainly occur in the distal aorta and the aortic bifurcation. Bilateral intermittent claudication is the chief symptom as more severe ischemia is prevented by good collateral pathways. The rare condition of aortic thrombosis may originate from atherosclerotic plaques. Predisposing factors are clotting disorders, paraneoplasia, and oral contraceptives. Aortic thrombi do not occlude the vessel but grow into the lumen in a cone-shaped manner. They become clinically apparent in most cases through embolization to peripheral arteries.

6.1.5.2 Visceral Arteries

Symptomatic mesenteric artery stenosis (abdominal angina) is rare. The prognosis of acute mesenteric artery occlusion crucially relies on the immediate diagnosis after hospitalization. The prognosis rapidly worsens within hours due to intestinal necrosis and short bowel syndrome even if patients are successfully operated on and survive the acute stage after bowel resection (Table 6.2).

Due to the unspecific clinical symptoms with severe abdominal pain (Table 6.3) but no other clinicopathologic

Table 6.2. Acute occlusion syndrome of the superior mesenteric artery. Mortality rates in relation to delay between onset of abdominal symptoms and surgery. (From Walter et al. 1992)

Time from initial symptoms to surgery [h]	[n]	Mortality
0 – 12	11	4 (36.3 %)
12 – 24	16	10 (62.5 %)
> 24	19	18 (94.7 %)
Total	46	32 (69.9 %)

Table 6.3. Acute occlusion syndrome of the superior mesenteric artery

	Initial stage 1 – 6 h	Silent interval 7 – 12 (24) h	Terminal stage > (12) 24 – 48 h
Clinical presentation	Initial triad: 1. severe abdominal pain without local or generalized signs of peritonitis, clinically normal abdomen 2. signs of shock in about 20 % of cases 3. diarrhea (anoxic)	Receding pain Mild local changes, deteriorating general state, onset of intestinal paralysis	Paralytic ileus Peritonitis Protracted shock
Laboratory findings	→ Progressive leukocytosis → → Increase of serum lactate level → → Increasing CK and LDH levels → → Progressive acidosis →		
Plain radiography	Negative	Typically negative	Increased air content, fluid levels
B-mode ultrasound	Negative	Negative	Thickened bowel loops, air inclusions, (sub)total ileus of small intestine
Revascularization possible	+++	++	(+)
Bowel resection necessary	–	(+)	++
Prognosis	→ Deteriorating →		

parameters at the initial stage and rapid progression within a few hours, prompt diagnosis and embolectomy are essential. The abdominal ultrasound examination performed in most patients for clarification of the abdominal pain should include (color) duplex scanning of the superior mesenteric artery. If the diagnosis of occlusion can be made with confidence by the spectral Doppler findings, immediate laparotomy can be performed without confirmatory angiography.

Visceral artery aneurysms are uncommon but significant because of their high risk of rupture (in particular aneurysms of the splenic and hepatic arteries). They are often discovered as incidental findings in patients undergoing an ultrasound examination for evaluation of abdominal complaints. On color duplex scanning, they are differentiated from other lesions, in particular pseudocysts of the pancreas, at first glance.

Stenoses of the celiac trunk may be caused by atherosclerosis (at origin) and rarely by fibromuscular dysplasia. External causes are compression by the arcuate ligament and the crura of the diaphragm. The significance of ligamentous stenosis of the celiac trunk, or arcuate ligament compression syndrome, is still controversial. The most important criterion for ligamentous compression is the respiratory variation in the degree of stenosis. The accompanying pain is most likely due to mechanical irritation of the celiac plexus. A reduction of perfusion resulting from intermittent compression seems unlikely as there is good collateralization of the visceral vessels. Intermittent compression may, however, damage the vessel wall and thus lead to secondary stenosis. This is also confirmed by studies investigating the outcome of surgery and showing good results especially in cases with a stable stenosis of the trunk largely unaffected by respiration and demonstration of a steal phenomenon by sonography and angiography (Walter et al. 1999). Surgery is indicated only in patients with epigastric pain and typical manifestations of abdominal angina such as postprandial symptoms and weight loss.

6.1.5.3 Renal Arteries

For proper therapeutic management of hypertension, it necessary to differentiate essential hypertension from secondary hypertension and, among the patients with secondary hypertension, identify those with renovascular hypertension, which is amenable to therapy (Table 6.4).

Table 6.4. Indications for ultrasonography of the renal arteries

- Workup of hypertension (atherosclerotic stenosis, fibromuscular dysplasia)
- Differentiation of < 50 % stenosis, higher-grade stenosis, and occlusion
- Follow-up after repair (operation, PTA with/without stenting)
- Suspected renal infarction
- Aortic aneurysm (spatial relationship to renal artery origins)
- Aortic dissection (possible involvement of renal arteries)
- Transplant kidney (anastomotic stenosis, rejection)

The average incidence of renovascular hypertension is 1 to 4 % in an unselected population (von Bockel et al. 1989; Foster et al. 1973; Olbricht et al. 1991) but incidences as low as 0.18 % and as high as 20 % have also been reported (Arlart and Ingrisch 1984; Tucker and Lebbarthe 1977). These discrepancies are due to the use of different screening methods and the investigation of different groups of the normal population and patients (presence of vascular risk factors and accompanying diseases, selected patient groups). Atherosclerotic stenoses virtually always occur at the origins of the renal arteries from the aorta or, very rarely, at the branchings into segmental arteries. They predominantly affect older males with other obstructive vascular diseases. In contrast, fibromuscular stenosis nearly exclusively involves the middle thirds of the renal arteries and primarily occurs in young women (Table 6.5). Hence, selective duplex scanning of the respective renal artery segment according to the suspected cause of stenosis can be performed.

In searching for a *renal artery stenosis* as a possible cause of hypertension in older patients with atherosclerotic vessel damage, the sonographer must pay special attention to the origins of the renal arteries, where the stenosis is likely to be located in over 95 % of this patient group. In younger patients in whom a suspected stenosis may also be due to fibromuscular hyperplasia, the entire course of the renal arteries is carefully evaluated, in particular the middle third (cf. Table 6.5). Numerous studies have confirmed the validity of duplex sonography in identifying renal artery stenoses (Table 6.7).

After a renal artery stenosis has been diagnosed by duplex scanning, no further diagnostic tests are needed prior to diagnostic angiography with simultaneous PTA. In patients having undergone PTA with or without stenting, ultrasound is also the method of choice to identify residual or recurrent stenoses.

Table 6.5. Fibromuscular and atherosclerotic renal artery stenoses

	Fibromuscular stenosis	Atherosclerotic stenosis
Proportion	< 10 %	> 90 %
Age	Typically < 40 years	Typically > 40 years
Sex	Predominantly women	Predominantly men
Preferred site	Typically middle and rarely distal third	Origin or proximal third
Poststenotic dilatation	Frequent	Rare
Repair method of choice	PTA Bypass, resection	PTA (middle and distal thirds) Reinsertion, bypass

6.1.6 Measurement Parameters, Diagnostic Criteria, and Role of Ultrasound

6.1.6.1 Renal Arteries

A wide range of different duplex scanning techniques and parameters have been proposed to differentiate normal findings and low-grade renal artery stenosis from hemodynamically significant higher-grade stenoses. This situation shows that all methods have their specific limitations, which one tries to overcome by different approaches. The fact that the poor visualization of the proximal and middle thirds of the renal arteries precludes velocity measurement for direct demonstration of a stenosis has prompted some investigators (Bönhof et al. 1990; Schwerk et al. 1994) to measure and compare peripheral resistance indices in both renal arteries. This is done by spectral Doppler sampling in the distal thirds of the arteries with scanning from the flank (Table 6.6).

In normal, unobstructed renal arteries, the resistance index (Pourcelot index) is roughly the same on both sides on condition that there is no unilateral damage of the kidney parenchyma, which would lead to more pulsatile flow and thus affect the Pourcelot index as well. Distal to a high-grade stenosis, flow is characterized by a delayed systolic increase and lower peak systolic velocity while diastolic flow is increased, resulting in a lower Pourcelot index. A Pourcelot index <0.5 determined in the distal renal artery at the hilum suggests postocclusive changes due to an upstream flow obstacle (cf. Fig. 6.6).

However, this method has a poor sensitivity in patients with more pulsatile flow and higher Pourcelot indices resulting from a loss of vessel elasticity due to atherosclerosis or medial sclerosis. Under such conditions, not even a high-grade stenosis is associated with a Pourcelot index <0.5. In contrast, it has been shown that a unilateral reduction of the Pourcelot index by over 0.05 (or over 10 %) compared to the contralateral side as a criterion for >70 % renal artery stenosis has a sensitivity of 82 % and a specificity of 92 % compared to angiography (Schwerk et al. 1994). This method takes into account elasticity losses as well as systemic factors such as the effects of hypercirculation or hypertension, which may be a source of error in flow velocity measurements for the quantification of stenoses.

Table 6.6. Different sonographic criteria used for diagnosing renal artery stenosis

- $V_{max} > 140$ cm/s (Schäberle 1988; duplex scanning) sensitivity 86 %, specificity 83 %
- $V_{max} > 180$ cm/s (Karasch 1993; color duplex scanning) sensitivity 92 %, specificity 90 %
- Renal-aortic ratio (RAR) >3.5 (Taylor 1988; duplex scanning) sensitivity 84 %, specificity 97 %
- Unilateral decrease in RI (Pourcelot) $>5-10$ % (Bönhof 1990; Schwerk 1994)

These indirect methods are limited by the fact that they will miss bilateral renal artery stenoses. Moreover, the results are influenced by the presence of parenchymal damage, which affects the resistance index. Although parenchymal damage with loss of parenchyma and renal atrophy can be identified by B-mode scanning and thus taken into account in the measurements, some uncertainty will remain. Parenchymal damage can also be caused by longstanding renal artery stenoses. In these cases, a high resistance index is an indicator of parenchymal damage and can be used to identify those patients who will not benefit from renal artery stenosis repair due to the extent of kidney damage that has already occurred at the time of diagnosis. This is assumed to be the case if the ipsilateral intrarenal Pourcelot index is $>0.8-0.85$.

The resistance index can be regarded as a sensitive indicator of an early, relevant loss of kidney function. In particular in patients with signs of a hepatorenal syndrome, higher-grade liver cirrhosis is associated with vasoconstriction in the renal cortex, which is reflected in an increased resistance index. In these patients with advanced liver cirrhosis, the resistance index is increased before laboratory tests will show impaired kidney function (Götzberger et al. 2003).

Ipsilateral comparison of Pourcelot indices at the renal artery origin and at its distal end near the renal hilum is a useful criterion for identifying fibromuscular stenosis if the middle third of the artery cannot be assessed properly due to overlying bowel gas or in obese patients. Obstruction by a high-grade stenosis will lead to more pulsatile flow with a higher Pourcelot index upstream and a lower index downstream due to a decreased peak systolic flow velocity and a corresponding increase in diastolic flow velocity (Fig. 6.7 a, b).

To take into account effects of hypertension (false-positive results) on the angle-corrected spectral waveform, it has been proposed to compare the peak systolic flow velocity in the aorta with that at the origin of the renal artery. The resulting renal-aortic ratio (RAR) is normally <3.5, with a ratio >3.5 indicating a hemodynamically significant renal artery stenosis (60 – 99 %). The RAR has been found to have a surprisingly high sensitivity of 83 – 100 % and a specificity of 73 – 97 % (Frauchinger et al. 1995; Taylor et al. 1988).

As with stenoses of the carotid system or peripheral arteries, it is also possible to demonstrate renal artery stenoses directly with a high degree of accuracy using the increase in peak systolic flow velocity above a specified threshold as determined from the angle-corrected Doppler waveform as a criterion.

Threshold velocities determined by means of ROC curve analysis always represent a compromise between sensitivity and specificity. A lower threshold increases sensitivity but decreases specificity while a higher threshold improves specificity but at the cost of sensitivity. Moreover, the ideal threshold determined varies with the accompanying diseases present in the study population. For instance, a higher cutoff value will be identified in a population with a larger proportion of diabetics with medial sclerosis and more pulsatile flow or in a population including subjects with high blood pressure values during the examination.

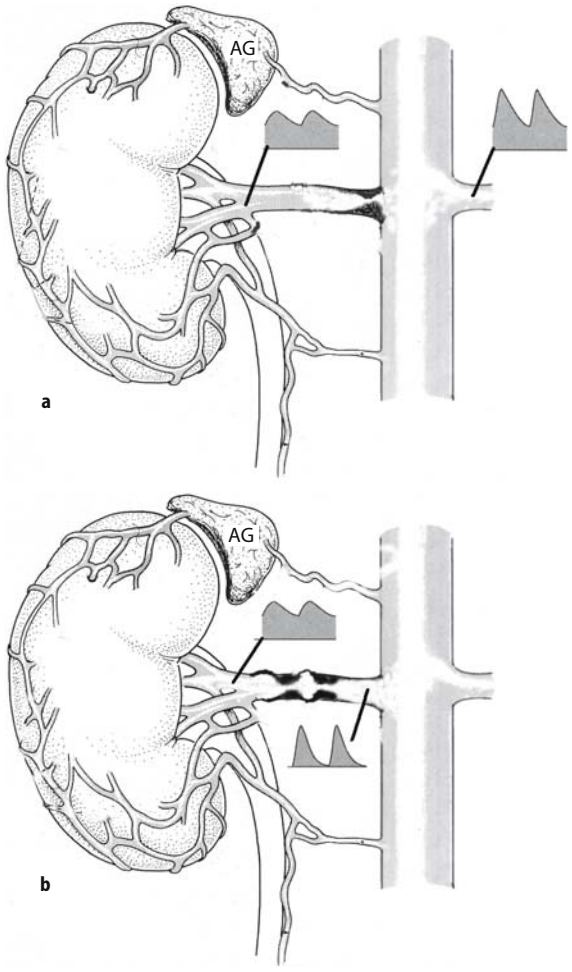

Fig. 6.7. a Atherosclerotic renal artery stenosis (at origin). Changes in postocclusive waveform: less pulsatile flow with delayed systolic upstroke, slower peak systolic flow velocity, and corresponding increase in diastolic component. Lower resistance index (Pourcelot index) as compared with nonstenosed, contralateral artery (cf. Figs. A 6.17 and 6.18). **b** Fibromuscular dysplasia of renal artery. Prestenotic and poststenotic waveforms with changes resulting from a stenosis in the middle third. Flow is more pulsatile upstream of the stenosis and becomes less pulsatile downstream with a markedly larger diastolic component and decreased resistance index (*AG* adrenal gland)

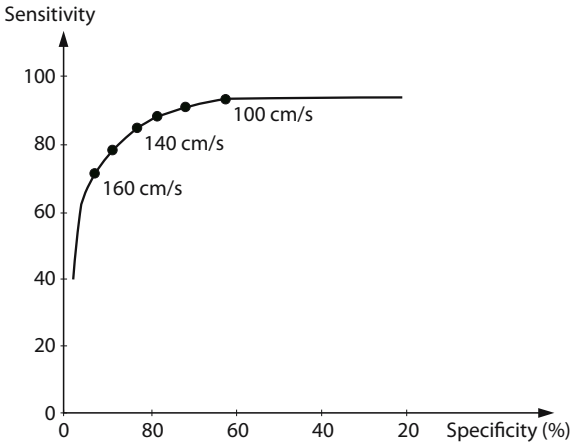

Fig. 6.8. Receiver-operating-characteristic (ROC) curve for identifying the optimal cutoff value (peak systolic velocity) for differentiating a normal renal artery or low-grade stenosis from hemodynamically significant stenoses (>50%). A threshold velocity of 140 cm/s yields a sensitivity of 86% and specificity of 83% compared to 75% and 93%, respectively, for a velocity of 160 cm/s (n=170 renal arteries, 44 with significant stenosis)

In a study by our group (1989), conventional duplex ultrasound already had a sensitivity of 86% and specificity of 83% compared to intra-arterial catheter angiography. Forty-four of 170 renal arteries were found to have a hemodynamically significant (>50%) stenosis. The relatively high prevalence of renal artery stenoses in this population was due to a selection bias (special angiology consultation service). In a receiver-operating-characteristic (ROC) curve analysis in that early study, we established a threshold of 140 cm/s to differentiate normal findings and low-grade stenoses from hemodynamically significant stenoses (Fig. 6.8).

In later studies (Karasch et al. 1993), in particular those using the color duplex mode for easier determination of an adequate Doppler angle (especially when insonating the slightly curved renal artery on the right), the cutoff value for a significant stenosis was corrected to a peak systolic velocity of 180 cm/s (Table 6.7).

Table 6.7. Studies investigating the sensitivity and specificity of (color) duplex ultrasound in identifying hemodynamically significant renal artery stenoses in comparison with angiography

Authors	Total No. of renal arteries/ No. of stenoses	Criterion Vmax [cm/s]	Sensitivity [%]	Specificity [%]	Reference angiography
Duplex scanning					
Avasthi 1984	52/26	100	89	73	IA
Kohler 1986	43/?	RAR >3.5	91	95	?
Ferretti 1988	104/27	>100	100	92	conv.
Taylor 1988	58/14	RAR >3.5	84	97	?
Strandness 1990	58/14	RAR >3.5	84	97	?
Hoffmann 1991	85/64	>180	95	90	?
Schäberle 1988	91/44	>140	86	83	IA, conv.
Color duplex scanning					
Breitenseher 1992	41/8	>120	17	89	IA
Karasch 1993	277/109	>180	92.7	89.8	conv., IA, IV
Spies 1995	268/42	–	93	92	IA

IA intra-arterial DSA; *IV* intravenous DSA, *conv.* conventional angiography

The study by Karasch et al. (1993) included 185 renal arteries examined by color duplex scanning, which was found to have a sensitivity of 92 % and specificity of 91 % using IA angiography and digital subtraction angiography (DSA) as reference methods.

Other study groups (Berland et al. 1990; Breitenseher et al. 1992; Desberg et al. 1990) used a threshold velocity of 100 – 120 cm/s to differentiate low-grade from hemodynamically significant stenoses (based on the threshold used for the internal carotid artery). The results of these studies are no longer valid in the light of more recent studies.

The poststenotic pressure drop with decreased perfusion after a higher-grade stenosis induces the affected kidney (renin-angiotensin system) to counterregulate the low systemic blood pressure. However, poststenotic perfusion will be decreased only in the presence of stenoses greater than 60 – 70 % with peak systolic flow velocities of over 200 to 220 cm/sec. In inconclusive cases, stenoses of this magnitude can be diagnosed by additionally taking into account indirect criteria of stenosis such as (audible) turbulence. From a clinical point of view, it is therefore less important to define a precise velocity threshold above which a stenosis becomes hemodynamically significant.

In diagnosing greater than 70 % renal artery stenosis using a peak systolic flow velocity of 200 cm/s, Olin et al. (1995) demonstrated a sensitivity and specificity of 98 % and Krumme et al. (1996) a sensitivity of 71 % and a specificity of 96 %. Surprisingly good results were reported by Baxter et al. (1996), who found a sensitivity of 100 % and a specificity of 95 % using a peak systolic velocity of 250 cm/s as a cutoff value.

In addition to a decreased resistance index (Pourcelot index), the acceleration time calculated from the poststenotic (damped) waveform at the renal hilum was proposed as another indirect criterion of stenosis. Using a value of less than 0.07 s as a criterion yielded sensitivities of 78 to 89 % and specificities of 92 to 98 % (Martin et al. 1991, Stavros et al. 1994, Nazzal et al. 1997). The indirect criteria are useful only for stenoses of 70 to 80 % and above because lower-grade stenoses do not affect the poststenotic waveform. Comparison of direct stenosis demonstration by color duplex using peak systolic flow velocity measurement and demonstration on the basis of indirect criteria (distal resistance index, acceleration time) with angiography showed a good correlation only for the direct approach (van der Hulst et al. 1996). This discrepancy is most likely due to parenchymal disease, vessel elasticity, and systemic cardiocirculatory factors. In conclusion, the diagnosis of renal artery stenosis should primarily be based on direct criteria and rely on additional indirect criteria only if the findings are inconclusive due to poor insonation conditions or methodological problems (cf. Fig. A 6.18).

To reduce measuring errors and misinterpretation of findings in the evaluation of stenoses, it is recommended to take into account systolic blood pressure as a systemic factor, to perform the measurements repeatedly, and to place the sample volume in a straight arterial segment. If a side-to-side comparison is done, vessels of the same order should be interrogated on both sides (segmental or interlobar arteries).

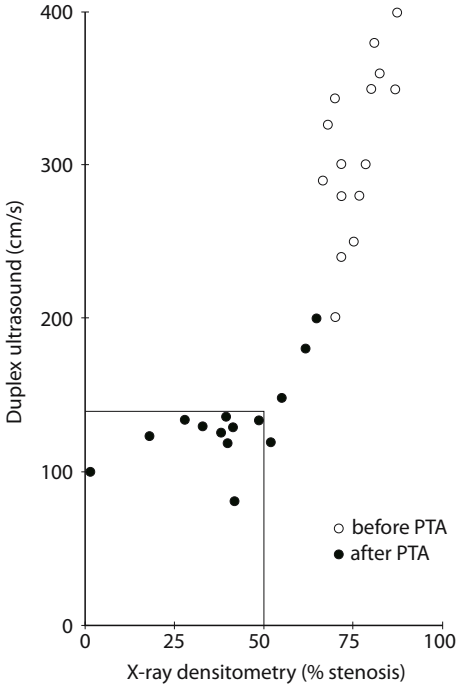

Fig. 6.9. Correlation of duplex ultrasonography and X-ray densitometry in 14 patients before and after PTA (R = 84). A hemodynamically significant stenosis is assumed at a velocity >140 cm/s for duplex scanning and at >50 % stenosis for X-ray densitometry

The *degree of stenosis* can likewise be estimated by duplex scanning on the basis of the increasing peak systolic flow velocity. In a study by our group, a good correlation was found between the peak systolic flow velocity determined by duplex sonography and the stenosis grade measured by X-ray densitometry with R = 0.84 (Schäberle et al. 1992; Fig. 6.9).

Two diagnostic modalities using different principles will necessarily yield slightly discrepant results. Angiography primarily relies on morphologic information and ultrasound on functional information.

The method of choice for follow-up after elimination of a renal artery stenosis (e.g. by PTA)) is duplex ultrasound (Schäberle et al. 1992). In this setting, the site to be evaluated is known, and the spectral waveform enables good quantification of the hemodynamic significance of a residual or recurrent stenosis. Moreover, the method allows good visualization of stents and stent complications.

Transplant Kidney

Two types of complications may occur after a kidney transplant: vascular complications and graft failure. Vascular complications comprise postoperative occlusion of the anastomosed artery or vein in the early postoperative course and stenosis of the renal artery (incidence of 2 – 25 %), aneurysm, and arteriovenous fistula as late complications. An anastomotic stenosis may occur as an early complication during the first weeks after surgery or after many years. The connection of the transplant artery to the iliac artery (cf. Fig. A 6.21) and the more superficial localization of the transplant vessels

make these more amenable to duplex scanning than native renal vessels. Stenosis criteria are the same as for native kidneys but indirect parameters should not be used. Instead, a stenosis must be demonstrated directly on the basis of an accelerated flow velocity at the anastomosis or along the course of the renal artery. An arteriovenous fistula mainly develops after needle biopsy and may resolve spontaneously. A persisting fistula can be identified by means of the typical color duplex criteria described in Ch. 4: mosaic-like color cloud (vibration artifacts) and pulsatile flow in the draining vein (cf. Fig. A 6.22).

Graft failure may occur immediately after transplantation (urine output less than 30 ml/hour and progressive elevation of retention values). The most common cause is acute tubular necrosis. Perfusion is preserved while an excessively high resistance index of over 0.9 may be noted.

Secondary failure after primary graft function is chiefly caused by acute rejection, infection, or nephrotoxic drug effects. Function may be impaired by stenoses of the graft artery or of the ureter. In addition, late failure may be due to chronic rejection.

Acute rejection typically occurs within the first 3 months of transplantation and may be of vascular or interstitial origin. The vascular form of rejection with intimal and medial thickening, fibrinoid necrosis, and subsequent thrombus formation in the small vessels can be identified by an early acute increase in the resistance index in the renal artery. In the interstitial form with tubulitis and interstitial lymphocyte infiltration and interstitial edema, there will be no significant increase in the resistance index of the renal artery despite incipient dysfunction. In vascular rejection, the resistance index may increase 1 – 5 days before the diagnosis can be made on clinical grounds; however, a reliable diagnosis of rejection in the case of an insidious increase in the resistance index can only be made through repeated determination, to then establish the indication for biopsy or therapy (Hollenbeck et al. 1994, Kubale et al. 1987, Rigsby et al. 1987).

6.1.6.2 Visceral Arteries

Celiac trunk. Stenoses of the celiac trunk are rare. They may be due to atherosclerosis or fibromuscular dysplasia. The rare arcuate ligament syndrome is characterized by intermittent compression of the celiac trunk by the diaphragmatic crura during expiration. Atherosclerotic stenosis will become clinically apparent only if several visceral arteries are affected.

Compression of the celiac trunk by the medial arcuate ligament of the diaphragm can lead to luminal narrowing identifiable by angiography and ultrasound. It is controversial whether the unspecific abdominal symptoms are due to hemodynamic disturbances or mechanical irritation of the celiac plexus. However, a primary vascular component of the compression syndrome is unlikely, given the rich collateral pathways.

The arcuate ligament syndrome has a characteristic angiographic appearance, namely a concave constriction of the origin of the celiac trunk from above. On color duplex scanning, the constriction produces a stenosis signal in the celiac trunk that varies with the respiratory movement of the diaphragm. The stenosis increases with expiration and decreases with inspiration and may completely disappear in deep inspiration.

Collateral pathways and the release of blood circulation during inspiration ensure adequate perfusion. Still, the intermittent compression can damage the vessel wall and trigger deposition of thrombotic material, resulting in a permanent stenosis and poststenotic dilatations as they are known from compression syndromes of other sites. The upper abdominal pain is most likely due to the pressure exerted by the arcuate ligament and the diaphragmatic crura on the vegetative nerves encircling the trunk.

Surgery of patients with the arcuate ligament syndrome is indicated in the presence of a so-called fixed stenosis, which is suggested if peak systolic flow velocities of over 280 cm/s are measured during inspiration as well as expiration. Moreover, the success of surgery with elimination of the symptoms induced by compression of the celiac trunk depends on the presence of a steal effect demonstrated by mesentericography or celiacography. Finally, the clinical findings must also be taken into account. These include abdominal angina with epigastric and postprandial pain and weight loss. Other causes of these symptoms such as tumor compression or chronic pancreatitis must be excluded (Fig. A 6.7).

Peak systolic flow velocities exceeding 220 – 250 cm/s (fasting) indicate hemodynamically significant stenoses greater than 50 %. However, in the celiac trunk, only higher-grade stenoses (> 70 %) with peak systolic velocities of over 280 – 300 cm/s will affect perfusion in a significant manner (see also Moneta et al. 1991). If there is occlusion of the celiac trunk, backward flow signals will be depicted in the splenic or hepatic artery, depending on whether collateral flow occurs via collaterals coursing to the splenic hilum or via the gastroduodenal artery. Flow velocities in the celiac trunk territory should be measured in a resting expiratory position to obtain a representative measurement).

Aneurysms of the hepatic and splenic arteries are rare and are conspicuous on B-mode scans as hypoechoic to anechoic round structures (Fig. A 6.12b). Mural thrombosis is seen as echogenic layering. Aneurysms are differentiated from tumors or pseudocysts of the pancreas by the depiction of flow signals in the color flow mode. Precise localization of a hepatic artery aneurysm is crucial for therapeutic decision making: Aneurysms proximal to the origin of the gastroduodenal artery from the common hepatic can be ligated without reconstruction because the liver will be supplied with blood via the gastroduodenal artery whereas restoration of the vessel is necessary after resection of a distal aneurysm from the proper hepatic artery. The surgical procedure is planned on the basis of the sonographically determined localization of the aneurysm and its relationship to the origin of the gastroduodenal artery (Fig. A 6.13).

Superior mesenteric artery. The wide variation in flow volumes and systolic and end-diastolic flow velocities in the mesenteric artery according to demand makes it necessary to scan patients in the fasting state in order to obtain standardized measurements and apply threshold velocities.

Quantitative determination of *blood flow* relies on the determination of the mean flow velocity and precise measurement of the vessel diameter. Diameter measurements in the superior mesenteric artery by our group demonstrated variations of about 10 % between systole and diastole with ensuing differences in the cross-sectional area of up to 35 %. Therefore, precise blood flow measurement makes it necessary to measure the systolic and diastolic vessel diameter separately and to calculate a mean vessel diameter according to the following formula, representing the two diameters according to their relative weight:

Mean vessel diameter R =
1/3 × (2 × R diastolic + R systolic)

For vessels up to 12 mm in diameter, the diameter can be measured most precisely using the leading-edge method (see Fig. 1.11) and scanning with a low transmit power. This method results in slight overestimation of the vessel diameter but, for diameters of up to 10 mm, the overestimation is less pronounced than the underestimation resulting from the inner-wall-to-inner-wall method. Also, the method enables systematization of the measurement error, which is important for follow-up measurements.

Color duplex scanning facilitates the identification of the mesenteric and renal arteries. Once the vessel has been brought into view, the Doppler spectrum is recorded for hemodynamic evaluation. Under good insonation conditions, color flow imaging will suggest a stenosis but verification by spectral Doppler is necessary. Depending on the clinical question to be answered, spectral Doppler tracings should be sampled at the vessel origins, the preferred sites of atherosclerotic stenoses of the visceral arteries.

Involvement of the peripheral branches is only seen in diabetics with generalized medial sclerosis. If there is high-grade atherosclerotic stenosis of only one of the three visceral artery origins, compensatory dilatation of the preformed *collateral pathways* will ensure adequate perfusion in most cases.

In general, *chronic intestinal ischemia* manifests as abdominal angina only if there is occlusion or stenosis of more than one visceral artery or in case of poor collateralization. The typical symptom is postprandial pain. *Calcified plaques* suggest a stenosis in the B-mode scan but definitive evidence is provided only by flow acceleration with turbulence or the absence of flow signals in case of occlusion.

In chronic mesenteric artery occlusion, ultrasound will often depict the main collateral vessels (gastroduodenal, splenic, and inferior mesenteric arteries) but angiography provides a better overview and enables more reliable evaluation of collateral pathways.

Chronic mesenteric artery occlusion is due to atherosclerosis and is associated with extensive collateralization through the celiac trunk (primarily the pancreaticoduodenal artery) and the inferior mesenteric artery (Riolan anastomosis). Since patients with chronic mesenteric occlusion are usually thin, the dilated gastroduodenal artery is visualized by duplex ultrasound at the pancreatic head. The superior mesenteric artery is filled distally and shows postocclusive flow with a delayed and reduced systolic rise and a decreased Pourcelot index.

A peak systolic flow velocity of over 200 cm/s in fasting patients suggests a *stenosis of the origin of the superior mesenteric artery*. The increase in peak systolic flow velocity is proportional to the degree of stenosis: > 280 cm/s corresponds to > 75 % stenosis (Fig. A 6.10). In a prospective study of over 100 patients with angiographically proven stenoses > 70 % in the superior mesenteric artery, duplex ultrasound with a cut-off value of 275 cm/s had a sensitivity of 92 % and a specificity of 96 % (Moneta et al. 1991, 1993). In the celiac trunk the sensitivity was 87 % and the specificity 80 % using a threshold of 200 cm/s for an angiographically proven stenosis greater than 70 % (Moneta et al. 1993). These data only apply to fasting subjects with normal vascular supply.

Acute mesenteric occlusion due to embolism is easily and reliably demonstrated by (color) duplex scanning as the absence of flow signals if the occlusion is located near the origin of the mesenteric artery from the aorta. Peripheral mesenteric artery occlusions pose a diagnostic problem. If there is extensive infarction of the small intestine but the main mesenteric artery is patent, the embolus is typically lodged at the divisions into jejunal branches or further distally at the origins of the ileocolic and right colic arteries. If there are patent branches such as the middle colic artery or proximal segments of the jejunal branches, the trunk of the mesenteric artery is patent as well. The overall reduction of blood flow and peripheral dilatation in the territory of the patent branches, which provide collateral flow via the arcades, is reflected in the spectral waveforms (cf. Figs. A 6.9 and A 6.10). Peak systolic flow

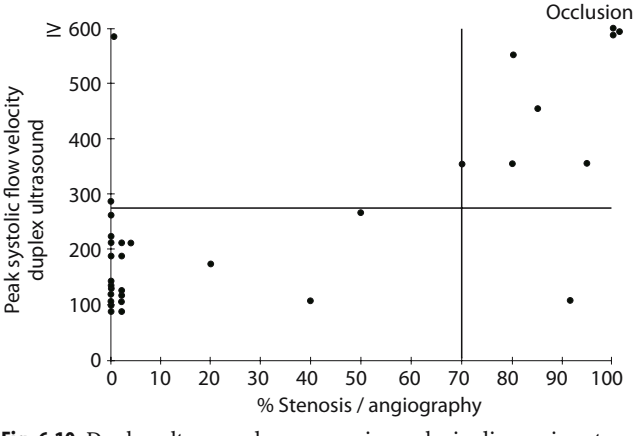

Fig. 6.10. Duplex ultrasound versus angiography in diagnosing stenosis of the origin of the superior mesenteric artery (from Moneta et al. 1993). The horizontal line represents the peak systolic flow velocity of 275 cm used as a threshold for angiographically proven stenosis of 70 %. The dots in the top right corner represent the mesenteric artery occlusions correctly diagnosed by duplex ultrasound. In the retrospective analysis, duplex ultrasound had a sensitivity of 89 % and a specificity of 92 % compared to angiography (n = 34)

velocity is reduced, and the lower peripheral resistance results in a larger diastolic component with a decreased Pourcelot index (Table 6.8).

The waveform changes become more pronounced with the number of occluded branches, which in turn increases the more proximal an embolus is located. However, the number of vessels involved has little clinical relevance and does not affect the patient's prognosis because the loss is compensated for by collateral flow through the patent branches and the arcades. In the worst case, short ischemic segments will persist and undergo necrosis in the further course, becoming clinically manifest as peritonitis (Fig. 6.11). Surgical resection of these short segments is indicated and has a good prognosis.

In summary, more central and hence prognostically relevant mesenteric occlusions can be identified as marked changes of the character of the spectral waveform sampled from the trunk of the superior mesenteric artery (cf. Fig. A 6.10). Consequently, if a patients shows the above-described decreases in the Pourcelot index and peak systolic flow velocity, the examiner must carefully evaluate the individual mesenteric branches distally in longitudinal and transverse planes in the color duplex mode in order to identify flow signals (Fig. 6.12). In the absence of flow, either emergency angiography is required or, if the ultrasound diagnosis can be made with confidence, immediate laparotomy for embolectomy of the affected branches can be performed.

The insonation conditions are rather poor in advanced occlusion due to overlying air, pain, and inability of the patient to cooperate. In these cases, however, the clinical symptoms will lead to surgery with ultrasound contributing only little to therapeutic decision making. The prognosis is

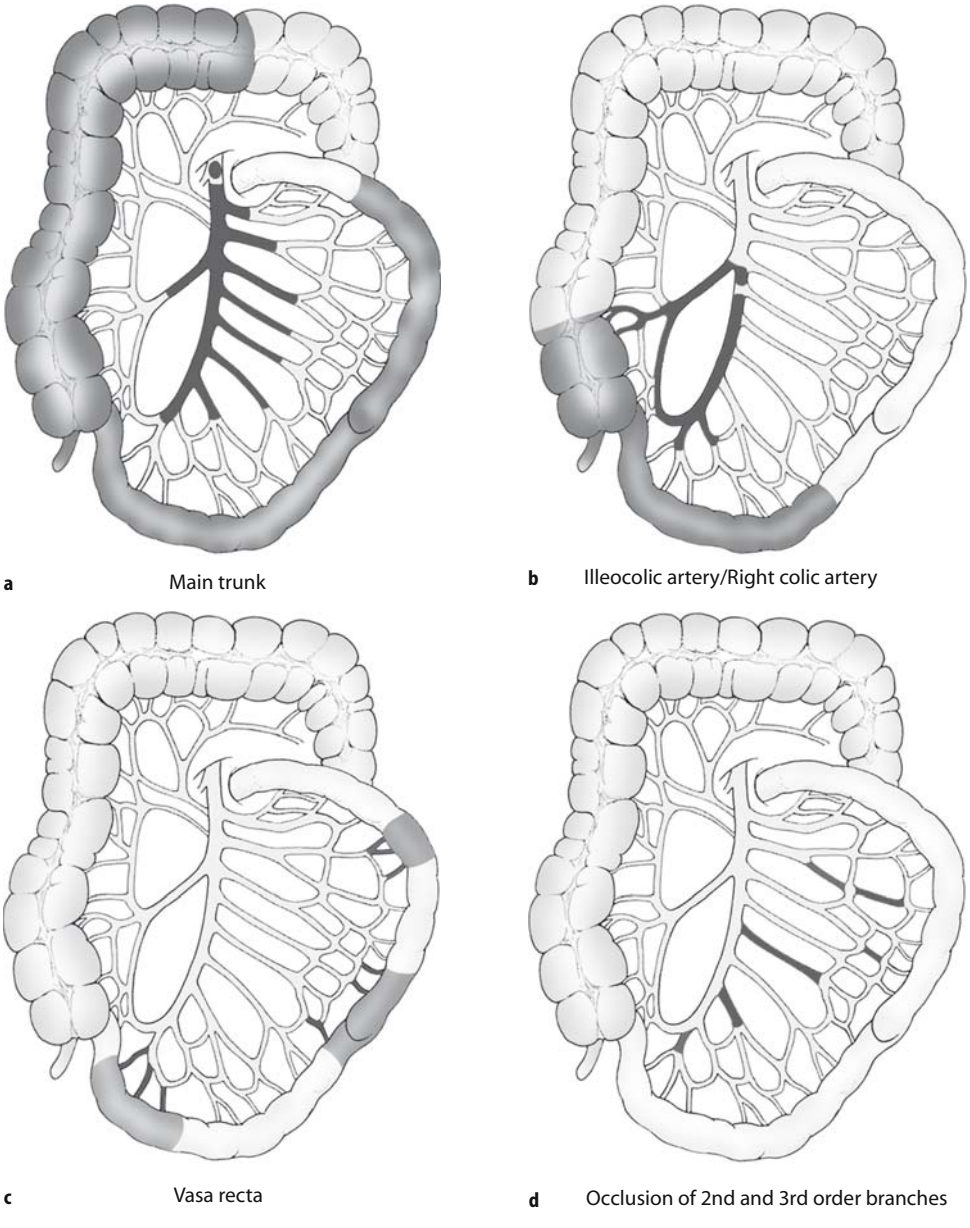

Fig. 6.11. Acute mesenteric artery occlusion. The extent of intestinal necrosis varies with the level of occlusion. Occlusion of individual jejunal branches only will not lead to acute intestinal ischemia as the arcades ensure collateral flow from patent jejunal branches (**d**). The vasa recta are involved in nonocclusive intestinal ischemia (**c**). Proximal occlusions in which the mesenteric trunk is still patent are associated with necrosis of long intestinal segments and have a poor prognosis. The Doppler waveform in the patent mesenteric artery shows abnormal changes (**a, b**). The patent branches dilate to provide maximum blood supply via the arcades, resulting in less pulsatile, low-resistance flow. Nevertheless, overall flow through the patent mesenteric trunk is reduced (decreased peak systolic velocity)

Table 6.8. Duplex ultrasound criteria for pathology of the superior mesenteric artery

Stenosis
- Peak systolic flow velocity > 280 cm/s (fasting)

Proximal occlusion
- Absence of flow signals

Distal occlusion
- Under good insonation conditions, absence of flow signal in occluded mesenteric branch
- Indirect signs of hemodynamically significant changes in waveform of proximal vessel segment:
  reduced peak systolic flow velocity
  reduced resistance index
  blunt waveform immediately before occlusion

poor. In early occlusion, when the clinical symptoms are not yet severe enough to warrant emergency surgery (cf. Table 6.3), the insonation conditions in most cases enable scanning of the main mesenteric artery and proximal divisions.

To confirm or exclude ischemia as the cause of ultrasonographically demonstrated thickening of bowel loops, the bowel wall and adjacent mesentery should be searched for flow signals using a high-resolution scanner operated with a high but artifact-free gain and low pulse repetition frequency. If flow signals detected in the color duplex mode are subsequently confirmed by spectral Doppler tracing, ischemia is excluded. A large diastolic component in the Doppler waveform is indicative of an underlying inflammatory condition (cf. Fig. A 6.11 d).

The resistance index (Pourcelot index) of the superior mesenteric artery is an unspecific parameter because it is also decreased in patients with abdominal conditions associated with peritonitis or in patients with sepsis. However, therapeutic decision making and the indication for surgery are based on the clinical findings in most patients while B-scan ultrasound or radiologic examinations are needed in inconclusive cases only. The spectral waveform in sepsis or peritonitis differs from that in distal mesenteric occlusion (decreased peak systolic velocity) in that the systolic rise is still relatively high and may be close to normal.

The indirect criteria cannot be quantified and, if present, should lead to further diagnostic testing (angiography) or laparotomy if warranted in conjunction with the clinical presentation. Hypotension and tachycardia as in septic shock or generalized peritonitis are also associated with marked hemodyamic changes in the mesenteric vessels and abnormal Doppler waveforms. Thus, the spectral waveform must always be interpreted in conjunction with the clinical presentation. However, a decreased Pourcelot index with a simultaneous decrease in peak systolic and mean flow velocities in the Doppler spectrum from the proximal superior mesenteric artery always indicates peripheral occlusion of a larger territory comprising several mesenteric branches (Table 6.9).

In acute intestinal ischemia, interpretation of the hemodynamic findings must also take into account the morphologic findings of B-mode scanning. Rapidly progressive wall edema

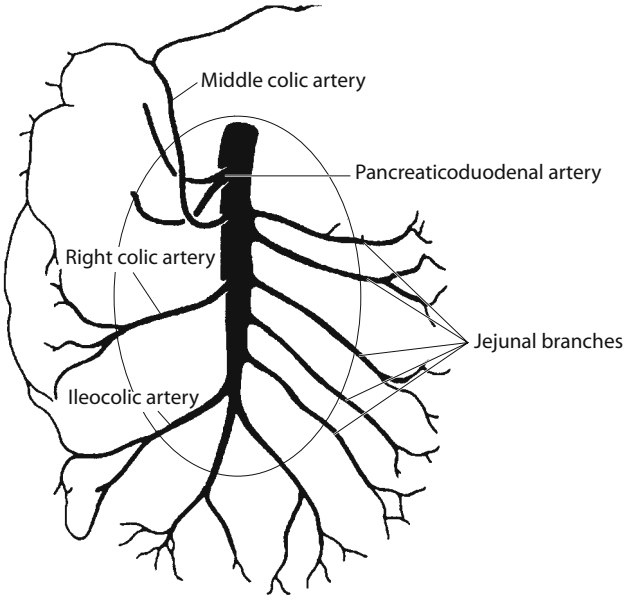

Fig. 6.12. Divisions of the superior mesenteric artery with side branches. Under optimal conditions, color duplex scanning visualizes the main trunk, the division into jejunal branches, the right colic artery, and ileocolic artery (visible area outlined). (According to Kubale 1994)

Table 6.9. Normal and abnormal changes of the spectral waveform from the superior mesenteric artery in relation to peripheral resistance

Decreased resistance index (Pourcelot) with absolute or relative increase in diastolic flow component
- With increase in mean flow velocity:
  postprandial
  drug-induced
  inflammatory
  tumor-related
- With decrease in mean flow velocity:
  distal mesenteric artery occlusion (dilatation of collaterals)

Increased resistance index (Pourcelot) with relative or absolute decrease in diastolic flow component
- Diabetes mellitus (medial sclerosis)
- Acute extensive mesenteric vein thrombosis

is identified by the typical bull's eye sign. The further course is characterized by intestinal wall necrosis and cessation of peristalsis. Progressive intestinal wall thickening and free fluid around affected bowel loops are identified sonographically as are air bubbles in the intestinal wall and portal vein that characterize the late stage.

If the hepatic artery arises from the superior mesenteric artery, the Doppler waveform obtained upstream of the origin will show a fairly large diastolic component with a decrease in the Pourcelot index, because the flow plattern in this case is affected by the supply of a parenchymal organ. This must be borne in mind in interpreting the findings.

Nonocclusive intestinal ischemia has a poor prognosis and frequently occurs in patients with considerable comorbidity.

The examiner must be aware of this condition as a differential diagnosis of proximal mesenteric occlusion. Circulatory insufficiency, sepsis, and diabetes mellitus are pathogenetic factors. Ultrasonography has no role in the diagnosis since only the smaller, distal mesenteric branches are affected while the superior mesenteric artery and the proximal segments of the main branches are patent. The diagnosis is confirmed angiographically before therapy with intra-arterial vasodilators is initiated.

An increased pulsatility of the mesenteric artery may be due to reduced wall elasticity in diabetes mellitus or indicate disturbed peripheral venous return, as in extensive mesenteric vein thrombosis.

The *diagnostic value of color duplex ultrasound* in evaluating infarction of the liver, spleen, or kidneys due to acute peripheral artery occlusion depends on the insonation conditions. The extent of infarction varies with the localization of the occlusion and blood supply through collateral routes. B-mode scanning shows poorly delineated, inhomogeneous, and hypoechoic areas, but only with a delay of 1 to 3 days after the acute event (Seitz and Rettenmaier 1994). There are some case reports describing the use of color duplex scanning in patients with renal or splenic infarction. However, ultrasound is most beneficial in guiding interventional procedures such as abscess drainage in superinfection of necrotic areas.

Aneurysms of the visceral arteries are very uncommon but tend to rupture. They are typically detected incidentally in patients undergoing B-mode ultrasound for diagnostic workup of abdominal complaints (which may be due to pressure). They are differentiated from pseudocysts or other cystic tumorous lesions of the upper abdomen by their characteristic color duplex appearance. Locating the aneurysm to the splenic, superior mesenteric, or hepatic artery is important for planning of the surgical procedure. As with all other vascular territories, the diagnostic evaluation of aneurysms falls in the domain of color duplex ultrasound: It enables reliable determination of the diameter, identification of thrombotic wall lining, and assessment of the patent residual lumen, not least of all because of the free selection of scanning planes with the transducer.

Aneurysms of the superior mesenteric artery are rare. Even less common are aneurysms of the gastroduodenal, pancreaticoduodenal, and inferior mesenteric arteries. They are typically mycotic aneurysms (staphylococci, salmonellae). Their localization and size are evaluated as with aneurysms of other vascular territories. For planning of the surgical procedure, it is crucial to exactly determine their course and their relationship to other vessels. Visceral artery aneurysms appear to be more common in patients with ectopic variants.

6.1.6.3 Aorta

Bilateral intermittent claudication may be caused by a stenosis of the distal aorta. Therefore, the aorta should be scanned if the spectral display of the iliac artery shows poststenotic changes. A high-grade stenosis of the aorta is indicated in the color duplex scan by a mosaic pattern resulting from perivascular vibration, as in an AV fistula. Severe atherosclerosis with calcified plaques impairs the detection of the high peak systolic flow velocity in the stenosis jet by duplex scanning. On the other hand, extensive plaques with acoustic shadowing and poor delineation of the lumen in the B-mode scan often suggest a high-grade stenosis of the aorta. The Doppler waveform sampled distal to the high-grade stenosis will show the typical postocclusive flow profile with a delayed systolic rise and large diastolic component.

Aortic stenoses chiefly occur in the distal infrarenal segment including the bifurcation. In this setting, collateral supply with refilling of the iliac system is mainly ensured by the inferior mesenteric artery, which will become dilated and show high systolic (often over 200 cm/s) and end-diastolic flow velocities (cf. Fig. A 6.36).

In acute obstruction of the terminal aorta (Leriche's syndrome), the lumen is discriminated in the B-mode scan by being filled with a hypoechoic material. If the occlusion is due to atherosclerotic stenosis, on the other hand, the aorta is difficult to differentiate from surrounding tissue. Flow is absent in both cases. In patients with poor visualization, chronic occlusion can be differentiated from high-grade stenosis by the absence of the mosaic pattern that is caused by perivascular vibration artifacts and is typical of stenosis.

Thrombosis of the aorta is depicted as a hypoechoic cone-like structure in the lumen. The tail of the thrombus is typically surrounded by flowing blood on all sides. Signs of luminal narrowing are seen on duplex scanning only when there is nearly complete occlusion. In most patients, aortic thrombosis becomes manifest through embolism, often to both legs. Under these conditions, the circular flow signal around the hypoechoic thrombus on color duplex differentiates thrombosis of the aorta from an embolizing aneurysm (cf. Fig. A 6.37).

The diagnosis of an aortic aneurysm including its localization and characterization (Table 6.10) falls in the domain of color duplex sonography.

While angiography only depicts the residual lumen of an aneurysm, ultrasound enables differentiation of mural thrombosis and residual lumen. The variable scanning plane

Table 6.10. Therapeutically relevant color duplex findings in aneurysm of the abdominal aorta

- Diameter of aneurysm (indication for surgery)
- Shape of aneurysm (saccular, spindle-shaped)
- Partial thrombosis
- Involvement of (common, internal) iliac arteries
- Infrarenal – suprarenal

Additional criteria if endovascular therapy is contemplated:

- Distance of proximal end of aneurysm to renal artery
- Degree of angulation in case of elongation of infrarenal aorta
- Conic neck of aneurysm
- Lumen of common femoral artery (large enough for stent insertion?)

of ultrasound relative to the course of the aneurysm facilitates determination of the true diameter compared to CT. Moreover, the use of standardized transverse sections as in CT may lead to overestimation of the aneurysmal diameter as a result of its elliptical profile in transverse orientation when there is concomitant elongation of the distal aorta, which is often associated with atherosclerotic aneurysm (cf. Fig. A 6.25). Ultrasonography does not have this methodological limitation as the transducer can be rotated to avoid oblique sectioning of the aortic lumen, thereby enabling more accurate diameter measurement.

Intraobserver as well as interobserver studies show good reproducibility of the results if these aspects are taken into consideration in sonographic diameter measurement. A standardized protocol is necessary to depict the true development of aneurysm size in follow-up examinations.

Embolizing aortic aneurysms and markedly saccular aneurysms require surgical management irrespective of their size. Saccular aneurysms tend to exhibit turbulent flow on color duplex scanning while laminar flow is more likely in smaller, spindle-shaped aneurysms. The local pressure peaks occurring in turbulent flow are associated with more rapid growth and a higher risk of rupture. In scanning patients with embolic occlusion of the leg arteries, thrombi in an aortic aneurysm should be excluded as a source of embolism (cf. Fig. A 6.24).

Rupture of an aneurysm is suggested by flank and back plain (occasionally abdominal pain), a palpable pulsating tumor, and shock. Gray-scale scanning depicts a hypoechoic structure of variable extent and comprising inhomogeneous or layered portions around the aorta in the retroperitoneum. Color duplex demonstrates paravascular flow signals in the leakage area in case of a contained perforation. Leakage must be differentiated from other hypoechoic periaortal structures such as retroperitoneal fibrosis, horseshoe kidneys, or lymphomas, which may be associated with an aneurysm (cf. Fig. A 6.31). An examiner performing ultrasonography on an emergency basis must pay special attention to such accompanying conditions as they have important implications.

If there is perforation into the duodenum, the intestine may appear fluid-filled. Fistular connections to the vena cava can be demonstrated by color duplex.

In a dissecting aneurysm, splitting of the arterial wall with tearing of the intima is suggested on gray-scale ultrasonography by the presence of a flap in the vessel lumen that is identified by its hyperechoic reflection and typical ondulating motion. Dissection is confirmed in the color mode by different flow velocities and directions in the true and false lumen. The power mode will help demonstrate slow flow in the false lumen and differentiate it from partial thrombosis. The color-coded flow directions contribute to the identification of the entry and re-entry sites. The relation of the origins of the visceral arteries and renal arteries to the true and false lumina is crucial for proper therapeutic management. As the dissected flap may extend into the groin, the iliac artery must be included in the examination (cf. Fig. A 6.32 and A 6.33).

Follow-up after surgical resection of an aneurysm or patch angioplasty of stenosis of the aorta is a domain of duplex ultrasonography. It ensures early identification of complications such as suture aneurysm, anastomotic stenosis, recurrent stenosis, or abscess. Hypoechoic structures around a prosthesis, particularly at the sites of anastomosis, must be checked for flow signals in the color mode to differentiate suture aneurysm from postoperative hematoma and abscess. Suture aneurysms are false aneurysms and hence are characterized by to-and-fro flow (steam engine sound) in the spectral waveform (recorded at the site of the wall perforation; cf. Fig. A 6.35). An abscess suspected on clinical grounds can be confirmed by ultrasound-guided fine-needle aspiration biopsy.

Color-coded duplex ultrasound is a highly valid follow-up modality for the identification of limb occlusions or endoleaks after stenting (Table 6.11). Depending on the ultrasound equipment used, the sensitivity for identifying endoleaks ranges from 77 – 96 % with a specificity of 90 – 94 % (D'Audiffret et al. 2001; Golzarian et al. 2002; Sato et al. 1998). The sensitivity for type II endoleaks is only 50 – 70 %. The sensitivity can be improved by the administration of echo enhancers, which are especially useful to identify type II endoleaks (Bendick et al. 2003; Böhm et al. 2000; Heilberger et al. 1997; McWilliams et al. 2002). However, the clinical significance of limb leaks (type II) continues to be controversial (Liewald et al. 2001; Parry et al. 2002; White et al. 2000). Type II endoleaks with little flow and slow flow velocities may undergo spontaneous thrombosis. Flow measurement by duplex scanning in the aneurysm in the presence of type II endoleak may contribute to therapeutic decision making. Another therapeutically relevant criterion is continuous growth of the aneurysm (measured in the B-mode) rather than shrinkage after stenting. Studies comparing follow-up after stenting by CT versus ultrasonography show very good correlations. In a pairwise comparison, an agreement of 93 % was found between CT and ultrasond (with an allowable tolerance < 5 mm).

Stents should be followed up at 6-month intervals with closer follow-up by noninvasive duplex scanning of type II endoleaks (of lateral branches, lumbar arteries, and the superior mesenteric artery) that do not require therapy. Type I (aorta-to-stent junction) and type III endoleaks are more readily identified sonographically due to faster flow. Nevertheless, computed tomography is the gold standard for the planning and follow-up of stent placement. Breaking and migration of a stent are reliably detected by conventional radiography.

Aortic wall thickening must be differentiated from perivascular, retroperitoneal processes by scanning of the aorta with special attention paid to the origins of branching vessels. Retroperitoneal lymphomas are circumscribed round lesions that may become confluent. Retroperitoneal fibrosis is typically depicted as a more hypoechoic structure covering the aorta from anteriorly and involving the vena cava. It tapers off laterally and may also surround and compress the ureter.

The course of the inferior mesenteric artery can help to differentiate wall thickening of the aorta and retroperitoneal fibrosis. In retroperitoneal fibrosis the proximal inferior mesenteric artery is pushed against the aorta and thus courses

Table 6.11. Therapeutically relevant sonographic criteria in the follow-up after treatment of aneurysms of the abdominal aorta

After surgical repair:
- Recurrent aneurysm – suture aneurysm
- Anastomotic stenosis (occlusion of Y-limb)
- Abscess

After endovascular stent placement:
- Endoleaks (types I, II, and III)
- Growth or shrinkage of the former aneurysm
- Stent migration
- Occlusion

between the aortic wall and the hypoechoic fibrosis for several centimeters before piercing through the hypoechoic fibrotic cap (cf. Fig. A 6.31). In inflammation of the aorta (e.g. giant cell arteritis), on the other hand, the inferior mesenteric artery pierces the hypoechoic layer around the patent lumen of the aorta directly at its origin to then course toward the left lower abdomen outside the hypoechoic thickening. Inflammatory wall thickening in aortitis and in inflammatory aortic aneurysm is fairly concentric and does not include the vena cava. The flexible selection of scanning planes with the ultrasound scanner facilitates determination of the relationships between the aorta, hypoechoic thickening, perivascular structures, and other vessels and thus aids in establishing the differential diagnosis.

6.2 Visceral and Retroperitoneal Veins

6.2.1 Vascular Anatomy

6.2.1.1 Vena Cava

The inferior vena cava ascends parallel to the course of the aorta and to the right of the vertebral column. It is a capacitance vessel with an elliptical cross-section and may vary in its anteroposterior diameter from 0.5 – 2.5 cm during the respiratory cycle. It is formed by the junction of the common iliac veins at the level of L4/L5 slightly below the aortic bifurcation.

Variants and anomalies of the inferior vena cava are seen in 1.5 – 4.0 % of the population. They result from errors in the complex embryonic development with a disturbance in the transition from the symmetric venous system to the predominantly right-sided, asymmetric secondary system. The congenital anomalies were classified by Chuang et al. as early as 1974 (Table 6.12).

6.2.1.2 Renal Veins

The right renal vein courses anterior to the renal artery and after 3 – 4 cm empties into the vena cava at the level of the L1 vertebra. The left renal vein runs anterior and somewhat

Table 6.12. Congenital anomalies of the inferior vena cava (classification by Chuang et al. 1974)

	Segment	
I	Postrenal	
	Type A:	Persistence of right posterior cardinal vein ("retro- or circumaortic ureter")
	Type B:	Persistence of right supracardinal vein ("normal inferior vena cava")
	Type C:	Persistence of left supracardinal vein ("left-sided inferior vena cava")
	Type BC:	Persistence of both supracardinal veins ("duplicated inferior vena cava")
II	Renal	Persistence of renal venous ring ("circumaortic ureter")
III	Prerenal or hepatic	Absence of hepatic segment ("azygos or hemiazygos vein continuation")

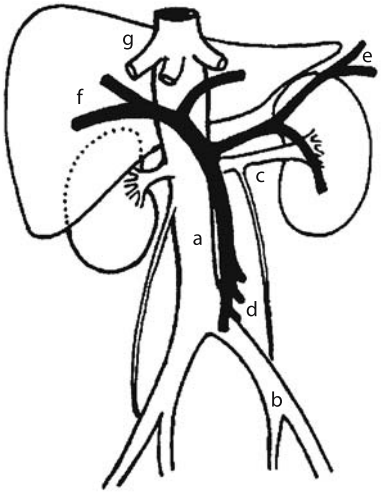

Fig. 6.13. Schematic representation of the large retroperitoneal and intra-abdominal veins (*black*) [*a* vena cava, *b* (common, external, and internal) iliac veins, *c* renal vein, *d* superior mesenteric vein, *e* splenic vein, *f* portal vein, *g* hepatic veins]

superior to the renal artery to then curve between the aorta and superior mesenteric artery and posteroinferior to the head of the pancreas on its way to the inferior vena cava. The left renal artery receives the ovarian or spermatic vein, which empty directly into the vena cava on the right (Fig. 6.13).

Variants include duplication of the renal veins and atypical openings that may even extend to the common iliac vein. Disturbed embryonic development may result in an atypical retroaortic course of the left renal vein.

6.2.1.3 Portal Venous System and Hepatic Veins

The *portal vein* is a thick trunk normally 6 – 8 cm long with a transverse, anteroposterior elliptical diameter of 8 –12 mm, rarely up to 16 mm. It shows relatively wide physiologic variation and passes through the hepatoduodenal ligament behind

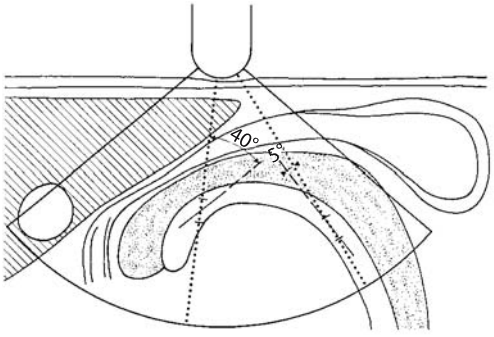

Fig. 6.14. Schematic cross-section of the splenic vein along its course from left to right to the neck of the pancreas, where it forms the portal vein together with the superior mesenteric vein

the proper hepatic artery and ascends to the porta hepatis taking an oblique lateral course. Intrahepatically, it follows the branches of the hepatic artery and the bile ducts. The branching pattern of the portal vein provides the basis for the anatomic segmentation of the liver. The branches of the hepatic veins are intersegmental vessels.

The *splenic vein* passes behind the pancreas from the hilum of the spleen to the neck of the pancreas, where it joins the superior mesenteric vein to form the portal vein (Fig. 6.14). The confluence of the two veins (cf. Fig. 6.13) is situated to the left of and behind the head of the pancreas, somewhat lateral and inferior to the origin of the mesenteric artery. The *superior mesenteric vein* courses to the right of the superior mesenteric artery and anterior to the aorta.

Blood is drained from the liver through the segmental branches into the three major veins that empty directly into the inferior vena cava.

6.2.2 Examination Technique

6.2.2.1 Vena Cava

The aorta can serve as a landmark in scanning the vena cava. When assessing the lower extremity vessels for thrombosis or in patients with pulmonary embolism, the vena cava is traced along its course after evaluation of the pelvic and leg veins. Evaluation in transverse orientation is followed by longitudinal scanning for recording of the Doppler spectrum. The confluence of the iliac veins at the level of the umbilicus can be identified using the aortic bifurcation at about the same level or slightly above for guidance.

In pelvic vein thrombosis, possible extension of the thrombus into the vena cava must be identified and the end of the thrombus evaluated for the presence of surrounding flow signals. Moreover, the respiratory variation in vena cava diameter is determined in transverse or longitudinal views. Diameter variation is absent in thrombosis.

Compression ultrasound is unreliable in the abdomen (where compression is limited by anatomy), which is why (color) duplex scanning is necessary to exclude thrombosis. Only in slender patients is it possible to reliably compress the vena cava. The flow velocity determined from the Doppler spectrum is likewise affected by respiratory variations and increasing cardiac pulsatility toward the heart. Below the kidneys, the liver serves as an acoustic window with the portal vein being located anterior to the vena cava at the hilum of the liver.

6.2.2.2 Renal Veins

The renal veins are scanned from the flank beginning at the hilum of the kidney and following their course toward the heart (cf. Fig. 6.5). While the shorter right vein can be scanned from this position throughout its course to the inferior vena cava, the left vein must be scanned from a medial approach in transverse orientation to visualize the segment between the aorta and superior mesenteric artery and its opening. In the search for thrombosis of the renal veins or intravascular tumor extension in the B-mode, the examiner must look for the absence of respiratory diameter fluctuations and the presence of echogenic intraluminal material dilating the vein. The absence of flow signals in the spectral Doppler tracing or color flow examination is diagnostic.

6.2.2.3 Portal Vein and Superior Mesenteric Vein

The course of the portal vein from below the head of the pancreas to the hilum of the liver is most easily accessible from a subcostal approach in an oblique plane through the right upper abdomen (Fig. 6.15). If visualization is impaired by overlying bowel gas, the hilum of the liver can be identified and the portal vein followed distally from an intercostal position (right flank) using the liver as an acoustic window. Portal vein thrombosis is suggested by the presence of echogenic material in the lumen and absent respiratory diameter variation in the B-mode scan and is subsequently confirmed by (color) duplex scanning.

The superior mesenteric vein courses to the right of the superior mesenteric artery with a position to the left suggest-

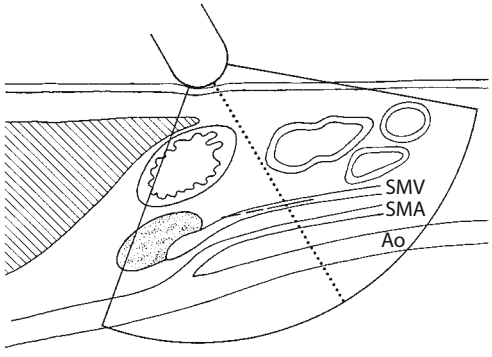

Fig. 6.15. Schematic representation of the course of the superior mesenteric vein (*SMV*; *SMA* superior mesenteric artery, *Ao* aorta)

ing malrotation. The criteria for diagnosing thrombosis are the same as in the portal vein. If mesenteric vein thrombosis is suspected, the vein should be traced to the level of the jejunal branches, the ileocolic vein, and right colic vein. This is most easily accomplished in transverse orientation with slight angulation of the transducer in the color duplex mode.

6.2.3 Normal Findings

6.2.3.1 Vena Cava and Renal Veins

The diameter of the vena cava varies from 0.5 – 2.5 cm with respiration. The respiratory variations are reflected in the Doppler frequency spectrum recorded longitudinally. Additional cardiac (atrial) modulation results in a W-shaped flow profile determined by the pressure changes in the right atrium. The first peak reflects the tricuspid valve movement during systole, followed by a decrease in flow velocity with increasing atrial filling and a second flow acceleration upon opening of the tricuspid valve, which produces the second peak. During atrial contraction, flow again becomes faster, sometimes with a short retrograde component.

The renal veins, in particular the right one, also show respiratory fluctuation of flow that is reflected in the Doppler waveform by an increase in flow velocity during inspiration and a decrease during expiration. The right renal vein also shows the atrial modulation. The left renal vein typically exhibits pulsatile variation due to brief compression of the vein during systole in the narrow passageway between the aorta and superior mesenteric artery. The left renal vein occasionally takes an atypical retroaortic course and very rarely multiple branches are present on the left (incidence of 4% versus about 20% on the right). If the left renal vein is not depicted between the aorta and superior mesenteric artery, the examiner must look for it behind the aorta at about the level of the origin of the left renal artery.

The major branches of the hepatic venous system and the right renal vein have the same flow character as the vena cava (cardiac (atrial) modulation and respiratory variation).

6.2.3.2 Portal Venous System

The normal portal vein is depicted by gray-scale sonography with an anechoic, smoothly delineated lumen below the liver and shows less pronounced respiratory caliber variation than the vena cava (usually 8 – 13 mm, larger caliber during deep inspiration). The (color) duplex mode depicts flow toward the liver with respiratory fluctuation. The flow velocity is 10 to 25 cm/s (Seitz and Kubale 1988) and may exceed 35 cm/s postprandially. Altogether, flow velocities in the portal system are characterized by wide interindividual variation and also increase after a meal as in the mesenteric circulation (two- to three-fold increase in the superior mesenteric artery and vein).

6.2.4 Documentation

The extent of documentation of the findings in the retroperitoneal veins as in the portal venous system depends on the clinical question to be answered. In addition to the B-scan findings and the Doppler waveform of the vein of interest, the perivenous findings should be documented as well. Specifically, vein compression and the extent of thrombotic changes must be recorded as well as collateral pathways in case of disturbed venous drainage, e.g. retroperitoneal and splenorenal shunts in renal vein thrombosis and gastric or umbilical shunts in portal hypertension (liver cirrhosis, Cruveilhier-Baumgarten syndrome).

6.2.5 Abnormal Ultrasound Findings, Measurement Parameters, and Diagnostic Role

6.2.5.1 Vena Cava

The complex embryonic development of the venous system results in numerous variants and malformations, all of which are rare. The vena cava can show the whole range of anomalies from aplasia to duplication.

Rare variants and atypical courses of the individual vessels are identified and differentiated from retroperitoneal lymph nodes by *color duplex scanning*. Compression of the vena cava is most commonly due to retroperitoneal lymph nodes or tumors, aortic aneurysm, or retroperitoneal fibrosis. Rare venous leiomyomas or leiomyosarcomas may also arise from the smooth muscle layer of the vena cava.

Since compression sonography is of limited use in demonstrating thrombosis of the retroperitoneal and visceral veins, *duplex scanning* and above all *color-coded duplex scanning* come in handy. However, criteria for *thrombosis* of the intra-abdominal or retroperitoneal veins are present on the *gray-scale scan* as well.

A thrombus may be visualized directly as a hyperechoic structure. In addition, thrombosis is suggested if the respiratory caliber variation typical of the larger retroperitoneal veins, in particular the vena cava, is lost. This finding is unspecific, however, since dilatation of the vena cava with reduced or absent caliber fluctuation may also occur in right ventricular failure. Thrombosis should always be excluded by color duplex scanning with a low pulse repetition frequency and high gain or by recording of a Doppler spectrum. Apart from thrombosis, venous drainage may be obstructed by tumor compression, tumor infiltration, or intravascular tumor extension.

The clinical symptoms of thrombosis depend on its localization, development, and collateralization. In particular in pelvic vein and *vena cava thrombosis*, there is a risk of embolism. Thrombosis of the vena cava is typically caused by an ascending thrombus from the pelvic and leg veins or extension of a tumor thrombus, for instance through the renal vein

in renal cell carcinoma. A fresh ascending thrombus is typically hypoechoic and may be difficult to identify on gray-scale scans in obese patients. In the further course, the thrombus undergoes hyalinization and becomes inhomogeneous. Thrombus organization with invasion of cells from the vessel wall and retraction of fibrin fibers results in increasing echogenicity and poorer delineation from the wall. Very old thrombi may undergo partial mural calcification.

Due to extensive collateralization, even occlusion of the vena cava may occasionally cause only few clinical symptoms. Venous return occurs predominantly through the paravertebral plexus, the ascending lumbar and azygos venous systems, the superficial veins of the abdominal wall, and the portal collateral route. Color duplex scanning enables good evaluation of the collateral pathways in thrombosis of the vena cava or pelvic vein, though the findings have no clinical relevance in most cases.

Disturbed drainage of the pelvic and leg veins demonstrated by spectral Doppler (continuous flow without respiratory fluctuation) may be due to central vena cava thrombosis caused by thrombus or tumor extension from the renal veins or compression of the vena cava by a retroperitoneal tumor or aortic aneurysm. Therefore, the examiner must carefully look for these possible causes. If the spectral waveform from the vena cava or pelvic veins shows pulsatile flow, a thorough search must be undertaken for an AV fistula, which may be caused by trauma, idiopathically, perforating aneurysm, or iatrogenically after surgery or puncture.

Tricuspid insufficiency or right ventricular failure affects caval blood flow, causing dilatation and abnormal changes of the Doppler waveform. Regurgitation into the right atrium in tricuspid insufficiency extends into the proximal vena cava where it becomes apparent in the waveform by a reflux component during systole.

Vena cava thromboses are typically due to ascending thrombosis of the pelvic and leg veins but may also be caused by local obstruction (external tumor compression or infiltration) as well as by thrombus or tumor extension from renal veins or thrombus extension from hepatic veins (Budd-Chiari syndrome).

6.2.5.2 Renal Veins

Just as in the inferior vena cava, *thrombosis* and central *tumor thrombi* of the renal veins can be identified sonographically under adequate insonation conditions. Therefore, preoperative *color duplex scanning* of the renal veins is sufficient prior to tumor nephrectomy. Venography has a similar diagnostic yield only if it is performed as venacavography with compression or provocative maneuvers. For this reason, contrast-enhanced CT is the primary alternative imaging modality in the routine clinical setting.

The nephrotic syndrome associated with glomerulonephritis is the most common cause of renal vein thrombosis. Predisposing factors are antithrombin III deficiency, sepsis, pregnancy, oral contraceptives, corticoid therapy, collagen diseases, and amyloidosis. Secondary renal vein thrombosis can be caused by obstruction due to retroperitoneal tumors, aortic aneurysm, or caval thrombosis as well as intravenous extension of renal tumors.

Renal vein thrombosis may already be apparent on the B-mode scan as a dilatation of the vessel lumen with a hypoechoic deposit with inhomogeneous portions (cf. Fig. A 6.48). However, only color duplex scanning is diagnostic and will also demonstrate partial thrombosis. An indirect sign of acute renal vein thrombosis in the arterial waveform is a marked reduction or even transient reversal of diastolic flow. This is due to a reflex vasoconstriction, and the flow pattern resembles that in rejection of a kidney transplant.

Prior to tumor nephrectomy, sonographic evaluation of the renal veins is necessary to plan the surgical procedure according to the *stage of venous tumor extension*:

- *Stage I* is characterized by a button-like protrusion of tumor from the renal vein into the vena cava (cf. Fig. A 6.49).
- In *stage II* the tumor extends farther into the vena cava but the upper margin is still below the level of the hepatic vein opening.
- In *stage III* the tumor extends to the level of the hepatic veins.
- In *stage IV* there is tumor extension to the atrium.

In most cases of stage I and II tumor extension, it is possible to enucleate the tumor thrombus when nephrectomy is performed.

Apart from an increased peripheral resistance reflected in the waveform from the renal artery, acute renal vein thrombosis can also cause kidney enlargement. The magnitude of these changes depends on the extent of collateral pathways of the thrombosed renal vein, which may involve splenorenal shunts or retroperitoneal routes such as venous connections to the adrenal gland. Recanalization after acute renal vein thrombosis is seen on color duplex as meander-like flow in an otherwise dilated and echogenic lumen.

Markedly slower flow in the renal vein with loss of cardiac and respiratory variations may also be seen in case of obstruction of the proximal inferior vena cava by a tumor or thrombosis or in right ventricular failure (acute: pulmonary embolism, chronic: tricuspid insufficiency).

6.2.5.3 Superior Mesenteric Vein

In rare cases, intestinal necrosis is caused by mesenteric vein thrombosis. Therefore, duplex scanning performed to exclude mesenteric artery occlusion in patients presenting with the respective clinical symptoms should be extended to the mesenteric vein to exclude thrombosis there as well. Edematous thickening of the intestinal walls is a conspicuous finding and will already be seen on the gray-scale scan.

Causes are hematologic diseases, clotting disorders, abscess or sepsis, and tumor occlusion. Apart from acute thrombosis presenting with acute symptoms of intestinal

necrosis, there may be chronic thrombosis with unspecific findings such as fever, leukocytosis, or thrombocytosis.

An abnormal course of the superior mesenteric vein suggests malrotation, which is confirmed if the superior mesenteric vein is to the left of the superior mesenteric artery. If the vein is anterior to the artery, malrotation is present in one third of the cases. These indirect signs of malrotation are easily detected by duplex scanning.

The severity of the clinical symptoms associated with mesenteric vein thrombosis depends on the extent and site of the thrombus and collateralization. Partial thrombosis of the superior mesenteric vein, for instance, may be fairly asymptomatic and present with the clinical signs of enteritis only. Conversely, patients with extensive central mesenteric vein thrombosis may present with an acute abdomen due to intestinal necrosis. Early diagnosis with initiation of anticoagulation therapy is essential to prevent further progression of thrombosis. Therefore, the mesenteric vein should be scanned in all patients with thickening of the intestinal wall on B-mode scanning. The criteria for thrombosis of the superior mesenteric vein are the same as in other vascular territories: dilatation of the vein, absence of respiratory diameter fluctuations, possibly depiction of the thrombus as an echogenic intraluminal structure on the B-mode scan, and absence of flow signals or only residual flow signals near the wall surrounding a central thrombus on (color) duplex scanning (cf. Figs. A 6.42 and A 6.43). An indirect sign apart from intestinal wall thickening on B-mode sonography is a more pulsatile flow in the arterial waveform in extensive mesenteric vein thrombosis (Table 6.13).

Abnormalities of the splenic vein (such as thromboses) are negligible both clinically and in terms of their therapeutic consequences because extensive collateral routes exist. Nevertheless, the splenic vein may be involved in patients with portal hypertension from liver cirrhosis and is therefore included in the examination in these cases.

Table 6.13. Mesenteric vein thrombosis

Risk factors
- Portal hypertension
- Sepsis
- Diverticulitis
- Paraneoplastic syndrome
- Autoimmune disease
- Clotting disorder

Clinical presentation
- From unspecific symptoms to acute abdomen (depending on the extent of collateralization)

Duplex ultrasound findings
- Hyperechoic thrombus
- Dilated vein
- No intraluminal flow signals
- Diastolic flow in the superior mesenteric artery may be reduced
- Thickening of bowel loops in gray-scale image

6.2.5.4 Portal and Hepatic Veins

Portal vein thrombosis is diagnosed using the same sonomorphologic criteria as for other sites: dilatation of the lumen, absent respiratory diameter variation, and no flow signals or only residual flow signals around the thrombus on (color) duplex scanning. Acute portal vein thrombi tend to be hypoechoic and are clearly delineated from perivascular structures whereas older thrombi contain more inhomogeneous and hyperechoic portions and their contours become blurred, resulting in poorer sonographic discrimination of the thrombotic vein. The Doppler spectrum sampled with an adequate angle will show absence of flow signals or more higher-frequency signals without respiratory variation around central thrombi surrounded by flowing blood. Recanalization or cavernous transformation is associated with meander-like, tortuous flow in the portal vein, appearing as antegrade and retrograde flow components.

Acute portal vein thrombosis, like acute proximal mesenteric vein thrombosis, is characterized by the sudden onset of clinical symptoms.

Collateralization in portal vein thrombosis is more extensive if the superior mesenteric vein is not involved; the collateral vessels in this case include the splenic vein and gastric veins, which can be depicted by duplex scanning.

The causes of portal vein thrombosis include liver cirrhosis, paraneoplasia, clotting disorders, and sepsis (Table 6.14). Similar to portal hypertension in liver cirrhosis, acute portal vein thrombosis is associated with widening of the veins serving as collaterals (splenic vein, esophagogastric vessels) and ascites, which can be identified sonographically as secondary signs.

The formation of collateral pathways in the liver hilum and partial recanalization of the thrombotic portal vein, so-called cavernous transformation, results in a wormlike meshwork of tortuous tubular structures, among which the former portal vein is no longer identifiable by color duplex scanning.

As with older thrombosis in other vessels, chronic portal thrombosis leads to shrinkage of the initially widened vessel

Table 6.14. Etiology of thrombotic changes in the portal venous system

- Acute pancreatitis
- Chronic pancreatitis (may be associated with pseudocyst)
- Cancer (hepatocellular carcinoma, metastases, pancreatic carcinoma)
- Idiopathic
- Abdominal infections
- Collagen diseases
- Myeloproliferative syndrome
- Trauma
- Status post splenectomy
- Pregnancy
- Pharmacologic therapy
- Liver disease, cirrhosis, thrombocytosis
- Antiphospholipid antibody syndrome
- Deficiency of AT3, protein C, protein S

with depiction of an inhomogeneous, more hyperechoic thrombus within the lumen. In contradistinction to acute portal thrombosis, the chronic form is associated with relatively unspecific, subacute clinical manifestations, in particular when it occurs secondary to liver cirrhosis.

In the detection of portal vein thrombosis, ultrasound has a sensitivity of 89 –100 % and a specificity of 95 – 100 %, which is comparable to its accuracy in the detection of deep pelvic vein thrombosis (Zwiebel 2000). Nevertheless, ultrasonography is limited by the fact that very slow flow with to-and-fro flow in pronounced portal hypertension may escape detection.

Portal hypertension secondary to liver cirrhosis is associated with widening of the portal vein and its distal tributary veins and of the collaterals (portocaval, gastroesophageal, splenorenal, umbilical), which may already be seen on B-mode scanning (Table 6.15). Moreover, respiratory diameter fluctuations are lost in the portal vein.

Atresia and hypoplasia of the portal vein are rare, as are atypical courses and malformations. In individuals with an extrahepatic congenital portocaval shunt, the portal venous blood from the mesentery and spleen is drained directly into the inferior vena cava. As a result of the direct connection between the splenic vein, superior mesenteric vein, and vena cava (gray-scale scan), the cardiac pulsatility of venous return in the vena cava is transmitted to the mesenteric vein and reflected in the Doppler waveform.

Aneurysms of the portal vein are likewise rare and must be differentiated from pseudocysts of the pancreas, choledochal cysts, and liver cysts by the demonstration of flow in the color duplex mode.

Portal hypertension can be caused by obstruction of the portal venous system at different levels (cf. Fig. A 6.1 b) and involves complex circulatory changes. The pressure in the portal vein is typically 2 – 4 mm Hg above that in the inferior vena cava and hypertension is defined as a pressure increased to over 11 mm Hg that persists for an extended period. *Indirect criteria* are dilatation of the superior mesenteric artery with loss of respiratory phasicity, an enlarged ventricular coronary vein diameter (> 4 mm), and patency of the umbilical vein with a high flow. The diameter of the portal vein is highly variable under normal conditions and therefore not helpful as an indicator of portal hypertension; only the loss of the normal elliptical transverse profile can serve as an indirect criterion.

The spectral waveform in portal hypertension shows a reduced mean flow velocity and loss of respiratory variation (cf. Table 6.15).

Depending on the severity of portal hypertension, spectral Doppler will demonstrate antegrade flow with a reduced velocity, to-and-fro flow, or flow reversal when pressure is increased to over 30 mm Hg. The normal triphasic waveform of the hepatic veins is lost in liver cirrhosis.

The main diagnostic role of *color-coded duplex ultrasonography* lies in the follow-up of portal hypertension with early identification of thrombosis as a possible complication. Moreover, it provides useful diagnostic information in presinusoidal, extrahepatic portal hypertension. The most common causes are primary or secondary tumorous thrombosis, inflammatory diseases like pancreatitis, and slow flow due to liver cirrhosis. Depending on its temporal course and collateralization, portal vein thrombosis may present with unspecific abdominal symptoms or an acute abdomen.

Table 6.15. Ultrasound findings in portal hypertension

B-mode	Ascites, splenomegaly Possibly cirrhotic changes of hepatic vessel architecture and parenchymal structure Signs of congestion of the gallbladder and stomach walls Dilated portal vein with change from elliptical to circular profile Portocaval collaterals Portal vein thrombus (echogenic)
Duplex	Reversed flow in portal vein Slower blood flow (diminished flow rate) Portocaval collaterals
Color duplex	Portocaval collaterals Stagnating/reversed blood flow Portal vein thrombosis

Table 6.16. Portocaval collaterals

Shunts draining toward center:
- Esophageal varices, gastric corpus and fundus varices (ventricular coronary vein – azygos vein, short gastric veins – azygos vein)
- Gastrosplenic shunts
- Portorenal and splenorenal collaterals
- Capsular veins of liver and spleen, diaphragmatic veins

Shunts draining toward periphery:
- Paraumbilical veins (Cruveilhier-Baumgarten syndrome)
- Splenolumbar shunts
- Mesenteric veins (superior and inferior mesenteric veins, ovarian vein, spermatic vein, rectal plexus)

The flow direction in the portal vein is determined not only by the severity of liver cirrhosis and the magnitude of portal blood pressure but also by the direction of collateral drainage (Table 6.16).

When the blood is chiefly drained through splenorenal shunts, flow in the portal vein is backward (hepatofugal), while normal, hepatopetal flow is preserved in the presence of a patent umbilical vein (Cruveilhier-Baumgarten syndrome).

Determination of volume blood flow relying on diameter determination is limited in veins by the fact that their diameter variation is very difficult to quantify. This also holds true for the portal vein, which varies widely in diameter between inspiration and expiration. Therefore, determination of mean blood flow velocity in the portal vein is a more suitable parameter to discriminate between healthy individuals and patients with portal hypertension. Note, however, that the mean flow velocity is also influenced by the extent of collateralization. For instance, pronounced flow in the patent and widened umbilical vein (Cruveilhier-Baumgarten syndrome) may mimic normal perfusion of the liver with a fairly normal

flow velocity in the portal vein because the blood is drained through the umbilical vein circumventing the sinusoids.

Although the variable collateralization leads to a wide variation in mean portal flow velocities both in intraindividual and interindividual comparison, significant differences are identified between healthy subjects and patients with portal hypertension when the mean values of larger study populations are compared. Several such studies demonstrated a statistically significant decrease from 15 cm/s in healthy subjects to half that value in patients with cirrhosis (Seitz and Kubale 1988). Though peak venous flow velocity is decreased to 7 – 15 cm/s (mean 10 cm/s) in patients with cirrhosis, there is wide interindividual variation and overlap with the flow velocities in normal subjects, which may lead to misinterpretation in individual cases.

Duplex scanning also demonstrates a decrease in portal blood flow associated with intake of beta-receptor blockers or somatostatin as well as an increase with eating and glucagon ingestion. The increase in portal flow velocity after a test meal is less pronounced in patients with cirrhosis.

Various tests have been proposed that promise more reliable discrimination of cirrhosis-induced portal hypertension from normal portal blood flow. Apart from the less marked increase of postprandial flow, drugs like beta-receptor blockers or nifedipine also have a less pronounced effect on the flow velocity in the portal vein in cirrhosis. Gaiani et al. (1989) compared 11 patients with liver cirrhosis and healthy controls 60 minutes after a test meal and found a markedly lower increase in diameter of 3 % in the patients compared to 14 % in controls and in flow velocity, which was 3.2 % versus 24 %. The volume flow rate after the test meal increased by only 8.5 % in the patients as opposed to 59 % in the controls. Such promising results were not always confirmed by other study groups.

Another approach combines the increased vascular cross-sectional area and the decreased flow velocity in the portal vein in portal hypertension in the so-called congestion index ($cm^2/cm/s = cm \times s$). Normal individuals have an index < 0.07 cm x s versus > 0.1 cm x s in portal hypertension associated with liver cirrhosis (Moriyasu et al. 1985; Siringo et al. 1994). Further studies are necessary to show whether glucagon-induced changes in portal venous flow can serve as an estimate of the hemodynamic reserve and whether measurement of portal flow velocity after propanolol administration may enable reliable identification of those patients requiring therapy for portal hypertension, although this parameter shows wide interindividual variation as well.

Endoscopic obliteration of esophageal varices and the TIPSS procedure (transjugular intrahepatic portosystemic shunt with stenting) have led to a decrease in portocaval and splenorenal shunt operations. An important preoperative question to be answered is whether the portal, mesenteric, and splenic veins are patent. There is good evaluability of these veins by ultrasonography, which is why color duplex scanning has evolved as the method of choice. In the postoperative follow-up, ultrasound enables direct evaluation of shunt patency. The cardiac fluctuation of blood flow in the vena cava is transmitted to the anastomosed portal vein through the shunt.

When a distal splenorenal shunt (Warren shunt) is created, the relief of the portal vein leads to flow reversal in the splenic vein (hepatofugal flow). In the TIPSS procedure, a short circuit is established between the hepatic vein and portal vein under ultrasound guidance. Color-coded duplex findings can shorten the puncture tract and this modality is also helpful in evaluating stent patency at follow-up.

A highly sensitive *direct sign* of portal hypertension is the presence of collateral routes, seen either as enlargement of the short gastric veins or coronary vein with venous drainage to the esophageal plexus or as a patent umbilical vein (Cruveilhier-Baumgarten syndrome). Other collateral routes that are less well amenable to sonographic evaluation include gastrorenal and splenorenal anastomoses and peripancreatic veins. The success of a therapeutic procedure can also be documented by sonographic follow-up of the collateral pathways.

Quantitative determination of blood flow is not necessary in the routine diagnostic workup of portal hypertension since there is no close correlation between portal blood flow and portal hypertension due to the highly variable and ramified collateral system.

On the one hand, the decreased portal blood flow in portal hypertension due to cirrhosis can lead to a compensatory increase in arterial perfusion that is detectable sonographically. The higher perfusion can result in an enlargement of the cross-sectional areas of the hepatic veins both within and outside the liver.

On the other hand, progressive cirrhosis is associated with an increased resistance in the peripheral hepatic artery branches, resulting in a more pulsatile flow profile with increased resistance indices of 0.8 to 0.9.

Like the vena cava, the hepatic veins are subject to both respiratory and cardiac variation. Besides prandial fluctuations, the flow velocity is determined by the pressure in the thorax, right atrium, and abdomen. Cardiac modulation results in a triphasic, W-shaped waveform reflecting the venous pressure variations during the cardiac cycle. The first velocity peak directed toward the vena cava occurs during systole and atrial filling. As the intra-atrial pressure increases, hepatofugal flow decreases in the hepatic veins and in the vena cava. Opening of the tricuspid valve leads to increased flow into the right ventricle and a second flow velocity peak in the hepatic veins and vena cava. During atrial contraction, there may be zero flow or retrograde, hepatopedal flow.

Another factor affecting the Doppler waveform of the hepatic veins is the consistency of the liver parenchyma. As elasticity is lost and the parenchyma becomes more rigid with progressive cirrhotic transformation, the waveform of the hepatic veins is increasingly flattened. This change is a diagnostic indicator of increasing tissue rigidity (cf. Fig. A 6.40 d, e) and also a prognostic factor with progressive phase loss of the waveform (Bolondi et al. 1991; Ohta et al. 1994). Cardiac pulsatility of blood flow is preserved in 30 – 50 % of patients with cirrhosis. Typically, however, the waveform becomes flattened with progressing parenchymal damage and a band-

like curve in the hepatic veins is associated with a life expectancy of less than 2 years. A markedly abnormal flow pattern in the hepatic veins was found to have a diagnostic accuracy in Child A cirrhosis (chronic hepatitis C) of 77 % (Colli et al. 1994) and a specificity of 78 %.

Since parenchymal damage also occurs in other liver conditions associated with pronounced fatty degeneration, flattening of the waveform in the hepatic veins is not a specific sign of liver cirrhosis. Moreover, there may be physiologic flattening in advanced pregnancy.

Duplex scanning is a valid modality for the routine diagnostic evaluation of portal hypertension including initial diagnosis, hemodynamic evaluation of the portal vein, and follow-up. Radiologic procedures are restricted to the examination of patients with poor insonation conditions (massive ascites, meteorism) and to answer specific diagnostic questions. The variable scan planes in ultrasonography enable hemodynamic assessment as well as precise determination of topographic relationships. This is an advantage of ultrasound over angiographic procedures as well as magnetic resonance imaging, especially with regard to the evaluation of blood flow rates and flow direction.

6.3 Atlas

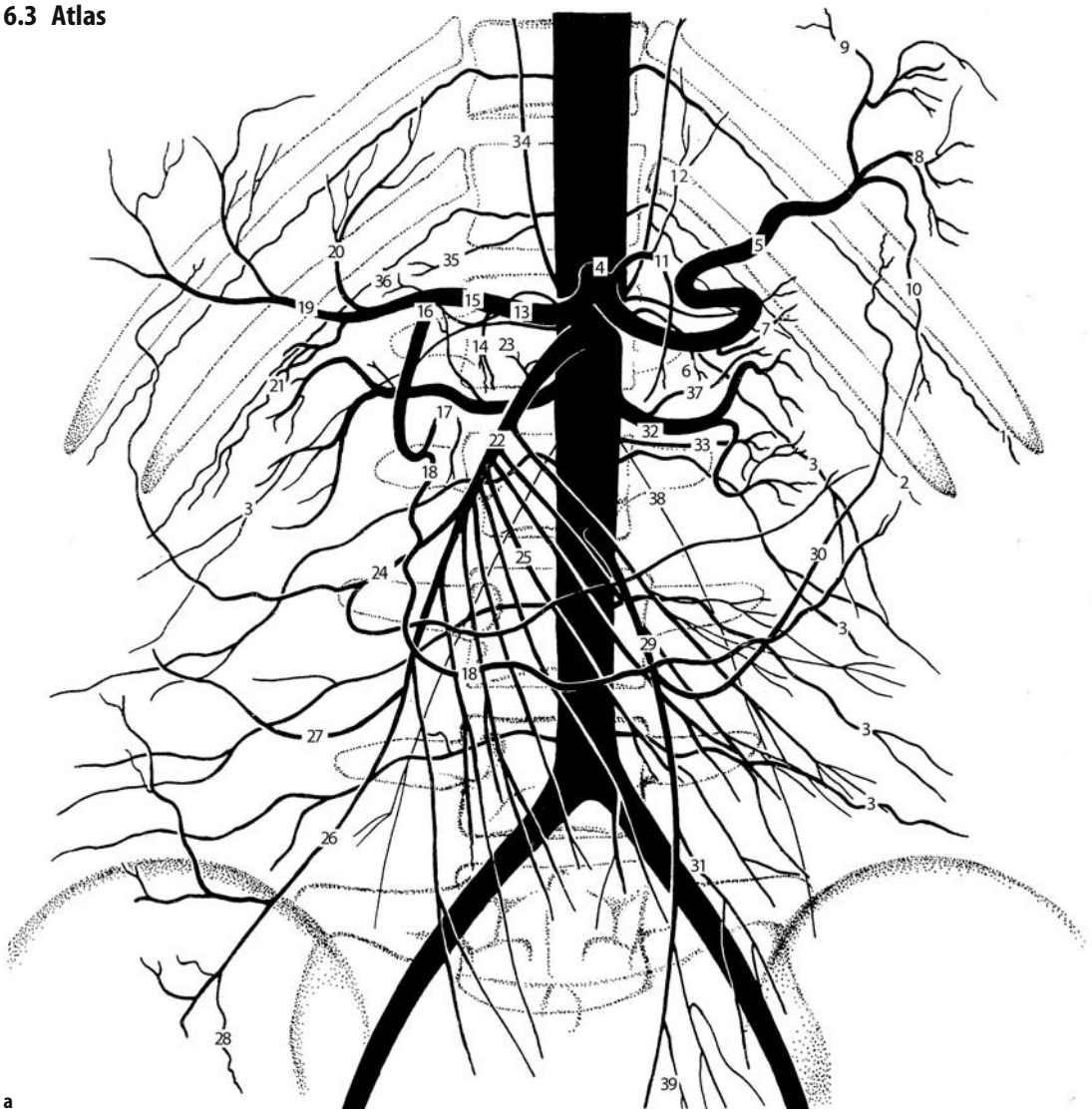

a

Fig. A 6.1 a, b
a Abdominal arteries (courtesy of Eastman Kodak)

1 Intercostal artery
2 Subcostal artery
3 Lumbar artery
4 **Celiac trunk**
5 **Splenic artery**
6 Dorsal pancreatic artery
7 Great pancreatic artery
8 Terminal branches of splenic artery
9 Short gastric artery
10 Left gastroepiploic artery
11 **Left gastric artery**
12 Esophageal branches of left gastric artery
13 **Common hepatic artery**
14 Right gastric artery
15 **Proper hepatic artery**
16 **Gastroduodenal artery**
17 Superior pancreaticoduodenal artery
18 Right gastroepiploic artery
19 Right branch of proper hepatic artery
20 Left branch of proper hepatic artery
21 Cystic artery
22 **Superior mesenteric artery**
23 Inferior pancreaticoduodenal artery
24 Middle colic artery
25 Jejunal arteries
26 Ileocolic artery
27 Right colic artery
28 Branch to appendix
29 **Inferior mesenteric artery**
30 Left colic artery
31 Sigmoid artery
32 **Renal artery**
33 Accessory renal artery
34 Inferior phrenic artery
35 Superior suprarenal artery
36 Middle suprarenal artery
37 Inferior suprarenal artery
38 Testicular artery (internal spermatic artery) or ovarian artery
39 Superior rectal artery

(Fig. A 6.1 cont.)
Portal venous system
b Portal hypertension – causes and collateral circulation (from Droste 1989)

Portal hypertension (> 15 cm H_2O in portal venous system)
Causes
A Prehepatic obstruction: thrombosis of portal or splenic vein, tumor of adjacent organ (e.g. pancreas, stomach, duodenum, gallbladder)
B Intrahepatic obstruction:
B_1 Presinusoidal: schistosomiasis, Wilson's disease, myeloproliferative diseases (intrasinusoidal: chronic hepatitis, fatty liver)
B_2 Postsinusoidal obstruction: liver cirrhosis (cause of portal hypertension in 90% of cases), cytostatic therapy, etc.
C Posthepatic obstruction: hepatic vein occlusion (Budd-Chiari syndrome), compression of inferior vena cava, constrictive pericarditis

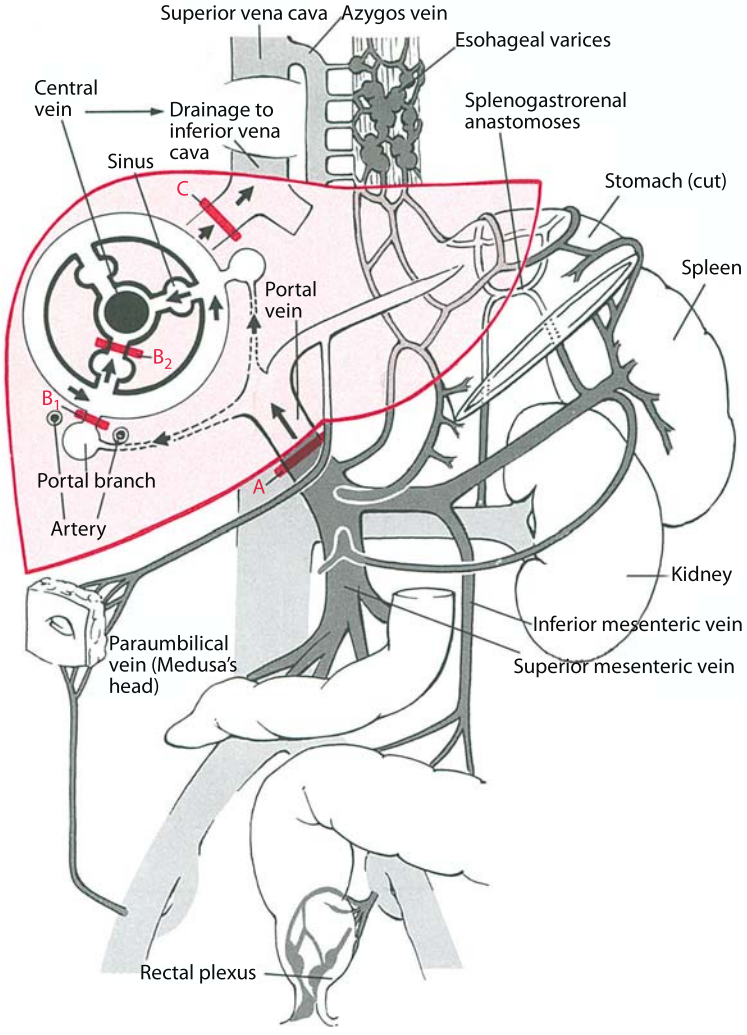

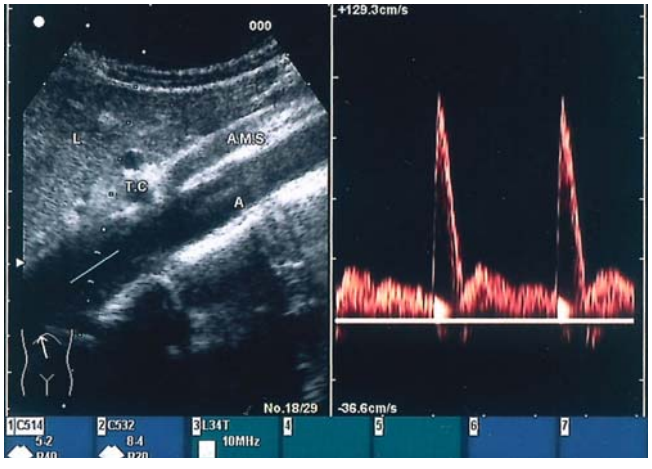

a

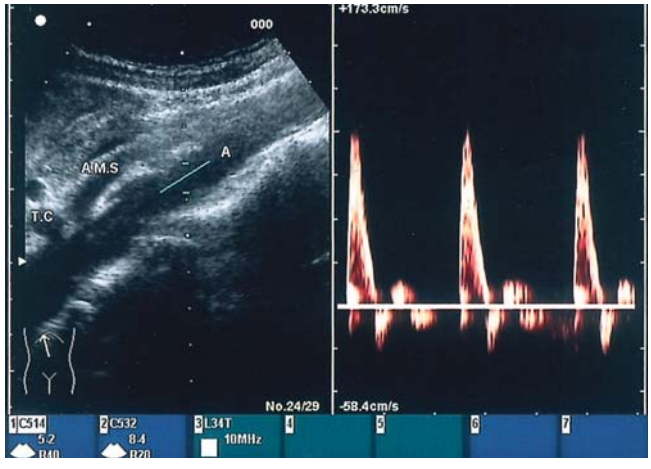

b

Fig. A 6.2 a, b
Flow profile of the aorta
a Proximal to the origins of the visceral arteries (*T.C* celiac trunk, *A.M.S* superior mesenteric artery), the flow profile of the aorta is predominantly determined by the supply of parenchymal organs. An incisure during early diastole is followed by constant diastolic flow

Flow in the aorta is of a mixed type resulting from blood flow to parenchymal organs (monophasic flow profile – low peripheral resistance) as well as flow to limbs (triphasic profile – high peripheral resistance)
b Distal to the origins of the visceral and renal arteries, the aorta has a triphasic flow profile (supply to limbs)

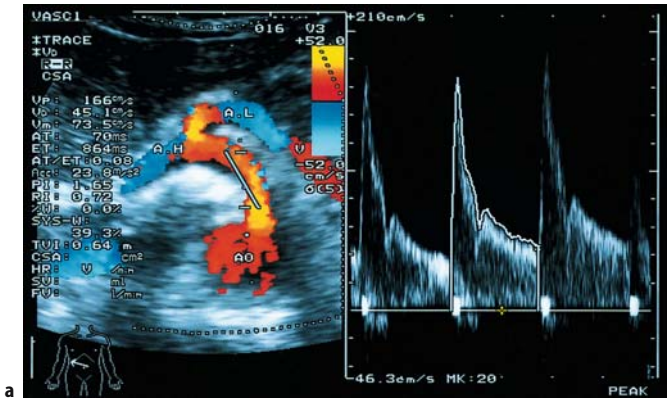

a

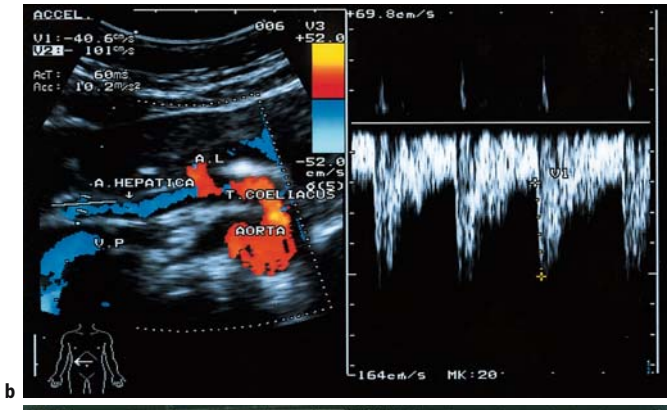

b

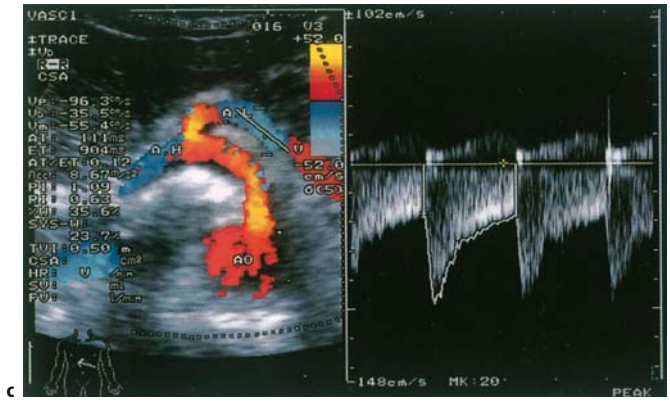

c

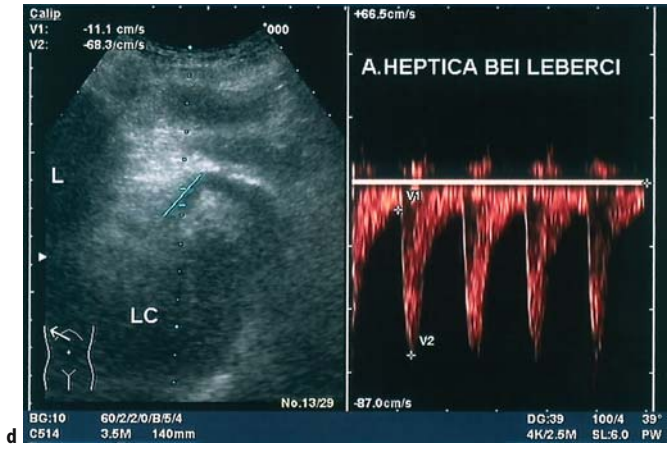

d

Fig. A 6.3 a–c
Celiac trunk

a Transverse view of the celiac trunk showing its origin from the aorta (*AO*) and division into the hepatic artery (*A.H*) and splenic artery (*A.L*). The bifurcation is said to resemble a palm leaf or gull's wings

Supplying parenchymal organs (spleen, liver), the celiac trunk, hepatic artery, and splenic artery show monophasic flow with a relatively large diastolic component, comparable to flow in the internal carotid. The aorta displayed in red gives off the celiac trunk anteriorly, likewise with flow depicted in red. The lighter color coding is not due to stenosis but to the angle of insonation

This is confirmed by the normal Doppler waveform with a peak systolic velocity of 165 cm/s and a peak end-diastolic velocity of 45 cm/s. Flow is synchronous with the cardiac cycle, exhibiting a low-frequency signal with a high amplitude due to wall motion in early systole

b The hepatic artery courses to the hilum of the liver along the posterior aspect of the lower liver margin. The artery is coded in blue, indicating flow away from the transducer. The high diastolic flow is due to the low peripheral resistance of the liver. The splenic artery *(A.L)* is shown to first course in an anterior direction (toward transducer, coded red) to then turn posteriorly (blue) toward the hilum of the spleen

c Splenic artery with typical Doppler waveform

Hepatic artery in liver cirrhosis

d Liver cirrhosis is associated with parenchymal transformation, resulting in an increase in flow resistance in the hepatic artery. This is reflected in an increased Pourcelot index, which correlates with the extent of parenchymal change. In the case presented, the index is markedly increased to 0.83 (same patient as in Fig. A 6.44 a–c). There is pronounced enlargement and hypoechogenicity of the caudate lobe (*LC*) as a sign of severe liver cirrhosis

Fig. A 6.4 a–c
Mesenteric blood flow

a Superior mesenteric artery with typical Doppler waveform of the mixed type. The end-diastolic flow component is intermediate between that of a peripheral artery and that of an artery supplying a parenchymal organ

24-year-old fasting subject: Normal blood flow in the superior mesenteric artery shortly after its origin with a peak systolic velocity of 128 cm/s, end-diastolic peak velocity of 21 cm/s, and pulsatile flow. Gray-scale scan depicts the superior mesenteric artery (*MS*) arising from the aorta (*A*) at an acute angle

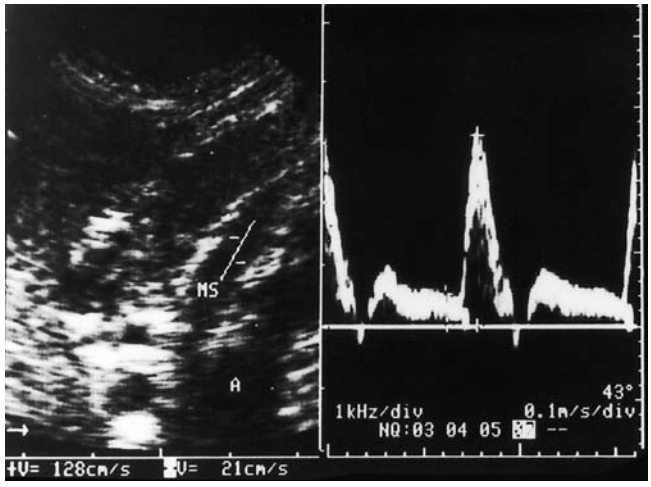

a

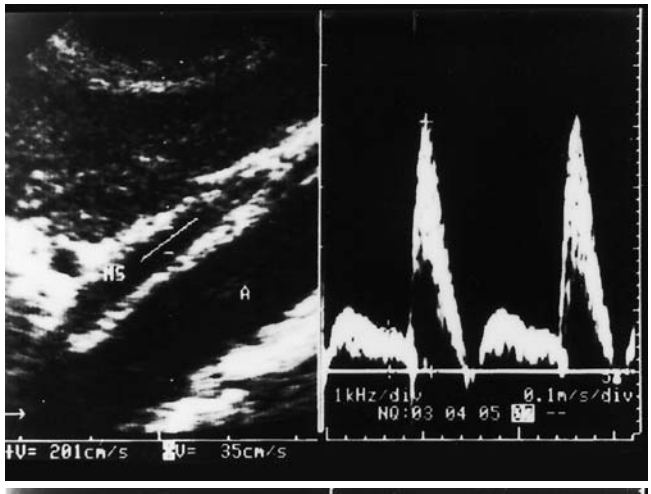

b

b Same subject as in **a**. Following administration of 20 mg of nifedipine, peak systolic flow velocity increases to 201 cm/s, end-diastolic velocity to 35 cm/s.

c Postprandial increase in mesenteric blood flow (peak systolic flow velocity of 227 cm/s, end-diastolic velocity of 73 cm/s). Assuming a threshold of 200 cm/s for >50% stenosis, the increased flow velocity observed after nifedipine administration and after eating would indicate a 50 – 60% stenosis in a fasting patient

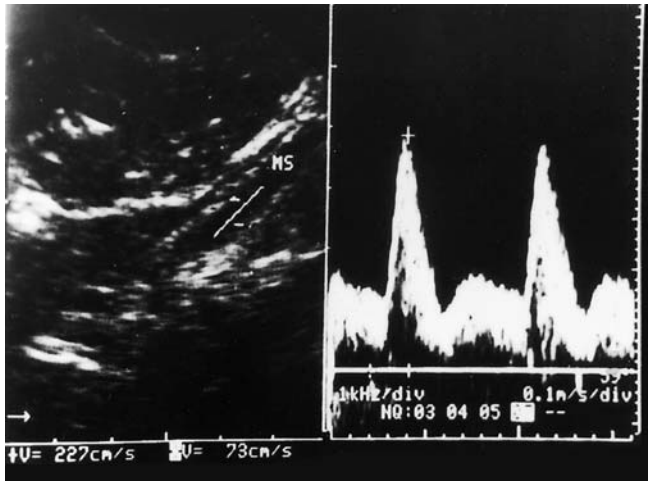

c

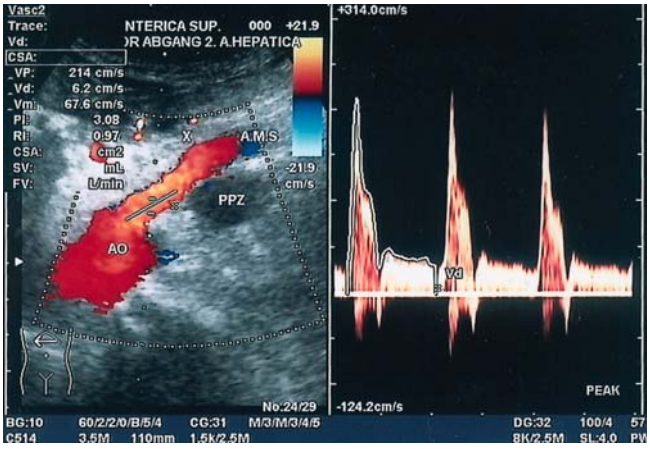

a

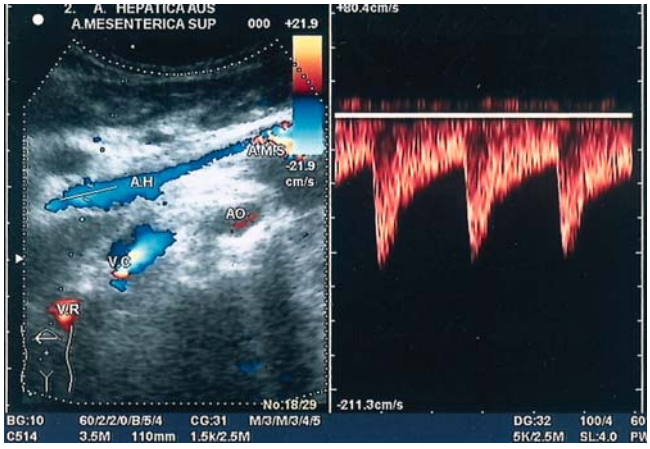

b

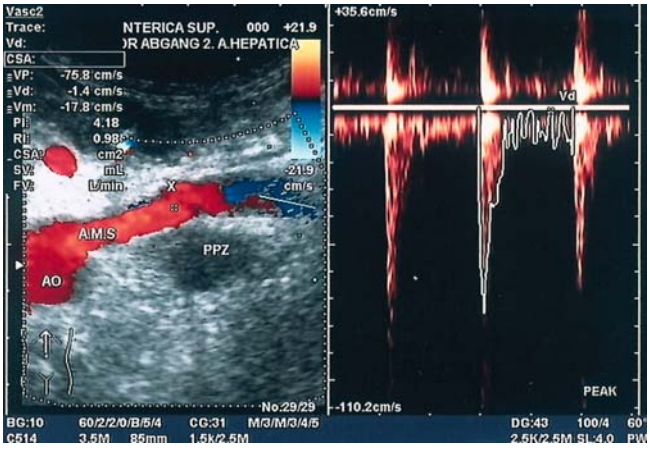

c

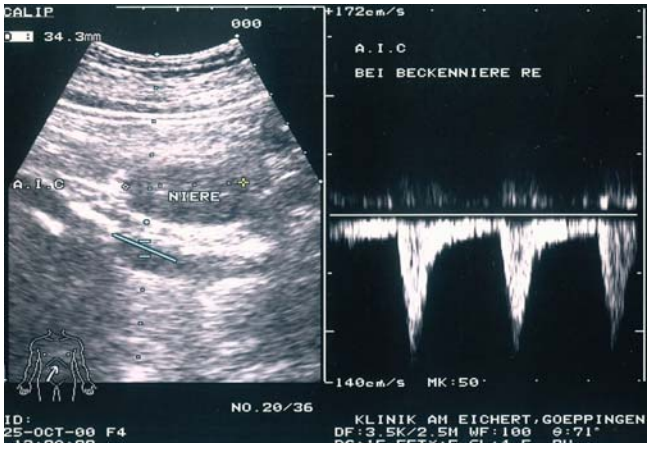

d

Fig. A 6.5 a–d Waveform patterns of anatomic variants

a Flow in a vessel as reflected in the Doppler waveform is determined by the organs it supplies. If the hepatic artery arises from the superior mesenteric, the peak systolic velocity will be high even in the absence of stenosis (fasting velocity of 214 cm/s in the case presented). The patient has chronic pancreatitis with depiction of a pancreatic pseudocyst (*PPZ*) between the aorta and the superior mesenteric artery. The cyst is hypoechoic on the B-scan and can be differentiated from an aneurysm in the color duplex mode

b In this rare case of duplication of the hepatic artery, the proximal superior mesenteric artery (transverse section through upper abdomen) gives off a hepatic artery (*A.H*) that courses to the right hepatic lobe along the anterior aspect of the vena cava (*V.C*). The left lobe is supplied by a normal hepatic artery arising from the celiac trunk

c Distal to the origin of the ectopic hepatic artery (at the level of the pancreatic pseudocyst, which serves as a landmark), the superior mesenteric artery shows flow with a smaller diastolic component and a reduced peak systolic velocity. Proximal to the hepatic artery origin, flow is of the mixed type due to supply to two organs (liver and bowel). The examiner must be aware of these variants in interpreting changes in the Doppler waveform

d In individuals with pelvic kidneys, as shown here (or in a transplant kidney anastomosed to the iliac artery), the normal Doppler waveform of the iliac artery proximal to the renal artery origin is monophasic rather than triphasic. The scan depicts part of the pelvic kidney above the common iliac artery. The monophasic waveform is due to blood supply to both the peripheral arteries and the renal artery and does not suggest postocclusive flow despite the presence of plaque proximal to the sample volume. Distal to the renal artery origin, the external iliac artery exhibits triphasic flow

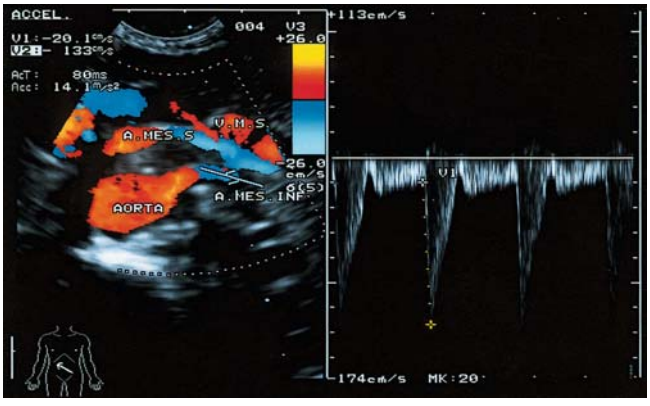

Fig. A 6.6
Inferior mesenteric artery

Origin of the inferior mesenteric artery from the aorta. The Doppler waveform resembles that of the superior mesenteric but may occasionally show a smaller diastolic flow component or even end-diastolic zero flow. Anteriorly, a jejunal branch is depicted (blue, away from transducer) distal to the division of the superior mesenteric artery. The superior mesenteric artery dividing into the ileocolic and right colic arteries is depicted anterior to the aorta with flow in the same direction coded in red. Directly anterior to the origin of the jejunal artery (displayed in blue), the jejunal vein with flow in the opposite direction (depicted in red) takes a course parallel to the artery and empties into the superior mesenteric vein (*V.M.S*)

Fig. A 6.7 a–e
Stenosis of celiac trunk

a The sample volume is placed in the celiac trunk (*T.C*) at its origin from the aorta. The Doppler waveform demonstrates a high-grade stenosis with a peak systolic flow velocity of over 4 m/s that does not change with inspiration and expiration. Differentiation of the cause of a stenosis (compression syndrome, atherosclerosis, fibromuscular dysplasia) is often difficult in the B-scan mode because wall assessment is impaired by the scan depth, the tangential angle of insonation relative to the vessel wall, and the presence of scatterers. The only differential diagnostic information that can be obtained by Doppler assessment is the variation of the stenosis grade with inspiration and expiration, which is indicative of the arcuate ligament syndrome

In the case presented, the hyperechoic plaques suggest an atherosclerotic process

b Schematic representation of the pathogenesis and morphology of celiac trunk stenosis

c Angiography showing the stenosis at the origin of the celiac trunk

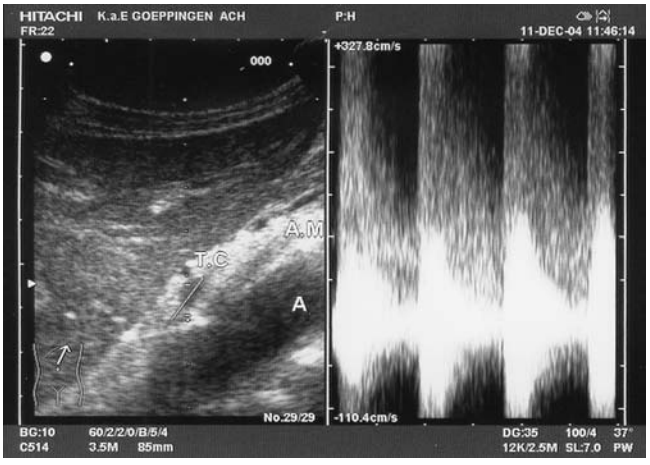

a

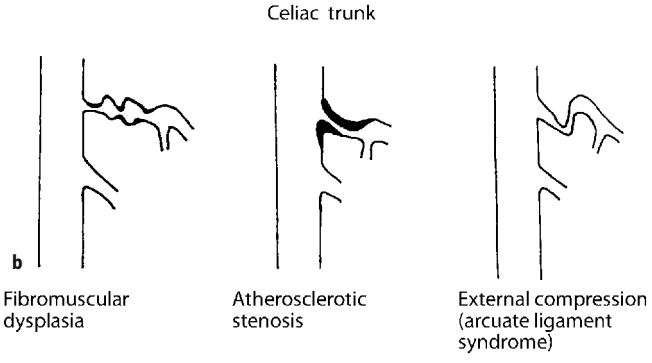

Mesenteric artery stenosis

d The superior mesenteric artery arises from the aorta at an acute angle and courses anteriorly. The origin appears somewhat narrowed in the gray-scale view and shows aliasing with the color coding changing from red, through yellow, to blue as a sign of marked flow acceleration in the color duplex image. The Doppler waveform depicts turbulent flow with an increased peak flow velocity of 285 cm/s in systole and 43 cm/s at end-diastole. Obtained in the fasting patient, this waveform corresponds to a stenosis of about 70 %. The color duplex scan additionally depicts the celiac trunk (*T.C.*) to the left of the mesenteric artery origin

e Angiography: Intermediate-grade stenosis of the superior mesenteric artery at its origin (*arrowhead*). Large-caliber inferior mesenteric artery acting as a collateral

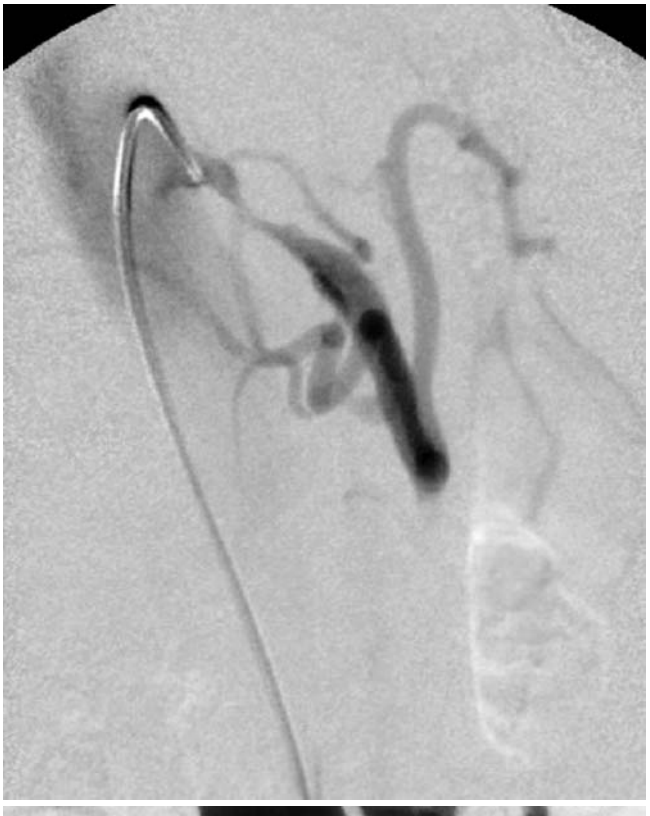

c

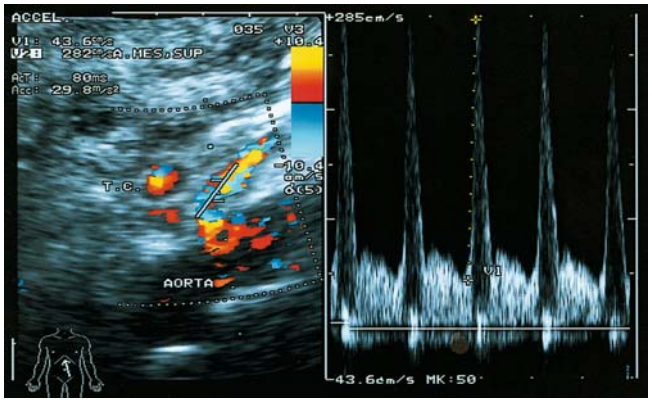

d

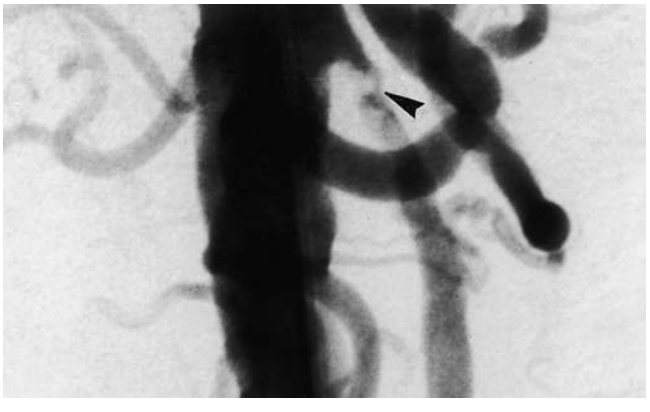

e

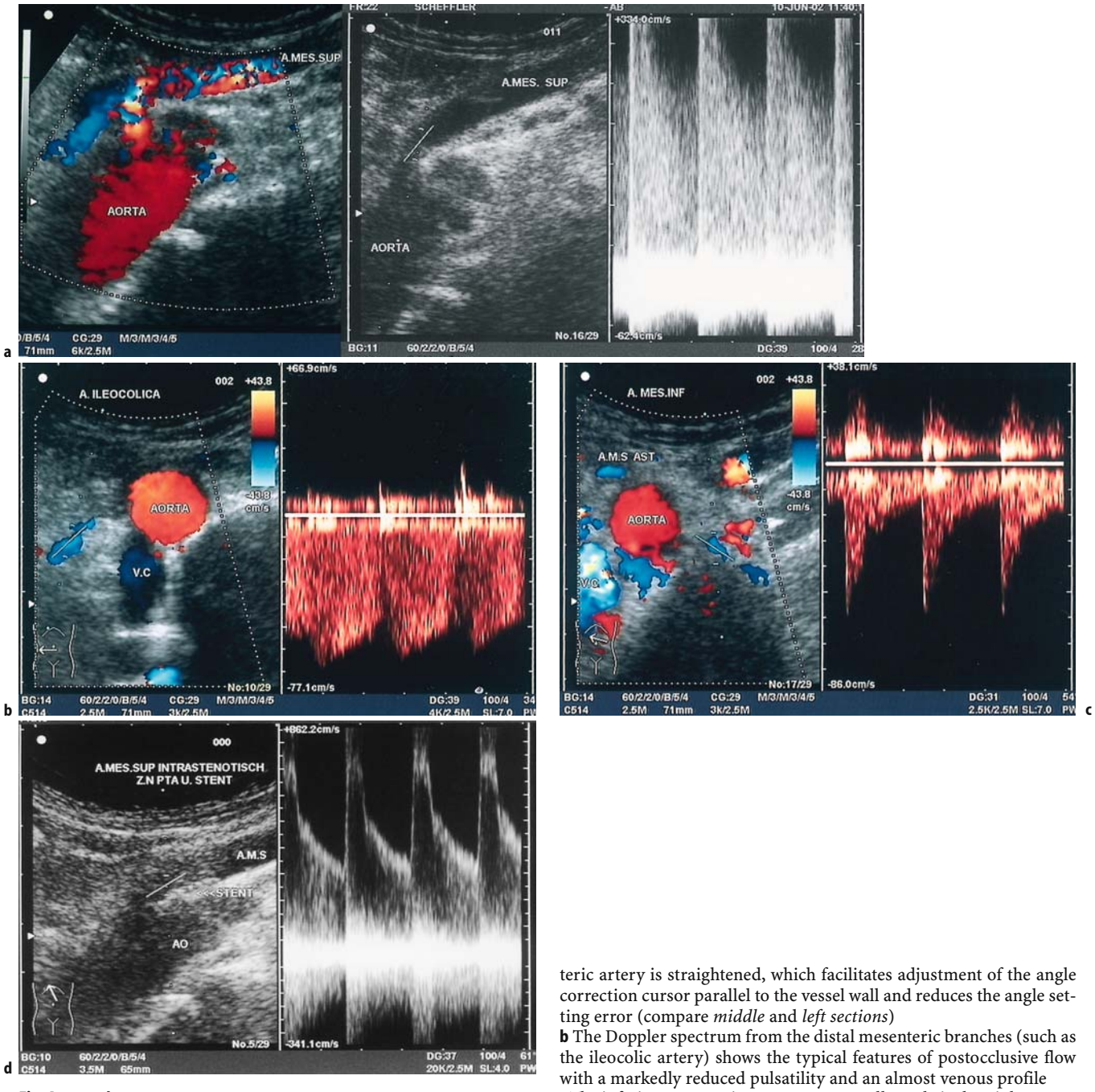

Fig. A 6.8 a–d
Mesenteric artery stenosis, high-grade
a Aliasing in the color mode suggests a high-grade stenosis at the origin of the superior mesenteric artery. The scanning conditions are usually good in the very thin patients presenting with suspected abdominal angina but the arched course of the superior mesenteric artery at its origin may impair adequate angulation of the Doppler beam (*left section*). In inspiration, this segment of the superior mesenteric artery is straightened, which facilitates adjustment of the angle correction cursor parallel to the vessel wall and reduces the angle setting error (compare *middle* and *left sections*)
b The Doppler spectrum from the distal mesenteric branches (such as the ileocolic artery) shows the typical features of postocclusive flow with a markedly reduced pulsatility and an almost venous profile
c The inferior mesenteric artery acts as a collateral via the Riolan anastomosis and hence shows an increased flow velocity, in particular in diastole
d Sonographic follow-up after 2 months identifies the stent as a mesh-like structure in the wall area of the superior mesenteric artery. The Doppler waveform is characterized by a high-frequency signal with an angle-corrected peak systolic flow velocity of over 8 m/s indicating recurrent, high-grade stenosis

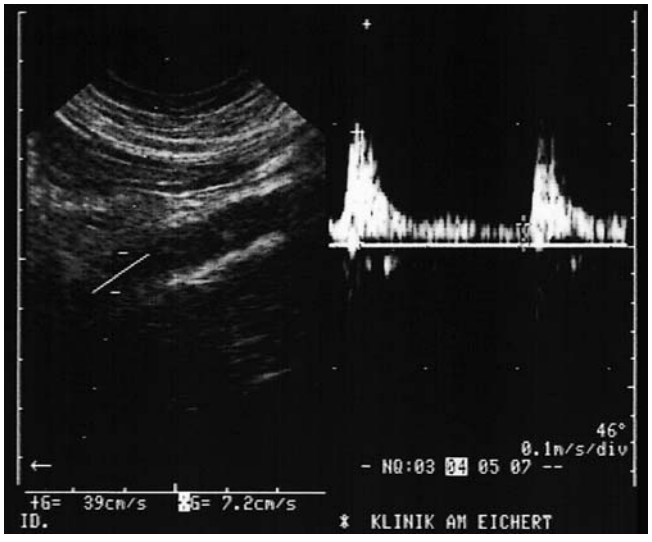

a

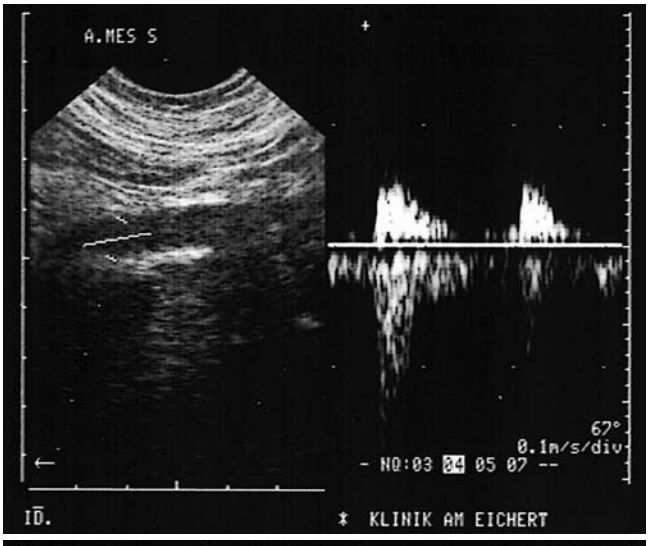

b

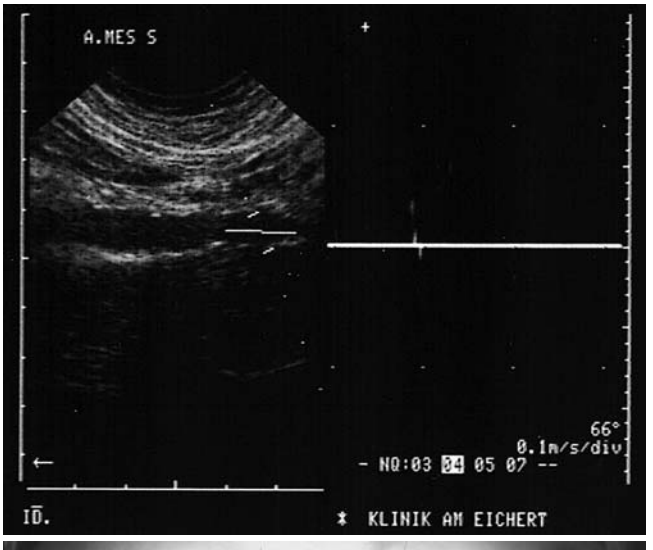

c

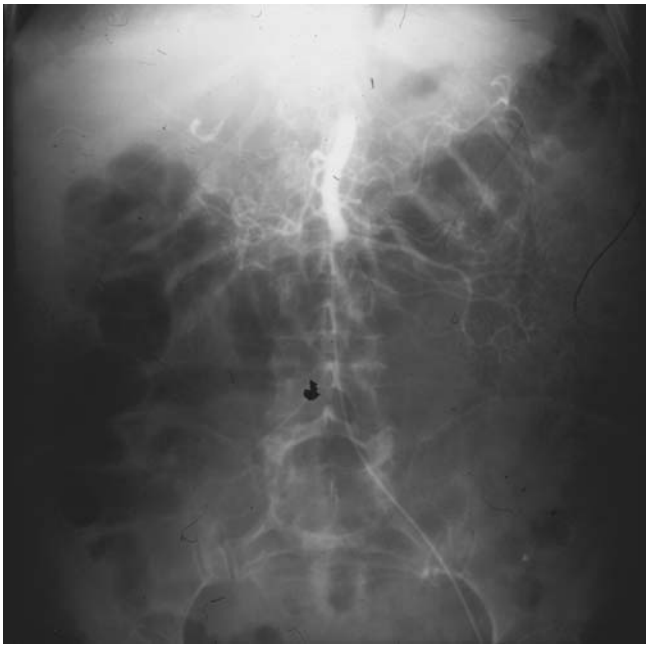

d

Fig. A 6.9 a–d
Mesenteric artery occlusion, acute
a Patient presenting with acute abdomen: abnormal Doppler waveform of the origin of the superior mesenteric artery with a decreased peak systolic flow velocity of 39 cm/s. The end-diastolic peak velocity is 7.2 cm/s; the Pourcelot index is reduced
b Continuous scanning of the superior mesenteric artery starting at its origin yields a flow profile more and more resembling a "knocking" waveform with a decreasing flow velocity and elimination of the end-diastolic flow component close to the occlusion. Flow in the mesenteric artery is toward the transducer and displayed above the baseline. The frequencies displayed below the baseline are from the middle colic artery, which arises near the sample volume
c More distally, the superior mesenteric artery is occluded with zero flow in the Doppler waveform despite a high gain
d Angiogram showing patency of the trunk of the superior mesenteric artery and occlusion distal to the origin of the middle colic artery

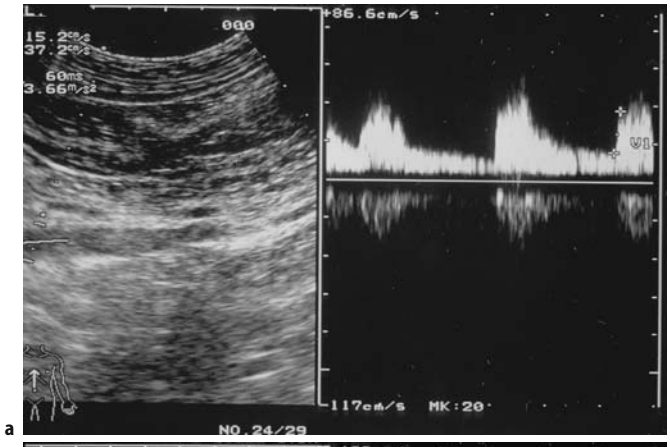

a

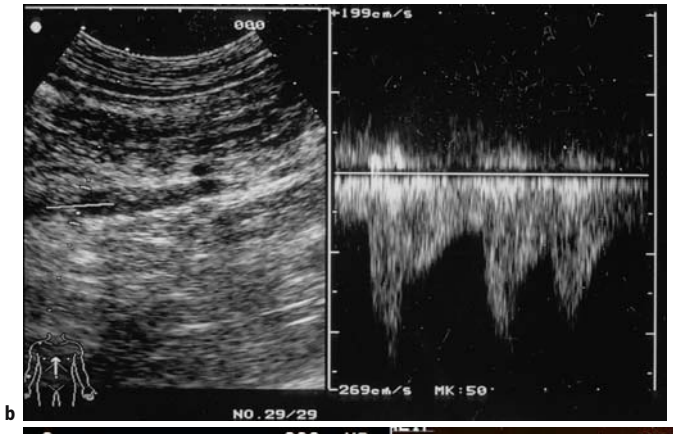

b

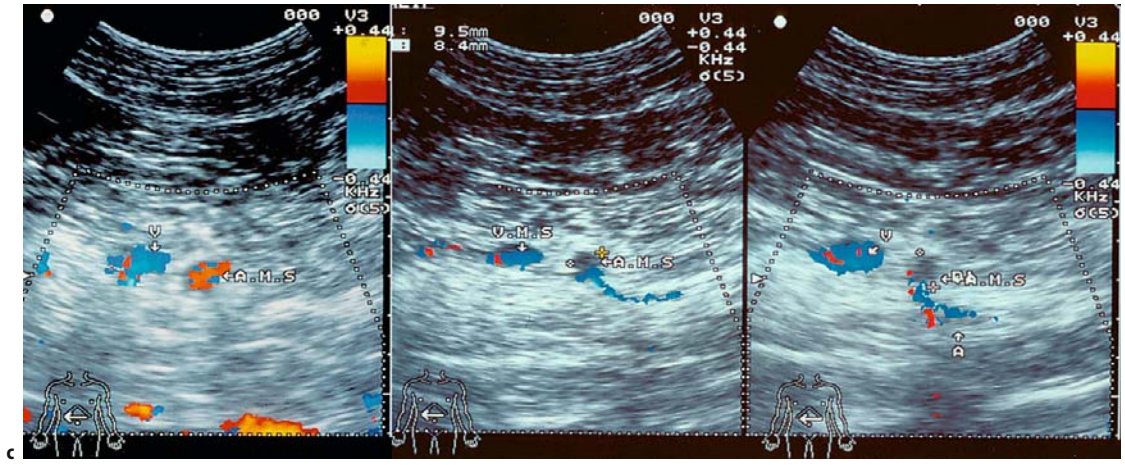

c

Fig. A 6.10 a–c
Acute mesenteric artery occlusion
a 42-year-old patient presenting with severe abdominal pain, partly of a cramping nature, having persisted for 3 hours. No abnormal laboratory values at this time (no leukocytosis, no acidosis, no elevated lactate level). The clinical examination demonstrates only mild tenderness, absence of peritonism, and diffuse abdominal pain. Normal B-mode ultrasound and radiologic examinations. No history of cardiac disease. Patient admitted to hospital in the evening with the tentative diagnosis of enteritis; analgesic therapy and follow-up contemplated. Additionally performed duplex scanning of the mesenteric arteries demonstrates an abnormal signal at the origin of the patent superior mesenteric artery. Peak systolic flow velocity is markedly reduced to 37.2 cm/s with a relatively large diastolic component of 15.2 cm/s, resulting in an abnormal resistance index of 0.59
b More distally, downstream of the origin of the middle colic artery, the Doppler spectrum of the mesenteric artery shows a blunt flow profile
c Color duplex scanning demonstrates a patent superior mesenteric artery to the level of the origins of the first jejunal branches. A proximal jejunal branch likewise shows color-coded flow signals. In the remainder of the superior mesenteric artery, neither color duplex nor spectral Doppler depict flow signals. Emergency embolectomy with complete revascularization was performed without the necessity for bowel resection

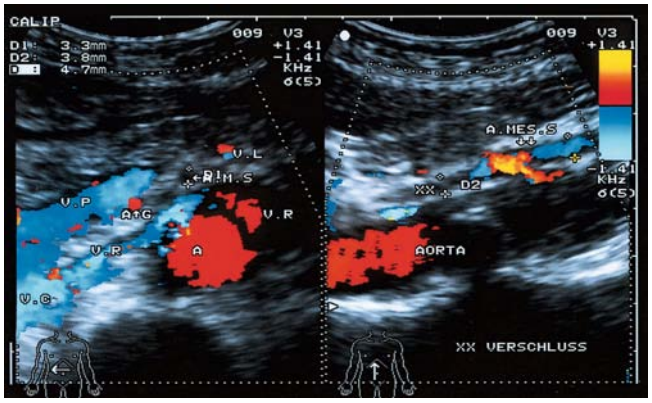

a

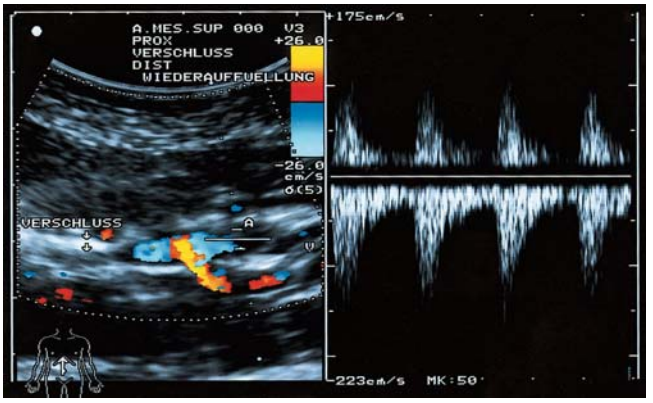

b

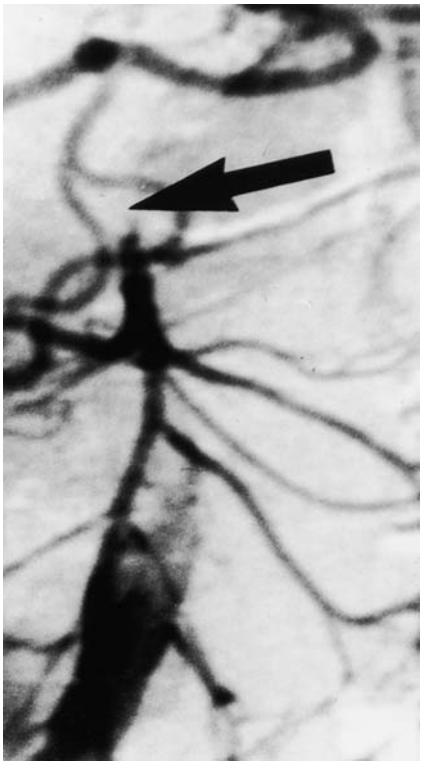

c

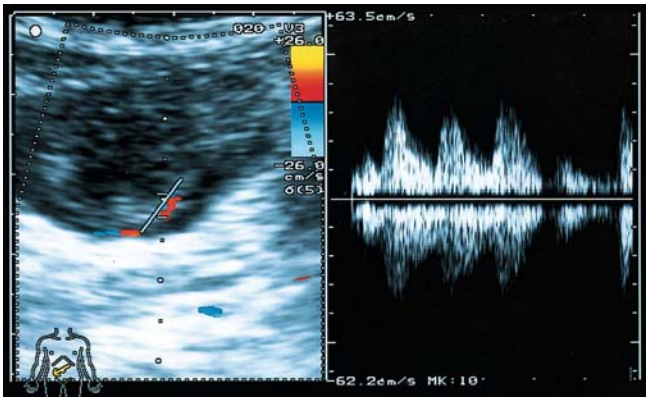

d

Fig. A 6.11 a–d
Mesenteric artery occlusion, chronic

a 50-year-old patient with symptoms of abdominal angina caused by proximal occlusion of the superior mesenteric artery with refilling through the gastroduodenal and pancreaticoduodenal arteries about 4 cm distal to its origin, as demonstrated by color duplex ultrasound. Transverse scan (*left section*) depicting the renal vein (*V.R*) and superior mesenteric artery (*A.M.S*) anterior to the aorta (*A*). Color duplex scanning fails to demonstrate flow in the occluded superior mesenteric artery (3.3 mm). More anteriorly, the splenic vein (*V.L*) is seen; the renal vein (*V.R*) including its opening into the vena cava (*V.C*) is depicted longitudinally with flow in blue to the left of the aorta sectioned obliquely. Anteriorly, the portal vein (*V.P*) is shown with blue-coded flow. Between the renal and portal veins, the cross-section of the red gastroduodenal artery is seen at its junction with the pancreaticoduodenal artery. It is depicted beneath the lower margin of the portal vein and marked (*A↑G*). In transverse orientation, this collateral pathway can be followed throughout including refilling of the superior mesenteric artery

The longitudinal scan (*right section*) depicts the superior mesenteric artery (*A.MES.S*) anterior to the obliquely sectioned aorta (red). Color signals are absent from the superior mesenteric artery segment in the left half of the scan (*XX*), where it is merely seen as a hypoechoic, tubular structure. Along its course to the right of the scan, it is refilled by the pancreaticoduodenal artery from posterolaterally (displayed in red, toward transducer). There is short backward flow in the unobstructed segment

b The Doppler spectrum shows fairly high flow in the postocclusive segment of the superior mesenteric artery (flow toward the periphery coded in blue in the color duplex image) with a postprandial peak systolic flow velocity of 120 cm/s and an end-diastolic velocity of 30 cm/s, suggesting good collateral flow through the gastropancreaticoduodenal artery (coded red in the color image). Proximal to the opening of this collateral, the occluded segment of the superior mesenteric artery is depicted as a hypoechoic, tubular structure. Near the opening of the collateral, flow is highly turbulent. The postocclusive waveform shows a somewhat delayed systolic rise, reduced pulsatility, and an increased end-diastolic component

c Angiography: Occlusion of the superior mesenteric artery at its origin (*arrow*) with refilling through the gastroduodenal and pancreaticoduodenal arteries. There is interference from the superimposed aorta at the lower margin. As a result of the delayed contrast medium passage through the collateral pathways after bolus administration, the contrast medium has already disappeared from the aorta at the level of the celiac trunk and origin of the superior mesenteric artery before opacification of the refilled superior mesenteric artery occurs

Inflammatory bowel disease

d Acute abdomen with wall thickening of bowel loops on B-mode ultrasonography. The depiction of flow signals in the bowel wall in the color duplex mode differentiates inflammatory thickening of the bowel wall from thickening due to acute ischemia or mesenteric vein thrombosis, which exhibit the characteristic bull's eye sign. The inflammatory origin is also underlined by the large diastolic component in the Doppler waveform

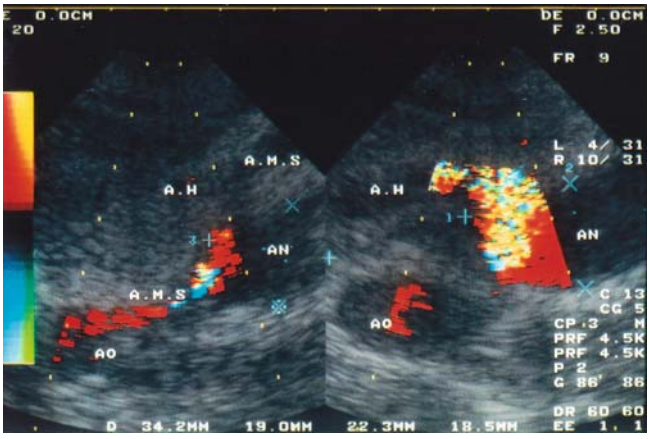

a

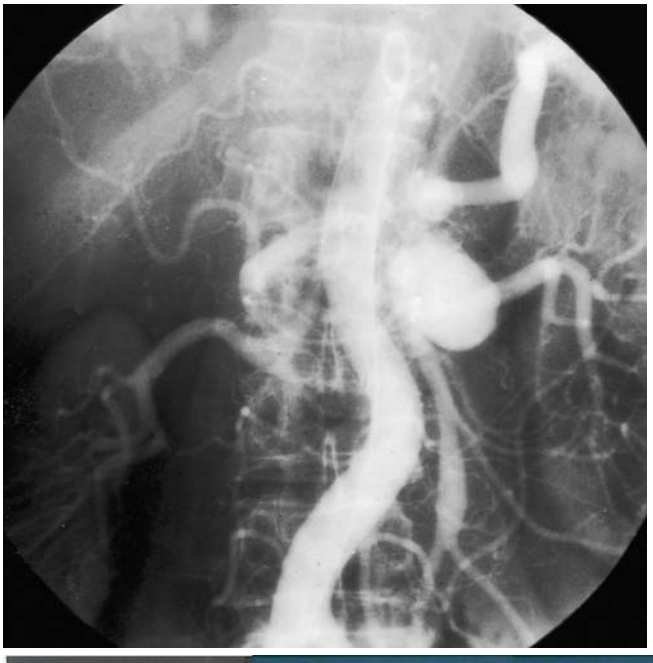

b

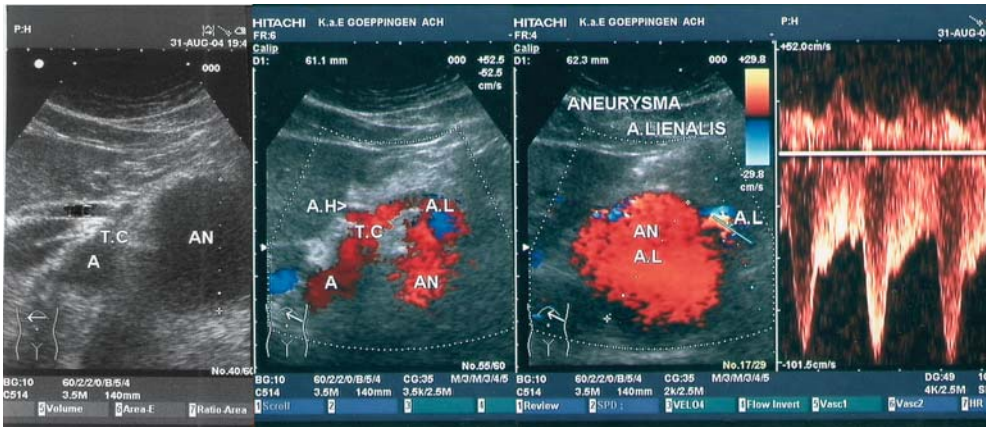

c

Fig. A 6.12 a, b
Superior mesenteric artery aneurysm

a The *left section* shows the red-coded superior mesenteric artery (*A.M.S*) with an aneurysmal dilatation (*AN*) approximately 2 cm distal to its origin from the aorta. The color box covers only the central part of the scan, which is why the vessel segments depicted at the margins show no color-coded flow signals. After moving of the transducer to an oblique plane (*right section*), the extent of the aneurysm can be evaluated; again only the medial segment is displayed with color coding due to the small color box. The hepatic artery (*A.H*) arises from the aneurysm (*AN*) and shows turbulent flow at its origin. In this case, the hepatic artery is involved because of its abnormal origin from the superior mesenteric artery. This information is important for planning of the surgical procedure because it means that the hepatic artery must be repaired as well. The aneurysm has a cross-sectional diameter of 22 mm and a longitudinal diameter of 34 mm

b Angiography: Aneurysm at the origin of the superior mesenteric artery. The overlying aorta obscures the origin of the hepatic artery from the aneurysm. The splenic artery arises from the aorta

Splenic artery aneurysm

c The B-mode scan depicts an anechoic cystic structure in the omental bursa (*leftmost*). The diagnosis of an aneurysm is suggested by the color coding in the duplex mode (*left center*). The junction of the aneurysm with the vessel is seen upon rotation of the transducer; in this example the splenic artery (*A.L*) shortly after its origin from the celiac trunk (*T.C*; *A* aorta, *A.H* hepatic artery). Moving the transducer laterally to the left (*right center*), the distal splenic artery (*A.L* with sample volume) can be traced along its course from the aneurysm (*A.N A.L*) to the splenic hilum. The vascular relationships of the aneurysm are thus determined sonographically prior to surgery. The Doppler waveform (*rightmost*) shows the typical low-resistance flow of the splenic artery

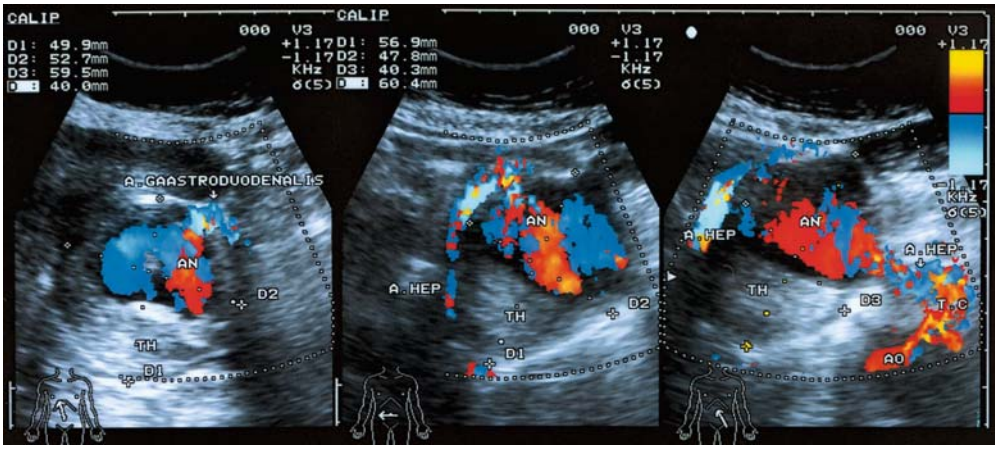

a

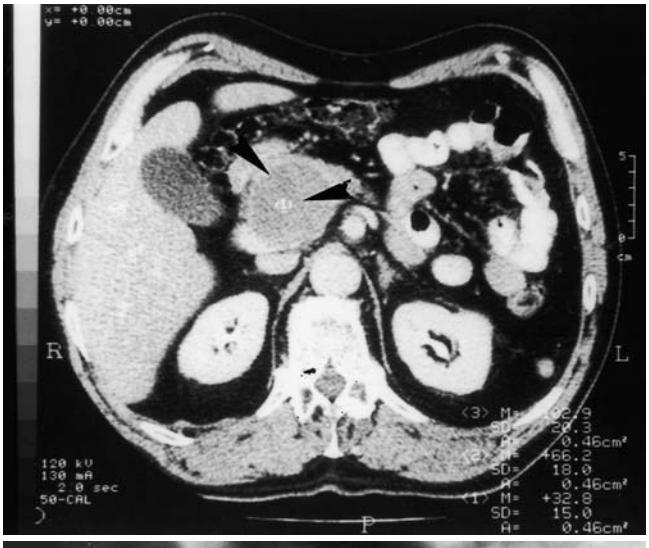

b

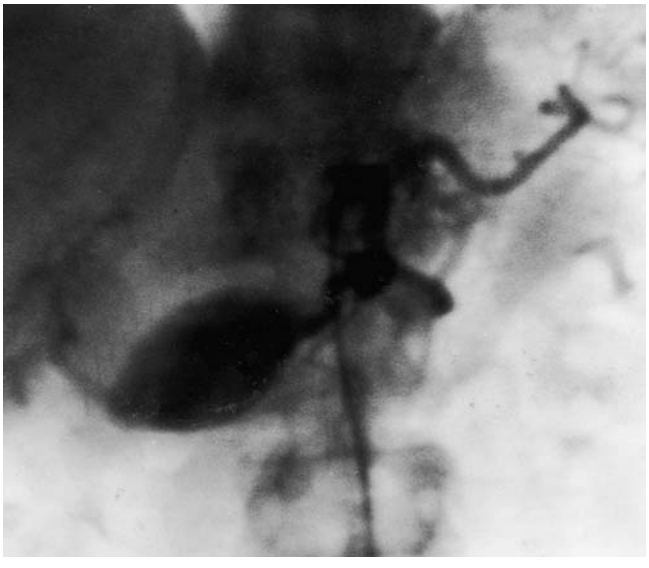

c

Fig. A 6.13 a–c
Hepatic artery aneurysm

a A structure of mixed echogenicity measuring 6 x 5 cm and showing flow signals in the color duplex mode is depicted in the portal hilum. A stagnation thrombus (*TH*) is seen in the posterior portion of the aneurysm. For the surgical procedure, it is important to precisely locate the vessels entering and arising from the aneurysm (*AN*), in particular the gastroduodenal artery, which is shown to arise from the anteroinferior aspect of the aneurysm (blue, *left section*). The *middle section* depicts the elongated proper hepatic artery (*A.HEP*) curving around the aneurysm. The *right section* shows the common hepatic artery (*A.HEP*) emptying into the aneurysm and arising from the celiac trunk (*T.C*) on the *right side* of the scan

As the hepatic artery aneurysm also involves the gastroduodenal artery, reconstruction of the hepatic artery is necessary after resection of the aneurysm. If the aneurysm were localized proximal to the gastroduodenal artery, the latter would ensure arterial supply of the liver

b Upper abdominal CT showing subhepatic mass (*arrowhead*): hepatic artery aneurysm with partial thrombosis (*arrowhead*)

c Angiography depicting hepatic artery aneurysm (*center*)

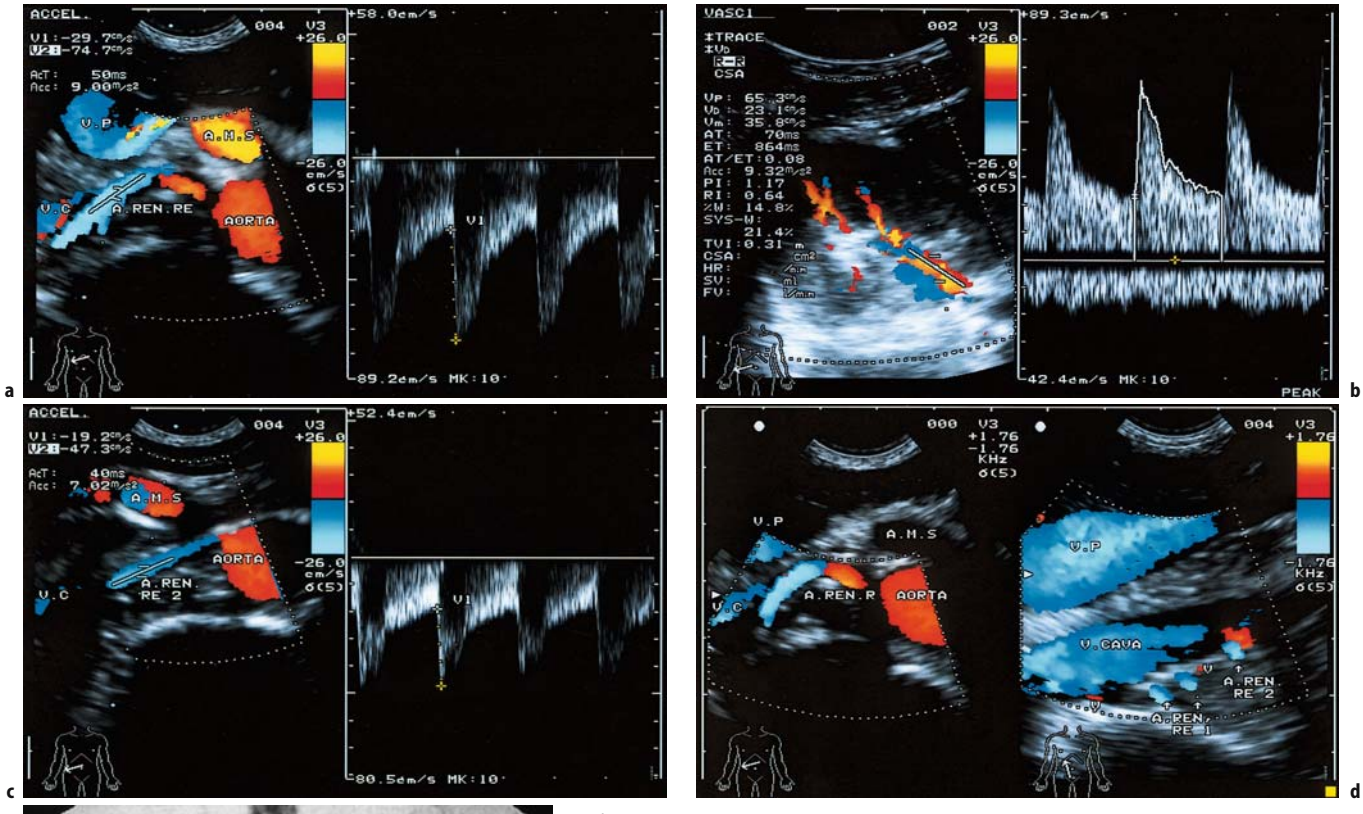

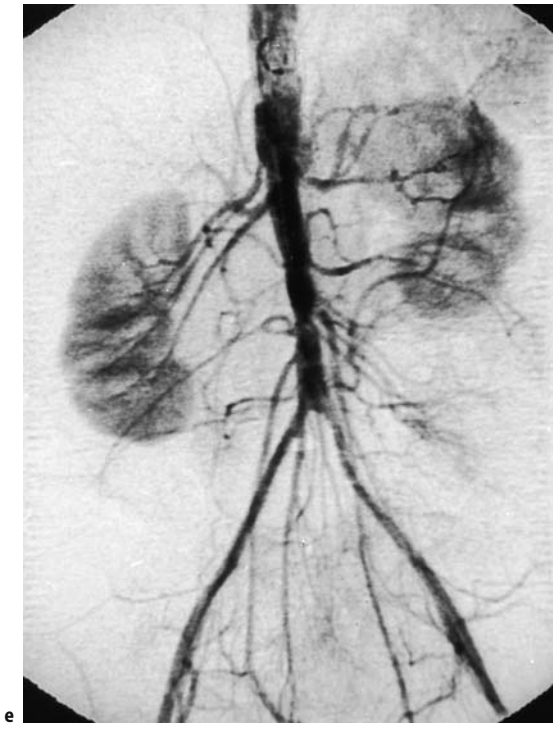

Fig. A 6.14 a–e
Course of renal arteries
a Adequate diagnostic evaluation for renal artery stenosis crucially relies on the meticulous depiction of the course of the renal artery. The transverse upper abdominal view on the *left* depicts the right renal artery (*A.REN.RE*) taking an arched course after arising from the aorta (proximal segment with flow in red toward transducer and distal segment with flow in blue away from transducer) below the vena cava (*V.C*). Anteriorly, the superior mesenteric artery (red, *A.M.S*) and portal vein (blue, *V.P*) are depicted. A Pourcelot index of 0.6 is calculated for the origin of the renal artery from a peak systolic flow velocity of 74.7 cm/s and an end-diastolic peak velocity of 29.7 cm/s
b Renal artery at the renal hilum in transverse orientation scanned from the flank with the beam striking the vessel at an adequate angle. The waveform and the Pourcelot index are the same at the hilum as at the origin, suggesting that no hemodynamically significant stenosis is present along the course of the renal artery between these two sampling sites
c Since 25 % of all kidneys are supplied by a paired renal artery and hypertension may be caused by a stenosis at the origin of the second branch, the sonographer must always look for a second renal artery branch by moving the transducer posteriorly in transverse orientation. In the case presented, a second renal artery depicted in blue arises from the aorta 1 cm away from the origin of the first one. The characteristic renal artery waveform confirms the identity of the vessel
d In longitudinal orientation, the renal arteries are located posterior to the vena cava. They are depicted in blue on the posterior aspect of the vena cava, likewise with blood flow in blue. Three branches of the renal artery with blood flow coded in blue are seen below the vena cava due to early division of the inferior renal artery
e Angiography: Two renal arteries arise from the aorta on the right with early division of the inferior branch

▷
Fig. A 6.15 a–e
Sonoanatomy of the renal arteries
a The left renal artery usually has a length of 5–6 cm from the aorta to the renal hilum. It is rarely possible to scan the left artery throughout its course in a single plane due to scattering by bowel gas. The *left section* depicts the renal artery with

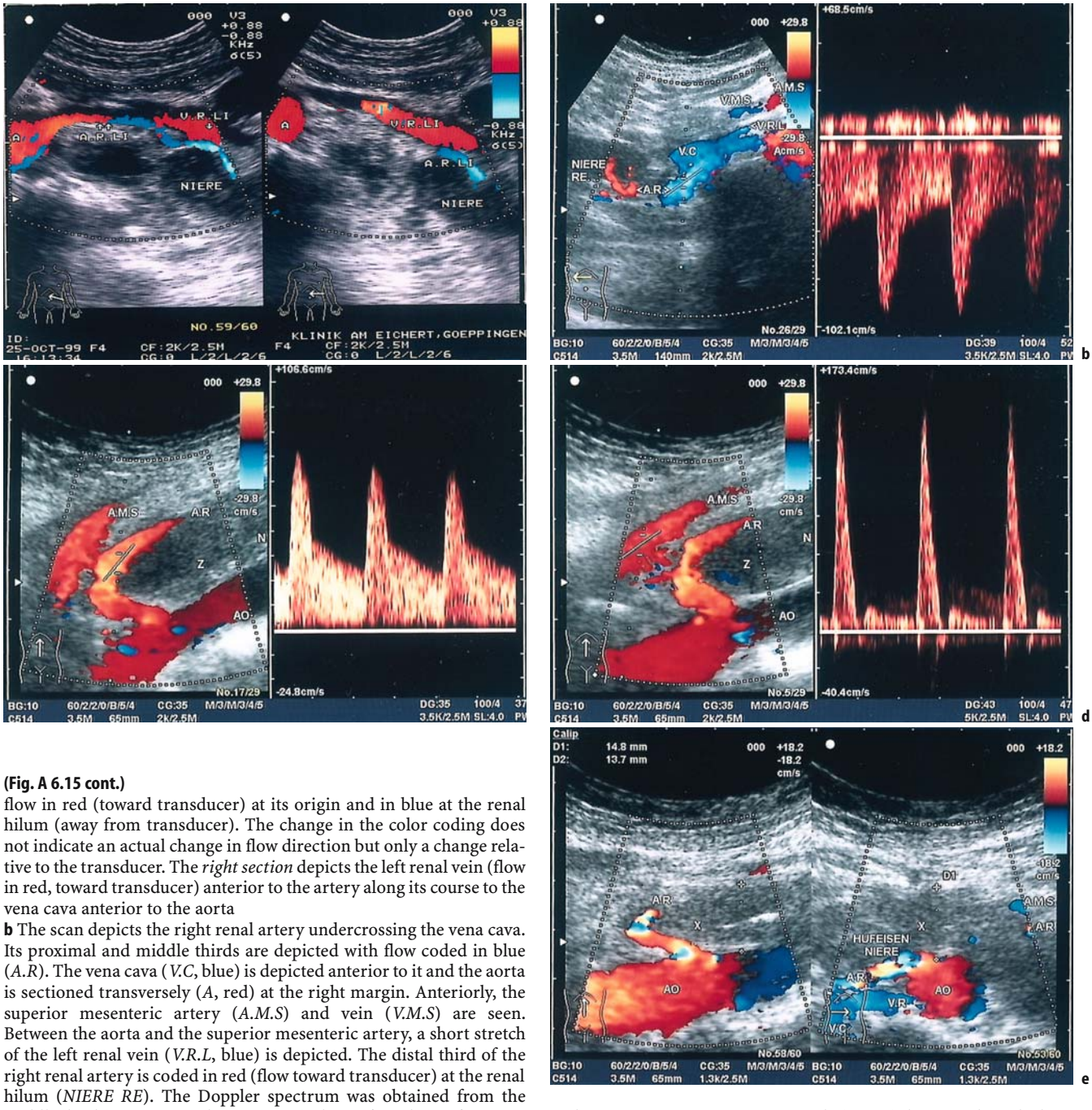

(Fig. A 6.15 cont.)
flow in red (toward transducer) at its origin and in blue at the renal hilum (away from transducer). The change in the color coding does not indicate an actual change in flow direction but only a change relative to the transducer. The *right section* depicts the left renal vein (flow in red, toward transducer) anterior to the artery along its course to the vena cava anterior to the aorta

b The scan depicts the right renal artery undercrossing the vena cava. Its proximal and middle thirds are depicted with flow coded in blue (*A.R*). The vena cava (*V.C*, blue) is depicted anterior to it and the aorta is sectioned transversely (*A*, red) at the right margin. Anteriorly, the superior mesenteric artery (*A.M.S*) and vein (*V.M.S*) are seen. Between the aorta and the superior mesenteric artery, a short stretch of the left renal vein (*V.R.L*, blue) is depicted. The distal third of the right renal artery is coded in red (flow toward transducer) at the renal hilum (*NIERE RE*). The Doppler spectrum was obtained from the middle third (posterior to the vena cava), the preferred site of stenosis in fibromuscular dysplasia

Horseshoe kidney

c Horseshoe kidneys have an atypical arterial and venous supply. Besides additional lower pole vessels, a 5th renal artery supplying the renal bridge overcrossing the aorta may be present as in the example shown. The young woman had an infected renal cyst (*Z*) in the preaortic bridge of the horseshoe kidney. Pus was drained from the cyst under ultrasound guidance. In inconclusive cases, the Doppler waveform can help to establish the identity of a vessel. Here, the inferior one of the two vessels coursing over the cyst (*Z*) and renal parenchyma displays the typical waveform of a renal artery and is thus identified as a supernumerary 5th renal artery (*A.R*)

d The artery coursing more superiorly (*A.M.S*) does not show the low-resistance flow typical of renal arteries but a mixed type characteristic of mesenteric arteries

e Closer inspection of the vascular supply (transverse scan on the *right*, longitudinal scan on the *left*) shows the right lower polar artery (*A.R*) with flow in blue. This artery takes an atypical course anterior to the vena cava on its way to the lower pole after arising from the aorta (*AO*). A retroaortic renal vein with flow coded in blue (*V.R*) passes from the left lower pole into the vena cava (*V.C*). There is aliasing in the renal artery due to the low pulse repetition frequency used to detect slow venous (and arterial) flow. The longitudinal scan on the *left* again shows the 5th renal artery (*A.R*) coursing to the renal parenchyma in front of the aorta (*AO*) after draining of the infected cyst (site indicated by the *X* in the kidney)

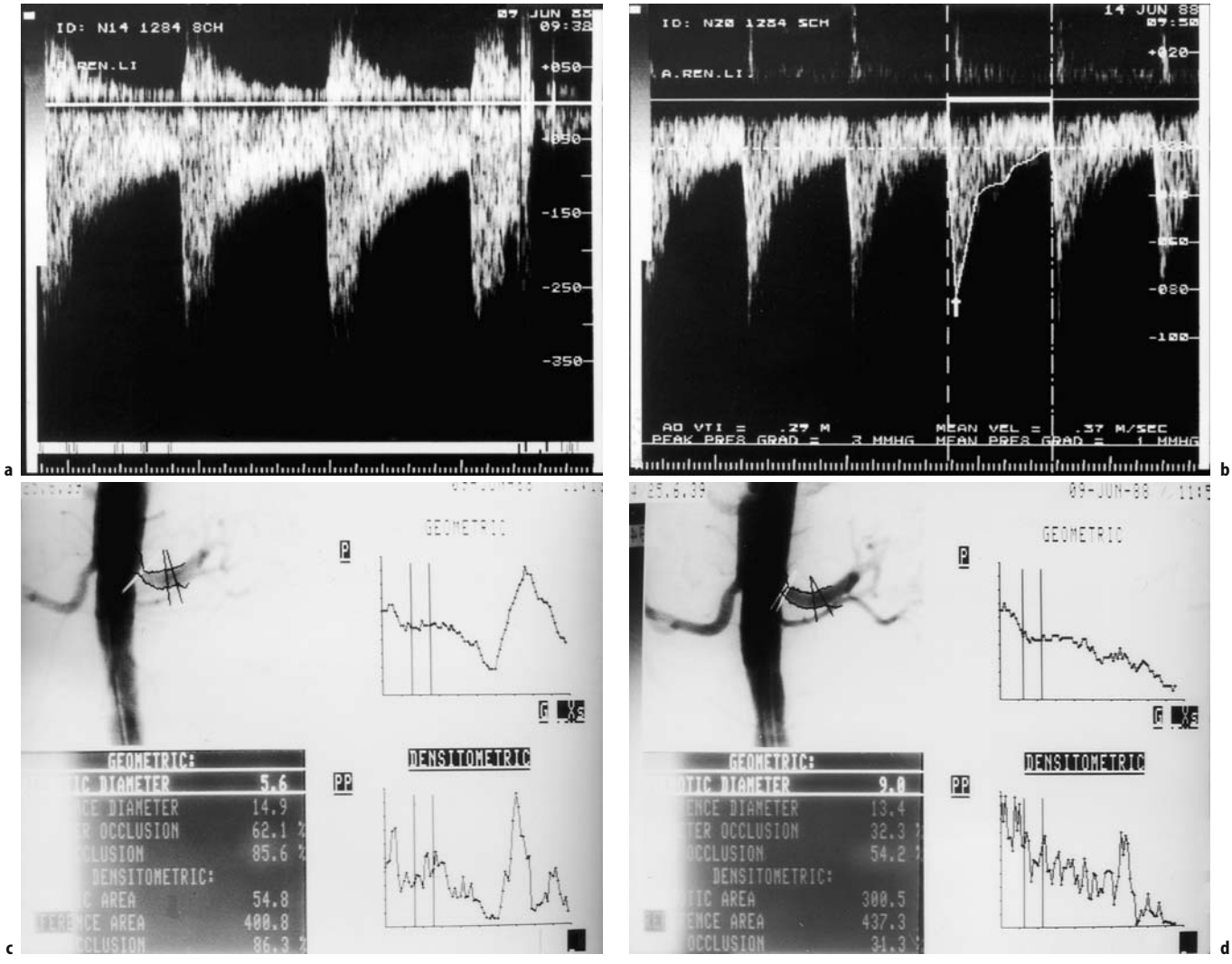

Fig. A 6.16 a–d
Renal artery stenosis – PTA
a Doppler waveform obtained in the presence of an intermediate- to high-grade stenosis at the origin of the renal artery with marked turbulence and a peak flow velocity of 310 cm/s during systole and 100 cm/s at end-diastole
b Doppler waveform from the same renal artery as in **a** after percutaneous transluminal angioplasty (PTA). Return to normal blood flow velocities (peak systolic velocity of 80 cm/s)
c X-ray densitometry (same patient as in **a**, before PTA): Measurement demonstrates a stenosis at the origin of the left renal artery with an area reduction of 86.3 %
d X-ray densitometry (same patient as before, after PTA; corresponding Doppler waveform in **b**): Residual stenosis with 31.3 % area reduction corresponding to a hemodynamically not significant stenosis with spectral broadening in the Doppler waveform but without accelerated flow

▷
Fig. A 6.17 a–f
Renal artery stenosis
a The waveform from the renal hilum on the left yields a peak systolic flow velocity of 85.7 cm/s and an end-diastolic peak velocity of 47.2 cm/s, from which a resistance index (Pourcelot index) of 0.64 is calculated

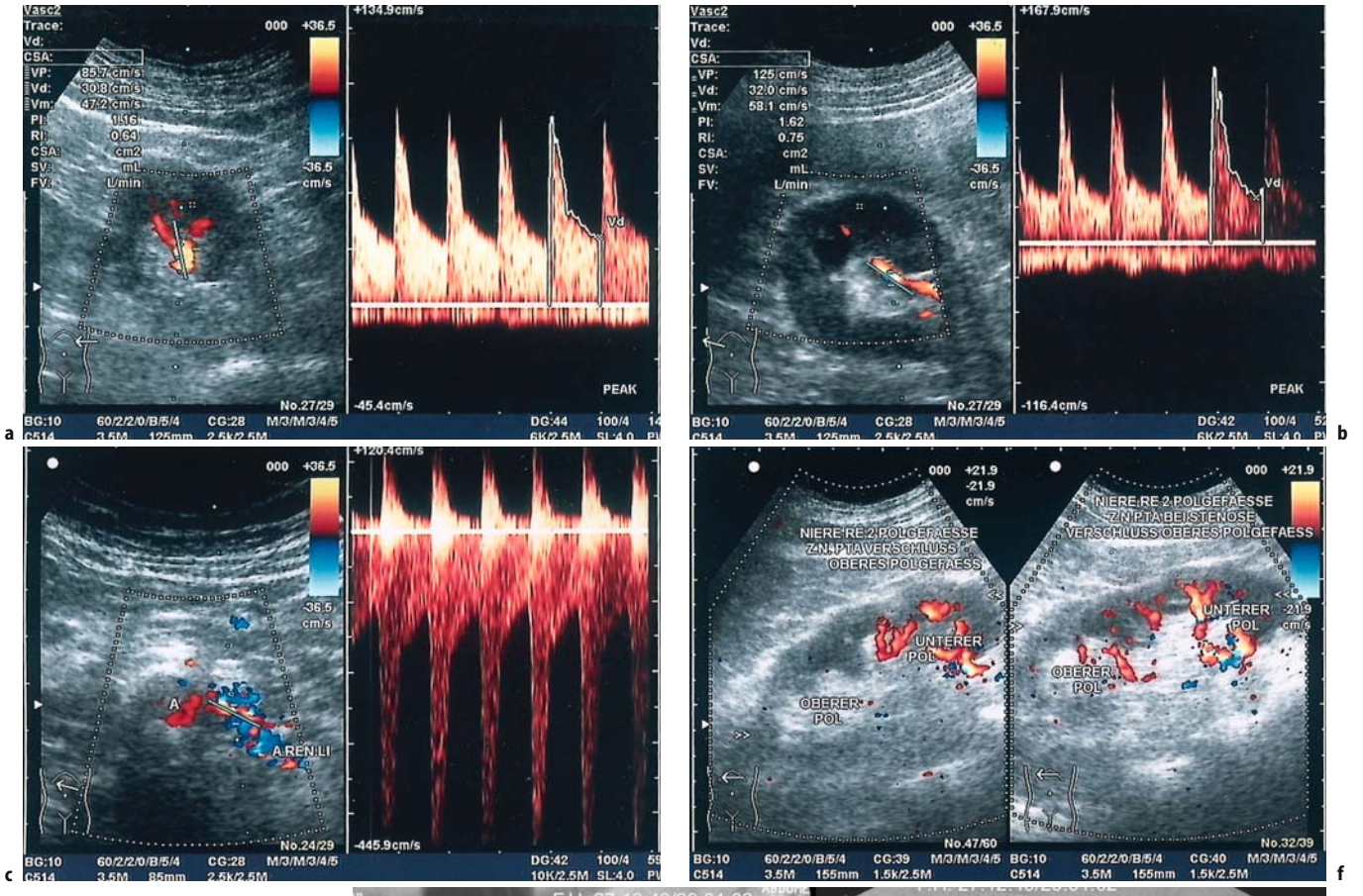

(Fig. A 6.17 cont.)

b The corresponding values in the right renal artery are: peak systolic velocity of 125 cm/s, peak end-diastolic velocity of 58.1 cm/s, and a resulting resistance index of 0.75. The difference of over 10 % indicates a renal artery stenosis on the left, where the decreased index indicates postocclusive flow

c The Doppler waveform from the origin of the left renal artery confirms a high-grade stenosis with a peak systolic flow velocity of over 4 m/s with the color duplex scan showing pronounced perivascular vibration artifacts (audible bruit on auscultation)

d Subsequent angiography with simultaneous PTA confirms high-grade stenoses of both polar arteries on the left

e Postinterventional control angiography demonstrates occlusion of the upper polar artery after PTA

f Renal infarction in the upper pole area is confirmed by the absence of color-coded vessels in the renal parenchyma on the color duplex scan (*left section*). Subsequent emergency angiography with reopening of the upper pole artery re-establishes flow in only some segmental arteries with rarefaction of the vessels in the renal parenchyma as shown on the duplex scan

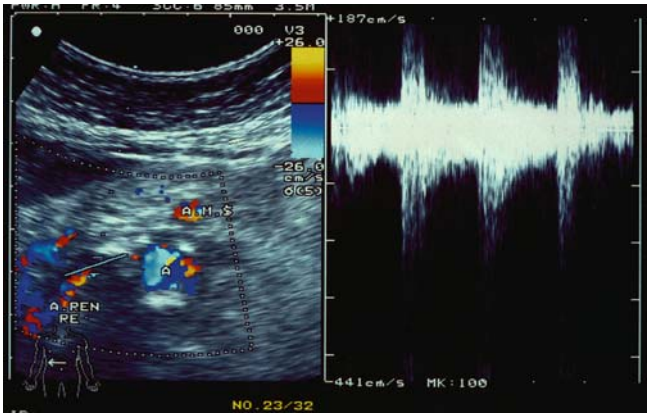

a

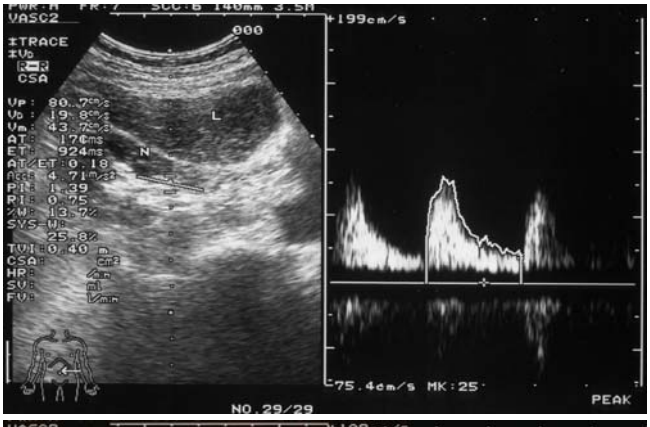

b

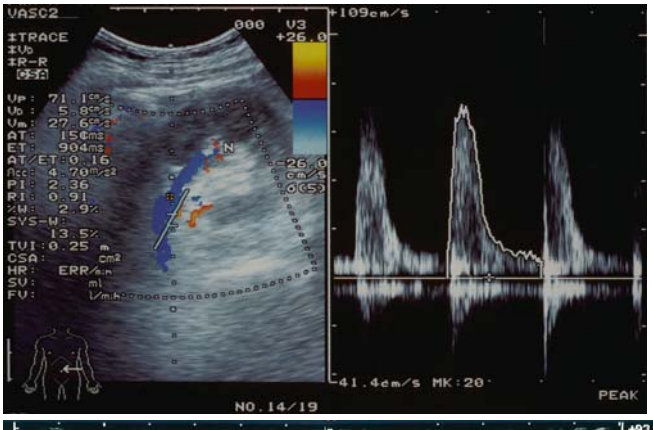

c

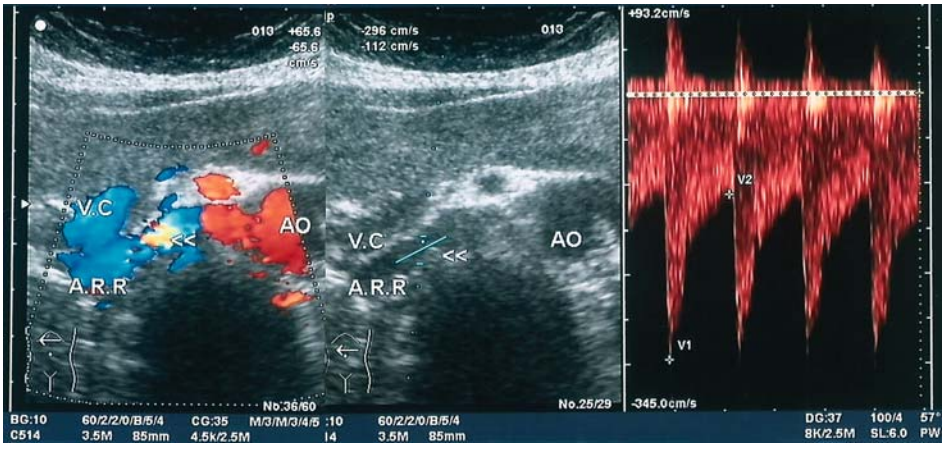

d

Fig. A 6.18 a–c
Renal artery stenosis in diabetes mellitus

a In a patient with a long history of insulin-dependent diabetes mellitus and macro- and microangiopathy, the Doppler waveform obtained at the origin of the right renal artery shows turbulence and accelerated flow indicative of a renal artery stenosis. (Color) duplex scanning provides no adequate information for estimating the degree of stenosis due to plaque with acoustic shadowing at the origin. In interpreting the peak systolic flow velocity of just over 2 m/s somewhat distal to the stenosis, one has to take into account possible hypertensive episodes during spectral Doppler sampling as well as the known higher pulsatility of blood flow with higher systolic peak velocities in diabetics. In the case presented, for instance, the resistance index (Pourcelot index) is calculated from the Doppler spectra of both hilar areas for confirmation of the hemodynamic significance of the stenosis

b The spectrum of the right hilum yields a peak systolic velocity of 80.7 cm/s and an end-diastolic peak velocity of 19.8 c m/s with a Pourcelot index of 0.75. The gray-scale scan depicts the liver (*L*) above the kidney

c The spectrum of the left hilum shows a clearly more pulsatile flow with a peak systolic velocity of 71.1 cm/s and an end-diastolic peak velocity of 5.8 cm/s with a Pourcelot index of 0.91. Compared to the spectrum recorded on the left side, the waveform of the right renal artery appears to be unusually normal, which is due to the fact that the effects of diabetes and stenosis cancel each other. The waveform of the left renal artery is too pulsatile for this vessel, which is attributable to medial sclerosis in longstanding diabetes mellitus and changes of the renal parenchyma. The much lower Pourcelot index of the right renal artery (over 10% in side-to-side comparison) is abnormal and indicates a hemodynamically significant proximal stenosis

Fibromuscular dysplasia

d 32-year-old patient with difficult-to-control hypertension. Color duplex scanning shows aliasing in the middle third (*arrow*) of the right renal artery (*A.R.R*) behind the vena cava (*V.C*) and 3 cm distal to its origin from the aorta (*AO*) as a sign of circumscribed flow acceleration. The Doppler spectrum yields a peak systolic flow velocity of 3 m/s in the area of the angiographically confirmed stenosis caused by fibromuscular dysplasia

Fig. A 6.19
Suprarenal aortic aneurysm
Sonographic evaluation of the renal artery is indicated to evaluate the relationship of its origin to an aortic aneurysm. Here, scanning of the upper abdomen in transverse orientation shows the right renal artery arising from an aortic aneurysm with partial thrombosis and a diameter of 4.5 cm at the level of the origin of the renal artery (hypoechoic, concentric thrombus also at the renal artery origin). In addition, there is high-grade stenosis of the renal artery with a peak systolic velocity exceeding 5 m/s

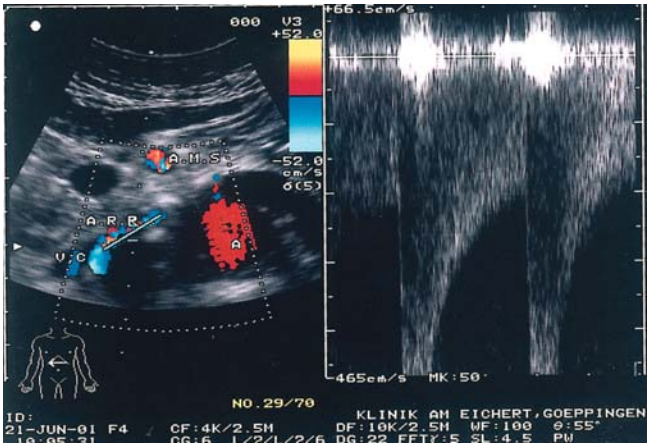

Fig. A 6.20 a, b
Vessel compression by tumor
a A sarcoma (confirmed by ultrasound-guided core biopsy) splays the vena cava (*V.C*) and aorta retroperitoneally. A long segment of the renal artery (*A.REN.RE*) running through the tumor is moderately constricted (peak systolic flow velocity of 250 cm/s in Doppler waveform). The vessels are located by color duplex scanning to avoid vascular damage by subsequent ultrasound-guided core biopsy. Anteriorly, the portal vein (*V.P*) is likewise compressed by the tumor

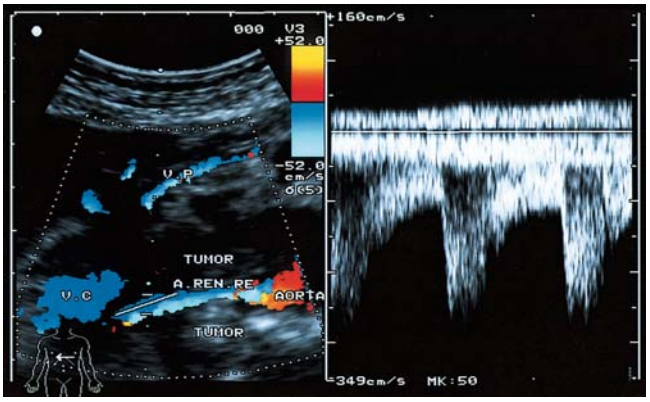

a

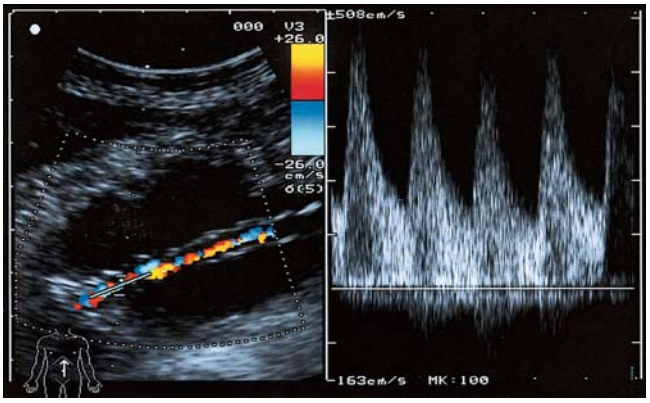

b

b The superior mesenteric artery encased by the tumor (sarcoma) at its root is also constricted along an extended segment (450 cm/s peak systolic velocity)

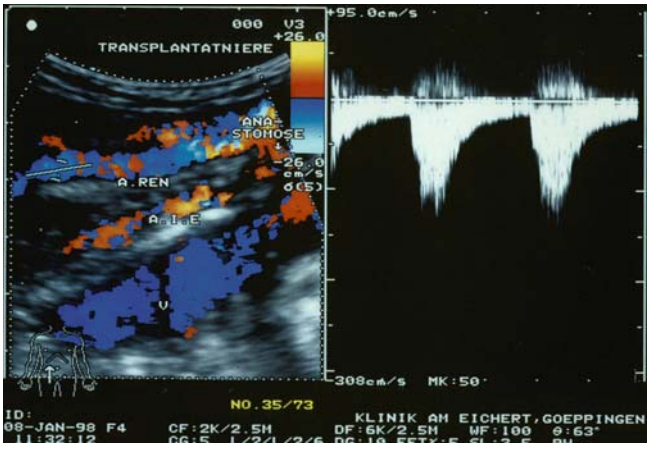

a

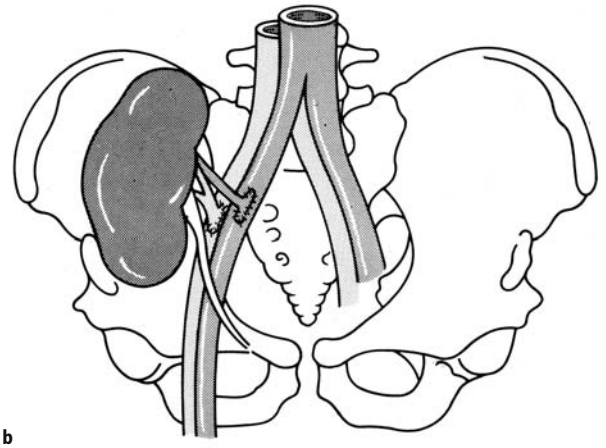

b

Fig. A 6.21 a, b
Transplant kidney
a Color duplex scan depicting the artery of the transplant kidney, anastomosed to the iliac artery, with flow coded in blue (flow away from transducer) while the iliac artery is shown with flow in red (toward transducer). The Doppler waveform has a large diastolic component and the typical pattern of low-resistance flow indicating a functioning graft without rejection
b Schematic representation of the connection of the renal transplant vessels to the iliac vessels

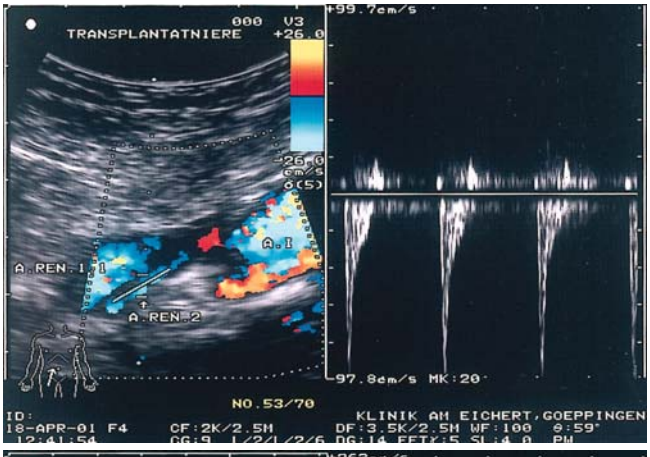

a

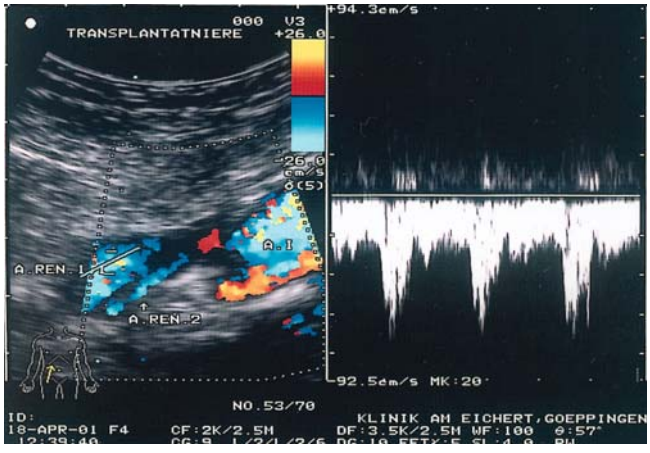

b

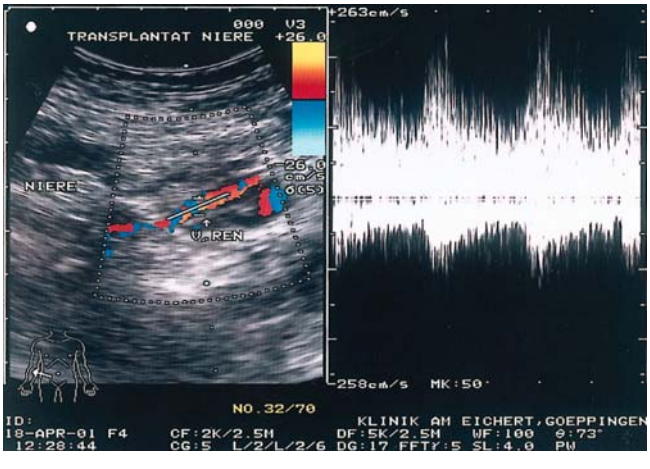

c

Fig. A 6.22 a–c
Transplant kidney – rejection – fistula
Analysis of the Doppler waveform from the renal artery is an integral component of the diagnostic evaluation of kidney graft function and rejection. The renal artery of a transplant kidney anastomosed to the iliac artery is often more easily accessible to sonographic evaluation than the native renal artery
a The two renal arteries supplying the kidney are depicted at their origins from the iliac artery (*A.I.*). A highly pulsatile waveform comparable to that of an extremity artery is obtained from the origin of the second renal artery (*A.REN.*2). This flow profile indicates rejection
b Surprisingly, the other transplant artery inserted somewhat higher has a monophasic waveform with the low-resistance flow typical of normal kidney function
c The Doppler waveform of the renal vein (flow toward transducer in the direction of the iliac vein) depicts a pulsatile flow profile with pronounced turbulence, which is typical of venous flow downstream of an AV fistula

Repeat biopsies performed in this patient for evaluation of transplant rejection led to the formation of a fistula, which explains why the artery (*A.REN.1*) supplying the fistula shows low-resistance flow despite rejection (as documented in *A.REN.*2)

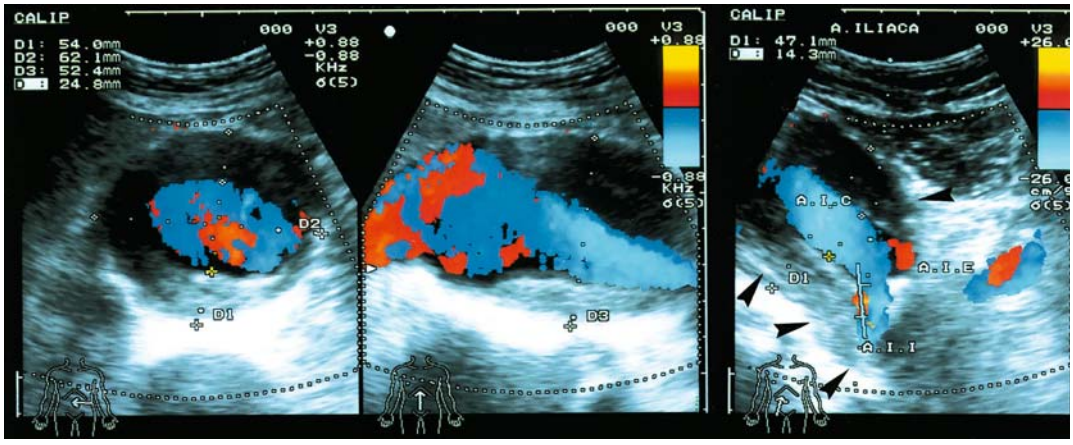

a

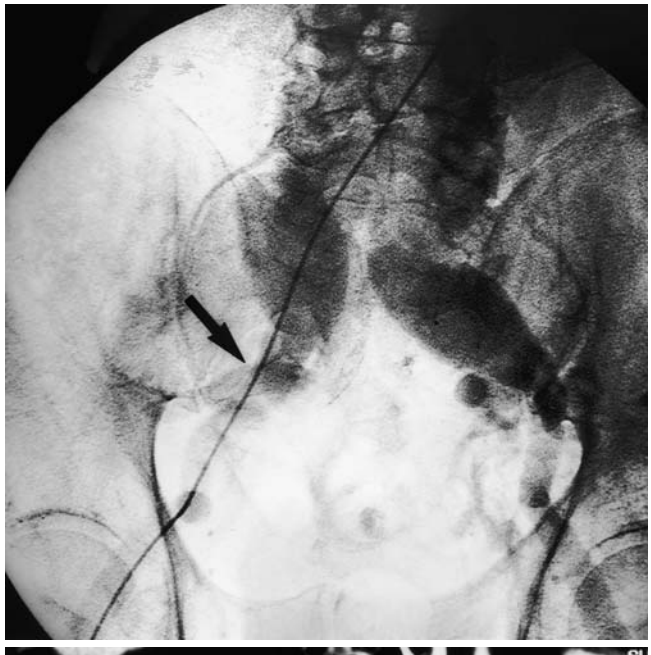

b

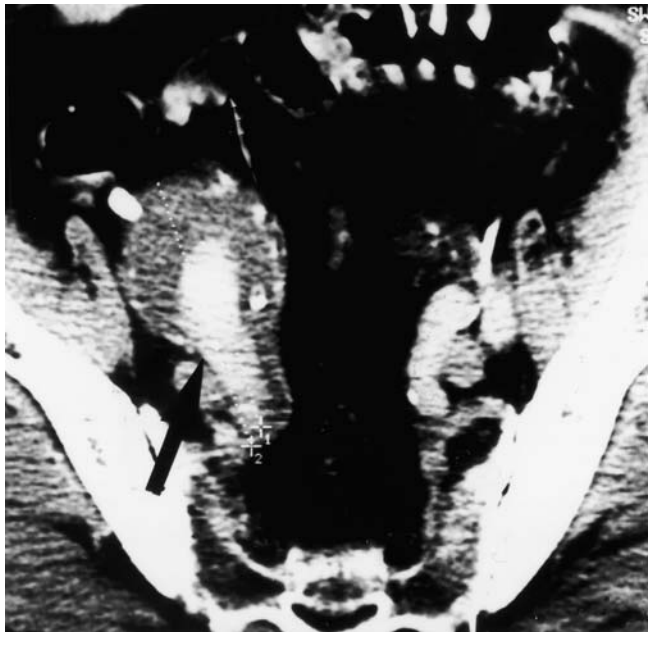

c

Fig. A 6.23 a–c
Aortic and iliac artery aneurysm

a Partially thrombosed aortic aneurysm with infrarenal extension shown in transverse orientation (*left section*) and longitudinally (*middle section*). Evaluation of the perfused lumen is improved in the color duplex mode. The total diameter of the aneurysm is 6.2 cm. The mural thrombosis lining the lumen appears hypoechoic around the patent lumen. The aneurysm (*right section*, *arrowheads*) extends into the common iliac artery (*A.I.C*) and the origin of the internal iliac artery (*A.I.I*). The elongated external iliac artery (*A.I.E*) leaves the scanning plane. The aneurysm has a total diameter of 47 mm with a patent lumen of 14 mm

b Angiography showing aneurysmal dilatation of the aorta and of the common iliac arteries. Due to mural thrombosis, the origin of the internal iliac artery on the right (*arrow*) seems not to be dilated

c Contrast-enhanced CT: Aneurysm on the right (*arrow*) extending into the origin of the internal iliac artery with mural thrombosis surrounding the perfused lumen. The internal iliac artery arises from the posterior aspect of the common iliac artery (cf. **a**)

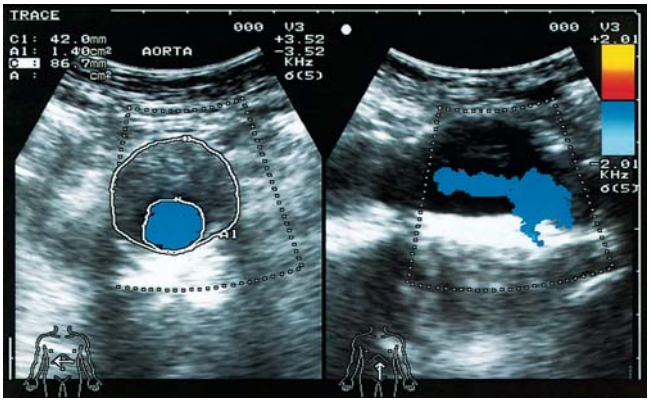

a b

Fig. A 6.24 a, b
Aortic aneurysm with arterial embolism
a While the risk of perforation correlates with the diameter of an aneurysm, the risk of embolism associated with the presence of thrombosis in an aneurysm is independent of its size. The saccular aneurym shown has a size of only 4 cm with mural thrombosis reducing the lumen to that of the normal vessel, especially in the saccular portion, but was the source of distal emboli (see **b**). This is an indication for surgery irrespective of aneurysm size. Angiography shows no abnormalities as the perfused lumen of the aneurysm corresponds to that of the normal width of the aorta. The white outline in the left scan indicates the extent of the aneurysm; the longitudinal scan on the right depicts the saccular anterior outpouching and the thrombotic lining
b Isolated occlusions of the profunda femoris artery with a patent superficial femoral artery (*A.F.S*) and common femoral artery (*A.F.C*) are typically due to embolism rather than atherosclerosis. Neither color duplex scanning nor the Doppler waveform demonstrates flow in the profunda femoris. The gray-scale mode shows not only a posterior plaque with acoustic shadowing but also hypoechoic thrombotic material extending from the profunda femoris artery (sample volume) into the bifurcation

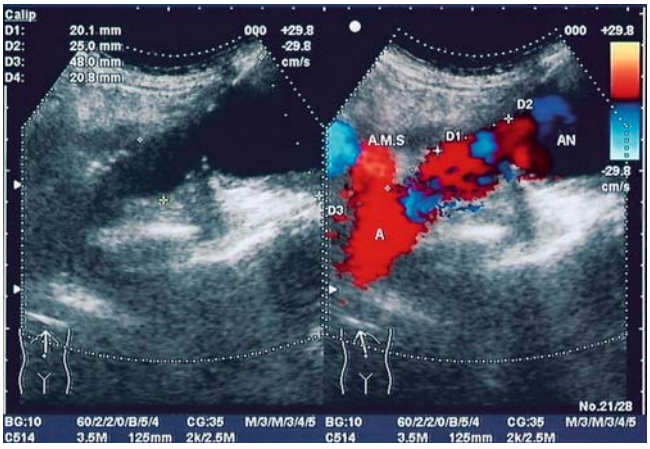

a b

Fig. A 6.25 a, b
Aortic aneurysm
a The therapeutic management of an aortic aneurysm is mainly dictated by its diameter, involvement of the iliac artery, presence of thrombosis, and infrarenal extent including the distance to the renal artery origins, which is important when stent placement is planned. Since the renal artery origins are best seen transversely and the segment between the origins and the end of the aneurysm in longitudinal section, it is helpful to first identify the superior mesenteric artery in the longitudinal view and to use this artery as a guiding structure. The renal arteries arise 1–2 cm distal to the origin of the mesenteric artery. The segment between the end of the aneurysm and the superior mesenteric artery origin can thus be measured in longitudinal orientation. This value minus 2 cm yields the distance between the renal artery origin and the aneurysm
b Whether surgical resection or stenting is the more suitable therapeutic approach primarily depends on the diameter of the aneurysm. Since a dilated aorta is also elongated (mostly with a left lateral convexity), imaging modalities with data acquisition in standardized transverse sections such as CT will lead to overestimation when the longest diameter of the elliptical lumen is measured (*right section*). To eliminate this source of error and perform a precise and reproducible cross-sectional diameter measurement (with little inter- and intraobserver variation) in repeat examinations, the sonographer must first identify the site of the largest diameter of the aneurysm. Next, the transducer is rotated in this position to identify the smallest transverse diameter (typically the luminal profile will change from elliptical to circular) to exclude overestimation resulting from oblique sectioning. In the example, the measured diameter is thus reduced from 61 mm in the elliptical configuration (transverse midabdominal scan) to the true value of 50 mm (*left section*)

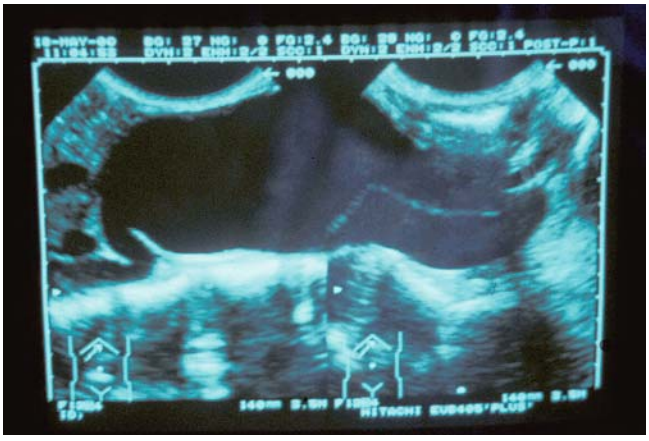

Fig. A 6.26
Aortic aneurysm of nonatherosclerotic origin
Aneurysms of nonatherosclerotic and nonbacterial/noninfectious origin can grow to gigantic proportions before they rupture. In this young African woman (examined in Uganda) who presented with a tense abdomen, an aneurysm with a cross-sectional diameter of over 15 cm arising from the infrarenal aorta and extending to the iliac bifurcation on both sides filled most of the intra-abdominal cavity. The aneurysm is shown on a composite scan in longitudinal orientation. There is suprarenal kinking of the aorta, which thus extends from the vertebral column to the abdominal wall. The intestine is pushed to the side. Further down in the lower abdomen, with the transducer slightly rotated, the common iliac artery is shown to be aneurysmatically dilated to the level of the origin of the external iliac artery (normal lumen). Posterior to the common iliac artery, the common iliac vein is dilated due to congestion. There are no atherosclerotic changes of the arterial wall

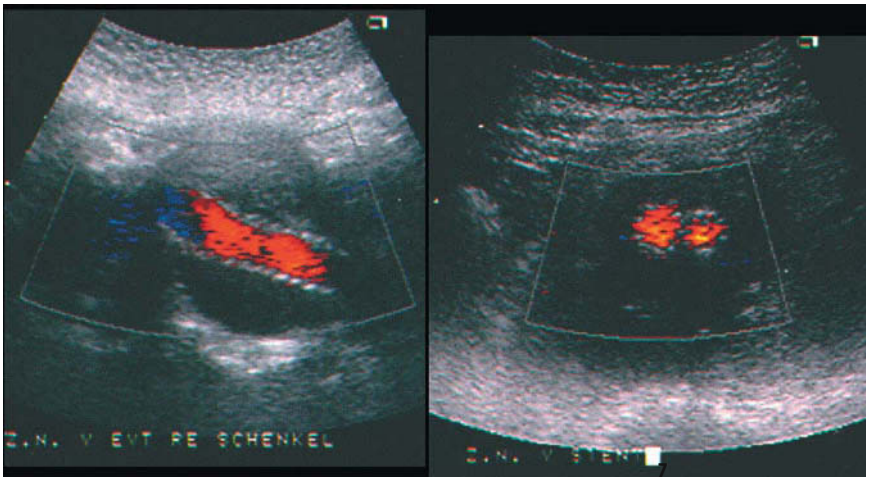

Fig. A 6.27
Stenting of aortic aneurysm
Depending on the design of the stent deployed, its echotexture may be visible on ultrasonography. The stent wall is always delineated as a hyperechoic structure within the aneurysm. The longitudinal scan on the *left* depicts one patent limb while the transverse scan on the *right* shows both patent limbs side by side with flow displayed in red within the hypoechoic aneurysm. There are no endoleaks. (Courtesy of P. Heilberger)

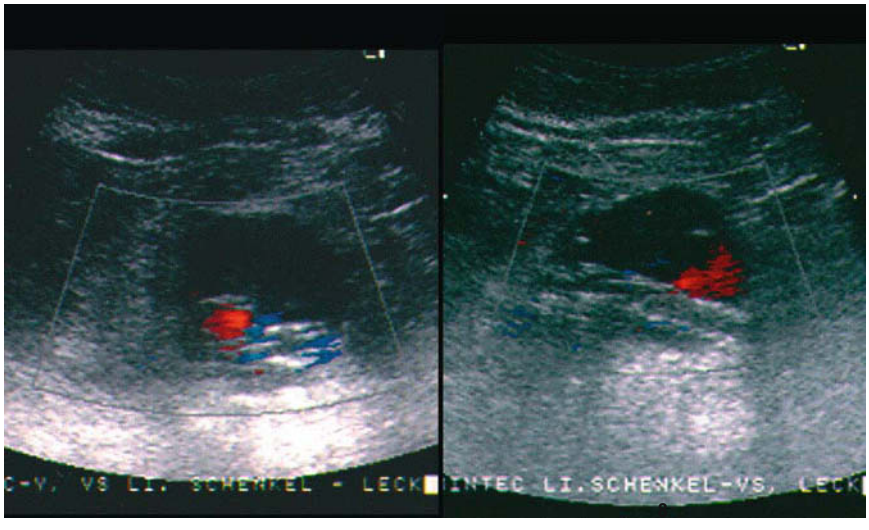

Fig. A 28
Type III endoleak
There is leakage at the site of sealing with patency of the right limb and occlusion of the left limb. The *left section* shows blue-coded flow signals around the stent in the hypoechoic lumen of the aneurysm as signs of the leak. The longitudinal scan on the *right* displays flow in red outside the stent in the lumen (type III endoleak). The absence of flow signals in the stent (posterior to the endoleak) is due to thrombosis

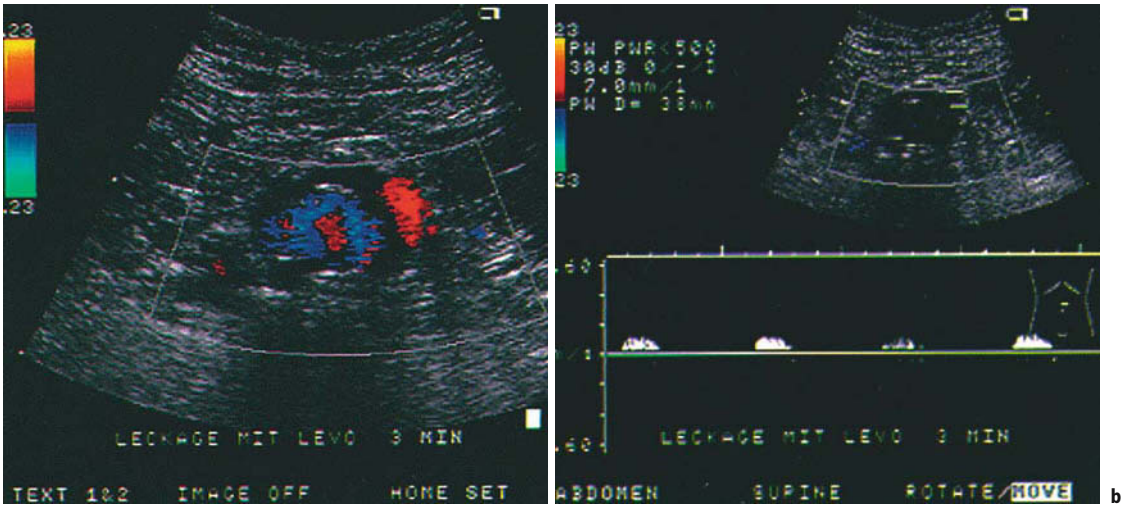

a b

Fig. A 6.29 a, b
Type II endoleak
a Red flow signals are depicted at the origin of the inferior mesenteric artery around the aortic stent in the hypoechoic aneurysm (type II endoleak)

b The Doppler waveform confirms the endoleak by the depiction of backward flow from the inferior mesenteric artery into the aneurysm

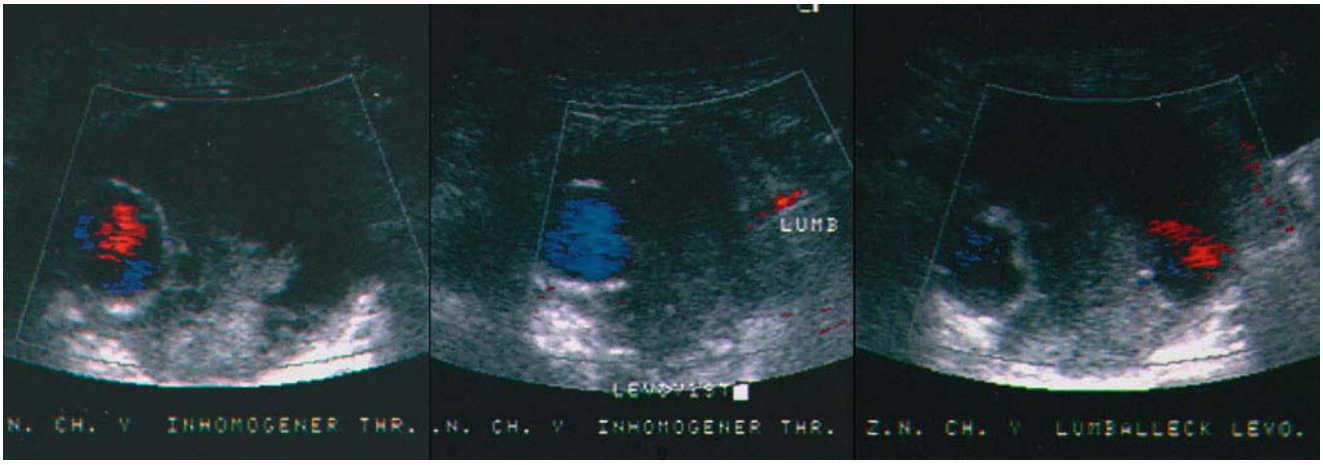

Fig. A 6.30 (courtesy of P. Heilberger)
Visualization of endoleak with echo enhancer
Patent stent in a hypoechoic aneurysm with an increase in size at follow-up. No flow signals are obtained from the aneurysmal sac without contrast medium (*left section*)

One minute after administration of an echo enhancer (Levovist), leakage is visualized on the left side of the aneurysm with red-coded flow from a lumbar artery (*middle section*)

The scan on the *right* shows good visualization of the type II endoleak due to retrograde flow in the patent lumbar artery (depicted in red at the right margin) 3 min after echo enhancer administration

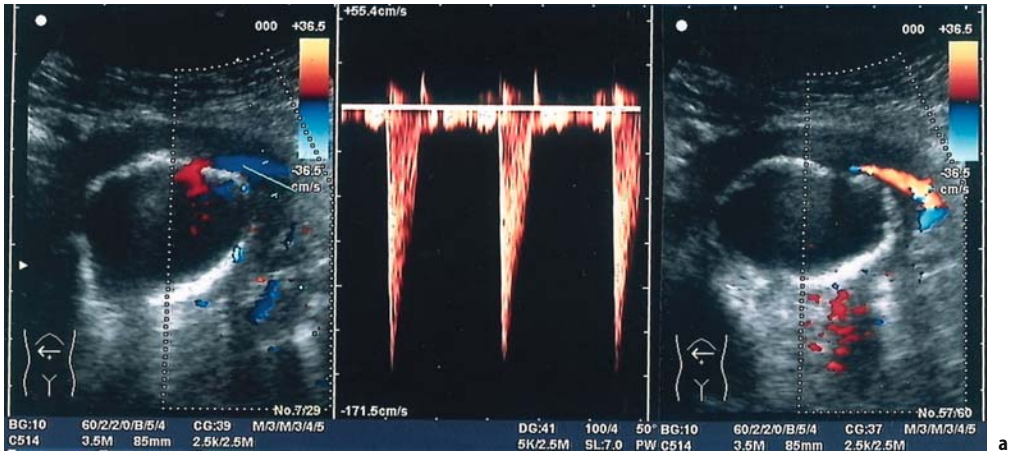

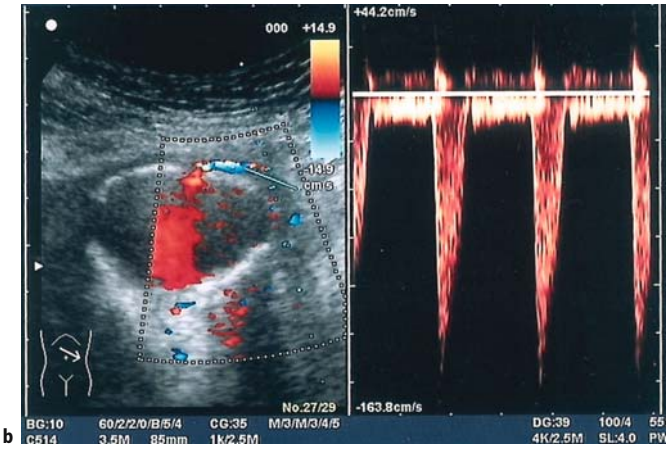

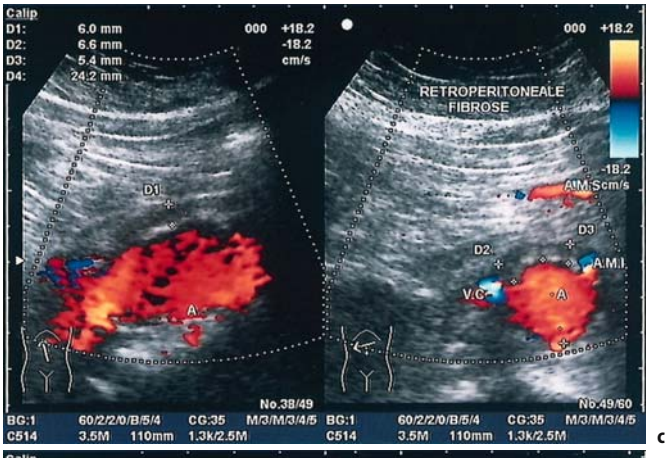

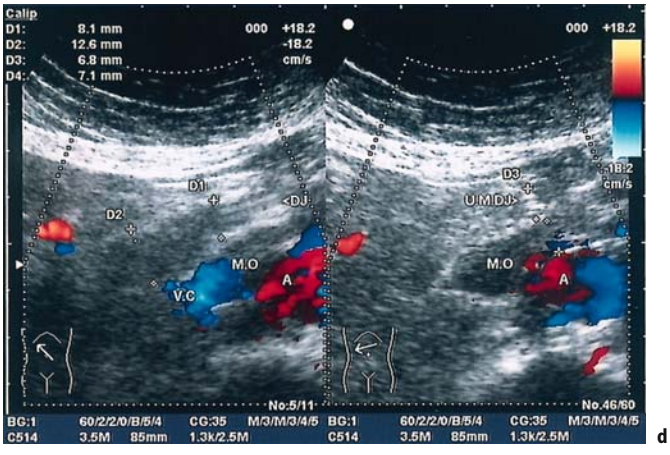

Fig. A 6.31 a–h
Retroperitoneal fibrosis, aortitis, inflammatory aortic aneurysm

a Retroperitoneal fibrosis in Ormond's disease may be visualized as a hypoechoic cap-like structure anterior to the aorta. This condition differs from aortitis and inflammatory aortic aneurysm in that the process also involves the vena cava, which is ensheathed by fibrotic tissue. The origin and proximal course of the inferior mesenteric artery are evaluated to establish the differential diagnosis. In the presence of retroperitoneal fibrosis, the mesenteric artery, after arising from the left lateral aspect of the aorta, is pushed against the aortic wall where it runs for some centimeters before piercing through the hypoechoic fibrotic layer and continuing its intra-abdominal course in the mesentery. The scan on the *left* depicts the inferior mesenteric artery arising from the aortic wall and the hypoechoic cap above. The scan on the *right* obtained in slightly oblique orientation documents the course of the inferior mesenteric artery with flow displayed in blue (away from transducer). It is pushed against the aortic wall by the hypoechoic structure. The *middle section* shows the corresponding Doppler waveform

b After a few months of cortisone therapy, the hypoechoic cap around the aorta and vena cava has markedly decreased in thickness, from 1 cm (cf. **a**) to 4 mm in the B-mode image, but the fibrotic tissue still pushes the inferior mesenteric artery against the aorta and its course remains unchanged. The Doppler spectrum sampled in the inferior mesenteric artery is presented on the *right*. Unchanged aneurysmal dilatation of the aorta with a diameter of 3.2 cm (not measured from the oblique scan shown, which was obtained for optimal evaluation of the superior mesenteric artery but is not suitable for diameter measurement because the aorta is sectioned obliquely)

Retroperitoneal fibrosis – vena cava compression

c Mild residual retroperitoneal fibrosis after therapy. The images illustrate the involvement of the vena cava, which is important for the differential diagnosis. The hypoechoic cap-like structure (marked with plus signs, 6 mm thick) covers the aorta and vena cava (*V.C*, with aliasing due to compression) at the level of the origin of the inferior mesenteric artery (*A.M.I*)

Retroperitoneal fibrosis with compression of ureter

d Another complication of retroperitoneal fibrosis is urinary tract obstruction with retention of urine. In the case shown, the slightly ectopic right ureter takes a more medial course overcrossing the aorta shortly before the bifurcation and is congested despite only mild ret-

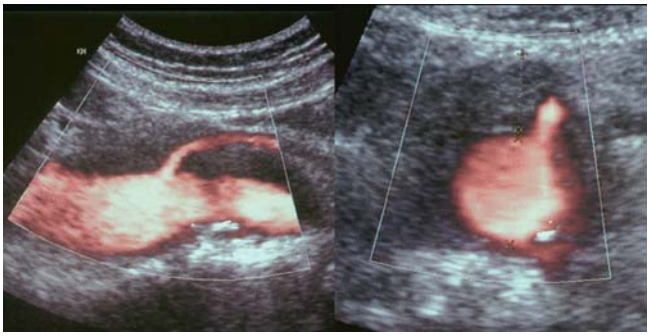

e

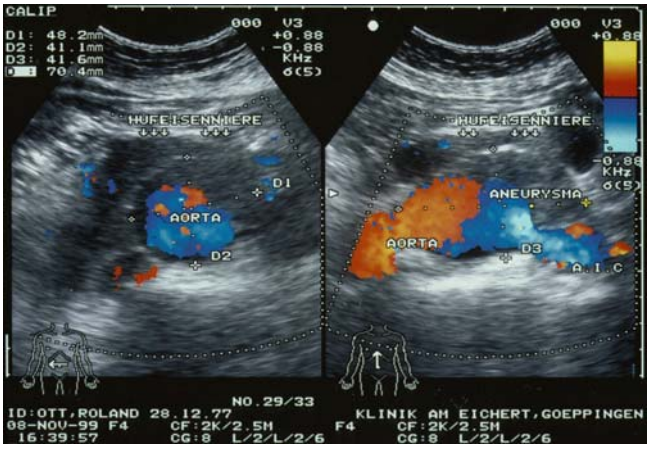

g

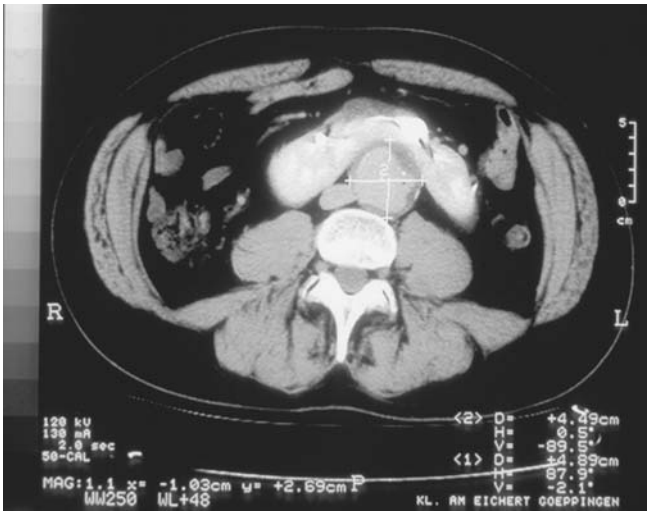

h

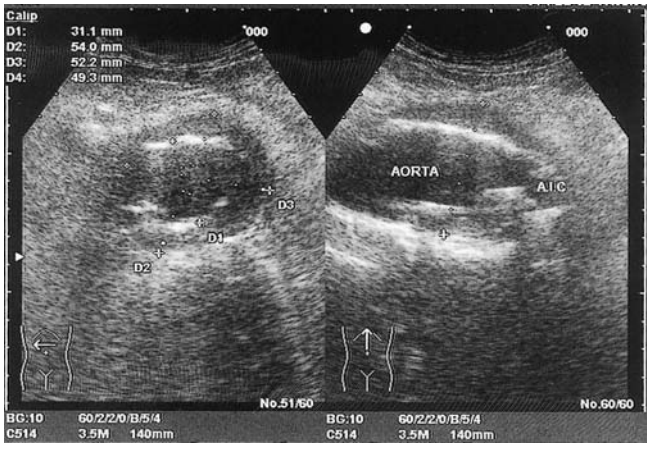

f

(Fig. A 6.31 cont.)
roperitoneal fibrosis. The oblique scan on the *left* depicts the dilated ureter (marked with *plus signs*; diameter of 12.6 mm at *D2*) with an indwelling double-J catheter (*DJ*, at level of *D1*). The *right section* depicts the ureter (marked with *plus signs*, *D3*) with the double reflection of the double-J catheter (*UMDJ*) medial to the transversely cut aorta (*A*). The residual fibrosis of Ormond's disease (*M.O*) is depicted as a hypoechoic para-aortic structure

e Aortic wall thickening in giant cell arteritis (longitudinal scan on the *left*, transverse scan on the *right*; scanning in the power mode). The course of the inferior mesenteric artery at its origin confirms the aortic wall process as the artery pierces the thickened wall directly at its origin without first coursing close to the aortic wall as in fibrosis. (Courtesy of K. Amendt)

f Transverse scan (*left*) and longitudinal scan (*right*) showing the typical appearance of an inflammatory aortic aneurysm. The aneurysm has a luminal diameter of 3.5 cm and exhibits atherosclerotic wall changes. The concentric hypoechoic layer (1 cm) around the aneurysm confirms the inflammatory origin of the aneurysm

Horseshoe kidney

g A horseshoe kidney is seen as a hypoechoic structure (cap) extending over the distal aorta. In the presence of a concomitant aortic aneurysm as in this case, the abnormal kidney must be sonomorphologically differentiated from the aortic wall as well as from other retroperitoneal structures or contained rupture of the aneurysm

h CT of the patient in **g** demonstrating the abdominal aortic aneurysm and the horseshoe kidney

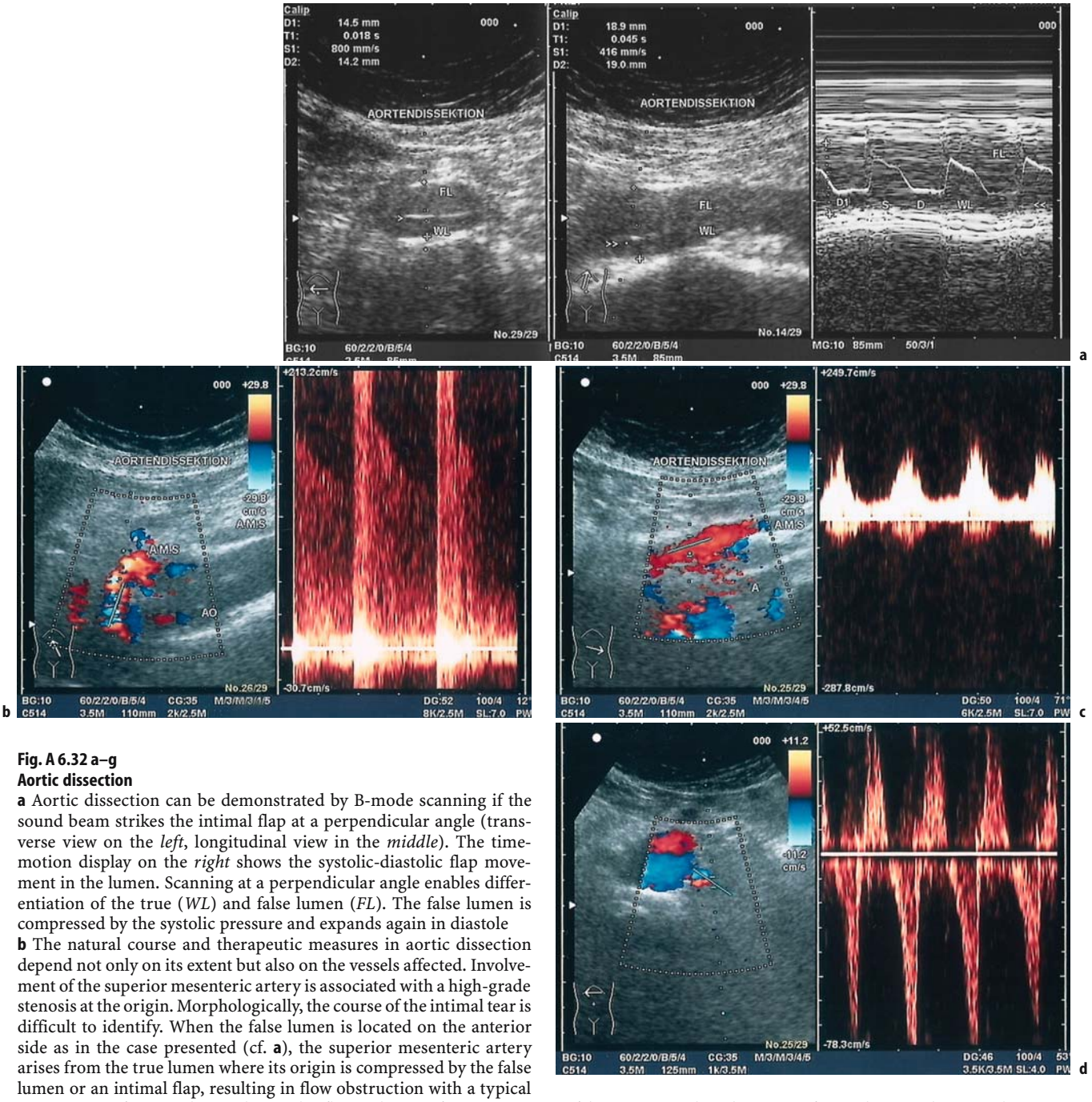

Fig. A 6.32 a–g
Aortic dissection

a Aortic dissection can be demonstrated by B-mode scanning if the sound beam strikes the intimal flap at a perpendicular angle (transverse view on the *left*, longitudinal view in the *middle*). The time-motion display on the *right* shows the systolic-diastolic flap movement in the lumen. Scanning at a perpendicular angle enables differentiation of the true (*WL*) and false lumen (*FL*). The false lumen is compressed by the systolic pressure and expands again in diastole

b The natural course and therapeutic measures in aortic dissection depend not only on its extent but also on the vessels affected. Involvement of the superior mesenteric artery is associated with a high-grade stenosis at the origin. Morphologically, the course of the intimal tear is difficult to identify. When the false lumen is located on the anterior side as in the case presented (cf. **a**), the superior mesenteric artery arises from the true lumen where its origin is compressed by the false lumen or an intimal flap, resulting in flow obstruction with a typical stenosis waveform and a peak systolic flow velocity of over 3 m/s (interpolation due to aliasing)

c Poststenotic Doppler waveform with the typical delay in systolic increase, turbulent flow, and a larger diastolic component. The color flow scan shows the aorta (*A*) with the flap away from the transducer

d If dissection involves the origin of a renal artery, there may be superimposition of the Doppler frequency spectra from the true and false lumina or – depending on the re-entry site or the position of the sample volume in the dissected segment – to-and-fro flow as in the left renal artery shown

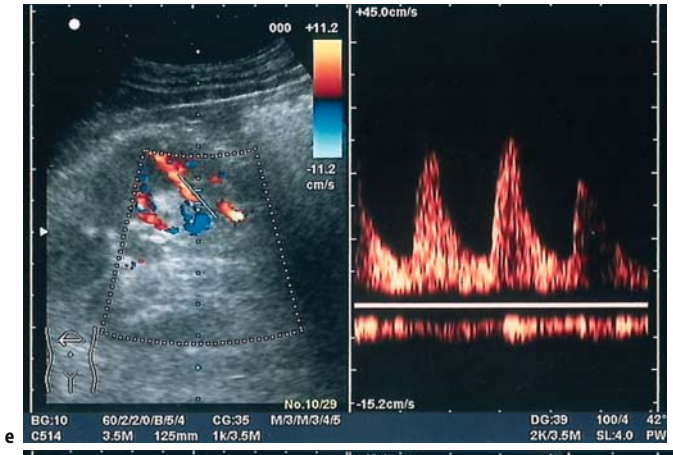

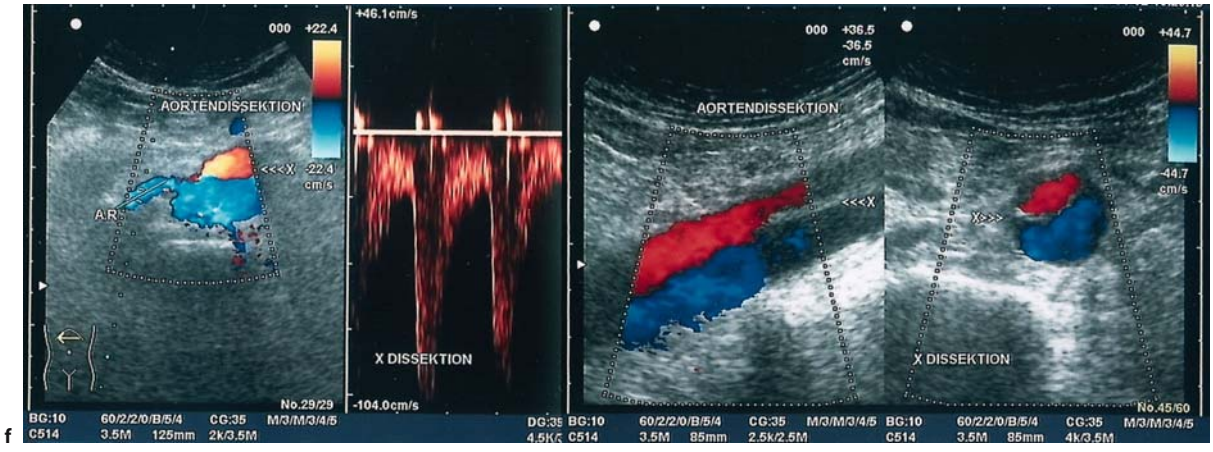

(Fig. A 6.32 cont.)
e The waveform from a segmental artery in the left renal hilum demonstrates the typical postocclusive flow pattern with a reduced systolic upstroke and low peak systolic velocity due to flow obstruction by the dissection
f The right renal artery is not involved in the dissection and has a typical monophasic waveform with a peak systolic flow velocity of 1 m/s. The further infrarenal course of the aortic dissection is shown in longitudinal (*right center*) and transverse planes (*rightmost*). The change in the color coding may be due to the position of the re-entry site or physiologic flow reversal (early diastolic reflux)

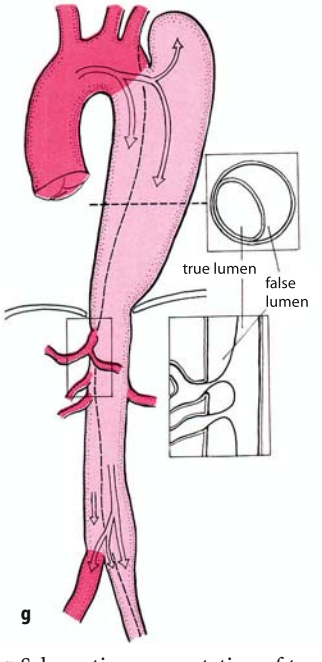

g Schematic representation of type III aortic dissection according to De Bakey (corresponding to **b** and **c**). The mesenteric vessels arising from the true lumen are compressed by the false lumen or the intimal flap. (From Heberer and van Dongen 1993)

▷
Fig. A 6.33 a–g
Aortic dissection
a Blood flow to the renal arteries is a crucial issue in the diagnostic evaluation of aortic dissection. At the level of the renal arteries (*left section*), both lumina of the dissected aorta exhibit antegrade flow and the left renal artery (*A.REN.LI*) is displayed with blue-coded flow. The scan on the *right* obtained 5 cm below clearly depicts the flap between the two lumina. The overall diameter is dilated to 42 mm due to aneurysmal changes
b CT scan of dissected aortic aneurysm with visualization of the intimal flap
c The second important diagnostic task in aortic dissection is to determine the relationship to the origins of the iliac arteries. Here, the dilated and dissected aorta with thrombotic wall deposits gives off the common iliac artery (*A.I.C*) on the right side and the dissected aneurysm (*A*) extends into the left common iliac artery. The gray-scale scan (*left section*) depicts the flap and the thrombotic portion while the color duplex scan (*right section*) shows the perfused lumina
d Aortic dissection as in the preceding example but with red-coded flow in the true lumen and blue-coded, retrograde flow in the false lumen. The scan on the *left* fails to depict the intimal flap about 3 cm below the origins of the renal arteries

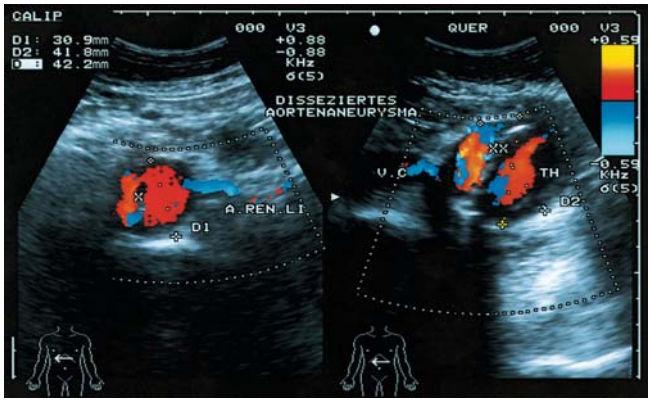

a

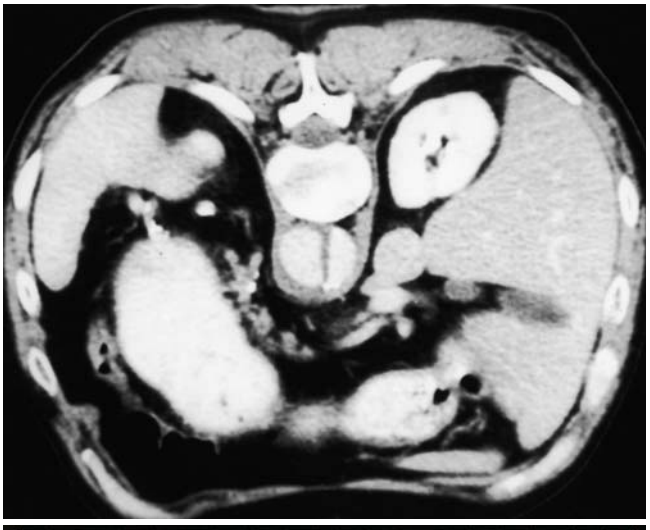

b

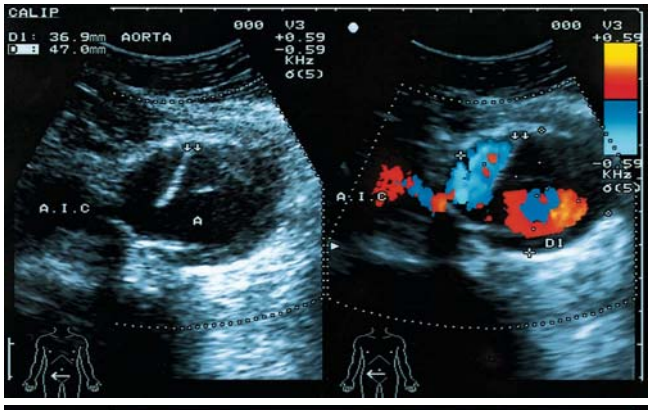

c

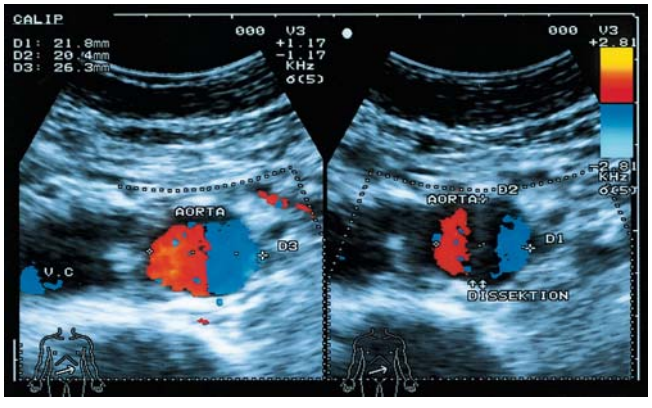

d

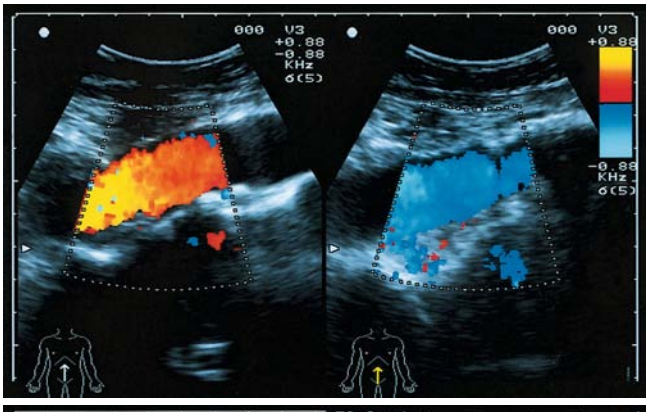

e

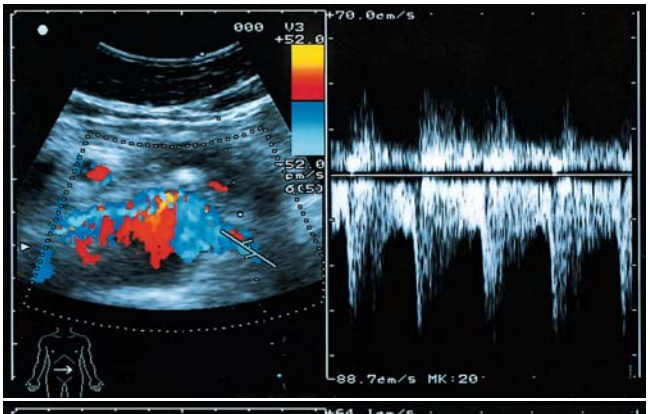

f

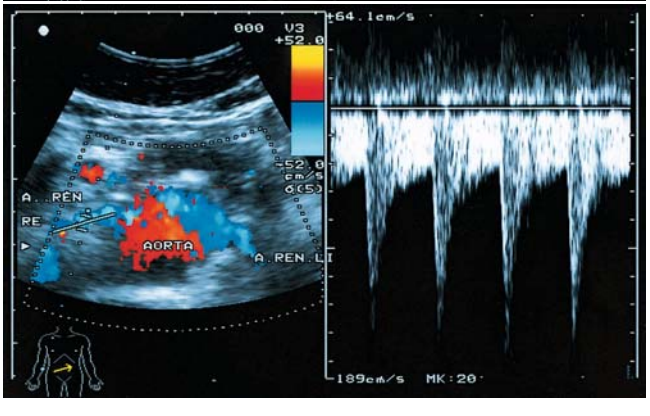

g

(Fig. A 6.33 cont.)
The scan on the *right* demonstrates partial thrombosis of the false lumen just above the bifurcation. This constellation reflects the status post surgery with closure of the thoracic entry

e Following closure of the thoracic entry, the false lumen supplying the renal artery is filled retrogradely through the abdominal re-entry. The longitudinal scan (*right section*) demonstrates forward, red-coded flow in the true lumen and retrograde, blue flow in the false lumen (transducer moved to the left side)

f Patency of the false lumen is maintained through the outflow of blood into the left renal artery arising from it. The false lumen and the left renal artery are depicted with flow coded in blue. Spectral analysis demonstrates decreased flow with a peak systolic velocity of 60 cm/s in the left renal artery compared to the contralateral side

g The true lumen (red) gives off the blue-coded right renal artery, which arises from the posterior aspect and has a peak systolic flow velocity of 165 cm/s and an end-diastolic velocity of 45 cm/s

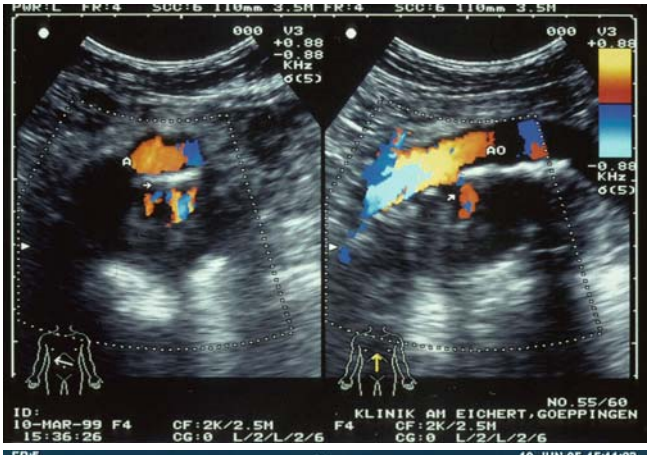

a

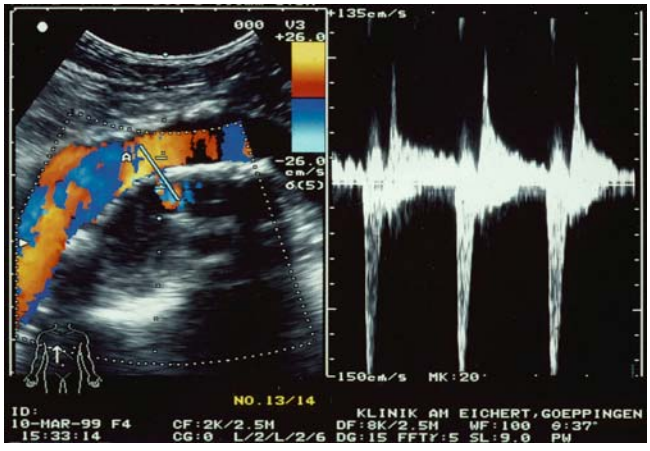

b

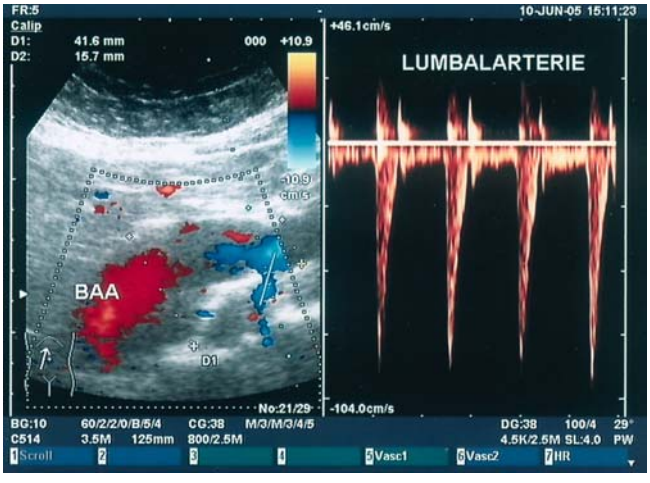

c

Fig. A 6.34 a, b
Aortic perforation
a Diagnostic evaluation of suspected perforations in the abdomen and pelvis may be impaired by a poor insonation window or the occurrence of artifacts. Color duplex scanning is useful for demonstrating leakage but the high susceptibility to artifacts in abdominal scanning makes it necessary to always confirm the color flow findings by spectral analysis. In the example, color duplex scanning of a patient presenting with back pain identifies a leak in the posterior aortic wall with color-coded flow signals distal to it. Alternatively, these signals may represent mirror artifacts caused by the strong reflection of the aortic wall
b The Doppler spectrum (*right section*) obtained from this area confirms the perforation by demonstrating to-and-fro flow (systolic influx with reflux throughout diastole), as it is also typical of false aneurysms

c Differential diagnosis: aortic perforation – lumbar artery
Dorsocaudal of a 41-mm infrarenal aortic aneurysm (*BAA*) a hypoechoic area is depicted adjacent to the aortic bifurcation (differential diagnosis: hematoma – retroperitoneal fibrosis – inflammatory vascular disease). As in **b** above, color flow imaging depicts blood flow signals coming out of the aorta (blue with sample volume) and passing the hypoechoic area (cf. Fig. A 6.31 a-h). However, the Doppler spectrum (*right section*) shows the typical waveform of a lumbar artery. The Doppler waveform thus excludes contained aortic perforation with typical to-and-fro flow as in example **b**. The lumen of the aorta is marked (41.6 mm in the aneurysm and 15.7 mm distal to it)

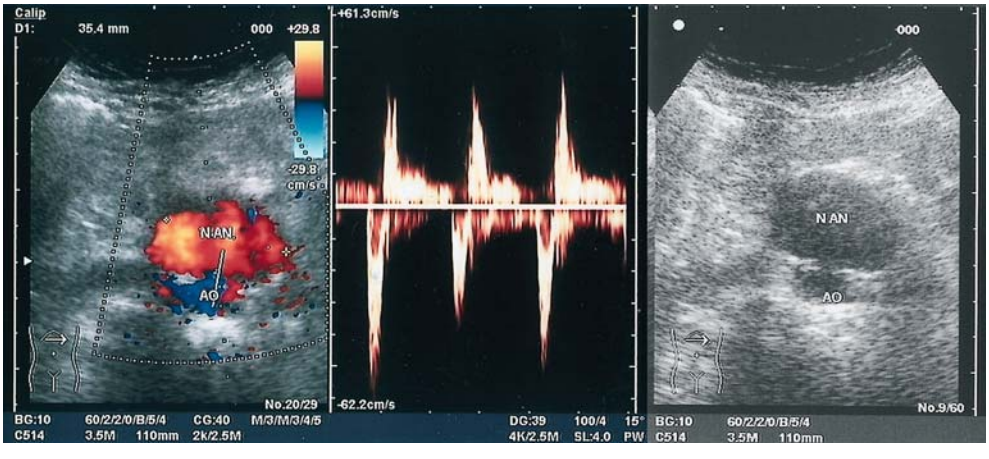

a

Fig. A 6.35 a–c: Suture aneurysm after placement of aortic prosthesis
a Sonographic follow-up after implantation of an aortic prosthesis (e.g. for aneurysm) is indicated at 6-month intervals because suture aneuryms, in particular at the superior anastomosis (*N.AN*), can cause life-threatening complications with possible perforation into the duodenum if they are not revised in time. The anastomoses are evaluated in longitudinal and transverse planes for the presence of hypoechoic mushroom-like structures indicating a contained perforation or suture aneurysm. A false aneurysm is indicated by color-coded flow signals originating from the anastomotic site and is confirmed by the typical Doppler waveform recorded near the wall

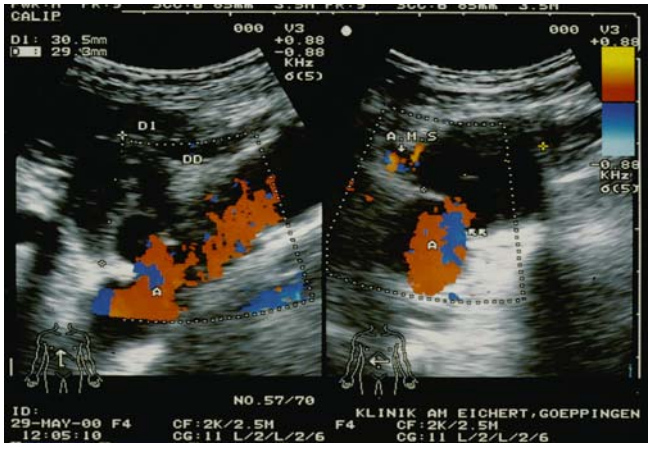

b

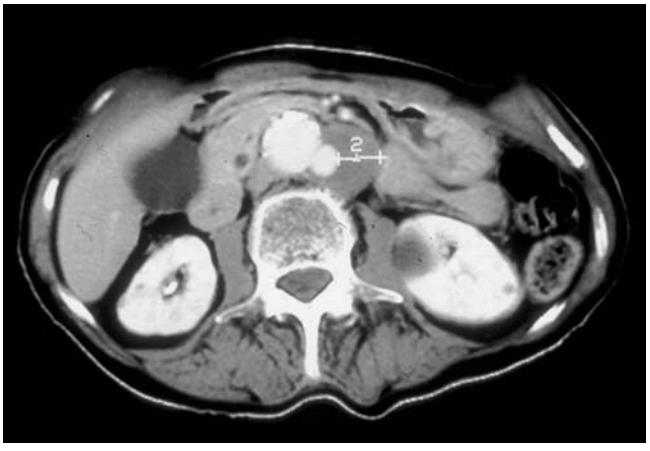

(Fig. A 6.35 cont.) b With progressive thrombosis, the color-coded area becomes smaller and the aneurysm is more difficult to differentiate from other hypoechoic perivascular structures. In this setting, a suture aneurysm is suggested by a color-coded area extending beyond the wall directly next to the suture line (*arrow*)

c CT confirming the suture aneurysm with nearly complete thrombosis (*2*)

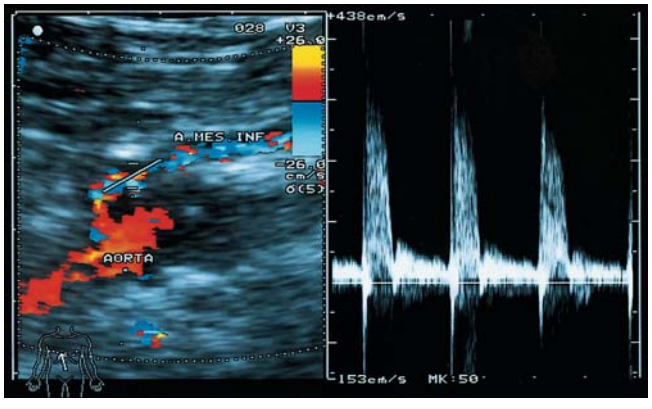

a

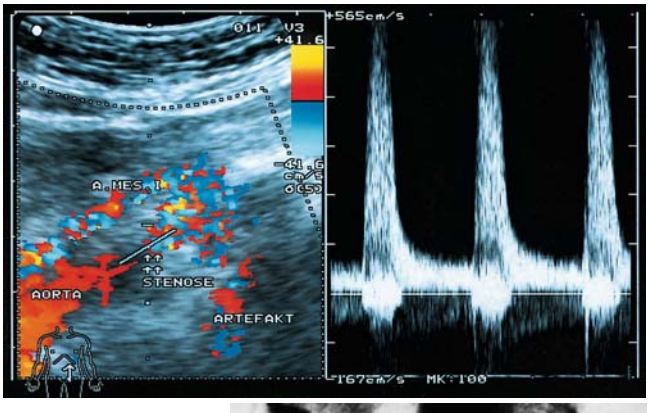

b

Fig. A 6.36 a–c
Collateralization of aortic stenosis
Aortic stenoses preferably involve the distal aorta including the bifurcation and the origins of the iliac arteries

a Mesenteric arteries serving as collaterals may exhibit criteria of stenosis in the color duplex scan and Doppler waveform although they are patent. In the example, color duplex scanning depicts turbulent flow with aliasing as a sign of accelerated flow in the inferior mesenteric artery (*A.MES.INF*), which collateralizes a stenosis in the aorta just distal to the origin of the inferior mesenteric. The Doppler spectrum shows peak systolic flow velocity to be increased to 300 cm/s

b When the transducer is rotated, the aorta (cf. **a**) comes to lie behind the inferior mesenteric artery (*A.MES.I*). There is acoustic shadowing due to plaques with partial elimination of the color signals but the stenosis is indicated by aliasing and perivascular vibration artifacts (mosaic-like color pattern). The artifacts continue posterior to the aorta. At the left margin, the inferior mesenteric artery passes through the aortic bifurcation and leaves the scanning plane. Due to stenosis, the peak systolic flow velocity in the aorta is increased to 570 cm/s with pronounced turbulence in the Doppler waveform

The origin of the inferior mesenteric artery is located at the *left margin* of the image but is obscured by the perivascular vibration artifacts caused by the aortic stenosis seen in the *middle* of the scan

c Angiography showing stenosis of the distal aorta with stenosis of the origin of the left common iliac artery and occlusion of the right common iliac artery. The large-caliber inferior mesenteric artery provides collateral flow via branches of the internal iliac artery

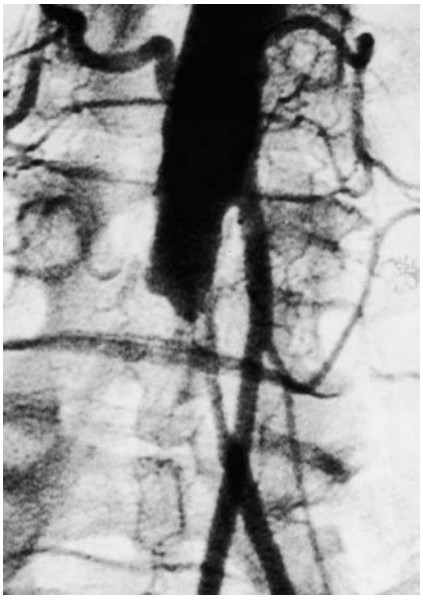

c

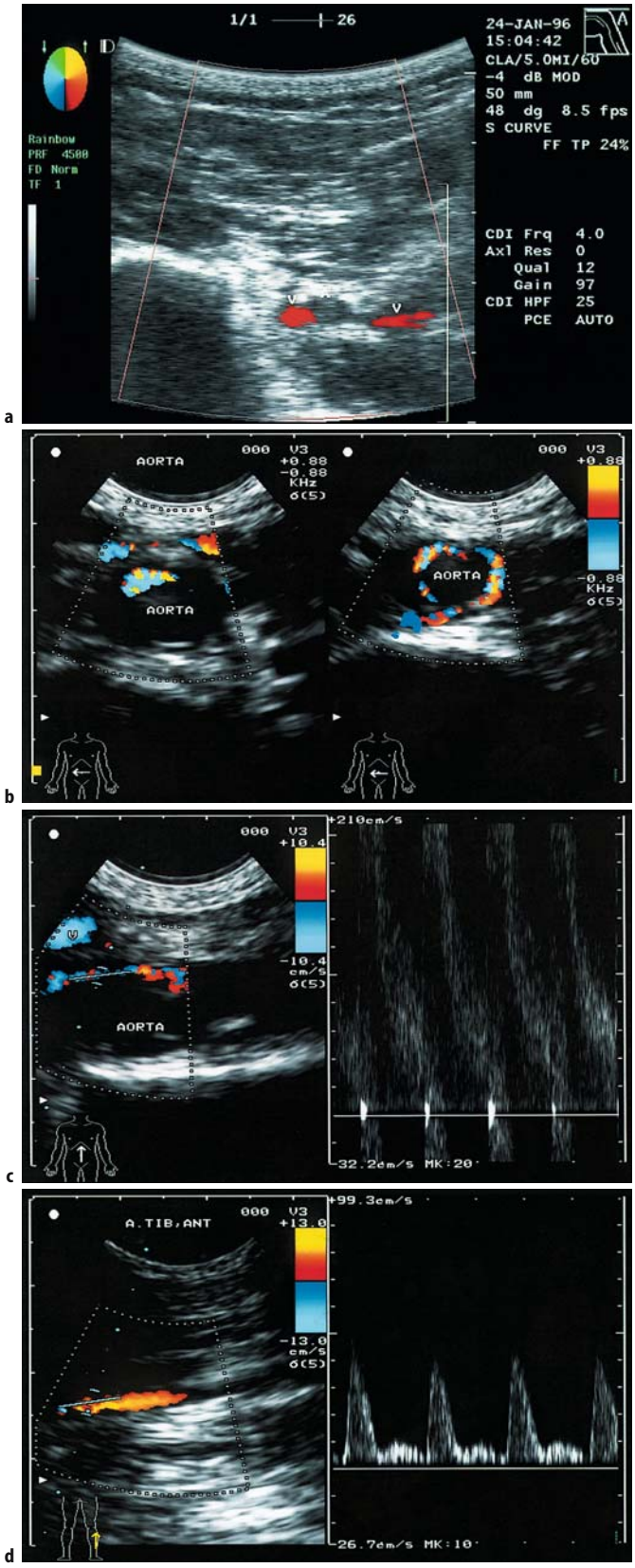

Fig. A 6.37 a–g
Aortic thrombus (thrombolysis) – aortic stenosis

a 35-year-old woman presenting with very severe acute pain of the feet and calves due to bilateral occlusion of the lower leg arteries. For illustration, the occlusion of the anterior tibial artery is presented in transverse orientation. The artery blocked by a hypoechoic thromboembolus exhibits no flow while there is flow coded in red in the anterior tibial vein (*V*) to the right and to the left. The acoustic shadow to the left of the tibial vein is caused by the fibula

b In this case, the embolic occlusion of the lower leg arteries is due to a thrombus in the distal aorta, just before the bifurcation. The transverse scan (*left*) depicts the thrombus 4 cm above the bifurcation. It is attached to the wall posteriorly with flow being confined to its anterior aspect (blue with aliasing)

The *right section* depicts the hypoechoic thrombus in the aorta shortly before the bifurcation surrounded by flow with turbulent and high-frequency components on all sides

c The longitudinal scan shows the thrombus occupying most of the aortic lumen with some residual flow anteriorly. The Doppler spectrum demonstrates pronounced flow acceleration with an end-diastolic velocity of 50 cm/s and a systolic velocity of 210 cm/s (aliasing); the waveform is monophasic. (Only the proximal segment of the aorta is depicted with color coding due to the small color box used)

d On the basis of the duplex findings obtained in this patient, angiography of the aorta was dispensed with because the manipulations might have triggered further distal embolism. Instead, bilateral intra-arterial thrombolytic therapy was initiated, which led to resolution of the thromboemboli in the lower leg arteries, as illustrated by the Doppler spectrum from the recanalized anterior tibial artery. The spectrum still shows abnormally increased diastolic flow, which is due to residual stenosis of the aorta and reactive hyperemia

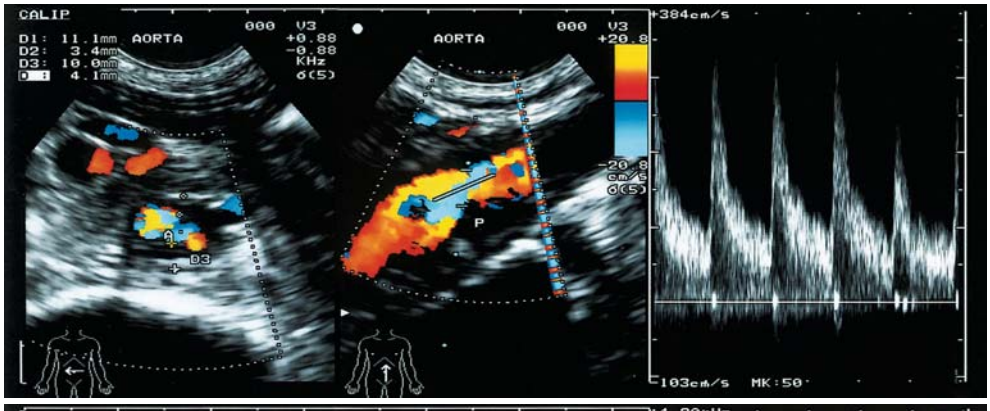

e

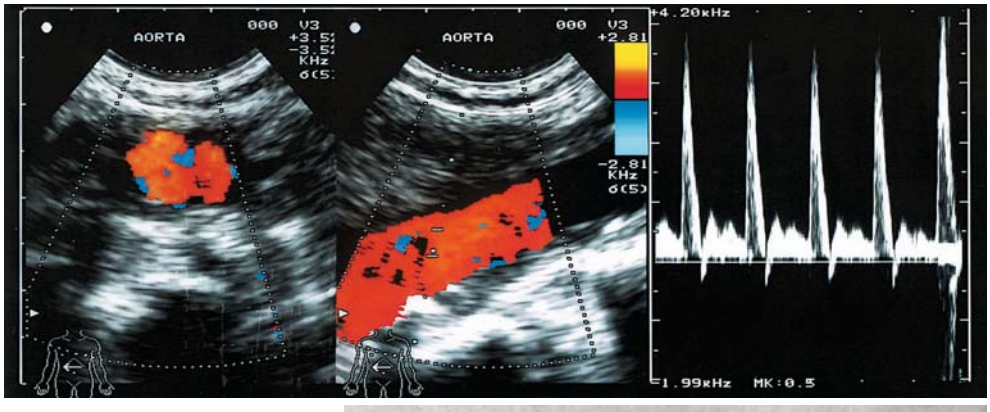

f

(Fig. A 6.37 cont.)

e Local thrombolytic therapy also had a systemic effect resulting in dissolution of the thrombus in the aorta. The transverse scan (*left section*) and longitudinal scan (*middle section*) still depict residual marginal thrombotic deposits. The color coding shows the patent lumen with aliasing (yellow – light blue) due to the residual stenosis. The Doppler spectrum indicates a high-grade residual stenosis with a peak systolic flow of 300 cm/s and a monophasic flow profile

f The patient refused further therapy. Follow-up 2 weeks later demonstrated autolysis of the residual thrombus in the distal aorta. The longitudinal scan (*middle section*) shows a hyperechoic posterior plaque and some residual, hypoechoic thrombotic deposits on the left wall with little luminal narrowing. Neither the Doppler spectrum nor color duplex scanning demonstrate a hemodynamically significant stenosis

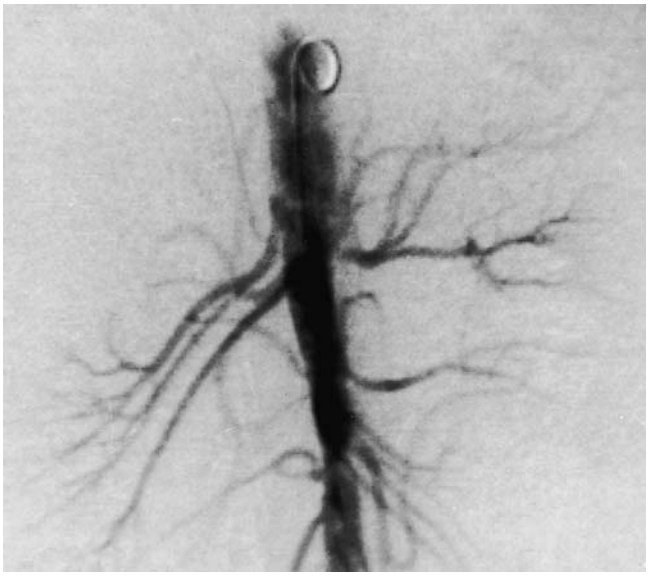

g

g Angiography confirms the residual stenosis of the distal aorta but with a lumen reduction $< 50\,\%$ (cf. **f**)

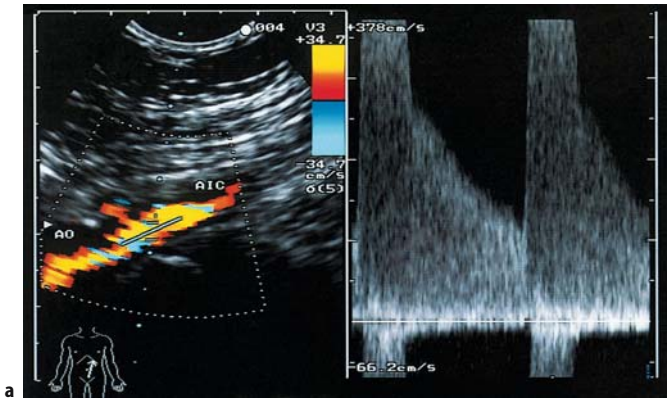

a

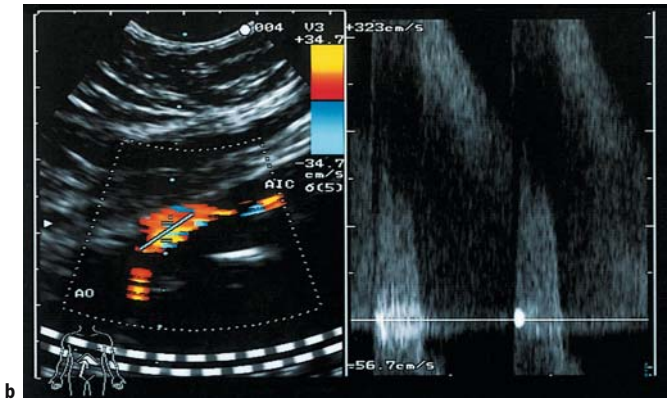

b

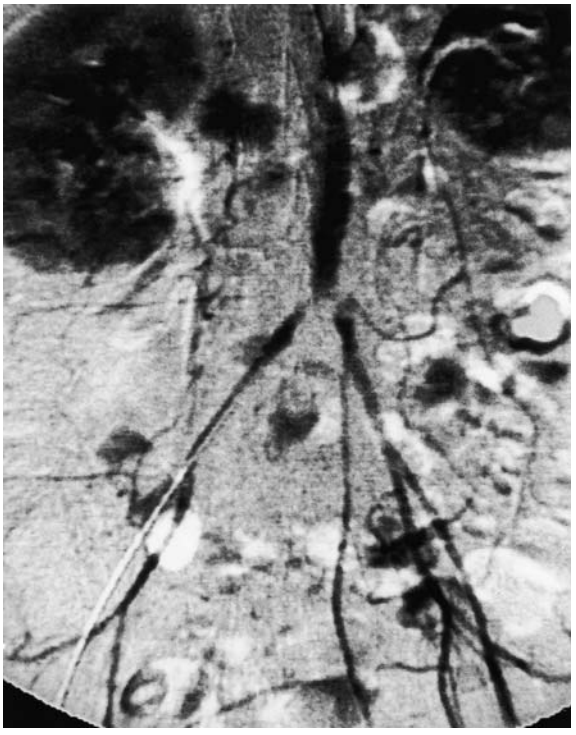

c

Fig. A 6.38 a–c
Stenosis of aortic bifurcation
a High-grade stenosis at the junction of the aorta (*AO*) with the common iliac artery (*AIC*) on the left, demonstrated by aliasing in the color duplex scan and flow acceleration with an end-diastolic velocity of 120 cm/s and a systolic velocity of over 370 cm/s (aliasing). The flow profile is monophasic
b (Color) duplex scanning demonstrates an additional high-grade stenosis at the origin of the common iliac artery on the right (aliasing)
c Angiography: High-grade stenosis of the aortic bifurcation

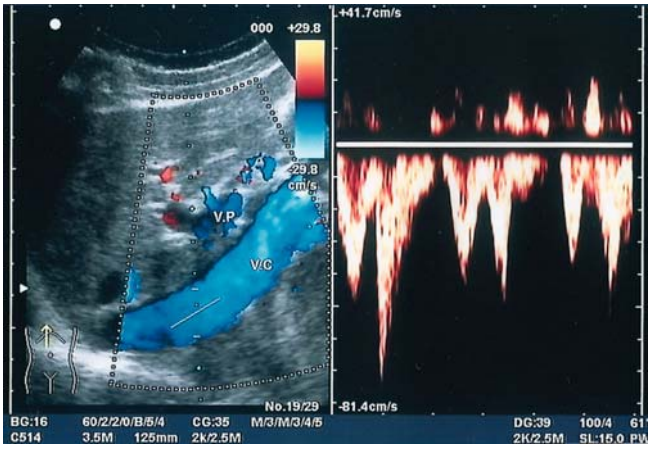

Fig. A 6.39
Vena cava
The cross-sectional area and blood flow velocity of the vena cava (*V.C*) vary with respiration. Flow is markedly faster during inspiration. In addition, the flow is subject to cardiac (atrial) modulation. The Doppler waveform typically shows two peaks, one during systole and the other upon opening of the atrioventricular valves. There is pronounced reduction, cessation, or even a short reversal of flow during atrial contraction

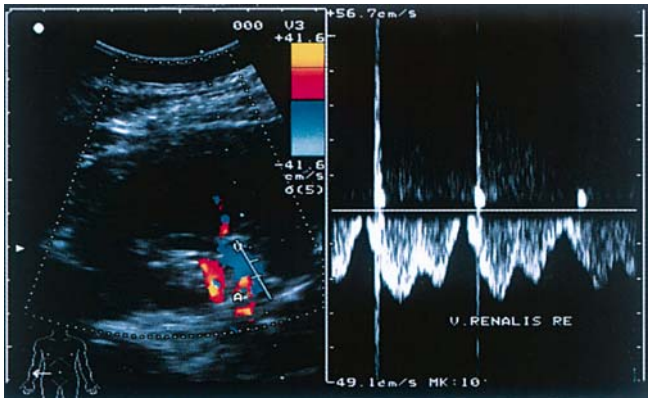

a

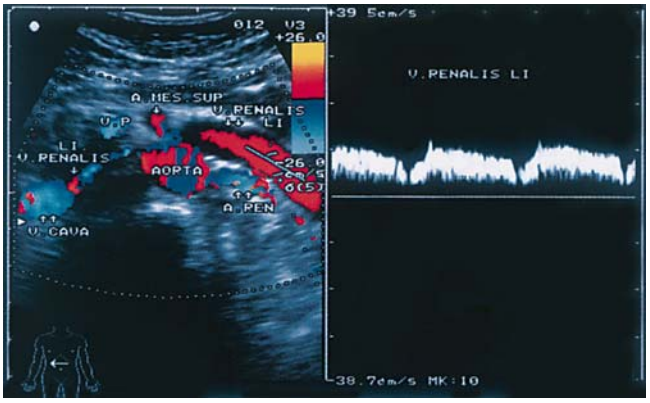

b

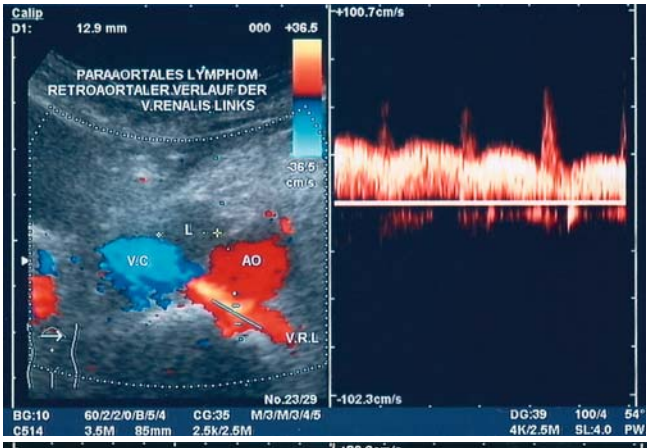

c

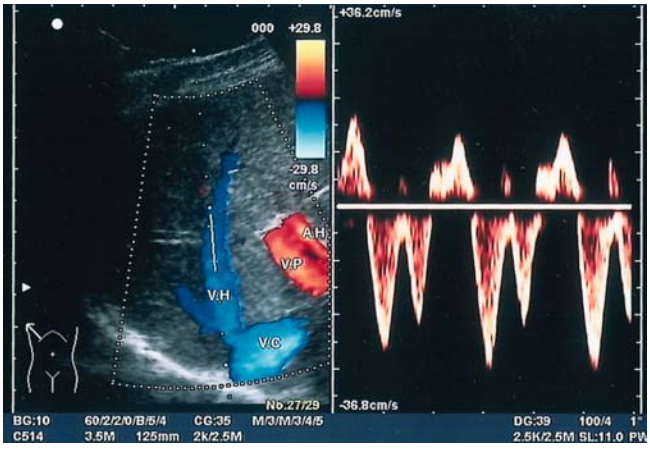

d

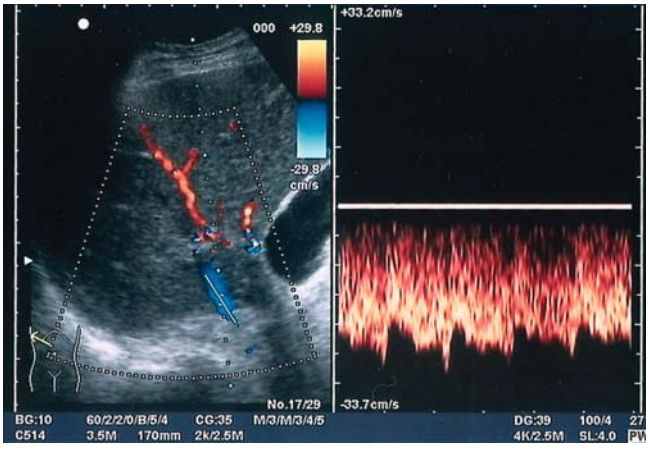

e

Fig. A 6.40 a–f
Right renal vein
a Cardiac and respiratory modulation of flow are transmitted as far as the right renal vein at the hilum (vein: blue, segmental artery: red)

Left renal vein
b Cardiac pulsatility is typically lost in the left renal vein due to the narrow passage between the superior mesenteric artery and aorta. Instead, its flow variation is determined by the aortic pulse. Posterior to the red-coded renal vein, the renal artery is depicted in blue. The blue-coded renal vein has a rather large caliber in front of the narrow passage and then continues as a relatively thin vessel to the vena cava

Retroaortic left renal vein
c If the left renal vein (*V.R.L*; red, flow toward transducer) is not identified between the aorta and superior mesenteric artery, the examiner must try and locate its opening into the vena cava (*V.C*) posterior to the aorta (*AO*). Identification of a retroaortic left renal vein is important prior to resection of an aortic aneurysm but is often an incidental finding, as in the case presented, where the atypical opening was identified in a patient in whom vascular sonography was performed prior to ultrasound-guided biopsy of a lymphoma (*L*)

Doppler waveform of hepatic veins
d W-shaped Doppler waveform with a first hepatofugal flow peak in systole, a second hepatofugal peak upon opening of the atrioventricular valves, and hepatopedal flow during atrial contraction. An abnormal spectrum resembling a sinus wave with to-and-fro flow in the extreme case is seen in patients with right ventricular failure

Abnormal waveform of hepatic veins in liver cirrhosis
e The right liver vein in a patient with Child A liver cirrhosis scanned from the intercostal approach shows only residual cardiac pulsatility. The rigidity of the liver parenchyma primarily prevents the decrease in flow velocity during atrial contraction, resulting in an increasingly band-like spectrum from the opening into the vena cava to peripheral branches (intermediate hepatic vein in blue, portal vein branch in red)

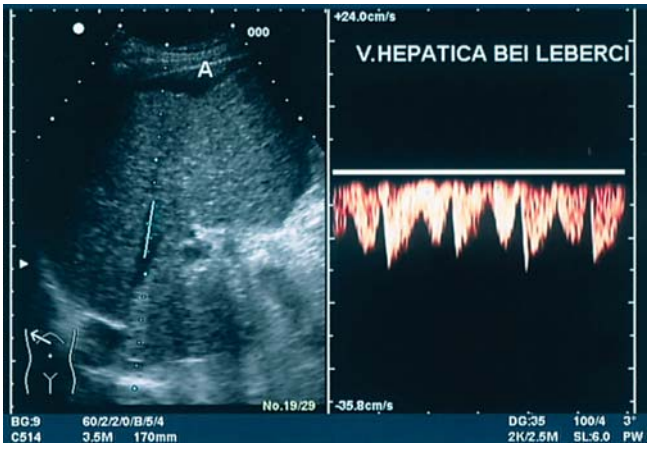

f

(Fig. A 6.40 cont.)
Waveform of hepatic vein in liver cirrhosis
f Nearly continous flow profile of the hepatic vein in liver cirrhosis (transducer in flank position) with less cardiac modulation. Though the curve is flattened due to the rigidity of the liver tissue, some residual cardiac pulsatility is still present, and the curve is not yet as flat as in **e** (*A* ascites)

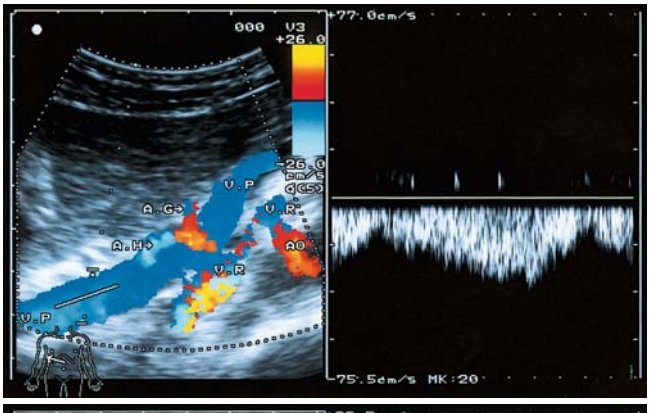

a

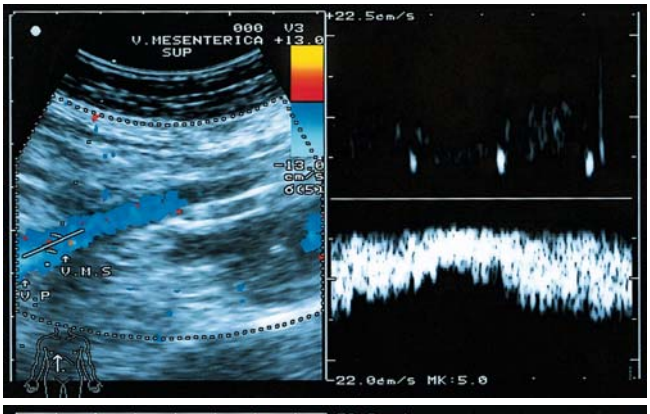

b

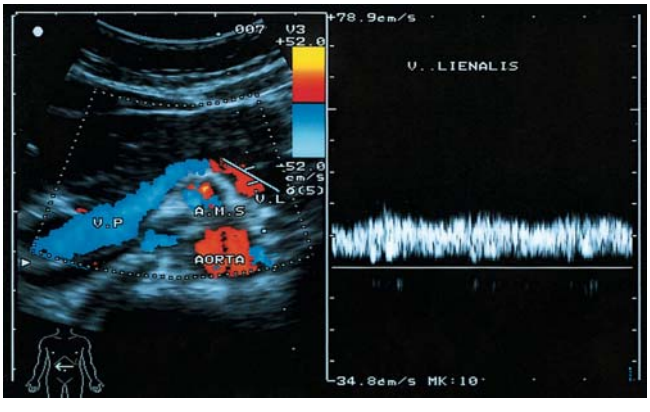

c

Fig. A 6.41 a–c
Portal vein and its tributaries
a The Doppler spectrum from the portal vein is characterized by relatively wide variation in flow velocity but flow is typically hepatocentral and slower in inspiration than in expiration
b The inspiratory and expiratory variation in blood flow velocity continues into the superior mesenteric vein, which is depicted to the right of the superior mesenteric artery
c The splenic vein (*V.L*) is depicted at the lower edge of the pancreas with flow in red. It crosses over the root of the superior mesenteric artery (*A.M.S*) to enter (displayed in blue) the portal vein (*V.P*). The respiratory variation in flow velocity may continue into the splenic vein

Fig. A 6.42 a–c
Mesenteric vein thrombosis

a The clinical manifestation of mesenteric vein thrombosis depends on the extent of thrombosis and may range from fairly unspecific symptoms to an acute abdomen with intestinal necrosis. In the example, a venous flow signal is obtained from the junction of the superior mesenteric artery with the portal vein depicted near the left margin of the gray-scale scan

b The longitudinal and transverse scans demonstrate occluding thrombosis (*TH*) of the superior mesenteric vein (*VMS*) that extends to its opening into the portal vein. The transverse scan (*left section*) depicts the superior mesenteric artery (*AMS*) adjacent to the occluded vein

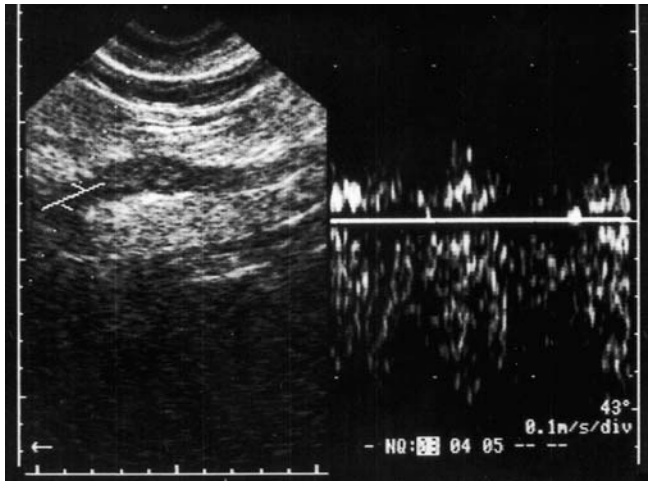

a

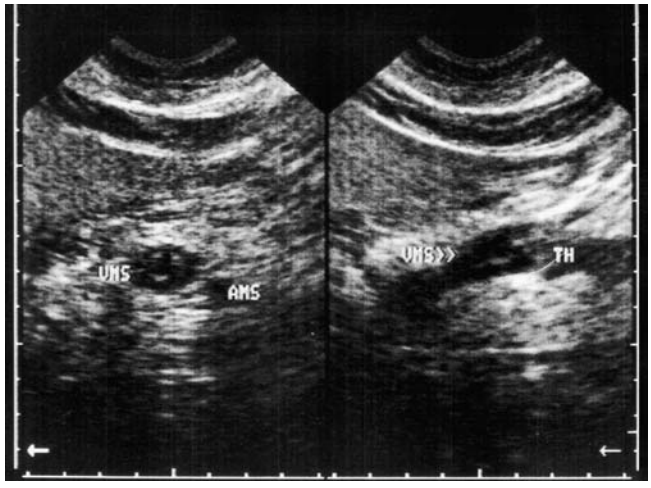

b

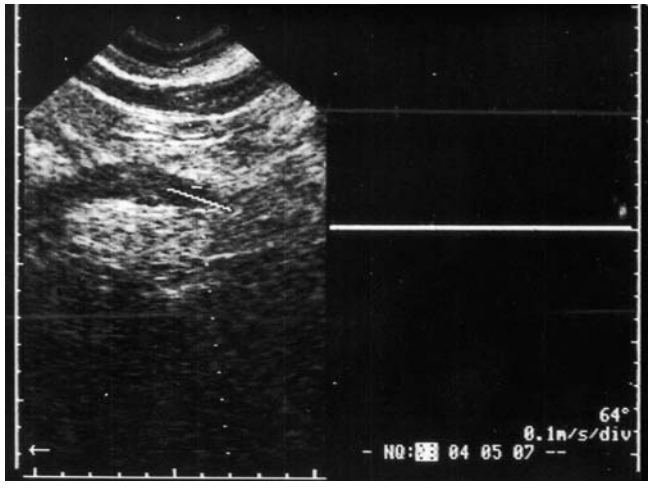

c

c The Doppler frequency spectrum obtained from the mesenteric vein in longitudinal orientation shows zero flow

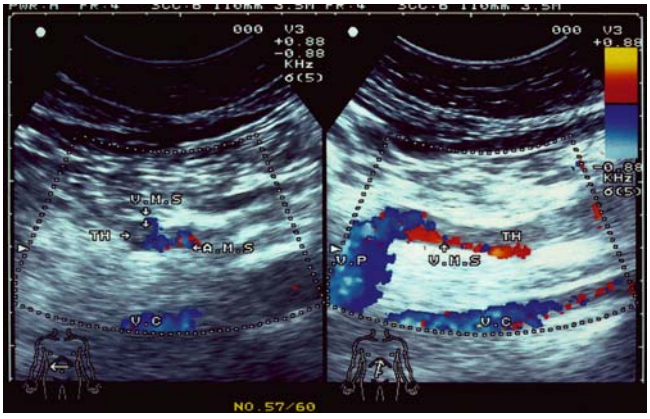

a

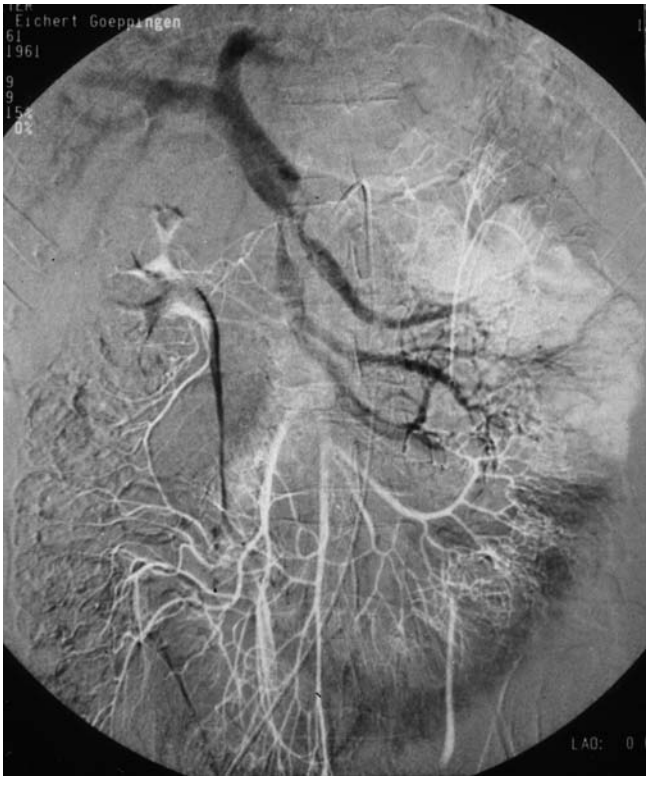

b

Fig. A 6.43 a, b
Mesenteric vein thrombosis
a The extent of thrombosis and collateralization determines whether the clinical manifestation will be mild with flu-like symptoms or severe with an acute abdomen due to intestinal necrosis. A 38-year-old patient with diffuse abdominal pain was treated conservatively for several days. Sonography was performed to exclude appendicitis and pancreatitis. Closer evaluation of the superior mesenteric vein by color duplex scanning revealed thrombosis of individual jejunal vein branches with protrusion of a thrombus into the trunk of the superior mesenteric vein. Mural mesenteric vein thrombosis causes obstruction of flow. Prompt initiation of full heparinization is necessary to prevent further appositional thrombus growth and subsequent intestinal necrosis
b Digital subtraction angiography confirms the partial mesenteric vein thrombosis

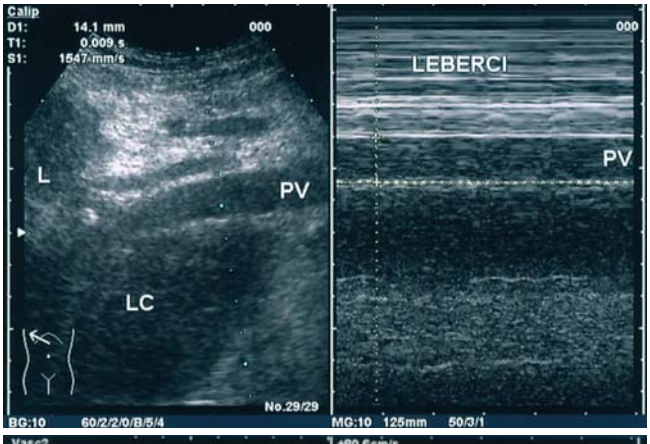

a

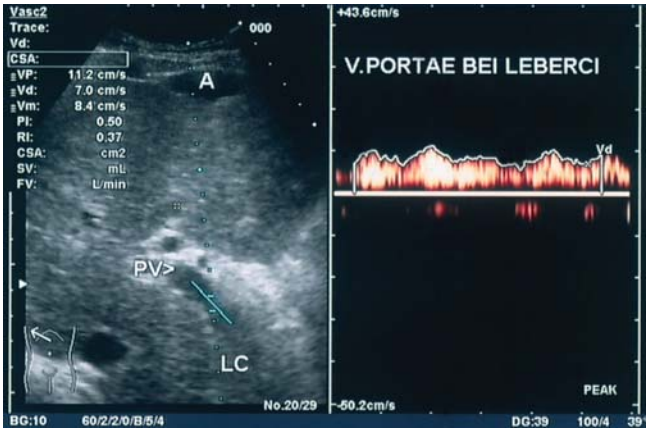

b

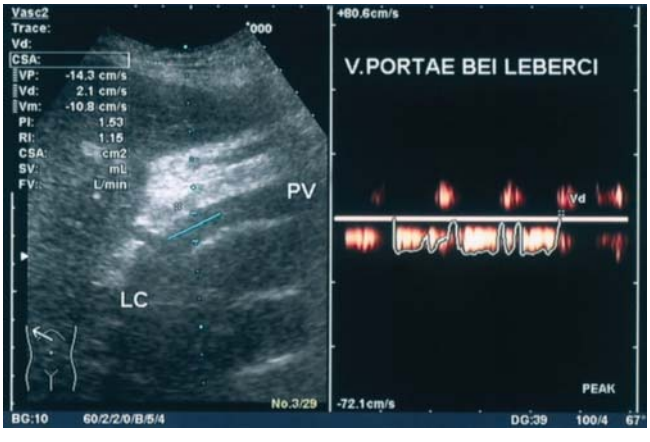

c

Fig. A 6.44 a–c
Portal hypertension
a Loss of respiratory diameter variation in gray-scale ultrasound is a sign of portal hypertension. In the example, the time-motion mode demonstrates a constant diameter of 14 mm of the portal vein (*PV*)
b The patient presented has portal hypertension due to Child C liver cirrhosis. The peak flow velocity is markedly reduced to 11.2 cm/s with a mean flow velocity of 8.4 cm/s (intercostal transducer position). Other signs of liver cirrhosis depicted by ultrasound are perihepatic ascites (*A*) and the enlarged caudate lobe (*LC*). The congestion index is markedly increased to 0.2 cm × s

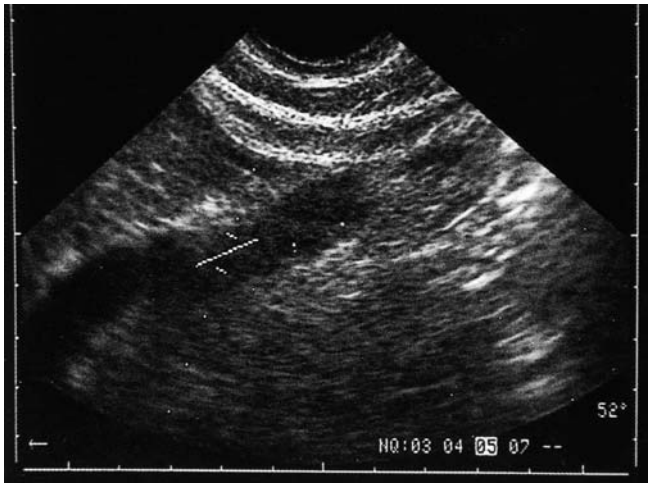

a

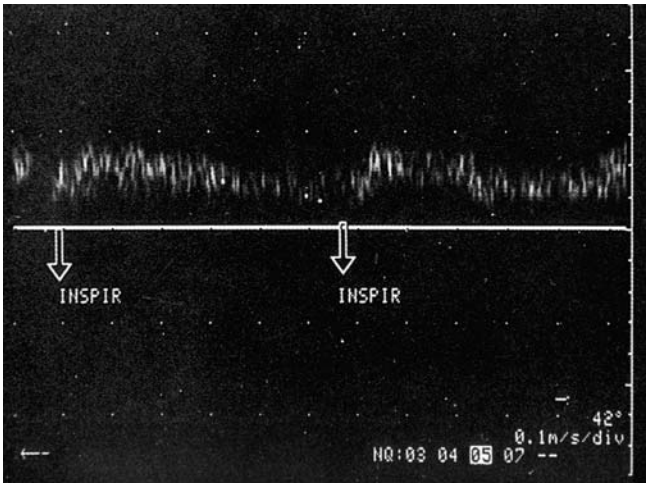

b

Fig. A 6.45
Collateral pathways in portal hypertension
Collateral flow in portal hypertension may occur chiefly through the patent umbilical vein (Cruveilhier-Baumgarten syndrome). In the example, the umbilical vein is seen coursing toward the abdominal wall along the lower edge of the liver. Its diameter is markedly increased to over 1.5 cm. Flow in the umbilical vein is hepatofugal. The faster flow during inspiration suggests a connection to the portal vein and a high shunt volume

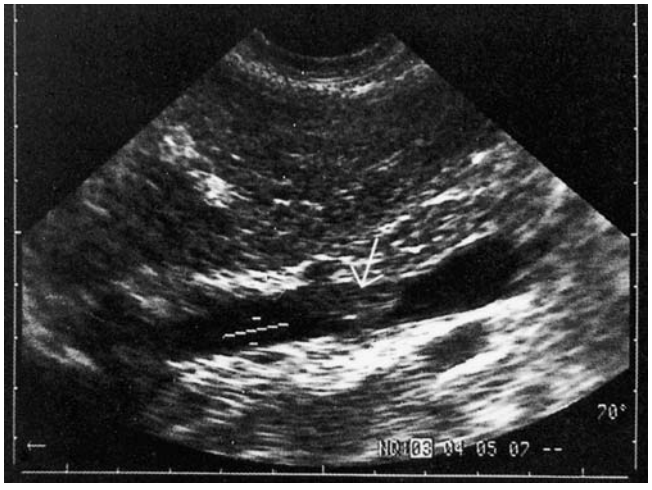

a

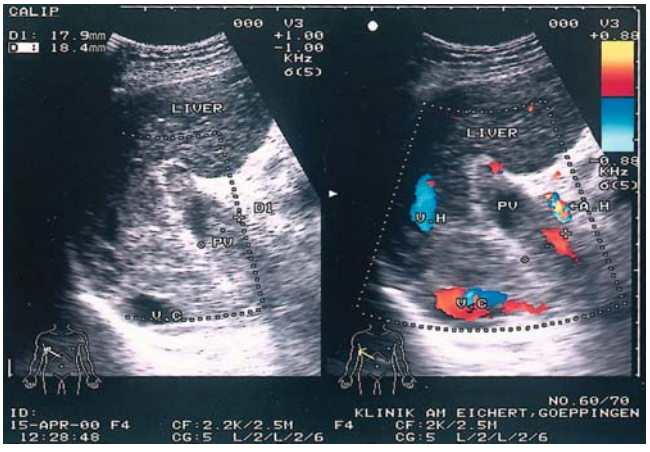

b

Fig. A 6.46 a, b
Portal vein thrombosis
a Development of a nonocclusive portal vein thrombus (*arrow*) following splenectomy due to hypersplenism with portal hypertension
b Like all venous thromboses, portal vein thrombosis may already be suggested in B-mode scanning by a dilatation of the vessel and the presence of hyperechoic deposits in the lumen. Color duplex scanning from the intercostal approach using the liver as an acoustic window depicts flow signals (red, toward transducer). There is nearly complete thrombosis with residual flow near the walls. The vena cava (*V.C*) is depicted posterior to the portal vein. Laterally, the hepatic artery (*A.H*) is sectioned, showing aliasing due to the low pulse repetition frequency (*V.H* hepatic vein)

◁
(Fig. A 6.44 cont.)
c A less pronounced increase in postprandial flow velocity (mean flow velocity: 10.8 cm/s) is another sign of portal hypertension

With an unchanged diameter of 14 mm, the postprandial flow volume increases by only 20 % (compared to a mean increase of over 60 % in normal individuals)

For didactic purposes, views of the portal vein from two transducer positions (**c**: subcostal; **b**: intercostal, from the flank) are shown with the sample volume placed at the same site within the vein. The intercostal approach enables smaller Doppler angles (in the example 38° versus 67°) and thus yields more accurate velocity measurements. Follow-up examinations should be performed with identical transducer positions

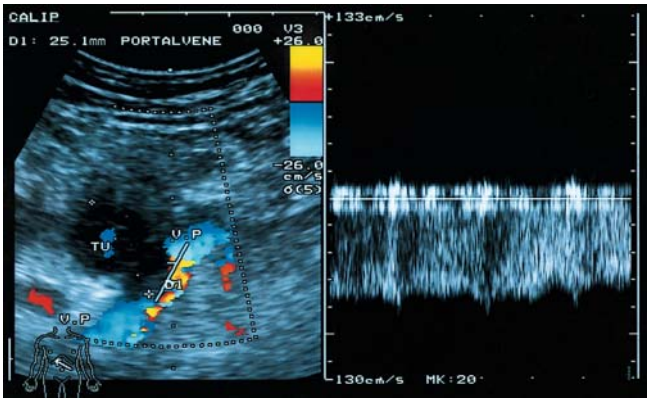

Fig. A 6.47
Tumor compression
Carcinoma of the head of the pancreas with infiltration of the portal vein (*V.P*). The wall is poorly delineated and the lumen is compressed. A stenosis is indicated by aliasing in the color duplex scan and in the Doppler waveform. Within the tumor (*TU*), a tumor vessel is depicted with flow in blue

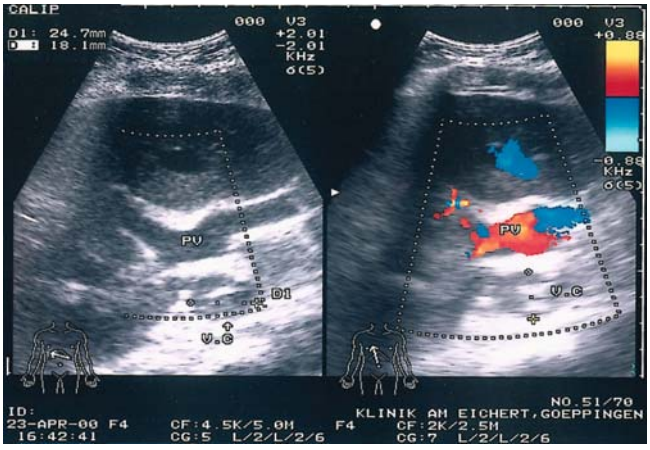

a

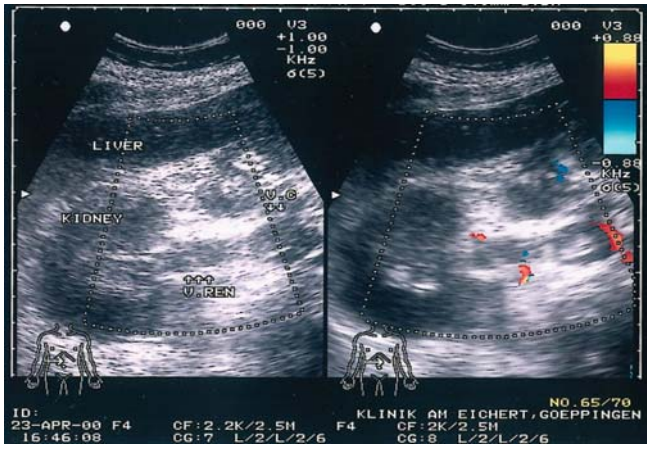

b

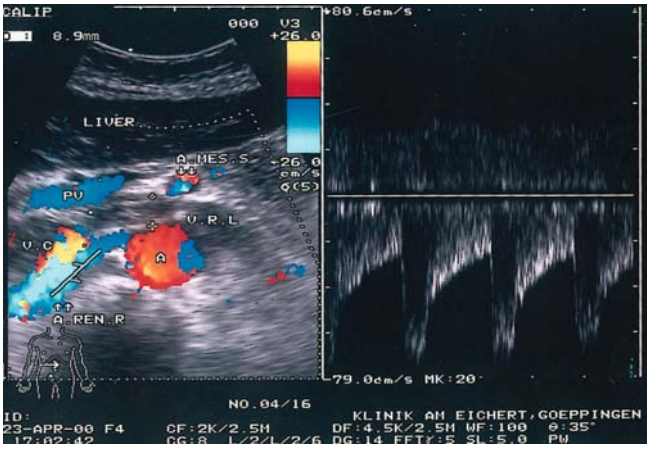

c

Fig. A 6.48 a–e
Vena cava thrombosis
Following laser-induced thermoablation of a large paracaval liver metastasis (presenting with upper abdominal pain on the right), the patient developed subcapsular liver hemorrhage and complete thrombosis of the vena cava as a result of the local heat effect

a B-scan (*left*) and color duplex scan (*right*) depicting the portal vein and vena cava (*V.C*) posterior to the liver hilum. The portal vein exhibits color-coded flow while the vena cava (*V.C*) is depicted with hyperechoic internal echoes but without flow signals
b The transverse view through the upper abdomen farther down shows residual flow near the walls displayed in red in the vena cava (right margin of *right section*) and no other flow signals. The scans also show the opening of the renal vein (*V.REN*) into the vena cava. The flow signals next to the renal vein indicate venous return through retroperitoneal collateral veins, chiefly the suprarenal vein
c A tubular, hypoechoic structure without flow signals is depicted in the typical location of the left renal vein (*V.R.L*) between the superior mesenteric artery (*A.MES.S*) and the aorta (*A*), indicating thrombosis of this vein. The vein is markedly widened and hyperechoic internal structures are depicted within the hypoechoic lumen. A vena cava thrombus next to the opening of the left renal vein is depicted with flow near the wall. Despite complete renal vein thrombosis, the right renal artery (*A.REN.R*) has a normal flow profile (*right section*). This arterial flow profile and the uneventful clinical course (no increase in creatinine or urea despite complete bilateral renal vein thrombosis) confirms the collateral function of the sonographically depicted retroperitoneal veins, in particular the suprarenal vein and the capsular veins

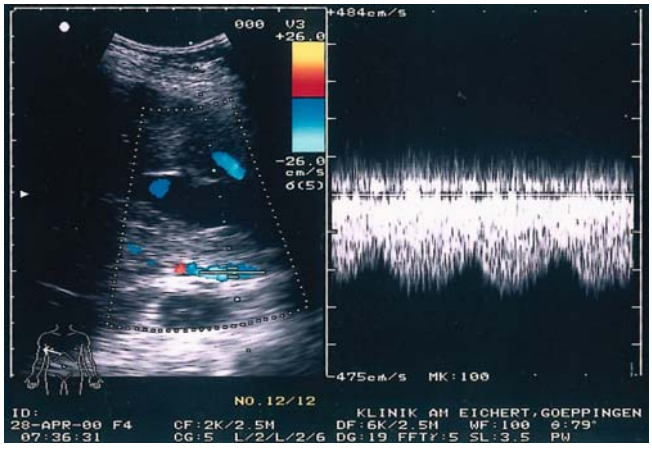

d

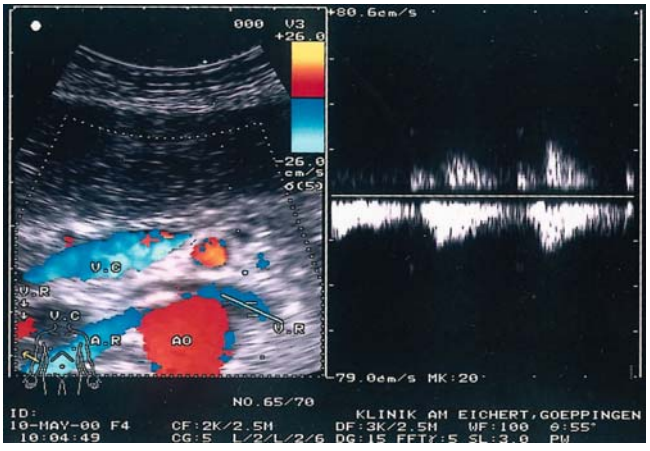

e

(Fig. A 6.48 cont.)

d Example of a retroperitoneal collateral vein with the typical venous flow signal depicted between the liver and the thrombosed vena cava (hypoechoic tubular structure posterior to the sample volume) in an oblique abdominal view

e Color duplex scanning 18 days later already demonstrates spontaneous recanalization of both renal veins with flow signals in the formerly completely thrombosed renal vein (*V.R*; cf. **c**) between the aorta and superior mesenteric artery, also confirmed by the Doppler spectrum. There is likewise flow in the right renal vein (*V.R*/*arrow*) depicted in red near the left margin

Fig. A 6.49 a, b
Renal vein thrombosis

a The right renal vein coursing below the liver is occluded by a thrombus protruding into the vena cava (renal cell carcinoma)

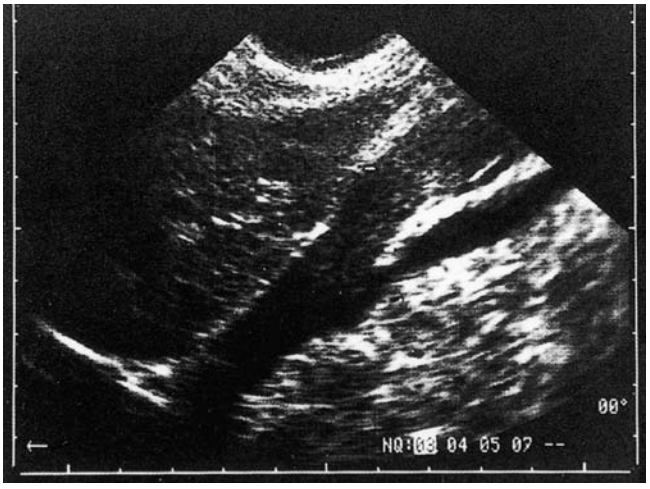

a

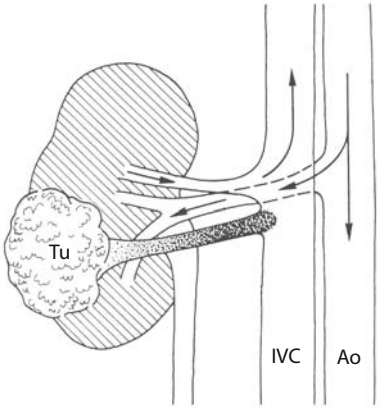

b

b Schematic representation of renal vein thrombosis due to tumor. Two renal veins are present and the drawing shows growth of a thrombus from a renal cell carcinoma into the vena cava through one of the veins

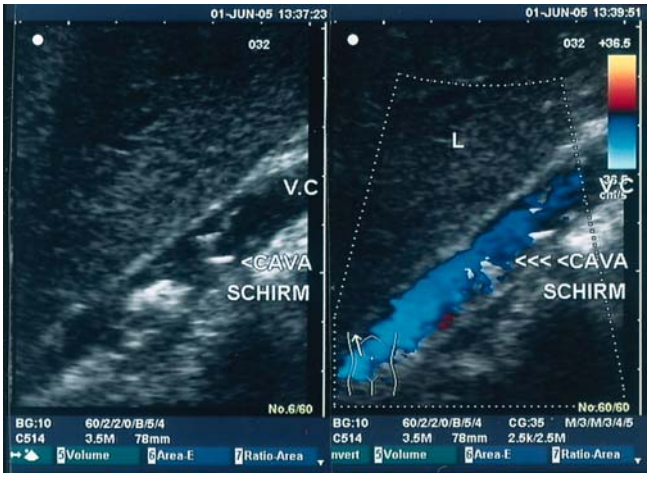

Fig. A 6.50
Caval umbrella
Placement of a caval umbrella is rarely indicated. Possible complications of the procedure like thrombotic deposits on the umbrella and vena cava thrombosis can be identified by ultrasound follow-up. The caval umbrella (*Cava Schirm*) is identified by hyperechoic spots in the lumen of the vena cava (*V.C.*) behind the liver (*L*) (*left section*). The color flow image shows that no thrombotic material is present and that the umbrella causes no flow disturbance (*right section*)

Penile and Scrotal Vessels

7

Erectile dysfunction is the lack of copulative power due to failure to initiate an erection or to maintain an erection. The causes of erectile dysfunction include psychologic, neurophysiologic, endocrinologic, and vasculogenic factors. The vascular mechanisms involved in the process of erection are an increased arterial inflow and reduced venous outflow. The incidence of erectile dysfunction due to vascular causes increases with age. About 10% of men suffer from erectile dysfunction.

7.1 Vascular Anatomy

7.1.1 Penile Vessels

The penis is supplied with blood by the internal pudendal artery, a branch of the internal iliac artery. The internal pudendal artery gives off scrotal branches and continues as the common penile artery, which divides into four terminal branches. These are the urethral or spongiosal artery, the dorsal penile artery (chiefly supplying the skin and glans penis), the bulbourethral artery, and the deep penile artery, which gives off branches to the corpora cavernosa (Fig. 7.1). These branches course centrally in the cavernous bodies, which become rigid and enlarged when arterial inflow through these branches is increased. The other arteries have no relevant role in the erectile process.

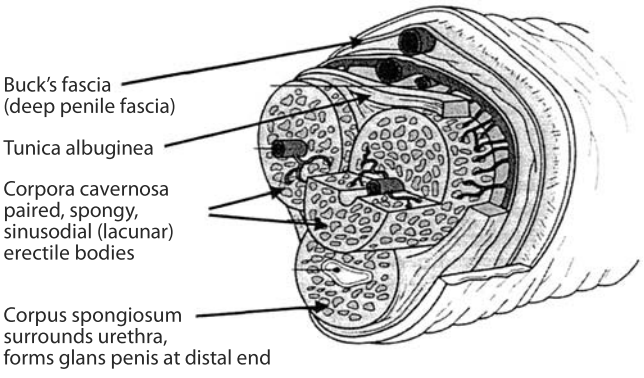

Fig. 7.1. Anatomy of the erectile bodies of the penis

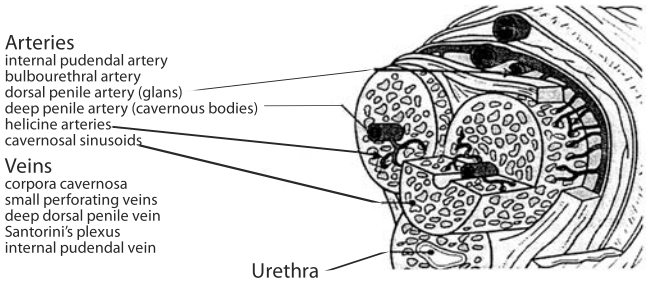

Fig. 7.2. Arterial supply to the penis with arterial branches and venous drainage

Blood from the distal and middle portions of the corpora cavernosa is drained through the emissary and circumflex veins into the periprostatic plexus and from the proximal portion through the deep penile vein into the internal pudendal vein. The blood from the superficial dorsal vein of the penis is primarily drained into the saphenofemoral junction through subcutaneous veins and the external pudendal veins. The blood from the deep penile vein flows out into the internal pudendal vein and the internal iliac vein (Fig. 7.2).

In the flaccid state, the arterioles (helicine arteries) and the sinusoids in the cavernous spaces are contracted. There is only little blood flow due to the high peripheral resistance. Conversely, the draining venules (emissary veins) are widely open; they drain the blood over a short stretch via the tunica albuginea into the circumflex vein and dorsal vein (Fig. 7.3 a, b).

7.1.2 Scrotal Vessels

The paired testicular artery arises from the abdominal aorta and courses from the retroperitoneum to the internal inguinal ring, from where it descends through the inguinal canal to the testis, surrounded by the veins of the pampiniform plexus and accompanied by the ductus deferens. The testicular veins drain the blood from the scrotum and testis via the pampiniform plexus. After having emerged from the internal inguinal ring, the right testicular vein courses to the inferior vena cava, the left testicular vein to the left renal vein.

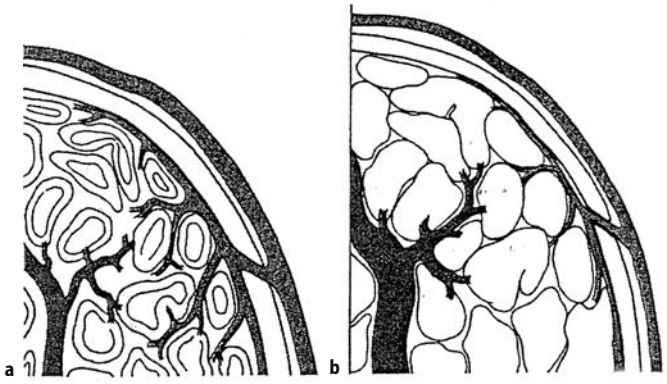

Fig. 7.3. a Mechanism of penile erection: In the flaccid state (detumescence), the helicine arteries and sinusoids are contracted while the subtonic emissary veins are open. **b** The initiating event of penile erection is relaxation of the smooth muscle of the helicine arteries, enabling increasing arterial inflow into the cavernous spaces. At the same time, venous outflow is increasingly blocked by compression of the emissary veins. Adequate closure of cavernosal outflow is crucial for maintaining an erection

7.2 Examination Technique

7.2.1 Erectile Dysfunction

The superficial course of the penile vessels enables their examination with a high-resolution, high-frequency transducer (7 – 10 MHz). The scanner must be adjusted to depict the slow flow by selecting a low pulse repetition frequency and a low wall filter.

With the patient in the supine position and the flaccid penis resting on the lower abdomen, the transducer is placed on the corpus carvernosum from a dorsal approach near the base in transverse orientation (Fig. 7.4). In this position, the B-mode examination is performed with special attention given to the thickness of the tunical albuginea and the penile septum. The color mode is then switched on and the deep penile artery is identified on both sides with slight angulation of the transducer. In the longitudinal plane, the Doppler spectrum is recorded from both arteries and the angle-corrected flow velocity is calculated. To depict the slow flow velocities, a low pulse repetition frequency and wall filter are necessary while the gain must be increased but without inducing artifacts.

Before scanning the penile vessels after administration of a vasoactive agent, written consent must be obtained from the patient after information about the examination and its possible side effects. For pharmacological induction of erection, prostaglandin (PGE1) or papaverine is injected into the left and right corpus cavernosum using a very fine (22 – 26 G) needle (Fig. 7.5). To avoid side effects due to overdosage, the examination should be performed on 2 days with increasing dosages, beginning with 40 mg papaverine or 10 µg PGE1. If no adequate erection is achieved, 80 mg papaverine or 20 µg PGE1 should be injected into the right or left corpus cavernosum. Immediate outflow of the injected agent is prevented by short venous compression at the root of the penis. The erect penis is examined 4 – 5 min after injection by color duplex scanning in the same way as in the flaccid state. Following identification of the deep artery in transverse orientation, a spectral Doppler tracing is obtained from the proximal third of the artery near the base in longitudinal orientation with angle-corrected measurement of peak systolic and minimum end-diastolic flow velocities. The flow velocity measurements are repeated every 2 to 3 min until full erection is achieved. Finally, venous outflow in the deep femoral vein may be measured (Table 7.1).

The pharmacologically induced erection should subside within 4 – 6 h. Immediate treatment is required in case of longer persistence or priapism, the most dreaded complication of PGE1 injection (Stief et al. 2000). This complication has an incidence of 1 – 4 % and chiefly occurs if the dose is too high and in young patients with psychogenic erectile dysfunction (Wagner and Kaplan 1993). Treatment consists in injection with a thin needle of 5 – 10 mg Effortil in 5 ml saline solution. If there is progression to priapism, the intracavernous blood must be drained by aspiration.

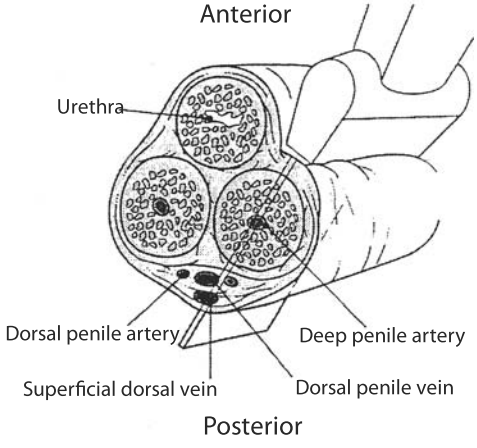

Fig. 7.4. Transducer position for evaluating arterial and venous perfusion. The penis rests on the patient's lower abdomen (as in erection)

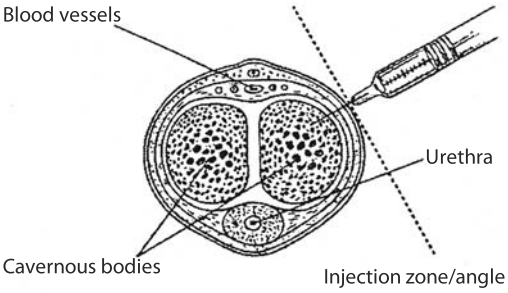

Fig. 7.5. Technique of intracavernous PGE1 or papaverine injection

Table 7.1. Pathophysiology of erectile dysfunction

50 – 70 % organic Chiefly vasculogenic	
Arterial	Stenosis, occlusion (risk factors: atherosclerosis, diabetes mellitus, hypertension, hypercholesterinemia, nicotine)
Venous Sinusoidal scar	Venous leakage Peyronie's disease, plaques – pain – detumescence

7.2.2 Scrotal Vessels

The principal vessels involved in scrotal and testicular perfusion, the testicular artery and vein, course close to the surface in the inguinal canal and are thus accessible to duplex scanning with a high-resolution transducer. The spermatic artery passes through the abdominal wall together with the ductus deferens at the inner inguinal ring and can be traced sonographically in the B-mode in the inguinal canal, through which it descends to the scrotum as part of the spermatic cord. The testicular artery and vein are identified in the transverse plane in the color duplex mode to then obtain spectral Doppler tracings in longitudinal orientation. In addition, in patients evaluated for the presence of varicocele, the diameters of the veins are determined in longitudinal and transverse planes and the vessels are tracked downward (pampiniform plexus).

7.3 Normal Findings

7.3.1 Penile Vessels

On B-mode scanning, the corpus cavernosum is depicted as a roundish structure of a fairly homogeneous texture and low echogenicity that is surrounded by the more echogenic tunica albuginea. The corpora are separated by a septum that is also echogenic.

In the flaccid state, the small-caliber deep artery of the penis may be difficult to identify in the B-mode. The Doppler spectrum recorded after identification of the artery in the color duplex mode shows a highly pulsatile flow due to the high peripheral resistance. Intracavernous injection of PGE1 induces dilatation of the deep artery (seen in the B-mode) with an increase in systolic and diastolic flow velocities (Heberner and 1994; Müller and Lue, 1988; Quam et al. 1989). Normal arterial inflow results in a peak systolic velocity of over 30 – 35 cm/s 5 – 15 min after injection. The initially low peripheral resistance during the early phase of erection is associated with a high diastolic flow (over 5 – 10 cm/s). The physiologic closure of venous drainage during erection increases the peripheral arterial resistance in the fully erected penis. This results in a marked decrease in the end-diastolic flow component, usually to zero (pulsatile flow), 5 – 25 min after injection. A value of 5 cm/s or above indicates venous insufficiency of the cavernous bodies.

The blood flow in the deep artery of the penis during tumescence is determined by arteriolar vasodilation and the changed pressure in the erectile tissue. The increasing filling of the cavernous spaces by inflowing blood results in a pressure increase in the corpora cavernosa as long as there is proper venous closure. The ensuing increase in arterial flow resistance in turn leads to a reduction of the diastolic flow component (more pulsatile flow).

7.3.2 Scrotal Vessels

The testicular artery has a flow profile typical of a parenchyma-supplying vessel but with a rather small diastolic component. In a study of 30 men, a peak systolic flow velocity of 14 cm/s (7.5 – 27.7 cm/s) and an end-diastolic velocity of 1.9 cm/s (0 – 4.7 cm/s) were found in the distal testicular artery. The resistance index (Pourcelot) was 0.84 (0.63 – 1; Middleton et al. 1989).

In the Valsalva test the testicular vein and pampiniform plexus veins exhibit zero flow after a brief reflux. Flow velocity varies with respiration; the normal diameter is less than 2 – 3 mm (Cvitanic et al. 1993).

7.4 Documentation

Transverse B-mode views of the penis depicting both cavernous bodies should be documented. The findings in the deep artery of the penis are documented together with the corresponding angle-corrected time-velocity spectra in longitudinal orientation in the flaccid state and in the same way at intervals of 2 – 3 min after PGE1 or papaverine injection. The spectra should document the increase in peak systolic and end-diastolic flow velocity following injection as well as the subsequent decrease in peak end-diastolic flow after full erection has been achieved.

The findings in the testicular artery are recorded at the level of the external inguinal ring in longitudinal orientation together with the spectral waveform. In the same way, the findings in the pampiniform plexus veins are documented with the patient breathing spontaneously and while performing the Valsalva maneuver. The diameter of the veins is measured and recorded in transverse orientation.

7.5 Clinical Role of Duplex Ultrasound

7.5.1 Erectile Dysfunction

Accurate data on the prevalence of erectile dysfunction is difficult to obtain due to underreporting because of embarrassment or because the problem is not considered worthy of medical attention. It is well established that the incidence

increases with age (Kinsey et al. 1948). Erectile problems are reported by 2 % of men up to 40 years of age, 7 % of men aged 41 to 50, 15 % of men aged 51 to 60, and 75 % of those over 70 years of age. In a population of 100 men (mean age 37 years), 7 % reported disturbed initiation of erection and another 9 % disturbed maintenance of erection (Frank et al. 1978). Until the end of the 1980s it was assumed that erectile dysfunction was of psychogenic origin in 90 % of cases (Borst 1987).

Various diagnostic procedures such as cavernosometry, cavernosography, CW Doppler, duplex scanning, and arteriography are available. They are used to measure intracavernosal pressure or perfusion parameters during erection or to detect arterial flow obstructions and demonstrate relevant organic abnormalities in 50 – 70 % of men presenting with erectile dysfunction (Stief et al. 1988; Tamura et al. 1993; Whitehead et al. 1990). This leaves a percentage of only 30 – 50 % with predominantly psychogenic dysfunction.

Apart from vasculogenic causes, organic erectile dysfunction may be of neurogenic, endocrine, or drug-induced origin. Other causes are lesions of the cavernous bodies such as penile induration (Peyronie's disease). As with diabetes mellitus, vascular changes (macro- and microangiopathy) may further aggravate a condition of primarily neurogenic origin (neuropathy of peripheral and autonomous nervous system). Vasculogenic erectile dysfunction may be caused by venous insufficiency of the corpora cavernosa with an incompetent veno-occlusive mechanism or by reduced arterial inflow due to stenosis or occlusion of the internal iliac artery or distal branches such as the pudendal artery (Table 7.2).

Prior to any examination, a detailed history must be obtained to identify possible nonvasculogenic causes of the patient's erectile problems. This includes information on drug intake as well as a sociopsychologic interview pertaining to the patient's social situation with special emphasis on the duration, severity, and character of the erectile dysfunction. Also important is a history of prior diseases and trauma including operations, in particular of the true pelvis, in order to obtain clues as to whether the erectile dysfunction is primarily organic or psychogenic in nature. Information must also be obtained on vascular risk factors and the subsequent clinical examination should be performed with special attention given to vascular disorders.

Precise determination of the cause is mandatory for successful treatment of erectile dysfunction. In patients in whom a nonpsychogenic cause has been identified, therapeutic management is initiated according to the algorithm presented in Fig. 7.7 and on the basis of the history, clinical findings, and invasive and noninvasive diagnostic tests. The therapeutic measures may include pharmacologic treatment and, in case of vasculogenic erectile dysfunction, venous resection or arterial revascularization based on the duplex sonographic findings.

Table 7.2. Sonographic criteria

B-mode scan (Longitudinal/ transverse)	Detumescence/erection Corpus cavernosum, homogeneous echotexture of normal tissue (scars) Atherosclerotic changes/plaques
Doppler	Spectral analysis Peak systolic flow velocity End-diastolic flow velocity Resistance index
Course of erection	Changes in Doppler waveform (chiefly diastolic component) and resistance index during: detumescence – tumescence – erection – full erection
Pharmacologically induced erection	Intracavernous injection: 10 µg PGE1 or 30 – 60 mg papaverine Spectral Doppler recordings every 3 to 5 min Both deep penile arteries and deep dorsal vein Maximum tumescence after 8 – 20 min

7.5.2 Acute Scrotum

In patients presenting with an acute scrotum, testicular torsion and inflammatory conditions such as epididymitis must be differentiated but this may be difficult on the basis of the clinical presentation and history alone. If either of these conditions is suspected, imminent loss of testicular function due to necrosis requires rapid intervention and may necessitate surgical exposure of the testis in inconclusive cases. Complete testicular torsion with arterial obstruction is distinguished from incomplete torsion. In the latter, only venous return is affected but the testis is likewise at risk. Noninvasive assessment by duplex scanning must therefore always include arterial inflow as well as venous outflow.

7.5.3 Varicocele

About 10 – 15 % of sexually mature men suffer from varicocele, among them 5 % with a severe form. Varicocele is a varicose condition of the veins of the pampiniform plexus that may be caused by valve incompetence of the spermatic vein. In addition, vascular anatomy also has a role in the pathogenesis since the majority of varicoceles occur on the left side. While the right spermatic vein empties directly into the vena cava, the left vein opens into the left renal vein. The higher hydrostatic pressure, compression by the inferior mesenteric artery, and an atypical course are among the factors that may predispose to the preponderance of left-sided varicocele. In a study of 45 patients with left-sided varicocele, 25 % were found to have a retroaortic course of the renal vein while a periaortic course was present in 31 cases (Justich 1982; outflow obstruction of renal vein).

Although the exact mechanism of how a varicocele affects the spermiogram is not yet fully understood (hyperthermia, endocrine regulation, hypoxia/adrenal reflux), it is implicated as a cause of infertility because 30 – 50 % of infertile men have a varicocele.

Surgery is indicated only in men with severe varicocele and manifest symptoms, unilateral testicular hypotrophy, or changes in the spermiogram with compromised spermiogenesis.

7.6 Abnormal Findings: Role of Duplex Ultrasound Parameters

7.6.1 Erectile Dysfunction

B-mode sonography depicts fibrosis in the homogeneously hypoechoic corpus cavernosum as hyperechoic strands. Fibrosis and calcifications of the tunica albuginea (Peyronie's disease) are reliably identified by thickening and an increased echogenicity.

Extensive obstructive processes of the upstream arteries (both iliac arteries or pudendal artery) will change the flow character in the deep penile artery (postocclusive flow profile with decreased pulsatility) and thus suggest a vasculogenic cause of erectile dysfunction already in the flaccid state.

Injection of PGE1 or papaverine will usually induce an increase in blood flow within 5 – 10 min (early tumescence phase) through a reduction of arterial resistance. This is reflected by a peak systolic flow velocity of over 30 – 35 cm/s, an increase in end-diastolic flow velocity, and a lower Pourcelot index. A pharmacologically induced peak systolic flow velocity of less than 30 cm/s in the deep penile artery suggests inadequate arterial perfusion. Studies demonstrated that a peak systolic velocity below 25 cm/s after intracavernous injection was due to vascular obstruction, which was confirmed as the cause of erectile dysfunction in 88 – 100 % of the patients by control angiography (Benson et al. 1993; Desai and Gilbert 1991; Quam et al. 1989). In another study of 42 patients with clinical signs of vasculogenic impotence, color-coded duplex sonography was found to have a sensitivity of 82 % and a specificity of 88 % compared to selective penile DSA (Brandstetter et al. 1993). A delayed systolic upstroke of the Doppler waveform is a further sign of a proximal flow obstruction.

Besides arterial causes, the failure to achieve or maintain an erection may be due to dysfunction of the veno-occlusive mechanism (Table 7.3). If the mechanism is intact, the rise in intracavernous pressure leads to an increase in peripheral resistance with a decrease in the diastolic flow component. Conversely, if there is venous cavernous insufficiency, the increased venous outflow results in persistent end-diastolic flow. An end-diastolic flow velocity of over 5 cm/s indicates venous leakage with a sensitivity of over 90 % (Quam et al. 1989). The magnitude of the end-diastolic flow velocity following maximum penile tumescence after intracavernous injection of a vasoactive agent correlates with the venous outflow resistance and thus with the severity of venous leakage. Duplex sonography is a highly accurate tool for determining hemodynamic parameters during pharmacologically induced erection in the diagnostic evaluation and differentiation of vasculogenic causes of erectile dysfunction.

Based on the findings of duplex scanning, further invasive diagnostic tests may be indicated according to the algorithm for step-by-step diagnostic management presented in Fig. 7.6. The therapeutic management depends on whether initial intracavernous self-injection (ICSI) is successful or not (Fig. 7.7). The duplex measurements assist in choosing the most suitable therapy.

Table 7.3. Erectile dysfunction (arterial – venous)

Erectile dysfunction	
Arterial incompetence:	
peak systolic flow velocity	< 25 cm/s: severe arterial incompetence acceleration time increased to over 120 ms 25 – 30 cm/s: moderate arterial incompetence
Note: limited diagnostic value in nervous patients and in psychogenic erectile dysfunction	
Venous erectile dysfunction	
Clinical presentation: poor rigidity despite normal arterial function	
Duplex scanning:	persistent diastolic flow > 5 cm/s resistance index (RI) < 1 evidence of flow in deep dorsal vein
Note: examination of venous competence only in patients with normal arterial function Duplex scan provides only tentative diagnosis of venous incompetence, which needs to be confirmed by cavernosometry, cavernosography	

7.6.2 Acute Scrotum

In patients presenting with an acute scrotum, duplex scanning excludes acute ischemia with a specificity of nearly 100 % (Fitzgerald and Foley 1991). Various studies performed in small study populations found sensitivities of 86 – 100 % and specificities of 100 % in the differentiation of acute testicular or epididymal inflammation with subsequent hyperemia from testicular torsion with signs of acute ischemia (De Wire et al. 1992; Lerner et al. 1990; Middleton et al. 1990; Ralls et al. 1990). Inflammatory changes are associated with a low peripheral resistance and a relatively high diastolic flow in the Doppler spectrum. In contrast, testicular torsion is characterized by the absence of arterial flow in the twisted vessel segment and highly pulsatile flow without a diastolic flow component and a reduced peak systolic flow velocity (compared to contralateral side) with a "knocking" waveform proximal to the lesion (in the inguinal ligament). The studies reported in the literature rarely address the problem of incomplete testicular torsion with disturbed venous outflow. To exclude testicular damage resulting from venous torsion, the vein must be evaluated by color duplex scanning from the scrotal compartment to the level of the inguinal ligament. The normal spectral waveform shows flow with respiratory phasicity.

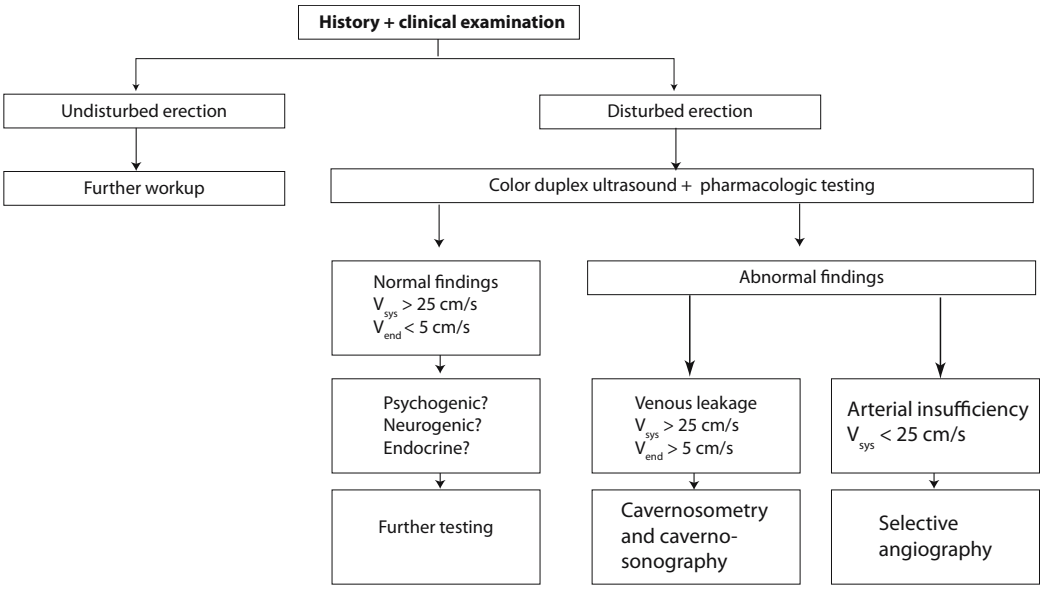

Fig. 7.6. Algorithm for the diagnostic management of patients with erectile dysfunction (V_{sys} and V_{end} systolic and end-diastolic velocity, respectively, measured by color duplex)

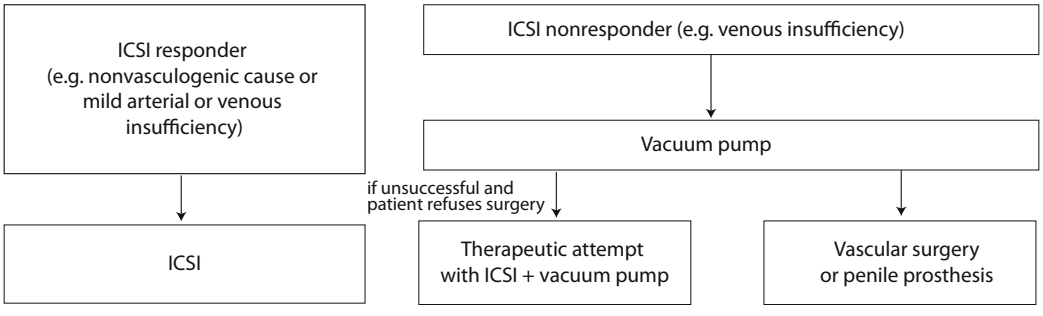

Fig. 7.7. Algorithm for the therapeutic management of patients with erectile dysfunction (*ICSI* intracavernous self-injection)

In a study of 31 patients, a cutoff value of 15 cm/s for peak systolic flow velocity was found to have an accuracy of 90% for identifying orchitis and of 93% for epididymitis (Brown et al. 1995). Another measure used was the quotient of peak systolic flow velocities on both sides with a quotient greater than 1.9 being defined as indicating epididymitis or orchitis.

Altogether, published results suggest a high validity of sonographic evaluation of testicular and penile perfusion and its abnormal changes but these findings remain to be confirmed in larger patient populations. Surgical exposure of the testis is still necessary in inconclusive cases.

7.6.3 Varicocele

Varicoceles are conspicuous as a convolution of veins in the scrotum. Dilatation of the veins of the pampiniform plexus with a diameter of over 3 mm is considered abnormal. The Valsalva test performed in the standing patient will induce continuous backward flow in the ectatic veins, which can be demonstrated by both color duplex sonography and in the Doppler waveform (Fitzgerald and Foley 1991). In a study of 63 infertile men, color duplex was found to be highly accurate in the diagnosis of varicoceles with a sensitivity of 97% and a specificity of 94% compared to venography of the spermatic vein (Trum et al. 1996). However, the clinical significance of a sonographically diagnosed varicocele must not be overestimated. In an investigation of 26 fertile men, 42% were found to have dilated pampiniform plexus veins with diameters of over 2–3 mm and signs of reflux (Cvitanic et al. 1993; Table 7.4).

Table 7.4. Sonographic criteria of varicocele

- Testicular size (>2 ml difference)
- Plexus veins (>3 mm diameter)
- (Color) duplex ultrasound: reflux during normal respiration in the standing patient

7.7 Atlas

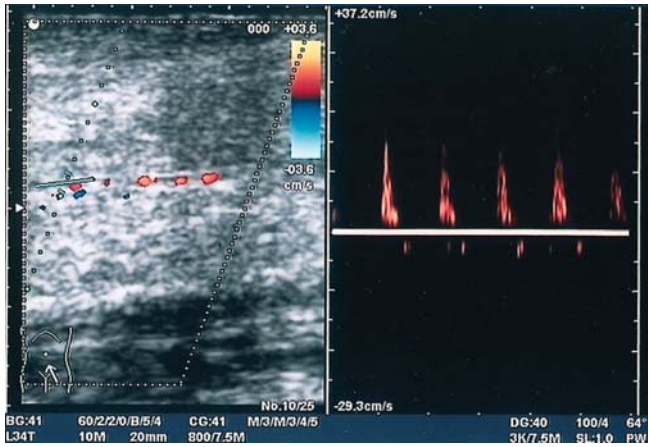

Fig. A 7.1
In the flaccid state (detumescence), the deep artery of the penis shows high-resistance flow with pulsatile systolic peaks but no significant diastolic flow

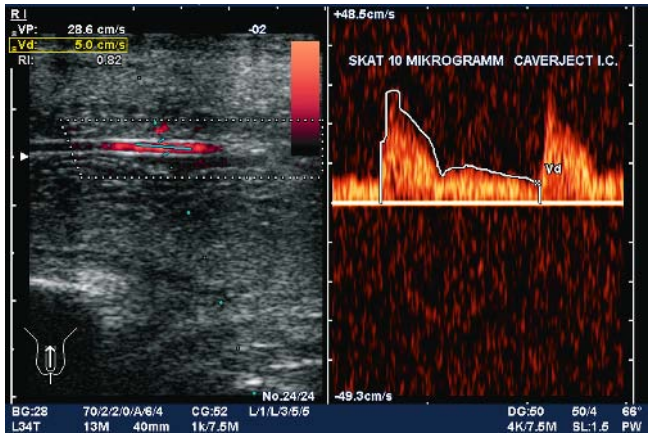

Fig. A 7.2
Markedly increased blood flow, especially in diastole, in the deep penile artery 10 – 15 min following injection of 10 µg PGE1 and relaxation of the smooth muscle of the sinusoids (low-resistance arterial inflow). (Courtesy of F. Trinkler)

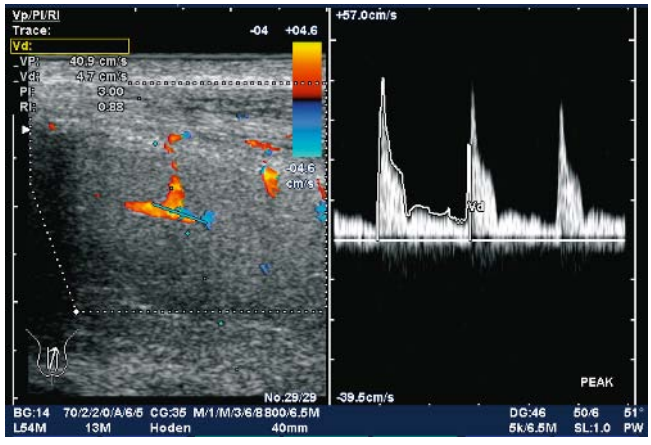

Fig. A 7.3
With increasing erection resulting from a continuous high arterial inflow, the sinusoids are filled and build up a counterpressure in the corpus cavernosum, which increases peripheral resistance and is associated with more pulsatile flow. The diastolic flow component decreases and approaches zero in the further course. A peak systolic flow velocity > 30 cm/s indicates normal arterial blood supply. In the example, the velocity is 40 cm/s. (Courtesy of F. Trinkler)

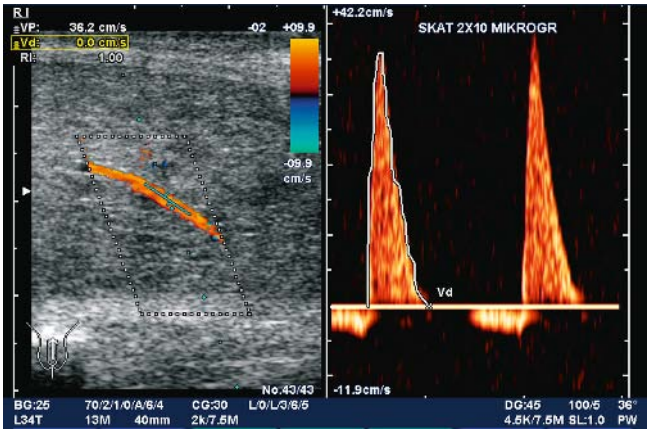

Fig. A 7.4
Flow decreases again due to the high intracavernous pressure in full erection with absence of flow or retrograde flow during diastole. This is associated with a decrease in peak systolic flow velocity. No flow is detected in the deep vein of the penis. (Courtesy of F. Trinkler)

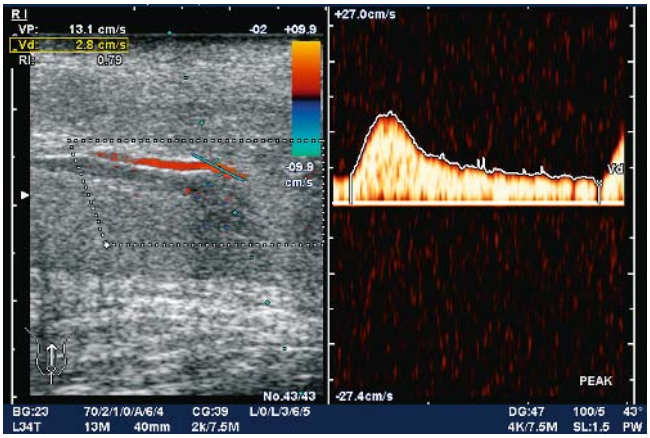

Fig. A 7.5
In the presence of inadequate arterial inflow, the increase in peak systolic flow in the deep penile artery is less pronounced. In severe insufficiency, the peak systolic velocity is less than 25 cm/s. In the case presented, intracavernous injection of 10 µg PGE1 does not induce erection and there is no adequate increase in flow during systole after a reasonable delay (5 – 15 min). The peak velocity of only 12 cm/s, the delayed systolic increase (prolonged acceleration time), and the larger diastolic component are typical signs of postocclusive flow; in the case presented caused by upstream atherosclerotic stenoses. Due to the high-grade arterial insufficiency in this case, it is not possible to reliably determine whether there is concomitant venous leakage

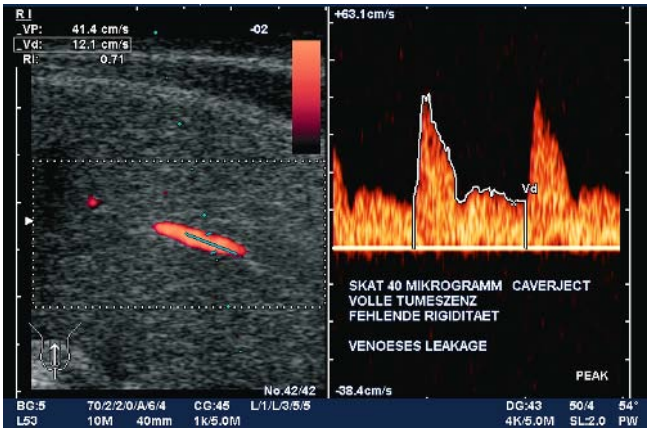

Fig. A 7.6
In patients with venous leakage, rigidity is inadequate although full tumescence is achieved. Following intracavernous PGE1 injection, the Doppler spectrum from the deep penile artery demonstrates an adequate systolic increase with a flow velocity of 41 cm/s but no reduction during diastole. The high diastolic flow velocity indicates low peripheral resistance to venous outflow

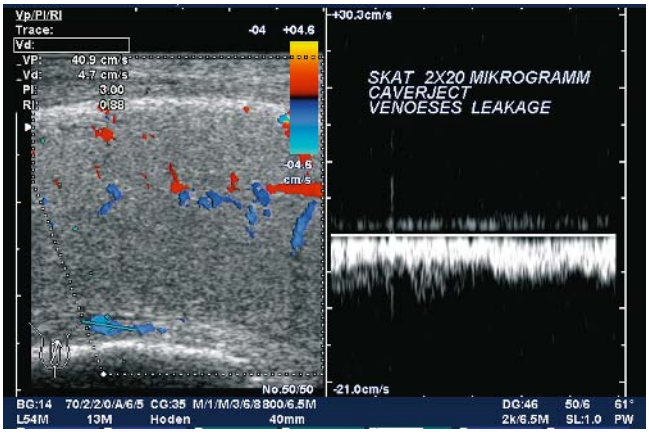

Fig. A 7.7
Under normal conditions, no venous flow signal is obtained from the deep dorsal vein in the phase of full tumescence. In the patient presented, venous leakage is suggested by the demonstration of venous flow with a velocity of 10 – 20 cm/s

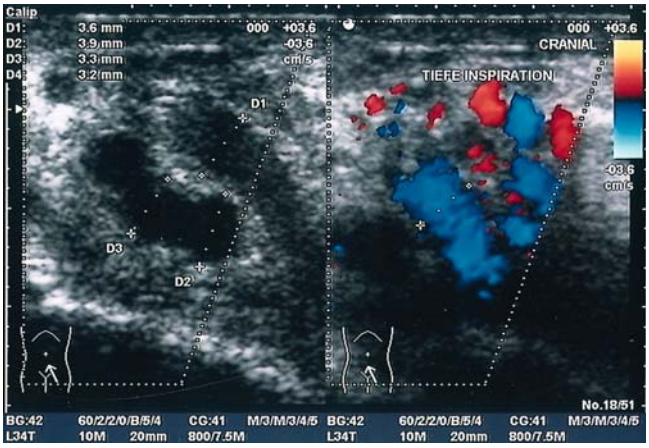

Fig. A 7.8
Varicocele
A varicocele is diagnosed by duplex sonography when there is dilatation of the veins of the pampiniform plexus to over 3 mm (*left section*) and backward flow toward the testes during deep inspiration or Valsalva's maneuver (color duplex scan, *right section*)

References

AbuRahma AF, Robinson P, Decanio R (1989) Prospective clinicopathologic study of carotid intraplaque hemorrhage. Ann Surg 55: 169–173

AbuRahma AF, Richmond BK, Robinson PA et al (1995) Effect of contralateral severe stenosis or carotid occlusion on duplex criteria of ipsilateral stenoses: comparative study of various duplex parameters. J Vasc Surg 22: 751–762

AbuRahma AF, Robinson PA, Killmer SM, Kioschos JM, Roberts MD (1996) A critical analysis of cerebral computed tomography scanning before elective carotid endarterectomy and its correlation to carotid stenosis. Surgery 119: 248–251

AbuRahma AF, Kyer PD, Robinson PA, Hannay RS (1998) The correlation of ultrasonic carotid plaque morphology and carotid plaque hemorrhage: clinical implications. Surgery 124: 721–728

ACAS (1995) Asymptomatic Carotid Atherosclerosis Study. JAMA 273: 1459–1461

Agrawal SK, Pinheiro L, Roubin GS et al (1992) Nonsurgical closure of femoral pseudoaneurysms complicating cardiac catheterization and percutaneous transluminal coronary angioplasty. J Am Coll Cardiol 20: 610–615

Ahmad S, Blagg CR, Scribner BH (1998) Center and home chronic hemodialysis. In: Schrier RW, Gottschalk CW (eds) Diseases of the kidney, 4th edn. pp 3281–3322

Aitken AGF, DJ Godden (1987) Real time ultrasound diagnosis of deep venous thrombosis: a comparison with venography. Clin Radiol 38: 309–313

Akbari CM, LoGerfo FW (1999) Diabetes and peripheral vascular disease. J Vasc Surg 30: 373–384

Akkersdijk GJM, Puylaert JBCM, Vries A (1991) Abdominal aortic aneurysm as an incidental finding in abdominal ultrasonography. Br J Surg 78: 1261–1263

Alanen A, Kormano M (1985) Correlation of the echogenicity and structure of clotted blood. J Ultrasound Med 4: 421–425

Albrecht T, Urbank A, Mahler M et al (1998) Prolongation and optimization of Doppler enhancement with a microbubble US contrast agent by using continuous infusion: preliminary experience. Radiology 207: 339–347

Albrecht T, Hoffmann CW, Schettler S et al (2000) B-mode enhancement at phase-inversion with US air-based microbubble contrast agent: initial experience in humans. Radiology 216: 273–278

Albrechtson LL, Olson QCG (1976) Thrombotic side effects of lower limb phlebography. Lancet II: 723

Alexandrov AV, Vital D, Brodie DS, Hamilton P, Grotta JC (1997) Grading carotid stenosis with ultrasound. Stroke 28: 1208–1210

Allard L, Cloutier G, Durand L-G, Roederer GO, Langlois YE (1994) Limitation of ultrasonic duplex scanning for diagnosing lower limb arterial stenoses in the presence of adjacent segment disease. J Vasc Surg 19: 650–657

Allenberg JR et al (1995) Endovascular reconstruction of infrarenal abdominal aortic aneurysm. Chirurg 66: 870–877

Allenberg JR, Kallinowski F, Schumacher H (1997) Stand der Chirurgie des infrarenalen Aortenaneurysmas: Prävalenz und Versorgungssituation. Dt Ärztebl 94: A2830-A2834

Alri M, Herba MJ, Reinhold C, Leclerc J, Ye S, Illescas FF, Bret PM (1996) Accuracy of sonography in the evaluation of calf deep vein thrombosis in both postoperative surveillance and symptomatic patients. AJR 166: 1361–1367

Alson MD, Lang EV, Kaufman JA (1997) Pedal arterial imaging. Vasc Interv Radiol 8: 9–18

Anderson IC, Baltaxe HA, Wolf GL (1979) Inability to show clot. One limitation of ultrasonography of the abdominal aorta. Radiology 132: 693

Anjaria PD, Vaidya PN, Vahia VN et al (1973) Venous aneurysms. J Postgrad Med 20: 142–144

Äppel RG, Bleyer AJ, Reavis S, Hansen KJ (1995) Renovascular disease in older patients beginning renal replacement therapy. Kidney Int 48: 171–176

Appelman PT, de Jong TE, Lampman LE (1987) Deep venous thrombosis of the leg. Ultrasound findings. Radiology 163: 747–746

Aprin H, Schwartz GB, Valderamma E (1987) Traumatic venous aneurysm. Clin Orthop 217: 243–246

Araki CT, Back TL, Padberg FT, Thompson PN et al (1993) Refinements in the ultrasonic detection of popliteal vein reflux. J Vasc Surg 18: 742–748

Arko FR et al (2003) Intrasac flow velocites predict sealing of type II endoleaks after endovascular abdominal aortic aneurysm repair. J Vasc Surg 37: 8–15

Arlart IP, Ingrisch H (1984) Renovaskuläre Hypertonie. Radiologische Diagnostik und Therapie. Thieme, Stuttgart

Ascer E, Lorenso E, Pollina RM, Gennaro M (1995) Preliminary results of a nonoperative approach to saphenofemoral junction thrombophlebitis. J Vasc Surg 22: 616–621

Ascer E, Pollina RM, Gennaro M, Lorensen E (1995) Noninvasive predictors of patency for infrapopliteal PTFE bypasses with combined arteriovenous fistula and vein interposition technique. Am J Surg 170: 103–105

Ascer E, Mazzariol F, Hingorani A, Dalles-Cunba S, Gade P (1999) The use of duplex ultrasound arterial mapping as an alternative to conventional arteriography for primary and secondary infrapopliteal bypasses. Am J Surg 178: 162–165

Atri M, Herba MJ, Reinhold C, Leclerc J et al (1996) Accuracy of sonography in the evaluation of calf deep vein thrombosis in both postoperative surveillance and symptomatic patients. Am J Roentgenol 166: 1361–1367

Aube C, Oberti F, Korali, et al (1999) Ultrasonographic diagnosis of hepatic fibrosis or cirrhosis. J Hepatol 30: 472–478

Aune S, Pedersen OM, Trippestad A (1998) Surveillance of above-knee prosthetic femoropopliteal bypass. Eur J Vasc Endovasc Surg 16: 509–512

Avasthi PS, Voyles WF, Greene ER (1984) Noninvasive diagnosis of renal artery stenosis by echo-Doppler velocimetry. Kidney Int 25: 824–829

Baker WH, Stoney RJ (1972) Acquired popliteal entrapment syndrome. Arch Surg 105: 780–781

Baker SR, Burnard KG, Sommerville KM, Thomas ML, Wilson NM (1993) Comparison of venous reflux assessed by duplex scanning

and descending phlebography in chronic venous disease. Lancet 341: 400–403
Banafsche R, Riester U, Bettolo W, Banafsche N, Motzkau D, Quendt J, Hupp T (1993) Wert der Erfassung von Karotisplaquemerkmalen mit B-Bild-Sonographie und farbkodierter Dopplersonographie. Gefässchirurgie 3: 92–100
Bandyk DF, Cato RF, Towne JB (1985) A low flow velocity predicts failure of femoropopliteal and femorotibial bypass grafts. Surg 98: 799–809
Bandyk DF, Scabrook GR, Moldenauer P et al (1988) Hemodynamics of vein graft stenoses. J Vasc Surg 8: 688–695
Bandyk DF, Schmitt DD, Seabrook GR (1989) Monitoring functional patency of in situ saphenous vein bypasses: The impact of a surveillance protocol and elective revision. J Vasc Surg 9: 286–296
Bandyk DF, Cato RF, Towne JB (1991) A low flow velocity predicts failure of femoropopliteal and femorotibial bypass grafts. Radiology 180: 379–386
Bärlin E, Schäberle W, Junge H, Seitz K, Rettenmaier G (1988) In-vitro-Untersuchung zur Meßgenauigkeit der mittleren Blutflußgeschwindigkeit bei Duplex-Geräten (abstract). Ultraschall Klin Prax Suppl 1: 69
Barnes RW (1985) Doppler ultrasonic diagnosis of venous disease. In: Bernstein EF (ed) Noninvasive diagnostic techniques in vascular disease. Mosby, Saint Louis, p 344
Barnes RW (1991) Noninvasive diagnostic assessment of peripheral vascular disease. Circulation 83 [Suppl 2]: 120–127
Barnes RW, Wu KK, Hoak JC (1975) Fallibility of the clinical diagnosis of venous thrombosis. JAMA: 605
Barnes RW, Nix ML, Barnes CL, Lavender RC et al (1989) Perioperative asymptomatic venous thrombosis: role of duplex scanning versus venography. J Vasc Surg 9: 251–260
Barrelier MT (1993) Superficial venous thromboses of the legs. Phlebology 46: 633–639
Bartels E (1992) Farbkodierte Dopplersonographie der Vertebralarterien. Vergleich mit der konventionellen Duplexsonographie. Ultraschall Med 13: 59–66
Bartels E, Flügel KA (1993) Advantages of color Doppler imaging for the evaluation of the vertebral arteries. J Neuroimag 3: 229–233
Barwegen MGMH, van Dongen RJAM (1987) Neurovaskuläre Kompressionssyndrome an der oberen Thoraxapertur und ihre vaskulären Komplikationen. In: Heberer G, van Dongen RJAM (eds) Gefäßchirurgie (Kirschnersche allgemeine und spezielle Operationslehre, vol 11). Springer, Berlin Heidelberg New York Tokyo, pp 571–584
Baumgartner I, Maier SE, Koch M et al (1993) Magnetresonanzarteriographie, Duplexsonographie und konventionelle Arteriographie zur Beurteilung der peripheren arteriellen Verschlußkrankheit. Fortschr Röntgenstr 159: 167–173
Baxter GM, McKechnie S, Duffy P (1990) Colour Doppler ultrasound in deep venous thrombosis: a comparison with venography. Clin Radiol 42: 32–36
Baxter GM, Aitchison F, Sheppard D et al (1996) Colour Doppler ultrasound in renal artery stenosis: intrarenal waveform analysis. Br J Radiol 69: 810–815
Beach KW (1992) 1975–2000: a quarter century of ultrasound technology. Ultrasound Med Biol 18: 377–388
Becker HM, Kortmann H (1987) Nahtaneurysmen. In: Heberer G, Van Dongen RJAM (eds) Gefäßchirurgie(Kirschnersche allgemeine und spezielle Operationslehre, vol 11). Springer, Berlin Heidelberg New York Tokyo, pp 178–184
Becker D, Strobel D, Hahn EG (2000) Tissue harmonic imaging und contrast harmonic imaging. Verbesserung der Diagnose von Lebermetastasen. Der Internist 41: 17–23
Beil PRF, Brennan J (1991) Vein graft surveillance by duplex scanning and pressure measurement. In: Greenhalg RM (ed) The maintenance of arterial reconstruction. Saunders, London, p 135
Belcaro G (1992) Evaluation of recurrent deep venous thrombosis using colour duplex scanning in comparison with venography. VASA 21: 22–26
Belcaro G, Nicolaides AN, Veller M (1995) Venous disorders. A manual of diagnosis and treatment. Saunders, London Philadelphia Toronto, p 99
Belkin M, Raftery KB, Mackey WC, McLaughlin RL, Umphrey SE, Kunkemueller A (1994) A prospective study of the determinants of vein graft flow velocity: implications for graft surveillance. J Vasc Surg 19: 259–267
Bendick PJ et al (2003) Efficacy of ultrasound scan contrast agents in the noninvasive follow-up of aortic stent grafts. J Vasc Surg 37: 381–385
Benson CB, Aruny JE, Vickers MA (1993) Correlation of duplex sonography with arteriography in patients with erectile dysfunction. AJR Am J Roentgenol 160: 71–73
Benvegna S, Cassina I, Giuntini G, Rusignuolo F, Talarico F, Florena M (1990) Atherothrombotic microembolism of the lower extremities (the blue toe syndrome) from atherosclerotic non-aneurysmal aortic plaques. J Cardiovasc Surg 31: 87–91
Berguer R, Hwang NHC (1974) Critical arterial stenosis. A theoretical and experimental solution. Ann Surg 180: 39–50
Berland LL, Koslin DB, Routh WD, Keller FS (1990) Renal artery stenosis: prospective evaluation of diagnosis with color duplex US compared with angiography – work in progress. Radiology 174: 421– 423
Bernardi E, Prandoni P, Lensing AWA, Agnelli G, Guazzaloca G, Scannapieco C, Piovella F, Verlato F, Tomasi C, Moia M, Scarano L, Girolami A (1998) D-Dimer testing as an adjunct to ultrasonography: prospective cohort study. BMJ 317: 1037–1040
Bettmann AM, Paulin S (1977) Leg phlebography. The incidence, nature and modifications of undesirable side effects. Radiol Diagn 122: 101
Bettmann M, Salzman E, Rosenthal D et al (1980) Reduction of venous thrombosis complicating phlebography. AJR 134: 1169–1172
Beven EG (1991) Thoracic outlet syndromes. In: Young JR, Graor RA, Olin JW, Bartholomew JR (eds) Peripheral vascular diseases. Mosby, St. Louis, pp 497–509
Biemans RGM (1987) Kompressionssyndrom der Arteria poplitea. In: Heberer G, van Dongen RJAM (eds) Gefäßchirurgie (Kirschnersche allgemeine und spezielle Operationslehre, vol 11). Springer, Berlin Heidelberg New York Tokyo, pp 593–599
Biland L, Lemgo E, Widmer LK (1987) Zur Epidemiologie der venösen Thromboembolie. Internist 28: 285
Blackshear WM, Phillips DJ, Chikos PM, Harley JD et al (1980) Carotid artery velocity patterns in normal and stenotic vessels. Stroke 11: 67–71
Blättler W (1993) Komplikationen der Thrombophlebitis superficialis. Schw Med Wschr 123: 223–228
Blättler W, Bulling B, Hertel T, Rabe E (1996) Leitlinien zur Diagnostik und Therapie der Thrombophlebitis. Phlebologie 25: 197–198
Blättler W, Linder C, Blättler IK et al (1996) Die ambulante Behandlung der akuten tiefen Beinvenenthrombose (TVT): eine randomisierte prospektive Studie. Schweiz Med Wochenschr 126 [Supp l]: 74
Blättler W, Partsch H, Hertel T (1996) Leitlinien zur Diagnostik und Therapie der tiefen Bein- und Beckenvenenthrombose. Phlebologie 25: 199–203
Bluth EL, Kay D, Merritt CRB, Sullivan M, Farr G, Mills NL, Foreman M, Sloan K, Schlater M, Stewart J (1986) Sonographic characterization of carotid plaque: detection of hemorrhage. AJR 146: 1061–1065
Bluth EL, Stavros AT, Marich KW, Wetzner SM, Aufrichtig D, Baker JD (1988) Carotid duplex sonography: a multicenter recommendation for standardized imaging and Doppler criteria. Radiographics 8: 487–506
Bock RW, Gray-Weale AC, Mock PA et al (1993) The natural history of asymptomatic carotid artery disease. J Vasc Surg 17: 160–171
Bodily K, Buttorff J, Nordesgaard A, Osborne R Jr (1996) Aortoiliac reconstruction without angiography. Am J Surg 171: 505–507

Böhm B et al (2000) Der Wert der farbkodierten kontrastmittelunterstützten Duplexsonographie bei der Erfassung von Endoleckagen nach Aortenstentimplantation im mittleren Nachuntersuchungszeitraum von 15 Monaten. Gefäßchirurgie 5: 225–231
Bollinger A (1979) Funktionelle Angiologie. Thieme, Stuttgart
Bollinger A, Franzeck UK (1982) Diagnose der tiefen Becken- und Beinvenenthrombose. Schweiz Med Wochenschr 112: 550–556
Bolondi L, Bassi SL, Gaiani S et al (1991) Liver cirrhosis: changes of Doppler waveform of hepatic veins. Radiology 178: 513–516
Bolondi L, Gaiani S, Gebel M (1998) Portohepatic vascular pathology and liver disease: diagnosis and monitoring. European J Ultrasound 7 [Suppl 3]: 41–52
Bommer WJ, Miller L (1982) Real-time two dimensional color flow Doppler: enhanced Doppler flow imaging in the diagnosis of cardiovascular disease (abstract). Am J Cardiol 49: 944
Bönhof JA, Meairs SP, Wetzler H (1990) Duplex- und Farbdopplersonographische Kriterien von Nierenarterienstenosen (abstract). Ultraschall Klin Prax 5: 187
Bonnefous O, Pasque P (1986) Time domain formulation of pulse-Doppler ultrasound and blood velocity estimation by cross correlation (Ultrasonic Imaging 8). Academic Press, pp 73–85
Bork-Wölwer L, Wuppermann TH (1991) Verbesserung der nichtinvasiven Diagnostik der V. saphena magna- und der Vena saphena parva-Insuffizienz durch die Duplex-Sonographie. VASA 20: 343–247
Börner N (1991) Diagnostische und prognostische Bedeutung der Echomorphologie tiefer Becken-Bein-Venenthrombosen. Habilitationsschrift Mainz
Börner N, Todt M, Schuter CJ, Meyer J (1987) Sonographie in der Diagnostik venöser Thromben. Klin Wochenschr 65 [Suppl 9]: 37
Boström A, Ljungman C, Hellberg A, Logason K, Bärlin T, Östholm G, Karacagil S (2002) Duplex scanning as the sole preoperative imaging method for infrainguinal arterial surgery. Eur J Vasc Endovasc Surg 23: 140–145
Bouchet C, Magne JL, Lacaze R, Lebrun D, Franco A (1986) L'anévrisme de la veine poplitée: une cause rare d'embolie pulmonaire à répétition. J Mal Vasc 11: 190–193
Bouhoutsos J, Daskalakis E (1981) Muscular abnormalities affecting the popliteal vessels. Br J Surg 68: 501–506
Bouhoutsos J, Martin P (1974) Popliteal aneurysm, a review of 116 cases. Br J Surg 61: 469–475
Bounameaux H (2002) Integrated diagnostic approach to suspected deep vein thrombosis and pulmonary embolism. VASA 31: 15–21
Bounameaux H, De Moerloose P, Reber G (1994) Plasma measurement of D-dimer as diagnostic aid in suspected venous thromboembolism: an overview. Thromb Haemost 71: 1–6
Bowersox JC, Zwolak RM, Walsh DB, Schneider JR, Musson A, LaBombard E, Cronenwett JL (1991) Duplex ultrasonography in the diagnosis of celiac and mesenteric artery occlusive disease. J Vasc Surg 14: 780–788
Brandl R, Orend KH, Becker HM (1993) Rekonstruktionsprinzipien bei peripherer arterieller Verschlußkrankheit der unteren Extremitäten. Dt Ärztebl 37: 1616–1620
Brandstetter K, Schwarzer JU, Bautz W, Pickl U, Lenz M (1993) Vergleich der Farbduplexsonographie mit der selektiven penilen DSA bei der Abklärung der erektilen Dysfunktion. Fortschr Röntgenstr 158: 405–409
Braun B, Scheffler P, Kiehl R, Wenzel E (1986) A duplex system for evaluation of venous function. In: Maurer PC, Becker HM, Heidrich H, Hoffmann G, Kriessmann A, Müller-Wiefel H, Prätorius C (eds) What is new in angiology? Trends and controversies, Proceedings. Zuckschwerdt, Munich
Braunwald E (1984) Heart disease. A textbook of cardiovascular medicine. Saunders, Philadelphia
Breitenseher M, Kainberger F, Hübsch P, Trattnig S, Baldt M, Barton P, Karnel F (1992) Screening von Nierenarterienstenosen. Fortschr Röntgenstr 156: 228–231
Brescia MJ, Cimino JE, Appel K, Burwich BJ (1966) Chronic hemodialysis using venipuncture and a surgically created arteriovenous fistula. New Engl J Med 275: 1089–1092
Brittinger WD, Twittenhoff W-D, Walker G, Konrad N (1966) Revaskularisation des Dialyseshunts. Nieren- und Hochdruckkrankheiten 25: 4–9
Brown JM, Hammers LW, Barton JW, Holland CK, Scoutt LM, Pellerito JS, Taylor KJ (1995) Quantitative Doppler assessment of acute scrotal inflammation. Radiology 197: 427–431
Bunk A, Buchcik R, Konopke R et al (2000) Farbdoppler, Power-Doppler, Echokontrastmittel. Verbesserung der perioperativen Diagnostik? Internist 41: 29–36
Burckhardt CB (1993) Signalverarbeitung in Ultraschallabbildung, Doppler und Dopplerabbildung. Ultraschall Med 14: 220–224
Bushong SC, Archer BR (1991) Diagnostic ultrasound. Physics, biology and instrumentation. Mosby Year Book, St. Louis
Buth J, Disselhoff B, Sommeling C, Stam L (1991) Color-flow duplex criteria for grading stenosis in infrainguinal vein grafts. J Vasc Surg 14: 716–726.
Calligaro KD, Musser DJ, Chen AY, Dougherty MJ, McAffee-Bennett S, Doerr KJ et al (1996) Duplex ultrasonography to diagnose failing arterial prosthetic grafts. Surg 120: 455–459
Calligaro KD, Syrek JR, Dougherty MJ, Rua I, McAffee-Bennett S, Doerr KJ et al (1998) Selective use of duplex ultrasound to replace preoperative arteriography for failing arterial vein grafts. J Vasc Surg 27: 89–95
Cardella JF, Young AT, Smith TP et al (1988) Lower extremity venous thrombosis. Comparison of venography, impedance plethysmography and intravenous manometry. Radiology 168: 109
Carpenter JP, Holland GA, Baum RA, Owen RS, Carpenter JT, Cope C (1993) Magnetic resonance venography for the detection of deep venous thrombosis: comparison with contrast venography and duplex Doppler ultrasonography. J Vasc Surg 18: 734–741
Carpenter JP, Lexa FJ, Davis JT (1995) Determination of sixty percent or greater carotid artery stenosis by duplex Doppler ultrasonography. J Vasc Surg 22: 697–705
Carr S, Farb A, Pearce WH, Virmani R, Yao JST (1996) Atherosclerotic plaque rupture in symptomatic carotid artery stenosis. J Vasc Surg 23: 755–766
CASANOVA Study Group (1991) Carotid surgery versus medical therapy in asymptomatic carotid stenosis. Stroke 22: 1229–1235
Chahlaoui J, Julien M, Nadeau P, Bruneau L, Roy P, Sylvestre J (1981) Popliteal venous aneurysm: a source of pulmonary embolism. AJR 136: 415–416
Chalmers RTA, Hoballah JJ, Kresowik TF, Sharp WJ, Synn AY, Miller E, Corson JD (1994) The impact of color duplex surveillance on the outcome of lower limb bypass with segments of arm veins. J Vasc Surg 19: 279–288
Chang BB, Leather RP, Kaufman JL, Kupinski AM, Leopold PW, Shah DM (1990) Haemodynamic characteristics of failing infrainguinal in situ vein bypass. J Vasc Surg 12: 596–600
Chawla Y, Santa N, Dhiman RK, et al (1998) Portal hemodynamics by duplex Doppler sonography in different grades of cirrhosis. Dig Dis Sci 43: 354–357
Chengelis DL, Bendick PJ, Glover PJL, Brown OW, Ranaval TJ (1996) Progression of superficial venous thrombosis to deep vein thrombosis. J Vasc Surg 24: 745–749
Chervu A, Moore WS (1994) Carotid endarterectomy without arteriography: personal series and review of the literature. Ann Vasc Surg 8: 296–302
Chuang VP, Mena CE, Hoskins PA (1974) Congenital anomalies of the inferior vena cava. Review of embryogenesis and presentation of a simplified classification. Br J Radiol 47: 206–213
Claudon M, Plouin PF, Baxter GM et al for the Levovist renal artery stenosis study group (2000) Renal arteries in patients at risk of renal arterial stenosis: multicenter evaluation of the echo-enhancer SHU 508 A at color and spectral Doppler US. Radiology 214: 739–746

Clifford TA, Back T, Padberg FT, Thompson PN, Duran WN, Hobson RW (1993) Refinements in the ultrasonic detection of popliteal vein reflux. J Vasc Surg 18: 742–748

Coelho JCU, Sigel B, Ryva JC, Machi J, Renigers SA (1982) B-mode sonography of blood clots. J Clin Ultrasound 10: 323–327

Cogo A, Lensing AWA, Koopman MMW, Piovella F, Siragusa S, Wells PS, Villata S, Büller HR, Turpie AGG, Prandoni P (1998) Compression ultrasonography for diagnostic management of patients with clinically suspected deep vein thrombosis: a prospective cohort study. BMJ 316: 17–20

Colli A, Cocciolo M, Riva C et al (1994) Abnormalities of Doppler waveform of the hepatic veins in patients with chronic liver disease: correlation with histologic findings. AJR 162: 833

Collin J, Auranja H, Sutton GLJ, Lindsell D, Oxford D (1988) Screening programme for abdominal aortic aneurysm in men aged 65 to 74 years. Lancet II: 613–615

Comerota AJ, Katz ML, Greenwald LL, Leefmans E, Czeredarczuk M, White JV (1990) Venous duplex imaging: should it replace hemodynamic tests for deep venous thrombosis? J Vasc Surg 11: 53–59

Connell J (1978) Popliteal vein entrapment. Br J Surg 65: 351

Correas J-M, Hélénon O, Pourcelot L, Moreau J-F (1997) Ultrasound contrast agents. Acta Radiologica 38 [Suppl 412]: 101–112

Cosgrove D (1997) Echo enhancers and ultrasound imaging. Eur J Radiol 26: 64–76

Cosgrove DO, Arger PH (1982) Intravenous echoes due to laminar flow – experimental observations. Am J Radiol 139: 953–956

Cosgrove DO, Blomley MJK, Jayaram V et al (1998) Echo-enhancing (contrast) agents. Ultrasound Quarterly 14: 66–75

Cossman DV, Ellison JE, Wagner WH, Carroll RM et al (1989) Comparison of contrast angiography to arterial mapping with color-flow duplex imaging in the lower extremities. J Vasc Surg 10: 522–529

Crawford ES, Hess KR (1989) Abdominal aortic surgery. N Engl J Med 321: 1040–1042

Croft RJ, Ellam LD, Harrison MJG (1980) Accuracy of carotid angiography in the assessment of atheroma of the internal carotid artery. Lancet I: 997–1000

Cronan J (1993) Venous thromboembolic disease: the role of US. Radiology 186: 619–630

Cronan J, Leen V (1989) Recurrent deep venous thrombosis: limitations of US. Radiology 170: 739–742

Cronan JJ, Dorfman GS, Scola FH, Schepps B, Alexander J (1987) Deep venous thrombosis. Ultrasonographic assessment using vein compression. Radiology 162: 191–194

Cronan JJ, Dorfman GS, Gusmark J (1988) Lower-extremity deep venous thrombosis: further experience with and refinements of ultrasound assessment. Radiology 168: 101

Cronenwett JL, Krupski WC, Rutherford RB (2000) Abdominal aortic and iliac aneurysms. In: Rutherford RB (ed) Vascular surgery, 5th edn. Saunders, Philadelphia, pp 1246–1280

Cvitanic OA, Cronan JJ, Sigman M, Landau ST (1993) Varicoceles: postoperative prevalence – a prospective study with color Doppler US. Radiology 187: 711–714

Dahl JR, Freed TA, Burke MF (1976) Popliteal vein aneurysm with recurrent pulmonary thrombo-emboli. JAMA 236: 3531–3532

Dasbach G, Schmitz I, Niehoff L, Edelmann M, Müller K-M (1998) Arteriosklerose der Karotisregion. Gefässchirurgie 3: 151–157

D'Audiffret A et al (2001) Follow-up evaluation of endoluminally treated abdominal aortic aneurysms with duplex ultrasonography: validation with computed tomography. J Vasc Surg 33: 42–50

Dauzat MM, Laroche J-R, Charras CC, Blin B, Domingo-Faye MM (1986) Real-time B-mode ultrasonography for better specificity in the noninvasive diagnosis of deep vein thrombosis. J Ultrasound Med 5: 625–631

Davidson JT, Callis JT (1993) Arterial reconstruction of vessels in the foot and ankle. Ann Surg 217: 699–708

Davies KN, Humphrey PR (1993) Complications of cerebral angiography in patients with symptomatic carotid territory ischaemia screened by carotid ultrasound. J Neurol Neurosurg Psychiatry 56: 967–972

De Bakey ME, Henly WS, Cooley DA et al (1965) Surgical management of dissecting aneurysms of the aorta. J Thorac Cardiovasc Surg 49: 130–148

De Bray JM, Glatt B (1994) Quantification of atheromatous stenosis in the extracranial internal carotid artery. Cerebrovasc Dis 5: 414–426

De Bray JM, Baud JM, Dauzat M on behalf of the Consensus Conference (1997) Consensus concerning the morphology and the risk of carotid plaques. Cerebrovasc Dis 7: 289–296

De Smet AA, Kitslaar PJ (1990) A duplex criterion for aorto-iliac stenosis. Eur J Vasc Surg 4: 275–278

De Smet AEA, Ermers EJM, Kitslaar PJ (1996) Duplex velocity characteristics of aortoiliac stenoses. J Vasc Surg 23: 628–636

De Valois JC, van Schaik CC, Verzijlbergen F, van Ramshorst B, Eikelboom BC, Meuwissen OJA (1990) Contrast venography: from gold standard to „golden backup" in clinically suspected deep vein thrombosis. Eur J Radiol 11: 131–137

DEGUM, Arbeitskreis Gefäßdiagnostik (1986) Richtlinien für die Durchführung dopplersonographischer Untersuchungen der Bekken- und Beinvenen. Deutsche Ges Angiologie, Mitteilungen 3. Demeter, Gräfelfing, Germany

DEGUM, Arbeitskreis Gefäßdiagnostik (1991) Richtlinien für die Durchführung doppler- und duplexsonographischer Untersuchungen peripherer Arterien und Venen, extrakranieller hirnversorgender Halsarterien und intrakranieller Arterien. Mitteil Angiol 1: 10–17

Delcker A, Diener HC (1992) Die verschiedenen Ultraschallmethoden zur Untersuchung der A. vertebralis: Eine vergleichende Wertung. Ultraschall Med 13: 213–220

Denzel C, Balzer K, Muller KM, Fellner F, Fellner C, Lang W (2003) Relative value of normalized sonographic in vitro analysis of arteriosclerotic plaques of internal carotid artery. Stroke 34: 1901–1906

Denzel C, Fellner F, Wutke R, Bazler K, Muller KM, Lang W (2003) Ultrasonographic analysis of arteriosclerotic plaques in the internal carotid artery. Eur J Ultrasound 16: 161–167

Desai KM, Gilbert HG (1991) Noninvasive investigation of penile artery function. In: Kirby RS, Carson CC, Webster GD (eds) Impotence: Diagnosis and management of male erectile dysfunction. Butterworth-Heinemann, Oxford, pp 81–91

Desberg AL, Paushter DM, Lammert GK et al (1990) Renal artery stenosis: evaluation with color Doppler flow imaging. Radiology 177: 749–753

DeWire DM, Begun EP, Lawson RK, Fitzgerald S, Foley WD (1992) Color Doppler ultrasonography in the evaluation of the acute scrotum. J Urol 147: 89–91

Diamaria G, Zittoun R, Reynes M (1981) Anévrisme veineux poplité révélé par une embolie pulmonaire. Ann Cardiol Angéiol 30: 337–338

Dion JE, Gates PC, Fox AJ, Barnett HJM, Blom RJ (1987) Clinical events following neuroangiography: a prospective study. Stroke. 18: 997–1004

Disselhof B, Buth J, Jakimowicz J (1989) Early detection of stenosis of femoro-distal grafts. A surveillance study using colour-duplex scanning. Eur J Vasc Surg 3: 43–48

Do DD, Zehender T, Mahler F (1993) Farbkodierte Duplexsonographie bei iatrogenen Aneurysmata spuria in der Leiste. Dtsch Med Wochenschr 118: 656–660

Donald IP, Edwards RD (1982) Fatal outcome from popliteal venous aneurysm associated with pulmonary embolism. Br J Radiol 55: 930–931

Dougherty MJ, Calligaro KD, DeLaurentis DA (1998) The natural history of „failing" arterial grafts in a duplex surveillance protocol. Ann Vasc Surg 12: 255–259

Droste C, von Planta M (1989) Memorix, 2nd revised edition. VCH Verlagsgesellschaft, Weinheim (Germany)

Dunant JH, Eugenidis N (1973) Cystic degeneration of the popliteal artery. VASA 2: 156–159ECST European Carotid Surgery Trialists Collaborative Group (1991) MRC European Carotid Surgery Trial: interim results for symptomatic patients with severe (70–90%) or with mild (0–29%) carotid stenosis. Lancet 337: 1235–1243

ECST Collaborative Group (1996) Endarterectomy for moderate symptomatic carotid stenosis: interim results from the MRC European Carotid Surgery Trial. Lancet 347: 1591–1593

Edmondson HT, Crowe JA (1972) Popliteal artery and venous entrapment. Ann Surg 38: 657–659

Edwards JM, Coldwell DM, Goldman ML, Strandness DE Jr (1991) The role of duplex scanning in the selection of patients for transluminal angioplasty. J Vasc Surg 13: 69–74

Effeney DJ, Fiedmann MB, Gooding GAW (1984) Iliofemoral venous thrombosis. Real-time ultrasound diagnosis. Normal criteria and clinical application. Radiology 150: 787–792

Eichlisberger R, Jäger K (1989) Beeinflussung der venösen Hämodynamik durch Venenpharmaka. Nachweis mittels Duplexsonographie. Was gibt es Neues in der Phlebologie (Kurzfassung)

Eisman BH, Legemate DA, de VosHJ, Mali WP, Eikelboom BC (1997) Hyperaemic colour duplex scanning for the detection of aortoiliac stenoses. A comparative study with intraarterial pressure measurement. Eur J Vasc Endovasc Surg 14: 462–467

El-Barghouti N, Geroulkas G, Nicolaides A, Androulakis A, Bahal V (1995) Computer-assisted carotid plaque characterization. Eur J Vasc Endovasc Surg 9: 389–393

El-Barghouti N, Nicolaides A, Bahal V, Geroulakos G, Androulakis A (1996) The identification of the high risk carotid plaque. Eur J Vasc Endovasc Surg 11: 470–478

El-Barghouti NM, Levine T, Ladva S, Flanagan A, Nicolaides A (1996) Histological verification of computerised carotid plaque characterization. Eur J Vasc Endovasc Surg 11: 414–416

Elias A, Le Croff G, Bouvier JL, Benichou A, Serradimigni A (1987) Value of real-time B-mode ultrasound imaging in the diagnosis of deep vein thrombosis of the lower limbs. Inter Angio 6: 175–182

Elsman BH, Legemate DA, van der Heyden FW et al (1996) The use of color-coded duplex scanning in the selection of patients with lower extremity arterial disease for percutanous transluminal angioplasty: a prospective study. Cardiovasc Intervent Radiol 19: 313–316

Engberding R (1990) Untersuchungstechniken in der Echokardiographie. Springer, Berlin Heidelberg New York, pp 183–193

Erickson SJ, Mewissen MW, Foley WD, Lawson TL, Middleton WD, Quiroz FA, Macrander SJ, Lipchik EO (1989) Stenosis of the internal carotid artery: assessment using color imaging compared with angiography. Am J Roentgenol 152: 1299–1305

Evers EJ, Wuppermann Th (1995) Ultraschalldiagnostik bei postthrombotischem Syndrom. Eine vergleichende Untersuchung mittels Farbduplex, CW-Doppler und B-Bildsonographie. Ultraschall in Med 16: 259–263

Evers EJ, Wuppermann Th (1997) Die Charakterisierung des postthrombotischen Refluxes mittel farbkodierter Duplexsonographie. VASA 26: 190–193

Evers EJ, Wuppermann Th (1997) Langzeitverlaufbeobachtung der venösen Hämodynamik bei postthrombotischem Syndrom mittels Farbdopplersonographie. Ultraschall 18 [Suppl 1]: 54

Falk E (1992) Why do plaques rupture? Circulation 86 [Suppl III]: III30-III42

Falk RL, Smith DF (1987) Thrombosis of upper extremity thoracic inlet veins: diagnosis with duplex Doppler sonography. Am J Radiol 149: 677–682

Faught WE, Mattos MA, van Bemmelen PS et al (1994) Color-flow duplex scanning of carotid arteries: new velocity criteria based on receiver operator characteristic analysis for threshold stenoses used in the symptomatic and asymptomatic carotid trials. J Vasc Surg 19: 818–828

Fay JJ (1985) Anévrisme veineux poplité. Thèse Médicine, No. 78, Lille

Federman J, Anderson ST, Rosengarten DS, Pitt A (1977) Pulmonary embolism secondary to anomalies of deep venous system of the leg. Br Heart J 39: 547–552

Feigenbaum H (1986) Echocardiography. Lea & Febiger, Philadelphia, pp 1–49

Feinstein SB, Cheirif J, ten Cate FJ et al (1990) Safety and efficacy of a new transpulmonary ultrasound contrast agent: initial multicenter clinical results. J Am Coll Cardiol 16: 316–324

Fell G, Phillips DJ, Chikos PM, Harley JD, Thiele BL, Strandness DE (1981) Ultrasonic duplex scanning for disease of the carotid artery. Circulation 64: 1191–1195

Fellmeth BD, Roberts AC, Bookstein JJ et al (1991) Post-angiographic femoral artery injuries: nonsurgical repair with US-guided compression. Radiology 178: 671–675

Ferrer EJM, Samso J, Serrando R et al (2000) Use of ultrasound in the diagnosis of carotid artery occlusion. J Vasc Surg 31: 736–741

Ferretti G, Salomone A, Castagno PL (1988) Renovascular hypertension: a non-invasive duplex scanning screening. Int Angiol 7: 219–223

Fisher AJ, Paulson EK, Kliewer MA et al (1998) Doppler sonography of the portal vein and hepatic artery: measurement of a prandial effect in healthy subjects. Radiology 207: 711–715

Fitzgerald SW, Foley WD (1991) Genitourinary system. In: Lanzer P, Yoganathan AP (eds) Vascular imaging by color Doppler and magnetic resonance. Springer, Berlin

Flanigan DP, Burnham SJ, Goodreau JJ et al (1979) Summary of cases of adventitial cystic disease of the popliteal artery. Ann Surg 189: 165

Fletcher JP, Kershaw LZ, Barker DS (1990) Ultrasound diagnosis of lower limb deep venous thrombosis. Med J Aust 153: 453–455

Flückiger F, Steiner H, Rabl H, Waltner F (1991) Zystische Adventitia-Degeneration der Arteria poplitea: Sonographische Sicherung der Diagnose. Ultraschall Med 12: 84–87

Fobbe F (1993) Periphere Venen. In: Wolf KJ, Fobbe F (eds) Farbkodierte Duplexsonographie. Thieme, Stuttgart New York, pp 114–129

Fobbe F, Wolf K-J (1988) Erste klinische Erfahrungen mit der Angiodynographie. Fortschr Röntgenstr 148: 259–264

Fobbe F, Koennecke H-C, El Bedewi M, Heidt P, Boese-Landgraf J, Wolf K-J (1989) Diagnostik der tiefen Beinvenenthrombose mit farbkodierter Duplexsonographie. Fortschr Röntgenstr 151: 569

Fobbe F, Ruhnke-Trautmann M, van Gemmeren D, Hartmann CA, Kania U, Wolf K-J (1991) Altersbestimmung venöser Thromben im Ultraschall. Fortschr Röntgenstr 155: 344–348

Foley WD (1991) Color Doppler flow imaging. Andover Medical Publishers, Boston

Foley WD, Middleton WD, Lawson TL, Erickson S, Quiroz FA, Macrander S (1989) Color Doppler ultrasound imaging of lower-extremity venous disease. Am Roentgenol 152: 371–376

Fontenelle LJ, Simber SC, Hanson TL (1994) Carotid duplex scan versus angiography in the evaluation of carotid artery disease. Ann Surg 60: 864–868

Forsberg F, Liu J-B, Burns PN, Merton DA, Goldberg BB (1994) Artifacts in ultrasonic contrast agent studies. J Ultrasound Med 13: 357–365

Forster S, Embree PM, O'Brien WD (1990) Flow velocity profile via time-domain correlation: error analysis and computer simulation. IEEE Trans Ultrason Ferroelect Freq Control 37: 164–175

Foster JH, Dean RH, Pinkterton JA Rhamy RK (1973) Ten years experience with the surgical management of renovascular hypertension. Ann Surg 177: 755–760

Francois GF, Jausseran JM, Giuly J (1988) Anévrisme veineux poplité. Presse Med 17: 755

Frank E, Anderson C, Ribinstein D (1978) Frequency of sexual dysfunction in „normal" couples. N Engl J Med 299: 111–115

Fraser JD, Anderson DR (1999) Deep venous thrombosis: recent advances and optimal investigation with US. Radiology 211: 9–24

Frauchinger B, Holtz D, Eichlisberger R, Jäger KA (1995) Duplexsonographie zur Abklärung der renovaskulären Hypertonie und bei Durchblutungsstörungen der Transplantatniere. In: Jäger KA, Eichlisberger R (eds) Sono-Kurs – Ein konzentrierter Refresherkurs über die gesamte Ultraschalldiagnostik. Karger, Basel, pp 114–127

Frimann-Dahl J (1935) Postoperative Röntgenuntersuchungen. Acta Chir Scand 76 [Suppl]: 36

Frühwald F, Blackwell DE (1992) Atlas der farbkodierten Dopplersonographie. Springer, Vienna New York, p101

Fürst G, Kuhn FP, Trappe RP, Modder U (1990) Diagnostik der tiefen Beinvenenthrombose. Farb-Doppler-Sonographie versus Phlebographie. Fortschr Geb Röntgenstr Neuen Bildgeb Verfahr 152: 151–158

Fürst G, Saleh A, Wenserski F et al (1999) Reliability and validity of noninvasive imaging of internal carotid artery pseudo-occlusion. Stroke 30: 1450–1455

Gaiani S, Bolondi L, Li Bassi S, Santi V, Zironi G, Barbara L (1989) Effect of meal on portal hemodynamics in healthy humans and in patients with chronic liver disease. Hepatology 9: 815–819

Gaiani S, Bolondi L, Fenyves D, Zironi G, Rigamonti A, Barbara L (1991) Effect of propranolol on portosystemic collateral circulation in patients with cirrhosis. Hepatology 14: 824–829

Gaitini D (1990) Late changes in veins after deep venous thrombosis: ultrasonic findings. Fortschr. Röntgenstr 153: 68–72

Gaitini D, Kaftori JK, Pery M, Weich YL, Markel A (1988) High-resolution real-time ultrasonography in the diagnosis of deep vein thrombosis. Fortschr Roentgenstr 149: 26

Galen SR, Gambino RS (1975) Beyond normality. The predictive value and efficiency of medical diagnoses. John Wiley and Sons, New York, pp 10–14

Gallacher JJ, Hageman JH (1985) Popliteal vein aneurysm causing pulmonary embolus. Arch Surg 120: 1173–1175

Galland RB, Simmons MJ, Torrie EPH (1991) Prevalence of abdominal aortic aneurysm in patients with peripheral vascular disease. Br J Surg 78: 1259–1260

Gartenschlager M, Klose KJ, Schmidt JA (1996) Diagnose flottierender venöser Thromben mittels Phlebo-Spiral-CT. Fortschr Geb Röntgenstr Neuen Bildgeb Verfahr 164: 376–361

Garth KE, Carroll BA, Sommer FG, Oppenheimer DA (1983) Duplex ultrasound scanning of the carotid arteries with velocity spectrum analysis. Radiology 147: 823–827

Geelkerken RH, Delahunt TA, Schultze Kool LJ et al (1996) Pitfalls in the diagnosis of origin stenosis of the coeliac and superior mesenteric arteries with transabdominal color duplex examination. Ultrasound Med Biol 22: 695–700

Geiger A, Hammel D, Scheld HH, Böcker W (1991) Fallbericht: Ungewöhnlich großer Tumor eines Glomus caroticum. Angio 13: 279–283

Gentile AT, Mills JL, Gooden MA, Westerband A, Cui H, Bermann SS et al (1997) Identification of predictors of lower extremity vein graft stenosis. Am J Surg 174: 218–221

Geroulakos G, Ramaswami G, Nicolaides A, James K, Labropoulos N, Belcaro G, Holloway M (1993) Characterization of symptomatic and asymptomatic carotid plaques using high-resolution real-time ultrasonography. Br J Surg 80: 1274–1277

Geroulakos G, Domjan J, Nicolaides A, Stevens J et al (1994) Ultrasonic carotid artery plaque structure and risk of cerebral infarction on computed tomography. J Vasc Surg 20: 263–266

Gerson L, Martin H (1981) Ectasie veineuse d'origine traumatique. Angiologie 33: 275–278

Gibson MHL, Mill JG, Johnson GE, Downs AR (1977) Ann Surg 185: 341–348

Giyanani VL, Krebs CA, Nall LA, Eisenberg RL, Parvey HR (1989) Diagnosis of abdominal aortic dissection by image-directed Doppler sonography. J Clin Ultrasound 17: 445–448

Glickerman DJ, 0bregon RG, Schmiedl UP, Harrison SD, Macaulay SE, Simon HE, Kohler TR (1996) Cardiac-gated MR angiography of the entire lower extremity: a prospective comparison with conventional angiography. AJR 167: 445–451

Golzarian J et al (2002) Evaluation of abdominal aortic aneurysm after endoluminal treatment: Comparison of color doppler sonography and biphasic helical CT. Am J Rad 178: 623–628

Gooding GAW, Perez S, Rapp JH, Drupski WC (1991) Lower-extremity vascular grafts placed for peripheral vascular disease. Prospective evaluation with duplex Doppler sonography. Radiology 180: 379–386

Gorenstein A, Katz S, Schiller M (1987) Congenital aneurysms of the deep veins of the lower extremities. J Vasc Surg 5: 765–768

Görtler M, Niethammer R, Widder B (1994) Differentiating subtotal carotid artery stenoses from occlusions by colour-coded duplex sonography. J Neurol 241: 301–305

Gramiak R, Shah PM (1968) Echocardiography of the aortic root. Invest Radiol 3: 356–366

Grant EG, Perrella RR (1990) Wishing won't make it so: duplex Doppler sonography in the evaluation of renal transplant dysfunction. AJR 155: 538–539

Grant EG, Duerinckx AJ, El Saden SM, Melany ML et al (2000) Ability to use duplex US to quantify internal carotid arterial stenoses: fact or fiction? Radiology 214: 247–252

Grassi CJ, Polak JF (1990) Axillary and subclavian venous thrombosis: follow-up evaluation with color Doppler flow US and venography. Radiology 175: 651–654

Gray-Weale AC, Graham JC, Burnett JR et al (1988) Comparison of preoperative B-mode ultrasound appearance with carotid endarterectomy specimen pathology. J Cardiovasc Surg 29: 676–681

Green RM, McNamara J, Ouriel K, DeWeese JA (1990) Comparison of infrainguinal graft surveillance techniques. J Vasc Surg 11: 207–214

Greenwood LH, Yrizarry JM, Hallett JW (1982) Peripheral venous aneurysms with recurrent pulmonary embolism: report of a case and review of the literature. Cardiovasc Intervent Radiol 5: 43–45

Grigg MJ, Nicolaides AN, Wolfe JHN (1988) Detection and grading of femorodistal vein graft stenoses: Duplex velocity measurements compared with angiography. J Vasc Surg 8: 661

Grigg MJ, Wolfe JHN, Tovar A, Nicolaides AN (1988) The reliability of duplex derived haemodynamic measurements in the assessment of femoro-distal grafts. Eur J Vasc Surg 2: 177–181

Grosser S, Kreymann G, Guthoff A, Taube C, Raedler A, Tilsner V, Greten H (1990) Farbkodierte Duplexsonographie bei Phlebothrombosen. Dtsch Med Wochenschr 115: 1939–1944

Grosser S, Kreymann G, Kühns A (1991) Duplex-sonographisch quantifiziertes Shuntvolumen und dessen klinische Relevanz. Angio Arch 22: 74–77

Gruss JD, Geissler C (1997) Über das Thoracic-outlet-Syndrom. Gefäßchirurgie 2: 57–64

Gruss JD, Bartels D, Kawai S, Karadedos C, Tsafandakis E, Straubel H, Ohta T (1989) Das Thoracic-outlet-Syndrom. Angio 2: 77

Gubler FM, Laan R, van der Veen F (1996) The value of palpation, varicoscreen contact thermography and colour Doppler ultrasound in the diagnosis of varicocele. Hum Reprod 11: 1232–1235

Haas SB, Tribus CB, Insall JN, Becker MW, Windsor RE (1992) The significance of calf thrombi after total knee arthroplasty. J Bone Joint Surg Br 74: 799 –802

Habscheid W (1988) Einsatz der Real-Time-Sonographie zur Diagnostik der tiefen Beinvenenthrombose auf einer internistischen Intensivstation. Intensivmed Notfallmed 25: 326

Habscheid W, Wilhelm T (1988) Diagnostik der tiefen Beinvenenthrombose durch Real-time-Sonographie. Dtsch Med Wochenschr 113: 586–591

Habscheid W, Landwehr P (1990) Diagnostik der akuten tiefen Beinvenenthrombose mit der Kompressionssonographie. Ultraschall Med 11: 268–273

Habscheid W, Becker W, Höhmann M (1989) Diagnostik der tiefen Beinvenenthrombose. Dtsch Med Wochenschr 114: 837

Habscheid W, Höhmann M, Klein S (1990) Kompressionssonographie

als Verfahren zur Diagnose der akuten tiefen Beinvenenthrombose. Med Klin 85: 6–12
Hach W (1981) Spezielle Diagnostik der primären Varikose. Demeter, Gräfelfing, Germany
Hach W, Hach-Wunderle V (1994) Die Rezirkulationskreise der primären Varikose. Springer, Berlin, Heidelberg
Hach W, Hach-Wunderle V (1996) Phlebographie der Bein- und Bekkenvenen. Schnetztor, Konstanz, pp 89–120
Hach W, Hach-Wunderle V (1998) Diagnostik der tiefen Bein- und Beckenthrombosen durch Phlebographie und Duplex-Sonograpie. Hämostaselogie 18: 11–17
Hach W, Girth E, Lechner W (1977) Einteilung der Stammvarikose der V. saphena magna in 4 Stadien. Phlebol Proktol 6: 116–123
Haerten R (1998) Power-Doppler-Verfahren. In: Bogdahn U, Becker G, Schlachetzki F (eds) Echosignalverstärker und transkranielle Farbduplex-Sonographie. Blackwell Wissenschafts-Verlag, Berlin Vienna, pp 93–99
Haerten R, Kim J (1993) Verfahren der Farbdoppler-Sonographie – Ein Methodenvergleich. Ultraschall Med 14: 225–230
Haimov H, Giron F, Jacobsen JH (1979) The expanded polytetrafluoroethylene graft. Three years' experience with 362 grafts. Arch Surg 114: 673–677
Haire WD, Lynch TG, Lund GB, Lieberman RP, Edney JA (1991) Limitations of magnetic resonance imaging and ultrasound-directed (duplex) scanning in the diagnosis of subclavian vein thrombosis. J Vasc Surg 13: 391–397
Hallam MJ, Reid JM, Cooperberg PL (1989) Color-flow Doppler and conventional dublex scanning of the carotid bifurcation: prospective double-blind correlative study. Am J Roentgenol 152:1101–1105
Hamann H, Cyba-Altunbay S, Schäfer H, Vollmar JF (1986) Asymptomatic carotid artery stenosis. Surgery versus medical treatment (Casanova Study). In: Maurer PC, Becker HM, Heidrich H, Hoffmann G, Kriessmann A, Müller-Wiefel H (eds) What is new in angiology? Zuckschwerdt, Munich, pp 305ff
Hamulyak K, Lensing AWA, van der Meer J, Smid WM, van Ooy A, Hoek JA (1995) Subcutaneous low molecular-weight heparin or oral anticoagulants for the prevention of deep-vein thrombosis in elective hip and knee replacement? Thromb Haemost 76: 1428–1431
Hankey GJ, Warlow CP, Sellar RJ (1990) Cerebral angiographic risk in mild cerebrovascular disease. Stroke 21: 209–222
Hansen LG, Boris P (1986) Aneurysma der Vena femoralis und poplitea. Radiologe 26: 210
Harnoss B-M, Keller F, Häring R, Distler A, Maurer PC (1991) Der Dialyseshunt als chirurgische und nephrologische Aufgabe. Angio Archiv 22
Harns PL, de Cossart L, Moody P, Douglas H (1988) How can we detect and manage fibrous strictures within new grafts? Are these more problematical with reversed than in situ bypass? In: Greenhalgh RM (ed) Limb salvage and amputation for vascular disease. Saunders, London, p 221
Harolds JA, Friedman MH (1977) Venous aneurysms. South Med J 70: 719–721
Hassler W, Steinmetz H, Pirschel J (1991) Transcranial Doppler study of intracranial circulatory arrest. J Neurosurg 71: 195–201
Hatle L, Angelson B (1985) Doppler ultrasound in cardiology. Lea & Febiger, Philadelphia, pp 22–26
Hatsukami TS, Prornozich JF, Zierler RE et al (1992) Color Doppler imaging of infrainguinal arterial occlusive disease. J Vasc Surg 16: 527–533
Hauser M, Brunner U (1994) Neue pathophysiologische und funktionelle Gesichtspunkte zur Insuffizienz der Vena saphena parva. VASA 22: 338–341
Heberer G, van Dongen RJAM (1993) Gefäßchirurgie (Kirschnersche allgemeine und spezielle Operationslehre, vol 11). Springer, Berlin Heidelberg New York Tokyo
Heilberger P et al (1997) Postoperative color flow duplex scanning in aortic endografting. J Endovasc Surg 4: 262
Heinrich U (1993) In-vitro-Untersuchungen an Gefäßstenosen mit der farbkodierten Duplexsonographie unter besonderer Berücksichtigung der Stenosegradbestimmung. Medical Thesis, Universität Würzburg, Germany
Hendrickx PH, Roth U, Brassel F et al (1990) Phantomuntersuchungen zur Wertigkeit der farbkodierten Doppler-Sonographie bei der arteriellen Verschlußkrankheit der unteren Extremitäten. Fortschr Röntgenstr 152: 1–5
Hendrickx PH, Roth U, von der Lieth H (1991) Wertigkeit der Angiodynographie zur Verlaufskontrolle chirurgischer Gefäßprothesen. Ultraschall Med 12: 188–192
Hennerici M, Neuerburg-Heusler D (1988) Gefäßdiagnostik mit Ultraschall. Thieme, Stuttgart
Henricksen JH, Moller S, Schifter et al (1999) Increased arterial compliance in decompensated cirrhosis. J Hepatol 31: 712–8
Herbener TE, Seftel AD, Nehra A, Goldstein I (1994) Penile ultrasound. Semin Urol 12: 320–332
Herzog P, Anastasiu M, Wollbrink W, Herrmann W, Holtermüller K-H (1991) Real-time Sonographie bei tiefer Becken- und Beinvenenthrombose. Med Klinik 86: 132–137
Hill SL, Donato AT (1994) Ability of the carotid duplex scan to predict stenosis, symptoms and plaque structure. Surgery 116: 914–920
Hirschl M, Bernt R (1990) Normalwerte, Reproduzierbarkeit und Aussagekraft duplexsonographischer Kriterien in der Venenfunktionsdiagnostik. Ultraschall Klin Prax 5: 81–84
Hoballah JJ, Nazzal MM, Ryan SM, Martinasevic M, Jacobovicz C, Rossley N et al (1997) Is color duplex surveillance of infrainguinal polytetrafluoroethylene grafts worthwhile? Am J Surg 174: 131–135
Hoffmann U, Edwards JM, Carter S, Goldman ML, Harley JD, Zaccardi MJ, Strandness DE Jr (1991) Role of duplex scanning for the detection of atherosclerotic renal artery disease. Kidney Int 39: 1232–1239
Hofmann W, Forstner R, Sattlegger P, Ugurluoglu A, Magometschnigg H (2001) Die bildgebende Diagnostik pedaler Anschlussgefäße, Gefäßchirurgie. Originalarbeit 6: 98–102
Hollenbeck M, Hilbert N, Meusel F, Grabensee B (1994) Increasing sensitivity and specificity of Doppler sonographic detection of renal transplant rejection with serial investigation technique. Clinical Investigator 72: 609–615
Hollerweger A, Macheiner P, Rettenbacher T, Gritzmann N (2000) Sonographische Diagnose von Muskelvenenthrombosen des Unterschenkels und deren Bedeutung als Emboliequelle. Ultraschall Med 21: 66–7 2
Horrow MM, Stassi J, Shurman A, Brody JD, Kirby CL, Rosenberg HK (2000) The limitations of carotid sonography: interpretative and technology-related errors. Am J Roentgenol 174: 189–194
Hull R, Hirsh, J, Sackett D et al (1981) Clinical validity of a negative venogram in patients with clinically suspected venous thrombosis. Circulation 64: 622–625
Hull R, Raskop G, Leclerc J, Jay R, Hirsh J (1984) The diagnosis of clinically suspected venous thrombosis. Clin Chest Med 5: 439–456
Hust MH, Schuler A (1992) Farb-Doppler-gesteuerte Kompressionstherapie eines großen Aneurysma spurium der Arteria femoralis nach Linksherzkatheterisierung. Dtsch Med Wochenschr 117: 1675–1678
Hust MH, Schuler A, Claußnitzer R, Wild K, Metzler B (1993) Farbdopplergesteuerte Kompressionstherapie. Dtsch Ärztebl 90: B2536-B2541
Idu MM, Buth J, Hop WC, Cuypers P, van de Pavoordt ED, Tordoir JM (1999) Factors influencing the development of vein-graft stenosis and their significance for clinical management. Eur J Vasc Endovasc Surg 17: 15–21
Ihlberg L, Luther M, Tierala E, Lepäntalo M (1998) The utility of duplex scanning in infrainguinal vein graft surveillance: results from a randomised controlled study. Eur J Vasc Endovasc Surg 16 : 19–27

Ikeda M, Fujimori Y, Tankawa H, Iwata H (1984) Compression syndrome of the popliteal vein and artery caused by popliteal cyst. Angiology 35: 245–251
Insua JA, Young JR, Humphries AW (1970) Popliteal artery entrapment syndrome. Arch Surg 101: 771–775
Irninger W (1963) Histologische Altersbestimmung von Thrombosen und Embolien. Virchows Archiv Path Anat 336: 220–237
Ishikawa K (1987) Cystic adventitial disease of the popliteal artery and of other stem vessels in the extremities. Jap J Surg 17: 221–229
Iwai T, Sato S, Yamada T et al (1987) Popliteal vein entrapment caused by the third head of the gastrocnemius muscle. Br J Surg 74: 1006–1008
Jack CR, Sharma R, Vemuri RB (1984) Popliteal venous aneurysm as a source of pulmonary emboli in a male. Angiology 35: 55–57
Jacob A, Stock KW, Proske M, Steinbrich W (1996) Lower extremity angiography: improved image quality and outflow vessel detection with bilaterally antegrade selective digital subtraction angiography. A blinded prospective intraindividual comparison with aortic flush digital subtraction angiography. Invest Radiol 31: 184–193
Jacobs NM, Grant EG, Schellinger D et al (1985) Duplex carotid sonography: criteria for stenosis, accuracy, and pitfalls. Radiology 154: 385–391
Jäger K (1987) Apparative Untersuchungen zur Diagnose der tiefen Venenthrombose. Internist 28: 299–307
Jäger K (1989) Neuere diagnostische Methoden zur nichtinvasiven Lokalisation und hämodynamischen Beurteilung arterieller Obstruktionen. Internist 30: 397–405
Jäger K, Bollinger A (1986) Blood flow velocity and diameter of the popliteal vein. Phlebology 85: 260–263
Jäger K, Philips DL Martin RL, Hanson C, Roederer GO, Langlois YE, Strandness DE (1985) Noninvasive mapping of lower limb arterial lesions. Ultrasound Med Biol 11: 515–521
Jäger K, Ricketts HJ, Strandness DE (1985) Duplex scanning for the evaluation of lower limb arterial disease. In: Bernstein EF (ed) Noninvasive diagnostic techniques in vascular disease. Mosby, St. Louis
Jäger K, Bollinger A, Siegenthaler W (1986) Duplex-Sonographie in der Gefäßdiagnostik. Dtsch Med Wochenschr 111: 1608–1613
Jäger K, Bollinger A, Valli C, Ammann R (1986) Measurement of mesenteric blood flow by duplex scanning. J Vasc Surg 3: 462–469
Jäger K, Seifert H, Bollinger A (1989) M-mode echovenography. A new technique for the evaluation of venous wall and venous valve motion. Cardiovasc Res 23: 25–30
Jäger K, Frauchiger B, Eichlisberger R, Beglinger C (1992) Evaluation of the gastrointestinal vascular system by duplex sonography. In: Labs KH, Jäger KA, Fitzgerald DE, Woodcock JP, Neuerburg-Heusler D (eds) Diagnostic vascular ultrasound. Arnold, London
Jäger K, Eichlisberger R, Frauchiger B (1993) Stellenwert der bildgebenden Sonographie für die Diagnostik der Venenthrombose. Hämostaseologie 13: 116–124
Johnson BF, Manzo RA, Bergelin RO, Strandness DE (1995) Relationship between changes in the deep venous system and the development of the postthrombotic syndrome after an acute episode of lower limb deep vein thrombosis: a one- to six-year follow-up. J Vasc Surg 21: 307–313
Johnston KW, Rutherford RB, Tilson MD et al (1991) Suggested standards for reporting on arterial aneurysms. Ad Hoc Committee on Reporting Standards, Society for Vascular Surgery and North American Chapter, International Society for Cardiovascular Surgery. J Vasc Surg 13: 459
Johnston DC, Chapman KM, Goldstein LB (2001) Low rate of complications of cerebral angiography in routine clinical practice. Neurology 57: 2012–2014
Jongbloets LM, Lensing AW, Koopman MM, Buller HR, Cate JW (1994) Limitations of compression ultrasound for the detection of symptomless postoperative deep vein thrombosis. Lancet 343: 114–144
Jorgensen JO, Hanel KC, Morgan AM, Hunt JM (1993) The incidence of deep venous thrombosis in patients with superficial thrombophlebitis of the lower limbs. J Vasc Surg 18: 70–73
Juenemann KP, Persson-Juenenemann C, Alken P (1990) Pathophysiology of erectile dysfunction. Semin Urol 8: 80
Jung M (1990) Diagnosis of deep leg vein thrombosis: can we dispense with phlebography? VASA [Suppl]: 30
Kakkar VV (1972) The diagnosis of deep vein thrombosis using 125I-fibrinogen test. Arch Surg 104: 152–159
Kaps M, Seidel G (1999) Echokontrastverstärkung in der neurologischen Ultraschalldiagnostik. Dt Ärztebl 96: A276–280
Karacagil S, Almgren B, Bergström R, Bowald S, Eriksson I (1989) Postoperative predictive value of a new method of intraoperative angiographic runoff assessment in femoropopliteal bypass grafting. J Vasc Surg 10: 400–407
Karacagil S, Löfberg AM, Almgren B et al (1994) Duplex ultrasound scanning for diagnosis of aortoiliac and femoropopliteal arterial disease. VASA 23: 325–329
Karacagil S, Löfberg. AM, Granbo A, Lörelius LE, Bergqvist D (1996) Value of duplex scanning in evaluation of crural and foot arteries in limbs with severe lower limb ischaemia – a prospective comparison with angiography. Eur J Vasc Endovasc Surg 12: 300–303
Karasch T, Rieser R, Grün B, Strauss AL, Neuerburg-Heusler D, Roth F-J, Rieger H (1993) Bestimmung der Verschlußlänge in Extremitätenarterien. Farbduplexsonographie versus Angiographie. Ultraschall Med 14: 247–254
Karasch T, Strauss AL, Grün B, Worringer M, Neuerburg-Heusler D, Roth F-J, Rieger H (1993) Farbkodierte Duplexsonographie in der Diagnostik von Nierenarterienstenosen. Dtsch Med Wochenschr 118: 1429–1436
Karasch T, Strauss AL, Worringer M, Neuerburg-Heusler D, Roth FJ, Rieger H (1993) Vergleich der Farbduplexsonographie mit verschiedenen angiographischen Verfahren in der Diagnostik arteriosklerotischer Nierenarterienstenosen und -verschlüsse. Ultraschall Klin Prax 8: 180
Karasch T, Strauss AL, Worringer M, Neuerburg-Heusler D, Roth FJ, Rieger H (1993) Normwerte farbduplexsonographisch ermittelter Strömungsgeschwindigkeiten in der A. renalis. VASA 41 [Suppl]: 67
Karasch T, Neuerburg-Heusler D, Strauss A, Rieger H (1994) Farbduplexsonographische Kriterien zur Diagnose arteriosklerotischer Nierenarterienstenosen und -verschlüsse. In: Keller E, Krumme B (eds) Farbkodierte Duplexsonographie in der Nephrologie. Springer, Berlin Heidelberg New York Tokyo
Kasai C, Namekawa K, Koyano R, Omoto R (1985) Real-time two-dimensional blood flow imaging using an autocorrelation technique. IEEE Trans Son Ultrason SU-32: 458–463
Kathrein H (1991) Duplexsonographie von Dialyseshunts. Springer, Berlin Heidelberg New York Tokyo
Kathrein H, König P, Dittrich P, Judmeier G (1988) Nichtinvasisve Beurteilung von Cimino-Brescia-Fisteln und PTFE-Shunts mit der Duplexsonographie. VASA 26 [Suppl]: 39–41
Katz ML, Johnson M, Pomajzl MJ et al (1983) The sensitivity of real time B-mode carotid imaging in detection of ulcerated plaque. Bruit 8: 13–16
Kearon C, Julian JA, Newnan TE, Ginsberg JS (1998) Noninvasive diagnosis of deep vein thrombosis. McMaster Diagnostic Imaging Practice Guidelines Initiative. Ann Intern Med 128: 663–677
Keleinouridis V, Eckstein MR, Dembner AG, Waitman AG, Athanasoulis CA (1985) The normal leg venogram: significance in suspected vein thrombosis. Int Angiol 4: 369–371
Keller F, Loewe HJ, Bauknecht KJ, Schwarz A, Offermann G (1988) Kumulative Funktionsraten von orthotopen Dialysefisteln und Interponaten. Dtsch Med Wschr 113: 332–6
Keller F, Harnoss B-M, Czerlinsky H (1991) Umfrageergebnisse zur Technik der Ciminofistel. Angio Archiv 22: 7–9.
Kerr ThM, Canley JJ, Johnson JR, Lutter KS, Riechmann GC, Cranley RD, True MA, Sampson M (1990) Analysis of 1084 consecutive

lower extremities involved with acute venous thrombosis diagnosed by duplex scanning. Surgery 108: 520–527
Kerr ThM, Lutter KS, Moeller DM, Hasselfeld KA, Roedersheimer LR, McKenna PJ, Winkler JL, Spirtoff K, Sampson MG, Cranley JJ (1990) Upper extremity venous thrombosis diagnosed by dublex scanning. Amer J Surg 160: 202–206
Kiews P-W (1991) Color velocity imaging – Ein Vergleich der Verfahren zur farbkodierten Sonographie. Roentgenstrahlen (Philips Medizin Systeme) 65: 1–6
Kiews P-W (1993) Physik und Technik der farblodierten Duplexsonographie (FKDS) In: Wolf KJ, Fobbe F (eds) Farbkodierte Duplexsonographie. Thieme, Stuttgart New York, pp 248–295
Killewich LA, Bedford GR, Beach, KW, Strandness DE Jr (1989) Diagnosis of deep venous thrombosis. A prospective study comparing duplex scanning to contrast venography. Circulation 79: 810–814
Killewich LA, Fisher C, Bartlett ST (1990) Surveillance of in situ infrainguinal bypass grafts: Convential vs colour flow duplex ultrasonography. J Cardiovasc Surg 31: 662
Killewich LA, Bedford GR, Beach KW, Standness DE (1998) Spontaneous lysis of deep venous thrombi: rate and outcome. J Vasc Surg 9: 89–97
Kimura K, Yasaka M, Moriyasu H, Tsuchiya T, Yamaguchi T (1994) Ultrasonographic evaluation of vertebral artery to detect vertebrobasilar axis occlusion. Stroke 25: 1006–1009
Kinsey AC, Pomeroy WB, Martin CE (1948) Sexual behavior in the human male. Saunders, Philadelphia, pp 218–262
Kirsch JD, Wagner LR, James EM, Charboneau JW, Nichols DA, Meyer FB, Hallett JW (1994) Carotid artery occlusion: positive predictive value of duplex sonography compared with angiography. J Vasc Surg: 19: 642–649
Koelemay MJ, Legemate DA, van Gurp J, Ponson AE, Reekers JA, Jacobs MJ (1997) Colour duplex scanning and pulse-generated runoff for assessment of popliteal and cruropedal arteries before peripheral bypass surgery. Br J Surg 84: 1115–1119
Koennecke HC, Fobbe F, Hamed MM, Wolf KJ (1989) Diagnostik arterieller Gefäßerkrankungen der unteren Extremitäten mit der farbkodierten Duplexsonographie. Fortschr Röntgenstr 151: 42–46
Kohler TR (1990) Evaluation of lower limb vessels. Clin Diagn Ultrasound 26
Kohler TR, Strandness DE Jr (1986) Noninvasive testing for the evaluation of chronic venous disease. World J Surg 106: 903–910
Kohler TR, Nance DR, Cramer MM et al (1987) Duplex scanning for diagnosis of aortoiliac and femoropopliteal disease: a prospective study. Circulation 76: 1074–1080
Koksoy C, Kuzu A, Kutlay J, Erden I, Ozcan H, Ergin K (1995) The diagnostic value of colour Doppler ultrasound in central venous catheter related thrombosis. Clin Radiol 50: 687
Koopman MMW, Prandoni P, Piovella F et al (1996) Treatment of venous thrombosis with intravenous unfractionated heparin administered in the hospital as compared with subcutaneous low-molecular-weight heparin administered at home. N Engl J Med 334: 677–681
Koppenhagen K, Fobbe F (1993) Diagnostik der tiefen Beinvenenthrombose. Hämostaseologie 13 [Suppl]: 12–14
Krause U, Kock HJ, Kröger K, Albrecht K, Rudofsky G (1998) Prevention of deep venous thrombosis associated with superficial thrombophlebitis of the leg by early saphenous vein ligation. VASA 27: 34–38
Kreitner KF, Kalden P, Neufang A et al (2000) Diabetes and peripheral arterial occlusive disease: prospective comparison of contrast-enhanced three-dimensional MR angiography with conventional digital subtraction angiography. AJR 174: 171–179
Kremkau FW (1990) Doppler ultrasound: principles and instruments. Saunders, Philadelphia
Kriessmann A, Bollinger A (1978) Ultraschall-Doppler-Diagnostik in der Angiologie. Thieme, Stuttgart
Kriessmann A, Bollinger A, Keller H (1982) Praxis der Doppler-Sonographie. Thieme, Stuttgart
Krings W, Adolph J, Diederich S, Urhahne S, Vassallo P, Peters PE (1990) Diagnostik der tiefen Becken- und Beinvenenthrombose mit hochauflösender real-time und CW-Doppler-Sonographie. Radiologe 30: 525–531
Krishnabhakdi S, Espinola-Klein C, Kurz G, Neufang A, Schmidt W, Oelert H (2001) Sonographisches Venenmapping – Stellenwert in der distalen Bypasschirurgie. Ultraschall in der Medizin 22 [Suppl]: 60
Krumme B, Lehnert T, Wollschläger H, Keller E (1995) Möglichkeiten und Grenzen der farbduplexgesteuerten Kompressionstherapie von punktionsbedingten Gefäßläsionen in der Leiste. Fortschr Röntgenstr 163: 158–162
Krumme B, Blum U, Schwertfeger E et al (1996) Diagnosis of renovascular disease by intra- and extrarenal Doppler scanning. Kidney Int 50: 1288–1292
Krysiewicz S, Mellinger BC (1989) The role of imaging in the diagnostic evaluation of impotence. Am J Roentgenol 153: 1133–1139
Kubale R (1987) Renovaskuläre Erkrankungen. In: Seitz K, Kubale R (eds) Duplex Sonographie der abdominellen und retroperitonealen Gefäße. Weinheim
Kubale R (1993) Abdominelle Venen, portalvenöses System und Leber. In: Wolf K-J, Fobbe F (eds) Farbkodierte Duplexsonographie. Thieme, Stuttgart, pp 158–184
Kubale R (1994) Abdominelle und retroperitoneale Gefäße. In: Rettenmaier G, Seitz KH (eds) Sonographische Differentialdiagnostik. Chapman & Hall, Weinheim, pp 865ff
Labs K-H (1991) Die Aussagekraft der Dopplerspektralanalyse für die praktische Diagnostik. VASA 32 [Suppl]: 72–84
Lagerstadt Cl, Olsson CC, Fagher BO, Öqvist BW, Albrechtsson U (1985) Need for long-term anticoagulation treatment in symptomatic calf-vein thrombosis. Lancet 2: 515–518
Landry GJ, Moneta GL, Taylor LM, McLafferty RB, Edwards JM, Yeager RA et al (1999) Duplex scanning alone is not sufficient imaging before secondary procedures after lower extremity reversed vein bypass graft. J Vasc Surg 29: 270–280
Landwehr P, Lackner K (1990) Farbkodierte Duplexsonographie vor und nach PTA der Arterien der unteren Extremität. Fortschr Röntgenstr 152: 35–41
Landwehr P, Tschammler A, Höhmann M (1990) Gefäßdiagnostik mit der farbkodierten Duplexsonographie. Dtsch Med Wochenschr 115: 343–351
Langholz JP (1997) Ultrasound contrast agents in peripheral vascular disease. In: Nanda NC, Schlief R, Goldberg BB (eds) Advances in echo imaging using contrast enhancement, 2nd ed. Kluwer Academic Publishers, Dordrecht, pp 543–560
Langholz J, Heidrich H (1991) Sonographische Diagnose der tiefen Becken-/Beinvenenthrombose: Ist die farbkodierte Duplexsonographie „überflüssig“? Ultraschall Med 12: 176–181
Langholz J, Schlief R, Heidrich H (1992) Verbesserung der farbcodierten Duplexsonographie durch Kontrastmittelgabe bei schwer untersuchbaren Regionen der peripher-arteriellen Becken-Bein-Strombahn. Ultaschall Med 13: 234–238
Langholz J, Maul R, Heidrich H (1994) Was ist eine „hypoplastische“ A. vertebralis? Überlegungen auf der Basis duplexsonographischer Untersuchungen (abstract). VASA 43 [Suppl]: 50
Langsfeld M, Hershey FB, Thorpe L et al (1987) Duplex B-mode imaging for the diagnosis of deep venous thrombosis. Arch Surg 122: 587–591
Langsfeld M, Gray-Weale AC, Lusby RJ (1989) The role of plaque morphology and diameter reduction in the development of new symptoms in asymptomatic carotid arteries. J Vasc Surg 9: 548–557
Lanzer P, Yoganathan AP (1991) Vascular imaging by color Doppler and magnetic resonance. Springer, Berlin Heidelberg New York Tokyo
Larch E (1993) Farbcodierte Duplexsonographie zur Beurteilung der Unterschenkelarterien bei peripherer arterieller Verschlußkrankheit. VASA 41 [Suppl]: 14

Larch E, Minar E, Ahmadi R, Schnurer G, Schneider B, Stumpflen A, Ehringer K (1997) Value of color duplex sonography for evaluation of tibioperoneal arteries in patients with femoropopliteal obstruction: a prospective comparison with anterograde intraarterial digital subtraction angiography. J Vasc Surg 25: 629–636

Laub G (1999) Principles of contrast-enhanced MR angiography. Basic and clinical applications. Magn Reson Imag Clin North Am 7: 783–795

Lausen M, Jensen R, Wille-Jorgensen P et al (1995) Colour Doppler flow imaging ultrasonography versus venography as screening method for asymptomatic postoperative deep venous thrombosis. Eur J Radiol 20: 200–204

Lee HM, Wang Y, Sostman HD et al (1998) Distal lower extremity arteries: evaluation with two-dimensional MR digital subtraction angiography. Radiology 207: 505–512

Lee VS, Hertzberg BS, Workman MJ, Smith TP et al (2000) Variability of Doppler US measurements along the common carotid artery: effects on estimates of internal carotid arterial stenoses in patients with angiographically proved disease. Radiology 214: 387–392

Legemate DA, Teeuwen C, Hoeneveld H, Eikelboom BC (1991) Value of duplex scanning compared with angiography and pressure measurement in the assessment of aortoiliac arterial lesions. Br J Surg 78: 1003–1008

Lensing AWA, Prandoni P, Brandjes D et al (1989) Detection of deep vein thrombosis by real-time B-mode ultrasonography. New Engl J Med 320: 342–345

Lensing AWA, Doris CI, McGrath FP, Cogo A, Sabine MJ, Ginsberg J et al (1997) A comparison of compression ultrasound with color Doppler ultrasound for the diagnosis of symptomless postoperative deep vein thrombosis. Arch Intern Med 157: 765–768

Lepore T, Savran J, van de Water J, Harrower H, Yablonski M (1978) Screening for lower extremity deep venus thrombosis. Am J Surg 135: 529–534

Lerner RM, Medorach RA, Hulbert WC, Rabinowitz R (1990) Color Doppler US in the evaluation of acute scrotal disease. Radiology 176: 355–358

Leu HJ (1973) Histologische Altersbestimmung von arteriellen und venösen Thromben und Embolie. VASA 2: 265–273

Leu HJ, Bollinger A, Pouliadis G, Brunner U, Soyka P (1977) Pathologie, Klinik, Radiologie und Chirurgie der zystischen Adventitia-Degeneration peripherer Blutgefäße. VASA 6: 94–99

Leung A, Hampson SJ, Singh MP et al (1983) Ultrasonic diagnosis of bilateral congenital internal jugular venous aneurysms. Br J Radiol 56: 588–591

Levine M, Gent M, Hirsh J et al (1996) A comparison of low-molecular-weight heparin administered primarily at home with unfractionated heparin administered in the hospital for proximal deep vein thrombosis. N Engl J Med 334: 677–681

Levy MM, Baum RA, Carpenter JP (1998) Endovascular surgery solely based on noninvasive preprocedural imaging. J Vase Surg 28: 995–1003

Lewis BD, James EM, Charboneau JW et al (1989) Current applications of color Doppler imaging in the abdomen and extremities. Radiographics 9: 599–631

Lewis BD, James EM, Welch TJ, Joyce JW, Hallett JW, Weaver AL (1994) Diagnosis of acute deep venous thrombosis of the lower extremities: prospective evaluation of colour Doppler flow imaging versus venography. Radiology 192: 651–655

Li R, Cai J, Tegeler C et al (1996) Reproducibility of extracranial carotid atherosclerotic lesions assessed by B-mode ultrasound: the ARIC Study. Ultrasound Med Biol 22: 791–799

Liewald F et al (2001) Influence of treatment of type II leaks on the aneurysm surface area. Eur J Vasc Endovasc Surg 21: 339–343

Ligush J, Reavis SW, Preisser JS, Hansen KJ (1998) Duplex ultrasound scanning defines operative strategies for patients with limb-threatening ischemia. J Vasc Surg 28: 482–491

Limberg B (1991) Duplexsonographische Diagnose der portalen Hypertension bei Leberzirrhose. Einfluss einer standardisierten Testmahlzeit auf die portale Hämodynamik. Dtsch Med Wochenschr 116: 1384–1387

Lindquist R (1977) Ultrasound as a complementary diagnostic method in deep vein thrombosis of the leg. Acta Med Scand 201: 435

Lippert H, Pabst R (1998) Arterial variations in man. Bergmann, Munich

Lohr JM, Kerr TM, Lutter KS, Cranley RD (1991) Lower extremity calf thrombosis: to treat or not to treat? J Vasc Surg 14: 618–23

Londrey GL, Hodgson KJ, Spadone DP, Ramsey DE, Barkmeier LD, Summer DS (1990) Initial experience with colour-flow duplex scanning of infrainguinal bypass grafts. J Vasc Surg 12: 284–290

Longo JM, Bilbao JI, Rousseau HP, et al (1992) Color Doppler guidance in transjugular placement of intrahepatic portosystemic shunts. Radiology 184: 281–283

Lopez JA, Espeland MA, Jarow JP (1992) Interpretation and quantification of penile blood flow Studies using duplex ultrasonography. J Urol 146: 1271

Ludwig M (1991) Quantitative Flußmessungen an Venen. Ultraschall-dreiländertreffen, Lausanne

Ludwig M, Stumpe KO (1994) Karotisultraschall in der Früherkennung der Atherosklerose. Dtsch Ärztebl 91: 745–746

Ludwig D, Schwarting K, Korbel CM, Bruning A, Schiefer B, Stange EF (1998) The postprandial portal flow is related to the severity of portal hypertension and liver cirrhosis. J Hepatol 28: 631–638

Lue TF (1991) Physiology of penile erection. In: Jonas U, Thon WF, Stief CG (eds) Erectile dysfunction. Springer, Berlin Heidelberg New York, pp 44–65

Lundell A, Lindblad B, Bergqvist D, Hansen F (1995) Femoropopliteal-crural graft patency is improved by an intensive surveillance program: A prospective randomized study. J Vasc Surg 21: 26–34

Lusby RJ (1993) Plaque characterisation: does it identify high risk groups? In: Bernstein EF, Callow AD, Nicolaides AN, Shifrin EG (eds) Cerebral revascularisation. Med-Orion, London Los Angeles Nicosia, pp 93–107

Luska G, Risch U, Pellengahr M, Boetticher HV (1990) Farbcodierte dopplersonographische Untersuchungen zur Morphologie und Hämodynamik der Arterien des Beckens und der Beine bei gesunden Probanden. Fortschr Röntgenstr 153: 246–251

Lutter KS, Kerr ThM, Roedersheimer LR, Lohr JM, Sampson MSG, Cranley JJ (1991) Superficial thrombophlebitis diagnosed by duplex scanning. Surgery 110: 42–46

MacMathuna P, Vlavianos P, Westaby D, Williams R (1992) Pathophysiology of portal hypertension. Dig Dis [Suppl 1]: 3–15

Marin J, Gosselin J, Khayat A (1978) A propos d'un cas d'anévrisme de la veine poplitée avec embolie pulmonaire. Phlébologie 31: 433–438

Markel A, Manzo RA, Bergelin RO, Strandness DE (1992) Valvular reflux after deep vein thrombosis: incidence and time of occurrence. J Vasc Surg 15: 377–384

Markel A, Manzo R, Bergelin RO, Strandness DE (1992) Pattern and distribution of thrombi in acute venous thrombosis. Arch Surg 127: 305–309

Marshall M (1990) Die Duplex-Sonographie bei phlebologischen Fragestellungen in Praxis und Klinik. Ultraschall Klin Prax 5: 51–56

Marshall M (1990) Sklerosierungsreaktion großer Varizen im hochauflösenden Ultraschallbild. Phlebol Proktol 19: 205–214

Martin RL, Nanra RS, Wlodarczyk J et al (1991) Renal hilar Doppler analysis in the detection of renal artery stenosis. J Vasc Tech 15: 173–130

Mattos MA, Londrey GL, Leutz DW et al (1992) Color-flow duplex scanning for the surveilance and diagnosis of acute deep venous thrombosis. J Vasc Surg 15: 366–376

May R, Mignon G (1976) Spindelförmiges Aneurysma der Vena fibularis. Fortschr Röntgenstr 25: 563–564

May R, Nissl R (1968) Aneurysma der Vena poplitea. Fortschr Röntgenstr 108: 402–403

May R, Nissl R (1973) Die Phlebographie der unteren Extremität. Thieme, Stuttgart New York

Mazzariol F, Ascher E, Salles-Cunha S, Grade P, Hingorani A (1999) Values and limitations of duplex scanning as the sole preoperative evaluation for popliteal and infrapopliteal bypasses. Ann Vasc Surg 13: 1–10

Mazzariol F, Ascher E, Hincorani A et al (2000) Lower-extremity revascularization without preoperative contrast arteriography in 185 cases: Lessons learned with duplex ultrasound arterial mapping. Eur J Vasc Endovasc Surg 19: 509–515

McWilliams RG et al (2002) Detection of endoleak with enhanced ultrasound imaging: comparison with biphasic computed tomography. J Endovasc Ther 9: 170–179

McLachan MSF, Thomson JG, Taylor DW, Kelly ME, Sackett DL (1979) Observer variation in the interpretation of lower limb venograms. Am J Radiol 132: 227–229

Meairs S, Hennerici M (1999) Four-dimensional ultrasonographic characterization of plaque surface motion in patients with symptomatic and asymptomatic carotid artery stenosis. Stroke 30: 1807–18 13

Meerbaum S (1997) Microbubbles fluid dynamics of echocontrast. In: Nanda NC, Schlief R, Goldberg BB (eds) Advances in echo imaging using contrast enhancement, 2nd ed. Kluwer Academic Publishers, Dordrecht, pp 11–38

Meissner MH, Caps MT, Zierler BK, Bergelin RO, Manzo RA Strandness DE (2000) Deep venous thrombosis and superficial venous reflux. J Vasc Surg 32: 48–56

Melany ML, Grant EG, Farooki S et al (1999) Effect of US contrast agents on spectral velocities: in vivo evaluation. Radiology 211: 427–431

Meltzer RS, Tickner EG, Sahines TP, Popp RL (1980) The source of ultrasound contrast effect. J Clin Ultrasound 8: 121–127

Mercer KG, Scott DJA, Turton EPL, Berridge DC, Weston MJ (1999) Can intra-operative flow measurements identify grafts for intensive duplex surveillance? St James University Hospital NHS Trust, Leeds, UK

Merritt CRB, Bluth EI (1992) Ultrasound identification of plaque composition. In: Labs KH et al (eds) Diagnostic vascular ultrasound. Arnold, London, pp 213–223

Metz V, Braunsteiner A, Grabenwöger F et al (1988) Farbcodierte Doppler-Sonographie der Becken-Bein-Arterien: Überprüfung der Wertigkeit der Methode im Vergleich zur Angiographie. Fortschr Röntgenstr 149: 314–316

Metz V, Dock W, Grabenwöger F et al (1992) Wertigkeit unterschiedlicher klinischer und bildgebender Verfahren für die postoperative Verlaufskontrolle extraanatomischer Bypasses. Fortschr Röntgenstr 154: 172–175

Mewissen MW, Kinney EV, Bandyk DF et al (1992) The role of duplex scanning versus angiography in predicting outcome after balloon angioplasty in the femoropoplital artery. J Vasc Surg 15: 860–86 6

Meyer P, Rudofsky G, Nobbe N (1986) Das Histogramm des Okklusionsmaterials – ein neuer Prognoseparameter der thrombolytischen Therapie bei tiefer Beinvenenthrombose. In: Hansmann M, Koischwitz D, Lutz H, Trier HG (eds) Ultraschalldiagnostik 86. Springer, Berlin Heidelberg New York Tokyo, p 138

Meyer Jl, Khalil RM, Obuchowski NA, Baus LK (1997) Common carotid artery: variability of Doppler US velocity measurements. Radiology 204: 339–341

Middleton WD, Siegel BA, Melson GL, Yates CK, Andriole GL (1990) Acute scrotal disorders: prospective comparison of color Doppler US and testicular scintigraphy. Radiology 177: 177–181

Miller N, Satin R, Tousignant L, Sheiner NM (1996) A prospective study comparing duplex scan and venography for diagnosis of lower-extremity deep vein thrombosis. Cardiovasc Surg 4: 505–5 08

Millner R (1987) Ultraschalltechnik, Physik. Weinheim, pp 41–46

Mills JL, Harris EJ, Taylor LM, Beckett WC (1990) The importance of routine surveillance of distal bypass grafts with duplex scanning: A study of 379 reversed vein grafts. J Vasc Surg 12: 379–3 86

Mills JL, Fujitani RM, Taylor SM (1993) The characteristics and anatomic distribution of lesions that cause reversed vein graft failure: A five-year prospective study. J Vasc Surg 17: 195–206

Mills JL, Bandyk DF, Gathan V, Esses GE (1995) The origin ot infrainguinal vein graft stenosis: A prospective study based on duplex surveillance. J Vasc Surg 21: 16–22

Mitchell DG (1990) Color Doppler imaging: principles, limitations and artifacts. Radiology 177: 1–10

Mödder U (1992) Farbcodierte Duplexsonographie (Angiodynographie). Fortschr Röntgenstr 157: 204–209

Mohan CR, Hoballah JJ, Schueppert MT, Sharp WJ, Kresowik TF, Miller EV et al (1995) Should all in situ saphenous vein bypasses undergo permanent duplex surveillance? Arch Surg 130: 483–487

Moll R, Habscheid W, Landwehr P (1991) Häufigkeit des Aneurysma spurium der Arteria femoralis nach Herzkatheteruntersuchung und PTA. Fortschr Röntgenstr 154: 23–27

Moneta GL, Taylor DC, Helton WS, Mulholland MW, Strandness DE (1988) Duplex ultrasound measurement of postprandial intestinal blood flow: effect of meal composition. Gastroenterology 95: 1294–1301

Moneta GL, Yeager RA, Dalman R et al (1991) Duplex ultrasound criteria for the diagnosis of splanchnic artery stenosis or occlusion. J Vasc Surg 14: 511–520

Moneta GL, Yeager RA, Antonovic R et al (1992) Accuracy of lower extremity arterial duplex mapping. J Vasc Surg 15: 275–284

Moneta GL, Edwards JM, Chitwood RW, Taylor LM et al (1993) Correlation of North American Carotid Endarterectomy Trial (NASCET) angiographic definition of 70% to 99% internal carotid artery stenosis with duplex scanning. J Vasc Surg 17: 152–159

Moneta GL, Lee RW, Yeager RA et al (1993) Mesenteric duplex scanning: a blinded prospective study. J Vasc Surg 17: 79–86

Moneta GL, Yeager RA, Lee RW, Porter JM (1993) Noninvasive localisation of arterial occlusive disease: a comparison of segmental Doppler pressures and arterial duplex mapping. J Vasc Surg 17: 578–582

Moneta GL, Edwards JM, Papanicolaou G, Hatsukami T, Taylor LM, Strandness DE, Porter JM (1995) Screening for asymptomatic internal carotid artery stenosis: duplex criteria for discriminating 60% to 99% stenosis. J Vasc Surg 21: 989–994

Monreal M, Montserrat E, Salvador R, Bechini J, Donoso L, McCallegos J, Foz M (1989) Real-time ultrasound for diagnosis of symptomatic venous thrombosis and for screening of patients at risk. Correlation with ascending conventional venography. Angiology 39: 527

Montefusco von Kleist CM, Bakal C, Sprayregen S, Rhodes BA, Veith FJ (1993) Comparison of duplex ultrasonography and ascending contrast venography in the diagnosis of venous thrombosis. Angiology 44: 169–175

Monzer MAY, Wiese JA, Shamma AR (1987) The to-and-fro sign: duplex Doppler evidence of femoral artery pseudoaneurysm. Am J Roentgenol 150: 632–634

Moore WS (2003) For severe carotid stenosis found on ultrasound, further arterial evaluation is unnecessary. Stroke 34: 1816–1817

Moriyasu F, Nishida 0, Ban N, Nakamura T, Sakai M, Miyake T, Uchino H (1985) „Congestion index“ of the portal vein. Am J Roentgenol 146: 735–739

Moucka J, Jäger K (1990) Rationelle Abklärung bei peripherer arterieller Verschlußkrankheit. Schweiz Rundsch Med Prax 79: 1553–1559

Mueller SC, Lue TF (1988) Evaluation of vasculogenic impotence. Urol Clin North Am 15: 65–76

Müller-Schwefe CH, Klinggräf G von, Riepe G, Schröder A (1991) Das inflammatorische Bauchaortenaneurysma. Ultraschall Med 12: 158–163

Müller-Wiefel H (1974) Untersuchungen zur Hämodynamik in den Venen der unteren Extremität. Physiologische, phathophysiologische und klinische Aspekte. Schattauer, Stuttgart

Mulligan SA, Matsuda T, Tanzer P et al (1991) Peripheral arterial occlusive disease: prospective comparison of MR angiography and

color duplex US with conventional angiography. Radiology 178: 695–700

Multicentre Aneurysm Screening Study Group: Multicentre aneurysm screening study (MASS) (2002) Cost effectiveness analysis of screening for abdominal aneurysms based on four year results from randomised controlled trial. BMJ 325: 1135 and Lancet 360: 1531–1539

Munda R, First MR, Alexander JW, Linnemann CC, Fidler JP, Kittur D (1983) Polytetrafluoroethyelene graft survival in hemodialysis. J Am Med Ass 249: 219–22

Murphy TP, Cronan JJ (1990) Evolution of deep venous thrombosis: A prospective evaluation with US. Radiology 177: 543–548

Naidich JB, Feinberg AW, Karp-Harmann H, Ka Tyma CG, Stein HL (1988) Contrast venography. Reassessment of its role. Radiology 168: 97

Nakamura T, Moriyasu F, Ban N, Nishida O, Tamada T, Kawasaki T, Sakai M, Uchino H (1989) Quantitative measurement of abdominal arterial blood flow using image-directed Doppler ultrasonography: superior mesenteric, splenic, and common hepatic arterial blood flow in normal adults. J Clin Ultrasound 17: 261–268

NASCET – North American Symptomatic Carotid Endarterectomy Trial Collaborators (1991) Beneficial effect of carotid endarterectomy in symptomatic patients with high-grade carotid stenosis. N Engl J Med 325: 445–453

Nazzal MM, Hoballah JJ, Miller EV, Sharp WJ, Kresowik TF, Corson J (1997) Renal hilar Doppler analysis is of value in the management of patients with renovascular disease. Am J Surg 174: 164–8

Neale ML, Chambers JL, KeIIy AT et al (1994) Reappraisal of duplex criteria to assess significant carotid stenosis from the North American Symptomatic Carotid Endarterectomy Trial and the European Carotid Surgery Trial. J Vasc Surg 20: 642–649

Neglen P, Raju S (1992) A comparison between descending phlebography and duplex Doppler investigation in the evaluation of reflux in chronic venous insufficiency: a challenge to phlebography as the gold standard. J Vasc Surg 16: 687–693

Neuerburg-Heusler D (1984) Dopplersonographische Diagnostik der extrakraniellen Verschlußkrankheit. VASA 12 [Suppl]: 59–70

Neuerburg-Heusler D, Hennerici M (1995) Gefäßdiagnostik mit Ultraschall. Doppler- und farbcodierte Duplexsonographie. Thieme, Stuttgart

Neuerburg-Heusler D, Karasch TH (1991) Farbkodierte Duplex-Sonographie – Erweiterung der gefäßdiagnostischen Möglichkeiten? In: Maurer PC, Dörrler J, von Sommogy ST (eds) Gefäßchirurgie im Fortschritt. Thieme, Stuttgart

Nevitt MP, Ballard DJ, Hallett JW Jr (1989) Prognosis of abdominal aortic aneuryms. A population-based study. New Engl J Med 321: 1009–1014

Nichols WN, O'Rourke MF (1990) McDonald's blood flow in arteries. Theoretical, experimental and clinical principles, 3rd edn. Edward Arnold, London, pp 54–76

Nicolaides AN (1995) Asymptomatic Carotid Stenosis and Risk of Stroke: identification of a high risk group (ACSRS): a natural history study. Int Angiol 14: 21–23

Nielsen TG, von Jessen F, Sillesen H (1993) Doppler spectral characteristics of infrainguinal vein bypasses. Eur J Vasc Surg 7: 610–615

Nielsen TG, Sillesn H, Schroeder TV (1995) Simple hyperaemia test as a screening method in a postoperative surveillance of infrainguinal in situ vein bypasses. Eur J Vasc Endovasc Surg 10: 298–303

Noon GP, Jose LZ, Graig M et al (1984) Popliteal vein pseudoaneurysm: a case report. Surgery 96: 942–945

Norris CS, Greenfield LJ, Hermann JB (1985) Free-floating iliofemoral thrombus. Arch Surg 120: 806–808

Numata K, Tanaka K, Kiba T et al (1999) Hepatic artery resistance after mixed-meal ingestion in healthy subjects and patients with chronic liver disease. J Clin Ultrasound 27: 239–48

Oates CP, Pickard RS, Powell PH, Murthy LNS, Whittingham TAW (1995) The use of duplex ultrasound in the assessment of arterial supply to the penis in vasculogenic impotence. J Urol 153: 354–7

O'Donnell TF Jr, Erdoes L, Mackey WC, et al (1985) Correlation of B-mode ultrasound imaging and arteriography with the pathologic findings of carotid endarterectomy. Arch Surg 120: 443–449

Ohta M, Hashizume M, Tomikawa M et al (1994) Analysis of hepatic vein waveform by Doppler ultrasonography in 100 patients with portal hypertension. AJG 89: 170–175

Olbricht CJ, Wanke B, Haubitz M, Koch KM (1991) Captopril spürt Stenosen der Nierenarterien auf. Med Trib 16: 27

O'Leary DH, Polak JF, Kronmal RA, Manolio TA et al (1999) Carotid-artery intima and media thickness as a risk factor for myocardial infarction and stroke in older adults. N Engl J Med 340: 12–22

Olin JW, Piedmonte MR, Young JR et al (1995) The utility of duplex ultrasound scanning in the diagnosis of renal artery stenosis. Ann Intern Med 122: 833–838

Olojugba DH, McCarthy MJ, Naylor AR, Bell PR, London NJ (1998) At what peak velocity ratio should duplex detected infrainguinal vein graft stenoses be revised? Eur J Vasc Endovasc Surg 15: 258–26 0

Owen WJ, McColl I (1980) Venous aneurysm of the axilla simulating a soft tissue tumour. Br J Surg 67: 577–578

Owen RS, Carpenter JP, Baum RA, Perloff U, Cope C (1992) Magnetic resonance imaging of angiographically occult runoff vessels in peripheral arterial occlusive disease. N Engl J Med 326: 1577–1581

Pages S et al (2001) Comparison of color duplex ultrasound and computed tomography scan for surveillance after aortic endografting. Ann Vasc Surg 15: 155–162

Papanicolaou G, Beach KW, Zierler RE, Strandness DE (1995) The relationship between arm-ankle pressure difference and peak systolic velocity in patients with stenotic lower extremity vein grafts. Ann Vasc Surg 9: 554–560

Parent FN et al (2002) The incidence and natural history of type I and II endoleak: a 5-year follow-up assessment with color duplex ultrasound scan. J Vasc Surg 35: 595–597

Park, AE, McCarthy, WJ, Pearce, WH, Matsumura, JS, Yao JST (1998) Carotid plaque morphology correlates with presenting symptomatology. J Vasc Surg 27: 872–879

Parry DJ et al (2002) Type II endoleaks: predictable, preventable, and sometimes treatable? J Vasc Surg 36: 105–110

Partsch H (1976) „A-sounds" or „S-sounds" for Doppler ultrasonic evaluation of pelvic vein thrombosis. VASA 5: 16–19

Partsch H (1996) Diagnose und Therapie der tiefen Beinvenenthrombose. VASA 46 [Suppl]

Partsch H, Lofferer O (1972) Die Doppler-Detektoruntersuchung als Suchtest und Verlaufskontrolle von Bein-Beckenvenenthrombosen. Wien Klin Wochenschr 84: 760–763

Partsch H, Mostbeck A (1979) Die Früherkennung der tiefen Unterschenkelvenenthrombophlebitis. VASA 8: 237–246

Partsch H, Oburger K, Mostbeck A et al (1992) Frequency of pulmonary embolism in ambulant patients with pelvic vein thrombosis: A prospective Study, J Vasc Surg 16: 715–722

Passman MA, Moneta GL, Nehler MR, Taylor LM et al (1995) Do normal early color-flow duplex surveillance examination results of infrainguinal vein grafts preclude the need for late graft revision? J Vasc Surg 22: 476–484

Patel KR, Semel L, Oauss RH (1988) Extended reconstruction rate for limb salvage with intraoperative prereconstruction angiography. J Vasc Surg 7: 531–537

Patriquin H, Lafortune M, Burns PN, Dauzat M (1987) Duplex Doppler examination in portal hypertension: technique and anatomy. Am J Roentgenol 149: 71–76

Pederson OM, Aslaksen A, Vik-Mo H, Bassoe AM (1991) Compression ultrasonography in hospitalized patients with suspected deep venous thrombosis. Arch Intern Med 151: 2217–2220

Pennestri F, Loperfido, Salvatori MP et al (1984) Assessment of tricuspid regurgitation by pulsed Doppler ultrasonography of the hepatic veins. J Cardiol 54: 363–8

Perko MJ, Just S, Schroeder TV (1997) Importance of diastolic velocities in the detection of celiac and mesenteric artery disease by duplex ultrasound. J Vasc Surg 26: 288–293
Perlin SJ (1992) Pulmonary embolism during compression US of the lower extremity. Radiology 184: 165–166
Perrier A, Bounameaux H (2001) Cost-effective diagnosis of deep vein thrombosis and pulmonary embolism. Thromb Haemost 86: 475–487
Perrier A, Desmarais S, Miron MJ, de Moerloose P, Lepage R, Slosman D, Didier D, Unger PF, Patenaude JV, Bounameaux H (1999) Noninvasive diagnosis of venous thromboembolism in outpatients. Lancet 353: 190–195
Persson BG, Donner M, Peterson B, Eklof B, Wintzell K (1980) Aneurysm of the popliteas vein as a cause of pulmonary embolism. Acta Med Scand 208: 407–410
Persson AV, Jones C, Zide R, Jewell Er (1989) Use of the triplex scanner in diagnosis of deep venous thrombosis. Arch Surg 124: 593
Petrick J (1996) Spektralanalyse von Ultraschall-Doppler-Signalen mit und ohne Ultraschallkontrastmittel an Modellen von Blutgefäßen. PhD Thesis Berlin 1995. Köster, Berlin
Petrick J, Schlief R, Zomack M, Langholz J, Urbank A (1992) Pulsatiles Strömungsmodell mit elastischen Gefäßen für duplexsonographische Untersuchungen. Ultraschall Med 13: 277–282
Petros JA, Andriole GL, Middleton WD, Picus DA (1991) Correlation of testicular color Doppler ultrasonography, physical examination and venography in the detection of left varicoceles in men with infertility. J Urol 145: 785–788
Pfeil W, Jacksch R, Kotzerke M, Störk T, Selbach J. Behandlung von Pseudoaneurysmen der Femoralarterie mit Thrombininjektion – Das deutsche Multicenter-Register. Cardio,-Angiologisches Centrum Be thanien, Frankfurt/M (DE); St. Vincenzkrankenhaus Essen (DE); Hegau Klinikum; Singen (DE); Karl Olga Krankenhaus; Stuttgart (DE); Caritas Krankenhaus; Bad Mergentheim (DE)
Ploenes C, Strauss A (1999) Die Wertigkeit der Farbduplexsonographie in der Diagnose von Nierenarterienstenosen und -verschlüssen. VASA 55 [Suppl]: 47
Podhaisky H, Hänsgen K, Seifert H, Taute BM (1996) Parameter und Einflußfaktoren der sonographischen Untersuchung des peripheren arteriellen Gefäßsystems. Herz/Kreisl 28: 129–133
Polak JF (1992) Peripheral vascular sonography: a practical guide. Williams & Wilkins, Baltimore
Polak JF, Cutter SS, O'Leary DH (1988) Doppler color flow imaging of the calf veins. Description of method and preliminary results (abstract). Radiology 169 [Suppl]: 318
Polak JF, Culter S, O'Leary D (1989) Deep veins of the calf: assessment with color Doppler flow imaging. Radiology 171: 481–485
Polak JF, Dobkin GR, O'Leary DH, Wang A-M, Cutler SS (1989) Internal carotid artery stenosis: accuracy and reproducibility of color-Doppler assisted duplex imaging. Radiology 173: 793–798
Polak JF, Donaldson MC, Dobkin GR et al (1990) Early detection of sphenous vein arterial bypass graft stenosis by color-assisted duplex sonography: a prospective study. AJR 154: 857–861
Polak JF, Magruder CD, Whittemore AD et al (1990) Pulsatile masses surrounding vascular prostheses: real-time US color flow imaging. Radiology 170: 363–366
Polak JF, Mitchell MI, Mannick JA, O'Leary DH, Donaldson MC, Whittemore AD (1990) Determination of the extent of lower-extremity peripheral arterial disease with color-assisted duplex sonography. Am J Roentgenol 155: 1085–1089
Polak KF, Karmel MI, Meyerowitz JA (1991) Accuracy of color Doppler flow mapping for evaluation of the severity of femoropopliteal arterial disease, a prospective study. J Vasc Interv Radiol 2: 471–476
Polak JF, Bajakian RL, O'Leary DH, Anderson MR, Donaldson MC, Jolesz FA (1992) Detection of internal carotid artery stenosis: comparison of MR angiography, color Doppler sonography, and arteriography. Radiology 182: 35–40
Polak JF, O'Leary DH, Kronmal RA et al (1993) Sonographic evaluation of carotid artery atherosclerosis in elderly: relationship of disease severity to stroke and TIA. Radiology 188: 363–370
Polak JF, Shemanski L, O'Leary DH, Lefkowitz D et al (1998) Hypoechoic plaque at US of the carotid artery: an independent risk factor for incident stroke in adults aged 65 years or older. Radiology 208: 649–654
Pomposelli FB Jr, Marcaccio EJ, Gibbons GW et al (1995) Dorsalis pedis arterial bypass: durable limb salvage for foot ischemia in patients with diabetes mellitus. J Vasc Surg 21: 375–384
Porst H (1987) Erektile Impotenz. Enke, Stuttgart, pp 73–77
Porter TR (1998) Transient response imaging. In: Bogdahn U, Becker G, Schlachetzki F (eds) Echosignalverstärker und transkranielle Farbduplex-Sonographie. Blackwell, Berlin Vienna, pp 192–203
Prandoni P, Cogo A, Bernardi E, Villalta S et al (1993) A simple ultrasound approach for detection of recurrent proximal vein thrombosis. Circulation 88: 1730–1735
Prandoni P, Polistena P, Bernardi E et al (1997) Upper-extremity deep vein thrombosis: risk factors, diagnosis and complications. Arch Intern Med 157: 357–362
Prountjos P, Bastounis E, Hadjinikolaou L, Felekuras E, Balas P (1991) Superficial venous thrombosis of the lower extremities co-existing with deep venous thrombosis. A phlebographic study on 57 cases. Int Angiol 10: 63–65
Quam JP, King BF, James EM, Lewis RW, Brakke DM et al (1989) Duplex and color Doppler sonographic evaluation of vasculogenic impotence. Amer J Roentgenol 153: 1141–1147
Quandalle P, Sandement A, Chambon JP, Wurtz A (1989) L'anévrisme des veines profondes des membres inférieurs. J Chir 126: 586–590
Raghavendra BN, Rosen J, Lam S, Riles T, Horii SC (1984) Deep venous thrombosis. Detection by high-resolution real-time ultrasonography. Radiology 152: 789
Ragavendra BN, Horii St, Hilton S, Subramanyam BR, Rosen RJ, Lam SL (1986) Deep venous thrombosis: Detection by probe compression of veins. J Ultrasound Med 5: 89–95
Rajfer J, Rosciszweski A, Mehringer M (1988) Prevalence of corporeal venous leakage in impotent men. J Urol 140: 69
Ralls PW, Jensen MC, Lee KP, Mayekawa DS, Johnson MB, Halls JM (1990) Color Doppler sonography in acute epididymitis and orchitis. J Clin Ultrasound 18: 383–386
Ranke C, Hendrickx PH, Brasel F et al (1990) Duplexsonographie: Genauigkeit, Reproduzierbarkeit und Fehlermöglichkeiten. Dtsch Med Wochenschr 115: 528–533
Ranke C, Creutzig A, Alexander K (1992) Duplex scanning of the peripheral arteries: correlation of the peak velocity ratio with angiographic diameter reduction. Ultrasound Med Biol 18: 433–440
Ranke C, Creutzig A, Becker H, Trappe HJ (1999) Standardization of carotid ultrasound. A hemodynamic method to normalize for interindividual and interequipment variability. Stroke 30: 402–406
Reid DB, Irshad K, Miller P, McKendrick M, Velu R (2005) Recent advances in intravascular ultrasound. Oral Presentation, International Congress 18 on Endovascular Interventions, Phoenix
Reilly LM (1990) Carotid intraplaque hemorrhage: noninvasive detection and clinical significance. In: Bernstein EF (ed) Noninvasive diagnostic techniques in vascular disease. Mosby, St Louis, pp 99–107
Reilly LM, Lusby RJ, Hughes L et al (1983) Carotid plaque histology using real-time ultrasonography: clinical and therapeutic implications. Am J Surg 146: 188–193
Reuther GR, Wanjura D, Bauer H (1989) Acute renal vein thrombosis in renal allografts: detection with duplex Doppler US. Radiology 170: 557–558
Rich NM (1982) Popliteal entrapment and adventitial cystic disease. Surg Clin North Am 62: 449–465
Rich NM, Hughes CW (1967) Popliteal artery and vein entrapment. Am J Surg 113: 696–698
Rich NM, Collins GJ, McDonald PT, Kozloff L, Clagett GP, Collins JT (1979) Popliteal vascular entrapment. Arch Surg 114: 1377–1384

Richter G, Böhm, S, Görg, DH, Schwerk WB (1992) Verlaufsbeobachtungen zur Echogenität venöser Gerinnungsthromben. Ultraschall Klin Prax 7: 69–73
Ricotta JJ (1990) Plaque characterization by B-mode scan. Surg Clin North Am 70: 191–199
Rieger H (1985) Durchblutungsstörungen. Adam Pharma Verlag GmbH, Essen
Rieger H, Schoop W (1998) Klinische Angiologie. Springer, Berlin Heidelberg New York, pp 627–666
Riehl J, Clasen W, Schmidt H, Kierdorf, H, Sieberth HG (1989) Altersabhängige Veränderungen der renalen Hämodynamik: Untersuchungen mittels Duplex-Sonographie. Ultraschall Klin Prax Suppl 1: 129
Rigsby Ch, Burns PN, Weltin GG, Chen B, Bia M, Taylor KJW (1987) Doppler signal quantitation in renal allografts: comparison in normal and rejecting transplants with pathologic correlation. Radiology 162: 39–42
Rofsky NM, Adelman MA (2000) MR angiography in the evaluation of atherosclerotic peripheral vascular disease. Radiology 214: 325–338
Rollins DL, Semrow CM, Friedell ML, Buchbinder D (1987) Use of ultrasonic venography in the evaluation of venous valve function. Am J Surg 154: 189–191
Roobottorn CA, Hunter JD, Weston MJ, Dubbins PA (1995) Hepatic venous Doppler waveforms: changes in pregnancies. J Clin Ultrasound 23: 477–82
Roos DB (1987) Thoracic outlet syndromes: update 1987. Am J Surg 154: 568
Roos DB (1989) Overview of thoracic outlet syndromes. In: Machleder H (ed) Vascular disorders of the upper extremity, 2nd revised ed. Futura Publishing Company, New York, p 155
Rose SC, Zwiebel WJ, Nelson BD et al (1990) Symptomatic lower extremity deep venous thrombosis: accuracy, limitations and role of color duplex flow imaging in diagnosis. Radiology 175: 639–644
Rosner NM, Doris PE (1988) Diagnosis of femoropopliteal venous thrombosis: comparison of duplex sonography and plethysmography. Am J Roentgenol 150: 623–627
Ross B, Sherriff L, Walton L (1984) Diagnosis of deep-vein thrombosis: comparison of clinical evaluation, ultrasound, plethysmography, and venoscan with X-ray venogram. Lancet 716–719
Ross GJ, Violi L, Barber LW et al (1988) Popliteal venous aneurysm. Radiology 168: 721–722
Rotter W (1981) Gefäßveränderungen bei frischer und älterer Thrombose. In: Vinazzer H (ed) Thrombose und Embolie. Anästhesie Intensivmed 134: 171–177
Rubin JM, Bude RO, Carson PL et al (1994) Power Doppler US: a potentially useful alternative to mean frequency-based color Doppler US. Radiology 190: 853–856
Rutherford RB, Flanigan DP, Gupta SK, Johnston KW, Karmody A, Whittemore AD (1986) Suggested standards for reports dealing with lower extremity ischemia. J Vasc Surg 4: 80–94
Rutherford RB, Baker D, Ernst C et al (1997) Recommended standards for reports dealing with lower extremity ischaemia: revised version. J Vasc Surg 26: 517–538
Saal JG, Dürk H (1994) Rationale Labordiagnostik in klinischer Immunologie und Rheumatologie. Internist 35: 633–639
Sabba C, Ferraioli G, Genecin P et al (1991) Evaluation of postprandial hyperaemia in superior mesenteric artery and portal vein in healthy and cirrhotic humans: an operator-blind echo-Doppler study. Hepatology 13: 114–118
Sacks D, Robinson ML, Marinelli DL, Perlmutter GS (1990) Evaluation of the peripheral arteries with duplex after angioplasty. Radiology 176: 39–44
Sacks D, Robinson ML, Marinelli DL, Perlmutter GS (1992) Peripheral arterial Doppler ultrasonography: diagnostic criteria. J Ultrasound Med 11: 95–103
Sacks D, Robinson ML, Summers TA, Marinelli DL (1994) The value of duplex sonography after peripheral artery angioplasty in predicting subacute restenosis. Amer J Radiol 162: 179–183
Sandler DA, Duncan JS, Ward P et al (1984) Diagnosis of deep vein thrombosis. Comparison of clinical evaluation, ultrasound, plethysmography and venoscan with x-ray venogram. Lancet II: 716
Sarap MD, Wheeler WE (1988) Venous aneurysms. J Vasc Surg 8: 182–183
Sarkar R, Ro KM, Obrand DI, Ahn SS (1998) Lower extremity vascular reconstruction and endovascular surgery without preoperative angiography. Am J Surg 176: 203–207
Sato S, Ohnishi K, Sugita S, Okuda K (1987) Splenic artery and superior mesenteric artery blood flow: Nonsurgical Doppler US measurement in healthy subjects and patients with chronic liver disease. Radiology 164: 347–352
Sato DT et al (1998) Endoleak after aortic stent graft repair: diagnosis by color duplex ultrasound scan versus computed tomography scan. J Vasc Surg 28: 657–663
Scarpato R, Gembarowicz R, Farber S, O'Donnell TF Jr, Kelly JJ, Callow AD, Deterling RA (1981) Intraoperative prereconstruction arteriography. Arch Surg 116: 1053–1055
Schäberle W (1992) Diagnosis of venous aneurysm by ultrasound examination (abstract). In: Eurodop 92, Br Med Ultrasound Soc, London, p 157
Schäberle W (1993) Ultraschall in der Venendiagnostik. Springer, Heidelberg
Schäberle W, Eisele R (1990) Duplexsonographische Kriterien eines distalen Mesenterialarterienverschlusses (abstract). Ultraschall Klin Prax 5: 197
Schäberle W, Eisele R (1991) Das sonographische Bild einer zystischen Adventitiadegeneration. VASA 33: 207–208
Schäberle W, Eisele R (1991) Duplexsonographie versus Phlebographie in der Diagnostik der tiefen Beinvenenthrombose. Phlebologie 5: 45
Schäberle W, Eisele R (1992) Duplexsonographische Diagnostik der Fossa poplitea zur Differenzierung seltener arterieller und venöser Gefäßerkrankungen. Ultraschall Klin Prax 7: 148
Schäberle W, Eisele R (1996) Die sonographische Diagnostik, Verlaufsform und Therapie der cystischen Adventitiadegeneration. Ultraschall Med 17: 131–137
Schäberle W, Eisele R (2001) Das venöse Aneurysma tiefer Beinvenen – Wertigkeit der Duplexsonographie in Operationsindikation und Therapieplanung. Ultraschall Med 22 [Suppl]: 60–61
Schäberle W, Neuerburg-Heusler D (1989) Wertigkeit der Duplexsonographie in der Diagnostik der Nierenarterienstenose. Klin Wochenschr 67 [Suppl XVI]: 177
Schäberle W, Seitz K (1988) Meßmethodische Probleme der Durchmesser- und Querschnittsbestimmung für die duplexsonographische Stromzeitvolumenmesseung. Ultraschall Klin Prax Suppl 1: 68
Schäberle W, Seitz K (1991) Duplexsonographische Blutflußmessung in der Arteria mesenterica superior. Ultraschall Med 12: 277–282
Schäberle W, Schock D, Eisele R (1992) Der isolierte Poplitealarterienverschluß: Wertigkeit der Duplexsonographie in Differentialdiagnose und Therapieplanung. VASA 35 [Suppl]: 69–70
Schäberle W, Strauss A, Neuerburg-Heusler D, Roth FJ (1992) Wertigkeit der Duplexsonographie in der Diagnostik der Nierenarterienstenose und ihre Eignung in der Verlaufskontrolle nach Angioplastie (PTA). Ultraschall Med 13: 271–276
Schäberle W, Ulrich Ch, Meyer H, Eisele R (1995) Großes Aneurysma spurium in der A. poplitea nach arthroskopischer Meniskektomie. Arthroskopie 8: 41–43
Scharnke W, Claußnitzer R, Wild K, Schuler A (1995) Aneurysma der V. poplitea als Ursache von Lungenembolien. Diagnose mittels FDS. Ultraschall Med 16: 114
Schatz IJ, Fine G (1962) Venous aneurysms. N Engl J Med 266: 1310–1312
Schellong SM (1993) Vaskulitiden. In: Alexander K (ed) Gefäßkrankheiten. Urban & Schwarzenberg, Munich Vienna Baltimore
Schellong SM, Schwarz T, Halbritter K et al (2003) Complete compression ultrasonography of the leg veins as a single test for the diagnosis of deep vein thrombosis. Thromb Haemost 89: 228–234

Schiff MJ, Feinberg W, Naidisch JB (1987) Noninvasive venous examinations as a screening test for pulmonary embolism. Arch Intern Med 147: 505
Schild H, Berg S, Weber W, Schmied W, Steegmüller KW (1992) Das Venenaneurysma. Aktuelle Radiol 2: 75–80
Schindler JM, Kaiser M, Gerber A, Vuilliomenet A, Popovic A, Bertel O (1990) Colour coded duplex sonography in suspected deep vein thrombosis of the leg. BMJ 301: 1369–1370
Schmidberger H, Hackl A, Ludwig G (1979) Aneurysma der Vena poplitea. Fortschr Röntgenstr 131: 553–554
Schmidt HE (1974) Möglichkeiten und Grenzen der antegraden Phlebographie. VASA 3: 440–445
Schmidt HE (1977) Aszendierende Phlebographie bei tiefer Beinvenenthrombose. Huber, Bern
Schmidt JA, Bierbrauer A, Wichert P (1993) Vaskulitiden großer Arterien. Internist 34: 615–621
Schneider JR, Walsh DB, McDaniel MD, Zwolak RM, Besso SR, Cronenwett JL (1993) Pedal bypass versus tibial bypass with autogenous vein: a comparison of outcome, and hemodynamic results. J Vasc Surg 17: 1029–1038
Schneider PA, Ogawa DY, Rush MP (1999) Lower extremity revascularization without contrast arteriography: a prospective study of operation based upon duplex mapping. Cardiovasc Surg 7: 699–703
Schöllhorn J (1985) Cystic adventitia degeneration as a cause of dynamic stenosis of the popliteal artery: a case report. Angiology 36: 809–814
Scholz H (1995) Der adäquate Gefäßzugang für die Hämodialyse. Bard, Impra, Munich
Schönhofer B, Bechthold H, Renner R, Bundschu HD (1991) Asymptomatische Lungenembolie bei Varikophlebitis der V. saphena magna: Sonographische Dokumentation von Wachstum und Ablösung eines Appositionsthrombus. Phlebologie 20: 48
Schönhofer B, Bechthold H, Renner R et al (1992) Sonographische Befunde bei Varikophlebitis der Vena saphena magna. Dtsch Med Wochenschr 117: 51–55
Schönhofer B, Bundschu HD, Wolf K, Grehn S (1992) Farbkodierte Duplexsonographie im Vergleich zur Phlebographie bei tiefer Bein- und Beckenvenenthrombose. Med Klin 87: 172–178
Schoop W (1988) Praktische Angiologie. Thieme, Stuttgart New York, pp 127f
Schopohl J, Haen E, Ullrich T, Gärtner R (2000) Sildenafil (Viagra). Dt Ärztebl 97: A-311–315
Schröder JO, Euler HH (1993) Systemischer Lupus erythematodes. Internist 34: 351–361
Schuler A, Wild K, Hofstätter F, Claussnitzer R, Blank W, Braun B (1993) Seltene Aneurysmalokalisationen – Farbdopplersonographische (FDS) Diagnostik. Ultraschall Klin Prax 8: 201
Schuler A, Claußnitzer R, Dinkelacker S, Blank B, Braun B (1995) Farbdopplersonographie bei ascendierenden Thrombophlebitiden der unteren Extremität. Ultraschall Med 16: 76
Schürmann R, Balzer TH, Schlief R (1992) Diagnostisches Potenzial von Ultraschall-Kontrastmitteln in der Gefäßdiagnostik. Ultraschall Med 13: 234–238
Schwartz RA, Kerns DB, Mitchell DG (1991) Color Doppler ultrasound imaging in iatrogenic arterial injuries. Am J Surg 162: 4–8
Schwarz T, Romahn K, Schellong SM (2004) The value of compression ultrasound of the calf veins in patients with acute pulmonary embolism. Haemostaseologie 24: 63
Schweizer J, Oehmichen F, Brandt HG, Altman E (1993) Farbkodierte Duplexsonographie und kontrastmittelverstärkte Duplexsonographie bei tiefer Beinvenenthrombose. VASA 22: 22–25
Schwerk WB, Restrepo IK, Stellwaag M et al (1994) Renal artery stenosis: grading with image-directed Doppler US. Evaluation of renal resistive index. Radiology 190: 785–790
Scoble JE (1996) The epidemiology and clinical manifestations of atherosclerotic renal disease: In: Novick A, Scoble J, Hamilton G (eds) Renal vascular disease. Saunders, London Philadelphia Toronto, pp 303–314
Seitz K, Kubale R (1988) Duplexsonographie der abdominellen und retroperitonealen Gefäße. VCH, Weinheim
Sieber CC, Jäger K (1992) Duplex scanning – a useful tool for noninvasive assessment of visceral blood flow in man. Vasc Med Rev 3: 95–114
Sieber CC, Beglinger C, Jäger K, Stalder GA (1992) Intestinal phase of superior mesenteric artery blood flow in man. Gut 33: 497–501
Sievers KW, Löhr E, Albrecht KH, Player T (1989) Diagnose einer Nierentransplantatstenose mit arteriovenöser Fistel durch die Duplex-Doppler-Sonographie. Ultraschall Klin Prax 4: 216–218
Sievers KW, Löhr E, Werner WR (1989) Duplex Doppler ultrasound in determination of renal artery stenosis. Urol Radiol 11: 142–147
Silverstein MD, Heit JA, Mohr DN, Petterson TM, O'Fallon WM, Melton LJ (1998) Trends in the incidence of deep vein thrombosis and pulmonary embolism. Arch Intern Med 158: 585–593
Silvestri M, Villain P, Boursier JL, Elias A (1987) L'anévrisme veineux poplité: une cause rare d'embolie pulmonaire. Presse Med 16: 2127
Siringo S, Bolondi L, Gaiani S et al (1994) The relationship of endoscopy, portal Doppler US flowmetry, and clinical and biochemical tests in cirrhosis. J Hepatol 20: 11
Sitzer M, Fürst G, Fischer H, Siebler M et al (1993) Between-method correlation in quantifying internal carotid stenosis. Stroke 24: 1513–1518
Sitzer M, Muller W, Siebler M, Hort W et al (1995) Plaque ulceration and lumen thrombus are the main sources of cerebral microemboli in high-grade internal carotid stenosis. Stroke 26: 1231–1233
Skillman JJ, Kent KC, Porter DH, Kim D (1990) Simultaneous occurrence of superficial and deep thrombophlebitis in the lower extremity. J Vasc Surg 11: 818–824
Smith H (1984) Quantitative Doppler flowmetry. I. Construction and testing of a duplex scanning system. Acta Radiol 25: 305–312
Smith H (1984) Quantitative Doppler flowmetry. II. Reliability of a duplex scanning system under in vitro conditions. Acta Radiol 25: 535–543
Sperschneider H, Stein G (1996) Update Nephrologie – Teil III. Nierenarterienstenose Rationelle Diagnostik. Med Klin 91: 517–520
Spies KP, Fobbe F, El-Bedewi M, Wolf KJ, Distler A, Schulte KL (1995) Color-coded duplex sonography for noninvasive diagnosis and grading of renal artery stenosis. Amer J Hypertens 8: 1222–1211
Stanziale SF, Wholey MH, Sheehan MK, Makaroun MS (2005) Assessing restenosis of stented carotid arteries by ultrasound criteria. Oral presentation, International Congress 18 on Endovascular Interventions, Phoenix
Stavros T, Harshfield D (1994) Renal Doppler: renal artery stenosis and renovascular hypertension: direct and indirect duplex sonographic abnormalities in patients with renal artery stenosis. Ultrasound Quart 12: 217–263
Steckmeier B, Spengel FA, Küffer G et al (1989) Richtlinien zur Diagnostik und Therapie des Kompressionssyndroms der A. poplitea. Angio 11: 105–113
Steinke W, Kloetzsch C, Hennerici M (1997) Carotid artery disease assessed by color Doppler flow imaging: correlation with standard Doppler sonography and angiography. Am J Roentgenol 154: 1061–1068
Sterpetti AV, Schultz RD, Feldhaus RJ, Davenport KL, Richardson M, Farina C, Hunter WJ (1988) Ultrasonographic features of carotid plaque and the risk of subsequent neurologic deficits. Surgery 104: 652–660
Sterpetti AV, Hunter WJ, Schultz RD (1991) Importance of ulceration of carotid plaque in determining symptoms of cerebral ischemia. J Cardiovasc Surg 32: 154–158
Stief CG (1993) Diagnostik und Therapie der erektilen Dysfunktion. Internist 34: 767–774
Stief CG, Wetterauer U (1988) Erectile responses to intracavernous papaverine and phentolamine: comparison of single and combined delivery. J Urol 140: 1415–1416

Stief CG, Bähren W, Scherb W, Gall H (1989) Primary erectile dysfunction. J Urol 14: 315–319
Stief CG, Truss MC, Becker AJ, Kuczyk M, Jonas U (2000) Pharmakologische Therapiemöglichkeiten der Erektionsstörung. Dt Ärztebl 97: A457–A460
Stiegler H, Weichhain B, Chatzopulos D, Mathies R, Standl R, Mehnert H (1991) Untersuchungen zur Häufigkeit und Symptomatologie der Lungenembolie in Abhängigkeit von der Lokalisation der tiefen Beinvenenthrombose. VASA 20: 119–124
Stiegler H, Rotter G, Standl R et al (1993) Wertigkeit der Duplexsonographie in der Diagnose insuffizienter Vv. perforantes (abstract). VASA 41 [Suppl]: 15
Stiegler H, Rotter G, Standl R, Mosavi S, von Kooten HJ, Wichenhain B, Baumann G (1994) Wertigkeit der Farbduplex-Sonographie in der Diagnose insuffizienter Vv. perforantes. VASA 23: 109–113
Stierli P, Aeberhard P, Livers M (1992) The role of colour flow duplex screening in infrainguinal vein grafts. Eur J Vasc Surg 6: 293–298
Strandness DE (1977) Thrombosis detection by ultrasound, plethysmography, and phlebography. Sem Nucl Med 7: 213–218
Strandness DE (1990) Duplex scanning in diagnosis of renovascular hypertension. Surg Clin N Amer 70: 109–117
Strauss AL, Beller KD (1996) Duplexsonographie mit Echokontrastmittel. Ultraschall Med 17: 260–265
Strauss AL, Beller KD (1997) Arterial parameters under echo contrast enhancement. Eur J Ultrasound 5: 31–38
Strauss AL, Schäberle W, Rieger H, Neuerburg-Heusler D, Roth F-J, Schoop W (1989) Duplexsonographische Untersuchungen der A. profunda femoris. Z Kardiol 78: 567–572
Strauss AL, Scheffler A, Rieger H (1990) Dopplersonographische Bestimmung des Druckabfalls über peripheren Modellarterienstenosen. VASA 19: 207–211
Strauss AL, Roth FJ, Rieger H (1991) Duplexsonographische Bestimmung des Druckabfalls über Iliakaarterienstenosen. Med Klin 86: 498–502
Strauss AL, Schäberle W, Rieger H, Roth F-J (1991) Use of duplex scan in the diagnosis of arteria profunda femoris stenosis. J Vasc Surg 13: 698–704
Strauss AL, Roth F-J, Rieger H (1993) Noninvasive assessment of pressure gradients across iliac artery stenoses: duplex and catheter correlative study. J Ultrasound Med 12: 17–22
Strauss AL, Weber G, Karasch T et al (1995) Quantifizierung hämodynamisch wirksamer Arterienstenosen mit Farbduplexsonographie. In: Ludwig M et al (eds) Doppler-/Duplex-Sonographie in der Intensivmedizin. Kagerer Kommunikation, Bonn, pp 18ff
Strauss AL, Ludwig M, Stein Hj, Horz R, Kopp H, Spengel F, Weber W für den Arbeitskreis Gefäßdiagnostik der Deutschen Gesellschaft für Ultraschall in der Medizin (DEGUM), Sektion Ultraschall der Deutschen Gesellschaft für Angiologie (DGA) und Kassenärztliche Vereinigung Koblenz (1999) Empfehlungen zur Qualitätssicherung in der Ultraschalldiagnostik der Gefäße (1996) VASA 28: 135–139
Streifler JY, Benavente OR, Fox AJ for the NASCET Group (1991) The accuracy of angiografic detection of carotid plaque ulceration. Results from the NASCET. Stroke 22: 149
Stritecky-Kähler T (1994) Chirurgie der Krampfadern. Thieme, Stuttgart New York
Sullivan DE, Peter DJ, Cranley JJ (1984) Real-time B-mode venous ultrasound. J Vasc Surg 1: 465
Sumner OS, Lamberth A (1979) Reliability of Doppler ultrasound in the diagnosis of acute venous thrombosis both above and below the knee. Am J Surg 138: 205
Talbot SR (1982) Use of real-time imaging in identifying deep venous obstruction: a preliminary report. Bruit 6: 41–42
Tamura M, Iriguchi H, Miyamoto T, Kimura K, Kawanishi Y et al (1993): Transition of diagnosis and treatment for impotence. Nippon Hinyokika Gakkai Zasshi 84: 1397 – 1403
Tartarini G, Bertoli D, Baglini R, Balbarini A, Mariani M (1988) Diagnosis of aortic dissection by color-coded Doppler. J Nucl Med 32: 127–130
Taylor DC, Kettler MD, Moneta GL et al (1988) Duplex ultrasound in the diagnosis of renal artery: a prospective evaluation. J Vasc Surg 7: 363–369
Taylor PR, Wolfe JHN, Tyrrell MR, Mansfield AO, Nicolaides AN, Houston RE (1990) Graft stenosis: justification for 1-year surveillance. Br J Surg 77: 1125–1128
Taylor PR, Tyrell MR, Crofton M et al (1992) Colour flow imaging in the detection of femoro-distal graft and native artery stenosis: improved criteria. Eur J Vasc Surg 6: 232–236
Taylor KJW, Burns PN, Wells PNT (1995) Clinical applications of Doppler ultrasound. Raven Press, New York, pp 1–33
Teichgräber U, Gebel M, Benter T, Manns MP (1997) Duplexsonographische Charakterisierung des Lebervenenflusses bei Gesunden. Ultraschall in Med 18: 267–271
Tellis VA, Kohlberg WI, Bhat DJ, Driscoll B, Veith FJ (1979) Expanded polytetrafluoroethylene graft fistula for chronic hemodialysis. Ann Surg 189: 101–105
Tessler FN, Gehring BJ, Gomes AS, Perrella RR, Ragavendra N, Busuttil RW, Grant EG (1991) Diagnosis of portal vein thrombosis: value of color Doppler imaging. Am J Roentgenol 157: 293–296
Theodotou BC, Whaley R, Mahaley MS (1987) Complications following transfemoral cerebral angiography for cerebral ischemia: report of 159 angiograms and correlation with surgical risk. Surg Neurol 28: 90–92
Thetter O (1987) Das Kompressionssyndrom des Arcus tendineus m. solei. In: Heberer G, Van Dongen RJAM (eds) Gefäßchirurgie (Kirschnersche allgemeine und spezielle Operationslehre, vol 11). Springer, Berlin Heidelberg New York, pp 600–602
Thiele BL, Bandyk DF, Zierler RE, Strandness DE Jr (1983) A systematic approach to the assessment of aortoiliac disease. Arch Surg 118: 477–481
Thomas ML, McDonald LM (1978) Complications of ascending phlebography of the leg. Br Med J 2: 317
Thomas CHR, Röder H-U, Möser GH (1989) Diagnostische Wertigkeit der Angiodynographie bei pulsierenden Raumforderungen. Fortschr Röntgenstr 150: 454–457
Thompson MM et al (1998) Comparison of computed tomography and duplex imaging in assessing aortic morphology following endovascular aneurysm repair. Br J Surg 85: 346–350
Tranquet T, Bescos JM, Reparaz B (1989) Noninvasive methods in the diagnosis of isolated superior mesenteric vein thrombosis: US and CT. Gastrointest Radiol 14: 321–325
Tratting S, Hübsch P, Schuster H, Pötzleitner D (1990) Color-coded Doppler imaging of normal vertebral arteries. Stroke 21: 1222–1225
Tratting S, Hübsch P, Schwaighofer B, Karnel F, Eilenberger M (1991) Vaskuläre Raumforderungen der Arteria carotis – Nachweis mit der farbkodierten Dopplersonographie. Ultraschall Med 12: 70–73
Tratting S, Schwaighofer B, Hübsch P, Schwarz M, Kainberger F (1991) Color-coded Doppler sonography of vertebral arteries. J Ultrasound Med 10: 221–226
Tratting S, Plötzleitner D, Hübsch P, Kaha K, Matula CH, Magometschnigg H (1992) Nicht-invasive Verlaufskontrolle mittels farbkodierter Doppler-Sonographie nach operativen Eingriffen an den extrakraniellen hirnversorgenden Arterien. Fortschr Röntgenstr 156: 224–227
Tratting S, Hübsch P, Frühwald F (1992) Farbkodierte Dopplersonographie der Vertebralarterien. In: Frühwald F, Blackwell DE (eds) Atlas der farbkodierten Doppersonographie. Gefäße und Weichteile des Halses und der oberen Extremität. Springer, Vienna New York, p 138
Treiman GS, Lawrence PF, Bhirangi K, Gazak CE (1999) Effect of outflow level and maximum graft diameter on velocity parameters of reversed vein grafts. J Vasc Surg 30: 16–25
Trodoir JHM, De Bruin HG, Hoeneveld H, Eikelboom BC, Kitslaar PJ (1989) Duplex ultrasound scanning in the assessment of arteriove-

nous fistulas created for hemodialysis access: comparison with digital subtraction angiography. J Vasc Surg 10: 122–128
Tucker RM, Lebbarthe DR (1977) Frequency of surgical treatment for hypertension in adults in the Mayo Clinic from 1973–1975. Mayo Clin Proc 52: 542–555
Tucker RM, Strog CG, Brennan LA, Sheps SG (1978) Renovascular hypertension: Relationship of surgical curability to renin-angiotensin activity. Mayo Clin Proc 53: 373–377
Twomey A, Twomey EM, Wilinks RA (1984) Unrecognized aneurysm disease in male hypertensive patients. Br J Surg 71: 307–308
UK Small Aneurysm Trial Participants (1998) Results for randomised controlled trial of early elective surgery or ultrasonographic surveillance for small abdominal aortic aneurysms. Lancet 352: 1649–1660
Umscheid T et al (2001) Nachuntersuchungen bei Patienten nach endovaskulärer Aortenprothesen-Durchführung, Anforderungen und Probleme, Gefäßchirurgie 6: 185–193
Urschel HC, Razzuk MA, Albers JE (1976) Reoperation for recurrent thoracic outlet syndrome. Ann Thorac Surg 21: 19
Valji K, Bookstein JJ (1993) Diagnosis of arteriogenic impotence: efficacy of duplex sonography as a screening tool. Am J Roentgenol 160: 65–69
Van Bemmelen PS, Bedford G, Beach K, Strandness DE (1989). Quantitative segmental evaluation of venous valvular reflux with duplex ultrasound scanning. J Vasc Surg 10: 425–431
Van Bockel JH, van Schilfgaarde R, Van Brummelen P, Terpsta JL (1989) Renovascular hypertension. Surg Gynecol Obstet 169: 467–478
Van Damme, H, Demoulin, JC, Zicot, M, Creemers, E, Trotteur, G, Limet, R (1992) Pathological aspects of Carotid plaques. J Cardiovasc Surg 33: 46–53
Van der Hulst VP, van Baalen J, Kool LS et al (1996) Renal artery stenosis: endovascular flow wire study for validation of Doppler US. Radiology 200: 165–168
Van der Zaag ES, Legemate DA, Nguyen T, Balm R, Jacobs MJ (1998) Aortoiliac reconstructive surgery based upon the results of duplex scanning. Eur J Vasc Endovasc Surg 16: 383–389
Van Gemmeren D, Fobbe F, Ruhnke-Trautmann M (1991) Diagnostik tiefer Beinvenenthrombosen mit der farbkodierten Duplexsonographie und sonographische Altersbestimmung der Thrombose. Z Kardiol 80: 5 23–528
Van Ramshorst B, Legemate DA, Verzijlbergen JF, Hoeneveld H, Eikelboom BC, de Valois JC, Meuwissen OJ (1991) Duplexscanning in the acute deep vein thrombosis of the lower extremity. Eur J Vasc Surg 5: 255–260
Van Ramshorst B, van Bemmelen PS, Hoeneveld H, Eikelboom BC (1994) The development of valvular incompetence after deep vein thrombosis: a follow-up study with duplex scanning. J Vasc Surg 20: 1059 1066
Vandendriessche M, Thiery L (1986) Aneurisma van de vena poplitea. Acta Chir Belg 86: 37–40
Vasdekis SN, Clarke GH, Nikolaides A (1989) Quantification of venous reflux by means of duplex scanning. J Vasc Surg 10: 670–677
Vasdekis SN, Clarke GH, Hobbs JT, Nicolaides AN (1989) Evaluation of non-invasive and invasive methods in the assessment of short saphenous termination. Br J Surg 76: 929–932
Vitovec J (1976) Aneurysma venae poplitae. Cesk Radiol 30: 328–340
Vogel P, Laing FD, Jeffrey RB Jr, Wing VW (1987) Deep venous thrombosis of the lower extremity: US evaluation. Radiology 163: 747–751
Vollmar J (1982) Rekonstruktive Chirurgie der Arterien. Thieme, Stuttgart, pp 137–202
Von Behren P (1998) Harmonic imaging. In: Bogdahn U, Becker G, Schlachetzki F (eds) Echosignalverstärker und transkranielle Farbduplex-Sonographie. Blackwell Wiss.-Verlag, Berlin Vienna, pp 183–191
Vosshenrich R, Kopka L, Castillo E, Bottcher U, Graessner J, Grabbe E (1998) Electrocardiograph-triggered two-dimensional time-of-flight versus optimized contrast-enhanced three-dimensionai MR angiography of the peripheral arteries. Magn Reson Imag 16: 887–892
Wagner G, Kaplan HS (1993) The new injection treatment for impotence. Brunner/Mazel, New York, pp 85–93
Waibel P, Fahrländer J, Ludin H (1966) Die chirurgische Behandlung der Angina abdominalis. Bedeutung der Diagnose in der Prophylaxe des arteriellen Mesenterialinfarktes. Schweiz med Wschr 96: 10
Wain RA, Berdejo GL, Delvalle WN et al (1999) Can duplex scan arterial mapping replace contrast arteriography as the test of choice before infrainguinal revascularization? J Vasc Surg 29: 100–107
Wallner B, Kratzsch G, Friedrich JM, Roth J (1989) Die intraarterielle DSA der Handarterien in der Diagnostik entzündlicher Bindegewebserkrankungen. RöFo 151: 565–568
Walter P, Lindemann W, Koch P, Feifel G (1992) Der akute Mesenterialinfarkt. Klinikarzt 21: 457–463
Walter P, Kubale, R, Gross, G, Beraneck E (1999) Das Kompressionssyndrom des Truncus coeliacus. Gefässchirurgie 4: 28–33
Ward B, Baker AC, Humphrey VF (1997) Nonlinear propagation applied to the improvement of resolution in diagnostic medical ultrasound. J Acoust Soc Am 101: 143–154
Watanabe F, Yoshida T, Akizuki M, Mukai M (1993) Development of multiple subcutaneous nodules in a patient with rheumatic arthritis during methotrexate therapy. Ryumachi 33: 74–79
Wauch J, Sacharias N (1992) Arteriographic complications in the DSA era. Radiology 182: 243–246
Weber J, May R (1990) Funktionelle Phlebologie. Thieme, Stuttgart
Weber G, Strauss AL, Rieger H, Scheffler A, Eisenhoffer J (1992) Validation of Doppler measurement of pressure gradients across peripheral model arterial stenosis. J Vasc Surg: 10–16
Wein AJ, van Arsdalen K, Hanno PhM, Levin RM (1991) Anatomy of male sexual function. In: Jonas U, Thon WF, Stief CG (eds) Erectile dysfunction. Springer, Berlin Heidelberg New York, pp 3–15
Weingarten MS, Branas CC, Czeredarzuk M, Schmidt JD, Wolferth CC (1993) Distribution and quantification of venous reflux in lower extremity chronic venous stasis disease with duplex scanning. J Vasc Surg 18: 753–759
Weinmann S, Sandbichler P, Flora G (1986) Aneurysma der Vena poplitea als Quelle der Lungenembolie. Langenbecks Arch Chir 367: 107–112
Welch HJ, Young CM, Semegran AB, Iafrati MD, Mackey WC, O'Donnell, TF (1996) Duplex assessment of venous reflux and chronic venous insufficiency: The significance of deep venous reflux. J Vas Surg 24: 755–762
Welger D, Müller JH (1988) Assoziierte thrombotische Prozesse des oberflächlichen, perforierenden und intramuskulären Venensystems bei Patienten mit akuter Phlebothrombose der unteren Extremitäten. Z Ges Inn Med Grenzgeb 43: 15–18
Wells DH (1992) Physical and technical aspects of colour flow ultrasound. In: Labs KH et al (eds) Diagnostic vascular ultrasound. Arnold, London, pp 145–152
Wells PS, Lensing AWA, Davidson BL, Prins MH, Hirsh J (1995) Accuracy of ultrasound for the diagnosis of deep venous thrombosis in asymptomatic patients after orthopedic surgery. Ann Intern Med 122: 47–53
Wells PS, Hirsh J, Anderson DR, Lensing AW, Foster G et al (1995). Accuracy of clinical assessment of deep vein thrombosis. Lancet 345: 1326–1330
Wells PS, Anderson DR, Bormanis J, Guy F, Mitchel M, Gray L, Clement C, Robinson KS, Lewandowski B (1997) Value of assessment of pretest probability of deep-vein thrombosis in clinical management. Lancet 350: 1795–1798
Wermke W, Gassmann B (1998) Tumordiagnostik der Leber mit Echosignalverstärker. Springer, Berlin Heidelberg New York Tokyo
Westerband A, Mils JK, Kistler S, Berman SS, Hunter GC, Marek JM (1997) Prospective validation of threshold criteria for intervention in infrainguinal vein undergoing duplex surveillance. Ann Vasc Surg 11: 44–48

Wheeler AHB (1985) Diagnosis of deep vein thrombosis. Am J Surg 150: 7–14
Whelan TJ (1984) Popliteal artery entrapment. In: Rutherford RB (ed) Vascular surgery. Saunders, Philadelphia
White GH et al (2000) How should endotension be defined? History of a concept and evolution of a new term. J Endovasc Ther 7: 435–438
Whitehead (1994) Implantation of penile prostheses. In: Whitehead ED, Nagler HM (eds) Management of impotence and infertility. Lippincott, Philadelphia, pp 27–54
Whitehead ED et al (1990) Diagnostic evaluation of impotence. Postgrad Med 88: 123–136
Widder B (1995) Doppler- und Duplexsonographie der hirnversorgenden Arterien. Springer, Berlin Heidelberg New York Tokyo
Widder B, Reutern GM von, Neuerburg-Heusler D (1986) Morphologische und dopplersonographische Kriterien zur Bestimmung von Stenosierungsgraden an der A. carotis interna. Ultraschall Med 7: 70–75
Widder B, Berger G, Bressmer H et al (1988) Reproduzierbarkeit sonographischer Kriterien zur morphologischen Beurteilung von Karotisstenosen. Ultraschall Klin Prax 5 [Suppl 1]
Widder B, Arnolds B, Drews S (1990) Terminologie der Ultraschallgefäßdiagnostik. Ultraschall Med 11: 214–218
Widder B, Berger G, Hackspacher J, Horz R, Nippe A, Paulat K, Schäfer H, Wieller C, Willeit J (1990) Reproduzierbarkeit sonographischer Kriterien zur Charakterisierung von Karotisstenosen. Ultraschall in Med 11: 56–61
Widder B, Paulat K, Hackspacher J et al (1990) Morphological characterization of carotid artery stenoses by ultrasound duplex scanning. Ultrasound Med Biol 16: 349–354
Widder B, Kleiser B, Hackspacher J, Reuchlin G, Dürr A (1992) Sonomorphological prediction of progressive carotid artery stenoses. In: Oka M et al (eds) Recent advances in neurosonology. Elsevier, Amsterdam, pp 425–429
Wilkinson R (1996) Epidemiology and clinical manifestation. In: Novick A, Scoble J, Hamilton G (eds) Renal vascular disease. Saunders, London Philadelphia Toronto, pp 171–184
Wilson YG, Davies AH, Currie IC, Morgan M, McGrath C, Baird RN (1996) Vein graft stenosis: incidence and intervention. Eur J Vasc Endovasc Surg 11: 164–169
Wixon CL, Mills JL, Westerband A, Hughes JD, Ihnat DM (2000) An economic appraisal of lower extremity bypass graft maintenance. J Vasc Surg 32: 1–12
Wolf KJ, Fobbe F (1993) Farbkodierte Duplexsonographie. Thieme, Stuttgart
Wolf Y et al (2000) Duplex ultrasound scanning versus computed tomographic angiography for postoperative evaluation of endovascular abdominal aortic aneurysm repair. J Vasc Surg 32: 1142–8
Wölfle KD, Neudert S, Mayer B, Storm G, Bruijnen H, Loeprecht H (1992) Duplexsonographische Überwachung von infrainguinalen arteriellen Rekonstruktionen: Kann dadurch ein drohender Bypassverschluss erkannt werden? Zentrbl Chir 117: 540–546
Wölfle KD, Bruijnen H, Mayer B, Loeprecht H (1994) Verlaufskontrolle infrainguinaler Bypassoperationen: Bedeutung von systolischer Spilzengeschwindigkeit und Arm-Knöchel-Index für die Bewertung femorodistaler Rekonstruktionen. VASA 23: 349–356
Wölfle KD, Bruijnen H, Limmer S, Loeprecht H (1999) Autologe Distal-origin-Bypasses zur Überbrückung infrapoplitealer Verschlussprozesse bei Diabetikern mit kritischer Fußischämie. Gefässchirurgie 4: 220–228
Woodcock JP, Fitzgerald DE, Labs KH et al (1992) Consensus on problem areas in diagnostic vascular ultrasound. In: Labs KH et al (eds) Diagnostic vascular ultrasound. Arnold, London, pp 321–325
Woods VL, Zvaifler NJ (1985) Pathogenesis of systemic lupus erythematosus. In: Kelly WN, Harris ED, Ruddy SR, Siedge CB (eds) Textbook of rheumatology, 3rd edn. Saunders, Philadelphia London Toronto, pp 1077–1100
Wuppermann T (1986) Varizen, Ulcus cruris und Thrombose. Springer, Berlin Heidelberg New York Tokyo
Wuppermann T, Exler U, Mellmann J, Kestilä M (1981) Noninvasive quantitative measurement of regurgitation insufficiency of the superior saphenous vein by Doppler ultrasound: a comparison with clinical examination and phlebography. VASA 10: 24–27
Wuppermann T, Knospe E, Reiss HD, Mellmann J (1981) Diagnostik insuffizienter Venae perforantes: Trefferquoten verschiedener Untersuchungsmethoden bei der primären Varikosis. In: May R, Partsch H, Staubesand J (eds) Venae perforantes. Urban & Schwarzenberg, Munich
Yao JST, Van Bellen B, Flinn WR, Bergan JJ (1982) Aneurysms of the venous system. In: Bergan JJ, Yao JST (eds) Aneurysms, diagnosis and treatment. Grune & Stratton, New York, pp 515–529
Yao JST, Flinn WR, McCarty WJ, Bergan JJ (1986) The role of noninvasive testing in the evaluation of chronic venous problems. World J Surg 10: 91–918
Yurcel EK, Fisher JS, Egglin TK, Geller SC, Waltman AC (1991) Isolated calf venous thrombosis: diagnosis with compression ultrasound. Radiology 179: 443–446
Zachrisson BE, Norback B (1974) Phlebographic diagnosis of a soleus vein aneurysm. VASA 3: 308
Zöllner N, Zoller WG, Spengel FA, Weigold B, Schewe CK (1991) The spontaneous course of small abdominal aortic aneurysms. Aneurysmal growth rates and life expectancy. Klin Wochensch 69: 633–6 39
Zuber M, Koch B, Gause A, Pfreundschuh M (1996) Diagnose- und Klassifikationskriterien in der Rheumatologie: Kollagenosen. Dtsch Med Wochenschr 121: 913–919
Zwiebel WJ (1987) Spectrum analysis in carotid Doppler sonography. Ultrasound Med Biol 13: 625–636
Zwiebel WJ (1997) Doppler parameters for carotid stenosis. Semin Ultrasound CT MR 18: 66
Zwiebel WJ (2000) Vascular disorders of the liver. In: Zwiebel WJ (ed) Introduction to vascular ultrasonography. Saunders, Philadelphia London Toronto, pp 431–454
Zwolak RM (2000) Arterial duplex scanning. In: Rutherford RB (ed) Vascular surgery, 5th ed. Saunders, Philadelphia London Sydney, pp 192–214
Zwolak RM, Fillinger MF, Walsh DB, LaBombard FE, Musson A, Darling CE, Cronenwett JL (1998) Mesenteric and celiac duplex scanning: a validity study. J Vasc Surg 27: 1078–108

Subject Index